CELEBRATING 50 YEARS

DEEP FOUNDATIONS INSTITUTE DFI

50th Annual Conference on Deep Foundations

October 20 - 23, 2025

Nashville Tennessee



2025 PROCEEDINGS

50 YEARS OF DEEP FOUNDATIONS EXCELLENCE

DOI:10.37308/DFI50.2025

Preface

The Deep Foundations Institute (DFI) proudly celebrates a historic milestone—the 50th Annual Conference on Deep Foundations. This event honors five decades of progress, collaboration, and innovation in our industry, while setting the stage for the future. On behalf of the 2025 Annual Conference Organizing Committee, we extend our sincere appreciation to all attendees, exhibitors, underwriters, speakers, presenters, session chairs, moderators, and volunteers whose contributions have made this gathering a tremendous success. We are excited to be part of this organization and come together with everyone to celebrate this year's annual conference.

Held in Nashville, Tennessee, from October 20–23, this year's conference theme, **"50 Years of Deep Foundations Excellence,"** reflects the remarkable journey of our profession. The program features a rich blend of technical sessions, case studies, and presentations covering the state of practice, emerging innovations, design and modeling advancements, equipment and testing technologies, software applications, and collaborative delivery methods. Keynote presentations and panel discussions from some of the industry's most influential voices will reflect on five decades of progress and share their visions for the future, offering inspiration and insight as we look ahead.

As Karl Terzaghi once observed, *"Unfortunately, soils are made by nature and not by man, and the products of nature are always complex… As soon as we pass from steel and concrete to earth, the omnipotence of theory ceases to exist."* This timeless insight reminds us why we gather—to share knowledge, solve complex challenges, and advance the art and science of deep foundations. It also speaks directly to DFI's mission: *To bring together multidisciplined individuals and organizations to find common ground and create a shared vision and a consensus voice for continual advancement in the deep foundations industry.*

This mission has guided DFI for 50 years and continues to unite contractors, consultants, suppliers, owners, and academics from around the world. We also recognize the extraordinary efforts of the sponsors, organizing committee, DFI staff, authors, reviewers, and all those who dedicated over a year of planning to bring this conference to life. Your commitment and collaboration are what make this event truly special.

Here's to honoring our legacy—and shaping the next 50 years of excellence in deep foundations.

Conference Chair: John Wolosick, P.E., S.E., BC.GE, F.ASCE, Keller North America

Program Co-Chairs: Lois Schwarz, Ph.D., Tensar A Division of CMC

Sam Sternberg III, P.E., BC.GE, Kiewit Infrastructure Engineers

Adam Hacker, P.E., HDR

Adventures in Karst Geology

Sinkhole Mitigation Using Compaction Grouting: A Case Study of Driveway Stabilization in Nashville, Tennessee
Hossein Alimohammadi, Ashfaq Memon *1*

Case Study- Effects of Undisclosed Large Diameter Sinkhole on Construction, Clearwater, Florida
Karl A. Higgins *10*

Sinkhole Whack-A-Mole - Lessons Learned Grouting a 25MGD Karstic Mine Leak
Kirk Roberts, Dustin Roberts, Brian Bucek *25*

Developments in Marine Projects

Enhancing Structural Performance of Monopiles Using Extenders: A Comparative Study on Lateral Pile Displacement and Load Capacity
Dhruvi Gondalia, Francisco Ciruela-Ochoa, Francesc Mirada *33*

Geo-Hazards (Seismic and Other Natural)

Calculated Load-Transfer Responses From Atypical Strain Readings Using the Incremental Rigidity Method
Van E. Komurka, Seth O. Robertson *43*

Experimental Curvature and Moment Response of Pile Foundations: Comparison With P-Y Predictions
William P. Shaffer, Rabie Farrag, Anne Lemnitzer *53*

Monte Carlo Simulation to Assess Soil Property Uncertainties for Seismic Evaluation of Existing Structures
Martin B. Hudson,, Kenneth S. Hudson *63*

Growth of Ground Improvement

Foundation Systems for Storage Tanks in Hydrocarbon Complexes: Critical Considerations and Case Studies
Sampat Raj, Sanjoy Bhowmik, VK Panwar *72*

Case Study of Small-Diameter Continuous Flight Auger Piles Tested By Bidirectional Static Load Tests in Tropical Soil
Yuri Barbosa, Alysson S. Resende, Marianna N. Carvalho, Nilton A. Chaves, J. R. Albuquerque, Marcos M. Futai *88*

The Impact of Rigid Inclusions on the Design of Footings and Slabs
Sonia Sorabella Swift *99*

Variability Assessment of Helical Piles Performance Via Geometric Conical Enhancement
Sara Heidarie Golafzani, Mostafa Nazmi, Abolfazl Eslami *111*

Benefits of a Construction Information Management System Applied to a Large Deep Soil Mixing Project
Will Tanner, Mohamed Elgouhary *122*

Application of Auger Cast-in-Place (ACIP) Piles in Urban Infrastructure: A Case Study of Philadelphia's Samuel S. Baxter Water Treatment Plant
Michael Whelan, Abhijit R. Sheth, Michael D. Bennett, Timothy J. Brennan *131*

Ground Improvement and Construction Challenges of Massive Fine-Grained Fill Embankments to Support Settlement Sensitive Structures
Carlos Dowell, Omar Conte, Roger Archabal *145*

Sacramento River East Levee Contract 4 – Seepage Cutoff Wall Construction Challenges and Solutions
Nagesh Malyala, Timothy Williams, Kimberly Brown *157*

Jet-Grouting: A Wide Range of Applications
Nathan P. Coughenour, Daniel G. Ruffing, Josh Bonetto *170*

Industry Evolution and Knowledge Transfer

Driven Precast Concrete Piles In lieu of Steel Piles at BlueScope Steel's Port Kembla Facility
Stephen Harkin, Wagstaff Piling *180*

Current Practice Concerning Drilled Shafts to Support Buildings in Japan
Yusuke Homma,, Yujiro Tanaka, Kentaro Oko *192*

Load Bearing Characteristics of Bored Precast Prestressed Nodular Piles
Yujiro Tanaka, Yusuke Homma, Kentaro Oko *202*

Low Carbon Initiatives at Euston Station HS2– The Environmentally Friendly Way of Pile Installation in the City of London
Franz-Werner Gerressen, Johann Kraxenberger, Deon Louw *213*

Suspension Underpinning of A Waterfront Chemical Facility
Michael Senior, Theodore Hudson, Samuel Hudson, Kirsten Grant *224*

The Evolution of Steel Piling Products Over the Last 50 Years
Pierre N. Werner, Dean Abbondanza *234*

Mass Concrete Drilled Shafts: Specification Landscape and Recommended Revisions
Andrew Z. Boeckmann, Paul J. Axtell, J. Erik Loehr *243*

Drilled Shaft Load Tests in Weakly Cemented Sandstone
David S. Graham, Paul J. Axtell *256*

Digitalization in Reverse Circulation Drill Rigs
Nikolas Schmitz, Lukas Biedak *267*

USACE-DFI Working Group on Seepage Control
Mary Ellen Bruce Large, David Paul, April Fontaine, Erik James *277*

Performance of Stone Columns With Alternate Granular Materials in Different Types of Soils
K. Kavinmalar, P. Kiruthika, A. Murali Krishna *287*

Geotechnical Monitoring Systems: The New Multi-Parametric DMS Columns - The Importance of the Testing in Lab and in Field For Reliability and Data Interpretation in the Early Warning Applications
Mario Lovisolo, L. Foglino *298*

Innovations and Quality in Equipment Design For Safety and Efficiency
Kai Fiand, Paul Doherty *310*

Slurry Wall Design Techniques and Construction Practices Over the Last 50 Years in Northeastern United States
S. Y. Fantaye, Ketan Trivedi Alex Ciamei, Lixun Sun *318*

Observations and Impact of Field Logging and Drilling Procedures on Site Characterization of Cambridge Argillite in Somerville, Ma
Udit S. Dasgupta, Andrew K. Keene *333*

Managing Risk with Testing and Data

Applying Machine Learning for SPT-N Prediction from Raw CPT Data
Milad Fatehnia, Schnabel, Sanaz Paran *345*

Applying The Incremental Rigidity Method To Static Load Tests Performed On All-Steel Piles
Joseph B. Mulcahey, Brett E. Belzer 356

Foundation Support of the Lilly Medicine Foundry in Lebanon IN
W. Morgan Nesmith, Jake K. McKean 369

Case Study - Statistical Analysis of Helical Pile Tests in a Power Transmission Line Project
Danilo Policastro 386

An Optimized Approach For Managing Overhead Transmission Line Foundation Design and Construction Risk
James P. Adams, Mariah Paz, Daniel Rosenbalm, Peter Kandaris 399

From Data to Action: Using Testing to Address MWD-Identified Deviations in Rigid Inclusion Installation
Chelsea Riddle, Keller North America, Kenneth T. Kniss, Keller North America 419

Foundation Design and Osterberg Cell Pile Load Testing in Brisbane, Australia
David Cunliffe, Daniel Schutt 429

Modeling the Past, Present and Future

Investigation of Limit Equilibrium Method and Finite Element Analyses for Ground Anchored Slopes
Farnyuh Menq, Daqing Xu, Luis Vasquez, Shin-Tower Wang 439

Improving the Reliability of Pile Drivability Studies by Explicitly Simulating Ground Disturbance
Edward J. Smith 451

Modern View of In-Situ Wall Prediction and Movement
Enrique Farfan, Adam Hacker, Tom Pace 466

Case History: Harbor Point Baltimore Evolution of Deep Foundations Over 40 years
Adam M. Dyer, Srinivas Yenamandra 478

Sustaining the Future

Sustainable Solutions For RCC Foundation Durability: Case Studies in Aggressive Subsoil and Groundwater Conditions
Geethanjali Koppolu, Sampat Raj, Sanjoy Bhowmik, VK Panwar 490

Conceptual Axial Stress-Strain Behavior Assessment of Drilled Displacement Piles Using Full-Scale Load Tests Database
Abolfazl Eslami, Arshiya Mehrazma, Amirhossein Ebrahimipour *502*

It's Not Delivery, It's Dynamic Compaction
Noah Miner,, Lisheng Shao, Jim Glider *513*

Sustainable Shoring
Chelsea N. Miller *521*

Transportation Application

A New Geomaterial for Roads Based on Mining Waste For Sustainability and Resiliency
Maria Vitoria Morais, Leonardo Marchiori, Luis Andrade-Pais, Antonio Albuquerque, Victor Cavaleiro *532*

The Foundations of the Railway Bridge Over the B25 in Donauwörth
Freddy Lopez, Tiroler Rohre, Erich Steinlechner, Tiroler Rohre *540*

Large Drilled Shaft Foundations and Bi-Directional Test Program For the West Seattle Link Extension Project
Dirk Bakker, Sound Transit, Yang Jiang, *550*

Performace of Muiti-bar GFRP Tiebacks
Mike Porco, Naji Shbaklo, Alireza Asadian, Rick V. Dozzi, Borna Hajimiragha *563*

Complex Logistical Constraints and their Technical Impact on A Deep Excavation Design, Ottawa, Ontario, Canada
Anna Crockford, Charles Luxford, amid Batenipour, Kristopher Burnham *575*

Reuse of Existing Piles Study – Hwy 417
Tony Sangiuliano, Nathan Bakker, Susan Ould-Brahim, Gregory Louisy, Paul Carnaffan *586*

Evaluation of Piles' Ultimate Capacity Utilizing Direct Cpt Methods Considering Consolidation and Aging Setup
Murad Y. Abu-Farsakh, Isam A. Khasib *598*

Finite Element Study on the Effect of Barge Impact on Bridges With Different Pile Group Configurations
Murad Y. Abu-Farsakh,Ahmad Souri, George Z. Voyiadjis *608*

Deep Foundation Design and Construction Challenges at Hunts Point Interchange in Bronx, New York

Alireza Ayoubian, Paul B. Pizzimenti, Jean Louis Locsin, Alfredas Daugiala *617*

Reliability Analysis of Drilled Shaft Resistance: A Case Study of the Circunvalacion Norte Viaduct Project
Bernardo Jiménez, Adrián Torrico Siacara *627*

North East Link Project, Melbourne, Australia Lower Plenty Road Interchange Diaphragm Wall Works
Z. El Hajj, Thadu Khin *640*

Design and Geotechnical Studies of Deep Foundations for Bridges in the Peruvian Lowland Rainforest
Jorge E. Alva, Miriam R. Escalaya, Alvaro J. Pérez *651*

Design & Construction Challenges of One the Deepest RCC Bored Cast-In-Situ Raker Pile
Naveen Govindaraju, Udaiveer Singh, Vikas C. Rane, Ramesh K. Shrivastava, *660*

Construction of a Retaining Structure Within Complex Site Conditions
Clayton Price *671*

Bridging Challenges: Creative Solutions For the I-81 Bridge Foundation Design
Ram K., Kamal R. *680*

Application of Random Fields in Commercial Finite Difference Software for Reliability Analysis of Laterally Loaded Piles
Adam Hassan, Ahmed Mahgoub, Don Dotson, D.V. Griffiths *690*

Construction Challenges of the Port Everglades Bypass Road on Highly Compressible Soils in Broward County, Florida
Gustavo J. Hernandez, Rafael, Matthew Meyer *701*

Subsurface Exploration for I-40 Reconstruction in the Pigeon River Gorge Post Hurricane Helene
Christopher J. Ramsey, Michael Senior *716*

Use of Nondestructive Testing to Establish Installation Disturbance Zone Criteria For Adjacent Continuous Flight Auger Pile Installation on Design Build Project
Saad Rehmatullah, Alfredas Daugiala, Les R. Chernauskas, William D. Oder *725*

Navigating Complexity: Engineering Solutions for I-81's CSX Railyard Bridge Expansion
Ram Kasturi, Eshana Kolli *738*

Application of Diverse Ground Improvement Techniques for the Stabilization of Reinforced Earth Wall Approach Ramps

Vijaya Bhushan Rao, Jason Redgers *748*

Multiobjective Optimization of Drilled Shafts in the Circunvalación Norte Viaduct Using Pareto-Front Analysis
Bernardo Jiménez, Adrián Torrico Siacara *760*

Sacramento River East Levee Contract 4 – Construction of Seepage Cutoff Wall
Pablo Bassola, Scott Gordon, Maurizio Siepi, Chris Hamilton *773*

Speedy Rebuilding of Earthquake-damaged Highway Embankment with Pressed-in Pipe Pile Wall
Takefumi Takuma, Shinya Kubo *784*

Innovative Bridge Pier Installation Using the Super Reach Attachment System: Insights from the design-build Jimmie Davis Bridge Replacement Project
Jewels Stover, Sean Pruet *794*

Underground and Tunneling

CSO 52 - Temporary Support of Excavation and Deep Foundations for Flood Protection
Garrison Mueller, Jake Coibion *804*

Mechanized Shaft Sinking With VSM: Safe and Resource-Saving Construction of Shafts and Foundations in Urban Surroundings
Stefan Frey, Julian Binder, Herrenknecht AG *815*

Adapting Diaphragm Wall Design for Post-Disaster Structures on Soft Ground: Challenges Under the 6th Generation Seismic Code
Atieh Shooshpasha, EllisDon, Amir Poshnejad, EllisDon *826*

Engineering Heritage: Integrating North America'S Largest Façade Retention System With Support of Excavation in the United Bldg. Project
Mark Reinders, Thomas Fiala, Lauren Speakman *837*

Modeling to Monitoring: Evaluating Adjacent Structures Feet from a Boston Excavation
Tyler M. Poggiogalle, Damian R. Siebert, Wystan Carswell *850*

Design, Construction, and Performance of a Sensitive Braced Excavation in Boston Blue Clay
Dylan W. Locke, Collin E. Sweeney, Jeffrey M. Taylor *859*

Performance of Rock Anchors for Underground Construction in Manhattan Schist – Influence of Geological Features
Chu E. Ho *870*

Innovative Approaches to Assessing Unknown Pile Lengths: Ensuring Clearance and Stability for Urban Tunneling Projects
Hamed Layssi, Farid Moradi, Mohammadhossein Afsharipour, Richard Malantic, Kambiz Daneshvar *884*

Innovative Secant Pile Excavation Support: Weapons Storage and Maintainance Facility – Malmstrom Air Force Base
Seth T. Hoffman, Bill Zietlow, Brendan Harkins *896*

NYCOT Builds a Bridge Under a Bridge Under a Bridge in Brooklyn
Anthony Loreto, Lisa Papandrea *906*

Working Platforms

Calculating the Load Capacity and Safety of Helix Piles
David A. Cabral, Flavia S. Cabral *919*

Panel Discussion

The Importance of Collaborative Project Delivery – Looking Back While Looking Forward
Luca Barison, Brad Long, Tom Pullen *931*

SINKHOLE MITIGATION USING COMPACTION GROUTING: A CASE STUDY OF DRIVEWAY STABILIZATION IN NASHVILLE, TENNESSEE

Hossein Alimohammadi, Ph.D., P.E., Terracon Consultants, Inc., Nashville, TN, USA
Hossein.Alimohammadi@terracon.com
Ashfaq Memon, P.E., Terracon Consultants, Inc., Nashville, TN, USA Ashfaq.Memon@terracon.com

ABSTRACT

Sinkholes present significant challenges to infrastructure, necessitating thorough investigation and effective remediation techniques. This paper examines a case study of a persistent sinkhole along a driveway in Nashville, Tennessee, where repeated pavement depressions occurred despite prior repair efforts. The study involved site inspections, drilling, analyses of soil and rock properties, and groundwater evaluations. Three repair methods were considered: traditional inverted rock filter, a land bridge construction, and compaction grouting. Taking into account technical feasibility, site-specific factors, and budget constraints, compaction grouting was selected as the most suitable approach. The paper details this solution, covering the grouting process, materials used, and construction specifications. The study's outcomes aim to inform and improve design standards and construction techniques for sinkhole repairs in Tennessee and comparable geological areas.

Keywords: sinkhole mitigation, compaction grouting, stabilization, case study

INTRODUCTION AND LITERATURE REVIEW ON SINKHOLE REMEDIATION METHODS AND CASE STUDIES

Sinkholes represent a significant geohazard with far-reaching implications for infrastructure integrity, public safety, and environmental stability, particularly in regions susceptible to subsidence. These phenomena typically occur due to natural geological processes such as the dissolution of soluble bedrock in karst terrains as well as anthropogenic activities, including mining, groundwater extraction, and construction (Waltham et al., (2005), Gutiérrez et al., (2008)). The unpredictable nature of sinkhole formation poses substantial challenges for risk assessment and mitigation, demanding innovative engineering solutions and site-specific remediation strategies.

A sinkhole forms when a subterranean void collapses, resulting in a sudden depression at the surface. Their sizes range from minor cavities to large craters capable of causing severe damage to roads, buildings, pipelines, and other critical infrastructure. Triggering mechanisms include heavy rainfall, groundwater level fluctuations, leakage from utility services, and vibrations from nearby construction (Parise et al. (2007), Brinkmann et al. (2008)). Due to their destructive potential, a wide body of research has focused on both proactive and reactive approaches to managing sinkholes. Proactive strategies emphasize hazard avoidance and risk reduction, encompassing detailed geotechnical investigations, remote sensing technologies, subsurface geophysical surveys (e.g., GPR, resistivity imaging), and continuous groundwater monitoring. Land-use planning and zoning regulations are also critical in limiting development in high-risk areas (Doctor et al. (2008), Kaufmann et al. (2013)).

Conversely, reactive strategies address sinkholes post-formation, aiming to stabilize ground conditions and repair affected infrastructure. These methods may involve compaction grouting, void filling with low-mobility grouts, underpinning structures, and rebuilding damaged facilities. In some cases, ecological restoration or bioengineering methods such as vegetative stabilization and hydrological balancing are used to enhance the sustainability and resilience of the remedial work (Yilmaz (2010), Gutiérrez et al. (2014)). Construction in karst-prone regions is particularly risky, necessitating meticulous planning and

 © Deep Foundations Institute 2025

execution. Key precautions include proper drainage design to prevent ponding, installation of stormwater management systems to control runoff, and continuous inspection during construction phases to identify early signs of ground instability. The involvement of geotechnical experts is essential throughout the project lifecycle to evaluate karst features and guide design adjustments as necessary.

Recent technological advancements have further expanded the toolkit for karst hazard management. Remote sensing platforms (e.g., LiDAR, InSAR) enable high-resolution terrain analysis, while numerical modeling tools facilitate prediction of subsidence patterns and ground deformation (Bennett et al. (2016)). Nature-based solutions, such as wetland restoration and soil bioengineering, offer environmentally friendly alternatives that integrate sinkhole mitigation with ecosystem restoration objectives (Paukstys et al. (2008), Galve et al., (2015)). Despite these innovations, challenges remain. Limited financial and technical resources, inadequate infrastructure, and conflicting land-use interests often hinder the effective implementation of comprehensive mitigation programs. Moreover, the dynamic evolution of karst systems—driven by hydrological and climatic variability—continues to complicate long-term hazard prediction and management (Ford et al., (2007)).

This paper provides a comprehensive synthesis of current sinkhole mitigation techniques and karst hazard management strategies. By integrating traditional engineering practices with cutting-edge technologies and sustainable approaches, it aims to contribute to a deeper understanding of best practices in reducing sinkhole-related risks and enhancing resilience in vulnerable landscapes. The study's outcomes aim to inform and improve design standards and construction techniques for sinkhole repairs in Tennessee and comparable geological areas (Alimohammadi et al., (2024)).

SITE DESCRIPTION AND PROBLEM HISTORY

The sinkhole located on Whispering Hills Drive, just north of Bonerwood Drive in Nashville, Tennessee, has become a source of persistent concern due to its ongoing subsidence and structural implications. Whispering Hills Drive is a two-lane asphalt roadway, approximately 9.14 meters in width, with a gentle downward slope toward the north-northeast. The affected area spans nearly 15.24 m along the travel lanes, exhibiting noticeable surface deformation and settlement. Of particular concern is a localized dropout measuring approximately 1.82m in diameter, situated in the eastern (northbound) lane. Subsurface utilities are present within the area of concern, including a 0.91m diameter water transmission main and a 0.30m water distribution line. Additionally, a storm drain traverses the depressed section of pavement near the eastern shoulder, while a stone-lined ditch runs parallel to the western side of the road. The combination of critical infrastructure and compromised subsurface conditions necessitates urgent and careful attention. This section of roadway has experienced recurring issues over an extended period. Historical accounts from Metro Public Works staff indicate that site inspections were conducted as early as the late 1990s, with intermittent dropouts and ground subsidence attributed to soil piping processes, a common mechanism in karst-prone regions where fine soils are washed into underlying voids, leading to surface collapse. In response to these issues, conventional sinkhole remediation measures have been employed multiple times, typically consisting of excavation of unstable materials and backfilling with crushed stone, followed by pavement restoration.

The most recent repair attempt occurred approximately four months prior to the current study (Alimohammadi et al. (2024)). At that time, the damaged asphalt pavement was removed, and soft subgrade materials were excavated to an unspecified depth. The undercut area was then refilled with crushed rock and overlaid with a thick asphalt surface course. Despite these efforts, the area again exhibited signs of significant settlement, culminating in a renewed dropout that prompted further investigation and a comprehensive mitigation strategy. Since late May 2009, the affected segment of Whispering Hills Drive has been closed to vehicular traffic due to safety concerns. Figure 1 presents an

overview of the dropout area within the roadway. Figures. 2a and 2b document current site conditions, including visible depressions and areas of pavement failure, illustrating the severity of the ongoing subsidence. The recurrence of sinkhole activity, despite repeated repairs, suggests that the underlying geotechnical and hydrological conditions have not been adequately addressed. This underscores the need for a more holistic and technically robust approach to evaluating the site, characterizing subsurface conditions, and implementing long-term remediation measures that account for the regional karst geology, utility interactions, and groundwater dynamics.

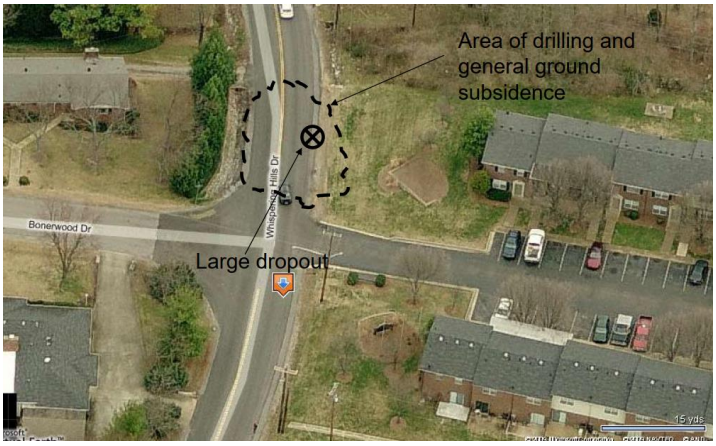


Fig. 1. The approximate location of dropout within the roadway



a) **b)**

Fig. 2. a and b) The existing site situations and dropouts within the roadway

FIELD EXPLORATION AND LABORATORY TESTING

The subsurface investigation was conducted in two primary phases to characterize the geotechnical conditions underlying the site, particularly in proximity to the observed sinkhole. The first phase occurred between April 24 and April 28, 2009, during which a total of seven borings were advanced within the affected area. Borehole depths ranged from approximately 5.18 to 14.78m below existing ground surface. A second phase of exploration was conducted on June 8 and 9, 2009, involving the advancement of five additional borings aimed at enhancing the spatial resolution of the subsurface profile and refining the geotechnical characterization.

 © Deep Foundations Institute 2025

Drilling operations employed both truck-mounted rotary drill rigs and all-terrain vehicle (ATV)-mounted rigs, each equipped with hollow-stem augers to facilitate advancement of the boreholes. Standard penetration tests (SPT) were performed in accordance with ASTM D1586 using a 5.08cm outside diameter (O.D.) split-barrel sampler. The number of blows required to drive the sampler the final 0.3m of an 0.45m penetration was recorded as the standard penetration resistance value (N-value). This data provided a basis for estimating the relative density of granular soils and the consistency of cohesive materials. All borehole activities, including sampling depths, penetration lengths, and SPT N-values, were meticulously documented in field logs. Recovered soil samples were sealed and transported to the laboratory for classification and testing. Field logs included preliminary visual-manual classifications of soil strata, as well as the drillers' interpretations of lithological transitions between sampled intervals. Final boring logs incorporated both field observations and laboratory data, with modifications applied where necessary based on laboratory results. Each boring was advanced to auger refusal, which generally occurred at depths ranging from 2.28 to 14.78m below ground surface. In seven of the twelve borings, underlying refusal materials were further penetrated using a double-tube core barrel system with an outer barrel fitted with a diamond bit. The high-speed rotating outer barrel facilitated rock cutting, while the inner barrel collected intact rock cores. After each core run, the barrel was retrieved and the rock cores were boxed, logged, and prepared for subsequent laboratory evaluation.

The geotechnical investigation involved detailed rock core classification, assessing percent recovery and Rock Quality Designation (RQD) to evaluate in-situ rock quality, alongside laboratory tests for natural water content and Atterberg Limits to characterize fine-grained soils. These findings, combined with Standard Penetration Test (SPT) data and soil classifications based on USCS standards, supported the evaluation of subsurface behavior and soil strength. Rock descriptions were primarily based on visual and tactile observations, although petrographic analysis via thin section microscopy was noted as a potential method for further lithologic identification, if warranted. All laboratory results and rock quality assessments were systematically documented on the finalized boring logs. These logs provide a comprehensive record of subsurface conditions, serving as the foundation for subsequent geotechnical analysis and design recommendations. The rock units underlying the site belong to the Ordovician-age Hermitage Formation, consisting of stratified limestone layers, phosphatic limestone, Coquina, laminated argillaceous limestone, and Curdsville Limestone, each with distinct physical characteristics. Weathering of these carbonate rocks produces residual silty, sandy clay soils, common in the site's boreholes. The site lies in a karst-prone region susceptible to sinkhole formation and soil piping, which threaten infrastructure stability. Although symptoms like pavement subsidence suggest ongoing karst activity, geotechnical tools currently lack precision in predicting such hazards. Field investigations included twelve borings (B-1 through B-12), strategically placed to assess subsurface conditions within the affected pavement area and adjacent right-of-way. Borings B-1 through B-8, B-11, and B-12 were located within the pavement footprint, where asphalt thickness varied from 9 to 61 cm. Borings B-9 and B-10, placed outside the pavement along the right-of-way, encountered 13 to 18cm of topsoil overlying deeper materials. Figure 3 represents location of the borings across the site and near the studied dropout and Table 1 illustrates auger refusal and fill depths in performed borings.

 © Deep Foundations Institute 2025

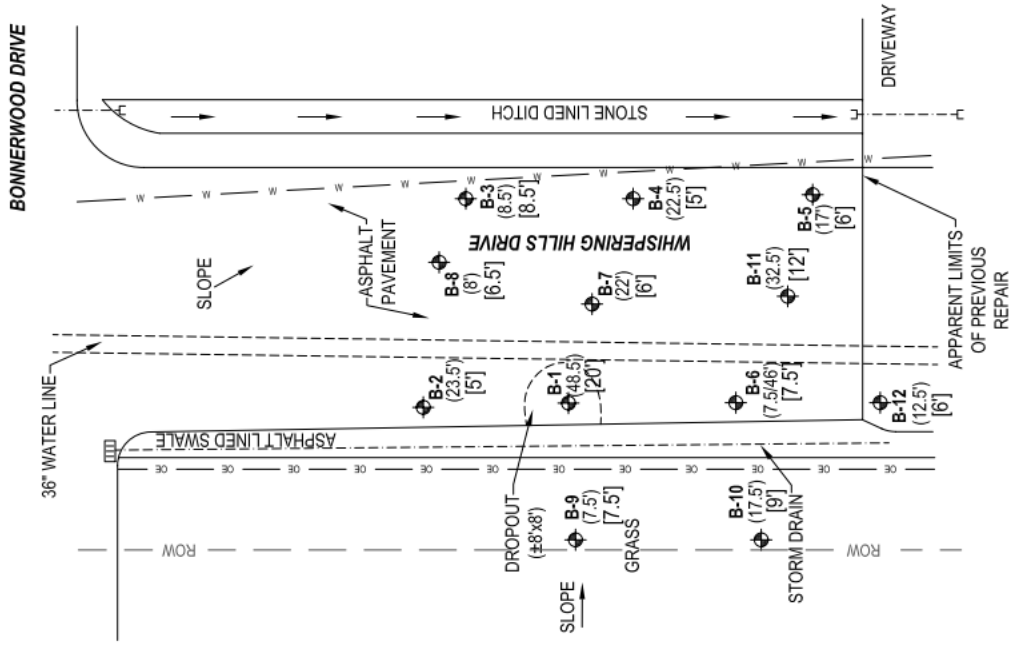


Fig. 3. Location of the borings across the site and near the studied dropout

Table 1. Auger refusal and fill depths in performed borings

boring	approximate fill depth (m)	approx. depth to refusal (m)	boring	approximate fill depth (m)	approx. depth to refusal (m)
B-1	6.1	14.78	B-7	1.82	6.70
B-2	1.52	7.16 *	B-8	1.98	2.43 *
B-3	2.59	2.59 *	B-9	2.28	2.28 *
B-4	1.52	6.85 *	B-10	2.74	5.33
B-5	1.82	5.18	B-11	3.65	9.9
B-6 **	2.28	14.02 *	B-12	1.82	3.81 *

* Boring where rock coring was performed

** Initial auger refusal occurred at a depth of about 2.28m on weathered limestone rock layer

Below the surficial cover, boreholes generally penetrated between 1.52 and 6.1m of fill material, typically overlying native lean to fat clay and limestone bedrock. At Boring B-1, located directly within a pavement dropout area, the fill extended to a depth of approximately 6.1m and consisted predominantly of crushed rock with varying degrees of clay content and minimal fines. Notably, Boring B-3 included mixed soil and rock, while B-9 and B-10 revealed large limestone fragments likely representative of shot rock fill. Natural cohesive soils underlying the fill included lean to fat clay of very soft to medium stiff consistency. Standard Penetration Test (SPT) values for the clay ranged from 0 to 6 blows, with occasional stiffer layers at B-4 and B-12. These soft conditions may signify prior solutioning and soil piping activity, typical indicators of developing karst voids and instability. Auger refusal, indicative of bedrock contact, occurred

 © Deep Foundations Institute 2025

at depths ranging from 2.28 to 14.78m below the existing surface. Deeper refusal zones were noted at Borings B-1 and B-6. A noteworthy anomaly was detected at B-4, where a 1-foot void was observed between the bottom of the asphalt and the top of the underlying crushed rock fill—highlighting ongoing subsurface erosion. The relative density of the fill materials was highly variable, ranging from very loose to medium dense, with SPT N-values between 0 and 23 blows. However, the presence of large limestone fragments likely exaggerated these blow counts, leading to potential overestimations of in-situ density and strength.

Selected borings (B-2 through B-4, B-6, B-8, B-9, and B-12) included rock coring to further characterize the bedrock at auger refusal. The retrieved core samples primarily consisted of light to medium gray limestone with thin to very thin bedding and weathered shaly seams. Core recovery was inconsistent, ranging from 30% to 100%, with particularly poor recovery noted at B-9 and B-12, possibly due to the fragmented or highly weathered nature of the bedrock. The quality of recovered rock, evaluated using Rock Quality Designation (RQD), varied from very poor to fair (0–75%). In Boring B-6, auger refusal occurred at 2.28m on weathered limestone, which extended to 4.26m in depth. Below this, the core barrel advanced with minimal resistance down to 4.26m, recovering no competent material suggesting the presence of a clay-filled solution channel, a hallmark of advanced karstification within the Hermitage Formation. At Boring B-9, coring revealed moderately to highly weathered limestone with numerous voids and crevices filled with concrete grout. Intriguingly, a 7.62cm thick piece of asphalt was encountered during coring at a depth of 3.65m, likely the remnant of previous compaction grouting efforts to remediate subsurface voids within the rock mass.

EVALUATION AND RECOMMENDATIONS

These findings affirm that the site is influenced by active karst processes typical of the Hermitage Formation, with evidence of solution cavities, clay infill, and variable rock quality. The presence of deeply weathered zones, fill over voids, and poorly recovered cores underscores the potential for subsurface instability and sinkhole formation. The detection of previous grouting remnants suggests that mitigation efforts may have occurred historically, albeit with limited documentation. Going forward, remediation strategies must account for the heterogeneous and karstic nature of the subsurface, employing both direct investigation and non-invasive geophysical techniques (e.g., electrical resistivity tomography, ground-penetrating radar) to delineate voids and assess risk zones. Engineering responses may include deep dynamic compaction, compaction grouting, or structural support systems tailored to the localized subsurface conditions.

Based on a comprehensive analysis of subsurface conditions, including geotechnical data and field observations, the observed pavement distress and localized ground dropout are attributed to ongoing soil piping and subsidence—strongly indicative of a developing or reactivated sinkhole feature. Prior repair efforts were largely superficial, failing to address the deeper, underlying mechanisms of instability. An initial remedial option considered was the conventional inverted rock filter method commonly used for sinkhole stabilization. However, successful implementation of this method requires excavation down to competent bedrock, estimated at a depth of approximately 14.78m. Given the proximity to adjacent properties and the confined work zone, this would necessitate extensive shoring of vertical sidewalls and the relocation of existing underground utilities. The logistical challenges and high costs associated with deep excavation and utility rerouting rendered this option infeasible.

A second option, constructing a structural land bridge over the compromised area, was evaluated. While theoretically viable, this approach was ultimately dismissed due to excessive projected costs and scheduling concerns. The extended design and construction timeline, spanning several months, posed unacceptable disruptions to stakeholders and project milestones. Following consultation with geotechnical

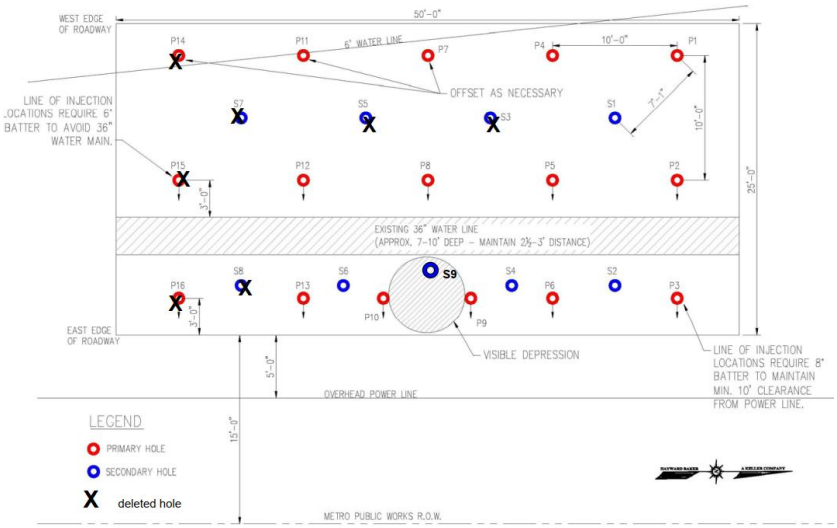
specialists and experienced grouting contractors, compaction grouting, also known as cap grouting, was identified as the most practical and cost-effective solution. This method involves injecting low-mobility, low-slump grout into the subsurface in a controlled, grid-based pattern. The grout displaces loose soils, fills interconnected voids, and creates a dense, stabilized matrix that provides long-term ground reinforcement. The primary objective of this technique is to form a continuous grout "cap" at or near the bedrock interface. This cap functions to seal off subsurface voids, prevent further migration of overburden into bedrock fissures, and reduce the likelihood of future subsidence events. Grouting is conducted from the base upward: as deeper zones are treated, casing is progressively withdrawn and grout is placed in lifts at designated intervals. This staged approach promotes uniform densification of the overburden while preserving permeability within the weathered bedrock, allowing for continued groundwater movement and minimizing hydraulic impacts on surrounding areas.

Grouting operations are expected to extend up to the invert elevation of the existing 0.91m diameter water line, approximately 2.43m beneath the road surface. All grouting activities will be performed by specialized contractors with proven experience in karst-related mitigation. Upon completion of the subsurface stabilization, the surface area will be undercut and reconstructed with engineered fill. This fill will comprise well-graded crushed stone and/or clean shot rock in accordance with TDOT Specification 903.05 (Type A, Grading D). The material will be placed in loose lifts not exceeding 25.4 cm and compacted to at least 95% of the standard Proctor maximum dry density. The upper 0.3m of the subgrade will be compacted to 100% of the same standard. Shot rock, when used, will be clean, angular, and durable, with individual fragment sizes not exceeding 0.45m and conforming to prescribed gradation and soundness criteria. Materials exhibiting unfavorable shape, excessive fines, or susceptibility to degradation are considered unsuitable and will be excluded.

Undercut material, comprising open-graded stone, fragmented limestone, and soil-rock mixtures, will be removed and not reused. The new fill will be benched into the existing subgrade to establish mechanical interlock and continuity. Final pavement grades will be designed to promote positive drainage, thereby reducing infiltration potential and prolonging the service life of the restored roadway. The proposed repair plan, including the use of compaction grouting, has been reviewed and accepted by the property owner. The necessary environmental permits have been submitted in accordance with regulatory requirements from the Tennessee Division of Water Resources. Bid documents are being prepared for contractor solicitation. This strategy has also been presented during a public meeting attended by local residents and representatives from the regulatory agency. The consensus supports the implementation of cap grouting as a durable and non-invasive solution to the current instability. Our previous experience supports its effectiveness in mitigating sinkhole activity and stabilizing infrastructure in karst environments. It is critical to note, however, that while this solution addresses the current hazard at the project site, it does not eliminate the broader risk of sinkhole formation throughout the vicinity. Karst terrains are inherently dynamic and susceptible to episodic collapse. As communicated to stakeholders, future sinkhole activity in adjacent public rights-of-way or private properties cannot be ruled out. Should additional events arise, they will need to be addressed independently.

In summary, the compaction grouting approach offers a balance of technical efficacy, cost-efficiency, and minimal disruption. It stabilizes the affected subgrade, supports the pavement structure, and mitigates the risk of future subsidence at the project location.

 © Deep Foundations Institute 2025



Notes
1. Sketch adapted from original grouting plan prepared by Hayward Baker dated August 10, 2009.
2. Injection holes/locations are approximate.

Fig. 4. The primary and secondary sinkhole locations within the site area.

CONCLUSIONS

This study presents a comprehensive investigation into the mechanisms, challenges, and mitigation strategies associated with sinkhole formation, with a focused case study on the persistent sinkhole along Whispering Hills Drive in Nashville, Tennessee. By employing an interdisciplinary methodology that integrated geotechnical investigation, geological mapping, and engineering analysis, the research offers critical insights into both the localized geohazard and broader sinkhole management practices. Extensive field investigations, including borehole drilling, standard penetration testing (SPT), and geophysical profiling, were conducted to characterize subsurface conditions. Laboratory testing further confirmed the presence of variable soil stratigraphy underlain by karst-prone limestone, with evidence of voids and soil piping—common indicators of subsurface instability in karst terrains. These findings underscored the limitations of traditional surface-based repair techniques and highlighted the need for a targeted, subsurface-oriented intervention. After evaluating multiple remediation alternatives, compaction grouting emerged as the most viable and cost-effective solution. This technique involves the controlled injection of low-mobility, low-slump grout to densify loose soils, fill subsurface voids, and arrest ongoing subsidence. The grout mix design, injection grid spacing, and pressure application parameters were developed based on site-specific geotechnical data to ensure optimal ground improvement and long-term stability. The proposed repair strategy not only addresses the immediate geotechnical distress but also emphasizes the importance of proactive sinkhole risk management through continued post-repair monitoring. Recommendations include the installation of piezometers and settlement markers to track groundwater fluctuations and surface deformation over time, measures essential for early detection of potential future failures. While this case study targets a specific urban site, the methodologies and findings are transferable to similar karstic settings globally. It reinforces the critical need for integrating geological and engineering knowledge in infrastructure planning, particularly in regions vulnerable to sinkhole activity. Furthermore, it highlights the necessity of involving stakeholders, such as municipal planners, utility providers, and local communities, in developing and implementing adaptive management strategies. The broader implications of this research lie in its contribution to the evolution of sinkhole remediation practices. By documenting the successful application of compaction grouting in a complex urban environment, this study supports its inclusion in the design guidelines and engineering standards for

karst-affected regions. The findings advocate for a shift toward more resilient and adaptable infrastructure systems, capable of withstanding the unique challenges posed by karst geomorphology.

In conclusion, the study underscores the critical role of interdisciplinary collaboration, site-specific analysis, and innovative engineering in addressing sinkhole hazards. Continued research, monitoring, and public engagement are imperative to advancing our understanding of sinkhole dynamics and promoting sustainable development in vulnerable terrains. The lessons learned from Whispering Hills Drive serve as a valuable reference for future projects and contribute meaningfully to the ongoing discourse on geohazard resilience in the built environment.

REFERENCES

Waltham, T., Bell, F., Culshaw, M., 2005. Sinkholes and subsidence: Karst and cavernous rocks in engineering and construction.

Gutiérrez, F., Parise, M., De Waele, J., Jourde, H., 2014. A review on natural and human-induced geohazards and impacts in karst. Earth-Science Reviews, Vol 138, pp. 61–88.

Parise, M., Gunn, J., 2007. Natural and anthropogenic hazards in karst areas: Recognition, analysis and mitigation. Geological Society, London.

Brinkmann, R., Parise, M., Dye, D., 2008. Sinkhole distribution in a rapidly developing urban environment: Hillsborough County, Tampa Bay area, Florida. Engineering Geology, Vol 99, pp. 169-184.

Doctor, D. H., Young, J. A., Weary, D. J., 2008. Incorporating karst groundwater vulnerability into watershed management planning. Environmental Geology, Vol 6, pp. 1233-1248.

Kaufmann, G., & Romanov, D., 2013. Geophysical and numerical investigation of subsurface cavity evolution in karst. Journal of Geophysical Research: Earth Surface, Vol 3, pp. 1713-1726.

Yilmaz, I., 2010. A case study from Turkey for the construction on a karst terrain. Engineering Geology, Vol 111, pp. 90–100.

Galve, J. P., Gutiérrez, F., Lucha, P., 2015. Sinkhole risk mitigation and land-use planning using sinkhole susceptibility maps. Engineering Geology, Vol 183, pp. 146–159.

Bennett, M. R., Doyle, P., & Mather, A. E., 2016. Geology and engineering: Mapping sinkholes using LiDAR. Quarterly Journal of Engineering Geology and Hydrogeology, Vol 49, pp. 51-62.

Ford, D., & Williams, P., 2007. Karst hydrogeology and geomorphology. Wiley.

Alimohammadi, H., Memon, A., 2024. Comprehensive Sinkhole Mitigation: A Case Study and Application of Compaction Grouting in Karstic Environments in in the State of Tennessee, USA. Journal of Civil Engineering Researchers, volume 6, issue 2, https://doi.org/10.61186/JCER.6.2.1

 © Deep Foundations Institute 2025

CASE STUDY: EFFECTS OF UNDISCLOSED LARGE DIAMETER SINKHOLE ON CONSTRUCTION, CLEARWATER, FLORIDA

Karl A. Higgins, III, P.E., BC. GE, Chief Operating Officer (COO), Hillis Carnes Engineering Associates, Inc. 100 Sparks Valley Road, Suite A, Sparks, MD USA, Tel: 410-375-3629, khiggins@hcea.com

ABSTRACT

Sinkholes are a common karst-related concern affecting many projects in the state of Florida. While the state of geotechnical practice in Florida generally applies best-practices to identify and characterize sinkholes and their risks to overlying construction, occasionally a deep, dormant, undisclosed, large diameter sinkhole is activated by changes in overlying conditions such as large grade changes associated with building construction. Such a condition occurred on a multi-family apartment construction project in Clearwater, Florida between first recognition of the problem in 2022 and the ultimate remediation of the sinkhole conditions in 2024.

Presentation of this case study should help future generations of geo-practitioners when faced with similar challenges. Excellent field measurement data existed for the evaluation of the sinkhole's impacts on construction, including deep vertical inclinometers, robotic total station measurements of impacted adjacent construction, traditional survey monitoring of settlement and, of course, many deep soil borings in the affected area. All of these measurements will be presented in the paper.

Initially the large diameter sinkhole only appeared to significantly impact an overlying, 18-ft tall segmental retaining wall and its nearby underground utilities (storm, sanitary and water). Wall settlement was as much as 5.5 feet, at which time the wall was declared severely damaged and likely to fail structurally. Supplemental borings in vicinity of the most severe wall settlement led to the characterization of a previously undiscovered, large diameter sinkhole. Initial remediation efforts included de-constructing the segmental wall and reconstructing the wall using lightweight aggregate.

Several months after the wall was reconstructed, top of wall settlement was observed again, and now measured ½ to 2 feet (less than initial wall). The engineers began to believe below grade, lateral soil movement was a contributing factor to settlement and installation of deep inclinometers began. Shortly after the inclinometers were installed, it was evident the larger soil mass underlying the wall and in the vicinity of the large diameter sinkhole was failing in a circular manner. The accumulation of earthen movements from the inclinometers and total stations allowed the geotechnical engineers to model future wall behavior using finite element methods, with the model calibrated by actual field measurements. With a confident finite element model, the engineers predicted the wall would eventually fail if not reinforced.

The second round of remediation was more robust than merely reconstructing the wall with lightweight aggregate and included very long, 110 ft sheet piles driven in front of the MSE wall, horizontally restrained with deadman anchors. The geotechnical engineers worked collaboratively on the design with a well-known geotechnical contractor and eventually stabilized the wall, verified with months of post-construction movement data. Adjacent buildings were impacted, requiring their underpinning and jacking to restore finish floor elevations and these remediation measures will also be presented.

 © Deep Foundations Institute 2025

INTRODUCTION

Sinkholes are a common karst-related concern affecting many projects in the state of Florida. While the state of geotechnical practice in Florida generally applies best practices to identify and characterize sinkholes and their risks to overlying construction, occasionally a deep, dormant, undisclosed, large diameter sinkhole is activated by changes in overlying conditions such as large grade changes associated with building construction. Such a condition occurred on a multi-family apartment construction project in Clearwater, Florida between first recognition of the problem in 2022 and the ultimate remediation of the sinkhole conditions in 2024.

PROJECT EXPLORATION AND GEOLOGY

Prior to the multi-family development construction, the site was developed as a mobile home park. It appeared that some fill grading was done during construction of the park along the eastern property line. Subsurface exploration began in 2020 and was conducted in two phases. The initial round of soil borings revealed organic soils near planned building #8 which was also near a wetland in the southeastern portion of the site. The organic soils (10-15 ft thick) were overlain by sandy fill soil; the organic soils extended to about 30 feet below grade. The site plan was re-configured, shifting buildings away from the wetland and organic soils. The organic soils were classified as Sandy Organic SILT (OL) whose moisture contents ranged from 350-495%, and whose organic content (by dry weight) ranged from 76-90%; Standard Penetration Test (SPT) N-values ranged from 3 to 5 blows/foot. Organic soils with these engineering properties indicates they are highly compressible under low to moderate load increases.

A final round of subsurface borings was performed with the new building configuration, and it was believed that all of the 10 apartment buildings were located outside the wetland area and the corresponding organic soil deposits. Some shallow fill and organic soils were identified along the southern property area, but they were removed and replaced during initial site grading. The final site characterization concluded that the soils beneath the apartment buildings consisted of about 35-50 feet of loose to medium dense SAND (SP, SP-SM, SM) underlain by the residual soils of highly weathered limestone. The residual soils were classified as SILT (ML) and CLAY (CH) with Standard Penetration Test N-values less than 30 blows per foot.

The soil borings aligned well with the published geologic unit consisting of undifferentiated upper marine soils (often sands) underlain by weathered limestone. The number and depth of soil borings well exceeded the local standard of care. While all of Clearwater is underlain by highly weathered limestone, a form of karst geology, the risk of sinkhole formation adversely affecting overlying construction was deemed low at the time of exploration.

FLORIDA KARST

Florida’s karst is unique compared to other karst formations in the United States. Karst is a geologic term used to describe underlying carbonate rock, in this case limestone, that can dissolve and/or erode to form voids. The voids are subject to raveling into void/collapse and the result can be sinkholes that express themselves at the ground surface. If the soil overburden above the void collapse is thick, the expression of the void collapse is large area, often circular depressions. It is these circular depressions, mapped in a variety of ways (LiDAR, aerial imagery, etc.) that often allow engineers/geologists to identify pre-

construction potential of sinkhole formation. Florida's karst is unique in the U.S. in that a layer of marine sediments (often sand) overlies the highly weathered, and potentially erodible, limestone. Karst features in say the mid-west, which are very common, consist of more cohesive residual soils (formed by the weathering on underlying limestone) underlain by less-weathered carbonate rock and less groundwater influences. The overburden soils in the mid-west karstic regions are less susceptible to raveling into voids created in the limestone and sinkhole formation is less dramatic than in Florida.

Floridian carbonate rock is so soft it is frequently impractical to core with the same methods used to core limestone bedrock in most of the U.S. as the sample would likely entirely degrade/erode during the coring/grinding process. Instead, most of Florida uses SPT N-values to categorize Limestone into two basic categories: A) N<50 bpf is considered "soft limestone" and B) N>= 50 bpf is considered "hard limestone" (ref. FDOT Soils and Foundation Handbook, historical convention).

While not unique to Florida, the predominate groundwater hydrology consists of an upper, surficial aquifer underlain by a deeper Upper Floridan Aquifer (and ultimately by a deeper Lower Floridan Aquifer). The deeper Upper Floridan Aquifer (not the surficial aquifer) is considered the primary source of drinking water in Clearwater and much of Florida. There are cohesive (less permeable) soil layers separating the aquifers and these cohesive soils are termed a "confining unit" (a layer of low hydraulic conductivity soil which restricts the flow of groundwater between aquifers). Confining soil units separate the aquifers into differing hydrostratigraphic layers.

Surface expressions of sinkholes in Florida are created when the confining unit between aquifers is breached, allowing the waters from the upper surficial aquifer to communicate with the groundwater of the Upper Floridan aquifer. This downward communication of ground water creates erosion of the confining unit followed by erosion (raveling) of the soils above the confining unit, resulting in the formation of sinkholes at the ground surface. Sinkholes can be very dramatic in appearance, such as those that open at the ground surface and are several hundred feet in diameter, or as benign as a small surficial depression of say several inches with a 6 feet diameter.



Fig. 1. – More dramatic, several hundred foot diameter sinkhole in Florida with surface expression. Source, Gainsville Sun Oct. 26, 2020

 © Deep Foundations Institute 2025

The vast majority of recorded sinkholes and problematic karst conditions in Florida is concentrated in the central and northwestern parts of Florida. Each yellow circle is a recorded incident.

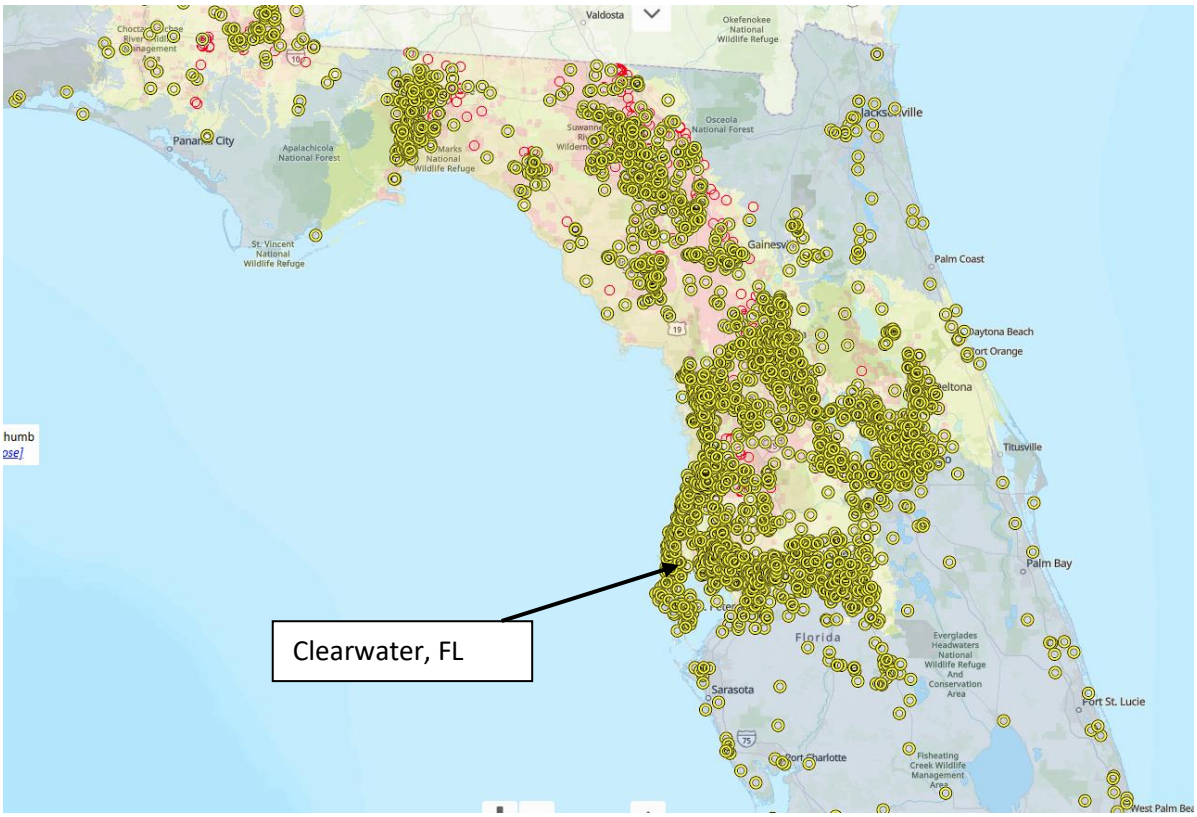


Fig. 2. – Florida Subsidence Incident Report Maps, developed by the Florida Department of Environmental Protection (FDEP) - Florida Geological Survey (FGS).

SHALLOW FOUNDATIONS

Consistent with local best practices in karst/sinkhole prone areas, a post-tensioned (PT) type-II monolithic slab foundation was chosen to support the 3-story, wood framed apartment buildings. Type II PT slabs have single post-tensioned tendons spaced about 3.5 feet on center in both N-S and E-W directions. The slabs themselves are about 4 inches thick, transitioning to drop-down interior and perimeter beams that support building walls. The beams are about 12-inches deep and 8 to 18 inches wide. Reinforcing is principally the post-tensioned tendons, but occasional normal rebar reinforcing is also used.

Foundation wall loads are modest when type II PT slabs are used, ranging from 2,600 lbs/ft to 3,600 lbs/ft (or bearing pressures of about 900 psf to 1,200 psf). While not strictly needed, post-tensioned foundations were chosen by the developer as a "best-practices" approach in the event a sinkhole does occur after construction. Conventional practice in Florida indicates that PT foundations are less likely to show the adverse impacts of differential settlement often associated with sinkhole formation, as the post-tensioning adds much more tensile capacity to the foundations versus traditionally reinforced shallow foundations and floating slabs. The decision to use PT slabs for this project as a "best practices" approach will prove to be a wise decision as explained later in the paper.

 © Deep Foundations Institute 2025

INITIAL CONSTRUCTION

Initial construction included demolishing the surficial infrastructure of the old mobile home park and grading the parcel per the civil plans. The shallow fill and organic soils were removed along the southern property boundary per the geotechnical report recommendations. The civil engineer elected to raise grades in the southern and eastern areas of the parcel, above the elevation of the mapped wetlands to the east. This resulted in a series of long retaining walls along the southern, eastern and northern property boundaries. As you recall, the site plan was initially re-configured to move buildings westward, away from the shallow organic soils and wetland that was noted in the first round of geotechnical exploration. Unfortunately, a portion of the MSE wall was selected directly above a prior area of concern, unbeknownst to the geotechnical engineer.

The tallest wall was about 18-feet; the owner selected traditional segmental block retaining walls that use geogrid reinforcing (or what is also referred to as a mechanically stabilized earth, MSE walls). Retaining walls this high are not common in Florida, where grade changes are often mild. At the time the geotechnical report was written, the geotechnical consultant was unaware of the significant grading changes and plans to use MSE walls and no design recommendations for the walls was provided. MSE wall construction was an early earthwork operation, so that the parcel infilling could occur.

After wall construction was completed along the parcel perimeter, underground utility work began along with shallow foundation construction. Much of this work was done in the Fall of 2021 and Winter of 2022.

INITIAL MSE WALL SETTLEMNT

The Figure below helps the reader orient themselves to the portion of the site impacted by the undisclosed sinkhole, the subject of this paper.

 © Deep Foundations Institute 2025

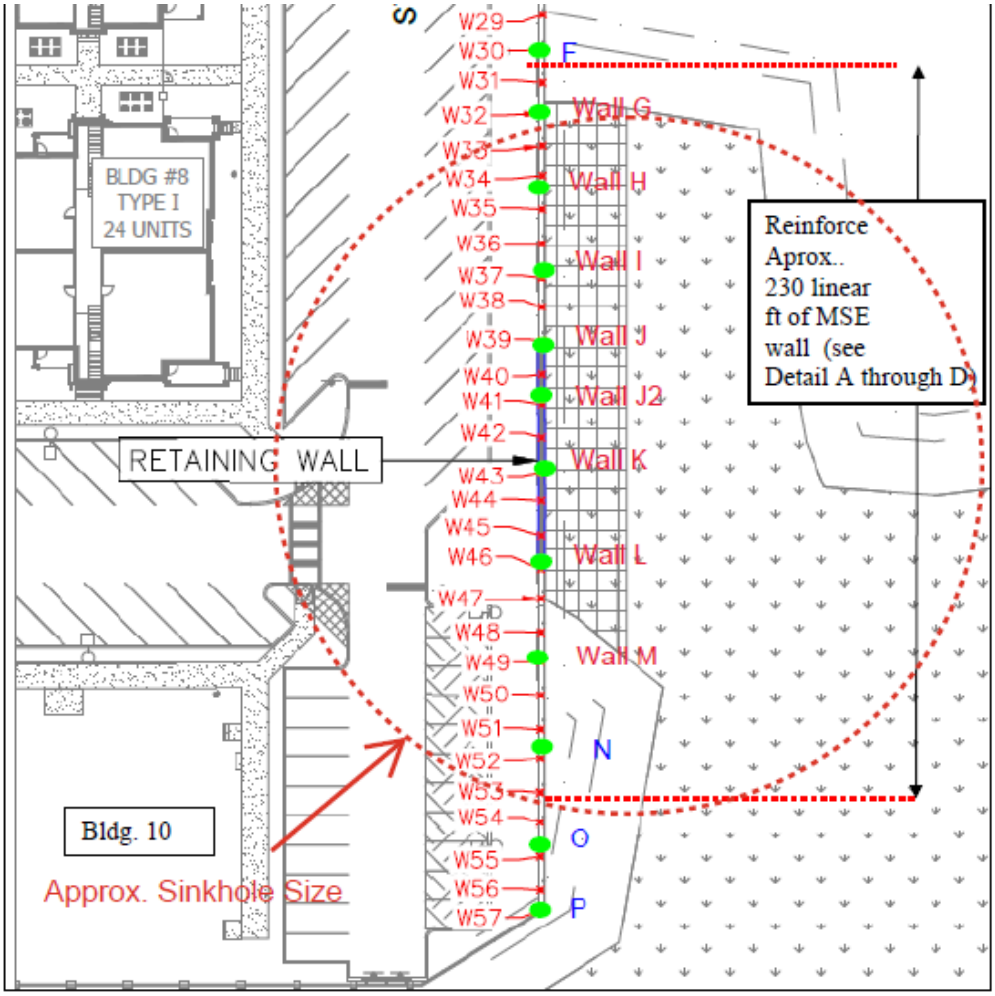


Fig. 3. – Southeastern Portion of the Site and vicinity of Large Diameter Sinkhole (Green dots are survey points)

In March 2022, the client visually observed significant settlement of MSE Wall #2 adjacent to buildings 8 and 10. The top of wall was initially surveyed in April 2022, and it was determined that about 230 linear feet of wall had settled 36 to 48 inches (less at the ends of the sinkhole diameter). Shortly after this information was conveyed to the geotechnical engineer, a site visit was performed to evaluate the wall condition. Visually, it was apparent that a 230-ft portion of wall had settled differentially from adjoining wall sections. Other visual observations included separation of MSE blocks at the wall face, loss of soil through the MSE block wall face, and some block cracking. Despite the obvious "sagging" of the wall, the wall was not in eminent collapse, a testament to how much deflection can occur in segmental block MSE walls without catastrophic outcomes. Clearly this amount of post-construction settlement is not acceptable for a final product, so the geotechnical engineer was engaged to conduct more subsurface exploration in the vicinity of the more significant wall settlement.

 © Deep Foundations Institute 2025

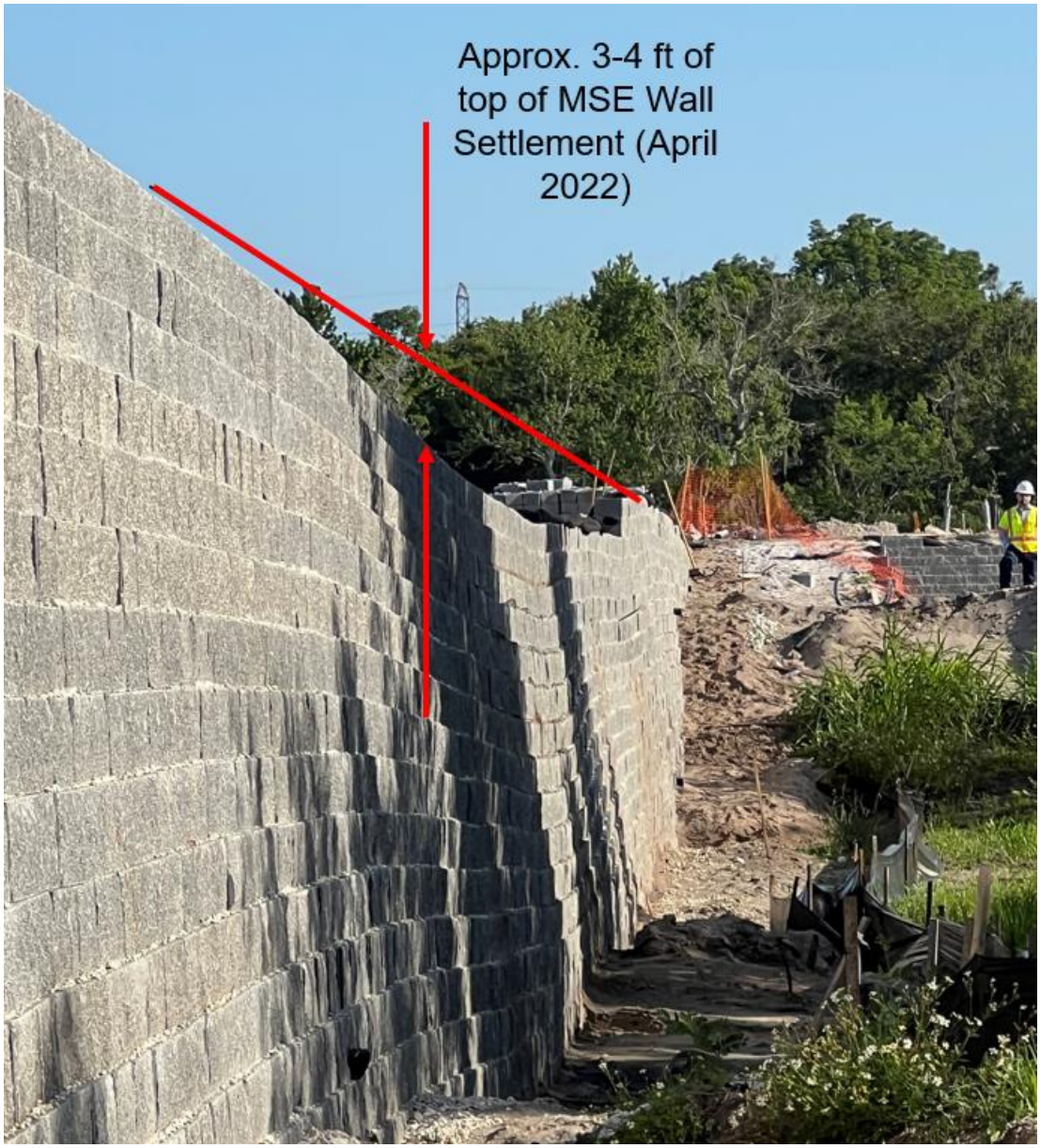


Fig. 4. – MSE wall Differential Settlement April 2022

FIRST ROUND OF SUPPLEMENTAL EXPLORATON

Four (4) deep soil borings were drilled in an alignment parallel to the wall just behind the geogrid reinforcing length, as well as two (2) deep soil borings in an alignment perpendicular to the wall in the direction toward building #8. The results of the borings were very different from the many soil borings drilled during two earlier phases of design geotechnical work. A 30-to-60-foot-thick layer of very soft organic soil (Organic SILT/CLAY, OL/OH) was discovered near the base of the MSE wall fill (EL. 47 feet) extending down to approximately EL. -10 feet. SPT N-values ranged from 0 to 3 bpf, with the 0 blows recorded as Weight of Hammer (WOH) or Weight of Rod (WOR). In the perpendicular direction, the depth to the bottom of the organic soils diminished in the direction towards the buildings. Wash

 © Deep Foundations Institute 2025

drilling techniques utilizing drillers mud were used to advance the borings, a common technique in this area and geologic setting.

The upper surficial aquifer was recorded at EL. 47 feet msl, and the drillers recorded loss of drilling fluid numerous times below EL. 47 feet. If groundwater was recorded as shallow as EL. 47 feet (0-10 feet below original site grades), then how do drillers lose drilling fluid at about EL. 20 ft? The answer likely is the upper surficial aquifer is connected to the lower Upper Floridan aquifer. When we examine the potentiometric surface elevation of the Upper Floridan aquifer, in the vicinity of the site, the potentiometric elevation is about EL. 10 feet (Florida's Water Management Districts, Florida Geologic Survey, United States Geologic Survey, SW Florida Water Management District 6/16/2017). In general, the potentiometric aquifer elevation is the highest elevation the Upper Floridan aquifer can be found at.

Although the aquifers appear to be connected hydraulically by mapping, there still likely exists a partial confining soil layers between these aquifers with varying hydraulic conductivities. If these partial confining layers are not fully saturated, drilling fluids can dissipate into these zones. The loss of drilling fluid in the confining layer demonstrates that the potential sinkhole mechanics are in place.

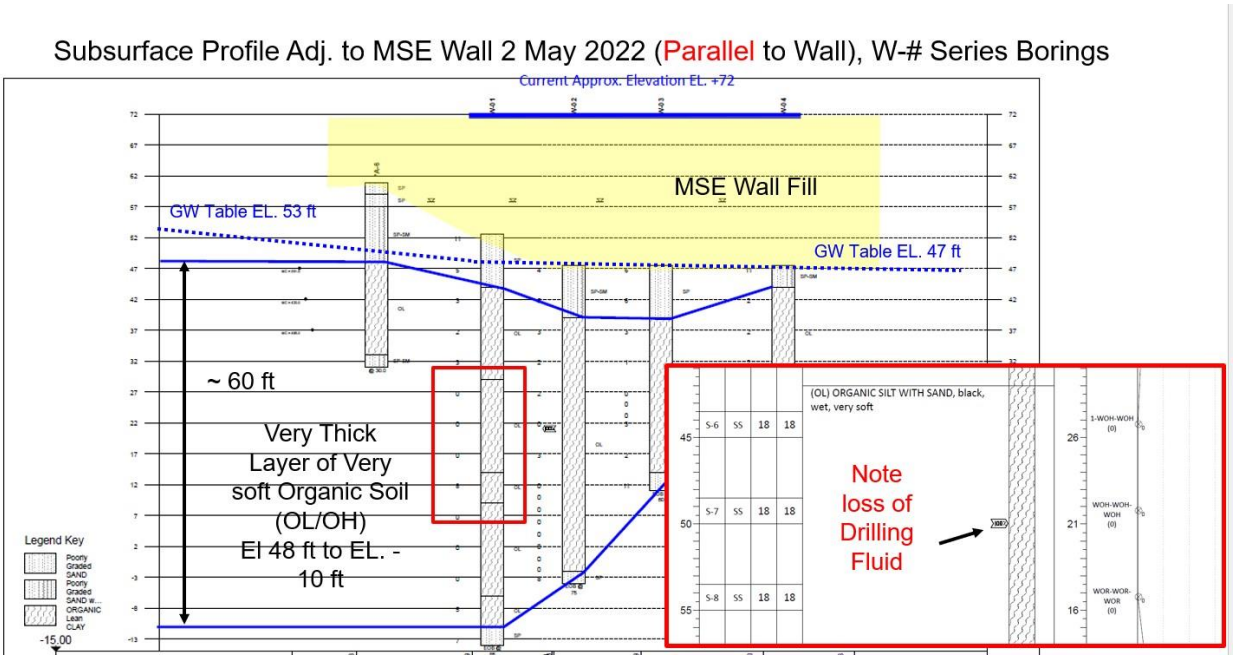


Fig. 5. – Subsurface Soil Profile Parallel to Wall where 36-48 inches settlement occurred

The results of these six (6) deep soil borings led to the characterization of a large diameter, relic sinkhole (paleosink) that was filled with the accumulation of organic soils and covered with a thin marine formation of sand; this type of sinkhole is referred to as a Cover-Subsidence variety (Sinclair, Stewart, Sinkhole Type, Development, and Distribution in Florida, U.S. Geological Survey, 1985). The overlying, 18-ft tall MSE wall settled adversely due to the loosely consolidated organic soils filling the throat of the relic sinkhole. It is surmised that the sinkhole initially formed likely long ago geologically and the throat of the sinkhole was filled with organic soils, probably deposited alluvially, wind or other as organic surface soil materials migrated toward the throat. Eventually the throat filled with predominately organic

 © Deep Foundations Institute 2025

soils (essentially sealing the sinkhole conduit), which was then covered with a sandy marine formation essentially concealing the oftentimes circular depressions we see at the ground surface.

NEXT STEPS

In June 2022, there was no indication that MSE wall settlement had adversely affected the adjacent buildings 8 and 10. The geotechnical engineer did start monitoring building 8 and 10 for settlement in early May 2022; the easternmost side of building 8 (the portion closes to the MSE wall) had settled (differentially from most of the PT slab) about 1 inch. No settlement of the PT slab was recorded for Building 10. Despite the 1-inch differential PT slab settlement, the structure was still performing adequately with no issues related to window or door closures. PT slabs can tolerate more differential settlement than traditionally reinforced footings and soil-supported slabs.

Sanitary sewer lines, water lines and storm sewer lines all ran parallel to the wall and in the space between buildings 8 and 10 and the MSE wall. These utilities were all surveyed to assess post-construction settlement concerns; closed-circuit TV camera surveys were also performed to look at the internal condition of the utilities. The storm and sanitary lines were impacted, and portions needed to be removed and reconstructed.

With no outward signs that building 8 or 10 was experiencing significant structural distress from the adjacent sinkhole activation, the project team evaluated options for repairing the approximate 230-ft long section of MSE wall. The owner had secured a sinkhole insurance policy before construction began, so the insurance carrier was now engaged. With the involvement of the design team, owner, contractor and insurance carrier, an agreement was reached to remove and replace about a 230-ft long section of the MSE wall, and then to reconstruct the wall using ultra-light-weight aggregate. The lightweight aggregate chosen was from AeroAggregates, which is created from recycled glass. The aggregate comes in a variety of gradations and has a unit weight as low as 15 pcf and a strength similar to natural aggregate. Initially, we proposed the entire MSE reinforced zone be comprised of ultra-light-weight material, but costs were substantial and it was decided to utilize this material for about 9 of the 18 feet, resulting in a reduction of total stress at the base of the MSE of 1,000 psf. The stress reduction was thought sufficient to avoid significant post-construction settlement once the wall was rebuilt. At this point in time, the MSE wall surcharge was in place for about 6 months before it was deconstructed and rebuilt with lightweight aggregate. We continued monitoring wall settlement prior to deconstruction and total settlement was recorded of at about 5.5 feet.

In July 2022, the affected portion of the MSE wall was reconstructed per plan. The work was complete, and the wall was measured and it appeared as designed with no sags. Six months later, in January of 2023, we were notified by the contractor/owner that the repaired section of MSE wall had settled again, this time about 1 to 2.5 ft, with the highest amounts in the middle of the wall.

BACK FOR MORE EXPLORATION

In February 2023, we re-mobilized to drill more deep borings and this time we converted several of the deep borings into vertical inclinometers. Inclinometers were needed to determine if lateral soil movement was a contributing factor to wall settlement. Soon after the inclinometers were installed and baseline measurements were made, these instruments were showing lateral movement of the wall face eastward

toward the wetland, away from buildings 8 and 10. We also re-convened the vertical settlement survey work on the PT slabs of both buildings and the MSE wall. Building 10 was largely unaffected, but more settlement was occurring at building 8, which was now expressing physical signs of significant differential settlement (gaps in siding, doors and windows not opening or cracked, obvious differential settlement of the PT slab of several inches).

In May-June 2023, after monitoring the deep inclinometers for several months, it was determined the soil mass beneath the MSE wall was failing in a rotational manner akin to a slope stability failure. Lateral soil movements were measured as deep as 58 feet from top of wall (or 40 feet below base of wall).

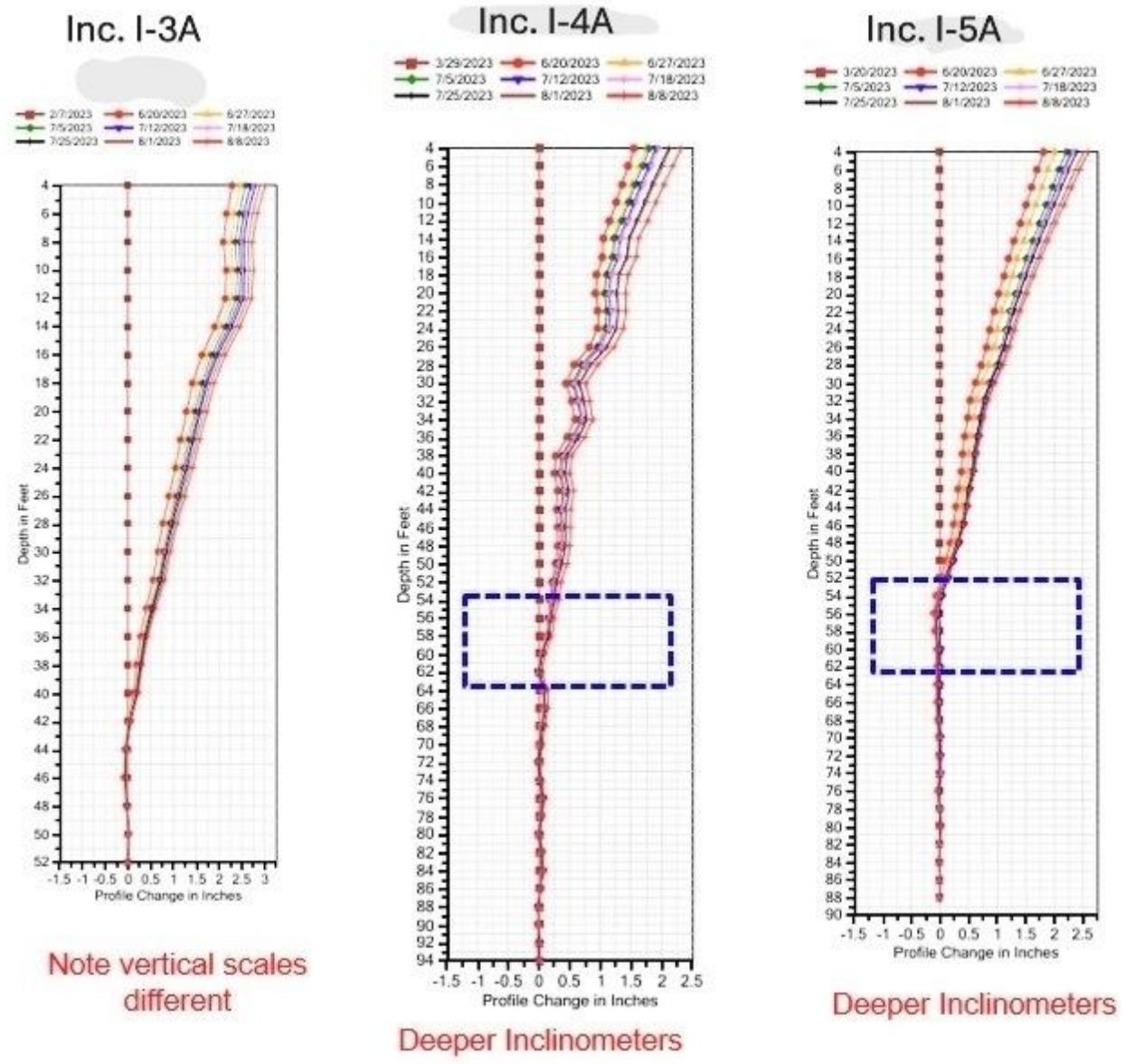


Fig. 6. – Example of Deep Inclinometer Data, February to August 2023

 © Deep Foundations Institute 2025

Based on the progression of lateral soil movement below the MSE wall, we predicted the wall would ultimately collapse. A more robust repair was needed beyond the initial efforts.

MODELING THE FAILURE, DERIVING ENGINEERING SOLUTIONS

The affected MSE wall segment and building movement data (vertically and laterally) provides a good source of data for finite element (FE) modeling. FE modeling is a late 20th century geotechnical engineering tool that helps us better understand complex soil-structure interaction. We first created a model of the current wall condition, developing soil parameters that matched well with measured soil/structure movements. This model along with the traditional inclinometer and survey data was the basis of the wall failure prediction. We then took those model parameters and used them to create potential engineering solutions for the failing MSE wall. Two concepts were derived: 1. 95 ft long continuous steel sheet pile wall driven in front of the MSE wall face; this concept also required ground anchors through the face of the sheet piles for adequate lateral resistance, and 2. 120-ft long "king piles, W 30 x 132 shape" spaced at 6 ft on center with interstitial steel sheet piles extending 20 ft below the organic layer. Option 2 did not require lateral soil anchors, but it did project more lateral movement than option 1. Along with lateral wall movement predictions, the FE software can also generate shear and moment estimates to determine structural steel needs. Both options were presented to the client who then directed us to work with a large geotechnical contractor who would then produce a design-build solution.

In the summer of 2023, we worked collaboratively with the owner's design-build contractor to come up with a final engineering solution. The contractor ultimately chose option 1 with some modifications. The contractor elected to use deadman anchors vs. grouted and stressed earth anchors, a solid contribution to option 1 that made the lateral anchoring easier and more effective to implement.

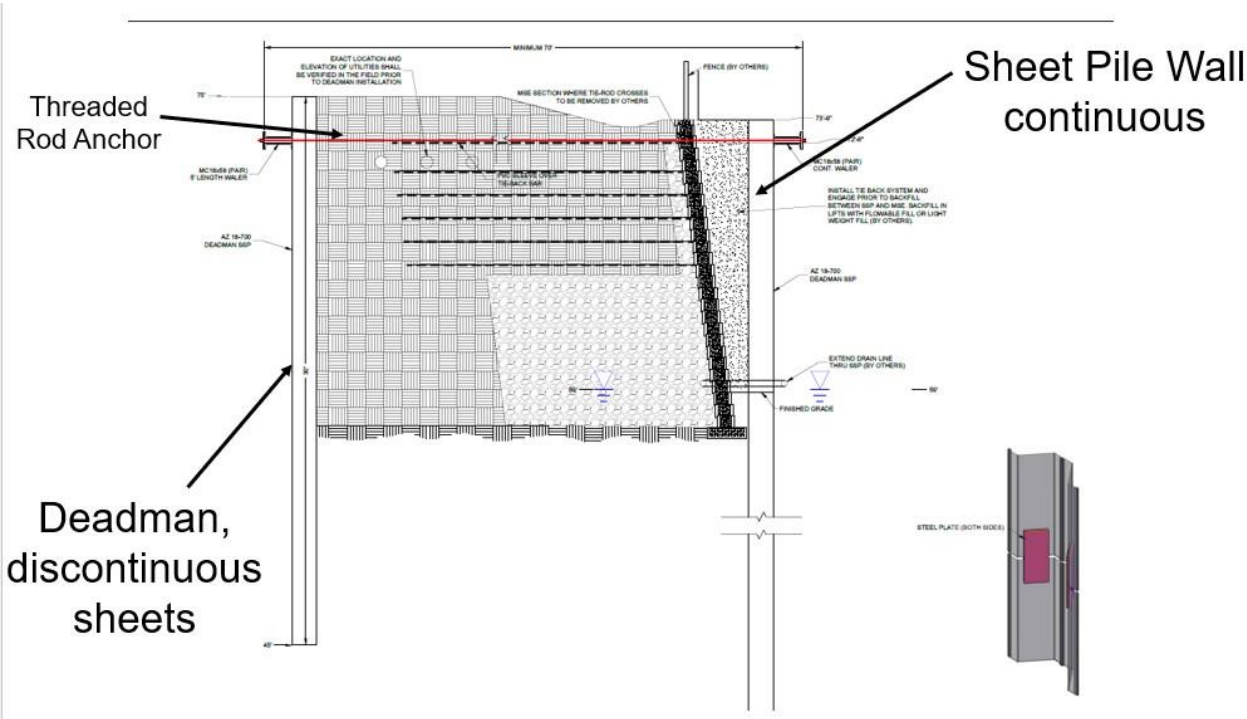


Fig. 7. – Final Design Configuration, care of Keller

 © Deep Foundations Institute 2025

The contractor started sheet pile driving in the summer of 2023 and the work proceeded for about 2 months until substantial completion. During this time, we also installed a robotic theodolite in the wetland area on a concrete pedestal. We affixed targets to the external top of sheet pile wall as well as along the eastern elevation of buildings 8 and 10. The robot shot these fixed targets at frequent intervals, and alarm threshold values were established to alert the team to any undesirable movements during sheet pile wall installation. We ultimately used the robotic data to confirm the design adequacy of the sheet pile wall system and monitor Building 8 during its repair.

BUILDING 8 REPAIRS

While the engineering work for the wall was proceeding, we were also working on a plan for building 8. In the summer of 2023, the easternmost portion of the PT slab had settled between 2 and 4 inches. This structure needed to be underpinned and jacked (if possible). Working with the structural engineer, we determined the perimeter wall loading where the settlement was most pronounced. We developed a preliminary scheme of closely spaced helical anchors along the perimeter exterior of the eastern foundation area. It was determined that 35-kip allowable anchors would be sufficient if spaced at 6-ft intervals. We then similarly collaborated with two potential design-build contractors, selecting one that had good experience jacking from helical anchors to restore foundation subgrade elevations. The interior partition walls were too challenging to get access to, so our work was focused along the building perimeter. Ultimately a plan was developed to install perimeter helical anchors utilizing a bracket configuration to allow upward jacking of the PT foundation.

The anchors were installed during the MSE wall stabilization work, but not jacked until after that work was done. Installation of the anchors was pursuant to the torque specifications required for the 35-kip allowable load. We established good best practices for monitoring building movement during jacking, to include traditional surveying and also monitoring the building via our robotic total station. Jacking operations were largely successful, and the foundation was restored to very near its original design elevation. Several helical anchor heads were overstressed during jacking, bending inward and thus determined to be unreliable and needing replacement. Supplemental helical anchors were installed where the damage during jacking occurred.

Below is a good representation of the robotic total station measuring upward movement of Building 8 during jacking.

 © Deep Foundations Institute 2025

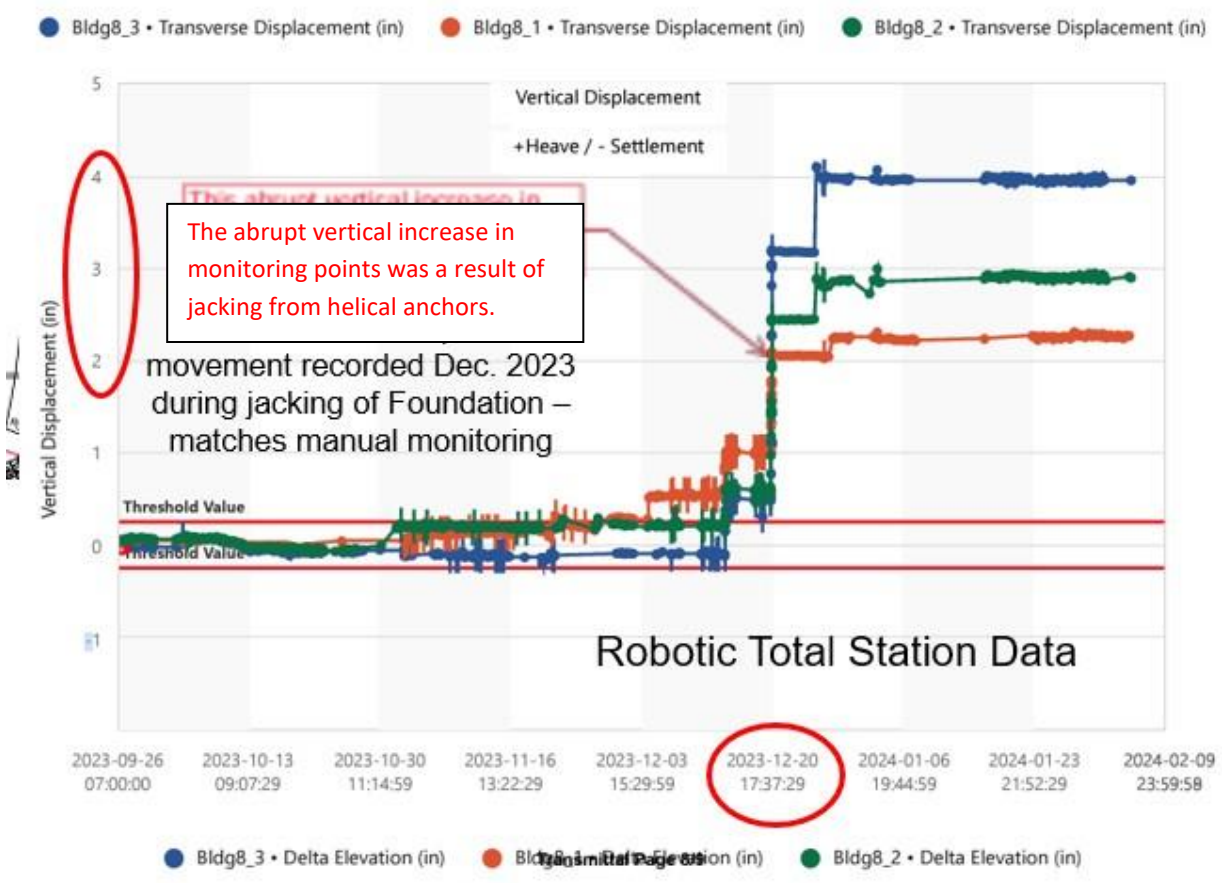


Fig. 8. – Vertical Data of Building 8 During jacking operations

Jacking of the PT slab created a void between the bottom of PT slab and the underlying soil. This void was anticipated, and the remediation effort also included drilling and grouting beneath the PT slab with "poly level" urethane. Holes were drilled at 3 feet on center, completely through the PT slab with care not to impact a PT cable. The PT cables were identified with ground penetrating radar (GPR) before drilling and grouting. The urethane was injected until the voids beneath that portion of the slab were filled. Volumes of urethane grout were recorded for contractor pay items. Grouting was conducted for about the eastern 1/3 of the building 8 footprint. Lastly, exterior building (windows, siding, doors) elements were repaired, and the building repairs were complete.

FINAL WRAP UP

The last bit of engineering was confirming that the sheet pile wall in fact stabilized the MSE wall. This was easily done, again with robotic total station data. Generally, the total wall movements were below the 1-inch design threshold, and the rate of lateral movement was very small at the end of monitoring. One might imagine that aesthetically this wall repair looked awkward; however, the final finished product looked quite professional. Unless someone pointed out the wall was reinforced, you would never know it (at least from the parking lot side of the project).

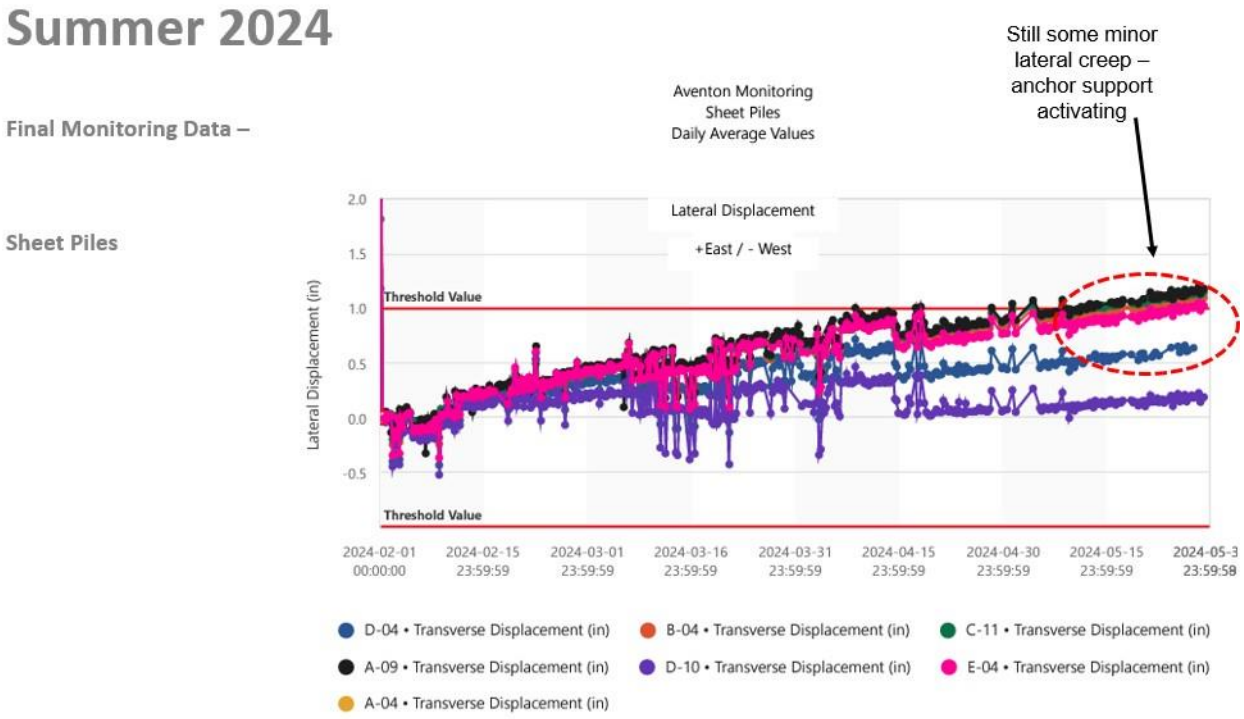


Fig. 9. – Lateral Sheet Pile Wall Movement Data after deadman anchor installation



Fig. 10. Photo – Final View of Sheet pile reinforced MSE Wall

The last little bit of unpleasantness was dealing with the insurance carrier. While the initial sinkhole claim and reconstructing the wall with lightweight fill was honored, the second round of repair work was contested and it took months for a successful resolution to be achieved. The client's choice of purchasing sinkhole coverage, particularly in this part of Florida, proved a wise choice.

 © Deep Foundations Institute 2025

So what are the lessons learned? Reviewing civil and structural plans after the geotechnical report is prepared is highly recommended; if significant differences between actual and report assumptions exist, they need to be addressed by the geotechnical engineer. In this example, seeing that a large retaining wall was planned in an area of the site that was deemed inappropriate for building construction could have resulted in site plan changes, grade changes and wall eliminations. On the subject of geotechnical exploration, particularly in karst terrain (sinkhole prone) areas of Florida, closely spaced and adequately deep borings or cone penetrometer tests (CPTs) are still the best method of sinkhole prediction. Geophysical techniques such as Ground Penetrating Radar and Electro Resistivity have mixed results historically in identifying potential future sinkhole activity.

REFERENCES

Fig. 1 Photograph, Gainsville Sun Oct. 26, 2020

Florida's Water Management Districts, Florida Geologic Survey, United States Geologic Survey, SW Florida Water Management District 6/16/2017

Sinclair, Stewart, Sinkhole Type, Development, and Distribution in Florida, U.S. Geological Survey, 1985

 © Deep Foundations Institute 2025

SINKHOLE WHACK-A-MOLE - LESSONS LEARNED GROUTING A 25MGD KARSTIC MINE LEAK

Kirk Roberts, CJGeo, Richmond, Virginia, USA, 757-592-0452, kirk@cjgeo.com
Dustin Roberts, CJGeo, Richmond, Virginia, USA, 757-592-8413, dustin@cjgeo.com
Brian Bucek, PE, CJGeo, Richmond, Virginia, USA, 804-223-2063, brianb@cjgeo.com

ABSTRACT

The Blue Ridge is famous in Virginia for Shenandoah National Park and the Blue Ridge Parkway. Less known is Virginia's extensive karstic geology west of the Blue Ridge, within the Valley and Ridge region, extending from Maryland to Tennessee, paralleling Interstate 81.

Various open pit and underground limestone mines operate in the area, including a limestone mine near Big Stony Creek in Blacksburg, which experienced a sudden increase in subterranean water inflow in March 2020. The water inflow exceeded the in-place dewatering system, resulting in water rising approximately 8 feet per day, or roughly 25 million gallons per day (GPD).

Previous flooding events were associated with sinkholes opening up in and adjacent to a stream flowing along the mine's service road and railway. Operators identified two different new sinkholes in the stream whose appearance was associated with the increase in inflow.

This paper will review the geology of the site, the sinkhole features which opened up, and repair methods evaluated. It will also review environmental constraints which significantly impacted the repair design process due to endangered fish in the stream.

Grouting of the sinkholes was performed using potable water certified plural component polyurethane. Polyurethane reduced environmental, covid-related logistics and on-site life safety risks. Lastly, the paper will review lessons learned during repair, and the dynamic environment encountered. This included multiple new sinkholes opening, two of which caused movement in adjacent bridge abutments, bringing VDOT into the process in the middle of the project.

REGIONAL GEOLOGIC & KARST TOPOGRAPHY REVIEW

Review of the Geologic Map of Virginia indicates the limestone mine lies within the Valley and Ridge physiographic province of Virginia. Available geologic references report that the mine is underlain by Ordovician-aged limestone of the Knox Group. Specifically within the Knox Group, the mine accesses a 500 meter unit of middle Ordovician limestone that is exposed at ground surface as the lower limb of the Butt Mountain Syncline, approximately 1,600 feet above sea level. The exposure of carbonates at low elevation relative to the local topography is dominated by karst. Karst is characterized by dissolution being the dominant regional weathering mechanism (Francisco, et al). In Karst regions such as Kimballton, VA, surface and subsurface geomorphology is controlled by the dissolution of carbonate rich rock. Dissolution occurs when water that has been acidified with CO_2 through interaction with soil and air, interacts with limestone breaking the calcium carbonate bonds. Acidified water infiltrates the

 © Deep Foundations Institute 2025

carbonate rock and travels through fractures that act as a conduit towards lower potential, continuing dissolution at a slower rate as saturation increases. A critical point is reached, where the conduit in the rock allows turbulent flow. Turbulent flow is characterized by the transportation of particles through the space causing mechanical erosion to assist in the conduit expansion. Depending on the amount of flow these conduits do not always remain open and can become inundated with soil and rock due to collapse or long term accumulation transported by groundwater. Sinkholes form when conduits grow close to the surface and the overburden collapses suddenly into the conduit (Waele, et al). Conduit collapse triggers the formation of sinkholes and caves which are common in this region.

FLOODING EVENT

In February 2020, Big Stoney Creek's catchment received higher than average rainfall causing flow in the creek to triple, increasing hydraulic pressure as well as erosional energy. Conduits close to the surface were found by cores drilled adjacent to the creek (Fig. 1). In the case of the Big Stoney Creek core logs found 27 individual conduits in a 90 feet bore. These conduits were mainly filled with loosely consolidated sediments and cobble. The cores were taken in January 2020, prior to the first sinkhole opening. The shifting overburden due to increased flow exposed the conduits just a few feet below the creek bed and water assumed the non-consolidated sediment filled space. As flow gradually increased more sediment was washed out and the conduits' ability to transport water increased. This rapid washout increased the system energy resulting in rapid growth of the surface features. Constant dewatering in the mine created a steep hydraulic gradient towards the shaft similar to a well drawing down the water table (Fig. 2). With the water table gradient increased between the recharge of the conduits and discharge in the mine, water flow in the conduits grew rapidly resulting in an increase from 4,000 gallons per minute (GPM) in February to 12,000 GPM in March.

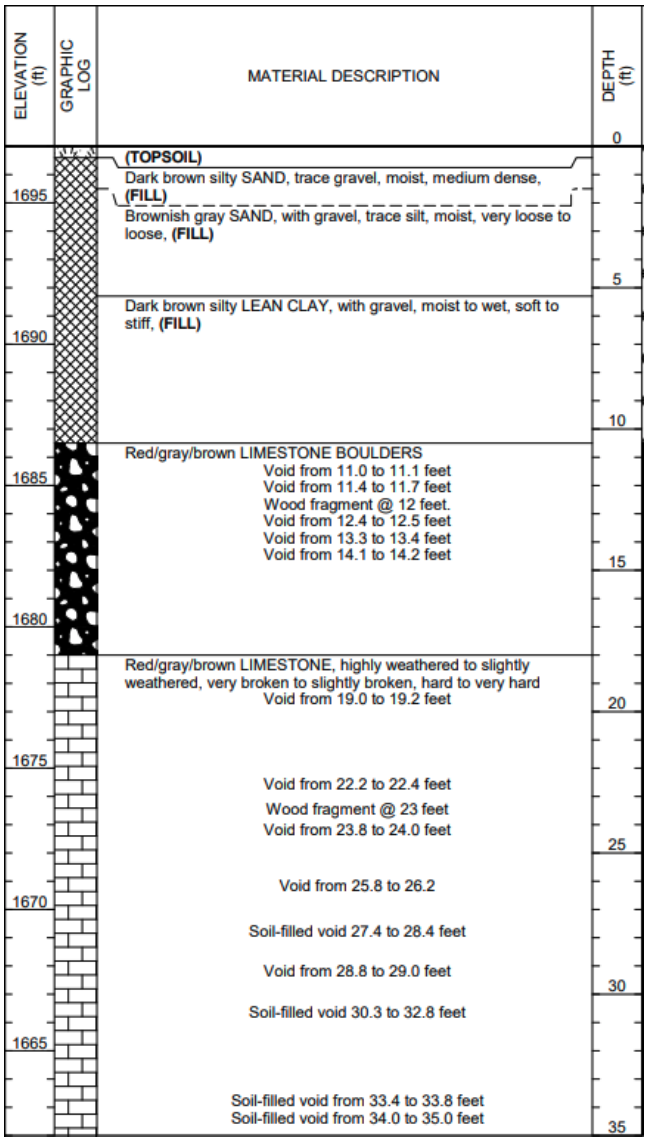


Fig. 1. Subsurface boring log information adjacent to creek

 © Deep Foundations Institute 2025

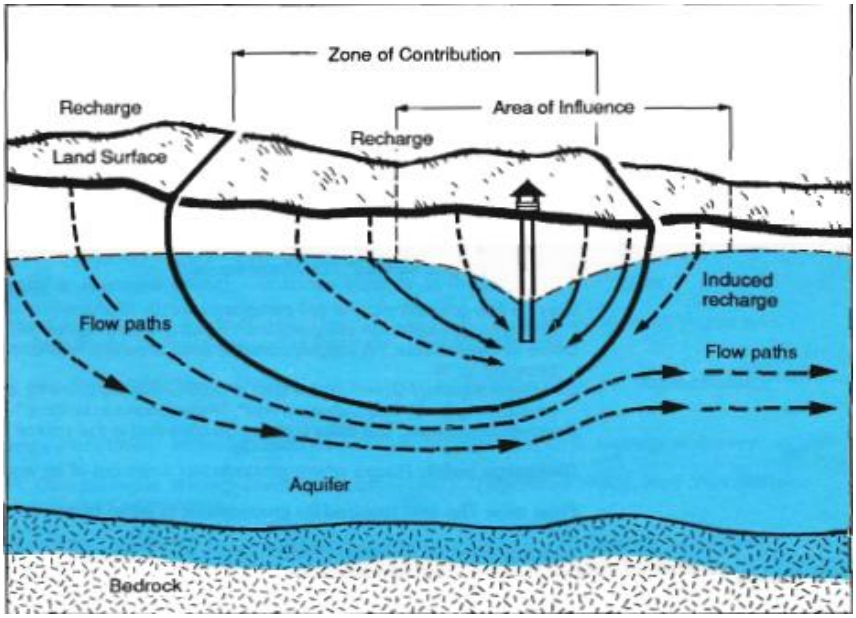


Fig. 2. Groundwater recharge gradient formed by well discharge similar to mine dewatering (Lyle et al. 2006)

GROUT PROGRAM DESIGN & CHALLENGES

The interaction between surface water and the underlying aquifer system meant grouting efforts needed not pose a risk of pollution or change of water pH. Material selection for the project had to meet Virginia Department of Transportation (VDOT) standards as well as Virginia Department of Game and Inland Fisheries (VDGIF). Stoney Creek is home to a large population of Candy Darter, a bottom feeding species of fish that was recently placed on the endangered species list. The creek bed is a spawning location for these fish in early spring. Flow decrease in the stream meant that the spawn could be affected physically and meant the material needed to be inert and cause no net pH change. VDOT was concerned with the Route 683 bridge footing that was washed out by Sinkhole 3. This added a further constraint in that the material needed to be DOT approved with a load bearing capacity sufficient for supporting the shallow footing.

Cementitious grouts were briefly considered, due to their higher strength capacities and heavier densities for placement into water. However, the risks to the endangered species associated with installation operations and potential seepage into the creek quickly eliminated using cementitious grouts as viable repair options. This meant using chemical grouts certified for potable water use had to be used. Mine personnel started to self perform the single component chemical grout installation, but was unsuccessful. Due to the high intensity water flow and the slow installation process, the chemical grout returned to the surface because it was not injected deep enough and its overall volume was not close to touching the size of sinkhole features that had opened up.

Ultimately, CJGrout 35NHV61 was selected due to its hydro-insensitive nature along with being NSF (potable water safe). This product is a hydrophobic grout with a high expansion rate of 20 times its original volume, and is inert upon reaction. The minimal water content of the cured foam prevents

shrinkage when water is no longer present and is a rigid foam ideal for void filling and compaction grouting. Compaction grouting results from the injection of a two component, fast set, high expansion structural foam. The act of expansion and pressure created allows the foam to assume the immediate void and compact surrounding sediments. The bearing capacity (between 45 psi and 65 psi (6,500 psf to 9,300 psf)) is rapidly increased and mobility decreases as the material solidifies. The reaction is temperature dependent, at 110 degrees (recommended mixing temperature) the reaction is complete in 49 seconds. Pumping into a cool aqueous environment effectively doubles the reaction time therefore increased reaction time required that water flow be temporarily decreased in order to prevent loss from washout. Physical properties of CJGrout 35NHV61 mixed at a 1/1 volume ratio are shown in (Table 1).

Table 1. CJGrout 35NHV61 Geotechnical Polyurethane Physical Characteristics

Physical Properties	Test Method	Free Rise	Restrained
Density	ASTM D1622	3.5 pcf	Packed to 5pcf
Compressive Strength	ASTM D1621	45 psi	65 psi
Compressive Modulus	ASTM D1621	750 psi	1300 psi
Tensile Strength	ASTM D1623	55 psi	78 psi
Tensile Modulus	ASTM D1623	800 psi	1200 psi
Water Absorption	ASTM D2842	≤ 0.08 lbs/ft²	≤ 0.06 lbs/ft²
Closed Cell Content		>92%	>94%
Max Service Temp		180°F	180°F
Elongation	ASTM D1623	5.5%	
Shear Strength	ASTM C273	55.2 psi	
Shear Modulus	ASTM C273	307 psi	
Flexural Strength	ASTM D790	68.4 psi	
Flexural Modulus	ASTM D790	1277 psi	

With the polyurethane grout approved, a grout program of using modified Platipus percussive driven earth anchors to depths of 35 feet below the water surface on a 3 foot grid spacing was proposed. The placement of the grout was verified by a combination of material return at the surface, decreased water flow in the mine, and gallons of grout placed.

GROUT PROGRAM IMPLEMENTATION

Grouting began late March 2020 at the first cluster of sinkholes (Fig. 3) that were consuming approximately 8,000 gallons per minute (GPM), significantly decreasing the creek water flow. 70 cubic foot super sacs were placed in the holes to slow water flow preventing mass washout and grout surface refusal. Using modified Platipus percussive driven earth anchors, a hydraulic ram (Fig. 5) drove ½-inch conduit to depths of 35 feet in 5 foot increments below the water surface on a 3 foot grid spacing. Large boulders from the creek bed and shifting cobble in the holes meant that a consistent grid spacing was not always achieved. The initial purchase order was for 4,000 gallons of grout with a weight of 9.5 lbs per gallon and a free rise density of 3.5 pcf. This equates to 307 cubic meters of fill and was divided among the sinkholes. Due to the unknown volume of void space, rapid sinkhole growth, and formation of new sinkholes additional purchase orders were necessary to control the flow. Sinkholes 1 through 3 as seen in

(Fig. 3) were grouted within the first 8 days. During the first 5 days of grouting water consumption continued to climb reaching 17,000 GPM. With a 36 hour delay between recharge of water to the karst conduit and discharge in the mine the daily effects of grouting were not immediately quantifiable. By the end of the 8th day the water level in the mine decreased due to the inflow rate dropping below the dewatering rate of 12,000 GPM.



Fig. 3. Drone image of Sinkholes 1,2 and 3's respective location in Stoney Creek adjacent to the Route 683 bridge.



Fig. 3. Drone image of sinkhole 1,2 and 3's respective location in stoney creek adjacent to the 683 bridge.

 © Deep Foundations Institute 2025



Fig. 4. Sinkhole 4 prior to grouting efforts with the Coffer dam partially erect.



Fig. 5. Sinkhole 4 during the grouting process with grout refusing to the surface

Significant flow change prompted a second purchase order of 2,000 gallons of grout (153 cubic meters) for two additional sinkholes that surfaced in close proximity. Sinkhole 4 appeared on the fringe of Sinkhole 1 and Sinkhole 5 formed 100 yards upstream in a branch of the creek. These features formed days after the capping of holes 1-3 resulting in an increase of flow into the mine. Sinkhole 4 and Sinkhole 5 did not form in the main channel of the creek bed allowing coffer dams to be constructed around these holes. The dams slowed recharge and decreased loss of foam injected from washout prior to reaction.

Each hole required 1,000 gallons of grout before leak down tests confirmed a stable and impermeable plug. Flow decreased to 7,000 GPM in the mine and a third grouting plan was constructed.

The third round of grouting aimed to further compact and fill the substrate surrounding Holes 1 through 3 as well support the footing of the bridge that was adjacent to Sinkhole 3. This purchase order included 1,500 gallons of grout (115 cubic meters) and was to be injected at any depth achievable. Due to the extensive and rigid cap of foam cemented cobble fewer grout casings were successfully installed as refusal was reached quickly. Injection depths were dictated by the ability to drive through the substrate and decreased rapidly from 35 feet to 10 feet below the creek bed as grouting continued. Water flow decreased to around 4,000 GPM with no visible sinkholes concluding the grouting efforts in the area.

LESSONS LEARNED

Polyurethane grouting as a mature geotechnical product provides a unique approach for sinkhole remediation. Permeation grouts due to their low viscosity, high expansion rate, hydrophobic nature and fast cure time can be used to not only cap but also fill underground cavities while also increasing the load bearing capacity. It is considered a long term fix when applied correctly and can be applied quickly minimizing interruption. Its ability to compact the substrate while encapsulating existing material allows it to stay intact for decades negating the need for regrouting. Grouting of the sinkholes reviewed above was a temporary fix due to limitations of the project. Core logs showed karst features extending 90 feet below the surface and without the ability to rapidly mobilize a large drill to place casings injection depths were limited to the depths of the formations. Grouting efforts had to be mobilized rapidly to restore flow in the creek, stabilize the bridge footing and reduce water flow in the mine. Wildlife concerns, bridge stability and reducing the flow from a peak of 17,000 GPM to 4,000 GPM into the mine allowed Lhoist North America time to either design a larger curtain grout plan to address the entire feature or cease mining operations. In the spring of 2021 new sinkholes formed in the area recharging the system, causing the mine to shut down indefinitely. To have prevented further sinkhole formation a curtain of grout would need to have been placed up to 90 feet deep, across the entire creek and flood plain. With this being an emergency grout project a grout curtain was not feasible most notably because drilling would need to occur in the creek bed to place grout casings. This not only would be extremely costly but a significantly slower process. Through this project polyurethane grout further proved its ability to stop leaks and void fill cavities in a dynamic environment and future curtain grout plans may be constructed with the material.

REFERENCES

De Waele, J., Gutiérrez, F., Parise, M., & Plan, L. (2011). Geomorphology and natural hazards in karst areas: a review. *Geomorphology*, *134*(1-2), 1-8.

Gutiérrez, Francisco, et al. “Review on Sinkhole Monitoring and Performance of Remediation Measures by High-Precision Leveling and Terrestrial Laser Scanner in the Salt Karst of the Ebro Valley, Spain.” *Engineering Geology*, vol. 248, 8 Jan. 2019, pp. 283–308., doi:10.1016/j.enggeo.2018.12.004.

 © Deep Foundations Institute 2025

Raymond, Lyle S. “What Is Groundwater.” *New York State Water Resources Institute Center For Environmental Research Cornell University*, July 1988.

 © Deep Foundations Institute 2025

ENHANCING STRUCTURAL PERFORMANCE OF MONOPILES USING HYBRID CONCEPTS: A COMPARATIVE STUDY ON LATERAL PILE DISPLACEMENT AND LOAD CAPACITY

Dhruvi Gondalia, Arup US Inc, New York, NY, Dhruvi.Gondalia@arup.com
Francisco Ciruela-Ochoa, Arup US Inc, New York, NY, Francisco.Ciruela-Ochoa@arup.com
Francesc Mirada, Arup US Inc, New York, NY, Francesc.Mirada@arup.com

ABSTRACT

Monopiles are the most prevalent foundation type for supporting offshore wind turbines in shallow to medium-depth waters, due to their ease of fabrication and installation. As offshore wind farms are increasingly located further from shore and wind turbines grow in size, larger monopiles are necessary to withstand the associated structural and environmental loads. However, the installation of these larger monopiles using current offshore technology is not viable. The transition to deeper waters for offshore wind energy installations necessitates innovative solutions to extend the applicability of monopile foundations beyond their traditional depth limits. This research presents the results of three-dimensional finite-element analyses comparing the performance of a hybrid monopile concept that may enhance standard monopile performance in relatively deep waters. The study focuses on understanding the load transfer mechanism in the hybrid monopile concept as a combination of passive resistance from the soil, friction at the base of the circular footing, and rotational restraint provided by the footings. The findings suggest that the hybrid monopile concept offers a viable alternative to cater the higher loads and leveraging existing monopile fabrication infrastructure. The research underscores the importance of innovative substructure solutions in advancing offshore wind energy capabilities and supporting the transition to deeper water installations.

Keywords: Hybrid monopile concept, offshore wind, lateral load capacity, wind turbine generator

INTRODUCTION

Over the past decade, the offshore wind (OSW) sector in the United States has experienced rapid growth, emerging as a competitive source of renewable energy. This growth has been fueled by technological advancements and increased investments following the advance of OSW at global level. Several foundation structures have been proposed to ensure the stable support of offshore wind turbines generators (WTG). Among these, large diameter monopiles, typically ranging from 4 to 8 m in diameter, have become the most widely used foundation type. This preference is due to the economic competitiveness of the solution, which is possible due to the relatively easier fabrication and the extensive experience in transportation and installation of monopiles across various soil conditions in different areas of the world. These monopiles are generally installed on the seabed using a driving method. To further enhance wind energy productivity, the size of the WTGs has progressively increased, necessitating the development of robust foundation systems capable of supporting the escalating associated loads.

Haiderali and Madabhushi (2016) conducted a comprehensive study to enhance the lateral capacity of large diameter monopiles in clay, which are commonly used as foundations for offshore wind turbines. The study utilized three-dimensional finite-element analyses to evaluate the effectiveness of various hybrid features and rock armor in improving monopile performance under combined vertical, lateral, and moment loads. The study assessed the effect of non-skirted reinforced concrete and steel footings, a skirted steel footing, and steel fins on the lateral response of a 5 m diameter monopile in clay and found the skirted steel footing and steel fins to be the most effective hybrid option for water depths of 30 m.

 © Deep Foundations Institute 2025

Bienen et al. (2012) have shown through centrifuge tests in medium dense sand that the pile head deflections can be reduced to approximately 50% by incorporating wings to monopiles for the same load level. However, these were prototype testing without any water levels. There have been other similar research articles like Lehane et al. (2010), Peng et al. (2010), Haiderali et al. (2013), Wang et al. (2018), Lee et al. (2023) studying the effect of external structures as an addition to the monopile to increase the lateral capacity through finite element analyses or centrifuge model tests.

The increasing need for installation of foundations in deeper waters, in combination with larger WTGs (15MW+), require monopiles of unprecedented size. This study considers a 12-m diameter monopile when used in combination with a solidary addition to conform the hybrid monopile concept. The concept involves two prefabricated reinforced concrete (RC) blocks forming a footings that can be grouted to the monopile.

MODEL GEOMETRY

Monopile

The monopile foundations consist of a large diameter open-ended steel tube driven into the seabed using hydraulic hammers, vibratory methods or a combination of both. For simplicity, the monopile in this study maintains a uniform diameter throughout its length and does not include a transition piece. The axial loads from the weight of the tower and turbine, and lateral forces due to wind and ocean waves and current have been applied at the top of MP.

The modeled monopile has an outer diameter (D) of 12 m, a wall thickness (t_p) of 110 mm, and total lengths (L_T) of 120 m for water depth of 50 m. The embedment length (L) is 50 m.

Hybrid Monopile Concept

Two circular RC footings have been modeled with a thickness of 4 m and 10 m, diameter of 48 m and 24 m respectively through which there was a 6 m dia. opening for the pile. The hybrid monopile concept has been illustrated in Fig. 1. The current assumption is that the monopile is connected to the circular footing monolithically.

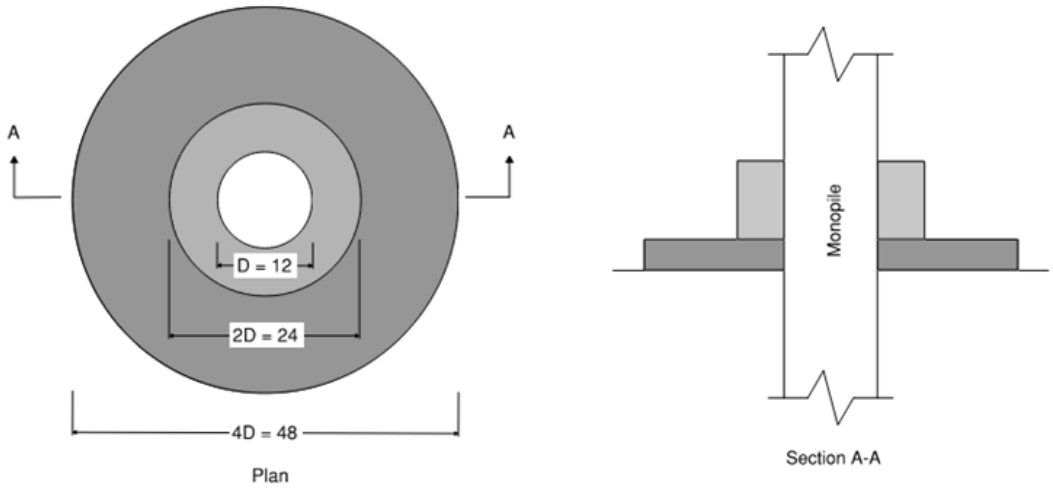


Fig. 1. Geometry of the hybrid monopile concept

 © Deep Foundations Institute 2025

Mesh geometry and software

In this study, the PLAXIS finite element software was utilized to model the behavior of monopiles with and without circular footings under various lateral loads. The model was executed with localized meshing around the pile and the circular footings, which significantly enhances the accuracy of the simulation results. The meshed model with the soil, monopile and circular footings is as shown in Fig. 2.

The soil block was rectangular with a length and width of 200 m, and height of 100 m. These dimensions were found to be adequate in preventing artificial boundary effects on the behavior of the hybrid monopile-soil system.

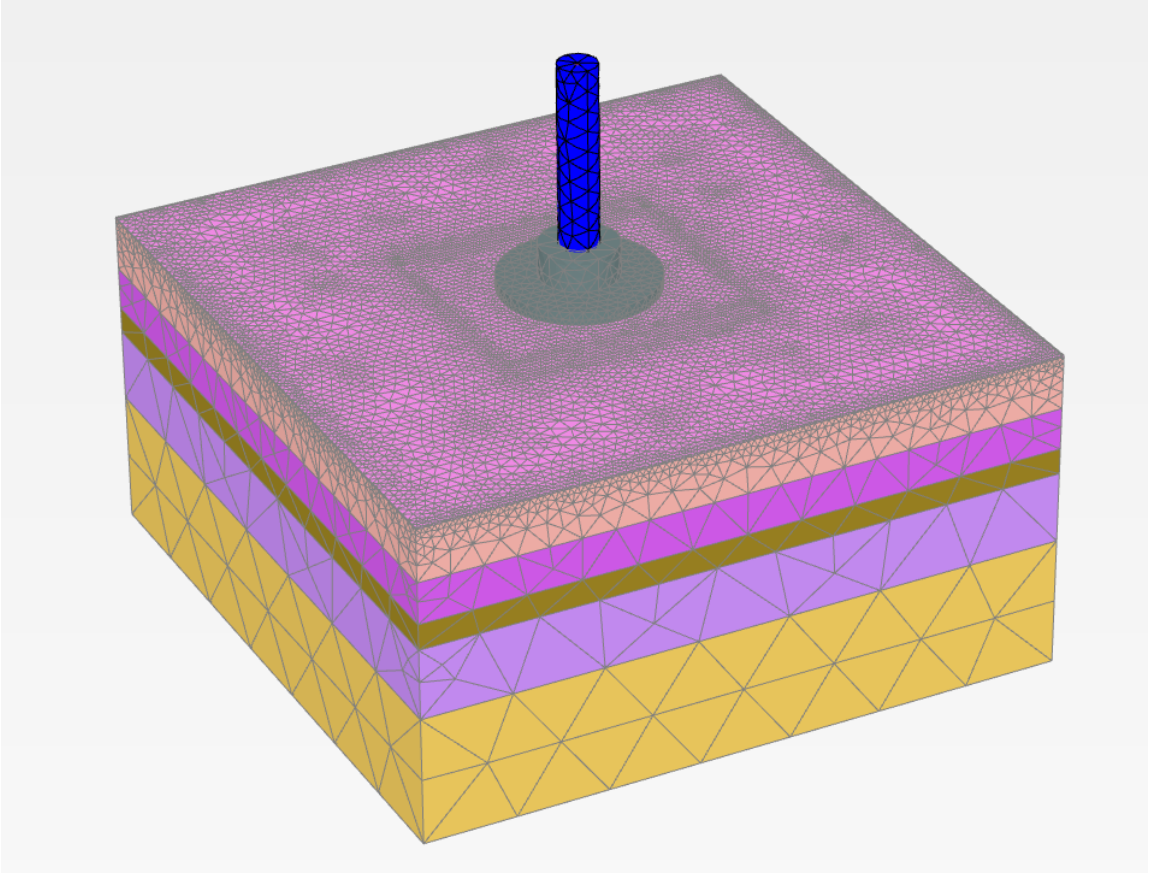


Fig. 2. Meshed Hybrid Monopile concept Plaxis Model

MATERIAL MODELS

Soil

A generic soil profile representation of an area of the East Coast of the United States was developed for modeling the hybrid monopile concept as illustrated in Fig. 3. The soils were modeled using Mohr-Coulomb failure criterion, which is widely employed in geotechnical engineering to describe the behavior of soil under shear stress. The Mohr-Coulomb model is characterized by its simplicity and effectiveness in capturing the essential mechanical properties of soils, including undrained shear strength, and internal friction angle. Each soil layer's properties, such as undrained shear strength (s_u), friction

 © Deep Foundations Institute 2025

angle (φ') derived from relative density D_r, shear modulus (G), were specified based on the data provided in Table 1.

The authors are aware that methods for soil-structure interaction (SSI) modeling of monopiles, such as those developed in the pile-soil analysis project (PISA, Taborda, D. M. G. et al. (2020)) or advanced constitutive models of soils, are the industry standard. However, for this proof-of-concept stage, a simplified approach has been adopted for modeling the response of soil to different loading conditions and understanding the mechanics of the load-transfer of this hybrid monopile concept.

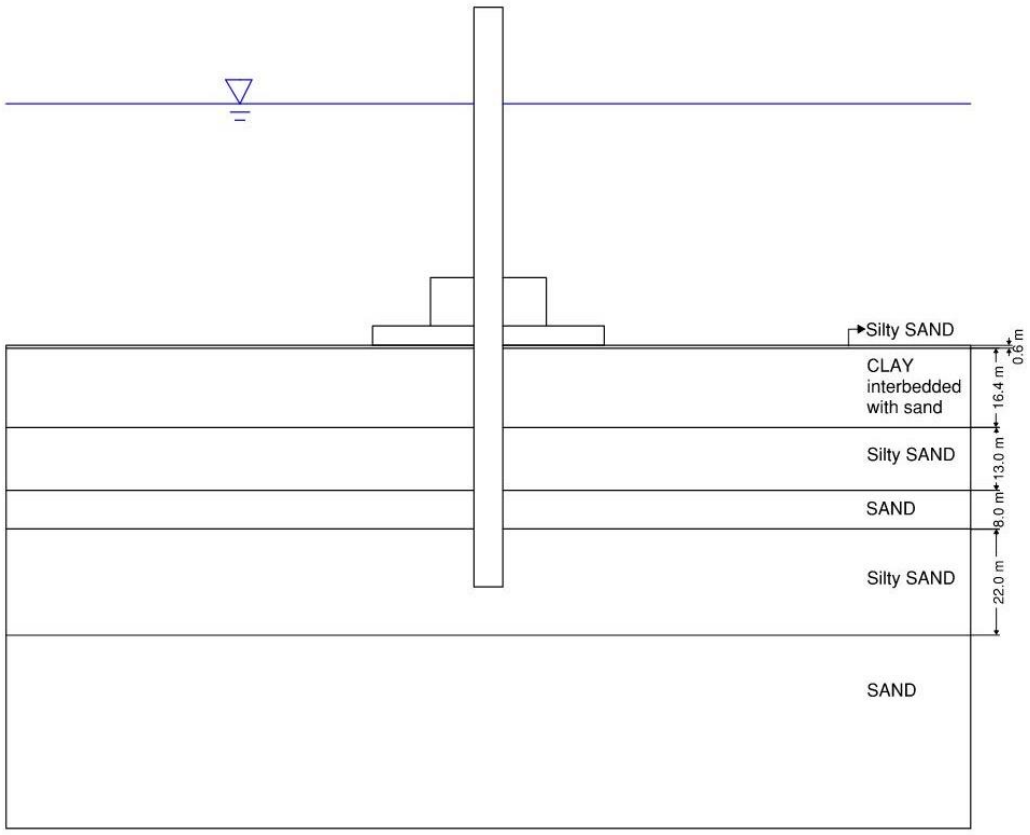


Fig. 3. Hybrid Monopile-Soil model

Table 1. Soil Profile and Geotechnical Parameters

Soil type	Depth Range (m BSB)	γ' (kN/m^3)	s_u (kPa)	D_r (%)	G_0 (MPa)
Silty SAND	0.0 - 0.6	8.5	-	-	2
CLAY interbedded with sand	0.6 - 17.0	8.5	60 to 130	-	36 -78
Silt, SAND	17.0 - 30.0	9	-	-	32
SAND	30.0 - 38.0	10.5	-	-	61
Silty SAND	38.0 - 60.0	10	-	-	49
SAND	60.0+	10.5	-	-	87

 © Deep Foundations Institute 2025

Monopile

The pile has been modeled as an elastic plate with a density of 7850 kg/m^3, Young's Modulus (E_p) of 210 GPa, and Poisson's ratio (ν_p) of 0.3.

Circular Footings

The concrete for the footing was modeled as a linear elastic non-porous soil volume with a density of 2500 kg/m^3, Young's Modulus (E_c) of 37 GPa, and Poisson's ratio (ν_c) of 0.15.

LOADING

After the soil had achieved equilibrium, the hybrid monopile system was subjected sequentially to gravity, axial, and lateral loads. For a typical monopile foundation, the vertical capacity is satisfactory if the requirements of lateral and overturning stabilities are guaranteed (Arany et al., 2017). A representative axial load of 5 MN was thereby applied at the center of the monopile head to account for the WTG loads.

A parametric study was undertaken to evaluate the effect of lateral load whilst maintaining all other loads and parameters constant. The analysis was conducted in the following sequence:

- Initial phase where the soil is considered to have equilibrium;
- Installation of monopile;
- Installation of the circular footings at the seabed around the monopile; and
- Application of axial and lateral forces at the pile head.

The lateral load was applied incrementally to get to the failure stage or reach the serviceability limit state.

RESULTS AND DISCUSSIONS

Three different runs have been undertaken at a water depth of 50 m to provide a comparative analysis and study the load transfer mechanism at the base of the hybrid monopile system: (1) Single monopile, (2) Hybrid monopile with base friction contribution (i.e., Plaxis interface reduction factor of 0.3), and (3) Hybrid monopile without base friction contribution (i.e., Plaxis interface reduction factor of 0.05). It should be noted that the reduction factor of 0.05 was set to achieve model convergence and is treated as if the friction contribution at the base was negligible. The monopile and circular footing geometry and parameters have been kept constants for all three runs.

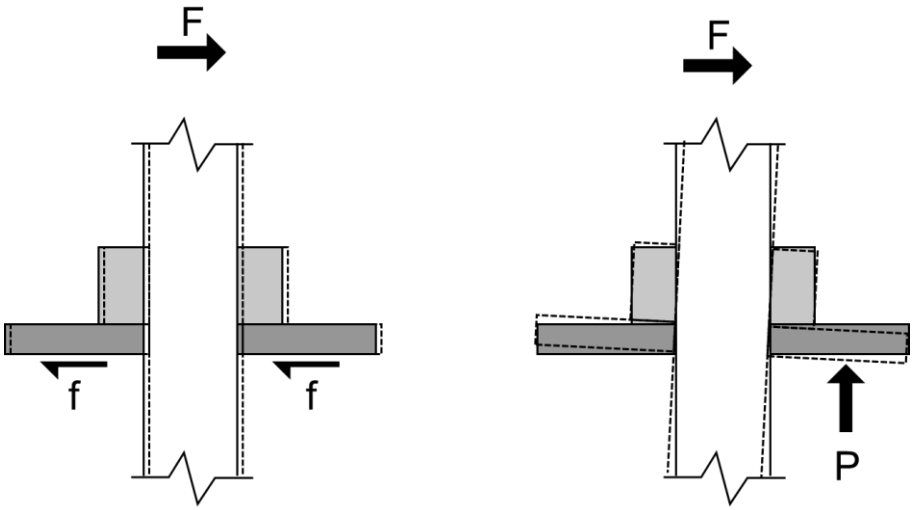
Load Transfer Mechanism

In single monopiles, the load transfer process is mainly governed by the passive resistance offered by the foundation soil. In the case of wind turbines supported by multiple foundations (i.e. jacket on piles), the load transfer mechanism is mainly through the push-pull action. In the Hybrid Monopile concept, the load transfer mechanism is expected to be a combination of the passive resistance offered by the foundation soil, the friction contribution of the base of the circular footing with the seabed and the rotation of the circular footing acting against the soil, this is illustrated in Fig. 4.

Figure 5 shows the shear stress at the base of the circular footing a lateral load of 20 MN applied in the positive X direction for (a) Hybrid Monopile with base friction – reduction factor = 0.3; and (b) Hybrid Monopile without base friction – reduction factor = 0.05. Due to the numerical reduction factor of 0.05, up to 2 kPa are observed for the case without friction between the base of the circular footing and the seabed (Fig. 6 (b)). Where the friction between the base of the circular footing and the seabed is

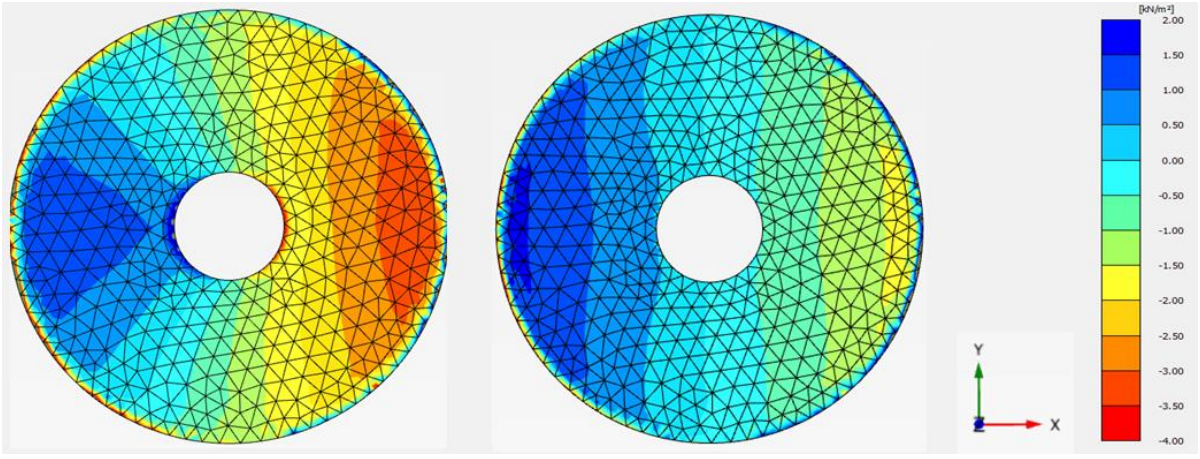
considered, a higher mobilized shear stress of up to 4 kPa is observed in the opposite direction of the lateral load. Provided the large area of the circular footing, these shear stresses are contributing to increase the lateral resistance of the hybrid monopile concept.

As illustrated in Fig. 6, the calculated lateral displacements of the pile at mudline are very similar for the case of the single monopile and hybrid concept without friction at the base. This is an indication that the increased lateral resistance of the hybrid monopile concept is mainly provided by the friction, which is expected given the very small rotation of the system. Figure 7 and Figure 8 show that the pile displacement at top of pile head and pile rotation at mudline, indicating that the push component of the Hybrid Monopile concept is providing rotational restraint as expected, however this relative contribution reduces as the lateral load increases (i.e. remains constant).



(a) (b)

Fig. 4. Load transfer mechanism (a) Base friction contribution; and (b) Circular footing 'push' contribution



(a) (b)

Fig. 5. Interface Shear Stress in the direction of loading for a lateral load of 20MN for (a) Hybrid Monopile w base friction – reduction factor = 0.3; and (b) Hybrid Monopile w/o base friction – reduction factor = 0.05

 © Deep Foundations Institute 2025

Lateral Pile Displacement at Mudline

The deformation of an offshore WTG can disrupt the mechanical system by imposing additional loads on the bearings, this is generally one of the controlling factors on the design of the foundations, and hence the performance of these hybrid monopiles is evaluated in terms of serviceability rather than ultimate state. The efficacy of the hybrid monopile in limiting the pile displacement is assessed by comparing the pile lateral displacement at mudline for monopile only and with monopile with hybrid monopile under varying lateral loads. Excessive lateral displacement at the mudline can compromise the structural integrity of the monopile, leading to increased bending moments and shear forces, potentially resulting in structural damage or failure. Therefore, controlling lateral displacement is essential to maintaining the integrity of mechanical system and ensuring the foundation's serviceability.

As illustrated in Fig. 6, the lateral load associated to about 120 mm (y_m/D = 1%) of lateral displacement increases by approximately 35% by employing circular footings as compared to having just the monopiles.

Figure 7 shows the lateral pile displacement at top of pile head vs the applied lateral load at that location. Comparing a representative lateral serviceability load H_{serv} of 18MN at the pile head, it is expected that the lateral displacements at the pile head will reduce up to 30% when using the hybrid monopile concept vs a standard monopile.

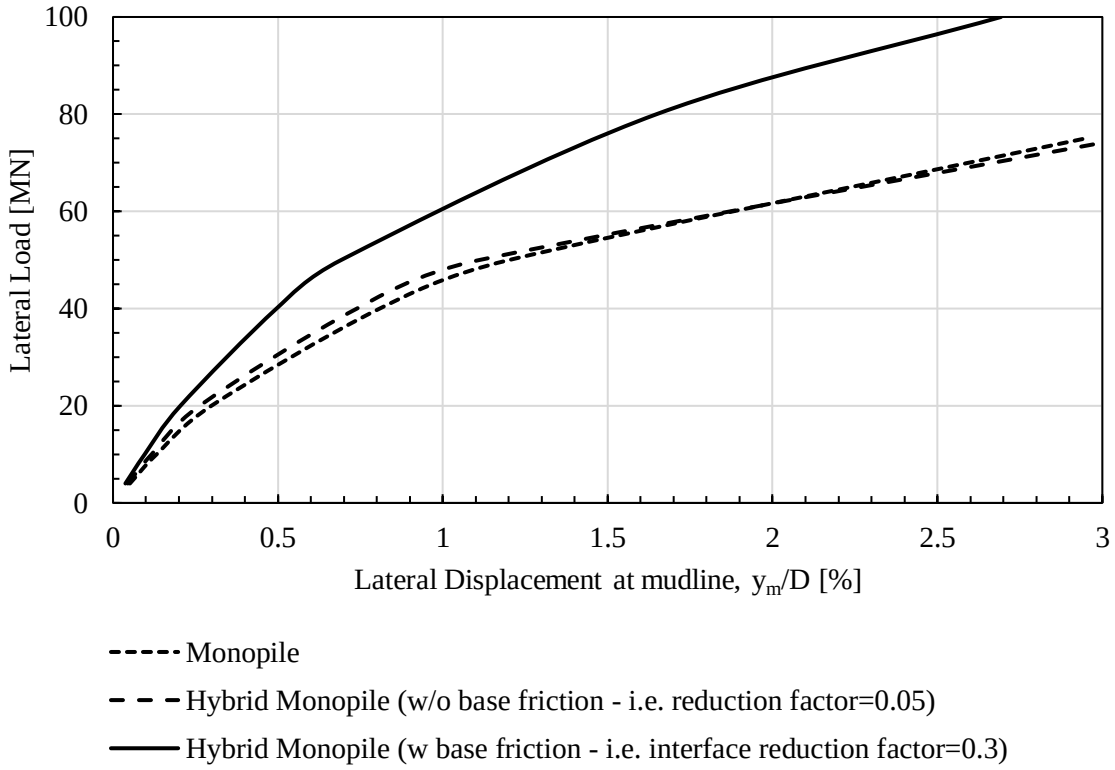


Fig. 6. Lateral Pile Displacement at Mudline vs Lateral Load

Pile Rotation

A comparison based on pile displacement may lead to overestimation of the effect of the circular footings as the point of rotation will shift up in the monopile with the circular footing due to increase in the flexural rigidity thereby increasing the pile rotation. Haiderali and Madabhushi (2016) suggested having

 © Deep Foundations Institute 2025

the serviceability criteria set as maximum allowed pile head rotation (θ_m) of 0.25° during the design life of a monopile. Therefore, a better performance indicator is the serviceability lateral pile capacity, H_{serv}, at which θ_m is equal to 0·25°.

Figure 8 shows the anticipated pile rotation vs an applied lateral load at the top of the pile. The results indicated a potential increase of over 30% in lateral resistance when the hybrid monopile with base friction is used vs a standard monopile.

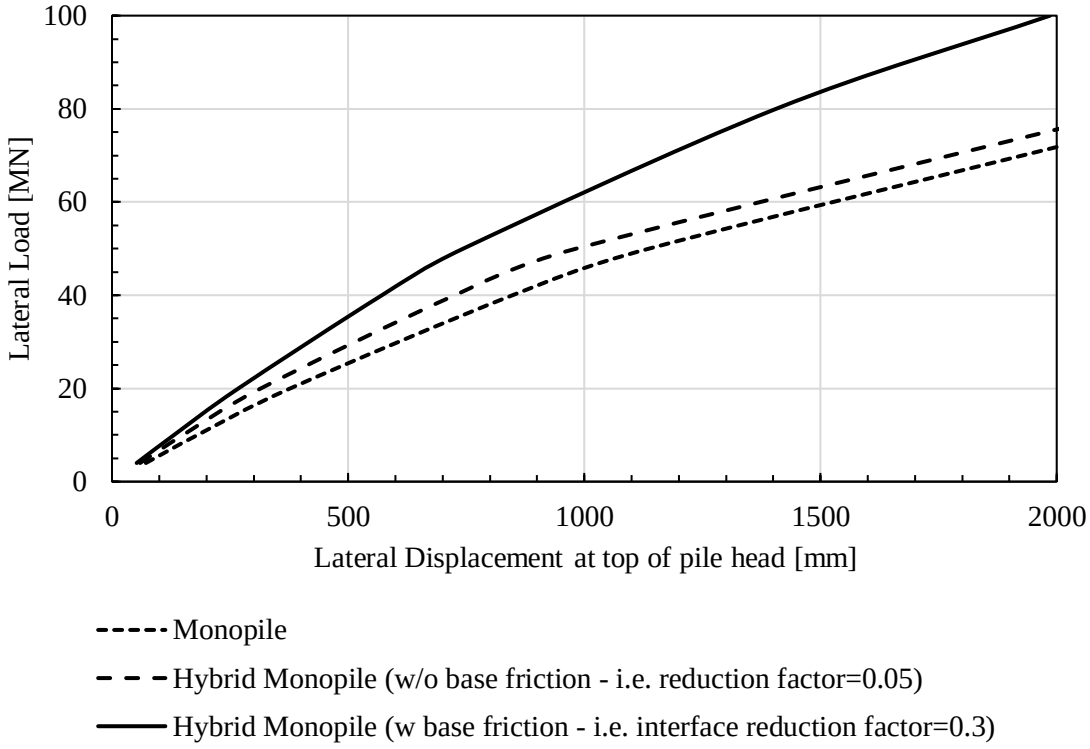


Fig. 7. Lateral Pile Displacement at top of pile head vs Lateral Load

 © Deep Foundations Institute 2025

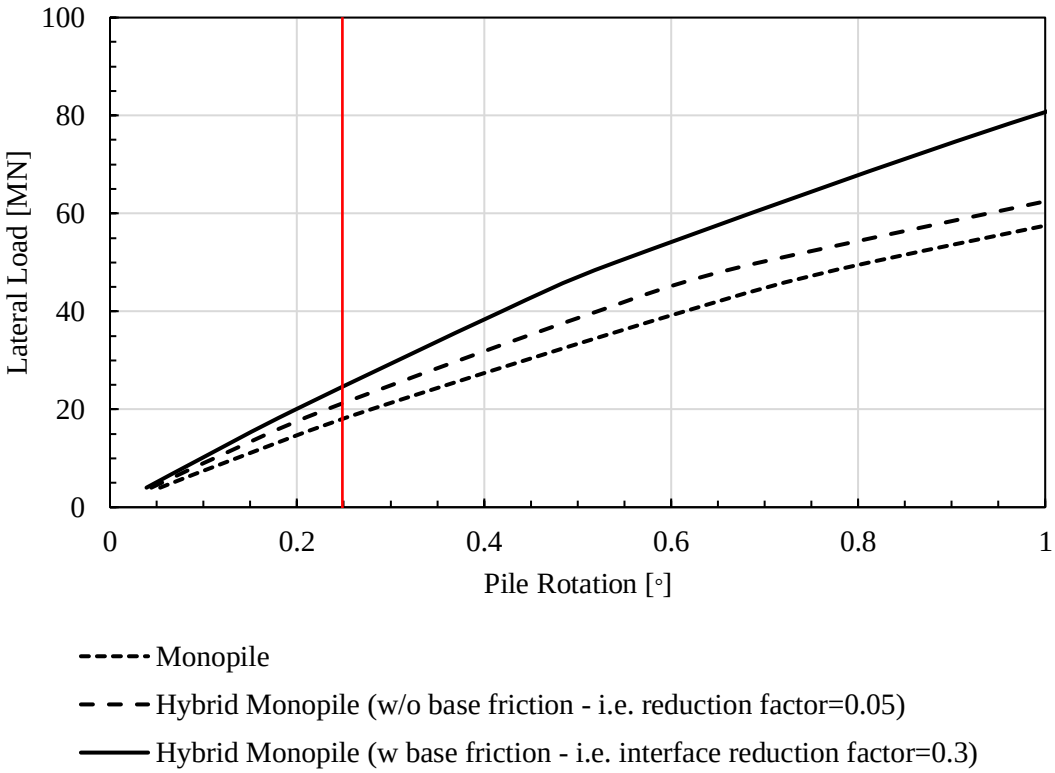


Fig. 8. Pile Rotation vs Lateral Load

CONCLUSIONS AND FUTURE WORK

This paper presents the first part of Arup's research work to investigate the enhancement of traditional WTG monopile foundations using hybrid monopile systems. This paper focuses on developing a proof-of-concept to understand the load transfer mechanisms of a hybrid foundation that uses circular footings when subject to varying lateral forces.

The analyses were performed using 3D finite element modeling and simplified generic soil strata and models. The study focused on a monopile with a diameter of 12 meters, embedded 50 m into the seabed, and with 50 m of water above the seabed.

The results of the study indicate that the hybrid monopile concept has the potential to resist larger lateral loads compared to traditional monopile foundations. It is also expected that the structural demands (moments and shears along the monopile) reduce given the reduce rotations and movements. The analyses also indicate that the hybrid monopile system benefits from a combination of passive resistance from the soil, friction at the base of the circular footing, and rotational restraint provided by the footings. This multi-faceted load transfer mechanism contributes to the enhanced performance observed in the hybrid monopile system.

The hybrid monopile concept offers a flexible and adaptable solution for supporting larger wind turbine generators (15MW+), addressing the increasing demand for higher offshore wind capacity in deeper waters. The ability to leverage existing monopile fabrication infrastructure further enhances the feasibility and economic competitiveness of this innovative foundation system.

 © Deep Foundations Institute 2025

Next stages of the projects will focus on better understanding the benefits of structural performance of the monopile and constructability of placing of the concrete footings at the base and preparing the base of the seabed to rely on the friction contribution provided by the base of the circular footing. These studies will be expanded with varying water depths and monopile diameters to understand if hybrid monopile systems maintain sufficient lateral capacity in deeper waters, which is essential for expanding offshore wind farms to new locations.

This study has highlighted the importance of the friction contribution of the base friction of the circular footings in the lateral capacity of the piles. The dimensions and geometry of circular footings should be optimized to maximize lateral capacity. This involves varying the dimensions and analyzing their correlation with the diameter and length of the monopile to develop guidelines for designing hybrid monopile concepts that provide the best performance. Furthermore, incorporating skirts into monopile footings should be assessed to determine their benefits in enhancing lateral capacity and stability.

REFERENCES

1. Arany, L., Bhattacharya, S., Macdonald, J., & Hogan, S. J. (2017). Design of monopiles for offshore wind turbines in 10 steps. *Soil Dynamics and Earthquake Engineering*, *92*, 126-152.
2. Bienen, B., Dührkop, J., Grabe, J., Randolph, M. F., & White, D. J. (2012). Response of piles with wings to monotonic and cyclic lateral loading in sand. *Journal of Geotechnical and Geoenvironmental Engineering*, *138*(3), 364-375.
3. Haiderali, A., & Madabhushi, G. (2016). Improving the lateral capacity of monopiles in submarine clay. *Proceedings of the Institution of Civil Engineers-Ground Improvement*, *169*(4), 239-252.
4. Haiderali, A., Cilingir, U., & Madabhushi, G. (2013). Lateral and axial capacity of monopiles for offshore wind turbines. *Indian Geotechnical Journal*, *43*(3), 181-194.
5. Lee, J. H., Kwak, T. Y., Jeong, Y. J., Park, J., & Kim, J. H. (2023). A Study on the Lateral Load Capacity of a Novel Hybrid Monopile via a Centrifuge Model Test. *Energies*, *16*(21), 7234.
6. Lehane, B., Powrie, W., & Doherty, J. (2010). Centrifuge model tests on piled footings in clay for offshore wind turbines. Frontiers in Offshore Geotechnics II, 623-628.
7. Peng, J. R., Rouainia, M., & Clarke, B. G. (2010). Finite element analysis of laterally loaded fin piles. *Computers & structures*, *88*(21-22), 1239-1247.
8. Taborda, D. M., Zdravković, L., Potts, D. M., Burd, H. J., Byrne, B. W., Gavin, K. G., ... & McAdam, R. A. (2020). Finite-element modelling of laterally loaded piles in a dense marine sand at Dunkirk. Géotechnique, 70(11), 1014-1029.
9. Wang, X., Zeng, X., Li, J., & Yang, X. (2018). Lateral bearing capacity of hybrid monopile-friction wheel foundation for offshore wind turbines by centrifuge modelling. *Ocean Engineering*, *148*, 182-192.

 © Deep Foundations Institute 2025

CALCULATING INTERNAL FORCES FROM ATYPICAL STRAIN READINGS

Van E. Komurka, P.E., BC.GE, F.ASCE, Life Member, GRL Engineers, Inc., Cleveland, Ohio, USA, (216) 868-6130, vkomurka@grlengineers.com
Seth O. Robertson, Ph.D., P.E., Dan Brown and Associates, LLC, Kingston, New Hampshire, USA, (603) 702-1259, SRobertson@DBA.World

ABSTRACT

A valuable objective of statically load testing deep foundations is to determine load-transfer response. Integral to this objective is determining internal forces at various elevations within the deep-foundation element. These internal forces are often calculated from strain readings (strain instrumentation does not determine internal forces directly). Strain readings can sometimes yield atypical results, with multiple strain gauges at a given strain-gauge level ("SGL") (i.e., the same elevation) providing significantly different individual readings, or the deep-foundation element changing effective rigidity during a static load test. A case history will be presented where a bi-directional static load test was conducted on a test shaft with strain gauges affixed to a center core beam. At multiple SGLs, the case-study test measurements indicated both: a) atypical strain readings occurred simultaneously, and b) effective rigidity changed during the test. The strain readings were evaluated using several methods, including the American Concrete Institute formula and the Incremental Rigidity ("I.R.") method. In addition, the I.R. method was employed to interpret the change in effective rigidity at the individual SGLs during the test. The resulting load-transfer responses are reasonable, and so exhibit the usefulness of applying the I.R. method to atypical strain readings, thus demonstrating a means of interpreting internal forces at SGLs which might otherwise have to be disregarded (i.e., a means of "salvaging" an SGL).

Keywords: Incremental Rigidity method, instrumented static load test, internal force, load transfer, static load test, strain gauges, strain readings

INTRODUCTION

Static load tests have an important role in the design and construction of deep foundations of all types: driven piles, augered cast-in-place ("ACIP") piles, drilled displacement piles ("DDP"), helical piles, drilled shafts, etc. For simplicity, all deep foundation types will be referred to herein as piles. Additionally, the types of static load tests addressed herein are axial, both head-down and bi-directional compressive, and tensile. The usefulness of static load tests, particularly in the design phase, is enhanced by determining load-transfer response during the test. Load-transfer response refers to the manner in which internal pile forces are transferred into the surrounding geomaterial, with the definitive result being the magnitudes of mobilized unit shaft resistances along the pile length versus relative soil-pile movement. Integral to this objective is determining internal forces at various locations within the deep-foundation element.

Load-transfer determinations can be obtained using several different types of instrumentation; two common types are telltales and strain gauges (Brown et al. 2018). Neither instrumentation type measures internal forces directly. When detailed load-transfer data are desired, telltale measurements alone are insufficient (Hannigan et al. 2016). Weldable strain gauges can be used on steel pipe and H-piles, and "sister-bar" strainmeters or concrete-embedment strain gauges can be installed in concrete(d) or grouted piles.

Embedded strain gauges are generally treated as reliable (even if unbeknownst they are not) in obtaining measurements characteristic of foundation response to applied load; converting strain readings to internal

 © Deep Foundations Institute 2025

pile forces is not necessarily straightforward, as it is a function of the pile's physical characteristics at the strain measurement location. This reality is at best misrepresented, and at worst misunderstood, by the notion that strain gauges measure internal forces (rather than provide readings that are an intermediate step in calculating internal forces). The physical characteristics required to convert strains to internal forces can vary by location within a pile, and during a static load test. Some physical characteristics can be measured, but are more often assumed, assigned presumptive values, estimated, based on constitutive relationships, or back-calculated. The methods used to determine a pile's physical characteristics can introduce significant error into internal pile force calculation, and therefore into determined mobilized unit shaft resistances.

Internal pile forces, F_i, at each strain-gauge level ("SGL") have conventionally been calculated using the strain reading (typically an average, if the SGL contains multiple strain gauges), ε_i, and the product of the pile's composite-section elastic modulus, E_i, and total cross-sectional area, A_i, by the following relationship (Greenspan 1943 & 1946; Pelecanos et al. 2017; Vable 2008):

$$F_i = E_i A_i \varepsilon_i \quad [1]$$

The Incremental Rigidity ("I.R.") method provides a means of quantitatively back-calculating a pile's physical characteristics (i.e., EA) from load-test measurements, and therefore more direct conversion of strain measurements to calculated internal forces (Komurka & Moghaddam 2020; Komurka & Robertson 2020). This method may also be used quantitatively in conjunction with other strain interpretive methods, or qualitatively to identify atypical structural stress-strain response to applied load. Piece-wise linear functions may be developed where the rigidity is defined by multiple interpretative methods over the strain history during a load test (Robertson 2024; Sinnreich 2011).

INCREMENTAL RIGIDITY METHOD OVERVIEW

During a static load test, strain is the measured parameter in Eq. 1, and conversion of measured strains to calculated internal forces conventionally involves determining the composite-section elastic modulus and total cross-sectional area at each strain-gauge level. Komurka and Moghaddam (2020) presented the Incremental Rigidity method, which determines the product EA, the foundation's ***axial rigidity***, at each interpretable SGL. For simplicity, EA will be referred to herein as rigidity. The Incremental Rigidity method is based on the Tangent Modulus method (Fellenius 1989, 2001, and 2019; Salem & Fellenius, 2017), but instead of relating changes in stress to changes in strain to determine a modulus relationship, the I.R. method relates changes in test load to changes in strain to determine an internal force relationship. In this way, the I.R. method offers more direct conversion of strains to calculated internal forces.

Integral to the I.R. method is routine application to field load-testing results, strain-gauge instrumentation layout optimization, and improved load-testing protocol beneficial to yield interpretable results. After shaft resistance between the test-load source and a strain-gauge level is essentially fully mobilized, the quotient of change in test load divided by change in strain ($\Delta Q/\Delta\varepsilon$) plotted against total strain for that SGL resolves into a virtually straight line, sloping from a larger rigidity to a smaller one with increasing strain (Komurka & Moghaddam 2020). A $\Delta Q/\Delta\varepsilon$ plot example is presented in Fig. 1. Strain-gauge levels where shaft resistance between the test-load source and that SGL is not essentially fully mobilized are non-interpretable using the I.R. method; calculating internal forces at these SGLs is addressed in Komurka & Robertson (2020).

Qualitatively, deviations in $\Delta Q/\Delta\varepsilon$ over the test duration may indicate variations in pile rigidity at specific strain magnitudes at a specific strain-gauge level. For example, if full composite-section action is not exhibited during initial test load increments, and assuming ΔQ remains constant throughout the test, $\Delta Q/\Delta\varepsilon$ may increase over several test load increments as strain becomes compatible over the pile's total

cross-section. Additionally, a reduction in ΔQ/Δε may indicate essentially full mobilization of geotechnical resistance between a SGL and test load location due to increased Δε, where the full change in test load is transferred to the specific strain-gauge level.

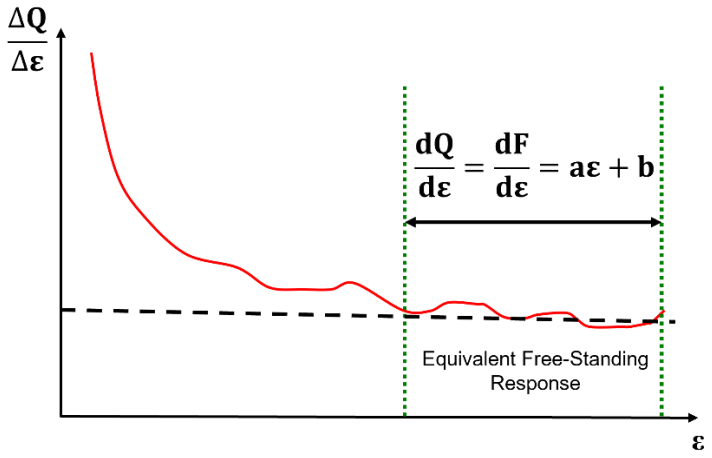


Fig. 1. Linearly resolved ΔQ/Δε plot for one interpretable strain-gauge level.

Quantitatively, a strain-dependent rigidity function can be defined as the "effective rigidity," whereas rigidity at a specific strain magnitude may not be easily defined based on conventional mechanics of fully composite materials. The term effective rigidity may be used to define the proportionality of a parameter to internal force (linear and non-linear proportionality), or conditions where strain compatibility is not a valid assumption over a load-test duration (and thus, the computed composite-section rigidity is not directly proportional to internal force).

The best-fit line coefficients from a linearly resolved ΔQ/Δε plot are used to calculate internal forces at an interpretable strain-gage level according to the following relationship (Komurka & Moghaddam 2020):

$$F_i = 0.5a_i\varepsilon_i^2 + b_i\varepsilon_i + c_i \quad [2]$$

Where for each interpretable SGL_i, a_i = y-intercept of the linearly resolved ΔQ/Δε plot, b_i = slope of the linearly resolved ΔQ/Δε plot, and c_i is the integration constant (since at zero internal force there is zero strain, c_i is equal to zero). Therefore, the linearly decreasing effective rigidity versus measured strain resolves to:

$$E_iA_i = 0.5a_i\varepsilon_i + b_i \quad [3]$$

A review of Eq. 2 indicates that to convert measured strains to calculated internal forces at interpretable SGLs, neither a pile's composite-section elastic modulus, nor its total cross-sectional area, need be known. In this way, the I.R. method offers more direct conversion of measured strains to calculated internal forces than the approach presented in Eq. 1.

CASE HISTORY

Test Pile Details

The test pile, designated TP-1, consisted of a concreted drilled shaft, having an embedded length of 60 feet. As-built diameters varied, from 33 inches from ground surface to 12 feet (in a temporarily cased section), tapering over the next six feet to 30 inches below. The results of two unconfined compressive strength tests performed the day of the test on four-inch-diameter cylinders averaged 6,605 pounds per

 © Deep Foundations Institute 2025

square inch ("psi"). The pile was bi-directionally statically load tested using a jack assembly with a fracture plane at a depth of 45 feet. A total of six strain-gauge levels were installed, four above and two below the jack assembly, with two strain gauges at each level mounted diametrically opposed, Fig. 2. The gauges consisted of Geokon Model 4911 36-inch-long vibrating-wire "sister-bar" rebar strainmeters constructed with #4 reinforcing bar. The strainmeters were installed between the flanges of a W16x31 core beam which was welded to the top and bottom of the jack assembly, and plunged into the fluid concrete, Fig. 3. Of interest for this case history is the measured strain response at SGLs A1 (above the jack assembly), and SGLs B1 and B2 (below the jack assembly). By inspecting these $\Delta Q/\Delta\varepsilon$ plots, other SGLs were considered uninterpretable, and the purpose of this paper is to address interpretation of atypical strain readings where feasible.

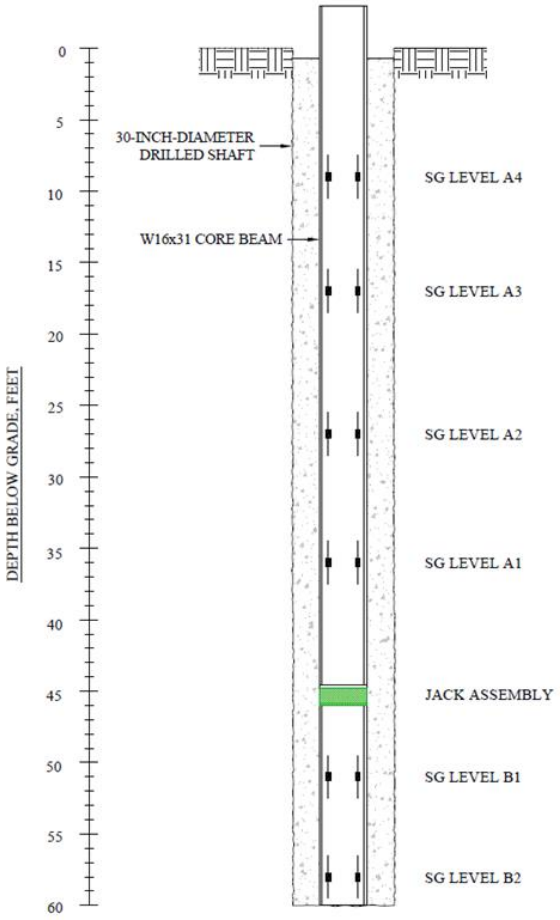


Fig. 2. Test pile schematic.



Fig. 3. Typical strainmeter installation.

Loading Sequence and Strain Responses

TP-1 was loaded in 22 load increments, and unloaded in 5 load decrements, Fig. 4. Early in the test, noteworthy upward shaft head displacement became apparent, risking significant reduction in the final number of load increments attainable. Accordingly, load increment magnitudes were decreased to increase the final number of load increments (a field decision to potentially provide better data interpretation). The strain responses from all strain-gauge levels are presented in Fig. 5.

 © Deep Foundations Institute 2025

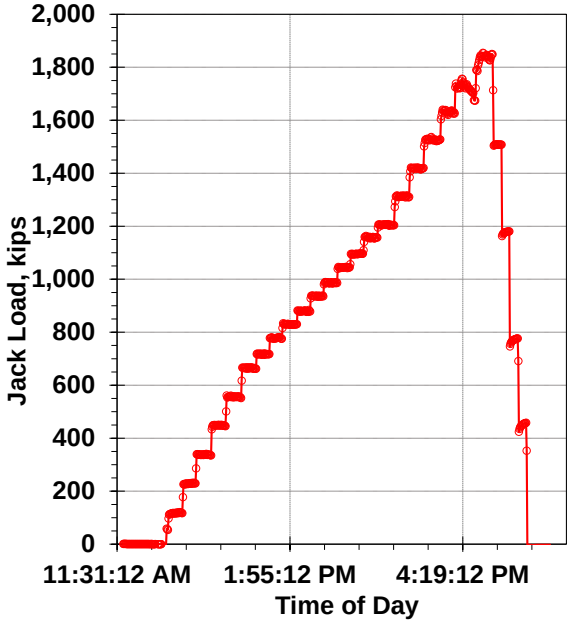


Fig. 4. Load vs. time.

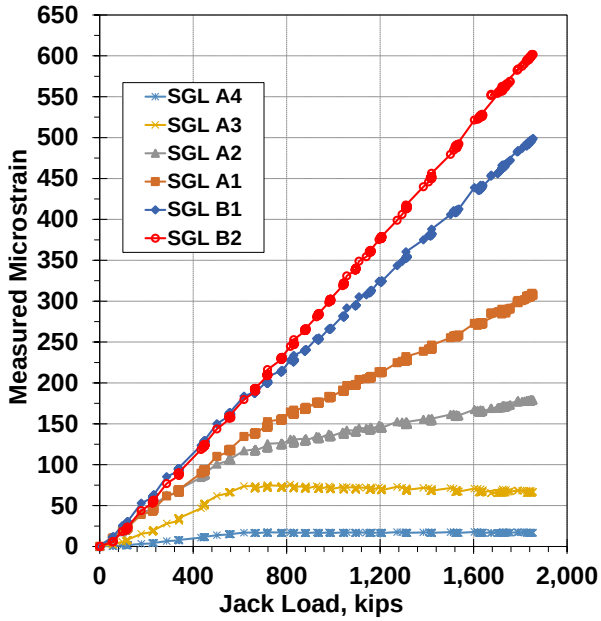


Fig. 5. Strain vs. load.

Incremental Rigidity Interpretations and Calculated Internal Forces

Incremental Rigidity evaluations presented herein are from strain readings from SGLs A1 (first level above the jack assembly), B1 (first level below the jack assembly), and B2 (second level below the jack assembly, near the shaft base).

Strain-Gauge Level B2 – The $\Delta Q/\Delta\varepsilon$ plot using average strains for SGL B2 is presented in Fig. 6. A review of Fig. 6 indicates that the $\Delta Q/\Delta\varepsilon$ plot for B2 resolved into two distinct interpretable linear responses (i.e., bilinear response), potentially indicating a change in effective rigidity during the test. This conclusion is reinforced with the indicated increase in $\Delta\varepsilon$ over the test duration (evidenced in Figs. 5 and 6 at approximately 250 microstrain), resulting in a decrease in $\Delta Q/\Delta\varepsilon$. The slopes and intercepts of the interpreted bilinear linear responses are reported on Fig. 6 (with bilinear responses, both equations are used to calculate internal forces, each being applied to the strain ranges over which they are presented on $\Delta Q/\Delta\varepsilon$ plots). When the bilinear $\Delta Q/\Delta\varepsilon$ strain responses determined from Fig. 6 were used to calculate internal forces at SGL B2, those calculated internal forces were nearly identical to downward test loads throughout the test, Fig. 7.

Strain-Gauge Level B1 – For B2's internal forces interpretation to be plausible, calculated internal forces at SGL B1 must also be nearly identical to downward test loads. The $\Delta Q/\Delta\varepsilon$ plot using average strains for SGL B1 is presented in Fig. 8. A review of Fig. 8 indicates that a) again the average strain readings exhibit bilinear response, and b) the resulting $\Delta Q/\Delta\varepsilon$ plots are somewhat "noisy." As at SGL B2, when the bilinear $\Delta Q/\Delta\varepsilon$ plot strain responses determined from Fig. 8 were used to calculate internal forces at SGL B1, calculated internal forces were nearly identical to downward test loads throughout the test, Fig. 9. This tends to validate the internal force interpretations at both SGLs B1 and B2. This indicates that a) the I.R. method can effectively model bilinear $\Delta Q/\Delta\varepsilon$ responses, indicative of change in effective rigidity during the test, and b) a $\Delta Q/\Delta\varepsilon$ plot can be interpreted to provide reasonable calculated internal forces even with somewhat "noisy" response, and so may not be as subjective as might be assumed.

 © Deep Foundations Institute 2025

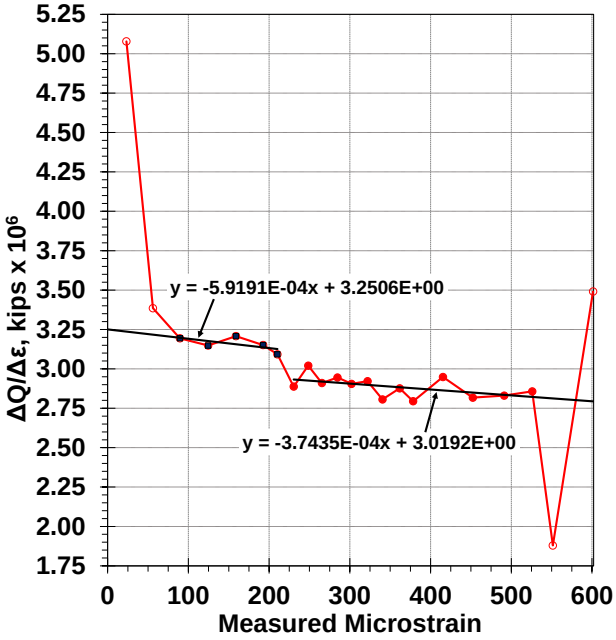


Fig. 6. Strain-Gauge Level B2 ΔQ/Δε plot.

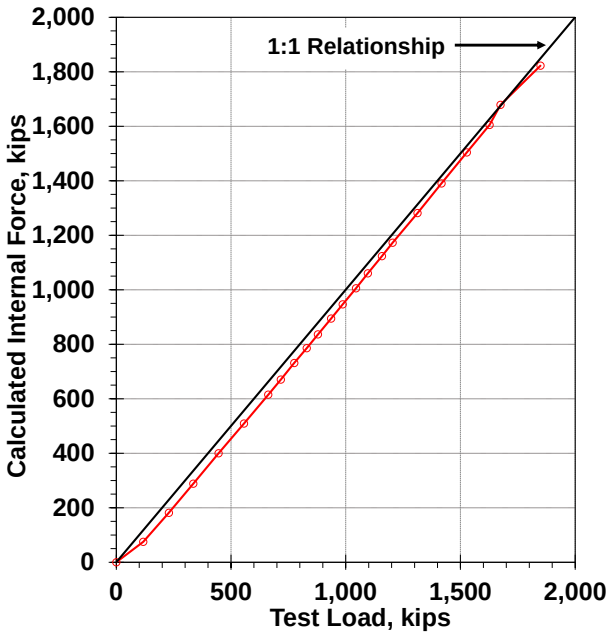


Fig. 7. Strain-Gauge Level B2 Calculated internal forces vs. downward test loads using the I.R. method and Eq. 2.

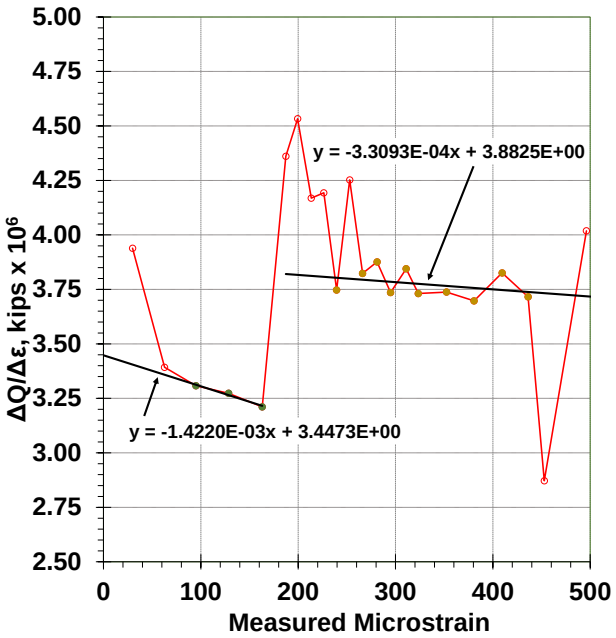


Fig. 8. Strain-Gauge Level B1 ΔQ/Δε plot.

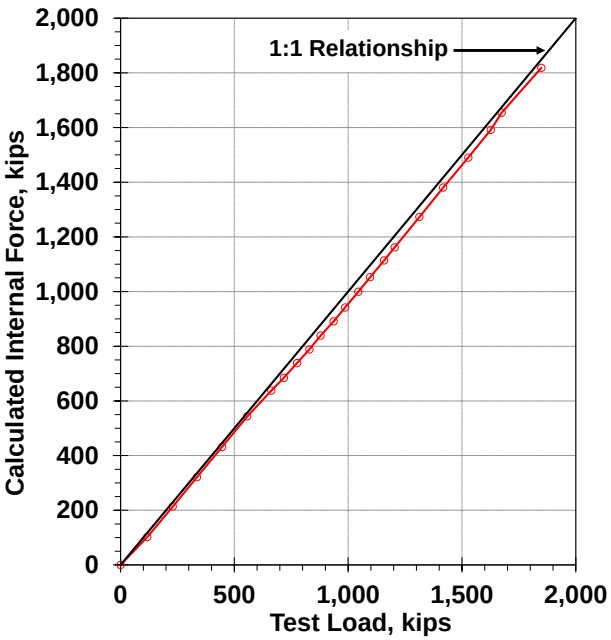


Fig. 9. Strain-Gauge Level B1 Calculated internal forces vs. downward test loads using the I.R. method and Eq. 2.

Strain-Gauge Level A1 – The ΔQ/Δε plot using average strains for SGL A1 is presented in Fig. 10. A review of Fig. 10 indicates that a) again the gauges' average strain readings exhibit bilinear response, and c) again the resulting ΔQ/Δε plots are quite "noisy." Linear interpretations of various slopes and intercepts for the average strain readings are reported on Fig. 10. As at SGLs B1 and B2, when the

bilinear ΔQ/Δε strain responses determined from Fig. 10 were used to calculate internal forces at SGL A1, calculated internal forces were nearly identical to upward test loads throughout the test, Fig. 11.

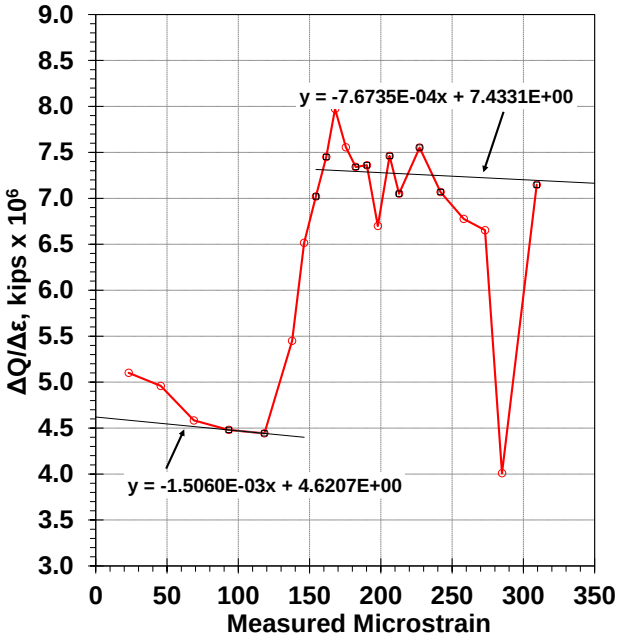


Fig. 10. Strain-Gauge Level A1 ΔQ/Δε plot.

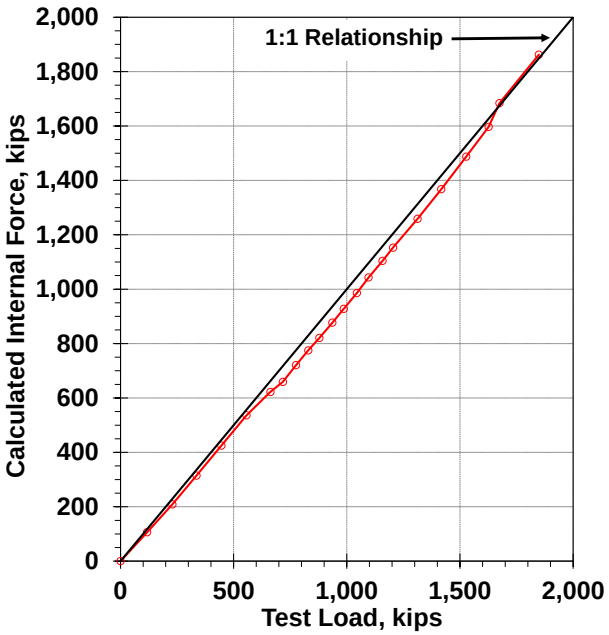


Fig. 11. Strain-Gauge Level A1 Calculated internal forces vs. upward test loads using the I.R. method and Eq. 2.

It should be noted that at all three evaluated strain-gauge levels, although strain readings yielded "noisy," bilinear ΔQ/Δε responses (i.e., experienced changes in rigidity during the test), in all cases the I.R. method accounted for these phenomena, and provided reasonable internal force interpretations.

Inherent in interpreting strain readings utilizing the I.R. method is the assumption that upstream side-shear resistance is essentially fully mobilized prior to developing the effective rigidity function. Therefore, the ΔQ/Δε interpretation could be misleading early in the loading phase, resulting in a higher axial rigidity than what would be otherwise computed if the pile were truly a free-standing column. However, this case study clearly demonstrates atypical strain readings, qualitatively identified via examining ΔQ/Δε over the test duration. Additionally, the results presented herein exhibit abnormal pile response to applied load, indicating either negligible pile-soil shear resistance in the lower foundation portion, and/or lack of composite action due to the instrumented core beam application. Further evaluation of the American Concrete Institute ("ACI") formula is presented in the following text for assessing the validity of a common interpretive method of converting measured strains to calculated internal forces.

The ACI Formula and Calculated Internal Forces

A number of empirical relationships exist to estimate concrete elastic modulus based on unconfined compression strength determined from test cylinders as reported in the American Concrete Institute ("ACI") Committee Report 363-10 (2010). One of the more popular relationships for normal-weight concrete is offered in the ACI 318-14 manual (2014), and is given by the following relationship:

$$E_{CONC} = 57{,}000(f'_c)^{0.5} \quad [4]$$

 © Deep Foundations Institute 2025

Where E_{CONC} = concrete elastic modulus, psi, and f'_c = concrete test cylinder unconfined compressive strength, psi. Komurka and Moghaddam (2020) provided a number of uncertainties regarding assessing the elastic modulus of concrete using the ACI formula. These uncertainties include (among others) the many ways in which the f'_c determined from concrete cylinders in the laboratory may not reflect the mass-concrete strength in the pile, (potentially owing largely to differences in curing conditions), and that Eq. 4 does not account for modulus strain dependency.

For comparison purposes, the ACI formula (Eq. 4) was used to estimate concrete modulus using the concrete test cylinders' average unconfined compressive strength. This concrete modulus, along with the pile's steel modulus and constituent concrete and steel cross-sectional areas, was used to calculate the pile's composite-section modulus. Plots of the resulting calculated internal forces vs. test loads using Eq. 1 and the constant (linear, strain-independent) concrete modulus estimated by the ACI formula (to determine the composite-section modulus) for the three SGLs are presented in Fig. 12. A review of Fig. 12, especially by comparison to Figs. 7, 9, and 11, indicates that calculated internal forces estimated using the ACI formula might have been misinterpreted as reasonable at SGLs A1 and B1. However, calculated internal forces at SGL B2 are greater than both the test loads and the calculated internal forces "upstream" (closer to the load source) at SGL B1, both of which are physical impossibilities.

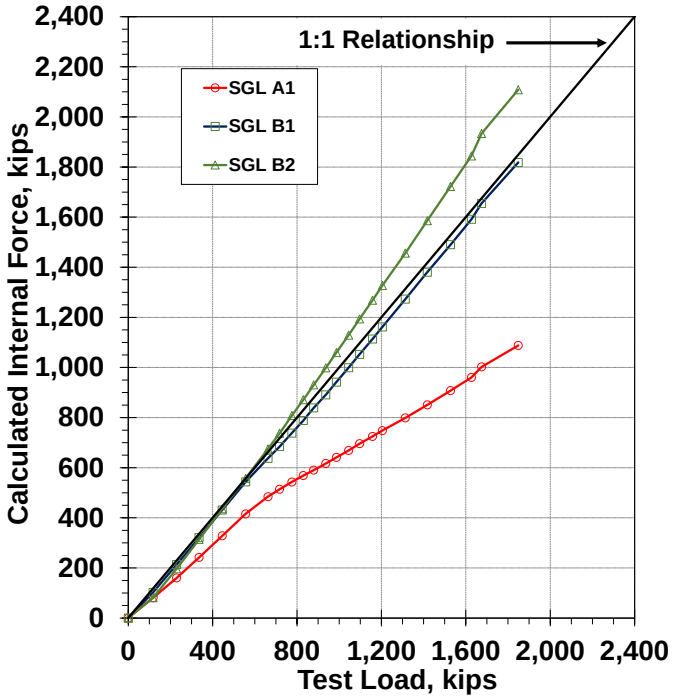


Fig. 12. Strain-Gauge Levels A1, B1, and B2 calculated internal forces vs. test load using the ACI formula (Eq. 4) and Eq. 1.

Potential Contributing Mechanisms to Bilinear ΔQ/Δε Responses

The methodology in applying the ACI formula to estimate the concrete modulus (to be used to calculate the composite-section rigidity) relies on the assumption of composite-section action and strain compatibility across the full pile cross-section at each SGL. Based on the results presented in Fig. 12, higher internal forces than the applied load are computed, as well as higher internal forces compared to an upstream location, both physical impossibilities. This suggests that either a) the ACI-formula-computed concrete elastic modulus is much greater than the actual elastic modulus, or b) composite-section action cannot be justified, which may result in a significantly lower effective rigidity. Utilizing an instrumented

core beam results in a high concentration of steel directly attached (welded) to the bi-directional jack assembly. It may be inferred that stress concentrates in the steel element (i.e., the foundation element does not have compatible strain over its full cross-section). Instrumented core beams must also have adequate concrete-steel development length adjacent to the jack assembly (above and below), such that the concrete-steel interfacial resistance is sufficient to transfer applied load to the surrounding substrate materials. These inferences cannot be readily assessed from strain readings alone, and if the underlying assumptions of the ACI formula are invalid, the ACI-formula-calculated internal forces are fundamentally invalidated.

Uncertainty lies in all methods for interpreting strain readings. The internal force computations presented herein (i.e., the I.R.-method and ACI-formula solutions) may indicate that applied loads are not adequately distributed to the surrounding substrate materials. Bilinear I.R.-method solutions may be applied to strain readings for more direct (i.e., without knowing EA), and more applicable (i.e., strain-dependent response) conversion of measured strains to calculated internal forces, thus demonstrating the inefficacy of the ACI formula under these scenarios. This is particularly important where a sudden change in $\Delta\varepsilon$ is exhibited during a load test, potentially indicating a change in effective structural rigidity rather than a change in resisting geotechnical forces. While the bilinear $\Delta Q/\Delta\varepsilon$ plot may not fully encompass the structural response to applied load, the I.R. method provides a reasonable assessment of the effective rigidity function over the load-test duration.

CONCLUSIONS

A general overview of the Incremental Rigidity method was presented for converting measured strains to calculated internal forces during a static load test with atypical strain readings. A case history presented interpretation of strain readings from a bi-directional static load test on a 30-inch-nominal-diamter concreted drilled shaft. The strain gauges were mounted in diametrically opposed pairs at various levels on a W16x31 core beam which was welded to the top and bottom of the jack assembly. Measured strains were converted to calculated internal forces at two SGLs below, and one SGL above, the jack assembly using the Incremental Rigidity method. At all three SGLs, the $\Delta Q/\Delta\varepsilon$ plots exhibited bilinear response, indicating a change in rigidity during the test. At two SGLs, the $\Delta Q/\Delta\varepsilon$ plots exhibited somewhat "noisy" responses. The I.R. method accounted for these phenomena, and provided reasonable internal force interpretations in all cases; application of the ACI formula did not. From this case history, the following conclusions are drawn:

- Mounting sister-bar strainmeters on a core beam for a bi-directional static load test risks obtaining atypical strain readings, and so should be avoided.
- At interpretable strain-gauge levels, the I.R. method can convert measured strains to calculated internal forces without knowledge of either a pile's composite-section modulus, or its total cross-sectional area. Limited uncertainty remains in defining an exact solution due to the mechanisms of load transfer during a static load test.
- The I.R. method can identify, and account for, a pile's change in rigidity during a static load test (i.e., model bilinear $\Delta Q/\Delta\varepsilon$ response) to yield reasonable calculated internal forces.
- The values presented on a $\Delta Q/\Delta\varepsilon$ plot ($\Delta Q/\Delta\varepsilon$ vs. ε) contain inherent inaccuracies resulting from uncertainties in test loads, strains, and potentially the stress history of both the pile itself and surrounding material. The I.R. method accounts for these inaccuracies by developing an "effective rigidity" (potentially not the pile's full composite rigidity), an internal force-strain relationship that accounts for these inherent inaccuracies, and provides reasonable internal force interpretation.
- Using the ACI formula to determine a constant (linear, strain-independent) concrete modulus used to convert measured strains to calculated internal forces provided unreasonable calculated internal forces; using the I.R. method is superior to using the ACI formula in this respect, particularly for atypical strain responses.

 © Deep Foundations Institute 2025

REFERENCES

ACI Committee, American Concrete Institute, & International Organization for Standardization (2014). Building Code Requirements for Structural Concrete (ACI 318-14) and Commentary. American Concrete Institute.

ACI Committee 363 (2010). Report on High-Strength Concrete (ACI 363R-10). ACI.

Fellenius, B.H. (1989). Tangent Modulus of Piles Determined from Strain Data. ASCE, Geotechnical Engineering Division, the 1989 Foundation Congress, F.H. Kulhawy, Editor, Vol. 1, pp. 500-510.

Fellenius, B.H. (2001). From Strain Measurements to Load in an Instrumented Pile. *Geotechnical News Magazine*, 19(1), pp. 35-38.

Fellenius, B.H. (2019). *Basics of Foundation Design, A Text Book*. Revised Electronic Edition, [www.Fellenius.net], pp. 484.

Greenspan, M. (1943). Axial Rigidity of Perforated Structural Members. *Journal of Research of the National Bureau of Standards*, *31*, pp. 305-322.

Greenspan, M. (1946). Theory for Axial Rigidity of Structural Members Having Ovaloid or Square Perforations. National Bureau of Standards Research Paper RP, 1737.

Hannigan, P., Rausche, F., Likins, G., Robinson, B., & Becker, M. (2016). Geotechnical Circular No.12, Design and Construction of Driven Pile Foundations, Volumes I and II, GEC 12: Report FHWA-NHI-16-010, US Department of Transportation, FHWA, Washington DC.

Komurka, V.E., & Moghaddam, R.B. (2020). The Incremental Rigidity Method – More-Direct Conversion of Strain to Internal Force in an Instrumented Static Loading Test. ASCE GeoCongress 2020, Minneapolis, MN.

Komurka, V.E., & Robertson, S. (2020). Results and Lessons Learned from Converting Strain to Internal Force in Instrumented Static Loading Tests Using the Incremental Rigidity Method. ASCE GeoCongress 2020, Minneapolis, MN.

Pelecanos, L., Soga, K., Chunge, M. P., Ouyang, Y., Kwan, V., Kechavarzi, C., & Nicholson, D. (2017). Distributed Fibre-Optic Monitoring of an Osterberg-Cell Pile Test in London. *Geotechnique Letters*, *7*(2), pp. 152-160.

Robertson, S. (2024). "Non-Linear Pile Rigidity Determined from Embedded Stressmeters in Instrumented Bi-Directional Static Load Test Piles", DFI 49th Annual Conference on Deep Foundations: Aurora, CO, October 2024.

Salem, H., & Fellenius, B.H. (2017). Bidirectional Pile Testing. What to Expect. *Proceedings of the 70th Annual Canadian Geotechnical Conference*, Paper 763, Ottawa, Canada, October 1-3, 7 p.

Sinnreich, J. (2011). "Strain Gage Analysis for Nonlinear Pile Stiffness." *ASTM Geotechnical Testing Journal*, Vol. 35, No. 2, pp. 367-374, doi: 10.1520/GTJ103412.

Vable, M. (2008). *Intermediate Mechanics of Materials*. New York: Oxford University Press.

 © Deep Foundations Institute 2025

EXPERIMENTAL CURVATURE AND MOMENT RESPONSE OF PILE FOUNDATIONS: COMPARISON WITH *P-Y* PREDICTIONS

William P. Shaffer, P.E., S.M.ASCE, Department of Civil and Environmental Engineering, University of California, Irvine, 4130 Engineering Gateway, Irvine, CA 92697; E-mail: wshaffer@uci.edu
Rabie Farrag, P.E., Ph.D., M. ASCE, WSP, Irvine, CA; E-mail: irabie@uci.edu
Carter Cox, P.E., HDR, Irvine, CA; E-mail: carter.cox@hdrinc.com
Anne Lemnitzer, Ph.D., A.M.ASCE, Department of Civil and Environmental Engineering, University of California, Irvine, 4130 Engineering Gateway, Irvine, CA 92697; E-mail: alemnitz@uci.edu

ABSTRACT

Large scale testing in controlled boundary conditions provides unique insights into pile performance through carefully selected and abundantly installed sensor instrumentation. Three 16ft long, 16-inch diameter pile elements with structurally unique properties were installed in loosely placed sand, and subjected to reverse cyclic lateral loading up to complete structural failure. The pile elements consisted of a reinforced concrete pile, a steel pipe pile, and a composite concrete-filled steel tube. The piles were instrumented with more than 50 sensors including strain gauges, LVTDs, string potentiometers, surface rosettes, and 3D strain sensors. This paper compares pile performance, and in particular the pile moment and curvature profiles with numerical predictions across a lateral displacement range of 0-5 inches. The global objective of this study is to examine existing spring formulations used to represent the soil resistance adjacent to the pile, as well as to propose alternative modeling input parameters, that consider the pile's structural behavior in a combined pile-soil model formulation, rather than treating pile and soil as individual components in a spring-based model. This paper presents the pile design, pile construction, and load deformation behavior, and compares experimentally obtained curvature and moment profile with traditionally predicted responses using the widely implemented *p-y* analysis. Findings suggest the *p-y* predictions consistently overestimate the internal curvature and moment compared to the experimental results.

INTRODUCTION

Deep foundations have repeatedly proven to be essential infrastructure components in resisting collapse and maintaining serviceability across both liquefiable and non-liquefiable soil environments. Pile designs are commonly selected based on regional geology, local construction practices, and availability of specialty contractors, design goals, and project-specific constraints. The use of simplified nonlinear soil models, particularly those based on *p-y* springs, has become the standard approach in lateral pile design. In a survey of U.S. practitioners, Lemnitzer (2018) reported that 92% of engineers relied on the *p-y* method for lateral pile analysis—underscoring its prevalence in everyday practice.

The *p-y* approach models lateral soil resistance (*p*) as a function of pile displacement (*y*), inherently linking it to the pile's bending behavior. Traditionally, the framework has assumed that piles within similar soil conditions will experience similar lateral soil resistance. However, this simplification often neglects the influence of pile curvature and moment profiles, which plays a pivotal role in how soil resistance is mobilized. Soil reaction varies not only with depth but also with but also with flexural behavior of the pile, such that a given soil response can vary depending on the pile type. Thus, curvature –

 © Deep Foundations Institute 2025

the second derivative of displacement – becomes an important measure for understanding the relationship between soil response and pile deformation.

While early *p-y* formulations (e.g., Matlock, 1970; Reese et al., 1974, 1975; O'Neill and Murchinson, 1983) provided foundational insight into soil-pile behavior, their application has since been extended far beyond the boundary conditions for which they were originally developed. The scarcity of high-quality curvature and moment data from large-scale pile tests has contributed to this broad extrapolation. This study seeks to evaluate the lateral performance of three pile specimens by comparing numerically predicted curvature and moment profiles against experimental data collected under controlled lateral loading. These results provide valuable insight into the limitations of current modeling techniques and contribute to the body of experimental evidence needed to refine soil-structure interaction models for future load demands.

EXPERIMENTAL PROGRAM

Three large-scale piles with different material properties were tested at the Structural Engineering Laboratory at UC Irvine. The test program included: a 16-inch reinforced concrete (RC) pile (SP4), a 16-inch concrete-filled steel tube (CFST, SP5), and a 16-inch hollow steel pipe pile (SP6). All three piles were embedded in a 14-foot-deep reinforced concrete soil chamber ("Soil Pit") with an 8-inch-thick concrete base (see Figs. 1 and 2). Each specimen was placed vertically in the empty soil pit, after which a poorly graded sand was pluviated (Fig. 2) around the specimens to achieve an average relative density of approximately 25% and an embedment of up to 14ft of soil. All piles were internally instrumented with strain gauges and inclinometers to record curvatures and displacements across the entire pile length. External instrumentation included linear variable differential transformers (LVDTs) and string potentiometers to monitor the head displacement above ground; load magnitudes were directly recorded from a 150kip MTS actuator, connected to the data acquisition system. Figure 1 provides a drawing (to-scale) of the experimental setup and also includes the location of the internal strain gauge instrumentation for all three test specimens.

Pile Design

Prior to the initiation of the experimental program, the lateral response of the piles was modeled using the commercial software LPILE (Ensoft, Inc., 2018). LPILE's analysis is based on the *p-y* curve method, which solves the equilibrium equation for pile deformations based on the Hetényi (1946) extension of Winkler's beam theory from 1867 using a finite-difference algorithm. Pile geometry and material properties were selected considering the general boundary and soil conditions in the pit (e.g., spacing, depth, sand properties, load application point). Even though many code standards suggest limiting lateral pile displacements to 1.0 inch (Parkes et al. 2018), the pile was pushed beyond its linear performance and up to complete structural failure. Analytical predictions suggested plastic hinging to be reached at approximately 0.5 inches of lateral displacement depending on the pile specimen.

The sand was modeled in LPILE using the API Sand model (O'Neill and Murchison, 1983) with a friction angle of 38.4° and an effective unit weight of 92 pcf, based on direct shear tests (ASTM D3080) performed on the same sand used during backfill. The 8" concrete base was modeled as a stiff boundary

using Reese's (1997) weak rock *p-y* curve with a rock mass modulus of 4,770 ksi, uniaxial compressive strength of 7 ksi, strain factor of 0.0005, and 100% RQD. Structural design of all piles followed ACI 318-14, AISC 360-16, and AASHTO LRFD (2017) provisions. The RC pile (SP4) and the steel tube pile (SP6) were designed to have similar initial bending stiffness ($EI \approx 77{,}000$ kip-ft²) −this represents the stiffness of SP4 prior to concrete cracking, while SP5 and SP6 shared identical exterior steel properties (pile-soil interface friction), but different structure stiffnesses due to the concrete infill in SP5.

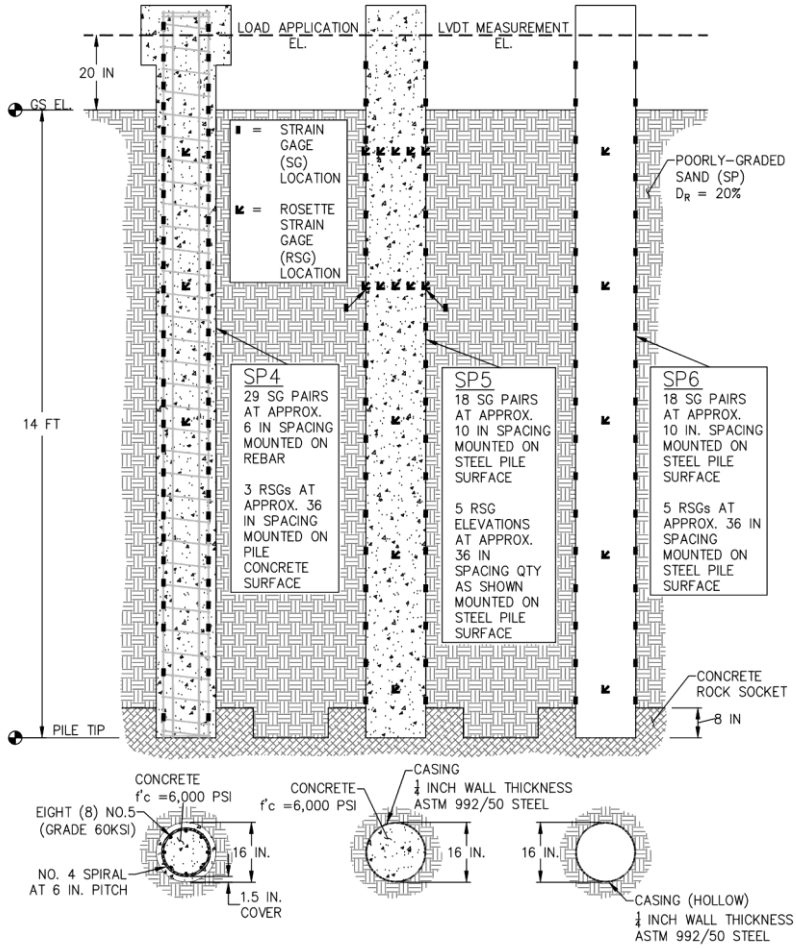


Fig. 1. Test Pile Configurations

Pile construction and materials

Figure 2 shows photographs during pile construction and instrumentation. Only the three specimens relevant to this study are described herein; other piles visible in the images of Fig. 2 were part of a concurrent test series involving rock-socketed piles (Farrag *et al*., 2020). The steel piles (SP5 and SP6) were fabricated from 16-inch diameter, 0.25-inch wall, Grade 50 steel pipes, generously donated by Nucor Skyline. The steel piles were placed in the soil pit and secured with wood framing until the small 8" concrete base was placed. Instrumentation included surface-mounted strain gauges (protected with half-pipe PVC channels) at 10 inch spacing, and string potentiometers at the pile top to record head load-displacements. Internal instrumentation furthermore included inclinometers, secured at the pile center

 © Deep Foundations Institute 2025

through wood bracing. The reinforced concrete pile (SP4) was cast using a sonotube shell and and furnished with 8 #5 longitudinal bars (1.23% reinforcement ratio) and spiral transverse reinforcement at 0.68% (6 inch pitch). The 28-day concrete compressive strength of SP4 was approximately 6 ksi, the rebar consisted of regular Grade 60 rebar. The two opposite longitudinal rebars were furnished with uniaxial strain gauges at 6 inch spacing (except for top and bottom gauges) to capture maximum strains in push and pull directions. Figure 1 provides detail on the instrumentation layout for each pile.

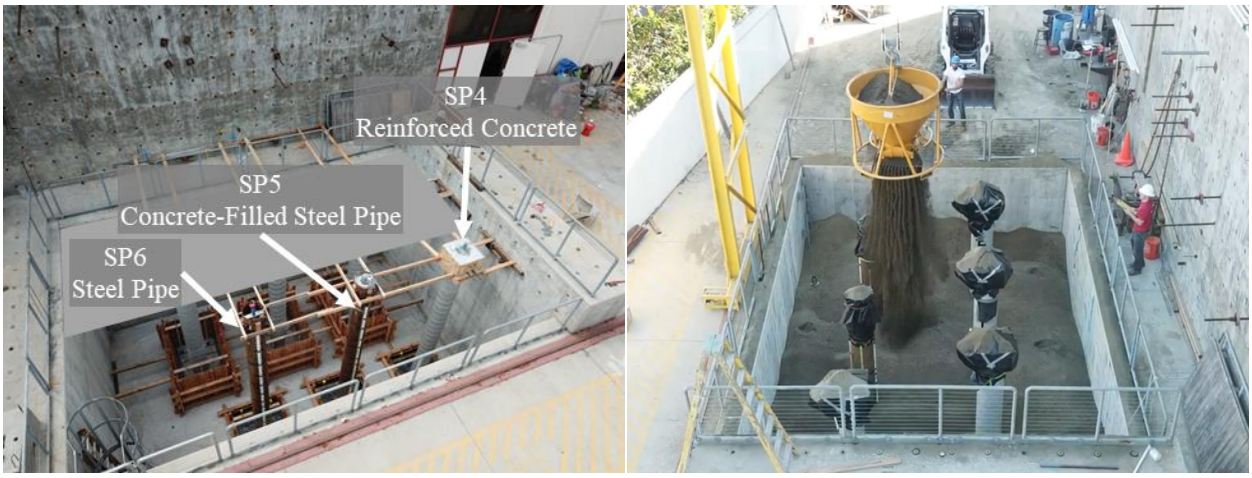


Fig. 2. Specimens SP4, SP5, and SP 6 in the soil pit (20 ft x 30 ft x 14 ft deep) prior to sand placement [left]; sand pluviation using a concrete hopper with a meshed bottom [right].

The backfill sand was placed using a controlled pluviation process, wherein sand was transferred by a skid steer into a hopper, lifted by the overhead crane and subsequently "rained" into the Soil Pit through a mesh screen. Prior to the placement of the soil, the drop height and mesh density were calibrated outside the soil pit to minimize particle segregation and target a relative density of approximately 25%. Field density was monitored throughout the entire sand placement using modified proctor molds and accompanying sand cone tests; post-fill geotechnical characterization included cone penetration testing (CPT) and dilatometer testing (DMT). The sand, classified as poorly graded (SP) per the Unified Soil Classification System, had a maximum dry density of 134 pcf (21 kN/m³) and an optimum moisture content of 8.8%. DMT results yielded a Dilatometer modulus E_D of 2.08 MPa (301 psi), corresponding to a back-calculated soil modulus E_S of approximately 1.89 MPa (274 psi). CPT/DMT-based friction angles ranged between 33° and 38°, depending on the correlation used (Kulhawy & Mayne, 1990; Robertson & Campanella, 1983). An aerial photo of the soil pit prior to sand placement is provided in Fig. 2. The full test dataset is hosted on NHERI's DesignSafe DataDepot and is described in detail in a companion data paper (Lemnitzer *et al*., 2025, under review).

Loading Protocol

All piles were subjected to a displacement-controlled, reversed-cyclic loading protocol. Three cycles per displacement level were applied to assess cyclic degradation and material damping. Each specimen was tested significantly beyond their typical code-permitted displacement (~1inch), and well beyond plastic hinging behavior. Maximum experimental displacements reached 10 inches for SP 5 and 6, and nine inches for SP4.

 © Deep Foundations Institute 2025

RESULTS AND DISCUSSION

Test Observations

A 6-inch by 6-inch reference grid (Fig. 3) was painted on the soil surface around each pile to provide visual reference for surface cracks, gapping, and the built-up of a circular crater upon reaching large lateral deformations. Field observations suggest clear evidence of gap initiation at small displacements—beginning as early as 0.5 inches—and progressive growth with each load step. For SP4 (reinforced concrete), a 6-inch-wide surface gap was visible at approximately 0.5 inches of lateral movement (Fig. 3 top). SP5 (composite pile) showed less initial separation, but a permanent 6-inch gap formed around 1.0-inch horizontal pile head displacement. The depth of subsurface gaps increased systematically from about 1-3inches at 0.5 inches of lateral displacement to over 1 foot at just 1.5 inches of lateral displacement. SP6 exhibited similar trends as SP5.

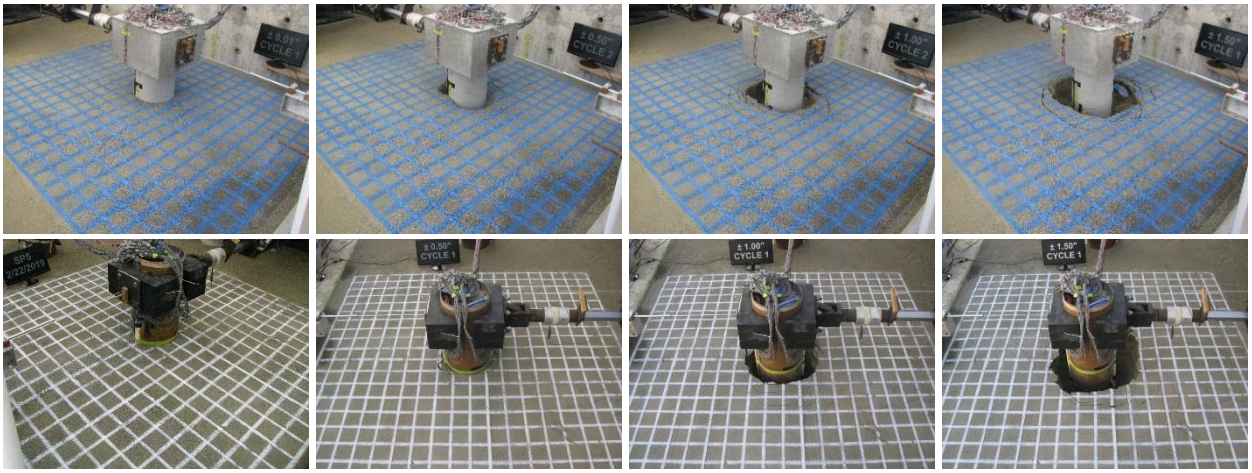


Fig. 3. Lateral load progression of SP4 (top) and SP5 (bottom) at the start of testing, 0.5, 1.0, and 1.5 inches of lateral displacement (left to right). The painted grid is on a 6 inch x 6 inch spacing

Pile head load vs displacement

Figure 4 shows a comparison of experimental backbone curves for SP4, SP5 and SP6 in the push direction. The backbone curves show a consistent over-prediction of the initial pile head stiffness by a factor of 2 to 3. Compared to their *p-y* predictions, the experimental maximum lateral pile load capacity is underpredicted for all specimens up to 20%. For SP4 (RC pile), yielding occurred at 3.0 inches of lateral displacement and 14 kips of load, with an ultimate capacity of 18 kips at 9 inches. SP5 (composite pile) yielded at 4.5 inches and 48 kips, reaching a peak capacity of 60.9 kips at 9 inches. Yielding in SP6 (hollow steel pile) was less distinct but estimated at 4.0 inches and 37.9 kips, with an ultimate capacity of 48.4 kips at 7 inches before significant strength loss. These yield displacements exceed their p-y predictions by 171%, 180%, and 160% for SP4, SP5, and SP6, respectively.

 © Deep Foundations Institute 2025

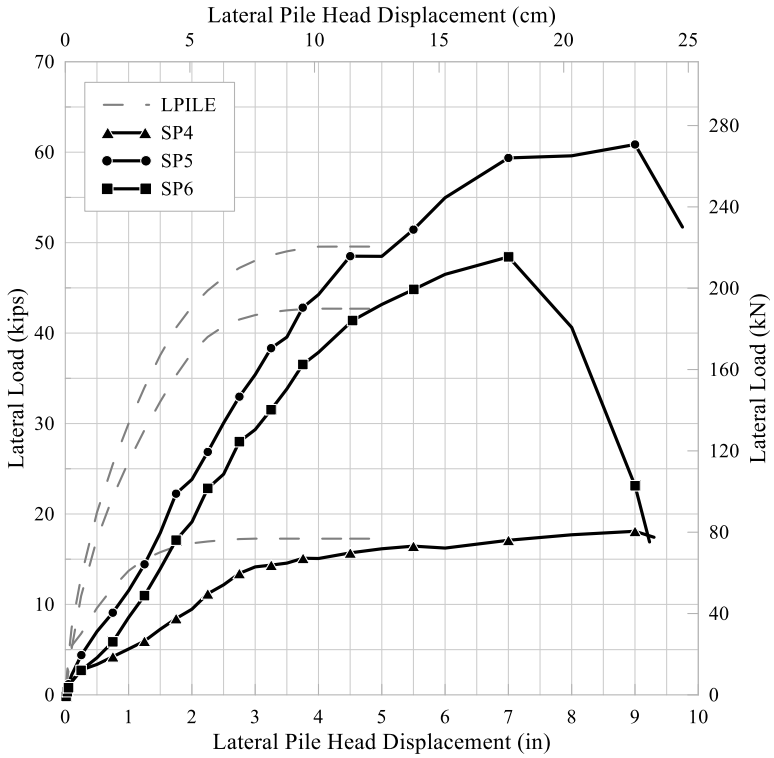


Fig. 4. Lateral load vs lateral pile head displacement curve in the push direction

Pile Curvature and Moment Behavior

Figures 5 and 6 compare the experimental pile curvatures obtained from strain gauge data with predicted curvatures using the *p-y* software LPILE for all three specimens at pile head displacements ranging from 0.05 to 2 inches. When the neutral axis is at the center of the pile (e.g. for SP4 and SP5 before cracking, and SP6 before yielding), the equation simplifies to the strain difference divided by the distance between the gauges and pile curvatures were calculated using Eq. 1:

$$\phi(z) = \frac{1}{2} * \left(\frac{\varepsilon_t(z)}{c_t} - \frac{\varepsilon_c(z)}{c_c}\right) \quad [1]$$

where $\phi(z)$ = pile curvature at depth z; ε_t and ε_c = measured tensile and compressive strain at depth z; c_t and c_c = the distances between strain gauge and neutral axis. For all other cases, i.e., when cracking in the concrete was reached, the location of the neutral axis was determined analytically using LPILE's section analysis, and applied to the distances c_t, and c_s, respectively. To facilitate an easier visual comparison, curvature profiles are grouped by pile head displacements into small (0.05 to 0.25 inches) and working load (0.5 to 2 inches) displacements.

Across all specimens and displacement levels, the *p-y* analysis consistently overpredicted internal pile curvatures, with discrepancies increasing at higher lateral displacements. The experimental curvature profiles show a much broader and more distributed curvature profile shape compared to the sharp peaks predicted by the *p-y* analysis. This broader shape suggests a more gradual formation of plastic hinges and strain redistribution along the pile length, and a potential higher degree of structural ductility than

 © Deep Foundations Institute 2025

obtained through the numerical analysis. At a lateral pile head displacement of 1.0 inches, the predicted curvature exceeds the measured curvature by a factor of 2.9 to 3.0 At 2.0 inches the overprediction reached a factor of 2.3 to 4.3, and at a lateral displacement of 5.0 inches this overprediction was 10 times. The curvature profiles for displacements larger than 2 inches are not shown, as the scaling of the graph and the overprediction of the analytical results depreciate the visual clarity of the graphs presented below.

Even though experimental results of the low displacement levels do not immediately suggest the location of the plastic hinge, the LPILE predictions captured the overall location well, as indicated by experimental results at larger lateral displacement levels. This component of the analysis is critical to future pile design.

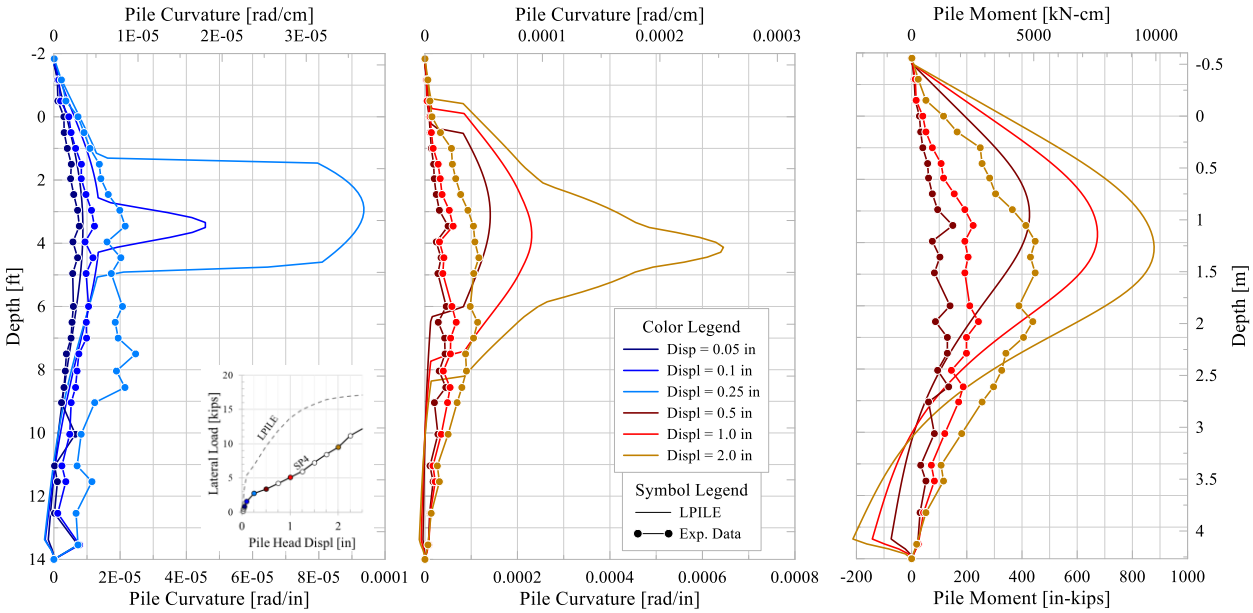


Fig. 5. SP4 (reinforced concrete pile) curvature and pile head load-displacement vs LPILE predictions

Curvature profiles are traditionally used to obtain pile bending moments. Using the nonlinear moment-curvature relationship (M-ϕ) from the structural engineering software SAP2000 by CSi, inc. shown in Fig. 7, the curvature profiles (both experimental and numerical) were translated into moment profiles along the pile depth. Moment curvature relationships generated in LPILE consider concrete cracking, while M-ϕ relationships obtained in SAP2000 only consider the cracked concrete. The M-ϕ relationship from LPILE was not used in the analysis because the flat portions of the curve associated with concrete cracking (pile curvature < 7E-05 for SP4 and < 2E-05 for SP5) produced unrealistic moment profiles. Additionally, it is evident from Figs. 5, 6, and 7 that LPILE does not strictly enforce its own M-ϕ relationship as demonstrated by the resulting smooth, and continuously changing moment profiles that lack the constant-moment regions expected where the M-ϕ curve indicates cracking. Table 1 shows the ratio of the predicted curvature to experimentally measured curvature, with the corresponding moment ratios in parentheses. Up to displacements of 2.0 inches, none of the curvature measurements are within the plastic hinging (i.e., flat portions of the M-ϕ curve), therefore the curvature and moment profiles take similar shapes.

 © Deep Foundations Institute 2025

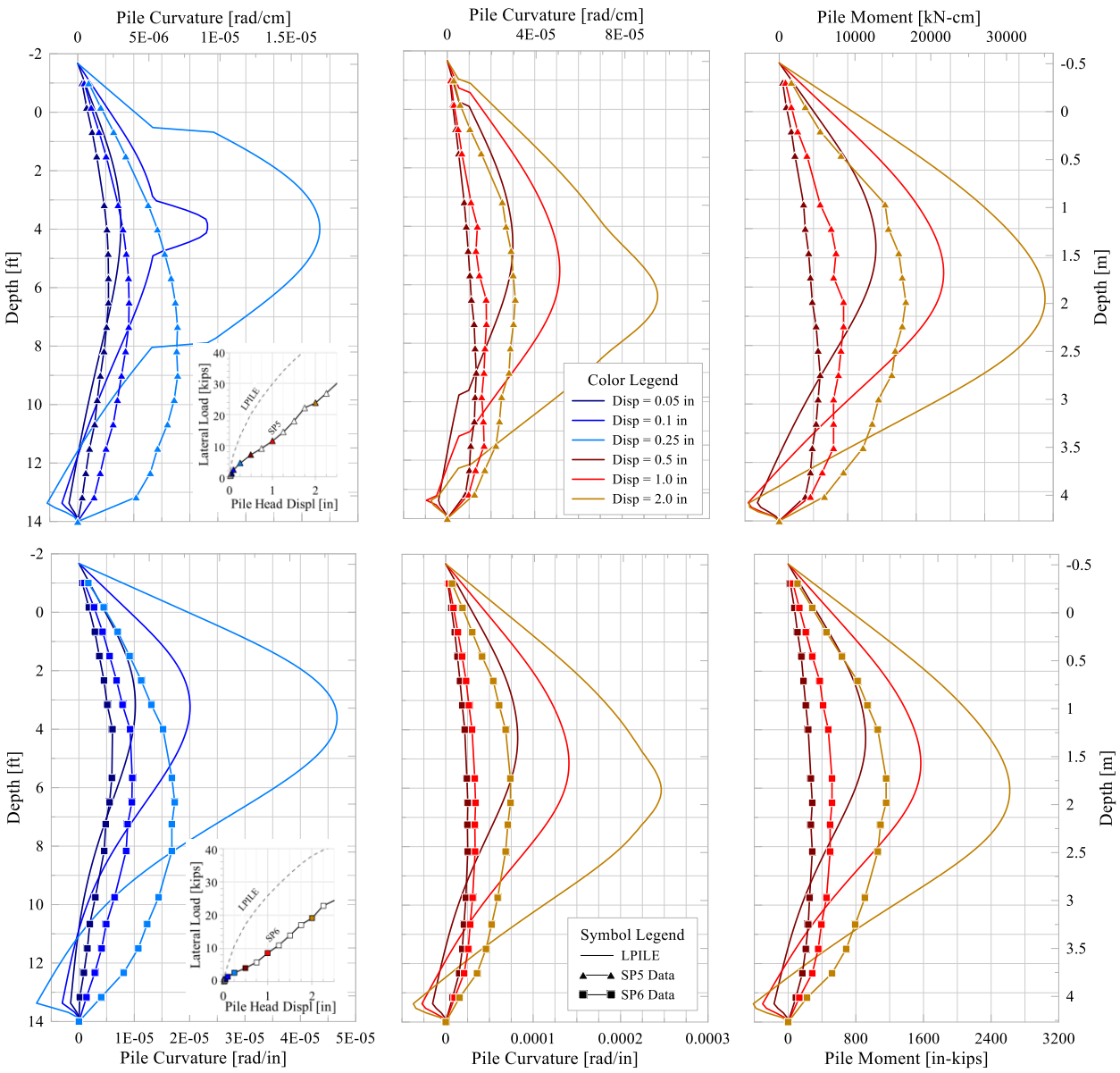


Fig. 6. SP5 – concrete filled steel pipe (top) – and SP6 – steel pipe (bottom) – curvature and pile head load-displacement vs LPILE predictions

As suggested by Figs. 4, 5, and 6, the numerically predicted moment profiles match the experimental location of maximum moments relatively well, despite the mismatch depths at low displacement levels. At lateral displacement levels of 0.5, 1.0 and 2.0 inch, the numerical moment overpredicts the experimental moment by a factor of two, and in some cases up to three.

 © Deep Foundations Institute 2025

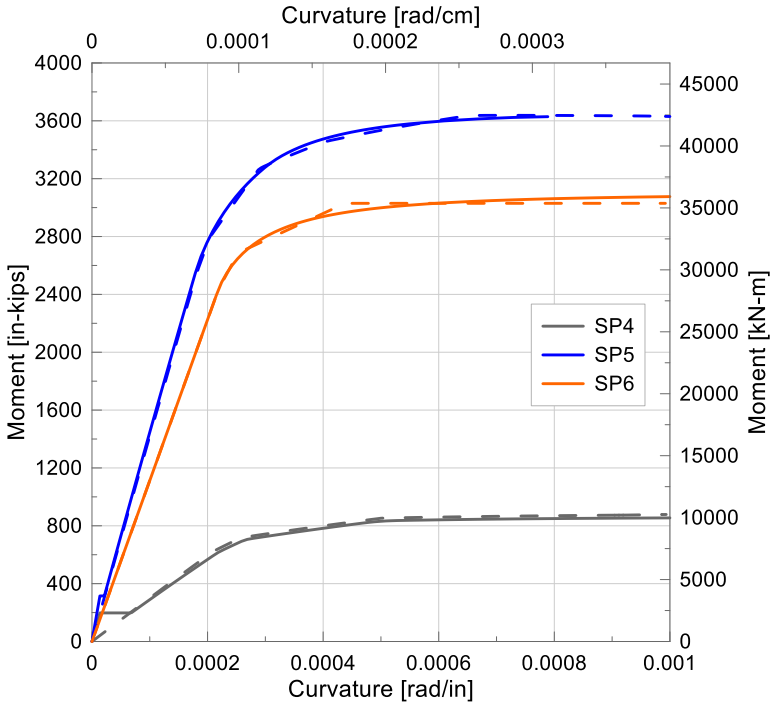


Fig. 7. Test specimen moment-curvature relationships (*M-ϕ* relationship from LPILE shown as a solid line and SAP2000 shown as dashed line)

Table 1. LPILE to experimental maximum curvature and moment ratios

$\varphi_{max,num}$ / $\varphi_{max,exp}$ ($M_{max,num}$ / $M_{max,exp}$)												
Test Specimen		Small Displacements						Working Load Displacements				
		0.05 inch		0.1 inch		0.25 inch		0.5 inch		1.0 inch		2.0 inch
SP4		1.1 (1.2)		3.7 (1.1)		3.8 (1.2)		2.8 (1.8)		2.9 (2.7)		4.3 (2.0)
SP5		1.4 (1.5)		2.5 (1.6)		2.4 (1.9)		2.3 (1.8)		2.4 (2.4)		2.3 (2.0)
SP6		1.7 (2.0)		2.1 (2.0)		2.7 (2.5)		3.3 (3.0)		3.0 (3.1)		2.4 (2.3)

SUMMARY

This study examines the discrepancies between experimental observations and numerical predictions obtained using the conventional *p–y* method. Although testing extended to 10 inches of lateral head displacement, the analysis emphasizes behavior up to 2 inches—considered the most relevant range for evaluating moment and curvature development. Strain gauge data revealed broader and more gradual curvature profiles compared to the sharp peaks predicted by the numerical model, indicating more ductile behavior than the *p–y* approach can capture. The *p–y* method consistently overpredicted curvature magnitudes, particularly at higher displacements. However, it reasonably approximated the depth of maximum curvature, especially as pile head displacement increased, which remains useful for identifying critical design sections. When curvature data were converted to moment using LPILE's nonlinear moment–curvature relationships, predicted maximum moments aligned more closely with experimental results in terms of shape. This agreement is attributed to the plateauing of moment response following the onset of plastic hinging. Overall, the findings underscore the limitations of simplified soil–pile

 © Deep Foundations Institute 2025

interaction models, which assume idealized soil behavior and neglect stress redistribution and gapping effects under large deformations. Based on the experimental observations presented in this paper, the authors suggest that cracked moment-curvature profiles be used for the entire analysis when translating experimental curvatures into moments.

REFERENCES

American Association of State Highway and Transportation Officials, AASHTO (2017). AASHTO LRFD 8th Bridge Design Specifications. Washington, D.C.

American Concrete Institute, (2019). Building Code Requirements for Structural Concrete (ACI 318-19) and Commentary (ACI 318R-19).

American Institute of Steel Construction, AISC. (2016). "Specifications for structural steel buildings." *ANSI/AISC Standard 360-16*. Chicago, Illinois.

American Petroleum Institute (API). (1993). "Recommended practice for planning, designing and constructing fixed offshore platforms." API recommended practice RP-2A, Wash., D.C.

Ensoft. (2018). "LPILE Version 10.0, A Program for the Analysis and Design of Deep Foundations Under Lateral Loads." Austin, Texas: Ensoft, Inc.

Farrag, R., Cox, C., Turner, B., & Lemnitzer, A. (2020). "Shear demands of rock-socketed piles subject to cyclic lateral loading." *DFI Journal – The Journal of Deep Foundations Institute*, 14(2), DOI: 10.37308/DFIJnl.20200526.223

Hetényi, M. (1946). "Beams on Elastic Foundation." University of Michigan Press, Ann Arbor, Michigan.

Kulhawy, F. H., & Mayne, P. W. (1990). Manual on estimating soil properties for foundation design (No. EPRI-EL-6800). Electric Power Research Inst., Palo Alto, CA (USA); Cornell Univ., Ithaca, NY (USA). Geotechnical Engineering Group

Lemnitzer, A. (2018). "Statistical assessment of uncertainties in soil resistance functions", PEER Researcher workshop, Berkeley, California, August 7th, 2018

Matlock, H. (1970). "Correlations for design of laterally loaded piles in soft clay." *Proc., 2nd Annual Offshore Technology Conf.*, OTC 1204, Houston, Texas, Vol. 1 577-594.

O'Neill, M. W., & Murchison, J. M. (1983). An evaluation of p-y relationships in sands. *Rep. PRAC 81-41-1* Prepared for American Petroleum Institute, University of Houston, University Park, Houston, TX.

Parkes, J., Castelli, R., Zelenko, B., O'Connor, R., & Godfrey, E. (2018). Geotechnical Engineering Circular: Design, Analysis, and Testing of Laterally Loaded Deep Foundations that Support Transportation Facilities (No. FHWA-HIF-18-031). United States. Federal Highway Administration.

Reese, L. (1997). "Analysis of laterally loaded piles in weak rock". *ASCE Journal of Geotechnical and Geoenvironmental Engineering*, Vol. 123, No. 11.

Reese, L. C., Cox, W. R., & Koop, F. D. (1975). "Field testing and analysis of laterally loaded piles in stiff clay." *Proc. 7th Offshore Technology Conf.*, OTC 2312, Houston, Texas, 2, 671-690.

Reese, L.C., Cox, W. R., & Koop, F. D. (1974). "Analysis of laterally loaded piles in sand." *Proc. 6th Annual Offshore Technology Con.*, OTC 2080, Houston, Texas, 2, 473-483.

Robertson, P. K., & Campanella, R. G. (1983). Interpretation of cone penetration tests. Part I: Sand. Canadian geotechnical journal, 20(4), 718-733.

Winkler, E. (1867). "Die Lehre von der Elastizität und Festigkeit." Dominicus Verlag, Prag.

 © Deep Foundations Institute 2025

MONTE CARLO SIMULATION TO ASSESS SOIL PROPERTY UNCERTAINTIES FOR SEISMIC EVALUATION OF EXISTING STRUCTURES

Martin B. Hudson, Hudson Geotechnics and UCLA, El Segundo, CA, USA, 424-220-4541, marty@hudsongeotechnics.com
Kenneth S. Hudson, Hudson Geotechnics, El Segundo, CA, USA, 424-658-4686, ken@hudsongeotechnics.com
Maikol Del Carpio, KPFF, Los Angeles, CA, USA, 213-310-8516, maikol.delcarpio@kpff.com
Jelisa Adams, Geocon West, Irvine, CA, USA, 949-346-1109, jelisa@geoconinc.com
Armand Terzian, KPFF, Los Angeles, CA, USA, 213-310-8562, Armand.Terzian@kpff.com

ABSTRACT

Seismic evaluations of structures are more frequently being performed in Los Angeles and other jurisdictions in California due to seismic retrofit ordinances and the desire of building owners to limit losses in the event of major earthquakes. The most common guideline used for evaluation of seismic performance of existing buildings is the ASCE 41 standard. There are uncertainties associated with evaluation of existing foundations, and uncertainties of soil properties are evaluated using the coefficient of variation (C_v) of properties to develop best estimate, lower bound, and upper bound values of strength and stiffness. Available geotechnical data at an example site is used to perform a probabilistic evaluation of the soil properties. Determination of strength and stiffness parameters require an understanding of the uncertainty of empirical relations and the dataset of soil properties. A Monte Carlo simulation is conducted to evaluate the likelihood of possible strength and stiffness parameters. Therefore, the footing bearing capacity, lateral capacity, and seismic lateral earth pressure (although this paper focuses solely on footing bearing capacity, the methods can be easily extended to those other topics) can be examined in a probabilistic manner, consistent with the methodology of ASCE 41. The evaluation can also be performed using analytical solutions via convolution of distributions for linear combinations and approximated using numerical integration where analytical convolution is intractable; we derive these solutions as well and validate the Monte Carlo simulations with the results. A comprehensive probabilistic evaluation provides the basis for a complete understanding of variability of the behaviour of a structure.

Keywords: Seismic rehabilitation, Monte Carlo Simulation, Los Angeles, statistics

INTRODUCTION

Structures built decades previously are increasingly being evaluated for seismic performance due to relatively recent seismic retrofit laws in various jurisdictions in California, or due to owners having the desire to provide more resilient and safer structures for their building inventory. However, there is sometimes a lack of geotechnical and/or foundation information compared to modern construction. This is especially true when the original geotechnical data was obtained using older techniques or does not contain currently used field and laboratory testing. The lack of information can be addressed by performing additional geotechnical explorations and testing as part of a seismic retrofit evaluation. In addition, where there is uncertainty in the original geotechnical data or lack of information, statistical analysis techniques can be used to augment the known data.

ASCE 41 (ASCE, 2017a) requires consideration of uncertainty of parameters in retrofit evaluations such as Section 8.4.1 – Expected Foundation Capacities. For example, foundation soil/rock stiffness and capacity must be evaluated using upper- and lower-bound values defined using a C_v with a default value of 1 and minimum value of 0.5. Quantification of C_v is often ignored or evaluated improperly in practice. Therefore, this manuscript describes methodologies for quantifying uncertainties in geotechnical parameters with an example project.

 © Deep Foundations Institute 2025

At the University of California (UC), there has been an on-going seismic retrofit program in progress since the 1980's (Carpio *et al.*, 2021). The Seismic Safety Policy (UC, 2024) states "The University must provide an acceptable level of earthquake safety for students, employees, and the public who occupy University Facilities within a reasonable time frame. The University must weight the probability and gravity of potential injury to persons foreseeably exposed to the risk of injury from a seismic occurrence against the practicality and cost of protecting against the risk of injury from seismic occurrences."

The subject of this paper involves an existing athletic facility at a UC campus built in 1969 and designed using the 1964 edition of the Uniform Building Code (ICBO, 1964). The stadium includes at-grade stadium seating constructed on a sloped ground surface, an at-grade concourse level at the top of the stadium seating, a long single-story restroom/concession building partially built into the hillside beyond the concourse at the top of the stadium seating along the west side, and a single-story ticket office/storage building. A plan view of the site is shown in Fig. 1. The seismic retrofit and evaluation is predominantly concerned with the long restroom-concession building. Based on the original building plans, the restroom/concession building and the ticket office/storage building structures are supported on shallow reinforced concrete strip footings (footings typically founded at a depth of 2 ft below lowest adjacent grade). A cross-section through the structure is shown in Fig. 2. The footings in a portion of the structure are shown in Fig. 3.

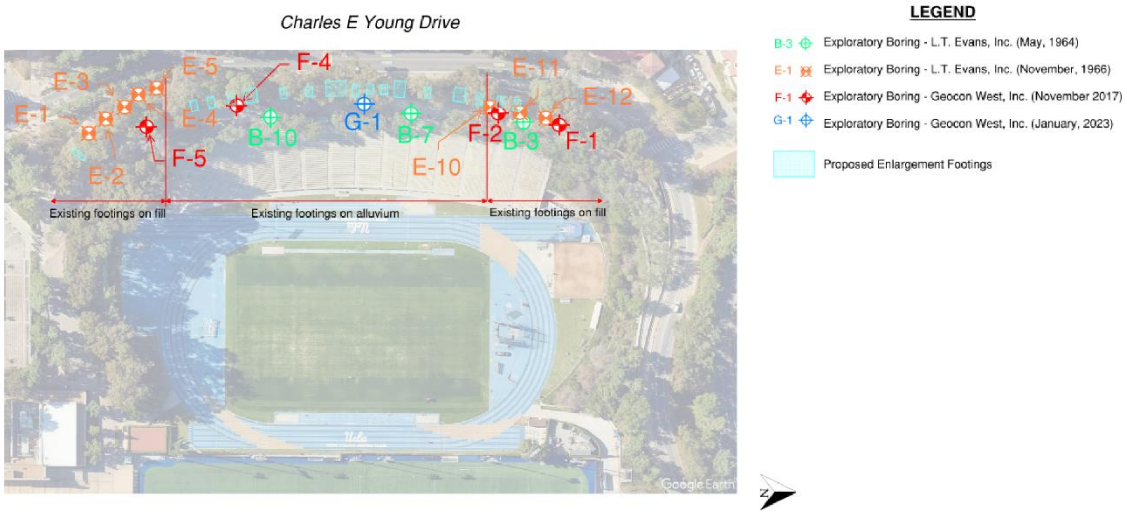


Fig. 1. Plan View of Site

The seismic performance evaluation project includes consideration of potential retrofit schemes. The nonlinear dynamic analysis performed by the structural engineers requires ground motion studies and development of acceleration-time series records in accordance with ASCE 41-17 (ASCE, 2017a) and ASCE-7-16 (ASCE, 2017b). Evaluation of the foundations and basement wall on one side of the restroom/concession building was performed by KPFF utilizing the ASCE 41 nonlinear dynamic procedure and soil-structure modeling necessitating axial and lateral soil springs to represent the foundations.

 © Deep Foundations Institute 2025

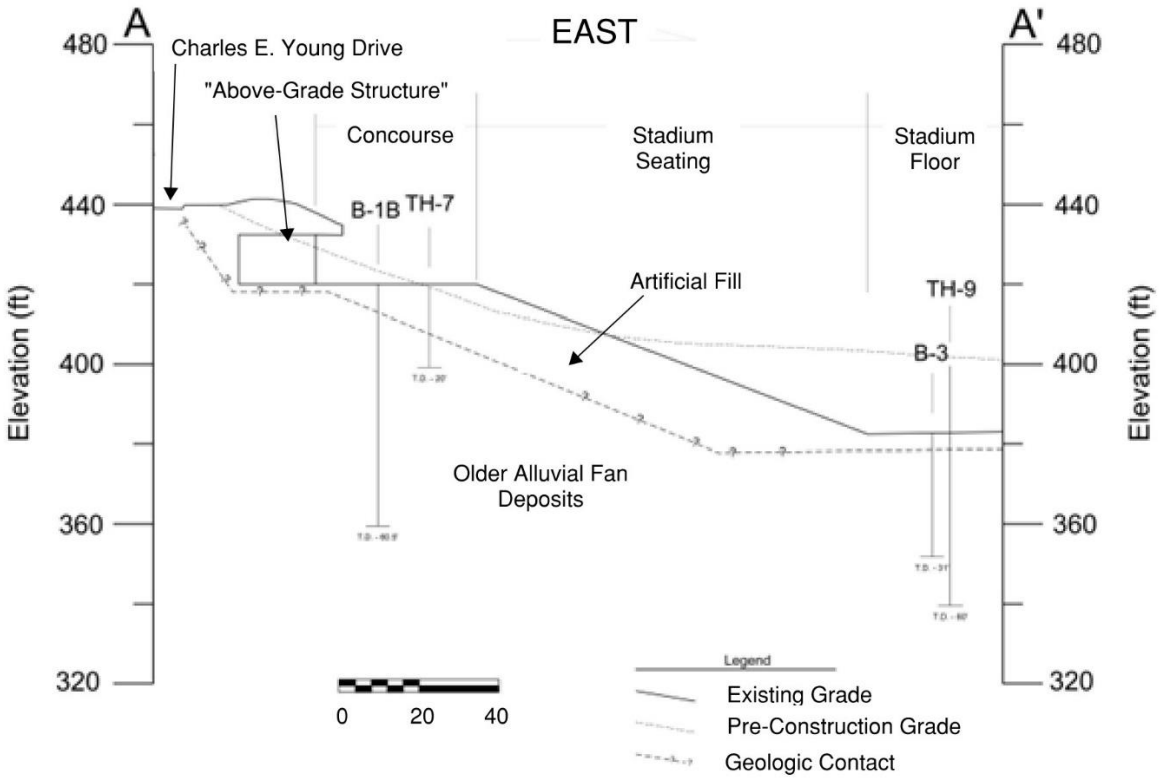
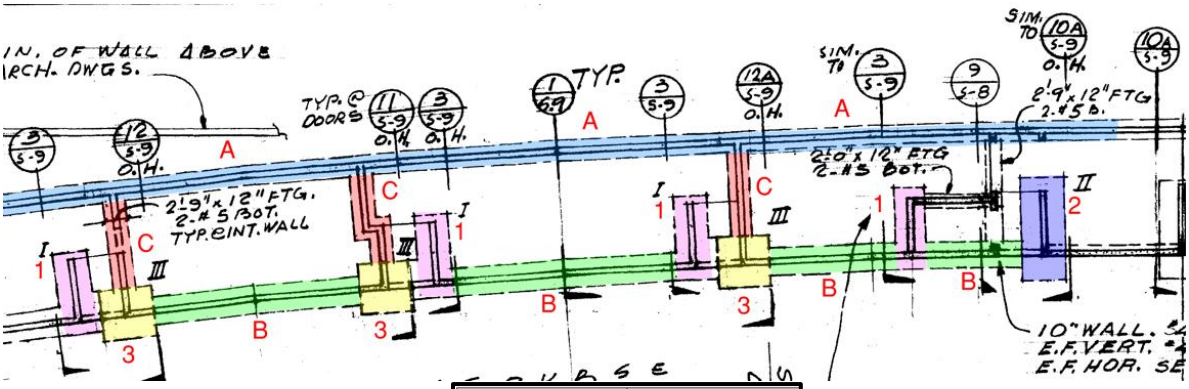


Fig. 2. Cross-Section A-A'



Footing Label	Footing Width (ft)
A	3.0
B	4.0
C	2.8
1	4.5
2	6.0
3	7.0

Note: footings typically founded at depth of 2 ft below lowest adjacent grade.

Fig. 3. Example of Spread Footings for Structure

 © Deep Foundations Institute 2025

GEOTECHNICAL CONDITIONS

The data obtained from the original geotechnical investigations at the project site and the additional investigation performed as part of the seismic evaluation indicate that the subsurface generally consisted of fill overlying alluvium containing predominantly sandy soils with various amounts of silt and clay. Artificial fill was encountered in the borings, with deeper portions of fill on the south side of the site. The fill extended to depths ranging from 2 feet to 20 feet below the approximate ground surface at Elevation 420 feet for the restroom and concession structure at the south side of the stadium. For the office structure, the fill is estimated to extend to an approximate depth of 12 feet below ground surface Elevation 420 feet. Groundwater was not encountered in the borings in the immediate vicinity of the subject structure. Groundwater was encountered in 1966 at approximate Elevations 392.5 feet and 400 feet within Boring 21 and Boring 15, respectively, both approximately 150 feet to the northeast of the structure. The locations of relevant borings are shown in Fig. 1.

SOIL STRENGTH PROPERTIES

For evaluation of foundation capacity, the soil strength parameters are estimated. In-situ testing was performed in the borings consisting of driven sample blow counts. The blow counts were obtained using California Modified Samplers N_{CalMod}.

Ordinarily, the blow counts are converted to equivalent Standard Penetration Test (SPT) blow counts (N) using an assumption that the conversion (N/N_{CalMod}) is 0.65. However, based on our prior experience in southern California where both Mod Cal and SPT samples are driven at the same site, there is a large uncertainty in this conversion. Based on past comparisons, the conversion factor is assumed to be a truncated normal distribution with a mean (μ) of 0.65, a standard deviation (σ) of 0.25, a minimum of 0.1, and no maximum. The uncertainty in the conversion is incorporated using the Monte Carlo method (Metropolis and Ulam, 1949): the normal distribution of the SPT/Mod Cal conversion factor is randomly sampled 4000 times and each sampled factor is multiplied to each measured blow count, resulting in 4000 sampled SPT N values. The sampled factors are presented in Fig. 4. A histogram is constructed from the resulting samples of N, its shape is examined, and, if a normal distribution is appropriate, a μ and σ are computed, quantifying the uncertainty in the conversion on the N values.

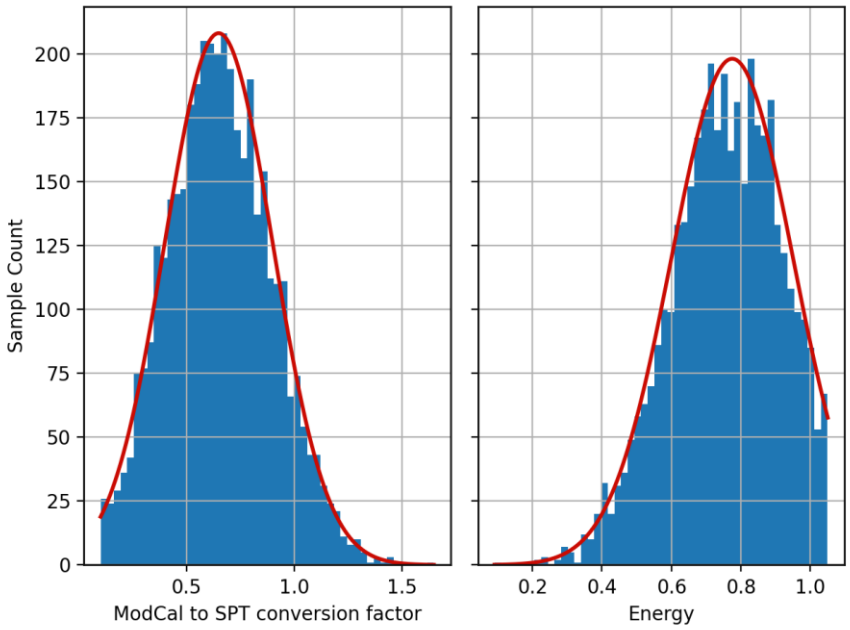


Fig. 4. Distribution of Blow Count Information

 © Deep Foundations Institute 2025

Next, the converted SPT N-values were converted to energy-corrected SPT values (N_{60}). Measurements of rig/sampler drive energy were not available for any of the borings. Therefore, based on our experience with rigs in southern California, we have assumed a truncated normal distribution of the energy with μ = 0.775, σ = 0.175, and maximum of 1.05. This is sampled similarly to the Mod Cal to N conversion and the distribution of samples is shown in Fig. 4.

The N_{60} values are converted to $(N_1)_{60}$. Finally, considering that the materials encountered consisted predominantly of sandy materials, the converted $(N_1)_{60}$ values are used to estimate friction angle φ' (Kulhawy and Chen, 2007). The mean conversion function was taken to be that of (Kulhawy and Chen, 2007), shown in Equation 1.

$$\varphi' = a + b * \log_{10}((N_1)_{60}) \quad (1)$$

To quantify the uncertainty in this conversion function, the intercept (a) and slope (b) of the relationship are assumed to be normally distributed and given μ of 27.5 and 9.2 and σ of 4.125 and 0.46, respectively. These parameter distributions are sampled, and each sample is applied to each measured blow count to produce a φ'. A visualization of the resulting data is presented in Fig. 5.

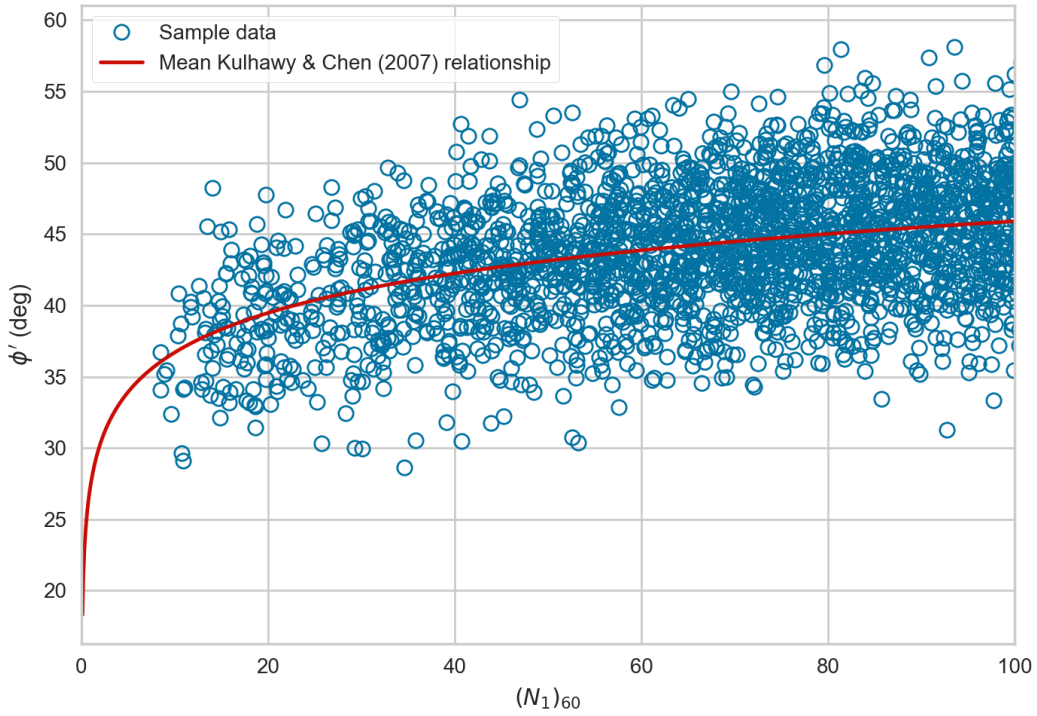


Fig. 4. Evaluation of Friction Angle

The resulting distribution of φ' is approximately normally distributed with μ and σ of 43.3 and 4.87 degrees, respectively, as presented in Fig. 6. This evaluation is for the alluvium at the site, the fill is analyzed in the same manner and results in a similar distribution, with μ and σ of 43.4 and 5.53 degrees, respectively.

 © Deep Foundations Institute 2025

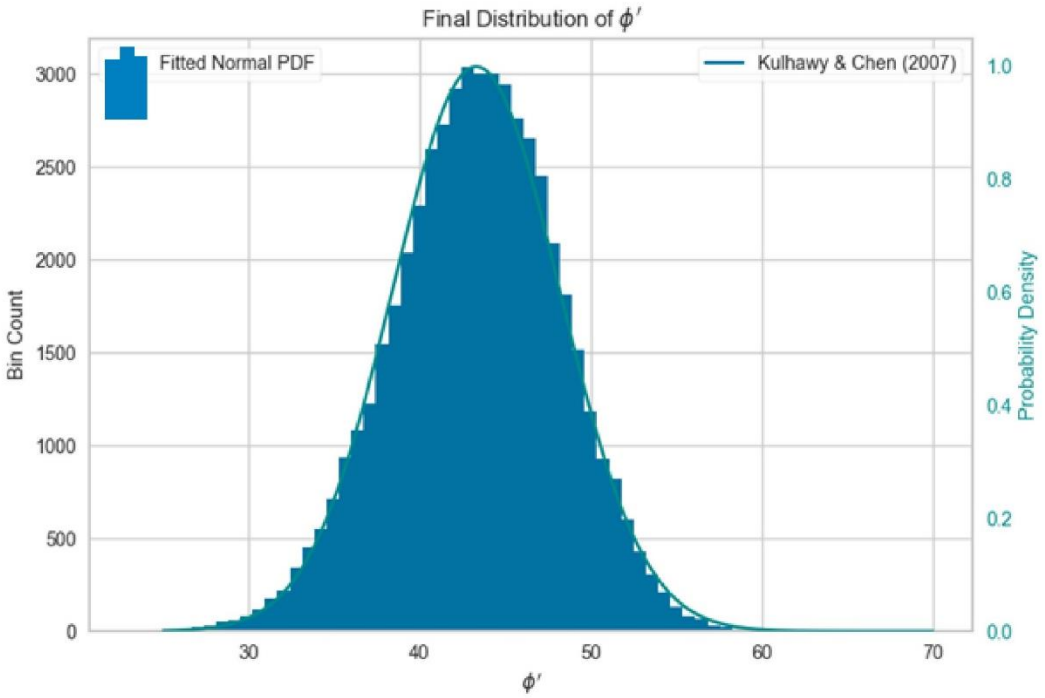


Fig. 5. Distribution of Friction Angle

ANALYTICAL SOLUTIONS FOR UNCERTAINTY

A more straight-forward approach would be to assign a probability density function (PDF), such as a normal distribution, to each variable and combine those PDFs to arrive at a PDF of the final parameter of interest. However, when evaluating functions more complex than arithmetic combinations (such as the geometric relationship between N_{CalMod} and N), there is no analytical solution to the combination of the normal distribution of N and the energy correction. Hence the above solution uses Monte Carlo simulations to achieve the result. However, if the distributions can be made log-normal, then the normal variables can be summed together, and an analytical solution can be achieved.

To accomplish this, the N_{CalMod} values at the site would need to be condensed to a single log-normal distribution. This is not compatible with the dataset because N_{CalMod} is dependent on the effective stress at the depth of the sample. Therefore, N_{CalMod} needs to be corrected for the stress effects before beginning the process. The N_{CalMod} data from the site is shown as a histogram and a fitted normal and log-normal distribution are plotted on top of it in Fig. 7. The sampling is not frequent enough to robustly determine a PDF, but either the normal or log-normal distribution looks like it may be appropriate. Therefore, the analysis proceeds with the log-normal distribution because it allows for the analytical solution.

 © Deep Foundations Institute 2025

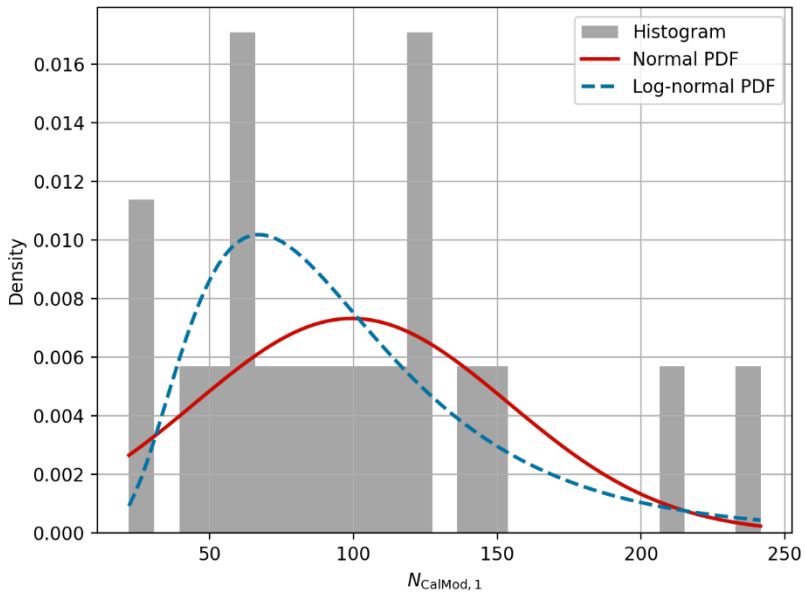


Fig. 6. Distribution of California Modified Sampler Blow Counts

The conversion factor from CalMod to SPT blow counts is based on a log-normal distribution, with its mean and standard deviation are used to define the parameters of the underlying normal distribution. Specifically, N/N_{CalMod} is characterized by a mean ($\mu_{N/NCalMod}$) of 0.65 and a standard deviation ($\sigma_{N/NCalMod}$) of 0.25, with a constraint that values must be at least 0.1 to ensure physical relevance. The log-normal parameters ($\mu_{\ln N/NCalMod}$) and ($\sigma_{\ln N/NCalMod}$) are computed as follows:

$$\sigma^2_{\ln \frac{N}{N_{CalMod}}} = \ln\left(1 + \frac{\sigma_{N/N_{CalMod}}{}^2}{\mu_{N/N_{CalMod}}{}^2}\right) \quad (2)$$

$$\mu_{\ln N/N_{CalMod}} = \ln\left(\mu_{N/N_{CalMod}}\right) - \frac{\sigma^2_{\ln \frac{N}{N_{CalMod}}}}{2} \quad (3)$$

The resulting PDF is truncated at 0.1 by normalizing by the complementary cumulative distribution function (CDF), (1 - CDF (0.1)), to enforce the minimum value constraint. Similarly, the energy correction factor, with a mean of 77.5% and a standard deviation of 17.5%, is modeled as log-normal, constrained to the range [0.1, 105] and normalized accordingly.

The combination of ($N_{CalMod,1}$) and N/N_{CalMod} yields the SPT blow count, $N_1 = N_{CalMod,1} * N/N_{CalMod}$. Since $N_{CalMod,1}$ and N/N_{CalMod} are log-normal, their product is also log-normal, with parameters derived from the sum of the logarithms' variances:

$$\sigma^2_{\ln N_1} = \sigma^2_{\ln N_{CalMod,1}} + \sigma^2_{\ln \frac{N}{N_{CalMod}}} \quad (4)$$

and mean adjusted for the product of the individual means. Subsequently, the energy-corrected blow count, $(N_1)_{60} = N_1 * Energy/60$, is computed. The log-normal nature of N_1 and energy ensures that $(N_1)_{60}$ is log-normal. The final parameter, the friction angle (φ'), is calculated using the (Kulhawy and Chen 2007) relationship (Equation 1). The PDF of (φ') is approximated by numerically integrating the joint distribution of the normal variables *a* and *b* and the log-normal $(N_1)_{60}$, accounting for the nonlinear

 © Deep Foundations Institute 2025

transformation induced by the logarithmic function. Each step preserves the analytical propagation of uncertainties, with the PDFs visualized in Fig. 8 to illustrate the evolution from input parameters to the final friction angle. This distribution is almost identical to the distribution achieved by the Monte Carlo simulations.

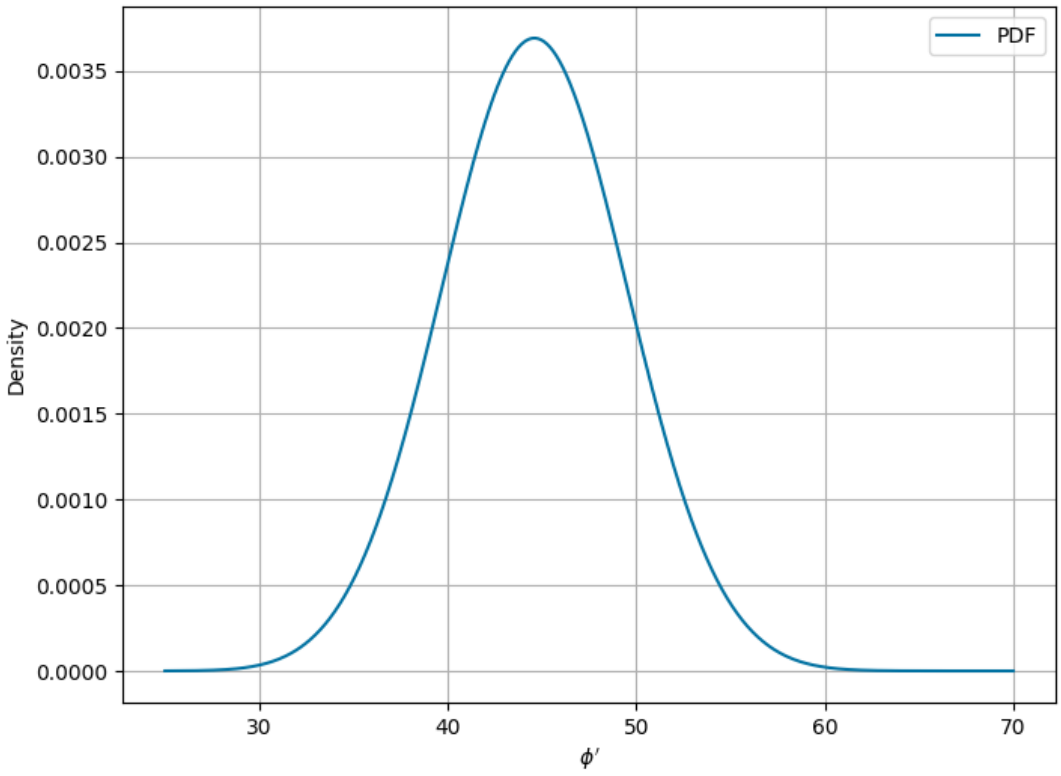


Fig. 7. Distribution of Friction Angle computed using analytical solutions

CONCLUSIONS

When evaluating seismic performance of existing structures, it is important to provide mean and variation estimates in parameters such as stiffness or strength. Underestimation of soil strength may not be "conservative" because softer soil-foundation springs might result in lower seismic demands on the structure. Therefore, more robust methods for evaluating best estimate and variability should be employed, such as the Monte Carlo technique, especially when using protocols such as ASCE 41 methodologies that explicitly require an estimate of C_v. Once the soil parameter mean and variability are obtained, design parameters such as bearing capacity, passive pressure, and foundation traction can be derived. Underestimates of design parameters such as bearing capacity can result in underestimates of seismic forces that are transferred during seismic excitation into the structure from the underlying soil.

REFERENCES

ASCE (American Society of Civil Engineers) (2017a). *Seismic Evaluation and Retrofit of Existing Buildings: ASCE/SEI 41-17*. Reston, VA: American Society of Civil Engineers.

 © Deep Foundations Institute 2025

ASCE (2017b). *Minimum Design Loads and Associated Criteria for Buildings and Other Structures: ASCE/SEI 7-16*. Reston, VA: American Society of Civil Engineers.

Carpio, M. D., L. Toranzo, and M. Hershberg (2021). "Performance Based Seismic Retrofit of an Older Non-Ductile Reinforced Concrete Building per ASCE 41-13 using Component Testing and Viscous Fluid Dampers." *Procedeedings Struct. Eng. Assoc. Calif. Annu. Conv.*

ICBO (International Conference of Building Officials) (1964). "Uniform Building Code, 1964 Edition."

Kulhawy, F. H., and J.-R. Chen (2007). "Discussion of 'Drilled Shaft Side Friction in Gravelly Soils' by Kyle M. Rollins, Robert J. Clayton, Rodney C. Mikesell, and Bradford C. Blaise." *J. Geotech. Geoenvironmental Eng.*, 133 (10): 1325–1328. American Society of Civil Engineers. https://doi.org/10.1061/(ASCE)1090-0241(2007)133:10(1325).

Metropolis, N., and S. Ulam (1949). "The Monte Carlo Method." *J. Am. Stat. Assoc.*, 44 (247): 335–341. https://doi.org/10.1080/01621459.1949.10483310.

UC (University of California) (2024). *Seismic Safety Policy*. 11. University of California.

 © Deep Foundations Institute 2025

FOUNDATION SYSTEMS FOR STORAGE TANKS IN HYDROCARBON COMPLEXES: CRITICAL CONSIDERATIONS AND CASE STUDIES

Sampat Raj, Engineers India Limited, New Delhi, India, 9560468440, sampat.raj@eil.co.in
Mriganabh Choudhury, Engineers India Limited, New Delhi, India, mriganabh.choudhury@eil.co.in
Sanjoy Bhowmik, Engineers India Limited, New Delhi, India, sanjoy.bhowmik@eil.co.in
VK Panwar, Engineers India Limited, New Delhi, India, vk.panwar@eil.co.in

ABSTRACT

Tanks are essential facilities in hydrocarbon complexes, used for storing various hydrocarbon products. These flexible structures can tolerate considerable settlement during loading without compromising performance. However, the higher allowable settlement often leads designers to overlook the need for detailed subsoil investigations and underestimate the importance of selecting an appropriate foundation system. This oversight can jeopardize the structural integrity and performance of tanks. This paper discusses various foundation types commonly used for tanks in refineries and petrochemical plants, along with selection criteria and critical considerations to equip engineers with the knowledge to make informed decisions during the design stage. Additionally, the paper presents case studies of seven floating roof tanks, with diameters ranging from 35 to 92 meters (115 to 302 ft) and heights from 14.8 to 20 meters (48.6 to 65.6 ft). The subsoil at the project sites predominantly consisted of fill overlying rock, organic soil underlain by medium to stiff clay, and silty sand followed by medium to stiff clay. These case studies illustrate the application of different foundation systems, including sand pads, pile foundations, and sand pads supported by improved ground using dynamic compaction and stone columns. The case studies highlight the critical appraisal of geological conditions and subsoil characteristics for selecting a techno-economic foundation system, along with design approaches, ground improvement techniques, and their associated limitations. Hydrotest results and performance analyses, including uniform settlement, planar tilt, and out-of-plane settlement, show that the observed settlements were within permissible limits. These results substantiate the effectiveness and continued relevance of ground improvement techniques, offering valuable insights into their application for tank foundations in challenging soil conditions.

Keywords: tank foundations, refineries and petrochemical plants, permissible settlement, ground improvement, sand pad foundations

1. INTRODUCTION

Oil refineries and petrochemical complexes play a vital role in the petroleum industry, converting crude oil into various useful end products. These sprawling industrial complexes comprise various oil processing units, storage tanks, and auxiliary facilities catering to essential requirements such as water, power, air, etc., for the operation of the plant. Among these, storage tanks are critical facilities used to store crude oil, petroleum intermediates, and end products. In oil processing refinery complexes, most of the area is occupied by these storage facilities.

Tanks in refineries and petrochemical plants are usually classified based on the type of roof—fixed roof or floating roof, determined by the flash point of the substance being stored. A fixed roof tank has a permanent, non-moving roof attached to the tank shell, while a floating roof tank has a roof that travels up and down along with the liquid level to trap vapor from low flash point fuels. The type of tank roof has a direct impact on the design and criticality of the foundation system, as different roof types impose varying structural and operational demands.

Typically, a storage tank consists of a cylindrical shell, bottom plates, connection of the shell to the bottom plates, and a roof, made of thin steel plates. For efficient tank performance, the structural integrity

 © Deep Foundations Institute 2025

of all these components is essential. Any distress induced in these components due to excessive total or differential settlement of the foundation may impair its integrity. Sometimes, such stresses create ovality in the tank shell, which may hamper the functioning of the floating roof. To avert such issues, thorough information about the geological formation and its engineering properties is imperative to ensure the adoption of a reliable foundation system. A guideline outlining the types of field tests and their quantities for assessing subsoil information necessary for tank foundation design is proposed by Raj et al. (2024). The foundation system should be selected based on a critical appraisal of the strength and deformation characteristics of the subsoil and the geo-hazard (if any) based on geographical location.

Differential settlement between two successive points along the tank's periphery plays a key role in selecting a suitable foundation type. According to the U.S. Army Corps of Engineers (1990), the limiting angular distortion for circular steel tanks on flexible bases is 1/125 for fixed-roof tanks and 1/300 to 1/500 for floating-roof tanks. However, in the hydrocarbon industry, due to the critical nature of stored substances, more conservative limits are typically adopted: 1/500 for floating-roof tanks and 1/300 for fixed-roof tanks (Bhandari et al., 1998). During the design stage, such settlement cannot be reliably determined, and the selection of foundation for tanks is generally carried out as per the estimated total settlement at the tank periphery. As per the industrial practice, the allowable total settlement at the tank periphery for tanks resting on the sand pad is 150 mm (5.9 in.) for floating roof tanks and 300 mm (11.8 in.) for fixed roof tanks. If the estimated settlement exceeds this limit, ground improvement becomes imperative to restrict the settlement within the permissible limits (Guber, 1974). Sometimes, the subsoil is so weak that even after the ground improvement, the estimated settlement exceeds the allowable limit, or the organic/peaty soil exists up to a substantial depth, which may cause large differential settlement, making ground improvement impractical. In such cases, pile foundations are adopted.

The selection of a foundation system for tanks in the hydrocarbon industry (i.e., flexible base or rigid raft) is generally based on factors such as tank size, the type of stored substances, and space availability. However, the integrity of the foundation system is ensured through appropriate ground improvement techniques or the use of piles, depending on the subsoil conditions. The choice of a suitable ground improvement method or pile-raft system depends on various factors, including geological formations, geotechnical properties, groundwater table conditions, cost, time constraints, and the availability of equipment and materials. However, limited information is available on the influence of these parameters in selecting foundation systems for tanks. This paper aims to address this gap by providing insights into the critical considerations for foundation system selection. Additionally, the effect of various factors is illustrated through two case studies. Case study 1 includes the use of pile foundations and ground improvement techniques such as stone columns and dynamic compaction. Field investigations like initial stone column load tests and confirmatory tests (e.g., post-treatment standard penetration tests) are discussed. Case study 2 presents the application of the soil replacement method for shallow-depth ground improvement. The performance of the tanks constructed on improved ground and pile foundations is evaluated based on hydrotest results.

2. TANK FOUNDATION TYPES AND ENGINEERING CONSIDERATIONS

Tank is a classic example of soil-structure interaction, where the structural response is closely linked to the performance of its foundation. The tank is made up of steel plates, which can tolerate significant settlement owing to their flexibility. However, this tolerance may sometimes lead designers to undervalue the importance of proper foundation design, potentially compromising the tank's performance. To avoid such issues, all geotechnical aspects must be carefully considered during the design stage, and the most suitable foundation system should be selected accordingly. This section discusses various tank foundation types and critical parameters to consider during their selection.

Tanks are typically supported on sand pad foundations, which consist of a mound of well-graded, clean sand or other suitable granular material placed over competent subsoil. These materials should be laid in approximately 150 mm (5.9 in.) thick layers and compacted thoroughly in accordance with industry standards. The outer sides of the sand pad should be covered with impermeable materials, preferably plain cement concrete (PCC), to protect it from erosion and prevent moisture ingress. The height of the sand pad is determined based on functional requirements, with a minimum height of 0.3 m (approximately 1 ft) as per API 650 (2020) to ensure proper drainage. In the hydrocarbon industry, the governing criterion for determining the height of the sand pad is the availability of an adequate Net Positive Suction Head (NPSH) to allow connected pumps to operate effectively and prevent cavitation.

The finished surface of the sand pad is usually elevated at the tank's center, sloping at one inch per ten-feet radius (API 650, 2020), extending from the tank center to the periphery. The purpose of it is to collect the impurities in oil near the shell of the tank. To maintain this slope post hydro-testing or during operation, the estimated settlements at both the tank center and periphery must be added to the initial sand pad levels.

For the sand pad foundations, the bottom plates of the tank rest directly on the pad. As these bottom plates are made of steel and susceptible to corrosion, it is imperative to provide an anticorrosive layer at the top of the pad. This layer serves as a protective barrier against corrosive elements, thereby prolonging the lifespan of the tank structure. The clean sand, cement-sand mixture (1:33), or other suitable materials can be used as an anti-corrosive layer. Additionally, the provision of a cathodic protection system as an additional safeguard against corrosion may be considered.

For optimum performance of the tank resting on a sand pad, the subgrade must have a uniform soil profile and properties. Sometimes, due to topographical conditions, the subgrade has part cut and part fill, which may induce differential settlement to the tank. For such conditions, a careful evaluation of the soil properties in both cut and fill areas shall be carried out, and suitable precautions shall be adopted. Bhandari et al. (1998) recommend replacing the entire soil in the fill portion with a suitable granular material having properties similar to the soil in the cut portion.

Large tanks with heavy shells and roofs impose substantial loads on the sand pad beneath the shell. As the tank shell is connected with flexible bottom plates, edge cutting may occur if the sand pad does not have adequate strength along the periphery. The edge cutting may cause an abrupt deflection of tank bottom plates from their original position, and in extreme cases, the welded connection between the tank shell and bottom plates may break. To prevent this, crushed stone or a concrete ring wall should be provided below the tank shell. The ring wall provides better distribution of the concentrated load of the shell, ensuring more uniform loading beneath the tank. The ring wall also serves functional purposes, such as anchoring needed to counter the uplift forces exerted due to wind, seismic activity, and stored substances. In cases where space constraints make a sand pad infeasible, ring wall foundations are utilized instead. The design of the ring wall should be carried out for the hoop stresses exerted by the soil filled in between and the stored product. It should be ensured that the base of the ring wall rests on competent strata with uniform properties along the periphery to prevent significant differential settlement.

A major drawback of ring wall footing is its inherent rigidity, which can induce stresses in the event of differential settlement. To mitigate this issue, a layer of asphalt with a minimum thickness of 150 mm (5.9 in.) should be laid on top of the ring wall. This layer allows the asphalt to follow the deformed profile in the event of differential settlement and ensures the uniform contact of the tank bottom to the ring wall. The minimum thickness of the ring wall should be 300 mm (11.8 in.), and the depth should be 0.6 m (approximately 2 ft) below the lowest grade level.

The subsoil beneath the sand pad or sand pad with a ring wall must be competent to bear the imposed load due to the self-weight of the tank, the stored substance, and the weight of the sand pad or sand pad with a

 © Deep Foundations Institute 2025

ring wall. The estimated settlement corresponding to this load must be within the permissible limits. When the bearing capacity of the soil is inadequate or the estimated settlement exceeds the permissible settlement limits, the subsoil should be improved using suitable ground improvement methods. Various ground improvement techniques, such as soil replacement, vibro-replacement (stone column), vibro-displacement, dynamic compaction, preloading with prefabricated vertical drains (PVD), etc., are widely used beneath storage tank foundations. The selection of appropriate ground improvement techniques depends on various factors, such as the tank's sizes and imposed loading, the type and depth of soil within the influence zone, the depth of the groundwater table, the availability of equipment/construction materials, time, cost, depth of treatment etc. The specific ground improvement methods used for some tank foundations are outlined in the case studies presented in the subsequent section.

When poor subsoil extends to substantial depths and ground improvement is not feasible, a pile foundation with a pile cap should be adopted. Pile cap is typically constructed using reinforced cement concrete, which makes the overall foundation system very costly. Alternative materials such as crushed stones and granular soil, along with high-strength geosynthetic materials like geogrid or geocell filled with granular materials, can also be explored to construct pile caps and make them economical. However, it must be ensured that the load is transferred to the piles without creating any undulations on the top surface during loading.

3. CASE STUDY-1

This case study presents the types of foundation systems adopted for tanks located in different geological conditions. The importance of the detailed geotechnical investigation, correct appraisal of subsoil data, geotechnical considerations while selecting the foundation system, design aspects, and performance evaluation are discussed.

3.1 General details

A mega refinery cum petrochemical complex has recently been constructed in the Southwest part of Nigeria. The site is situated along the shoreline of the Atlantic Ocean, and most of the plant area is surrounded by lagoons. Previously, the plant site area was covered by densely forested water mangroves as shown in Fig. 1, which were removed during site grading to construct the plant. The original ground levels varied from RL 0.5 m to RL 4.5 m (1.6 to 14.8 ft), and most of the area was low-lying. Areas having RL 0.5 m to RL 1.5 m (1.6 to 4.9 ft) were mostly waterlogged and swampy. Since the substantial area was low-lying, a huge earth-filling was carried out to achieve the finished grade level of RL 3.0 m (9.8 ft). The filling was carried out by dredged sea sand extracted from the Atlantic Ocean.



Fig. 1. Site conditions before dredging work

This plant consists of several storage tanks with diameters ranging from 20 m to 92 m (66 to 302 ft) and heights varying from 10 m to 20 m (33 to 66 ft). For the present case study, three tanks T-1, T-2, and T-3 are considered. The details of these tanks are shown in Table 1.

 © Deep Foundations Institute 2025

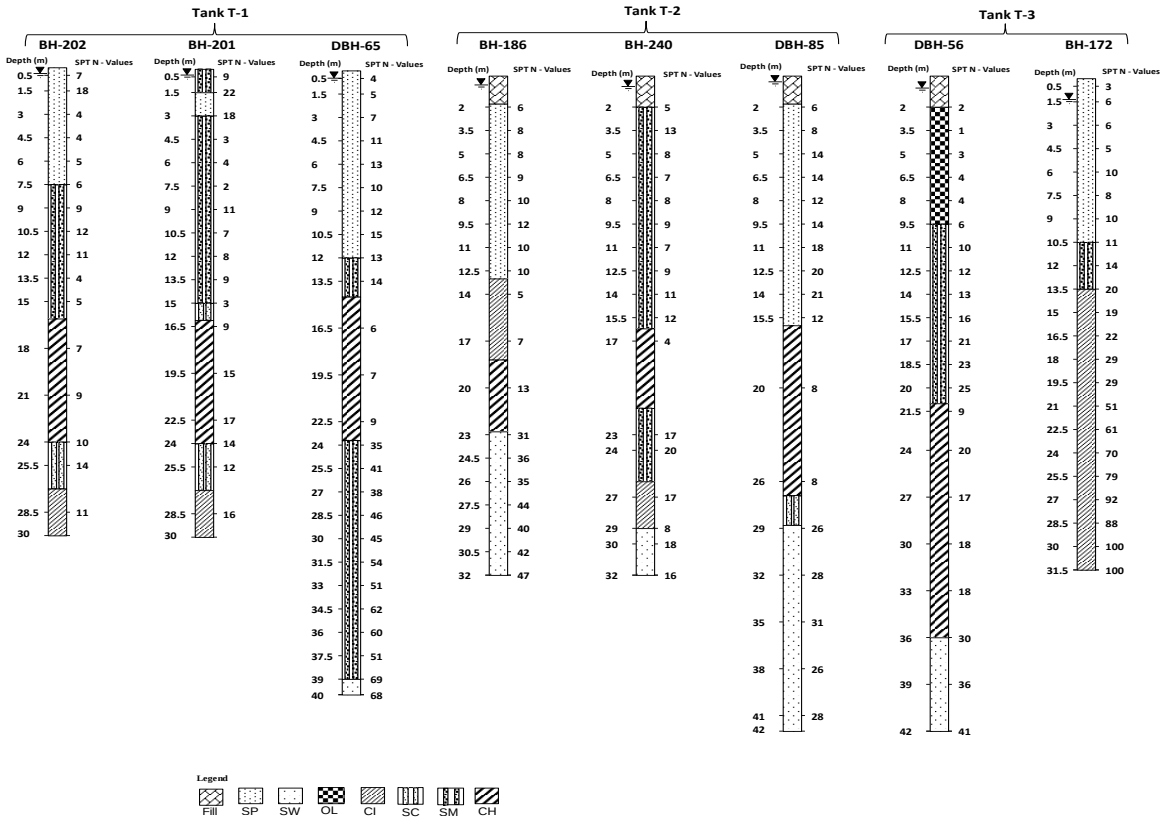
Table 1. Tank details

Tank No.	Diameter of Tank (m)	Height of Tank (m)	Roof Type
T-1	92	20	Floating roof
T-2	57	14.8	Floating roof
T-3	47.9	18.6	Floating roof

3.2 Stratigraphy of soil

A detailed subsoil investigation, consisting of boreholes and laboratory testing, was conducted to characterize the subsoil and determine the engineering properties of soil layers. The subsoil profiles of the tanks, depicted in Fig. 2, indicate that at T-1 and T-2 locations, the top layer consists of loose to medium-dense silty sand/sand, with a thickness varying from 13 m to 16.50 m (43 to 54 ft) below the existing ground level. The subsequent strata comprise medium to stiff clay, with SPT N values ranging from 4 to 17, and the extent of this layer varies from 22 m to 29 m (72 to 95 ft) below the existing ground level. This layer is underlaid by medium-dense to very dense silty sand/sand extending up to the termination depth of the borehole. Additionally, at a few locations, an intermediate layer of stiff clay was also encountered.

At the T-3 location, some parts of the area were low-lying, with ground levels varying from RL 1.0 m to 3 m (3.3 to 9.8 ft). During site grading, a maximum filling of about 2 m (6.6 ft) was carried out. The soil profile revealed that the topsoil is fill in some portions of the tank location, followed by loose to medium dense silty sand up to a depth of 13.50 m to 21.50 m (44 to 71 ft) below existing ground levels. However, in some parts of the tank area, especially in low-lying areas, organic soil was encountered, with a thickness of 7.50 m (24.6 ft). Subsequent strata consist of stiff to hard clay up to a depth of 36.0 m (118 ft), followed by dense to very dense sand extending up to the termination depth of the borehole.



 © Deep Foundations Institute 2025

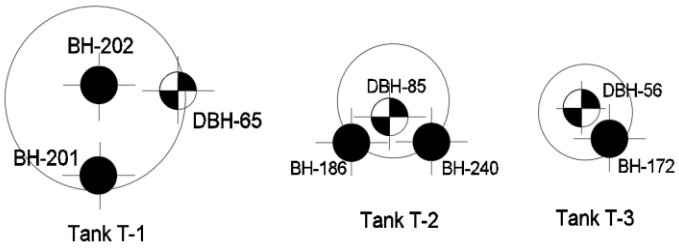


Fig. 2. Soil profile and boreholes locations

3.3 Selection Criteria for Foundations

These tanks were proposed to be constructed on a sand pad foundation; however, the subsoil beneath the sand pad was not competent to support the superstructure load. A detailed settlement analysis was carried out for all the tanks using the commercially available software Geo5. The analysis was performed using the Oedometric modulus method and the coefficient of restriction of the influence zone was 15% of the stresses. The estimated settlements are shown in Table 2. The estimated settlement was more than the specified permissible limits, i.e., 300 mm (11.8 in.) at the tank center and 150 mm (5.9 in.) at the tank peripheral area. Therefore, it was imperative to improve the subsoil by suitable ground improvement methods. Various ground improvement methods were explored, and taking due cognizance of subsoil, techno-economic considerations, and availability of equipment, it was decided to use vibro-stone columns and dynamic compaction methods.

Dynamic compaction and stone column are widely used ground improvement techniques for large-area stabilization that densify the subsoil beneath the tank, thus improving the bearing capacity of soil and decreasing the total and differential settlements under applied loading. Dynamic compaction is a ground improvement method in which heavy weight is repeatedly dropped on the ground surface from a height ranging from a few meters to tens of meters. The degree of improvement depends upon the type of subsoil, groundwater conditions, hammer weight, the height of fall, and no. of repetition. This method is suitable mainly for granular subsoil having low fine contents (IS 13094, 2021; Lukas 1995), and ground improvement up to about 30 m (98 ft) depth can be achieved (IS 13094, 2021).

Ground improvement using vibro stone columns is a method in which stone aggregates are poured into the ground using vibrating tools to form a vertical column. Besides, densifying the subsoil, stone columns also act as a vertical drain, assist in dissipating excess pore water pressure in the event of an earthquake and mitigating liquefaction susceptibility. This method is suitable mainly for soft clays and alluvial deposits (IS 13094, 2021).

Table 2. Estimated settlement at tank center and at periphery corresponding to hydrotest loading for the unimproved ground

Tank No.	Estimated Settlement		Remarks
	at tank center (mm)	at tank periphery (mm)	
T-1	430	235	
T-2	332	182	
T-3	232	127	The area where organic soil did not exist.
	1677	922	The area where organic soil existed. Secondary consolidation settlement is not considered.

 © Deep Foundations Institute 2025

Tank T-1 has a very large diameter and height, which imposes a substantial load on the ground surface. The depth of the influence zone was also significant, resulting in a larger settlement. The existence of cohesive soil strata mainly contributed to this settlement. Therefore, improving the subsoil up to the bottom of this stratum was imperative. Considering the greater depth required for ground improvement in cohesive soils, stone columns were adopted.

For tank T-2, the estimated settlement slightly exceeded the permissible settlement limits. Therefore, ground improvement up to a shallower depth was deemed adequate to keep the estimated settlement within permissible limits. Considering the presence of granular soil, specifically sand/silty sand, ground improvement using dynamic compaction was chosen. The main advantage of dynamic compaction over stone columns is that it is a sustainable solution requiring small quantity of foreign materials, is economical, and takes less time to execute.

For tank T-3, the subsoil beneath the tank footprint area exhibited high variability, with organic materials encountered on one side of the tank, which would settle excessively. Moreover, under loading conditions, these organic materials were prone to lateral movement, leading to significant total and differential settlements, thereby compromising their performance. To assess the viability of ground improvement under such challenging soil conditions, an initial group stone column load test was conducted near the tank foot print area. The spacing and depth of the test columns were kept at 1.60 m (5.25 ft) and 25 m (82 ft), respectively. The applied pressure-settlement behavior of the initial stone column group test is presented in Fig. 3, which shows that settlement was higher than the settlement criteria (25-30 mm [0.98–1.18 in.] at design load for three column group test) stipulated by IS 15284 Part 1 (2003). Moreover, the settlement did not stabilize with time, indicating the ineffectiveness of this method in organic soil with substantial thickness.

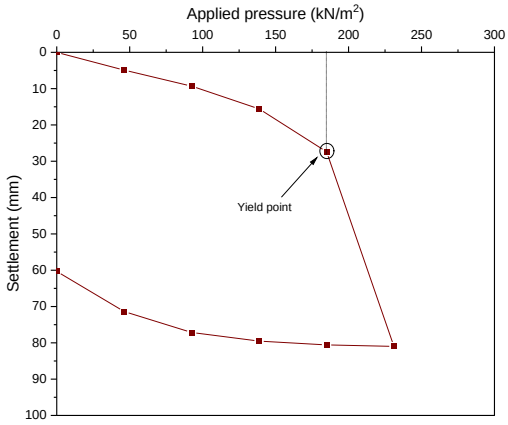


Fig. 3. Pressure-Settlement curve for stone column group test

The option of replacing these unserviceable materials with structural fill was also explored; however, considering the large size of the tank, significant depth of replacement, and the presence of groundwater at a shallower depth, this method was not considered suitable. Consequently, a pile foundation system was chosen for this tank.

The different foundation systems adopted for the tanks within a site indicate that selecting an appropriate foundation system depends on a correct appraisal of the subsoil conditions, its engineering properties, the suitability of ground improvement methods for the prevailing subsoil types, acceptance limits, and the availability of time and cost.

 © Deep Foundations Institute 2025

3.4 Design Approach for Ground Improvement using Stone Columns at T-1 Location

The degree of improvement relies on various factors such as column spacing, subsoil parameters, column diameter, etc. The length and spacing of stone columns were carefully determined to achieve optimal densification, with the primary objective of limiting settlement within acceptable limits. The length of the stone columns was 25 m (82 ft), and the spacing was 2.20 m (7.2 ft) inside the tank shell and 1.80 m (5.9 ft) along the tank periphery. The diameter of the stone columns was 900 mm (35.4 in.) with a triangular grid pattern to yield the densest packing (IS 15284 Part 1, 2003; Mohapatra et al. 2017). The spacing along the tank shell was reduced to cater to the additional stresses induced by the weight of the tank shell. The area replacement ratio, representing the quantity of soil replaced by stones, was 15.17% inside the tank periphery. The layout of stone columns, illustrating their arrangement both inside the tank periphery and along the tank periphery, is depicted in Fig. 4.

The degree of improvement post-installation was estimated using the procedure suggested by Priebe (1995). Post-ground treatment, the estimated settlements at the tank center and periphery were about 250 mm (9.8 in.) and 138 mm (5.4 in.), respectively. The settlement was within the specified settlement limits (i.e., 150 mm [5.9 in.] at the edge of floating roof tank).

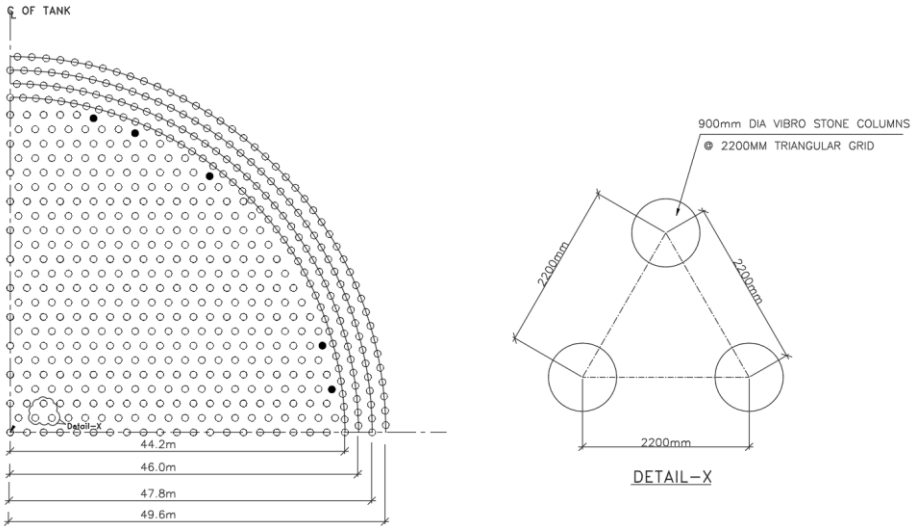


Fig. 4. Stone column layout

3.5 Design Approach for Ground Improvement using Dynamic Compaction at T-2 Location

Dynamic compaction at the tank location T-2 was carried out in two stages, i.e., point tamping and full tamping. For the point tamping, the entire area was divided into grids at a spacing of 8 m (26.2 feet) on both sides. The hammer weight was 475 kN (106,784 lbf), and the height of the fall was 16.85 m (55.3 ft). The total energy per blow at the ground surface was 8004 kNm (5.9 million ft-lbf), and the minimum no. of strikes were eight. The set criteria for each tamping location were decided as a maximum 200 mm (7.87 in.) average settlement of the last two strikes. Initially, primary tamping was performed across the entire area, followed by secondary tamping at intermediate locations. During tamping, a cumulative depression ranging from 198 to 300 cm (6.5 to 9.8 ft) occurred, which was subsequently filled with sand and rammed suitably. Post first stage tamping; the entire area was compacted using full tamping methods for which falling energy at the surface was 4000 kNm (2.95 million ft-lbf). The layout of dynamic compaction is illustrated in Fig. 5.

 © Deep Foundations Institute 2025

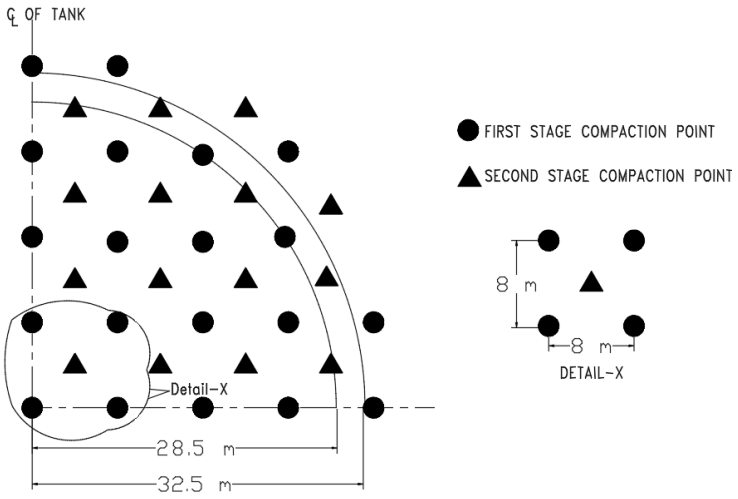


Fig. 5. Layout of dynamic compaction scheme

Post dynamic compaction, performance testing was carried out by conducting standard penetration tests to assess degree of improvement of the subsoil. The depth of the boreholes was decided based on the estimated depth of compaction, i.e., 12 m (39.4 ft). A total of six boreholes were executed at various locations beneath the footprint area of the tank. The improvement in field SPT N values post dynamic compaction is shown in Fig. 6, which indicates that substantial improvement in the ground resistance was observed. The maximum improvement occurred at shallower depths and the degree of improvement decreased with depth. The results indicate that for depth up to 7 m (23 ft) below the ground surface, an improvement factor of 3-6 in the SPT N values post improvement was observed as compared to the unimproved ground. At depth beyond 7 m (23 ft), improvement factor of 1.5 was observed. The ground improvement up to 10-12 m (32.8–39.4 ft) depths was achieved. Based on the depth of improvement as shown in Fig. 6, the empirical coefficient (n) was back calculated by using equation 1. The calculated range of n value was 0.37-0.45, which can be used for the saturated non plastic silty sand. The improvement in ground resistance substantiates the efficacy of the dynamic compaction in the silty sand.

$$D = n(WH)^{0.5} \quad [1]$$

Where D = depth of improvement, W = weight of hammer, H = height of fall, and n = empirical coefficient.

Based on the improved soil parameters, settlement analysis was reperformed, and total settlement at the tank center and the edge was estimated as 194 mm (7.6 in.) and 107 mm (4.2 in.), respectively. The estimated settlement post-ground improvement was within the specified settlement limits.

 © Deep Foundations Institute 2025

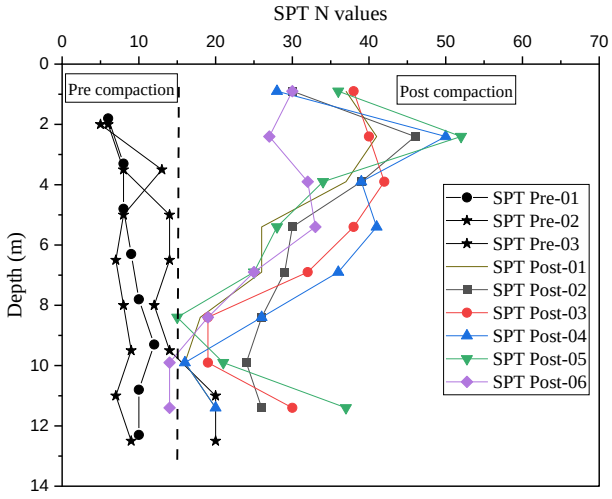


Fig. 6. SPT N values pre and post ground improvement

3.6 Design Approach for Pile Foundation at T-3 Location

Due to the presence of organic soil extending to significant depths, ranging from 2.5 to 9 m (8.2 to 29.5 ft) below the grade level in some portions of the tank location, and considering the findings of the initial stone column load test as shown in Fig. 3, the tank T-3 was constructed on a pile foundation. Driven cast-in-situ RCC piles, each with a diameter of 500 mm (19.7 in.) and approximately 22 m (72.2 ft) in length, were installed using a vibratory pile driving hammer. These piles were terminated in a competent soil stratum, and the termination of each pile was established according to the specified pile termination criteria. A concrete pile cap with a ring beam was constructed above these piles. The tank was subsequently constructed on this foundation system.

3.7 Hydro-test Results and Performance Analysis

A hydro-test is the ultimate check for any tank to check the leak proofness, determine its behavior during loading, and validate the design considerations. All three tanks were subjected to hydro-testing up to a specified height using water. Hydro-testing was carried out in four stages, i.e., 25%, 50%, 75 and 100 % water filling, and the rate of filling and retention of water at each stage were held as per the hydro-test procedure. The settlement measuring points were D/10, where D is the diameter of the tank in feet, and marked along the tank periphery to monitor the settlement at each stage of loading (API 650, 2020). The measured settlements along the tank periphery at 100% loading for tanks T-1, T-2 and T-3 are shown in Fig. 7, showing maximum total settlement of 89 mm (3.5 in.), 39 mm (1.5 in.) and 18 mm (0.7 in.), respectively. The maximum differential settlements were 1 in 1204, 1 in 710, and 1 in 557 for T-1, T-2 and T-3, respectively. The observed total and differential settlements between consecutive peripheral points were meeting the specified settlement criteria, i.e., maximum total settlement of 150 mm (5.9 in.) and differential settlement of 1 in 300 to 1 in 500 along the tank periphery.

The performance analysis of the tank T-1 based on the hydrotest results was also carried out as per the provisions of API 653 (2014). The investigation focused on planar tilt and out-of-plane settlement, which are critical factors affecting the tank's structural integrity and operational efficiency. The planar tilt is the rotation of the tank in the tilted plane. It causes an increase in the liquid level and, thereof, an increase in the hoop stress in the tank shell. Also, excessive tilting can cause the binding of peripheral seals in a floating roof and inhibit roof travel.

Planar tilt $(\delta) = (S_1\text{-}S_2)/D$ [2]

 © Deep Foundations Institute 2025

Where S_1, S_2 = settlement of two diametrically opposed points at the tank periphery, in mm, and D = tank diameter, in mm.

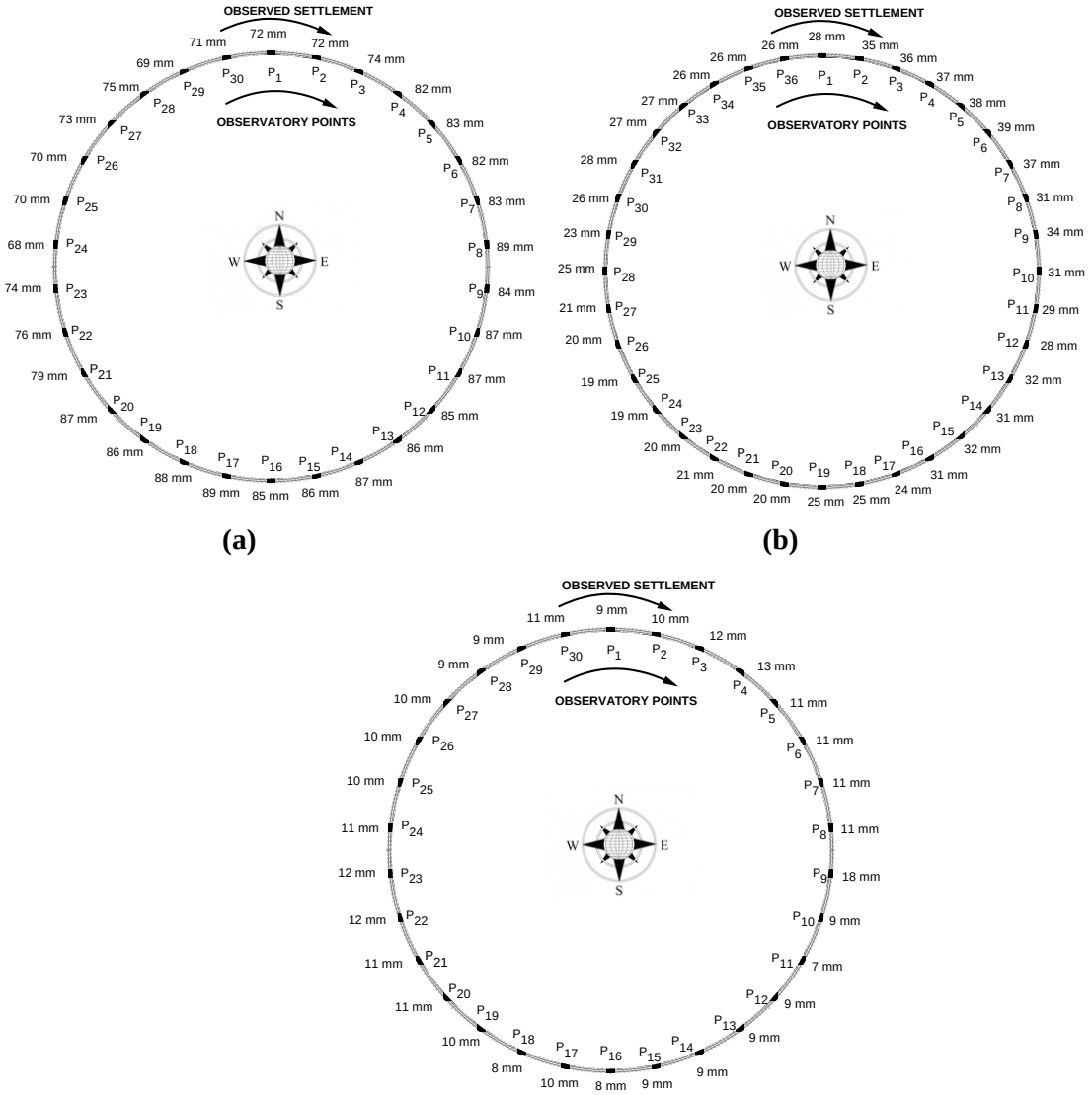


Fig. 7. Hydrotest results of: (a) T-1 (b) T-2 and (c) T-3

Greenwood (1974) has proposed acceptable limits for planar tilt in steel storage tanks as D/200, whereas, Japanese fire defence agency (1977) have proposed D/100, with D being the tank's diameter in mm. Langeveld (1971) proposed acceptable limit as 500 mm (19.7 in.) for planar tilt (δ_{max}). The maximum observed differential settlement between two diametrically opposite points that is P_8 and P_{24} was 21 mm (0.8 in.), within permissible limits.

The out-of-plane settlement is a critical component to determine and evaluate in order to ensure the structural integrity of the tank shell and bottom. The out-of-plane settlement at the bottom edge leads to a lack of circularity at the top of the tank. The out-of-plane settlement was determined by drawing the plane of rigid tilt considering the observed edge settlement. The vertical distances between the plane of rigid tilt

and the observed edge settlement are known as the out-of-plane settlement. The out-of-plane settlement curve, shown in Fig. 8, was studied, and it was found that the calculated out-of-plane maximum settlement was 7 mm (0.3 in.), safely below the permissible limit of 40 mm (1.6 in.) for floating roof tanks. The maximum estimated out of plane deflection was 5.4 mm (0.2 in.), which was also fell within the permissible limit of 32 mm (1.3 in.) calculated by the following formula (API 653, 2014).

$$\text{Maximum permissible out-of-plane deflection } |S| \leq \frac{(L^2 \times Y \times 11)}{2[(E \times H)]} \quad [3]$$

Where S = deflection, in feet (ft); L = arc length between measurement points, in feet (ft); Y = yield strength of the shell material, in pound force per square inch (lbf/in.^{2}); H = tank height, in feet (ft).

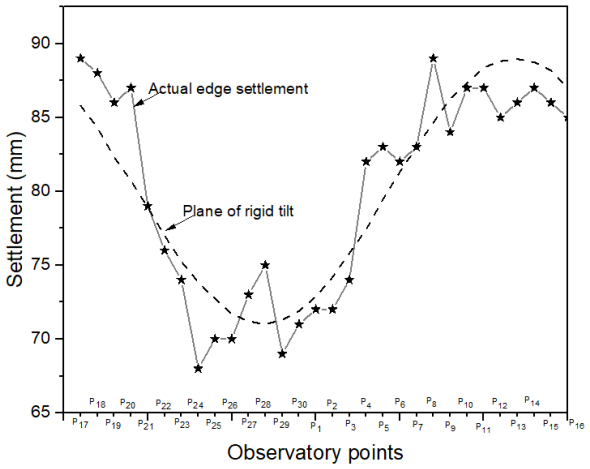


Fig. 8. Out-of-plane settlement curve

The performance analysis based on the hydrotest results show that the overall performance of the tank was found to be in order, and tanks were released for storing the end products.

4. CASE STUDY-2

4.1 General Details

Four nos. of tanks, namely 03A/B/C/D, were proposed to be constructed at one of the refinery sites in the state of Maharashtra, India. Each tank's diameter and height were 35 m (114.8 ft) and 20 m (65.6 ft), respectively. The type of roof was the floating roof. Figure 9 shows the satellite image of all these tanks. The proposed area was occupied earlier by an industrial plant, which was later dismantled, and the debris was deposited as a fill inside the plant boundary.



Fig. 9. Satellite image of tanks

 © Deep Foundations Institute 2025

4.2 Stratigraphy of Soil

A detailed soil investigation, including boreholes, and laboratory testing, was conducted to characterize the subsoil. The soil profile, as depicted in Fig. 10, revealed that the uppermost strata generally comprised filled-up soil with boulders (debris), with the thickness of this layer varying from 3 m to 8.5 m (9.8 to 27.9 ft) below the existing ground level. Subsequent layers consisted of very stiff to hard murrum, ranging from 1 m to 8 m (3.3 to 26.2 ft) thick, with SPT N values ranging from 20 to 81. This layer was underlain by basalt rock of varying weathering grades, with core recoveries ranging from 5% to 87% and RQD ranging from 0% to 87% along the depth. It extends up to the termination depth of the boreholes. The groundwater table was encountered at a depth ranging from 6.50 m to 8.0 m (21.3 to 26.2 ft) below the ground level.

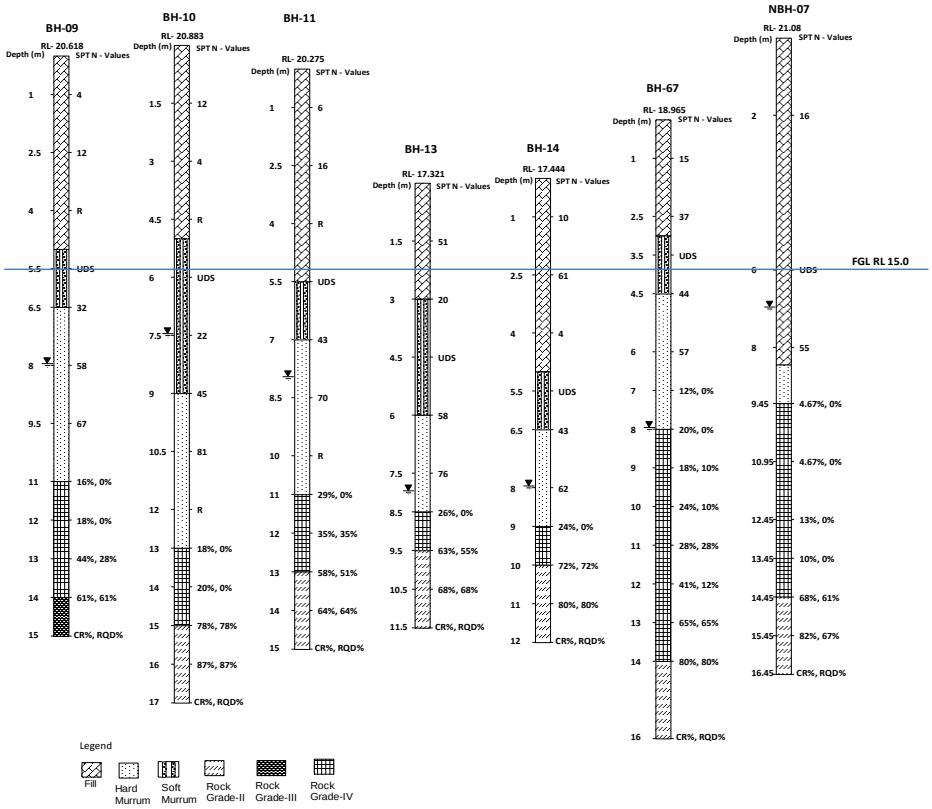


Fig. 10. Subsoil profile

4.3 Selection Criteria for Foundations

The ground levels before site grading varied from RL 16.9 m to RL 22.1 m (55.4 to 72.5 ft), whereas the finished grade level (FGL) was RL 15 m (49.2 ft). Therefore, the proposed area was cut to reach the finished grade level. Post-site grading, the maximum depth of filled-up soil was approximately 2.6 m (8.5 ft) below FGL.

The existing fill beneath the grade level was heterogeneous, and its thickness varied below the footprint area of the tank. The presence of such loosely dumped material beneath the tank could have adversely affected its performance, leading to unacceptable total and differential settlement if not addressed appropriately. This heterogeneous material required special engineering consideration, and therefore, it was removed entirely and replaced with sand gravel mix (1:1) laid in layers of 200 mm (7.9 in.) loose

 © Deep Foundations Institute 2025

thickness and compacted to 85% relative density. The bottom level of the ground improvement was kept uniform to avoid the possibility of differential settlement. The sand pad was constructed with sand conforming to zones II and III as specified in IS 383 (2016), as shown in Fig. 11. A stone ring wall was provided below the tank shell area to prevent edge settlement.

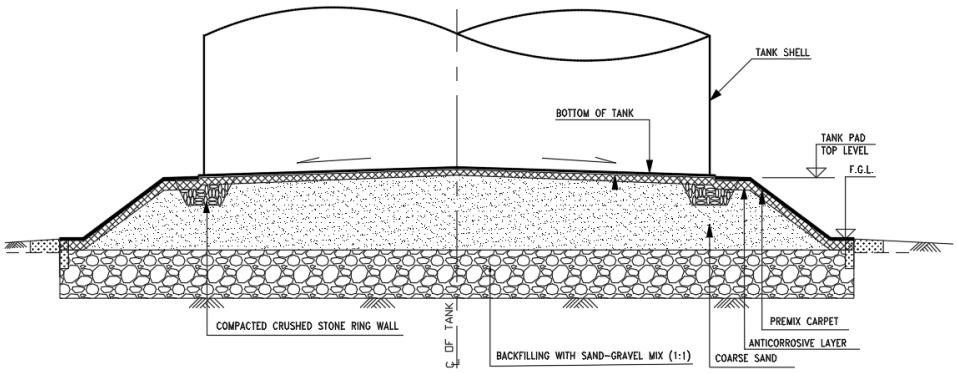


Fig. 11. Sand pad foundation over compacted fill

4.4 Hydro-test Results

Settlement post ground improvement was estimated for all tanks corresponding to hydrostatic loading of 190 kPa (27.6 psi). It varied from 41 mm to 68 mm (1.6 to 2.7 in.) at the tank center and 23 mm to 37 mm (0.9 to 1.5 in.) at the tank edge. Post-construction, these tanks were subjected to hydro-testing as per the approved procedure. Each tank was gradually filled with water in four increments, with each load maintained for 24 hours before the next increment was added. Settlement of the tanks was measured at eight equidistant peripheral points. The observed settlements for each tank are presented in Fig. 12, showing that the settlements ranged from 3 mm to 14 mm (0.12 to 0.55 in.), well within the permissible limits at the tank periphery. The observed settlement was lower than the estimated settlement because a portion of the settlement had already occurred during construction due to the overburden pressure of the sand pad and the self-weight of the tank.

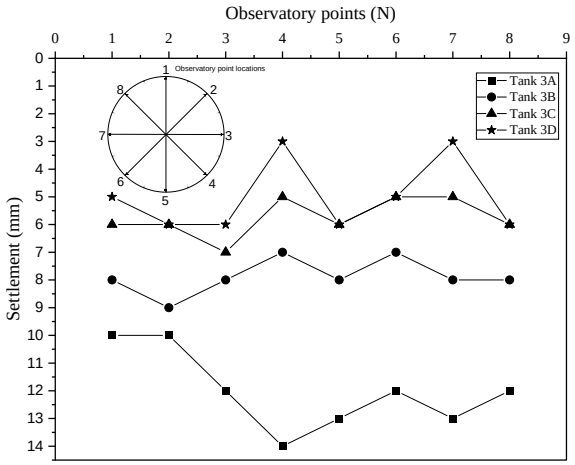


Fig. 12. Observed peripheral settlement

The case study underscores the viability of soil replacement with compacted fill beneath sand pad or ring wall foundations, particularly when treatment depth is shallow, and groundwater tables are at deeper depths. Typically, soil replacement up to 6 m (19.7 ft) below grade level proves commercially feasible.

 © Deep Foundations Institute 2025

5. CONCLUSIONS

This paper highlights the key aspects of foundation selection for storage tanks in refineries and petrochemical complexes, offering insights into various foundation types and the engineering considerations involved in determining the optimal foundation system.

The first case study demonstrates the effectiveness of dynamic compaction as a ground improvement technique for cohesionless soils with fine content below 20%. Post-treatment performance testing confirmed its suitability up to 12 m (39.4 ft) depth in saturated, non-plastic silty sand. An empirical coefficient *(n)* in the range of 0.37–0.45 was established for such soils, aiding in design validation and future applications.

Ground improvement using stone columns proved effective for cohesive soils with high fine content. The hydrotest results and the performance analysis for tank T-1 resting on the improved ground show its effectiveness for large-area improvement. However, its application in organic soils with significant thickness showed ineffectiveness, as highlighted by the initial group load test results.

The second case study emphasized the viability of soil replacement with compacted fill beneath sand pad or ring wall foundations, particularly when treatment depth is shallow, and groundwater tables are at deeper depths.

This paper provides valuable insights and practical recommendations for optimizing foundation systems in hydrocarbon complexes, offering a comprehensive guide for engineers and stakeholders involved in storage tank construction projects. By incorporating these critical considerations and leveraging case study insights, practitioners can ensure the longevity and stability of storage tank foundations, mitigating risks and enhancing operational efficiency.

ACKNOWLEDGEMENTS

The authors express their gratitude to the management of Engineers India Limited for granting permission to publish this paper.

REFERENCES

1. American Petroleum Institute (API) 650, 2020. Welded Tanks for Oil Storage. 13th Edition, American Petroleum Institute.

2. American Petroleum Institute (API) 653, 2014. Tank Inspection, Repair, Alteration, and Reconstruction. 5th Edition, American Petroleum Institute.

3. Bhandari, R.K.M., Asha, S.R., Nanda, A., and Malhotra, V.K., 1998. Foundation for large steel oil storage tanks. Indian Geotechnical Conference, New Delhi, India.

4. Greenwood, D.A., 1974. Differential settlement tolerance of cylindrical steel tanks for bulk liquid storage. Proceedings of the conference on settlement of structures, Cambridge University, British Geotechnical Society, A Halsted Press Book, John Wiley and Sons, Inc., New York, N.Y., pp. 35-97.

5. Guber, F.H., 1974. Design engineering contributions to quality tankage. I.I.W. Annual Assembly, Budapest, 99–129.

6. IS 383, 2016. Coarse and fine aggregate for concrete – specification.

 © Deep Foundations Institute 2025

7. IS 13094, 2021. Selection of ground improvement techniques for weak soils-guidelines.

8. IS 15284 (Part 1), 2003. Indian standard for design and construction for ground improvement-guide lines.

9. Langeveld, J.M., 1971. The design of large steel storage tanks for crude oil and natural gas. Proceedings of the annual meeting of the International Institute of Welding, pp. 35-95.

10. Lukas, R. G., 1995. Dynamic compaction. Report FHWA-SA-95-037. Federal Highway Administration.

11. Mohapatra, S.R., Rajagopal, K., Sharma, J.S., 2017. 3-Dimensional numerical modeling of geosynthetic-encased granular columns. Geotextiles and Geomembranes, 45, pp. 131–141. https://doi.org/10.1016/j.geotexmem.2017.01.004.

12. Priebe, H.J., 1995. The design of vibro replacement. Ground Engineering, 28(12):31–37.

13. Raj, S., Choudhury, M., Panwar, V.K., and Bhowmik S., 2024. Enhancing Tank Reliability: Performance Evaluation of Distressed Foundation Systems - A Case Study. In Proc. of the DFI-India, 13th Annual Conference.

14. Regulations for Tanks, 1977. Japanese Fire Defense Agency.

15. U.S. Army Corps of Engineers, 1990. Engineering and Design: Settlement Analysis. Engineer Manual 1110-1-1904, Washington, DC.

 © Deep Foundations Institute 2025

CASE STUDY OF SMALL-DIAMETER CFA PILES TESTED BY BIDIRECTIONAL LOAD TESTS IN TROPICAL SOIL

Yuri Barbosa, University of São Paulo, São Paulo, Brazil, +55 (19) 97118-4154, yuri.barbosa@usp.br
Alysson S. Resende, ARCOS Engineering, Belo Horizonte, Brazil, alysson@arcos.eng.br
Marianna N. Carvalho, University of São Paulo, São Paulo, Brazil, mariannacarvalho@usp.br
Nilton A. Chaves, ARCOS Engineering, Belo Horizonte, Brazil, alysson@arcos.eng.br
Paulo J. R. Albuquerque, University of Campinas, Campinas, Brazil, pjra@unicamp.br
Marcos M. Futai, University of São Paulo, São Paulo, Brazil, futai@usp.br

ABSTRACT

Bidirectional load tests are alternatives to conventional load tests that do not require a reaction system, making them highly applicable to large-diameter piles. This procedure, when performed on small-diameter piles, is still scarcely explored in the literature, especially in the context of tropical soils. The objective of this paper is to present a case study involving five continuous flight auger (CFA) piles with diameter of 0.50 m in the Federal District of Brazil, where the soil is frequently characterized as lateritic. The pile lengths ranged from 14 to 19 meters, with the expansive cell assemblies installed at distances of 2 to 4 meters from the tip. Load-displacement results for the shaft and base resistance components of each pile are presented, which—due to the significant displacements reached during testing for most of the piles—allowed the conclusion that failure occurred at small displacements, less than 10% of the diameter. Considerations were raised regarding the possible presence of loose material in one of the analyzed cases. The ultimate load results were compared with nine methods for estimating shaft, base, and total pile resistance based on the SPT, showing that most of them proved to be conservative for the present case study.

Keywords: bidirectional static load test, small-diameter piles, tropical soils, load capacity estimative

INTRODUCTION

The concept of the bidirectional load test was first introduced in the 1980s by Silva (1986), in Brazil. At the time, the author aimed to develop an execution procedure that would be economically viable and would not interfere with the construction schedule—these being the main reasons for the lack of load testing in foundation elements in the country. Another goal was to meet the demands of the civil construction sector, which was responsible for the construction of large structures that, in turn, required large reaction systems, increasing both the cost and the risks involved in conducting conventional load tests. Thus, Silva (1983; 1986) described in his work the creation of the Hydrodynamic Expanding Cell, or *expancell*. The novelty of this method lay in the installation of the expanding cells inside the pile, dividing it into two segments (upper and lower, above and below the cell assembly, respectively), which would then react against each other, thereby eliminating the need for a full reaction system composed of beams, anchors, piles, etc. Another innovative aspect was the fact that the cell was actuated by water instead of oil, making it possible to reuse the tested elements since the procedure allowed the cavity created by the device to be filled with grout at the level of the cell assembly, sealing the opening. The test only gained worldwide recognition in the 1990s, after the procedure was patented by Osterberg (1989).

 © Deep Foundations Institute 2025

By dividing the pile into two segments, the bidirectional load test has the main advantage of separating the resistance components of the pile without the use of extensometers along its length. When the expanding cell assembly is installed directly at the pile tip, a direct response of the shaft resistance (above the cell assembly) and the base resistance (below the cell assembly) is obtained. On the other hand, when the cell assembly is installed at a certain distance above the pile tip, the resistance response obtained for the segment below the installation level is the sum of the shaft resistance and the actual base resistance of the pile. The bidirectional test also allows for more than one installation level of the expanding cell assembly, providing better discretization of the pile's mechanical behavior along its depth (Niazi and Mayne 2014; Wan et al. 2018). The test procedure is conducted in the same manner as a conventional load test, with the application of loads in stages followed by displacement readings, which are made possible through the installation of tell-tales on the upper and lower plates of the cell assembly. The result of the bidirectional load test is the development of two load-displacement curves, each corresponding to one segment of the pile when there is only a single level of expanding cell assembly (the most common test scenario) (Silva 1986; Osterberg 1989). The displacement at the pile head is also feasible in the bidirectional test, and the measurement of the elastic shortening of the upper segment is given by its difference from the displacement at the top of the cell assembly. Also, more load-displacement curves are obtained in cases with multiple levels of expanding cells. In the interpretation of bidirectional load tests, it is common practice to convert the resulting curves into an equivalent curve representative of a conventional static load test. Several methodologies for this conversion are available in the literature. Among these, the traditional method proposed by Silva (1986) and Osterberg (1989) is noteworthy, as it simplifies the analysis by neglecting elastic shortening and treating the pile as a perfectly rigid element.

Installing the loading system within the pile results in its permanent loss after the test, as it is embedded in the reinforcement and concreted in place. Although recent alternatives have been proposed to overcome this issue — such as bidirectional load tests employing recoverable cells (Dai and Gong 2012) and cell assemblies installed at the pile head (Moghaddam et al. 2021) — the methodology involving subsequent disposal of the system remains the most widely used. The loss of this component is the main factor contributing to the increased cost of performing bidirectional load tests on small-diameter piles. For this reason, this type of test is generally recommended for high-capacity piles (England 2003), which limits the number of case studies available in the literature for large-diameter bored piles. However, Brazilian practice has demonstrated that bidirectional tests can be both technically and economically feasible for smaller-diameter piles, particularly in cases involving a greater number of tested elements (Resende et al. 2022). These smaller-diameter piles, unlike their large-diameter counterparts, allow for a higher degree of mobilization of individual resistance components. Typically, full mobilization occurs in only one of the two segments (in cases with a single level of cell installation), due to the inherent difficulty in predicting the ideal location of the cell assembly to ensure both segments of the pile reach failure. Accordingly, this study presents a case history involving the interpretation of five bidirectional load tests performed on continuous flight auger (CFA) piles constructed in tropical soil in Brasília, Federal District, Brazil. The local subsoil is typically characterized as lateritic, with a reddish coloration. The tested piles had diameters of 0.50 m and lengths ranging from 14 to 19 m, with the expansive cell assemblies installed 2 to 4 meters above the pile base. One of the tests exhibited a high degree of mobilization in both segments, while three others showed significant loading in only one segment, with the other exhibiting moderate mobilization. Different curve extrapolation methodologies were applied, and considerations were made regarding the failure mechanisms of this type of pile in the local soil and the effects of excavation. The suitability of various load capacity prediction methods was also evaluated based on the interpretation of the field test results.

METHODOLOGY

The present case study concerns the foundation system of a residential complex located in the Guará neighborhood of Brasília, Federal District, Brazil. Five continuous flight auger (CFA) piles with a diameter of 50 cm—designated PCE-01 through PCE-05—were subjected to bidirectional static load tests. The piles were designed for working loads of 1080 kN (PCE-01, PCE-04, and PCE-05) and 1000 kN (PCE-02 and PCE-03). The tests were conducted using a quick maintained load procedure, in accordance with the Brazilian standard NBR 6122 (ABNT 2022). Table 1 summarizes the main characteristics of the piles and the load tests performed:

Table 1. Summary of the performed bidirectional load tests

Load Test	Pile displacement measurement	Diameter (m)	Segment length (m)	Maximum load test (kN)	Maximum displacement (mm)
PCE-01	Pile head	0.50	15	1120.14	14.39
PCE-01	Top of cell set	0.50	15	1120.14	25.97
PCE-01	Bottom of cell set	0.50	3	1120.14	126.41
PCE-02	Pile head	0.50	16	1092.20	61.61
PCE-02	Top of cell set	0.50	16	1092.20	63.02
PCE-02	Bottom of cell set	0.50	2	1092.20	63.51
PCE-03	Pile head	0.50	14	1270.00	0.73
PCE-03	Top of cell set	0.50	14	1270.00	2.21
PCE-03	Bottom of cell set	0.50	3	1270.00	14.15
PCE-04	Pile head	0.50	12	1280.16	52.76
PCE-04	Top of cell set	0.50	12	1280.16	54.12
PCE-04	Bottom of cell set	0.50	2	1280.16	5.65
PCE-05	Pile head	0.50	15	1092.20	25.00
PCE-05	Top of cell set	0.50	15	1092.20	27.26
PCE-05	Bottom of cell set	0.50	4	1092.20	110.22

Figure 1 presents the Standard Penetration Test (SPT) results obtained closest to each tested pile. According to the figure, a well-defined stratum primarily composed of clay can be observed, with increasing compactness with depth. The presence of gravel was identified at depths greater than 11 meters, and the groundwater level was recorded at 11.5 meters in all five boreholes presented. All samples collected during the SPTs exhibited a reddish coloration, which is a typical characteristic of the lateritic soils found in the Brasília region (Monteiro et al. 2021; Bernardes et al. 2024).

 © Deep Foundations Institute 2025

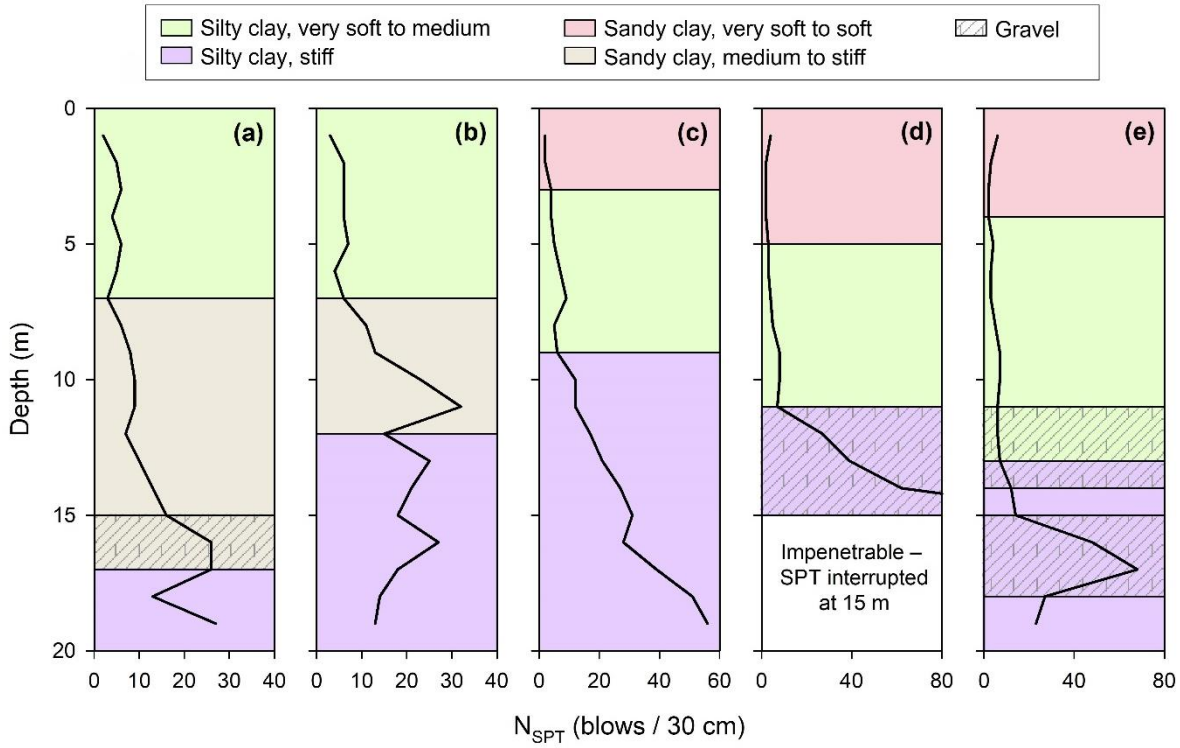


Fig. 1. SPT results near the piles (a) PCE-01, (b) PCE-02, (c) PCE-03, (d) PCE-04, and (e) PCE-05

RESULTS AND DISCUSSIONS

The load–displacement responses obtained from the tests are presented in Fig. 2. In the figure, the corrected curves for the upper segments were obtained by subtracting the submerged unit weight of these portions—considering the groundwater level at a depth of 11.5 m—from the load–displacement curve corresponding to the applied loads during testing. No correction was applied to the curves of the lower segments, in order to produce conservative results. According to the data, the lower segments of piles PCE-01, PCE-02, and PCE-05, as well as the upper segments of piles PCE-02 and PCE-04, reached displacements of 50 mm, corresponding to 10% of the pile diameter (D), a commonly adopted criterion for defining pile capacity (Fellenius 2021). The upper segments of tests PCE-01 and PCE-05 also exhibited significant displacements, on the order of 5% D. Another noteworthy aspect in the figure is the behavior observed for the PCE-02 test (Fig. 2b), in which an abrupt increase in displacement occurred in both segments starting at 800 kN, followed by a return to a stiffer response at loads of approximately 840 kN and 920 kN for the upper and lower segments, respectively. This type of load-transfer mechanism is typical of piles with the presence of loose material along their length, which can lead to a misinterpretation of the load–displacement curve as indicative of failure, when it may actually reflect the compaction of a weaker zone along the pile shaft. Once this portion is fully mobilized, the initial stiffness is regained, and the structural performance prior to the sudden displacement increase is restored (Resende et al. 2022).

 © Deep Foundations Institute 2025

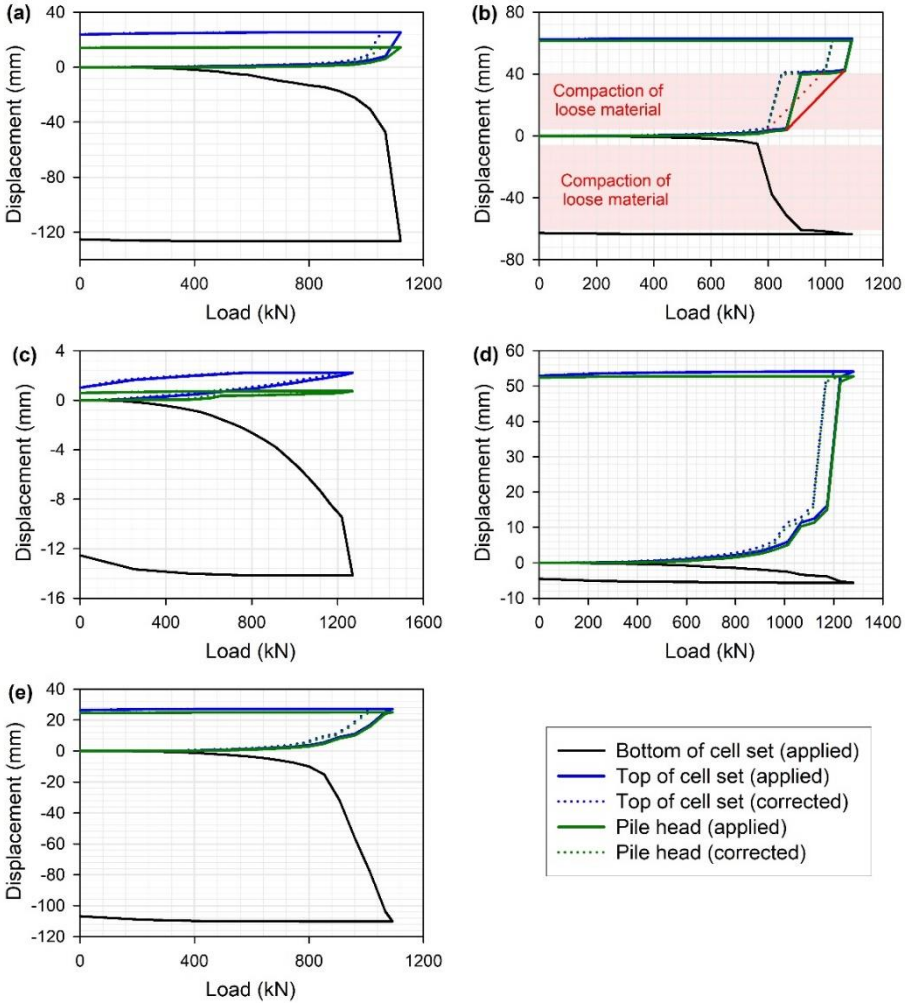


Fig. 2. Load-displacement responses for (a) PCE-01, (b) PCE-02, (c) PCE-03, (d) PCE-04, and (e) PCE-05

For the cases that were not mobilized up to the displacement value corresponding to 10% D, four extrapolation techniques were used for estimation: Décourt (1996), Chin (1970), Van der Veen (1953), and Aoki (1976). The results of the extrapolated curves for the not-fully-mobilized segments are presented in Fig. 3 below. From the figure, it is noticeable that the behavior of the methods proposed by Décourt (1996) and Chin (1970) are similar, since the theory behind the former is analogous to that of the latter, with the difference that Décourt (1996) analyzes the load/displacement ratio, while Chin (1970) investigates the displacement/load ratio. A similar relationship is observed between the methods of Aoki (1976) and Van der Veen (1953), as the methodology of the former is a correction proposal to the hyperbolic equation that describes the load-displacement behavior in load tests as suggested by the latter. A high level of convergence was found for the upper segments of tests PCE-01 and PCE-05, indicating that the maximum mobilization of 25 mm displacement (around 5% D) was sufficient to reach failure for these segments—half of the typically employed 10% D. For the lower segments of test PCE-03, some differences were found between the pairs of extrapolation methods, although not very significant because for a displacement of 50 mm, the methods of Décourt (1996) and Chin (1970) resulted in resistances around 1410 kN, while the approaches by Van der Veen (1953) and Aoki (1976) yielded values of 1287 kN—approximately 9% lower. The same behavior was observed for the lower segment of PCE-04, with a resistance of 1540 kN for the first two methods and 1325 kN for the latter two, 14% lower. The greatest discrepancy was found in the upper segment of the PCE-03 test, with a resistance of 2080 kN obtained

 © Deep Foundations Institute 2025

using the first two methodologies, and 1420 kN with the other two. Nevertheless, in all three cases, the methods of Décourt (1996) and Chin (1970) proved to be less conservative.

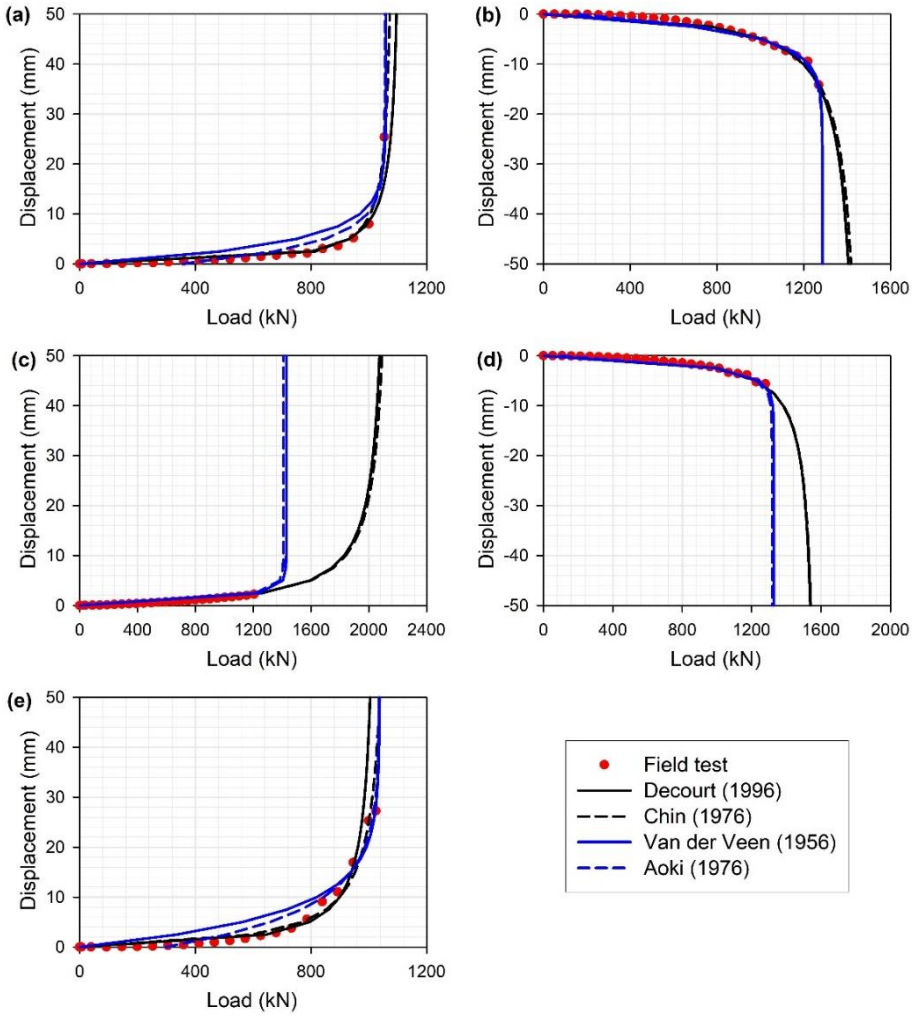


Fig. 3. Extrapolation of segments mobilized at displacements below 10% of the pile diameter during bidirectional testing: (a) upper segment of PCE-01, (b) lower segment of PCE-03, (c) upper segment of PCE-03, (d) lower segment of PCE-04, and (e) upper segment of PCE-05

The results for lateral, tip, and total loads resisted in the bidirectional load tests, considering the load corresponding to 10% D displacement as the failure criterion, are presented in Table 2 below. It is important to note that, in the present study, the total bearing capacity was determined using the traditional methodology (Silva 1986; Osterberg 1989), that is, obtained by directly summing the lateral and tip resistances at the specified displacement, assuming a rigid pile and negligible elastic shortening. Elastic shortening is given by the difference between the displacements measured immediately above the assembly of expansive cells and those measured at the pile head, which, according to Fig. 2, was on the order of 1.5 mm for the vast majority of loading stages in this case study, except for the final stage of test PCE-01. Near the displacement corresponding to 10% D, the average shortening found was negligible, and thus the cited methodology was adopted. For the segments that required extrapolation, the average of the estimated loads was adopted, except for the upper segment of test PCE-03, in which only the average of the Van der Veen (1953) and Aoki (1976) methods was considered, in favor of safety.

 © Deep Foundations Institute 2025

Table 2. Lateral, tip and total resistance for 10% D load failure criteria

Resistance	PCE-01	PCE-02	PCE-03	PCE-04	PCE-05
Lateral	1071	1080	1420	1230	1029
Tip	1067	860	1350	1432	950
Total	2138	1940	2770	2662	1979

For comparison purposes, the failure criterion defined by NBR 6122 (ABNT 2022) was used, in which the ultimate load is defined as the intersection between the load-settlement curve and the straight line described by Eq. 1, as follows:

$$Q_f = \frac{QL}{EA} + \frac{D}{30} \quad [1]$$

where Q_f = failure load, Q = applied load in test, L = pile length, E = elasticity modulus, A = pile section area and D = pile diameter. The choice of this methodology, although commonly used in Brazilian practice, is considerably conservative when compared to the 10% D criterion, since the failure loads in this case study were reached at displacements around 20 mm. Table 3 presents the bearing capacity values for the lateral, tip, and total components for the five tests performed. The table also shows, in percentages, a comparison with the values obtained using the 10% D failure criterion displayed in Table 2. With the exception of the lateral resistance in PCE-02 and the tip resistance in PCE-01, all other cases showed values above 90% when compared to this criterion, supporting the hypothesis that the failures observed in this study were reached at small displacements under loading. These failures also occurred in an abrupt manner, as noted by Monteiro et al. (2021) for piles constructed in the lateritic soil of the same region.

Table 3. Lateral, tip and total resistance for NBR 6122 load failure criteria

Resistance	PCE-01*	PCE-02*	PCE-03*	PCE-04*	PCE-05*
Lateral	1040 (97%)	880 (81%)	1420 (100%)	1120 (91%)	965 (94%)
Tip	920 (86%)	780 (91%)	1280 (95%)	1393 (97%)	863 (91%)
Total	1960 (92%)	1660 (86%)	2700 (97%)	2513 (94%)	1828 (92%)

* The percentages in parenthesis refer to the load failure criteria of 10% D in Table 2.

Figure 4 presents the comparison between the load capacities estimated by different semi-empirical methodologies and those measured experimentally through bidirectional load tests conducted in this study. The plots include the lateral, tip, and total resistance components for the five tests performed (PCE-01 to PCE-05) considering the NBR 6122 load failure criteria. The solid line represents the ideal condition in which the estimated values coincide with the measured ones (Estimated = Measured), while the dashed lines indicate a ±20% deviation. The methods proposed by Aoki and Velloso (1976), Meyerhof (1976), Milititsky and Alves (1985), and Robert (1997) tended to considerably underestimate the majority of the load estimates, with very few points falling within the ±20% range. This conservative behavior had already been noted by Décourt (1996), especially for lateritic soils typically found in tropical regions. It was also observed that the methodologies of Teixeira (1996) and Lobo (2005) showed the best performances, with most of the points located close to the reference line or within the ±20% range, for both lateral and tip components, indicating good predictive capability. The Décourt and Quaresma (1978) methodology also proved to be promising, particularly in the estimation of lateral and total resistances of some load test while the tip capacity was underrated. On the other hand, the propositions of Karez and Rocha (2000) and Shioi and Fukui (1982) tended to overestimate the load capacities.

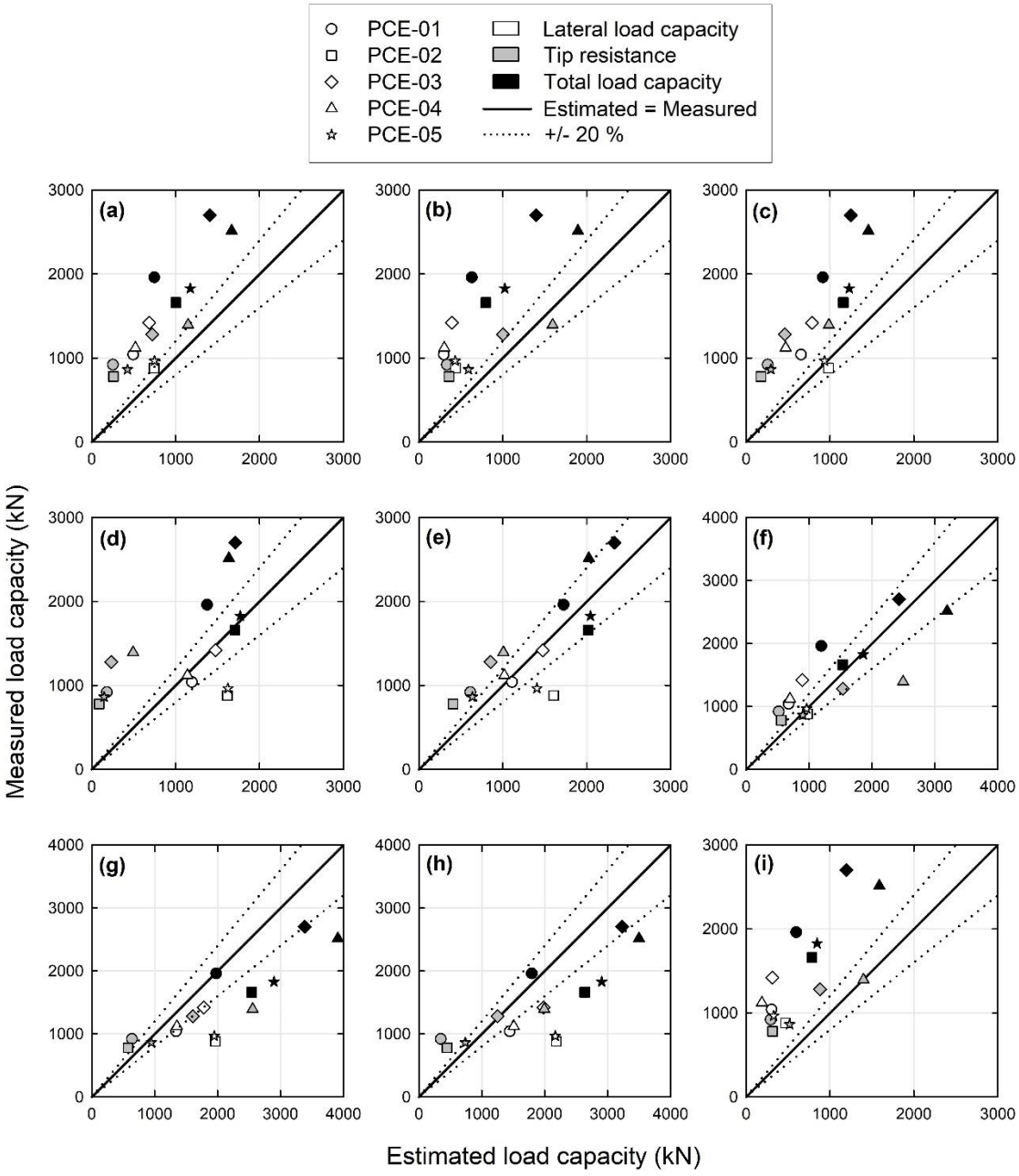


Fig. 4. Estimated *vs.* measured lateral, tip and total load capacities by semiempirical methodologies: (a) Aoki and Velloso (1976), (b) Meyerhof (1976), (c) Milititsky and Alves (1985), (d) Décourt and Quaresma (1978), (e) Teixeira (1996), (f) Lobo (2005), (g) Karez and Rocha (2000), (h) Shioi and Fukui (1982) and (i) Robert (1997)

CONCLUSIONS

This study presented the results of five bidirectional load tests conducted on continuous flight auger installed in tropical lateritic soils. Through detailed analyses of load–displacement responses,

extrapolation techniques, and comparisons with national and international design methodologies, the following conclusions were drawn:

1. **Load–displacement behavior and mobilization**: Most test segments reached displacements of at least 50 mm (10% of pile diameter), allowing for a well-defined identification of failure loads. For segments that did not reach this displacement, extrapolation methods proved effective, often resulting in similar predictions and confirming their reliability for practical use. The occurrence of abrupt displacement increases followed by stiffness recovery, as observed in test PCE-02, highlights the importance of correctly interpreting anomalies in the load–displacement curve;
2. **Bearing capacity estimation**: The total load capacities were calculated using the classical approach of summing the tip and lateral components, based on the 10% D displacement criterion and assuming negligible elastic shortening. Comparisons with the failure criterion suggested by NBR 6122 (ABNT 2022) showed that most failure loads occurred at displacements around 20 mm, indicating that the piles mobilized their ultimate resistance at relatively small displacements, with abrupt failure mechanisms consistent with previous findings of small-diameter piles under bidirectional loading tests in lateritic soils;
3. **Performance of predictive methodologies**: Among the semi-empirical methods assessed, those of Teixeira (1996), Lobo (2005), and Décourt and Quaresma (1978) showed the best agreement with the measured values, with most predictions falling within a ±20% range, especially for lateral and total resistances. In contrast, the methodologies of Aoki and Velloso (1976), Meyerhof (1976), Milititsky and Alves (1985), and Robert (1997) tended to be overly conservative, substantially underestimating pile capacities. Conversely, the approaches by Karez and Rocha (2000) and Shioi and Fukui (1982) often led to overestimations;
4. **Implications for design in lateritic soils**: The results reinforce the need for careful selection and calibration of design methods when applied to tropical soils. While conservative approaches ensure safety, they may lead to uneconomical designs. The observed consistency between measured and predicted values using updated or regionally calibrated methods suggests their suitability for similar geotechnical contexts.

REFERENCES

Aoki, N. 1976. Considerações sobre a capacidade de carga de estacas isoladas. Lecture Notes, Universidade Gama Filho, Rio de Janeiro.

Aoki, N. and Velloso, D.A. 1975. An approximate method to estimate the bearing capacity of piles. Proceedings of 5th Congreso Panamericano de Mecanica de Suelos y Cimentaciones, Buenos Aires, Sociedad Argentina de Mécanica de Suelos y Ingenieria de Fundaciones, pp. 367-376.

Bernardes, H.C., Cunha, R.P., Cruz Jr., A.J., Sales, M.M., and Rebolledo, J.F.R., 2024. Analysis of the geotechnical behavior of a piled raft in tropical lateritic soil based on long-term monitoring of columns, piles, and raft–soil interface. Canadian Geotechnical Journal, 61(4) 627-648.

Chin, F.K. 1970. Estimation of the ultimate load of piles not carried to failure. Proceedings of 2nd Southeast Asia Conference on Soil Engineering, Singapore, pp. 81-90.

Dai, G. and Gong, W., 2012. Application of bi-directional static loading test to deep foundations. Journal of Rock Mechanics and Geotechnical Engineering, 4(3) 269-275.

 © Deep Foundations Institute 2025

Décourt, L. 1996. A ruptura de fundações avaliada com base no conceito de rigidez. Proceedings of Seminário de Engenharia de Fundações Especiais 3, São Paulo, ABMS, pp. 215-224. [in Portuguese]

Décourt, L. and Quaresma, A.R. 1978. Capacidade de carga de estacas a partir de valores de SPT. Proceedings of 6th Congresso Brasileiro de Mecânica dos Solos e Engenharia Geotécnica, Rio de Janeiro, ABMS, pp. 45-53. [in Portuguese]

England, M. 2003. Bi-directional static load testing – state of the art. Proceedings of International Geotechnical Seminar on Deep Foundations on Bored and Auger Piles, Rotterdam, Millpress, pp. 309-313.

Fellenius, B.H. 2025. Basics of foundation design. A text book. http://www.fellenius.net/papers. 574 p. Accessed 01-04-25.

Lobo, B.O. 2005. Método de previsão de capacidade de carga de estacas: aplicação dos conceitos de energia do ensaio SPT. MSc. Thesis, Universidade Federal do Rio Grande do Sul, Porto Alegre, 121 p. [in Portuguese]

Meyerhof, G.G. 1976. Bearing capacity and settlement of pile foundations. Journal of the Geotechnical Engineering Division, 102(3) 197-228.

Milititsky, J. and Alves, I. 1985. Discussions – Section 3.3: building foundations. Proceedings of 1st International Conference on Geomechanics in Tropical Lateritic and Saprolitic Soils, Brasília, ABMS, pp. 45-48.

Moghaddam, R.B., Hannigan, P.J., and Rausche, F., 2021. Top-loaded bi-directional test, a new approach to deep foundations load testing. https://www.grlengineers.com/wp-content/uploads/2022/09/Top-Loaded-BiDirectional-Test-A-New-Approach-to-Deep-Foundations-Load-Testing-1.pdf. 13 p. Accessed 01-04-25.

Monteiro, F.F., Cunha, R.P., Aguiar, M.F.P., and Silva, C.M., 2021. Settlement of bored piles with expander body system in lateritic soils. International Engineering Journal, 74(3) 309-318.

NBR 6122: Projeto e execução de fundações, 2022. Associação Brasileira de Mecânica dos Solos, ABMS Publisher, Rio de Janeiro, 120 p. [in Portuguese]

Niazi, F.S. and Mayne, P.W., 2014. Axial pile response of bidirectional O-Cell loading from modified analytical elastic solution and downhole shear wave velocity. Canadian Geotechnical Journal, 51(11) 1284-1302.

Karez, M. and Rocha, E.A.C. 2000. Estacas tipo hélice continua: previsão da capacidade de carga. Proceedings of 4th Seminário de Engenharia de Fundações Especiais, São Paulo, ABMS, pp. 274-278. [in Portuguese]

Osterberg, J.O. 1989. New device for load testing driven piles and drilled shafts separates friction and end bearing. Proceedings of 14th International Conference of Piling and Deep Foundations, London, CRC Press, pp. 421-427.

Resende, A.S., Barbosa, Y., Chaves, N.A., and Albuquerque, P.J.R., 2022. Avaliação de desempenho de estacas escavadas em ensaios bidirecionais – Análise de resultados. Proceedings of XX Congresso Brasileiro de Mecânica dos Solos e Engenharia Geotécnica, Campinas, ABMS, pp. 1-6. [in Portuguese]

Robert, Y.A. 1997. Few comments on pile design. Canadian Geotechnical Journal, 34(4) 560-567.

Shioi, Y. and Fukui, J. 1982. Application of N-value to design of foundations in Japan. Proceedings of the 2nd European Symposium on Penetration Testing, Amsterdam, pp. 159-164.

Silva, P.E.C.A.F. 1986. Célula expansiva hidrodinâmica: uma nova maneira de executar provas de carga. Proceedings of XVIII Congresso Brasileiro de Mecânica dos Solos e Engenharia Geotécnica, Porto Alegre, ABMS, pp. 223-241. [in Portuguese]

Teixeira, A.H. 1996. Projeto e execução de fundações. Proceedings of 3rd Seminário de Engenhaira de Fundações Especiais e Geotecnia, São Paulo, ABMS, pp. 33-50. [in Portuguese]

Van der Veen, C. 1953. The bearing capacity of pile. Proceedings of 3rd International Conference of Soil Mechanics and Foundation Engineering, Zurich, ICOSOMEF, pp. 84-90.

Wan, Z., Dai, G., and Gong, W., 2018. Full-scale load testing of two large-diameter drilled shafts in coral-reef limestone formations. Bulleting of Engineering Geology and the Environment, 77(3) 1127-1143.

 © Deep Foundations Institute 2025

THE IMPACT OF RIGID INCLUSIONS ON THE DESIGN OF FOOTINGS AND SLABS

Sonia Sorabella Swift, P.E. and Jules Petrella

ABSTRACT

Rigid Inclusions (RIs), typically fully-grouted columns, used to reduce settlement and increase bearing capacity, are versatile ground improvement elements widely used to support structures. RIs supporting buildings are often located under footings and slabs (referred to herein as foundations), often separated by a load transfer platform (LTP). The purpose of the LTP is to create a physical separation between the RIs and the foundations and to distribute the load from the RI to the underside of the foundation. RI-supported foundations are typically designed for uniform bearing. However, RIs do create stress concentrations on foundations, the magnitude of which varies based on applied loading, soil conditions, the spacing of RIs, LTP thickness, stiffness and consistency, and other factors. The impact of these stress concentrations on the supported foundations is a major question within our industry. The purpose of this paper is to show the impact of RIs on foundations using simple statics analysis and the results of finite element modeling and establish thresholds beyond which uniform conditions may not be assumed for structural design.

While the impact of these stresses may changes to the foundation design, it is rare in cases where the RI design follows traditional ground improvement methodology. Where the RIs act more like deep foundation elements than ground improvement, the stress concentrations from the RIs should be evaluated by the RI designer and, if required, the impact on the foundation design should be evaluated by the structural engineer.

In this paper, we will show the results of 2D and 3D PLAXIS models evaluating the conditions beneath RI-supported foundations. Our slab models evaluate the bending moment in the slab with changes in soil profile and LTP thickness. Our footing models compare the bending moment and shear in the footing supported by RIs with those in the footing supported by a composite (uniform) soil for various RIs layouts.

INTRODUCTION

Rigid inclusions (RIs) are a common type of ground improvement used to reduce settlement and increase bearing capacity. While they are often confused with piles, they are markedly different with rigid inclusions not being structurally connected to the superstructure and often being separated from the superstructure by a load transfer platform (LTP). RIs are columns that are significantly stiffer than the surrounding soils. RIs have primarily been grout or concrete elements ranging from 280 to 450 mm (11 to 18 inches) in diameter. More recently, RIs are comprised of other materials that have typically been thought of as deep foundation elements such as ductile iron piles (DIPs), timber piles, small-diameter steel piles, H-piles, and more. While this is a natural evolution for RIs, it is critical to understand the differences between RIs and piles to properly design RIs, regardless of what material they are made of.

RIs can be used in a wide range of applications from sites where little ground improvement is needed to sites that are ideal for deep foundations. The RI spectrum conceptualizes the broad range of RI application (Swift and Pearlman, 2024). Because of this spectrum, RI design requires an understanding of how the RIs interact and share load with the soil and the subsequent impact, if any, on the superstructure. There is no one-size-fits-all approach to ground improvement design, which can make it difficult to develop rules for RI design, as flexibility and optimization are key factors in the use of RIs. Figure 1 shows the RI spectrum along with the general trend for various components of an RI design with respect to their place on the spectrum.

 © Deep Foundations Institute 2025

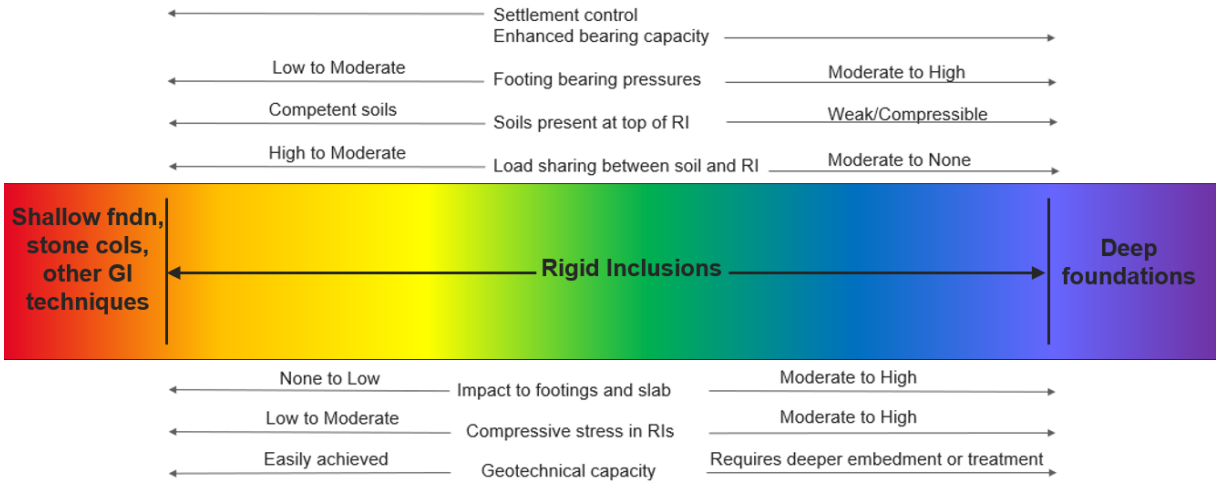


Figure 1. The Rigid Inclusion Spectrum (Swift and Pearlman, 2024).

LOAD TRANSFER PLATFORM

The load transfer platform (LTP) is a critical element of the RI system design, construction, and long-term performance. The LTP generally consists of well-graded aggregate, crushed stone, lime-or cement-treated soils, or cementitious materials. Regardless of the material used, the LTP allows for appropriate load transfer to the RIs, reduces lateral loads transferred to the RIs, and reduces stresses on the base of the supported foundation. The thickness and composition of the LTP is determined by the RI designer depending on the specific project details. In the US, LTPs below footings are generally 150 to 300 mm (6 to 12 inches) thick while LTPs below slabs are generally 0.6 to 1.2 meters (2 to 4 feet) thick. Cementitious materials are often used as LTP below footings when compaction of the subgrade soils cannot be otherwise achieved. Cementitious materials are not often used as LTP beneath slabs.

The load transfer that occurs through the LTP requires some small movement to occur; thereby increasing the total settlement of the system. The need for and thickness of the LTP, especially below slabs, is commonly questioned to reduce cost. While reducing LTP thickness or using a wider RI spacing under slabs can reduce costs of the RIs, it will likely come at the cost of a thicker slab-on-grade. Optimization of the LTP and slab thickness must be evaluated on a case-by-case basis.

The modelling and analyes presented in this paper assume an LTP that is competent and can transfer load from the structure to the RIs without significant deformation. The design and construction of the LTP is crucial to the behavior of the RIs. The type of material used and the testing required during placement should be part of the RI design and should be strictly adhered to. Failure to provide an LTP that can adequately transfer load to the RIs may result in behavior different than what we assumed for our models and the conclusions provided herein may not be appropriate.

Soil Profiles Modeled

To demonstrate the impact RIs on slabs and footings, we modeled two RI-reinforced soil profiles in PLAXIS 2D. The two profiles shown in Figure 2 represent profiles that fall on different ends of the RI spectrum shown in Figure 1. We selected these profiles because the proximity of the soft clay to the ground surface will impact the load transfer and the load sharing between the soil and the RI.

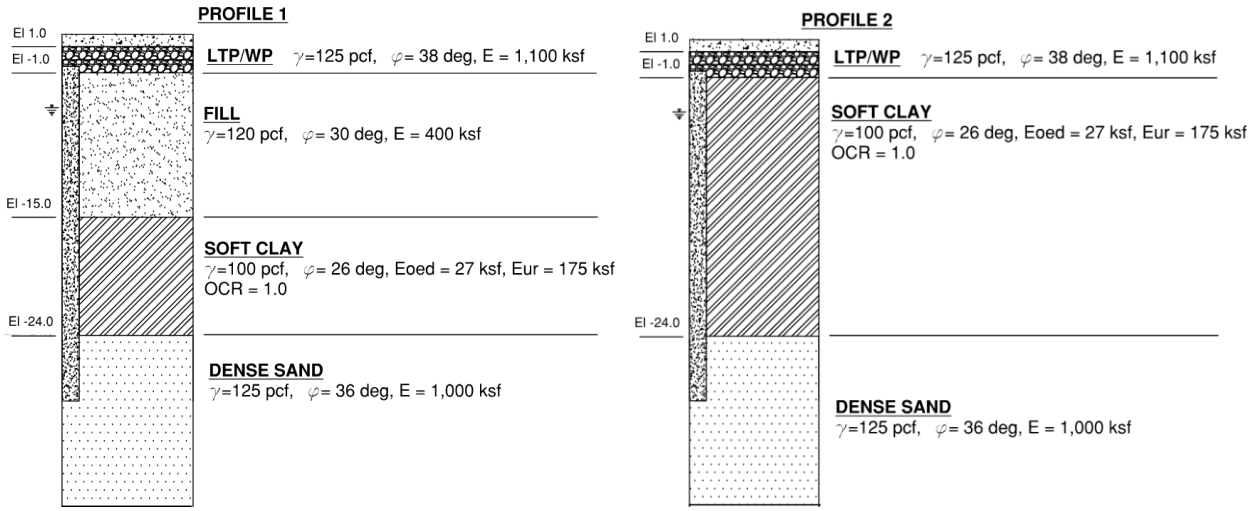


Figure 2. Soil Profiles Modeled.

SLABS-ON-GRADE

RIs below slabs-on-grade are generally placed in square grids ranging from 1.5 to 3.0 meters (5 to 10 feet). The use of a slab-on-grade in conjunction with an LTP is one of the main differentiators between RIs and piles. Slabs-on-grade used with RIs are typically thinner (130 to 230 mm (5 to 9 inches)) than structural slabs used with piles (250+ mm (10+ inches)). Slabs-on-grade are also not typically part of a building's structural system and often designed based on past experience and local practice. This is especially true for structures designed for uniform loading (residential buildings, office space, parking garages, commercial centers, schools) whereas slabs for structures with rack loading are often designed based on the specific loading provided. Common practice is to design slabs as uncracked, unreinforced elements. Steel mesh or rebar is often provided to control cracking, but it is not accounted for in the design of the slab.

The slab is designed for a uniform subgrade and the structural engineer is not accounting for the impact of the RIs during slab design. If the LTP thickness is sufficient, the load will distribute between the top of the RI and soil so designing for uniform bearing is appropriate. However, if the LTP is too thin with respect to the spacing of the RIs and the stiffness of the soils, then the RI causes a stress concentration at the bottom of the slab. Stress concentrations result in tensile stresses at the top of the slab. If the slab is designed to remain uncracked as unreinforced concrete, then the tensile stresses imparted on the slab by the RI can be compared to the modulus of rupture of the concrete. Increased stress concentrations at the bottom of the slab may require changes to the thickness or strength (f'c) of the slab. As the slab is not part of the structural system of the structure, a cracked slab poses no risk to occupancy safety but is generally undesirable for aesthetic reasons.

RI interaction with Slabs

We modeled the soil profiles in Figure 2 with RIs spaced 3 m (9.75 ft) apart and a slab ranging in thickness from 130 to 200 mm (5 to 8 inches). We varied the distance between the bottom of the slab and the top of the RI between 150 mm and 910 mm (0.5 ft and 3 ft) and applied a uniformly distributed load of 7.2 kPa (150 psf) to the top of the slab.

Figure 3 shows the tensile stress estimated in the slab based on the results of the PLAXIS model and the method of additional bending moments described in ASIRI Section 3.4.3. We compare the stresses to the modulus of rupture in the unreinforced concrete, which represents the maximum allowable tensile stress in the concrete, calculated based on a 27,600 kPa (4,000 psi) concrete strength and the equations and reduction factors given in ACI 318-14 for plain concrete.

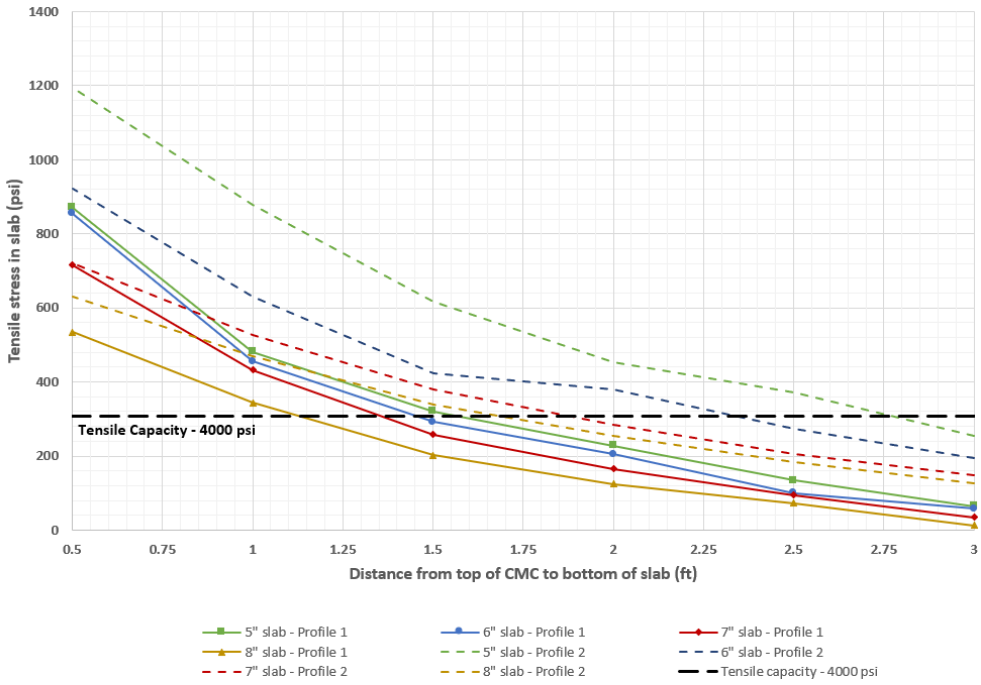


Figure 3. Tensile Stresses in Slab-on-Grade.

Figure 3 shows that the thickness of the LTP has a significant impact on the tensile stress in the slab. The tensile capacity of the slab is more easily exceeded in thinner slabs. It also shows that Profile 2 (softer soils near the ground surface - located on the right half of the RI spectrum) will produce larger tensile forces when compared to the same conditions for Profile 1 (more competent soils near the ground surface – located on the left side of the spectrum). Therefore, thinner slabs are more susceptible to damage when combined with thin LTPs, especially on soft soil sites. From Figure 3 and based on our past experience, we recommend checking the tensile stresses in the slab in cases where the thickness of the LTP is less than 610 mm (2 ft) for with competent soils near the ground surface or 910 mm (3 ft) for loose or soft soils near the ground surface. The results in Figure 3 were generated using a 3 m (9.75 ft) spacing, on the wider end of the spacings currently used for RIs. More tightly spaced RIs would likely result in lower stresses in the slab than those shown; therefore, these recommendations are conservative.

Figure 3 also shows that a thicker LTP will reduce the stress concentration and produce more uniform stresses at the bottom of the slab. The solution for a given project may be the use of a thin slab combined with a thick LTP or thick slab combined with a thin LTP. The RI designer can also modify their design to reduce the impact on the slab, such as cutting off the RI lower or tightening the RI spacing. Many different conditions can be designed for and result in acceptable performance of the RI system. However, if the project team chooses an LTP that is too thin for the RI spacing and soil conditions without evaluating the impact of the RIs on the footing, the risk of cracking the slab increases significantly.

FOOTINGS

Individual spread and strip footings are also typically designed as bearing on uniform support. The design of the footing and its reinforcement does not account for any point loads or stress concentrations at the bottom of the footing. The footing is designed for the moment, one-way shear, and two-way shear applied by the column loads as if it were sitting on a uniform elastic subgrade.

However, as RIs are rigid elements placed near the bottom of the footing, structural engineers often question whether the design of the footing is appropriate or whether it needs to account for the point loads from the RIs. The simple answer to this question is that based on significant modelling performed within Menard

globally and our past experience, uniform bearing is an appropriate assumption for most footing designs. We have found that if the footing is designed for the moment, one-way shear, and two-way resulting from uniform bearing, the design will be conservative. However, there are limitations to that assumption and in cases with obviously non-uniform conditions or elements with varying stiffness beneath a single footing (as in the case of existing foundations combined with new foundations), the structural engineer should check the forces in the footing due to the proposed support.

Geometric layout

Our past research has shown that the magnitude of the moment and shear forces in the footing are tied to the geometric location of the RIs with respect to the center of the footing. To avoid exceeding the moment and shear force generated by uniform soil conditions, follow these rules when placing RIs below footings whenever possible:

- lay out the RIs so that they are within B/4 of the center of the footing (where B is the footing width),
- place an RI in the center of the footing,
- lay out the RIs in radial patterns, as shown in Figure 4 instead of in grids.

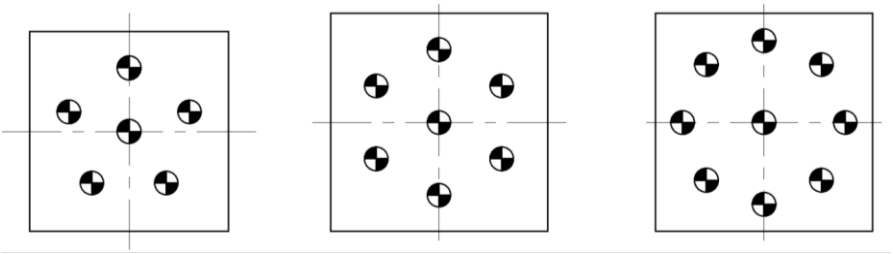
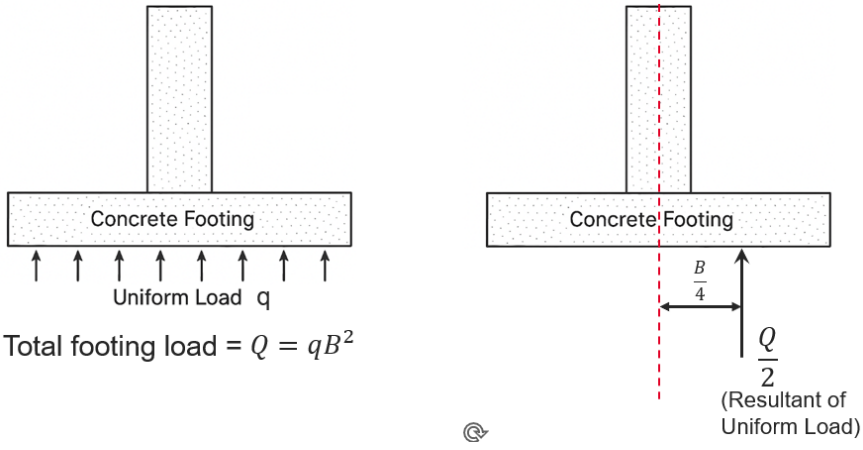


Figure 4. Example of radial patterns for RI layout under footings.

Understanding the role of the geometry of the RI layout on the forces in the footing is a key component to understanding and explaining the interaction between the structure and its support system. Consider the uniform support provided to a footing (of width B) and the resultant force on that footing shown in Figure



5

Figure 5. For simplicity, assume that the moment will be calculated at the center of the footing, though there are usually code allowances to reduce the moment based on the size of the base plate or column.

 © Deep Foundations Institute 2025

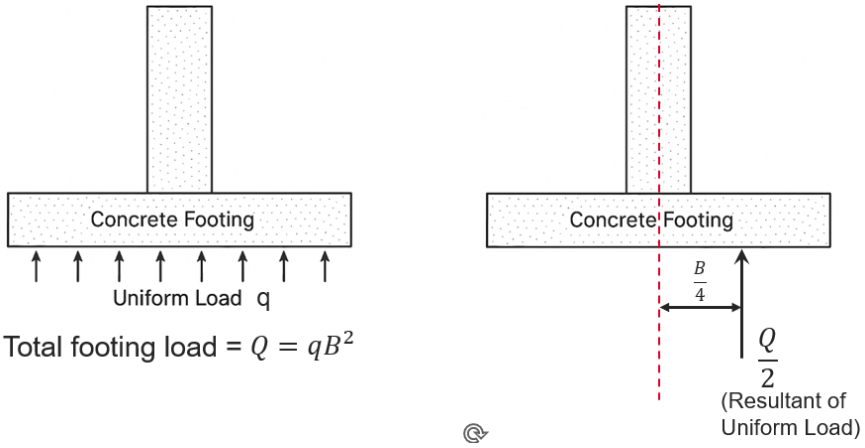


Figure 5. Footing supported uniformly by soil and corresponding resultant force

The moment caused by the uniform load is equal to the magnitude of the resultant of the uniform load times the distance from the center of the footing. Now consider the footing (of width B) supported by RIs and the resultant force on that footing shown in Figure 6. The resultant force is the same. Therefore, if the distance from the center of the footing to the center of the RI is less than or equal to B/4, the RI support will result in smaller moments than uniform support. These same rules also holds true for one-way shear, though the equations are different. See ACI 318-14 for the proper location of the moment and shear planes.

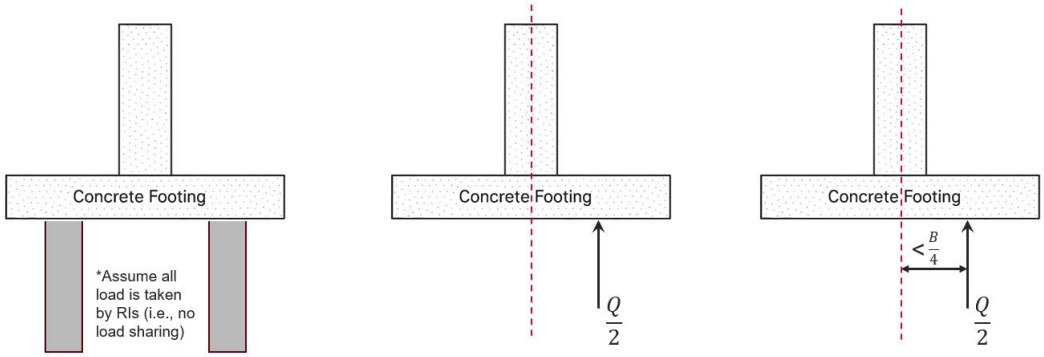


Figure 6. Footing supported by RIs and corresponding resultant force

For the example above, we assumed that all the load is taken by the RIs; however, typically, RIs are separated from the footing by an LTP, which allows for some load sharing. The same concepts apply but the calculations need to account for both the load in the soil and the RI. While the conditions under an RI-supported footing are not fully uniform, the presence of the LTP softens the response from the RIs and as you thicken the LTP, the response approaches uniform conditions.

FINITE ELEMENT MODELING

Although we can do simple calculations about the support provided by uniform conditions and RIs, the interaction between the RI and the soil is critical to the observed behavior. Thererfore, we modeled RI-supported footings to evaluate the behavior with different support conditions. We modeled five different footings, each supported by a different number of RIs, as described below and shown in Figure 7Figure 7:

- 1.5-meter-square (5-foot-square) footing supported by a single RI in the center
- 2.7-meter-square (9-foot-square) footing supported by a two or three RIs
- 3.0-meter-square (10-foot-square) footing supported by four or five RIs

 © Deep Foundations Institute 2025

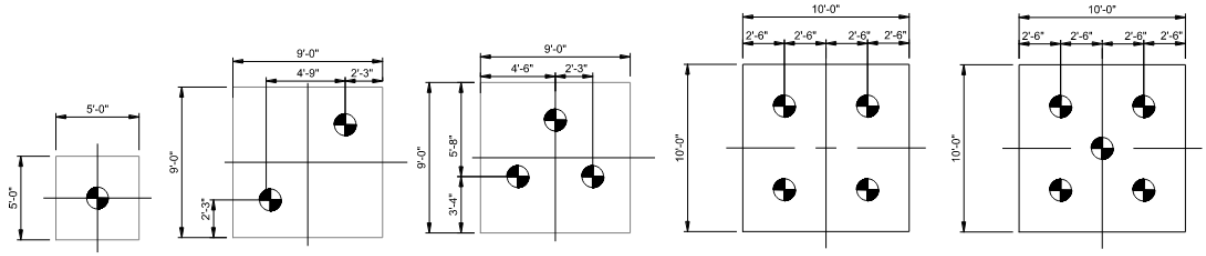


Figure 7. Footing and RI Geometries for 1, 2, 3, 4 and 5 RIs.

We used Soil Profile 1 and 2 for these analyses, as shown in Figure 2. We ran the models with RI reinforcement and uniform support, which was modeled using a composite soil. The composite soil was a column of linear-elastic soil directly below the footing extending to the bottom of RIs. We modeled the composite soil as linear elastic with a modulus value that resulted in equal footing settlement to the footing supported by RIs for each condition we evaluated. See Figure 8 for a visualization of the composite column versus the RI support.

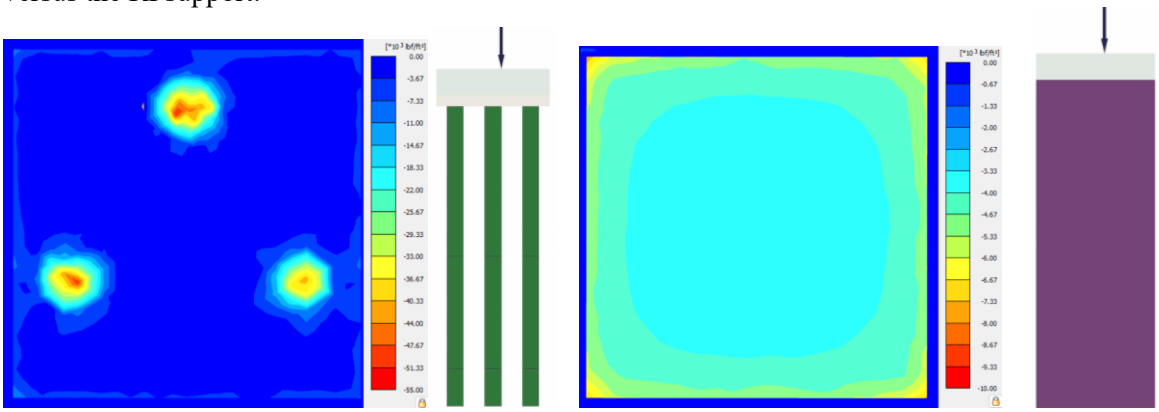


Figure 8. Vertical effective stress (ksf) at the bottom of a footing supported by RIs(left) and uniform soil (right).

We placed a dummy plate in the center of the footing to determine the shear force and bending moment within the footing. We placed a 610-mm x 610-mm (2-ft x 2-ft) plate centered on the top of the footing and applied a pressure equal to the plate equal to the total footing load, which was equal to 192 kPa (4,000 psf) times the area of the footing, for each condition modeled. We modeled the LTP as a 150-mm-thick (6-inch-thick) layer below the entire footing area and evaluated the conditions using the properties of a traditional dense-graded aggregate (DGA) and a cementitious lean mix, which we refer to as a mudmat. We also ran the models assuming no LTP, i.e., the RIs are touching the bottom of the footing.

RESULTS

We plot the bending moment and shear force across the footing in one direction. PLAXIS 3D provides the shear and bending moment in the plate in two directions assuming one-way action. For the symmetric layouts, the forces are the same in both directions. In practice, the moments and shear forces in the footing may be smaller than what is estimated by PLAXIS because of two-way action of the footing. However, the focus of this study is to compare the RI-supported footings with the uniformly-supported footings; therefore, we will focus on the relative behavior of the bending moment and shear forces. In the figures that follow, we only show one composite case because all of the composite cases, regardless of soil profile or LTP, were nearly identical. We also plot bending moment and shear forces across the entire footing. For design according to ACI 318-14, you are permitted to evaluate bending moment and shear beyond the center of the footing, based on the geometry of the column and base plate, which would result in lower moments in the footing than shown in Figure 9 through Figure 14.

 © Deep Foundations Institute 2025

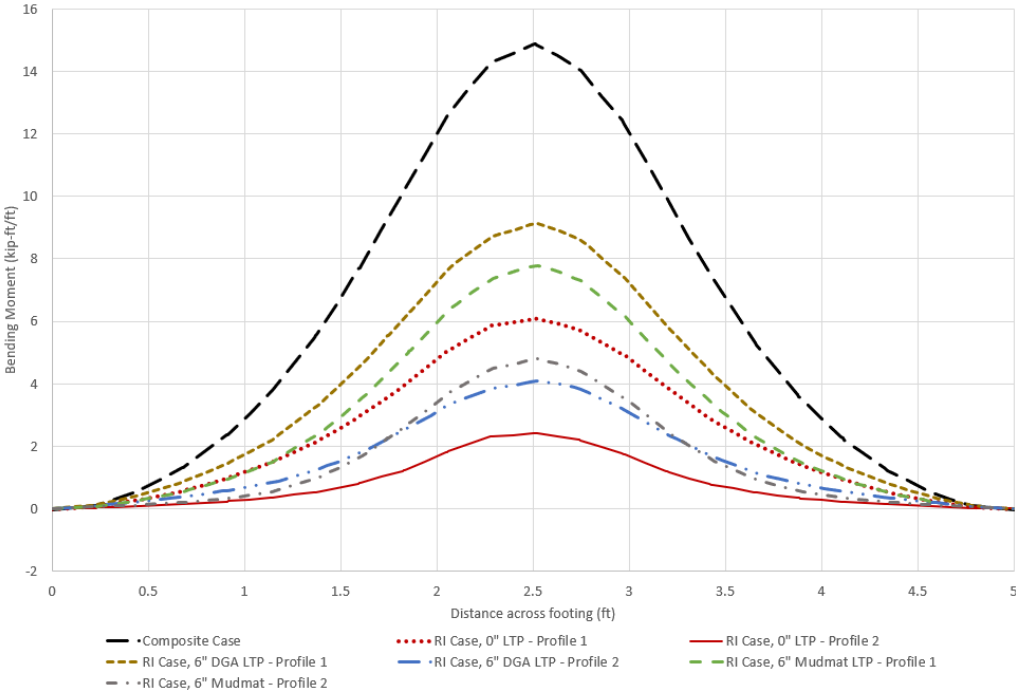


Figure 9. Bending moments for 5-ft x 5-ft footing supported by a single RI – Profiles 1 & 2.

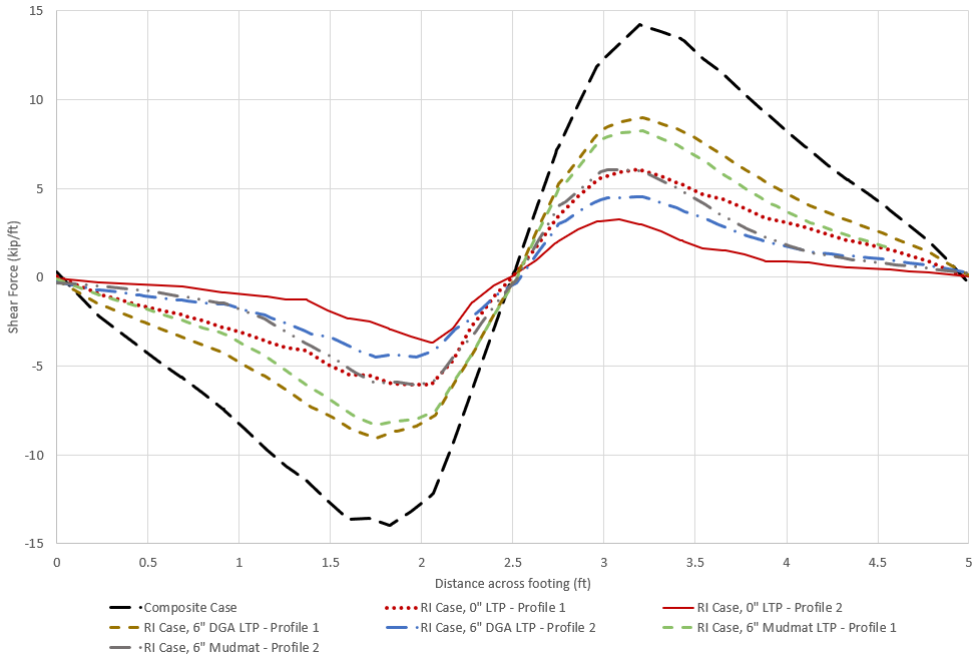


Figure 10. Shear forces for 5-ft x 5-ft footing supported by a single RIs – Profiles 1 & 2.

 © Deep Foundations Institute 2025

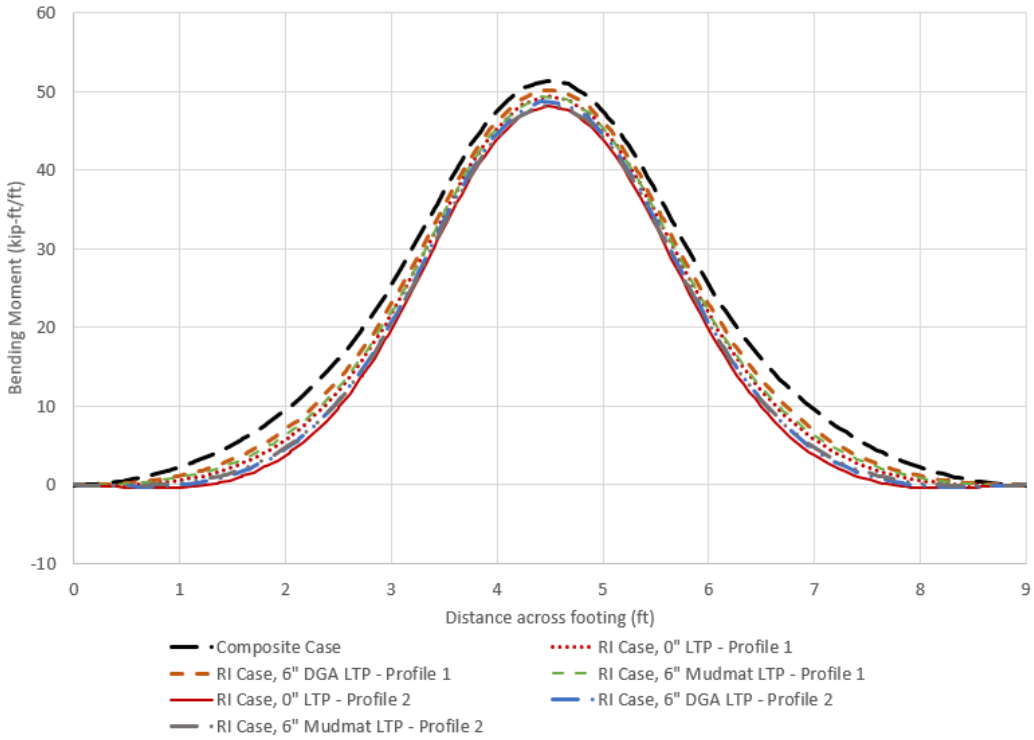


Figure 11. Bending moments for 9-ft x 9-ft footing supported by two RIs – Profiles 1 & 2.

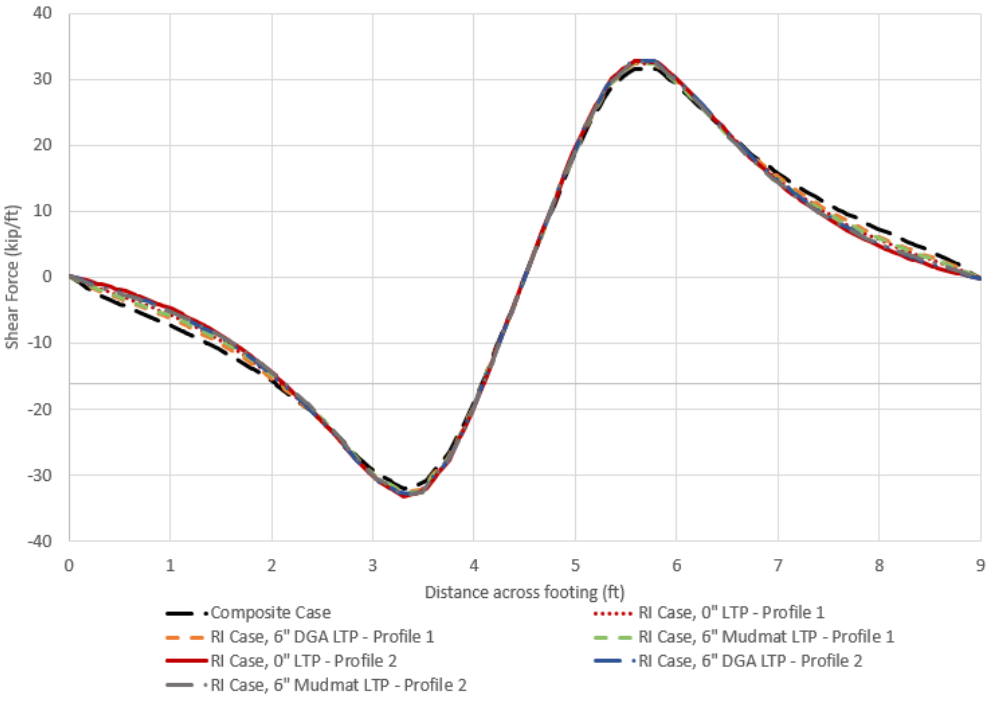


Figure 12. Shear forces for 9-ft x 9-ft footing supported by two RIs – Profiles 1 & 2.

 © Deep Foundations Institute 2025

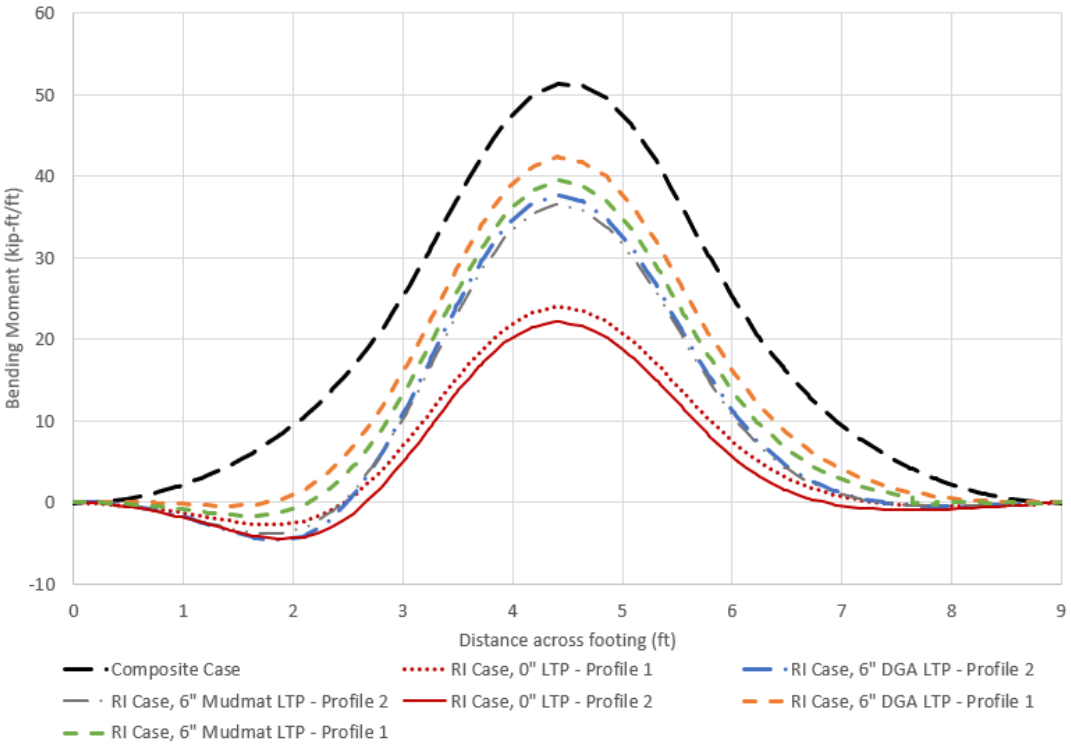


Figure 13. Moment for 9-ft x 9-ft footing supported by three RIs - Profiles 1 & 2.

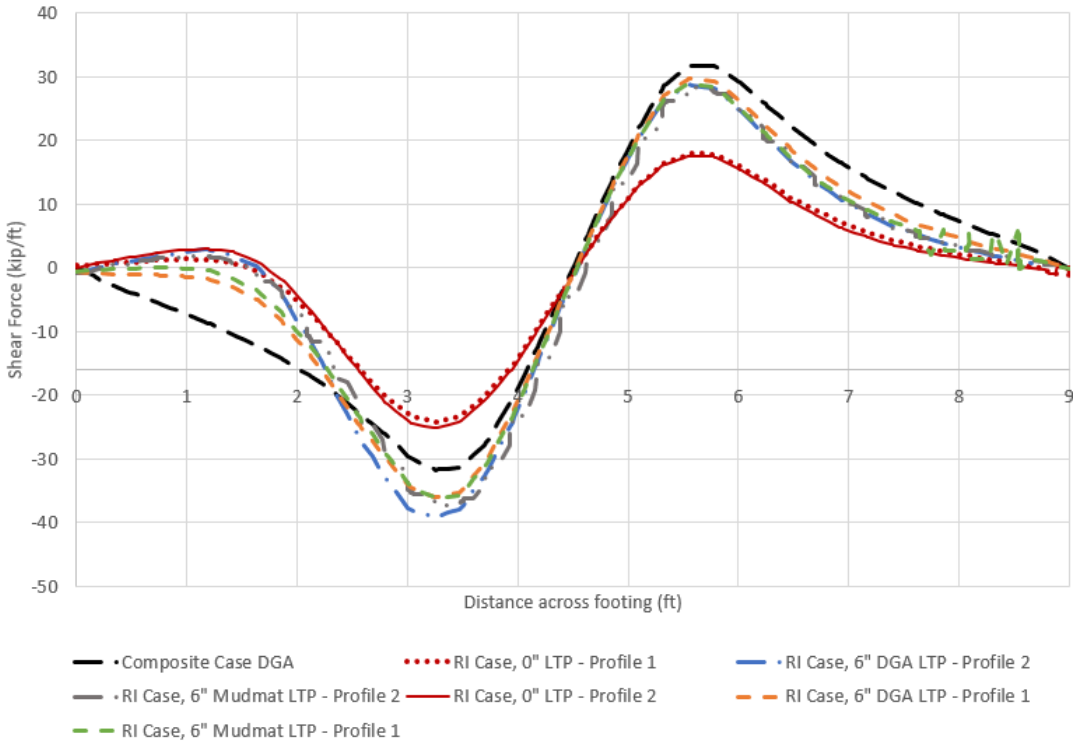


Figure 14. Shear forces for 9-ft x 9-ft footing supported by three RIs - Profiles 1 & 2.

Figures 9 through 14 show that the composite cases produce higher moments and shear forces in the footings than any of the RI cases.

 © Deep Foundations Institute 2025

Where the footing is supported by 1 RI, the results show that there is some impact on the response based on the soil profile and the type of LTP used. However, the magnitude of both the moment and the shear forces internal to the footing are lower in the RI-supported case than in the composite support case.

For the footing supported by 2 RIs, the response for all cases is nearly identical and similar to that of the composite case. The behavior is not greatly impacted by the type of LTP or the soil profile.

For the case of a footing supported by 3 RIs, the response is different depending on which direction you cut a cross section through the footing. We present the results from the direction that produced the larger moments and shear forces. Again, the magnitude of the moment internal to the footing is lower in the RI-supported case than in the composite support case. However, the shear forces in the RI-supported cases are slightly higher than they are in the composite case when an LTP is used. Placement of the RIs may impact the magnitude of the shear forces, so we recommend additional evaluation of footings supported by 3 RIs when an LTP is used and the footing design doesn't have excess shear capacity. The shear forces for the conditions we evaluated were 10-20% larger for the RI-supported case depending on the soil conditions at the ground surface.

We evaluated footings supported by 4 and 5 RIs and found that that results were consistent with those for 1 to 3 RIs - the moment and shear forces footing in the RI-supported cases did not exceed those of the composite case. We do not show those results for brevity.

In Figures 9 through 14 the moment and shear forces caused by the case with no LTP (RI Case – 0" LTP) produces the smallest moments and shear forces while the uniform case produces the largest moments and shear forces. That results from the load being supported entirely by the RIs with no soil contribution, as shown in Figure 6, so the moment is based only on the magnitude of the force in the RI and the location of the RI. However, as you increase the LTP and therefore the load in the soil, the moment accounts for the load distribution between the RIs and the soil. As the LTP becomes thicker, the load in the RI decreases and the load in the soil increases as you approach uniform support.

CONCLUSIONS

The interaction between RIs and the structure they support needs to be considered during design by the RI designer and the structural engineer. The impact of the RI on the structural design of the footing or slab will vary depending on the soil conditions, the load sharing between the RI and the soil and other project-specific factors.

Slabs-on-grade tend to be more sensitive to the impact of RIs than footings because they are thinner and often designed as unreinforced elements. The thickness and composition of the LTP are critical factors in determining whether the RI will act as a point load below the slab and result in bending of the slab or whether its impact will be distributed throughout the LTP. Thicker LTPs will better distribute the load from the RI so that the stress on the bottom of the slab is relatively uniform. However, when thinner LTPs are used, the impact of the RI on the slab may result in bending of the slab that may exceed the tensile capacity of the slab. The authors recommend that the RI designer and/or structural engineer check the impact of the RI on the slab in cases where the thickness of the LTP is less than 2 ft for soil profiles with competent soils near the ground surface or 3 ft for soil profiles with soft or loose soils near the ground surface or where other conditions may warrant a check.

Footings tend to be less sensitive to the impact of the RIs; however, the interaction is of significant concern to the structural engineer. Based on our results, the moment and shear resulting from RI support is less than or similar to that of uniform support. Based on the modelling we have presented in this paper and other modeling that has been performed in the past by Menard, the authors recommend the following:

- lay out the RIs so that they are within B/4 of the center of the footing (where B is the footing width),
- place an RI in the center of the footing,
- lay out the RIs in radial patterns instead of in grids.
-

While the impact of RIs on footings is an important consideration for design, it's also notable that Menard, in the US and Worldwide, has never been involved with a project where the footings did not perform as expected because of the impact of the RIs. However, as we use RIs more often and in more creative ways, it's important to be aware of the potential impacts on the structural design of the footing and consider them during design.

REFERENCES

American Concrete Institute (2019). ACI318-19: Building Code Requirements for Structural Concrete.American Concrete Institute.

ASIRI National Project (2012). ASIRI National Project, Recommendations for the design, construction and control of rigid inclusion ground improvements. Presses des Ponts and IREX.

European Committee for Standardization (CEN) (2004). EN1997-1:Eurocode 7 -Geotechnical design – Part 1:General rules. CEN.

Swift S. and Pearlman S. (2024, May 10). *Rigid Inclusions: A Spectrum of Applicability* [Conference presentation], IFCEE 2024, Dallas, Texas, USA.

 © Deep Foundations Institute 2025

VARIABILITY ASSESSMENT OF HELICAL PILES PERFORMANCE VIA GEOMETRIC CONICAL ENHANCEMENT

Sara Heidarie Golafzani, Assistant Professor, Amirkabir University of Technology, Tehran, Iran. Email: s_heidari@aut.ac.ir
Mostafa Nazmi, Research Assistant, Amirkabir University of Technology, Tehran, Iran. Email: eng.m.nazmi@aut.ac.ir
Abolfazl Eslami, Professor, Amirkabir University of Technology, Tehran, Iran. Email: afeslami@aut.ac.ir

ABSTRACT

Although helical piles are effective for both onshore and offshore structures under axial loads, their performance can be compromised due to installation-induced soil disturbance. Among enhancement methods, expanded piles, post-grouting, geometric modifications, conical helices offer recent promise. This study investigates the impact of conical helix geometry on soil disturbance, and axial performance. Six full-scale static load tests were conducted on helical and conical helical piles under both compressive and pullout loads at a coastal site. The test program considered two helix spacing-to-diameter ratios (S/D = 1.5 and 3) and different helix configurations. Ultimate load capacities were interpreted using multiple established criteria and further analyzed using probabilistic methods, incorporating Monte Carlo simulations to account for inherent soil variability. The results demonstrate that conical helical piles enhance load-bearing capacity and reduce installation disturbance, particularly under pullout loading at S/D = 1.5 and compression at S/D = 3. Compared to conventional helical piles, conical variants exhibited higher initial stiffness and limit loads. Moreover, reliability-based design (RBD) analysis revealed that the cylindrical shear method provides more conservative and consistent predictions than the individual plate approach. The investigation concluded that incorporating conical geometry variations minimizes soil disturbance, simplifies installation processes, and enhances the load-bearing capacity of these foundation systems.

Keywords: **Conical Helical Piles, Field Testing, Inherent Soil Variability, Geometric Enhancement, Reliability**

INTRODUCTION

Helical piles are commonly used in various onshore and offshore projects. In onshore environments, these applications include reinforcing the foundations of lightweight structures, supporting energy transmission structures, stabilizing excavation walls, and maintaining the stability of underground pipelines (Perko 2009). Probable applications in marine environments include using foundations for bridges, anchoring for aquaculture applications, and supporting the foundations of offshore wind turbines (Lutenegger 2011a; Gallant 2020; Byrne and Houlsby 2015; Spagnoli 2013; Ebrahimipour and Eslami 2024).

One of the limitations and challenges in helical piles realized as linear foundation units (Eslami et al. 2025) is the influence of pile geotechnical performance reduction, due to soil disturbance as emphasized in several research works (Tsuha et al. 2012; Spagnoli and Tsuha 2020; Fateh et al. 2017). Performing the post-grouting is the most common method to deal with this issue. However, this approach comes with high costs and practical challenges (Nabizadeh and Choobbasti 2017; Mansour and El Naggar 2022). Another proposed solution involves using helical piles with tapered central shafts, enhancing soil properties, partially mitigating the issue (Bak et al. 2021; Fahmy and El Naggar 2017; Esmailzadeh and Eslami 2025). However, this method is associated with higher material consumption and a notable rise in required torque. Furthermore, incorporating self-expanded sections has been recognized as an efficient

 © Deep Foundations Institute 2025

idea for model piles (Shojaei et al. 2021). However, their actual feasibility has not been thoroughly studied. Another method, less challenging than the other ones, is conical helical piles, where the helix diameters are gradually increased downward. A few relevant research works are (Lutenegger 2011b, Nazmi and Eslami 2025, Tsuha et al. 2015, Ghazavi et al. 2023). Figure 1 illustrates a schematic of soil disturbance around the various helical piles.

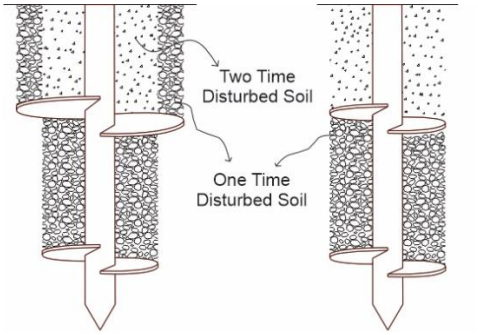


Fig. 1. Schematic illustration of soil disturbance around the various helical piles; (a) conical helical pile and (b) typical helical pile.

Despite the occurrence of soil disturbance during installation of helical piles, another issue affecting the bearing capacity is embedded uncertainties, including inherent soil variability, measurement error, and model uncertainty (Phoon and Kulhawy 1999a, b). Tang and Phoon (2018) evaluated model uncertainties in the design of axially loaded helical piles using extensive field data, focusing on reliability-based methods like the torque-correlation and individual plate bearing approaches. Their research calibrates resistance factors for LRFD using Monte Carlo simulations. It underscores the need for further investigation into large-diameter piles and time-dependent soil behavior to refine design practices.

As reviewed and based on the existing published research works, limited records are available on full-scale comparative load tests on helical and conical helical piles. In this regard, the current research work is devoted to the comparison and contrast of the geotechnical performance of helical and conical helical piles under both compressive and pullout loads. Full-scale field tests have been selected as the primary method because of their precision and effectiveness in evaluating the behavior of deep foundations. In this regard, one helical pile with an S/D (spacing-to-diameter ratio) of 3 and two conical helical piles with S/D of 1.5 and 3 were installed and tested in a coastal research site, and their behaviors were compared. Furthermore, to assess the performance of these piles regarding inherent soil variability, shear strength parameters were considered as random variables and generated. The bearing capacity of the investigated helical piles was predicted considering the generated random variables and compared with the measured ones from available load-displacement diagrams.

SITE GEOTECHNICAL CHARACTERISTICS

The current research site is in Babolsar, a city on the southern coast of the Caspian Sea. (Fig. 2). Since in-situ tests play a pivotal role in soil characterization and estimation of engineering parameters (Eslami and Fellenius 1997), a field study program included standard penetration tests (SPT) and laboratory tests. Two boreholes were drilled to a depth of 10 meters to perform the SPT. Additionally, SPT samples were taken at depths of 2, 4, 6, 8, and 10 meters from the ground surface using a sampler in accordance with ASTM D1586. Following this, laboratory tests were carried out on these samples to determine their physical and chemical properties.

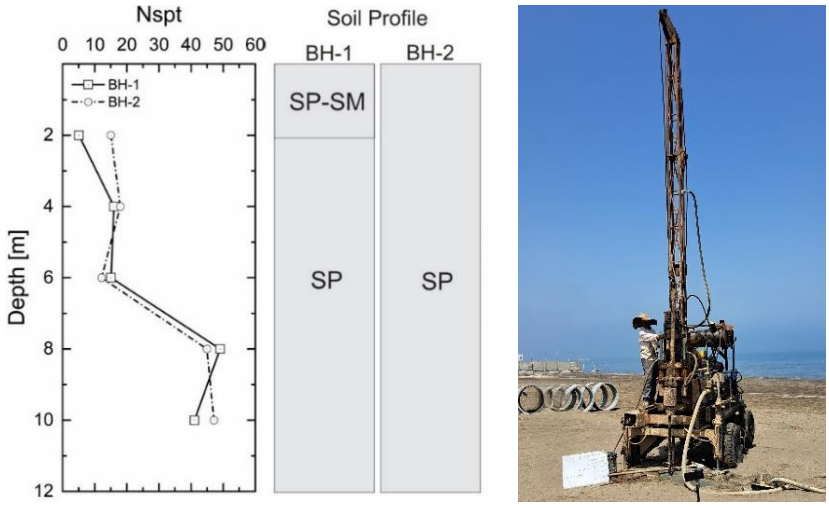
 © Deep Foundations Institute 2025



(a) **(b)**

Fig. 2. Research site: (a) Geographical location, (b) Satellite photo

In borehole number 1, the soil profile from the ground surface to a depth of 2 meters is comprised of well-graded sandy silt, classified as SP-SM by the Unified Soil Classification System. The Standard Penetration Test (SPT) value, denoted as N_{SPT}, is recorded as 5 for this layer. Between depths of 2 meters and 10 meters, the soil transitions to poorly graded sand (SP), exhibiting N_{SPT} values that vary from 18 to 49. Borehole number 2 presents a similar composition, with soil extending from the ground surface to a depth of 10 meters, also categorized as poorly graded sand (SP); the N_{SPT} values in this borehole range from 12 to 46. Detailed representations of the SPT results and the soil profile for the site and the testing equipment are illustrated in Fig. 3.



(a) **(b)**

Fig. 3. Site investigation; (a) SPT blow number and soil profile, (b) testing equipment

PILE INSTALLATION AND LOADING

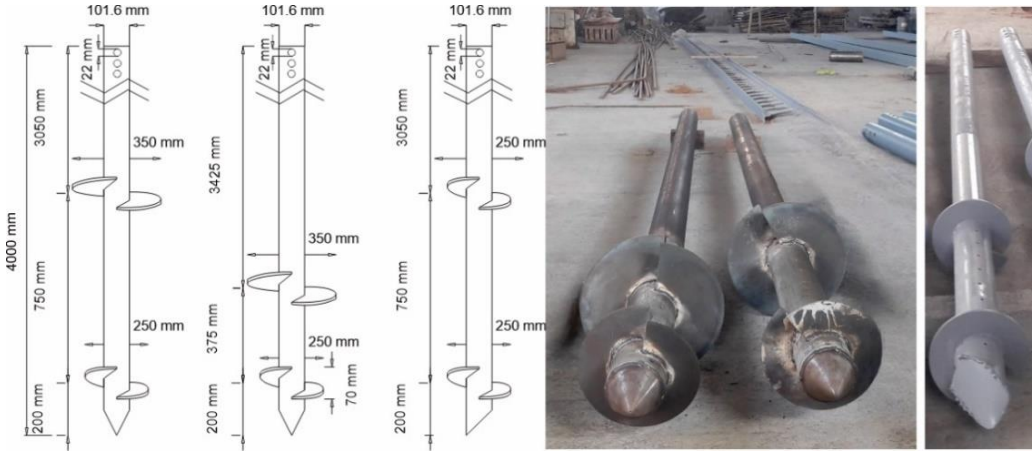
The central shaft of all piles is constructed from ST37 steel. This material is chosen as a seamless welded pipe with a diameter of 101.6 mm and a wall thickness of 4 mm. The helices, which have diameters of 250 mm and 350 mm and a thickness of 8 mm, were connected using S/D ratios of 1.5 and 3. These helices were welded to the central shaft. To improve the pile's penetration into

 © Deep Foundations Institute 2025

the soil, a conical segment with a 60-degree apex angle was welded to the tip of each pile. Additionally, to compare the behavior of helical piles and conical helical piles, a helical pile featuring two helices, each with a diameter of 250 mm and an embedment depth of 3500 mm, was also constructed alongside the previously mentioned piles. Figure 4 provides a visual representation of the mentioned piles, and their geometric specifications are presented in Table 1. As illustrated in Fig. 4a, three rows of 22 mm holes have been implemented for proper attachment of pile head and connector.

Table 1. Full-scale helical piles configuration

Pile Name		No. helix	Length	Embedded Depth	Shaft diameter	Helix diameter	S/D	Pitch
Short ID	**Descriptive ID**	**-**	**(mm)**	**(mm)**	**(mm)**		**-**	**(mm)**
CHP-1.5	**Conical Helical Pile, 250-350, S/D = 1.5**	2	4000	3500	101.6	250,350	1.5	70
CHP-3	**Conical Helical Pile, 250-350, S/D = 3**	2	4000	3500	101.6	250,350	3	70
HP-3	**Helical Pile, 250-250, S/D = 3**	2	4000	3500	101.6	250,250	3	70



(a) **(b)**

Fig. 4. Piles geometry: (a) Schematic (b) Prototype

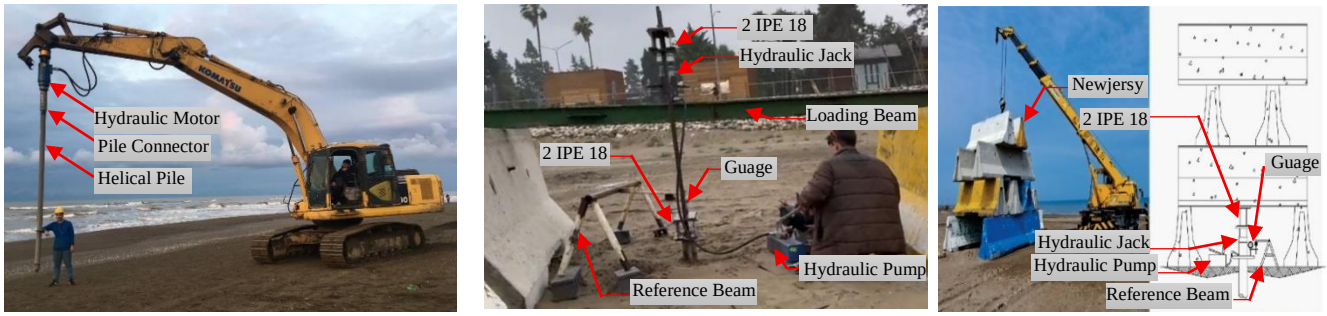
Helical piles are typically installed by applying mechanical torque at the pile head using a rotary hydraulic head. By monitoring the torque required for helical pile installation, it is possible to identify structural failures, changes in soil composition, or fluctuations in groundwater levels.

The hydraulic motor is connected to the pile head through a drive and several pins. One of the helical piles is placed vertically in the designated location and is continuously rotated, with torque applied at a rate of less than 30 rotations per minute, gradually driving it into the soil to a depth of 3,500 mm. Figure 5a shows the equipment used for installing helical piles.

Compression and pullout loads are applied in increments of 5% of the estimated pile load, at 10-minute intervals, as specified in ASTM D1143-D3689, respectively. In the compression setup, the required gravity load is provided using nine New Jersey barriers. The axial load is applied to the piles with a 50-

 © Deep Foundations Institute 2025

ton hydraulic jack. For the pullout setup, a 6-meter-long steel beam supports the load beam, which is placed on two New Jersey barriers. The same 50-ton hydraulic jack is used to apply the load to the pile. The displacement of the pile head during both compression and pullout loading conditions is measured using a digital gauge with an accuracy of 0.01 mm. Figures 5b and 5c illustrate the pullout and compression loading setups, respectively.



(a) **(b)** **(c)**

Fig. 5. Installation and loading setups; a) installation equipment, b) pullout setup, c) compressive setup

LOAD-DISPLACEMENT AND ANALYSIS

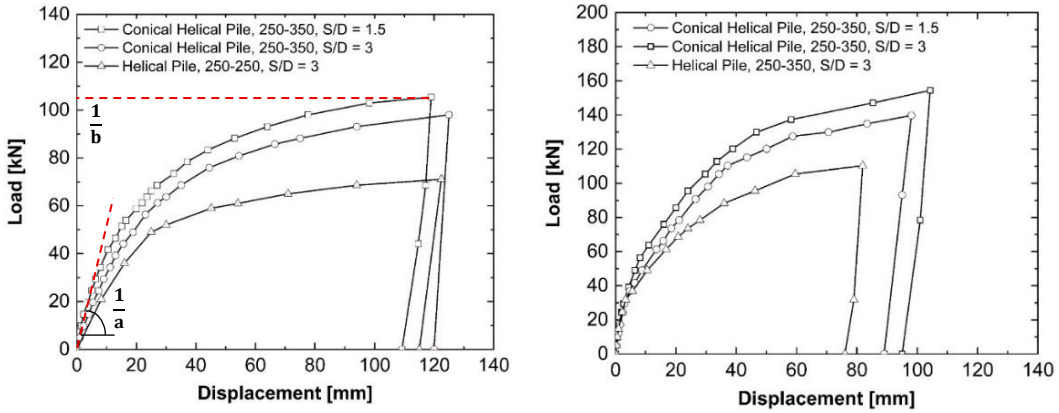
In this study, the ultimate load capacities of both helical and conical helical piles have been determined using four commonly used interpretation methods: Reese and O'Neill (1988), ISSMFE 1985 (ISSMFE 1985), Brinch-Hansen 80%, and maximum measured load. Figure 6 depicts the load-displacement of helical and conical helical piles under pullout and compressive loads. Table 2 details the ultimate load and corresponding displacement for the helical and conical piles under both pullout and compressive loading conditions. Additionally, the parameters 1/a, representing initial stiffness, and 1/b, representing the asymptotic or limit load, were determined by fitting the hyperbolic functions to these diagrams (Eslami and Ebrahimipour 2024; Arjmand et al., 2025), and are provided in Table 2 and Fig. 6. According to Fig. 6, and Table 2, under pullout loading, the Conical helical pile with dimensions 250-350 and an S/D of 1.5 exhibits the highest initial stiffness, limit load and maximum measured load, followed by the same Conical helical pile at an S/D of 3, and the Helical Pile with dimensions 250-250 at an S/D of 3. Conversely, in compressive loading, the Conical helical pile, 250-350, S/D = 3, demonstrates the greatest initial stiffness, limit load, and maximum measured load, followed by the Conical helical pile, 250-350, S/D = 1.5, and the Helical Pile, 250-250, S/D = 3. The increase in the 1/a ratio indicates enhanced initial stiffness against settlement, while the rise in the 1/b ratio signifies improved ultimate capacity. This enhancement can be attributed to a more advantageous stress distribution and more effective engagement of the surrounding soil with the conical helical pile.

Overall, the findings indicate that conical helical piles demonstrate superior pullout and compressive capacities, along with enhanced initial stiffness, when compared to typical helical piles for the research site and the piles examined.

According to Perko (2009), the disturbance factor (DF)—defined as the ratio of pullout to compression capacity—indicates that a higher DF ratio correlates with less disturbance during installation. The data presented in Table 2 confirm that the average DF for conical helical piles not only exceeds that of standard helical piles but also emphasizes that conical helical piles experience substantially less disturbance during installation at the research site.

RELIABILITY BASED ANALYSIS REGARDING INHERENT SOIL VARIABILITY

To assess the impact of inherent soil variability on the bearing capacity of helical piles, 100000 random shear strength parameters—specifically, cohesion (c) and friction angle (φ)—were generated using Monte Carlo Simulation (MCS). The bearing capacity of the examined helical piles was then predicted using two methods: (a) Individual plate bearing (Chance 2003) and (b) Cylindrical shear methods (CFEM 2006) and considering the effect of friction and cohesion, simultaneously. It was assumed that these parameters were inversely correlated, with a correlation coefficient of -0.5, and they followed a log-normal distribution (Eslami et al., 2016). The mean value and coefficient of variation (COV) for cohesion were determined to be 15 kPa and 25%, respectively, while the mean value and COV for the friction angle were found to be 30° and 10%, by the geotechnical site investigation report.



(a) **(b)**

Fig. 6. Load-displacement of helical and conical helical piles: a) pullout b) compression

Table 2. Ultimate load and relevant displacement for helical and conical helical piles

Piles ID		5% D		10% D		Brinch-Hansen 80% (1963)		Maximum Measured		Hyperbolic parameters	
		Load (kN)	δ (mm)	Load (kN)	δ (mm)	Load (kN)	δ (mm)	Load (kN)	δ (mm)	$\frac{1}{a}$	$\frac{1}{b}$
Pullout	CHP-1.5	45.6	12.5	66.1	25	112.6	219	105.4	119	5.8	123.9
	CHP-3	37.8	12.5	58.8	25	106.4	245	98	125	4.4	120.3
	HP-3	29.2	12.5	49	25	73.9	182.8	71	122.4	4.1	83.9
Compression	CHP-1.5	58.6	12.5	87.3	25	160	244	139.7	98	7.8	170.2
	CHP-3	67.4	12.5	97.5	25	171.7	212	154.4	104.2	9.4	178.9
	HP-3	52.9	12.5	74.81	25	121.1	189.3	110.3	81.9	8.3	126.4
Disturbance Factor	CHP-1.5	0.78		0.76		0.7		0.75		-	
	CHP-3	0.56		0.6		0.62		0.64		-	
	HP-3	0.55		0.65		0.61		0.64		-	

For each combination of cohesion (c) and friction angle (φ), the axial compression bearing capacity of the three investigated helical piles was predicted and compared with the ultimate bearing capacity of each pile based on various interpretation methods. To enhance the understanding of soil inherent variability, the model factor or resistance bias factor (λ_R)—defined as the ratio of measured to predicted capacity—

 © Deep Foundations Institute 2025

was calculated along with its statistical properties, as illustrated in Table 3. To calibrate the resistance factor for each helical pile, the combined dead and live loads were assessed using the AASHTO strength limit I framework (AASHTO, 2012) with the modified First Order Second Moment (FOSM) method (Heidarie Golafzani et al., 2020). According to AASHTO (2012), the dead (Q_D) and live (Q_L) load factors were established at 1.25 and 1.75, respectively. The bias and coefficient of variation (COV) for the log-normally distributed dead and live loads were assumed to be 1.05 (0.1) and 1.15 (0.2), respectively. The LRFD calibration was conducted for a Q_D/Q_L ratio of 3, with target reliability index set at 3, as recommended by Tang and Phoon (2018). Subsequently, the efficiency ratio (ER = φ/λ_R), which represents the ratio of the resistance factor to the bias resistance factor, and the actual factor of safety (AFS = FS*λ_R) were computed. The factor of safety (FS) is determined by calibrating the resistance factor through fitting to allowable stress design (ASD) (Allen, 2005; Heidarie Golafzani et al., 2020).

The bias ratios (λ_R) for both individual and cylindrical methods reveal a consistent underestimation of actual helical pile capacity, with mean values frequently exceeding unity across most interpretation methods. Figure 7 depicts a comparison of the model parameter ratio Q_m/Q_p between two analysis approaches—Individual and Cylindrical—across four load test interpretation methods: 5%D, 10%D, BH80%, and Max. The ratio indicates how closely the model-predicted capacity (Q_p) aligns with the interpreted bearing capacity from load tests (Q_m), with a value of 1 representing perfect agreement. Results show that both models overestimate capacity under the 5%D criterion, with increasing ratios toward the Max interpretation, where underestimation becomes more apparent—especially in the cylindrical model. The cylindrical approach consistently yields higher and more variable values than the individual model for all three investigated piles, particularly for the Brinch-Hansen 80% and Maximum measured criteria, highlighting the influence of the chosen interpretation method on perceived model accuracy and bias.

Table 3. The variation of bias resistance factor statistics for different load-displacement interpretation criteria

Piles ID	Statistics	Individual Plate Bearing Method				Cylindrical Shear Method			
		%5D	%10D	Brinch-Hansen80%	Maximum measured	%5D	%10D	Brinch-Hansen80%	Maximum measured
CHP-3	Mean (λ_R)	0.67	0.97	1.71	1.54	0.86	1.25	2.20	1.98
	COV	0.25				0.22			
CHP-1.5	Mean (λ_R)	0.55	0.82	1.50	1.31	0.84	1.25	2.29	2.00
	COV	0.25				0.21			
HP-3	Mean (λ_R)	0.53	0.75	1.21	1.10	0.71	1.00	1.61	1.47
	COV	0.25				0.22			

 © Deep Foundations Institute 2025

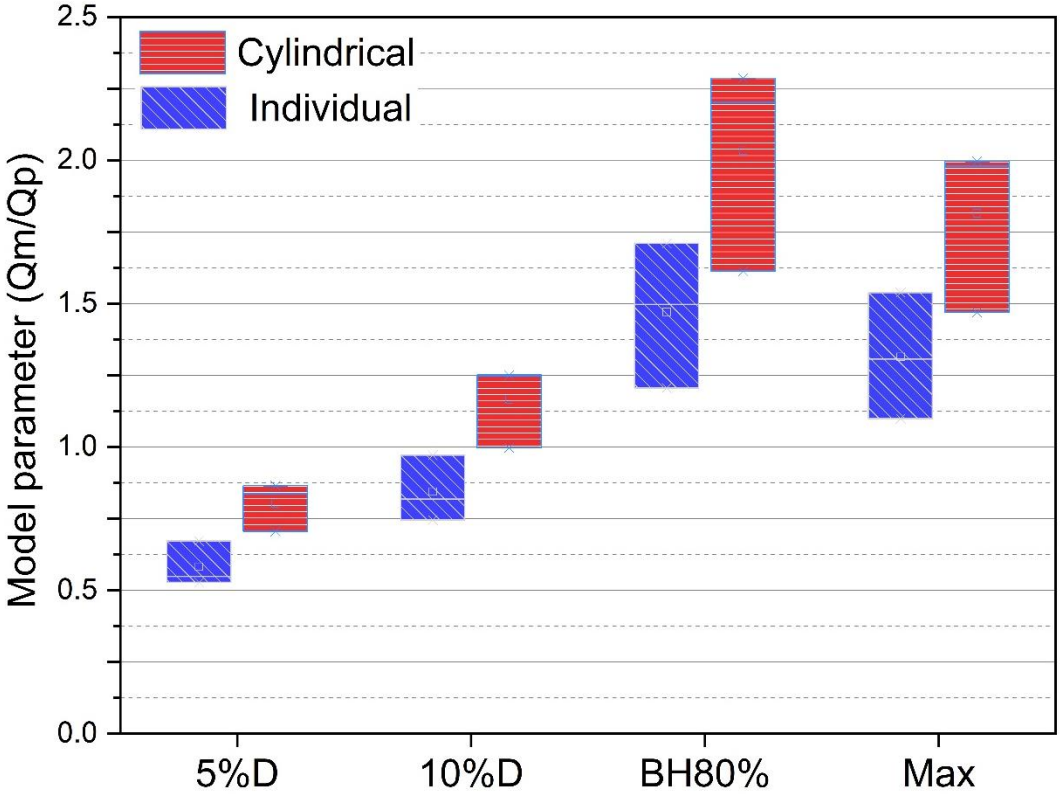
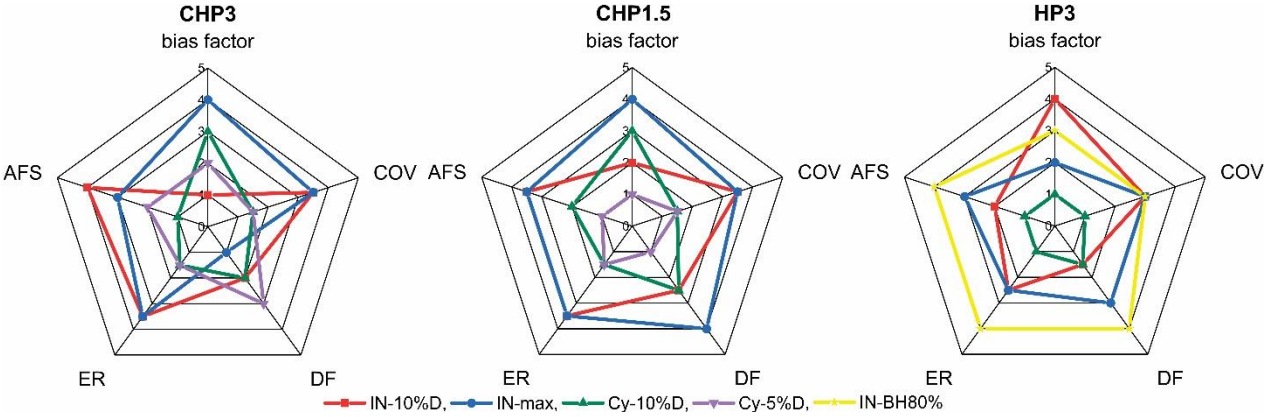


Fig. 7. Performance assessment of two implemented approaches for each criterion

Figure 8 illustrates a comparative performance analysis of four better interpretation criteria regarding Table 3, for three different pile types: CHP-3, CHP-1.5, and HP-3. The data is conveyed through radar charts, wherein each axis delineates a key performance attribute, including model bias factor (λ_R), coefficient of variation (COV), disturbance factor (DF), efficiency ratio (ER), and actual factor of safety (AFS). This analysis aims to achieve a reliability index of $\beta = 3$. In each radar plot, smaller polygon areas indicate better overall performance, meaning that the interpretation method leads to more accurate, consistent, and efficient design outcomes. For the conical pile with S/D = 3 (CHP-3), the cylindrical shear method under the 10%D criterion yields the most favorable results, followed by other methods with larger polygon areas, indicating relatively weaker performance.

For the conical pile with S/D = 1.5 (CHP-1.5), the 5%D criterion, combined with the cylindrical approach, yields the best performance, highlighting the effectiveness of this low-displacement threshold in minimizing uncertainty and maximizing safety. Similarly, for the standard helical pile HP-3, the cylindrical method, under the 10%D criterion, again delivers the best balance among all five evaluated parameters. Figure 8 highlights that cylindrical shear methods consistently outperform the individual plate bearing approach across different investigated pile configurations and at the research site. It also demonstrates the critical role of selecting appropriate interpretation criteria—particularly those based on smaller displacement thresholds—for achieving reliable, efficient, and disturbance-minimizing foundation designs.

 © Deep Foundations Institute 2025



(a) (b) (c)

Fig. 8. Comparing the performance of different interpretation criteria for (a) CHP-3, (b) CHP-1.5 and (c) HP-3

CONCLUSIONS

This study investigated the geotechnical performance and reliability of helical and conical helical piles through full-scale field tests and reliability-based analysis, addressing both load-bearing behavior and the influence of inherent soil variability. The research focused on two key geometric parameters: the helix configuration (typical vs. conical) and the spacing-to-diameter ratio (S/D = 1.5 and 3). A total of six full-scale axial load tests (compression and pullout) were conducted on three pile types—standard helical and two conical helical variants—installed at a coastal site characterized by stratified sandy soils. The piles' performance was evaluated using multiple load-displacement interpretation methods (5%D, 10%D, Brinch-Hansen 80%, and Maximum Measured), and their ultimate capacities were compared through both deterministic and probabilistic approaches. The significant findings are as follows for the investigated helical piles in the research study area:

- The results confirm that conical helical piles substantially outperform standard helical piles in terms of both initial stiffness and ultimate load capacity under pullout and compressive loads. Notably, the CHP-1.5 pile demonstrated the best pullout resistance, while CHP-3 performed superiorly in compression, indicating that optimized conical geometry combined with appropriate S/D ratios enhances axial capacity and minimizes installation-induced disturbance.
- Monte Carlo simulations incorporating correlated shear strength variability revealed that the cylindrical shear method provides a more conservative and reliable prediction of pile capacity compared to the individual plate bearing approach. Furthermore, performance metrics such as bias factor, efficiency ratio, and actual factor of safety confirmed the superiority of cylindrical methods, particularly when combined with lower displacement-based interpretation criteria (5%D and 10%D).

Eventually, this research highlights the benefits of geometric enhancement through conical helices as a viable alternative, underscoring the importance of selecting suitable interpretation and design methods that account for both field variability and reliability performance. These findings contribute to advancing the design framework for helical foundation systems, particularly in offshore and coastal environments where minimizing soil disturbance and ensuring load predictability are critical.

REFERENCES

AASHTO. 2012. AASHTO LRFD bridge design specifications. 6th ed. Washington, DC: AASHTO.

Allen, T.M., Nowak, A.S. and Bathurst, R.J., 2005. Calibration to determine load and resistance factors for geotechnical and structural design. *Transportation Research Circular*, (E-C079).

 © Deep Foundations Institute 2025

Arjmand, A., Eslami, A., Ebrahimian, P., Golafzani, S.H. and Ebrahimipour, A., 2025. Appraisal of load-displacement behavior of granular Columns: Data-Centric approach. *Ocean Engineering*, *339*, p.122110.

Bak, H.M., Halabian, A.M., Hashemolhosseini, H. and Rowshanzamir, M., 2021. Axial response and material efficiency of tapered helical piles. *Journal of Rock Mechanics and Geotechnical Engineering*, *13*(1), pp.176-187.

Byrne, BW, and GT Houlsby. 2015. Helical piles: an innovative foundation design option for offshore wind turbines. *Philosophical Transactions of the Royal Society A: Mathematical, Physical and Engineering Sciences* 373 (2035):20140081.

Canadian Geotechnical Society. 2006. Canadian Foundation Engineering Manual (4th ed.). Canadian Geotechnical Society

CHANCE®. 2003. Civil Construction Helical Systems CC Catalogue. Centralis, Missouri, USA. On CD.

Ebrahimipour, Amirhossein, and Abolfazl Eslami. 2024. Analytical study of piles behavior for marine challenging substructures. *Ocean Engineering* 292:11651.4

Eslami, Abolfazl, and Bengt H Fellenius. 1997. Pile capacity by direct CPT and CPTu methods applied to 102 case histories. *Canadian Geotechnical Journal* 34 (6):886-904.

Eslami, A., Heidarie Golafzani, S. and Jamshidi Chenari, R., 2016. Assessment of Babolsar concrete pedestrian bridge failure for 1964 flood event and retrofitting practice. *Engineering Failure Analysis*, *68*, pp.101-112.

Eslami, Abolfazl, and Amirhossein Ebrahimipour. 2024. Load-displacement appraisal and analysis for driven piles; a data-centric approach. *Computers and Geotechnics*, 171, 106377.

Eslami, A., Ebrahimipour, A., Imani, M., Imam, R., Mo, P., 2025. Form and load transfer aspects of foundation systems: case-based implementation and adaptation for buildings. Deep Undergr. Sci. Eng 1–17. https://doi.org/10.1002/dug2.12146.

Esmailzade, M. and Eslami, A., 2025. Experimental study on performance and enhanced methods of helical piles using Frustum Confining Vessel in Anzali Sand. Ocean Engineering, 324, p.120624.

Fahmy, A. and El Naggar, M.H., 2017. Axial performance of helical tapered piles in sand. *Geotechnical and Geological Engineering*, 35, pp.1549-1576.

Fateh, Amir Mansour Askari, Abolfazl Eslami, and Ahmad Fahimifar. 2017. Study of soil disturbance effect on bearing capacity of helical pile by experimental modelling in FCV. *International Journal of Geotechnical Engineering* 11 (3):289-301.

Gallant, Aaron. 2020. Assessing Helical Anchors for Aquaculture Applications.

Ghazavi, Mahmoud, Yasaman Ghomi, Parisa Heidari, and Bahram Mohammadzadeh Jelogir. 2023. "Effects of helix shapes and locations on compression capacity of helical piles for offshore foundations." *Marine Georesources & Geotechnology* 41. 634-647

Hansen, J Brinch. 1963. Discussion of “Hyperbolic stress-strain response: cohesive soils”. *Journal of the Soil Mechanics and Foundations Division* 89 (4):241-242.

Heidarie Golafzani, S., Eslami, A. and Jamshidi Chenari, R., 2020. Probabilistic assessment of model uncertainty for prediction of pile foundation bearing capacity; static analysis, SPT and CPT-based methods. *Geotechnical and Geological Engineering*, *38*(5), pp.5023-5041.

ISSMFE Subcommittee on, Field and Laboratory Testing. 1985. Axial pile loading test—Part 1: Static loading. *Geotechnical Testing Journal* 8 (2):79-90.

Lutenegger, Alan J. 2011a. Historical development of iron screw-pile foundations: 1836–1900. *The International Journal for the History of Engineering & Technology* 81 (1):108-128.

Lutenegger, Alan J. 2011b. Behavior of multi-helix screw anchors in sand. In *Proceedings of the 14th Pan-American Conference on Soil Mechanics and Geotechnical Engineering*.

Mansour, Mohamed A, and M Hesham El Naggar. 2022. Optimization of grouting method and axial performance of pressure-grouted helical piles. *Canadian Geotechnical Journal* 59 (5):702-714.

Nabizadeh, Farhad, and Asskar Janalizadeh Choobbasti .2017. The performance of grouted and un-grouted helical piles in sand. *International Journal of Geotechnical Engineering.*

Nazmi, Mostafa, and Abolfazl Eslami. 2025. Conical helical piles behavior assessment through physical modeling and field testing. *Transportaion Infrastructure Geotechnology*. https://doi.org/10.1007/s40515-025-00601-z

Perko, Howard A. 2009. *Helical piles: a practical guide to design and installation*: John Wiley & Sons.

Phoon, Kok-Kwang, and Fred H, Kulhawy., 1999a. Characterization of geotechnical variability. *Canadian Geotechnical Journal*. https://doi.org/10.1139/t99-038

Phoon, Kok-Kwang, and Fred H, Kulhawy., 1999b. Evaluation of geotechnical property variability. *Canadian Geotechnical Journal*. https://doi.org/10.1139/t99-039

Shojaei, Ebrahim, Abolfazl Eslami, and Navid Ganjian. 2019. "Self-expanded piles: A new approach to unconventional piles development. *Marine Georesources & Geotechnology* 39 (1):115-128.

Spagnoli, G. 2013. "Some considerations regarding the use of helical piles as foundation for offshore structures." *Soil mechanics and foundation engineering* 50 (3):102-110.

Spagnoli, Giovanni, and Cristina de Hollanda Cavalcanti Tsuha. 2020. A review on the behavior of helical piles as a potential offshore foundation system. *Marine Georesources & Geotechnology* 38 (9):1013-1036

Standard Test Method for Standard Penetration Test (SPT) and Split-Barrel Sampling of Soils ," ASTM D1586/D1586M-18e1, ASTM International, 2022.

Standard Test Method for Particle-Size Analysis of Soils," ASTM D 422 – 63, ASTM International, 2002.

Tang, C. and Phoon, K.K., 2018. Statistics of model factors and consideration in reliability-based design of axially loaded helical piles. *Journal of geotechnical and geoenvironmental engineering*, *144*(8), p.04018050.

Tsuha, C.D.H.C., dos Santos Filho, J.M.S.M. and Santos, T.D.C., 2015. Helical piles in unsaturated structured soil: a case study. *Canadian Geotechnical Journal*, *53*(1), pp.103-117.

Tsuha, Cristina de Hollanda Cavalcanti, Nelson Aoki, Gérard Rault, Luc Thorel, and Jacques Garnier. 2012. "Evaluation of the efficiencies of helical anchor plates in sand by centrifuge model tests." *Canadian Geotechnical Journal* 49 (9):1102-1114

 © Deep Foundations Institute 2025

BENEFITS OF CONSTRUCTION INFORMATION MANAGEMENT SYSTEMS (CIMS) APPLIED TO A LARGE DEEP SOIL MIXING PROJECT

Will Tanner, Geosyntec Consultants, Inc., Kennesaw, GA 30144, 770-789-6563, wtanner@geosyntec.com
Mohamed Elgouhary, Treviicos, Charlestown, MA 02129, 617-594-1780, melgouhary@treviicos.com
Bhrugesh Patel, Geosyntec Consultants, Inc., Toronto, ON, 416-306-8317, bpatel@geosyntec.com

ABSTRACT

As a part of the process of environmental site closure, an industrial waste impoundment required the construction of a large gravity earth retention system built from the top-down using the deep mixing method (DMM). The earth retention system (DMM Wall) is 3,155 feet long and consists of 4,613 individual DMM columns arranged in a cellular configuration, installed to a maximum depth of 83 feet. The project team utilized a construction information management system (CIMS) with customized automated processes to: (i) rapidly prepare as-built reports; (ii) track the constructed position of each DMM column in three dimensions and perform calculations regarding verticality and overlap with adjacent columns; and (iii) collect and display other QA/QC data such as unconfined compressive strength. CIMS process outputs were displayed in near real-time on a data management and visualization platform. CIMS allowed for expedited acceptance of DMM columns and rapid identification, evaluation and resolution of over 50 non-conformities resulting in uninterrupted construction workflow and no schedule delays.

BACKGROUND

An existing industrial waste basin is closing by relocating most of the waste material to an onsite lateral landfill expansion. The removal of the waste material in the basin requires the construction of a large retention structure to support an existing landfill, which occupies a portion of the basin footprint, while excavation of waste material progresses in the open basin. The retaining structure has a maximum height of 80-ft and extends over 3,000-ft in length. The retaining structure was designed as a gravity retaining system using the Deep Mixing Method (DMM) in the waste material deposit. The total volume of DMM materials within the structure is approximately 620,000 cubic yards and consists of over 4,600, 8-ft diameter, individual DMM elements.

REPORTING REQUIREMENTS

Project reporting requirements included submission of three dimensional positional, geometric, and other operational data for each individual DMM element including calculations for verticality and overlap with adjacent columns within 72-hours of the end of each workday. Given the large number of DMM elements and high daily production, the contractual reporting timeframe created a challenge for typical more manual-based data post-processing. During construction it became apparent that the only way to meet these reporting requirements was to move to a more automated data processing and report system. Therefore, Treviicos teamed up with Geosyntec to create a Construction Information Management System (CIMS) to address this need.

CONSTRUCTION DATA SOURCES AND INITIAL MANUAL PROCESSING

The project generated various types of data which were initially all managed manually. The center of the data was an Excel file with over ten worksheets including data for columns' design and as-built information, grout plant information, summary data, survey instruments data, etc. The master sheet included all raw and calculated information associated with each column such as column location, depth, diameter, drilling phase date and times, grout mix, injected grout volume, etc. The data arrived

 © Deep Foundations Institute 2025

fragmented from various instruments and field logs where engineers and technicians manually transcribed and copied them into the Excel file. This was further complicated by staggered data entry for each given column due to their various sources, and corresponding quality control processes.

The subsequent challenge involved various data analyses needed for the final column reports. This included verticality and overlap checks at one foot depth intervals, theoretical and actual injected grout volume calculations, tip and top treatment depth calculations, blade rotation number calculations, a QA/QC checklist, wet grab sample results, obstruction reports, associated photos, etc.

Compliance with the project requirements demanded that the DMM Contractor compile all these items into a single submission package as a final column report for approval from the Owner. Manually compiling, processing, and calculating the information and generating the necessary reports for high daily production would have been unachievable without a team of individuals exclusively tasked with data management.

CIMS IMPLEMENTATION

Automation of processes and workflows from a single source is a major advantage of CIMS, as shown conceptually in Fig. 1. For this project, the CIMS consisted of four elements: (i) an Enterprise Database (EDB); (ii) data collection using electronic field forms; (iii) a system of automated and semi-automated data processing pipelines; and (iv) a reporting platform.



Fig. 1. SharePoint Site as a platform for data entry, storage and centralization.

Enterprise Database

The first step involved collection and centralization of data coming from the field to create a "single source of truth", or an EDB. This is a vital step in the creation of any IMS and consists of storing all raw data in a single location to minimize the risk associated with versioning and fragmentation of the data. Importantly, Excel file data management does not address this risk. Therefore, the authors created an SQL server database to store all project related data. This allowed processing of large amounts of data at very high speed, which was critical to the project.

Data Collection – Electronic Field Forms

The next steps involved getting the data from the field into the EDB. Electronic field forms designed using off-the-shelf technology, such as Survey123 (see Fig. 2), streamlined this process. The electronic field forms compiled information such as location, rig used, mix design, top and bottom treatment information, column deviation, grout volume, obstructions, and relevant photographs. The field forms had some clear advantages like cost effective design and deployment time, full customization, and data logic support such as default values, calculations, data validation and design data displayed alongside collected

user data for basic quality control. Field personnel used these forms with ease which supported accurate and seamless data transition.

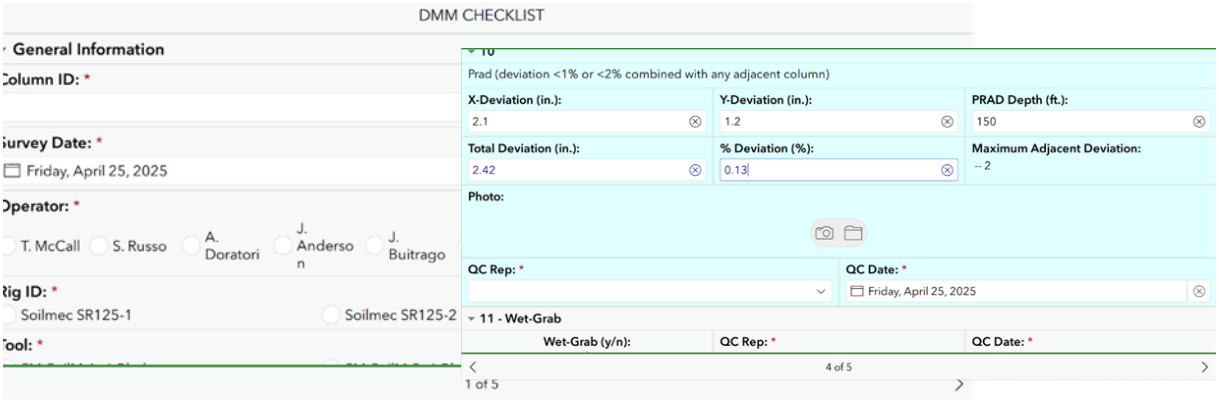


Fig. 2. Custom electronic field form for data collection and live calculations.

Automated Data Pipelines

While some field data were collected using electronic field forms apps, others, such as verticality data, were being generated in CSV format and as-built information for a column was being extracted from the rigs and added manually into an Excel sheet. Still other information was being generated by software in PDF reports. Therefore, the authors designed and implemented automated data pipelines to process the data coming from the field by various methods.

All data files were uploaded to a OneDrive cloud folder to organize and share. The automated data pipelines extracted these data files, processed the data to perform necessary calculations, reformatted the data and uploaded them to the EDB in appropriate structures. These pipelines were set to execute at a set interval throughout the day to capture any new information available.

Reporting Platform

The primary objective of the CIMS system was the production of a complete column report for each column in accordance with the 72-hour window established in the specifications. Each report consisted of many components such as: (i) a DMM column report; (ii) a rig drilling report; (iii) column identification and construction notes; (iv) a grout volume report; (v) a verticality report; (vi) an overlap report; (vii) and other various pieces of data such as testing data, etc. Given that the final report combined data from multiple sources (i.e., drill rigs, field forms, etc.), the CIMS was designed to automatically integrate the multiple data streams. The responsibilities of the contractor were reduced to uploading the rig generated PDFs and data files to the shared cloud drive and submitting field collection data entered into the electronic field forms.

The final manual step consisted of alerting the CIMS that a final report could be generated by marking a column as “ready”. This step was built into the process since the comprehensive data sets could vary slightly from one column to another. Once the column was marked “ready”, the CIMS would automatically generate the report. Parts of an example report are shown in Figs. 3 through 6. This step also supported an on-demand report generation option in case a report needed to be regenerated.

 © Deep Foundations Institute 2025

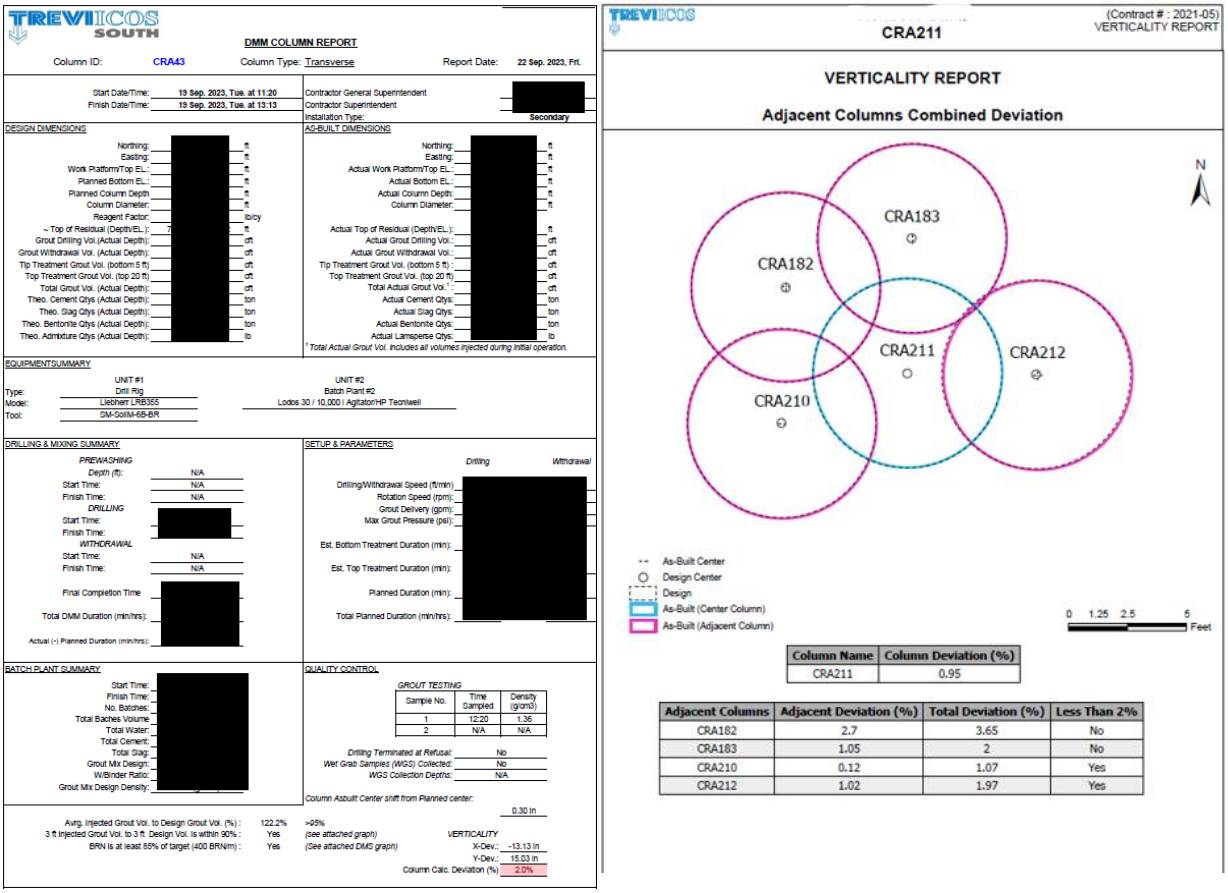


Fig. 3. Typical column report.

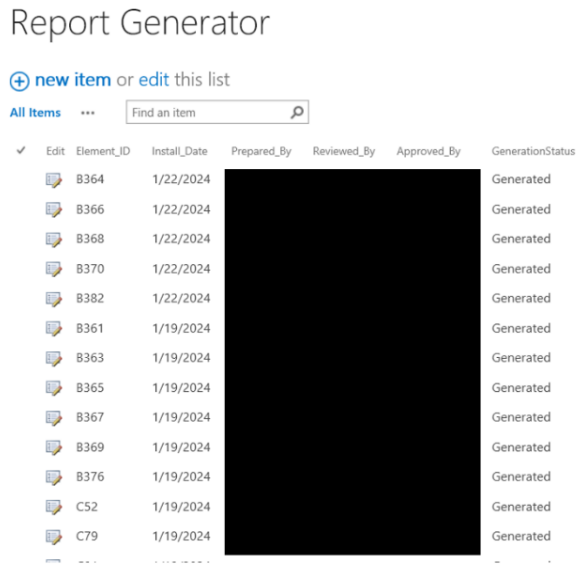


Fig. 4. On demand report generation form.

 © Deep Foundations Institute 2025

TREVIICOS SOUTH

DMM OBSTRUCTION

Column ID: A48 **Report Date:** 06-01-2023

OBSTRUCTION SUMMARY

Installed On: 06-01-2023	**Work Platform El:** 479.1
Obstruction Top EL: None	**Obstruction Bottom EL:** None
Top of Obstruction Depth: None	**Bottom of obstruction Depth:** None
~ Obstruction Start Time: 11:17	**~ Obstruction Stop Time:** None
Obstruction Material: Plastic/ Rubber mat	
Remarks: Plastic/ rubber mat attached on tool from unknown depth after withdrawal.	

OBSTRUCTION PHOTOS



Fig. 5. Obstruction report.

TREVIICOS SOUTH

DMM CHECKLIST

GENERAL INFORMATION	
Column ID: CRA43	Survey Date: 2023-09-19
Operator: [redacted]	Rig ID: LiebherrLRB355
Tool: SM-SoilM-6B-BR;6Blades;BottomRing	
Design Northing: 993628.6	Design Easting: 1981114.597
Design Elevation (ft): 479.9	Design Depth (ft): 77.7
Adjacent Depths	
Construction Sequence Type: Secondary	
Mix Design: 240-50L-150-2B-06L	
Avg. Adjacent Residual Depth (ft): 74.95	Avg. Adjacent Final Depth (ft): 82.25
Max. Adjacent Residual Depth (ft): 75.5	Max. Adjacent Final Depth (ft): 83
Min. Adjacent Residual Depth (ft): 74.4	Min. Adjacent Final Depth (ft): 81.5
QC Rep: [redacted]	QC Date: 2023-09-19
As-built Information	
Real-time Readings from Leica MC1 display at start of column.	
Northing: 993628.56	Easting: 1981114.56
Heading (degrees): 319.24	Elevation (ft): 480.33
Is element < 2" from Design? (as indicated by Leica): yes	
Leica Photo: No Section 2 Photo	
QC Rep: [redacted]	QC Date: 2023-09-19
PRE-WASH	
Pre-Wash Available? no	
Start Time: / End Time: / Depth (ft):	
QC Rep:	QC Date:
DRILL MIXING PHASE	
Start Time: 11:20	End Time: 13:01

Fig. 6. DMM checklist.

ADDITIONAL AUTOMATED PROCESSES USING CIMS DATA

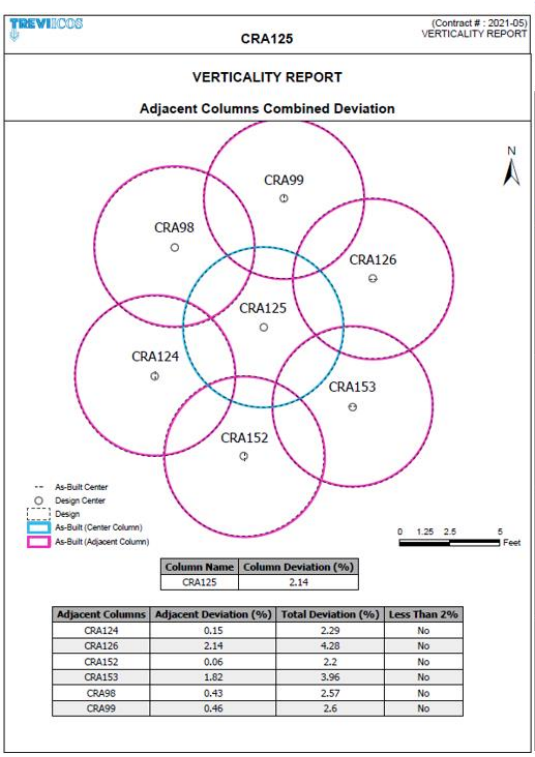
In addition to the basic design and function of the CIMS as discussed above, the authors established several other automated processes to enhance the presentation and interpretation of important data. These processes included: (i) DMM column verticality and overlap with adjacent columns; (ii) grout volume evaluation; (iii) a weekly construction progress report; (iv) a live interactive web map; and (v) a reporting dashboard used exclusively by the DMM contractor to perform quality control in real time.

DMM Column Verticality and Overlap

One of the most important components of the column report was verticality and overlap analysis. The specifications required that each column meet at least one of the following three conditions: (i) maintain a vertical alignment of less than or equal to one percent deviation from vertical; or (ii) maintain contact at the column base with each adjacent column; or (iii) any two adjacent columns shall have a maximum combined deviation from vertical of two percent in aggregate. These calculation results had to be reported at a maximum interval of 5 feet in depth.

Typically, this would be achieved using CAD drawings of as-built column data but in this case the production of drawings was not possible within the reporting time limit. To overcome this problem, the authors wrote algorithms into the report generation that used the data available in the EDB to perform verticality as well as overlap calculations. By combining Geographical Information Software (GIS) with the EDB these automated scripts calculated the verticality and generated the overlap report for each column. The reports showed the design placement, as built placement, vertical deviation and adjacent

column overlap every 5 feet in depth. If necessary, these automated calculations could be performed at 1-foot intervals. Examples of the results are shown in Figs. 7 through 9.



Column Name	Column Deviation (%)
CRA125	2.14

Adjacent Columns	Adjacent Deviation (%)	Total Deviation (%)	Less Than 2%
CRA124	0.15	2.29	No
CRA126	2.14	4.28	No
CRA152	0.06	2.2	No
CRA153	1.82	3.96	No
CRA98	0.43	2.57	No
CRA99	0.46	2.6	No

Fig. 7. Overlap report.

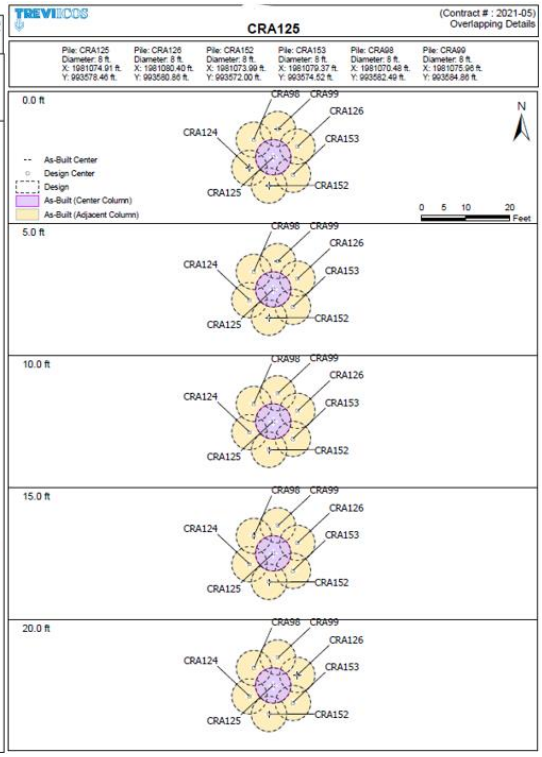
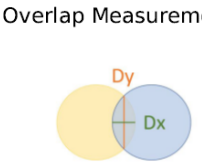


Fig. 8. Overlap report showing 5 ft cuts.



Element ID	Adj. Element ID	Depth (ft)	Dx (ft)	Dy (ft)
A136	A126	0.0	1.74	4.98
A136	A126	5.0	1.75	4.99
A136	A126	10.0	1.79	5.04
A136	A126	15.0	1.84	5.11
A136	A126	20.0	1.88	5.16
A136	A126	25.0	1.93	5.2
A136	A126	30.0	1.98	5.27
A136	A126	35.0	2.04	5.33
A136	A126	38.19	2.08	5.38

Fig. 9. Overlap values table.

Grout Volume Evaluation

In addition to verticality and overlap, the specifications required a check on the injected grout volume versus the theoretical grout volume and generate a graphical representation report to demonstrate that the average injected grout volume is greater than or equal to 95 percent of the theoretical volume for the entire column and greater than or equal to 90 percent for any 3-foot interval of the DMM column length.

 © Deep Foundations Institute 2025

The authors defined an automated process within CIMS to import raw data from the drill rigs and generate the graphs. A sample is shown below in Fig. 10.

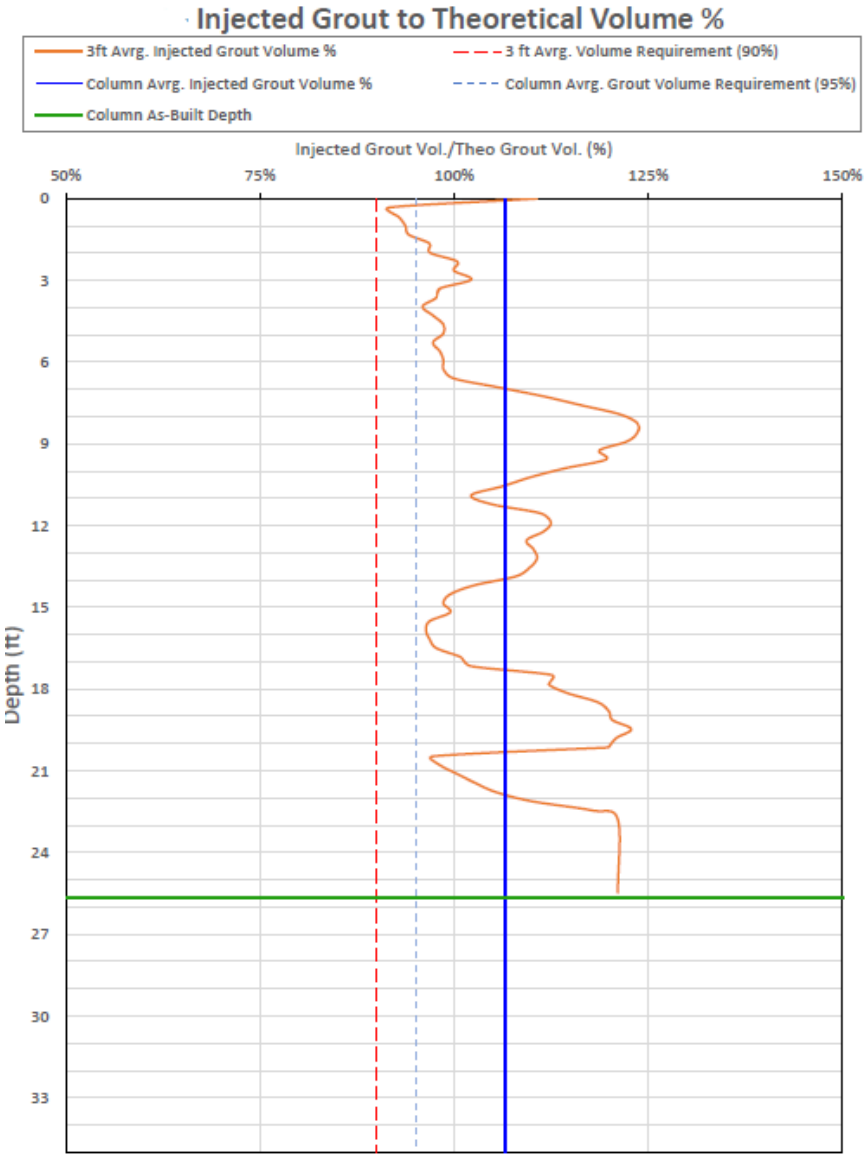


Fig. 10. Grout volume report.

Weekly Construction Progress Report

Another submission consisted of a weekly construction progress drawing report, shown in Fig. 11, for each zone of the overall DMM structure. The figure shows proposed columns and constructed columns to graphically summarize construction progress in plan view. It also displays the locations where verification coring was performed, and wet grab samples taken.

 © Deep Foundations Institute 2025

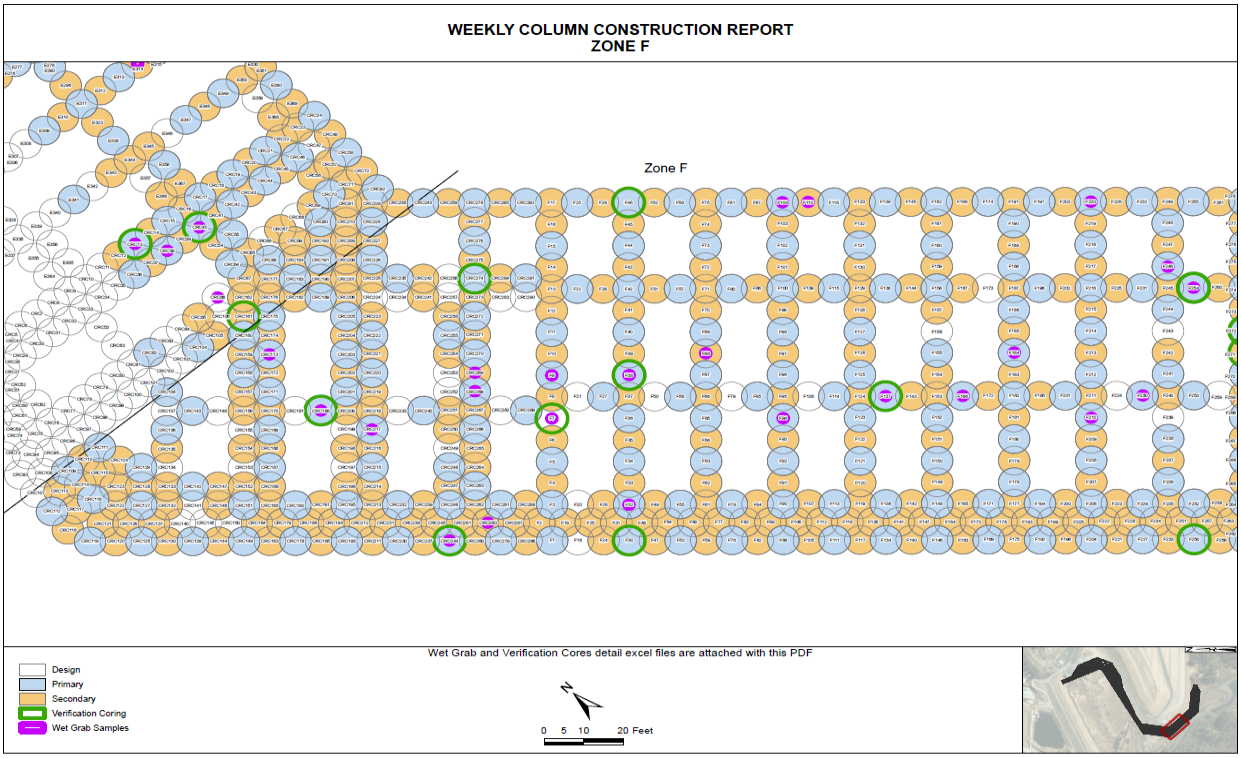


Fig. 11. Weekly construction progress report.

Live Web Map

Beyond the automated reports, CIMS had one more critical system consisting of a live web map, a screenshot of which is shown in Fig. 12. The web map showed all columns on an interactive platform along with data such as design placement, as-built placement, cross sections of each column at every 5-feet in depth, overlap information, verification coring placement, wet grab sampling, boring locations and depth targeting map. The web map was connected to the database which allowed it to show the construction data within an hour of receiving them. The web map served as a single interface comprehensive summary for construction progress and was used extensively by the design team to evaluate nonconformities and RFI's in near real-time.

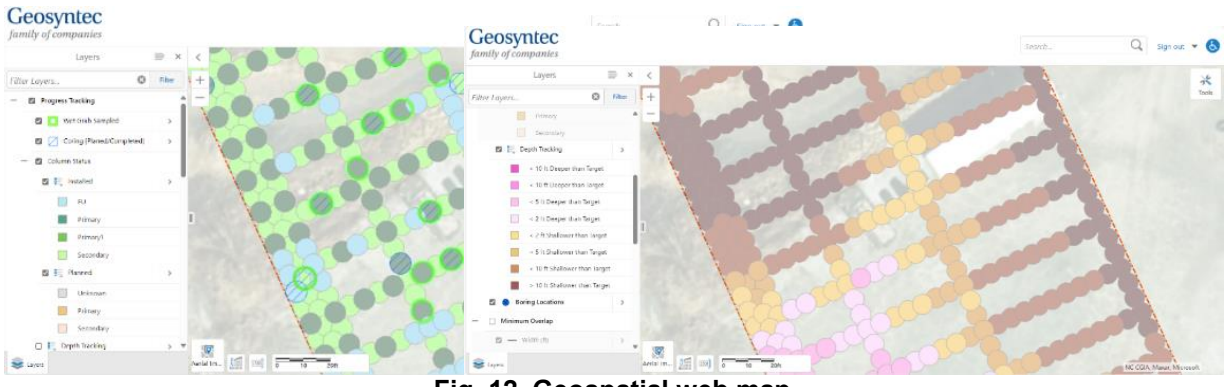


Fig. 12. Geospatial web map.

 © Deep Foundations Institute 2025

Reporting Dashboard for Contractor Quality Control

The final automated process using CIMS consisted of a web-based reporting dashboard (Fig. 13). The dashboard was not part of reporting requirement but was used by the contractor to track progress. The dashboard included various reports presented at different levels (i.e., in details or as a summary) including daily and cumulative construction progress, verticality and QC testing summary data. The dashboard provided all of the contractor's team members with real-time status progress.

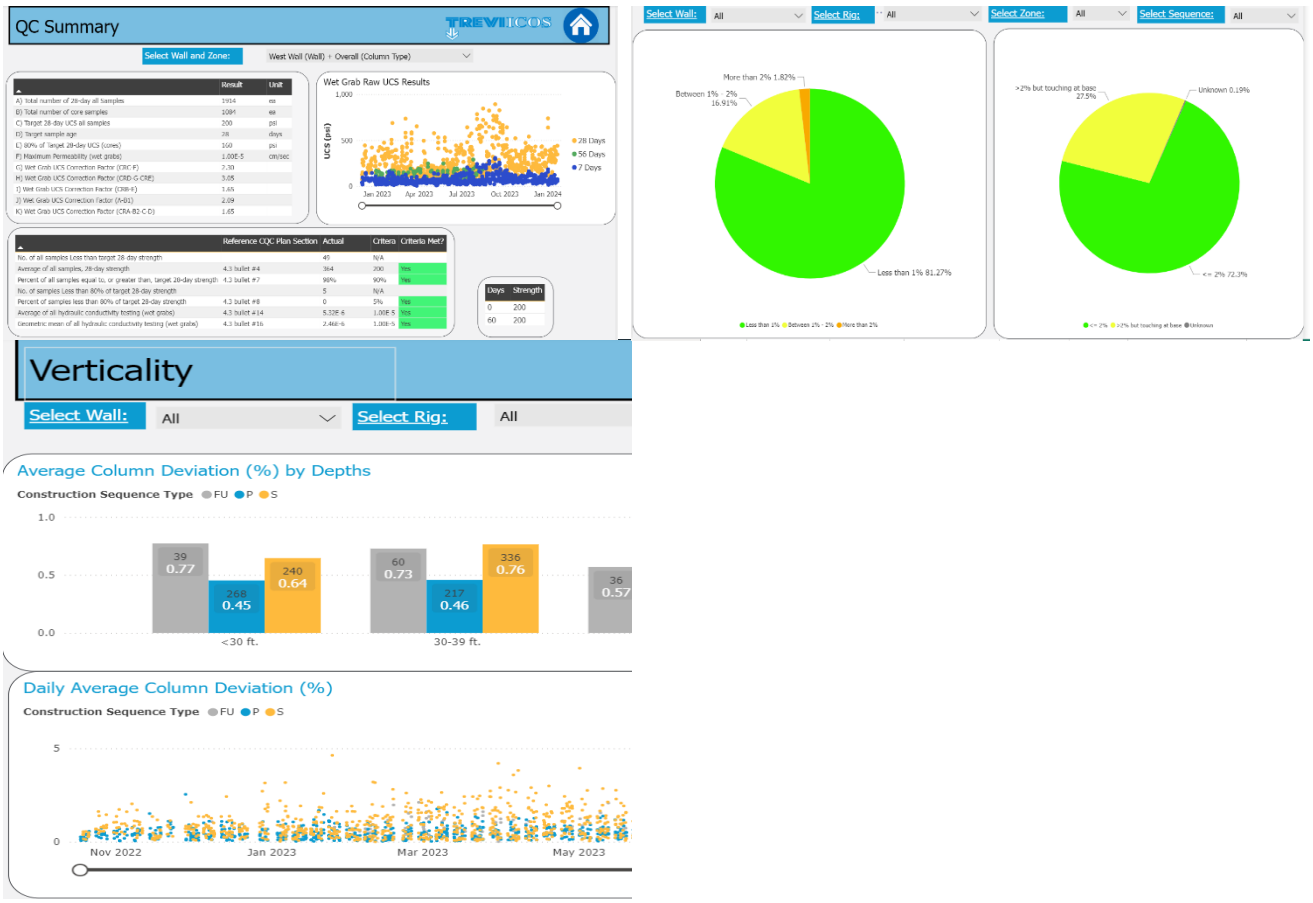


Fig. 13. QC summary.

CONCLUSIONS AND RECOMMENDATIONS

The CIMS provided tremendous support in keeping the project on track within its strict timeline and reporting requirements (e.g., column report, verticality analysis, overlap report, and weekly progress report), which would have otherwise significantly impeded progress. It enabled the QC team to perform their tasks in a more efficient fashion and allowed the team to examine and analyze data rather than focusing on data entry, collection and processing. It offered significant value by automating data collection, processing, and reporting, thereby saving time and reducing errors. The system ensured that data was accurate, reliable, and easily accessible, which was crucial for meeting the project's stringent reporting requirements. It allowed for rapid engineering review, assessment and acceptance of the overall structure based on the as-built condition. Additionally, the CIMS offered valuable insights beyond the requirements through a dashboard that provided real-time updates on field production progress and QC data statistics during construction.

APPLICATION OF AUGER CAST-IN-PLACE (ACIP) PILES IN URBAN INFRASTRUCTURE: A CASE STUDY OF PHILADELPHIA'S SAMUEL S. BAXTER WATER TREATMENT PLANT

Michael Whelan, P.E., Assistant Manager of Facilities Design, Philadelphia Water Department (PWD), Philadelphia, PA, USA, (215) 685-6300, michael.whelan@phila.gov

Abhijit R. Sheth, P.E., Principal Geotechnical Engineer, GFT, Valley Forge, PA, USA, (610) 783-3853, asheth@gftinc.com

Michael D. Bennett, P.E., Doctoral Student, Virginia Tech, Blacksburg, VA, USA, (540) 231-6635, mdb927@vt.edu; formerly Project Geotechnical Engineer, GFT, Valley Forge, PA, USA

Timothy J. Brennan, P.E., Principal Project Manager, GFT, Valley Forge, PA, USA, (610) 783-3751, tbrennan@gftinc.com

NOTE: On April 28, 2025, Gannett Fleming, Inc. and TranSystems rebranded as GFT Infrastructure, Inc. (GFT) following their merger. Gannett Fleming performed all project activities described in this paper prior to the merger.

ABSTRACT

The reconstruction of Clear Well Basins (CWB's) 3 and 4 at the Philadelphia Water Department's (PWD's) Baxter Water Treatment Plant exemplifies the robust use of auger cast-in-place (ACIP) piles for urban infrastructure. The Plant sits along the Delaware River near Philadelphia's northeast boundary and has supplied drinking water to the city for over 100 years. Increasingly stringent water treatment standards and aging facilities have made upgrades necessary. The new CWB's are side-by-side underground 5-million-gallon cast-in-place concrete water storage basins. Geotechnical investigations of the site revealed challenges such as deep alluvial deposits, a high groundwater table and buoyant uplift forces, widely variable weathering of the underlying Wissahickon Formation, and potential impacts on the adjacent foundations of recently constructed CWB's 1 and 2. Ultimately, the project team selected a foundation design for CWB's 3 and 4 that utilized approximately 2,100 ACIP piles, many socketed into weathered Wissahickon schist. The case study examines the advantages of ACIP piles in complex geotechnical conditions, focusing on pile design, load testing, construction monitoring, and installation challenges. It also highlights the importance of robust QA/QC procedures, effective stakeholder management, and comprehensive planning and coordination in successfully delivering a critical infrastructure upgrade.

Keywords: Auger cast-in-place (ACIP) piles, infrastructure, weathered rock, load test, QA/QC

INTRODUCTION AND PROJECT HISTORY

PWD operates three water treatment facilities to ensure a reliable water supply for the City of Philadelphia, Pennsylvania. These facilities are strategically designed for system flexibility and redundancy. The Queen Lane and Belmont Water Treatment Plants draw water from the Schuylkill River, while the Samuel S. Baxter Water Treatment Plant draws from the Delaware River. The largest of the three plants, the Baxter Plant plays a critical role supplying approximately 60 percent of the city's drinking water with the capacity to supply 100 percent if needed.



Fig. 1. Aerial site location map.

 © Deep Foundations Institute 2025

Upgrades to the Baxter Plant have included the construction of four new Clear Well Basins (CWB's) in a multi-phase program to replace the facilities' original clear well basin constructed in 1902. Construction of CWB's 1 and 2 was completed in 2022 as the design of CWB's 3 and 4 was completed. The CWB's 3 and 4 project site is located along Pennypack Street adjacent to the Delaware River in Philadelphia, Pennsylvania. The Aerial Site Location Map is shown in Fig. 1.

Clear Well Basins (CWB's) 3 and 4

The site of the four new clear well basins was historically occupied by the Baxter Plant's prefilters, a relic of former treatment processes, prior to their demolition in 2014. The bottom of the prefilter basins were approximately El. 220 (PWD datum, feet) with the ground surface around El. 234. The site was then used as a stockpile for material excavated during the construction of CWB's 1 and 2. The site is bounded by CWB 2 to the north, a private gun club to the south, a PWD residuals lagoon to the east and a PWD access road to the west. Figure 2 shows an overall Site Plan of the CWB's 3 and 4 site.

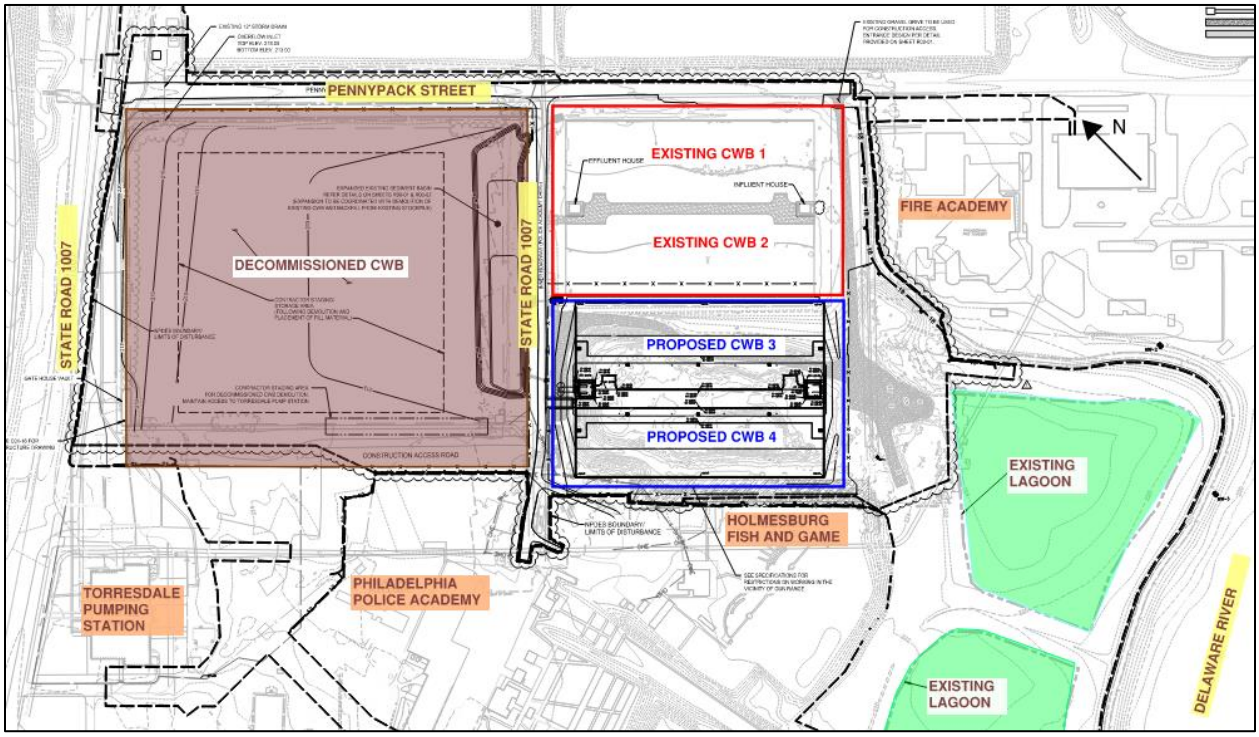


Fig. 2. Site plan of CWB's 3 and 4.

CWB's 3 and 4, like CWB's 1 and 2, consist of two 5-million-gallon side-by-side below-ground cast-in-place concrete basins, influent and effluent control gate houses, and 10-foot-diameter influent conveyance piping. The total basin footprint will be approximately 500 feet by 350 feet and will have a bottom of foundation elevation of El. 195, with the exterior finished grade approximately El. 216. Anticipated loads for the CWB's range from 2,500 to 3,000 pounds per square foot (psf) for the tanks and 4,500 psf for the influent and effluent houses.

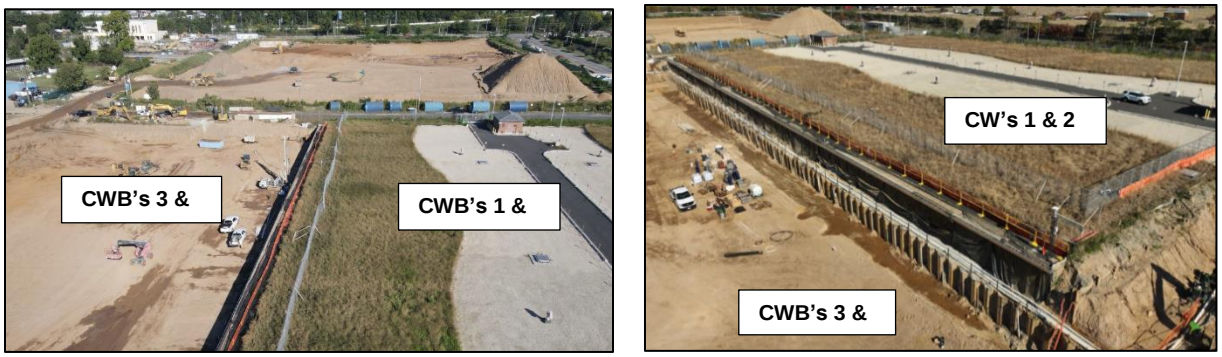


Fig. 3. Site prior to construction, September 2024.

SUBSURFACE INVESTIGATION

PWD engaged GFT to evaluate the foundation design alternatives to support the underground water tank. GFT began its geotechnical design with a desktop exploration study. The site is underlain by the Trenton Gravel, a Quaternary alluvial formation roughly 30 feet thick consisting of gravelly sand interbedded with assorted cohesive layers. The Trenton Gravel overlies the Wissahickon Formation, which consists of interbedded schist and gneiss often highly weathered to a significant depth (Geyer and Wilshusen 1982).

The subsurface exploration program consisted of a total of 23 borings to characterize soil conditions and evaluate bedrock quality within the footprint of the proposed structures. Rock coring was performed in 12 of the borings. Figure 4 shows a Boring Location Plan for the subsurface exploration program at CWB's 3 and 4.

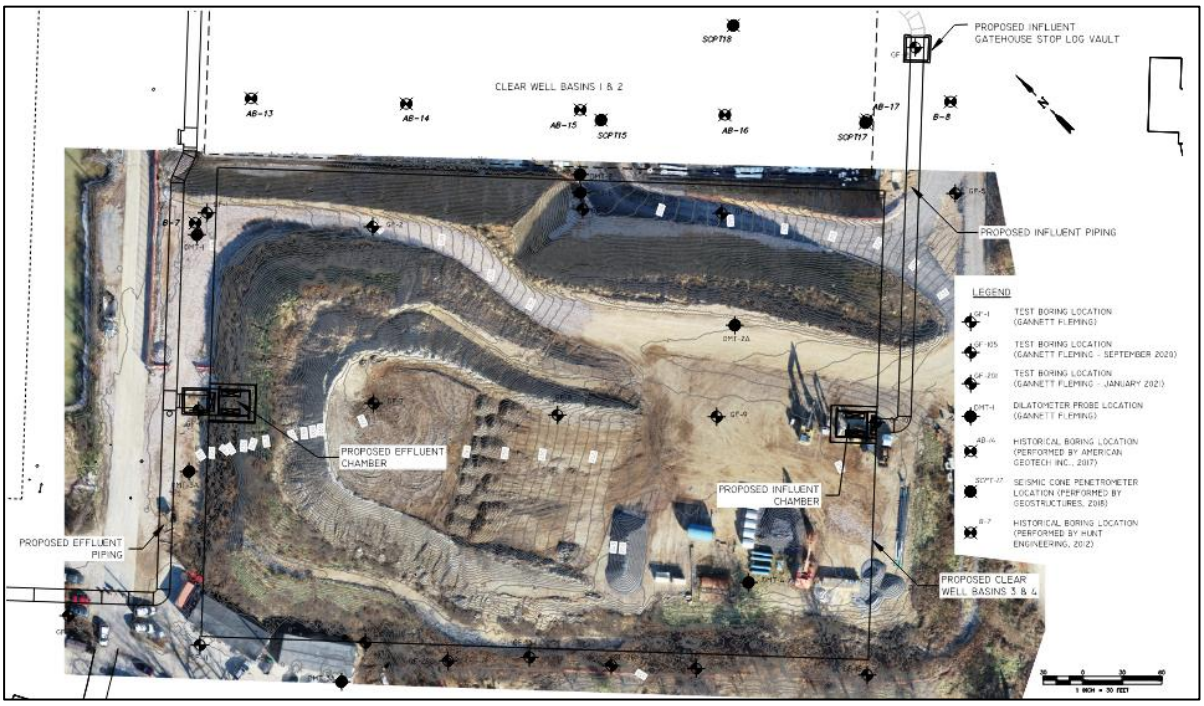


Fig. 4. Boring location plan for CWB's 3 and 4 (Gannett Fleming 2022).

At the time of the subsurface exploration program, the soil stockpile occupying the area from the site preparation and excavation of CWB's 1 and 2 varied in elevation from El. 264 to El. 196, with most of the

 © Deep Foundations Institute 2025

area ranging from El. 260 to El. 240. Table 1 shows the general strata encountered in the borings while Fig. 5 shows a typical subsurface profile.

Table 1 - Soil Strata

Stratum	Soil/Rock Material	Depth Below Ground Surface	Soil Density/ Consistency
A – Fill	Brown and gray, Silty SAND (SM), Sandy SILT (ML), Poorly Graded SAND (SP), and Poorly Graded GRAVEL (GP) containing concrete and boulders	1 to 52.5 feet	Very loose to dense
B-1 – Alluvium (Trenton Gravel)	Brown, Silty SAND (SM) and Poorly Graded SAND (SP) with varying amounts of gravel	Below Stratum A and interbedded with Stratum B2 to depths of 26 to 84 feet	Medium dense to very dense
B-2 – Alluvium (Trenton Gravel)	Gray, Sandy SILT (ML), SILT (ML), Silty CLAY (CL-ML), and Sandy Lean CLAY (CL) with varying amounts of sand, trace gravel, and minor wood fragments	Below Stratum B-1 in Borings GF-1 through GF-4, GF-6 through GF-8, GF-11 through GF-13, and GF-16 to depths of 37 to 96.5 feet	Soft to hard and very loose to loose
C – Residuum	Brown and gray, Silty SAND (SM), Clayey SAND (SC), and Sandy SILT (ML), contains mica and varying amounts of rock fragments	Below Stratum B-1 and B-2 to depths of 28 to 102 feet	Medium dense to very dense
D – Saprolite (highly/partially weathered rock)	Gray, Silty SAND (SM) and Clayey SAND (SC), contains mica and varying amounts of rock fragments	Below Stratum C to depths of 50 to 99 feet	Very dense
E – Rock	Gray, SCHIST Very soft to medium hard, completely weathered to moderately weathered	Below Stratum D in Borings GF-1, GF-3, GF-5, GF-6, GF-8, GF-11, GF-12, and GF-16 to maximum depth of exploration, 104 feet	REC: 0 to 100% RQD: 0 to 57%

Groundwater elevations at the site ranged from El. 188.7 to El. 203.1; the average value was El. 196.0. Thus, the average groundwater level at the site is roughly 2 feet above mean sea level as defined by NGVD29 (Gannett Fleming 2022).

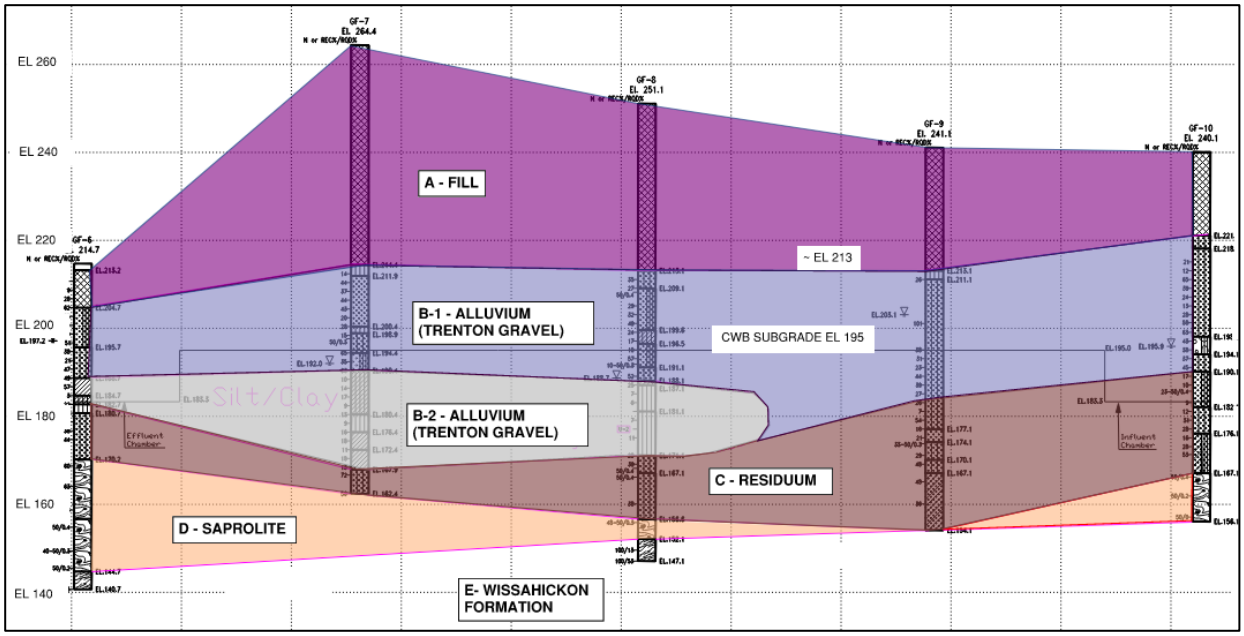


Fig. 5. Typical subsurface profile. Source: Gannett Fleming (2022).

 © Deep Foundations Institute 2025

FOUNDATION DESIGN

The findings of the geotechnical exploration raised two major, though expected, concerns among the design team members. First, the groundwater level at the site was higher (average El. 196) than the anticipated Bottom of Footing Elevations (BFE's) for CWB's 3 and 4, planned to be at approximately El. 195. The problem would be even more severe at the influent and effluent houses, which would have lower anticipated BFE's. Therefore, the site would require dewatering to maintain safe, stable working conditions during construction, and uplift pressures would need to be considered for operating conditions.

The second major issue at the site concerned cohesive alluvium interbedded in the Trenton Gravel layer. This material varied in thickness from 6.0 to 22.5 feet across the site. It was recognized even during site investigation that this problem would be particularly tough, as pocket penetrometer readings ranged from approximately 0.5 to 4.0 tons per square foot (tsf), indicating a highly variable consistency. Figure 6 shows a contour map indicating the variation in thickness of the cohesive stratum across the site.

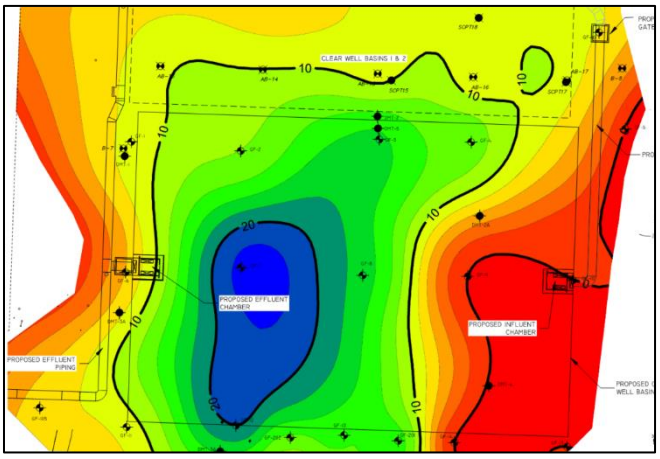


Fig. 6. Contour map of thickness of cohesive layer. Source: Gannett Fleming (2022).

Overall challenges that were considered in evaluating feasible foundation types included:

- Difficult subsurface conditions including:
  - Presence of a cohesive alluvium stratum with varying depths
  - Varying depth to competent bedrock
  - Varying thickness of highly weathered rock (saprolite)
  - Scattered cobble/boulder layers
- Presence of a shallow groundwater table
- Hydrostatic uplift pressures
- Proximity of adjacent CWB 1 and 2 foundations
- 100-year structural design service life
- Critical infrastructure classification of Category IV for the facility
- Historic nature of the site
- Site logistics, including staging of various construction activities
- Expected volume of soil cuttings from ground improvement and related spoils management
- QA/QC related to specialty foundation installation

Evaluation of Foundation Alternatives

Spread footings were the first foundation alternative considered, as they provide a feasible, cost-effective solution for transferring structural loads to the underlying bearing stratum. However, using them for CWB's 3 and 4 would have required excavating and replacing the cohesive stratum extending approximately 12 to 27 feet below the BFE. Therefore, this option would have been very difficult and cost prohibitive and was not investigated further.

 © Deep Foundations Institute 2025

The next option considered was a mat foundation supported on medium dense to very dense alluvium. The team considered a mat measuring approximately 500 feet by 350 feet. The limited depth to bedrock beneath the proposed BFE's relative to the size of the proposed mats would have resulted in only minimal dissipation of loading beneath them. Therefore, the team evaluated both elastic and consolidation settlements.

Elastic settlement was anticipated in the cohesionless Stratum B-1 and residual Stratum C, while consolidation settlement (primary and secondary) was confined to the cohesive Stratum B-2. Laboratory testing established that this stratum was characterized by slightly overconsolidated soils. Since the mat foundation dimensions are large (approximately 350 feet wide x 500 feet long) compared to zone of influence (~30 to 60 feet), the foundation vertical stress was not assumed to dissipate with increasing depth below the mat. Therefore, only recompression (Cr) of the cohesive layer, estimated to be 0.05, was considered in the analysis, since the proposed loading will not exceed the preconsolidation pressure. In many cases the existing fill layer provided overburden pressure more than the design bearing pressure. Settlement estimates varied across the site depending upon the depth of Stratum B-2. Total settlements ranged from approximately 0.9 inches in areas with no cohesive layers to approximately 4.8 in. where Stratum B-2 reached 22 feet thick. Differential settlement was estimated to be approximately 3 inches, yielding an angular distortion of 0.002 inches/inch, which was within tolerable limits. The testing showed that 90% primary consolidation, aided by double drainage, could be achieved within 36 days, while secondary settlement was projected over 50 years. Based on the subsurface exploration data and consolidation settlement magnitudes, the team decided that the high total settlements anticipated in areas with thicker cohesive layers would necessitate the use of ground improvement to transfer the CWB structural loads to a firmer underlying bearing stratum.

Ground improvement options considered beneath the mat foundation included: Aggregate piers; Driven piles; Drilled shafts; Drilled-displacement piles or auger displacement pile and Augered cast-in-place (ACIP) piles

Aggregate piers were technically feasible but presented construction concerns. The team considered it distinctly possible that the extensive vibrations involved in installing aggregate piers could disturb the foundations of adjacent active CWB's 1 and 2 and might induce liquefaction of the saturated granular soil within the Trenton Gravel alluvium. Neither would the aggregate pier system address the buoyancy uplift force that the completed CWB's 3 and 4 would experience; tiedown anchors would be needed to counteract this force. While aggregate piers and tie-downs were technically feasible and had been utilized on CWB's 1 and 2, PWD requested a foundation for CWB's 3 and 4 which eliminated penetrations through the mat slab to the tank interior, as would be required for tie-downs. Aggregate piers were thus ruled out. Driven piles were also ruled out due to their potential for excessive construction vibration.

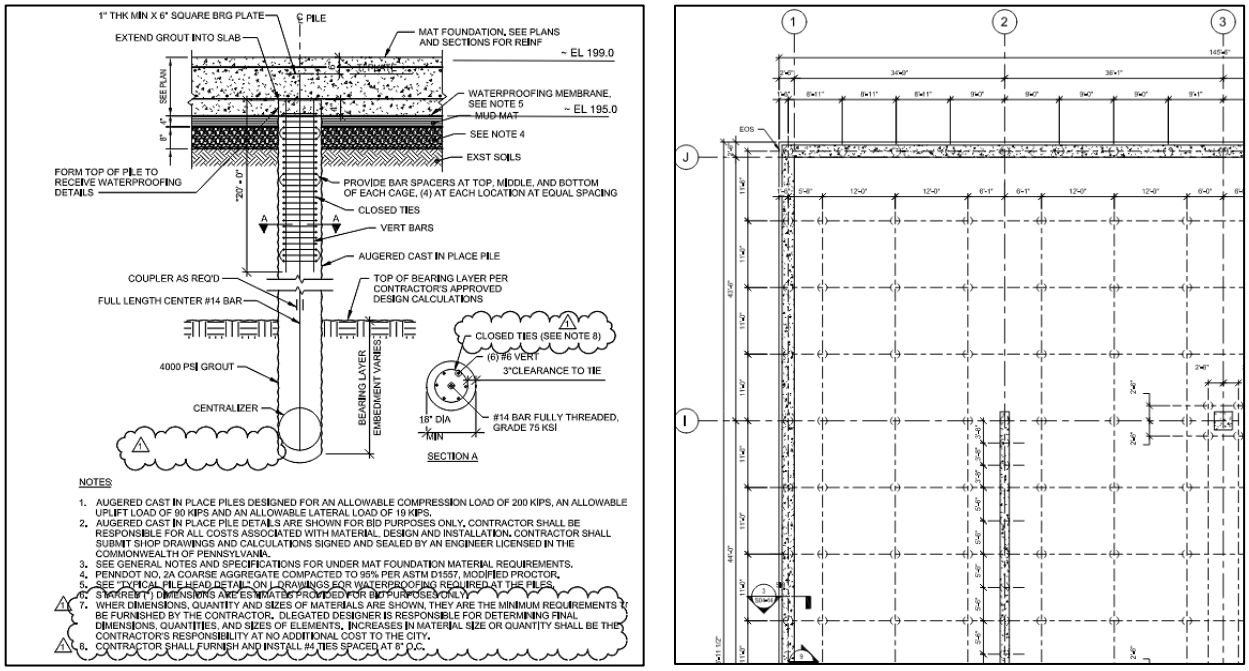
The design team next considered drilled shaft foundations. These were also technically feasible and would eliminate concerns about construction vibration. However, traditional drilled shafts at the site would require significant and costly, albeit constructable, modifications. The high groundwater levels at the site would require the use of temporary casing during installation, and the uplift forces from the completed structure would have necessitated rock sockets. The team therefore decided against this alternative as well.

After ruling out the above foundation options, the design team turned to ACIP piles. These are installed by drilling a continuous flight auger into the ground while simultaneously injecting grout, creating a high-capacity, low-vibration foundation element. ACIP piles offered several advantages for CWB's 3 and 4. First, their installation generates minimal vibrations and limits disruption to surrounding infrastructure, which is critical given the CWB's proximity to operational pumping stations, adjacent CWB's 1 and 2 foundations, and other critical components of the Baxter Plant. Second, these foundation elements provide

desired load-bearing capacity, ensuring the structural integrity of the new basins under the fluctuating loads imposed by water storage and distribution operations. Third, these piles do not always need to be socketed into rock, provided they are embedded in a relatively dense stratum capable of providing resistance to buoyant uplift loads. Finally, ACIP piles are adaptable to challenging subsurface environments, making them ideal for a site with a history of industrial use, urban fill, and varying geotechnical conditions. Based on GFT's experience with the City of Philadelphia and construction near the Delaware River, the team concluded that ACIP piles were the most feasible option from a constructability and cost standpoint.

Delegated ACIP Design

GFT collaborated closely with the project's structural engineer, Arcadis, to confirm the suitability of ACIP piles for the proposed structure, evaluate preliminary designs for them, and provide recommendations for final foundation design. The axial capacity of ACIP piles followed GEC No. 8 (FHWA, 2007). 18-inch diameter ACIP piles were evaluated for use with a maximum allowable axial compressive design load of 100 tons and a design uplift capacity of 45 tons. The lateral capacity demand for each pile was 9.5 tons, with a maximum lateral deflection not exceeding 1.0 inch. To achieve the design load capacity, the piles needed to be socketed 20 to 30 feet into residuum and saprolite (highly/partially weathered bedrock) of Strata C and D, respectively, corresponding to depths of 30 to 60 feet below BFE. The design recommended a full-depth, high-strength (75 ksi), all-thread reinforcing bar extending 6 inches into the mat foundation and secured by a bearing plate system to develop the design uplift capacity. The design evaluation confirmed that this configuration met the project's structural requirements while accommodating the site's geotechnical challenges. Settlement analyses further validated the design, predicting total settlement of CWB's 3 and 4 to be less than 1 inch, with differential settlement below 0.5 inches. These values indicate minimal risk of structural distress, ensuring long-term performance of the basins and associated infrastructure. Figure 7a shows the contract pile detail and Figure 7b shows a contract partial plan view of the pile layout.



Figs. 7a/7b. Contract ACIP pile detail and partial plan view of pile layout (GF/Arcadis, 2022).

 © Deep Foundations Institute 2025

Once the preliminary ACIP pile design was confirmed, the project was put out for bid. The contract documents required delegated final design of the ACIP piles. Ultimately, Daniel J. Keating Company (DJK) was awarded the general construction contract, and subcontracted Keller for dewatering, Schnabel Foundation for jet/permeation grouting at the influent and effluent pipes, and Berkel & Company (Berkel) for ACIP pile installation. Berkel used GFT's preliminary analyses to finalize the delegated ACIP pile design. Their design verified the contract minimum pile properties, detailed pile reinforcing requirements, and established pile termination criteria. The nearly 2,100 ACIP piles expected to be used were estimated to total over 96,000 linear feet. The contract required Low Strain Pile Integrity Testing (PIT) testing on 10 percent of production piles, which was performed by Berkel's subcontractor, D.W. Kozera, Inc. Each 18-inch diameter pile would be constructed of 4,000 psi grout reinforced with both a full-length, high-strength, all-thread No. 14 center rebar and a 23'-3" rebar cage consisting of five No. 6 rebars joined with a No. 3 spiral tie. Figure 8 shows the production pile detail.

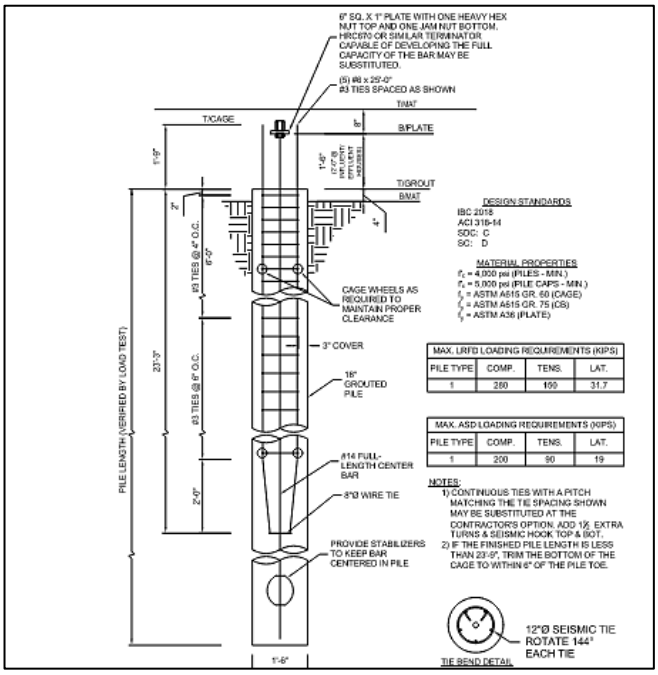


Fig. 8. Production pile detail (Berkel, 2024).

INDICATOR PILES AND FIELD LOAD TESTING

Per contract specifications, Berkel installed nine sacrificial indicator piles in late October 2024 to determine actual production pile lengths and refine installation procedures and pile termination criteria before going into full-scale production. Three indicator piles were load-tested – two in compression (IPC-1A and IPC-2) and one in tension (IPT-1). The test piles were installed to practical refusal, defined by a penetration rate of < 1 foot per minute, in the vicinity of Borings GF-11, GF-15, and GF-3, respectively. The total depth of these piles were 43 feet, 60 feet and 33 feet, respectively. The tensile test was performed on a shallow pile to ensure it had sufficient uplift capacity. The load tests were conducted in accordance with ASTM D1143, Procedure A, to 250 percent of the design load under observation of a GFT geotechnical engineer. Each pile was instrumented with four strain gauges mounted on sister bars. Figure 9 shows the location of indicator and test piles.

 © Deep Foundations Institute 2025

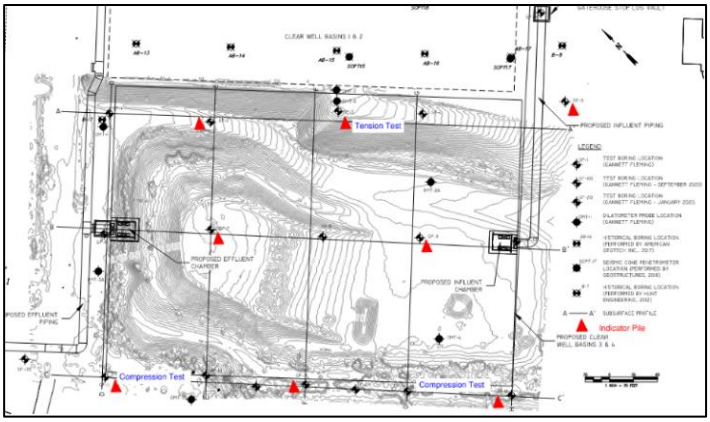


Fig. 9. Indicator pile and test pile location.



Fig. 10. Rig set-up on an indicator pile.





Fig. 11. Site overview and load test set-up.

Figures. 10 and 11 show the indicator pile installation and load test processes, respectively. Figure 12 shows the plotted load versus displacement for compression test pile IP(C)-1A, drilled to a depth of 43 feet. It exhibited a displacement of 0.09 inches at its design load of 100 tons and of 0.28 inches at its maximum load of 250 tons. The pile showed no sign of either structural or geotechnical failure, as its displacement was primarily elastic. Figure 13 shows the load distributions over depth, estimated using strain gauge data, for each increment of the IP(C)-1A load test. The load distribution curves confirmed that the residuum and saprolite layers generated most of the side resistance, although the Trenton Gravel alluvium contributed some additional side resistance.

 © Deep Foundations Institute 2025

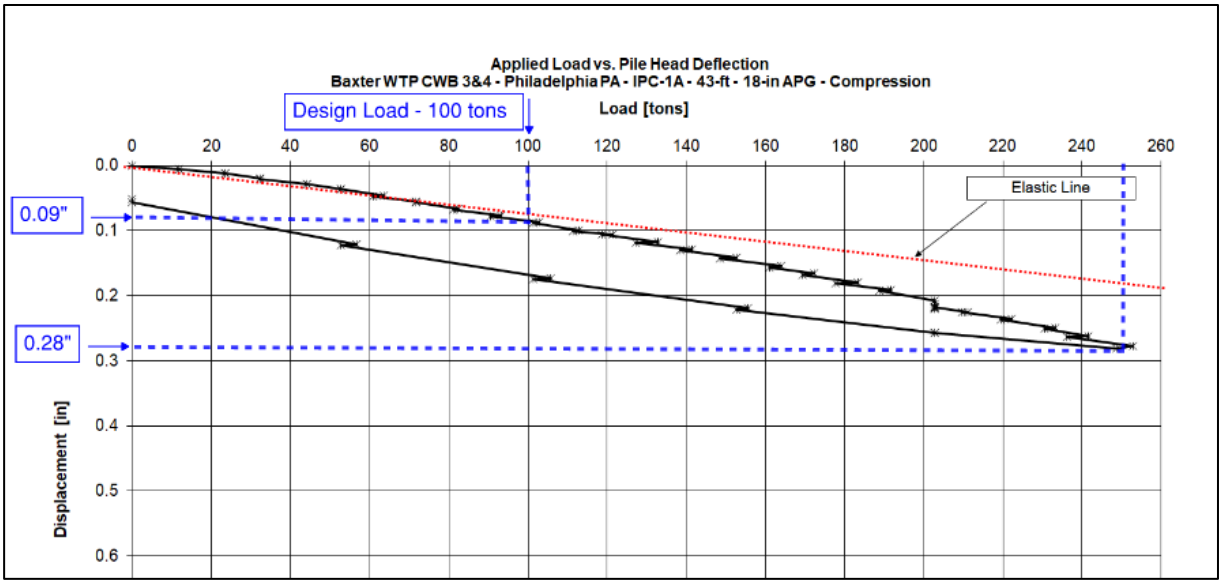


Fig. 12. Load-displacement plot for pile IP(C)-1A compression test. Source: Berkel (2024).

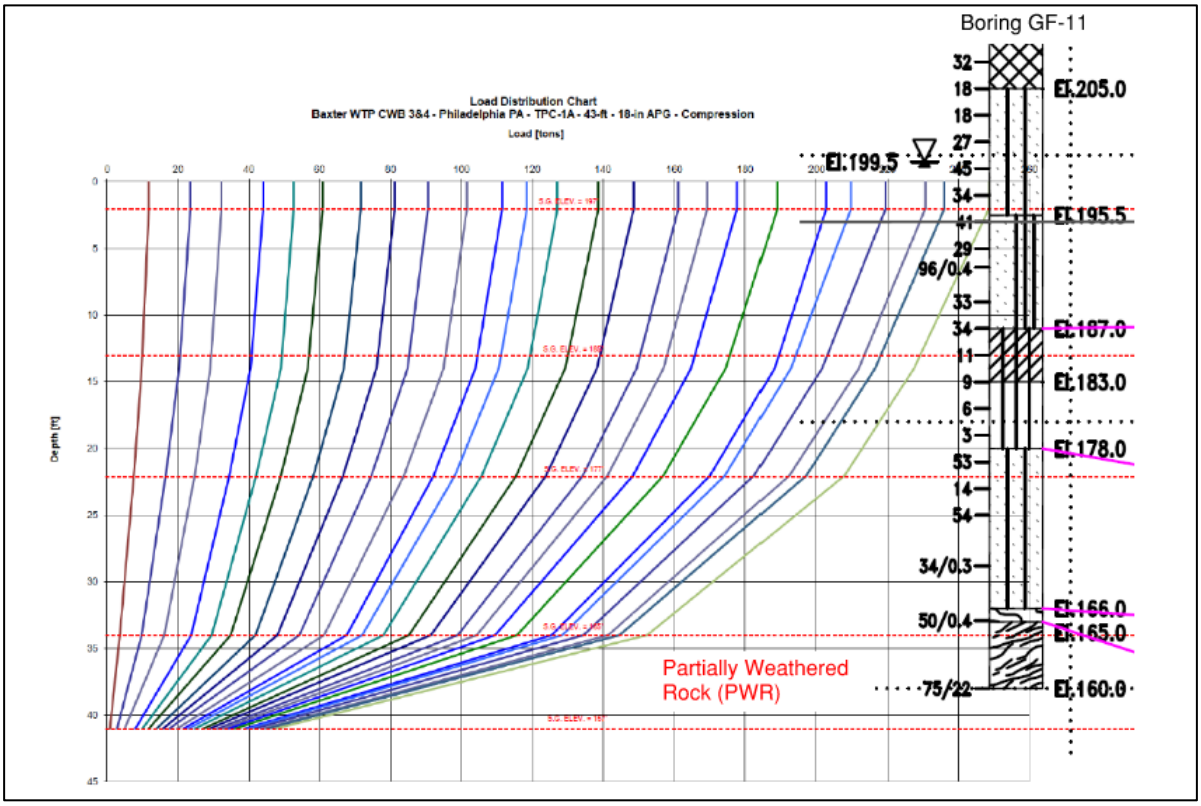


Fig. 13. Load distribution over depth for pile IP(C)-1A compression test. Source: Berkel (2024).

DESIGN PILE INSTALLATION CRITERIA

Installation data from the indicator piles confirmed the variable depth to the saprolite layer, a critical factor in determining pile termination depths. Therefore, GFT, DJK, and Berkel held several meetings to establish robust termination criteria for ACIP pile installation. This ensured that they could provide

adequate design capacity given the site's complex subsurface conditions. Ultimately, three pile termination criteria tied to refusal, defined as 1 foot or less of auger advancement per minute, were provided by Berkel and agreed upon by the design team and PWD:

- Criterion A: Piles could be terminated from 22 to 30 feet in length if they were drilled both to refusal and at least 5 feet into PWR or competent bedrock.
- Criterion B: Piles could be terminated from 30 to 35 feet in length if they were drilled both to refusal and at least 3 feet into PWR.
- Criterion C: Piles could be terminated at 35 feet or more in length once they met any of the following sub-criteria: 1) Refusal, 2) 15 feet embedment in PWR, or 3) Pile length of 65 feet.
- Modified versions of these criteria would be used for the ACIP piles at the influent and effluent houses, where BFE would be at El. 183 compared to El. 195 for CWB's 3 and 4.

Notably, for Criterion A piles, where rock was encountered relatively shallow and PWR criteria could not be met, Berkel recommended socketing the piles into 5 feet of competent bedrock to meet the design uplift capacity rather than increasing their diameter.

PRODUCTION PILE INSTALLATION AND QA/QC

As the Geotechnical Engineer of Record for the PWD at the Samuel S. Baxter Water Treatment Plant CWB's 3 and 4, GFT provided full-time inspection of the ACIP pile installation. Berkel began installing production ACIP piles in November 2024, at a rate of 10 to 12 piles per day. Installation of all 2,100 production piles was completed on August 1, 2025, over a duration of approximately 10 months. Construction of the other components of CWB's 3 and 4 is ongoing, with the clear wells expected to become operational in 2027.



Fig. 14. Drone view of ACIP pile installation. Source: DJK (November 2024).

 © Deep Foundations Institute 2025

As with any construction project, the design, inspection, and contractor teams at CWB's 3 and 4 faced some challenges during the installation of ACIP piles. A critical finding early in pile installation was the initial disparity between depth to saprolite as defined by the inspectors' observations of penetration depth versus drilling time and that defined by the penetration rates recorded by the drill rig's automated monitoring equipment (AME). To correlate these, the team systematically compared manual depth estimates from the inspectors with AME logs over several weeks. This iterative process of clear communication reconciled differences in these assessments, enabling the team to achieve consistent, relatively accurate saprolite depth estimates and to ensure that contract requirements were met.

Based on these observations, the project team agreed on three "rules of thumb" for deciding when the saprolite layer had been reached. The first was the auger penetration rate falling below a certain threshold compared to overlying materials. A value of 6 feet per minute was used as a starting point and adjusted as needed based on observed penetration rates and those of surrounding piles. The second rule of thumb was the appearance of cuttings brought up by the auger, and the third was the rig chatter during drilling. Figures. 14 and 15 show pile installation in action.



Fig. 15. Drone view of ACIP pile installation (DJK, April 2025).

Other challenges encountered during ACIP pile installation included:

- Control of grout cover over reinforcement cages: The contract specification required a minimum 3 inches grout cover, with the American Concrete Institute (ACI) allowing for a -0.5-inch tolerance. During installation, some piles were observed to have 2 to 2.5 inches of cover. Because the reinforcing cage contributes to pile's lateral capacity, this condition prompted additional structural analysis. Berkel's structural engineer took a conservative approach by omitting the shear contribution of the affected piles and redistributing the shear demand to the remaining piles in the mat, which had ample reserve capacity. This approach eliminated the need for mitigation. To

further enhance quality, specialty centering devices were employed to consistently achieve a minimum of 2.5 inches of grout cover. Further engineering evaluations confirmed that nearly all affected piles satisfied project design requirements, with only one location requiring supplemental piles. Berkel also strengthened its QC program by adding a dedicated QC team for the remainder of the installation, ensuring alignment with Owner's expectations.

- Bent rebars/central bar: Cage and/or center bars on some installed piles were bent by equipment working in the vicinity. Rebars bent less than 30 degrees were manually bent back into position. In the few cases where the bend exceeded 30 degrees, the bar was cut and a new straight piece of bar was installed via a mechanical coupler Moreover, DJK and Berkel added additional QA/QC safeguards that included a site walk by the QA/QC team before turning over an area of the mat foundation to the project's structural inspector for the next construction activity.
- Elevation of influent and effluent house piles: At the influent and effluent house locations, the proposed subgrade elevation (~El. 186.0) was approximately 9 feet below the BFE of CWB's 3 and 4 (~El. 195.0). Since all piles were drilled from the CWB 3 and 4 BFE, the piles at the influent/effluent house areas had to be exposed to the proposed subgrade elevation after drilling and then chipped down to the design elevation. This was quite challenging considering the high groundwater table and concurrent construction activities. DJK coordinated excavation, dewatering, and pile chipping operations effectively with no major setbacks.
- Grout logistics: The contract required stringent grout placement times, requiring grout to be placed within 60 minutes of mixing in one continuous operation to ensure pile integrity. However, grout delivery times were impacted by challenging cold weather conditions. Through collaboration, the design team, general contractor, and client came to a consensus of extending the delivery window to 120 minutes, provided that the grout met the contract requirements.
- Constrained working environment: As ACIP pile and tank slab construction progressed, there was a constant need to coordinate work to allow all trades to advance their tasks. ACIP installation was coordinated with DJK's floor slabs sequencing, allowing DJK's vehicles and equipment to reach slab locations while minimizing impacts to ongoing ACIP operations. This allowed the ACIP drill rig to advance drilling while gradually working backwards out of the work zone.

SUMMARY AND CONCLUSIONS

The implementation of an ACIP pile foundation system to support Clear Well Basins 3 and 4 at the Baxter Water Treatment Plant has proven the foundation system's capability to support the dynamic nature of this critical infrastructure's design loads. The indicator pile and load test program validated the ACIP piles' ability to penetrate complex geologic conditions with minimal vibrations, while achieving the required load capacity, primarily through unit side shear resistance developed in the residuum and partially weathered rock strata.

The authors would like to emphasize the importance of load test program for a project of this magnitude. Load tests are costly to conduct, so selecting suitable locations based on site-specific conditions is important for successful implementation of ACIP pile foundations. Notably, tension tests, though less common for ACIP piles, are recommended when a structure is designed to carry uplift loads, such as in this project. The authors would like to emphasize the importance of QA/QC for specialty foundation systems, particularly when dealing with complex geology, site constraints, and infrastructure demands for sustainability and resilience. The QA/QC is among the most important aspects of successfully executing an ACIP pile foundation project. Through effective communication, design refinements, and enhanced QA/QC inspection protocols, the project team successfully addressed field challenges ensuring the foundation's stability and contributing to sustainable infrastructure solutions under complex geotechnical conditions.

 © Deep Foundations Institute 2025

ACKNOWLEDGMENTS

The GFT authors are grateful to the Philadelphia Water Department for the opportunity to collaborate and for entrusting to GFT the role of Geotechnical Engineer of Record for Samuel S. Baxter Water Treatment Plant CWB's 3 and 4. All authors extend their appreciation to their partner firms for their expertise and collaboration in successfully executing this critical infrastructure project: Arcadis, Berkel & Company, Daniel J. Keating Company, GeoStructures (King of Prussia, PA), D.W. Kozera, Inc., In-Situ Soil Testing, Keller, Navarro & Wright Consulting Engineers, Pennoni, SANO Drilling, and Schnabel Foundation.

REFERENCES

Berkel (Berkel & Company). 2024. Technical Submittal: APG Element Load Test Results and Analysis, Baxter WTP Clear Well Basins 3 & 4 – Philadelphia PA, Berkel Reference No. 22-157. Berkel & Co., Atlanta, GA, 53 p.

Federal Highway Administration (2007), Geotechnical Engineering Circular No. 8: Design and Construction of Continuous Flight Auger Piles.

Gannett Fleming. 2022. Samuel S. Baxter Water Treatment Plant, Clear Well Basins 3 and 4: Geotechnical engineering report, Philadelphia, Pennsylvania. Gannett Fleming, Audubon, PA, 391 p.

Geyer, A.R., and Wilshusen, J.P. 1982. Engineering characteristics of the rocks of Pennsylvania. Pennsylvania Geological Survey, Harrisburg, PA, 316 p.

PWD (Philadelphia Water Department). 2025. "Brief history of the Philadelphia Water Department." PWD. https://water.phila.gov/wp-content/uploads/files/brief-history-of-pwd.pdf. Accessed Apr. 14, 2025.

Rinde, M. 2024. "The times they are a-changin': Here's how Philly's evolved over the last 75 years." Billy Penn at WHYY, Jan. 17. https://billypenn.com/2024/01/17/philly-by-the-numbers-pew-charitable-trust/. Accessed Apr. 6, 2025.

Schmidt, S. 2023. "Sam Baxter: The complex legacy of the man behind the water treatment plant." WHYY, Apr. 25. https://whyy.org/articles/samuel-baxter-philadelphia-history-water-treatment/. Accessed Apr. 6, 2025.

 © Deep Foundations Institute 2025

GROUND IMPROVEMENT AND CONSTRUCTION CHALLENGES OF MASSIVE FINE-GRAINED FILL EMBANKMENTS TO SUPPORT SETTLEMENT SENSITIVE STRUCTURES

Carlos Dowell, Langan. Panama City, Panamá, cdowell@langan.com
Omar Conte, P.E., Langan, West Palm Beach, Florida, oconte@langan.com
Roger Archabal, P.E., Langan, Miami, Florida, rarchabal@langan.com

ABSTRACT

Design and construction of massive thick fills over compressible clayey soils in a highly variant topography is a challenge in itself. Additionally, when the use of on-site fine-grained soils (that would typically be discarded) is required, the geotechnical challenges increase. This paper presents the soil investigations, geotechnical design evaluations, ground improvement recommendations, quality assurance program and post-construction settlements measurements for several large warehouses within a 300-acre logistic complex in Costa Rica. This site required thick fills between 5 to 8 meters (15 to 25 feet) to be constructed in order to create large building pads, roads and parking areas. Due to the large warehouse areas between 8,000 to over 20,000 m^2 (86,000 to 215,000 ft^2) and varied topography, the necessary earthwork operations had to be performed utilizing primarily onsite soils to make the project economically feasible. A comprehensive QA/QC program was developed and executed during the filling process to minimize the risk associated with the fine-grained fill materials (volcanic clays/silts). Additionally, post-fill confirmatory field tests (e.g. CPT, plate load test) were performed to validate the strength and modulus values of the compacted fill.

The native subsurface conditions consisted of soft, clayey soils, with thicknesses ranging from 2.5 to 5.5 meters (8 to 18 feet). Given the large footprints of the warehouses and relatively high structural loads at the columns and floors; a combination of several cost-effective ground improvement techniques were recommended to minimize settlements. This included preloading with heights between 2 and 3 meters (6.5 to 10 feet) to simulate future footing stresses and floor loads. A detailed stress distribution modelling analysis was performed to minimize the soft native soil removal and replacement depths (and areas) beneath the footings. Settlement plates were installed prior to fill placement to monitor the required fill and the different recommended preload heights. These plates also provided real-time settlements during the filling process and beyond, allowing for back-calculation of the soil's deformation parameters. This information was used to refine our design calculations and estimate future settlements more accurately. Post-shell construction settlement measurements confirmed our settlement predictions and models.

PROJECT OVERVIEW

Central American nations, particularly Costa Rica, have established Free Trade Zones (FTZs) to attract investment and boost economic growth. These zones offer various incentives, including tax exemptions and streamlined trade procedures, making them attractive for businesses seeking to establish operations or export to international markets. These free trade zones are usually developed on large undeveloped areas near highways and reliable infrastructure. The development of this specific FTZ complex is composed of very large warehouses with footprints ranging between 7,000 to 15,000 m^2 (75,000 to 170,000 ft^2) with access roads, truck parking areas and other sensitive infrastructure.

The project site is located inside of a newly developed worldclass FTZ with a total area of 124 hectares (306 acres) in San José, Costa Rica. This FTZ is one of the largest infrastructure and mass gradings projects being developed in the region. The topography of the area is composed of several hills and valleys with significant topographic relief. The overall FTZ is being developed in phases, and Langan has

 © Deep Foundations Institute 2025

been providing civil engineering mass-grading and geotechnical consulting services since the onset of development. Because of the difference in elevations with the original topography of the site, the development required cuts and fill of up to 10 meters (32.8 ft.) depending on the location of the different parcels. For one of the parcels already developed, the required fill heights vary between 0 to 8 meters (0 to 26.2 feet) and cuts were up to 15 m (49.2 ft.) deep. A section of the mass grading cut and fill drawing for one of the parcels within the development is presented in Fig. 1 to exemplify the extent of the massive fills required.

The required earthwork volume necessary to develop the numerous large plateaus for the different phases of the project is massive (greater than 1,300,000 cubic meters). Due to the amount of earthwork required and to make the development economically feasible, the majority of the fill to be used needed to be onsite soils. Based on the several geotechnical investigations performed around the entire property and subsequent more detailed geotechnical investigations for each warehouse parcel, the onsite soils are composed of primarily clays and silts of volcanic rock origin with varying consistency. These fine-grained soils are generally very soft within 1 to 3 meters of the surface in most areas. Seams within these silts and clays layers were classified as high-plasticity (CH and MH) and had to be discarded during earthwork operations as they were not recommended to be re-used.

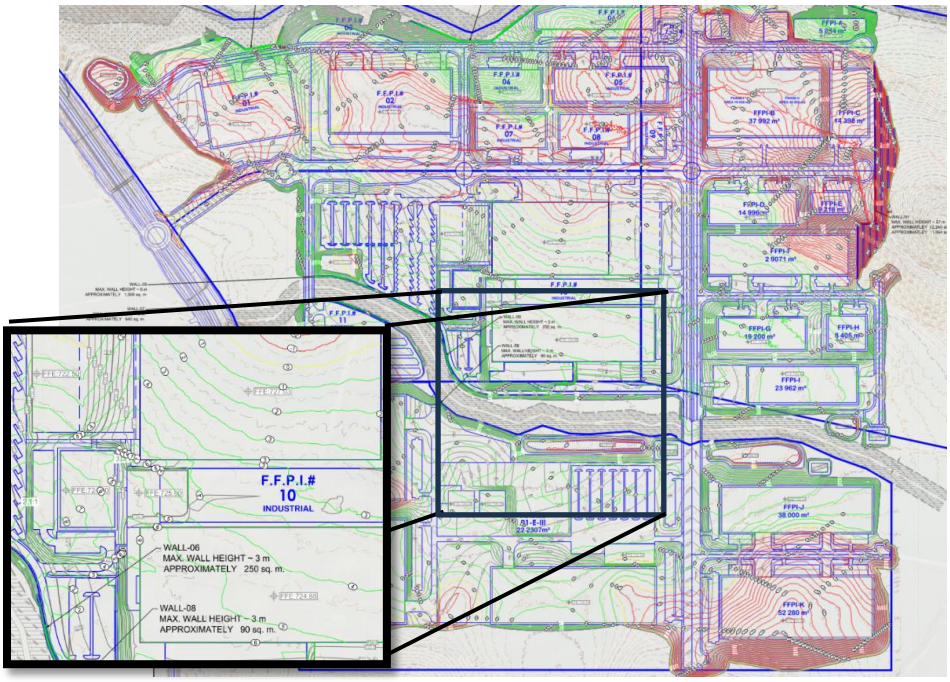


Fig. 1. Cut and Fill Plan for a Section of a Parcel within the Overall Development.

The common structural floor loads for the constructed warehouses range between 2 to 5 ton/m^2 (400 to 1,000 psf) and the column loads vary between 15 to 20 ton/m^2 (3,000 to 4,200 psf). The large areal loads from the fill and warehouse floor plus the proposed columns loads in combination with the poor in-situ geotechnical conditions, along with the required use of onsite fill; makes the development of this project a geotechnical challenge. Contrary to the footings at column locations, the floor loads will not dissipate stresses at shallow depths. In fact, the soil/rock layers below the warehouses will experience stress dissipation up to a depth of "2B" where "B" is the width of the warehouse (100 to 300 m [300 to 900 ft]). In addition, the fine-grained soils need to be stabilized to minimize swelling and settlement potential. Due to the warehouse size, shallow foundations with or without ground improvement is the preferred foundation alternative. Pile support and structural slabs are not considered feasible foundation alternatives for warehouses as it will make the project economically nonviable.

 © Deep Foundations Institute 2025

GEOLOGICAL SETTING

Volcanic soils are common in some areas of Central and South America, especially near mountains and volcanic regions. The majority of the onsite soils present within the overall development are silts and clays of volcanic rock origin. Most of these volcanic soils are composed of volcanic vents, fragments formed from the break-up of moving lava, or fragments of dust, ash or pumice which fall around the vent of the volcano or are carried to a distance by wind. Additionally, they may be also formed by the weathering and erosion of lava flows or consolidated pyroclastic debris. In general, volcanic soils have relatively high shear strength and permeability in relation to their particle size, plasticity and mineral composition. Furthermore, volcanic soils exhibit a quite low compressibility under relatively low stress increments (Bommer et all, 2002). This is an advantage for the development as most of the onsite soils need to be re-used as fill during the mass-grading phase of the project. Volcanic clays appear visually similar to alluvial clays. However, the geotechnical properties differ from other type of clays, especially of marine origin that are often related to major settlements of coastal or near-coastal developments.

Volcanic clays and marine clays differ in their formation, composition, and properties. Volcanic clays, are derived from volcanic ash reacting with alkaline groundwater, often forming in areas with volcanic activity. Marine clays, on the other hand, form in marine environments from various sources, including the weathering of rocks, and organic matter. Marine clays are often found in coastal and offshore areas and can be a mixture of different clay minerals, including kaolinite, montmorillonite, and illite, along with non-clay minerals like quartz and feldspar. Volcanic clays, while also containing clay minerals, often have a unique composition with non-crystalline components like allophane and imogolite.

SUBSURFACE CONDITIONS

Several initial geotechnical explorations have been conducted to date in the general area of the overall FTZ development. The geotechnical campaigns included Standard Penetration Test (SPT), Cone Penetration Test (CPT) and geophysical surveys. Subsequent and more specific geotechnical investigations are performed at the time of development of the individual parcels. Specific subsurface investigations were planned to obtain the necessary geotechnical information for the varied parcels. The investigations considered the size of the parcels, the findings during the initial geotechnical investigation, the required grading fills/cuts, the anticipated site layout and structural loads. Depending on the different factors mentioned, the number/depth of borings, CPT and in-situ testing were determined. Additionally, soil sampling was performed for laboratory tests. Sieve Analysis (ASTM D6913, 2021), Atterberg Limits (ASTM D4318, 2021), Swell Potential (ASTM D4546) and Standard Proctor (ASTM D1557, 2021) tests were among the most common laboratory tests performed. Based on all the geotechnical investigations performed to date, the general subsurface conditions throughout the site can be summarized as follows:

Topsoil (Organic Silt):

This layer consists of a black or dark brown clayey silt with a high organic content, depth ranging from 0 to 1.0 m (0 to 3.28 ft), with an average depth of 0.45 m (1.48 ft). Overall, this layer is characterized by a consistency that varies from very soft to soft, with SPT-N values between 0 and 9, with an average of 3.

High Plasticity Clay:

A layer of potentially expansive gray and/or grayish-brown clay, with high to very high plasticity, and a very soft to stiff consistency. SPT-N values for this layer ranged from 0 to 22 blows per 30 cm, with an average of 6. This layer is found between 1.35 and 3.15 meters (4.4 to 10.3 ft.) deep. The

 © Deep Foundations Institute 2025

expansion/settlement potential of this layer presents a risk that must be assessed due to the potential impact on the proposed structures.

Clayey Silt:

This stratum consists of clayey silt, some brown (sometimes dark) sand, and rock blocks. This stratum is generally found from the soil surface to a depth of 5 to 12 m (16 to 40 ft.) below the surface. SPT-N values in these soils generally increase with depth. Therefore, it can be subdivided into two strata: an upper stratum with SPT-N values ranging from 1 to more than 43 blows, with an average of 9 blows; and a lower, more consistent stratum with SPT-N values between 10 and 100, with an average of 57 blows. In isolated areas, pockets of soft clay were found with blow counts of less than 4.

Volcanic Rock Formations

Hard to very hard tuffaceous volcanic rocks ("tuffs") were found beneath the soil layers, ranging from a depth of approximately 5 to 17.5 m (16.4 to 57.4 ft.).

Groundwater Level:

The water table has been documented at widely varying levels. In some areas, the water table was observed near the surface, and in other areas at depths up to 6.3 m (20.1 ft). This might be attributed to the presence of aquitards due to the low permeability clay layers near the surface.

SOIL IMPROVEMENT PROGRAM

Based on subsurface conditions observed during the geotechnical investigations phase and the proposed thick fills and structural floor/column loads, a combination of ground improvement programs have been used on different parcels throughout the overall development. In most cases, the combination of discrete removal and replacement in isolated areas (below footings) in combination with ground improvement techniques have been utilized to improve the compressible layers at the site and minimize structure settlement.

Before earthwork operations started at each parcel location, the topsoil layer was removed and disposed off-site or stockpiled to be used in future green landscape areas. The soft clay layer, underlain the topsoil layer, was not uniform, and some areas with deeper pockets of this material, could cause more settlement compared to areas where this layer was found to be thinner.

Granular soils from quarries are an available and preferred source for fills during any embankment construction. However, due to the size and fill thickness required during the mass-grading phase of the project; the import of granular soils (fill) needs to be limited in order to make the project economically viable. In addition to the cost of granular fill material, the disposal of onsite soils and related environmental and transportation fees need to be considered in detail while evaluating ground improvement alternatives such as remove and replace.

In general, the earthwork sequence consisted of the removal of topsoil, the placement and compaction of the on-site fine-grained fill until a pre-determined depth below Finished Floor Elevation (FFE). This was followed by the placement and compaction of a minimum design thickness of imported granular fill material (locally known as “lastre”) up to FFE followed by the recommended preload height.

The granular fill, “lastre,” was used for the upper layers below and within structure areas until the finished grade was achieved. A design thickness was required to counteract potential swelling of the

 © Deep Foundations Institute 2025

onsite fill and to be used as a seal to minimize the water content changes. In addition to the technical viability of materials, the practicality of material placement and compaction during the varied seasons had to be considered. For instance, on-site fine-grained fill was placed and compacted until the rainy season prevented its effective use. The on-site fill layer thickness varied but were typically between 2 to 4 meters (6.5 to 15.2 ft) thick. On top of the on-site fill, imported granular fill was placed and compacted. This granular “lastre" layer thickness varied from approximately 4 m to 6 m (15.2 ft to 19.7 ft) on some parcels and between 1.5 to 3 m (4.9 to 10 ft) on other parcels. An aerial picture during earthwork operations and construction of the massive fill required is presented in Fig. 2.



Fig. 2. Earthwork and Preload Operations.

Due to the marginal geotechnical properties of the onsite fine-grained fill materials, swell tests were recommended and performed. Initial tests of the clayey soils resulted in a swell potential range classified as “medium to moderately high”. However, additional swell tests were done to similar materials, but on remolded samples compacted with a higher moisture content than the optimum. This condition was recommended to better mimic the actual field conditions associated with use of the material as fill and to minimize the swelling potential. These supplemental swell tests resulted in swelling percentages between 0.28% and 0.32%, which classifies as “low” swelling potential. These swell test results are more aligned with the field conditions as most of the density compaction results measured during the filling process were at or above the optimum water content.

Furthermore, since this fine-grained fill material was placed as the first layers of the fill, underlying the thick imported granular backfill, the swelling potential would be further minimized due to the granular fill load. Nonetheless, to counteract any swelling potential of fill materials with fines (clays and silts), we recommended that the fine-grained fill soils be compacted to at least 95% of the Proctor Standard (ASTM D698, 2021), at about 2% to 4% above the optimal moisture content (wet side) and to maintain moisture in the material at the time of compaction.

Ground Improvement for Fill and Floor Loads

Given the presence of the native soft silts and clays which could lead to settlement under the average 4 meters of fill required, as well as the stresses from the floor and slab loads of the structure, we recommended soil improvement through "preloading." Based on the significant volume of earthworks occurring onsite, preloading was determined to be the most cost-effective soil improvement technique for this development. The preload heights varied among the different parcels. The design preload height is a function of the proposed floor loads, column loads, distance to the compressible layer and thickness of the compressible layer. In most cases, a 2 m (6.5 ft.) preload height was recommended over the entire area of the structure. In some cases where a larger footing (3x3, [9.8x9.8 ft.]) was required to accommodate the column loads in the main axis of the warehouse, a 3 m (9.8 ft.) preload height by 5 meters in width preload strip section was recommended. In parking areas, the recommended preload height was 1 m (3.28 ft.) The stresses induced by the preloading would be equal to or greater than those of the structural and fill

loads. Likewise, the surcharge was extended at least 1.5 m (4.9 ft.) in directions where future structures are not anticipated. However, in locations where adjacent future structures could be built, the surcharge zone was extended 5 meters to minimize future differential settlements.

All suggested preload surcharge heights are considered above the final grade level. The preloads were monitored by at Settlement Plates (SP), which were placed at strategic points based on the silt/clay thicknesses observed in the geotechnical explorations and the required fill heights. Considering the geotechnical and consolidation characteristics of the volcanic origin silt/clay soils, our analysis indicates that the preload will need to be sustained for only a few weeks following the completion of construction. The purpose of the preload was to over-consolidate the soft clay layer to an Over Consolidation Ratio (OCR) above approximately 1.5. Based on our experience and data published by Yu (1993) an OCR greater than 1.5, results in the accomplishment of the primary settlements and most of the secondary settlements. This results in negligible settlements during the life of the structure.

Field observation by means of topographic surveying of installed settlement plates was implemented, to monitor soil deformations during fill placement. Topographic readings began at the start of fill placement, and readings continued thereafter until preload was placed and settlements had stabilized. Elevations of each settlement plate were measured twice every week during fill and preload construction and once per day after post-surcharge top-out.

The survey data measured vertical deformations (settlements) ranging from 2.5 to 5 cm (1 to 2 in) during the fill placement process until the design Finish Floor Elevation (FFE) had been reached. After fill construction reached FFE, the surcharge phase started. Due to the client´s scheduling and desired expedited schedule, preloading occurred in localized areas, at different times, prioritizing areas that had to be cleared first. Once the desired preload thicknesses were achieved (above FFE), additional vertical deformations ranging between 2.5 to 4 cm (1 to 1.6 in) were measured from the settlement plate readings. Total settlements varying between 5 to 9 cm (2 to 3.5 in) was achieved during fill and preloading activities. The settlement readings for two of the parcels developed is presented in Figs. 3 and 4.

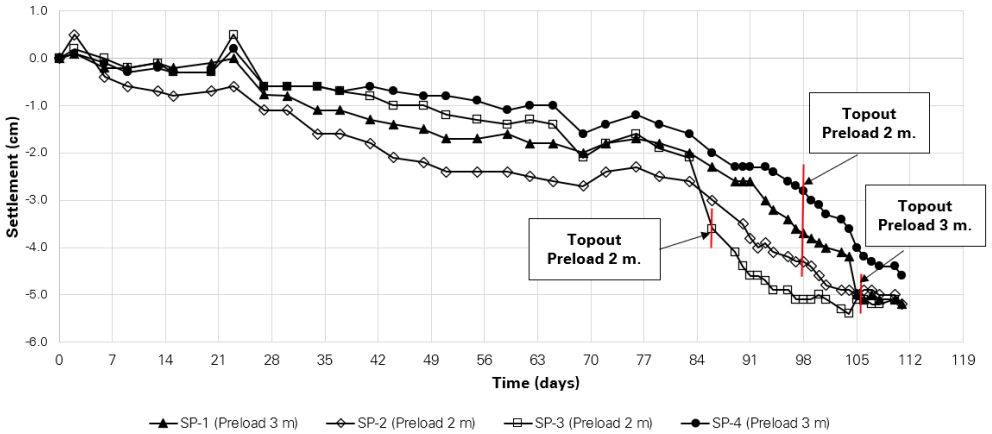


Fig. 3. Measured Settlement during Surcharge Program for Parcel A

 © Deep Foundations Institute 2025

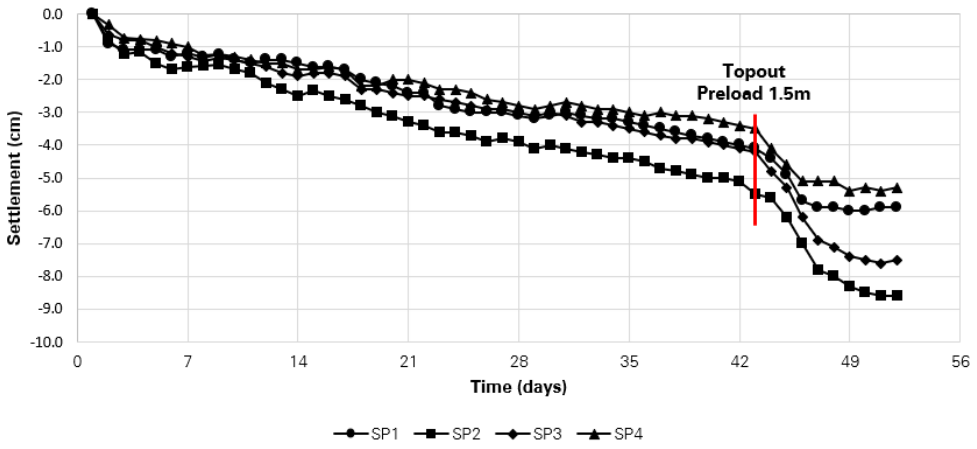


Fig. 4. Measured Settlement during Surcharge Program for Parcel B

Although the measured settlements are not extreme, structures and slabs subjected to these movements will experience deformation and cracking. Specifically, the potential differential settlement due to the different fill heights and compressible layer thickness can result in detrimental distortions to concrete floors. Warehouses are especially susceptible to settlement distress as there may be impacts beyond structural damage such as sensitive assembly line equipment, storage racks and sensitive equipment mobility.

Ground Improvement for Footings

Bearing capacity and settlement were the two main factors controlling the footing design for the proposed warehouses. In general, the footing bearing elevations were within the massive fills or in cut areas in native soils. Ground improvement at the isolated footing locations was performed to minimize potential settlements and ensure an adequate bearing material The ground improvement at each footing location consisted of "removal and replacement" with low-strength grout ("Tobacemento"), after the preload program was completed. The use of grout allowed for vertical cuts to be performed at footing locations and to over-excavate below the proposed footing bearing depth. The over-excavation depth below the proposed bearing depth was calculated depending on the size of the footing, distance to in-situ compressible layers, load and consistency of the partially improved soil (fill or onsite) beneath the footing. The preload and surcharge program described on the previous section was mainly performed to simulate the proposed floor loads, however; some of the over-stress from the preload program was considered during each footing evaluation. More details regarding the foundation evaluations and recommendations are presented in the following sections.

QUALITY CONTROL AND QUAILTY ASSURANCE DURING EARTHWORK

Prior to the placement of the fill at the project site, the topsoil and soft soils (clays and silts) that were encountered, were removed and replaced with approved on-site fine-grained soil fill material from cut areas within the overall site. All earthwork and mass-grading operations were performed under full time inspection of a geotechnical representative. The quality control program consisted of using field density testing (nuclear gauges), to measure the degree of compaction and optimum water content of the placed fill in every lift. Furthermore, due to the massive fills, part of the QA/QC program involved performing CPTs and plate load tests post-filling to confirm the load carrying capabilities of the fill. Fill operations continued using the on-site fill once above ground surface, up to about 4 meters (13.1 ft) in some areas.

 © Deep Foundations Institute 2025

The overall quality control program for fill compaction consisted of performing a density testing (ASTM-D6938) at a standard frequency of about one test on every 500 m^2 (5,380 ft^2) area per vertical lift. The testing followed a grid pattern throughout the site, documenting precise test locations within the project. The results were well documented and summarized. Due to the subtle variation in characteristics of the on-site fill material, a family of Proctor curves (soil moisture versus density laboratory graphs) were used in the field to document test results.

Once over-excavation was finished (if needed) and the lower fill layers were placed and compacted up to a height of approximately 3 to 4 m (9.84 to 13.1 ft) (using on-site fine-grained fill), the granular "lastre" material was imported to the site for the upper layer of the required fill. The granular fill in the upper layers and closer to the final grade were also compacted up to a minimum of its 95% maximum dry density, but for these materials using a greater energy according to the Modified Proctor ASTM D1557. This layer was also suggested as a cap layer to prevent large moisture changes within the on-site fill, further minimizing swelling potential.

Due to the overall fill having a total height of approximately 4 meters (13.1 ft) above existing grade/working surface subgrade, some settlements were still expected due to the elastic compression/consolidation processes. These settlements were monitored using settlement plate devices and topographic survey techniques. Settlement plates were installed soon after backfilling the areas where the topsoil and some the soft clayey soil were partially removed and replaced, to monitor settlements of the existing native soil. The settlement plates allowed us to obtain real measurements and to validate when settlements caused by the fill loads and preload had stabilized and better understand the compression behavior of the existing soils. Elevations of each settlement plate were measured twice every week for a period of three months and once per day during the following month.

POST-SOIL IMPROVEMENT TESTING

The standard quality control during regular filling operations is the density compaction testing, as this activity sets the consistency of the known fill material properties. As an additional confirmatory measurement, several post-filling field tests were performed onsite. In addition to the rigorous quality control program established during the construction of the fill, a series of plate load tests were performed at different stages, to determine the load capacity of the fill. Due to the client's scheduling and desired expedited schedule, on-site fill began in areas that were a priority to be developed. After the on-site fill was finished in these specific areas, plate load tests were performed at this interim level (before placement of the granular fills). Once the granular fill was placed, additional plate load tests were performed near final grades. Plate load tests performed on the on-site fill resulted in a soil reaction modulus, k_s, that varied between 4.90 to 6.40 kg/cm^3 (177.0 to 231.2 pci) for a 1.25mm deflection (0.05 inch). These values correspond to bearing pressures of 10 ton/m^2 (2,080 psf) for a deflection of approximately 0.2cm (0.08 inch) which is an acceptable subbase value for this type of structures. On the other hand, plate load tests performed on the imported granular fill, ranged from 12.20 kg/cm^3 to 25.30 kg/cm^3 (440.8 to 914.0 pci) for 1.25mm (0.05 inch) deflection [bearing pressures between 15 ton/m^2 (3,120 psf) to 31 ton/m^2 (6,450 psf) at 1.25mm (0.05 inch) deflection]. We understand fill earthwork activities were observed and inspected by qualified geotechnical personnel from local consultants.

As another subsurface investigation tool, several CPTs were performed at the site at the interim of the on-site fill application, before the imported granular fill was placed. These CPTs were performed to verify the soil parameters through continuous tip resistance and friction ratio measurements. These estimated soil parameters were then utilized to further evaluate bearing capacity of the soil improvement zone, as well as, to obtain soil parameters of the deeper soil profile for settlement calculations.

FOUNDATION ANALYSIS

On this project, all footings were embedded within the fill and in cut areas within native soils. For footings bearing in native soils, a detailed analysis was performed at each column/footing location to determine the depth and size of ground improvement (removal and replacement) required. A detailed stress dissipation evaluation was performed at each footing location to determine the depth where the footing stress will dissipate to a pressure level below the allowable bearing capacity of the onsite fill or improved soil beneath the footing. Additionally, the replacement area below the footing was also enlarged in most cases to allow for better dissipation of stresses. The removed soil underneath the footings was replaced by grout locally known as "Tobacemento", which allowed not only for vertical cuts at the isolated footing locations, but also to use a 2:1 stress dissipation model (Fig. 5).

Settlement calculations and modeling was performed to estimate settlements underneath footings. Critical and average scenarios/cases were evaluated for each warehouse. The critical case was defined by the footings with the highest load and with the closest proximity to the compressible in-situ layer; while the average scenario/case was the condition widely observed throughout the warehouse. Based on the preload program data, it was observed that settlements occurred rather quickly compared to other fine-grained soils and associated consolidations process. Hence, a "composite elastic modulus" was back-calculated utilizing the preload settlement data. The estimated settlements for the average and critical conditions were very low and under the structural threshold. The estimated settlements were below 1.5 cm (0.6 in) as presented in Fig. 6. The actual measured settlements during the construction of the shell were negligible and within the precision of the survey equipment as presented in the following section.

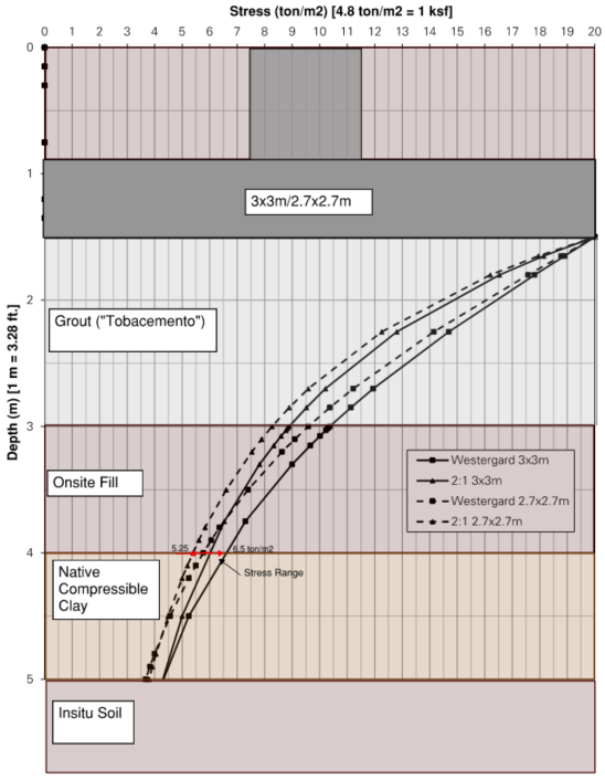


Fig. 5. Stress Dissipation Analysis for Footings.

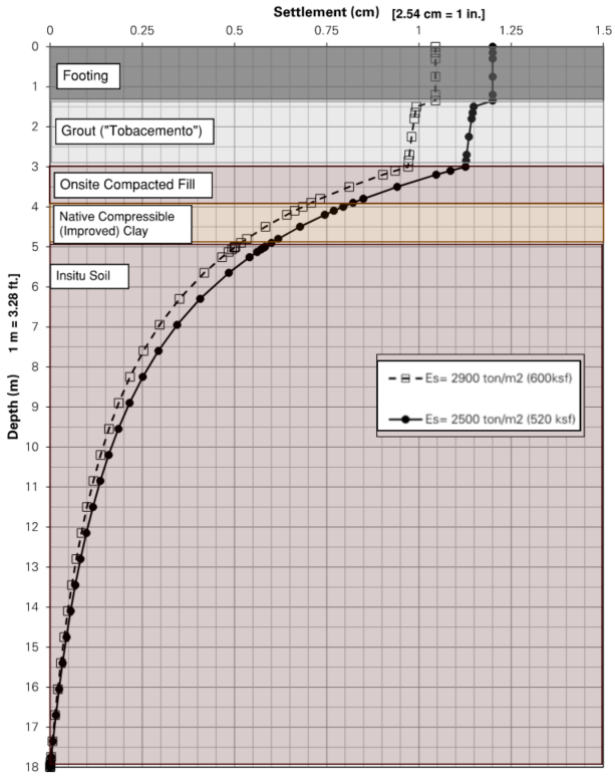


Fig. 6. Settlement Estimate with Composite Es.

The borings and CPT tests performed after fill and the preload or post-ground improvement were used to determine the allowable bearing capacity with depth underneath each footing. Calculations were

 © Deep Foundations Institute 2025

performed using the Meyerhoff bearing capacity method, based on the undrained shear strength and unit weights obtained from CPT tests, considering a purely cohesive soil with no friction angle. Based on the results of our evaluations, the allowable bearing capacities reported were adequate compared to the values measured with the CPT results. In fact, in some instances, the measured bearing capacities for the on-site fill and the natural soil had the potential to be increased, but we originally proposed capacities satisfying the structural needs. Allowable bearing capacity from the results of select CPT tests vs. the stress dissipation curve from a generalized footing is presented in Fig. 7. As observed on Fig. 7, the average allowable bearing capacity within the onsite fine grained fill ranges between 15 to 25 ton/m^2 (3 to 5 ksf); however, allowable bearing capacity within the native compressible layer ranges between 5 to 10 ton/m^2 (1 to 2 ksf). The allowable bearing capacity is greater than the dissipated stress from the footing with depth.

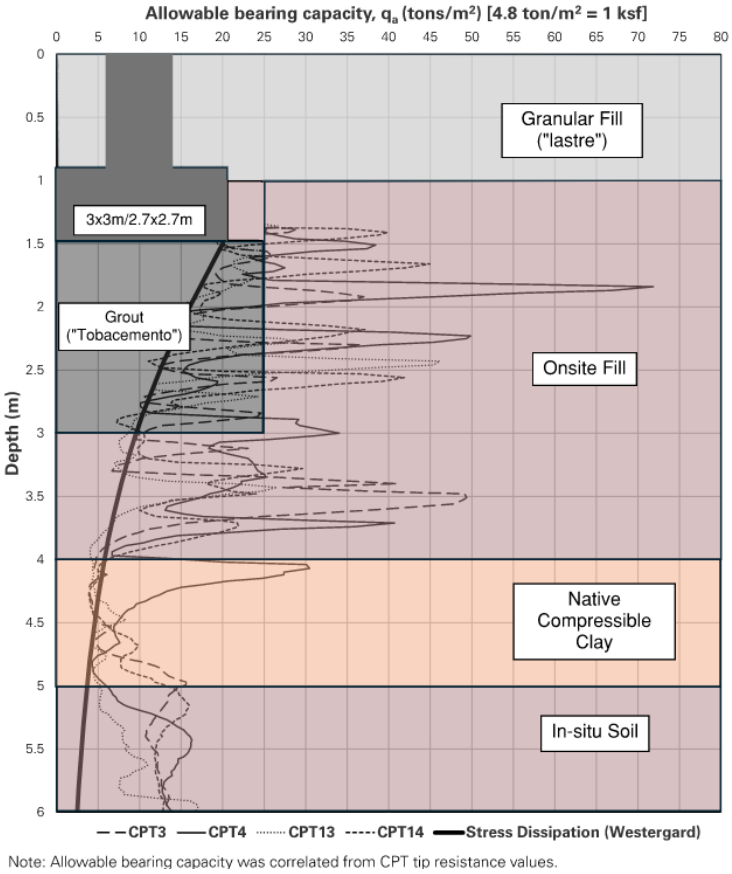


Fig. 7. Allowable Bearing Capacity (from CPT results) vs. Stress Dissipation with depth

POST CONSTRUCTION SETTLEMENT MONITORING

To confirm the success of the soil improvement program implemented within the project, control points were installed at each column location (34 columns total) of one of the warehouses constructed. Survey measurements were obtained for a period of five months (1 months after completion of the shell). The loads applied at this stage are those belonging to the shell itself or dead loads. Settlements experienced in the columns ranged from 0 to -0.009 cm (0 to -0.004 inch). The magnitude of these settlements is negligible and could be attributed to survey equipment precision. An aerial picture of the warehouse columns with the survey monitoring points installed is presented on Fig. 8. The initial and final readings taken throughout a 5-month period at each of the column locations are shown in Fig. 9.



Fig. 8. Aerial Picture during Shell Construction

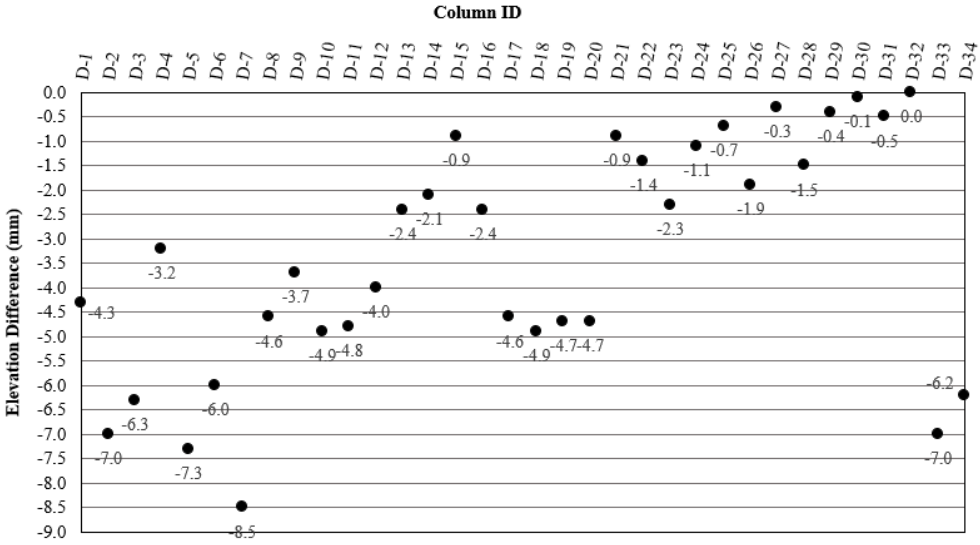


Fig. 9. Graph of settlement differences between initial and final readings for each column.

CONCLUSION AND LESSONS LEARNED

Embankments for structure support are usually constructed using granular soils; however, during massive embankment construction, such as the ones required for this site, the client's needs and feasibility of fill materials needed to be further analyzed. As stated previously, these type projects are only economically viable if on-site material, produced from cuts within the site, are used as fill material to create these massive warehouse platforms. Given the fact that these emerging FTZs host and service high-end international corporations, the structures' performance must comply with high construction standards. Because on-site material consisted mostly of plastic silts and clays (fine grained soils) highly susceptible to volume change when exposed to moisture change, and that these fine-grained fill materials were underlain by layers of soft compressible clays and silts of volcanic origin, a comprehensive geotechnical understating of these soils was necessary to comply with the construction standards required for the project.

Manipulating fine-grained soils during earthwork and segregating undesirable material from usable material can be a challenge, especially in tropical countries such as Costa Rica where weather dictates field operations. However, if field operations are carried out with a stringent and comprehensive QA/QC program, the project can be a success. This case study demonstrated that by performing an appropriate

geotechnical investigation, preloading program, followed by an in-depth and comprehensive settlement and footing stress dissipation analyses the use of fine-grained soils on massive fills up to 8 m (25 feet) is possible. Settlements were originally estimated to range between 5 to 12 cm (2 to 5 inch) for the overall structure prior to ground improvement. Post-ground improvement settlement were measured up to 9 cm (3.5 inches) with the proposed preload program. Settlements measured on control/monitoring points installed at column locations resulted in a maximum settlement of 9 mm (0.4 inch) after shell construction. These measured settlements fall within the precision of a total station which was the survey equipment of preference for these projects.

In conclusion, in order to construct massive fine-grained soil fill embankments for high-end structure support, it is important to: understand the subsurface conditions and the load/stresses that the underlying soil layers will be subjected too, understand the behavior and engineering properties of the soils being used as fill material, perform an adequate ground-improvement program, coordinate a quality control and quality assurance program during fill applications, and perform post-construction testing to provide adequate foundation recommendations and performance.

REFERENCES

ASTM Standard D1557-12, 2021. "Standard Test Methods for Laboratory Compaction Characteristics of Soil Using Modified Effort (56,000 ft-lbf/ft3 (2,700 kN-m/m3))," ASTM International, West Conshohocken, PA, 2003, DOI: 10.1520/D1557-12R21.

ASTM Standard D698-12, 2021. "Standard Test Methods for Laboratory Compaction Characteristics of Soil Using Standard Effort (12,400 ft-lbf/ft3 (600 kN-m/m3))," ASTM International, West Conshohocken, PA, 2003, DOI: 10.1520/D0698-12R21.

ASTM Standard D4318-17e1, 2018. " Standard Test Methods for Liquid Limit, Plastic Limit, and Plasticity Index of Soils," ASTM International, West Conshohocken, PA, 2003, DOI: 10.1520/D4318-17E01.

ASTM Standard D6913-04, 2009. “Standard Test Methods for Particle-Size Distribution (Gradation) of Soils Using Sieve Analysis," ASTM International, West Conshohocken, PA, 2003, DOI: 10.1520/D6913-04R09E01.

Yu, Peter K., 1993. Site Stabilization in Hurricane Region. 3rd International Conference on Case Histories in Geotechnical Engineering, St. Louis, Missouri, USA.

 © Deep Foundations Institute 2025

SACRAMENTO RIVER EAST LEVEE CONTRACT 4 – SEEPAGE CUTOFF WALL CONSTRUCTION CHALLENGES AND SOLUTIONS

Nagesh Malyala, PE, Stantec, Sacramento, California, 916-418-8297, Nagesh.Malyala@stantec.com
Chris Hamilton, US Army Corps of Engineers Sacramento District, Sacramento, California, 916-557-7612, Christopher.E.Hamilton2@usace.army.mil
Timothy Williams, PE, GE, Kleinfelder, Rancho Cordova, California, 916-366-1701, twilliams@kleinfelder.com
Kimberly Brown, PE, Kleinfelder, Rancho Cordova, California, 916-366-1701, kbrown@kleinfelder.com

ABSTRACT

Sacramento River East Levee (SREL), part of the American River Common Features (ARCF) 2016 Project, is being executed by USACE under four different contracts (Contract 1 through Contract 4). The project is adjacent to Sacramento, California and is important for public safety and asset protection. Contract 4 included construction of seepage cutoff walls at 4 separate locations in 2023 and 2024. Contract 4 flood protection features are intended to reduce the flooding risk to critical infrastructure in Sacramento, California. The project was constructed through a USACE Sacramento District contract and was supported by Kleinfelder and Stantec, who provided design and engineering during construction services related to civil and geotechnical engineering.

This paper discusses the challenges encountered and solutions adopted during jet grout and Deep Mix Method (DMM) cutoff wall construction. Triple fluid jet grouting was selected to close a 200-foot-long gap beneath a 100-foot-deep existing seepage cutoff wall, which required a vertical and horizontal overlap. Challenges included jet grouting to a depth of 140 feet through gravels, cobbles, and buried trees and verification of the required overlaps. A second triple fluid jet grout cutoff wall was constructed through a 100-year-old levee breach adjacent to a hotel and restaurant facility. Jet grouting through the breach fill was problematic with grout losses, shallow sinkholes, and difficult drilling conditions. Supplemental single fluid jet grout stabilization columns, staged grouting, and extensive monitoring were performed to help prevent damage to the hotel and restaurant. DMM was used to replace a proposed open trench soil-bentonite cutoff wall and to replace a proposed jet grout cutoff wall. In each case, accessibility and reduced schedule were the main drivers for the replacement. Contract flexibility was important to allow for these changes. Jet grout cutoff wall verification was done through verticality readings of each column, graphical overlap reports, coring, and in situ testing. The paper emphasizes the importance of collaboration during construction, construction sequencing, challenges created by triple fluid jet grouting in levee breach fill, and the solutions developed to overcome those challenges.

Keywords: jet grout, deep mix method (DMM), cutoff wall, verification coring

PROJECT OVERVIEW

Sacramento River East Levee (SREL) levee improvements, part of the American River Common Features (ARCF) 2016 Project, were constructed along the Sacramento River in Sacramento County, California, to reduce the flooding risk to the critical infrastructure in urban areas of Sacramento. The work on which this paper focuses consisted of several short work areas over a 15-mile-long portion of the Sacramento River between the Sacramento Railyards just south of the American River to Cliff's Marina just south of Freeport, California. This paper focuses on discussion of construction related issues for short cutoff wall segments using deep mix method (DMM) and jet grout methods to address specific high-risk areas at Edwards Break/Little Pocket (1,237-foot cutoff wall), Sump 132 (deepening an existing 200-foot long DMM cutoff wall), and Cliff's Marina (a 365-foot long cutoff wall and seepage berm) for levee breach risk remediation.

 © Deep Foundations Institute 2025

Edwards Break/Little Pocket

Edwards Break was a levee breach that occurred in 1904 on the north side of the Little Pocket area of Sacramento where the river makes a westward turn resulting in a scour hole and landward scour pond. The breach was closed and a large landside berm, about 500 feet along the river by 200 feet wide, was constructed behind the levee. Since the landside berm was constructed, it has been occupied by various businesses and roads and is currently occupied by a privately owned hospitality facility and associated drive lanes and parking lots, as shown in Fig. 1.

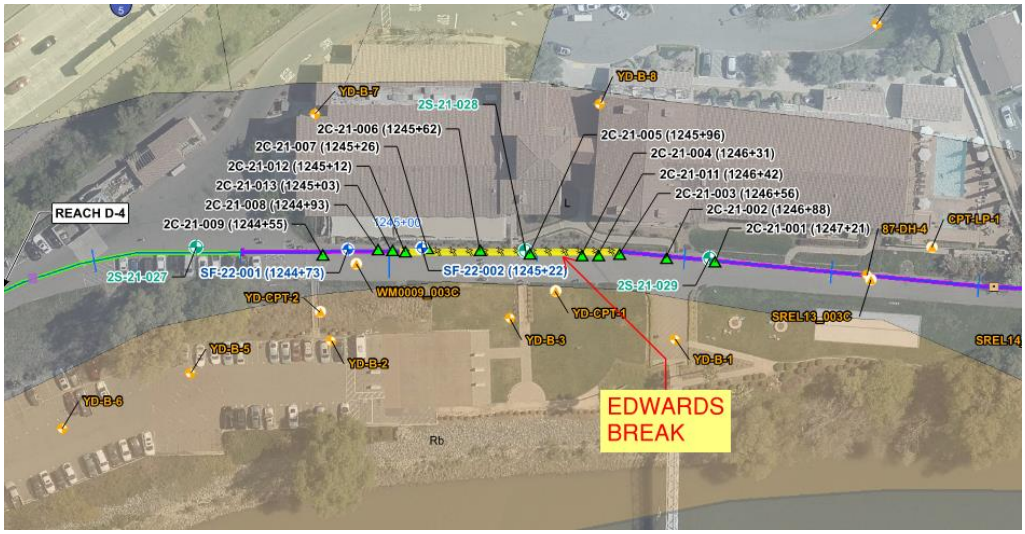


Fig. 1. Plan View of Edwards Break

A series of sonic borings and cone penetration tests (CPTs) were advanced to investigate the limits of the breach fill debris and to characterize the breach fill material. A schematic of the subsurface profile is shown in Fig. 2; the depth of the breach appears to vary between 20 feet and 64 feet below the levee crest. The upper part of the breach fill consisted of sand fill (loose to medium dense poorly graded to silty sand) 5 to 20 feet thick that was underlain by debris fill (poorly graded gravel with cobbles, rock fragments and wood fragments). The driller reported the material was loose and recovery varied from 25% to 56%.

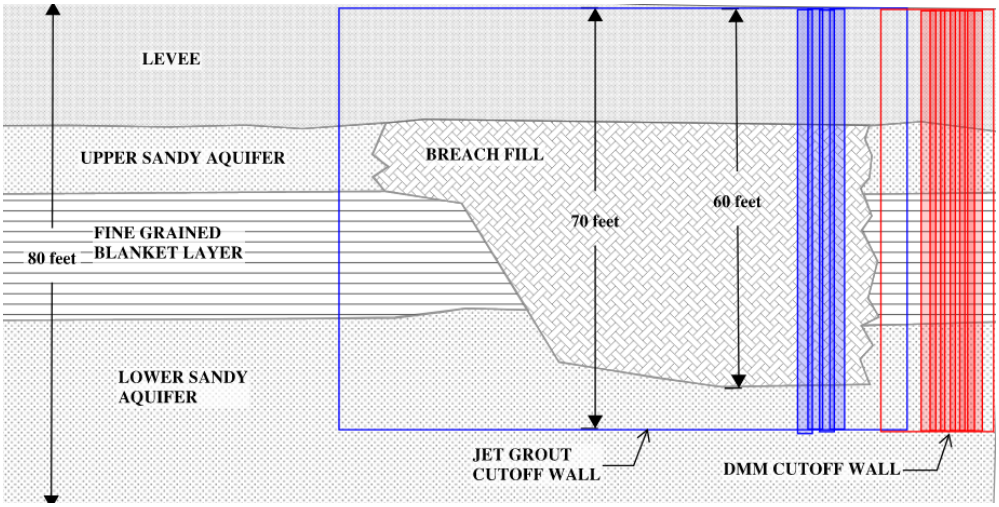


Fig. 2. Schematic Profile View of Subsurface around Edwards Break with 2024 Cutoff Walls

SREL downstream of the raised berm area was found to not meet project levee design criteria (see USACE EM 1110-2-1913) and a cutoff wall was recommended. To prevent seepage from flowing around the upstream end of this cutoff wall through the breach fill, which could cause levee instability, the downstream end of the cutoff wall was extended upstream to cutoff the debris fill.

Due to the debris at Edwards Break and adjacent hospitality buildings, jet grout was selected for the cutoff wall through the breach fill since it was considered to have less of an impact to adjacent structures (e.g. ability to work from the existing bike path elevation without degrading the levee and less noise and vibration) and was considered easier to adjust to the uncertain ground conditions at the site. The contractor was given the option to use DMM or open trench soil-bentonite for the Little Pocket cutoff wall downstream of the Edwards Break/hospitality building and of using DMM or jet grout to connect the Edwards Break cutoff wall and the Little Pocket cutoff wall. The contractor selected DMM for these purposes since the DMM batch plant could be located on a berm constructed on the degraded levee crown and slurry ponds for a slurry trench would be difficult to fit within the work area and DMM had a shorter schedule.

Construction adjacent to an operating hospitality facility was a challenge. A sound barrier wall was constructed in front of the structures to serve as a visual and sound barrier. Structural inspections were performed, and monitoring points were established on the major structures that were tracked for movement during construction. A parking lot for the facility located on the waterside of the levee was used for jet grout batch plants and spoils handling.

Sump 132

Sump 132 is the largest pump station in the City of Sacramento and drains the Pocket Area, a large residential neighborhood in Sacramento, California. Constructed in the early 1970s when the former agricultural area was developed, the facility consists of a pile supported pump station with 8 pumps, an inlet channel at about Elevation -3 feet, and a wet well at about Elevation -15 feet, which is about the same elevation as the bottom of the river. The pump station was located at the site of a former agricultural drainage pump station, which was located on an old slough that drained into the river that had been closed during levee construction in the late 1800s and early 1900s. Significant boils occurred in the inlet channel during flood events in 1986 and 1997. After the 1997 flood, a weighted filter (rip rap over geotextile) was constructed within the intake channel, extending about 100 feet upstream from the concrete intake apron. However, during later high-water events, clear water could be seen flowing between the concrete apron and the weighted filter. In 2003, improvements consisting of connecting the weighted filter to the concrete apron with a wood header and construction of a DMM cutoff wall about 400 feet long along the crest of the levee to a depth of about 105 feet (Elevation -70 feet) to cutoff off potential seepage pipes (note: it did not penetrate an aquiclude and was a ‘hanging’ wall) and relief wells next to and along the intake channel.

Sump 132 geotechnical explorations indicated the presence of a sandy levee underlain by a silt and clay blanket over about 80 to 90 feet of sand with deeper gravel layers. There were four deep mud rotary and sonic explorations up to 170 feet deep and four shallower, roughly 100-foot-deep borings and CPTs. There were notes such as rootlets and minor organics on a few of the boring logs. The boring logs also included comments on gravel and some cobbles and high sampler penetration blow counts. Based on the explorations included in the Contract documents, some minor organic/wood material and dense sands and gravel with some cobbles were to be expected.

In 2020, a fully penetrating DMM cutoff wall that connected to the south side of the 2003 DMM cutoff wall was constructed for the SREL project. In 2022, additional work in the vicinity included construction of a fully penetrating DMM cutoff wall that connected to the north side of the 2003 DMM cutoff wall. These cutoff walls extended to about 145 feet (Elevation -110 feet). As a result, a window had been formed beneath the 2003 cutoff wall that was about 400 feet wide and 40 feet tall (Fig. 3) that was located in a sand and gravel layer. This resulted in a potential for concentrated flow through the window and reactivation of the boils from 1986 and 1997. To remediate this concern, the cutoff wall was deepened to match the upstream and downstream DMM cutoff walls (labeled SREL C1 DMM (2020) and SREL C3 DMM (2022) in Fig. 3, respectively). Since this decision was made while the upstream SREL C3 DMM wall was still under construction, the upstream and downstream walls were able to be extended roughly 200 feet to partially close the roughly 400-foot-long gap in the area outside of the pipe zone, which were significant savings in schedule and cost to the project.

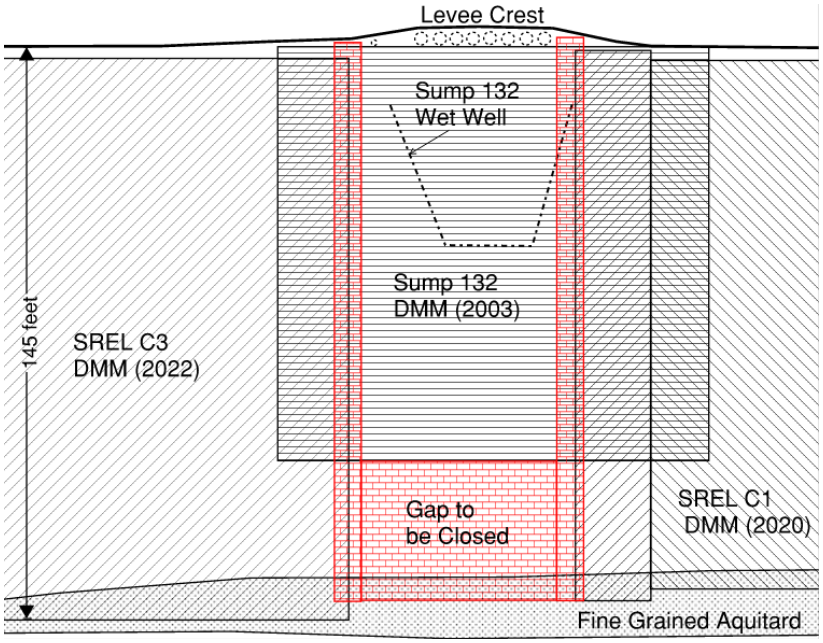


Fig. 3. Sump 132 Existing and SREL C4 2023 (in red) Cutoff Walls

A DMM type cutoff wall would necessitate removal and replacement of the 8 drainage pipes through the levee crown. Since the steel pipes were over 50 years old, it was likely complete removal to the pump station would be required. This would be costly and extend the schedule in order to fabricate the pipes and associated backflow prevention valves. A jet grout type cutoff wall was selected since jet grout columns could be constructed between the pipes, allowing the pipes to remain in place.

Cliff's Marina

The SREL ARCF project ends at the intersection of the SREL with the Morrison Creek Beach Lake levee at Cliff's Marina, south of Freeport, California. SREL downstream of Cliff's Marina was a rural, delta levee that was not built to meet the same design criteria as the upstream urban levees (see EM 1110-2-1913). Therefore, there is the potential for the levee to fail immediately south of the levee intersection sooner than it would within the urban system. This could result in a breach hole eroding upstream and compromising the urban levee system by removing the levee intersection and causing flooding into the Sacramento urban area. Remediation was recommended to improve the levee extending 750 feet downstream of the levee intersection. This consisted of 365 feet of the cutoff wall that would cross State Route 160 and be constructed primarily at the landside levee toe with the remainder of the improvement consisting of a stability/seepage berm, which was significantly lower in cost than a cutoff wall. Jet grout was recommended since the cutoff wall would cross the Cliff's Marina parking lot and State Route 160; however, once construction started, the contractor proposed to change from the jet grout method to the DMM method to save schedule, which was accepted.

DEEP MIX METHOD CUTOFF WALLS

The 80-foot deep, 1,107 linear feet length of cutoff wall downstream of Edwards Break was constructed using DMM based on the availability of a six-auger DMM rig, which allowed faster DMM construction than a standard three-auger DMM rig would; avoiding slurry mixing ponds and a soil-bentonite mixing pad; less off haul of slurry affected soils; and schedule savings from no soil-bentonite settlement period and capping the DMM cutoff wall after 3 days. The contractor felt these factors outweighed the higher costs associated with DMM (e.g. large volumes of cement and the need for specialized equipment). The DMM method of construction uses specialized equipment to mix in place water, cement, bentonite, and soil to construct a uniform, low permeability, soil cement bentonite (SCB) seepage cutoff wall through and beneath the levee. The six-auger DMM rig provides an element geometry as shown in Figs. 4 and 5 below. Each element is overlapped by the next in a primary-secondary sequence.

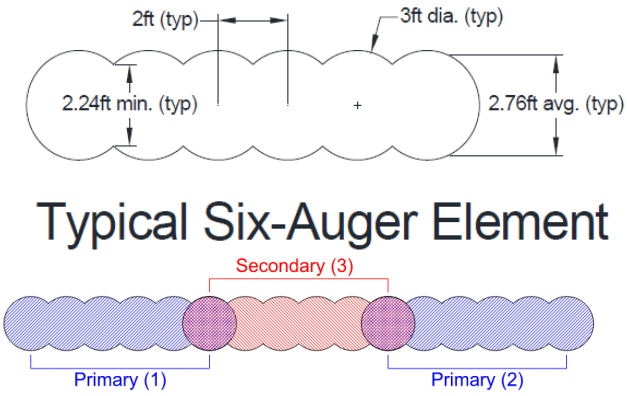


Fig. 4. Typical six-auger DMM element detail (Raito, 2023)



Fig. 5. Six-auger DMM rig in action downstream of Edwards Break

Similarly, the 47-foot deep, 365-foot-long section of jet grout cutoff wall design at Cliff's Marina that was awarded to the contractor as jet grout was converted to DMM after the contractor provided a value engineering proposal. The contractor indicated they had a plan to work within State Route 160 and the Cliff's Marina parking lot and that the DMM would be faster and could start sooner than jet grouting, which benefited the project. This change avoided jet grout cutoff wall installation problems and delays.

Problems with Coring and In-situ Testing

The DMM subcontractor for this contract had performed similar work in previous SREL contracts. This experience was used as justification for the contractor's request not to perform a mix design (an existing mix design would be used) or the demonstration section (e.g. a short section of cutoff wall used to test the proposed construction parameters), which were required by the specifications. The project delivery team (PDT) accepted this request on the condition that verification coring and in-situ water testing would be performed for every 250 linear feet of cutoff wall (for a total of six coring locations). The results of all but one coring location met the specification requirements. One corehole had a rising head test hydraulic conductivity of 4.60E-05 cm/sec, while the requirement is a hydraulic conductivity of no greater than 1x10-6 cm/sec. The contractor contributed the failing test to excessive horizontal corehole deviation, with the corehole being too close to the outer wall of the cutoff wall to properly test, which was likely since the contractor took several attempts to core the failed test's location. The contractor had decided to place the

 © Deep Foundations Institute 2025

soil cap over the cutoff wall prior to coring and testing it. By covering the cutoff wall, the contractor was then unable to visually verify that the marked coring location was centered in the wall. This resulted in failed coring attempts that punched out of the DMM wall into surrounding soil. The PDT required core sample laboratory testing for unconfined compressive strength (ASTM D2166) and permeability (ASTM D5084, Method C). The core sample tests had satisfactory results, and the DMM cutoff wall was accepted.

Cavities in the Top of DMM Cutoff Wall

After the Edwards Break/Little Pocket DMM wall was constructed and prior to the levee rebuild, the uppermost foot of the DMM wall was removed and a cap of sandy lean clay was compacted over the top. The top of the wall was visually inspected and probed to verify the quality of the treatment. During this inspection, several shallow cavities (generally less than 3 feet deep) within the treatment were observed. An example of a cavity found is shown in Fig. 6.



Fig. 6. Example of DMM wall cavity found after removing the temporary cap

It was determined tracked equipment driving over the top of the newly constructed cutoff wall likely pushed soil cap material into the top of the cutoff wall before is reached the initial cure stage. Each cavity was excavated, vacuumed, and backfilled with approved controlled low strength material (CLSM).

JET GROUT CUTOFF WALL CHALLENGES AND SOLUTIONS

Difficult Site Conditions at Sump 132

The triple fluid jet grout method of construction was used at Sump 132, whereby a drill string with nozzles for cement grout, compressed air, and water is inserted into a previously drilled pilot hole and rotated to form a column up to 10 feet in diameter. The water nozzle cuts the soil, the compressed air lifts the spoils, and the grout fills the eroded matrix and mixes with the remaining soil resulting in a soil cement column. The contractor can adjust the installation procedures to expand or decrease the diameter of the column. Spoils were collected in a trough at the top of the column and pumped to a processing facility to remove the water. Water was discharged to the sanitary sewer system and dry cuttings were taken to a landfill.

During jet grouting, the contractor encountered several issues that affected production.

- Woody vegetation was observed in multiple jet grout columns (at various locations and depths) during installation. The contractor stated that “wood, in the most variable forms, sizes, and quality: chips, fresh, carbonized, large size wooden logs/planks, etc. have been identified during drilling and/or jet grouting on almost all JG elements at Sump 132.” The wood was encountered in the pilot holes as well in the spoils trough, which caused out-of-specification vertical alignment and issues with pumps and lines to the spoils processing facility. It is theorized that this wood was a result of trees and associated roots and old piers/wharves that were buried during levee construction in the late 1800s and early 1900s.

- Although the contractor was required to have equipment for cobbles and cobbles were noted on the boring logs, the contractor reported that “Hard layers of large size gravel or cobbles rocks

have been encountered during the drilling of both test, and production elements at Sump 132." Cobbles, gravel, and dense layers at depth were more abundant than anticipated which slowed production.

- A 10-foot vertical overlap was specified between the jet grout wall and the 2003 DMM cutoff wall, which proved to be an issue for the contractor. The Contractor was responsible for locating the existing 2003 DMM cutoff wall, which was potholed in advance of construction. Unfortunately, as-built records of the 2003 DMM cutoff wall were not available. In addition, cutoff walls tend to widen or 'mushroom' at the top. As a result, a cutoff wall may be several feet wider than designed when the top is exposed. To maintain connection between the DMM and jet grout cutoff walls, the center of the jet grout columns had to be drilled no further than 2.5 feet from the center of the DMM cutoff wall, see Fig. 7. The jet grout pilot holes contacted the top of the DMM cutoff wall, which caused verticality issues.

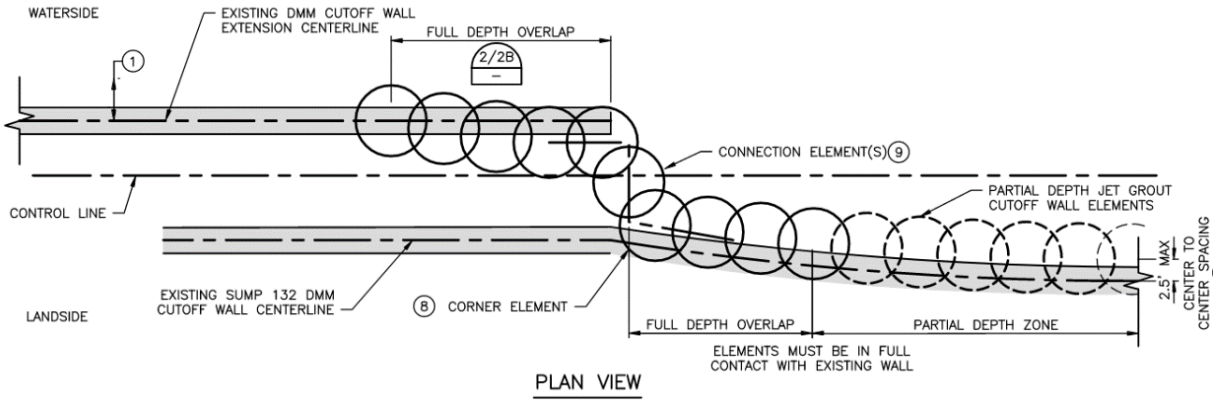


Fig. 7. Typical Jet Grout Column Overlaps

Jet grout column pilot bores were checked for verticality after drilling with an inclinometer. This serves as the basis for column and existing cutoff wall overlap. There were multiple columns that had to be redrilled to achieve the specified verticality, which the contractor attributed to the presence of wood, cobbles, and/or the existing 2003 DMM cutoff wall. The contractor was able to work through these issues; however, construction of the Sump 132 jet grout cutoff wall took about 100 days longer than originally planned.

Difficult Site Conditions and Jet Grouting Issues at Edwards Break

As discussed above, the Edwards Break breach fill was loose and included rock fragments, wood fragments, and gravel pieces with variable sample recovery, all of which affected jet grout construction. The jet grout method was able to construct columns, but not without challenges. The contractor elected to use a Wassara water-activated hammer to drill the jet grout columns and utilized triple fluid methods to construct 8-foot diameter columns. Several test columns developed shallow sinkholes at the ground surface, which are discussed further below.

Jet grouting using triple fluid and single fluid systems are typically open system grouting with continuous circulating drill and jet grout cuttings. Issues such as cross-hole communication, loss of grout in the formation, loss of cutting returns, and settlement of grout are not typically expected to be encountered in jet grouting due to expected continuous circulation. The issues encountered during drilling and grouting in the Edwards break are summarized below:

Wood in drilling and jet grout cuttings: A significant amount of wood was encountered in the drill and jet grout returns (see Fig. 8), primarily in the Edwards Break area leading to repeat jet grouting of the same column. Occurrence of wood hampered the jetting process and choked the suction pumps pumping the drill cuttings to the treatment plant resulting in stoppage of drilling and jetting leading to significant downtime and impacting the overall project schedule. Wood was encountered between depths of 8 feet and 87 feet, though mostly at deeper depths in the middle of the breach and at shallower depths at the outer extents of the breach, which indicates wood may have been used or been buried when the breach was filled.



Fig. 8. Wood screened from jet grouting spoils

Loss of drill and jet grout cutting returns: Multiple instances of complete loss of returns during the drilling and grouting phase were documented. Loss of returns were documented between depths of 23 feet and 81 feet but were predominantly concentrated between 40 feet and 60 feet between boreholes for WH-A16 and WH-A22. An action plan was provided by the PDT for instances of drilling and grouting fluid loss. The plan included options of breaking up column construction into phased pieces, as well as significantly increasing the grout treatment in problematic grouting zones.

Grout communication: Two instances of cross-hole grout communication (grout flowing between adjacent columns) were documented, which highlight the permeable nature of the subsurface.

Sinkholes: The above issues led to multiple sinkholes, which led to the adjustment of jet grouting to a stage-based approach. The sinkhole formation was predominantly observed within the extents of the Edwards Break area (see Fig. 9). This issue is discussed in further detail below.



Fig. 9. Sinkhole on waterside from WH-A24 to WH-A26

Repeat drilling and grouting of the columns: Multiple iterations of drilling and grouting were performed on the jet grout columns. Repeat drilling and grouting were associated with hole deviations and issues encountered during drilling and grouting. Interruptions in jet grouting have the potential to create distinct joints between column phases, and such joints are a potential defect in the cutoff wall. A minimum 6-1/2-foot vertical overlap was utilized by the contractor to mitigate the potential of a distinct joint between column phases.

Sinkholes and Stabilization at Edwards Break

A pre-production test section involving three separate column pairs (six columns total) was installed to show that the contractor's proposed injection parameters would provide a cutoff wall meeting the specified acceptance criteria. During construction of the test section, several sinkholes developed alongside and under the concrete spoils trench and guide wall. These sinkholes indicated a risk to site stability and required a method to improve stabilization prior to cutoff wall production. These sinkholes were backfilled with jet grout slurry placed via a tremie pipe or with CLSM.

 © Deep Foundations Institute 2025

To address the potential for damage to the adjacent structure, the contractor proposed a method of single fluid stabilization columns on the landside of the alignment that would reduce the jetting energy of the production columns in the upper 20 feet of the subsurface. The idea was that by reducing the energy in this zone, sinkholes would be less likely to develop. The proposal shown in Fig. 10 was accepted, with the modification that the landside row of stabilizing columns was reduced from four feet in diameter to three feet in diameter.

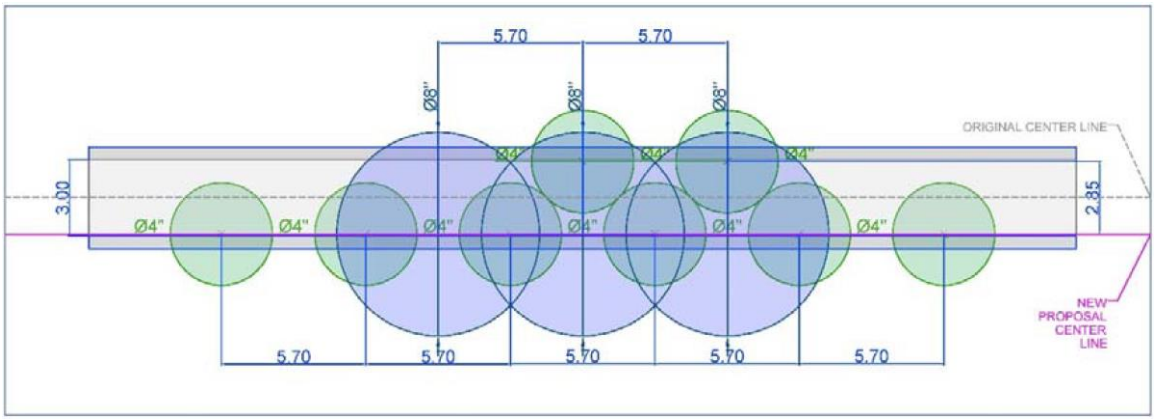


Fig. 10. Contractor proposal to add stabilizing single fluid jet grout columns at Edwards Break

In addition to installation of single fluid stabilization columns, the PDT added installation of four inclinometers to the contract. Inclinometers were measured three times per shift when jet grouting was done within 50 feet of them. This provided a means to monitor for subsurface deformation. Work was halted in a 100-foot radius when large movements (more than 1 inch from prior movement) were measured. This occurred twice when jetting was occurring near inclinometer casings, was investigated and found to be related to jets moving the inclinometer casing and not larger ground movements, and jet grouting continued

Continued sinkhole development led the contractor to propose an alternative jet grouting method employing two phases of jet grouting, as outlined below.

- *By splitting the column into two stages (4-foot with single fluid and immediately after, the 8-foot with triple fluid), the column will be installed following a progression, in which the second step will compensate potential instabilities created during the first step.*
- *Additionally, during the first step with single fluid, we have the possibility to monitor instability and fluid loss in a limited volume with reduced risks.*
- *The sequence of work can be described as follows:*
  1. *Drill using the WASSARA hammer down to design level.*
  2. *Withdraw and switch to single fluid monitor.*
  3. *Drill to 15 meters (or 49 ft) depth using grout and start jetting bottom to top (parameters for the 4-foot columns) up to the bottom of the trough (3 feet below ground level).*
  4. *Switch the monitor to triple fluid.*
  5. *Drill down again to the bottom design level using grout and start jetting bottom to top (parameters for the 8-foot columns) up to 6 meters below ground level.*

 © Deep Foundations Institute 2025

6. *Switch off water and air pressure and re-inject with 4-foot parameters the last 5 meters (up to bottom of trough).*

This alternative method was accepted to construct the remaining production columns. Minor sinkholes developed while using this alternative method, but it otherwise seemed to reasonably mitigate the risk.

Potential Fluid Escape into the Sacramento River at Sump 132

As the contractor installed the jet grout cutoff wall columns at Sump 132, there were instances of air bubbles rising within the Sacramento River. Air bubbles could indicate fluid escape, which posed an environmental concern and had to be mitigated. Jet grouting was determined as the cause since triple fluid jet grouting uses several liters per minute (about 0.5 gallon per minute) of compressed air flow, and the bubble flow ceased when jet grouting was stopped. When the contractor noticed the air bubbles in the river, they notified the PDT and coordinated an adjustment to the work plan to move from the downstream location where the bubbles appeared to a location further upstream, which was accepted to reduce schedule impact. The contractor continually monitored the river for signs of air or grout releases and would implement a water testing protocol when bubbles or turbidity were noticed. No grout releases occurred. In addition, the contractor was provided with an alternate construction method when air bubbles were noticed in the river by onsite personnel. The outline discussed with the contractor is as follows:

- *Above 80-foot depth – From the crown surface, inject with the PS-TC1/PS-TC2 triple fluid "no air" parameters.*
- *Below 80-foot depth - "Pre-treat" the column with low-pressure grout and no water/air from the depth air bubbles are observed at to the top of the column. Return to the column and complete at a later date after the grout has had time to strengthen. Complete by drilling through to a few feet below the depth injection stopped at and continue injection up to the top of column.*
- *For multi-stage columns (i.e. columns completed over more than one day), complete the upper part of the column from a depth of 25 meters or greater from the levee crown surface. This will address potential problems caused by woody debris encountered around 20-23 meter depth.*

Raw Data Processing and Analysis

Once the contractor demonstrated that the chosen jetting parameters (hydraulic horsepower (HHP) for the water and cement pumps, and pounds of cement injected per linear foot) produced a compliant soil-cement material, then the production columns must have not less than 90 percent of the selected values. Once these limits were established, they had to be maintained during production and verified using the data acquisition system at the drill and grout batch plant.

To verify that the specification was met, the PDT processed the raw data collected by the jet grouting monitor and developed statistical summary tables and normal distribution curves. These tables and plots were used to verify that the target parameters (water jet and grout jet specific energies in particular) were met for each column. Columns that had relatively lower specific energies, as shown by developed tables and plots, were often prioritized as coring locations. Examples of statistical tables and plots used for quality assurance purposes are shown below in Figs. 13 and 14.

Column WH-A12	Parameter							
	Air Pressure	Air Flow	Water Pressure	Water Flow	Grout Pressure	Grout Flow	Jetting SE	Grouting SE
Unit	bar	L/min	bar	L/min	bar	L/min	MJ/M	MJ/M
Target	13	6000	430	485	180	432	189	70
Min	4	4509	323	378	137	342	149	53
Median	8	7903	458	467	209	433	194	82
Mean	8	7998	458	468	208	433	194	82
Stdev.P	1	845	3	10	2	12	4.10	1
Max	12	17569	466	619	233	1486	234	140

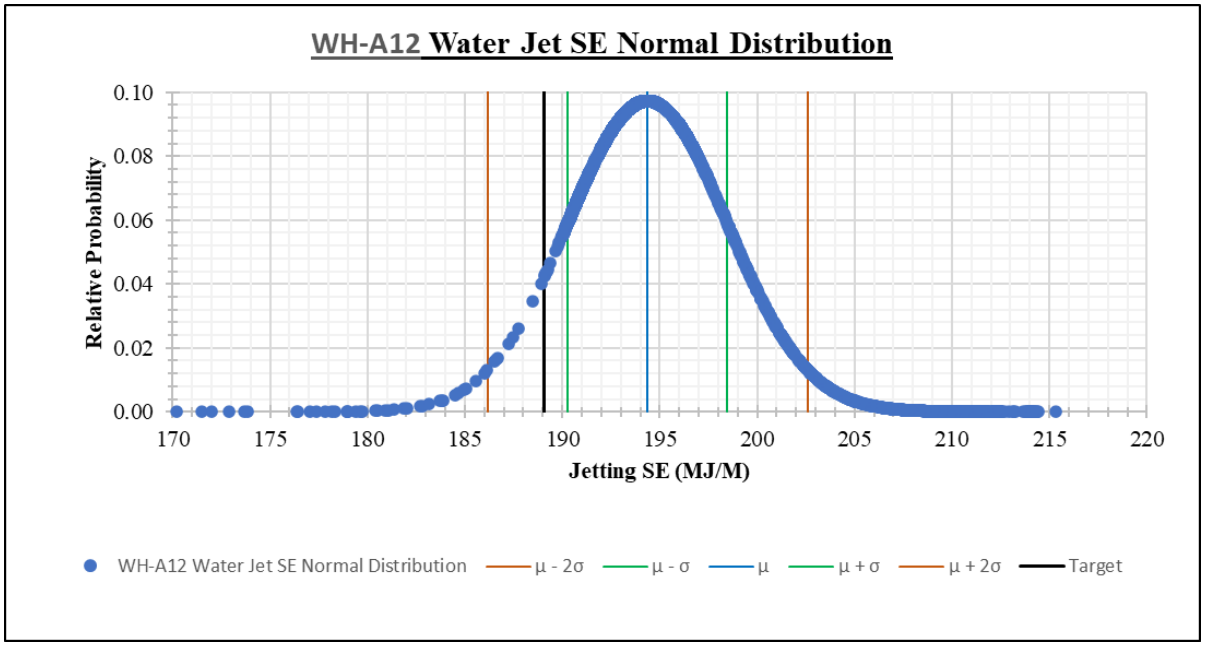


Fig. 13. Example of a triple fluid jet grout column's water jet specific energy raw data normal distribution curve after data processing

 © Deep Foundations Institute 2025

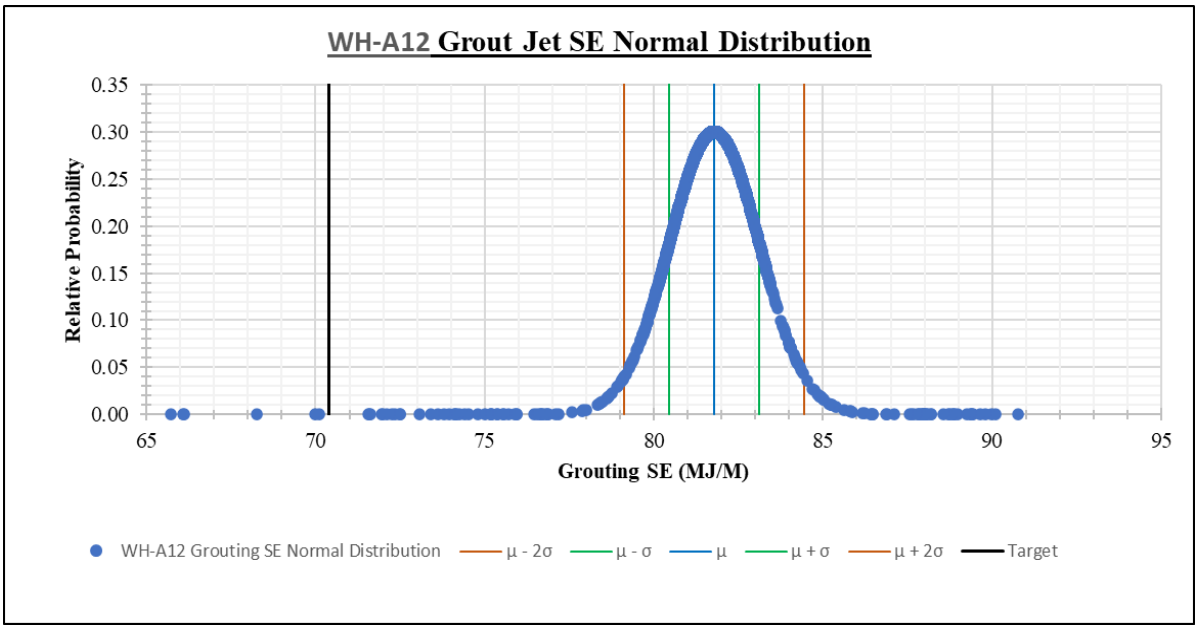


Fig. 14. Example of a triple fluid jet grout column's grout jet specific energy raw data normal distribution curve after data processing

Additional Verification Coring and Testing

The project specifications required coring and in-situ testing at a rate determined by the Contracting Officer with a minimum of 10 percent of the production cutoff wall columns to be cored. The total amount of coring at the Edwards Break heading was doubled to 20 percent of the production cutoff wall columns. With a total of 46 production columns, this increased the number of coring locations from five to nine. This modification was made to better assess the treatment in this problematic heading. The additional cores were located in column overlaps that were expected to have defects based on construction records and provided data on whether there was in fact a physical defect that required repairs.

SUMMARY

The work along the SREL system had many unique challenges. Jet grouting is a labor-intensive operation that is used for specialized applications. As a result, each site required adaptation to site conditions and alterations of plans and schedules to get the project done. The work had unanticipated site conditions, unexpected equipment issues, and was in an urban environment with limited access including existing private structures/businesses and residential backyards that backed up to the construction limits. As discussed in this paper, many issues arose during construction that required a quick response by the team. The engineering and contractor teams worked closely to identify these issues, develop solutions, and implement those solutions. By maintaining a collaborative work environment and close communication between the contractor and the design, quality assurance, construction engineering, and construction oversight teams, the work was successfully completed.

ACKNOWLEDGEMENTS

The authors would like to sincerely thank the U.S. Army Corp of Engineers for the support extended through the execution of the SREL Contract 4 design and Engineering during Construction (EDC) effort.

 © Deep Foundations Institute 2025

Cooperation and assistance from the Sacramento Area Flood Control Agency, the City of Sacramento Department of Utilities, and State of California Department of Water Resources were important to project execution.

The project could not have been completed without the hard work and effort by Maloney Odin, A Joint Venture, the prime contractor and their major subcontractors Treviicos, Inc., (subcontractor for jet grouting) and Raito, Inc. (subcontractor for DMM).

REFERENCES

EM 1110-2-1913, Design and Construction of Levees. United States Army Corps of Engineers. Dated April 30, 2000.

Plans- Sacramento River East Levee, Contract 4, American River Common Features 2016, Sacramento, California. Solicitation No.: W91238- 23-B-002. Contract No.: W91238-23-C-004. Prepared by Kleinfelder and Stantec for United States Army Corps of Engineers, Sacramento District. Issue Date: 20 January 2023.

Technical Specifications. American River Common Features 2016, Sacramento River East Levee, Contract 4, Sacramento County, California. Project No. 456852, Specification No. 2440, Design File No. 6-04-2304. United States Army Corps of Engineers, Sacramento District.

Design Documentation Report. American River Common Features 2016, Sacramento River East Levee, Contract 4, Sacramento County, California. Project No. 456852, Kleinfelder in association with Stantec, January 27, 2023.

 © Deep Foundations Institute 2025

JET GROUTING: A WIDE RANGE OF APPLICATIONS

Nathan P. Coughenour, P.E., M.ASCE, Geo-Solutions Inc., New Kensington, PA USA, 724-335-7273, ncoughenour@geo-solutions.com
Daniel G. Ruffing, P.E., M.ASCE, Geo-Solutions Inc., New Kensington, PA USA, 724-335-7273, druffing@geo-solutions.com
Josh Bonetto, EIT, Geo-Solutions Inc., New Kensington, PA USA, 724-335-7273, jbonetto@geo-solutions.com

ABSTRACT

Jet grouting, a ground improvement technique with wide application for solving geotechnical and geoenvironmental problems, has been around for over 50 years. At a high level, jet grouting is a cross between soil mixing and grouting that utilizes a high-pressure fluid stream to erode and mix the soils with grout.

What makes jet grouting so unique and widely applicable is the highly customizable implementation. Jet grouting provides the ability to install relatively large subsurface elements (commonly 1 to 3 meters, or even larger) combined with the flexibility associated with a small drilling rig with small physical tooling (typically 70 to 120 mm).

The purpose of this paper is to provide an overview of different applications of jet grouting, including case study examples. The applications and case studies covered include mass stabilization/solidification (ISS), groundwater cutoff walls, and targeted jet grouting used in conjunction with slurry trenching and soil mixing techniques.

INTRODUCTION

Jet grouting is a versatile ground improvement technique used to enhance soil properties. The process differs from soil mixing in that the mixing is performed with a high-pressure fluid stream, not an auger, and differs from traditional grouting in that the grout is pumped into cavities created by the process, not existing voids. The process results in a soil-cement column that exhibits improved strength and reduced permeability relative to the soils alone. The design of jet grout columns is based on soil properties, selection of grout, and grouting parameters (Evans et al, 2021). Jet grouting serves the dual purpose of soil densification through rearrangement and cohesive strength improvement. The process has evolved to address diverse soil types and challenges, with significant developments in equipment and methodology over the years. Case studies illustrate the successful application of jet grouting in various projects, emphasizing its role in solving diverse problems with soil and groundwater. All the case studies presented were performed by Geo-Solutions, Inc. (GSI).

JET GROUTING TECHNIQUES

The jet grouting process involves the use of high-pressure jets to erode soil while simultaneously injecting grout which mixes with the in-situ material to form solidified columns with enhanced strength and reduced permeability. This technique begins with drilling to the desired depth. Once the target depth has been reached, the grout injection begins through a nozzle at high velocity and pressure. The high-pressure fluid grout erodes and mixes with the soil. The resulting soil-cement mixture hardens to create a column that can be used for various applications, including foundation support, slope stabilization, and groundwater control. Jet grouting is adaptable to different soil types and site conditions, making it a versatile solution in geotechnical and geo-environmental engineering (Evans et al, 2021).

 © Deep Foundations Institute 2025

Jet grouting systems are categorized into single, double, and triple fluid methods. The single fluid system uses neat cement grout, injected at high pressure/velocity through horizontal nozzle(s), that erodes and mixes with the in-situ soil. The double fluid system combines grout and a second fluid, typically air, that is used to enhance the erosion and mixing process. Double fluids systems are typically desirable for jet grouting in cohesive soils. The triple fluid system utilizes one fluid, typically water, assisted by a second fluid, typically air, to erode the in-situ soil, while a separate nozzle placed lower on the drill stem delivers the cement grout, to mix with the in-situ soil (ASCE - GI, 2016). These systems allow for precise control over the geometry and properties of the treated soil, enabling their use in various geotechnical and geo-environmental applications (Gurpersaud, et. al, 2019).

Jet grouting offers several advantages over other ground improvement techniques, such as its versatility in treating a wide range of soil types, including silts and clays, and its ability to create strong, low permeability soil-cement columns. This method is particularly effective in confined spaces and complex site conditions, making it suitable for urban construction and environmental remediation projects (Evans et al, 2021). However, jet grouting can be more expensive and time-consuming compared to other grouting or soil mixing methods. This is mostly due to the high-pressure injection process requiring specialized equipment and expertise which can increase project costs (Evans et al, 2021).

IN-SITU STABILIZATION/SOLIDIFICATION (ISS) OF CONTAMINATED SOILS

In-situ soil solidification/stabilization (ISS) is an environmental remediation technique that involves the addition of binding agents to contaminated soil to immobilize hazardous constituents and improve soil properties (US EPA 1991). This process increases the strength and reduces the permeability of the treated soil, making it suitable for future construction while solving the environmental issue (US EPA, 2006). ISS is particularly effective in treating heavy metals and organic contaminants, providing a cost-effective and less disruptive alternative to excavation and ex-situ treatment (US EPA, 2006). The technique also offers other benefits such as reduced waste generation and lower overall project costs (US EPA 1991).

ISS is typically performed using soil mixing but can also be performed using jet grouting. Previous literature has highlighted the use of jet grouting for mass/block ISS, including Gazaway and Jasperse, 1992 and Day et. al. 1997. The following section provides brief examples of jet grouting utilized for ISS applications.

Case Study Example – MGP ISS

As part of an overall site remediation plan for a former MGP site, jet grouting was utilized to stabilize the annular space between a brick outer wall and steel inner wall of a former subsurface gas holder. The 18-inch gap around the perimeter of the 105-foot diameter holder was filled with a combination of impacted soils and coal tar. Due to the limited space between the inner and outer gas holder walls, neither removal of the soils or traditional ISS methods were viable, so jet grouting was selected for the ISS implementation in this zone. Figure 1 shows the jet grouting ISS being performed. In total, over 100 jet grout columns were installed to 22’ deep on a 3-foot spacing to create a stabilized monolith in the annular space. All jet grouting ISS quality control samples met the project requirements of greater than 50-psi UCS and less than 5x10^-6 cm/sec permeability.

 © Deep Foundations Institute 2025



Fig. 1. Jet grouting ISS of MGP impacted soils

Case Study Example – Mercury ISS

Jet grouting was utilized at a former Superfund site in the Northeastern US, focusing on solidifying mercury-contaminated soils beneath existing building footers. Mercury impacted soils on the interior of the site, including beneath interior footers, were removed, treated ex-situ, and disposed of as part of earlier remedial actions. However, the mercury impacted material beneath the footers of the perimeter retaining wall would have been costly to remove due to the complex excavation and shoring that would have been required adjacent to and beneath a city sidewalk, street, and utility corridor. As an alternative to removal, ISS was used to stabilize the mercury in place. For implementing the ISS, jet grouting was selected due to the ability to implement at angles and to complete the work from within the site footprint with limited to no disturbance of an adjacent retaining wall or the sidewalk and utilities exterior to the retaining wall.

 © Deep Foundations Institute 2025

A field demonstration test was completed on the interior of the site to test multiple jetting parameters and mix designs prior to full scale implementation. Test columns were exposed via excavation and column diameters were assessed. Nine-foot diameter columns were achieved which helped eliminate the need for jetting outside of the site footprint.

Figure 2 below shows the jet grouting configuration and orientation utilized to stabilize the impacted soils beneath the footer. In addition, to increase the coverage below the footers, a sonic drill rig was utilized to create pilot holes through the footer which allowed the jet grout tooling to pass through. These columns were drilled at an angle which allowed the jet nozzles to extend laterally below the footers and create additional coverage/treatment.

A drill setup for jet grouting and a high-pressure jet grouting pump were used to perform the work using a specially formulated grout mixture of Portland Cement, Bentonite, Sulphur, MercLok™, and water. A total of 14 columns were installed to ensure full treatment below 5 perimeter footers. Spoil trenches were excavated before installation of columns and the spoils were diverted into a poly cast pond to maintain a clean site. Following the initial cure/set period, the spoils were relocated to a load out zone and shipped to a disposal facility specializing in handling mercury contaminated waste. Given the short duration of onsite work, this project required a quick turnaround time for analytical spoils data to meet the transport and disposal schedule.

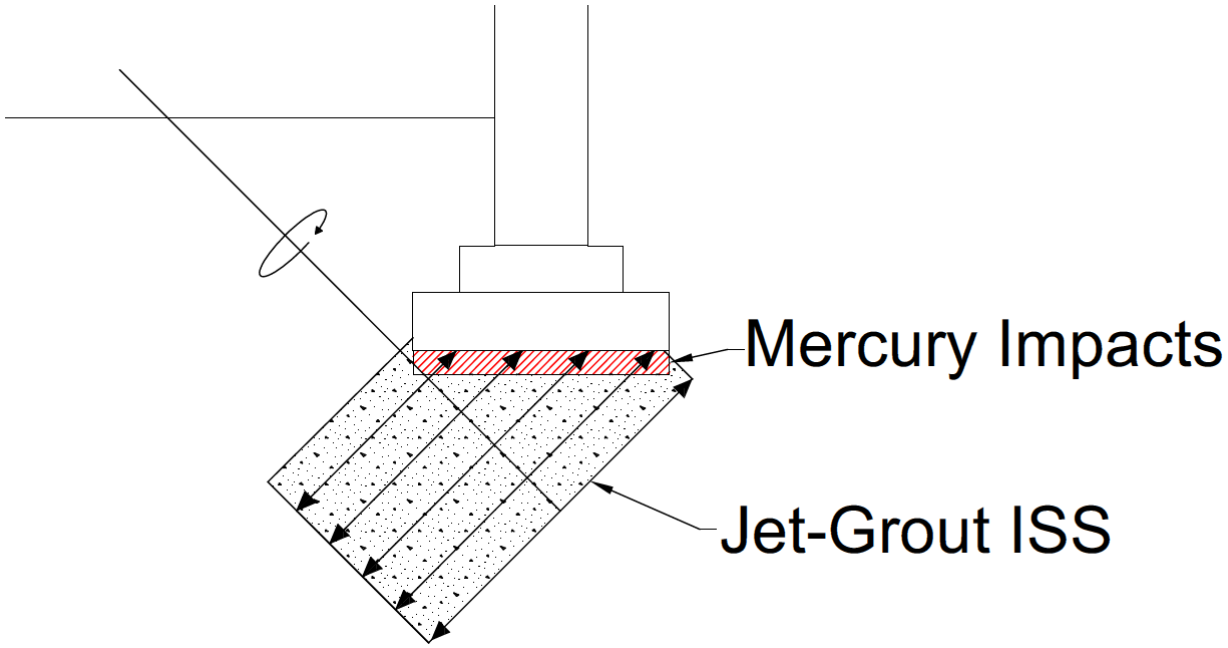


Fig. 2. Installation geometry for jet grouting of mercury impacted soils beneath retaining wall footer

Figure 3 shows the mercury stabilization via jet grouting being performed on one of the five footers. Wet grab samples were taken during the jet grouting work and achieved the project requirements for UCS (minimum 25 psi) & hydraulic conductivity (average $< 1\times10^{-6}$ centimeters per second (cm/sec). Following the completion of ISS work, approximately 5,100 tons of stone was imported and compacted at 1-foot lifts at 95% compaction across the work area prior to turning the site back to the Owner.

 © Deep Foundations Institute 2025



Fig. 3. Jet grouting of mercury impacted soils beneath retaining wall footer

GROUNDWATER CUTOFF WALL INSTALLATIONS

Groundwater cutoff walls, installed using various methods, are a common tool for environmental containment or to slow water flow for geotechnical objectives. These cutoff walls are installed to cut off or slow horizontal groundwater flow. Jet grouting's adaptability to various soil types and its ability to form continuous, low-permeability walls make it a valuable tool in groundwater control applications such as excavations that need to be carried out below the water table (Amatya, et. al., 2015) and to seal areas between retaining walls and bedrock, ensuring dry excavation conditions (Lundberg, A.B., et al. 2024).

Case studies have demonstrated success in creating hydraulic seals for excavations and other subsurface structures (Klein et al, 2006) and for effectively controlling groundwater flow and preventing contaminant spread at contaminated sites, including but not limited to, Gazaway and Jasperse, 1992. Another case study for jet grouting in this application is presented below.

Case Study Example – Environmental Cutoff Wall

277 jet grout columns were installed to a maximum depth of 40 feet below ground surface, creating 595 linear feet of cutoff wall at a Former Manufactured Gas Plant in New Jersey. The project site was an active facility with critical infrastructure that required uninterrupted operations throughout the remediation work. All site Contractors were required to coordinate the sequencing of the work with the owner such that the Owner’s active operations were not impacted.

Jet grout columns were installed from existing grade to refusal at the top of weathered bedrock. A single row of jet grout columns was installed along with a cement bentonite slurry wall as part of the barrier wall

 © Deep Foundations Institute 2025

construction. Approximately 15,000 vertical square feet of jet grout barrier wall was installed. The jet grouting process involved columns ranging from 4 to 6 feet in diameter, with several columns installed within 2 feet of active underground utilities, including gas lines. Utilities were exposed and protected to ensure safety during grouting. Spoil trenches were excavated before column installation, and a vac truck was utilized for spoil management to maintain a clean site. Wet grab samples and full-depth cores were taken throughout the project for UCS and hydraulic conductivity testing, all of which were accepted by the Geotechnical Engineer. This phase of the project required careful coordination around active construction and utilities, highlighting the complexity and precision of jet grouting in an active facility. Figure 4 shows the jet-grout cutoff wall being installed in one of the planned locations.



Fig. 4. Jet grout cutoff wall installation

GROUNDWATER CUTOFF FOR DEEP EXCAVATIONS

Deep excavations require consideration of how to keep the soil sidewalls stable and manage groundwater while the excavation is "open". Cutoff walls are a cost effective and technically sound solution for assisting with groundwater management and may even be incorporated into the shoring system used for sidewall support. Jet grouting is a practical method for constructing groundwater cutoff walls for deep excavations, particularly in urban environments where space is limited and precise control over the geometry and properties of the treated soil is required. In this application, columns are interconnected to form continuous cutoff walls, effectively sealing the excavation from surrounding groundwater (Evans et al, (2021). Case studies have demonstrated its success in preventing groundwater intrusion in deep excavation projects, highlighting its versatility and effectiveness (Johansson & Spånér 2020). Another case study for jet grouting in this application is presented below.

 © Deep Foundations Institute 2025

Case Study Example – Deep Excavation Groundwater Cutoff & SOE Wall

170 jet grout columns were installed to a maximum depth of 17.4 meters below ground surface at a project site in Ontario, to create a subsurface groundwater barrier as part of a support of excavation (SOE) system. Jet grout columns along with drilled caissons provided a combination cutoff wall and SOE system for the construction of elevator shafts allowing additional access to the subway station below grade. The project involved jet grouting within close proximity to an active subway tunnel, residential walkways and houses, and various underground utilities, including gas, water, and sewage lines. Utilities were exposed and protected with demarcations or steel plates to serve as drill guides. A field demonstration test was completed prior to full scale production to verify column diameters and jetting parameters. In addition to the jet grouting, the project scope, including spoil management using excavated trenches and a vac truck. Due to the small footprint of the project site, multiple spoils staging areas were required and extensive coordination between deliveries, spoils disposal, and the jet grouting operation was conducted daily. Traffic control was required for entering and exiting the site and for maintaining access to the active subway station entrance. For QA/QC, wet grab samples, full-depth cores, and in-situ packer testing were conducted, with all results accepted by the Geotechnical Engineer. The jet grouting portion of the project required careful coordination around active construction and utilities in a densely populated area. Figure 5 shows the jet grouting being implemented on the tight urban site.



Fig. 5. Jet grouting for groundwater control of future deep excavation

 © Deep Foundations Institute 2025

JET GROUTING COMBINED WITH OTHER TECHNIQUES

Jet grouting is a highly effective tool for use with other techniques in targeted applications around utilities or obstructions, providing precise improvement in challenging conditions (Gurpersaud, et. al, 2019). This method is particularly useful for urban projects where space is limited, and utilities such as gas, water, and sewage lines must be protected and/or where other obstructions limit the applicability of other techniques such as soil mixing or sheet piles. Jet grouting allows for the creation of subsurface barriers without disturbing existing infrastructure, ensuring safe and efficient construction. Case studies have demonstrated the success of jet grouting in stabilizing soils and controlling groundwater flow around critical utilities and structures including the following.

Case Study Example – Targeted Jet Grouting Around Utilities for Groundwater Cutoff

Jet grout columns were installed to create a cutoff wall surrounding active utility corridors at a site in New York. The jet grouting program connected two segments of a slurry wall, avoiding contact with utilities that could not be terminated or relocated. A blend of Portland Cement and Blast Furnace Slag was used to achieve the groundwater cutoff, with columns extending to a target depth of 32 feet below ground surface. This method ensured the creation of an effective subsurface barrier while protecting existing utilities and maintaining site integrity.

The jet grouting process involved precise construction operations to connect the slurry wall segments without disturbing the active utilities. The project required careful coordination and planning to manage the work in proximity to multiple utilities, including water, gas, electric, and sewage lines. The approach included exposing utilities and using protective measures such as steel plates to guide drilling and prevent damage.

Case Study Example – Targeted Jet Grouting Around Utilities for Perimeter Containment System

As part of a perimeter containment system, jet grouting was performed around utility crossings and sheet piles in New Jersey. The project involved using a single fluid jet grout system to install 13 four-foot and 2 five-foot diameter jet grout columns to a maximum depth of 80 feet below ground surface. The jet grouting parameters were carefully selected to ensure the formation of columns with diameters between 4 and 5 feet in the expected soil conditions. The key objectives of the project were to achieve a complete tie-in between sheet pile walls on both sides of the utilities and between the sheet pile bottom and bedrock, ensuring the jet grout barrier had a permeability less than 1x10^-6 cm/s. Figure 6 shows a few example plan drawings of the jet grout column layout.

Challenges included achieving full tie-in around utilities due to the high prevalence of subsurface obstructions and working immediately adjacent to the river. Despite these challenges, the subsurface jet grouting barrier was successfully installed on schedule, demonstrating the versatility of jet grouting in complex geotechnical conditions for environmental sites. The QC samples resulted in an average unconfined compressive strength (UCS) of grab samples of 800 psi, and average hydraulic conductivity of $5x10^{\wedge -8}$ cm/s after 28 days.

 © Deep Foundations Institute 2025

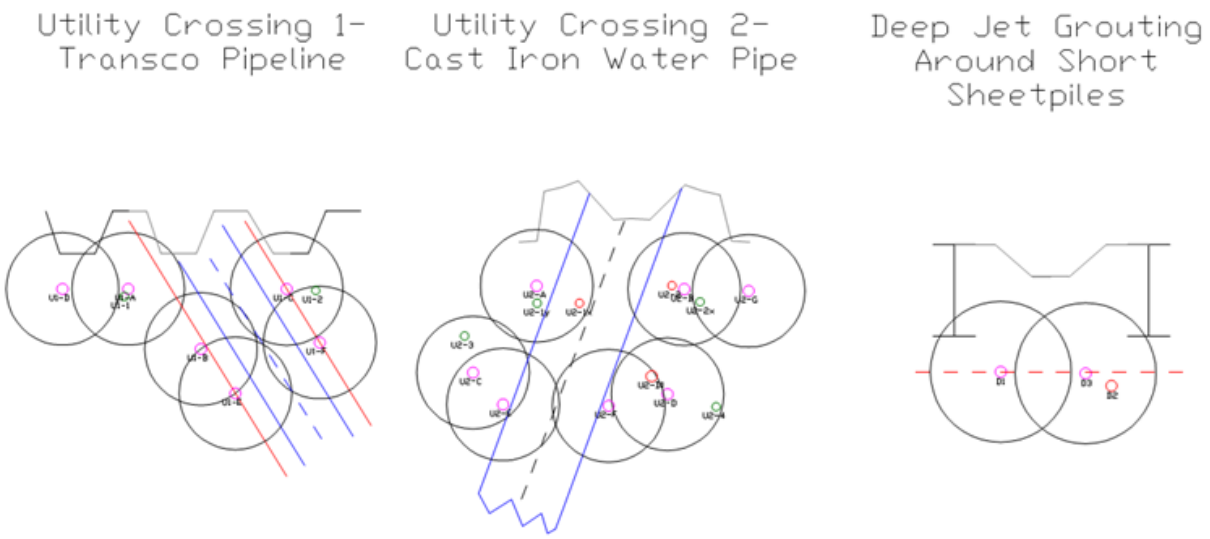


Fig. 6. Jet grouting layout around utilities and sheet piles

CONCLUSION

Jet grouting is proven to be a versatile and effective ground improvement technique with a wide range of applications in geotechnical and geo-environmental engineering. Its ability to create strong, low permeability soil-cement columns makes it suitable for solving various challenges, including soil stabilization, groundwater control, and foundation support. The adaptability of jet grouting to different soil types and complex site conditions, such as urban environments with limited space and the presence of utilities, further enhances its usefulness. Case studies have demonstrated the successful implementation of jet grouting in projects involving mass ISS, groundwater cutoff walls for environmental and hydrogeologic applications, and targeted applications around utilities or obstructions.

Looking ahead, future developments in jet grouting technology may focus on improving efficiency and reducing costs. Advancements in equipment and methodology could enhance the precision and effectiveness of jet grouting, making it an even more valuable tool for addressing geotechnical and geo-environmental challenges. Continued research and innovation will likely expand the range of applications for jet grouting, ensuring its relevance in modern construction and environmental remediation projects. As the field evolves, jet grouting will remain a crucial technique for creating stable and sustainable ground conditions in diverse engineering scenarios

REFERENCES

Amatya, S., Haberfield, C.M, Zhan, R., 2015, Assessing Probability of Not Achieving Column Overlap in Jet Grout Applications. 12th Australia New Zealand Conference on Geomechanics and was edited by Graham Ramsey. ISSMGE.

ASCE G-I Grouting Committee - Jet Grouting Task Force, 2016. Jet Grouting Guide Specification. Geo-Institute of ASCE.

Day, S., Zarlinkski, S., and Jacobson, P., 1997. Stabilization of Cadmium-Impacted Soils Using Jet-Grouting Techniques. ASCE Specialty Conference, In-Situ Remediation of the Environment.

 © Deep Foundations Institute 2025

Evans, J., Ruffing, D., & Elton, D. (2021). Fundamentals of Ground Improvement Engineering (1st ed.). CRC Press. https://doi.org/10.1201/9780367816995

Gazaway, H.N., & Jasperse, B.H., 1992. Jet Grouting in Contaminated Soils. Grouting, Soil Improvement and Geosynthetics, 206-214.

Gurpersaud, N., Lees, D., and Han Z., 2019. Specialty Grouting Techniques: Technical Considerations and Applications. GeoSt. John's, 73rd Canadian Geotechnical Conference, St John's, NL.

Johansson, L., Spånér, F., 2020. Preventing Groundwater Intrusion in Piled Excavations Using Jet Grouting. Chalmers University of Technology, Department of Architecture and Civil Engineering.

Klein, E., Andromalos, K., and Trimble, J., 2006. Soil Nail and Jet Grouted Excavation Support Wall At Peirce Mill Dam. Deep Foundations Institute, 2006.

Lundberg, A.B., et al., 2024. Modelling the Permeability of a Jet-Grouted Cut-Off Wall." NGM2024, 2024.

US EPA., 2006. In Situ Treatment Technologies for Contaminated Soil. United States Environmental Protection Agency – Solid Waste and Emergency Response. EPA 542/F-06/013.

US EPA., 1991. Solidification/Stabilization Resource Guide. United States Environmental Protection Agency – Office of Solid Waste and Emergency Response. EPA/542-B-99-002.

 © Deep Foundations Institute 2025

DRIVEN PRECAST CONCRETE PILES IN LIEU OF STEEL PILES AT BLUESCOPE STEEL'S PORT KEMBLA FACILITY

Stephen Harkin – BE(Civil), MIEAust, CPEng (Civil/Structural/Geotech), NER, APEC Engineer IntPE(Aust)
Business Development Manager, Wagstaff Piling, Sydney, NSW, Australia. s.harkin@wagstaffpiling.com.au

ABSTRACT

In the heart of New South Wales's (NSW) steel manufacturing territory, the BlueScope Steel Port Kembla facility, approximately 100km south of Sydney on the east coast of NSW, Wagstaff Piling was successful in providing an alternate foundation solution comprised of driven, segmental precast concrete piles in lieu of the traditionally used foundation system of driven steel piles for the No. 6 Blast Furnace Reline project. The alternate solution of concrete piles not only provided design parity but also such significant program, cost and construction advantages to the project that the big steel manufacturer shifted away from what it had always done to a more innovative solution of using precast concrete piles. Until that point in time, Wagstaff Piling had only carried out minor projects using driven precast concrete piles within the Port Kembla facility, however, the successful outcomes of these projects along with the historical pile load testing data provided compelling evidence of the suitability of the alternative foundation solution for the major project works. Wagstaff Piling worked collaboratively with BlueScope Steel and their structural and geotechnical engineering design consultants to develop robust and efficient foundation solutions for the various structures within the facility.

Key Words: Dynamic, Precast, Driven, Piling

INTRODUCTION

While the Illawarra region of the NSW South coast has always been a coal mining and processing district due to the prevailing geotechnical conditions, steel manufacture did not start in earnest in Port Kembla until the late 1920's when the Hoskins family relocated their operations from the upper Blue Mountains. This was not only to gain access to a deep water port but to be closer to the coal supply with easier transport and big business opportunities in Sydney. Since that time, it has become the largest manufacturing facility in NSW producing steel plate products and covers an area of approximately 760 hectares. Blast furnaces are used at Port Kembla to produce iron, which is the first part of the steel manufacturing process, from iron ore and coke.

The number 6 blast furnace at Pt Kembla has been offline since 2011, however, in 2023 the 6BF Reline project was announced to reline the blast furnace so it could be brough back online.

A geotechnical profile of deep alluvial soils and an existing steel manufacturing facility meant that the preferred pile type in and around the facility had always been driven steel piles. Predominately, universal bearing piles (UBPs) or universal columns (UC's) have been driven for all the structures and services throughout the plant and its surrounds.

While well versed in driving steel piles as a foundation solution, Wagstaff Piling offered an alternative design solution consisting of driven, segmental, precast concrete piles in lieu of steel piles. The precast concrete pile installation process requires similar piling equipment, but fewer processes and site labour. This is because the concrete piles have a mechanical joint to connect pile segments, rather than requiring a welded splice as steel piles do. This efficiency in installation was a major factor in BlueScope Steel to moving away from their traditional steel piles and engage Wagstaff Piling on a design, construct and certification contract basis.

 © Deep Foundations Institute 2025

This project case study discusses the design and manufacture of the precast concrete piles along with the installation of the piles using various piling rigs and hydraulic hammer sizes as well as the innovative techniques used to overcome some of the site constraints. Results of pile load testing, analysis and reporting will also be presented and examined. The paper also covers the unique construction and design challenges of working within an a live steel production and manufacturing facility.

SITE LOCATION AND DESCRIPTION

Port Kembla is located approximately 100km south of Sydney on the south coast of NSW and directly south of the city of Wollongong. A coal mining region from the mid 1850's the Illawarra region progressed along a typical path incorporating deep water port facilities, steel manufacturing and processing plants along with their respective supporting trades and service providers accounting for a big proportion of the employment and vocational pathway opportunities in the area.

SUBSURFACE CONDITIONS

The prevailing geotechnical conditions throughout the BlueScope facility at Port Kembla is a profile of made ground consisting of gravelly, sandy filling and coal wash with a capping layer of slag which is a byproduct of the iron making processes in the blast furnaces on site. The thickness of this filling in general, ranges between 1.5 and 4m but in localised areas up to 8m from surface level. The fill overlies estuarine clays and sands then alluvial clays over residual clay grading to slightly weathered sedimentary or metamorphic rock. The depth to this rock, and hence driven pile length varied from approximately 17 to 22m from surface level.

The slag filling layers through the site presented an interesting challenge for the pile installation. While the slag can be compacted quite well and then become effectively cemented together and as such act as a fantastic working platform for plant, equipment and subgrade for roads and light structures, it is this very useful property which prevents piles from being easily driven through it. As such a process of pre-drilling and pre-digging of each pile location was undertaken in the upper filling to allow the concrete piles to be installed without overstressing the piles or causing damage. This pre-drilling also reduced the transfer of surface vibrations from the pile driving.

The geotechnical investigation reports had a suite of cone penetrometer tests (CPTs) and cored boreholes to assess the insitu strengths and stiffnesses of the soils and strength and weathering of the rock. The estuarine clays and sands were generally firm to stiff and very loose to loose and the deeper alluvial and residual clays were very stiff to hard. The bedrock, irrespective of if it was sedimentary or metamorphic (sandstone or latite) had a shallow weathering profile of less than 1m before the rock became at least medium if not high to very high strength.

This combination of stiff and very stiff clays at depth and good quality founding rock conspired to produce very good geotechnical capacities for the piles in both compression and tension. These capacities were proven with dynamic pile load testing using Pile Diving Analyser (PDA) and analysed with the signal matching software CAPWAP. These testing results are discussed later in this paper.

Image 1 below shows a typical subsurface profile.

 © Deep Foundations Institute 2025

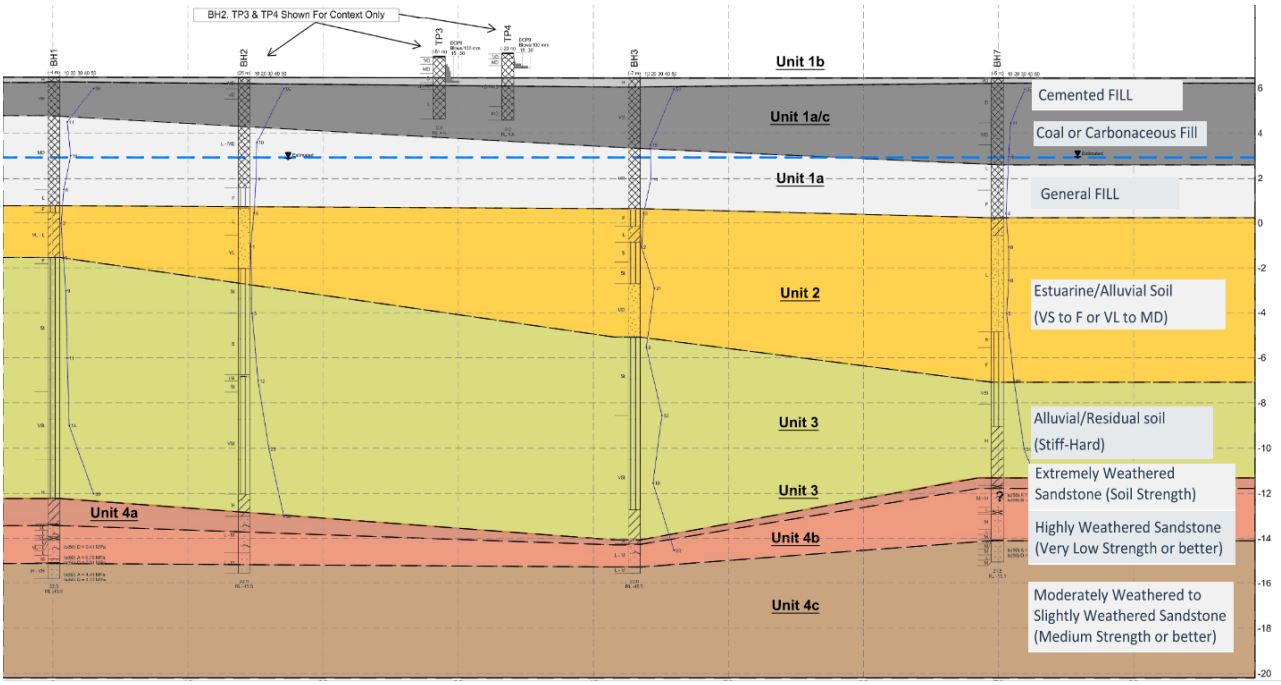


Image 1 – General Geotechnical Profile

DESIGN PROCESS

As previously discussed, BlueScope Steel's decision to move towards a driven precast concrete pile foundation solution in lieu of their traditional steel pile solution was a relatively large step. In doing so it also challenged some of the rigid design processes that have been used at the facility. Strong specifications and detailed processes are essential at a large facility to ensure conformity in construction and robustness of design. One of these specifications deals specifically with pile design, installation and quality control. The document itself nominates the maximum axial and lateral loads that can be apportioned to steel piles subject to their section size and length. This allows a fairly simple process for the structural consultants to apportion a number and size of piles required to carry the design actions from the buildings they are designing.

The move to precast concrete piles meant that the structural and geotechnical design of the piles now rested with the piling contractor, it also required the structural designers to provide pile loads at each pile location for the design process to develop. The BlueScope Steel project team initiated this process with a series of introductory meetings between the Wagstaff Piling design engineers and the five respective structural consultants that were engaged by BlueScope Steel. Each of these consultants were looking at separate sub-projects within the 6BF Reline project and were all focused on their own individual requirements and design criteria for their structures. These structures were as follows:

- Top Gas Recovery Turbine,
- Slag Handling Area,
- Waste Gas Recovery,
- Excess Gas Bleeder,
- Primary Ferrous Area.

 © Deep Foundations Institute 2025

The design process started with the Top Gas Recovery Turbine (TRT) structure. The structural consultant provided a suite of axial and lateral actions in both ultimate limit state (ULS) and service limit state (SLS) for the piles. These varied subject to the location of the piles and the nature of what the structure above required from the foundation.

A detailed design covering both geotechnical and structural aspects of the piles was then undertaken. The geotechnical analysis of the piles subject to lateral actions was either carried out using L-Pile for individual pile actions or with PIGLET for pile groups. Both of these design programs are widely used in the foundation industry and have good correlation with pile test data. Once the geotechnical design was carried out, the bending moments induced by the lateral loading acting on the piles were combined with the structural actions and an allowance for positional tolerance and checked using the structural design program RC Column.

The design report also covered the general detailing of the piles and their connection to the pile caps along with the durability of the concrete piles. The subsurface soils at the site had been classified in the geotechnical investigation reports as mildly aggressive to concrete structures. As Wagstaff Piling manufacture their piles with 60MPa concrete and 40mm cover to reinforcing it meant that the piles are suitable for a 50 year design life in compliance with the project design specification.

In addition to the above, the report detailed the requirements for dynamic pile load testing to prove geotechnical capacity. This was set at 5% of piles in each work area to give good level of confidence for the design. It is worth noting here that as all the piles on the project were driven to refusal on rock, settlement of the piles under compression loading was not an issue.

Following an internal design review by a senior engineer withing the Wagstaff Piling NSW office, the report was finalised and submitted to BlueScope for a third-party review to be carried out by their design consultants. This step-by-step process of consultation, design, review then amendment (if required) before a submission of a design report allowed for the design procedure to develop a robust and efficient foundation solution for the entire project.

The design process not only dealt with the structural and geotechnical design of the piles, but it also had to contend with some construction restrictions which were imposed by the proximity of the new and existing structures. An example of this was the initial design work for the TRT area which initially had a group of approximately 47 piles in a central group under a large pile cap. Within this group there were pairs of piles set at opposed rakes (1 in 4) to resist lateral loads. This posed two distinct issues, firstly being able to position the 25m long mast of the piling rig to align with the rake of the pile and not clash against the existing buildings and elevated pipework and secondly to ensure that the pile could be installed with a level of confidence such that it wouldn’t contact existing vertical piles for the surrounding structures. Image 2 show a layout of the pile group with the raking piles highlighted in pale blue then Image 3 shows a 3D model of the position of the piling rig mast (in red) for the raking piles and the surrounding buildings which demonstrates an inevitable clash with the piling rig mast and the buildings adjacent to the pile cap.

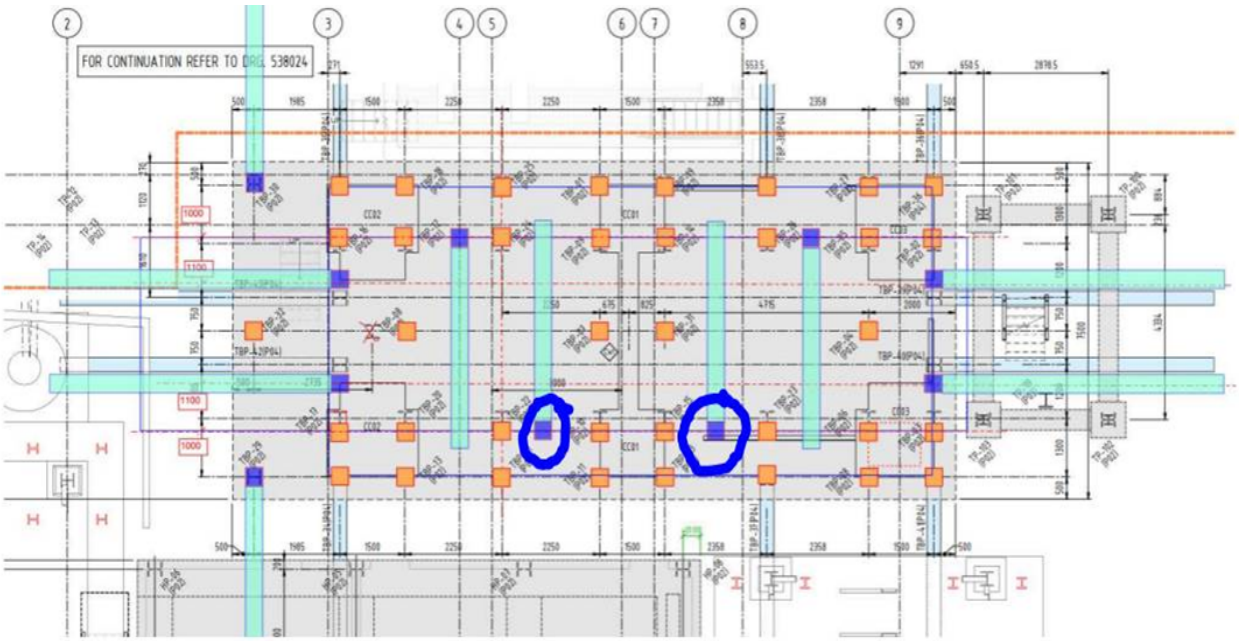


Image 2 – TRT pile group with raking piles

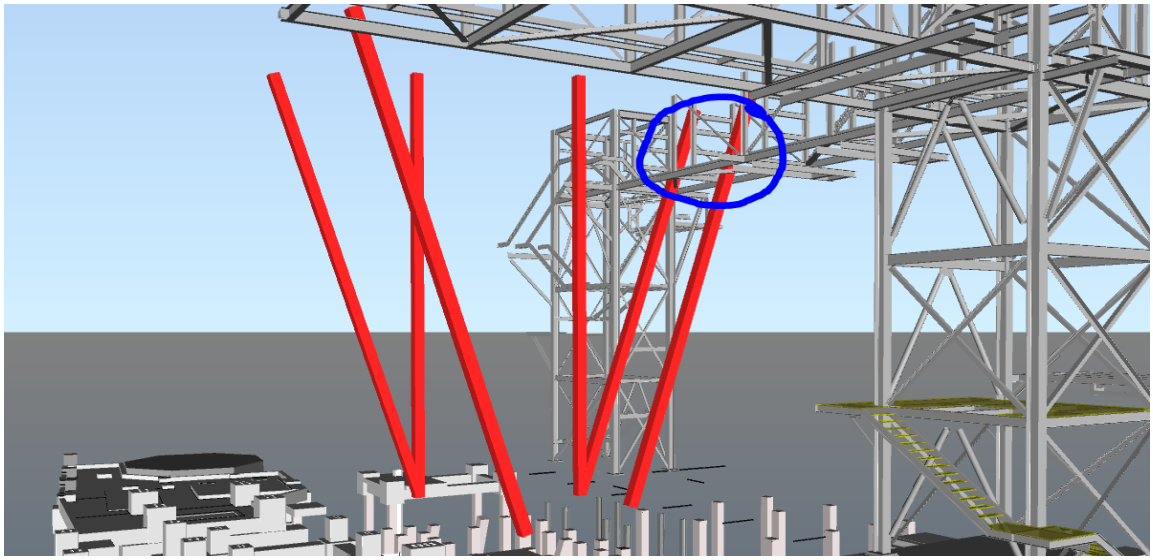


Image 3 – Location of the piling rig mast for raking piles in the TRT pile group.

The constructability of the design should always be front of mind for any designer and so the loading within the pile cap was amended to remove the reliance on raked piles for lateral stability. This meant the vertical piles carried an increased lateral load. This, then led to another four piles in the pile group, however, it allowed for the piles to be installed without the risk of clashing with existing piles or the surrounding structure and services.

The challenges of working with multiple consultancies was alleviated by the work of BlueScope's project teams who made concerted efforts to streamline the design processes and allow for continuity of the pile

 © Deep Foundations Institute 2025

design. Early design lessons learnt were rolled into subsequent packages to assist all the parties who had a vested interest in the design development to flow smoothly.

PRECAST CONCRETE PILE MANUFACTURE

Wagstaff Piling operates three casting yards, one each in Queensland, Victoria and Western Australia. Due to the prevailing geotechnical conditions in and directly around Sydney being more suited to drilling piles rather than driving them, NSW had not had a permanent casting yard. The pile sections for this project were manufactured in the Queensland casting yard and transported to site on semi-trailers.

Wagstaff Piling manufactures pile sections with 60MPa concrete and 40mm clear cover to reinforcing as standard. The concrete mix had been developed and refined with its concrete supply partner over decades and has remained basically the same for a long time apart from minor adjustments to suit occasional project specification or ground condition requirements. The standard pile concrete mix has approximately 25% fly ash as a supplementary cementitious material, maximum aggregate size of 20mm and a design slump of 220mm $\pm$ 40mm. It exhibits high early strength gain, which is important for removing the piles from their moulds after one day and allowing transport to site at as early as seven days, or once a minimum compressive strength of 40MPa has been reached. The piles are cast in mould beds and covered, then stacked and air cured. Images 4 and 5 below show 400mm square precast piles ready for casting with reinforcing cages, pile joints and lifting hooks in position and then finishing the tops of the piles after they have been poured.





Images 4 & 5 – Pile pre and post casting

CONSTRUCTION

The first delivery of piles to site started in October 2024 to the TRT area approximately 75No 350mm and 400mm square piles, 18No of which had restricted headroom with an operating height of either 8 or 12m underneath elevated service structures.

As mentioned in the introduction, one of the main advantages that driven precast concrete piles have over steel piles from a construction perspective is when it comes to splicing the piles together. Splicing is the process of joining pile sections together to extend the length of the pile. Steel piles longer than 15m normally need to be welded together on site, requiring the section ends to be prepared with the top of the bottom section to be flat and the bottom of the top section with bevelled edges to allow the weld material

to fill the space and fuse the two sections. Welding of 310UC158 sections can be slow as the flanges and webs are 25 and 15mm thick respectively. A good boilermaker will complete three welds per shift with everything running smoothly. In addition to the welders and time, the top section of the pile needs to be held in place during the welding, this requires additional service cranes, operators and ground crew to working with the splicing crews. Once the welding has finished there is a time delay before the pile can be re-driven to allow the weld material to cool thoroughly, normally 24 hours is an appropriate time, but individual specifications can vary. A weld inspection and testing regime is also normally specified, anywhere from 25 to 100% of welds depending on the specification. Welded splicing of raked steel piles adds extra complexity to the process as gravity is working against the welder who is trying to join the steel sections together. Another intricacy comes about with sequencing of pile installation to allow access for the piling rig back to the welded steel pile to finish driving it to depth.

The Wagstaff Piling segmental precast pile joints remove the welding process and its constraints entirely. The joint pins are locked into place with wedges that allow for full load transfer between pile sections. Splicing a precast concrete pile with one of these joints takes approximately five to ten minutes and is done with the piling rig and the offsider, no additional personnel or plant are required.

As the ground conditions were assessed as mildly aggressive the long-term durability and performance of the pile joint was not in question.



Images 6 & 7- Splicing precast concrete piles

This splicing process was brought into critical focus for the piles in low headroom conditions. As some of the pile locations were restricted by existing site infrastructure, pile section lengths were limited to 3 or 6m long, hence considering a pile length of between 18 and 21m long the difference between three or five welded splices on steel piles and the same number of precast pile joints was an enormous program and cost saving. It also reduced the amount of people and plant require to do the work and in a site with restricted space, reducing the interaction between people and plant is a very positive safety outcome.

 © Deep Foundations Institute 2025



Images 8 & 9 – A Banut 500 series rig installing 6m long pile sections in low headroom conditions

The nature and age of the BlueScope facility in Port Kembla means that there are not just above-ground restrictions, but areas with subsurface services and easements that limit access to track-mounted piling rigs. In this particular case, for the Excess Gas Bleeder Area, a different solution for installing the piles was proposed. A series of service pipes meant that the 80tonne piling rig could not track up to the pile locations, hence these piles were installed with a “hanging hammer” held by a service crane. The hanging hammer operated an eight-tonne block actuated by a remote hydraulic power pack. The service crane pitched the bottom pile section into a predrilled pile hole then lifted the hammer on top of the pile, then the power pack was used to operate the hydraulics and drive the pile section down. The top section was then lifted into place and spliced with wedges and the hammer lifted on top of it and the piles was driven to design depth. While this as a much slower process than using a standard piling rig, the innovative method allowed the piles to be installed in their design location without disruption to the site services and without significant design changes to the superstructure which would have been required if the piles could not be installed in the intended locations.

 © Deep Foundations Institute 2025





Images 11 & 11 – Using a hanging hammer to install pile sections in locations not accessible to a standard piling rig.

While these restrictions provided some challenges, the majority of pile locations were unrestricted and the Banut 655 piling rig had no such concerns installing the piles, be they vertical or raked.

 © Deep Foundations Institute 2025





Images 12 & 13 – Banut 655 piling rig pitching and installing pile section at 1 in 6 rake with the Bluescope Steel facility in the background.

PILE LOAD TESTING

As part of the design verification process, Wagstaff Piling carried out dynamic load testing with the Pile Driving Analyser (PDA) from Pile Dynamics (PDI). This equipment is a vital tool in assessment and confirmation of pile capacity and structural integrity. It allows for remote access to the pile data during testing which is important for a national company like Wagstaff Piling. It also provides an assessment of driving stresses, hammer efficiency and importantly PDA testing measures actual transferred energy, unlike theoretical calculations which rely on potential energy and assumptions.

The testing was carried out as both end of drive testing and restrike testing. End of drive testing, means as it sounds, that gauges are attached to the pile as it is being driven and a final set taken, whereas restrike testing happens any time after the pile has been driven to its final set.

Following PDA testing, CAPWAP analysis was carried out on the data. CAPWAP (also a PDI product) is a signal matching software used to analyse PDA data, it allows for a detailed assessment of shaft capacity along the pile and toe resistance and can provide a prediction of load displacement behaviour. Using this software was a vital step in the verification process because the analysis allows the engineer to separate the shaft capacity (skin friction) from the end bearing capacity and as such confirm the pile geotechnical tension capacity.

The restrike testing demonstrated only a minor increase in shaft capacity with time. Known as set up, this phenomenon occurs mainly in cohesive soils and is where the soil tends to re-mould around the pile surface increasing the skin friction. In general, there was a 10 to 15% increase in shaft capacity with restrike testing.

 © Deep Foundations Institute 2025

It is worth noting here that the restrike testing occurred normally within four to five days after initial driving, so this percentage estimate may be conservative, but as the piles easily achieved the design capacities required, there was no need to carry out longer duration testing.

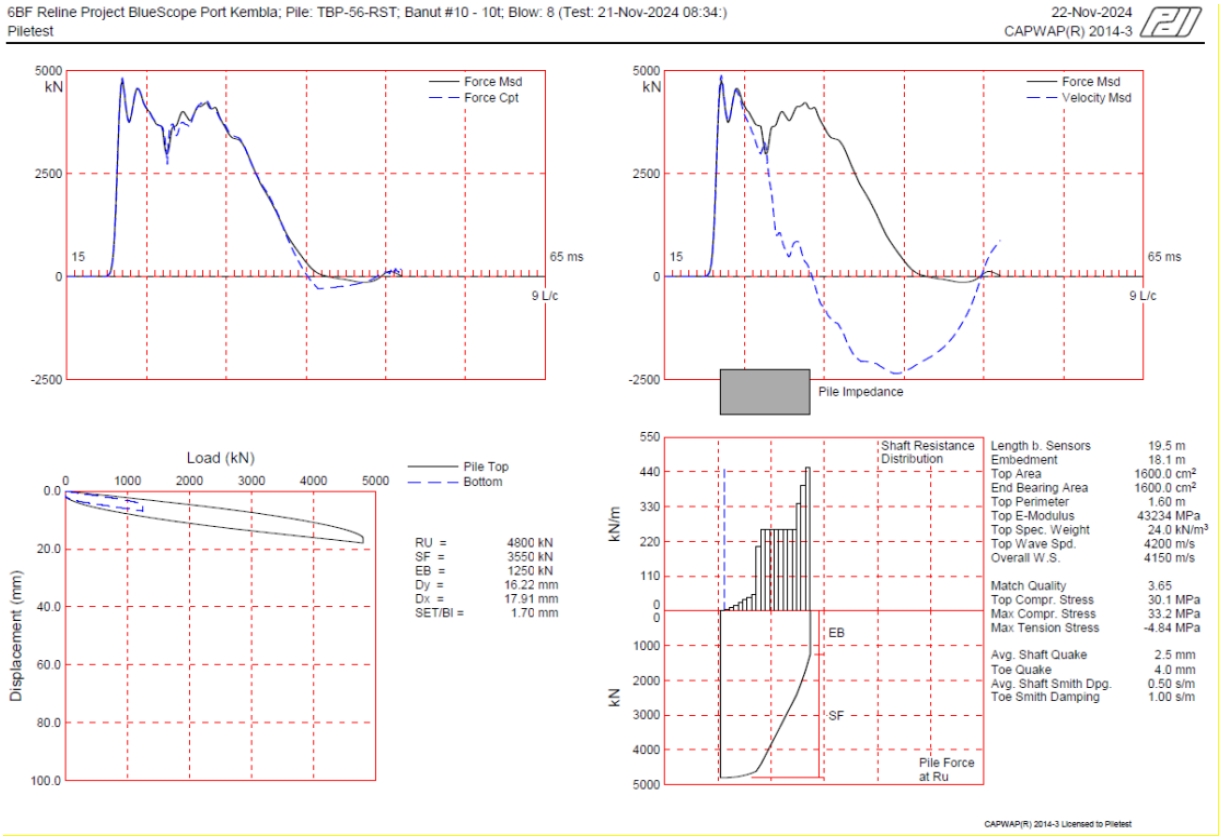


Image 14 – An extract CAPWAP Analysis reporting showing load displacement and the split of skin friction and end bearing

Account also needed to be made within the load testing for piles installed and then tested with different weight hammers which also operated at different maximum drop heights. While our full height rig operated a 10t hammer with a maximum drop height of 1.2m, our low-headroom rig operated a 6t hammer with a 0.75m maximum drop height. These hammers deliver different maximum energies to the piles they are driving or testing. But again, as the piles were all driven to refusal on rock and the pile loads were not extremely high, the testing regime did not require enormous amounts of energy from the hammers to prove pile capacities.

CONCLUSION

BlueScope Steel's 6BF Reline project is part of a large capital spend and upgrade program that is being carried out in their Port Kembla facility on the NSW south coast. Wagstaff Piling was successful in an open tender process with an alternate foundation solution of using driven precast concrete piles in lieu of the steel piles. The use of driven segmental precast concrete piles has proven on this site to be a more efficient and cost-effective solution that the traditionally used driven steel piles. The ability to use innovative design and construction solutions to overcome some of the specific constraints of working within an operational steel manufacturing facility made the precast concrete pile solution a more compelling foundation system at this site.

 © Deep Foundations Institute 2025

The driven piles were designed, manufactured, installed and tested by Wagstaff Piling personnel and have proven to be a robust and efficient foundation system at Port Kembla for BlueScope's 6BF Reline project.

ACKNOWLEDGEMENTS
The author wishes to thank BlueScope Steel for the opportunity to write and present on this case study. Wagstaff Piling Pty Ltd and Piletest Pty Ltd for their assistance and guidance in the development of the project and of this paper and presentation.

 © Deep Foundations Institute 2025

CURRENT PRACTICE CONCERNING DRILLED SHAFTS TO SUPPORT BUILDINGS IN JAPAN

Yusuke Homma, JAPAN PILE CORPORATION, 36-2 Nihonbashi Hakozakicho, Chuo-ku, Tokyo, Japan, +81(0)3 5843 4196, yusuke_honma@japanpile.co.jp
Yujiro Tanaka, JAPAN PILE CORPORATION, 36-2 Nihonbashi Hakozakicho, Chuo-ku, Tokyo, Japan, +81(0)3 5843 4196, yujiro_tanaka@japanpile.co.jp
Kentaro Oko, ASIA PILE HOLDINGS CORPORATION, 36-2 Nihonbashi Hakozakicho, Chuo-ku, Tokyo, Japan, +81(0)3 5843 4173, kentaro_oko@asiapile-hd.com

ABSTRACT

Development of construction methods for installation of drilled shafts to support high rise buildings is being actively pursued in Japan. Of particular interest are the large diameter (about 1 to 3 meters) drilled shafts with the bottom enlarged to diameters of about 4 to 6 meters (13 to 20 feet) to provide large end bearing resistance, and drilled shafts with multi-stage enlarged nodules along the shaft in order to resist the large uplift (pull-out) force. These distinctive drilled shafts developed in recent years are found to be preferred foundation option to support high rise buildings in Japan. In this paper, we present various drilled shaft methods and types and introduce an example of a building that uses a drilled shaft with enlarged bottom in combination with multi-stage enlarged nodules.

Keywords: drilled shafts, large end bearing capacity, large pull-out resistance

INTRODUCTION

In Japan, the design practice for architecture (building structures) and civil engineering (public works) are governed by different set of design codes. As a result, the design requirements for structures related to civil engineering such as tunnels, bridges, railways, roads etc. are different from those for architecture involving privately owned building structures such as office buildings, condominiums, commercial facilities, factories hospitals etc. That is, the evaluation method for the soil bearing resistance as well as the structural strength of the pile body for a given site condition will differ in Japanese practice depending on the design code applicable to structure. For example, Table.1 shows the recommended bearing capacity of drilled shafts in sandy soils in civil engineering and architecture disciplines. As may be noted, there are different formulations recommended depending on the discipline and design standards and guidelines. In general, the end bearing capacity of drilled shafts in Japan is obtained by multiplying the bearing capacity coefficient α (60~150) by the average N value (standard penetration blow count) around the pile tip region and the base area A_p. In civil engineering discipline, only straight drilled shafts are used, but in architecture discipline, the use of drilled shafts with an enlarged bottom is permitted. While multiple piles beneath a foundation is common in civil engineering discipline, each pillar supported on single pile is often adopted in architecture discipline in view of its economic efficiency.

In this paper, we describe the use of drilled shafts in Japan in the architecture discipline. The alluvial plains where the densely populated cities are located in Japan consist of soft alluvial deposits where foundation piles with large bearing capacity are required to support building structures. In particular, for high rise buildings, drilled shaft foundations are the preferred foundation option. As a result, the development of

 © Deep Foundations Institute 2025

drilled shafts with an enlarged bottom has been actively pursued in order to derive large end bearing resistance. In addition, Japan is an earthquake-prone country, and it is mandatory to design piles to resist seismic forces. Earthquake-resistant drilled shafts that can resist a large bending moment due to the inertia force of the building during an earthquake by providing a steel casing in the upper part below the pile head, and by including multi-stage enlarged nodules along the shaft to improve shaft friction to resist large uplift (pull-out) forces have been developed. This paper presents such developments in drilled shaft foundations for buildings in Japan and introduces an example of a building that uses a drilled shaft with enlarged bottom in combination with multi-stage enlarged nodules.

Table 1. Bearing capacity of the drilled shaft in Japan

Discipline		Bearing capacity (kN) = $\alpha \cdot N \cdot A_p$
Architecture	Building Standards Act	150・N・A_p N：Average of N values around the pile tip 1D above and 4D below the tip (D：pile tip diameter)
Architecture	Recommendations for design of building foundations	120・N・A_p N：Average of N values around the pile tip 1D above and 1D below the tip
Civil Engineering - Roads	Specifications for highway bridges	Sand ：110・N・A_p （≦3300 A_p） Gravel：160・N・A_p （≦8000 A_p） N：Average of N values over 3D below the tip
Civil Engineering - Railways	Design standards for railway structure and commentary	Sand ：60・N・A_p （≦3500 A_p） Gravel：60・N・A_p （≦7500 A_p） N：Minimum of N values over 3D below the tip

TRENDS IN DRILLED SHAFTS CONSTRUCTION METHODS IN JAPAN

The primary methods of drilled shafts construction in Japan consist of the earth drill method, the reverse circulation method, and the all-casing method in both civil engineering and architecture disciplines. Figure 1 shows the records of the three construction methods in 2021 (April 2021~ March 2022) indicating the dominance of earth drill method.

Figure 2 shows the distribution of shaft diameters and the presence or absence of an enlarged bottom based on the results of a survey conducted by the Japan Foundations Engineering Association. In civil engineering

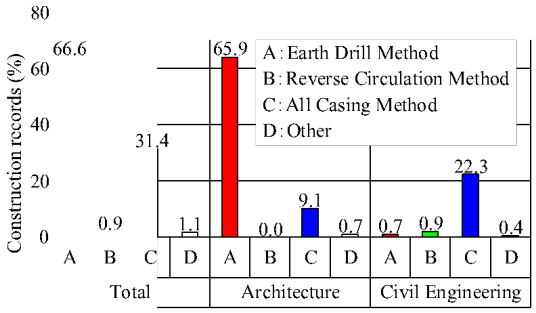


Fig. 1 Records of dilled shaft Installations

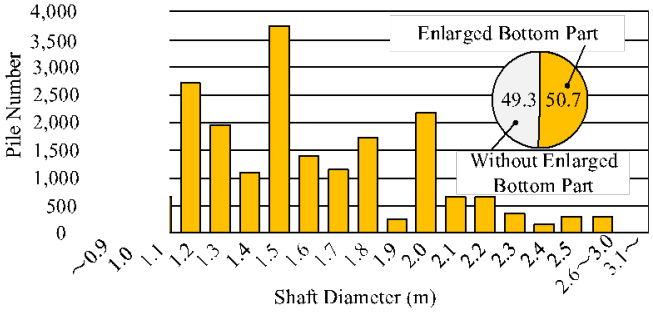


Fig. 2 Drilled shaft diameters and bottom enlargement

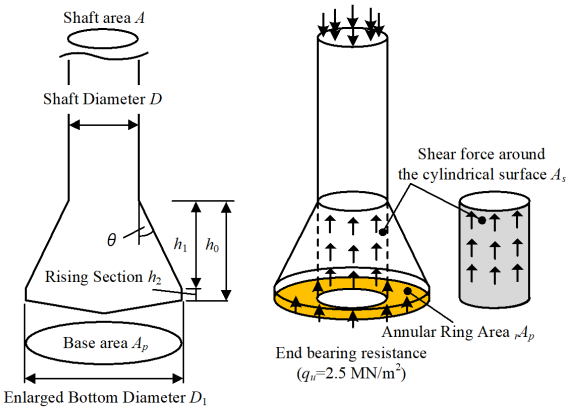
 © Deep Foundations Institute 2025

discipline, all-casing method is the mainstream, but in architecture discipline, the earth drill method accounts for about 70%, half of which have an enlarged bottom part. About 60% of the shaft diameters are in the range of 1.0 m ~ 1.5 m, with remaining generally in the range of 2.6 m ~ 3.0 m.

TRANSITION IN DRILLED SHAFTS WITH ENLARGED BOTTOM

In Japan, manual excavation for deep foundations started from around 1930s, and by 1960s, drilled shafts with enlarged bottom by mechanical excavation had developed. In the beginning, bottom enlargement was achieved by initially excavating a straight shaft to a predetermined depth, and using a drilling system that extends the blades by hydraulic mechanism, and then lifting the soil cuttings from the bottom by a reverse circulation method. In 1984, an enlarged bottom pile with mechanical excavation by the earth drill method was developed. The earth drill method involves two enlargement blades that are gradually expanded with the excavated soil cuttings stored in the central drum that gets lifted to ground level. Since the construction equipment for earth drill method is simpler it has mostly replaced the reverse circulation method.

In early days, the Building Center of Japan, which was conducting evaluations related to the development of drilled shafts, specified limits on shape and dimensions of enlarged bottom based on the compressive strength of concrete as illustrated in Fig. 3. Based on this, the enlarged bottom diameter was to be 4.1 m or less, the enlargement ratio (defined as the ratio of effective base area A_p to shaft cross-sectional area A) was to be 3.2 or less, the inclination angle of the enlarged bottom part was to be 12 degrees or less, and the compressive stress of concrete was between 18 and 32 MN/m^2. In addition, the upper limit of the long-term(static) allowable end bearing resistance that can be adopted was limited to 2.5 MN/m^2 assuming that it was supported by soil layer with N value of 50 or more. The rationale for limiting the inclination angle



・The diameter (D_1)of the enlarged part be 4.1 m or less.
・The base enlargement ratio (= effective base area / shaft cross-sectional area) shall be 3.2 or less.
・The inclination angle (θ) of enlarged part shall not exceed 12°.
・The length (h_2) of the rising part of the enlarged part shall not be less than 0.3 m.
・The compressive strength (F_c) of concrete shall be 18 MNm^2 ≦ F_c ≦ 32 MN/m^2.

○The Rationale of enlargement ratio 3.2

Long-term allowable bearing resistance ${}_aR_t = A_p \cdot q_u$
Compressive strength of shaft ${}_aR_p = 1/4 \cdot F_c \cdot A$
${}_aR_p > {}_aR_t$
The Maximum F_c=32 MN/m^2
The Maximum D_1= 4.1m
${}_aR_t = A_p \cdot q_u = 4.1^2 \cdot \pi/4 \cdot q_u = 13.2 \cdot 2.5 = 33$ MN
$A = 4 \cdot {}_aR_t / F_c = 4 \cdot 33/32 = 4.125$ m^2
Enlargement ratio = A_p/A =13.2/4.125 = 3.2

○The Rationale of The angle θ =12 degree

Long-term allowable end bearing resistance ${}_aR_g = {}_rA_p \cdot q_u$
Shear force around cylindrical surface ${}_aS = \tau_c \cdot A_s$
${}_aS > {}_aR_g$
F_c=32 MN/m^2, h_2=1.0m, θ =12 degree
D_1= 4.1m , enlargement ratio 3.2 (D≒2.3m)
The shear stress (τ) of concrete in Japan
τ =min{ F_c /40, ¾(0.49+F_c /100)}=0.61MN/m^2
${}_aR_g = {}_rA_p \cdot q_u = (4.1^2 - 2.3^2)\,\pi/4 \cdot q_u = 9.05 \cdot 2.5 = 22.6$ MN
${}_aS = \tau_c \cdot A_s = \tau_c \cdot \{(D_1 - D)/2/\tan 12° + h_2\} \cdot D \cdot \pi = 23$ MN
${}_aR_g / {}_aS = 23 / 22.6 > 1.0$

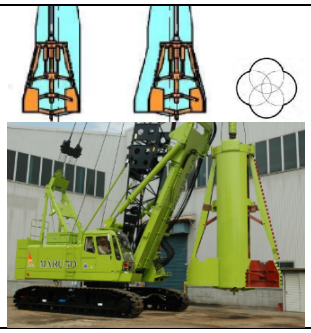
Fig. 3 Specification of enlarged bottom pile and ground reaction force transmission

 © Deep Foundations Institute 2025

to 12 degrees was in consideration of the transfer of end bearing resistance from the bottom to the drilled shaft. As illustrated in Fig. 3, if the end bearing resistance (equal to 2.5 MN/m^2) acting on the annular ring area of the enlarged shaft is to be borne by the shear force around the cylindrical surface, the inclination angle needs to be limited to about 12 degrees in the case of a concrete strength of 32 MN/m^2. This was the rationale for limiting the angle of inclination to 12 degrees based on the strength of the concrete. The rationale for the enlargement ratio of 3.2 or less is also provided in Fig. 3.

However, in 2002 the limits on the shape and dimensions of enlarged bottom of drilled shafts as well as the concrete strength consideration was abolished, and drilled shafts with an enlarged bottom diameter of more than 4.1 m began to be developed. Recent technological developments in enlarged bottom piles are symbolized by the increase in the enlarged bottom diameter, the increase in the enlargement ratio by reducing the shaft diameter, and the accompanying increase in concrete strength. Table.2 is a list of the main large-diameter drilled shafts with enlarged bottom in recent years. Here, we will introduce the enlarged bottom pile (new ACE construction method) developed by four Japanese companies as a representative, which is classified as an earth drill method.

Table 2. Main large-diameter enlarged bottom piles of recent years in Japan

Method Name	Petal enlarged bottom pile	NEW-EAGLE pile	new ACE
Shaft diameter (m)	1.8～4.3	0.7～4.0	0.8～4.7
Enlarged bottom diameter (m)	3.5～6.7	0.9～5.5	0.8～4.8
Maximum enlargement ratio	–	7.29	4.62
Inclination angle	12°	21.1°	12°
Concrete strength (MN/m^2)	$18 \leqq F_c \leqq 80$	$18 \leqq F_c \leqq 60$	$24 \leqq F_c \leqq 60$
Enlarged bottom bucket			

NEW ACE CONSTRUCTION METHOD

new ACE is a construction method in which the drilling excavation corresponding to the planned shaft diameter extends to bearing after which further excavation is completed by the new ACE bucket to construct a cone-shaped enlarged part. The dimensions of the pile are shown in Table.2. The maximum enlargement ratio is 4.62 when the shaft diameter is 2.0 m and the base diameter is 4.4 m. The construction procedure is illustrated in Fig. 4.

 © Deep Foundations Institute 2025

The construction equipment consists of the new ACE excavator and the new ACE bucket as shown in Fig. 5. The new ACE excavator provides construction performance of an earth drilling method, and is equipped with features (hydraulic pump, oil transmission device, etc.) for the operation of enlargement blades. In addition, the new ACE bucket is equipped with two enlargement blades that open up or close in using the hydraulic system.

As part of the development this enlargement method, an excavation investigation was completed to confirm the excavated shape of the enlarged bottom (Fig. 5).

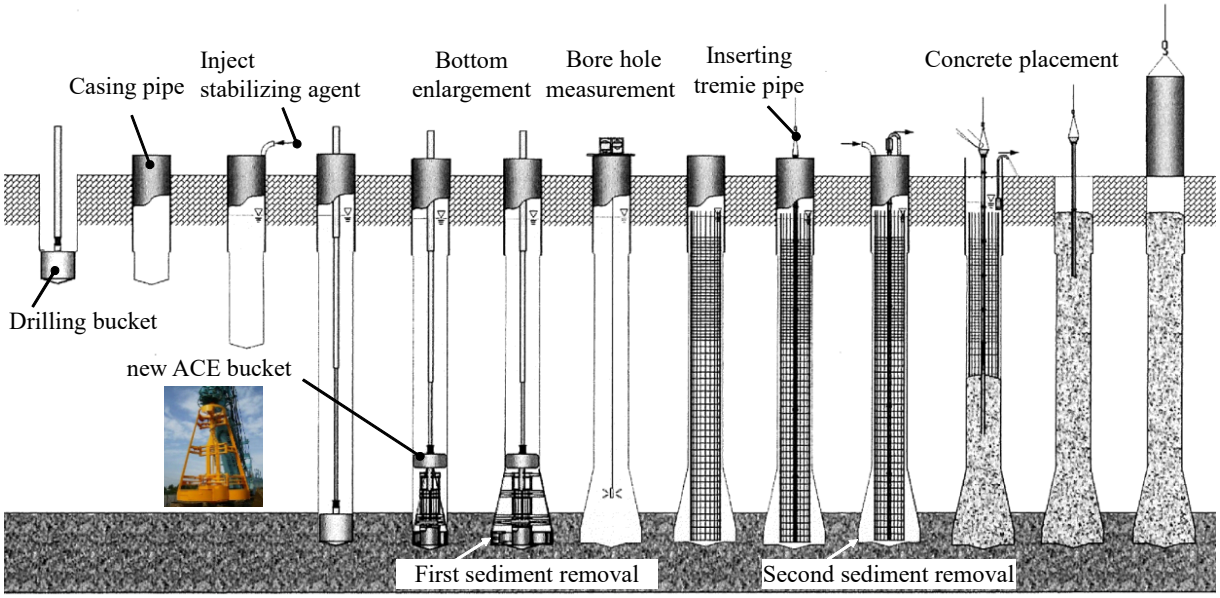


Fig. 4 Construction procedure of new ACE construction method

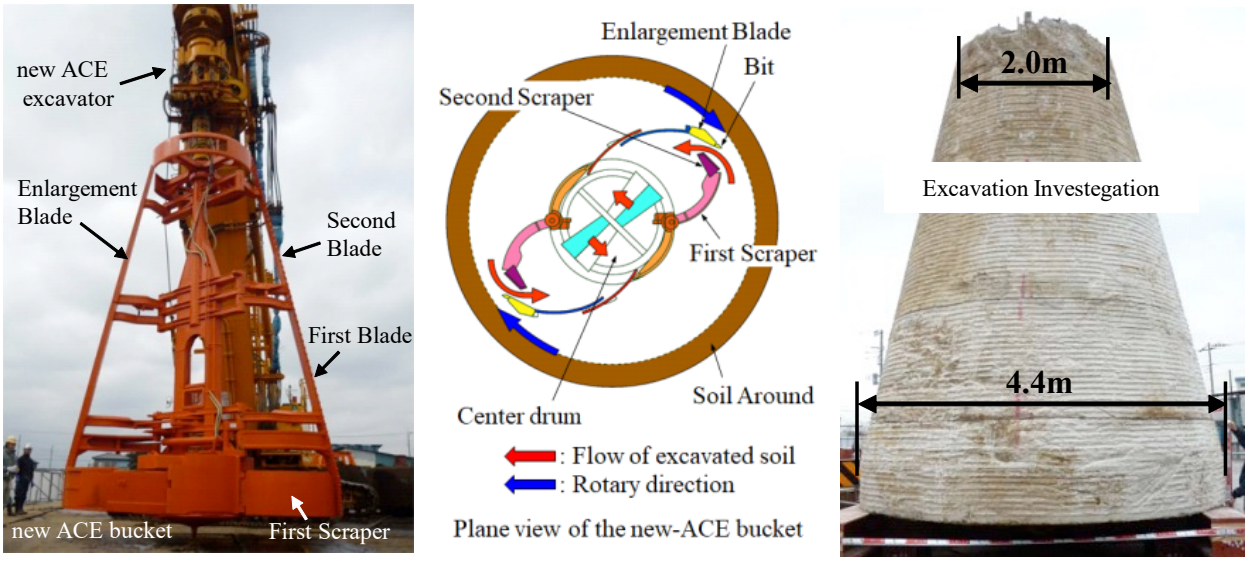


Fig. 5 Construction equipment and a result of excavation investigation

 © Deep Foundations Institute 2025

DRILLED SHAFTS WITH MULTI-STAGE-ENLARGED NODULES

Japan is well known as one of the most seismically active regions in the world. While the development of drilled shafts with enlarged bottom is primarily to resist a large compressive loads, there is also the demand for pull-out resistance under earth loading. The pull-out resistance is normally limited by available shaft friction and often results in the design of longer drilled shafts and/or larger diameters to meet the demand. Such increase in depth and/or diameter of drilled shafts start reaching practical limits as the demand increases with the need to design for higher seismic hazards prescribed by newer building codes. Faced with such circumstances, the method of evaluating the pull-out resistance of piles was revised in the Building Standards Law in 2001. With this revision, it has become possible to evaluate the unique pull-out resistance by considering the shape of the pile and the construction method. In the case of drilled shafts, a large number of drilled shafts with multi-stage-enlarged nodules have been developed in which not only the enlarged bottom part but also the enlarged nodules in the middle part are constructed to increase the shaft frictional resistance in additoin to the enlarged bottom part.

ME-A CONSTRUCTION METHOD

In this paper, we introduce the drilled shafts with multi-stage-enlarged nodules (Me-A construction method) developed by a group of nine Japanese companies. Figure 6 illustrates the general features of a drilled shaft installed by Me-A method. In this method, the drilled shaft is constructed with enlarged parts in the middle of the shaft in addition to the tip using earth drill method.The construction procedure of this method is shown in Fig. 7. The enlarged middle parts are constructed using the new ACE bucket, and then lower excavation is performed with Me ACE bucket that provides a slope to prevent sediment.

AN EXAMPLE OF A BULDING THAT USES A DRILLED SHAFT WITH ENLARGED BOTTOM IN COMBINATION WITH MULTI-STAGE ENLARGED NODULES

Outline of a building and ground overview

This is an office building with 1 basement floor and 23 floors above ground located in Japan. Considering that the facility is located directly above the station, a seismic control system has been adopted in this structure to ensure human safety and basic functions when large earthquakes occur.

Figure 8 shows a soil boring log together with drilled shaft configurations. Soft alluvium consisting mainly of clay deposits exist up to a depth of about 27 m, underlain by alternating gravel and clay. The liquefaction potential in the layer designated A_s is small, and the clay layers designated A_{c2} and D_{c2} are overconsolided. It was judged that the sand and gravel layer between depths of 28 m ~ 36 m was not suitable for bearing support layer due to inadequate layer thickness, and the sand and gravel layer at a depth of 45 m or more was adopted as the bearing stratum for the piles.

 © Deep Foundations Institute 2025

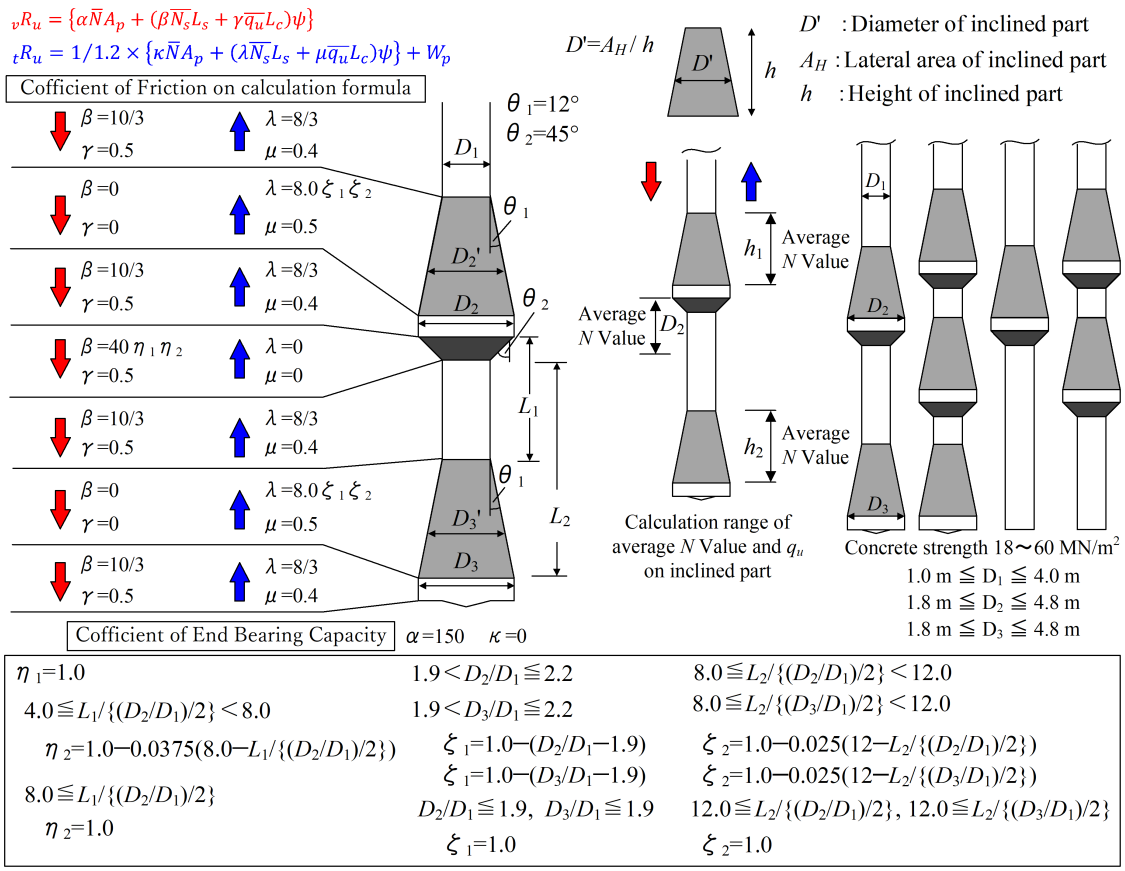


Fig. 6 Figure and specifications of Me-A

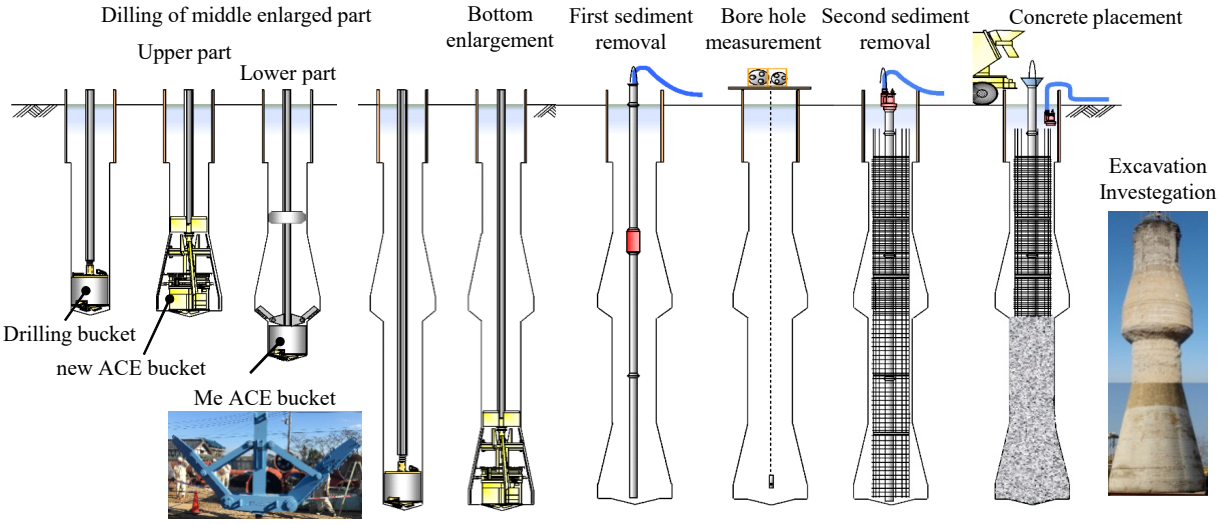


Fig. 7 Construction procedure of Me-A

 © Deep Foundations Institute 2025

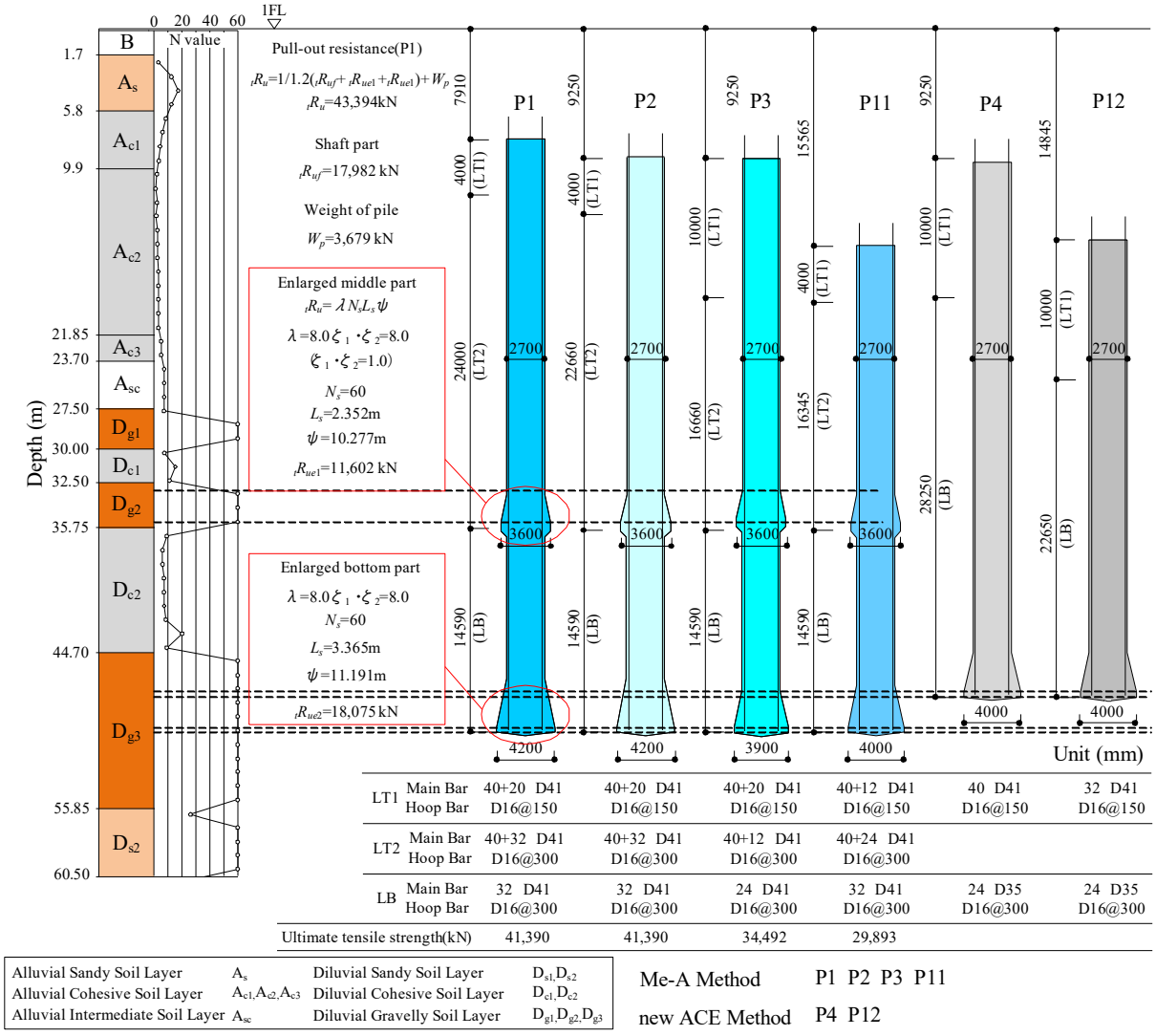


Fig. 8 Soil boring log and pile list

Design axial load and foundation structure

A pile foundation plan is shown in Fig. 9, and ultimate axial loads are shown in Table 3. The shape of the building is 22.69m in the short side (Y direction) while the long side (X direction) is about 107 m. During an earthquake, large compressive loads (50 MN ~ 80 MN) and uplift loads (−6 MN ~ −35 MN) act on the piles in the outer periphery of the building. It is possible to resist compressive loads by using a enlaregd bottom pile (new ACE construction method), but shaft friction resistance alone is not sufficient to resist uplift loads. Therefore, we adopted a drilled shafts with multi-stage-enlarged nodules (Me-A method) and provided a enlarged part in the gravel layer at a depth of 32m~36m to provide sufficient pull-out resistance.

 © Deep Foundations Institute 2025

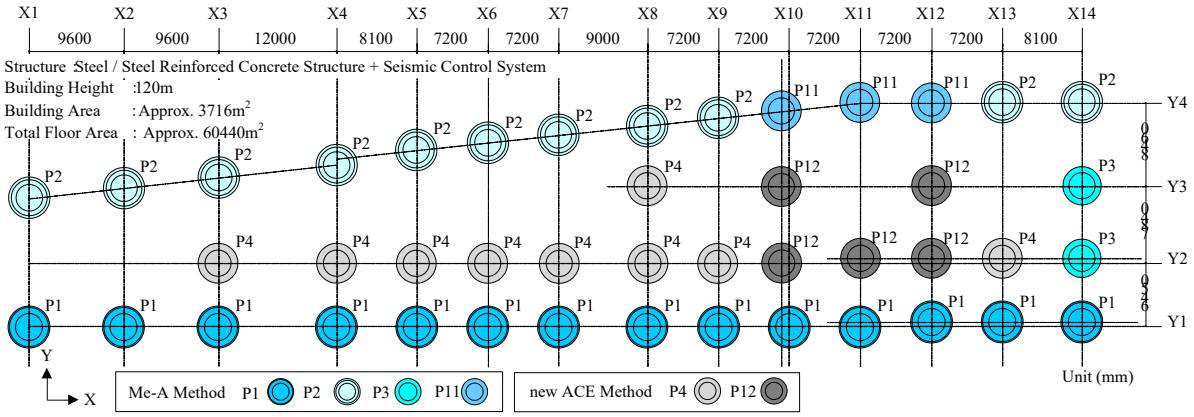


Fig. 9 Pile foundation plan

Table 3. Ultimate axial load and design values of compressive and pull-out resistance

	Pile	Axial Load (MN)			Calculation Value (MN)			Demand to Capacity Ratio		
	No	N_l	N_{min}	N_{max}	${}_vR_a$	${}_tR_u$	${}_vR_u$	$N_l/{}_vR_a$	$N_{min}/{}_tR_u$	$N_{max}/{}_vR_u$
Y1-X1	P1	29.2	-27.4	83.5	34.6	-41.3	103.8	0.84	0.66	0.80
Y1-X2	P1	26.6	-25.7	75.8	34.6	-41.3	103.8	0.77	0.62	0.73
Y1-X3	P1	25.8	-30.1	77.5	34.6	-41.3	103.8	0.74	0.73	0.75
Y1-X4	P1	24.4	-33.1	75.1	34.6	-41.3	103.8	0.71	0.80	0.72
Y1-X5	P1	22.6	-30.4	68.9	34.6	-41.3	103.8	0.65	0.74	0.66
Y1-X6	P1	21.9	-27.8	66.7	34.6	-41.3	103.8	0.63	0.67	0.64
Y1-X7	P1	22.3	-26.8	67.9	34.6	-41.3	103.8	0.64	0.65	0.65
Y1-X8	P1	22.2	-30.6	69.1	34.6	-41.3	103.8	0.64	0.74	0.67
Y1-X9	P1	21.0	-31.6	67.1	34.6	-41.3	103.8	0.61	0.77	0.65
Y1-X10	P1	20.0	-30.2	66.8	34.6	-41.3	103.8	0.58	0.73	0.64
Y1-X11	P1	18.7	-28.7	61.9	34.6	-41.3	103.8	0.54	0.69	0.60
Y1-X12	P1	18.2	-27.9	63.2	34.6	-41.3	103.8	0.52	0.68	0.61
Y1-X13	P1	17.3	-31.4	59.9	34.6	-41.3	103.8	0.50	0.76	0.58
Y1-X14	P1	18.3	-34.6	68.0	34.6	-41.3	103.8	0.53	0.84	0.65
Y2-X3	P4	24.0	19.6	33.4	34.6	-41.3	103.8	0.69	-	0.32
Y2-X4	P4	22.4	12.5	34.0	34.6	-41.3	103.8	0.65	-	0.33
Y2-X5	P4	20.6	15.8	28.3	34.6	-41.3	103.8	0.59	-	0.27
Y2-X6	P4	20.2	20.2	26.7	34.6	-41.3	103.8	0.58	-	0.26
Y2-X7	P4	20.4	19.1	25.9	34.6	-41.3	103.8	0.59	-	0.25
Y2-X8	P4	18.9	18.1	23.0	34.6	-41.3	103.8	0.55	-	0.22
Y2-X9	P4	17.1	16.3	21.3	34.6	-41.3	103.8	0.49	-	0.21
Y2-X10	P12	19.7	16.6	26.9	34.6	-18.3	93.9	0.57	-	0.29
Y2-X11	P12	19.8	18.4	22.0	34.6	-18.3	93.9	0.57	-	0.23
Y2-X12	P12	20.7	15.5	25.8	34.6	-18.3	93.9	0.60	-	0.27
Y2-X13	P4	16.4	12.8	24.6	31.3	-22.9	94.2	0.52	-	0.26
Y2-X14	P3	17.3	-22.7	49.1	31.2	-34.4	89.4	0.56	0.66	0.55
Y3-X8	P4	18.4	12.9	27.0	31.3	-22.9	94.2	0.59	-	0.29
Y3-X10	P12	19.6	8.6	36.6	31.4	-18.3	93.9	0.63	-	0.39
Y3-X12	P12	20.5	10.0	37.3	29.8	-18.3	93.9	0.69	-	0.40
Y3-X14	P3	18.9	-6.4	46.5	31.4	-34.4	89.4	0.60	0.19	0.52
Y4-X1	P2	28.8	-25.5	83.0	31.3	-41.3	103.8	0.92	0.62	0.80
Y4-X2	P2	26.8	-25.3	75.5	31.3	-41.3	103.8	0.86	0.61	0.73
Y4-X3	P2	26.8	-21.0	74.8	29.8	-41.3	103.8	0.90	0.51	0.72
Y4-X4	P2	24.4	-24.1	71.1	34.6	-41.3	103.8	0.70	0.58	0.68
Y4-X5	P2	23.6	-24.8	68.5	34.6	-41.3	103.8	0.68	0.60	0.66
Y4-X6	P2	23.2	-20.4	66.6	34.6	-41.3	103.8	0.67	0.49	0.64
Y4-X7	P2	21.1	-24.9	62.5	34.6	-41.3	103.8	0.61	0.60	0.60
Y4-X8	P2	19.9	-23.8	59.2	34.6	-41.3	103.8	0.57	0.58	0.57
Y4-X9	P2	23.2	-25.4	71.5	34.6	-41.3	103.8	0.67	0.61	0.69
Y4-X10	P11	22.4	-21.7	65.0	31.4	-29.8	94.2	0.71	0.73	0.69
Y4-X11	P11	23.4	-22.2	69.2	31.4	-29.8	94.2	0.75	0.74	0.73
Y4-X12	P11	23.4	-22.2	69.2	31.4	-29.8	94.2	0.75	0.74	0.73
Y4-X13	P2	22.7	-23.8	64.8	34.6	-41.3	103.8	0.66	0.58	0.62
Y4-X14	P2	22.9	-25.5	68.2	34.6	-41.3	103.8	0.66	0.62	0.66

※${}_vR_a = 1/3\ {}_vR_u$ N_l : Long-term axial load , N_{min} : Axial ultimate load (tension) , N_{max} : Axial ultimate load (compression)

Evaluation of the bearing capacity of the Me-A method

The ultimate compressive bearing capacity ${}_vR_u$ and the ultimate pull-out resistance ${}_tR_u$ determined from the ground resistance of the drilled shaft by Me-A method are obtained using the calculation formula shown in equations [1] and [2] respectively. For evaluation of the end bearing capacity and the resistance of the enlarged middle part, consideration is given to the influence of (1) the diameter enlargement ratio and (2) the enlargement interval ratio, by allowing for the resistance of the inclined part in the enlarged parts in formulating the friction resistance. As for the compressive bearing capacity, there is no effect of the enlargement ratio, and the effect of the enlargement interval ratio is considered. From the experimental results, it was confirmed that the bearing capacity tended to decrease when the enlargement interval ratio fell below 8.0, so the reduction factor η_2 was set as shown in Fig. 6. As for the pull-out resistance, since both effects were confirmed from the experimental results, the reduction coefficients ζ_1 and ζ_2 were set. Each cofficient and reduction factor is shown in Fig. 6.

 © Deep Foundations Institute 2025

$$ {}_vR_u = \{\alpha \overline{N} A_p + (\beta \overline{N_s} L_s + \gamma \overline{q_u} L_c)\psi\} \quad [1] $$

$$ {}_tR_u = 1/1.2 \times \{\kappa \overline{N} A_p + (\lambda \overline{N_s} L_s + \mu \overline{q_u} L_c)\psi\} + W_p \quad [2] $$

Where α, κ = cofficient of end bearing capacity, $\overline{N}$ = average of N value around the pile tip (Blow 1D, Upward 4D from the tip (D : pile tip diameter)), A_p= effective area of pile tip, β, λ =cofficient of friction of sand, $\overline{N_s}$ = average of N value of sandy ground around the pile, L_s = total length on sandy ground, γ, μ = cofficient of friction of clay, $\overline{q_u}$ = average of compressive strength of clay ground around the pile, L_c = total length on clay ground, ψ = length of the circumference of pile, W_p = effective dead weight of pile.

Result of compressive bearing capacity and pull-out resistance

A list of compressive bearing capacity and pull-out resistance capacity are shown in Table 3. The adopted calculation values is the smaller of the compressive bearing capacity or pull-out resistance determined from the ground resistance and the compressive strength or tensile strength of the pile cross-section. In addition, the demand to capacity ratio of the axial force of each column position to the adopted bearing capacity is shown in Table 3. By adopting the Me-A, we were able to keep pulling within 0.85 of the demand to capacity ratio.

CONCLUSION

The latest drilled shafts in Japan were explained. An example was shown in which it was difficult to design economically without adopting drilled shaft with enlarged bottom in combination with multi-stage enlarged nodules.

REFFERENCES

Kuwabara Fumio, 2009. Recent Trends and Issues of drilled shafts, The foundation engineering & equipment, Monthly, Vol.37, No.8, Japan, pp.2-7 (in Japanese).

new ACE construction method, 2007. fondation evaluation committee, The Building Center of Japan, BCJ evaluation-FD0277-01 (in Japanese).

Drilled shafts with enlarged middle and bottom part (Me-A construction method), 2019. evaluation report, Center for Better Living, evaluation CBL FP033-18 (in Japanese).

 © Deep Foundations Institute 2025

LOAD BEARING CHARACTERISTICS OF BORED PRECAST PRESTRESSED NODULAR PILES

Yujiro Tanaka, Japan Pile Corporation, 36-2 Nihonbashi Hakozakicho, Chuo-ku, Tokyo, Japan, +81(0)3 5843 4196, yujiro_tanaka@japanpile.co.jp
Yusuke Homma, Japan Pile Corporation, 36-2 Nihonbashi Hakozakicho, Chuo-ku, Tokyo, Japan, +81(0)3 5843 4196, yusuke_honma@japanpile.co.jp
Kentaro Oko, ASIA PILE HOLDINGS CORPORATION, 36-2 Nihonbashi Hakozakicho, Chuo-ku, Tokyo, Japan, +81(0)3 5843 4173, kentaro_oko@asiapile-hd.com

ABSTRACT

Precast nodular piles, used in Japan for almost a century, are high-strength concrete spun piles with fixed-interval nodules. In the early days these piles were driven with a mound of crushed stone around the pile such that the crushed stone space, between nodules around the shaft as the pile penetrated into the ground. The installation method shifted to bored precast methods after 1970 due to regulations restricting noise pollution from impact driving. Bored precast piling involves placing piles in drilled holes, grouting with cement grout that enhances shaft friction. Recently, nodular piles are also used as bearing resistance piles. A base-enlarged pre-boring method, with an enlarged base at the pile toe, increases bearing resistance capacity. Combined with base enlargement, bored precast piles provide high axial load resistance for buildings. This paper explores the history, development, load transfer analysis, and design practice of bored prestressed high-strength concrete (PHC) nodular piles in Japan.

Keywords: Nodular Pile, Bearing Capacity, Settlement, Loading Tests, Load Transfer Analysis.

INTRODUCTION

In 1923, Shojiro Takechi developed the nodular pile in Osaka, Japan. Initially developed as a 350 mm (1.15 ft) square pile, this evolved to hexagonal and heptagonal sections before the current, circular spun precast piles with nodules at every 1000 mm (3.28 ft) spacing. In general, use of precast nodular piles in Japan went through various changes in shape and installation methods over the past 80 years. With the availability of larger machinery, lager diameter nodular piles have been developed, and are considered well suited to provide higher friction resistance to support low to mid-rise structures.

TRANSITION OF NODULAR PILE CONSTRUCTION METHODS

Around the 1930s, manual drop hammers were used to drive nodular piles with a pile of crushed rock around the pile such that the space between nodules got packed with crushed rock as it penetrated into the ground (Photo 1). By the 1960s, diesel/hydraulic hammers replaced drop hammers, the crushed rock packing approach continued as a means of soil improvement and providing drainage for excess porewater pressure through the crushed rock to serve as liquefaction mitigation. From 1960 to 2000, regulations on noise and vibration became stricter, and alternatives to impact driving for installation of piles were developed. One of the recent installation methods as an alternative to impact driving is the Geo Mixing

 © Deep Foundations Institute 2025

Takechi Original Pile (GMTOP) method (2000) that installs piles in cement-mixed soil holes. Another method known as the Hyper Mega (HM) method (2006), combines the MEGA Takechi Original Pile (MEGATOP) method (2003) with an enlarged base. The HM method allows 1200 mm (3.94 ft) nodule diameter nodular pile and straight shaft connections, enhancing end bearing resistance as well as the shaft friction (Fig. 1). In 2024, the HM method was used in over 4000 projects in Japan (Photo 2).



Photo 1. Nodular pile installation using a drop hammer in the 1930s

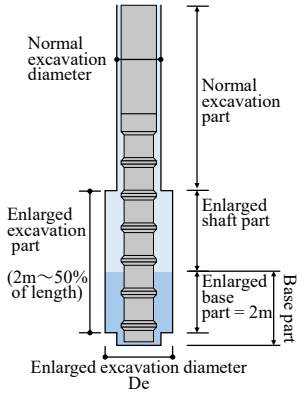


Fig. 1. Image of Pile material and Excavation of the HM method



Photo 2. Nodular pile installation using the HM method

OVERVIEW OF THE HM METHOD

Applicable piles

The HM method is applicable to various pile types, including nodular piles with a maximum node diameter of 1200 mm (3.94 ft), and straight piles like PHC, PRC, SC, and steel pipe piles, also up to 1200 mm (3.94 ft) in diameter, which can be spliced with nodular piles. These piles can be combined to suit specific design conditions. Figure 2. illustrates 1000-800 mm nodular piles (nodule diameter-shaft diameter). Enhanced horizontal and axial bearing capacity can be achieved by using an enlarged upper section, joining straight piles larger than the lower nodular pile. Piles with concrete strengths of 85, 105, and 123 N/mm² are utilized.

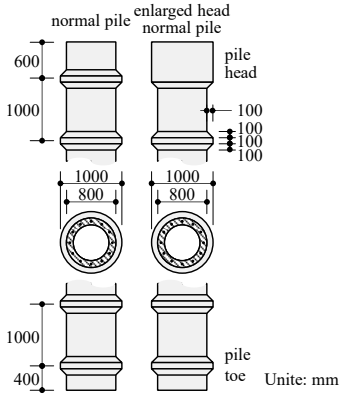


Fig. 2. Configuration of a 1000-800 mm Nodular Pile with Enlarged Head

 © Deep Foundations Institute 2025

Ground conditions and installation depth

The ground to which the HM method can be applied is sandy soil, gravelly soil, and clay (including silty soil) near the pile tip, and sandy soil (including gravelly soil) and clay around the pile tip. The current maximum depth of installation is 68.5 m. In ground with liquefaction potential, a separate study is required.

Overview of construction procedures

An overview of the installation procedure for the HM method is illustrated in Fig. 3. There are two types of auger heads used for bottom expansion: a mechanical type that expands cutting blades by rotating in the opposite direction and a hydraulic type that expands the cutting blades hydraulically. If the standard excavation diameter (diameter at the nodule + 50 mm) is D_s, and the enlarged excavation diameter is D_e, then the enlargement factor ω is defined as $\omega = D_e/D_s$. Work monitoring is extremely important to ensure the quality of the pile at the base enlarged pre-boring and grouting method. The key points especially are checks to confirm that the expanded blade has correctly expanded and the grout has been properly pumped. These critical items are measured and monitored by devices integrated with the construction machinery.

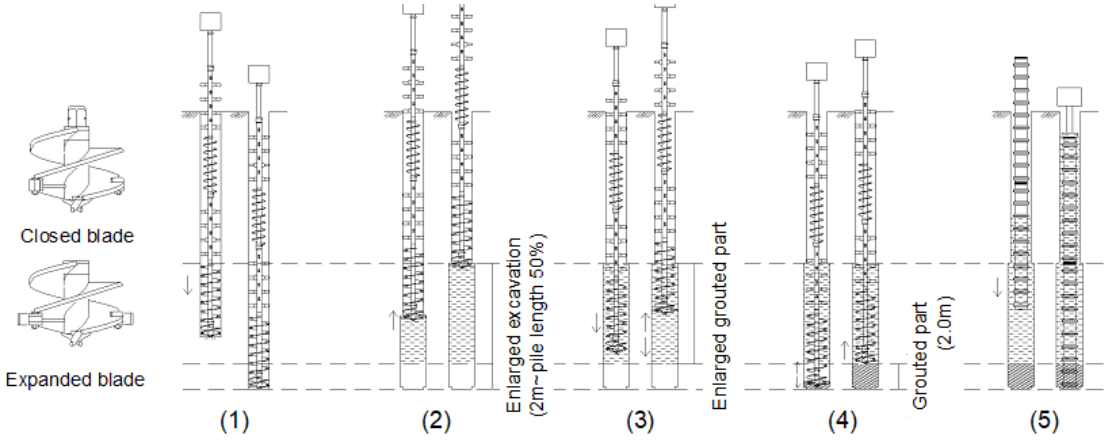


Fig. 3. Installation sequence

AXIAL BEARING CAPACITY

Bearing resistance

As shown in Fig. 4, the end bearing capacity P_p is evaluated as the axial resistance at a position 2000 mm (6.56 ft) above the pile toe in this HM method. This evaluation position of 2000 mm above the pile toe is set to broadly consider the influence of the ground near the pile tip. For this reason, the “bearing capacity” includes the shaft friction of the 2000 mm grouted base in addition to the load bearing capacity at the bottom face of the grouted base. As the two components are not evaluated separately in the conventional design methods, these components have remained unclear in terms of the bearing capacity mechanism.

 © Deep Foundations Institute 2025

End bearing capacity P_p in the HM method is the sum of the resistance P_{pp} at the pile toe (bottom) face and the shaft friction of the grouted base P_{pf} above the bottom. For P_{pp}, the axial force at the lowermost node position (about 350 mm above the pile toe face) is used.

To derive the equations for the bearing capacity of piles installed by the HM method, the diameter of the grout base should be considered to vary in the range of 1 to 2 times that of the standard excavation diameter (in the upper part). This range is selected based on the constructability considerations. The conventional α is expressed by equation [1], and the factor a, b, c are determined from the data of loading tests.

$$\alpha = \alpha_p + \alpha_f = a\omega^b + c\omega \quad [1]$$

Where α_p = Bearing capacity factor due to load bearing capacity at the pile toe face (lowermost node bottom face); α_f = Bearing capacity factor due to shaft friction resistance of grouted base; ω = Enlargement ratio = D_e / (D_o + 0.05); D_e= Enlarged excavation diameter (grouted base diameter) (m); D_o = Nodal diameter at the grouted base position (m)

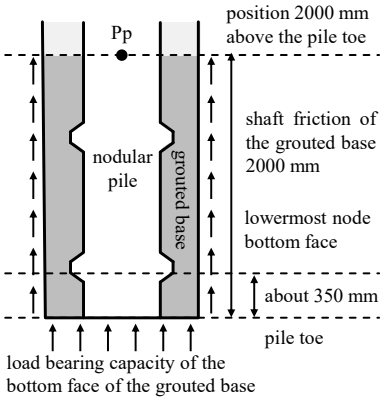


Fig. 4. Evaluation position of pile bearing resistance capacity P_p

Detailed analysis process is omitted. On the basis of the above analysis from load test results with a strain gauge, the equations of α for sandy/gravelly and clayey soils (including silty soils) are given by equations [2] and [3] respectively.

$$\alpha = 240\omega^{1.5} + 90\omega \quad [2]$$

$$\alpha = 210\omega^{1.25} + 90\omega \quad [3]$$

When ω = 2.0, the value of α for sandy/gravelly soil is 858 (kN/m^2) and for clayey soil it is 679 (kN/m^2). Figure 5 shows the relationship of α with ω compared with load test data for sandy and gravelly soil. The values in the data for both types of soil exceed those obtained from the equations.

 © Deep Foundations Institute 2025

Shaft friction resistance

Empirical equations for estimating the shaft friction resistance are derived using the friction resistance f_s and f_c, determined from the results of loading tests. The calculation equations are as shown in [4] to [7].

$$P_{fs} = f_s L_s D\pi \quad [4]$$

$$f_s = \beta N_s \quad [5]$$

$$P_{fc} = f_c L_c D\pi \quad [6]$$

$$f_c = \gamma q_u \quad [7]$$

Where P_{fs} = Shaft friction resistance of sandy soil (kN); f_s = Shaft friction in sandy soil (kN/m^2); L_s = segment length of pile in contact with sandy soil (m); D = Pile diameter in meter (nodule diameter of nodular pile); β = Shaft friction resistance factor of sandy soil; N_s = Average N-value (N60) of sandy soil; P_{fc} = Shaft friction resistance of clayey soil (kN); f_c = Shaft friction in clayey soil (kN/m^2); L_c = segment length of pile in contact with clayey soil (m); γ = Shaft friction resistance factor of clayey soil (kN); q_u = Measured unconfined compression strength (kN/m^2). Values of shaft friction resistance at ultimate load bearing capacity from equations are compared with the loading test data.

In the case of nodular piles, the occurrence of the slip surface between the pile shaft and the cement grout cannot be considered owing to the bearing resistance at nodules and their effect of integrating the pile with the cement grout. Moreover, the occurrence of the slip surface between the cement grout and the soil is observed during loading tests. Accordingly, the shaft friction resistance of nodular pile is decided by the frictional resistance between the cement grout and the soil, and is considered to be proportional to the outer diameter (excavation diameter) of the cement grout. Thus, the shaft friction stress of a nodular pile was estimated using the excavation diameter (taken as ωD_o) and not the nodal diameter D_o.

Figure 6 shows the f_s - N_s relationship of sandy soil around the pile. These data were obtained from various ground conditions across Japan. Since the equation for (mean - 1.06σ) is $f_s/\omega = 30.3 + 5.50\ N_s$, the relatioship for β is expressed by equation [8]. Fig. 7 also shows the f_c - q_u relationship for clayey soils. Since the equation for (mean - 1.06σ) is $f_c/\omega = 23.12 + 0.510\ q_u$, the relationship for γ is expressed by equation [9]. The friction resistance of a Straight pile is considered that there is a case where the slip occurs between the cement grout and the pile body. This phenomenon has been confirmed in loading tests. Thus, the data is estimated by the pile diameter (not by the excavation diameter).

 © Deep Foundations Institute 2025

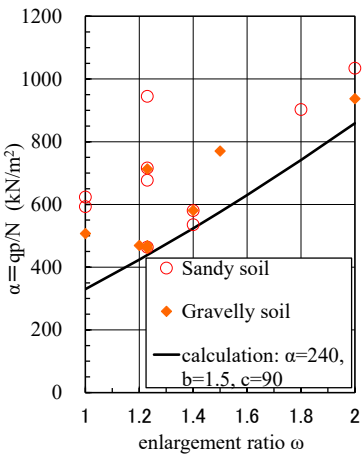


Fig. 5. *α-ω* relationship (sandy and gravelly soil)

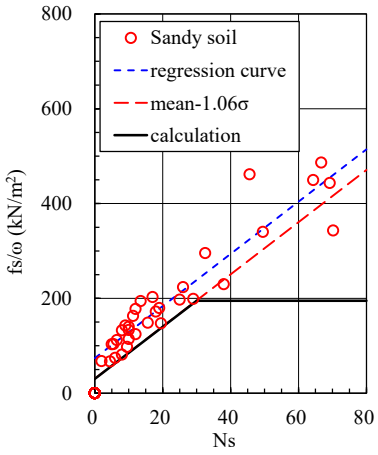


Fig. 6. f_s-N_s relationship (nodular pile; sandy soil)

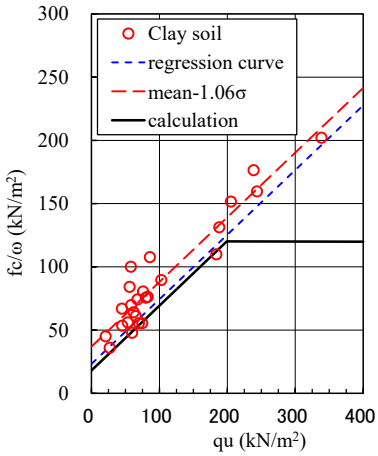


Fig. 7. f_c-q_u relationship (nodular pile; clayey soil)

$$\beta\overline{N_s} = (30 + 5.5\overline{N_s})\omega \quad [8]$$

$$\gamma\overline{q_u} = (20 + 0.5\overline{q_u})\omega \quad [9]$$

COMPARISON OF BEARING CAPACITY CHARACTERISTICS

Outline of comparison conditions

The ultimate bearing capacity (measured value) obtained from the loading test results of the HM method is compared with the calculated value. Fig. 8 and Table 1 show the conditions of the ground and pile specifications used for the comparison. These ground conditions and pile specifications are selected from the results of loading tests on the piles installed by the HM method. The pile tip ground conditions are sand (tip N-value 13.6), gravel (tip N-value 33.3), and clay (tip N-value 10.0). The *N*-value is one of the indices representing ground strength, obtained through a ground investigation called the Standard Penetration Test. The Standard Penetration Test, along with the Cone Penetration Test, is widely used in Japan as part of geotechnical exploration. The conditions of the pile specifications are: pile lengths of 26 to 32 m, nodal piles with diameters 500-400 mm to 800-600 mm, and expansion ratios of 1.80 to 2.00.

 © Deep Foundations Institute 2025

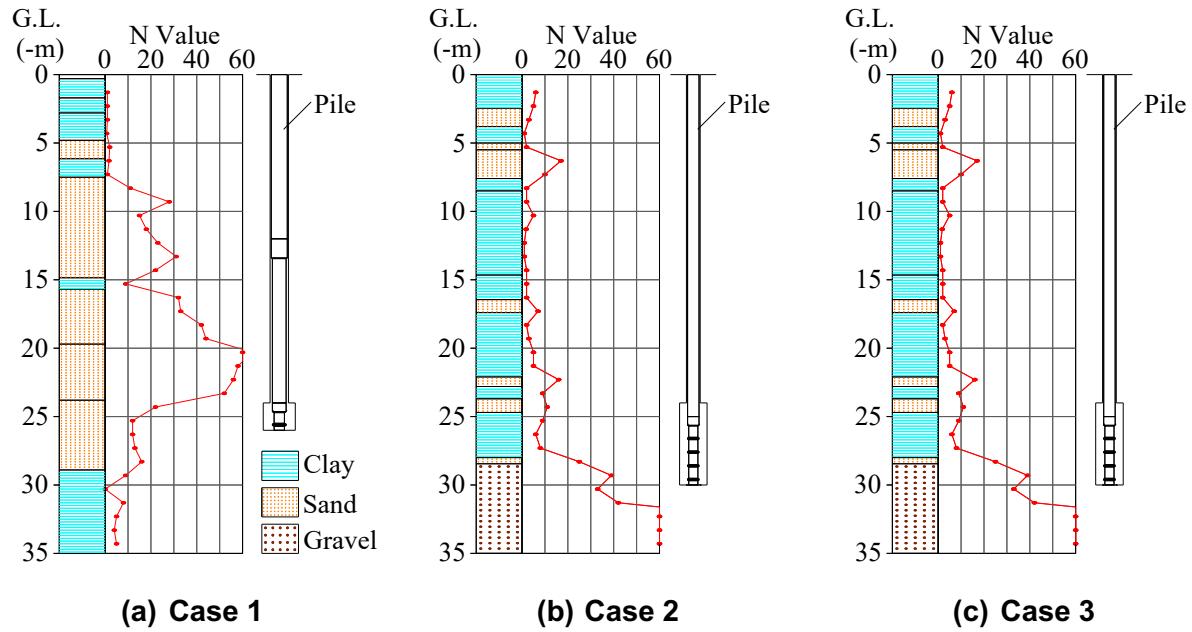


Fig. 8. Soil and pile condition for calculation case study

Table 1. Soil and pile condition for calculation case study

Test Case	Case 1	Case 2	Case 3
Soil at the pile tip	sand	gravel	clay
Nodular pile (nodule-shaft diameter in mm)	600-450	500-400	800-600
Overall pile length (m)	26	30	32
Enlargement ratio	1.80	2.00	1.80

Comparison results

Table 2 shows the results of the comparison between the measured and calculated values of the ultimate bearing capacity. The ratio of measured to calculated values are in the range of 1.13 to 1.63. It was confirmed that the measured values were higher or well above the calculated values. As shown in Figs. 5-7, the parameters α, β, and γ are set on the conservative side, which results in the measured values higher than the calculated values.

Table 2. Comparison of ultimate bearing capacity

Test Case	Case 1	Case 2	Case 3
Measured Value from load test (kN)	14,400	9,800	18,600
Calculated Value from equation (kN)	12,700	6,900	11,400
Measured / Calculated	1.13	1.42	1.63

 © Deep Foundations Institute 2025

COMPARISON OF LOAD-SETTLEMENT CHARACTERISTICS

Verification summary

The load-settlement relationship at the pile head and axial force distribution obtained from the loading test results of the HM method are compared with the analytical values. The ground conditions and pile specifications used in the comparison are the same as Fig. 8 and Table 1 above. The calculation method of the analytical values is described in the next section.

Analysis model overview

The analytical values are obtained using a load transfer analysis. Load transfer analysis is a method for analytically determining the load-settlement relationship of a single pile based on the pile tip resistance-tip settlement relationship and the shaft resistance-settlement relationship of the pile obtained from previous loading test results. Specifically, as shown in Fig. 9, the pile body is assumed to be elastic and divided into several pile elements, and the analytical model considers friction springs along the pile shaft and an axial vertical spring at the pile tip. The hyperbolic curves expressed in Equations [10] and [11] are used to represent the friction spring between the pile shaft and the surrounding soil and an axial spring between the pile tip and the ground below.

$$q_p = S_p/\left(a_p + b_p S_p\right) \quad [10]$$

$$f_i = S_i/\left(a_f + b_f S_i\right) \quad [11]$$

a_p, b_p, a_f and b_f are the respective coefficients, the reciprocals $1/a_p$ and $1/a_f$ of which are the initial tangential slopes of the respective hyperbolic curves, and the reciprocals $1/b_p$ and $1/b_f$ are the asymptotic values (see Fig. 10). The coefficients a_p, b_p, a_f and b_f are obtained using regression lines with the N values for each soil type obtained from numerous loading test results of the pre-boring method (Table 3).

The regression lines with the N values for the coefficients a_p, b_p, a_f and b_f are given in reference (Ito A., 2008). The respective coefficients were calculated from the excavation diameter and excavation cross section. Therefore, the compressive deformation of the pile body was evaluated assuming that the entire excavation diameter, including the cement grout and the pile body. The modulus of elasticity, E_p, of the uniformly elastic body is obtained from Equation [12]. The modulus of elasticity of the pile body and cement grout were adopted as typical values of E_c=40000 N/mm^2 and E_m=4000 N/mm^2, respectively. A_c is the cross-sectional area of the pile shaft section and A_m is the cross-sectional area of the cement grout section.

 © Deep Foundations Institute 2025

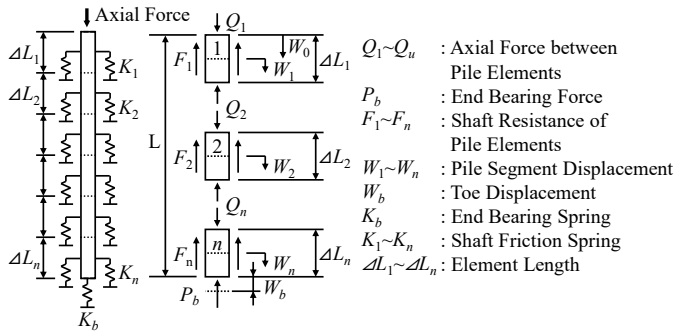


Fig. 9. Load Transfer analysis model

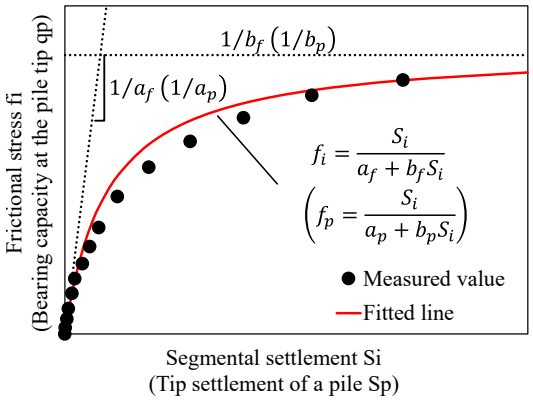


Fig. 10. Overview of hyperbolic approximation

Table 3. Regression line of hyperbolic constant

(a) q_p-S_p Curve

Soil	Constant	Regression equation
Sand	$1/a_p$	18200N+13700
	$1/b_p$	243N+49.4
Clay	$1/a_p$	12400N+67500
	$1/b_p$	38.0N+1000

(b) f_i-S_i Curve

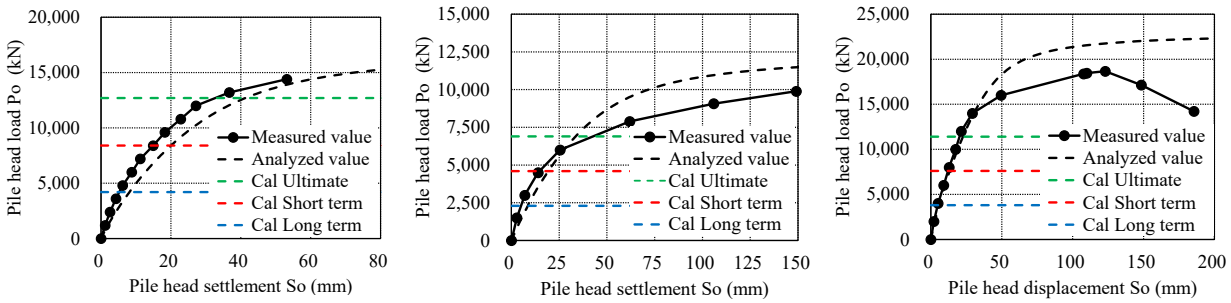
Soil	Constant	Regression equation
Sand	$1/a_f$	1580N+10900
	$1/b_f$	243N+67.1
Clay	$1/a_f$	1750N+15000
	$1/b_f$	4.40N+50.1

$$E_p = (E_c A_c + E_m A_m)/(A_c + A_m) \quad [12]$$

Results of verification

Fig. 11 shows the comparison of pile head load-settlement relationships and Table 4 shows the comparison of pile head settlement at each design load (Long-term, Short-term, and Ultimate). It can be seen that the load transfer analysis was able to reproduce the load-settlement relationships of the piles obtained from the loading tests. The measured/analytical values of the pile head settlement at each design load range from 0.78 to 1.72. Fig. 12 shows the comparison results of axial force distribution (Long-term, Short-term, and Ultimate). The load transfer analysis successfully reproduces the pile's axial force distribution as observed in the loading test. While a discrepancy exists between the measured and analyzed values at ultimate load, this analytical accuracy is deemed sufficient when considering the inherent uncertainties of the ground.

 © Deep Foundations Institute 2025

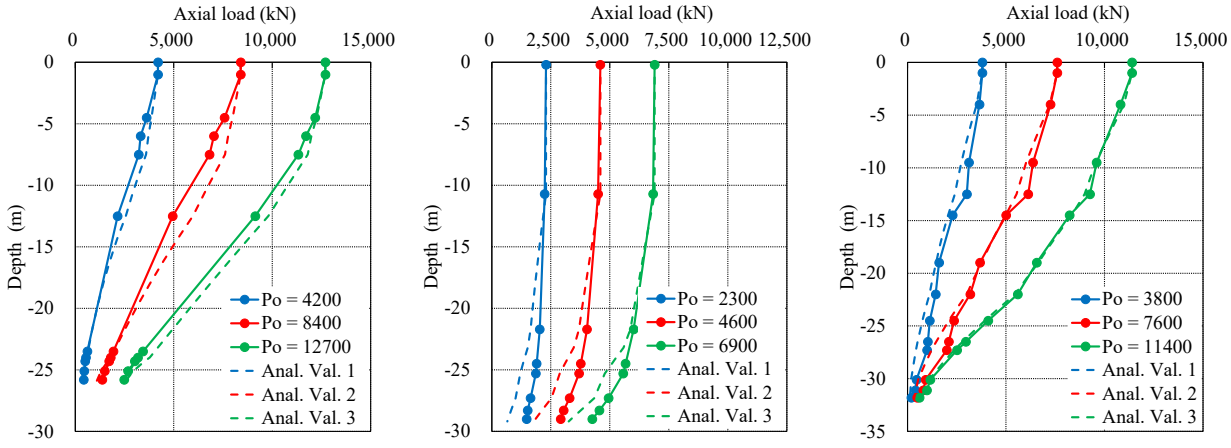


(a) Case 1 (b) Case 2 (c) Case 3

Fig. 11. Pile Head Load-Settlement Relationship

Table 4. Comparison Measured Values and Analyzed Values (pile head settlement S_o(mm))

Test Case	Case 1			Case 2			Case 3		
State	Long term	Short term	Ultimate	Long term	Short term	Ultimate	Long term	Short term	Ultimate
Measured Values	5.2	14.9	32.7	5.0	14.7	42.8	4.8	12.1	20.2
Calculate Values	8.1	19.8	39.5	8.6	19.3	33.5	5.8	13.3	22.4
Measured/Calculated	1.55	1.32	1.21	1.72	1.31	0.78	1.21	1.09	1.11



(a) Cace 1 (b) Case 2 (c) Case 3

Fig. 12. Axial distribution curves

CONCLUSION

In this paper, an overview of the HM method and its bearing capacity evaluation equation are described, and the measured and calculated load bearing and load transfer mechanisms of the HM method are compared. The results showed that the load transfer analysis effectively replicates the pile's load-settlement characteristics and axial force distribution derived from the loading test results. Continuing with further load testing on fully instrumented piles will help expand the dataset and contribute to improved reliability

 © Deep Foundations Institute 2025

of the design approached developed for specific installation methods and pile types.

REFERENCES

Toyoshima, M.: Special Course on Foundations by Illustrations, Building Material Research Association, 1975 (in Japanese).

Ogura, H. Komatsu, G. Manabe, M. Oshima, A. Chikusa, N. Hosoda, Y. Sumi, M. and Mimura, T.: Enlarged Boring Diameter and Vertical bearing Capacity Installed by Root Enlarged and Solidified Pre-boring Method of Precast Pile, GBRC, Vo.32, No.1, pp.10-21, 2007 (in Japanese).

Japanese Society of Soil Mechanics and Foundation Engineering: Design and Explanation of Pile Foundations, Chapter 5 Calculation of Axial Bearing Capacity of Piles, 1985 (in Japanese).

Ito A., Ogura H., Tanaka Y. and Han H.: Estimation of Load-Settlement Relations on Pre-boring Nodular Piles, J. Struct. Constr. Eng., AIJ, No. 628, pp.907-913, Jun.,2008 (in Japanese).

Architectural Institute of Japan: Recommendation for Design of Building Foundation, pp.222-224, 2019.11 (in Japanese).

 © Deep Foundations Institute 2025

LOW CARBON INITIATIVES AT EUSTON STATION HS2 – ENVIRONMENTALLY FRIENDLY WAY OF PILE INSTALLATION IN THE CITY OF LONDON

Franz-Werner Gerressen, BAUER Maschinen GmbH, Germany, Franz-Werner.Gerressen@bauer.de
Johann Kraxenberger, BAUER Maschinen GmbH, Germany, Johann.Kraxenberger@bauer.de
Matthew Gregory, Cementation Skanska, UK, matthew.gregory@skanska.co.uk
Deon Louw, Cementation Skanska, UK, deon.louw@skanska.co.uk
Robert West, Cementation Skanska, UK, robert.west@skanska.co.uk

ABSTRACT

The pile installation at Euston Approaches was carried out with the full focus on lowering carbon emissions. Several initiatives were implemented, starting with the preparation of the piling location using a low carbon guide wall, where the incorporation of basalt reinforcement replaces traditional steel. The pile installation itself was then carried out using the world's first electric, grid-powered, large rotary drilling rig eBG33. Instead of a diesel engine, the eBG33 has a powerful electric drive. Furthermore, the concreting of the piles was completed using low carbon concrete. The low carbon concrete mix delivers a 45% reduction in the embodied carbon of the main piling concrete. To finalize the pile installation, the Zero Trim Pile Technique was used. A technique, which eliminates the need for pile cropping/trimming. The solution contributes significantly to the reduction of embodied carbon and has demonstrable safety benefits including reduced noise, vibration, and dust. The paper will expand on the construction process, the specific challenges and experiences made under these circumstances.

Keywords: Electric driven drill rig, drilled piles, low carbon concrete, low carbon guide wall, zero trim pile, basalt reinforcement

INTRODUCTION

High Speed Two (HS2) is a major high-speed railway project in the UK connecting London to the West Midlands. The 13 mi (21 km) of twin-bore tunnels in London include numerous geotechnical structures and extensive foundation works, such as embedded retaining walls and cut-and-cover box structures. For the contiguous retaining wall and bearing piles in the Euston Station Approaches alone, there are approximately 1800 No. rotary bored piles. Piles are constructed mainly in the London Clay Formation and Lambeth Group some, however, were advanced to the Thanet Sand Formation at approximately 160 ft (49m) from ground level. The diameter of these piles ranges from 29 – 71 in (750 - 1800 mm) and most are constructed using a polymer support fluid to stabilise the soils during boring. Pile cut off level was located within the cohesive soils of the London Clay Formation with each pile reinforced with a full-length cage. Striving to achieve low carbon solutions to typical operations on the site, several innovations were conceived.

LOW CARBON GUIDEWALL

Secant and contiguous bored piled walls often require a reinforced guidewall to ensure the plan position and verticality. The guide wall is a cast in place using a low strength concrete and reinforcement bars to ensure its integrity during piling operations, Fig. 1 shows this typical detail. A guide wall is a low-risk item of temporary works that is removed and demolished therefore serving as the perfect ‘sandbox’ for trialling innovative materials.

Using Basalt Fibre Reinforced Polymer (BFRP) and a high Ground Granulated Blast-Furnace Slag (GGBS) replacement concrete mix, a low carbon guide wall alternative was implemented. BFRP, derived from basalt rock, offers superior strength, durability, and corrosion resistance. Basalt fibres and other composites are often used in various materials to boost tensile strength, thermal stability, and overall performance. Table

 © Deep Foundations Institute 2025

1 presents the properties of the BFRP that was placed in the guide walls in place of conventional grade steel (500N/mm^2).

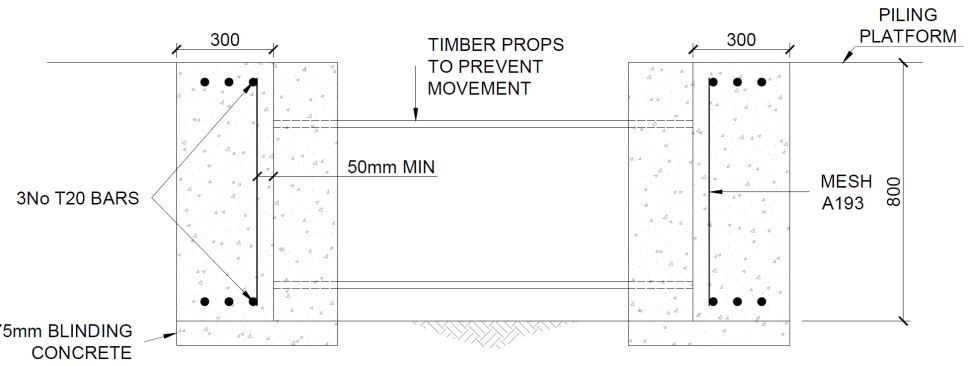


Fig. 1. Typical guide wall section.

Table 1 – Properties of Basalt Bar

Diameter (mm)	Tensile Strength (MPa)	Elasticity Modulus (MPa)	Density (kg/m^3)
8	1430	50,000	2000
16	1200	50,000	2000

BFRP offers a sustainable alternative to traditional materials like steel due to the abundance of basalt rock and its reduced embodied carbon. To put this into context the global warming potential of 6mm BFRP bars, measured as kgCO_2e, excluding transport, is 74% lower than that of steel, 22% lower than steel with 100% recycled content, 49% lower than galvanised steel, 88% lower than stainless steel and 44% lower than GFRP (Pavlovic, Donchev, Petkova, & Staletovic, 2022). The amount of carbon savings that can be achieved when looking at replacing conventional reinforcement bars with BFRP is presented in Table 2. This simple assessment considers equal steel replacement, the area of steel required is constant for both scenarios. The carbon factors used in the table below are from the cradle to the gate (A1 – A3) which can account for 50% of the embodied carbon life cycle (Orr, Gibbons, & Arnold, 2020).

Table 2 - Embodied Carbon Comparison (Reinforcement)

Type	Area of Steel (m^2/m)	Density (kg/m^3)	Weight (kg/m)	A1-A3 ECF (kgCO_2e/kg)	Embodied Carbon (kgCO2e)
Steel	0.469	7750	36.37	0.787[1]	28.62
Basalt, BFRP	0.469	2000	9.39	1.82[2]	17.08
Notes: [1] (CARES, 2023), [2] (Basalt Technologies UK Ltd, 2022)					

As shown in Table 1, simply swapping reinforcement bars for BFRP can save around 40% of embodied carbon alone, without considering the benefits that can be gained from adopting a low carbon concrete mix combined with the superior properties of BFRP to value engineer the structure. Typically, lower strength concrete, C20/25, is placed in traditional guide wall design however, to enhance the overall carbon saving, a CIII/B 80% high GGBS mix was placed. Table 3 provides a comparison between the two mixes that were used at the project.

By adopting a higher GGBS replacement mix we were able to save approximately 23,553kgCO2e or 20% per metre run of the guide wall. Combined savings, when considering the traditional guide wall and the low

 © Deep Foundations Institute 2025

carbon guide wall, was approximately 23,564kgCO2e per metre run. Approximately 4,430 ft (1,350 linear metres) of low carbon guide wall has, and is forecasted, to be installed at the Euston Approaches site equating to a saving of 31,811tCO2e.

Table 3 - Embodied Carbon Comparison (Concrete)

Type	Volume per m run of guidewall (m^3/m)	Density (kg/m^3)	Weight (kg/m)	Embodied Carbon of concrete, A1- A3 [1](kg/m^3)	Embodied Carbon A1 – A3 ($kgCO_2e$)
CEMIII/A 50% GGBS (C20/25)	0.48	2293	1100	108[1]	118869
CEMIII/B 73% GGBS (C20/25)	0.48	2364	1134	84[1]	95316
Notes: [1] ICE Database – Embodied Carbon Model of Cement, Mortar and Concrete (Jones & Hammond, 2011)					

BFRP is light, safe to handle, and can be cut with regular tools, reducing sparking risks. It's versatile and can be moulded into conventional shape codes without mechanical aid (even curved, as shown in Fig. 2). When discarded, the concrete-BFRP mix can be crushed; BFRP breaks down into fibres for recycling, negating the need to separate it from concrete. Low carbon concrete has slower strength gain and takes longer to set before formwork removal. A C20/25 mix reaches design minimum strength about 5 days quicker than low carbon concrete.



Fig. 2. Basalt reinforcement and a completed section of guide wall

LOW CARBON CONCRETE

Concrete, particularly Ordinary Portland Cement (OPC) production, significantly contributes to piling work's carbon footprint. A high replacement concrete mix was developed with suppliers in attempt to reduce this impact at a project level by replacing the typical piling mix, Mix A (Table 4) in permanent works piles.

Table 4: Concrete Specification of Mix A

Strength:	C40/50		Maximum Water/Cement Ratio:	0.38
Cement Class:	CIIIA + SR		Carbonisation Class	XC2
Consistence:	F5		Chloride Class:	XD2
MCC:	380		Chemical Class:	DC2

 © Deep Foundations Institute 2025

Initial trials tested varying cement categories (380-420, 435 and 485kg/m3) and GGBS replacements (50 – 85%). All cement types passed fresh property tests providing confidence in the concept. Five mixes were chosen for batch plant trials based on lab performance, strength, and carbon reduction potential for HS2 S1's remaining concrete needs. Fig. 3 shows the recorded strength gain with varying GGBS and Cement Contents. All the results show the compressive strength reaching a minimum of 50N/mm^2 by 28 days except for the 85% GGBS mix (red line).

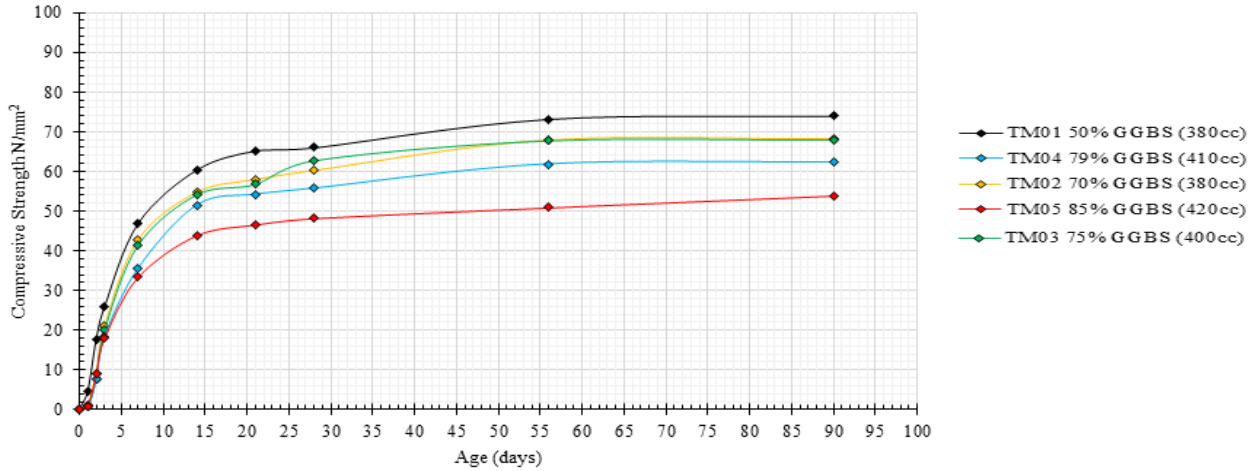


Fig. 3. Recorded strength gain of trial mixes 1 to 5 (380 – 430cc) over 90 days

Whilst several low carbon concrete mixes were trialled, significant progress was made on a 79% high GGBS replacement mix (HC79).

The mix was designed to meet all the concrete specifications requirements in Table 5 whilst still delivering a significant reduction in the embodied carbon. Cradle to gate carbon factors were calculated with the ICE Concrete Model created by Dr Craig Jones of Circular Ecology. The suppliers declared carbon certificates revealed embodied carbon values that correspond to those calculated by the project team, independently reviewing the values provided in Fig. 4.

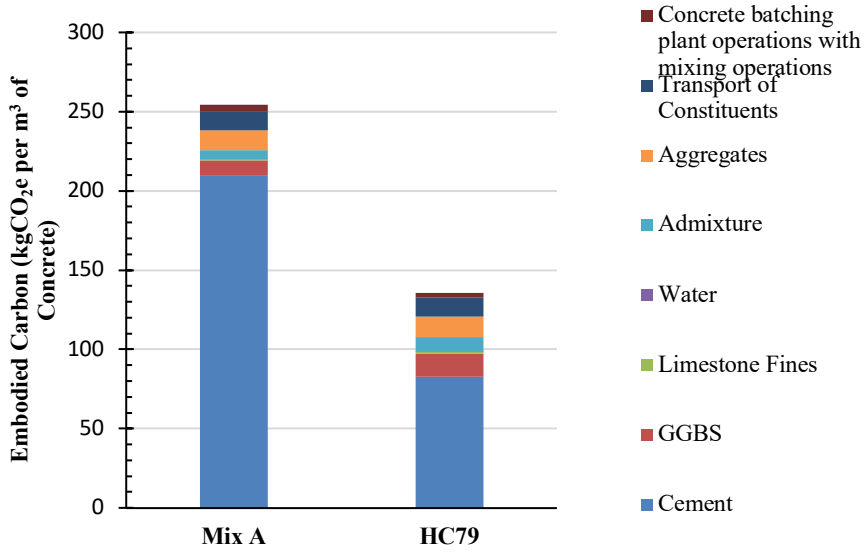


Fig. 4. Cradle to gate embodied carbon contribution per constituent and process.

 © Deep Foundations Institute 2025

The mix was designed to meet all the concrete specifications requirements in Table 5 whilst still delivering a significant reduction in the embodied carbon. Cradle to gate carbon factors were calculated with the ICE Concrete Model created by Dr Craig Jones of Circular Ecology. The suppliers declared carbon certificates revealed embodied carbon values that correspond to those calculated by the project team, independently reviewing the values provided in Fig. 4.

The HC79 concrete mix, with a 45% reduction in embodied carbon compared to Mix A, passed plant trials, and met specification requirements. Despite initial concerns about workability and bleed characteristics during site trials in 131 ft (40m) deep temporary piles, adjustments to the sand, aggregate grading, and limestone fines addressed these issues. Unfortunately, this change in composition yielded a 4-month delay in the implementation due to the testing periods required to achieve the various durability requirements. As a result, it was not possible to realise the full carbon savings that were originally forecasted for this phase of works. Fortunately, 1.05 million cu ft (30,000m^3) of concrete is still to be placed at Euston Approaches site when works resume.

The final HC79 mix is stable, high-flow, low-to-zero bleed, high-strength, durable and suitable for various placement methods including tremie in dry piles, under support fluid and by pump. HC79 was accepted by the client and replaced Mix A for permanent works. A comparison between the original piling mix, Mix A, and the approved HC79 mix based on what was delivered to site and what is still left to complete on the project has been provided in Table 5.

Table 5: Concrete embodied carbon saving following the introduction of HC79

Name	Concrete consumption (m^3)		Embodied carbon ($kgCO_2e$ per m^3)	Total Carbon (tCO_2e)
HC79	Placed	2900	136	394
	Forecasted[1]	33000	136	4488
Mix A	Total[2]	35900	255	9154
Notes: [1]This is the remaining theoretical volume of concrete required to complete the piling scope (April 2024). [2] This is the total of the forecasted and placed concrete from HC79 mix to provide comparison.				

The adoption of the HC79 low carbon concrete mix emits a total of 4882tCO_2e which was a total saving of 4272tCO_2e or 46% reduction when compared against the same quantity of concrete Mix A if its use had continued.

ZERO TRIM PILE TECHNIQUE

The innovative ‘zero-trim pile’ technical project was extensively covered in a paper, Introducing the zero-trim pile technique: a more sustainable alternative to pile cropping (Lo, Bailie, Louw, & Piper, 2023) which form the basis of this section.

The technique eliminates the need for cropping by sucking out wet concrete above cut-off level. It enhances safety, minimizes noise, saves time, boosts accuracy, and prevents cracking. During the construction of a rotary bored pile, concrete is traditionally over-poured and then trimmed down to design cut-off level. This over pour surges any interface material (a mix of concrete, support fluid & soil particles) that has collected at the top of the concrete column insuring sound concrete at the finishing level. Creating sound, homogenous concrete at pile cut-off level is crucial for effective load transfer in piling works. It's often

overlooked because the piling specialist usually demobilises after completing the pile to its casting level, leaving the pile cropping to others. This approach doesn't consider the full construction sequence, hindering efficiency. A visualisation of the pile construction is provided in Fig. 5.

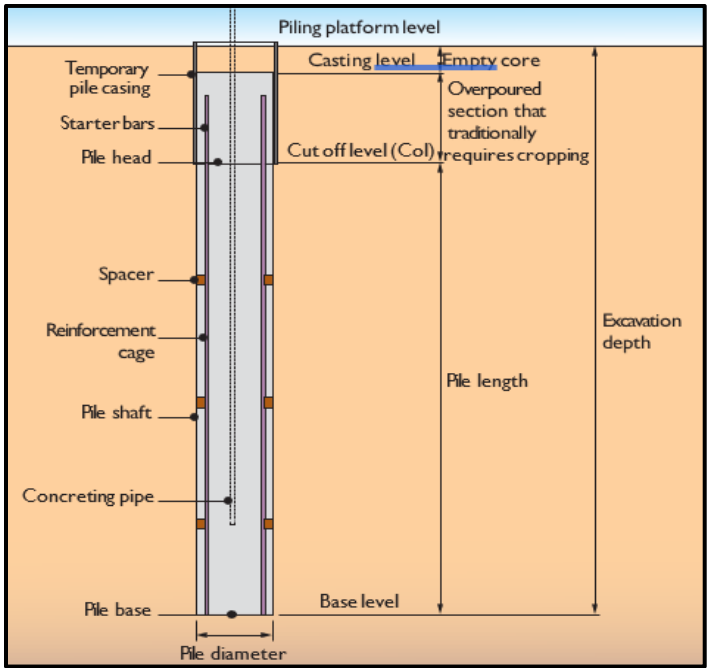


Fig. 5. Rotary bored piling terminology and trial pile cross-section (Lo, Bailie, Louw, & Piper, 2023).

The traditional method of concrete over-pour breakdown using hand-held pneumatic breakers can lead to health issues like hand-arm vibration syndrome, along with dust and noise pollution. The alternative, using pile croppers attached to excavators, is more efficient and safer. They use a hydraulic jaw system to cut piles producing a level finish. However, they're less effective on pile retaining walls due to space constraints between the piles. Both methods can cause damage to the structural integrity of the pile reinforcement.
The project team, considering the large-scale work, planned to avoid traditional pile-breaking methods in pre-construction. They collaborated early with supply chain partners to improve piling methods holistically. They aimed to find an alternative that would eliminate saw cutting, drilling, breaking, and cropping, reduce over-pour and cut down on time and costs.

The team found that manipulating concrete before it cures is easier since its strength increases exponentially once curing starts. To avoid traditional pile cropping, a foundation specialist proposed using a vacuum excavator to remove wet concrete from the pile head before hardening. Two options were considered for the construction technique but only one of the two adhered to industry wide best practices and guidance. The sequence was to over-pour the concrete (concrete poured using a tremie) and remove the excess with a vacuum excavator to cut- off level before the concrete has set as shown in fig. 6.

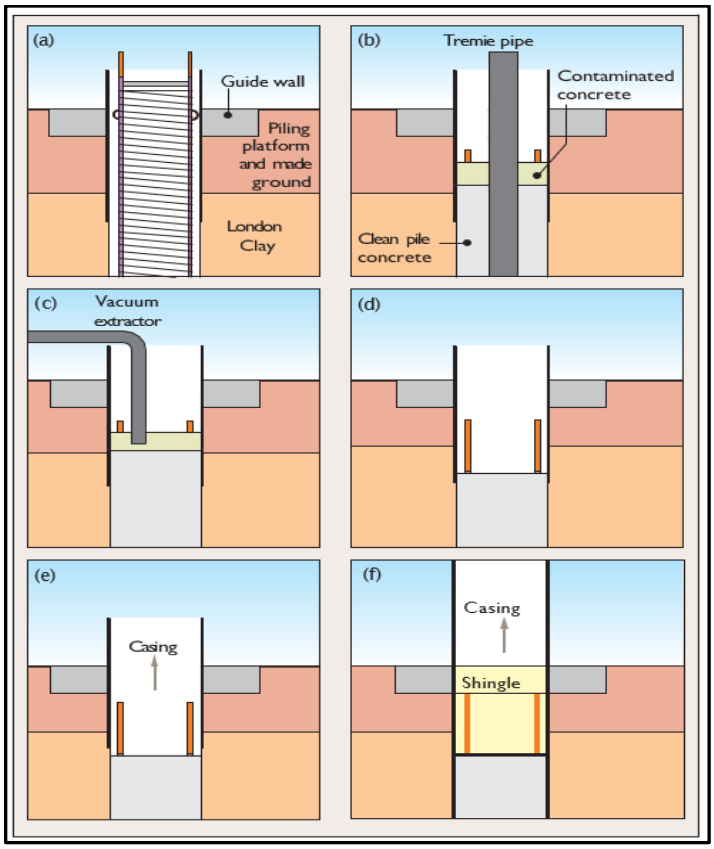


Fig. 6. Zero-trim pile technique sketch: (a) stage 1, day 1, reinforcement cage lowered into pile bore; (b) stage 2, day 1, concreting through tremie pipe to 24 in (600 mm) above cut-off level;(c) stage 3, day 1, vacuum excavator pipe lowered down bore to remove the casing; (f) stage 6, day 2, pile backfilled with shingle and casing extracted by rig (Lo, Bailie, Louw, & Piper, 2023)

The team, after a successful trial, applied the procedure to permanent work piles. Initially, 15 piles were completed traditionally without Zero-Trim for comparison. The results are shown in Fig. 7, with the photo on the left showing Zero-Trim and the right showing over pour and manual breaking. Some of the key benefits identified during the trials and the implementation across the project have been discussed.



Fig. 7. Zero-Trim and traditionally constructed piles after excavation

HEALTH AND SAFETY

Adopting a fit-for-purpose pile preparation technique can minimise health and safety risks associated with:

- Hand arm vibration syndrome

 © Deep Foundations Institute 2025

- Lifting of heavy concrete blocks
- Dust and Noise

The project site was in a highly populated residential area of London, it was crucial for the project team to respect the neighbours by minimising the noise and dust produced. Zero-trim piles eliminate the risks at the source and for this project, saved over 60,000 hazardous working hours involved in traditional trimming methods.

SUSTAINABILITY

Through the PAS 2080 (BSI, 2016) carbon dioxide management principles, embodied emissions calculations were undertaken by multiplying the estimated quantity by a carbon factor (kgCO2e per kg of material) for the different life-cycle stages, this equated to a saving of over 800 000 kgCO2e from the reduced over-pour.

QUALITY

Traditional pile-cropping methods often lead to reinforcement damage. The challenge in managing mechanical pile croppers during the cropping phase can lead to replacement or repair of the reinforcement. This not only adds to the expense and alters project timelines, but it can also cause clashes between pile and capping beam reinforcement.

PROJECT PERFORMANCE

The advantages of using the vacuum excavator in terms of cost and schedule were quite pronounced from a project performance standpoint. Although it had an initial hiring cost, it essentially eradicated the expenses linked with pile cropping. In the construction sequence, the piling contractor needed extra time to properly position the casing for the vacuum excavator to work efficiently. However, the vacuum excavator made it possible to eliminate excess concrete and polymer in just a few minutes. This process added less than an hour to the piling construction process which was offset by significant time savings in omitting the manual break down of cured piles. The zero-trim piles method was substantially quicker in reaching the cut-off level compared to traditional mechanical breaking. Consequently, this greatly sped up preparations for pile-cap construction and saved the project as much as 36 weeks on the overall programme.

PILE INSTALLATION BY USING ELECTRIC DRIVEN DRILL RIG

Noise and emissions on jobsites get more and more in focus. Neighbours are more sensitive for pollution and traffic noise. A close by jobsite normally increases this. To keep the additional pollution to a minimum the choice for the drilling rig was to go for an electric one. The Bauer eBG 33 helps to minimize the additional exposure in both ways to a minimum.

The eBG 33 is contributing to the reduction of CO2 and noise emissions on projects. It is the world's first electric, grid-powered, large diameter drilling rig. Permanently connected to the grid it allows all kind of drilling methods to be done. The execution of the piling works at Euston Approaches using the eBG33 will be the focus of this article.

At Euston Approaches piling works the eBG33's electric drive was powered by a dedicated on-site sub-station. As a result, the machine was able to operate with zero local emissions reducing the CO2 emissions. The eBG33 was tasked with working in an area of the project that was near occupied residential properties (Fig. 8). Compared to the diesel-powered equivalent piling rig, the eBG33 base carrier noise levels were 50% less. This significantly reduced the disruption allowing residents to remain in their properties whilst piling works were in operation.



Fig. 8. eBG 33 working close to adjacent structures.

For the rig operator, there is no difference between the eBG and BG drilling rig. Some additional considerations are required prior to operation of the eBG, some of which are below:

- Early liaison with the electricity supplier to arrange 800 kVA grid connection,
- Advanced planning to get the power supply in time and in position,
- Cable connection hover needs special attention,
- Logistics planning incorporating the power cables to avoid damages (Effective cable layouts utilise the site boundaries to remove risk of damages and allow free flow of traffic),
- Power cable protection.

Especially in narrow projects with close adjacent housing the advantages of the e BG come into full effect. Following the works at Euston Station Approaches, some real advantages were identified:

Local zero CO2 emission

Connected to the grid the overall CO2 emission of the eBG depends on how the electric power is produced (i.e., selecting renewable energy suppliers is key).

Reduction noise emission

In standard measurement, the sound power level of the eBG is reduced by 50% in comparison to BG rigs in the same torque class. The production of a pile does not only consist of drilling works. Rig idle times during cage installation and concreting also have an impact. Compared to diesel engines, which produce C02 and noise as soon as they have been started, the electro motor is almost silent. Process noise is unavoidable. However, the features of the eBG33 help limit noise to a minimum. For example, the spoil discharge assistant can be optimised such that the tool and ground conditions can be aligned. In addition,

the B-Tronic screen has a tool filling indicator or “helper” which gives the operator visual advice of the optimum filling of the tool. This achieves the best drilling performance and minimum time loss during discharging.

SUMMARY AND CONCLUSIONS

Innovative approaches such as low carbon guide walls, low carbon concrete, and zero-trim technology significantly contribute to minimising the overall carbon emissions on the project. The use of an electrically powered piling rig that is continuously connected to the grid can achieve local zero carbon emission. Table 6 presents the total savings for each of the four initiatives presented in this paper.

Table 6. Total Carbon Savings (tCO_2e)

Element	Type	Total Carbon Saving (tCO_2e)
Low carbon guide walls (A1 – A3)	Actual & forecasted	38110
Electric driven rig (A5a)	Actual[1]	28
Low carbon concrete (A1 – A4)	Actual & forecasted	4272
Zero Trim	Actual & forecasted	800
Notes:[1] Whilst all infrastructure is in place to successfully operate the eBG33 at Euston Approaches, actual use of the rig will depend on the number of piling rigs and their availability. To maintain the integrity of the calculations the forecasted saving has not been included in the estimated total savings.		

The total carbon savings that could be achieved at Euston Approaches when implementing the low carbon initiatives presented in this paper would equate to 38110tCO_2e which is the equivalent to powering 4509 homes for one year (United States Environmental Protection Agency, 2024). The paper has demonstrated that small, considered, changes to everyday operations can have a significant impact on reducing the overall carbon emissions of a project.

ACKNOWLEDGEMENTS

The authors would like to thank Skanska, Costain and Strabag (SCS), Skanska Technology, Basalt Technologies, Heidelberg Materials UK, and Hercules Site Services for their contribution to the low carbon initiatives presented in this paper.

REFERENCES

Basalt Technologies UK Ltd. (2022). *Environmental Product Declaration* . Wing, UK: Basalt Technologies UK Ltd.

BSI. (2016). *PAS 2080: Carbon management in buildings and infrastructure.* London, UK: BSI.

CARES. (2023). *Statement of Verification: EPD 000125.* Watford: BRE Global.

Department for Environment, Food and Rural Affairs. (2023). *UK Government GHG Conversion Factors for Company Reporting.* London, UK: UK Governmemt.

 © Deep Foundations Institute 2025

Jones, C., & Hammond, G. (2011). *The Inventory of Carbon and Energy (ICE).* Bracknell: BSRIA.

Lo, H., Bailie, P., Louw, D., & Piper, L. (2023). Introducing the zero-trim pile technique: a more sustainable alternative to pile cropping. *Proceedings of the Institution of Civil Engineers*.

Orr, J., Gibbons, O., & Arnold, W. (2020). A brief guide to calculating embodied carbon. *The Structural Engineerm Volume 98, Issue 7*, 6.

Pavlovic, A., Donchev, T., Petkova, D., & Staletovic, N. (2022). Sustainability of alternative reinfrocement for concrete structures: Life cycle assessment of basalt FRP bars. *Construction and Building Materials 334 (2022) 127424*.

Protchenko, K., Zayoud, F., Urbanski, M., & Szmigiera, E. (2020). Tensile and Shear Testing of Basalt Fiber Reinforced Polymer (BFRP) and Hybrid Basalt/Carbon Fiber Reinforced Polymer (HFRP) Bars. *Materials (Basel)*, 13, 5839.

Siemens Gamesa Renewable Energy. (n.d.). *Environmental Product Declaration SG 8.0-167 DD.* Vizcaya, Spain: Siemens Gamesa Renewable Energy.

United States Environmental Protection Agency. (2024, January). *Greenhouse Gas Equivalencies Calculator*. Retrieved from United States Environmental Protection Agency: https://www.epa.gov/energy/greenhouse-gas-equivalencies-calculator#results

 © Deep Foundations Institute 2025

SUSPENSION UNDERPINNING OF A WATERFRONT CHEMICAL FACILITY

Michael Senior, PE, Schnabel Engineering, Seattle, WA, USA, 206-573-5190,
msenior@schnabel-eng.com
Theodore Hudson, Project Engineer, Commerce Construction, Cherry Hill, NJ, 267-565-7737
tjh@commerceconstruction.com
Samuel Hudson, Construction Manager, Commerce Construction, Cherry Hill, NJ 856-498-8275
Ssh@commerceconstruction.com
Kirsten Grant, PE, Schnabel Engineering, Lexington, KY, USA, 859-469-6340,
kgrant@schnabel-eng.com

ABSTRACT

A chemical facility was constructed in the early 1900's along the Delaware River in Philadelphia to allow for movement of chemical products through the waterway. The facility was constructed with a roughly 152 meter (500 foot) long timber relieving platform, including timber decking and timber piles extending into marine soils and backfill atop the platform. The facility includes two containment slabs on grade that house a majority of the piping and mechanical equipment, multiple storage structures, and 14 columns that support the overhead piping across the length of the platform. The columns are supported on spread footings bearing on the fill material that was placed above the timber decking. A dive inspection of the platform was performed in 2022 and concluded that the timber decking and piles had notable deterioration. It was also noted the relieving platform, and site in general, required rehabilitation to support further operation of the plant. Rehabilitation activities included replacement of the platform decking and construction of a new structure. The facility needed to be kept operational during construction to support plant production, therefore bypass systems and temporary underpinning was required to keep pipes and instrumentation in operation. Given an allowable deformation of 6 mm (1/4 inch) for overhead utilities and site constraints such as an reduced capacity of the existing timber platform, soft marine soils, and restricted working room, an unconventional underpinning method was required. As opposed to supporting the structures from the bottom as seen in conventional techniques, the structures were picked up from the top using a series of steel members and jacks, and suspended in air during construction. This paper will focus on the design and successful implementation of the innovative techniques. Implementation of these techniques provides more opportunities to perform underpinning at locations where typical underpinning is impractical.

Keywords: underpinning, deep foundations, marine, innovative

INTRODUCTION

A rehabilitation project for a chemical company's dock facility was initiated based on recommendations from dive inspection reports in 2022 detailing the deteriorating condition of the existing timber relieving platform. Historic records of original construction do not exist, but it is speculated that the dock was constructed in the early 1900's with notable upgrades in the 1970's and 1990's.

After the dive inspection, an evaluation was performed by the owner to understand the impacts of performing rehabilitation to the existing facility or building a new facility that would lead to operational downtime; the chemical company chose to move forward with rehabilitation of the existing facility.

 © Deep Foundations Institute 2025

The function of the dock is for loading chemical materials and products made at the chemical facility for transportation on the Delaware River. A pipe system from the dock to the chemical company's facility has two hook-up connections at the dock, for each chemical material, cumene and phenol. These are referred to as the Cumene and Phenol Manifolds throughout this paper. Rehabilitation activities were required to be performed while one of the hook-up connections was still active to allow for continuation of plant usage. This requirement meant logistically that all structures related to the transportation of the chemical elements would need to be minimally impacted during construction. The owner restricted deformation of structures and utilities to a maximum of ¼ inches (6.35 mm) during construction. Additionally, the site itself was constraining, with tight spaces between structures and limited access. Due to such an old site with a storied history of upgrades there was a lot of miscellaneous, yet functional and active, equipment and instrumentation connected to the structures that was grandfathered in and needed to be worked around.

Innovative underpinning techniques were required to allow for rehabilitation activities at the dock while leaving the structures and pertinent mechanical features in-place. Construction phasing and coordination between the contractor and underpinning designer were critical to providing support to the structures during construction in tight confinements. Design changes were frequent during construction to support structures that either differed from available existing condition drawings or were unknown prior to excavation.

PROJECT OVERVIEW

Site Layout

The dock is approximately 500 feet (152 m) long and 60 feet (18.3 m) wide, with a laydown yard adjacent to the site. The site extents are shown in Fig. 1 below with the overhead piping illustrated in isometric view. The piping is approximately 17 feet (5.2 m) above existing grade and spans the length of the site, then turns inland to the chemical facility. The boundary conditions of the site relevant to this paper are a continuous concrete seawall along the waters edge, an existing timber sheet pile wall about 23 feet (7 m) inland from the seawall, and a timber-relieving platform about 8 feet (2.4 m) below grade that is supported on a field of timber piles. The tidal fluctuation for any given day was about 6.5 feet (2 m).



Fig. 1. General Site Layout (isometric view from Google Earth)

Notable existing structures on the site are shown in Fig. 2 and include the cumene manifold, phenol manifold, dock house, scrubber tank, and pipe supports (seen in yellow). These structures are founded on old backfill atop the timber relieving platform. The backfill was generally poorly graded silty sand with gravel with large river rock that was likely old dredge material.



Fig. 2. Existing Structures

Pipe Supports: 14 pipe supports (PS) that hold up overhead utility pipes transporting chemicals. The pipe supports consist of 8" diameter steel columns coated in fireproofing and supported on concrete spread footings, with bottom of footing at 2.25 feet (0.7 m) above the top of the existing timber deck. The existing footings ranged in shape (rectangle and circle) and sizes from 4 feet (1.2 m) by 5 feet (1.5 m) wide to 4 feet (1.2 m) x 6 feet (1.8 m) and thickness of 3 to 4 feet (0.9 to 1.2 m).

Dock House: Concrete hollow block (CHB) building supported on reinforced concrete strip footings with instrumentation and boiler equipment inside. The strip footings are 2 feet (0.6 m) wide and 1 feet (0.3 m) thick with bottom of footing located 3 feet (1 m) below grade.

Scrubber Tank: The tank bears on a pile-supported spread footing and is bounded by a slab-on-grade and concrete containment wall with a strip footing. On the east (water) side the strip footings are 1.5 feet (0.45 m) wide and 9 inches (23 cm) thick with bottom of footing located about 2.5 feet (0.8m) below grade. The wall was 6 inches (15.2 cm) thick with #4 bars at 12 inch (30.5 cm) spacing each way.

Phenol Manifold: The phenol manifold is adjacent to the existing dock house and located up against the existing concrete seawall. The phenol manifold consists of a 64 foot (19.5 m) by 13 foot (4 m) containment area with the following structures: three pipe supports of varying foundation sizes; concrete

 © Deep Foundations Institute 2025

sump pit; 23 foot (7 m) tall steel tower with spread footings; two HSS columns with spread footings for loading trucks from the tower; sloped concrete slab with welded wire mesh (WWM) reinforcement; and miscellaneous equipment on top of the slab to remain. The slab was later found to be two separate slabs stacked on top of each other.

*Cumene Manifold**:***
The cumene manifold is on the south end of the site and located up against the existing concrete seawall. The cumene manifold consists of a 44 feet (13.4 m) by 15 feet (4.6 m) containment area with the following structures: two pipe supports of varying foundation sizes; concrete sump pit; sloped concrete slab with welded wire mesh (WWM) reinforcement; and miscellaneous equipment on top of the slab to remain.

Dive Inspection

Divers were used during the triennial dock inspection to evaluate the condition of the existing timber piles and timber low deck system that supports the aforementioned structures. During the inspection, the timber piles supporting the timber low deck were observed to have corrosion and deterioration in the hardware at timber pile and timber pile clamp connections, as well as general separation between the pile clamp bearing locations on the timber pile shoulders. Localized sections of the timber low deck system were observed to be yielding 1 to 2 inches during the dive inspection. The observed conditions in the dive inspections led to the allowable loading over top the timber relieving platform during construction to be 150 psf by the owners Engineer.

Part of the contractor's scope of work in the dock rehabilitation project was to perform a secondary inspection and advise which locations require hardware extraction and replacement per the Engineers inspection criteria. The contractor was to also identify the areas separation at the timber pile clamp and timber shoulder and install timber wedges at the identified locations so the clamps could achieve full bearing on the timber piles shoulders. The timber pile rehabilitation work had to be completed prior to the underpinning work of the individual pipe supports and the phenol manifold, adding a complex sequential planning effort to help advance the critical underpinning scope of work.

Permanent Repair Overview

To prolong the life of the facility, the owner's Engineer designed the following structural rehabilitation elements. The temporary underpinning discussed in this paper had to be located and detailed as to avoid the new structures.

- A new NZ26 Steel sheet pile bulkhead, battered HP14x89's for lateral support, and a reinforced cast-in-place concrete pile cap at the convergence point of the two steel members to replace the existing tongue and groove timber sheeting wall;
- Placement of a new 18" reinforced cast-in-place concrete structural slab over top of the existing timber low deck in the tidal zone;
- Demolition of existing 245'-0" Long pile supported timber high deck structure, including decking, bracing, and pile cap removal, as well as extraction of 50+ timber piles from the

 © Deep Foundations Institute 2025

riverbed. Subsequent installation of a new 250'-0" pile supported Steel High Deck Structure, including providing and installing HP14x89's driven piles, HP14x89 prefabricated truss's, super arch fenders, and new galvanized deck grating; and

- Repairs to cracks in the existing concrete seawall, including chipping out latent concrete, installing new epoxy coated wire mesh, and pouring new self-consolidating concrete at crack locations.

UNDERPINNING DESIGN

The manifolds, pipe supports, dock house, and scrubber tank required temporary underpinning during excavation of the soil atop of the relieving platform to install the new concrete decking. The project team evaluated various underpinning methods for this project ranging from simple methods like traditional pit underpinning to more expensive methods like grouting. The project site had numerous variables that had to be worked around. Table 1 below summarizes the comparison between the alternatives, showing that suspension underpinning was the advantageous method.

Deformation Criteria: Maximum ¼" movement of existing structures and utilities.

Equipment Restriction: Allowable 150 psf surcharge on the existing timber deck. It was decided by the design team that we did not want to load the deck at all based on yielding and deterioration of the timber.

Soft Soils: The geotechnical conditions of the site are typical to riverfront relieving platform projects. The alluvium below the platform is Sandy Silt to Silt (ML) with trace clay, gravel, and organics up to depths of above 55 feet (16.8 m) before transitioning to a weathered schist.

Interference: The system would have to adapt around existing timber piles, new driven piles, new steel sheeting, existing timber sheeting, and existing mechanical equipment and instrumentation surrounding the existing structures.

Table 1. Summary of Underpinning Options

Type	Traditional Pit	Micropiles	Jet Grout	Suspension
Deformation Criteria		X	X	X
Equipment Restriction	X			X
Soft Soils	X			X
Interference	X		X	X

The typical suspension underpinning system used in the project is shown in Figs. 3 and 4. The system includes picking up the structure (pipe support foundation shown in the figures) from the top using post-installed concrete anchors, two steel beams, and supports on either end. Figure 3 illustrates a tension connection to the concrete while Fig. 4 is a shear connection. On the water side the forces transfer through the steel leveling beam to the existing concrete seawall. The existing concrete from the inspection was deemed inconsequential to distributing vertical forces through the wall. The width of the seawall base

 © Deep Foundations Institute 2025

helped to distribute low pressures to the timber deck. The inland side of the beams were supported on driven HP14 piles. The piles were driven a few feet (1 m) outside of the extent of the existing timber sheeting. By spanning between the seawall to just outside of the timber sheeting the structure could be lifted without loading the timber deck. The beams were braced laterally to account for wind loading on the overhead utilities/structures. The vertical loading of the pipe supports ranged from 30 to 66 kips (133.4 to 293.6 kN) with a wind included moment of around 40 kip-ft. To avoid an immediate settlement of the structure once the soil below the foundation was removed the beams were hydraulically jacked and shimmed at each end prior to excavation. A 10-ton jack and a temporary jacking beam are shown in Fig. 3.



Fig. 3. Typical Suspension Underpinning

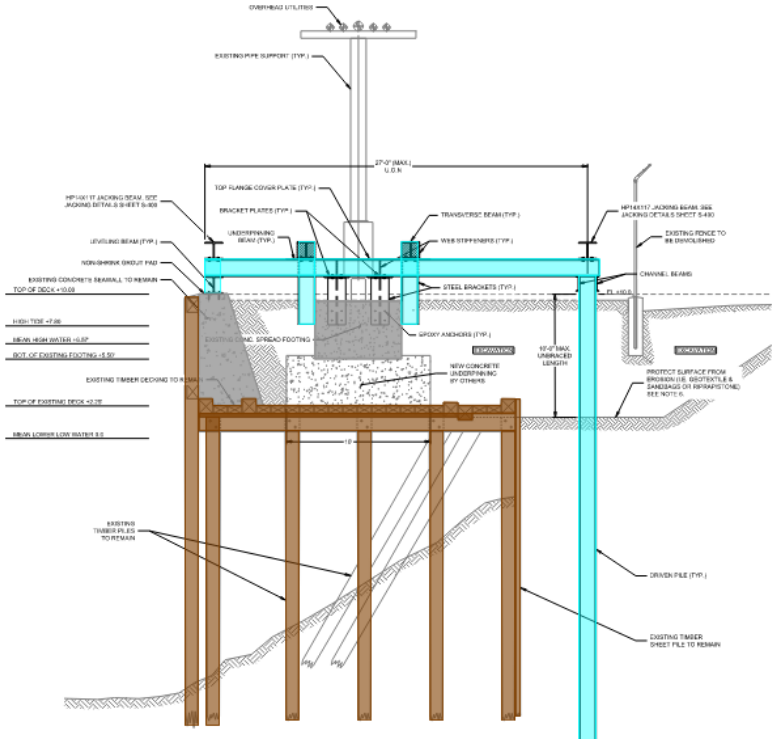


Fig. 4. Typical Suspension Underpinning Section View

 © Deep Foundations Institute 2025

The above concept where the seawall supported one end and driven piles the other was generally used for the remaining structures including the scrubber tank and manifolds. The concept adapted to the structure-specific features such as strip footings, sump pits, and steel towers. Figure 5 below shows the underpinning for the scrubber tank. Due to the proximity of two pipe supports to the scrubber tank the system was altered to underpin all three structures at once. Tension connections were used for the rectangular pipe support footing, shear connections for the circular footing, and knee braces for the concrete strip footing of the scrubber tank containment wall. Heavy 35-foot (10.7 m) long W24x192 beams ran parallel to the seawall to limit deflections of the beam supporting the footings. Due to the presence of an existing concrete bollard, the southernmost reaction beam was connected to the face of the bollard with shear anchors (Fig. 5, right) as an modification to the originally schemed bearing on the seawall.



Fig. 5. Scrubber Tank Underpinning (Left) prior to excavation (Right) after excavation

The support of the dock house and phenol manifold were combined into a single system since they were only about 10 feet (3 m) away from each other. The dock house was first laterally supported with a traditional HP14x117 soldier pile and timber lagging wall. The piles were generally placed on 8 foot (2.4 m) centers with the exception of a 15 foot (4.6 m) span in the center of the alignment where the overhead pipe bridge runs from the manifold to the dock house. Already subject to lateral load from dock house footing surcharge and earth pressures, the soldier pile wall then served as the inland support foundation for the phenol manifold underpinning, replacing the driven piles shown in Fig. 4. The dock house piles were left sticking up at higher elevations to connect to the phenol manifold underpinning beams at their respective elevations. Due to site restrictions with working around existing instrumentation or miscellaneous mechanical equipment underpinning beams ranged from bearing on top of the seawall to a height of 10 feet (3 m) above top of seawall.

 © Deep Foundations Institute 2025

Since the existing manifold slab was only 8 inches (20.3 cm) thick with temperature WWM reinforcement the underpinning system was designed to pick everything up off the slab first, then pick up the slab where the only loading is essentially its dead weight. Figure 6 below shows a schematic of the different underpinning beam systems used and the relationship between the phenol manifold underpinning system and the dock house soldier pile wall. Pipe supports PS-7, PS-8, and the sump pit were supported using the typical concept shown in Fig. 3. The steel tower, pipe support PS-9, and the concrete slab itself were supported in different ways.

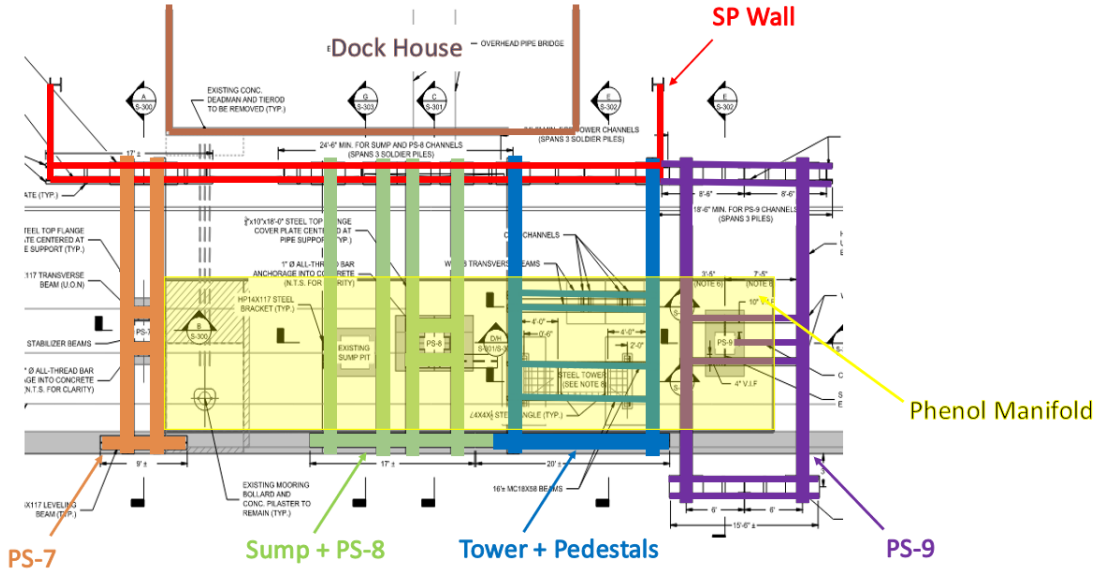


Fig. 6. Phenol Manifold Underpinning Beam Schematic

Pipe Support PS-9: Due to existing instrumentation along the height of the vertical column and around the footing, the connection had to be made at 8 feet (2.4 m) above grade. The pipe support was picked up by locally removing the fireproofing and extending a steel plate through the existing steel column. Due to existing equipment on the seawall piles were driven in the river to act as the waterside support. The driven piles were laterally braced and structurally connected to the seawall to provide rigidity during a wind event.

Steel Tower: For similar reasons as listed above for PS-9 the connection to the tower was restricted to 10 feet (3 m) above grade. The tower is made up of small steel members albeit channels or angles. The tower was picked up by connecting steel beams to the existing steel columns of the tower. The existing foundation connection was analyzed for tension.

Concrete Slab: The concrete slab was supported using a combination of post-installed epoxy anchors and pre-stressed steel chains with bearing plates and tapcon anchors. The epoxy anchors were used where overhead beams were able to be installed from the top of the seawall. This kept all-thread rods at shorter lengths. The pre-stressed chains were used around the steel tower and PS-9 where the overhead beams were 8 to 10 feet (2.4 to 3 m) above ground surface which allowed for faster construction and allowed for an even load distribution over the surface area of the slab. A concern of the design team's during the

layout of the chains was potential rotation (swing-like movement) of the slab if picked up unevenly. The slab was know to be sloping due to its function as a containment basin for chemicals.

Figure 7 below shows a construction photo of the phenol manifold underpinning beams from the point of view of a barge (left) and from the north end of the dock (right). The steel tower beams can be seen up high while adjacent pipe support beams are lower based on interference with existing structures and utilities. Pre-stressed chains (pre-stressed to 5 kips with a ratchet) are seen extending down from the steel tower underpinning beams to the top of the concrete slab.



Fig. 7. Phenol Manifold Underpinning

For brevity in this paper the cumene manifold design and construction is not discussed. The cumene manifold is similar to the phenol manifold with support of a lightly reinforced concrete slab, a pipe support, and concrete sump pit.

CONSTRUCTION

The construction and underpinning design process was intimately intertwined for this project as new foundation shapes were unearthed and as the owner made decisions on what structures, equipment, and instrumentation was to remain or allowed to be removed and replaced. It was typical for an underpinning system to be redesigned as excavation took place due to a change in conditions from the historic drawings.

A 275 Ton conventional crawler crane was used to support landside construction activities including pile driving, structural steel placement, and demolition. A 240 Ton, barge mounted, crawler crane was used to support waterside underpinning execution. Various pieces of earth moving equipment were utilized for

excavation around and underneath the existing pipe supports and the underpinning structural steel systems, including conventional excavators, mini-excavators, skid steer loaders, and hydrovac trucks. The conventional and mini excavators were used for initial excavation to expose the top of the pipe supports, and the hydrovac truck and skid steer loaders were used to excavate the areas adjacent to and underneath the pipe support where load restrictions applied. All piles associated with typical pipe support underpinning, phenol manifold underpinning, and the dock house soldier pile and lagging wall were installed with an Ice Model 44B vibratory diesel hammer.

All the new underpinning foundations (see Fig. 4) were poured within the tidal influence of the Delaware River, restricting the crew to four hours per shift when the tide dropped below the timber relieving platform water. The excavation also faced the same constraints.

The facility in which the underpinning scope of work took place was active during construction and was a relatively small and confined project site in general. Construction activities had to be carefully planned around typical plant operations, vessel traffic, and hot work restrictions.

CONCLUSIONS

To rehabilitate an old timber relieving platform supporting a chemical facility underpinning of existing structures and equipment was required. Variables in the selection of the underpinning system included weight restrictions on a deteriorated timber decking, tidal fluctuations, soft marine soils, conflict with existing and new structures and/or equipment, and allowable deformation criteria of structures to be supported. After careful consideration of different underpinning techniques including traditional pit underpinning, micropiles, and grouting, the team selected to use suspension underpinning techniques.

The suspension underpinning system allowed for structures and equipment to be picked up from the top using an array of steel beams, piles, and anchors. The beams connected to the structure were hydraulically jacked to mobilize the structure and prevent an immediate settlement from occurring during initial excavation of the backfill atop the platform. The suspension underpinning concept was adaptable, being used to support slabs, sump pits, spread footings of varying shapes, strip footings, and miscellaneous mechanical equipment.

ACKNOWLEDGEMENTS

Our team would like to acknowledge the senior leadership in Allen Cadden and Phil Shull who were essential in developing the underpinning concepts on this complicated site, the dock builders out of the local 474 union, and operating engineers local 452 union for helping in the execution of the work.

 © Deep Foundations Institute 2025

THE EVOLUTION OF STEEL PILING PRODUCTS OVER THE LAST 50 YEARS

Pierre N. Werner, ArcelorMittal Sheet Piling, Luxembourg, pn.werner@arcelormittal.com
Dean Abbondanza, JD Fields & Company, Inc., Houston TX, dabbondanza@jdfields.com

ABSTRACT

This paper highlights the significant evolution in steelmaking methods and looks back at how steel sheet piling has changed and improved over the last 50 years. The traditional blast furnace production route – once the only way to make steel – has largely given way to more modern and environmentally friendly methods such as direct reduction of iron and the electric arc furnace, using recycled scrap metal as a raw material. These methods have revolutionized the production of steel construction products, including sheet piles, and have made production more flexible while reducing its carbon footprint.

The last 50 years have also seen some significant changes to sheet pile sizes, dimensions, and interlock geometry, providing the industry access to ever more efficient products with improved reliability and strength. In parallel, the development of new solutions (such as watertightness systems) allowed increased tailoring to specific applications and new use cases. Combined wall systems (based on H-beam or tubular king piles) paved the way for ever deeper excavations, port drafts and the most challenging retaining structures required by today's infrastructure projects. Steel grades also have evolved over this same period with a clear move to higher yield-strength steels needed to meet the increased bending moments associated with deeper retaining structures. The paper discusses the development and adoption over time of new ASTM standards for grades with improved resistance against (atmospheric and marine) corrosion. The world of steel piling products has seen significant disruption and evolution over the last 50 years, which has given rise to safer, more efficient, and stronger retaining solutions to meet today's high demands on retaining structures.

Keywords: sheet piling, steel, steel grades, combined walls, improvements, efficiency, CO_2

EVOLUTION IN STEELMAKING

The blast furnace ('BF') was once the only way to make hot metal as input for steelmaking. Its basic function is to reduce mined iron ore to iron by mixing it with coke (produced from coal) and providing the right temperature and environment for the carbon atoms in the coke to remove the oxygen atoms from the iron ore, leaving pure iron. The resulting liquid iron (also called 'hot metal') is then treated in a Basic Oxygen Furnace (BOF) to produce steel. Fundamentally, the BF-BOF process necessarily emits significant quantities of carbon dioxide (typically more than 2 tons of CO_2 per ton of steel produced), and consequently the steel industry is among the top worldwide emitters of man-made carbon dioxide.

As early as the 1950s, alternative direct reduction processes were being developed, and by the 1970s and 1980s, the direct reduction of iron (DRI) with natural gas started to become economically viable. One of the benefits of this process are the significantly lower carbon dioxide emissions, which are about halved compared to the blast furnace production route.

In parallel, the Electric Arc Furnace (EAF) was developed (pioneered by Nucor) in the United States in the 1970s. These new types of furnaces were able to melt the iron pellets coming out of the DRI installations, but interestingly they could also be used to melt ferrous scrap, completely bypassing primary steel production by taking advantage of the inherent circularity and recyclability of steel. End-of-life steel (meaning recyclable ferrous scrap contained within obsolete items or structures), which was now starting to become available in sufficient quantities to generate a market dynamic of its own, has the advantage of being easy to collect and separate from other waste materials thanks to its magnetic characteristics.

 © Deep Foundations Institute 2025

The new EAF route provides a further step-change as far as carbon emissions of steelmaking are concerned, especially if the electricity used to power the installation was not generated from fossil fuels (which would simply shift the emissions from direct to indirect). Indeed, finished steel produced in an EAF can reduce CO_2 emissions of the order 0.5 tons CO_2 / ton of steel. This emission rate corresponds to half of the emissions associated with natural gas based DRI and less than a quarter of traditional BF-BOF-produced steel.

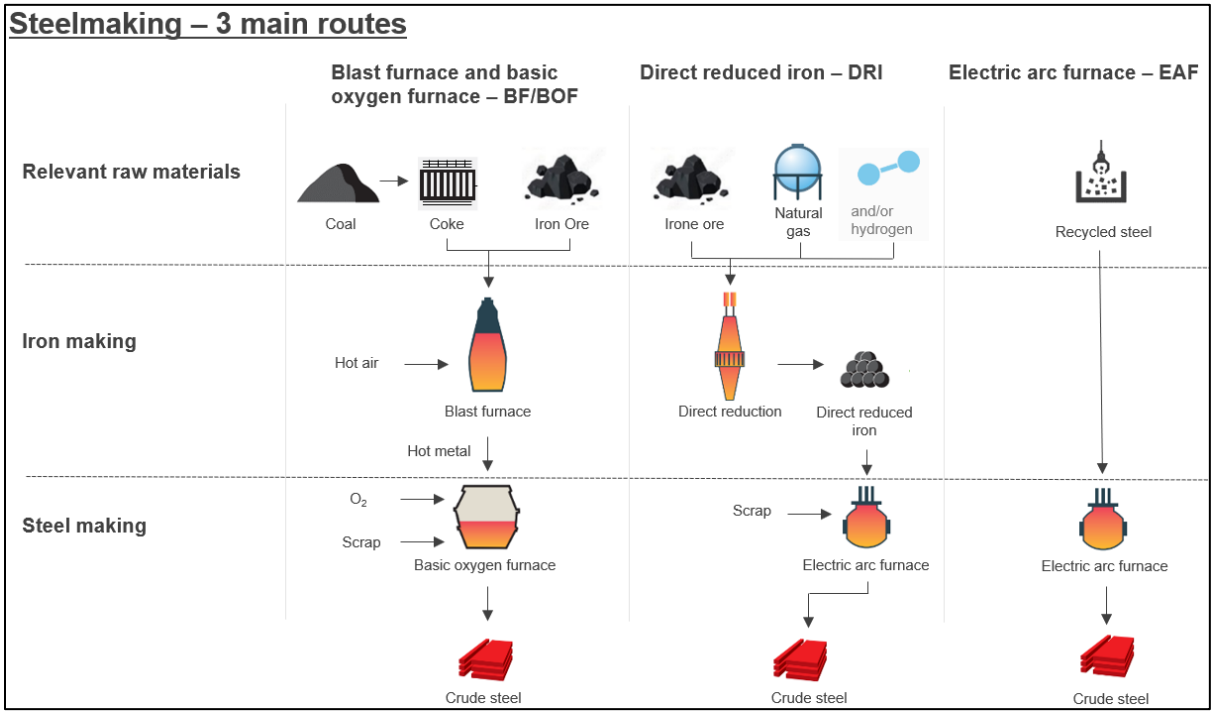


Fig. 1. the 3 main steelmaking routes (source: ArcelorMittal Sheet Piling)

Not every steel product can be produced by melting down scrap in an EAF. For some applications such as sheets for the automotive industry and appliances, a high steel product purity is required, which excludes EAF-made steel due to the presence of residual elements in the scrap raw materials. This, however, is not a problem for the majority of construction products including sheet piles. Consequently, in many parts of the world the EAF has become the production method of choice for steel sheet piling.

Over the last 50 years, technological advances in steelmaking have allowed steel sheet pile producers to significantly lower their carbon footprint,. Other than improved climate-change credentials, the EAF route has also allowed producers to reduce dust emissions, water use, as well as improve other environmental factors (see for example "NUCOR – The Circularity in Steel Series, Part 3: Benefits of Electric Arc Furnace (EAF) Steelmaking").

EVOLUTION IN SHEET PILING SIZES AND GEOMETRY

Moving on from the basic technology of steelmaking, there have also been some major changes in the piling products themselves. The last 50 years have seen significant evolution of sheet pile sizes, dimensions, and interlock geometry, providing the foundation construction industry access to ever more efficient products with improved reliability and strength. The first interlocking steel sheet piles were produced in the United States by the Lackawanna Steel Company around 1910. This was closely followed in Europe by the

 © Deep Foundations Institute 2025

introduction of the Ransome Z-type sheet pile in 1911 and the Larssen U-type sheet pile in 1914. By the 1930s, these initial narrow and very shallow sections had been replaced by the wider and deeper PZ sections in the United States (with a single pile projected width of 18") and BZ sections in Europe, with a similar width of 500mm, in the search for greater efficiency, higher stiffness and faster installation. Figure 2 presents examples from vendor catalogs of sheet pile sizes and styles available over 50 years ago, and Table 1 gives an overview of the main types of sheet pile designations cited in this paper, along with their respective manufacturers.

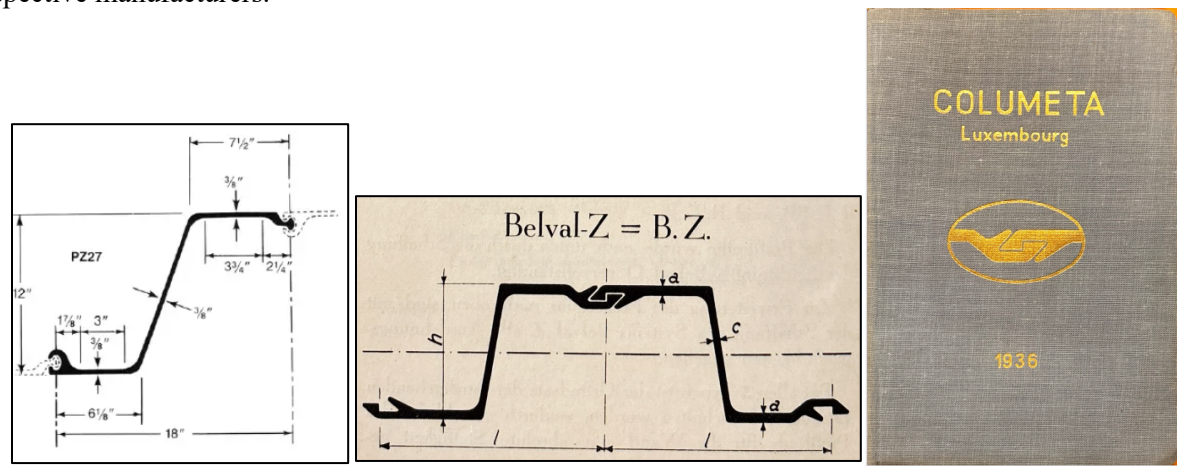


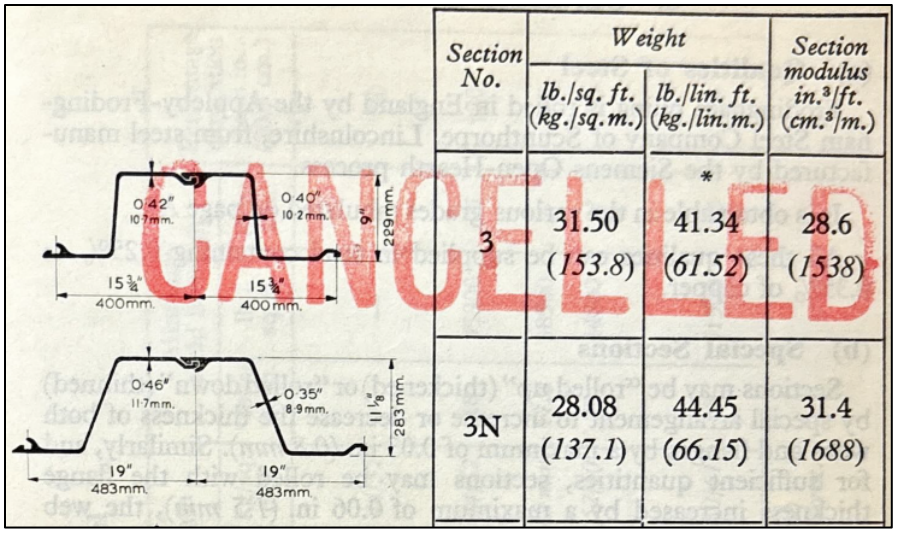
Fig. 2. PZ27 (left, old Bethlehem Steel catalogue, unknown year) and BZ sheet pile (middle & right, COLUMETA Luxembourg catalogue, 1936)

Table 1: overview (non-exhaustive) of the main historical and current types of sheet pile designations mentioned in this paper (in alphabetical order)

Sheet pile designation	Manufacturer
AZ	ArcelorMittal (Luxembourg)
BZ (historical)	ARBED (Luxembourg)
HZ / HZM	ArcelorMittal (Luxembourg)
NZ	Nucor (USA)
PZ	Nucor (USA)
PZC	Gerdau (USA)

Another good example of this drive for efficiency can be seen in the extract from the British Steel Piling Handbook (1969) shown in Fig. 3. In this example, sheet pile section no. 3, originally produced by the Appleby Frodingham Steel Co. Ltd., which was incorporated into British Steel in 1967 (Pocock et al (1990)) was cancelled from the production program and replaced by the wider 3N model, resulting in a weight saving of 11% per unit area of wall, while simultaneously increasing section modulus by 10%.

 © Deep Foundations Institute 2025



Section No.	Weight lb./sq. ft. (kg./sq.m.)	Weight lb./lin. ft. (kg./lin.m.)	Section modulus in.³/ft. (cm.³/m.)
3	31.50 (153.8)	41.34* (61.52)	28.6 (1538)
3N	28.08 (137.1)	44.45 (66.15)	31.4 (1688)

CANCELLED

Fig. 3. Frodingham sheet pile sizes 3 and 3N as published in the British Steel Piling Handbook (1969)

More than 20 years later the next significant developments took place, again on both sides of the Atlantic. New generations of sheet piles (AZ followed by PZC sections) were put on the market with nominal widths of the order of 25 inches (630mm). Further notable advances in sheet pile widths occurred in 2004 with the AZ-700, followed by the NZ in 2014 and the AZ-800 in 2015, each time increasing the sheet pile width and adapting the overall geometry and distribution of material to make the piles more efficient in terms of weight of steel required per surface area of retaining wall, for a given section modulus (See Fig. 4). This constant effort to produce wider, deeper, and stiffer sheet piles was driven (a) by the needs of sheet piling application in terms of height of earth retention, and (b) by the desire to offer more efficient sheet piles to the market, therefore becoming increasingly competitive compared to alternative materials such as concrete.

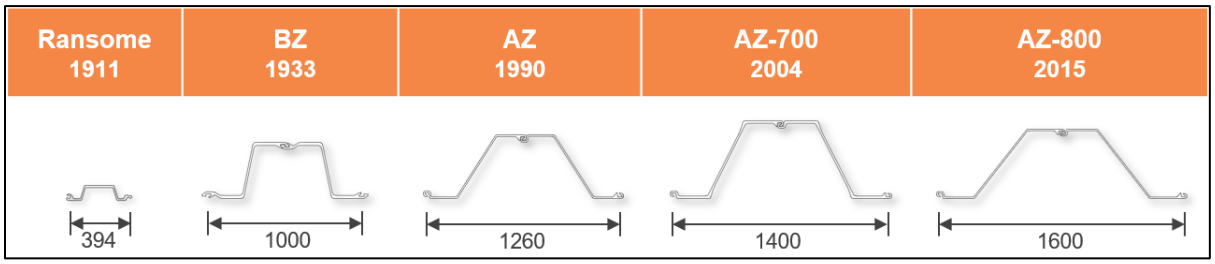


Fig. 4. Evolution of Z-type sheet piling width in mm (source: ArcelorMittal Sheet Piling)

As applications continued to evolve (e.g., towards deeper excavations or quay walls with deeper drafts), increasingly high modulus solutions were required. British Steel was among the first manufacturers to sell a 'combined wall' system, which required welding a Frodingham Z-type section to the outside flange of a hot-rolled beam, offering a section modulus range not previously available on the market (see Fig. 5).

 © Deep Foundations Institute 2025

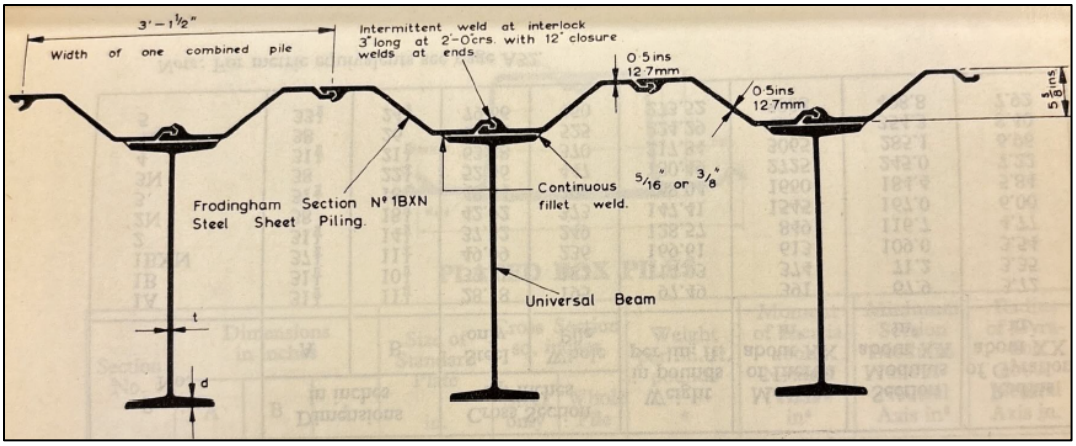


Fig. 5. British Steel high-modulus wall system (British Steel Piling Handbook 1969)

The first HZ-ZH combined wall system was introduced in the 1970s by ARBED (Luxembourg), with the particularity that it did not reply on any structural welding, thanks to rolled-in notches on the tips of the flanges of the king piles, which were attached to the intermediary Z-type sheet piles by hot-rolled connectors (see Fig. 6).

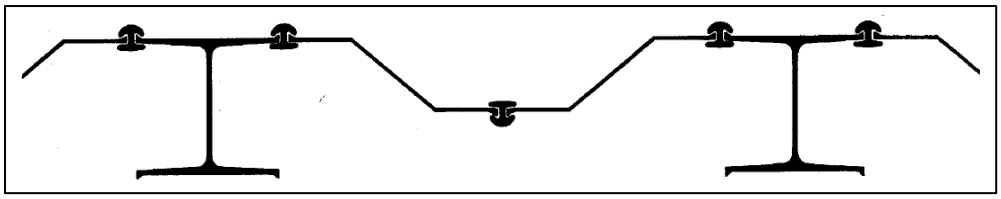


Fig. 6. HZ-ZH combined wall system (source: TradeARBED catalogue 1986)

This solution was upgraded to the HZ-AZ system in the 1990s, which added the possibility to combine the H-beam king pile sections with the newly created AZ range (source: ArcelorMittal HZM catalogue), and then again in 2008 to the HZM-AZ system offering deeper and heavier beams (see Fig. 7). By the 2000s, the introduction of spiral-welding had also allowed the straightforward fabrication of large diameter steel pipe at competitive cost and provided an additional option for high-modulus combined walls (Fig. 8).

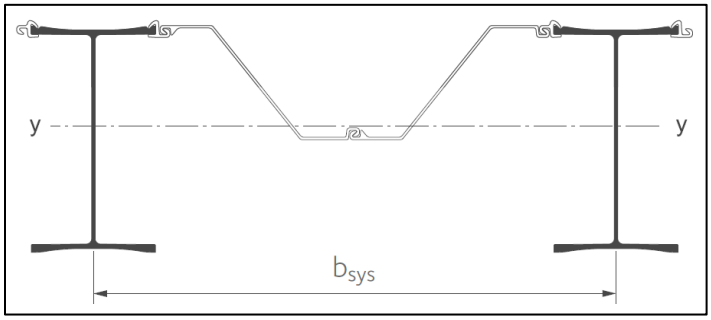


Fig. 7. HZM-AZ combined wall system (source: ArcelorMittal Sheet Piling general catalogue 2024)

 © Deep Foundations Institute 2025

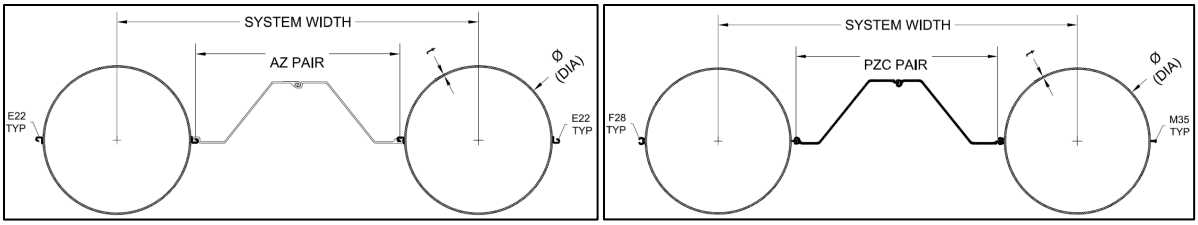


Fig. 8. Two options of tube combined wall systems (source: JD Fields & Company catalogue 2024)

As a final thought in this chapter on sheet pile geometry, let us consider the specific shapes of the interlocks. With the exception of the loosest interlock types, designed primarily for easy driving and multiple reuse, most types of sheet piles benefit from relatively good watertightness straight out of production, thanks to the careful and precise design of the interlocks. The natural plugging effect that can occur in fine soils will typically further improve water tightness over time. However, more advanced use cases, such as containment of polluted soils, or permanent basements and underground car parks, require more stringent permeability properties. To this end, over the years, various producers have introduced sealant systems capable of withstanding varying water pressure gradients and guaranteeing high levels of impermeability. This has given rise to new application possibilities for sheet piling products.

EVOLUTION IN STEEL GRADES

The last 50 years have seen a clear move to higher yield-strength steels needed to meet the increased bending moments associated with deeper retaining structures. The specification of higher strength and high-quality steels observed in different regions of the world, not only allows for designs to be weight-optimized, potentially offering substantial savings to end users, but the additional strength can also help improve resistance of the material during installations in hard driving conditions.

The steel pile fabrication industry has also seen the development and adoption of new ASTM standards for grades with improved resistance against (atmospheric and marine) corrosion. The following discussions present standards advancements in different world regions.

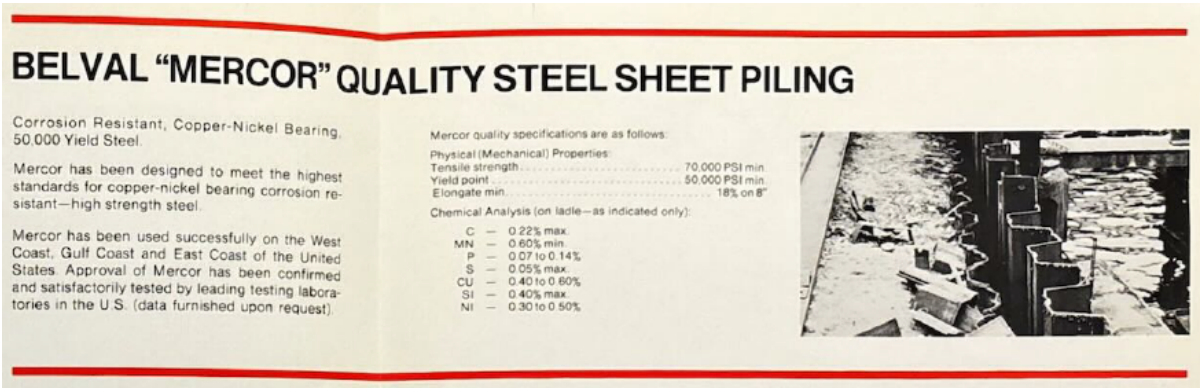
United States. 50 years ago, steel sheet piles in the fell under the ASTM product standard A36, “Standard Specification for Carbon Structural Steel”, which was first published in 1960 and included a single steel grade for all structural shapes with a minimum yield point of 36 ksi (250 MPa) (source: Handbook of Steel Construction, 8th Edition, CISC, 2004). In 1966, as metallurgical advances allowed new alloying elements to be used to give more strength to steel, ASTM first published the now ubiquitous standard A572, “Standard Specification for High-Strength Low-Alloy Columbium-Vanadium Structural Steel”, initially specifying only grade 42 and 50 options (requiring a minimum yield point of 42 and 50 ksi, respectively). Eventually grades 55, 60 and 65 were added to the standard, the latter being officially adopted for sheet piling as recently as 2018. On a practical level, the sheet piling market in the United States was primarily using grade 50 steel until the early 2010s, when the standard gradually shifted towards the higher strength grade 60.

Steel sheet pile users often need to consider corrosion in addition to strength. Various solutions exist today to optimize durability. Initially covered through proprietary developments (e.g. the ‘Mercor’ grade, see Fig. 9), the pursuit of steel chemistries with enhanced corrosion resistance eventually reached the ASTM, which introduced standards with specifications for improved corrosion resistance under atmospheric exposure (A588 introduced in 1968, commonly referred to as ‘weathering steel’) and in marine environments (A690 introduced in 1988). In the 2010s, one sheet pile manufacturer introduced a proprietary steel grade with enhanced corrosion resistance in the low water and permanent immersion zones. In parallel to specific steel grades to reduce

corrosion rates, there has also been progress in protection systems, from specialized coatings to cathodic protection (including the impressed current and sacrificial anode systems). Lifetimes of steel sheet pile structures of up to 100 years are no longer in the realm of science fiction.

Canada. The Canadian Standards Association (CSA) followed a similar approach, with dated CSA standards from the 1950s such as G40.4 (Medium Structural Steel) and G40.6 (Structural Silicon Steel) prescribing steel with yield points of 33 and 44 ksi, respectively. These standards eventually gave way to the current general requirements for rolled or welded elements, CSA G40.21 (Structural Quality Steel), which includes grades up to a minimum yield point of 480 MPa (70 ksi) and optional impact testing at different temperatures.

Europe. The European standard for sheet piling is EN 10248, "Hot rolled sheet piling of non-alloy steels", exists in two parts – Part 1: Technical delivery conditions, and Part 2: Tolerances on dimensions and shape. This standard was first published in 1995, replacing and harmonizing a series of individual national standards in Europe, and was recently updated in 2023-24 as part of a major overhaul and modernization. While the 1995 version (long used as the main reference in many parts of the world) only included steel grades up to a minimum yield point of 430 MPa (approximately 62 ksi), the most recent version recognizes advances in steelmaking by adding new grades with a minimum yield point of 460 and 500 MPa (66 and 72 ksi, respectively). In addition, the chemical composition table includes new requirements to ensure better weldability (maximum carbon and carbon equivalent content), as well as more stringent conditions on residual elements such as sulfur and phosphorus, and there is a new requirement on toughness, with compulsory Charpy V-notch impact testing.


BELVAL "MERCOR" QUALITY STEEL SHEET PILING

Corrosion Resistant, Copper-Nickel Bearing, 50,000 Yield Steel.

Mercor has been designed to meet the highest standards for copper-nickel bearing corrosion resistant—high strength steel.

Mercor has been used successfully on the West Coast, Gulf Coast and East Coast of the United States. Approval of Mercor has been confirmed and satisfactorily tested by leading testing laboratories in the U.S. (data furnished upon request).

Mercor quality specifications are as follows:

Physical (Mechanical) Properties:

Tensile strength	70,000 PSI min.
Yield point	50,000 PSI min.
Elongate min.	18% on 8"

Chemical Analysis (on ladle—as indicated only):

C	0.22% max.
MN	0.60% min.
P	0.07 to 0.14%
S	0.05% max.
CU	0.40 to 0.60%
SI	0.40% max.
NI	0.30 to 0.50%

Fig. 9. Published proprietary specification for "MERCOR" grade sheet piles (source: Skyline Industries brochure, est. 1970s)

OTHER IMPROVEMENTS

Considering the evolution of sheet piling products mentioned herein, installation equipment has also needed to adapt along the way to wider, longer, and heavier sheet piles and combined wall systems. Around the world, diesel impact hammers are increasingly giving way to double-acting hydraulic impact hammers, leader rigs are being used to improve precision of installation, double clamps are now available for vibratory hammers to handle wider sheet piles, and vibration-less press-in technologies have been developed to minimize disruption in proximity to existing infrastructure and critical urban locations. These ae just a few ways in which equipment manufacturers and piling contractors have contributed to the continuous improvement of the industry.

 © Deep Foundations Institute 2025

Piling equipment is not the primary focus of this paper, but some interesting resources on the evolution of installation machinery can be found for example in the publication 'Basic Principles of Hammers for Sheet Pile Installation' by the PDCA (Pile Driving Contractors Association, 2021), and in a number of resources available on the website of the UK-based 'Steel Piling Group', which has a similar mission to that of the PDCA.

SUMMARY AND CONCLUSIONS

From the narrow and shallow early models produced in the most basic construction grades, the market over the past 50 years has evolved to larger steel sheet pile members with significantly greater capacity. Suppliers are now able to offer state-of-the-art piling solutions, including advanced combined wall systems that can withstand the soil pressures resulting from the construction of the deepest bulkheads, designed for post-Panamax vessels. In parallel, installation equipment manufacturers have adapted to these changes to facilitate the installation process.

Sheet piles have become much more sustainable, not only due to considerably lower embedded carbon dioxide than 50 years ago, but also because higher strength steels and optimized geometries have increasingly allowed the use of lighter and more efficient piles in designs, reducing the resources required to achieve the same technical performance.

Advanced sealant systems for sheet pile interlocks can now provide reliable environmental containment solutions, and a multitude of corrosion resistance options have allowed engineers to design marine structures with 100-year lifetimes.

The DFI has come a long way in 50 years – the authors hope that readers will agree that the same can be said for the humble sheet pile.

ACKNOWLEDGEMENTS

The authors wish to thank Boris Even, General Manager, ABM Coordination & Product Development, ArcelorMittal Sheet Piling, for his input and review.

Google AI and Microsoft Copilot have been used to identify and research further sources of information and background reading in the preparation of this paper. Specific sources identified and used in this way are listed in the references below.

REFERENCES

ASTM standards : www.astm.org

British Steel Piling Handbook (1969)

Canadian standards : www.csagroup.org

COLUMETA Luxembourg catalogue, 1936

European standards : www.cencenelec.eu

Handbook of Steel Construction, 8th Edition, CISC, 2004

NUCOR – The Circularity in Steel Series, Part 3: Benefits of Electric Arc Furnace (EAF) Steelmaking

 © Deep Foundations Institute 2025

PDCA : Basic Principles of Hammers for Sheet Pile Installation (2021)

PileBuck Magazine : Sheet Pile Design. Chapter 1 – Overview of Sheet Piling (https://pilebuck.com/sheet-pile-design-by-pile-buck/chapter-1-overview-sheet-piling/)

Pocock, D. C. D. (1990), Ellis, S.; Crowther, D. R. (eds.), "The Development of Scunthorpe"

Steel Piling Group (UK), Downloads & Resources (https://www.steelpilinggroup.org/downloads/)

TradeARBED HZ-ZH catalogue (1986)

Vulcan Hammer website : Sheet pile designations (https://vulcanhammer.info/2017/06/29/vulcan-onshore-tip-51-sheet-pile-designations/)

 © Deep Foundations Institute 2025

RECOMMENDED SPECIFICATION PRACTICES FOR MASS CONCRETE DRILLED SHAFTS

Andrew Z. Boeckmann, Dan Brown & Associates, St. Louis, MO USA, 573-424-0017, aboeckmann@dba.world
Paul J. Axtell, Dan Brown & Associates, Overland Park, KS, USA, 816-210-1954, paxtell@dba.world
J. Erik Loehr, University of Missouri, Columbia, MO, USA, 573-882-6380, eloehr@missouri.edu

ABSTRACT

The last ten years have seen a rapid increase in the number of public agencies applying mass concrete provisions to drilled shafts, with at least one third of state departments of transportation now considering large-diameter shafts as mass concrete. The provisions that are applied vary widely among agencies and from project to project. The resulting specification landscape is surrounded by many open and consequential questions. This paper draws from recent experience developing thermal control plans for 11 different drilled shaft projects to evaluate the major questions, documenting the range of practices with respect to maximum internal temperature, maximum temperature differential, monitoring requirements, and other important provisions. For each specification topic, the paper also presents recommended practices. The recommended practices are intended to satisfy the legitimate demand for durable drilled shafts while accounting for the unique environment of underground concrete and the practical realities of drilled shaft construction. The paper also addresses the practice of limiting temperature to prevent reduction in compressive strength.

Keywords: drilled shaft, concrete, mass concrete, temperature, durability

INTRODUCTION

It has become cliché to comment on the trend toward using large diameter drilled shafts; nevertheless, the trend often bears mentioning because it continues to produce unique challenges for the foundation industry. The trend has coincided with the evolution of mass concrete specifications among owners using structural concrete for large elements. Many owners have recently started designating drilled shafts as mass concrete. In addition, the American Concrete Institute (ACI) recently updated its mass concrete guide (207.1-21, 2022) to include a new definition of mass concrete that designates virtually all drilled shaft, auger-cast-in-place pile and diaphragm wall elements as mass concrete.[i] The application of mass concrete provisions to deep foundations raises many questions with significant consequences for constructability, risk, and cost.

The questions are reflected in the variation of provisions among the drilled shaft mass concrete specifications that have been applied. This paper uses experience developing thermal control plans for nine drilled shaft projects and performing thermal analysis for two additional projects to identify the major questions pertaining to mass concrete provisions for drilled shafts and characterize the variability of provisions regarding each of the major questions. The eleven projects represent ten unique owners: two federal agencies, two state transportation agencies, five local or regional transportation agencies, and one private developer. The local or regional transportation agencies generally referred to corresponding state agency specifications. Three of the owners referenced American Concrete Institute (ACI) specifications.

For each question, recommendations regarding the most sensible provisions are provided. The recommendations are intended to satisfy the legitimate demand for durable drilled shafts while accounting for the uniqueness of underground concrete and tremie concrete placement. Among the relevant unique aspects of drilled shaft concrete compared with above-ground mass concrete are:

 © Deep Foundations Institute 2025

- Boundary conditions consist of geologic materials (often with a thin steel casing), not air. For drilled shafts supporting bridges over water, shafts typically extend up through a water column, and the water may be flowing, possibly both above and below the mudline.
- The effect of any of these boundary conditions is difficult to predict because of uncertainties in thermal properties. Generally, however, geologic materials are effective insulators that produce lesser temperature differentials than would be observed in similarly sized elements above ground. Flowing water, either surface water or groundwater, is a significant exception.
- Curing techniques (e.g. insulated formwork, burlap, curing compounds etc.) are not applicable to drilled shafts (with exceptions for the portion above the ground surface).
- Concrete placement for large-diameter shafts is challenging and puts significant demand on fresh concrete. For most large diameter shafts, the concrete must flow long distances under pressure, displace support fluid, flow through congested reinforcing cages, produce intimate contact with the sides of the excavation, and maintain the workability necessary to address these challenges over a long-duration placement.
- The demands of concrete placement place significant constraints on the concrete mixture design, reducing flexibility for mass concrete considerations. Techniques to satisfy the demands include characteristics that produce high heats of hydration (e.g., relatively high cement content) and others that increase uncertainties in the heat of hydration (e.g., heavy reliance on admixtures, the tendency for significant bleed).
- Cooling pipe networks are not practical. They interfere with tremie operations, exacerbate challenges with congested reinforcement, and introduce a significant risk for injecting pressurized water into the fresh concrete.
- Drilled shaft concrete cannot be seen after placement, with exceptions for shafts extending above ground without permanent casing.
- Removing and replacing drilled shaft concrete is generally not a practical option. Rejected drilled shafts often lead to expensive, time-consuming, and complicated remediation foundations.

These aspects are considered in the development of recommendations for the six major questions addressed in this paper. For each question, background information is presented before characterizing the state of practice and then providing recommendations.

SHOULD DRILLED SHAFTS BE EXEMPT FROM MASS CONCRETE SPECIFICATIONS?

Background

Whether drilled shafts should be considered mass concrete is the first major question. Opponents often point to the lack of evidence of any drilled shafts having experienced mass concrete damage as justification for excluding shafts. Opponents will also note many of the items in the bullet list from the Introduction as mitigating factors and considerations that make application of mass concrete provisions impractical and risky. Proponents typically note that drilled shafts are unique, but not so unique as to be immune from any threat of thermal damage. Proponents also note that investigations to examine shafts for thermal damage have not been completed, and that some thermal damage could take years to manifest.

State of Practice

The number of owners who opt to designate drilled shafts as mass concrete has increased in recent years. As shown in **Error! Reference source not found.**, a 2018 survey by the National Concrete Consortium (Marsten, 2018) found 12 of 33 (36%) responding transportation agencies have designated drilled shafts as mass concrete. This is most likely an underrepresentation: at least two agencies who indicated in 2018 that they do not consider drilled shafts as mass concrete have since applied mass concrete provisions based on experience documented in this paper.

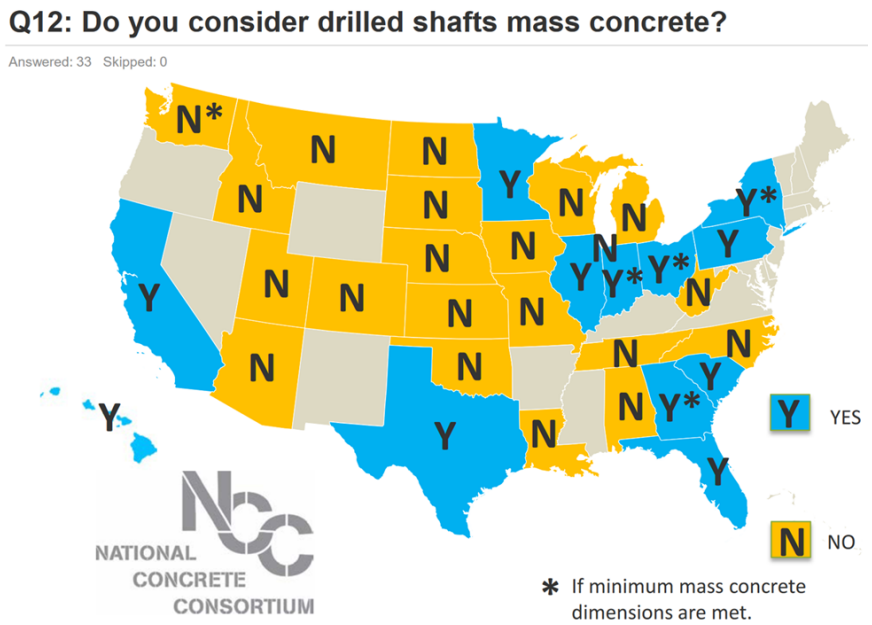


Fig. 1. Results of 2018 survey of state transportation agencies and toll authorities regarding designation of drilled shafts as mass concrete. Adapted from Marsten (2018).

Recommendations

Drilled shafts should not be exempt from mass concrete specifications. There is no reason to believe the most concerning form of thermal damage, Delayed Ettringite Formation (DEF; discussed in the next section), is not applicable to drilled shafts, even if it has never been documented. Although it is inappropriate to completely exclude drilled shafts from mass concrete provisions, many of the provisions commonly applied in mass concrete specifications should not be applied to drilled shafts. Information in the remaining sections demonstrates how simply adopting above-ground mass concrete provisions for drilled shafts leads to unnecessary challenges and risks.

WHAT SHOULD THE MAXIMUM TEMPERATURE LIMIT BE?

Background

Ettringite is a mineral found in Portland cement concretes. Ettringite in its early form, or "primary ettringite," is a needle-shaped crystal that benefits plastic concrete due to its ability to regulate early hydration reactions to prevent flash setting, increase early strength development, and reduce drying shrinkage (Portland Cement Association (PCA), 2001). Although ettringite formed at early ages is beneficial, high internal temperatures during curing may lead to DEF, which PCA defines as the "potentially deleterious reformation of ettringite in moist concrete, mortar, or paste after destruction of primary ettringite due to high temperatures." Subsequent exposure of concrete to water enables the delayed formation of ettringite, potentially causing expansion and cracking of the concrete, with attendant concerns for concrete strength and durability. It is important to emphasize that development of high temperatures in concrete elements does not necessarily mean that DEF will occur. Instead, temperature limits are imposed because limiting the maximum temperature for concrete has been demonstrated to prevent DEF from occurring.

Section 6.2.2 of ACI 201.2 *Durable Concrete Guide* (2023) provides a thorough review of literature documenting the development of maximum temperature limits to prevent DEF. For concrete mixtures consisting of ordinary Portland cement, 158 °F is believed to be a safe threshold below which DEF is

 © Deep Foundations Institute 2025

sufficiently unlikely to occur. The guide cites studies that have demonstrated concrete mixtures with certain supplementary cementitious materials (SCMs) are less susceptible to DEF, stating "the risk of expansion of heat-cured mortars and concrete can be effectively eliminated by the incorporation of enough of the appropriate SCMs." These studies are the basis for permitting temperatures up to 185 °F for concrete mixtures satisfying any of the criteria listed in **Error! Reference source not found.**. Of relevance for drilled shaft concrete are items 3a and 3c (highlighted). Drilled shaft concrete mixtures appropriate for placement by tremie commonly satisfy these criteria because of the workability, workability retention, long-term strength, and durability benefits of fly ash and slag.

Table 1. ACI recommended measures for reducing DEF potential. Reprint of Table 6.2.2.2, ACI 201.2-23

Maximum Concrete Temperature, *T*	Prevention Required
$T \leq 158$ °F	No prevention required.
158 °F $< T \leq$ 185 °F	Use one of following to minimize risk of expansion: 1. Low-alkali Portland cement having moderate or high sulfate resistance (ASTM C150/C150M) 2. Portland cement with 1-day mortar strength ≤ 2850 psi (ASTMC109/C109M) 3. Portland cement in combination with the following SCMs a. ≥ 25 % Class F fly ash (ASTM C618) b. ≥ 35 % Class C fly ash (ASTM C618) c. ≥ 35 % slag cement (ASTM C989/C989M) d. ≥ 5 % silica fume (ASTM C1240) with ≥ 25 % slag cement e. ≥ 5 % silica fume (ASTM C1240) with ≥ 20 % Class F fly ash f. ≥ 10 % metakaolin (ASTM C618) 4. Blended hydraulic cement with SCM content listed in Item 3 (ASTM C595/C595M or ASTM C1157/C1157M).
$T >$ 185 °F	Not permissible under any circumstances.

State of Practice

Among the 11 sets of specifications considered in this paper, eight limit the maximum temperature to at most 158 or 160 °F, regardless of SCM content. The other three (Illinois DOT 2022 Standard Specification, Illinois Tollway special provision, and South Carolina DOT special provision) permit temperatures of 180 or 185 °F with SCM content consistent with the ACI 201 guidance. Among the eight owners who limit maximum temperature to 158 or 160 °F in all cases, several have cited concerns regarding strength as justification. Potential strength loss from high temperatures is addressed in the final topic of this paper.

Recommendations

The maximum temperature limit for drilled shafts should be established from the ACI 201 guidance document. The literature review presented in ACI 201 provides convincing support for application of the 185 °F limit to concrete mixtures with sufficient SCMs. It is also noteworthy the ACI 201 guidance is presented as applying when temperatures greater than 158 °F are "unavoidable." The unique characteristics of drilled shaft concrete listed in the Introduction speak to the unavoidability of elevated temperatures within many large diameter drilled shafts.

 © Deep Foundations Institute 2025

WHAT SHOULD THE MAXIMUM TEMPERATURE DIFFERENTIAL BE?

Background

As concrete hydrates and heat accumulates, the surface of concrete elements cools at a faster rate than the interior as heat transfers to surrounding materials. As a result, the temperature of the concrete decreases with distance from the element center, which produces a temperature difference within the concrete member. Temperature differences produce tensile stresses in the concrete, which can result in cracking.

A common mass concrete provision is to limit temperature differentials to 35 °F to prevent thermal cracking. This approach is conservative in two regards. First, the value of 35 °F is a lower bound for all concrete mixtures. The value was developed empirically based on unreinforced concretes from Europe in the 1950s (Gadja and Vangeem, 2002). The temperature differential for incipient cracking can be predicted more precisely by considering concrete properties. Most important are elastic modulus and coefficient of thermal expansion, both of which can be predicted based on the type of aggregate used in the concrete mixture. For concrete mixtures without the most expansive aggregates, differentials greater than 35 °F can be withstood without cracking.

Second, the design posture of preventing thermal cracking altogether is conservative. ACI 224R (2001) suggests a limiting crack width of 0.3 mm for concrete exposed to soil, although smaller limiting crack widths may be considered in aggressive ground conditions or based on consideration of anticipated service life. Similarly, for substructures exposed to water (i.e., Class 2 exposure), AASHTO specifies a crack width of 0.013 in. (0.32 mm) in design criteria for control of cracking (2024; Section 5.6.7).

A procedure for establishing allowable temperature differentials to control cracking in drilled shaft concrete is presented in Boeckmann, et al. (2021). The methodology is adopted from guidance published by the UK-based CIRIA (Bamforth, 2018). For a 10-ft diameter shaft with 6-inch cover and 1% longitudinal reinforcement (relatively light reinforcement, which is conservative), the procedure produces allowable temperature differentials that vary from about 250 °F for concrete mixtures with the least expansive aggregate (3 με/°F) to about 100 °F for mixtures with highly expansive aggregate (8 με/°F). Measured temperature differentials for all projects included in the analysis of this paper are less than 100 °F.

Another concept from the CIRIA guidance is relevant to considerations of durability. Regarding thermal cracking, Bamforth writes “surface cracks that may initially exceed the allowable width are likely to close as the element cools down.”

State of Practice

Among the 11 sets of specifications, provisions for the maximum temperature differential vary widely, as shown in **Error! Reference source not found.**. The most conservative approach, limiting differentials to 35 °F, is the most common approach and was specified for four of the 11 projects. Five other projects specified higher values, ranging from 45 to 60 °F, with some imposing time- or calculation-based qualifications. Specifications for another project required a differential value intended to prevent cracking to be established in the thermal control plan, a provision based on Caltrans standard specifications. Finally, one project did not apply a maximum temperature differential to drilled shafts with permanent casing in accordance with South Carolina DOT standard specifications. Two noteworthy data points regarding the state of practice not reflected in the project experience are the 2022 version of the Illinois DOT standard specifications and the 2018 mass concrete special provision from Minnesota DOT, both of which exempt drilled shafts from temperature differential requirements.

 © Deep Foundations Institute 2025

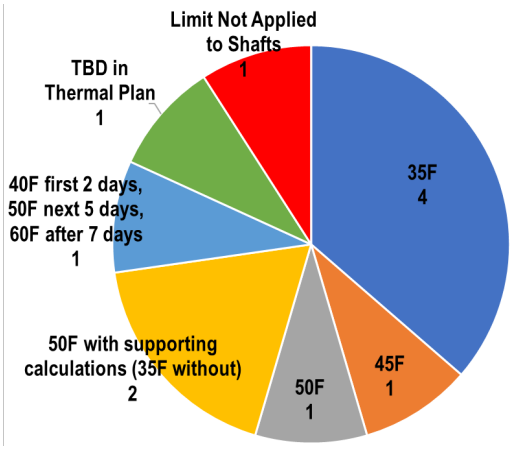


Fig. 2. Maximum temperature differential specified in 11 different project specifications.

Recommendations

The following provisions are recommended regarding the maximum temperature differential for drilled shafts:

- Temperature differential provisions should never apply within a permanent steel casing. Durability is inherently satisfied if shaft is permanently cased with steel.
- For most (i.e., "non-aggressive") ground conditions, temperature differentials should not apply to shafts without permanent steel casing. Temperature differentials for permissible crack widths per AASHTO and ACI are so large as to make the calculation and monitoring effort unnecessary.
- For drilled shafts in aggressive ground conditions and without permanent casing, allowable temperature differentials should be established to prevent thermal cracking in accordance with the procedures established in Boeckmann, et al. (2021). The resulting allowable differential values should only apply to portions of the shaft that are uncased.

HOW LONG SHOULD MASS CONCRETE SHAFTS BE MONITORED?

Background

Execution of a thermal control plan requires monitoring temperatures within the concrete element to compare measured temperatures and differentials with established limits. The duration of monitoring should be sufficient to capture the period during which the maximum temperature or temperature differential could exceed the established limits. For above-ground concrete, this period can extend beyond the point at which the mass concrete element temperatures have started to decrease to account for the possibility that low ambient temperature conditions will result in increasing temperature differentials, even after the concrete begins cooling. Duration provisions therefore are often based on ambient temperature conditions, e.g. "until the difference between the internal concrete temperature and the average daily ambient temperature is less than 35 °F."

Duration requirements based on ambient temperature are not rational for drilled shaft concrete. Drilled shaft temperature differentials are governed by temperature of the surrounding soil, rock, or water, which typically does not fluctuate over the timescale of cement hydration. Moreover, because the ground generally serves as an effective insulator, the internal temperature of drilled shaft concrete tends to decrease rather slowly. With low ambient temperatures, satisfying monitoring duration requirements based on comparison with ambient temperature can therefore lead to months of monitoring for each shaft, which unnecessarily

increases costs with no benefit. When drilled shaft concrete extends through water, and the insulation offered by the surrounding soil or rock is not present, a permanent steel casing is necessary, which alleviates any concern of differential cracking in that zone (see above).

State of Practice

Specifications for seven of the 11 projects included requirements for monitoring duration that are based on ambient conditions. The other four either referenced times of removing formwork (also not applicable to drilled shafts) or deferred the monitoring duration to the approved thermal control plan.

Recommendations

Mass concrete drilled shaft temperature monitoring should be performed until at least 24 hours after values of concrete temperature at the center of the shaft (in plan view) have reached their maximum value and are less than the allowable value. If specifications include provisions regarding temperature differential, monitoring should be performed until 24 hours after both the center temperature and the temperature differential have reached their maximum values and are less than the allowable values. (If a temperature limit is exceeded, monitoring should continue until temperature values are less than the limit, even if the 24-hour criterion is satisfied.)

WHAT SHOULD THE CONSEQUENCES OF TEMPERATURE EXCEEDANCES BE?

Background

Mass concrete provisions sometimes include language regarding the consequences of temperature exceedances, i.e. the required actions when measured temperatures are greater than maximum temperature or maximum temperature differential limits. A common provision is to require revisions to the thermal control plan to prevent future exceedances. Provisions regarding the in-place, non-conforming concrete are less common, more variable when included, and often of much greater consequence.

State of Practice

As shown in **Error! Reference source not found.**, more than half of the drilled shaft mass concrete specifications reviewed do not address the consequences of exceedances, other than to require revisions to prevent future exceedances. Two of the 11 reviewed specifications require the thermal control plan to include provisions regarding how any potential damage will be addressed. Another two deem the concrete unacceptable and require removal and replacement, and the remaining specification requires an engineering assessment.

 © Deep Foundations Institute 2025

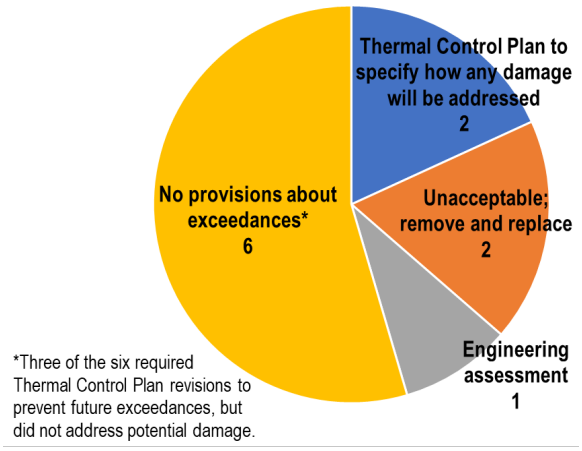


Fig. 3. Consequences of temperature exceedance in 11 different project specifications.

Recommendations

A series of recommendations are offered to improve specification provisions regarding consequences of temperature exceedances:

- All mass concrete provisions, especially those applied to drilled shafts, should be explicit about the range of potential consequences of temperature exceedances for the non-conforming concrete, even if a specific consequence is not included.
- If the concrete mixture includes sufficient SCM content to withstand 185 °F per ACI 201, the drilled shaft should be acceptable for mass concrete purposes so long as observed temperatures are less than 185 °F, even if the specification limit is 160 °F.
- If the concrete mixture does not satisfy ACI 201 requirements and exceeds 160 °F, or if the concrete mixture does satisfy ACI 201 but exceeds 185 °F, the drilled shaft concrete should be deemed unacceptable, unless a case for acceptance can be justified and is approved by the Engineer of Record. Considering the potential consequences of DEF, it is difficult to envision such a case for drilled shaft concrete, although the presence of permanent steel casing could be a mitigating factor.
    - The consequences of this can be enormous for large diameter drilled shafts, and well beyond the cost and schedule burdens associated with exceeding the peak temperature limit for above grade structures. Often, large diameter drilled shafts are initially positioned exactly where they need to be to address multiple design considerations, and abandoning a location can have substantial ripple effects on a project.
    - In addition, the thermal control plan should be revised to prevent exceedances for the remaining mass concrete shafts.
- If a temperature differential limit is specified and is exceeded, the drilled shaft concrete should not be deemed unacceptable for mass concrete purposes, but the thermal control plan should be revised to prevent exceedances for the remaining mass concrete shafts.

WHAT ABOUT POTENTIAL STRENGTH LOSS DUE TO ELEVATED TEMPERATURES?

On several of the 11 projects, owner's engineers have cited concerns about potential reductions in concrete strength as a result of elevated temperatures. The concerns are in addition to durability concerns related to DEF, and have been used to justify maintaining the 160 °F limit for projects where a limit of 185 °F should be acceptable to prevent DEF per ACI 201. This section explains the strength reduction concerns, describes the problems with using those concerns to justify a blanket 160 °F limit, and provides three alternative approaches that would be more effective for addressing concerns regarding strength reduction.

 © Deep Foundations Institute 2025

Background

Although DEF is the predominant motivation for maximum temperature limits, concerns about reduction in strength are sometimes cited as a justification for imposing maximum temperature limits in mass concrete specifications (e.g., ACI 301, 2020). Strength concerns date back at least as far as the 1960s with research at the Portland Cement Association (e.g., Verbeck and Helmuth, 1968; Verbeck and Copeland, 1972). The research is based on tests of cement paste specimens cured at a range of temperatures. Results, for example those shown in **Error! Reference source not found.**, suggest that at early ages, higher curing temperature is associated with greater strength, but long-term strength is diminished by higher curing temperature.

Empirical data tracking production concrete compressive strength data over time also suggest an effect of temperature on strength (e.g., Dodson and Rajagopalan, 1979; Petscharnig, 1987, as summarized by Neville, 2011). The empirical studies take advantage of natural variation in mean temperature over the course of a calendar year, demonstrating that higher 28-day strength values are generally observed for specimens cured in winter months and lower values for specimens from summer months. The effect demonstrated in the empirical data varies but is less severe than that from **Error! Reference source not found.**.

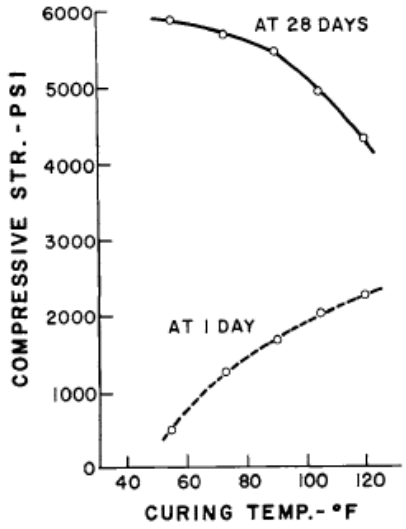


Fig. 4. Effect of curing temperature on compressive strength of cement paste at 1 and 28 days (Verbeck and Copeland, 1972).

More recent research by Chini, et al. (2003) for the Florida Department of Transportation evaluated the effect of elevated curing temperature on durability and strength. The research included strength testing of concrete specimens cured at room temperature (73 °F) and two elevated temperatures: 160 and 180 °F. Results from the research are shown in **Error! Reference source not found.**. Both plots in the figure show compressive strength on the vertical axis versus curing temperature on the horizontal axis. Compressive strength is presented as a ratio of the strength at 28 days for the specimen cured at 73 °F. The first plot is for a concrete mixture without fly ash; the second plot is for a concrete mixture with 18% fly ash (as a percentage of the total cementitious content weight). In both plots, three lines are shown: strength at 7 days, strength at 28 days, and strength at 91 days. Consistent with previous research, the results indicate a negligible or beneficial effect of elevated curing temperature for 7-day strength. At 28 and 91 days, there is a significant loss of strength for specimens cured at the higher temperatures.

Two observations are relevant, and noteworthy. First, the magnitude of strength reduction at 28 and 91 days for elevated curing temperature is less for mixtures with fly ash than those without (about 8% versus 15%, respectively). Second, for the mixture with fly ash, there is no significant difference in strength for specimens cured at 160 °F versus those cured at 180 °F (0% at 28 days, 1% at 91 days).

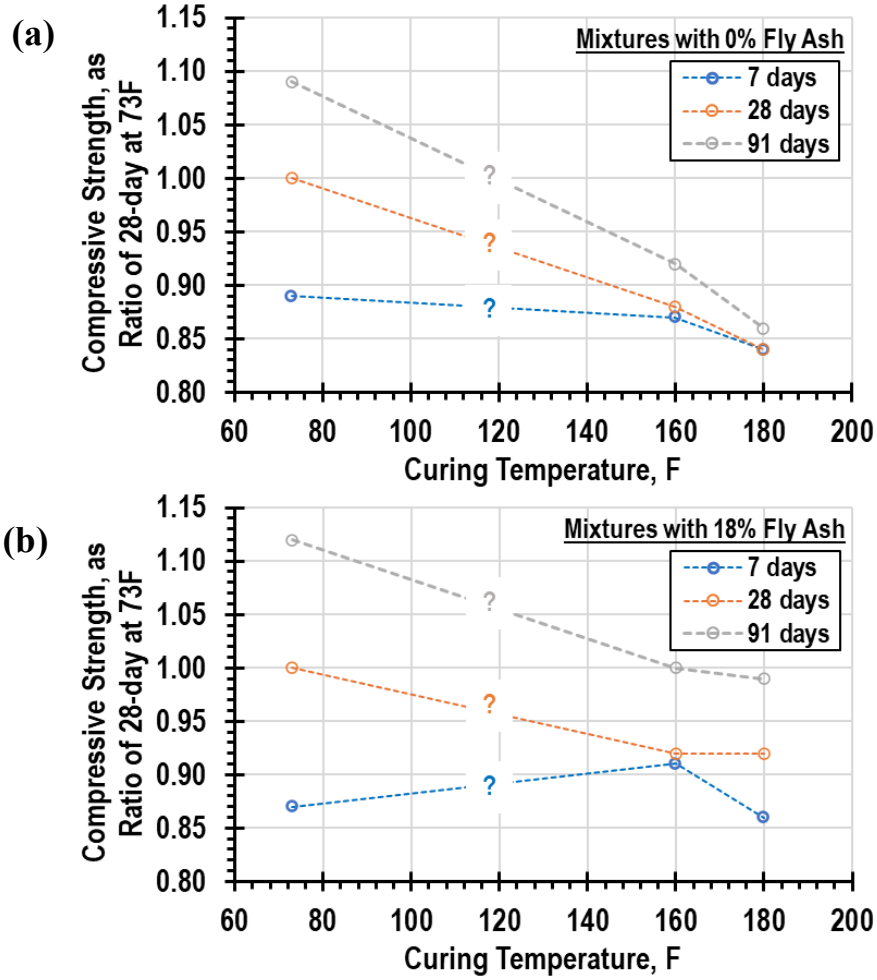


Fig. 5. Compressive strength versus curing temperature for concrete mixtures with (a) no fly ash and (b) 18% fly ash. Data are presented as a ratio of the 28-day strength of specimens cured at 73 °F. Based on data from Chini, et al. (2003).

In summary, there is ample evidence to support the notion that long-term strength is reduced by high curing temperatures. However, the magnitude of strength loss varies considerably from one study to the next, with the available data suggesting the effect is diminished for concrete mixtures with SCMs. In addition, the magnitude of strength loss varies as a function of temperature; there is no practical threshold below which strength loss is not a concern. Instead, a common method to at least partially address the effect is to field cure concrete specimens. However, field curing does not mimic curing temperatures experienced in mass concrete members, which are governed by the heat of hydration. In rare cases, strength specimens for mass concrete specimens are match cured, wherein the curing temperature within the specimen storage container follows measured temperatures within the element. However, this approach is only commonly used for precast members.

Problems with Limiting Temperature to Prevent Strength Loss

 © Deep Foundations Institute 2025

A logical but wholly impractical conclusion one could reach based on the data regarding the effect of curing temperature is that the curing temperature should be limited to 73 °F. A more realistic conclusion is that some reduction in strength occurs as the curing temperature increases above 73 °F, but there is insufficient evidence to justify any definitive reduction in allowable maximum temperature. Indeed, this conclusion is consistent with recommendations from the FDOT report, itself, which called for additional research and did not recommend imposition of a 160 °F limit. (It also seems relevant that FDOT's mass concrete specifications include a temperature limit of 180 °F for mixes with sufficient SCM content.) The recommendation for additional research is wise considering significant uncertainty in the topic, the potential consequences of strength loss, and the constructability challenges often associated with a strict 160 °F limit.

To explain the reduction in strength at high temperature, the hypothesis from Verbeck and Helmuth (1968) and repeated by others (e.g. Chini, et al., 2003; Neville, 2011) is that the rapid hydration encouraged by high curing temperatures leads to a more porous structure that is inherently weaker than less porous structures formed under lower curing temperatures. Questions arise in applying this hypothesis to drilled shaft concrete, which is necessarily cured under significant fluid pressure because of shaft geometry. Fluid pressure would be expected to diminish the formation of voids associated with porous structure. Such speculation should not imply there is no temperature effect on strength development for drilled shaft concrete. Rather, the speculation points again to the uniqueness of drilled shaft concrete, which also typically includes significant dosages of retarding and workability admixtures not included in most of the research mixtures. The effect of temperature on strength is poorly defined, generally; for drilled shafts, it is especially uncertain.

Alternative Approaches

There is no rational basis for limiting the maximum temperature to 160 °F based on strength concerns. Instead, two possible explanations explain the "stickiness" of the 160 °F limit for mixes with sufficient SCM content:

(1) Engineers sincerely concerned about strength reductions have simply borrowed the limit that developed rationally from research on DEF, despite the lack of evidence supporting 160 °F (or any other value) as a safe limit for strength-reduction purposes.
(2) Engineers philosophically opposed to any relief on the temperature limit have used potential strength effects to justify maintaining the 160 °F limit, despite DEF research supporting raising the limit for mixes with sufficient SCM content.

Either explanation is incompatible with a logical evaluation of the available evidence.

If structural engineers designing drilled shafts are truly concerned about the effect of high temperatures on strength, there are at least three ways this could be achieved more effectively than applying a blanket 160F limit:

(1) Specify concrete strength values in the construction documents that exceed the value used to design the drilled shaft by a marginal value that accounts for temperature effects.
(2) During trial batching, cure strength specimens at 185 °F and 73 °F (or another standard temperature) to quantify the temperature effect and adjust the acceptance value accordingly.
(3) During construction, match cure strength specimens to account for any strength loss in the acceptance protocol. This approach may warrant designing the concrete mixture to account for potential losses.

Instead, the status quo for engineers concerned with strength losses is to assume the strength loss will not occur and impose maximum temperature limits to provide reassurance regarding that assumption. There

are two problems with the status quo approach. First, as explained above, the experimental evidence does not support the assumption that the strength reduction will not occur at 160 °F. Second, for drilled shafts, the imposition of a 160 °F limit is difficult and, in some cases, impossible to satisfy in a manner compatible with best tremie concrete placement practices. The status quo therefore represents an inequitable and cost ineffective transfer of risk wherein the designer attempts to reduce design uncertainty by imposing temperature limits that introduce significant construction risks for the contractor. It would be easier, more reliable, and more practical to specify higher strength to account for potential loss than to specify temperature limits to prevent the loss.

SUMMARY OF RECOMMENDATIONS

Recommendations regarding six major questions for drilled shafts as mass concrete have been provided in this paper:

- Drilled shafts should not be exempt from mass concrete provisions, altogether, but mass concrete provisions applied to drilled shafts should be carefully crafted and include appropriate exemptions as noted in subsequent recommendations. Engineers or owners should not blindly apply mass concrete provisions developed for above grade structures to drilled shafts.
- The maximum temperature limit should be 185 °F when the concrete mixture includes SCM content satisfying the provisions in ACI 201.
- Except in cases of uncased drilled shafts in aggressive ground conditions, temperature differential limits should not apply to drilled shafts, and should never apply to permanently cased shafts. For uncased shafts in aggressive ground conditions, allowable temperature differentials to prevent thermal cracking should be established in accordance with procedures in Boeckmann, et al. (2021).
- The duration of monitoring should not be linked to the ambient temperature. Temperature monitoring for mass concrete drilled shafts should cease 24 hours after the maximum temperature has been observed and has been observed to be less than the allowable value.
- Mass concrete provisions should be explicit about consequences of exceedance for the non-conforming concrete.
- If a shaft constructed with a concrete mixture that does not satisfy ACI 201 requirements has temperatures exceeding 160 °F, or if the concrete mixture does satisfy ACI 201 but temperatures exceed 185 °F, the drilled shaft concrete should be deemed unacceptable, unless a case for acceptance can be justified and is approved by the Engineer of Record.
- Concerns about strength loss due to elevated curing temperatures should not be addressed via mass concrete temperature criteria. Alternative approaches such as incorporating tests in the trial batch program are more rational and cost effective.

ACKNOWLEDGEMENTS

The authors are grateful for the technical support and feedback from colleagues and industry friends, especially Mark Madgett, Ben Turner, and Patrick Earney.

REFERENCES

AASHTO. (2024). *AASHTO LRFD Bridge Design Specifications*, American Association of State Highway and Transportation Officials, 10th Edition. 2024.

ACI 201.2-23. (2023). *Durable Concrete-Guide*, American Concrete Institute, Farmington Hills, MI, 99 p.

ACI 207.1-21. (2022). *Mass Concrete-Guide*, American Concrete Institute, Farmington Hills, MI, 34 p.

 © Deep Foundations Institute 2025

ACI 224R-01. (2001). *Control of Cracking in Concrete Structures (Reapproved 2008)*, American Concrete Institute, Farmington Hills, MI, 45 p.

ACI SPEC-301-20. (2020). *Specifications for Concrete Construction*, American Concrete Institute, Farmington Hills, MI, 69 p.

Bamforth, P.B. (2018). *Control of Cracking Caused by Restrained Deformation in Concrete*, C766, CIRIA, London.

Boeckmann, A.Z., El-tayash, Z., & Loehr, J.E. (2021). Establishing and Satisfying Thermal Requirements for Drilled Shaft Concrete Based on Durability Considerations. *Transportation Research Record*, Vol. 2675, No. 8, 13 p.

Chini, A.R., Muszynski, L.C., Acquaye, L., & Tarkhan, S. (2003). *Determination of the Maximum Placement and Curing Temperatures in Mass Concrete to Avoid Durability Problems and DEF*, Final Report to the Florida Department of Transportation, 165 p.

Dodson, C.J. & Rajagopalan, K.S. (1979). Field Tests Verify Temperature Effects on Concrete Strength. *Concrete International,* Vol. 1, No. 12, 23-30.

Gajda, J., & Vangeem, M. (2002). Controlling Temperatures in Mass Concrete. *Concrete International*, 59–62.

Masten, M. (2018). State Reports Summary: Types of Reinforcement and Mass Concrete. Presentation to National Concrete Consortium.

Neville, A.M. (2011). *Properties of Concrete*, 5th Ed., Pearson, New York, 846 p.

Petscharnig, F. (1987). Einflüsse der jahreszeitlichen Temperaturschwankungen auf die Betondruckfestigkeit. *Zement und Beton*, Vol. 32, No. 4, 162-163.

Portland Cement Association. (2001). *Ettringite Formation and the Performance of Concrete*. PCA R&D Serial No. 2166, IS417.01, 16 p.

Verbeck, G.J., & Copeland, L.E. (1972). Some physical and chemical aspects of high pressure steam curing. *ACI Symposium*, SP32-01, 14 p.

Verbeck, G.J., & Helmuth, R.A. (1968). Structures and physical properties of cement paste. *Proceedings of the 5th International Symposium on the Chemistry of Cement*, Tokyo, Vol. 3, 1-32.

[i] The updated mass concrete definition considers both element dimension and equivalent cement content. For elements with equivalent cement content of 700 lbs per cubic yard, a diameter of 2-ft or greater is considered mass concrete.

 © Deep Foundations Institute 2025

DRILLED SHAFT LOAD TESTS IN WEAKLY CEMENTED SANDSTONE

David S. Graham, P.E., BC.GE, Dan Brown and Associates, Chattanooga, Tennessee, USA, 205-427-0682, dgraham@dba.world
Paul J. Axtell, P.E., BC.GE, Dan Brown and Associates, Overland Park, Kansas, USA, 816-210-1954, paxtell@dba.world

ABSTRACT

Bi-directional load tests on three, large diameter drilled shafts in weakly cemented sandstone at three different sites demonstrate that weakly cemented sandstone can provide significant geotechnical axial resistance in both side and base resistance. Load tests from sites in Minneapolis, Minnesota, Oak Park Heights, Minnesota, and Lansing, Iowa, are presented. The Paleozoic sandstone bedrock at these sites is difficult to sample due to the weak cementation. Despite the best efforts of site characterization, determining representative uniaxial compressive strength for design correlation is difficult due to low or no sample recovery and poor sample quality. Visual observation of the rock socket drilling, performed with traditional rotary tools for these three projects, also produced spoils that resemble uncemented sand rather than intact sandstone. However, despite the apparent weakness, full-scale load tests demonstrate that the in-situ bedrock can resist large axial loads exceeding the capacity of the bi-directional jacks for properly constructed drilled shafts. Furthermore, load test results confirm side and base resistance in the weak sandstone bedrock are simultaneously mobilized at compatible displacements. This paper presents the subsurface conditions, a summary of the construction, details of bi-directional load test setup, and load test results for each site. The load test results are compared. Recommendations are made for future projects with similar geologic conditions.

Keywords: Drilled Shaft, Rock Socket, Bi-directional, Load Test, Sandstone

INTRODUCTION

Paleozoic sandstone is the surficial bedrock across a significant portion of the Upper Midwestern United States, including Southeastern Minnesota, Northeastern Iowa, and Western Wisconsin. Much of this sandstone is weakly cemented and highly friable. Friability makes the sandstone easy to excavate but difficult to sample, test, or otherwise characterize for geotechnical evaluation. Due in part to the difficulty in sampling and testing, bi-directional load tests have been performed on three large diameter drilled shafts in weakly cemented sandstone at three different bridge sites between 2007 and 2024. The sites are: 1) I-35W St. Anthony Falls Mississippi River Bridge in Minneapolis, Minnesota, 2) St. Croix Crossing Bridge over the St. Croix River between Oak Park Heights, Minnesota, and St. Joseph, Wisconsin, and 3) IA-9 Black Hawk Mississippi River Bridge, between Lansing, Iowa, and De Soto, Wisconsin. The dimensions of the rock sockets and other basic test shaft information are summarized in Table 1. Bedrock data from borings at the test shaft locations are presented in Fig. 1.

At the Black Hawk Bridge site, rock core samples were not successfully recovered in any borings near the test shaft location on the Wisconsin side of the Mississippi River despite various attempts with various types of rock core sampling equipment by two different geotechnical drilling contractors. Some rock core samples were recovered on the Iowa side of the river in different

 © Deep Foundations Institute 2025

sandstone strata at higher elevations than the test shaft rock socket. These sandstone core samples exhibited variable recovery between 0% and 100% with an average of 47% and low rock quality designation (RQD) between 0% and 70% with an average of 18%. Uniaxial compressive strength (UCS) on sandstone samples from these cores ranged from 98 psi to 1,300 psi with an average of 910 psi. Although these data are not from the same strata as the test shaft rock socket, they are the only sandstone rock core data available from the Black Hawk site.

Table 1. Basic test shaft information

Project	Location	Test Date	Bi-Directional Jacks	Rock Socket Diameter (ft)	Base Load Plate Diameter (ft)	Rock Socket Length (ft)
I-35W St. Anthony Falls Mississippi River Bridge	Minneapolis, MN	November 22, 2007	2 levels of 4 26-inch jacks at the base and 10.0 ft above the base	6.5	5.4	39.9
St. Croix Crossing Bridge	Oak Park Heights, MN	August 27, 2012	3 34-inch jacks 4.8 ft above the base	7.5	-	46.8
IA-9 Black Hawk	Lansing, IA	February 13, 2024	3 24-inch jacks at the base	8.5	6.0	30.9

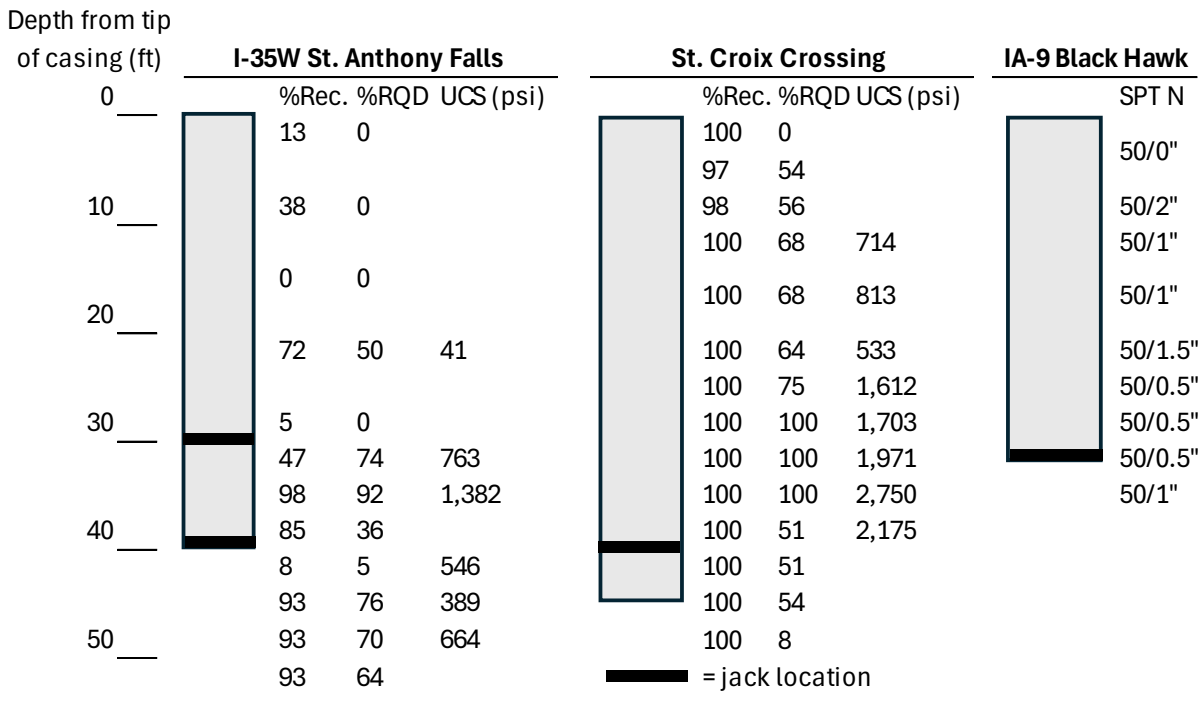


Fig. 1. Rock socket schematic with bedrock data

The St. Anthony load test was a multi-stage test with two levels of bi-directional jacks. The test was conducted in the following stages:

 © Deep Foundations Institute 2025

Stage 1: The lower jacks were loaded with the upper jacks fully closed.
Stage 2A: The upper jacks were loaded with the lower jacks allowed to freely close until a gross bi-directional load of 8,000 kips was reached.
Stage 2B: The upper jacks were loaded beyond 8,000 kips with the lower jacks locked, engaging base resistance.

CONSTRUCTION

All three drilled shafts included permanent steel casing installed into bedrock. The rock sockets for all three test shafts were excavated using traditional rotary drilling equipment consisting of various augers, core barrels, and cleanout buckets driven by crane-mount or hydraulic-crawler type drill rigs. The resulting spoils typically take the form of uncemented sand (Fig. 2). Occasionally, cemented pieces of rock are extracted.



Fig. 2. Typical uncemented sand spoils on a rock auger from the Black Hawk Bridge Test Shaft

Artesian groundwater conditions were encountered within the sandstone rock sockets at the St. Anthony test shaft and the St. Croix test shaft. The artesian condition at St. Anthony was approximately 14 ft above ground level. The contractor had to work from aerial lifts with an extended casing to counteract the artesian pressure and maintain a positive support fluid head. The artesian head at St. Croix was approximately 3 ft above river level and was counteracted by maintaining a higher than planned support fluid level in the casing. Artesian groundwater was not encountered at the Black Hawk test shaft.

All three test shafts were constructed with polymer slurry as the support fluid. While it may have been possible to construct the sockets with water as the support fluid. Polymer slurry was used for several reasons, including better ability to provide excavation support, preservation of sidewall integrity, and reduced fluid loss. Cleanout at St. Croix and Black Hawk included a full exchange of the polymer slurry with an airlift.

 © Deep Foundations Institute 2025

Base cleanliness was inspected using a miniature shaft inspection device (mini-SID) at all three sites. The St. Anthony test shaft had approximately 1 inch of sediment across its base prior to concrete placement. The St. Croix Crossing test shaft had approximately ½ inch of sediment across approximately 33% of its base with the remainder of the base having less than ½ inch of sediment. The Black Hawk test shaft had less than ½ inch of sediment across its entire base.

All three test shafts were poured in the wet with a tremie. The concrete mixes were highly workable and appropriate for tremie placement in a drilled shaft. The concrete placement at the Black Hawk bridge was initiated with approximately 10 yd^3 of neat cement grout having the same 28-day design strength as the ensuing concrete.

LOAD TEST RESULTS

Gross bi-directional load versus displacement, "butterfly" plots, are presented in Fig. 3. Upward and downward resistance are relatively well balanced, mobilizing at small and similar displacements for the St. Croix and Black Hawk tests. The St. Anthony test was less well balanced, particularly for Stage 1 of the multi-stage test. Figure 4 presents unit base resistance versus normalized displacement, where displacement is expressed as a percentage of loaded base diameter. Note that for the St. Anthony and Black Hawk test shafts, the loaded base plate diameter is smaller than the rock socket diameter, as indicated in Table 1. The St. Croix test shaft did not have the jacks at the base, and the loaded diameter is the rock socket diameter. All three load tests demonstrate relatively similar maximum unit base resistance between 389 and 444 ksf, a 13.2% difference. Mean maximum mobilized unit base resistance is 410 ksf and none of the tests reached a strength limit state or nominal resistance although it is possible the St. Anthony test was approaching the limit in base resistance. Mobilized base resistance is limited by the capabilities of the bi-directional jacks. All test results exhibit relatively linear base response stiffness that begins mobilizing immediately; however, the stiffness varies between the three tests. Surprisingly, the Black Hawk load test, which appears to have the poorest quality sandstone, exhibits the stiffest base response of the three. Base response stiffness correlates with base cleanliness observed with the mini-SID.

Unit side resistance interpreted from the load tests is presented in Table 2 and Fig. 5. Unit side resistance varies both from test to test and among segments of each test shaft on the basis of inferred load shed from recorded strain gage data. The St. Anthony test shaft was able to achieve greater displacement due to the two-level, multi-stage test setup. Average unit side resistance performance in the rock sockets considering all three tests is approximately 25 ksf at approximately 1/3-inch displacement based on mean values in Table 2. Visual inspection of the results in Fig. 5, considering some extrapolation for the St. Croix and Black Hawk results leads to similar values.

 © Deep Foundations Institute 2025

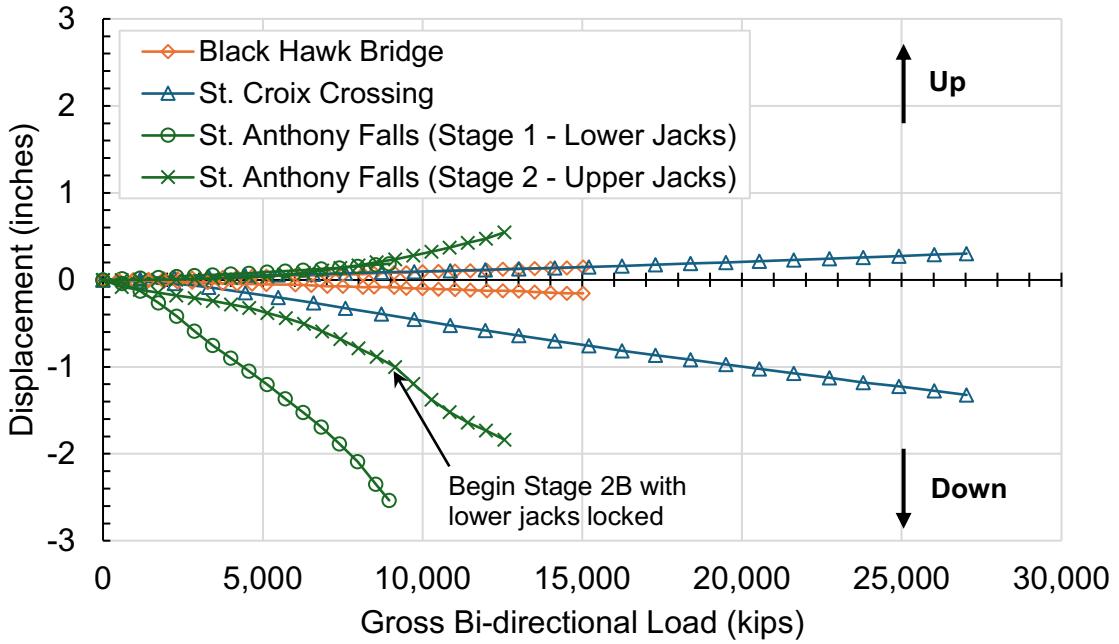


Fig. 3. Gross bi-directional load versus displacement

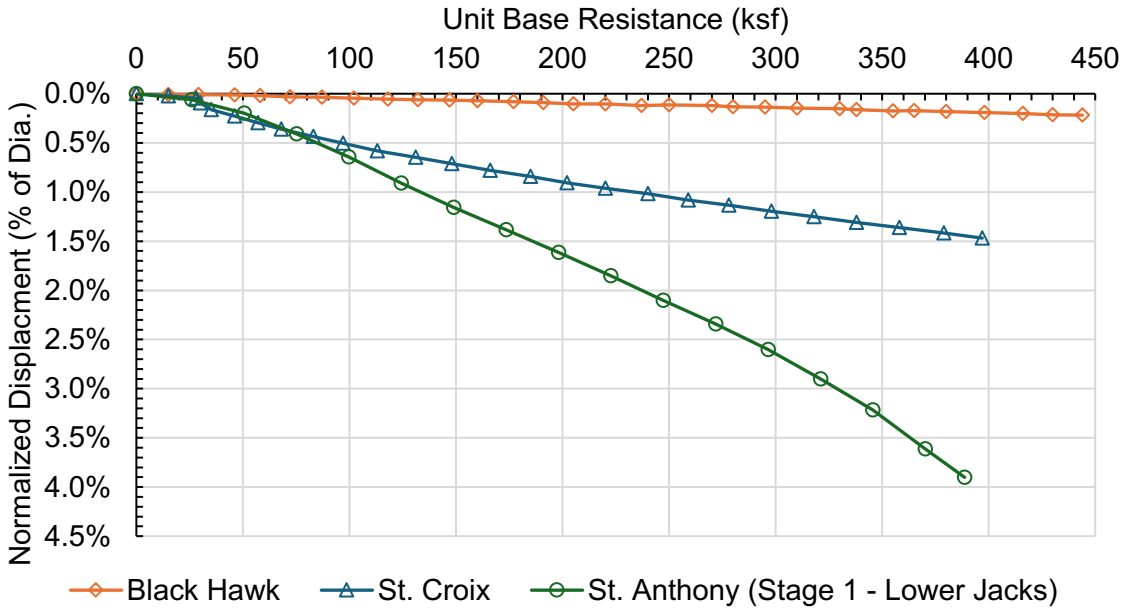


Fig. 4 – Unit base resistance versus displacement normalized as percentage of loaded area diameter

Table 2. Rock Socket unit side resistance

Project	Average Maximum Mobilized Unit Side Resistance (ksf)	Maximum Mobilize Unit Side Resistance, Single Segment (ksf)	Displacement at Maximum Mobilized Unit Side Resistance (ksf)
St. Anthony Falls (Stage 2 – Upper Jacks)	31.3	54.2	0.64
St. Croix Crossing	25.2	47.9	0.27
Black Hawk Bridge	16.6	30.3	0.14

COMPARISON TO EMPIRICAL ESTIMATES

The following equation is commonly used to estimate unit side resistance in "normal" rock, as is recommended in AASHTO, *Bridge Design Specifications* (2020) and FHWA, *Drilled Shafts: Construction Procedures and LRFD Design Methods* (2018):

$$\frac{f_{SN}}{p_a} = C\sqrt{\frac{q_u}{p_a}} \quad [1]$$

Where f_{SN} = nominal unit side resistance, C = empirical regression coefficient (1.0 for "normal" rock), q_u = mean UCS, and p_a = atmospheric pressure in the same units as q_u.

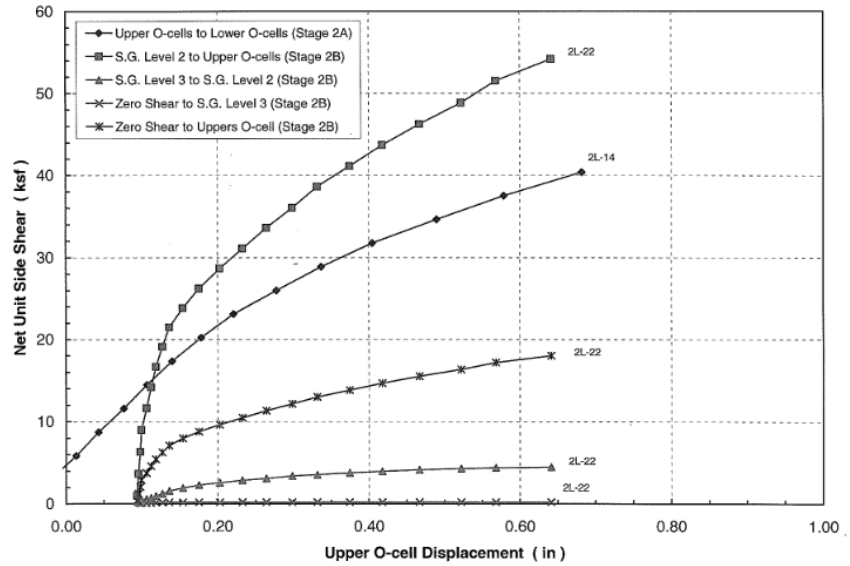
"Normal" rock sockets are defined as rock sockets constructed with traditional rotary equipment and resulting in nominally clean sidewalls without resorting to special procedures or artificial roughening. According to the definition, all three rock sockets described herein are "normal." Although it is only recommended for unstable rock that is susceptible to caving without support, many designers use the following equation for any rock that is weak or fractured:

$$\frac{f_{SN}}{p_a} = 0.65\ \alpha_E\sqrt{\frac{q_u}{p_a}} \quad [2]$$

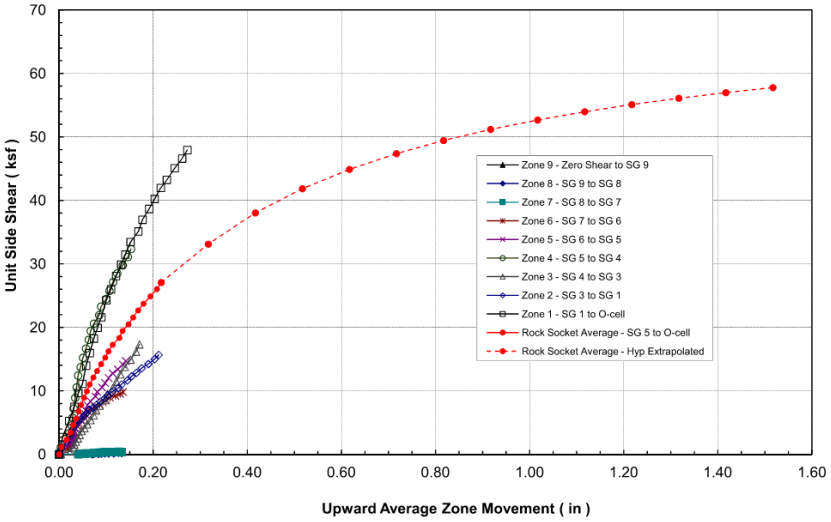
Where α_E = empirical coefficient based on RQD and joint condition, and the other parameters are the same as defined for Equation 1.

Where UCS and RQD data are available, the results from the load tests are compared to predicted values calculated using Equations 1 and 2. The predicted values and measured values are compared in Table 3 and Figs. 6 and 7. The measured values are only from the St. Anthony and St. Croix load tests, as UCS and RQD are not available for the Black Hawk test shaft due to the inability to recover rock core samples. Equation 1 is a better predictor of the measured unit side resistance than Equation 2 for all six rock socket segments. Both equations underpredict the maximum measured unit resistance in most cases. Equation 1 overpredicts in one case. However, it should be noted that displacement at the St. Croix load test was not sufficient to fully mobilize the nominal unit side resistance.

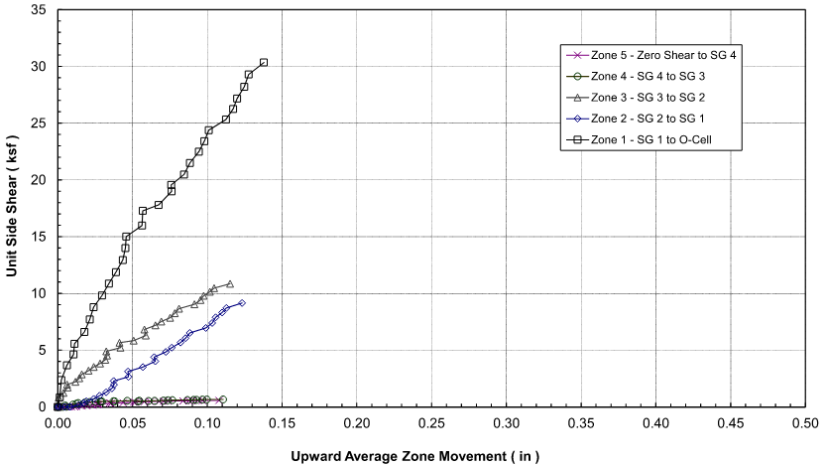
 © Deep Foundations Institute 2025



(A)



(B)



(C)

Fig. 5. Unit side resistance versus displacement, (A) St. Anthony, (B) St. Croix, and (C) Black Hawk

 © Deep Foundations Institute 2025

Table 3. Unit side resistance empirical predictions versus load test measured

Project, Rock Socket Segment	Average q_u (psi)	Average RQD (%)	α_E (unitless)	Unstable Rock, Equation 2 Predicted (ksf)	Normal Rock, Equation 1 Predicted (ksf)	Load Test Measured (ksf)
St. Anthony, SG 3 to SG 2	41	17	0.38	0.9	3.5	4.5
St. Anthony, SG 2 to Upper Jacks	763	37	0.49	4.8	15.3	54.2
St. Anthony, Upper Jacks to Lower Jacks	1,382	67	0.81	10.8	20.5	40.4
St. Croix, SG 5 to SG 4	764	45	0.58	5.7	15.3	32.3
St. Croix, SG 4 to SG 3	1,073	64	0.65	7.6	18.1	17.3
St. Croix, SG 3 to SG 1	2,009	92	0.96	15.4	24.7	15.7
St. Croix, SG 1 to Jacks	2,175	48	0.59	9.9	25.7	47.9

The following equation is commonly used to estimate unit base resistance in "normal" rock and is recommended in AASHTO and FHWA:

$$q_{BN} = N^*_{cr} q_u \quad [3]$$

Where q_{BN} = nominal unit base resistance, N^*_{cr}= empirical bearing capacity factor (2.5 for "normal" rock), and q_u = mean UCS below shaft base.

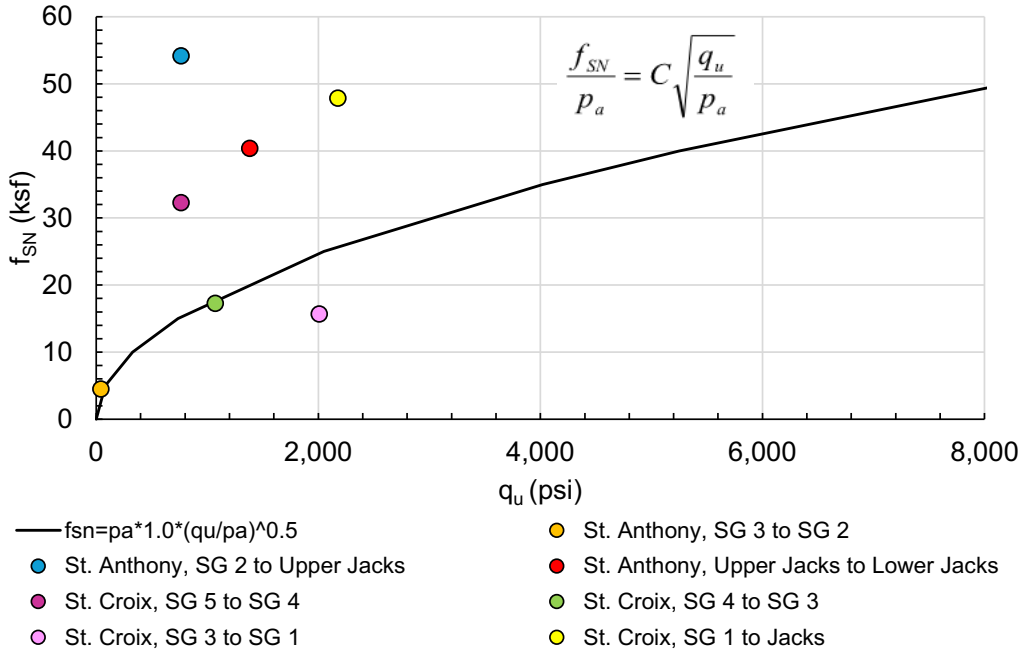


Fig. 6. Predicted and measured unit side resistance versus average uniaxial compressive strength, normal rock equation

 © Deep Foundations Institute 2025

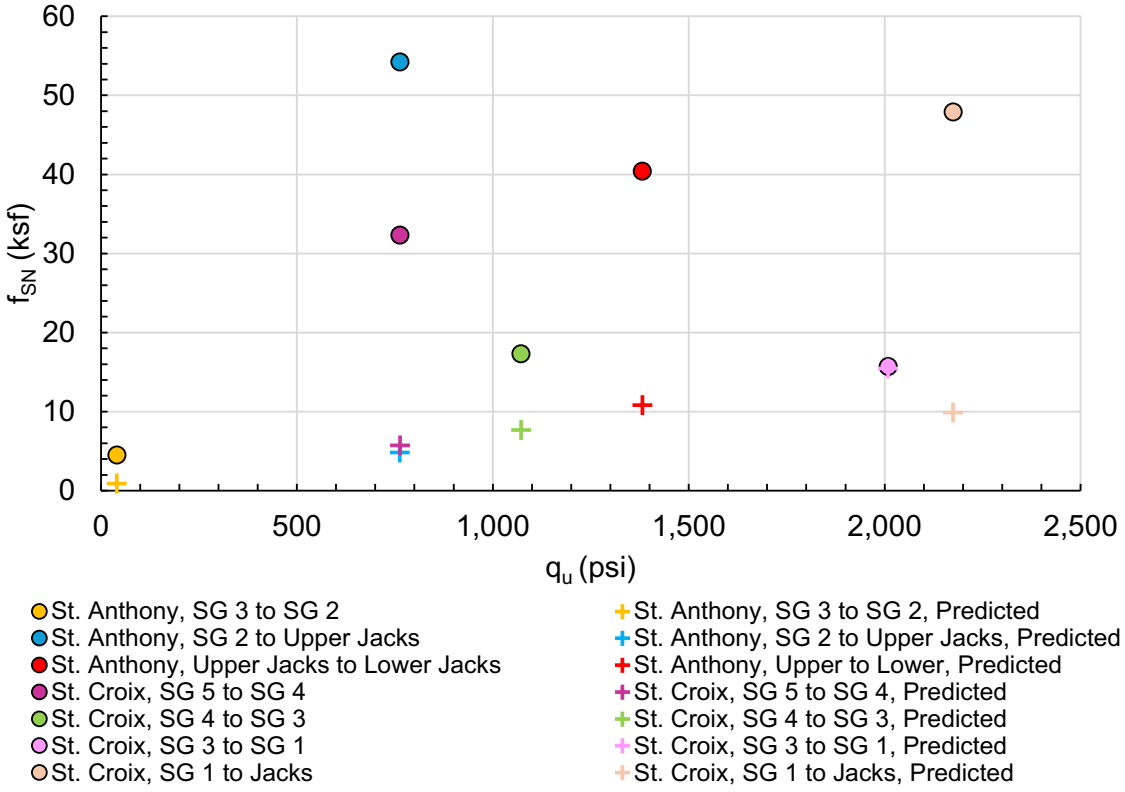


Fig. 7. Predicted and measured unit side resistance versus average uniaxial compressive strength, unstable rock predicted values

The predicted values are compared to those measured at St. Anthony an St. Croix in Fig. 8. The equation underpredicts unit base resistance for the St. Anthony Falls test, while it overpredicts unit base resistance for the St. Croix test. However, base displacement at the St. Croix test was significantly less than achieved at St. Anthony, and greater unit resistance could have been demonstrated since the strength limit state was not achieved, i.e., the mobilized unit base resistance is well below the nominal value based on visual inspection of the data.

There is an AASHTO and FHWA recommended equation for base resistance on fractured rock. It is a function of UCS, vertical effective stress, and Geologic Strength Index (GSI), which is somewhat subjective. Thus, an objective comparison to the measured values is difficult. Regardless, the range of reasonable GSI for the sandstone at these sites would result in significant underprediction compared to the measured unit base resistances.

 © Deep Foundations Institute 2025

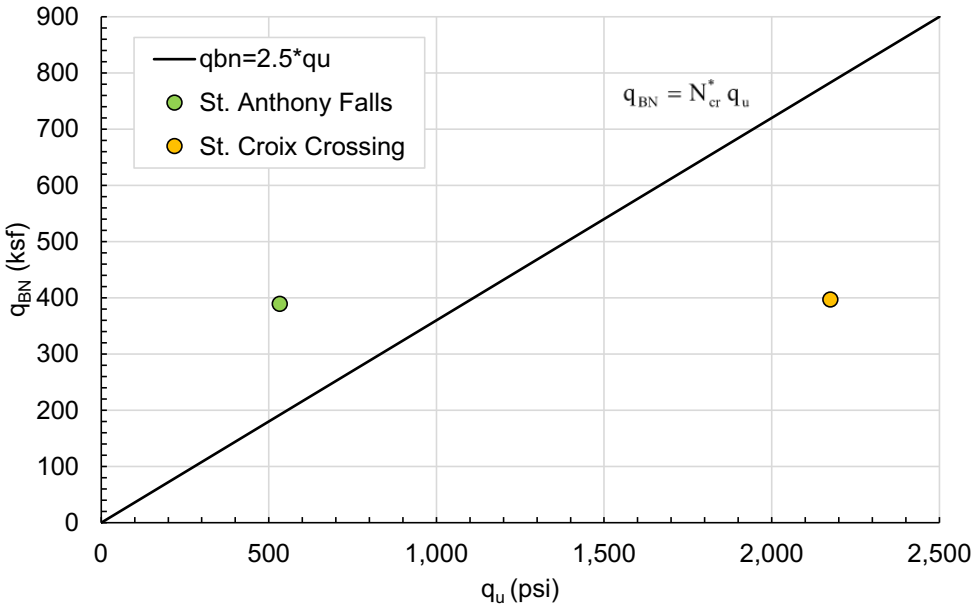


Fig. 8. Predicted and measured unit base resistance versus average uniaxial compressive strength, normal rock predicted values.

DISCUSSION

While these load tests indicate that the axial resistance in weakly cemented sandstone can be substantial and greater than empirical equations indicate, it should be noted that construction practices have a significant influence on axial performance. At the St. Croix site in 1995, a bi-directional load test was performed on a drilled shaft that did not perform nearly as well. The difference in performance is attributed to several differences in the construction and inspection practices (Axtell et al. 2013). Additionally, if groundwater conditions are not properly managed, particularly artesian conditions, axial performance can be impacted. Support fluid management, cleanout, proper reinforcing cage design, proper concrete mix design, concrete placement, and quality management are critical to axial performance in weakly cemented sandstone.

These load tests allowed production drilled shaft rock socket lengths to be reduced compared to what they would have been based on empirical design methods due to the better than anticipated axial performance and the allowed use of a higher axial resistance factor associated with performing a load test. The conditions at these sites favor load testing due to the difficulty in collecting bedrock data representative of the in-situ conditions. Because construction has a significant influence on performance in weakly cemented sandstone, constructing a non-production test shaft has the added benefit of serving as a demonstration shaft to validate means and methods.

SUMMARY AND CONCLUSIONS

These full-scale load tests demonstrate that weakly cemented sandstone can resist large axial loads exceeding the capacity of the bi-directional jacks for properly constructed drilled shafts. Furthermore, the load tests confirm side and base resistance are mobilized simultaneously at compatible displacements, a conclusion that is supported by the Axtell et al. 2022. Traditional

empirical design methods generally underestimate the unit side and base resistance that can be provided by rock sockets in weakly cemented sandstone. Where axial resistance controls, a drilled shaft design in similar material may benefit significantly from axial load testing, as it is the only reliable means of assessing axial performance in material that is so difficult to sample or properly characterize. Proper design, including comprehensive understanding of the subsurface conditions and groundwater pressures, proper construction, and informed quality verification are necessary to achieve the results demonstrated by these load tests. If drilled shafts are properly constructed in similar sandstone, similar axial performance may be expected.

ACKNOWLEDGEMENTS

The authors would like to thank all the people and organizations that contributed to these projects, including but not limited to Braun Intertec, Carl Bolander and Sons, Flatiron, Fugro-Loadtest, IaDOT, Keller (Case Foundation Company), Kraemer North America, Stalworth Underground, MnDOT, and Parsons.

REFERENCES

AASHTO. (2020). LRFD Bridge Design Specifications, 9th Edition.

Axtell, P.J., Brown, D.A., Lamb, R.A., D.G., Lamb, R.L., Graham, D.S., and Ryan, W.G. (2013) "St. Croix Bridge, Minnesota: The Influence of Construction on the Axial Resistance of Drilled Shaft Foundations in Weak Sandstone," Proceedings of the DFI 38th Annual Conference on Deep Foundations. Phoenix, AZ, USA. 25-28 September 2013.

Axtell, P., Turner, J., Turner, B., Jacobs, S., McIntosh, K., Vega, B., Hertlein, B., and Gomez, J. (2022) "Combined Side and Base Resistance in Rock-Socketed Drilled Shafts – A State of the Art Consensus," J. of Deep Foundations Institute, Vol. 16, No. 2, pp. 1-9.

Brown, D.A., Turner, J.P., and Castelli, R.J. (2018). Geotechnical Engineering Circular No. 10 (GEC 10) - Drilled Shafts: Construction Procedures and LRFD Design Methods, FHWA-NHI-18-024.

Gebhard, J.A., Lamb, R.A. (2009). "St. Anthony Falls, I-35w Bridge Drilled Shaft Load Test Program," Proceedings of the DFI 34th Annual Conference on Deep Foundations. Kansas City, MO, USA. 20-23 October 2010.

Glisson, M., Race, M., and Komurka, V.E. (2017). "Using Load Testing to Save Money and Time on the I-35W Bridge Project," Proceedings of the 34th Annual International Bridge Conference, The Engineers' Society of Western PA. National Harbor, MD, USA. 5-8 June 2017. pp. 662-667.

LOADTEST, Inc. (2007). Report on Drilled Shaft Load Testing (Osterberg Method): Test Shaft 2 – I-35 W over Mississippi River, Minneapolis, MN (LT-9401). November 26, 2007.

LOADTEST USA. (2012). Report on Drilled Shaft Load Testing (Osterberg Method): Test Shaft 1 – St. Croix River Bridge, Washington Co., MN (LT-9616). September 7, 2012.

LOADTEST, a division of Fugro USA Land Inc. (2024). Report on Drilled Shaft Load Testing (Osterberg Method): TS-1 - IA 9 Mississippi River Bridge Project, Allamakee County, IA (LT-238460-1). February 20, 2024

 © Deep Foundations Institute 2025

DIGITALIZATION IN REVERSE CIRCULATION DRILL RIGS

Nikolas Schmitz, HMH, Erkelenz, Germany, +49 2431 83-345, nikolas.schmitz@hmhw.com
Lukas Biedak, HMH, Houston, TX, USA, +17134173107, lukas.biedak@hmhw.com

ABSTRACT

The integration of digital technologies into reverse circulation drilling (RCD) rigs represents a pivotal advancement in the drilling industry, facilitating semi-automated operations with potential upgrades for full automation. This paper explores these innovations and evaluates their contribution to efficiency and safety enhancements. Automation of essential processes significantly reduces setup times and maximizes machine uptime, boosting operational efficiency. Furthermore, it allows remote rig operation enhancing safety, particularly in challenging site conditions. Central to these advancements is a logging tool that continuously records machine and drilling data. Logged data, coupled with sensors providing real-time feedback, form the basis for our advanced assistance tool that offers operators optimized drilling parameters, leading to maximized performance, enhanced safety, and reduced carbon footprint. Furthermore, it enables automatic adjustments to drilling parameters. The logged data is accessible from any device, supporting comprehensive reporting and analysis. Additionally, an analytics tool provides deep insights into drilling operations, generating reports on machine condition, suggesting optimized handling strategies, and providing borehole certificates stating verticality and depth. Another improvement includes the advanced Hydraulic Power Pack Control, which dynamically adjusts its performance based on real-time drilling needs, contrasting with traditional constant high-performance operations that consume more fuel.

Keywords: Digitalization, RCD, Reverse Circulation Drilling, Safety, HSE

OPERATIONAL MODES OF DRILLING

Currently, RCD rigs are operated manually, which means that drilling performance is significantly influenced by the operator's skills. However, modern control and automation technologies offer a solution to this reliance on human skills. By retrofitting the rig's hydraulics, sensors, and actuators and integrating state-of-the-art control system technology, it is possible to automate critical drilling processes via closed-loop controlled drives. In other complex drilling applications such automated strategies have been long established, and the drilling process can be controlled automatically with appropriate sensors and actuators.

While drilling a borehole, a fixed feed rate can be set and maintained by a drive system. This operational mode is known as “Rate of Penetration” (ROP). Throughout drilling, the force exerted on the drill bit is continuously monitored. If a disturbance occurs, like encountering hard geological formations, it is detected by an increase in contact pressure on the drill bit, prompting the system to automatically decrease the feed rate. Thus, this drilling technique is a position or speed control with active force monitoring.

Another type of automatic drilling is "Weight on Bit" (WOB). In this method, drilling is regulated based on the force at the drill bit on the borehole surface. The feeding unit is controlled to ensure that the drill bit follows a predetermined target force. Meanwhile, specific limits, such as the current feed rate, are continuously monitored. Should these limits be exceeded due to actual drilling conditions—such as when drilling into a cavity—the system automatically limits the feed rate. This process is a force control with speed monitoring.

 © Deep Foundations Institute 2025

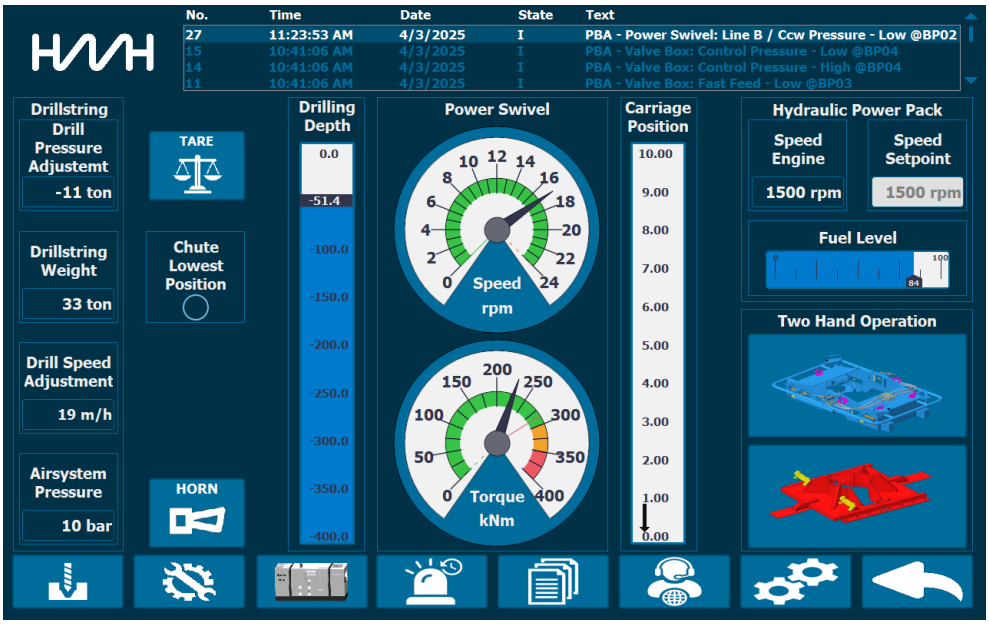


Fig. 1. Drilling Modes in RCD Rigs

In the operation of an RCD rig, another drilling mode focuses on monitoring and controlling the torque at the drill bit. The drilling torque is generated by the power swivel, a hydraulically driven rotary motor located in the drill mast and is transmitted to the drill bit via the drill pipe. The torque is maintained at a set value by adjusting the feed movement, ensuring consistent torque during drilling.

The RCD rig's drive system comprises two vertically arranged hydraulic feed cylinders within the mast, linked to the power swivel by a carriage. By integrating these two cylinders into a servo-hydraulic control loop, all the aforementioned automatic drilling operations can be executed on an RCD rig.

Control system upgrades in the RCD Rig

Once the cylinders, carriage, and power swivel of the RCD rig are managed with position and force control, it not only enables automated and efficient drilling, but also enables the automation of secondary processes, such as the automated installation or removal of drill pipes. The long-term objective is to develop a fully automated and controlled drilling plant.

To ensure precise displacement or speed control, dynamic proportional valves are required as hydraulic actuators, and the cylinders are to be equipped with a displacement measuring system. For force control, which is crucial for WOB, pressure sensors are placed on the ring and bottom sides of the feed cylinders. These sensors provide the pressure readings necessary to directly determine the force exerted by the two cylinders.

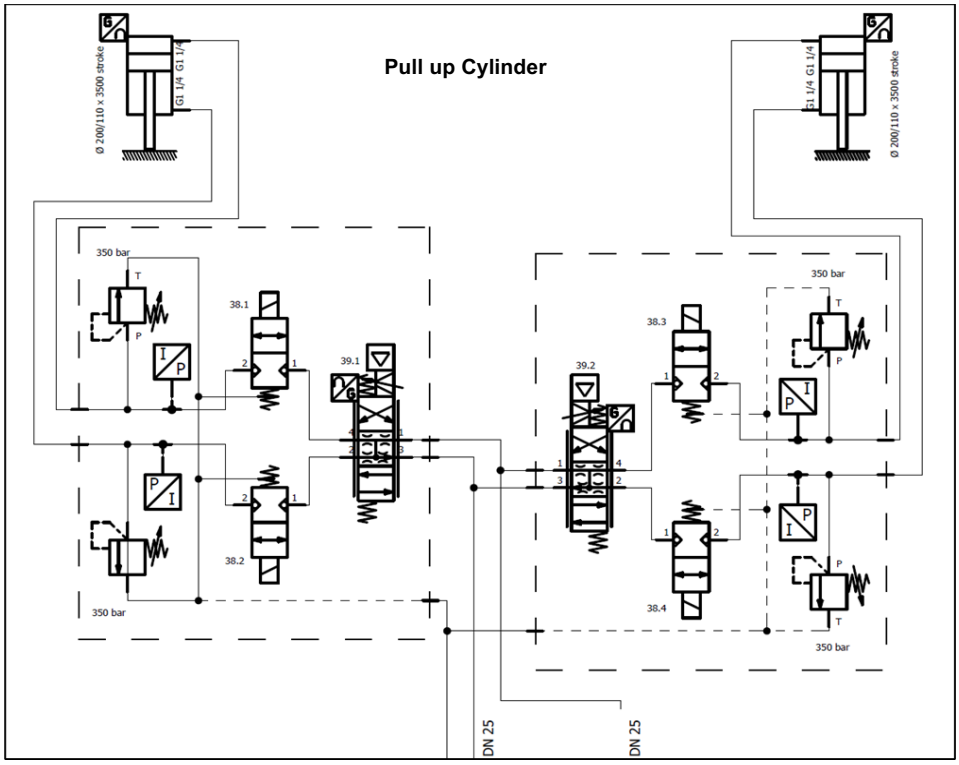


Fig. 2. Servo hydraulic control of the pull up cylinders

Figure 2 illustrates the main components of the hydraulic control circuit. In addition to the two servo valves, four pressure sensors determine the force balance on the two cylinders. Displacement measuring systems are installed on each cylinder to accurately track their position. Additional safety functions are provided by other valves, such as blocking or pressure relief valves.

In addition to the hydraulic actuators and the sensors, an appropriate control concept is required to implement the described functions. The control system must at least contain the following functionalities:

- Position and speed control
- Force control
- Synchronization control between the two cylinders
- Switchover between position and force control
- Setpoint generators for force and displacement control

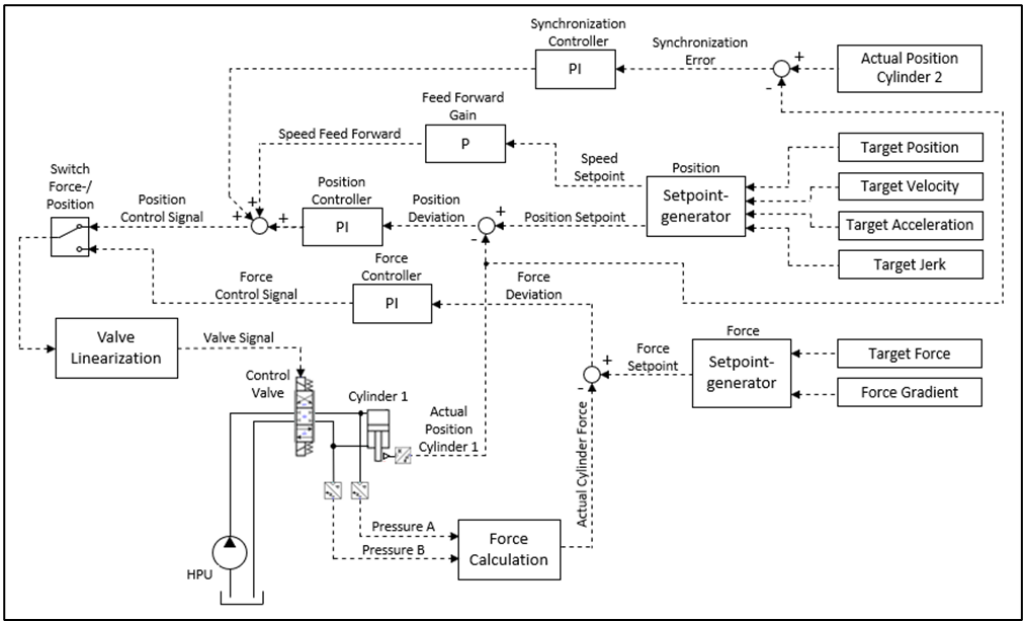


Fig. 3. Controller structure for one cylinder

Figure 3 illustrates the control concept for a cylinder axis, consisting of a switchable position and force controller. Another controller is implemented between the two axes to support accurate synchronization of the cylinders. The controller structure for the second cylinder is identical and thus not depicted. A crucial aspect of stable position control is the generation of the setpoint signal. For this purpose, a setpoint generator has been developed to determine a continuous trajectory of movement in form of setpoint acceleration, velocity and position. The acceleration as such does not allow any spikes or jumps. This can be achieved by limiting the derivative of the acceleration, i.e. the jerk.

In the current configuration, desired movement trajectories can be generated based on freely parameterizable maximum speed, maximum acceleration and maximum jerk. The control system was developed and optimized during the early development phase using dynamic system simulation. Below are results from the simulation, offering insights into the expected system behavior and anticipated control accuracy. Figure 4 depicts the movement sequence based on the positioning of the drill head and drill pipe. The trajectory specified by the setpoint generator when lifting the load by 0.4 m is illustrated in red, while the actual position of the drilling equipment, based on the position of cylinder 1, is shown in green. The control deviation, which is the difference between the setpoint and the actual position, is depicted in the figure below for cylinders 1 and 2. It shows that the control deviation reaches a maximum of 10 mm during the cylinders' movement. Once the setpoint has reached the target value of 1.4 m, the controller rapidly pulls the axes to position, reducing the control deviation to near zero within a few seconds.

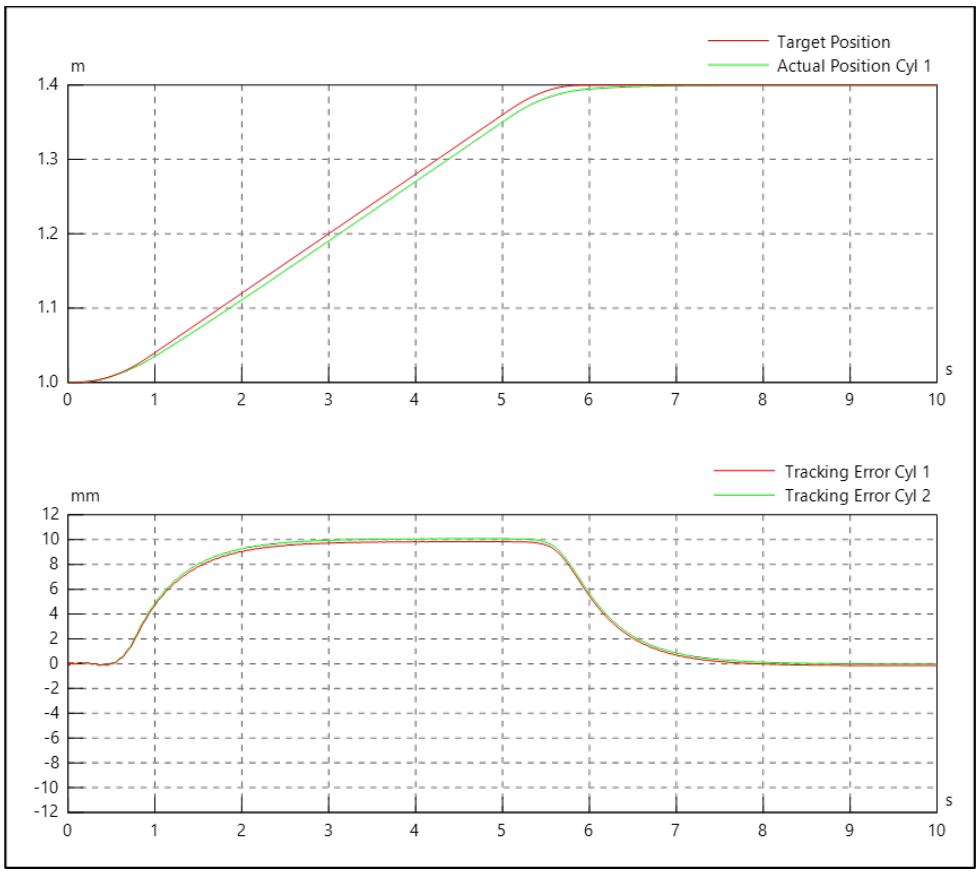


Fig. 4. Lifting movement of drill string – positions (top) and control deviations (bottom)

The comparison of the cylinders' control deviations shows the synchronization error, i.e. the deviation of the cylinder positions from each other. This error is notably minimal, measuring less than one millimeter. Whereas in previous systems cylinder's synchronization is forced by the mechanical connection of the cylinder and the drill mast, position differences are now automatically corrected. This automatic compensation reduces mechanical stress on the drill mast and the crossbeam between the cylinders.

In addition to position control and force control, also switching between the two types of controllers have been investigated. Figure 5 illustrates, in the upper section, the target and the actual position of the drill bit. Below this, the target force of the drill bit is depicted in red, the current contact force is displayed in green. The force threshold for deactivating position control and activating force control is represented by a blue line, set at 20 kN in the diagram. The target force is 400 kN and the force gradient to approach the target force was parameterized to 200 kN/s.

 © Deep Foundations Institute 2025

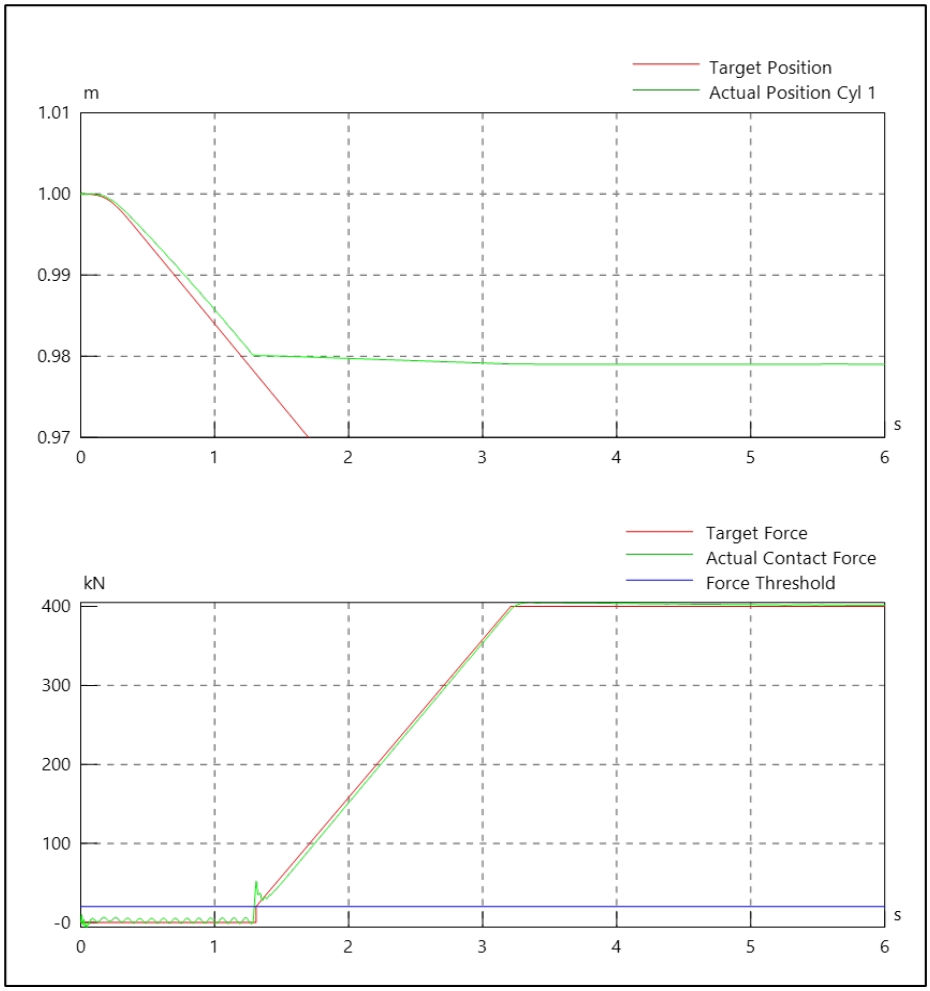


Fig. 5. Switchover from position to force control

At time t = 0 seconds the drill bit is positioned 20 mm above the borehole surface. With a target speed of 0.02 m/s the drill bit then slowly moves towards the ground. The contact force of the drill bit is constantly monitored and measured via the cylinder pressures. At t = 1.3 seconds, contact occurs between the ground and the drill bit, resulting in a rapid increase of contact pressure (WOB). Once the force reaches 20 kN, the control signals of the control valves are no longer influenced by the position controller but by the force controllers of the two cylinders. The target force then increases linearly from the force threshold to the target force using the defined force gradient.

As previously described for position control, force control also demonstrates very good and stable control behavior with only minor deviations. Further simulations for different operations and scenarios have been performed. Switching between the WOB mode and the ROP mode also performs robustly and satisfactorily.

IMPROVEMENTS OF AUTOMATION FOR RCD OPERATIONS

Performance improvements

The new RCD rig's key enhancements include electrically controlled valve systems, process instrumentation, a state-of-the-art machine controller, and drilling operations via a touch control panel.

 © Deep Foundations Institute 2025

These components are managed through a programmable logic controller (PLC), enabling both partially and fully automated processes. Additionally, a digital Human Machine Interface (HMI) and electric joystick control provide more intuitive and ergonomic operation.

During drilling, different sensors provide continuous feedback to automatically maintain parameters such as WOB. This results in increased penetration, reduced wear and tear and consequently a faster drilling process and higher machine uptime.

The automation of core processes, such as adding drill pipes or stabilizers, reduces set-up times, increases machine uptime for drilling, thus enhancing efficiency. Partially automated piping is now possible, allowing predefined positions to be automatically reached using position sensors. This enables faster and parallel movements of the power swivel.

Moreover, a wireless remote-control panel is available for operations such as easier piping connection. This wireless control allows the operator to be close to precise and critical operations, improving visual control and sensitivity. Consequently, less manpower is required for tasks such as connecting the drill pipes or stabilizer.

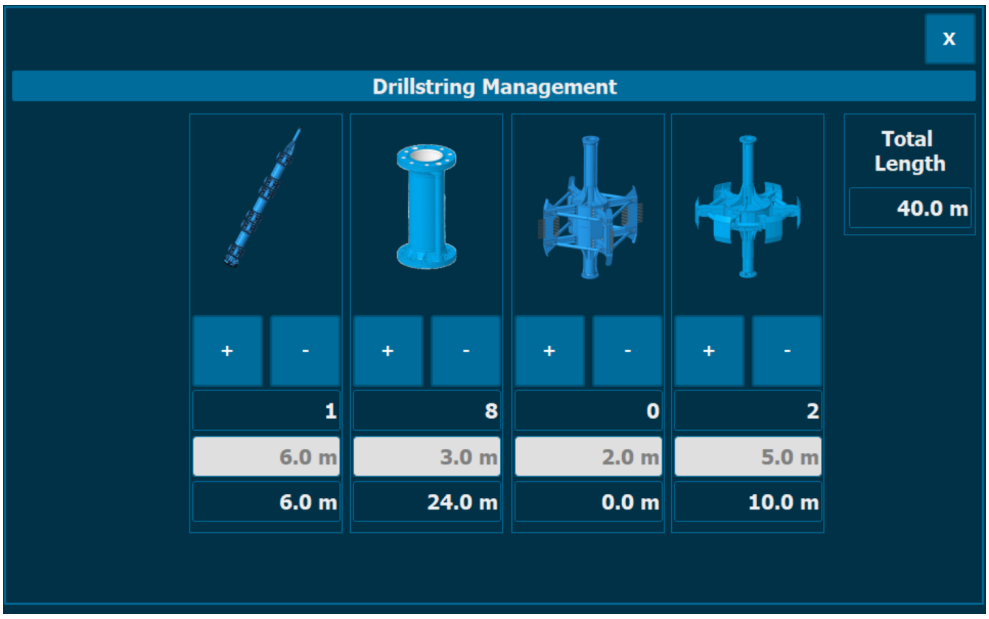


Fig. 6. Drillstring Management

A drill string management system calculates the length of the drill string and stores the position of each component in the string, as illustrated in Fig. 6. This allows the operator to know precisely when to add or remove a stabilizer. Automatic balancing of the drill string is achieved by measuring the pressure difference between the two mast cylinders and the position of the carriage. The display at the HMI clearly visualizes functionalities such as automatic balancing, reducing the chance of misinterpretation compared to traditional pressure gauges and symbols. Additionally, automatic alignment of the work platform for inclined structures is possible through a tilting sensor. Controlled flow of compressed air is also facilitated to ensure optimal removal of cuttings from the borehole.

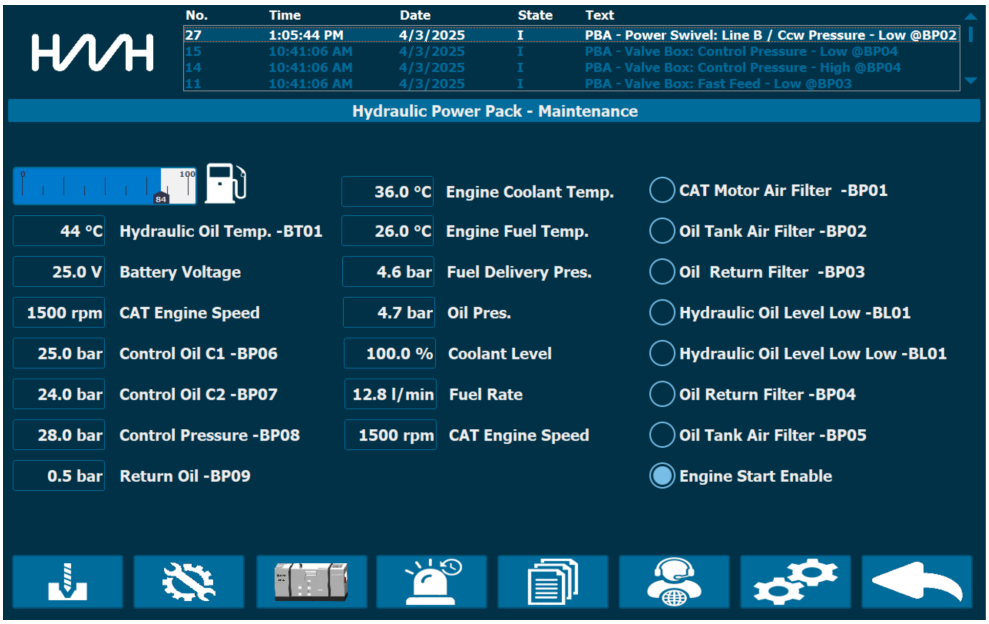


Fig. 7. Hydraulic Power Unit

A new touch panel within the hydraulic power unit (HPU) enables selection of appropriate pressure limits for different types of machines. This panel can also be used for HPU maintenance or for the overview of all parameters and sensors inside the HPU, as illustrated in Fig. 7.

The automated control of the hydraulic oil coolers ensures optimal oil temperature, even at low temperatures. Activity of the cooling fan is adjusted to actual requirements, thereby reducing noise level and speeding up the operational readiness of the RCD rig, even in cold conditions.

Data recording/Use of data

All measured values can be displayed and evaluated on a trend screen, which also includes historical data. Drilling trends and processes are recorded and stored, such as drilling depth, thrust, torque, WOB, ROP, rpm of the power swivel, angle deviation of the drill bit, improving control of the drilling direction and angle. Such functionality is essential for maintaining borehole verticality, especially in applications like secant wall drilling.

All stored data can be exported in raw, csv or pdf formats. The HMI provides documentation that includes the user manual, hydraulic and electrical schematics for easy maintenance. Additionally, videos for detailed introductions to specific operations or processes can be included.

 © Deep Foundations Institute 2025

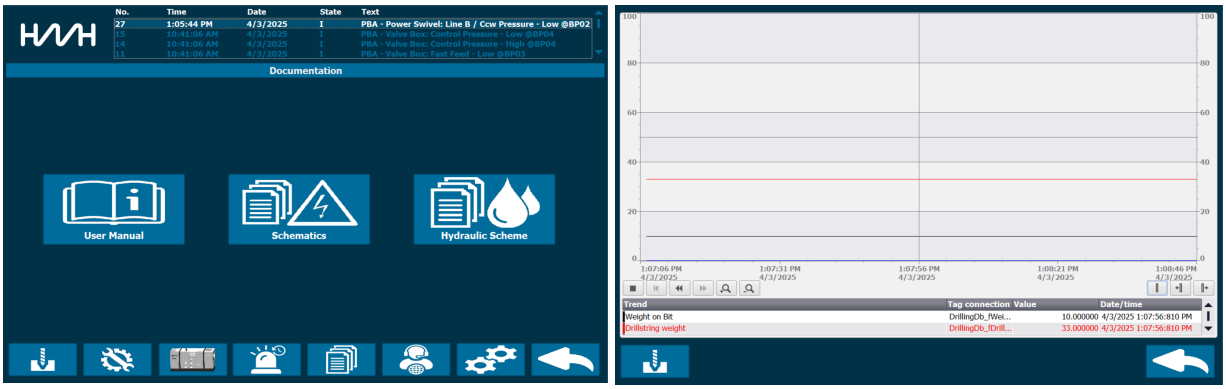


Fig. 8. Access to data

Remote support via remote access

Remote support for the RCD rig is available through the Global System for Mobile Communications (GSM), Wi-Fi or Ethernet. All available machine and drilling data are stored and illustrated within a cloud-based application, accessible at any time to both customer and supplier's service personnel. This results in continuous improvement of the software through drilling data analysis, as well as predictive maintenance, enhanced machine productivity, and reduced unplanned downtime with better insights and faster access. All data provided within the cloud-based dashboard can be used in real time by the customers for warnings, status and instructions to resolve an issue or to improve current process.

Insights into all machine data for all machines are provided within a single cloud-based platform. A smartphone and tablet app are also available, and software updates can be performed at any time on the construction site.

Fuel consumption

With the RCD rig's control system upgrade, the HPU can achieve a fuel reduction of between 8% to 22%, depending on the type of HPU. In the past, HPUs were typically operated at a constant high-performance level with related high fuel consumption. Now, a new interface between the machine controller and the power unit has been established, allowing performance regulation of the HPU according to actual drilling operation needs. Monitoring hydraulic oil flow and pressure throughout the whole system enables performance-related control of the diesel engine and connected hydraulic pump. This ensures the optimal working range of the engine and reduces fuel consumption. Before increasing diesel engine speed, the hydraulic pump is fully utilized to its performance limit by controlling the pump swivel angel to maintain fuel consumption as low as possible. Improved air coolers control further reduces the required engine capacity.

Health, Safety and Environment (HSE) aspects

Since operating conditions are continuously monitored, critical conditions can be easily recognized at an early stage. If the operator does not respond to messages or indications, the machine automatically reacts and initiates a safe state. A loss of tension at the clamping device initiates a stop of operation.

Operator usability is significantly improved with an ergonomic joystick, touch panel and radio remote panel, as illustrated in Fig. 9. The radio remote panel not only improves overview for the operator but also allows to remotely operate the rig in challenging site conditions, such as clamping the rig onto the casing without the operator being on the platform.

The PLC-controlled drilling process reduces noise and vibration of the RCD rig. As explained in the previous chapter, dynamic control of the diesel engine minimizes fuel consumption and noise level of the HPU.

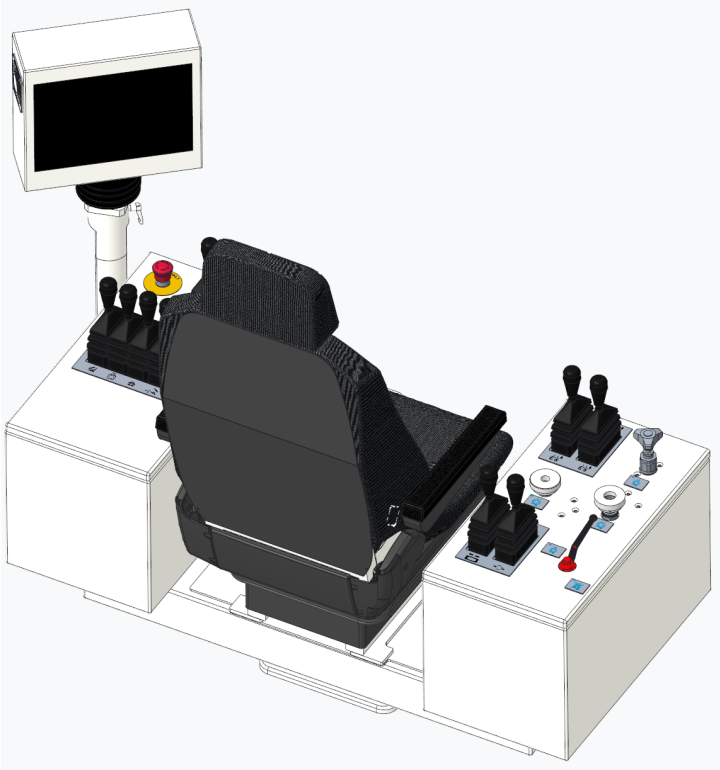


Fig. 9. Operator Chair

SUMMARY AND CONCLUSIONS

The integration of advanced digital technologies and automation into reverse circulation drilling (RCD) rigs signifies a transformative step in the drilling industry. This paper has illustrated how these innovations enhance the reliability and precision of operations, bolster safety, and reduce fuel consumption. By automating essential drilling processes, enabling real-time data analysis and feedback, and introducing dynamic control of resources, RCD rigs can better meet the rigorous demands of modern drilling activities.

The improvements in control systems allow for seamless, exact operation modes like "Rate of Penetration" (ROP) and "Weight on Bit" (WOB), while the enhanced HSE features substantially mitigate operational risks, particularly in challenging environments. The dynamic adjustment of the Hydraulic Power Pack ensures optimal fuel efficiency, aligning with sustainable industry practices.

This advancement not only maximizes operational efficiency and safety but also paves the way for future developments in fully automated drilling operations.

 © Deep Foundations Institute 2025

USACE-DFI WORKING GROUP ON SEEPAGE CONTROL

Mary Ellen Bruce Large, P.E., BC.GE, Nicholson Construction Company, Canonsburg, Pennsylvania, USA, +1 (412) 997-4829, maryellen.large@nicholsonconstruction.com
David Paul, P.E., Paul Geotek Engineering, LLC, Denver, Colorado, USA, paulgeotekeng@comcast.net
Gianfranco Di Cicco, GDCONSULTING, LLC, Tampa, Florida, USA, GDCons2015@gmail.com
April Fontaine, P.G., U.S. Army Corps of Engineers, Washington, District of Columbia, USA, april.l.fontaine@usace.army.mil
Erik James, P.E., G.E., P.G, U.S. Army Corps of Engineers, Sacramento, California, USA, Erik.W.James@usace.army.mil

ABSTRACT

Since 2011, Deep Foundations Institute (DFI) has enjoyed a collaborative relationship with U.S. Army Corps of Engineers (USACE) and other federal agencies aimed at aligning expectations and promoting mutual understanding between industry and the government on seepage control projects for dams and levees. The working group activities started with a technology transfer workshop to support USACE's plan to contract hundreds of millions of dollars to construct seepage barriers for the rehabilitation of dams and levees, and their planned development of a seepage control guidance manual. The success of this workshop led to a series of other activities that have further cemented a relationship between government engineering agencies and industry contractors, engineers, and material/equipment suppliers. This paper will present the working group activities conducted over the past 14 years and highlights the results of this very successful, mutually beneficial, and engaging collaboration. It is hoped that this innovative and committed working relationship will inspire other groups to work together in similar ways.

Keywords: working group, government, collaboration

INTRODUCTION

In May 2011, USACE representatives met with contractors and equipment manufacturers in Europe to learn about new cutoff wall technologies. This visit was intended to collect information to be incorporated into a USACE-wide engineering manual and establish relationships with parent companies of U.S.-based specialty contractors being retained for high profile domestic cutoff wall projects. During this trip, DFI Trustee Gianfranco DiCicco met with Dave Paul (at that time USACE Lead Engineer for Dam Safety, now also DFI Trustee) and suggested that DFI would be eager and able to collaborate with the USACE. The goals were to create a forum to discuss state of cutoff wall practices, provide information on new technologies for input to the manual, and introduce advancements for the planned major dam rehabilitation projects in the U.S. This initial suggestion started the ball rolling toward what would become a long-lasting and successful partnership. Over the past 14 years, the USACE-DFI Working Group has focused efforts on aligning expectations and promoting mutual understanding between industry and the government on seepage control projects for dams and levees.

The working group has solicited involvement over the years from other government agencies, including U.S. Bureau of Reclamation (USBR), Tennessee Valley Authority (TVA), National Resource Conservation Service (NRCS), Federal Emergency Management Agency (FEMA), and Federal Energy Regulatory Commission (FERC). This collection of agencies was originally organized to share technical, contractual, quality, and research information broadly to improve practices and limit litigation on large seepage cutoff projects. Through DFI-organized conferences, sessions at military and other external events, meetings, signed memoranda of understanding between USACE and DFI, and two additional workshops (2016 and 2023), the working group addressed challenging practices that inhibit progress and execution of seepage control projects and promote safety, quality, equitable risk sharing, and technical success.

 © Deep Foundations Institute 2025

This paper archives the working group activities conducted over the past 14 years and highlights the results of this successful, mutually beneficial, and engaging collaboration. It is hoped that this innovative and committed working relationship will inspire other groups to work together in similar ways.

THE FIRST WORKSHOP (2011, DEERFIELD BEACH)

In 2011, David Paul was serving as Lead Engineer for Dam Safety at USACE. As an active participant in the European working group for cutoffs, together with Di Cicco, they suggested continuing the technical exchange between USACE and DFI. They suggested organizing a technology transfer workshop to present updated and innovative methods and practices used for constructing seepage control barriers. The workshop was prompted by USACE's plan to contract hundreds of millions of dollars to construct seepage barriers for rehabilitating dams and levees, and their planned development of a seepage control guidance manual. In addition to broad representation from USACE, the workshop attendance (Fig. 1) was expanded to include USBR, TVA, and NRCS and FERC with the intent of providing an industry-wide forum for discussion of technologies, quality assurance and control methods, and research needs for seepage control practices.



Fig. 1. Attendees first USACE-DFI workshop (Deerfield Beach, 2011).

DFI specialty contractor, engineering, and manufacturer members involved in cutoff wall construction for dams and levees were invited to attend. The meeting topics were discussed among the DFI and government attendees, and while maintaining a strong desire for state-of-the-art technical presentations, the planning discussions also revealed significant interest in receiving contractor input on quality assurance/quality control (QA/QC) and acceptance criteria methods, specifications, and contractual/ procurement practices. It was acknowledged that the "best jobs" are those on which the USACE and the contractor adopted a team/partnering attitude. It was agreed that a collaborative pursuit of successful projects includes applying a partnering approach, and encouraging mutual understanding of goals, technologies, appropriate specification models, responsible contracting and procurement processes, and effective QA/QC procedures. A partnering approach results in safer, higher quality, less costly projects while reducing possible claims and delays during project execution.

Representatives from each agency presented their technical programs for dam and levee safety, and DFI contractor and engineer members presented on the following topics:

- State-of-the-art of cutoff wall technologies.
- QA/QC methods and acceptance criteria.

- Specifications and standards.
- Contracting and procurement practices.

The workshop topics were sequenced from technical to contractual with the goal of fostering an atmosphere of open sharing that would promote good communication and improved cooperation between the stakeholders. Invited contractor presentations progressed from outlining best practices and successes (what works) to topics that require further research or study (what does not work). DFI invited contractors to collaborate on technical content such that an industry perspective was presented. Presenters served as spokespersons for the industry, as opposed to representatives of individual companies. This may have been one the first times for such a cooperative approach, and this collaboration would continue. DFI coordinated the presentations, incorporating minority and majority opinions thereby giving rise to a lively discussion. USACE remained open to constructive discussion and potential improvements to the standard contract documents and technical specifications.

The cooperative and constructive atmosphere that was created allowed frank and open discussion of stakeholder goals. Strong facilitators guided discussions and encouraged constructive results. DFI developed detailed notes and the guts of a strategic plan for a collaborative forum for developing tools for delivery improvement and an improved process for future projects.

PARTNERSHIP ESTABLISHED

DFI and USACE signed the first memorandum of understanding (MOU) in 2013. This agreement was re-signed in 2018 and 2023, each with a 5-year duration. The MOU states that the purpose of the MOU is to "establish a cooperating relationship to address our mutual participation in the Nation's dam and levee safety programs. Our common goal is to enhance the safety of dams, levees and coastal area construction and rehabilitation projects to improve quality and safety while lowering project risk and cost."

The MOU outlined the following understanding for dam, levee, navigation, coastal area performance for the national infrastructure:

USACE

- Encourage continuing dialogue between USACE and DFI on issues of importance.
- Promote a comprehensive approach to sustainable development.
- Advance the state-of-practice through innovative rehabilitation solutions.
- Promote professional, ethical, and sustainable practices.
- Enhance the public image of all parties involved.
- Identify research and development needs.

DFI

- Facilitate communication among deep foundations industry practitioners.
- Promote qualifications-based selection procurement.
- Promote development and use of peer review and consensus standards and guidelines for design and construction.
- Increase diversity of the dam safety engineering profession.
- Promote the foundation construction industry to young people as a rewarding career.
- Promote the importance of maintaining and rehabilitating the nation's water infrastructure.
- Encourage these activities through promoting DFI membership, continuing education, professional registration and development.

BROADENED OUTREACH

United States Levee Safety Coalition

Recognizing the aligned work and contributions of other professional organizations, DFI joined the United States Levee Safety Coalition (Coalition) in 2013. This group is led through Association of State Dam Safety Officials (ASDSO) (https://damsafety.org/levee-safety), and includes American Society of Civil Engineers (ASCE), DFI, National Association of Flood and Stormwater Management Agencies (NAFSMA), United States Society on Dams (USSD), and American Council of Engineering Companies (ACEC). The primary focus of this group is life safety, and the mission is to advance levee safety across the country through good engineering practices, sound public policy, and increased awareness and education within communities of practice and the public. The root causes of many of the levee rehabilitation issues that lead to life threatening levee situations exist below ground, and DFI member companies develop the foundation solutions to address these challenges. Through DFI's technical committee structure, DFI supports the Coalition's policymaking, negotiations, and advocacy with technical expertise that promotes projects with high quality, increased safety, improved communication, more sustainable practices, and increased cost effectiveness.

The Coalition has been active in meeting with U.S. Congress representatives to support legislation that funds dam and levee safety programs. In 2019, the Coalition (Fig. 2) met with House and Senate appropriators to reinforce the life safety importance of this work and encourage full funding ($79 million) of the National Levee Safety Program (NLSP). The NLSP was authorized under the Water Resources Reform and Development Act (2014) and reauthorized through 2023 by America's Water Infrastructure Act (2018) to promote consistent safety standards, create levee safety guidelines, and provide funding assistance to states and regional districts for establishing participant levee safety programs.



Fig. 2. U.S. Levee Safety Coalition members on Capitol Hill (2019).

 © Deep Foundations Institute 2025

Midwest Levees Technical Exchange (2014, St. Louis)

DFI prepared a session at the Midwest Levees Technical Exchange in 2014 in St. Louis. The goal of the session was to share with government agencies (USACE, Society of Military Engineers) new technologies for levee repair and rehabilitation and to highlight the role of DFI in supporting the entire geo-foundation industry to improve cooperation and partnership for promoting enhanced quality, safety, durability, and sustainability. Presentations covered the working group activities, ground improvement techniques, slurry trenching, sheet piling, self-hardening slurry, and trench mixing applications.

DISASTER RESPONSE

Hurricane Sandy (2012)

Hurricane Sandy devastated communities and coastal areas along the Atlantic region of the United States in October 2012. In August 2014, USACE provided a briefing of rehabilitation plans for DFI members including impacts, legislation, recovery project overviews, and agency objectives. The meeting was held to emphasize that the recovery program was one of USACE's top priorities and that they would continue to work closely with partners to complete the recovery mission and sustain open communication and transparency. DFI members were honored to be part of these discussions.

Levee and Coastal Restoration Conference (2014, Miami)

The extent of the Hurricane Sandy disaster, which followed the devastating effects of Hurricane Katrina six years earlier, prompted DFI and the working group to lead an industry-wide levee and coastal restoration conference. This event brought together nationwide organizations to share and discuss programs and practices for seepage cutoff and ground improvement/foundation strengthening projects for levee and coastal restoration. The program was one of the first times that a DFI conference focused on agency presentations to solicit input from DFI members on planning requirements and technical needs.

Agencies provided updates on specific project recovery work, including Hurricane Sandy, Katrina rebuild and Lower Mississippi levee issues, Gulf Coast restoration programs, and Sacramento Area Flood Control projects. Representatives from USACE, USBR, NRCS, and FERC provided additional overarching agency program overviews, and DFI members presented relevant technique presentations and case histories. The goal of the conference was to connect agencies with DFI members who have specific technical expertise to meet the demands of the recovery work.

DFI 41st Annual Conference (2016, New York)

DFI's Annual Conference in 2016 marked the first time DFI's annual conference was expanded to include a successful parallel track, focusing on seepage control and lead by Dave Paul with the support of Mary Ellen Large (at the time with DFI, now with Nicholson Construction Company) and Gianfranco Di Cicco. The program included keynote presentations from USACE and from the World Bank on their policy, strategy and lessons learned. The seepage control technical track covered international case histories on barrier wall applications executed through a broad variety of foundation techniques. This was the first time the DFI annual conference reach the 1000 attendees mark thanks to the additional track.

DFI 49th Annual Conference (2024, Denver)

As the working group began rekindling it energy, DFI organized the annual conference in 2024 to have a second water-related track. The conference was titled, "Water-Resiliency-Infrastructure," and the water-

related track showcased programs, practices and projects focused on groundwater and surface water. Keynote lectures and panel discussions presented agency perspectives on advances and resiliency of water infrastructure. Involvement from USACE, USBR, TVA, FERC and private water generators presented the owner viewpoints that the industry needs to hear to be positioned to respond to needs and demands.

TECHNICAL INPUT TO FEDERAL GUIDANCE

Engineering Manual on Cutoff Walls

USACE included DFI input to their developing engineering manual on cutoff technologies. The manual will cover all cutoff wall technologies, including panels, secant walls, deep mixing, jet grouting and grout curtains. USACE provided the draft manual to DFI committee members for a thorough review, and DFI engineers, contractors, equipment manufacturers, material suppliers, and researchers provided hundreds of comments reflecting an industry-wide perspective. Working group members met in Nashville, Tennessee to review and respond/resolve each comment. The level of teamwork and focus on a common goal was outstanding, a testament to the trust that had been building through the working group.

At the same time, DFI's Slurry Wall Committee (now called DFI Structural Slurry Wall and Seepage Control Committee) was preparing a document titled, "Guidelines for Selecting Cutoff Wall Systems," (published 2021). Due to the alignment of the content, the USACE members provided reciprocal feedback on the development of the DFI document. Recognizing that the documents served different audiences (public/private), the content was not made the same in all areas. The documents are compatible and not conflicting.

Technical Guide Specifications

In 2023, working group members along with DFI Committees on Soil Mixing and International Grouting provided detailed comments to USACE on guide specifications for foundation grouting, limited mobility grouting in soil, and deep mixing. DFI members provided consensus comments aimed at ensuring the specifications represent the state of the practice.

WORKING GROUP MEETINGS AND WORKSHOPS

Working Group Meeting – San Francisco – Deep Mixing Conference (2015, San Francisco)

In conjunction with DFI's Deep Mixing Conference in San Francisco in 2015, the working group held a meeting with the USACE Sacramento District to identify specific project issues related to the Natomas/American River projects and discuss general cutoff wall practice issues. The discussions were aimed at defining topics for a detailed program agenda for a follow up workshop to the Deerfield Beach event). The topics of the meeting focused on specifications, materials/longevity/permanence, QC/QC, alternative technologies, mix designs, sampling methods (wet grab/coring), bentonite slurry hydration, and others.

Second Working Group Workshop, Sacramento 2016

The second working group workshop was held in Sacramento, California on November 15-16, 2016. Over eighty engineers, contractors, and researchers from USACE and industry attended (Fig. 3). The primary goals of the workshop were to

- Identify and discuss technical topics, contractual issues and procedures where USACE specifications differ from responsible, conventional and customary practice.

- Recommend changes to specification language and practices that will improve communication and quality, and reduce delays, confusion, and litigation on seepage control projects.
- Identify research needs or other actions required to implement recommended changes.



Fig. 3. Attendees second USACE-DFI Workshop (Sacramento, 2016).

DFI members, USACE and regional engineering consultants developed workshop presentations on the following main topic areas:

- Design considerations.
- Products.
- QC/QA testing requirements.
- Roles and responsibilities of designers and construction managers.
- Acceptance criteria.
- Long term performance.

DFI members worked together again to prepare consensus presentations, and workshop discussions outlined proposals for practice changes and associated processes and timelines.

Third Working Group Workshop (2023, Denver)

The third USACE-DFI Workshop on Seepage Control Practices was held at USACE's Risk Management Center in Lakewood, Colorado, on November 15-17, 2023. Sixty attendees joined the 2½- day workshop, comprising USACE representatives from 13 districts, USBR, FERC, and DFI contractor and engineering consultant members (Fig. 4).

A team of USACE representatives and DFI members led the workshop organization, including April Fontaine (USACE, Headquarters), Erik James (USACE, Sacramento), Gregg Batchelder-Adams (USACE, RMC) David Paul (Paul GeoTek Engineering, LLC), Gianfranco Di Cicco (DFI President at the time, now GD Consulting, LLC), Mary Ellen Large (Nicholson Construction), and Theresa Engler and Matt Glisson (DFI). The leaders met weekly for several months to develop the workshop agenda, and they facilitated broader meetings with members to prepare industry-consensus presentations for the workshop.



Fig. 4. Attendees third USACE-DFI workshop (Denver, 2023).

This workshop was aimed at rekindling relationships between DFI leaders/members and government agencies. The hope was to reestablish the forum which had lost momentum after the 2016 workshop and then stalled during COVID. The group was ready to get jump started again, tackle some of the unaddressed topics from the 2016 workshop, and find new topics. Topics focused on project quality and included parallel presentations from the government agencies and industry to highlight different views and priorities. Topics included recent challenges and successes, newly developed guidance, data management, plastic concrete, materials selection, quality control/assurance and testing methodologies, and long-term performance. Attendees participated in active breakout sessions with discussion and debate. Each breakout had the directive to define the next steps and timelines to implementing improvements to seepage control practices. The following facilitators from DFI and USACE led these breakout sessions to productive conclusions:

- Design and geotechnical pre-construction data – Mark Stanley (HDR), Gregg Batchelder-Adams (USACE, RMC), and Mark Petersen (Black & Veatch)
- QC/QA and Acceptance Criteria – Michael Arnold (Bauer Foundations) and Steven Shifflett (USACE, Louisville)
- Data management practices – Jamey Rosen (Geosyntec), Laurel Robison (USACE) and Jeff Burton (ACT)
- Materials, products and plastic concrete – Dominic Parmantier (Condon Johnson), John Murphy (USACE ERDC) and Gilbert Tallard (Liquid Earth Support)
- Specifications – Luca Barison (Nicholson) and Bill DeBruyn (USACE, Dam Safety Modification Mandatory Center of Expertise)
- Long term performance – John Rice (Utah State University), Erik James, (USACE, Sacramento) and Mark Petersen (Black & Veatch)

The product from this workshop is intended to be a series of flyers that present industry-agreed practice on seepage control issues. It is envisioned that these flyers are downloaded and used to support specification development and technical processes on seepage control projects. DFI and USACE representatives volunteered to serve on task forces to further discussions on the topics identified in the workshop and develop the flyers. The task forces meet monthly to create and debate content and prepare these publications. The flyer topics include:

Specifications

- Company and personnel requirements (key personnel) need to be reasonable and achievable by the industry.
- Out-of-date specifications that do not represent current materials or practices.
- Specialty subcontractors need to be included in discussions between prime contractors and owners that pertain to the subcontractor's work.

QA/QC/Acceptance Criteria

- Verticality limit is not applicable to all techniques, and element overlapping needs to govern.
- Testing cored samples in low strength materials can be problematic.
- Vague and subjective criteria are not enforceable.
- In situ permeability testing procedures cause debate.
- Statistically based specifications should be used.

Materials

- Reduce minimum solids in fresh self-hardening slurry.
- Define impacts of industry changes in cementitious materials.

Data Management

- Deliver data fast enough in a usable format where possible and practical.
- Provide data in accordance with specified dictionaries/schemas.
- Data may not be applicable to current data management specifications.
- Provide data in consistent format for QA/QC comparison.
- Emphasize immediate benefit of data management to get contractor buy-in.

Long Term Performance

- Define how cutoff wall properties have changed over the life of the wall.
- Provide instrumentation to improve monitoring performance.
- Evaluate cracking effects.

Design and Geotechnical Investigation

- Current design and construction contracting scheduling and scoping are not adequate to meet current needs for both the designer and cutoff wall contractor to reduce risk and improve quality during construction.
- Is there a need for a designer to identify changes in geology and multiple mix. designs/demonstration sections?
- Rectify inconsistent use of Geotechnical Data Reports.

Mini Workshop October 2024

In conjunction with DFI's 49th Annual Conference, 20 working group members attended a 4-hour mini-workshop (Fig. 5) as a follow up to the November 2023 workshop. The goals of this smaller workshop were to reconnect the working group members together in person and online to keep our group's working relationship active, address a handful of comments on the USACE's draft 65% DMM Specifications that warranted detailed discussion, review the progress and content from the consensus flyers we had worked on this year, and develop a plan for publishing the flyers.

FINAL REMARKS

It has been our privilege to work with the dedicated and committed members of the USACE-DFI Working Group on Seepage Control. Our thanks go out to DFI, USACE, USBR, TVA, NRCS, and FERC for

supporting this forum. The success and longevity of this working group are the result of the commitment and dedication of the members who represent their organizations with an optimistic outlook toward improvement, and the patience, forward thinking, and trust required to listen and consider alternative perspectives and experience.



Fig. 5. Attendees mini workshop (Denver, 2024).

 © Deep Foundations Institute 2025

PERFORMANCE OF COPPER SLAG IN GRANULAR INCLUSION METHOD OF GROUND IMPROVEMENT

K. Kavinmalar, Indian Institute of Technology Tirupati, Andhra Pradesh, India, yeskayyen464@gmail.com
P. Kiruthika, Indian Institute of Technology Tirupati, Andhra Pradesh, India, ce20d502@iittp.ac.in
A. Murali Krishna, Indian Institute of Technology Tirupati, Andhra Pradesh, India, amk@iittp.ac.in

ABSTRACT

Granular column inclusions are an effective ground improvement technique, enhancing soil strength, promoting densification, and radial consolidation. Ideally, well-graded granular materials are preferred for column inclusions; however, there is growing interest in the utilization of sustainable alternatives such as shredded tire chips, crushed concrete, copper slag, and other recycled materials owing to their environmental and economic benefits. This study explores the potential of copper slag as an alternative column material. Numerical analyses are performed using PLAXIS 2D to compare copper slag columns (CSC) with ordinary granular columns (OGC) under various subsoil conditions including loose sand, soft clay, and layered profiles. The study considers mechanical and hydraulic performance of columns and also examines the influence of different column length-to-diameter (L/D) ratios and evaluates the extent of bulging along the column length. Results show that CSCs consistently perform as well as OGCs in reducing settlement, despite exhibiting approximately 13% greater bulging. Additionally, variations in L/D ratio have minimal impact in cohesionless soils due to their immediate drained response under loading. Overall, copper slag proves to be a viable, sustainable alternative for granular columns, offering improved performance and contributing to effective waste management.

Keywords: granular inclusion, copper slag, bulging, consolidation, PLAXIS 2D

INTRODUCTION

The growing demand for infrastructure in urban and industrial areas has driven the need for ground improvement, particularly for land reclamation projects. The cost of conventional foundation systems, coupled with environmental constraints, has significantly promoted the in-situ improvement of weak soil deposits as a more sustainable and economical alternative. A range of geotechnical methods are employed to improve the performance of weak or soft soils. The selection of an appropriate technique depends on several factors, including soil type, existing ground conditions, site size, treatment area, location, and design loads. Stone columns serve as an effective ground improvement technique by enhancing both the strength and deformation characteristics of soft soils. They function primarily through reinforcement, densification, and drainage. During installation, the densification of surrounding soil leads to an increase in overall unit weight, while the columns facilitate rapid dissipation of excess pore water pressure and increases the ground stiffness. Primarily, the granular inclusion method, such as stone columns, conventionally rely on natural resources like sand and gravel. However, the depletion of these natural resources is closely associated with rising population, economic development, and technological progress. As a result, the demand for primary raw materials and the volume of waste generated are expected to rise significantly in the coming decades (Kuiper et al., 2018; Velenturf et al., 2019). However, the researchers have increasingly explored alternative, specifically sustainable materials for use in the stone columns. These includes fly ash, recycled aggregates, tire chips, pulverized fuel ash (PFA), silica-manganese slag and other materials (Zukri et al., 2000). Despite considerable research being conducted to assess the viability of various manufactured and recycled materials as alternatives to conventional aggregates in stone column construction, there remains a continued need to explore new materials, as much of the existing research focuses on a limited set of alternatives.

 © Deep Foundations Institute 2025

Copper being one of the most extensively produced metals globally, is accompanied by a substantial generation of copper slag waste. According to the International Copper Study Group (ICSG) report in 2019, global copper consumption rose significantly from 5,000 metric tonnes in 1900 to 17,888 metric tonnes in 2008, and further to 24,500 metric tonnes by 2018. This trend reflects a compound annual growth rate (CAGR) of approximately 3.4% over the observed period, highlighting the increasing global demand for copper across various industries as shown in Fig. 1 (Jena et al., 2022). Despite efforts to repurpose copper slag, a substantial amount continues to be disposed of in landfills or stockpiles, occupying vast tracts of land and posing long-term environmental risks.

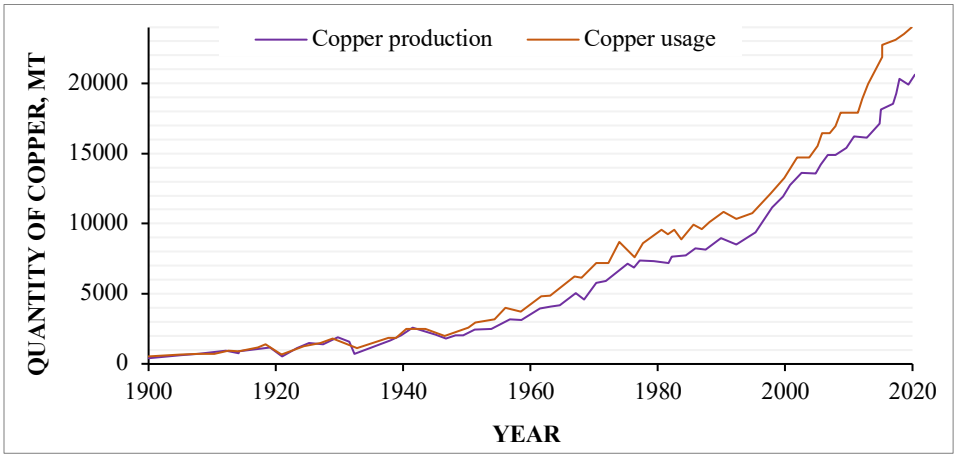


Fig. 1. Global copper production and usage for 1900–2020 (after Jena et al., 2022)

Copper slag is a glassy, granular material with high specific gravity and notable angularity, composed mainly of iron, silicon, and aluminium oxides. It is produced in significant quantities in copper producing countries such as India, Chile, and China. Numerous studies have explored the potential for recycling and reusing copper slag as a component in mortar and concrete, aiming to enhance sustainability in construction practices (Pavez et al., 2018; Rashad et al., 2016; Shi et al., 2008; Al-Jabri et al., 2009). Although its use has been explored in abrasive tools, road construction, cement, and concrete applications, the potential of copper slag in geotechnical engineering remains relatively untapped. Considering its favourable engineering properties such as high shear strength, low water absorption, and durability, copper slag presents a promising alternative to natural aggregates in ground improvement techniques. Furthermore, copper slag has been classified as non-toxic and environmentally safe, with leaching tests such as TCLP and acid extraction confirming minimal heavy metal release and long-term stability, thereby supporting its suitability for use in construction applications (Shanmuganathan et al., 2008).

Although extensive research exists on the parametric study of stone columns in homogeneous soil conditions, there remains a notable lack of studies addressing their behaviour in stratified soil profiles which replicate real field conditions more accurately and helps in practical implementation. This gap becomes particularly significant when introducing alternative materials into ground improvement techniques, where a detailed and methodical analysis is required to evaluate their suitability and performance across varying geotechnical conditions. In this context, the present study investigates the feasibility of using copper slag as a sustainable material in the granular inclusion method of ground improvement. A comprehensive analysis is conducted considering critical parameters including soil type and stratification, length-to-diameter ratio, and the bulging behaviour of the column, all of which significantly influence the overall effectiveness of granular columns. The pore pressure dissipation through radial consolidation provided by OGC and CSC is also studied. The research highlights the potential of copper slag to enhance both the

 © Deep Foundations Institute 2025

mechanical and hydraulic properties of treated soils, while simultaneously addressing environmental challenges such as industrial waste utilization and the conservation of natural aggregates.

PROPERTIES OF COPPER SLAG

The properties of copper slag were evaluated through laboratory experiments using material sourced from Sterlite Copper, a unit of Vedanta Limited in Thoothukudi, Tamil Nadu, which primarily produces copper via pyrometallurgical processes. The specific gravity of the copper slag has been determined to 3.7, indicating its dense nature. Figure 2 and figure 3 illustrates the physical appearance of copper slag and its gradation respectively. Relative density and direct shear tests were conducted to evaluate the strength characteristics of copper slag which are tabulated in table 1.



Fig. 2. Copper slag aggregate

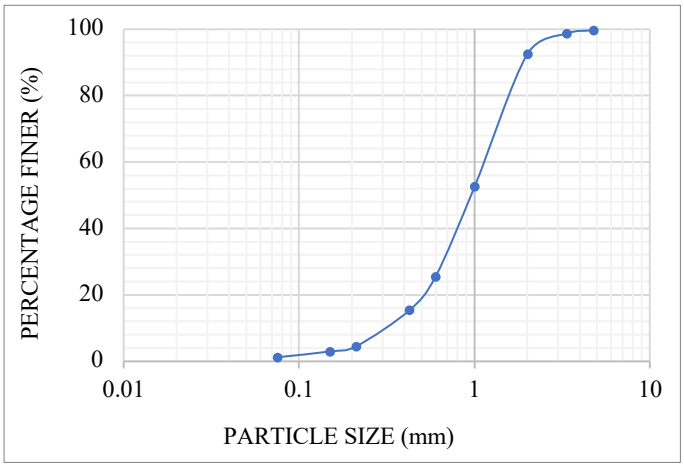


Fig. 3. Grain size distribution of copper slag

Table. 1. Results of Direct Shear and Relative Density Tests on Copper Slag

Max unit weight (kN/m^3)	26.67
Min unit weight (kN/m^3)	20.71
Max void ratio	0.76
Min void ratio	0.61
Angle of internal friction, φ (degrees)	46

NUMERICAL MODELLING

To evaluate and compare the performance of ordinary granular columns (OGC) with copper slag columns (CSC), numerical analysis was conducted using PLAXIS 2D finite element software. The study was confined to two-dimensional modelling. The analysis is structured around three distinct ground conditions, both without and with ground improvement: (1) homogeneous sandy soil (HSS), (2) homogeneous clayey soil (HCS), and (3) two-layered site stratification. The layered soil condition is further classified as Case 1, where sand overlies clay, and Case 2, where clay overlies sand. The influence of critical parameters such as the length-to-diameter (L/D) ratio, bulging effects of the column, and the consolidation behaviour of the surrounding soil is investigated to provide a comprehensive understanding of the ground response under varying subsurface conditions and column configurations.

 © Deep Foundations Institute 2025

Validation study

The numerical model was validated by simulating the load–settlement behaviour of a single stone column, based on the experimental study conducted by Narasimha Rao et al. (1992). In the experimental analysis, a test tank with a diameter of 650 mm was used, containing a clay bed of 350 mm height. A stone column with a diameter of 25 mm and height of 225 mm was installed at the center of the clay bed and subjected to loading through a circular plate with a diameter twice that of the column. An axisymmetric finite element analysis was performed in PLAXIS 2D using 15-node triangular elements, as illustrated in Fig. 4. The soil and stone column materials were modelled using Mohr-Coulomb failure criterion, assuming elastoplastic behaviour and all materials were considered under drained conditions. The material properties used in the simulation are reported in table 2. The comparison between the model results and experimental data presented in Fig 5 shows a close agreement, confirming the reliability of the numerical approach.

Table. 2. Material properties of validation model

Property	Material	
	Clay	Stones
Modulus of elasticity, E (kPa)	4000	45000
Poisson's ratio, μ	0.45	0.3
Cohesion, c_u (kPa)	20	0
Angle of internal friction, φ (degrees)	0	38

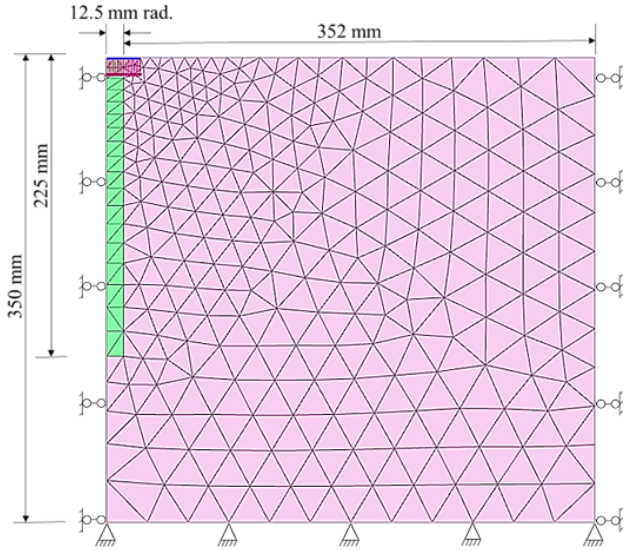


Fig. 4. Finite-element discretization of model test by Narasimha Rao et al., 1992

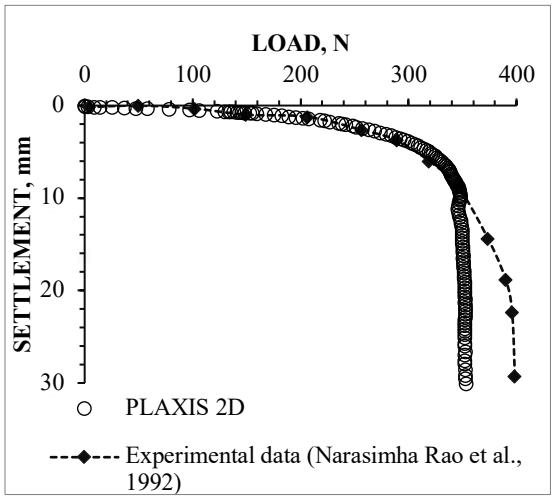


Fig. 5. Validation results of PLAXIS

Numerical modelling for present study

The stone column was simulated under axisymmetric conditions, and the soil and column materials were modelled using a 15-node triangular finite element mesh. In the numerical analysis, an elementary boundary condition was adopted, wherein radial deformation ($u_x = 0$) was restricted along the vertical boundaries, while vertical settlement was permitted. The base of the model was fixed in both horizontal and vertical directions ($u_x = 0$, $u_y = 0$). The installation effects that occur during the construction of the columns were not incorporated in the analysis. The Mohr-Coulomb failure criterion, assuming elasto-perfectly plastic behaviour is adopted, which defines soil failure governed by effective cohesion (c_u) and the angle of internal

 © Deep Foundations Institute 2025

friction (φ). No interface elements were used between the stone column and surrounding clay, as deformation was primarily governed by radial bulging, with minimal shear development expected. Moreover, due to the uncertain nature of shear strength properties in the mixed zone formed during column installation, the interface was idealized as fully bonded. This modelling approach is supported by previous studies such as Mitchell and Huber (1985) and Saha et al. (2000), which also neglected interface elements in similar analyses. A prescribed vertical displacement of 30 mm was applied to simulate loading conditions and assess the resulting settlement behaviour. Dilatancy angle is considered as $\psi^o = \varphi' - 30^o$.

The input properties of copper slag are sourced from Ahirwar and Mandal (2018) and the surrounding soil materials are sourced from the study by Kiruthika et al. (2022), which considered a real-time subsoil profile from a port located on the eastern coast of India. The site stratigraphy comprised medium dense to dense, poorly graded sand with Standard Penetration Test (SPT) N-values ranging from 11 to 63, overlaying a soft clay layer. A depth ratio of 1:1 between the sand and clay layers was identified. A similar stratigraphic profile was adopted in the present study, appropriately scaled down to suit the dimensions of the numerical model. Permeability of copper slag at D_r = 50% is considered from Das et al. (1983) and of other materials were sourced from Waltham (1994). The angle of internal friction for copper slag has been reported to range between 40° and 53°, as noted in studies by Gorai et al. (2003) and Das et al. (1983). In comparison, IS 15284: Part 1 (2003) specifies the internal friction angle for conventional columnar materials to lie between 38° and 42°. The average value within the specified range has been adopted for the column material to ensure consistency and realistic representation of material behaviour. The configuration of the column installed in layered soil strata is illustrated in Fig. 6 and the input properties are tabulated in table 3.

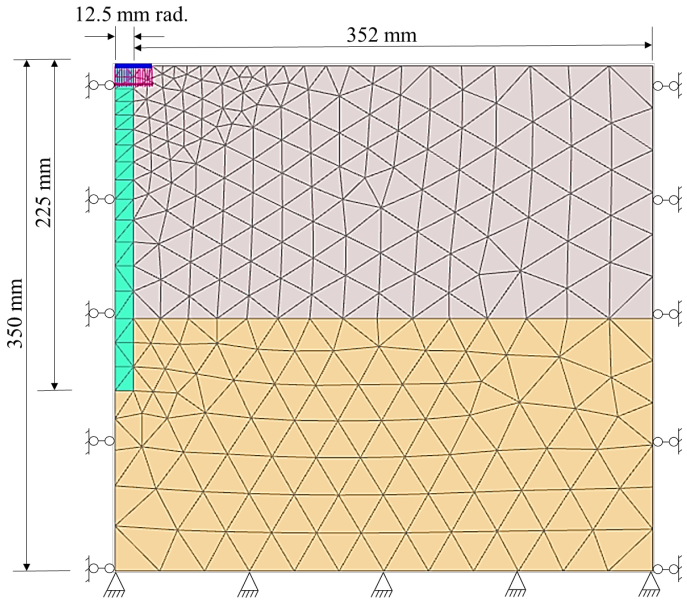


Fig. 6. Generated mesh for stratified soil profile

 © Deep Foundations Institute 2025

Table. 3. Material properties

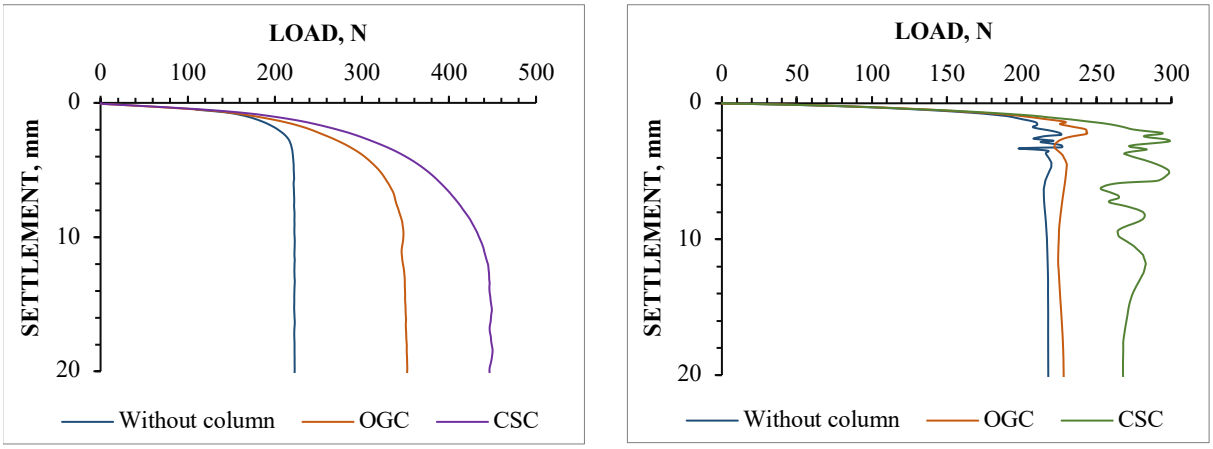
Property	Material			
	Sand	Clay	Stones	Copper slag
Modulus of elasticity (kPa)	17000	4000	45000	20000
Poisson's ratio, μ	0.3	0.45	0.3	0.35
Cohesion, c_u (kPa)	-	20	-	-
Angle of internal friction, φ (degrees)	35	-	40	46.5
Permeability (m/s)	2.3×10^{-5}	2.3×10^{-9}	3.5×10^{-3}	0.47×10^{-3}

RESULTS AND DISCUSSION

The load-bearing and hydraulic behaviour of columns were investigated under various ground conditions, including homogeneous sandy soil, homogeneous soft clay, and stratified soil profiles. The study on stratified soil conditions includes two distinct cases to assess the influence of soil layering on column performance. In Case 1, a layer of sand overlies clay, while in Case 2, clay is placed over sand.
According to IS 15284-1 (2003), the failure mechanism of a single stone column loaded over its area significantly depends on the column length. Columns having lengths greater than a critical length, approximately four times the column diameter typically fails through bulging in the case of end-bearing columns. This highlights the importance of evaluating bulging for longer columns, especially when using alternative materials with high specific gravity like copper slag. Thus, the critical influencing factors were analyzed to compare the performance and efficiency of copper slag columns with those constructed using conventional materials.

Effect of varying subsoil profiles

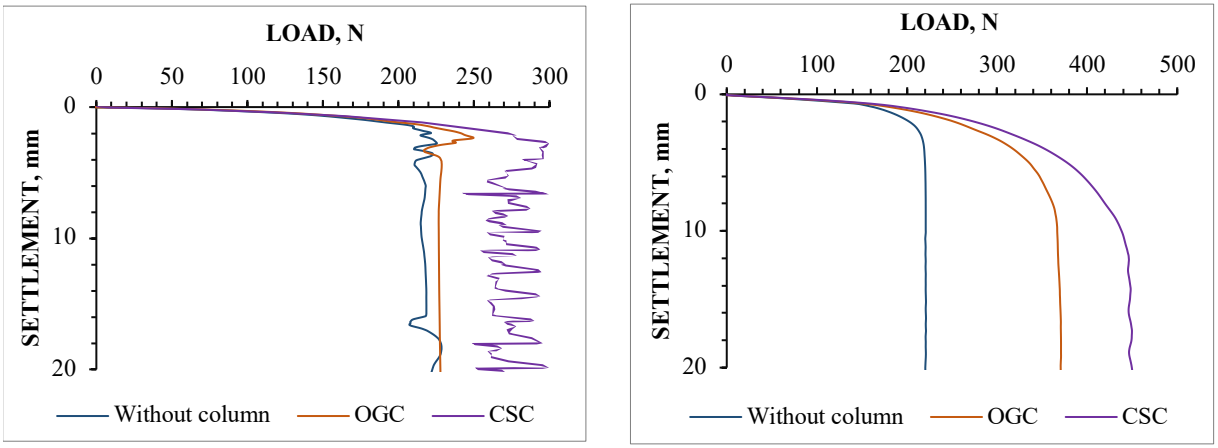
The performance CSC and OSC in homogeneous and layered soils is presented in Fig. 7 and Fig. 8 respectively. In homogeneous clayey soils, OGCs show a 66.8% improvement in load-bearing capacity, whereas CSCs demonstrate a significantly higher improvement of 102.7%. In homogeneous sandy soils, OGCs yields an improvement of 4.3%, while CSCs achieve a considerably greater enhancement of 25.5%. These results highlight the superior performance of CSCs across both soil types, with particularly notable effectiveness in cohesive soils.



a) Columns in homogenous clayey soils **b) Columns in homogenous sandy soils**

Fig. 7. Load bearing capacity of columns under homogenous soils

 © Deep Foundations Institute 2025

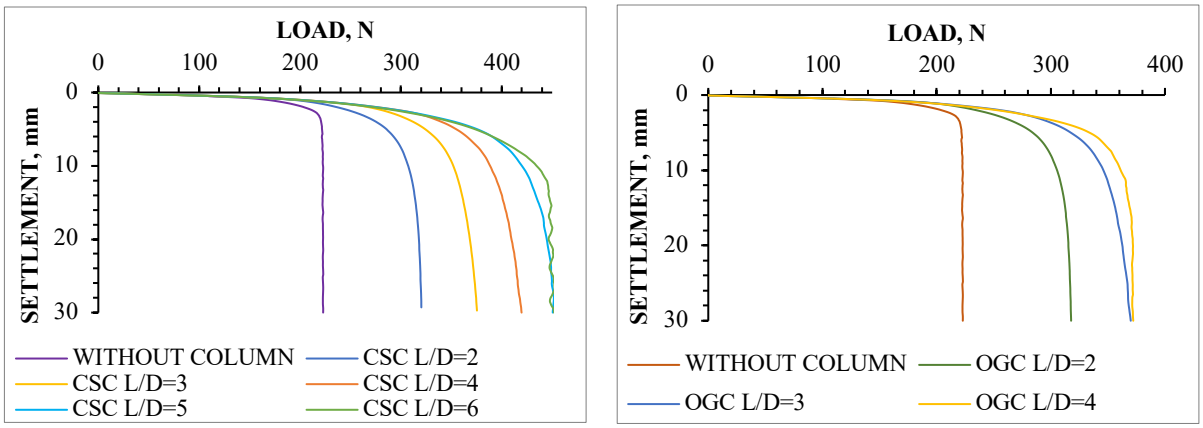


a) Columns in layering case 1 **b) Columns in layering case 2**

Fig. 8. Load bearing capacity of columns under layered soils

Effect of L/D ratios of the column

The influence of the length-to-diameter (L/D) ratio on the performance of copper slag columns (CSCs) and ordinary stone columns (OSCs) in homogenous clay is illustrated in Fig. 9. In general, an increase in the L/D ratio leads to an enhancement in the load-carrying capacity of the column, due to improved confinement and deeper stress distribution. However, beyond a certain critical L/D ratio, further increases do not significantly contribute to performance improvement. From the analysis, the critical L/D ratio is observed to be 5 for copper slag columns and 3 for ordinary granular columns. Beyond these values, the efficiency of ground improvement remains relatively unchanged, indicating an optimal design threshold for each material. The effect of varying length-to-diameter (L/D) ratios in cohesionless soils is not considered, as sand exhibits an immediate drained response under loading, where the footing and column–sand system deform simultaneously.



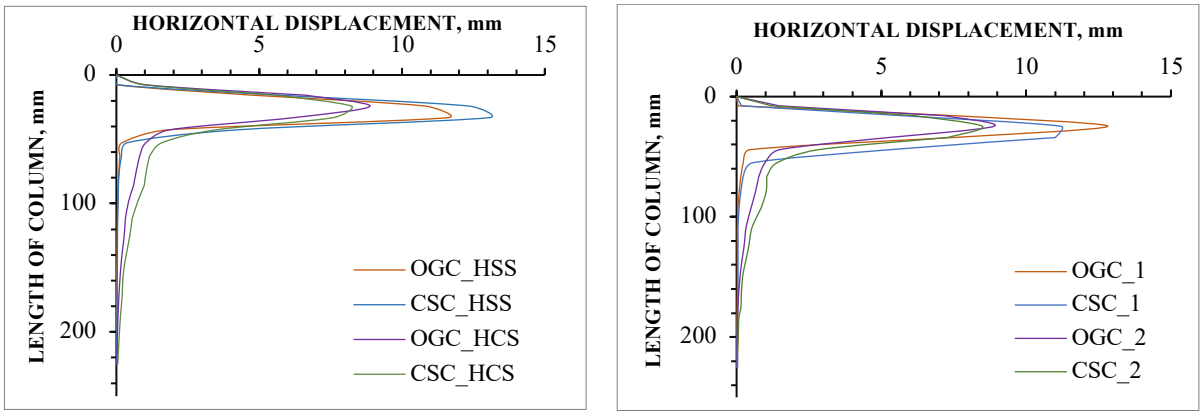
a) Influence of L/D ratio of CSC **b) C Influence of L/D ratio of OGC**

Fig. 9. Influence of L/D ratios of columns in homogenous clayey soils

 © Deep Foundations Institute 2025

Bulging characteristics of columns

The effect of bulging is evaluated by analyzing the horizontal displacement along the column length, as shown in Fig. 10. Both columns exhibit peak bulging at similar depths and follow a comparable bulging pattern. In homogenous sandy soils (HSS), copper slag columns show approximately 13% greater bulging than conventional stone columns; however, this increased deformation does not affect their mechanical performance. In contrast, under homogenous clayey soils (HCS), and layered soils, copper slag columns display slightly lower peak bulging compared to ordinary granular columns which is due to the cohesion of clay that offers more resistance to the bulging limiting the lateral displacement.



a) Columns in homogenous soils **b) Columns in layered soils**

Fig. 10. Bulging characteristics of columns

Drainage characteristics

Figure 11 illustrates excess pore water pressure dissipation over time for untreated clay, OGC and CSC modelled for 99% degree of consolidation in PLAXIS. The inclusion of columns significantly enhances consolidation by accelerating radial drainage. OGC shows the fastest dissipation due to its higher permeability followed by CSC which is 3.5×10^{-3} and 0.47×10^{-3} respectively. Compared to untreated clay, the time to reach near-zero excess pore pressure is reduced which demonstrates the effectiveness of granular inclusions in improving drainage characteristics and expediting consolidation in soft clay.

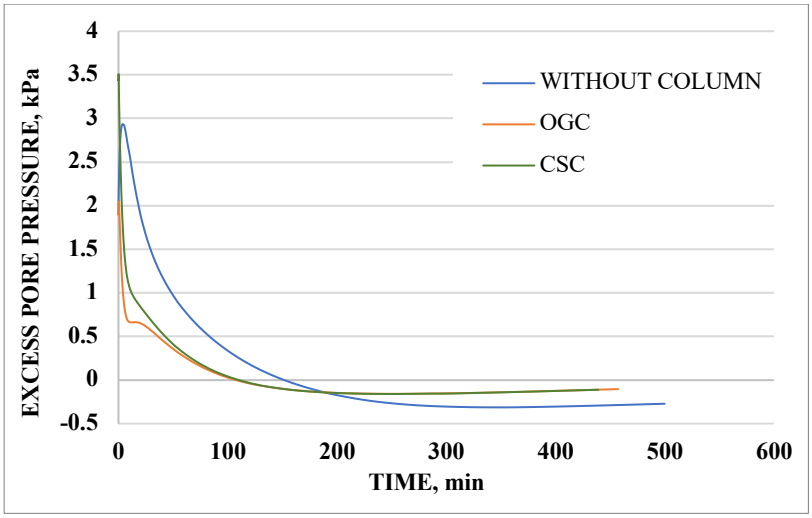


Fig. 11. Improvement in drainage characteristics

 © Deep Foundations Institute 2025

CONCLUSION

This study evaluates the performance of copper slag as a sustainable alternative to conventional materials in granular column applications for ground improvement. Using numerical modelling in PLAXIS 2D, the mechanical and hydraulic behaviour of copper slag columns (CSCs) was compared with ordinary granular columns (OGCs) under homogeneous and stratified soil conditions. The key findings are summarized below.

i) CSCs consistently demonstrate superior performance over OGCs in terms of load-bearing capacity and settlement reduction, particularly in cohesive soils. This enhanced mechanical behaviour is primarily attributed to the higher angle of internal friction of copper slag, which promotes greater shear resistance and interlocking with the surrounding soil, thereby improving load transfer.

ii) Although CSCs exhibit slightly greater bulging in cohesionless soils, this deformation remains minimal. The increased bulging is associated with the higher unit weight of copper slag, which generates greater radial stress in the surrounding soil.

iii) CSCs effectively facilitate radial consolidation, with performance closely approaching that of conventional granular columns (OGC). This indicates that CSCs serve as a viable alternative for enhancing drainage characteristics in soft soils.

iv) The influence of the column length-to-diameter (L/D) ratio is evident in cohesive soils, leading to better ground response with increasing L/D until the critical value. The analysis identifies a critical L/D ratio of 5 for CSCs and 3 for OGSs.

v) The study of stratified soil layers of sand over clay and clay over sand demonstrates that soil layering significantly influences column performance. Overall, copper slag emerges as a technically viable and environmentally responsible material for use in granular column ground improvement, contributing to both natural resource conservation and effective industrial waste utilization.

FUTURE SCOPE

Future research should focus on validating the numerical findings through large-scale experiments and field studies, assessing the long-term durability and potential breakdown of copper slag under environmental and cyclic loading conditions. The influence of construction techniques, which significantly affect column densification and lateral stresses, must be examined through advanced modelling and testing. Additionally, studies on complex soil profiles, groundwater variations, and comprehensive life-cycle assessments will provide deeper insights into the technical, environmental, and economic feasibility of copper slag columns for sustainable ground improvement.

REFERENCES

Ahirwar, S.K., & Mandal, J.N. (2017). Finite element analysis of flexible pavement with geogrids. *Procedia engineering*, *189*, 411-416.

Al-Jabri, K. S., Al-Saidy, A. H., & Taha, R. (2011). Effect of copper slag as a fine aggregate on the properties of cement mortars and concrete. *Construction and Building Materials*, *25*(2), 933-938.

Ambily, A.P., & Gandhi, S.R. (2007). Behavior of stone columns based on experimental and FEM analysis. *Journal of geotechnical and geoenvironmental engineering*, *133*(4), 405-415.

 © Deep Foundations Institute 2025

ASH, S. (2024). 2019 Minerals Yearbook. *US Geological Survey*.

Das, B. M., Tarquin, A. J., & Jones, A. D. (1983). Geotechnical properties of a copper slag. *Transportation Research Record*, (941).

Gorai, B., & Jana, R. K. (2003). Characteristics and utilisation of copper slag—a review. *Resources, conservation and recycling*, *39*(4), 299-313.

Indian Standards IS. 2003. "Indian standard code of practice for de sign and construction for ground improvement-guidelines. Part 1: Stone columns." IS 15284 (Part 1), New Delhi, India.

Jena, S. S., Tripathy, S. K., Mandre, N. R., Venugopal, R., & Farrokhpay, S. (2022). Sustainable use of copper resources: Beneficiation of low-grade copper ores. *Minerals*, *12*(5), 545.

Kiruthika, P., Banerjee, S., Murali Krishna, A., & Boominathan, A. (2022). Performance of stone columns in multi-layered soils system. In *Geo-Congress 2022* (pp. 50-60).

Kuipers, K. J., van Oers, L. F., Verboon, M., & van der Voet, E. (2018). Assessing environmental implications associated with global copper demand and supply scenarios from 2010 to 2050. *Global Environmental Change*, *49*, 106-115.

Look, B. G. (2007). *Handbook of geotechnical investigation and design tables*. Taylor & Francis.

Madheswaran, C. K., Ambily, P.S., Dattatreya, J. K., & Rajamane, N. P. (2014). Studies on use of copper slag as replacement material for river sand in building constructions. *Journal of the Institution of Engineers (India): Series A*, *95*, 169-177.

Mitchell, J. K., & Huber, T. R. (1985). Performance of a stone column foundation. *Journal of Geotechnical Engineering*, *111*(2), 205-223.

Murari, K., Siddique, R., & Jain, K. K. (2015). Use of waste copper slag, a sustainable material. *Journal of Material Cycles and Waste Management*, *17*, 13-26.

Pavez, O., Rivera, O., Toledo, I., & Nazer, A. (2018). Use of copper slag as fine aggregate and partial replacement of cement. *HOLOS*, *34*(4), 31-45.

Phiri, T. C., Singh, P., & Nikoloski, A. N. (2022). The potential for copper slag waste as a resource for a circular economy: A review–Part I. *Minerals Engineering*, *180*, 107474.

Rashad, A. M. (2016). A Brief Review on Blast-Furnace Slag and Copper Slag as Fine Aggregate in Mortar and Concrete Based on Portland Cement. *Reviews on Advanced Materials Science*, *44*(3).

Saha, S., Santhanu, S., and Roy, A. 2000. "Analysis of stone column in soft ground." Proc., Indian Geotech. Conf., Bombay, India, 297–300.

Saxena, S., & Roy, L.B. (2022). Suitability analysis of stone column materials with PLAXIS. *Engineering, Technology & Applied Science Research*, *12*(2), 8421-8425.

 © Deep Foundations Institute 2025

Shanmuganathan, P., Lakshmipathiraj, P., Srikanth, S., Nachiappan, A. L., & Sumathy, A. (2008). Toxicity characterization and long-term stability studies on copper slag from the ISASMELT process. *Resources, Conservation and Recycling*, *52*(4), 601-611.

Shi, C., Meyer, C., & Behnood, A. (2008). Utilization of copper slag in cement and concrete. *Resources, Conservation and recycling*, *52*(10), 1115-1120.

Shivashankar, R., Dheerendra Babu, M. R., Nayak, S., & Rajathkumar, V. (2011). Experimental studies on behaviour of stone columns in layered soils. *Geotechnical and Geological Engineering*, *29*, 749-757.

Sivapriya, S.V., Gunalan, S., Mugesh, A., Niranjan, J., & Yuvaraj, K. (2023). Investigating the advantage of copper and steel slags as partial replacement material in a sand compaction column in stabilizing the soft clay. *International Journal of Geotechnical Engineering*, *17*(5), 510-518.

Tandel, Y.K., & Patel, J.B. (2009). Review of utilisation of copper slag in highway construction. *Australian Geomechanics*, *44*(3), 71.

U.S. Geological Survey. Mineral Commodity Summaries 2020; U.S. Geological Survey: Reston, VA, USA, 2020; p. 204.

Velenturf, A. P., Archer, S. A., Gomes, H. I., Christgen, B., Lag-Brotons, A. J., & Purnell, P. (2019). Circular economy and the matter of integrated resources. *Science of the Total Environment*, *689*, 963-969.

Zukri, A., & Nazir, R. (2018, April). Sustainable materials used as stone column filler: A short review. In *IOP conference series: materials science and engineering* (Vol. 342, No. 1, p. 012001). IOP Publishing.

 © Deep Foundations Institute 2025

GEOTECHNICAL MONITORING SYSTEMS: THE NEW MULTI-PARAMETRIC DMS® COLUMNS - THE IMPORTANCE OF LAB AND TESTING FIELD FOR RELIABILITY AND DATA INTERPRETATION IN EARLY WARNING APPLICATIONS

L. Foglino, C.S.G. Srl, Italy
M. Lovisolo, C.S.G. Srl, Italy

ABSTRACT

Increased sensitivity regarding hydrogeological and residual risk has led to considering continuous geotechnical stability monitoring as a mitigation factor, using dedicated models and specific early warning techniques.

Moreover, geotechnical design guidelines highlight the importance of applying the observational method to monitor stability in particular context complexity, in all phases including design, construction, structural testing, and post-construction. The answer to these guidelines may come through modern geotechnical monitoring systems using multi-parametric instrumentation.

C.S.G. leads the field in multi-parametric monitoring for early warning applications. In 2000, we obtained the first patents that introduced the multi-inclinometer and the multi-parametric systems. The Differential Monitoring of Stability (DMS®) is an automatic, in-place, 2D/3D, geotechnical monitoring system that provides real time stability monitoring of landslides, cuttings and engineering works. It can be installed up to 250 meters and higher depths, and it is fully instrumented for early warning applications.

The instruments are an evolution of the traditional in-place inclinometer (IPI) with added columnar instruments which make it possible to overcome the limit of zone extension limitations. However, due to column length and the freedom from the inclinometric pipe grooves, new generation geotechnical monitoring systems are not compatible with traditional instrument testing procedures. Special attention is required during the construction phase and specific testing/calibration needs to be conducted in the lab and during field testing. This paper describes techniques specifically developed to address line connection alignment problems that may arise when there are numerous inclinometric sensors. It also addresses the design and construction of specific machines for mechanical assembly and automatic joint alignment by using specific software procedures to calibrate and test sensors.

Keywords: multi-parametric, geotechnical monitoring system, overall calibration, EW systems

INTRODUCTION

Increased sensitivity regarding hydrogeological and residual risk has led to considering continuous geotechnical stability monitoring as a mitigation factor, using dedicated models and specific early warning techniques. (*Blikra et al 2013, Giuffredi et al. 2003, Lovisolo et al. 2003).*

Moreover, recent legislative guidelines (national laws and standards UNI EN ISO 18674, Eurocodes, etc.) require new geotechnical monitoring improvements that fundamentally support various stages of design, survey, construction, testing, and post-construction. These important new guidelines, along with advancements in sensor, digital communication systems, and remote data transmission monitoring, have led to the creation of in-column instrumentation. In real time, they manage multiple sensors, especially inclinometer sensors, and allow continuous soil and rock deformation reconstruction along the entire vertical section under investigation.

 © Deep Foundations Institute 2025

These instruments are an evolution of the traditional in place inclinometers (IPI) with the aim to overcome their constrains related mainly to the limited multi-gauge active lengths, vulnerability of the electrical cable/connections, and the specific requirements for the four grooves inclinometric casing. These limits, in fact, have a significant impact in applying the IPI, especially related to early warning because the zone monitored/monitorable is limited compared to the entire depth of interest (deep-seated landslides, multi-sliding zones etc). The advantageous results include no longer having a dependence on the standard inclinometric casing, an increased ability to evaluate the horizontal displacement, and a longer-term operation extended to possible damaged conditions at the level of casing, when not recoverable with standard IPI or probe instrumentation/survey.

With the realization of the columnar instruments, it is possible to overcome these limitations in terms of the length of the investigated segment since the connection between the various modular elements allows considerable depths to be reached, fully instrumented. However, because of the column length and the lack of grooves, this new generation of geotechnical monitoring tools is not compatible with testing procedures used for the traditional instrument, both the inclinometer probe and IPI. This requires special attention during the construction phase and proper specific testing/calibration during field testing. This paper specifically addresses the alignment problems that may arise in the connection line of numerous inclinometric sensors.

Since 2000, C.S.G. Srl, has manufactured their patented DMS® system to solve also these problems by designing and constructing specific machines for mechanical assembly and automatic joint alignment, along with specialized software for sensor calibration and testing.

FROM INCLINOMETRIC SURVEY TO MULTI-INCLINOMETRIC AUTOMATIC MONITORING

Measuring the horizontal displacements using inclinometric data collected along the vertical investigation using the classic method (Fig. 1) and precise trigonometric functions, can be summarized as follows:

$$x = OP = NPsen\alpha_x \quad (1)$$

$$y = OQ = NQsen\alpha_y \quad (2)$$

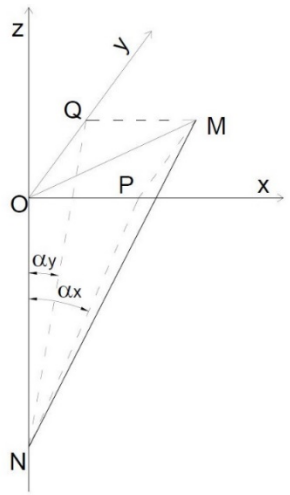


Fig. 1. Horizontal displacements calculation

 © Deep Foundations Institute 2025

x = lateral deviation of the pipe along the x axis

y = lateral deviation of the pipe along the y axis

α = inclination of the pipe at a given depth

MN = probe length

NP = MN orthogonal projection onto the xz-plane

NQ = MN orthogonal projection onto the yz-plane

For small angles:

$$NP = NQ \cong MN$$

Inclinometric measures are affected by systematic, random, and accidental errors. When using an inclinometer probe, it is possible to compensate for systematic errors by performing measurements along the same plane 1-3, reversing the probe, and assuming the bias remains constant in the two series of measures 1 and 3. Classifying accidental errors is more complex as it is difficult to identify and quantify the uncertainties. The main problems with the inclinometer probe are linked to the borehole near-verticality requirement, the probe repositioning in time, and the coupling wheel carriage/grooves which significantly increases systematic errors (Mikkelsen 2003).

With the IPI, the device generally uses standard inclinometric casing as a guide pipe and can be removed for repairs and re-calibrations (Dunnicliff 1988). The IPI being in place reduces both systematic and accidental errors. Systematic errors can be considered constant over time (intervenes a very important factor since the positioning of the instrumentation inside the borehole remains the same). Accidental errors are also lessened because the "operator" component is limited, there is no instrument repositioning, and digital instrumentation allows several measurements to be made.

The main limitation of IPI is that it provides a limited approach in addressing an issue because it is often unfeasible to install a sequence of individual IPI to monitor. For example, the entire landslide body or a general vertical of investigation because many installations are limited by gage length and the number of sensors in the chain. Usually, the monitored zone is limited to a known or supposed sector, overlooking large portions that may be the onset of neo-kinematics (new potential sliding zones). To obviate, at least in part, this problem it is customary to periodically extract the instruments and proceed with reading the entire vertical of investigation with the inclinometer probe. This repositions the IPI, if necessary, in a way more consistent with the deformation (Simeoni & Mongiovì 2003). This activity is not feasible in the presence of large casing deformations because there is a risk of getting the instrument stuck, losing the borehole at the same time. This can result in significant damage and increased cost for the client, especially for boreholes drilled in harsh environments and when long term and continuous monitoring is needed. This is typically related to early warning projects. These limits can easily be overcome with multi-inclinometer monitoring that allows for continuous measurements to be taken, in real time, for the entire borehole.

Multi-inclinometric columns are an evolution of IPI systems as they are in-place monitoring tools made up of a sequence of inclinometric modular elements joined together to reach the desired length.

Currently, different companies produce some type of multi-inclinometric system that differ in sizes, maximum length, materials, and sensors. These instruments commonly use micro-electro-mechanical systems (MEMS) technology. It is a modular structure composed of parts, flexible elements, and use free from traditional inclinometer casing installation due to being able to operate without grooves. This last characteristic distinguishes this type of instrument from IPI because it can operate inside a pipe, without inclinometric grooves, thanks to an internal sensor axes alignment along the column.

The flexible connection element in these systems play a key role since it allows for column deformation while maintaining the directionality of the sensor axes. However, it must also be particularly robust to withstand the tensile stress put on the instrument and adequately protect the internal electrical cable connections.

DMS® GEOTECHNICAL MONITORING COLUMNS: MECHANICAL ALIGNMENT AND OVERALL CALIBRATION

For the past 25 years, C.S.G. Srl has perfected their production process by conducting a series of tests designed to ensure that a high-quality and robust product is offered to clients. (Lovisolo & Della Giusta 2005).

DMS® instrument is made by mechanical assembly of modular elements consisting of a rigid part in grinded stainless-steel pipe containing digital sensors, mainly MEMS sensors, and a flexible part able to copy soil/rock deformations, as shown in Fig. 2.

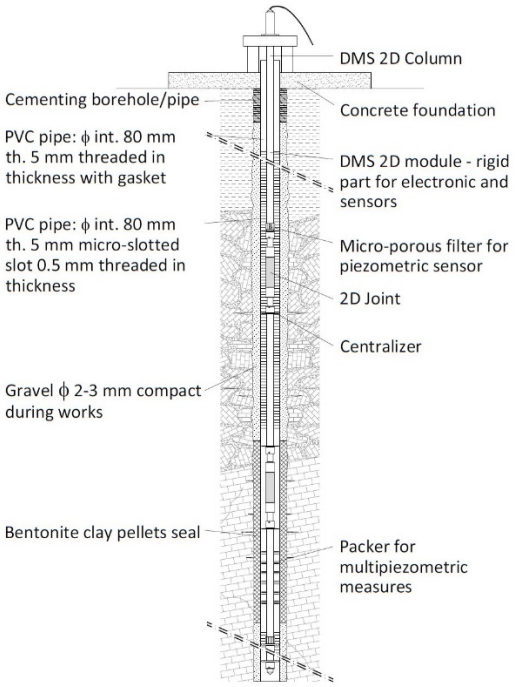


Fig. 2. DMS® Multi-parametric Column In-place Sketch

The flexible part houses the electric power and data transmission cables to allow both electrical and mechanical connections to the successive module. A special feature of these tools is the ability to monitor the deformation, even within smooth pipes without grooves, thanks to the internal reference system that is fixed in the assembly phase.

This characteristic is particularly useful for developing multi-parametric systems where piezometric sensors are placed in the same column, also at different levels separated by packers, strain gauge sensors, accelerometers etc. that would not find a proper application in standard inclinometric pipes.

The series of modular elements containing inclinometric sensors allows the vertical deformation and then the displacements/deformations quantification to be determined (Fig. 3). The cumulative deformation is determined by the following equations:

$$D_x = \sum_{i=1}^{n} L_i \cdot sin\alpha_{x,i} \quad (3)$$

$$D_y = \sum_{i=1}^{n} L_i \cdot sin\alpha_{y,i} \quad (4)$$

where:

D_x = cumulative displacements along the x axis.

D_y = cumulative displacements along the y axis.

α_x = rotation angles of the modular element around the y axis.

α_y = rotation angles of the modular element around the x axis.

n = number of modular elements.

i = i-th modular element, numbered from the bottom of the column (i = 1 for the modular element at the bottom of the column, i = n for the modular element at the head of the column).

The connection of various modular units allows instruments assembly with very high lengths. This assembly process, seemingly simple and easy to complete, must be particularly accurate and requires technologies, appropriate construction methods, and rigorous testing. Since spiralling needs to be controlled, this avoids any elements mutually rotating during the connection that could cause misalignment/spiralling of the column. As for the traditional inclinometer probe, through a process of testing and eventual compensation, the generation of systematic and accidental errors are circumvented that could potentially affect the measurement and compromise the subsequent data interpretation.

For the DMS® columns production, C.S.G. Srl has developed special equipment and procedures for the automatic and in-phase control joint assemblies for individual sensor calibration. Also, specific procedures for proprietary software have been created for final testing of the entire column using a special testing field.

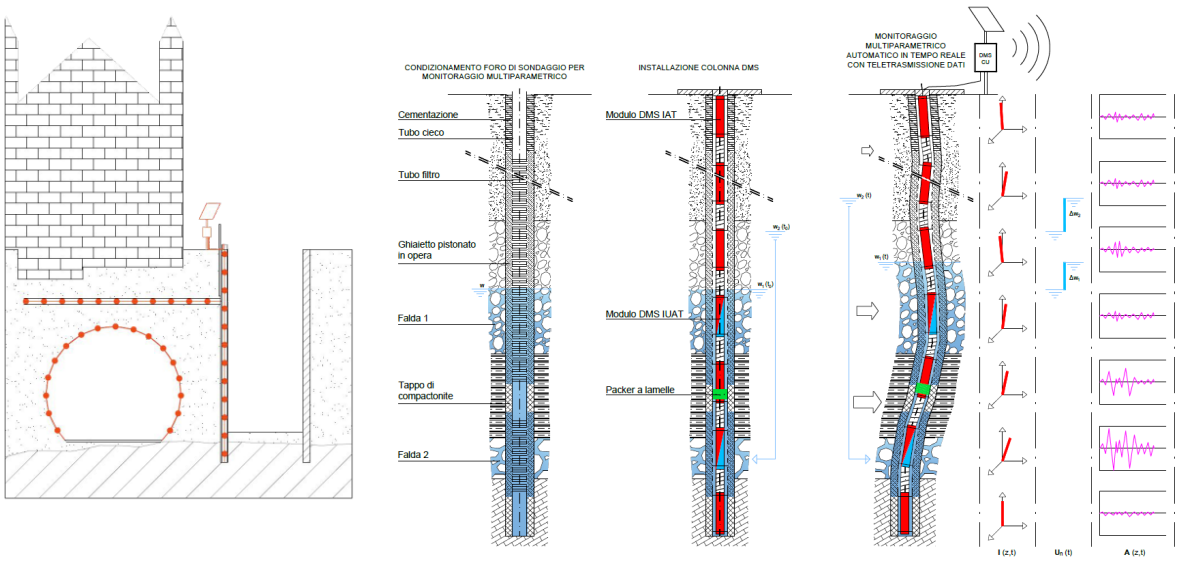


Fig. 3. How DMS® works

 © Deep Foundations Institute 2025

Mechanical Alignment with JM Machine

Mechanical alignment of the modular elements forming a column is guaranteed by mechanical M/F references placed at the joint ended parts and the stainless-steel pipe. Furthermore, mechanical alignment is also ensured by grinding the stainless-steel pipe which is necessary to avoid any possible deviation of the pipe along its own axis.

The joint is composed of two rigid terminal parts for connection to the tubular elements and a central part in high-resistance, reinforced rubber that ensures necessary column flexibility. The joints tensile strength may vary, depending on the models, from 20 to 50 kN. Their flexibility, depending on the models, varies from ± 90 ° to ± 120 °.

The joints are realized using a Joint Machine (JM) as shown in Fig. 4, which automatically assembles various components with a working cycle that ensures perfect terminal parts alignment. The machine assembles the terminal parts with the reinforced rubber element and then presses everything together.

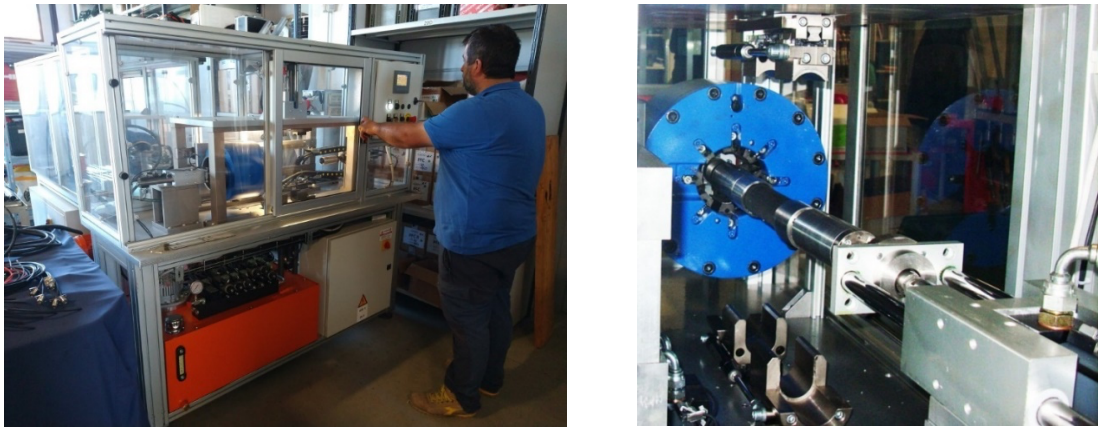


Fig. 4. DMS® Joint Assembling with JM Machine

The joint terminal parts are designed specifically to house the sensor support, the control electronics, protected by the rigid tubular element and the M/F connection.
The control electronics and sensors are installed on one of the joint terminals while the other terminal houses the electrical connection.

Inclinometric Sensors Calibration

The industrial sensors are generally accompanied by the manufacturer's certificate of compliance based on statistical parameters. The performances of the sensors therefore fall within a Gaussian distribution, or within a range of values ±x, which does not identify the specific value of accuracy of the single sensor.

To identify any outliers and to connote specific individual sensor characteristics, it is necessary calibrate each sensor. The set joint-sensors-control electronics is then fixed on a bi-axial rotary table for the inclinometric sensors' setting and calibration procedure (Fig. 5). This process is fully automatic using specialized software that provides both bi-axial rotary table cyclic automation of the data collected and sensors' calibration/setting.



Fig. 5. Sensors Calibration Using the Bi-axial Rotary Table

Once calibration is completed, joints are assembled to the tubular rigid elements and then connected to form the designed length column. The column is then moved to the thermo-controlled testing field using a special hydraulic DMS® Reeler and installed inside the boreholes both vertically and inclined for axes direction control and for long-term stability tests through specific procedures. In the following paragraph, the alignment testing is described and the compensation procedure of possible spiralling.

Testing in Thermo-controlled Testing Field

One of the most delicate and complex aspects to be considered in the construction phase of these instruments is the axes iso-orientation of the individual inclinometric sensors. In other words, for the entire instrument to provide consistent and reliable data, it is crucial that all the axes of each biaxial inclinometric sensor are perfectly oriented in the same way to avoid spiralling errors. Practically speaking, each modular element connection must not generate a torsional component between the elements that could generate orientation errors in the direction of displacement of the individual sensors/modules. This could then cause significant errors when evaluating the displacement.

To better understand the scope of this problem, consider an instrumented column 100 meters long (1 module/m). The connections between the various elements total are 198. If there were a misalignment error between two consecutive connections of 0.05 mm, it would result in a total misalignment, assuming that the rotation is in the same direction, between the ended parts of the instrument of $0.05 \cdot 198 = 9.9$ mm. Assuming a tool external diameter of 40 mm, the phase angle $\vartheta = \frac{9.9 \cdot 360°}{40 \cdot \pi} = 28.4°$. This error is largely unacceptable for a measuring instrument in terms of the resultant magnitude and the movements direction. Clearly, the error is proportional to the number of connections and external diameter. Assuming, for instance, a column 100-meters-long and modular elements 0.5-meters-long, the connections are 398 with a possible misalignment of 19.9 mm corresponding to a rotation of 57°. These simple considerations lead to the conclusion that the problem is not a small one but needs to be addressed with particular care in terms of mechanical precision in constructing and assembling the individual components, especially the union between various modular elements. Testing and software calibration of the sensors using a suitable thermo-controlled test fields becomes especially indispensable for columns of considerable length. It should be noted that the phase shift/spiralling is not detectable during the installation inside vertical boreholes, (Fig. 6), since the horizontal displacement is zero or close to zero, or when variously inclined boreholes orientation is not known. It could trigger an accuracy error that can significantly affect the results of monitoring and make the movements inconsistent with the real ones.

 © Deep Foundations Institute 2025

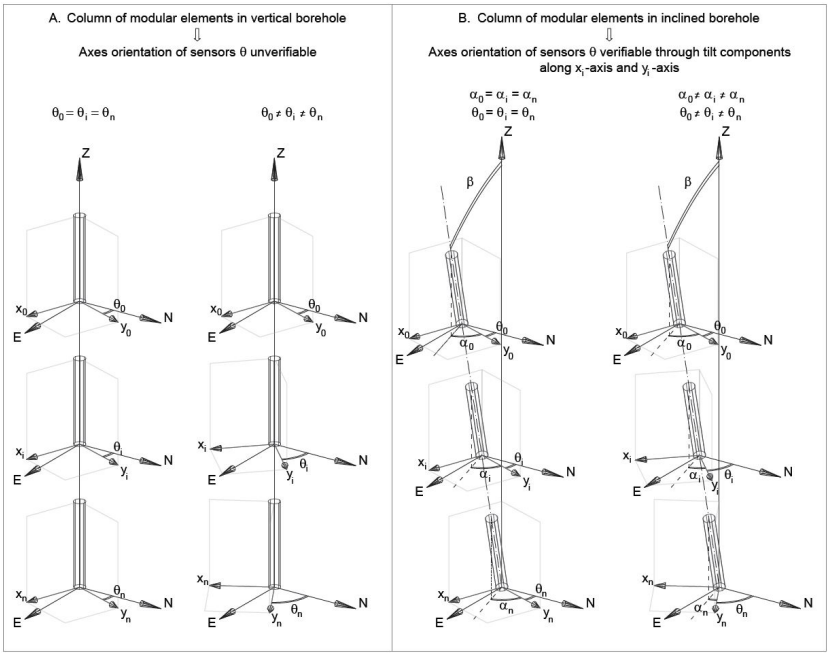


Fig. 6. Comparison Between the Column Behaviour in a Vertical Borehole or in an Inclined Borehole with Known Layout. A. Column of Modular Elements in Vertical Borehole: Axes Orientation of Sensors θ Unverifiable. B. Column of Modular Elements in Inclined Borehole: Axes Orientation of Sensors θ Verifiable through Tilt Components Along x_i-axis and y_i-axis

To limit measurement errors, C.S.G. has developed a series of mechanical and software controls and procedures involving the entire construction process. In addition to this, a specific operating procedure and software for instruments testing in the specific thermo-controlled tests field has been established (Fig. 7).



Fig. 7. Thermo-controlled Testing Field. Construction Phase and Installation of a DMS® Column Inside the 10° Inclined Borehole 220-meters-long For the ARC Test With DMS® Reeler

At the end of the assembly phase, the final assessment is completed in the thermo-controlled testing field through an "ArcTest" that recognizes and assesses phase shifts. In detail, the column is inserted into an inclined borehole having a known inclination (10°) requiring that the individual column modules measure the inclination x and y components. C.S.G. Srl proprietary software reconstructs the borehole layout measured by the column. This layout is automatically compared with the known profile and through a

misalignment correction process of the axis's orientation, the software evaluates the possible phase shifts with respect to the known direction and provides to their correction.

The software tool calculates the horizontal displacement along x and y axes, P_i, and R_i respectively, from the pitch (rotation around the y axis) and roll (rotation around the x axis) rotations, for each i-th module using the following equations:

$$P_i = L_i \cdot sin(\alpha_{pitch}) \tag{5}$$

$$R_i = L_i \cdot sin(\alpha_{roll}) \tag{6}$$

where:

P_i = displacements component along x axis.

R_i = displacements component along y axis.

L_i = modular element length.

α_{pitch} = rotation angle around the y axis (pitch).

α_{roll} = rotation angle around the x axis (roll).

Displacement resultant D_i is calculated as:

$$D_i = \sqrt{(P_i)^2 + (R_i)^2} \tag{7}$$

The software then proceeds to evaluate the azimuth angle of the direction of inclination of each module according to internal reference system, in other words assuming north coincides with the y axis:

$$\alpha_i = arctan\left(\frac{P_i}{R_i}\right) \qquad if\ R_i > 0\ and\ P_i > 0 \tag{8}$$

$$\alpha_i = arctan\left(\frac{P_i}{R_i}\right) + 180° \qquad if\ R_i < 0\ and\ P_i <> 0 \tag{9}$$

$$\alpha_i = arctan\left(\frac{P_i}{R_i}\right) + 360° \qquad if\ R_i > 0\ and\ P_i < 0 \tag{10}$$

Once calculated α for each module, the software evaluates the possible offset between the direction of the head of the column α_n and the direction α_i of the i-th module, as follows:

$$offset_i = \alpha_n - \alpha_i \tag{11}$$

To consider the less than perfect linearity of the test borehole and its possible deformation in time, the real layout of the borehole is detected by an inclinometer probe survey at periodical frequency and then used for the offset evaluation.

Fig. 8 shows an example of alignment for a 100-meter-long column following the installation inside the inclined borehole. It is possible to detect the spiralling of the column and the normalised profile after the Arc-Test procedure.

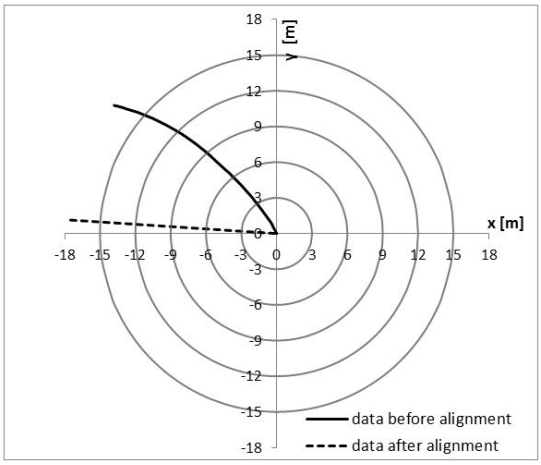


Fig. 8. Alignment. Data Diagram Before and After Alignment with Arc-Test Software

The offset value could be used during the final installation phase at the client's site as an overall certification of the multi-inclinometer instrumentation.

See below for a DMS® column with an active instrumented length of 250 meters installed in a vertical hole for a continuous monitoring for early warning after two years of full operation. The data highlights the column directed with and without the application of the Arc-Test calibration where an overall misalignment of about 50° is represented (Fig. 9).

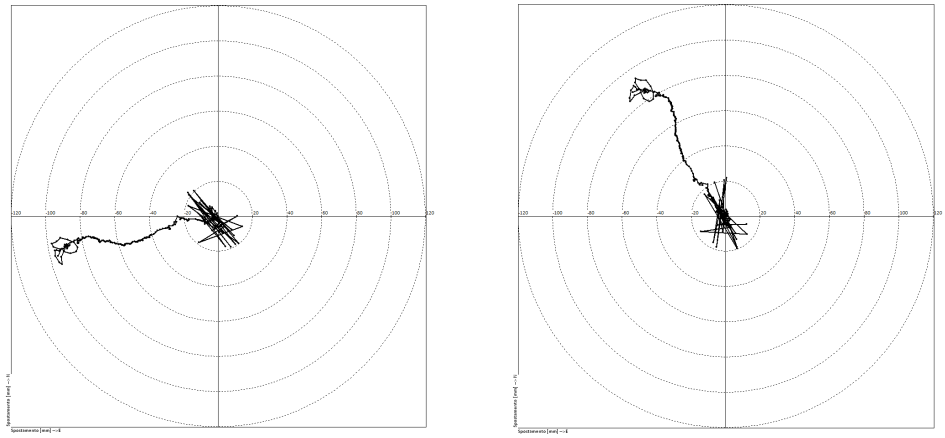


Fig. 9. Polar Plot Diagram of a DMS® Column 250 meters Fully Instrumented with and Without Alignment Application of Arc-Test Calibration in an EW Project

CONCLUSION

The multi-inclinometric monitoring columns and even more multi-parametric columns can substantially enhance geotechnical monitoring. They enable continuous, automatic, and real time displacement detection, and other important geo-indicators, simultaneously along an entire vertical investigation that is difficult to monitor with traditional instruments. Multi-inclinometric and multi-parametric columns may also be particularly useful for continuous monitoring of deep-seated landslides, up to considerable depths for automatic early warning management, as a relevant risk mitigation factor.

 © Deep Foundations Institute 2025

The quality and technical reliability of these new types of instruments can be defined by more than the accuracy of individual sensors. As is the case with traditional inclinometric instruments, it is essential to standardise the minimum quality requirements related to stability and accuracy (Dunnicliff & La Fonta 2001, La Fonta & Beth 2002, Mikkelsen 2003, UNI EN ISO 18674) and extending them to multi-inclinometric columns. Consideration must be given to their potential high depths (up to 250 meters, continuous, fully instrumented), as well as tensile strength, watertight seal, correct alignment of the reference system. Correct alignment and overall accuracy are essential for precise interpretation and data usage because the use of this instrument is no longer tied to traditional inclinometric pipes with grooves (Lovisolo & Della Giusta 2005). It should not be overlooked that a multi-inclinometric chain is not just a simple, repeated connection of sensors, but a complex, unique instrument. Its construction requires particular care regarding sensor selection, onboard electronics, mechanics, and column assembly methods. Moreover, it is essential that the assembly phase includes all calibrations and tests necessary to ensure proper functionality of individual electronic components and their correct integration with the mechanics. Finally, at the end of the construction phase, it is important to have careful, comprehensive calibration and testing procedures for the entire column using a specific thermo-controlled testing field. These steps can be accomplished by the DMS® Reelers, a self-propelled tracked unit developed for installing and maintaining the DMS® monitoring columns, which allows the DMS® columns' calibration phases up to hundreds of meters long in the testing field's boreholes. The goal is to provide the most accurate and reliable geotechnical monitoring data for correct data interpretation. Oftentimes the focus is on the amount of data collected rather than having accurate data, especially in terms of direction of displacements or consistency between the real direction of deformation and the one measured by the instrument. Lost in this perspective is the true purpose of geotechnical monitoring.

REFERENCES

Blikra, L. H., Kristensen, L., Lovisolo, M. 2013, 'Subsurface monitoring of large rockslides in Norway: a key requirement for Early Warning', International Conference Vajont 1963-2013. Thoughts and analyses after 50 years since the catastrophic landslide, Italian Journal of Engineering Geology and Environment, Università Sapienza di Roma, pp. 307-314.

Dunnicliff, J 1988-2003, *Geotechnical instrumentation for monitoring field performance*, John Wiley & Sons, New York.

Dunnicliff, J & La Fonta, JG 2001, 'In place inclinometers. A significant test program', *Geotechnical News*, vol. 19 no. 1, pp 33-34.

Giuffredi, F, Zanolini, L & Foglino, L 2003, 'Application of a new integrated multi-parametric monitoring system for the analysis of micro-movements in the Civil Protection activities: An example', in F Myrvoll (eds), *Field Measurements in Geomechanics*, A.A. Balkema Publishers, Lisse, pp. 61-66.

La Fonta JG & Beth MB 2002, *In place inclinometers, a significant test program,* Soldata – France, Unpublished.

Lovisolo, M & Della Giusta, A 2005, 'Precision of D.M.S. columns from real time in-place measurements and improvement in micro-movements analysis with early warning function', in CA Brebbia & GM Carlomagno (eds), *CMEM XII Twelfth International Conference on Computational Methods and Experimental Measurements*, WIT Press, Southampton, pp. 177-186.

Lovisolo, M, Ghirotto, S, Scardia, C & Battaglio, M 2003, 'The use of Differential Monitoring Stability (DMS®) for remote monitoring of excavation and landslide movements', in F Myrvoll (eds), *Field Measurements in Geomechanics*, A.A. Balkema Publishers, Lisse, pp. 519-524.

 © Deep Foundations Institute 2025

Mikkelsen, PE 2003, ‘Advances in inclinometer data analysis’, in F Myrvoll (eds), *Field Measurements in Geomechanics*, A.A. Balkema Publishers, Lisse, pp. 555-567.

Simeoni, L & Mongiovì, L 2003, ‘The problematic management of the displacement monitoring system of a landslide’, in F Myrvoll (eds), *Field Measurements in Geomechanics*, A.A. Balkema Publishers, Lisse, pp. 673-680.

UNI EN ISO 18674 Geotechnical Investigation and testing. Geotechnical monitoring by field instrumentation. Part 1 general rules, July 2015

 © Deep Foundations Institute 2025

INNOVATIONS AND QUALITY IN EQUIPMENT DESIGN FOR SAFETY AND EFFICIENCY

Kai Fiand, CAPE Holland B.V. Beilen, Netherlands, +1 346 290 3874 kai.fiand@capeholland.com
Bartjan van den Berg, CAPE Holland Inc., Houston, Texas, USA, bartjan.vandenberg@capeholland.com
Paul Doherty, Venterra Group, London, UK, paul.doherty@venterra-group.com

ABSTRACT

Vibro piling equipment has existed for decades and has been used extensively onshore for sheet pile installation amongst other foundation solutions. This silent method of foundation installation brings great benefits for urban areas as well as in environmentally sensitive areas to mitigate impacts on wildlife (e.g. marine mammals). By combining this technology with other innovative ideas, the safety and efficiency of foundation installation can be elevated to a much higher level. For instance, combining the functionality of a certified pile lifting device to allow upending and placing the pile allows tool changes at height to be avoided. Mitigating the need for rigging adjustments (eg. disconnecting slings) in unstable conditions does not only increase the speed of foundation installation but also avoids safety hazards. Triggered by offshore safety standards these innovative ideas are now also available for coastal/onshore projects to increase safety and efficiency and ultimately lead to cost savings by improving productivity. The ability to accurately predict pile vibro driveability also ensures that the right tooling can be selected for the project (hammer size / frequency) and that we can quantify the penetration depth to ensure the selected vibro hammer is capable of installing the pile to a stable depth.

Keywords: pile driving, foundation installation, lifting, safety, efficiency, vibratory hammer, piling equipment

INTRODUCTION

Vibro pile installation has seen significant advancements in recent years, driven by innovations in equipment, monitoring technology, and understanding of the soil-structure interaction allowing for better predictability of pile driveability. As an essential foundation method used in onshore infrastructure as well as offshore construction, vibro piling offers an efficient, low-noise alternative to traditional impact pile driving. The latest technological developments focus on improving installation speed, reducing environmental impact, and enhancing pile performance in various soil conditions. The most significant advances in installation equipment have been driven by the specific needs of the offshore wind sector. However, the technology enhancements can also benefit to onshore infrastructure projects such as major river crossings or port structures.

The offshore wind sector requires a stable fixed-bottom foundation capable of supporting an offshore wind turbine of up to 20MW capacity in water depths of up to 80m. The primary foundation options are Monopiles and Jackets for most fixed-bottom sites. Monopiles, which make up the vast majority of foundations installed to date comprise a single steel tube of up to 30 feet diameter driven or vibrated into the seabed to a penetration of circa 100 to 150 feet, depending on the ground conditions. Jackets comprise a 3- or 4-legged lattice structure formed from welded tubular steel elements, supported on pre or post installed piles supporting each leg (typical jacket piles are in the 48 to 150 inch diameter range). The need to minimize offshore operations, reduce the cycle times and streamline activities to reduce the vessel costs, which can be circa USD 500,000 per day, demands that piling equipment is reliable. As a result, vibro hammers have been developed to mitigate the need for separate lifting tools – these Vibro Lifting Tools (VLTs) facilitate safe and efficient offshore operations, significantly de-risking these multi-billion dollar

 © Deep Foundations Institute 2025

offshore wind energy projects. These tools also mitigate the potential for pile free run where piles can suddenly experience an uncontrollable penetration into the seabed which can damage the crane/vessel as well as resulting in a non-compliant foundation due to tolerance issues, etc. Another advantage of adopting vibro technology offshore is to mitigate the underwater noise impacts on marine mammals, which can be a major concern for impact pile driving in certain jurisdictions. While developed specifically for the offshore wind sector, the specific features of these VLTs can now also be applied to onshore infrastructure projects where similar benefits can be experienced in terms of safer operations and higher production rates achieved through simpler piling processes. This paper provides an overview of the recent technological advancements as well as introducing some relevant project case studies where the improvements in the VLT were experienced firsthand.

BACKGROUND: EQUIPMENT EVOLUTION

Vibratory driving is a technique which has been widely and very successfully applied for the installation of low-displacement piles such as sheet piles, H-beams, and small diameter tubular piles. In Europe, about 80% of sheet piles are driven by vibratory hammers. The remainder are either pushed or driven by an impact hammer (Azzouzi, 2003). Traditionally, vibro hammers have also had the auxiliary role of bringing the pile to a stable depth before driving it to final depth with an impact hammer, thus avoiding the need for temporary support frames. Vibrators operate with continuous vibrations of higher frequencies (20-40 Hz) compared to impact pile drivers, which typically have strike rates between 30-60 blows per minute for heavy hammers and 30-120 blows per minute for light hammers.

The vibratory driving technique dates to the early 1930's when it was simultaneously developed in a number of countries, including Germany and Russia. The Russian soil dynamics researcher Pavyluk observed that soil resistance could be reduced by using vibrations during pile installation (Pavyluk, 1969). Extensive research on the effects of vibratory sheet-pile driving on soils, led to acceptance of vibratory sheet-pile installation as an effective and economical method. During the 1980s and 1990s, research projects related to the driveability of piles were conducted in the Department of Structural Dynamics at the Dutch Organisation for Applied Scientific Research (TNO) and the Department of Soil Mechanics and Execution Techniques at the Belgian Building Research Institute (BBRI) (BBRI, 1994). However, a limited number of publications about this research work can be found in the public domain. The work by Jonker and Middendorp (1988) to account for soil fatigue as a result of the cyclic loading of the vibratory hammer has been a major contribution in driveability modelling and predictions. Extensive laboratory studies on the three different components (i.e., vibratory-driver, soil, and pile) that influenced both the driveability and the bearing capacity of vibro installed piles have been conducted at the University of Houston, Texas (USA) (O'Neill and Vipulanandan, 1989). The history of vibratory pile driving has been extensively discussed by various researchers (e.g. Viking, 2002) and is outlined in El Kanfoudi (2016).

Research continued at both practical and theoretical levels for different industries. Viking (2002), Middendorp and Verbeek (2004) and Vanden Berghe (2001) have provided an extensive review on vibratory installation methods and have demonstrated the successful use of vibratory drivers for the installation of piles in a variety of situations. Strong interest in the application of vibratory hammers to install steel tubular monopiles for the offshore wind industry was supported by a successful installation of a 90 ft diameter tubular pile with a length of 130 ft by vibratory hammers in Hong Kong, China in 2011.

The more recent advances in vibro installation equipment over the past decade have been driven by the needs to install large diameter piles for offshore wind farms in a safe and efficient manner. CAPE Holland

have developed a suite of Vibro Lifting Tools (VLTs) that have facilitated the installation of offshore Monopiles greater than 30 ft in diameter at the Moray West project in Scotland, Jacket Pin piles for a variety of offshore support structures and onshore piles for applications that includes bridges, quay walls and jetties. Key features of the new equipment include safer and more efficient operations due to the ability to pick the piles from a horizontal position and pitch them into a vertical position without manual intervention and then install them to a stable depth without the need for templates and guide structures. The flexibility offered by the VLTs also mean that piles can be extracted and/or repositioned if needed. This allows piles and sheets, or combi walls, to be installed temporarily for applications such as ground improvements or pipeline starter piles where structures are only needed temporarily and will need to be removed later.

The improvements in pile handling translate to dramatically increased productivity with installation times often reduced by 50% compared to other pile installation methodologies.

INSTALLATION PROCESS AND PRIMARY BENEFITS OF THE VLT

Vibro pile installation has seen significant advancements in recent years, driven by innovations in equipment as well as better predictive models for the soil-structure interaction that allow the right tooling to be selected for a particular set of site conditions (soil and pile combination). The image below demonstrates the simplicity of the tool, where the ability to connect the VLT in a horizontal position and upend the pile without the need for manual intervention and complex rigging clearly saves time and improves reliability as well as safety. In an offshore environment, efficient and safe operations are critical as the cost of the vessel drives the overall project costs – therefore every minute saved in the installation operations adds up to significant overall savings when amplified by the vessel costs. Reliability is also critical as equipment breakdown can pause all operations and lead to substantial cost overruns. Offshore projects also demand a very high standard of Health & Safety, where certified lifting tools are a requirement. The VLTs are therefore designed as certified lifting tools as well as pile installation tools. The design, fabrication, and assembly follow a detailed third-party certification process to ensure reliability and predictability of response. Being able to install one pile faster is useful, but consistently being able to install 1000 piles faster allows saving significant amount of time and money.

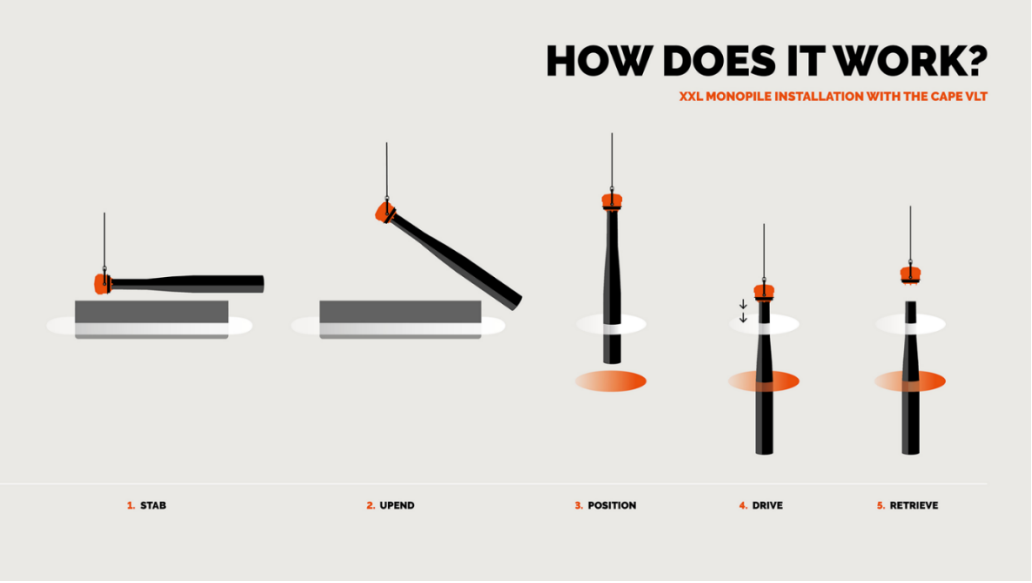


Fig. 1. Pile installation methodology using the VLT

 © Deep Foundations Institute 2025

While these equipment enhancements have been very much driven by the needs of the offshore sector, they can also be leveraged for onshore and nearshore projects. This extrapolation of technology to onshore conditions gives the same safety and productivity benefits. The predictability of response not only allows for a much faster installation schedule, the predictability of the response allows the overall program to be reduced by removing some of the float between dependent activities.

For onshore applications, conventional pile handling requires more complex handling, rigging with shackles and guide ropes and multiple operators needed to upend piles and guide them into position. Furthermore, tool changes often require operators working at height in man riding baskets or cherry pickers in order to connect/disconnect shackles, etc. All of these operations have been undertaken in this manner for decades as it is deemed the "normal" operating procedure – however, many of these risks can be avoided through the use of the VLT.

PREDICTING PILE INSTALLATION BEHAVIOUR AND LIMITATIONS OF VIBRO DRIVEN PILES

Vibro pile installation has seen significant advancements in recent years, driven by innovations in equipment but this has also been mirrored by better theoretical models to estimate the installation of the pile to a given set of site conditions including changes in soil conditions and variable pile geometries. The installation behaviour is a function of a wide range of variables including the hammer frequency, the hammer power, the pile geometry and associated pile frequency, the soil conditions, the water conditions, etc. The inhomogeneous nature of soils also means that at most sites it is necessary to predict the response for a range of different soil conditions (sands, clays, etc.). While outside the scope of this paper, there have been significant improvements in predicting the likely penetration depths and penetration rate when using a specific VLT with a particular pile geometry. This allows the selection of the right size VLT for any given project and also to determine whether additional equipment such as an impact hammer is needed to finish the piles to a target penetration depth. The more widespread use of the VLT both onshore and offshore has created a wider dataset of use cases which in a simple manner allows for anecdotal identification and cross reference of where specific tools can be used successfully but this dataset also allows for updating and validation of the analytical predictive installation models.

OFFSHORE CASE STUDY – MORAY WEST

Vibro pile installation has seen significant advancements in recent years, driven by innovations in equipment. Modular tooling allows for large single piece monopiles to be installed in a single lift operation. The VLT technology enabled the installation of 41 monopiles with a weight of up to 2,000 metric tons and a pile top diameter of 24 ft during the winter period in the North Sea, known for rough weather conditions. The efficient installation method allowed the use of smaller weather windows and reduced project risks. One major risk that was identified for the project was the potential pile run. By always keeping tension in the crane wire and having the VLT clamped on to the flange of the monopile full control was maintained at all times during the installation through instable soil layers until stability was reached.



Fig. 2. VLT-640 Triple installing large monopiles at the Moray West Offshore Wind Project

ONSHORE CASE STUDY – RGLNG TERMINAL

By scaling down the CAPE offshore technology to facilitate onshore operations, allows the VLTs to be deployed for a wide range of infrastructure projects including major river crossings, port developments, LNG terminals and soil enhancement for tunnel constructions.

CAPE Holland has successfully contributed to the Rio Grande LNG (RGLNG) terminal project by providing its advanced VLT-80 Vibro Lifting Tools (VLTs) for the installation of 307 piles. The RGLNG terminal, located on the Brownsville ship channel in Texas, is an essential project for the US natural gas export industry. The terminal's first phase includes the construction of three liquefaction trains, two storage tanks, and two marine berths.

 © Deep Foundations Institute 2025



Fig. 3. VLT-80 upending a pile on the RGLNG project

CAPE Holland supplied two VLT-80 units for the project, allowing for the efficient upending and installation of each pile in a single operation. These innovative Vibro Lifting Tools are designed to handle large, heavy piles, optimizing the installation process and reducing project timelines.

The piles installed at the terminal support several critical structures:

- **Marine Berths**: 184 piles were installed to support the two marine berths, where LNG carriers will dock to load and unload cargo.
- **Mooring Dolphins**: 60 piles were installed for the mooring dolphins, providing secure docking facilities for LNG vessels and ensuring safe operations.
- **Materials Offloading Facility (MOF)**: 53 piles were installed to support the MOF, which is vital for the reception and offloading of materials used in terminal operations.

The use of CAPE Holland's VLT-80 units played a key role in enabling Bechtel to meet important project deadlines while ensuring the safety and quality of the installation. This collaboration highlights CAPE Holland's expertise in providing reliable and efficient foundation installation solutions for large-scale infrastructure projects.

 © Deep Foundations Institute 2025



Fig. 4. VLT-80 upending a pile on the RGLNG project

As can be seen from the image above, the piles were pitched and lifted in a simple and safe operation which saved significant time. The quick cycle time allowed multiple piles to be installed in a day, dramatically improving the overall delivery schedule when compared to more traditional approaches that would involve significantly more manual intervention, rigging, etc.

FUTURE OUTLOOK: THE TECHNOLOGY ROADMAP FOR THE VLT

The technological advancements in recent years to enable projects like Moray West and the RCLNG terminal to be completed are impressive and demonstrate a huge step forward in the capabilities of piling equipment, however recent advancements have also helped to highlight that continued improvement in the VLT technology could unlock even further savings in both onshore and offshore projects. Some future equipment developments that are being progressed include:

- Higher frequency gearbox to facilitate deeper penetrations as well as mitigating potential resonance issues for some specific pile-hammer-soil conditions;
- Variable frequency gearbox for adaptability in different ground conditions;
- Combination with other technologies such as jetting to facilitate deep penetrations in challenging ground conditions;
- Different clamping arrangements to facilitate simple pitching and lifting of a range of pile geometries.

 © Deep Foundations Institute 2025

As well as specific equipment upgrades that are currently being planned, there is an ongoing engineering effort to further enhance the accuracy of driveability analysis and noise predictions. There is a significant role for real time measurements during pile installations to help validate and calibrate both driveability models and noise propagation models and to improve the predictability of the pile-soil-hammer response to the specific site conditions. The development and validation of better predictive tools is helpful to demonstrate the value of adopting vibro technologies on new projects.

CONCLUSION

The offshore wind sector has spawned the development of a novel set of Vibro Lifting Tools (VLTs) designed and constructed by CAPE Holland in order to maximise the efficiency of offshore operations. These tools have now been deployed on onshore infrastructure and coastal projects where the benefits have also been realized. Some of these advantages include:

- Safe handling, minimizing the need for rigging
- Automatic pitching and tilting of the pile, reducing the need for manual interventions
- Less people resources required due to the safer and simpler operations
- Quiet installation compared to impact only driving
- Faster installation schedules due to improved productivity
- More predictable and controllable response, mitigating issues such as pile free run
- Ability to extract piles or adjust piles if required.

LITARATURE CITED

[1] Azzouzi S. [2003]. “Intrillen van stalen damwanden in nietcohesieve gronden”, GeoDelft NL &. TU. Delft NL

[2] N. P. Pavlyuk [1969]. "Vibration of a solid body resting on an elastic base” Gosstroiizdat

[3] Jonker, G., Middendorp, P., [1988]. Subsea installations using vibratory piling hammers, 20th OTC, Houston, Texas

[4] O'Neill and Vipulanandan, [1989]. Laboratory Modeling of Vibro-Driven Piles, Journal of Geotechnical Engineering, Volume 116, Issue 8

[5] El Kanfoudi [2016]. On modelling the lateral behaviour of vibratory driven monopile foundations for offshore wind turbines, TU Delft Repository

[6] Viking, K. [2002]. Vibro-Driveability—A Field Study of Vibratory Driven Sheet Piles in Non-Cohesive Soils. Ph.D. Dissertation, Department of Civil and Architectural Engineering Royal Institute of Technology (KTH), Stockholm, Sweden.

[7] Vanden Berghe, J.-F. [2001]. Sand Strength Degradation within the Framework of Vibratory Pile Driving. PhD Dissertation, The Faculty of Applied Science, Universite Chatolique de Louvain, Belgium.

 © Deep Foundations Institute 2025

SLURRY WALL DESIGN TECHNIQUES AND CONSTRUCTION PRACTICES OVER THE LAST 50 YEARS IN NORTHEASTERN UNITED STATES

S. Y. Fantaye, P.E., Principal, Mueser Rutledge Consulting Engineers, NY, NY, USA
Ketan Trivedi P.E., Senior Associate, Mueser Rutledge Consulting Engineers, NY, NY, USA
Alex Ciamei P.E., Senior Associate, Mueser Rutledge Consulting Engineers, NY, NY, USA
Lixun Sun, PhD., Lead Engineer, Mueser Rutledge Consulting Engineers, NY, NY, USA

ABSTRACT

Slurry walls, also known as diaphragm walls, were first introduced to the United States in the early 1960s for deep excavation projects. The technology was patented in the late 1940s by ICOS in Italy. The first major application of slurry wall technology occurred in the mid-1950s for the Paris Metro Line 8, where the technique was used to create a 100 feet (30.5 m) deep excavation. The slurry wall was laterally supported by bracing and tieback anchors. After a decade of successful development and demonstration, slurry walls were introduced to the U.S. in the early 1960s. The first major U.S. application of slurry walls took place in the late 1960s for a 70 feet (21.3 m) deep excavation in Lower Manhattan, New York City, during the construction of the foundations and below-grade structures for the original World Trade Center Towers. The slurry wall was supported by multiple levels of high-capacity strand tieback anchors installed in rock. The construction proved successful, providing lateral support for deep excavation and effective groundwater control, enabling foundation construction in the dry. Following the success of the World Trade Center project, slurry wall technology was widely adopted in major U.S. cities. Slurry walls became particularly essential for constructing tall buildings requiring significant below-ground space for parking and other facilities, deep subway stations, and shafts for launching and retrieving tunnel boring machines. The technology allowed for safe excavations, worker protection, and the safeguarding of adjacent structures, reducing construction risks for contractors, owners, and the public. This paper explores the advancements in slurry wall analysis, design, and construction methods over the past 50 years, with a focus on case histories from northeastern U.S. cities, particularly Boston, New York City, Baltimore, and Washington, D.C.

Keywords: Limit Equilibrium Method, Finite Element Method, Clough and O'Rourke's Method, Clamshell, Hydromill, Hydrofraise, AI

INTRODUCTION

History and Development of Diaphragm Wall Analysis and Design

Slurry wall construction was first introduced to the United States in the late 1960s. At the time, almost all of the analysis was being performed by hand calculations aided by slide rules and the most basic of electronic calculators. Engineers spent countless hours calculating lateral pressure diagrams and analyzing the slurry wall as if it were a structural beam. This method of analysis, also known as the Limit Equilibrium Method, considers the actual excavation process whereby the load is applied to the beam element at various stages of excavation from existing grade down to the final subgrade, moment equilibrium, shear and factor of safety against toe stability (wall rotation), are calculated by hand.

 © Deep Foundations Institute 2025

Limit Equilibrium Method

The design process begins with identifying the soil layers and their properties, such as unit weight, cohesion, internal friction angle, groundwater depth, depth of excavation and identifying constraints such as adjacent structures followed by assuming the geometry of the slurry wall including the thickness of wall, bracing levels, wall depth of embedment below the excavation level. Then, the lateral earth pressures acting on both sides of the wall are calculated (Fig. 1), using active earth pressure coefficients (Ka), retained side, and passive earth pressure coefficients (Kp), excavated side. Other load effects such as surcharge loads at the ground surface on the retained side that contribute to the lateral earth pressures such as weight of existing buildings founded at shallower depth than the proposed excavation and or ground pressures from construction equipment are included in the calculation. Additionally, if groundwater is present, the hydrostatic pressures acting on the wall both on the retained and excavated sides are calculated.

The first stage of analysis in a multi-staged slurry wall is the stage prior to installation of the uppermost brace level, where the slurry wall acts as a cantilever beam. For this stage, force equilibrium equations, sum of horizontal forces, active (driving) and passive (resisting), and moments caused by these forces are summed about an assumed base of wall because wall embedment provides the primary support for a cantilever wall (Fig. 2) (NAVFAC, 1982). The assumed wall embedment is iteratively adjusted as the sum of driving and resisting moments must equal zero for the wall to be in equilibrium. Then, the wall embedment is increased or checked to ensure adequate factor of safety. The factor of safety is typically calculated by comparing the resisting forces (passive earth pressures) to the driving forces (active earth pressures and external loads). Once equilibrium is reached, wall internal forces moment and shear for this stage of excavation are calculated by cutting a section through the wall and setting up a free body diagram of the segment and analyzing the sum of external and internal forces about the cut using equilibrium equations (Fig. 2). Wall deflection is typically calculated assuming a fixed cantilever beam where the effect of the passive soil springs is ignored. Alternatively, charts developed by Clough and O'Rourke (Clough et al, 1990) are used in estimating wall deflection.

In the second stage (Fig. 4), the upper brace is installed, and excavation has progressed to just below the second brace level. Moments due to the opposing forces are summed about the brace level to calculate a safety factor against toe kickout, followed by calculation of moment and shear in the wall using equilibrium equations described above. Wall deflection is typically calculated assuming a "hinge" support at the point of zero net pressure and analyzing a structural beam for deflection.

$$\sum M_1 = 0$$
$$\sum V_1 = 0$$
$$\sum N_1 = 0$$

 © Deep Foundations Institute 2025

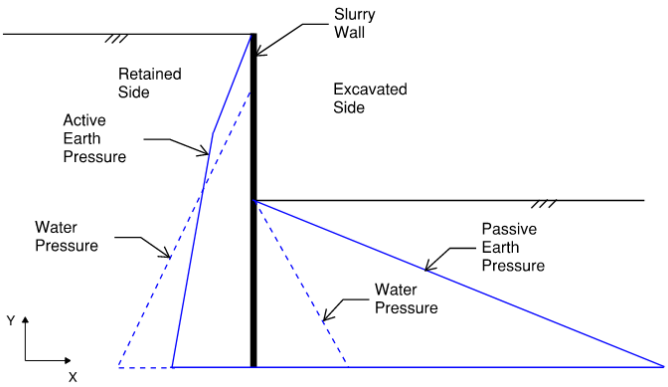


Fig. 1. Pressure Diagrams for Limit Equilibrium Method

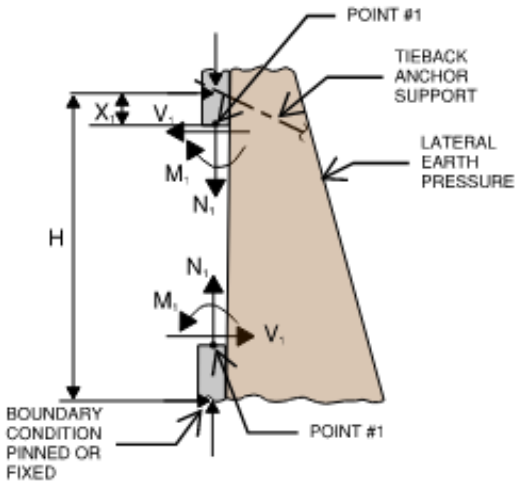


Fig. 2. Free body diagram of slurry wall with one level of support

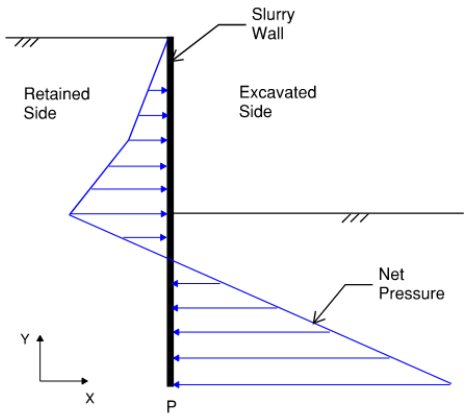


Fig. 3. Net Pressure Diagram for 1st Excavation Stage (Cantilever)

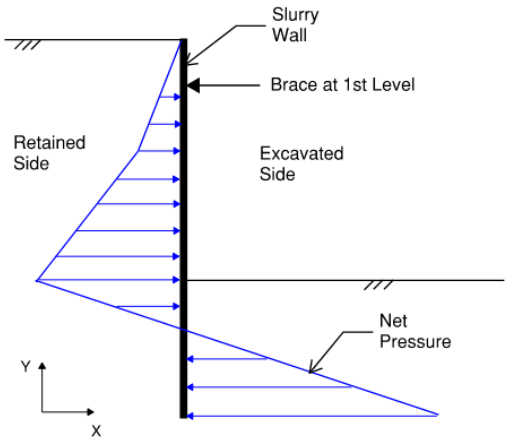


Fig. 4. Net Pressure Diagram for 2nd Excavation Stage (One Level Brace)

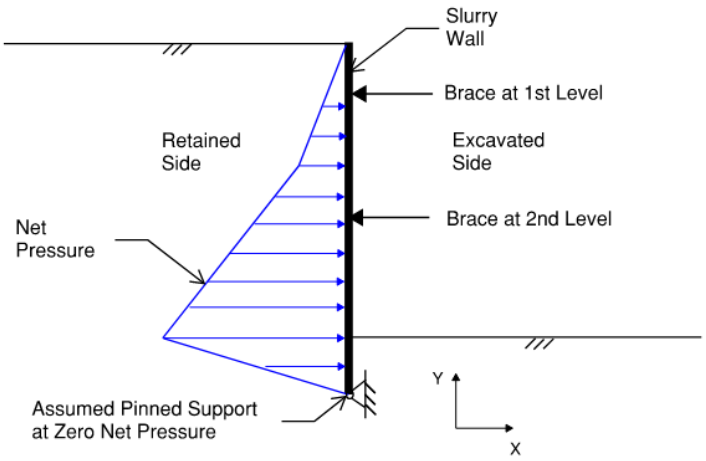


Fig. 5. Net Pressure Diagram for 3rd Excavation Stage (Two Level Braces) Brace)

 © Deep Foundations Institute 2025

For third and subsequent stages (Fig. 4 and Fig. 5), net pressure diagrams resulting from the sum of driving and resisting forces, either from a triangular Rankine (NAVFAC, 1982) or Apparent Earth Pressure diagrams are then applied on the wall assuming the wall is a continuous structural beam with multiple supports (NAVFAC,1982).

Lateral pressure diagrams were usually simplified into rectangular blocks for ease of analysis. A continuous beam model was then created with rectangular block loadings. To analyze the beam model, the widely used method of analysis was “moment distribution.” This method assumes rigid multiple support, which usually is not the case with lateral bracing systems (tiebacks, cross lot struts and rakers) for slurry walls.

During the 1960s and 1970s, computer programs such as FORTRAN and STRESS which were used mostly in universities and large organizations became available for use by consulting engineering firms. Fortran, short for "Formula Translation," was developed by IBM and first released in 1957 (Backus, 1998). The program was widely adopted in various engineering and scientific fields due to its efficiency in handling complex numerical computations. STRESS (Structural Engineering System Solver) is a programming system for the solution of structural engineering problems (Fenves, et.al.,1964). These programs were general structural engineering computer programs that simply transformed what was once performed by hand into a routine effort computed by a computer. The programs used the principles of equilibrium equations and Direct Stiffness Method or matrix methods of structural analysis which are highly suitable for computers (Matrix Analysis of Frame Structures), as the underlying method. The advantages of these programs were not limited to simply automating the analysis process but also allowed the user to input trapezoidal and triangular soil pressure diagrams instead of simplifying it and allowed for variable stiffness of the slurry wall along its depth, although not needed for a slurry wall. While these programs were a huge leap forward compared to the tedious hand calculations used to analyze a slurry wall, their major deficiency was that they lacked the ability to represent the soil-structure interaction in the calculation of internal forces and deformation of the wall. In essence soil springs could not be entered into these programs.

During the late 1960’s and 1970s, BMCOL was one of the first programs that attempted to consider soil-structure interaction became available to consulting engineering firms. The BMCOL program was developed as part of a cooperative highway research program at the University of Texas at Austin and was designed to assist engineers in analyzing beam-columns under various loading conditions (Matlock, et. al.,1968). BMCOL, which used a beam model with spring supports, was inspired by the Winkler Spring Method. This was essentially a structural analysis program with “structural” springs. However, user intervention was required for the soil-structure interaction part. Lateral braces were modelled as structural springs with corresponding stiffness. Passive pressure below subgrade was modelled as a series of closely spaced springs, based on the modulus of horizontal subgrade reaction, K_h) (NAVFAC, 1982). The program provided the spring forces, but because BMCOL was a structural program, it made no consideration whether the soil springs below subgrade could provide the required passive force equal to the calculated spring force. This is where user intervention was required. The user would have to manually calculate the passive force corresponding to each spring, and where the calculated spring force exceeded the available passive resistance, those particular springs were removed and replaced with an equivalent resisting force. The program was then rerun and the process repeated until all soil springs were subject to a force no greater than the resisting passive force.

During the 1990s, as desktop computers became more common and commercial engineering analysis and design software became more readily available and affordable, the above programs, both structural and soil-structure interaction, were more frequently used. As computers evolved and their computing capacities significantly increased, the use of finite element analysis (FEA) was introduced to the field of consulting engineering.

Finite Element Methods

FEA for geotechnical engineering applications is a computational method for determining stresses and deformations in selected domain by breaking it down into small/finite elements. These elements are typically in simple geometric shapes, like triangles and quadrilaterals in 2D, or tetrahedrons and bricks in 3D (Fig. 6). Each element is governed by the equations that describe its stress and deformation characteristics. These equations are then assembled into large matrix equations and solved collectively on a computer. FEA has been becoming a powerful analysis tool in geotechnical consulting engineers in the last three decades with the availability of commercial software and increasing computing power. During this period, FEA was also becoming more frequently used in slurry wall design.

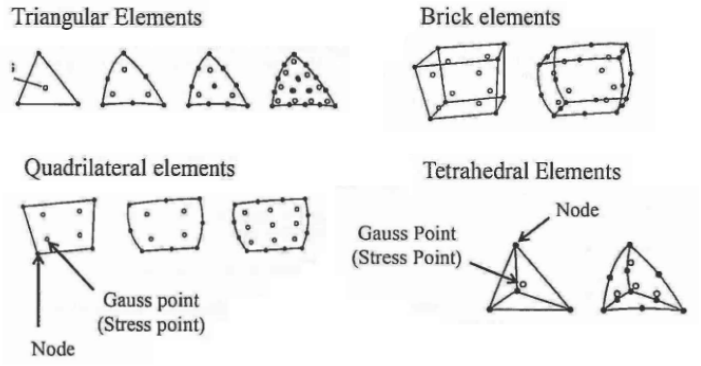


Fig. 6. Types of Elements Used in Finite Element Analysis

The advantages of using FEA in slurry wall design include its capabilities of modeling complex geometry, simulating the excavation stages and accounting for the soil-structure interaction. In a typical FEA on support of excavation (SOE) system, the soil can be modeled as volume elements and the structural components, such as the slurry wall and brace systems, can be modeled as structural elements. The structural elements can fully interact with the surrounding soil elements. To realistically model the soil-structure interaction, the interface elements can be adopted between the structure and sounding soil. The interface elements can simulate the relative displacements, like slide and separation, between the structure and soil. Also, with the advanced soil constitutive models, FEA can simulate the soil's nonlinear behavior, drained and undrained material behaviors, and the consolidation procedures with reasonable accuracy. Figure 7 shows a typical FEA/Plaxis 2D mesh used for a SOE system with 3-level braces of tieback.

 © Deep Foundations Institute 2025

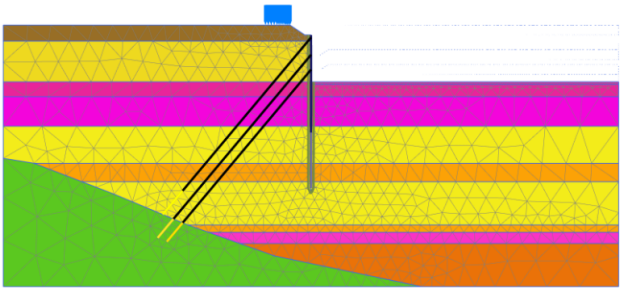


Fig. 7. A Typical FEA/Plaxis 2D Mesh for SOE Analysis

A salient application of FEA in slurry wall design is to evaluate the impacts of SOE system on the adjacent structures and facilities, such as building, subway tunnel and utility line etc. These impacts were basically estimated by the empirical approaches, such as Clough and O'Rourke's method, before FEA became a major analysis tool in geotechnical engineering. Currently, the impacts of SOE systems on the adjacent structures and facilities are mostly conducted by FEA.

Comparison of Limit Equilibrium Method (LEM) and Finite Element Methods (FEM)

A comparison of wall internal force results for LEM and FEM methods for two different walls are presented in Fig. 8 and Fig. 9. Initial brace results from LEM were used in the FEM model for design section N1A. Then these brace results were preloaded to fifty percent of the estimated only. A comparison of the moment diagram for these two methods indicates a redistribution of moment.

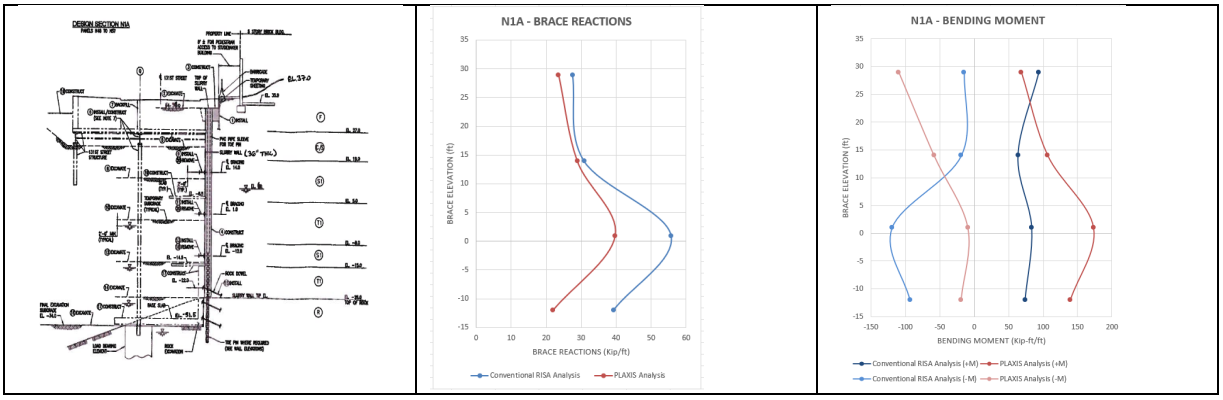


Fig. 8. Comparison of Brace Loads and Wall Moments – Case 1
(Note wall is supported by preloaded internal bracing)

Similarly, initial brace results from LEM were used in the FEM model for design section N1B. Then these brace results were preloaded to one hundred percent of the estimated to minimize wall displacement and associated settlement of adjacent structures. A comparison of the moment diagram, as shown in Fig. 8 and 9, for these two methods indicates a redistribution of moment with generally increased values from the FEM.

 © Deep Foundations Institute 2025

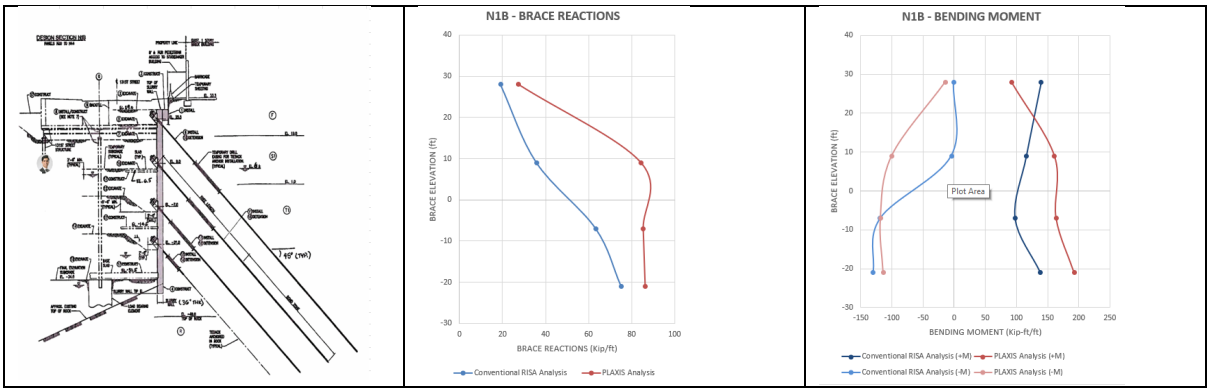


Fig. 9. Comparison of Brace Loads and Wall Moments – Case 2
(Note wall is supported by preloaded tieback anchors)

Future of Diaphragm wall analysis and design

In recent years and up to today (2025), the common method of analysis is the traditional computer aided moment distribution method in conjunction with FEA. The reason why many engineers prefer the two methods is simple, the traditional moment distribution method has a proven track history whereas the FEA method is still evolving. From our experience, we have seen significant divergence between the methods. We have not observed any generalized trends such as consistently higher or lower brace loads or wall moments, except for wall deflection calculated using the FEA method correlates better with observed wall deflection from inclinometer data.

Continued review of monitoring data, including optical survey and inclinometer data, as well as load cell data should be performed to compare the actual loads and deflections against those predicted by calculations. The soil-structure interaction models should then be calibrated. The calibrated results should then be used for future projects to minimize the divergence between actual vs predicted loads and deflections.

We are currently not aware of the use of AI in slurry wall design, however it is our opinion that in the not-too-distant future, that the FEA method, aided by AI (artificial Intelligence) will become the method of choice. But until then, the slurry wall designers should continue to use the two methods described herein. Design brace loads, moments and shear in the wall should be the higher of values obtained by the two methods. Wall deflection as well as movements of nearby structures and utilities should be based on the FEA method.

CONSTRUCTION METHODS

Panel Excavation

From inception to current state of practice of slurry wall construction, panel excavation equipment and methods have evolved. The initial method of excavation involved a cable suspended mechanical clamshell bucket (Fig. 10) and percussion chisel (Fig. 11), from a crane. Impresa Costruzioni Opere Specializzate (ICOS) is credited with the invention of the mechanical clamshell in early 1950s. These tools and methods of excavation are still in practice fully and in combination with advanced systems. The mechanical

clamshell bucket is controlled by the cables which open and close the bucket. Digging the slurry-mix stabilized panel is carried out by lowering and dropping the clamshell and biting into the material by pulling on one of the cables and closing the jaws of the clamshell. This process is repeated to advance the excavation below the bottom of the guide wall to either final subgrade, top of rock or dense to very dense stratum or until an obstruction is encountered. Where it is necessary to dig through dense to very dense stratum or an obstruction or key the bottom of the slurry wall into rock, a chisel weighing 5 to 15 tons (DFI, 2005) dropping from a height of 10 to 25 feet is used to loosen up the material before it is removed with the clamshell. One of the advantages of this system is its simplicity, in that it is operated using a cable system, its own weight and gravity, which significantly minimizes downtime due to few moving parts. Its disadvantages include less vertical control with depth and impacts on the environment such as noise & vibrations at the ground surface. The dropping of the clamshell and chisel cause relatively high levels of noise and vibrations that may exceed certain acceptable levels in urban environments. In general, mechanical clamshell buckets can be used on most geologic formations up to approximately 150 feet deep.

The hydraulic clamshell system (Fig. 12) was introduced as an enhanced method of slurry wall panel excavation in the early to mid-1970s. There is no literature which attributes the invention of this system to any one company except companies such as ICOS and Soletanche-Bachy which have played pivotal roles. This clamshell in general performs similar tasks to the mechanical clamshell. However, it typically performs panel excavation with better precision (less vertical deviation with panel depth), higher efficiency digging in denser soils than mechanical clamshells. The main advantage of the hydraulic over the mechanical clamshell is the controlled opening and closing of the jaws using hydraulic means and its ability to adjust vertical control. The clamshell is typically lifted and positioned into the panel with either a cable or Kelly-bar attached to a crane. Unlike the mechanical clamshell, the hydraulic is lowered, positioned and the jaws hydraulically operated to perform controlled excavation.

Hydrofraise was developed in Europe by Soletanche-Bachy in the early 1970s (Fig 13). This equipment performs similar excavation, although with differing methodology than the mechanical and hydraulic clamshells, however it is superior to both due to its efficiency, vertical control and ability to excavate in all formations including rock. Its efficiency can be attributed to the continuous removal of the soil by the rotary digging action of the cutter wheels that rotate in opposite directions, where the spoils are mixed with the slurry and removed via reverse circulation. Soletanche-Bachy has continuously advanced its equipment and technology with on-board data acquisition systems including a triaxial gyroscope system used for verticality and position control. Unlike mechanical and hydraulic clamshells, the Hydrofraise cutters do not have to be withdrawn from the panel to remove the spoils. Some disadvantages of this equipment include: (1) it requires to be inserted into a pre-excavated panel equivalent to a minimum depth, so it is fully submerged in the slurry including its verticality sensors, which is about 30 feet (9.1 m) depth. Panel pre-excavation requires either a mechanical or hydraulic clamshell; (2) In geologic formations such as glacial till, the presence of certain size cobbles and boulders may clog the cutter wheels. When clogging occurs, the cutter wheels must be withdrawn from the panel to remove the obstructions by rotating the cutter wheels in the opposite direction (Fig. 14). If frequent clogging occurs, the unclogging operation could significantly adversely impact production efficiency.

Hydromills perform identical tasks to the Hydrofraise, except that these machines were introduced after the Hydrofraise to the market by different companies such as Bauer, Casagrande and Soilmec. In 1984, German

contractor Bauer A.G., Schrobenhausen, used one of such trench cutters to build a 131 feet (39.9 m) deep wall in sandstone at the country's Brombach reservoir (Reina, 2012). A performance comparison of slurry wall panel excavation equipment is provided in Table 1.

Table 1. Performance Comparison of Slurry Wall Panel Excavation Equipment

Equipment	Geologic Formation	Panel Depth Range FT, (m)	Vertical Control Adjustment	Obstructions[2]	Productivity	Cost
Mechanical Clamshell	Loose to medium dense	50 to 140[1] (15.2 to 42.7)	No	Requires chisel	Slightly less efficient than other systems	Less than other systems
Hydraulic Grab	Loose to dense to very dense	50 to 140 (15.2 to 42.7)	Yes	May require chisel	Slightly more efficient than clamshell[3]	More than mechanical but less than Hydromill/ Hydrofraise
Hydromill/ Hydofraise	Loose to dense to very dense	100 to 240 (30.5 to 73.2)	Yes	Wheels may lock up, may slow production	More efficient than mechanical and hydraulic clamshells	More than other systems

[1] The information provided in Table 2 is based on the authors experience
[2] Obstructions are defined as nested cobbles and boulders commonly found in glacial formations.
[3] Equipment experiences more downtime than clamshell due to frequent hydraulic system maintenance requirements



Fig. 10. Mechanical Clamshell



Fig. 11. Drop chisel

 © Deep Foundations Institute 2025





Fig. 12. Hydraulic Clamshell. **Fig. 13. Hydrofraise** **Fig. 14. Cutter Wheel Unclogging**

Diaphragm wall panel joint construction methods

Early diaphragm wall panel joint construction methods included installation of wide-flanged members or removable pipe at the ends of panels. Wide flanged beams serve as panel end stops, because they adhere to the fresh concrete and provide an armored joint. These end stops are installed after panel excavation, prior to cage installation and concrete placement, with blocking installed between the flanges against the unexcavated panel end. Circular pipes also serve as panel end stops by forming a half-circular shape when the pipe is removed after the concrete initial set. Unacceptable levels of groundwater leakage through these joints led to the development of a patented relatively watertight joint system known as Continuous waterstop (CWS) joints depicted in Fig. 15 and 16. This construction method involves wedging a rubber waterstop into a steel end-stop mechanism which is inserted into the panel prior to reinforcing cage installation and concrete placement. After the adjacent panel is excavated, the steel end-stop is removed leaving behind the waterstop as shown on Fig. 16. An “overbite” construction joint is another joint construction method that can be used with a hydromill or hydrofraise, cutting a key into the previously concreted panels. In this method, the panels are laid out such that the secondary panels (panels between previously constructed primary panels) are narrower than the length of the cutting wheels, thereby overcutting into the concrete of the adjacent primary panels to form a keyed joint, improving the quality of the joint.



Fig. 15. Waterstop installation at end stop



Fig. 16. CWS joint at a completed panel

Slurry wall reinforcing

Slurry walls are reinforced by steel rebar cages or structural steel beams (soldier piles). Reinforcing cage fabrication requires significant laydown space. Therefore, depending on the availability of space at the project site, reinforcing cages may be fabricated on or off-site. The cage can be lifted utilizing a tilt table (Fig. 17) or with one or two cranes with rigging to lift and up-end the cage (Fig. 18). To alleviate constraints posed by reinforcing cage construction and delivery, alternative slurry wall reinforcing such as wide flange steel beams can be used when availability and cost permit. A slurry wall with wide flange steel beam reinforcing is also known as Soldier Pile Tremie Concrete (SPTC) wall is usually considered for temporary applications such as deep support of excavations because the concrete between the beams is unreinforced.

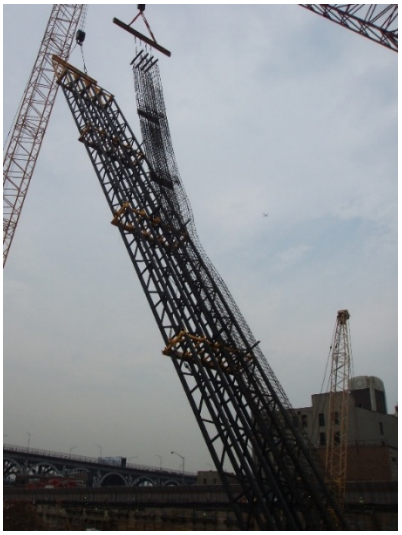


Fig. 17. Tilt-Table for lifting rein. cage



Fig. 18. T-panel reinforcing lift with 2 cranes

 © Deep Foundations Institute 2025

QUALITY CONTROL AND ASSURANCE

Slurry walls serve as lateral earth pressure support and groundwater cutoff systems for temporary deep excavations for construction of subway tunnels, multilevel building basements, utility shafts, tunnel boring machine launching and retrieving shafts and other similar applications. As analysis and design methods have advanced along with construction methods, slurry walls are being incorporated as permanent structural walls. The analysis, design and construction of slurry walls require thorough quality control and assurance as these structures are essential, provide worker protection, and safeguard adjacent structures such as existing buildings and utilities. Quality control and assurance of these structures vary by project. Where a slurry wall is proposed to serve as temporary and permanent structure for a deep excavation in an urban environment, peer review of the analysis and design are frequently required to satisfy quality control and assurance requirements. Similarly, during construction thorough inspection by experienced engineers is essential for the successful completion of such projects. Quality control and assurance of slurry wall construction is a broad topic that cannot be adequately discussed in this paper. Therefore, the related items stated herein are salient features only including:

- Thorough review of slurry wall submittals such as pre-trenching methods, guide wall shop drawings, slurry mix design, panel excavation methods, panel layout shop drawings, reinforcing cage shop drawings, concrete mix designs and methods of repair and sealing leaks. This is essential to ensure the wall is constructed in accordance with Contract Documents.
- Careful and detailed daily logging of activities is essential because the document serves as the record of as-built conditions and may be used to examine any conditions that may be uncovered during excavation.
- Daily sampling and testing of the slurry mix to measure density, viscosity, pH and filtrate loss to ensure the slurry properties are within minimum ranges. This is essential because if the properties of the slurry mix are compromised, the trench could be at risk of collapse as has been observed at some projects.
- Inspecting/observing panel excavation including proper documentation of method of excavation, quality and level of slurry mix within the trench, type and quantity of material being excavated, verticality, sounding of panel bottom with a weighted tape. This is critical because volume of excavated material in excess of anticipated is an indication of over excavation and potential bulge(s) in the wall. Out-of-plumbness of the panel beyond the tolerance may cause structural deficiency. Early detection of excess volume and out-of-plumbness can mitigate unnecessary and costly repair.
- Reinforcing cages inspection to confirm steel bar size, grade, quantities, and overall cage geometry including lifting and insertion methods. Embedded elements such as plates and trumpets for bracing installation and block-outs such as for permanent slab to wall connection must be verified to ensure misalignment does not occur. Improperly constructed reinforcing cages and inadequate lifting plans have led to distortion or failure of cages in some instances leading to worker safety concerns.
- Spacing between reinforcing bars is critical for concrete placement.
- Accurate surveying of reference elevations, typically the top of guide wall, are essential to verify proper placement of reinforcing cage. This is critical because it can avoid costly future repair due to misalignment of the cage and associated embedded elements.

 © Deep Foundations Institute 2025

- Concrete sampling and testing are essential because poor quality concrete can compromise the structural integrity of the wall. In addition to concrete compressive strength testing, the slump and workability of the mix is critical for proper placement.
- Inspecting/observing concrete placement is crucial because the tremie pipe must remain embedded within the concrete as the slurry mix is being displaced. Accidental lifting of the tremie pipe above the top of concrete being placed creates a breach where concrete will mix with the slurry. A tremie pipe breach often causes concrete segregation and/or trapping of laitance. In some projects, where tremie pipe breach has occurred, local panel blowout has been observed.
- To avoid accidental lifting of the tremie pipe out of the freshly placed concrete, sections of the tremie pipe being removed should be tracked and maintained an appropriate depth within the concrete.

REPRESENTATIVE SLURRY WALL PROJECTS

The authors had a unique opportunity to have collectively worked on 15 projects located in NYC, Boston, Washington D.C., and Baltimore, and have closely reviewed 5 projects out of over 100 projects the firm has worked in between the 1960's and 2025. Table 2 below provides a sample of the projects, for which the provided information has been verified with available records and provides valuable information to guide slurry wall designers in the selection and early planning of slurry walls for similar applications.

Table 2. Representative Slurry Wall Projects

NAME[1]	PERIOD	LOCATION	PURPOSE	GEOLOGICAL CONDITIONS	WALL PROPERTIES			LATERAL WALL SUPPORT	CONSTR. METHOD	ANALYSIS METHOD
					THICK.	DEPTH				
					PANEL FT (m)	PANEL FT (m)	EXCAV. FT (m)			
Manhattanville, Columbia University	2008-2025	NY, NY	Excavation Support & Perm. Wall	Fill, Organic, Sand, Varved, Till, Decomposed/Weathered Rock, Bedrock	Rectangular: 3 to 4 (0.9 to 1.2), T-panels: 3 (0.9)	140 (42.7)	40 (12.2)	Permanent Floor Slabs, Tiebacks, Cross Lot Bracing	Top-Down / Conventional	Limit Equilibrium, FEM
World Trade Center Post 9/11 Recovery	2001-2006	NY, NY	Excavation Support & Perm. Wall	Fill, Organic, Sand, Till, Decomposed Rock, Bedrock	3 (0.9)	100 (30.5)	80 (24.4)	Tiebacks	Conventional	Limit Equilibrium, FEM
World Trade Center Vehicle Security Center	2007-2014	NY, NY	Excavation Support & Perm. Wall	Fill, Organic, Sand, Decomposed Rock, Bedrock	3 (0.9)	100 (30.5)	60 to 100 (18.3 to 30.5)	Tiebacks, Raker / Butress panel, Permanent Floor Slabs	Conventional	Limit Equilibrium, FEM
Gowanus Canal CSO	2019-2025	NY, NY	Excavation Support & Perm. Wall	Fill, Organic, Sand, Till, Decomposed/Weathered Rock, Bedrock	T-panels: 3 (0.9)	210 (64.0)	30 (9.1)	Cross Lot Bracing, Permanent Floor Slabs	Conventional	Limit Equilibrium, FEM
New York Law School	2004-2008	NY, NY	Excavation Support & Perm. Wall	Fill, Sand, Till, Decomposed Rock, Bedrock	3 (0.9)	100 (30.5)	65 (19.8)	Permanent Floor Slabs	Top-Down	Limit Equilibrium
63rd St. Line to Queens Blvd. Subway Extension	1994-1996	NY, NY	Excavation Support	Fill, Varved, Sand, Bedrock	3 (0.9)	35 to 80 (10.7 to 24.4)	35 to 80 (10.7 to 24.4)	Tiebacks	Conventional	Limit Equilibrium
National WWII Monument	1999-2002	Washington, DC	Excavation Support & Perm. Wall	Fill, Sand, Bedrock	3 (0.9)	30 to 40 (9.1 to 12.2)	15 to 30 (4.6 to 9.1)	None	Conventional	Limit Equilibrium
Boston Marine Industrial Park Tunnel	1991-1992	Boston, MA	Excavation Support	Fill, Blue Clay, Bedrock	3 (0.9)	70 to 100 (21.3 to 30.5)	40 to 60 (12.2 to 18.3)	Cross Lot Struts / Pin Piles	Conventional	Limit Equilibrium
Four Seasons Hotel and Legg Mason Headquarters	2006-2008	Baltimore, MD	Excavation Support & Perm. Wall	Fill, Alluvial Silt/Clay, Potomac Sediments, Residual Soil, Weathered Rock, Bedrock	2.5 (0.8)	70 to 100 (21.3 to 30.5)	55 (16.8)	Tiebacks, Permanent Floor Slabs	Conventional	Limit Equilibrium, FEM
30 Hudson Street Office Complex	1999-2002	Jersey City, NJ	Excavation Support & Perm. Wall	Fill, Organic, Sand, Till, Decomposed Rock, Bedrock	2.5 (0.8)	35 to 65 (10.7 to 19.8)	45 (13.7)	Tiebacks, Permanent Floor Slabs	Conventional	Limit Equilibrium

 © Deep Foundations Institute 2025

Note: 1) In general, estimated and where available measured lateral deformations and ground settlement closely corelate and were in the range of 1 to 2.5 in (2.5 to 6.4 cm), with the upper bound deformations corresponding to the deeper excavations and challenging site soil conditions. (Fantaye, 2008).

FUTURE ADVANCEMENTS IN SLURRY WALL CONSTRUCTION

Advancements in material science such as high strength reinforcing steel, high compressive strength concrete, concrete admixtures such as plasticizers and fluidifiers, Ultra-High-Performance Concrete (UHPC), steel fiber reinforcing and pre-stressed precast concrete technologies when adopted for slurry wall construction can significantly advance the industry.

SUMMARY AND CONCLUSIONS

Slurry wall analysis has evolved significantly over the decades. Initially, analysis was based on the limit equilibrium method without considering soil-structure interaction. Wall lateral displacement was estimated based on the principles of statics assuming the wall as a continuous beam, but estimates of ground settlement adjacent to the excavation, shallowly founded buildings or structures and utilities were difficult until empirical methods were developed by Clough et al. The method of Clough and O'Rourke outlined in the paper 'Construction Induced Movements of In-situ Walls', was based on observation of lateral wall movement and associated ground settlement for different types of excavation support walls in sand, and various types of clay (Clough et al, 1990). While the method of Clough and O'Rourke was a groundbreaking approach for estimating lateral wall movement and ground settlement associated with deep excavations, reasonably predicting adjacent structure movement (settlement, planar movement and angular distortion) were difficult until finite element methods which consider soil-structure interaction were developed

As the computing capacity of computers developed the use of powerful finite element soil-structure interaction tools, such as the Plaxis or Midas software, made the prediction of slurry wall and adjacent structure movement reasonable and practical. On projects where panels were instrumented, monitoring data collected corroborated the predicted values from the analysis.

Current state of slurry wall analysis and design includes limit equilibrium methods to develop wall properties, geometry, required levels of bracing, bracing size and stiffness and initial estimate of bracing preloading. The initial results from limit equilibrium are used as input into the finite element analysis model, refined through iterative analysis to predict wall internal force, lateral movements and adjacent structure movement.

The methods of analysis and design continue to evolve as monitoring data from previous projects and lessons learned are incorporated into the design of new projects in similar conditions. With the advent of data science and Artificial Intelligence (AI), the observational approach will lead to practical, efficient and safe design.

Similarly, advancement in material science such as high strength reinforcing steel, high compressive strength concrete, concrete admixtures such as plasticizers and fluidifiers, Ultra-High-Performance Concrete (UHPC), steel fiber reinforcing and pre-stressed precast concrete technologies when adopted for slurry wall construction can significantly advance the industry.

REFERENCES

Backus, John, 1998. The History of Fortran, II and III", IEEE Annals of the History of Computing, Vol. 20, No. 4, 66-77

Clough, G.W., O'Rourke, T.D. 1990. Construction induced movements of in-situ walls. Design and Performance of Earth Retaining Structures, ASCE, GSP 25: 439-470

Deep Foundation Institute, 2005. Industry Practice Standards and DFI Practice Guidelines for Structural Slurry Walls, 5-12.

Fantaye, S.Y. et.al., 2008. Diaphragm wall for deep basement provides efficient use of waterfront property at Harbor East in Baltimore, Deep Foundations Institute.

Fenves, Steven, et.al.,1964, STRESS: A Reference Manual, The M.I.T. Press, 1-7

Matlock, H., Taylor, T.P, 1968. A Computer Program to Analyze Beam-Columns Under Movable Loads, Center for Highway Research, The University of Texas at Austin, 1-21

NAVFAC, 1982. Design manual 7.2" foundations and earth structures, Dept. of the Navy, U.S. Government Printing Office, Washington, D.D., 59-111, 235

Panak, John J., 1973.Development of Methods for Computer Simulation of Beam-Columns and Grid-Beam and Slab Systems, Center for Highway Research, the University of Texas at Austin, Research Project 3-5-63-56. 1-3

Reina, Peter, 2012. Soilmec Hydromill Shatters Slurry-Wall Records, Engineering News-Record.

 © Deep Foundations Institute 2025

OBSERVATIONS AND IMPACT OF FIELD LOGGING AND DRILLING PROCEDURES ON SITE CHARACTERIZATION OF CAMBRIDGE ARGILLITE IN SOMERVILLE, MA

Udit S. Dasgupta, Arup US Inc, New York, NY, Udit.Dasgupta@arup.com
Andrew K. Keene, Kiewit Engineering Group Inc, Lone Tree, CO (formerly with Arup US Inc, New York, NY), Andrew.Keene@kiewit.com

ABSTRACT

This paper presents key observations from a geotechnical investigation (GI) program conducted in Somerville, Massachusetts (MA). The investigation involved borehole drilling with standard penetration tests (SPT) to identify subsurface conditions. The GI program was carefully developed based on a thorough review of available existing geotechnical and geologic information for the area with an emphasis on accurate in-situ site characterization through best-practice field logging, drilling procedures, and laboratory testing. The primary bedrock formation encountered in the region was the Cambridge Argillite which has been known to be highly variable spatially and show a wide range in terms of geotechnical properties. Field observations and laboratory testing showed that the formation is highly sensitive to moisture content and the impact of drilling on drilled shaft side shear resistance should be considered. The primary conclusions were that in-situ moisture preservation of the bedrock and the remolded shear strength of the completely weathered bedrock is critical for accurate geotechnical site characterization for design.

Keywords: ground investigation, site characterization, geology, argillaceous, SPT, direct shear test, remolded shear strength, moisture preservation, pile resistance, design, variability

INTRODUCTION

The primary bedrock formation in the Somerville, MA is the Cambridge Argillite. This complex geologic formation has been studied extensively by geologists and geotechnical engineers in the Boston, MA area. It is a type of weakly metamorphosed argillaceous shale with varying levels of weathering and alteration ranging from unweathered to a residual soil. The geotechnical properties as well as stratigraphy are known to be highly variable, which makes the material challenging to characterize. (Kaye, 1967; Johnson, 1989; Hassan and O'Neill, 1997; Brown et al., 1999). Argillaceous materials, both in decomposed and intact rock form, have been seen to exhibit sensitivity to moisture content and wetting-drying cycles (Corominas et al., 2015; Martin et al., 2016).

Site investigations are a critical item in the foundation design process. Given the complexity of the Cambridge Argillite formation, this paper illustrates the importance of a well-planned ground investigation (GI) program comprising of best practices in drilling, field logging, and laboratory testing in order to characterize its geotechnical properties. The findings of this study are based upon the observations and testing results obtained from a GI program performed on an approximately 15 acre project site in the Somerville, MA area as shown in Fig. 1.

 © Deep Foundations Institute 2025

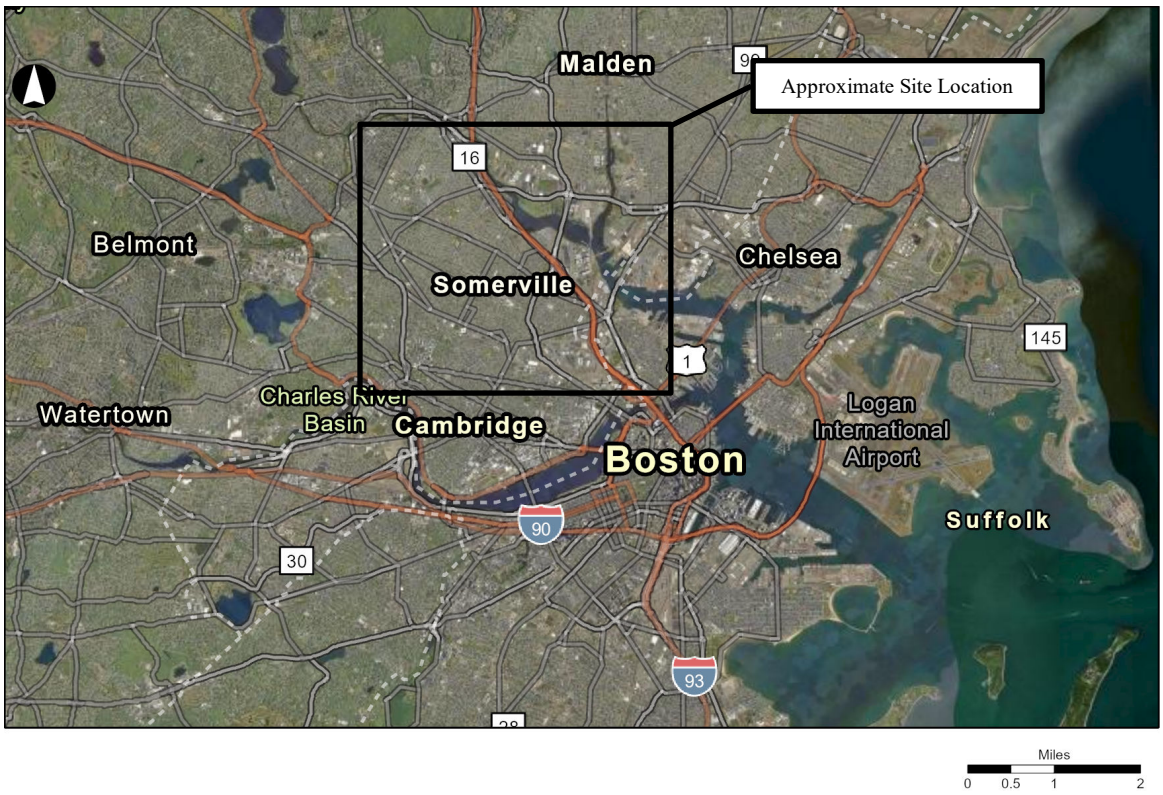


Fig. 1. Approximate site location

GEOLOGY

The site in consideration is located in the Boston sedimentary basin formed in the Pre-Cambrian era. Folding, faulting and slight metamorphosis of the sedimentary rocks occurred by colliding of the North American and African Plates during the Late Paleozoic. These influences coupled with subsequent plate separations produced bedrock fractured at high angles with intrusive dikes. Subsequent glacial activities produced thick till deposits followed by marine deposits of Boston Blue Clay, although this formation was not encountered in any of the boreholes that are considered a part of this study.

The major structural characteristics of the Boston Basin trend east-northeast. These characteristics include the folds, major faults and slatey cleavage. The bedrock is the Cambridge Argillite which is highly variable blue gray to brown gray fine grained clayey rock derived from siltstone, claystone, or shale, and occasionally consists of sand, with some diabase, felsites or andesite. The primary intrusive rock consists of an unweathered to highly weathered, gray and green, igneous diabase rock which intrudes the argillite in the form of dikes.

The Cambridge Argillite is underlain by the Roxbury Conglomerate, Mattapan Volcanic Complex, and the Dedham Granite as the basement rock as shown in Fig. 2 and Fig. 3. The Roxbury Conglomerate comprises of a very hard, durable stone, mottled brown in color, with embedded round to angular pebbles in a silt, sand and clay matrix, and resembles a dense concrete material. The scope of this study is limited to the Cambridge Argillite. Near surface conditions at site are typical of the Boston area that is located outside the old colonial shoreline. The overburden soils consist primarily of miscellaneous fill, marine sand, marine clay, glacial till, and weathered and decomposed bedrock (Zen et al., 1983; Hatch, 1991; Connors, 1993; Barosh and Woodhouse 2012).

 © Deep Foundations Institute 2025

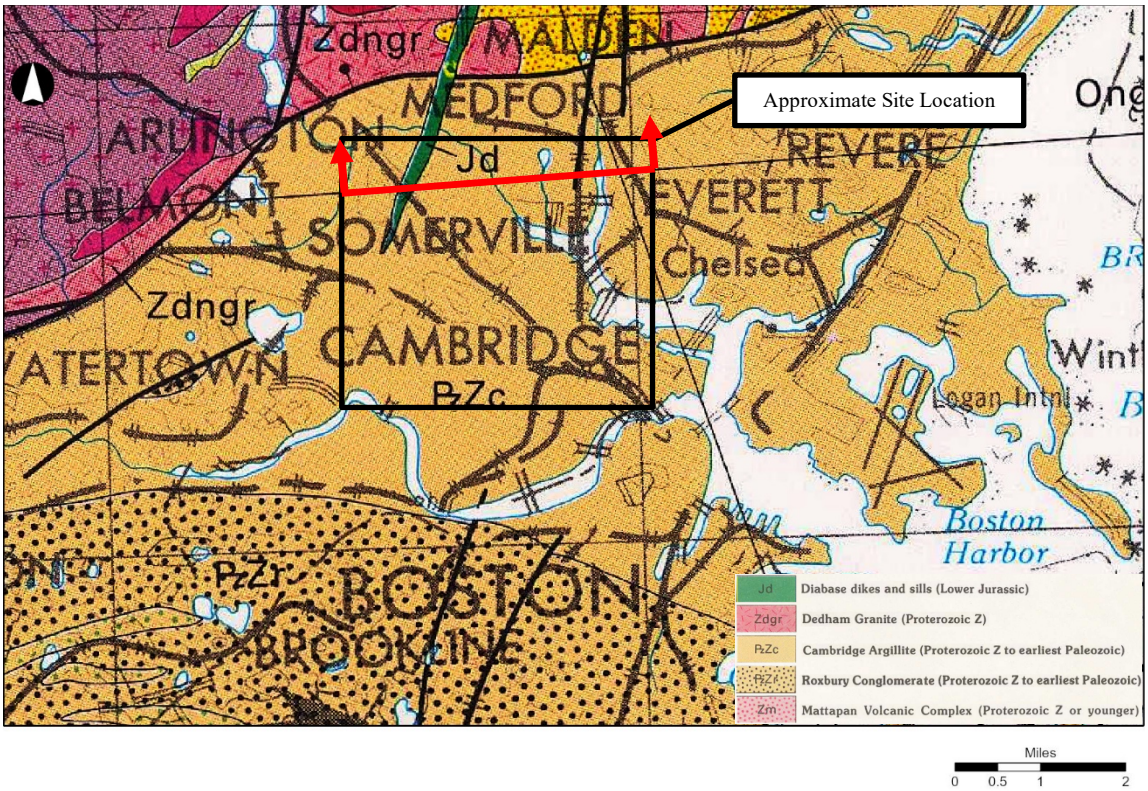


Fig. 2. Bedrock geology map with approximate section location (Zen et al., 1983)

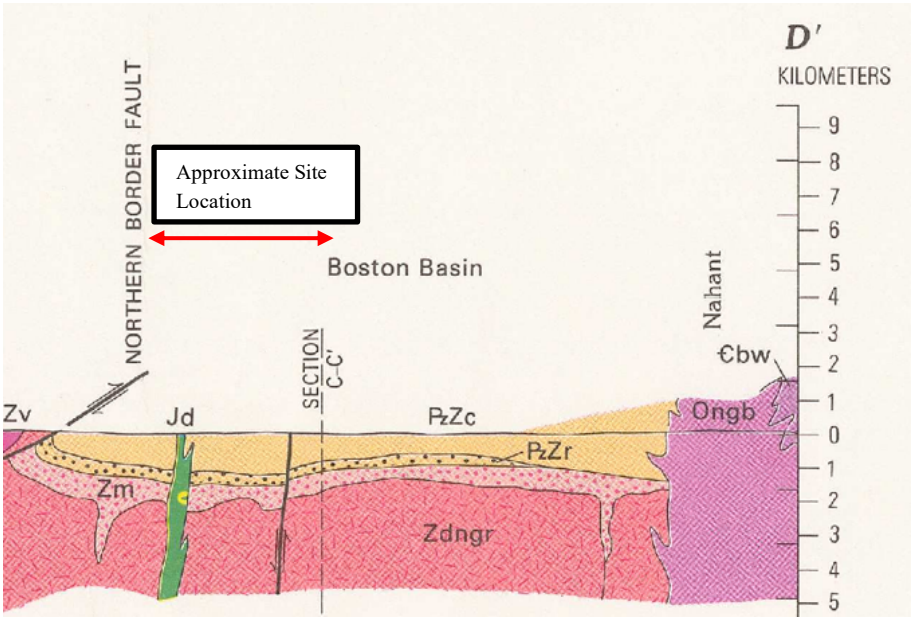


Fig. 3. Geologic section with approximate site location (Zen et al., 1983)

 © Deep Foundations Institute 2025

GROUND INVESTIGATION (GI) PROCEDURE

FIELD PROCEDURES

A GI program considered for this study was executed on a project site in Somerville, MA and comprised on 7 Standard Penetration Test (SPT) boreholes ranging in depths from 57ft below ground surface (bgs) to 161.6ft bgs.

Standard Penetration Tests (SPTs) were conducted in all boreholes in accordance with ASTM D1586/1586M. These tests involved the utilization of a 2-inch (in) outer diameter (O.D.) split-spoon sampler 24in long, driven by a 140-pound hammer free falling 30in. All rigs were equipped with automatic hammers. Samples were classified as per the USCS classification system in accordance with ASTM D2487. Best-practice field logging techniques were employed as per ASTM D2488.

Rock coring was performed in all boreholes as bedrock was encountered. Rock core samples, up to 5ft long, were obtained utilizing rock coring techniques within a NX-size, double-tube core barrel and were classified according to their geologic origin. The rock cores were assigned a recovery and rock quality designation (RQD). Coring time for each 1ft interval was recorded. In anticipation of encountering the Cambridge Argillite during the GI, special care was taken to preserve the in-situ moisture state of the cored rock as per the procedures outlined in ASTM D5079.

LABORATORY TESTING

A laboratory testing program tailored to the project requirements was executed for the soil and rock and the testing relevant to this paper include:

- Soil Index Property Testing: Moisture content tests in accordance with ASTM D2216; Gradation of soil in accordance with ASTM D6913; Gradation of fine-grained soils (Hydrometer) in accordance with ASTM D7928; Atterberg limits tests in accordance with ASTM D4318
- Soil Shear Strength: Direct Shear Test in accordance with ASTM D3080
- Rock Testing: Moisture content tests in accordance with ASTM D2216; Slake durability in accordance with ASTM D4644; Compressive strength of rock in accordance with ASTM D7012 (Method C and D)

MOISTURE PRESERVATION OF BEDROCK

In order to maintain the in-situ moisture state of the Cambridge Argillite the following procedure, in accordance with ASTM D5079, was performed in preparation of the core samples and core:

- Prior to coring, the core box was lined with an outer layer of aluminum foil followed by a layer of saran wrap.
- The rock core was placed in the core slots and the saran wrap and aluminum foil was tightly wrapped around the core. The cores were wet in a timely manner prior to sealing to prevent moisture loss.
- The core boxes were sealed and were protected from direct sunlight prior to shipping to the testing laboratory.

FACTUAL RESULTS

SITE CHARACTERISTICS

The typical subsurface profile encountered across the site comprises of the following, listed from shallowest to deepest:

 © Deep Foundations Institute 2025

- Uncontrolled manmade fill: Uncontrolled fill material comprising silty sand, sandy clay, and silty clay with variable gravel percentages was encountered in all the boreholes across the site.
- Cohesive layer: Underneath the uncontrolled fill, a layer of stiff to hard silty clay and clayey silt was encountered. This layer was encountered in all the boreholes across the site and has a typical thickness of 1 to 7ft.
- Glacial Till: Typically encountered below the cohesive layer, the natural deposits are typically classified as medium dense to very dense silty to clayey sands, and silty to clayey gravels when non-cohesive and stiff to hard sandy silts, and silty to sandy clays when cohesive. These deposits are typically encountered at a depth of 5 to 24ft bgs and has a typical thickness of 2 to 28ft.
- Decomposed Rock: Decomposed rock is encountered below the Glacial Till, and is typically classified as very dense silty to clayey sands; and stiff to hard sandy to silty clays. The parent material is typically fine argillite across the site, except for an isolated borehole where decomposed diabase is encountered. This layer is interbedded with the weathered rock and bedrock.
- Weathered Rock: Typically encountered beneath the decomposed rock layer, weathered fine argillite is typically encountered across the site, except for an isolated borehole where weathered diabase is encountered. This layer is interbedded with weathered rock and bedrock.
- Bedrock: Bedrock was typically encountered underlaying the weathered rock. Fine argillite was encountered in all other boreholes except an isolated borehole where diabase was encountered. It should be noted that in the boreholes adjacent to the borehole with diabase, poor quality argillite metamorphized and mixed with diabase was encountered. This aligns well with the documented geologic conditions in the region (Brown et al., 1999).

FIELD CONDITIONS

The primary field observations made during the drilling and logging of the boreholes which are of significance to this study are:

- The site was relatively flat with ground surface elevations ranging from +8.5 to +11ft.
- Groundwater depths, based on overnight borehole observations, were recorded as ranging from approximately 2 to 5ft bgs (below ground surface), when perched on the shallow cohesive layer. The groundwater depths measured when the hole was cased to bedrock ranged from 4 to 9ft bgs.
- Depth to the decomposed bedrock varied between 18 to 44ft bgs, with a median of 29ft bgs.
- Depth to core-able bedrock, where encountered, varied between 37 to beyond 70ft bgs, with a median of 52ft bgs.
- The rock core was found to be easily susceptible to mechanical breaks while retrieving the cores from the core barrel due to its fragile nature. These mechanical breaks were carefully demarcated in an effort to document in-situ jointing in the rock.
- The stratigraphy varied greatly from borehole to borehole and with depth within each borehole as well. The weathering profile in the bedrock varied between unweathered to highly weathered to decomposed in an inconsistent manner from core run to core run. Although there was some improvement in quality of bedrock at greater depths, this improvement was not reliably consistent within the range of depths explored.
- The decomposed bedrock had variable quantities of sand, silt, and clay. Field procedures including the jar test, dilatancy test, and plasticity test, in accordance with procedures outlined in ASTM D2488 were conducted at each sample to accurately discern the correct USCS classification. The samples were pulverized prior to classification. The field estimated percentages of fine sand vs fines content were often close to 50-50 on many samples. The field classification was further verified with laboratory index testing.
- Core barrel jams were frequently encountered when the material changed from unweathered to highly weathered or decomposed, or if high angle fractures were encountered.
- Average core times per foot of coring in the unweathered bedrock was between 1.5 to 3 minutes.

Evidence of a core barrel jam was seen when the core times exceeded this range.
- Occasionally, the core times would be low (<=1 minute) which would be accompanied by core loss. This evidenced the washing away of soil like materials encountered in the bedrock during coring.
- Recovery in the bedrock for 5ft core runs ranged from 0% to 100% with a median of 98%; and Rock Quality Designation (RQD) ranged from 0% to 79% with a median of 32%.

LABORATORY TESTING RESULTS

The laboratory testing results for the decomposed rock material are presented in Table 1. The laboratory testing results for the bedrock are presented in Table 2. The unconfined compressive strength (UCS) test of the rock samples were conducted on two moisture states to assess the impact of moisture content on strength – As-received and Air-dried. The air-dried samples were dried out for a minimum of 4 days under ambient conditions after preparation into the UCS sample. For the direct shear testing, samples were pulverized and remolded to in-situ moisture contents and compacted to a target density of 135 pcf. The tests were performed at three normal stresses – at 0.5 times vertical effective stress ($0.5*\sigma'_v$), at vertical effective stress (σ'_v), and at 2 times vertical effective stress ($2*\sigma'_v$).

Table 1. Soil Laboratory Results for Decomposed Rock

Material	USCS	Fines %	Moisture Content (%)	Liquid Limit (%)	Plastic Limit (%)	Plasticity Index (%)	Apparent Cohesion, c' (psf)	Apparent Friction Angle, φ' (degrees)
Granular Decomposed Rock	SM, GM	21.4-35	14.5-19.9	Non-Plastic	Non-Plastic	Non-Plastic	1130	28.6
Cohesive Decomposed Rock	SC, ML, MH, CL, CH	36.3-99.4	14.3-25	32-62	27-34	5-34	1.97-655	25.2-27.4

Table 2. Rock Laboratory Results

Material	Total Unit Weight (pcf)	Compressive Strength (psi)	As-Received Moisture Content (%)	Slake Durability Index (%)
Argillite – As-received	154-167	253-1879	3.1-7.1	92-98.8
Argillite – Air-dried	153-164	1048-3368		
Diabase – As-received	189	10421	-	-
Diabase – Air-dried	185	15341		

FINDINGS

CHALLENGES WITH CAMBRIDGE ARGILLITE

Based on the field observations and laboratory testing results, the following challenges were encountered with the characterization of the Cambridge Argillite:
- Remolding of decomposed rock to clay-like paste from drilling – The decomposed rock tends to form into a clay-like paste when altered by drilling action and contact with drilling fluid. Similar conditions are anticipated when a drilled shaft is constructed through the material. A considerable impact on the shear resistance is anticipated when the material gets remolded during drilling operations. This impact of drilling is discussed further below.

- High spatial variability in stratigraphy – The rock showed high spatial variability both in depth and in plan as evidence by Fig. 4 which shows the distribution of recoveries and RQDs. In complex stratigraphy, such as conditions highlighted in this study, there should be a borehole for each drilled shaft or group of drilled shafts, and the design should be borehole specific rather than developing a site wide idealized stratigraphy (Brown et al., 1999).
- Rock strength dependent on moisture content – The laboratory test results showed that there is a considerable impact on the strength of the argillite depending on if the cores were tested wet as-received versus air-dried. In contrast, not much impact is seen for the diabase rock. These results are discussed further below.

DESIGN CONSIDERATIONS – DECOMPOSED ROCK

The primary deep foundation type typically suggested for high column load demands in the Boston, MA region is a drilled shaft (Johnson, 1989). The risk of boulders in the overlying glacial till, high blow counts in the argillite layers, and variability in the rock, make driven piles a poor foundation option in the geology.

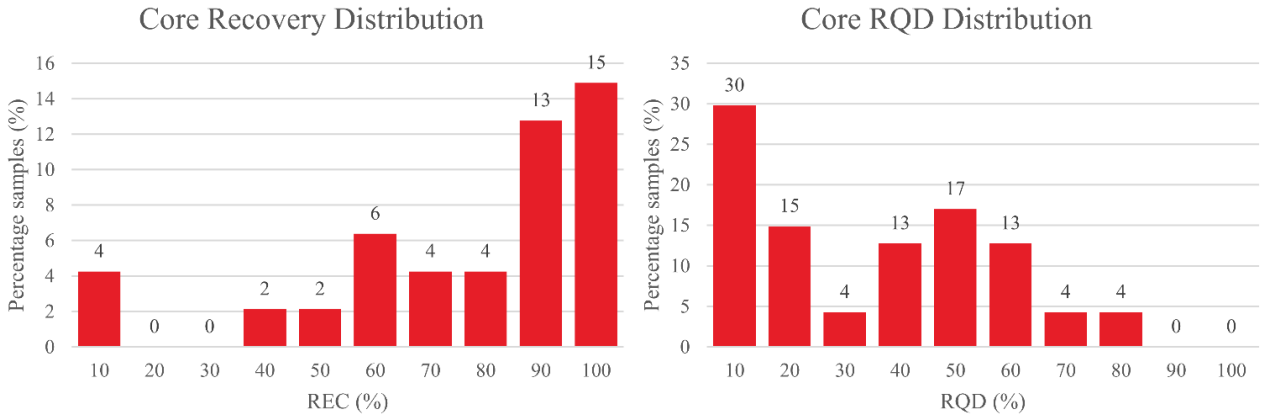


Fig. 4. Recovery and RQD Histograms

The Cambridge Argillite is known to exhibit hydrothermal weathering in certain zones, which manifests as kaolinization of the material (Kaye 1967; Brown et al., 1999). The results from the Atterberg testing supports this based on the commonly observed ranges for different clay mineralogy as shown in Fig. 5 (Martin et al., 2016). When drilled through this material exhibits a different side shear-transfer mechanism in drilled shafts where the material behaves like a remolded clay (Hassan et al., 1997).

 © Deep Foundations Institute 2025

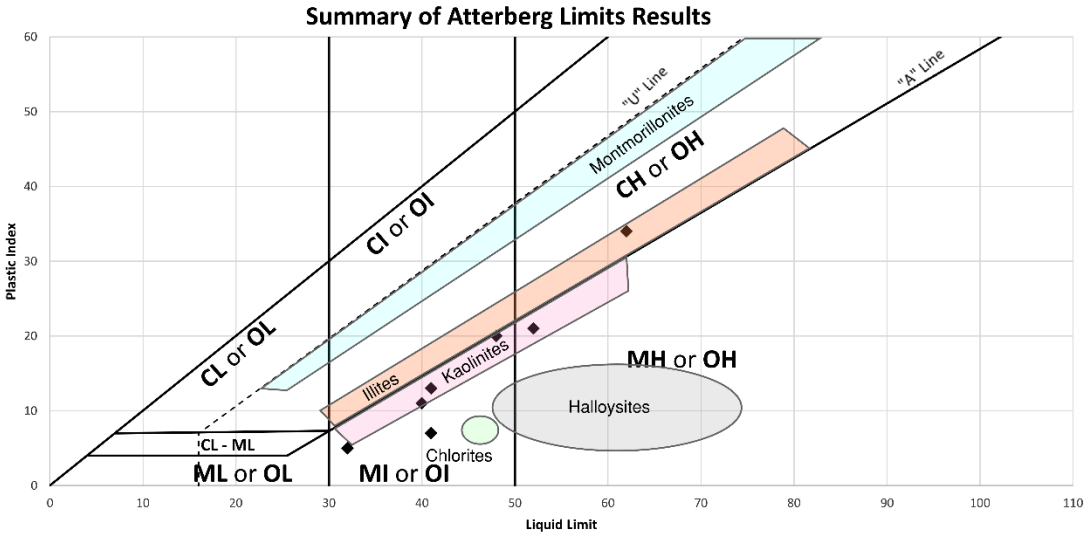


Fig. 5. Atterberg limits test data of decomposed rock compared to ranges for common clay mineralogy (adapted from Martin et al. 2016)

To inform the design of side resistance of the decomposed rock for drilled shafts, three approaches were compared: a correlation based on Standard Penetration Test N-values (SPTN) (Peck et al., 1974); assuming decomposed rock to be normally consolidated with a strength profile given by SHANSEP (Ladd and Foott, 1974); and a remolded strength obtained from direct shear testing. The shear strength profiles based on the three approaches are shown in Fig. 6. The results indicated that the decomposed rock that exhibited cohesive index properties had a significant reduction in strength on remolding and shear testing when compared to the in-situ SPT values correlated shear strength. Interestingly, there is good agreement with the SPT correlation and direct shear testing when the decomposed rock did not exhibit cohesive behavior based on index testing.

Based on these findings, a residual side resistance in the decomposed argillite can be estimated with detailed characterization of the material with index testing and direct shear testing. SPT N correlations in the weathered layer should not be utilized unless index testing in the layer shows that the material is clearly cohesionless. Even if the material is found to be cohesionless, it is recommended that remolded direct shear testing be performed to validate the use of SPT correlations for estimating side shear resistance.

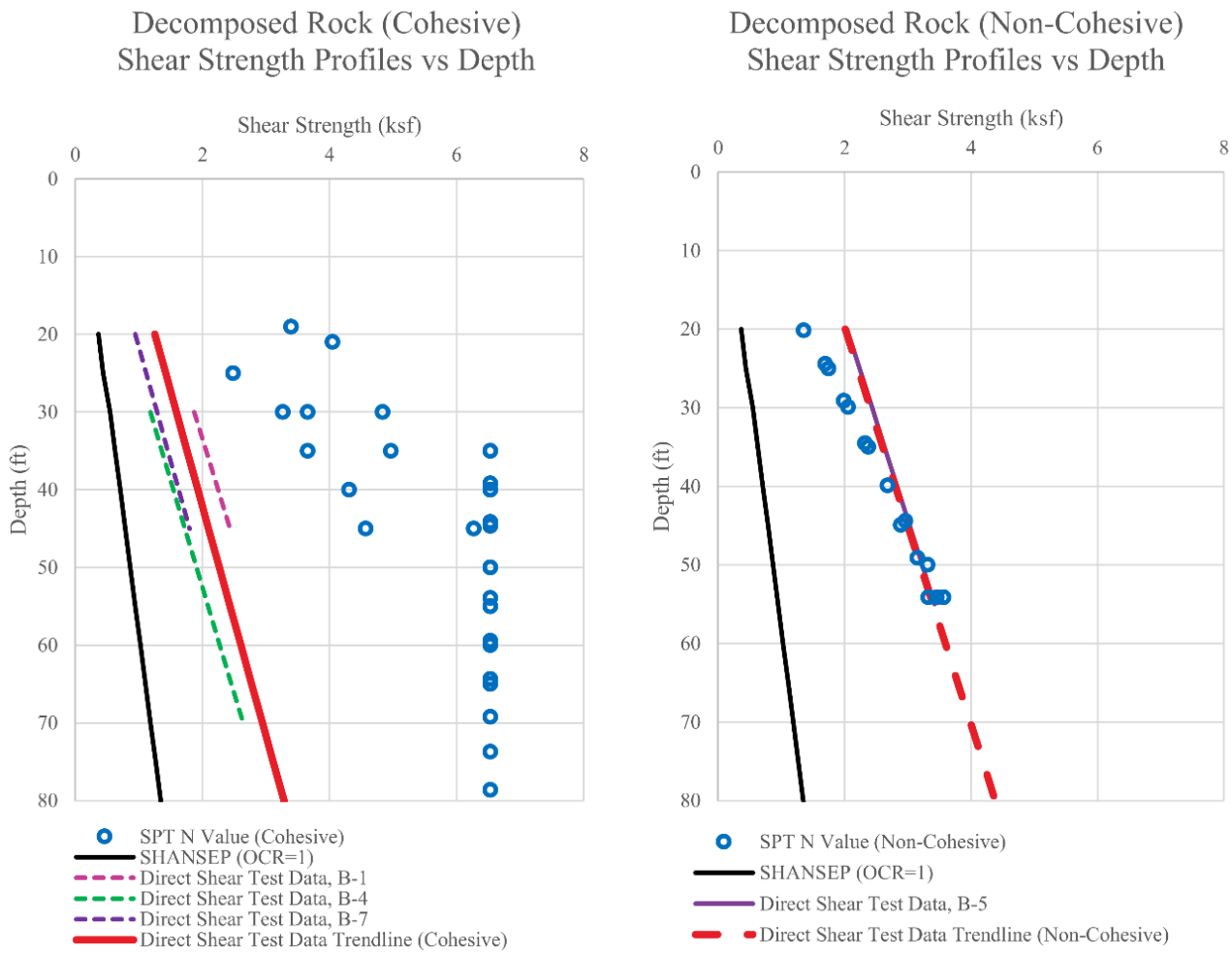


Fig. 6. Shear strength profiles of the decomposed bedrock based on SPT N correlations, Direct Shear Test data, and SHANSEP for non-cohesive and cohesive samples

DESIGN CONSIDERATIONS – UNWEATHERED ROCK

The laboratory test results on the rock indicate that the rock is sensitive to moisture content when testing of Unconfined Compressive Strength (UCS). Tests were performed on core samples across the different boreholes. Results for specific samples where the as-received and air-dried states tests were in close proximity by depth are shown in Table 3.

Table 3. Impact of Drying Out of Rock Cores

Sample	Compressive Strength – As-received (psi)	Compressive Strength – Air-dried (psi)	Multiple Increase in Strength (-)
Core Run 1	1392	2374	1.7
Core Run 2	294	1048	3.6
Core Run 3	991	3070	3.1
Core Run 4	253	3368	13.3

The results show that an artificial increase in strength ranging from 1.7 to 13.3 times the in-situ strength occurs when the samples are tested after allowing to dry out. The slake durability testing indicates that the rock material is prone to weathering on repeated wetting and drying cycles. Moreover, these results highlight that the behavior of the Cambridge Argillite are in line with published literature on the behavior of weak shales (Martin et al., 2016). In practical terms, rock core collected in the field and allowed to go through multiple wetting-drying cycles prior to laboratory testing may greatly vary from its in-situ state.

If the core samples are not treated with due care during the site investigation, as outlined above and in ASTM D5079, the testing results are likely to not be representative of in-situ conditions increasing uncertainty in the design and making judgements more challenging.

Given the challenges of correctly characterizing the soil and rock encountered in the Cambridge Argillite, when permissible, the best approach to verifying design assumptions prior to construction is to conduct full-scale load tests at drilled shaft locations.

GI BEST PRACTICES FOR CAMBRIDGE ARGILLITE

The testing results presented in this paper underscore the importance of implementing best-practice measures for the drilling and logging of GI in the Cambridge Argillite. These best-practice measures are summarized as follows:

- Field Classification Best Practices as per ASTM D2488: The decomposed bedrock had variable quantities of sand, silt, and clay. Field procedures including the jar test, dilatancy test, and plasticity test, in accordance with procedures outlined in ASTM D2488 should be conducted at each sample to accurately discern the correct USCS classification. The field classification should be verified with laboratory index testing.
- Core Barrel Choice: At a minimum, the swivel-type double-tube core barrel should be used in rock core sampling for the Cambridge Argillite. The triple-tube core barrel can be used to increase sample recovery in inferior-quality rock or partially cemented soils, with the additional advantage of minimizing sample handling and disturbance during removal from the core barrel. Wireline based core barrels are preferred due to the possibility of encountering deep weathered zone. This helps prevent the likelihood of hole collapse when coring through these weathered zones.
- Core Progress Monitoring: Core times should be recorded in minutes per foot of advancement of the core barrel and noted on the borehole logs. These observations along with notes about core loss and/or core barrel jams provide strong evidence of how the bedrock stratigraphy varies with depth within a core run.
- Moisture and Sample Preservation: Moisture preservation is critical when sampling in the Cambridge Argillite. The rock should be sealed with a tightly fitting wrapping of a plastic film, such as vinylidene chloride (for example, saran or similar material). Over this, another tight wrapping of aluminum foil is placed, so that as little air as possible is trapped beneath the wrappings. The ends of the wrappings should be overlapped over the ends of the sample and folded over so as to seal the ends of the sample. As an additional sealant, a few coats of a plastic microcrystalline wax may be applied (ASTM D5079).

SUMMARY AND CONCLUSIONS

This paper presents the findings of a GI campaign in the Somerville, MA area which evidence the need for high quality GI drilling and logging practices when attempting to characterize the Cambridge Argillite Formation for geotechnical design. Direct shear testing of the remolded samples of the decomposed rock indicated that there is a considerable loss in shear strength on remolding due to drilling operations. This impact is seen when the decomposed rock shows the properties of cohesive materials discerned from

index testing. A residual side resistance in the decomposed argillite can be estimated with detailed characterization of the material with index testing and direct shear testing. SPT N correlations in the weathered layer greatly overestimate the shear strength when the material is cohesive and should not be used without verification with remolded direct shear testing. Additionally, there is a considerable impact on UCS of the rock depending on whether testing is performed on wet as-received core samples versus air-dried core samples. Care should be taken to preserve the moisture of the rock samples collected in-situ. Due to the high variability in properties and spatially, design stratigraphy based on drilled shaft specific boreholes as well as load testing, when permissible, is warranted before finalizing design.

REFERENCES

AASHTO, 2024. LRFD Bridge Design Specifications. Tenth Edition. Washington, DC.

ASTM Standard D1586/D1586M, 2018. Standard test method for Standard Penetration Test (SPT) and split-barrel sampling of soils. ASTM International, West Conshohocken, PA.

ASTM Standard D2113, 2014. Standard practice for rock core drilling and sampling of rock for site exploration. ASTM International, West Conshohocken, PA.

ASTM Standard D2216, 2019. Standard test method for laboratory determination of water (moisture) content of soil and rock by mass. ASTM International, West Conshohocken, PA.

ASTM Standard D2487, 2017. Standard practice for classification of soils for engineering purposes (Unified Soil Classification System). ASTM International, West Conshohocken, PA.

ASTM Standard D2488, 2017. Standard practice description and identification of soils (Visual-Manual procedures). ASTM International, West Conshohocken, PA.

ASTM Standard D3080/D3080M, 2023. Standard test method for direct shear test of soil under consolidated drained conditions. ASTM International, West Conshohocken, PA.

ASTM Standard D4318, 2017. Standard test methods for liquid limit, plastic limit, and plasticity index of soils. ASTM International, West Conshohocken, PA.

ASTM Standard D4644, 2016. Standard test method for slake durability of shales and other similar weak rocks. ASTM International, West Conshohocken, PA.

ASTM Standard D5079, 2008. Standard practices for preserving and transporting rock core samples. ASTM International, West Conshohocken, PA.

ASTM Standard D6169/D6169M, 2021. Standard guide for selection of subsurface soil and rock sampling devices for environmental and geotechnical investigations. ASTM International, West Conshohocken, PA.

ASTM Standard D6913/D6913M, 2017. Standard test methods for particle-size distribution (gradation) of soils using sieve analysis. ASTM International, West Conshohocken, PA.

ASTM Standard D7012, 2023. Standard test methods for compressive strength and elastic moduli of intact rock core specimens under varying states of stress and temperatures. ASTM International, West Conshohocken, PA.

 © Deep Foundations Institute 2025

ASTM Standard D7928, 2021. Standard test method for particle-size distribution (gradation) of fine-grained soils using the sedimentation (hydrometer) analysis. ASTM International, West Conshohocken, PA.

Barosh, P.J., Woodhouse, D., 2012. Geology of the Boston Basin. Civil Engineering Practice, 26-27, pp.100-236.

Brown, L.M., Soydemir, C., Parkhill, S.T., Lally, M.J. and Smith, A.D., 1999. Bedrock characterization and design considerations for rock socketed caissons in the Greater Boston area. 14th International Conference on Soil Mechanics and Foundation Engineering, Hamburg, Germany (pp. 959-962).

Connors, P. J., 1993. Geological background and engineering parameters of Boston Blue Clay. University of Massachusetts at Lowell.

Corominas, J., Martínez-Bofill, J. and Soler, A., 2015. A textural classification of argillaceous rocks and their durability. Landslides, 12, pp.669-687.

Duncan, J.M., Wright, S.G. and Brandon, T.L., 2014. Soil strength and slope stability. John Wiley & Sons.

Hatch, N.L., 1991. The bedrock geology of Massachusetts. U.S Geological Survey Professional Paper 1366-E-J. US Government Printing Office.

Hassan, K.M. and O'Neill, M.W., 1997. Side load-transfer mechanisms in drilled shafts in soft argillaceous rock. Journal of geotechnical and geoenvironmental engineering, 123(2), pp.145-152.

Hassan, K.M., O'Neill, M.W., Sheikh, S.A., and Ealy, C.D., 1997. Design method for drilled shafts in soft argillaceous rock. Journal of geotechnical and geoenvironmental engineering, 123(3), pp.272-280.

Johnson, E.G., 1989. Geotechnical characteristics of the Boston area. Civil Engineering Practice, 4(1), pp.53-64.

Kaye, C.A., 1967. Kaolinization of bedrock of the Boston, Massachusetts, area. US Geological Survey Professional Paper 575-C, pp. C165-C172.

Ladd, C.C. and Foott, R., 1974. New design procedure for stability of soft clays. Journal of the geotechnical engineering division, 100(7), pp.763-786.

Martin, C.D., Giger, S. and Lanyon, G.W., 2016. Behaviour of weak shales in underground environments. Rock Mechanics and Rock Engineering, 49, pp.673-687.

Peck, R.B., Hanson, W.E., and Thornburn, T.H., 1974. Foundation Engineering. First Edition. John Wiley & Sons, NY.

Terzaghi, K. and Peck, R., 1967. Soil Mechanics in Engineering Practice. John Wiley & Sons, NY.

Zen, E-an, Goldsmith, Richard, Ratcliffe, N.M., Robinson, Peter, Stanley, R.S., Hatch, N.L., Shride, A.F., Weed, E.G.A., and Wones, D.R, 1983. Bedrock geologic map of Massachusetts, Scale: 1:250,000. U.S. Geological Survey, Arlington, VA.

 © Deep Foundations Institute 2025

APPLYING MACHINE LEARNING FOR SPT-N PREDICTION FROM RAW CPT DATA

Milad Fatehnia, Ph.D., P.E., Schnabel, Marietta, GA, USA, milad.fatehnia@schnabel.com
Sanaz Paran, Ph.D., Everfi, Alpharetta, GA, USA, sanaz.paran@everfi.com

ABSTRACT

In geotechnical engineering, the Cone Penetration Test (CPT) is a commonly employed technique for evaluating soil properties. Similarly, the Standard Penetration Test (SPT) is a widely used in-situ test that provides critical data on soil strength, density, and stratification, playing a key role in foundation design, site characterization, and geotechnical analysis. This study employs Machine Learning (ML) methods to predict corrected SPT-N values from raw CPT data, leveraging a dataset from the I-405 Freeway expansion in Orange County, California, which includes CPT soundings, SPT boreholes, and laboratory testing. The anticipated findings offer promises for improving geotechnical characterization, assisting practitioners in infrastructure projects, and advancing ML applications in geotechnical engineering, thereby enhancing the quality, resilience, and efficiency of geotechnical projects.

Keywords: Cone Penetration Test, SPT-N, Machine Learning, Random Forest, eXtreme Gradient Boosting

INTRODUCTION

Geotechnical engineering is increasingly relying on data for smarter decision-making and advanced techniques. Engineers are integrating new data management tools to gather, analyze, and interpret geological data more effectively. These tools enhance decision-making and streamline workflows, improving precision and efficiency in geotechnical practices. Leveraging data-driven methods improves geotechnical risk assessment and strengthens infrastructure resilience. Field testing, instrumentation, and data management play a crucial role in risk mitigation (Fatehnia and Deaton, 2023; Fatehnia and Deaton, 2022).

The Standard Penetration Test (SPT) is a common in-situ test used to evaluate soil strength, density, and stratification by measuring the resistance of a split-barrel sampler driven into the soil using a standard hammer. SPT-N is the recorded blow count, representing the number of hammer blows required to advance the sampler 12 inches, providing a measure of soil density and strength. The Cone Penetration Test (CPT), offering more consistent and detailed soil profiling, is increasingly preferred for site characterization and design. Establishing correlations between SPT-N and CPT data is essential for improving soil property assessments and ensuring reliable geotechnical analysis. Correlations between SPT-N and CPT data are essential for evaluating soil properties when either test is unavailable (Akca, 2003; Jarushi et al., 2015; Lu et al., 2022).

This study highlights the application of Machine Learning (ML) methods in geotechnical analysis, demonstrating their potential to optimize data utilization and enhance safety and efficiency in infrastructure projects. Utilizing machine learning methods, this research focused on developing predictive models for SPT-N values based on raw CPT data. The dataset originated from a geotechnical investigation for the expansion of the I-405 Freeway in Orange County, California. It comprises raw CPT data, corrected SPT-N values, and soil classifications following ASTM Unified Soil Classification System (USCS) standards, drawn from 90 CPT soundings and their adjacent SPT boreholes. The raw CPT data and corresponding corrected SPT-N values were prepared for training the ML techniques. The objective is to showcase the effectiveness of these techniques by creating predictive models for corrected SPT-N values from raw CPT data, ultimately enhancing soil property estimation.

 © Deep Foundations Institute 2025

CONE PENETRATION TEST (CPT)

CPT is a widely employed in-situ geotechnical investigation method for evaluating subsurface soil and rock properties. During the test, a cone-shaped penetrometer is systematically advanced into the ground at a consistent pace using hydraulic or mechanical means, with the encountered resistance recorded as raw data. Three primary parameters derived from the CPT include Cone Tip Resistance (qc), Sleeve Friction (fs), and Pore Pressure Reading (u2). qc measures soil resistance at the cone's tip, indicative of load-bearing capacity and typically quantified in units like psi, tsf, or MPa, with a pressure transducer at the cone tip recording advancement force. fs, or sleeve resistance, assesses frictional forces along the cone's sleeve during penetration, reflecting soil shear strength and aiding in identifying stratification variations. The u_2 sensor in CPT testing measures pore water pressure within the soil, providing insights into drainage conditions and groundwater presence. Negative readings may indicate partial drainage or soil consolidation under loading, particularly in overconsolidated or unsaturated soils (Fatehnia et al., 2024). "Figure 1" illustrates the CPT instrument and its installation on project sites.

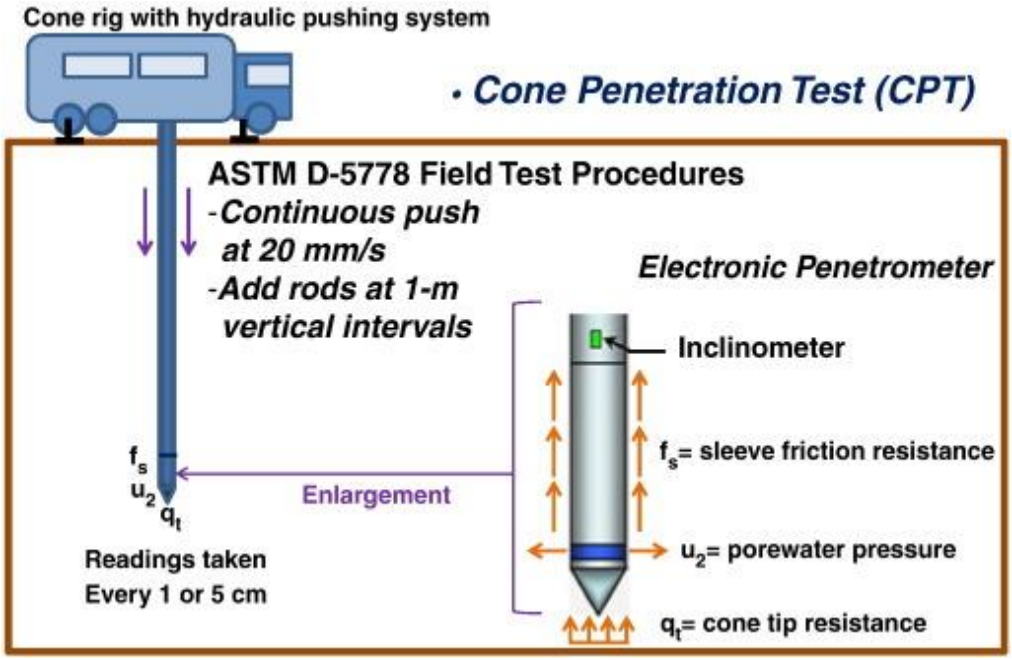


Fig. 1. CPT instrument details and installation (Ku et al., 2016)

DATA SOURCE AND PROJECT OVERVIEW

The data utilized in this research was obtained from a geotechnical investigation conducted for the expansion of a 16-mile stretch of the San Diego Freeway (I-405) in Orange County, California, near the Los Angeles County border. The project's objectives included the addition of general-purpose and toll lanes, as well as the replacement, widening, or construction of new bridges and Earth Retaining Systems (ERS) along the corridor. To ensure the successful execution of the widening project, a comprehensive data collection initiative was undertaken. This effort resulted in a significant number of in situ soil tests, including CPT soundings and SPT soil borings, to characterize the subsurface conditions across the project area. As shown in "Fig. 2A" and "Fig.2B", a total of 581 exploratory points, comprising 207 CPTs and 374 soil borings were utilized in this study.

 © Deep Foundations Institute 2025

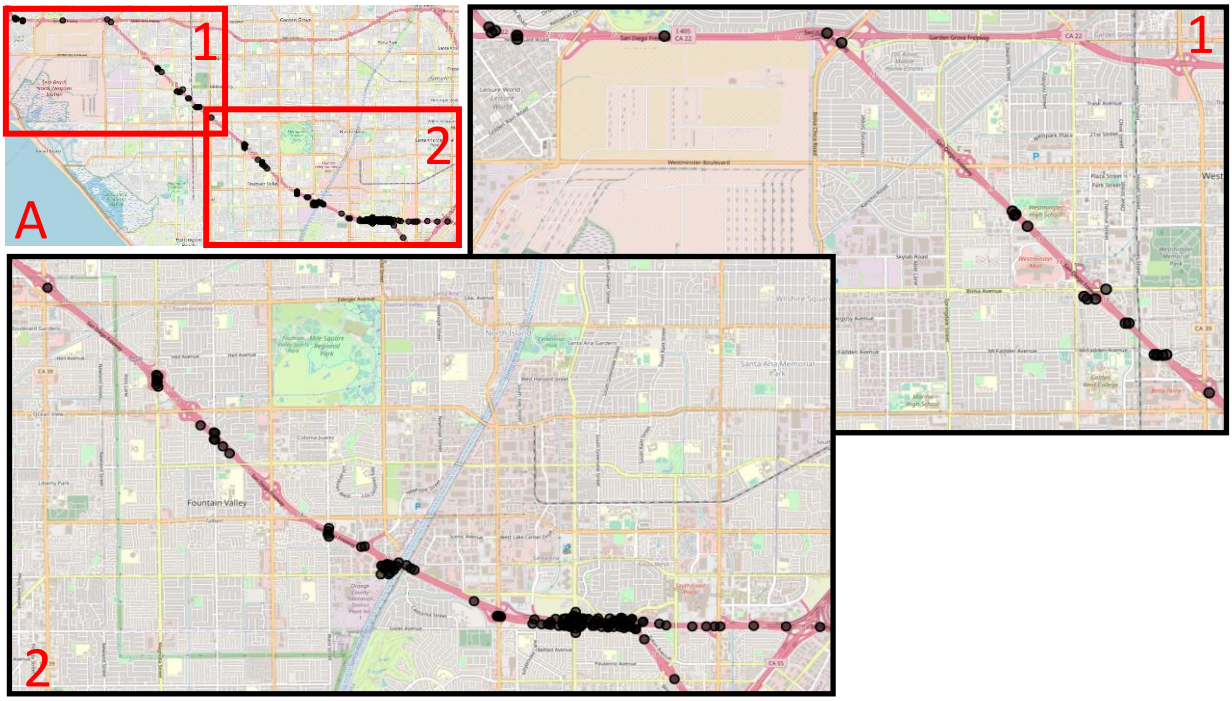


Fig. 2A. CPT sounding's locations over the project alignment (Fatehnia et al., 2024)

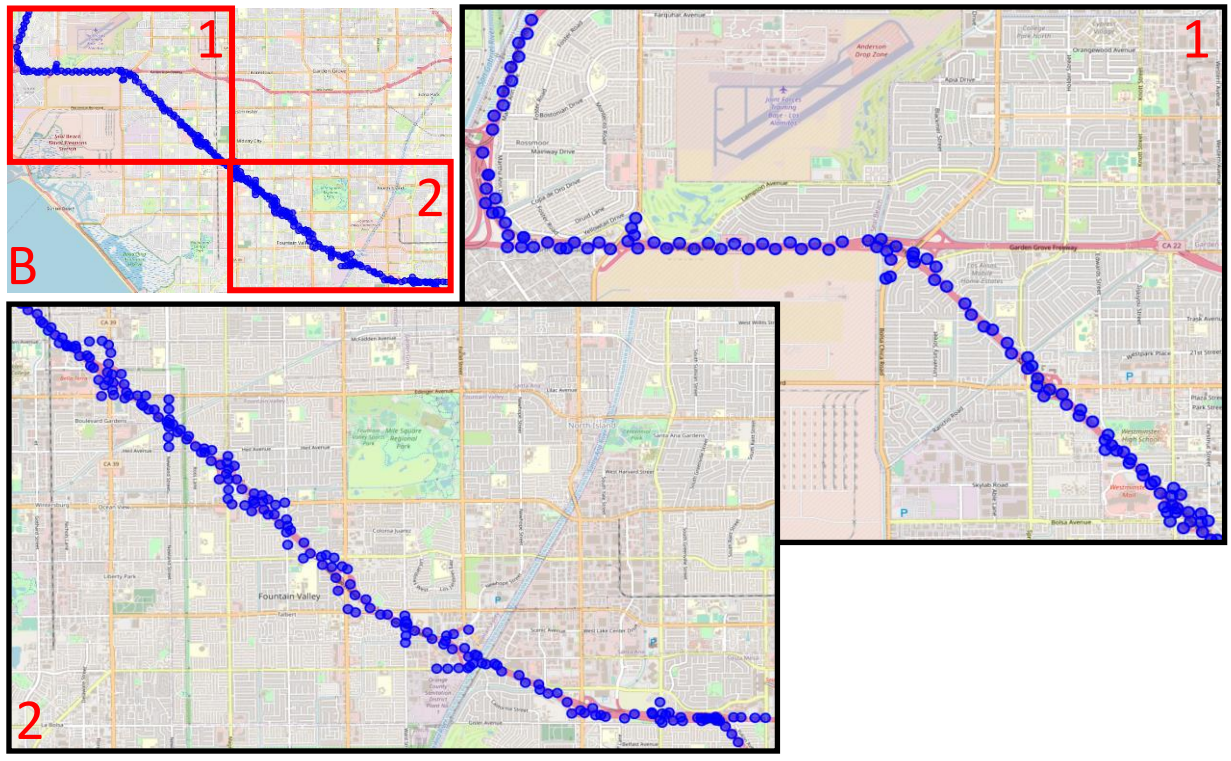


Fig. 2B. Soil boring's locations over the project alignment (Fatehnia et al., 2024)

 © Deep Foundations Institute 2025

DATA PREPROCESSING

Data preprocessing is essential for maintaining the accuracy and reliability of collected data. This section delineates the fundamental procedures for data cleansing when comparing CPT data with corrected SPT-N values derived via Rotary Wash or Hollow Stem Auger methods. Both borehole and CPT data were stored as distinct gINT projects. We extracted the data from multiple gINT projects and imported them into a single OpenGround cloud project to facilitate visual examination of test locations. Subsequently, we calculated the distances between adjacent boreholes and CPTs, identifying instances of missing data in both boreholes and CPTs. We then filtered the dataset to extract CPT data, corrected SPT-N values, and laboratory-tested soil classifications from relevant test locations, ensuring that CPT soundings and adjacent SPT boreholes were within 50 feet of each other. The data were extracted in comma-separated value (CSV) format, priming them for ML analysis.

Procedures applied to 581 exploratory points, including 207 CPTs and 374 soil borings, involved several data refinement steps. Boreholes and CPT soundings missing coordinates were excluded to enable precise geospatial analysis. Incomplete CPT data and borehole profiles were removed to maintain dataset integrity, while boreholes with incomplete soil classifications were discarded to ensure reliable geotechnical information. Only boreholes within 50 feet of CPT soundings were selected for direct comparisons. Outliers were identified and removed to preserve dataset quality, unit consistency across CPT data was ensured, and soil classifications and interpretations were verified for accuracy and reliability.

Python was employed for preprocessing and integrating CPT data, Corrected SPT-N values, and USCS Group Names for ML analysis, sourced from adjacent CPT soundings and boreholes. A Python script facilitated data extraction and integration by aligning specific columns from exported CPT data files with corresponding Corrected SPT-N values and soil classifications based on depth conditions. This ensured comprehensive data compilation by merging individual files and excluding rows with missing values. A selection of 90 pairs of CPT soundings and boreholes that were completed within a 50 ft proximity (180 total test locations) was made from available data to ensure accuracy and consistency in analysis. Since SPT-N values represent a specific depth range, the corresponding CPT data within that range were aggregated and assigned to the respective SPT-N value for analysis.

The depth of the processed data ranged from 2.56 ft to 126.21 ft. Following data cleansing and the removal of incomplete records, a total of 43,520 entries comprising raw CPT data, Corrected SPT-N values, and soil classifications remained. This refined dataset used for subsequent ML modeling and analysis. "Table 1" presents the statistical summary of the finalized data.

Table 1. Summary statistics of the complete dataset

Statistical Param.	Depth	qc (tsf)	fs (psi)	u2 (psi)	Corr. SPT-N
Count	43520	43520	43520	43520	43520
Mean	50.54	111.86	1.45	0.74	16.41
Standard Deviation	30.64	138.67	1.33	4.86	22.33
Minimum	2.56	0	0	-0.95	0
Maximum	126.21	887.72	15.61	231.58	100

In total, the records encompassed 30 distinct USCS soil types. "Table 2" illustrates the diversity of classifications, along with their occurrence counts and corresponding percentages within each record.

 © Deep Foundations Institute 2025

Table 2. Classification distribution and occurrence percentage of the complete dataset

USCS Group Name	Occurrence Count	Occurrence Percentage
Silty sand	9728	22.35
Lean clay	5107	11.73
Sandy lean clay	4811	11.05
Fat clay	3608	8.29
Clayey sand	3225	7.41
Silty clay	2489	5.72
Poorly graded sand with silt	2416	5.55
Poorly graded sand with clay	2137	4.91
Sandy silt	1867	4.29
Lean clay with sand	1547	3.55
Poorly graded sand	1271	2.92
Silt	881	2.02
Silty clayey sand	700	1.61
Silt with sand	672	1.54
Poorly graded sand with silt and gravel	507	1.16
Poorly graded sand with gravel	474	1.09
Clayey sand with gravel	456	1.05
Silty clay with sand	349	0.80
Silty sand with gravel	270	0.62
Poorly graded gravel with sand	223	0.51
Poorly graded gravel with clay	161	0.37
Sandy lean clay with gravel	129	0.30
Poorly graded gravel	120	0.28
Silty clayey sand with gravel	99	0.23
Lean clay with gravel	84	0.19
Gravelly lean clay with sand	60	0.14
Sandy silty clay	53	0.12
Poorly graded gravel with silt	45	0.10
Sandy fat clay	23	0.05
Asphalt Concrete	8	0.02
Total	43520	100

In the next process, we divided the dataset into two distinct subsets: one comprising sandy soils and the other consisting of clayey soils. This filtering process sought to eliminate records with USCS Group Name values not falling within these designated categories, enabling an assessment of the ML method's efficacy across varied soil types. Consequently, two new datasets were generated, each containing a refined subset of data exclusively pertaining to the specified categories. "Table 3" illustrates the distribution of classifications and their occurrence percentages within the sandy soils' dataset, while "Table 4" presents the distribution and occurrence percentages within the clayey soils' dataset.

 © Deep Foundations Institute 2025

Table 3. Classification distribution and occurrence percentage of the sandy soils' dataset

USCS Group Name	Occurrence Count	Occurrence Percentage
Silty sand	9728	45.71
Clayey sand	3225	15.15
Poorly graded sand with silt	2416	11.35
Poorly graded sand with clay	2137	10.04
Poorly graded sand	1271	5.97
Silty clayey sand	700	3.29
Poorly graded sand with silt and gravel	507	2.38
Poorly graded sand with gravel	474	2.23
Clayey sand with gravel	456	2.14
Silty sand with gravel	270	1.27
Silty clayey sand with gravel	99	0.47
Total	21283	100.00

Table 4. Classification distribution and occurrence percentage of the clayey soils' dataset

USCS Group Name	Occurrence Count	Occurrence Percentage
Lean clay	5107	27.97
Sandy lean clay	4811	26.35
Fat clay	3608	19.76
Silty Clay	2489	13.63
Lean clay with sand	1547	8.47
Silty Clay with Sand	349	1.91
Sandy lean clay with gravel	129	0.71
Lean clay with gravel	84	0.46
Gravelly lean clay with sand	60	0.33
Sandy Silty Clay	53	0.29
Sandy fat clay	23	0.13
Total	18260	100

MACHINE LEARNING MODELS

ML algorithms can analyze vast datasets, uncovering patterns and relationships between input and output variables. Their effectiveness has been demonstrated in various geotechnical applications, including predicting soil liquefaction (Garcia et al., 2012), assessing slope stability (Cho, 2009; Peng et al., 2014), classifying soil types (Bhargavi and Jyothi, 2011; Fatehnia et al., 2024), evaluating pile foundation load-bearing capacity (Fatehnia and Amirinia, 2018), and improving site characterization (Ghaderi et al., 2019; Kohestani et al., 2015; Zhang et al., 2022).

Python was employed in this study to develop ML models. The predictive modeling performed using Random Forest (RF) and eXtreme Gradient Boosting (XGBoost). The analysis focused on predicting corrected SPT-N values from the four parameters: depth, qc, fs, and u2.

Random Forest (RF)

Random Forest (RF) is a powerful ensemble learning technique widely applied across various fields for predictive modeling. By combining multiple decision trees, RF enhances accuracy and robustness compared to individual tree-based models. A key characteristic of RF is its use of randomly selected input variables for each tree, promoting model diversity and reducing overfitting, which improves generalization to unseen data. RF has demonstrated strong predictive capabilities in geotechnical engineering, where it has been successfully applied to various tasks, including soil classification, estimation of undrained shear strength, assessment of seismic-induced settlement, prediction of shallow foundation settlement, evaluation of pile drivability, and determination of liquefaction potential based on CPT and shear wave velocity data. Its ability to handle complex relationships within geotechnical datasets makes it a reliable tool for advanced predictive modeling in this domain (Fatehnia et al., 2024; Liu and Macedo, 2011; Pham et al., 2022; Shoarinejad et al., 2018; Zhang et al., 2021).

In this study, RF was implemented with 100 decision trees, each trained on randomly selected subsets of features to enhance model diversity. The Gini index was used as the splitting criterion to minimize impurity at each node. Final predictions were made by aggregating the outputs from all trees, improving accuracy and stability. The dataset was divided into 80% for training and 20% for testing, with a random state of 42 to ensure reproducibility.

eXtreme Gradient Boosting (XGBoost)

XGBoost is a widely used machine learning algorithm known for its high efficiency and strong predictive capabilities in both regression and classification tasks. As an ensemble learning method, it enhances predictive accuracy by combining multiple weak decision trees. Its scalability, computational efficiency, and built-in regularization techniques have made it a valuable tool across various scientific and analytical domains. Key features, such as early stopping, robust handling of missing data, and feature importance evaluation, contribute to its reliability and adaptability in diverse applications. In geotechnical engineering, XGBoost has gained significant traction due to its ability to efficiently process complex datasets and deliver precise predictions. It has been successfully applied to predict critical geotechnical parameters, including pile-bearing capacity, slope stability, undrained shear strength, and subsurface geology. Its capability to handle intricate relationships within geotechnical data makes it a preferred choice for researchers and practitioners seeking advanced data-driven modeling approaches (Amjad et al., 2022; Bharti et al., 201; Fatehnia et al., 2024; Shi and Wang, 2021; Zhang et al., 2021).

In this study, the XGBoost model was implemented with 100 trees and a learning rate of 0.1, allowing for iterative refinement of predictions. The model was trained with a random state of 42 to ensure reproducibility. The dataset was split into 80% for training and 20% for testing, ensuring robust model evaluation.

PERFORMANCE EVALUATION METRICS

Model performance was evaluated using four metrics: Mean Absolute Error (MAE), Mean Squared Error (MSE), Root Mean Squared Error (RMSE), and R^2 Score. MAE measures the average absolute difference between predicted and actual values, with lower values indicating better accuracy. MSE calculates the average of squared differences, penalizing larger errors more significantly, which is useful for minimizing large deviations. RMSE, the square root of MSE, gives the error in the same units as the target variable and is commonly used in regression problems. R^2 Score indicates how well the model explains the variability in the target, where a value of 1.0 represents a perfect model, 0 indicates no explanatory power, and negative values suggest the model is worse than using the mean as a predictor. These metrics allow

for a comprehensive evaluation of model performance by quantifying both error magnitude and the model's ability to explain variance in the data.

RESULTS

The results, as shown in "Table 5" and "Table 6", indicate that Random Forest consistently outperforms XGBoost across all datasets, demonstrating lower error values and higher predictive accuracy. For the complete dataset, Random Forest achieves lower MAE, MSE, and RMSE values, along with a higher R^2 score of 0.9173. In contrast, XGBoost produces higher error values and a lower R^2 score of 0.7871, suggesting that it captures less variability in the data. A similar pattern is observed in the sandy soil dataset, where Random Forest again provides better predictive performance. The MAE, MSE, and RMSE values are lower for Random Forest, and the R^2 score of 0.9415 indicates strong model reliability. XGBoost, on the other hand, exhibits higher error values and an R^2 score of 0.8566, showing reduced predictive accuracy compared to Random Forest. In the clayey soil dataset, Random Forest demonstrates the best overall performance. It achieves the lowest MAE of 2.1839 and the smallest RMSE of 5.0309, along with an R^2 score of 0.8347. XGBoost performs less effectively in this dataset, with higher errors and an R^2 score of 0.6847, indicating weaker predictive capability. The sandy soil dataset yields the highest R^2 values for both models, suggesting that corrected SPT-N values in sandy soils are more predictable based on CPT data. The complete dataset follows, with slightly lower R^2 values, while the clayey soil dataset produces the lowest R^2 scores. This trend suggests that soil type influences the effectiveness of ML-based predictions, with clayey soils presenting greater complexity and variability that both models struggle to capture.

We analyzed the importance of four parameters—depth, qc, fs, and u2—in predicting the corrected SPT-N using feature importance techniques based on a Random Forest Regressor. Feature importance reflects the contribution of each input variable to the model's predictions. After training the model, we extracted the importance scores for each parameter. The results, shown in the pie charts in "Fig. 3," revealed that for both the sandy and clayey soil datasets, depth had the highest importance, followed by qc. In contrast, for the complete dataset, qc had the highest importance. Across all datasets, fs had the least importance.

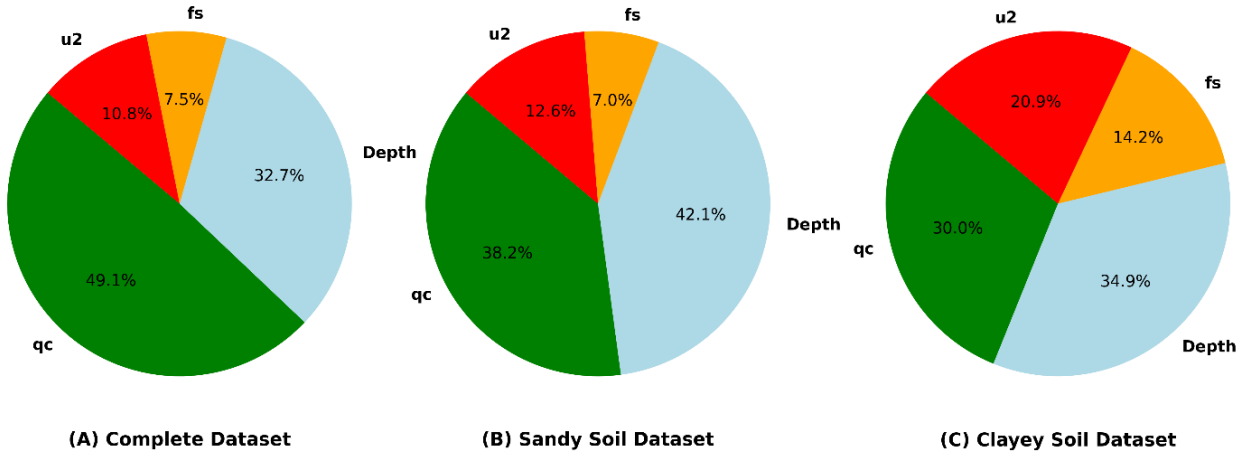


Fig. 3. Importance of parameters in predicting corrected SPT-N for the applied datasets

 © Deep Foundations Institute 2025

Table 5. Performance Comparison of Random Forest Model

Dataset	MAE	MSE	RMSE	R^2 Score
Complete	3.3818	42.2434	6.4995	0.9173
Sandy Soil	3.2789	43.6314	6.6054	0.9415
Clayey Soil	2.1839	25.3102	5.0309	0.8347

Table 6. Performance Comparison of XGBoost Regression Model

Dataset	MAE	MSE	RMSE	R^2 Score
Complete	7.5931	108.687	10.4253	0.7871
Sandy Soil	7.5501	106.9706	10.3427	0.8566
Clayey Soil	4.4661	48.2875	6.9489	0.6847

CONCLUSION

This study demonstrates the effectiveness of ML techniques in predicting corrected SPT-N from raw CPT data, enhancing property estimation. By applying Random Forest and XGBoost regression models, we establish a predictive framework that bridges the gap between these soil investigation methods. Analyzing data from a geotechnical investigation for the I-405 Freeway expansion in Orange County, California, we identify key correlations between CPT parameters and SPT-N values across different soil types. Our findings indicate that Random Forest consistently outperforms XGBoost, achieving higher predictive accuracy with lower error metrics and higher R^2 scores across all datasets. The sandy soil dataset exhibits the best model performance, with both methods achieving their highest R^2 values, whereas clayey soils present greater complexity, leading to reduced predictive accuracy. Depth and cone tip resistance remain the most significant predictors across all datasets. While Random Forest proves to be a robust and reliable choice for predicting SPT-N values, model performance varies by soil type, emphasizing the influence of subsurface conditions on ML-based predictions. Future research should focus on improving model generalizability through expanded datasets, hybrid modeling approaches, and integration of additional geotechnical parameters to enhance predictive reliability in diverse soil conditions.

REFERENCES

Akca, N. (2003). “Correlation of SPT-CPT data from the United Arab Emirates.” Engineering Geology, 67, 219-231.

Amjad, M., Ahmad, I., Ahmad, M., Wróblewski, P., Kamiński, P., and Amjad, U. (2022). “Prediction of pile bearing capacity using XGBoost algorithm: modeling and performance evaluation.” Applied Sciences, 12(4).

Bhargavi, P., and Jyothi, D. S. (2011). “Soil classification using data mining techniques: A comparative study.” International Journal of Engineering Trends and Technology, 55-59.

Bharti, J. P., P. Mishra, V. E. Sathishkumar, Y. Cho, and P. Samui. (2011). “Slope stability analysis using RF, GBM, CART, BT, and XGBoost.” Geotechnical and Geological Engineering, 39(5), 3741-3752.

Cho, S. E. (2009). “Probabilistic stability analyses of slopes using the ANN-based response surface.” Computers and Geotechnics, 36(5), 787-797.

 © Deep Foundations Institute 2025

Fatehnia, M., and Amirinia, G., (2018). “A review of genetic programming and artificial neural network applications in pile foundations.” International Journal of Geo-Engineering, 9(2), 1-20.

Fatehnia, M. and Deaton, S. (2023). “A Geotechnical Data Archive Isn't Geotechnical Data.” GeoStrata Magazine Archive, 27(5), https://doi.org/10.1061/geosek.0000500.

Fatehnia, M. and Deaton, S. (2022). “Geotechnical Data Analytics and Data Mining Using Microsoft Power BI.” Proc. Geo-Congress, 553-560.

Fatehnia, M., Mahmoudabadi, V., Amiri, S., (2024). “Utilizing Machine Learning for Cone Penetration Test-Based Soil Classification.” Transportation Research Records, 2678 (11), 1639-1648.

Garcia, S., Ovando-Shelley, E., Gutierrez, J. and Garcia, J. (2012). “Liquefaction assessment through machine learning.” 15 WCEE, Lisboa.

Ghaderi, A., Abbaszadeh Shahri, A., and Larsson, S. (2019). “An artificial neural network-based model to predict spatial soil type distribution using piezocone penetration test data (CPTu).” Bulletin of Engineering Geology and the Environment, 78(6), 4579–4588.

Jarushi, F., AlKaabim, S. Cosentino, P., (2015). “A New Correlation between SPT and CPT for Various Soils.” International Journal of Geological and Environmental Engineering, 9(2), 101-107.

Kohestani, V. R., Hassanlourad, M. and Ardakani, A. (2015). “Evaluation of liquefaction potential based on CPT data using random forest.” Natural Hazards, 79(2), 1079–1089.

Ku, T., Moon, S.W., Gutierrez, B.J., (2016). “Advanced application of seismic cone penetration test at complex ground conditions.” Engineering Geology, 210, 140-147.

Liu, C., and J. Macedo. (2022) “Machine learning-based models for estimating seismically-induced slope displacements in subduction earthquake zones.” Soil Dynamics and Earthquake Engineering, 160, 107323.

Lu, Y. C., Liu, L. W., Khoshnevisan, S., Ku, C. S., Juang, C. H., & Xiao, S. H. (2022). “A new approach to constructing SPT-CPT correlation for sandy soils.” Georisk: Assessment and Management of Risk for Engineered Systems and Geohazards, 17(2), 406–422.

Peng, M., Li, X. Y., Li, D. Q., Jiang, S. H. and Zhang, L. M. (2014). “Slope Safety Evaluation by Integrating Multi-Source Monitoring Information.” Structural Safety, 49, 65-74.

Pham, T. A., and Tran, V. Q. (2022) “Developing random forest hybridization models for estimating the axial bearing capacity of pile.” PLOS ONE, 17(3). https://doi.org/10.1371/journal.pone.0265747.

Shi, C., and Wang, Y. (2021). “Development of subsurface geological cross-section from limited site-specific boreholes and prior geological knowledge using iterative convolution XGBoost.” Journal of Geotechnical and Geoenvironmental Engineering, 147(9).

Shoarinejad, A., Güler, E. and Özturan, M. (2018). “Evaluation of liquefaction potential using random forest method and shear wave velocity results.” Proc., International Conference on Applied Mathematics & Computational Science (ICAMCS.NET), 23–26.

 © Deep Foundations Institute 2025

Zhang, W., C. Wu, H. Zhong, Y. Li, and L. Wang. (2021). “Prediction of undrained shear strength using extreme gradient boosting and random forest based on Bayesian optimization.” Geoscience Frontiers, 12(1), 469–477.

Zhang, J. Z., Zhang, D. M. Huang, H. W. Phoon, K. K. Tang, C. and Li, G. (2022). “Hybrid machine learning model with random field and limited CPT data to quantify horizontal scale of fluctuation of soil spatial variability.” Acta Geotechnica, 17(4), 1129–1145.

 © Deep Foundations Institute 2025

APPLYING THE INCREMENTAL RIGIDITY METHOD TO STATIC LOAD TESTS PERFORMED ON ALL-STEEL PILES

Joseph B. Mulcahey, E.I.T., RESPEC, Rapid City, South Dakota, USA, 605-646-4571, joseph.mulcahey@respec.com
Brett E. Belzer, P.E., RESPEC, Rapid City, South Dakota, USA, 605-394-6548, brett.belzer@respec.com

ABSTRACT

Appropriately calculating internal forces from measured pile strains is critical to the success of any instrumented static load test, and knowing the pile's axial rigidity (composite-section Young's modulus, E, times total cross-sectional area, A, together EA) is required. In recent years, the Incremental Rigidity (I.R.) method (Komurka & Moghaddam, 2020) has proven to be a robust tool for converting static load test strain-gauge data for piles with cementitious content, as the I.R. method provides a direct relationship between strain and internal force without requiring knowledge of either E or A. It is commonly assumed that the I.R. method need not be applied to all-steel piles due to presumably uniform axial rigidity values. Instead, a constant EA factor is usually used. This paper provides a brief overview of the I.R. method, discusses sources of uncertainty in EA and static load testing, and shows results from applying the I.R. method to numerous static load tests performed on all-steel piles. Interpreted internal-force values derived from the I.R. method are compared to conventionally interpreted static and dynamic load testing results and validate the robustness of the method. The benefits, limitations, and recommended best practices for applying the I.R. method to all-steel piles are discussed.

Keywords: incremental rigidity, H-piles, driven piles, steel piles, static load test, CAPWAP, strain gauges, unit soil resistance

INTRODUCTION

In recent years, the Incremental Rigidity (I.R.) method has proven to be a robust tool for calculating internal force from strain readings collected during an instrumented static load test (Komurka and Moghaddam, 2020; Komurka and Robertson, 2020; Robertson et al., 2021; Sinnreich, 2022; Ambaliya et al., 2023; Robertson and Komurka, 2023). The I.R. method provides a direct relationship between strain, ε, and internal force, F, without requiring knowledge of the composite-section Young's modulus, E, or the total cross-sectional area, A, of the pile, a useful advantage when dealing with piles where one or both of those parameters are variable and uncertain (e.g., drilled and bored piles, and other piles containing cementitious content, such as prestressed concrete and concrete-filled pipe). In the case where E and A are known, internal pile force is calculated from pile strain by Equation 1 below:

$$F_i = E_i A_i \varepsilon_i \quad [1]$$

Where at each Strain-Gauge Level I, F_i = Internal pile force, E_i = Pile composite-section Young's modulus, A_i = Pile total cross-sectional area, and ε_i = Pile strain

 © Deep Foundations Institute 2025

The use of Eq. 1 to calculate internal force shall be hereafter referred to as the "conventional method." It may be commonly assumed that all-steel piles need not undergo analysis via the I.R. method due to the pile's uniform axial rigidity (i.e., the product of E and A, or EA). Additionally, the variance in both E and A for all-steel piles tends to be very small. However, there can be considerable uncertainty in the measured strain-gauge values, applied loads from hydraulic jack, and soil-structure interaction (e.g., soil plugging), etc. This paper demonstrates that performing the I.R. method on all-steel piles can provide more reliable internal pile force calculations from strain than the conventional method (i.e., Eq. 1) and is therefore a worthwhile endeavor. The following sections present results comparing internal forces calculated from the conventional method and the I.R. method from 19 static load tests performed on all-steel piles. These results demonstrate that the I.R. method resolves certain nonsensical or obviously erroneous strain-gauge readings, accounts for other possible soil-structure-interaction phenomena and reveals greater uncertainty in load-transfer results when using the conventional method than is typically recognized.

BACKGROUND

Theory

The I.R. method is derived from the theoretical response of a free-standing pile under axial load. When the shaft resistance between a test load source and a given point along a pile is fully mobilized, the incremental change in test load, ΔQ, is equal to the incremental change in internal force, ΔF, at that given point along the pile. It follows that a strain gauge at this location would then be measuring changes in elastic compression as though the pile were a free-standing column with no shaft resistance. In this case, Eq. 1 may be divided by the incremental change in strain, Δε, to give the following relationship:

$$\frac{\Delta Q}{\Delta \varepsilon_i} = \frac{\Delta F_i}{\Delta \varepsilon_i} = (EA)_i \quad [2]$$

While shaft resistance is less than fully mobilized, internal force would not equal test load initially. As the test load increases, more shaft resistance is mobilized. Once shaft resistance has been fully mobilized between a test load source and a given point in the pile, any incremental increases in test load would have to pass through that point to further "downstream" (further from the load source) in the pile (assuming the remainder of the pile is able to provide sufficient resistance). In this scenario, the incremental change in test load is equal to the incremental change in internal force (i.e., ΔQ = ΔF). ΔQ/Δε may be plotted against total pile strain for a given strain-gauge level in an all-steel pile as shown in Fig. 1 below.

 © Deep Foundations Institute 2025

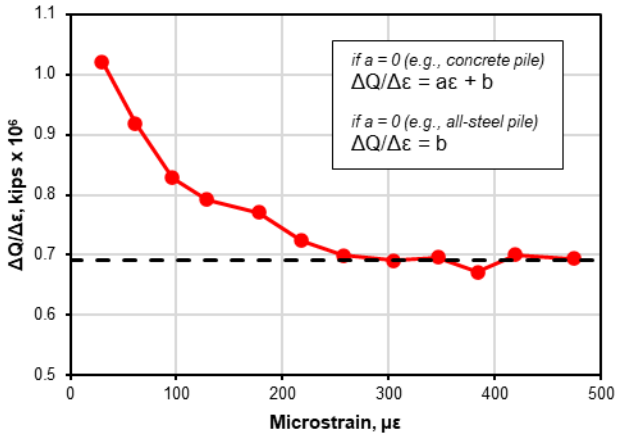


Fig. 1. Example ΔQ/Δε plot and linear fit at one strain-gauge level for an all-steel pile

The linear portion of the ΔQ/Δε plot is the portion of the test where all shaft resistance has been mobilized and the pile is exhibiting a free-standing response. Thus, Eq. 2 is valid. The linear portion is fit (as shown by the dashed line in Fig. 1) and integrated with the following relationship posed by Komurka and Moghaddam (2020), which is based on the Tangent Modulus Method (Fellenius 1989, 2001, and 2019; Salem and Fellenius, 2017):

$$F = 0.5a\varepsilon^2 + b\varepsilon = (0.5a\varepsilon + b)\varepsilon = (EA)\varepsilon \quad [3]$$

Where a = slope of the ΔQ/Δε plot linear fit, and b = intercept of the ΔQ/Δε plot linear fit. Note that combining Eq. 1 and the third equality in Eq. 3 yields a strain-gauge-location-specific EA value in terms of the ΔQ/Δε response, thus providing a more direct calculation of internal force from measured pile strain. A more thorough treatment of the theory supporting the I.R. method may be found in Komurka and Moghaddam, (2020). Another advantage of the I.R. method is that it accounts for strain-dependent behavior (if any) of the pile material (captured by the "a" term in the linear fit of the ΔQ/Δε plot). All-steel piles, however, exhibit strain-independent behavior, and EA is expected to be constant throughout a static load test. Therefore, the theoretical response of a ΔQ/Δε plot for a steel pile should have a zero slope (i.e., a = 0) and a simplification can be made to Eq. 3:

$$F = b\varepsilon = (EA)\varepsilon \quad [4]$$

Eq. 2 and Eq. 4 show that the theoretical ΔQ/Δε value for a free-standing column would be the same as the theoretical rigidity (i.e., EA value) of the pile, as ΔQ/Δε = b = EA. This is assuming that E does not change with strain (i.e., is strain-independent, as with an all-steel pile). Therefore, this paper shall hereafter refer to ΔQ/Δε and pile rigidity or EA interchangeably. However, it is crucial to recognize that this equality does not hold true for piles containing cementitious content (i.e., strain-dependent piles), as Fig. 1 and Eq. 3 show that ΔQ/Δε ≠ EA when a ≠ 0. Note that the theoretical ΔQ/Δε (EA) value for each tested pile is shown as a black dashed line in the following figures.

 © Deep Foundations Institute 2025

Variability and Uncertainty of E and A

It is well known that of all modern construction materials, steel is one of the most consistent. Typically, steel sections vary little across different fabricators and batches. However, steel mill tolerances allow for some variability in the pile area. AISC [2023] permits a tolerance of -2.5% to +3.0% for the cross-sectional area of HP piles. Statically tested all-steel piles also include a welded steel channel (also with a tolerance of -2.5% to +3.0%) to protect strain gauges during driving, which may influence pile rigidity. A 3"x3"x1/4" channel has an area of 1.44 in^2, which would account for 6.7% to 11.6% of the area of the various HP sections included in this paper. All area values reported in this paper include the area of the channel. While AISC provides a Young's modulus, E, of 29,000 ksi to be used for design, some variability could be expected based on slight variations in its metallurgy (e.g., chemical composition). Commonly assumed values for Young's modulus, which may vary among analysts, range from 29,000 to 30,000 ksi, varying by only 3.4%.

Though the error attributed to EA for steel may contribute to the overall uncertainty involved with a static load test, it is anticipated to be dwarfed by other sources of error (discussed in the next section). Rigidity as a property is intrinsically extensive (i.e., related to the size of the system), and its value depends on its constitutive material(s), shape, and boundary conditions (Komurka and Moghaddam, 2020). Particularly, the fact that rigidity is influenced by boundary conditions implies that the quantity is not to be strictly defined by pile properties. Instead, rigidity inherently relies on components of the static load testing system outside of the pile itself (e.g., soil resistance, stress history, and deformation properties). Therefore, the definition of rigidity for the calculation of internal forces ought to consider other sources of influence beyond pile material and geometry.

Other Sources of Uncertainty in a Static Load Test

It is no mystery that geotechnical engineering hosts a great deal of uncertainty with regard to analysis and design, and instrumented static load tests are no exception. It is important to recognize that a static load test is a complex system that has numerous possible reasons for results to be different than expected. Besides the relatively small uncertainty and variability derived from E and A of an all-steel pile, a comprehensive but by no means exhaustive list of other possible sources of error and uncertainty is provided below:

1) Load cell and jack pressure error – Fellenius [1984] found that load cell measurements erred by 10-20% compared to jack pressure. Additionally, load cell readings are sensitive to end conditions (i.e., stress distribution in plates) and alignment during loading, both of which are dependent on test setup and not calibration or precision of the load cell itself. It should be noted that using jack pressure to determine applied load also has error for similar reasons as load cells (e.g., end conditions, alignment) but tend to be more reliable in field settings.
2) Strain gauges – for vibrating-wire gauges, strains are converted from vibration frequency to digits, then from digits to microstrain via calibrated gauge factors. Operators may make errors in programming calibration values. Additionally, numerous factors such as the act of pile driving or improper installation can influence readings or cause malfunctions.
3) Uncertain localized soil conditions – though soil borings and other characterization efforts are performed to understand site-specific soil conditions, the exact conditions at the pile location are

uncertain, and the act of driving alters those conditions compared to what a boring or CPT may have encountered. The unknown presence of boulders/cobbles, soil plugs, etc. introduce uncertainty.

4) Pile driving – numerous factors about pile driving can impact the load test response. Some examples include damaging the pile during driving, introducing pile batter or sweep, and residual stresses, potentially in both the pile and surrounding soil.

Test Database

Table 1. Test Pile Database

Pile I.D.	Pile Section	Depth, feet	Geology
Corson TP-2	HP 12x74	35.0	Shale
Lincoln TP-1	HP 12x74	60.5	Glacial Till
Lincoln TP-2	HP 12x74	41.7	Glacial Till
Fall River TP-2	HP 10x57	37.8	Shale
Spink TP-1	HP 10x42	41.0	Glacial Till
Spink TP-2	HP 10x42	31.3	Glacial Till
Minnehaha TP-3	Pipe 16" x 0.25"	39.2	Glacial Till
Minnehaha TP-4	Pipe 16" x 0.25"	32.5	Glacial Till
Buffalo TP-2	HP 10x42	43.1	Shale
Buffalo TP-3	HP 10x42	42.5	Shale
Brookings TP-1	HP 14x73	75.0	Glacial Till
Brookings TP-2	HP 14x73	65.0	Glacial Till
Meade TP-1	HP 12x53	29.0	Siltstone
Meade TP-2	HP 12x53	25.0	Siltstone
White River TP-1	HP 12x53	39.0	Shale
White River TP-2	HP 12x53	35.0	Shale
White River TP-3	HP 12x53	41.0	Shale
Harding TP-2	HP 12x53	55.0	Shale
Keldron TP-1	HP 12x53	35.0	Shale

The database presented in this paper consists of 19 static load tests performed in South Dakota soils to aid the South Dakota Department of Transportation (SDDOT) in refining their deep foundation design procedures for driven pile for bridge abutments. The load tests consist of 17 H-piles and 2 closed-ended pipe piles terminating in a variety of geologic formations (mostly shales and glacial till), with embedded depths ranging from 25 to 75 feet. All test sites contained 0 to 20 feet of weak soil overlying soils of geotechnical interest. Table 1 provides a summary of the piles tested. All test piles contain at least one soil segment (i.e., pile segment between two strain gauges) in the noted geologic formation. The instrumentation design, installation, and testing were performed by a third-party contractor, and strain-gauge data were provided for analysis. Typically, four strain gauges were installed along the pile length, though not all strain gauges for each test survived. Strain gauges are labeled with ascending depth (e.g., SG-1 is nearest to the ground surface). Specifically, the original test database included 30 tests, but only 19 produced usable strain-gauge data for a thorough I.R. analysis. For each test pile, high-strain dynamic pile testing (HSDPT) was performed for the full depth of driving, and a Case Pile Wave Analysis Program

(CAPWAP®) analysis was performed on a representative blow from end of initial drive (EOID) and beginning of restrike (BOR). Restrikes were typically performed on test piles seven days after installation, and static load tests were typically performed seven days after restrike (14 days after pile driving).

Analysis Approach

Equation 4 was used for interpreting $\Delta Q/\Delta\varepsilon$ plots for all static load tests presented in this research. In other words, each $\Delta Q/\Delta\varepsilon$ plot was fit with a zero-slope line. The last several recorded test loads and measured strains were averaged for each load step (Komurka and Robertson, 2020). Each strain-gauge level was analyzed via the I.R. method, but a $\Delta Q/\Delta\varepsilon$ relationship was only used to calculate internal force for a strain-gauge level if the strain-gauge level was judged to be interpretable (i.e., above the resistance balance point). The resistance balance point is defined as the point along the pile where the soil is providing equal resistance above and below that point. If a strain gauge was judged to be non-interpretable, the most believable rigidity value derived from interpretable strain-gauge levels for that pile was used to calculate internal force for non-interpretable levels under the assumption that the pile's rigidity was uniform along its length.

TEST CASE RESULTS

Numerous valuable conclusions can be made about applying the I.R. method to all-steel piles. This section examines three test cases in-depth to demonstrate the 1) validity of the zero-slope assumption, 2) ability of the I.R. method to reasonably interpret improperly calibrated/erroneous strain-gauge readings, and 3) ability of the I.R. method to more-accurately estimate toe resistance than the conventional method.

Validation of Zero-Slope Assumption

Figure 2 depicts the $\Delta Q/\Delta\varepsilon$ plots for each strain gauge and the internal force profiles for the maximum test load calculated by conventional and I.R. methods for Lincoln TP-2. The internal force profile from the CAPWAP analysis at BOR is included for reference. This HP 12x74 pile was driven approximately 41 feet deep in entirely glacial till. Examining the $\Delta Q/\Delta\varepsilon$ plots in Fig. 2a reveals three things about the static loading response of this pile:

1) SG-2 is observed to mobilize shaft resistance early on in the test and resolve to a near-zero-slope line at approximately 250 microstrain ($\mu\varepsilon$). It resolves to an intercept magnitude approximately equal to the theoretical $\Delta Q/\Delta\varepsilon$ value for an HP 12x74 pile.
2) SG-1 exhibits a near-zero-slope response, but at higher $\Delta Q/\Delta\varepsilon$ values than SG-2. SG-1 was placed within 1 foot of the ground surface.
3) SG-3 and SG-4 do not resolve linearly at a near-zero-slope line, indicating that shaft resistance above did not fully mobilize before test completion.

The good agreement between SG-2 and the theoretical EA for this pile provides some confidence that the I.R. method provides a reasonable result. As noted above, it would generally be expected that the pile rigidity would vary little along its length for a given pile section, and it would be expected that SG-2 would fully mobilize shaft resistance since it is relatively near the surface and therefore expected to be above the resistance balance point in the pile.

 © Deep Foundations Institute 2025

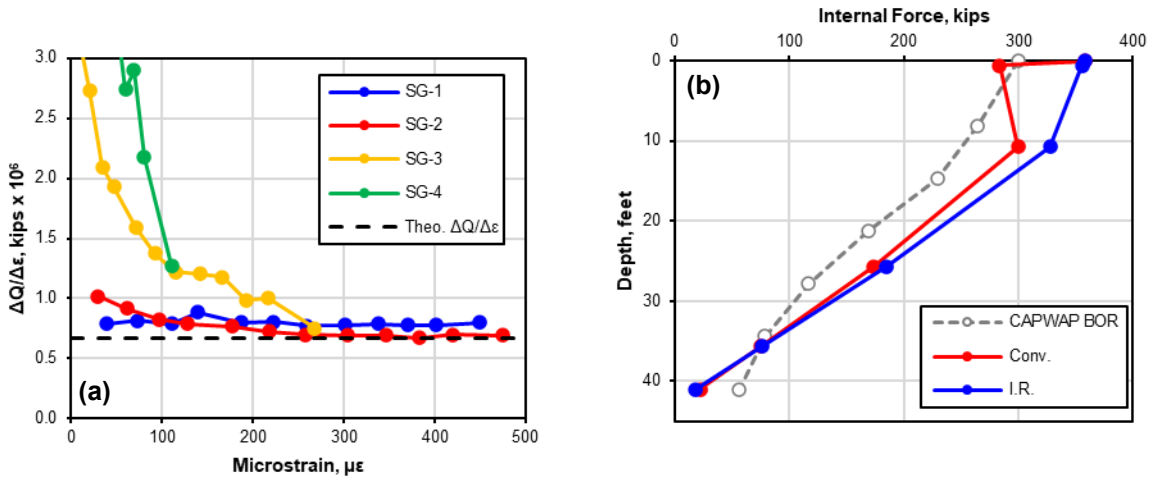


Fig. 2. (a) ΔQ/Δε plots for all strain-gauge levels and (b) internal force profiles from conventional and I.R. methods for the maximum test load for Lincoln TP-2

In this case, using the I.R. method to calculate internal forces at the maximum test load for this pile provides a nearly identical result as the conventional method, as shown in Fig. 2b, with the exception of SG-1. Using the conventional method yields an internal force from SG-1 that is smaller in magnitude at a shallower depth (i.e., "upstream) – a physically impossible result – essentially rendering the load-transfer data from that soil segment useless. It is generally recommended to install strain gauges far enough away from the pile boundary to ensure a plane-strain loading condition (Sinnreich, 2022). In this case, SG-1 was installed 2.9 feet from the load cell and embedded only 0.6 feet in the soil. Therefore, it is likely that other mechanical phenomena (e.g., bending, stress concentrations, eccentric loading) are contributing to the higher ΔQ/Δε values of SG-1. Whatever the reason, the unique load-strain response at SG-1 is captured by the I.R. method, and a more reasonable internal force is calculated at SG-1 as shown in Fig. 2.

Resolution of Improperly Calibrated Strain Gauges

Figure 3 depicts the ΔQ/Δε plots for each strain gauge and the internal force profiles at the maximum test load calculated by conventional and I.R. methods for White River TP-1. The internal force profile from the CAPWAP analysis at BOR is included for reference. This HP 12x53 pile was driven approximately 39 feet deep and terminated in 21 feet of shale, overlain by 18 feet of weak sand and clay.

Examining the internal force profile derived from the conventional method in Fig. 3b (red curve) reveals a highly suspicious result. The internal force calculated at SG-1 near the ground surface is approximately 25% of the applied test load. The remaining strain gauges yield similarly small internal forces, though the shaft resistance distribution below SG-1 makes sense proportionally given the site conditions. The ΔQ/Δε plots in Fig. 3a reflect this discrepancy between the conventional and I.R. method internal force profiles, as the ΔQ/Δε values derived from the top three strain gauges are 4 to 5 times greater than the expected theoretical rigidity for this pile. It is worth noting that the top three strain gauges exhibit a nearly identical zero-slope response. It is suspected that the cause of the great discrepancy in the theoretical and effective

rigidities could be improperly calibrated or converted strain-gauge measurements, though this suspicion could not be confirmed due to not possessing the raw frequency measurements from the vibrating-wire sensors. Regardless, using the I.R.-method-derived ΔQ/Δε values to calculate internal forces yielded a much more believable result that agrees better with the site conditions, including the internal force profile obtained from the CAPWAP. This testifies to the I.R. method's ability to salvage data that is either erroneous or presented in alternative units (e.g., digits, volts).

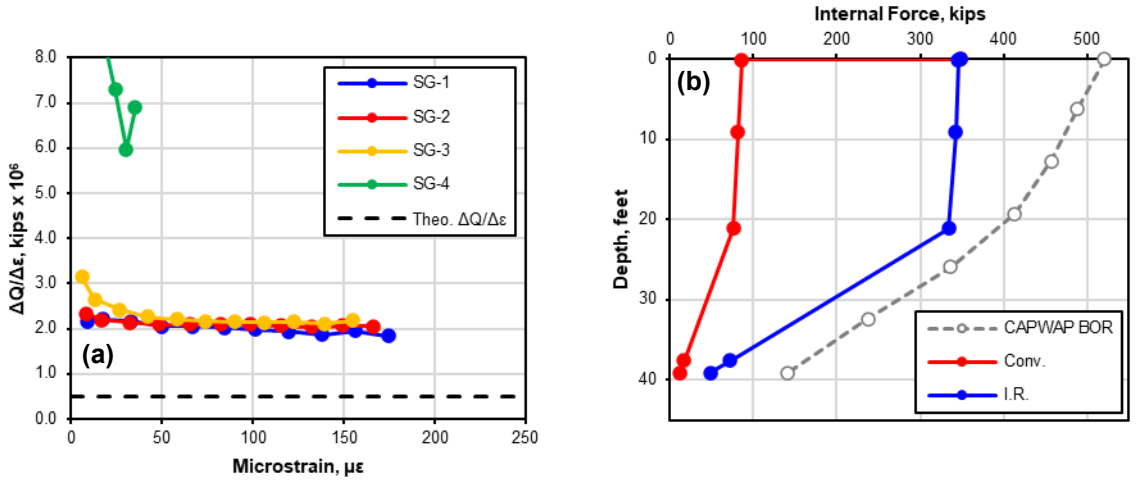


Fig. 3. (a) ΔQ/Δε plots for all strain-gauge levels and (b) internal force profiles from conventional and I.R. methods for the maximum test load for White River TP-1

Underestimated Unit Toe Resistance

Figure 4 depicts the ΔQ/Δε plots for each strain gauge and the internal force profiles for the maximum test load calculated by conventional and I.R. methods for Meade TP-2. The internal force profile from the CAPWAP analysis at BOR is included for reference. This HP 12x53 pile was driven approximately 25 feet deep and terminated in 8 feet of siltstone, overlain by 8 feet of sand and gravel, overlain by 9 feet of clay fill.

Examining the internal force profile derived from the conventional method in Fig. 4 reveals a similarly suspicious result as White River TP-1. Namely that the top soil segment appears to provide the greatest magnitude of shaft resistance, though that layer is expected to be geotechnically weak. Also, like White River TP-1, the ΔQ/Δε plots of the top three strain gauge levels resolve to a nearly identical zero-slope line. SG-4 appears to resolve linearly as well, though at higher ΔQ/Δε values.

It is possible that strain gauge calibration error is contributing to these results, but two additional pieces of data must be considered. First, BOR CAPWAP analysis showed that the nominal pile resistance was estimated to be toe-resistance dominated (35.3% shaft resistance). Conversely, the conventional method shows that the pile is shaft-resistance dominated (64.1% shaft resistance). The BOR penetration resistance was approximately 27 blows per foot (bpf), indicating that restriking the pile likely mobilized the full available pile resistance during dynamic testing, and thus the CAPWAP force profile is assumed to be

 © Deep Foundations Institute 2025

reasonably accurate. Second, telltale data indicated significant toe settlement relatively early in the test, with approximately 0.10 inch of toe settlement at a test load of 200 kips (58.8% of the total head settlement of 0.17 inch). These two facts combined suggest that excessive toe settlement is causing the pile to "relax," and the strain gauges therefore are measuring smaller strains than if the toe settled less. The I.R. method presents this phenomenon as higher $\Delta Q/\Delta\varepsilon$ values, since if $\Delta\varepsilon$ is reduced, the quotient $\Delta Q/\Delta\varepsilon$ is increased. Calculating internal force using the I.R. method with the higher $\Delta Q/\Delta\varepsilon$ values derived from all strain gauges are more congruous with the other available data. Specifically, the I.R. method calculates 15.1% shaft resistance in the pile, which agrees better with the CAPWAP, especially in segmental shaft resistance distribution at portions deeper than 8 feet along the pile, as shown in Fig. 4.

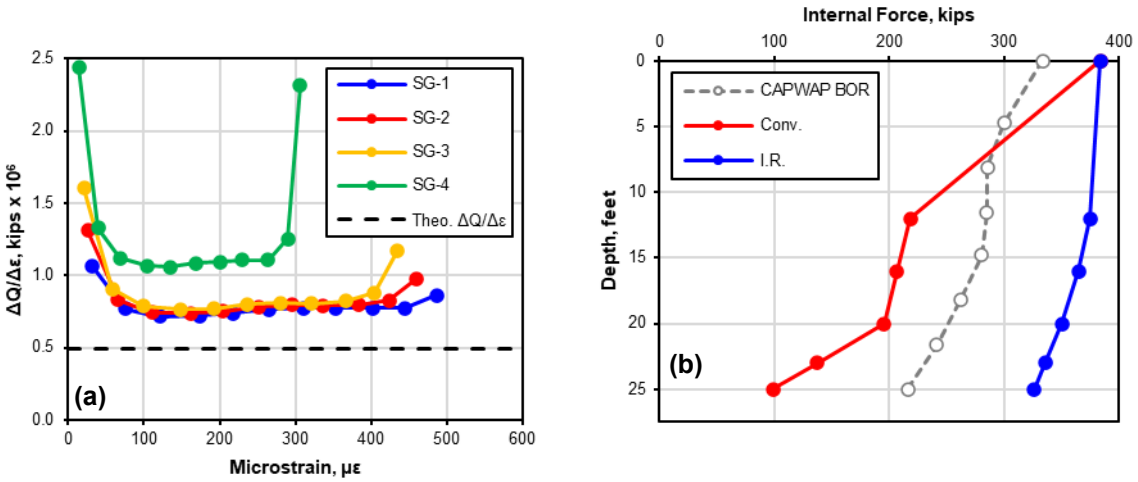


Fig. 4. (a) ΔQ/Δε plots for all strain-gauge levels and (b) internal force profiles from conventional and I.R. methods for the maximum test load for Meade TP-2

It is worth noting that the fit from the $\Delta Q/\Delta\varepsilon$ plot for SG-4 was used, though it appears to respond differently than the other three gauges. There were two reasons why it was judged as trustworthy, despite the different response. First, it resolved on a zero-slope line, indicating that the shaft resistance is fully mobilized above the gauge. Second, when the average $\Delta Q/\Delta\varepsilon$ fit for SG-1 through SG-3 is used to calculate internal force at SG-4, the I.R. analysis shows the soil segment between SG-3 and SG-4 has an unbelievably large unit shaft resistance value compared to typical unit shaft resistance values in siltstone. Additionally, the shaft resistance distribution from the I.R. analysis agrees better with the CAPWAP when the fit from the $\Delta Q/\Delta\varepsilon$ plot for SG-4 was used to calculate internal force, as previously mentioned.

UNIT RESISTANCE COMPARISON

The three test cases demonstrate some of the unique benefits of using the I.R. method; this section aims to demonstrate how the I.R. method performs compared to conventional analysis ($F = EA\varepsilon$) overall for all-steel piles. Unit shaft and toe resistance values were calculated from the internal forces derived from both the conventional and I.R. methods. The average (AVG), standard deviation (SD), and coefficient of variation (CV, computed as SD divided by AVG) of unit resistance values for all test piles are given in Table 2 for various soil types. Additionally, Figure 5 plots unit resistance versus depth for both the

 © Deep Foundations Institute 2025

conventional and I.R. methods. Data points are plotted by site and colored by dominant geology, where shales are orange, tills are green, and siltstones are purple. Weak overburden soils at all sites are included in their own category (black points in Fig. 5). Within each geologic setting, similar soil types are expected to have similar resistance values.

Table 2. Unit Resistance Comparison of Conventional and I.R. Methods for Different Soil Types

Parameter	Metric	Weak Soils		Shales Only		Tills Only	
		Conv.	I.R.	Conv.	I.R.	Conv.	I.R.
# of Tests (Shaft Segments)		19 (27)		9 (14)		8 (21)	
Unit Shaft Resistance (psi)	AVG	10.6	1.8	14.5	18.9	16.2	11.9
	SD	15.8	1.9	7.5	9.8	22.9	9.4
	CV	1.49	1.02	0.52	0.52	1.41	0.79
Unit Toe Resistance (ksf)	AVG	-	-	497	630	658	580
	SD	-	-	261	252	800	485
	CV	-	-	0.53	0.40	1.21	0.84

Examining Table 2 and Fig. 5 reveals three things:

1) The I.R. method results have reduced variability (i.e., smaller CV values) for unit shaft and toe resistance compared to the conventional method. The only exception is shale unit shaft resistance, which has similar variability. These results suggest that I.R. gives greater confidence in characterizing unit resistance parameters.
2) Weak overburden soils differ the most between conventional and I.R. methods. I.R. shows that these soils have weak unit shaft resistance as expected, whereas the conventional method indicates that these weak soils provide substantial unit shaft resistance. The I.R. method results for weak overburden soils agree with other available site data (e.g., CAPWAP force profiles, small Standard Penetraion Test (SPT) N-values, weak penetration resistance during driving while in those layers, etc.)
3) Figure 5 illustrates for unit shaft resistance that I.R. analysis generally gives increasing unit shaft resistance values with increasing depth as expected. Conversely, the conventional method tends to have greater scatter, especially for weak overburden soils. These results reinforce that I.R. gives greater confidence in characterizing unit resistance parameters.

Figure 6 shows the proportional (i.e., percent) shaft resistance for the I.R. and conventional methods compared to that of the CAPWAP BOR results. Note that outlined data points convey values where the penetration resistance was greater than 120 bpf during restrike, indicating that the dynamic test may not have mobilized all available pile resistance. The correlations (i.e., R-squared values) presented only consider points where penetration resistance was less than 120 bpf. It is observed that the I.R. method and conventional method had correlations of 0.610 and 0.035 with CAPWAP-estimated percent shaft resistance, respectively. The better correlation from the I.R. method strongly suggests that the method more accurately delineates the load-transfer response than assuming a constant EA and using the conventional method. Additionally, the disparity between conventional and I.R. methods appears to be greatest for lesser percent shaft resistance values. This lends more credence to the theory that toe resistance is underestimated from the pile relaxing from greater toe settlement, as asserted when discussing Meade TP-2 previously.

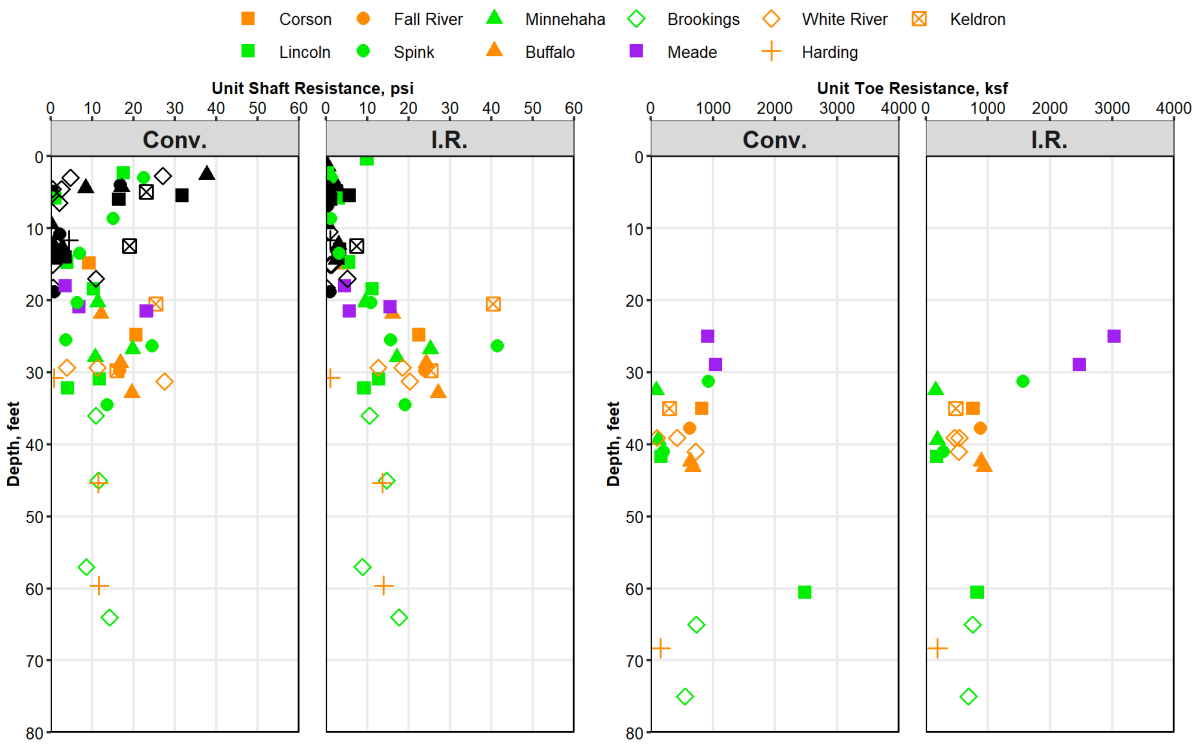


Fig. 5. Unit shaft and toe resistance versus depth comparing conventional and I.R. methods

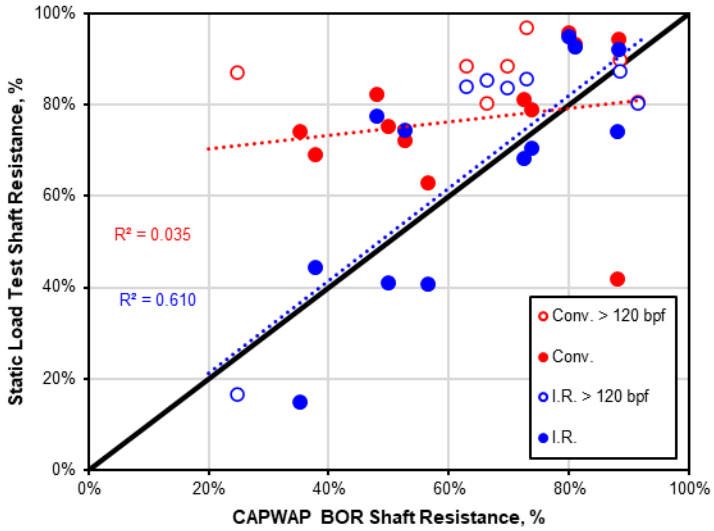


Fig. 6. Correlation of percent shaft resistance between CAPWAP and static load testing

SUMMARY AND CONCLUSIONS

The I.R. method has proven to be a robust tool for calculating internal force from strain-gauge data collected during instrumented static load tests, but no literature exists confirming its validity for all-steel

piles. Despite the well-known and relatively consistent material (E) and geometric (A) properties for all-steel pile sections, other possible sources of error could affect the pile's rigidity during a static load test which could lead to miscalculating internal pile forces and soil unit resistance by simply assuming E and A. The strain-independent character of steel deformation allows for a simplification to fitting $\Delta Q/\Delta\varepsilon$ plots, namely that a zero-slope may be assumed as shown in Eq. 4.

Examining specific test cases confirm that this "zero-slope" assumption is reasonable when compared to the theoretical $\Delta Q/\Delta\varepsilon$ for most tests (Lincoln TP-2). The results of these $\Delta Q/\Delta\varepsilon$ plots demonstrate that soil segments that fully mobilize shaft resistance resolve approximately to a zero-slope line for all-steel piles. Additionally, whether it is dealing with strain-gauge calibration error (White River TP-1) or accounting for other possible pile-soil-interaction phenomena (Meade TP-2), the I.R. method is able to salvage reasonable internal force values from otherwise suspect load-test data or unusable strain-gauge data. Unit resistance values derived from the I.R. method and conventional method were compared for different soil types. It was found that the I.R. method had reduced or similar variability for unit shaft and toe resistance compared to the conventional method. The I.R. method's delineation of load transfer response agrees better with dynamic load testing done for each pile compared to the conventional method, as shown in Fig. 6. These results strongly suggest that the I.R. method gives more confidence in characterizing the load-transfer response than the conventional method for all-steel piles.

Overall, the I.R. method is a valuable analytical tool that should be applied to strain-gauge data from static load tests performed on all-steel piles. Though conducting the I.R. method contains some application of engineering justification and requires more effort than a conventional analysis, it is the opinion of the authors that the favorable results presented in this paper validate the use of the I.R. method compared to simply calculating internal force from an assumed EA. It is also worth noting that, whether analysists acknowledge it or not, assuming E and A for calculation of internal force also requires application of engineering justification, albeit to a lesser degree. Regardless, prudent engineering justification must be exercised in interpreting $\Delta Q/\Delta\varepsilon$ plots, as numerous potential sources of error during a static load test exist. In step with this truth, it is believed that I.R.-analysis quality is enhanced by scrutinizing site- and test-specific data to substantiate calculated internal forces. Additionally, it is advised to always compare internal forces calculated by the conventional method and the I.R. method and determine which are most appropriate for use in design. However, the results in this paper exhibit that the I.R. method generally appears to yield more accurate interpretations of strain-gauge data than the conventional method and should thus be the go-to method for calculating internal forces for all-steel piles.

ACKNOWLEDGEMENTS

We would like to offer special thanks to Van E. Komurka, P.E., D.GE, F.ASCE, for answering our questions about the I.R. method and offering his experience and expertise pertaining to reducing strain - gauge data and the deep-foundations-load-testing industry as a whole. We are incredibly grateful for the time, mentorship, and review effort he has generously offered. We would also like to thank the SDDOT for their collaboration in this static load testing project. We hope these findings serve the SDDOT well in better understanding South Dakota's unique soil conditions for pile design.

REFERENCES

AISC “Steel Construction Manual,” 16th Edition, American Institute of Steel Construction, Chicago, 2023.

Ambaliya, S.K., Kulkarni, S. & Robertson, S., 2023. Determination of Internal Force Distribution Using the Incremental Rigidity Method on Instrumented Static Load Tests in India. DFI-India Annual Conference, pp. 213-225.

Fellenius, B.H., 1984. Ignorance is bliss—and that is why we sleep so well. Geotechnical News, Canadian Geotechnical Society and United States National Society for Soil Mechanics and Foundation Engineering, Vol. 2, No. 4, pp. 14-15.

Fellenius, B.H., 1989. Tangent Modulus of Piles Determined from Strain Data. ASCE, Geotechnical Engineering Division, the 1989 Foundation Congress, F.H. Kulhawy, Editor, Vol. 1, pp. 500-510.

Fellenius, B.H., 2001. From Strain Measurements to Load in an Instrumented Pile. Geotechnical News Magazine, 19(1), pp. 35-38.

Fellenius, B.H., 2019. Basics of Foundation Design, A Text Book. Revised Electronic Edition, [www.Fellenius.net], 484 p.

Komurka, V.E., & Moghaddam, R.B., 2020. The Incremental Rigidity Method – More-Direct Conversion of Strain to Internal Force in an Instrumented Static Loading Test. ASCE GeoCongress 2020, Minneapolis, MN.

Komurka, V.E., & Robertson, S., 2020. Results and Lessons Learned from Converting Strain to Internal Force in Instrumented Static Loading Tests Using the Incremental Rigidity Method. ASCE GeoCongress 2020, Minneapolis, MN.

Robertson, S.O., Bixler, M.G. & Komurka, V.E., 2021. Bi-Directional Static Load Testing Results of an Augered Cast-In-Place Pile and a Drilled Displacement Pile. In IFCEE 2021, pp. 128-142.

Robertson, S. & Komurka, V.E., 2023. Converting Strain to Internal Force in Instrumented Static Load Tests on Cast-In-Place Grouted Piles. DFI 48th Annual Conference, pp. 29-38.

Sinnreich, J., 2022. Perspective Chapter: Interpretation of Deep Foundation Load Test Data. In New Approaches in Foundation Engineering. IntechOpen.

Salem, H., & Fellenius, B.H., 2017. Bidirectional Pile Testing. What to Expect. Proceedings of the 70th Annual Canadian Geotechnical Conference, Paper 763, Ottawa, Canada, October 1-3, p. 7.

 © Deep Foundations Institute 2025

FOUNDATION SUPPORT OF THE LILLY MEDICINE FOUNDRY IN LEBANON IN

W. Morgan Nesmith, BERKEL, Atlanta GA USA, +1 770-739-3561, morgan@berkelandcompany.com
Jake K. McKean, BERKEL, LaGrange KY, +1 502-225-0053, jmckean@berkelandcompany.com
Nicholas Zadd, BERKEL, +1 502-225-0053, nzadd@berkelandcompany.com

ABSTRACT

Eli Lilly and Company are investing $4.5 billion to create the Lilly Medicine Foundry, a new center for advanced manufacturing and drug development, combining research and manufacturing in a single location. The Medicine Foundry is in Indiana's LEAP Research and Innovation District in Lebanon, Indiana and will expand the company's investment there to more than $13 billion.

Multiple new facilities are planned for the manufacture of a range of bioactive compounds for use in pharmaceutical therapeutics. Distinct compounds include Peptides (short chains of amino acids that are involved in many physiological processes and biochemical functions), Oligonucleotides (short chains of nucleotides that can be made of DNA or RNA) and Small Molecules (with a molecular weight of < 900 Da). A Central Utility Building (CUB) with an extensive array of pipe and utility racks is planned to support the manufacturing facilities. The facilities are being constructed on pads of structural fill approximately 5-ft to 15-ft above the natural ground surface. Native soils are generally up to 35 feet of soft to stiff (generally highly weathered) glacial deposits with stiff to very hard glacial deposits underlying the site. Column loads for manufacturing facilities typically ranged from 400 to 1000 tons with 4000 psf design bearing pressures for large floor areas in numerous facilities to accommodate the relatively heavy manufacturing equipment at each facility.

Project requirements include a maximum of 3/4 in total settlement of the structures. Given the size and overall weight of the structures and the large area loads of the manufacturing equipment within the structures, this specification became the primary design consideration for foundation support of most of the structures. The manufacturing facilities will be supported on a combination of Augered-Cast-in-Place (ACIP) piles under building columns and augered, Rigid Inclusions (RIs) under the floors. The CUB facility will be supported by a range of RIs under columns and floors depending on the required support across the facility. To date, approximately 6,500 ACIP piles and 4,700 RIs have been installed to support these facilities.

This paper addresses the design and construction of the referenced ACIP piles and RIs with particular regard to the behavior of the foundation elements in the glacial till deposits underlying the site. Geotechnical site characterization information included logs of several borings and the results of cone penetration tests (CPT) performed to up to 100-ft below grade across the entire project site. The boring logs included visual classifications and Standard Penetration Test (SPT) results. Results of laboratory tests performed on collected samples were also included in the report. The results of several seismic CPTs were also provided. The shear wave velocity profile information indicated stiffnesses in the till deposits that were significantly greater than might be indicated by the CPT and boring data. The anticipated soil stiffnesses were verified by the pile and RI performance testing program, allowing the project team to economize the foundation design for pile capacity, but more significantly for the estimation of overall structure settlement.

Keywords: Augercast, ACIP Piles, APG piles, Rigid Inclusions

BACKGROUND

In a landmark development for pharmaceutical manufacturing infrastructure, Eli Lilly and Company has committed $4.5 billion to establish the Lilly Medicine Foundry, an innovative center that seamlessly

 © Deep Foundations Institute 2025

integrates advanced manufacturing capabilities with drug development operations. This strategic investment, situated within Indiana's LEAP Research and Innovation District in Lebanon, Indiana, represents a significant expansion of Lilly's presence in the region, bringing their total investment to more than $13 billion.

The ambitious scope of this project encompasses multiple specialized manufacturing facilities designed for the production of three distinct pharmaceutical components: Peptides (short chains of amino acids crucial to physiological processes and biochemical functions), Oligonucleotides (short nucleotide chains composed of either DNA or RNA), and Small Molecules (compounds with molecular weights less than 900 Da). Supporting these production facilities, a comprehensive Central Utility Building (CUB) and an extensive network of pipe and utility racks ensure seamless operations across the manufacturing complex. The construction sequence incorporated elevated building platforms, with facilities being erected on structural fill pads positioned 10 to 15 feet above the natural ground surface.

Berkel was initially contracted to provide Rigid Inclusion (RI) support for the CUB facility. Based on the effectiveness of this solution, the contract was subsequently expanded to include deep foundation and RI support for the additional manufacturing facilities. These additional facilities were in early phases of development when Berkel was integrated into the project team, and included unknown final utility locations, unknown final equipment loads and locations, and preliminary structure loads. The early involvement of the foundation contractor enabled a rapid response to accommodate facility design modifications as these, and other details were finalized.

LOCAL GEOLOGY

The project site is situated within the Tipton Till Plain section of the Central Till Plain physiographic region of Indiana. This area falls within the limits of Wisconsin and Pre-Wisconsin glacial depositions, which have significantly influenced the regional geology and soil characteristics. The Tipton Till Plain section is, in general, topographically homogeneous. However, several glacial features are common throughout the landscape which result in subtle variations in subsurface profiles and groundwater conditions observed across the site.

The predominant soil type in the project site is reported as silt or silty clay loams of the Crosby-Treaty Association. The parent materials of these soils are described as silty materials or loess over loamy till, which is consistent with the glacial deposition history of the region. These soil associations typically exhibit moderate drainage characteristics and are known for their relatively high clay content.

Regional bedrock mapping indicates that the project site is underlain primarily by the Devonian-Mississippian aged New Albany Shale formation. This formation consists predominantly of organic-rich black shale with minor amounts of greenish-gray shale and dolostone. Bedrock elevations in the project vicinity are reported as ranging from El. 700 to El. 750 ft, while the site surface elevation is approximately El. 920 ft. This indicates a significant overburden of glacial and post-glacial deposits above the bedrock surface. It should be noted that neither borings nor soundings conducted during the site investigation encountered any bedrock, as these investigations did not extend to the expected bedrock depths.

SITE-SPECIFIC PROFILE

Site preparation for the project involved the placement of engineered fill to reach design levels of El. 925 ft for the Central Utility Building (CUB) and El. 928 ft for the Peptide 1 facility. Prior to the placement of this fill, the existing ground level across the site was approximately El. 915 to El. 920 ft, with natural

 © Deep Foundations Institute 2025

groundwater levels observed between El. 915 ft and El. 918 ft. Table 1 is a generalization of the subsurface profile including the engineered fill, a shallow cultivated zone and the underlying glacial till.

Glacial till deposits consisted predominantly of lean clays (CL), silty clays (CL-ML), and interbedded sands (SM and SP-SM) that extended to depths exceeding 100 ft below the exploration level. The glacial till was generally described as exhibiting varying shades of brown, brown and gray, or gray, with distinct weathering characteristics at different depths throughout the profile (noted in Table 1).

Interbedded in both the upper and lower till were deposits of silty sands (SM), occasionally containing gravel, and poorly graded sands with silt and gravel (SP-SM). These granular deposits likely represent glaciofluvial sediments deposited by meltwater during glacial retreat phases. SPT N-values in these materials ranged from 2 bpf to 45 bpf, indicating very loose to dense relative densities, with the density generally increasing with depth.

Table 1. General Subsurface Profile

Elevation [ft]	
925 to 928 (Final Grade)	ENGINEERED FILL: primarily on-site natural soils processed and compacted to meet project specifications.
915 to 920	CULTIVATED ZONE: (historic and active row cropping agricultural activities). Typically, dark brown lean clay containing variable amounts of sand, root hairs, and organic content (1.2 percent to 2.7 percent). **Removed** prior to the placement of the engineered fill mentioned above.
914 to 917	GLACIAL TILL: highly weathered, in soft or loose (to occasionally hard) conditions indicative of intense weathering processes, including freeze-thaw cycles, oxidation, and biological activity, resulting in reduced strength and increased compressibility compared to deeper materials. Low plasticity lean clays with varying amounts of sand and sandy lean clays (CL). Standard Penetration Test (SPT) N-values ranged from 0 to 80 blows per foot (bpf), reflecting the heterogeneous nature of glacial deposits. Natural moisture contents ranged from 8.1 percent to 26.2 percent, with the higher moisture contents generally corresponding to the softer consistency materials.
890	GLACIAL TILL: moderately weathered, firm/stiff or medium dense. Transition between the highly weathered near-surface materials and the less weathered deeper deposits with properties ranging from those described above and below. Low plasticity sandy silty clays (CL-ML). SPT N-values ranged from 3 to 60 bpf, indicating soft to hard consistency, though generally exhibiting greater stiffness than the upper till materials. Natural moisture contents ranging from 9.0 percent to 13.2 percent, consistent with their greater density and lower void ratio.
870	GLACIAL TILL: stiff/hard or dense/very dense, with generally increasing stiffness and density with depth reflecting the reduced weathering and larger overburden pressure.
850	GLACIAL TILL: very hard, minimally weathered with significant overconsolidation
800	Approximate Extent of Exploration

 © Deep Foundations Institute 2025

DESIGN REQUIREMENTS

General

The owner's primary objective was centered on achieving production readiness by a specific target date. To meet this critical timeline, the project team adopted a conservative approach to floor load support. This strategy included designing support for a broader potential support area to accommodate uncertainty in the final positioning of heavy manufacturing and production equipment. Additionally, due to the precise tolerances required by sensitive manufacturing equipment, a maximum total facility settlement of 3/4-inch was established as a design constraint.

Cub Facility

Project documentation specified design bearing pressures for spread footings in the CUB facility ranging from 4000 psf to 6500 psf (Fig. 1). Additional design floor loads were subsequently incorporated into the requirements:

- Column Line C-1 to C-4.1: up to 450 psf
- Column Line C-4.1 to C-12: between 1000 psf to 1900 psf as determined by the project team

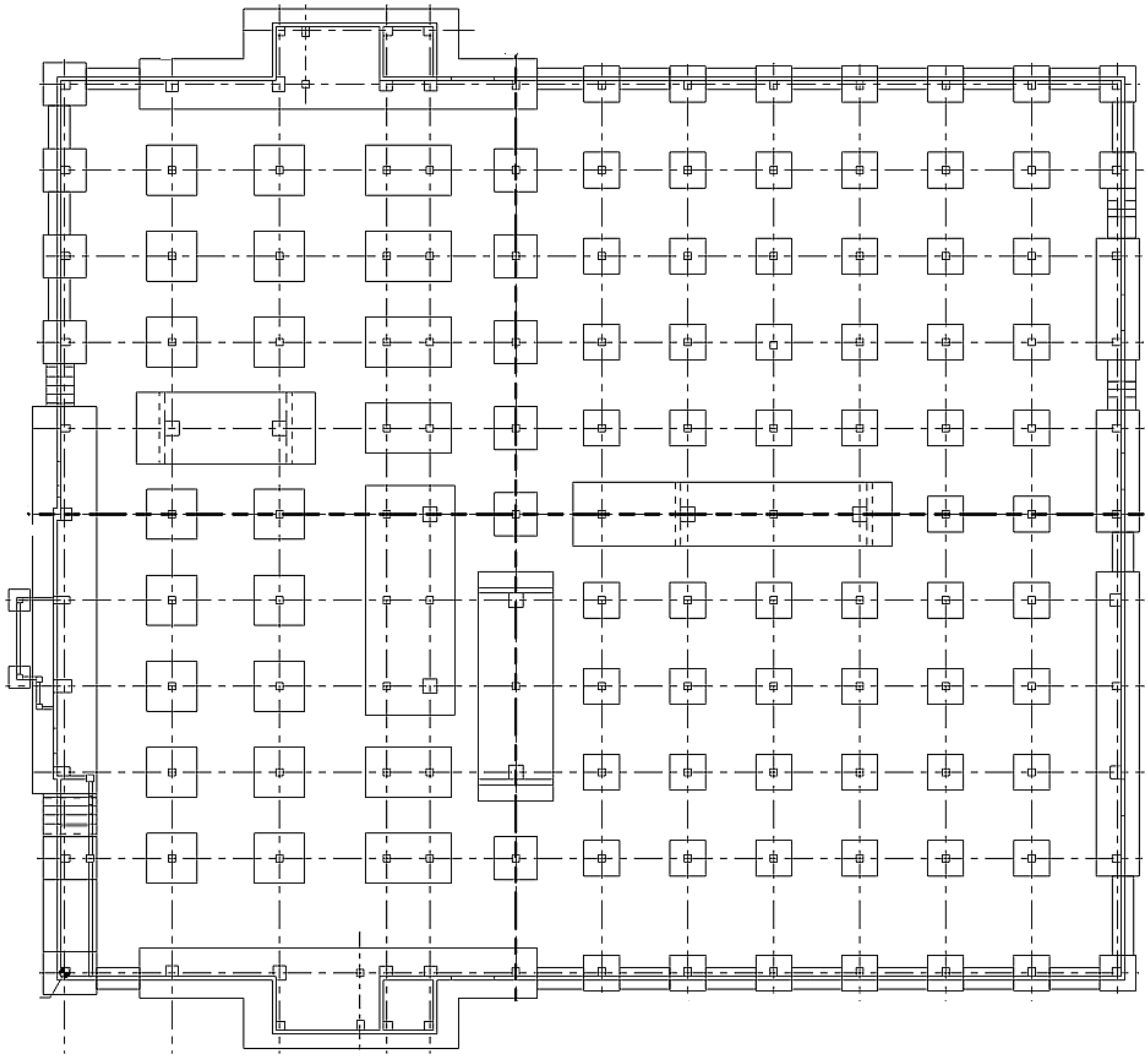


Fig. 1. CUB Facility Footings and Floor

 © Deep Foundations Institute 2025

Peptide 1 Facility

Design reactions for columns to be supported at the Peptide 1 facility were provided by the project team (Fig. 2). The evaluation of these reactions indicated that piles would be necessary for column support due to the relatively high lateral demands. Individual 20-in diameter ACIP piles were specified to provide resistance for up to 210 tons compression, 50 tons tension, and 11 tons lateral load. Additionally, the project team specified the following floor loads to be supported:

- Row P1-M to P1-C: up to 4000 psf
- Row P1-C to PO1-A: up to 1000 psf

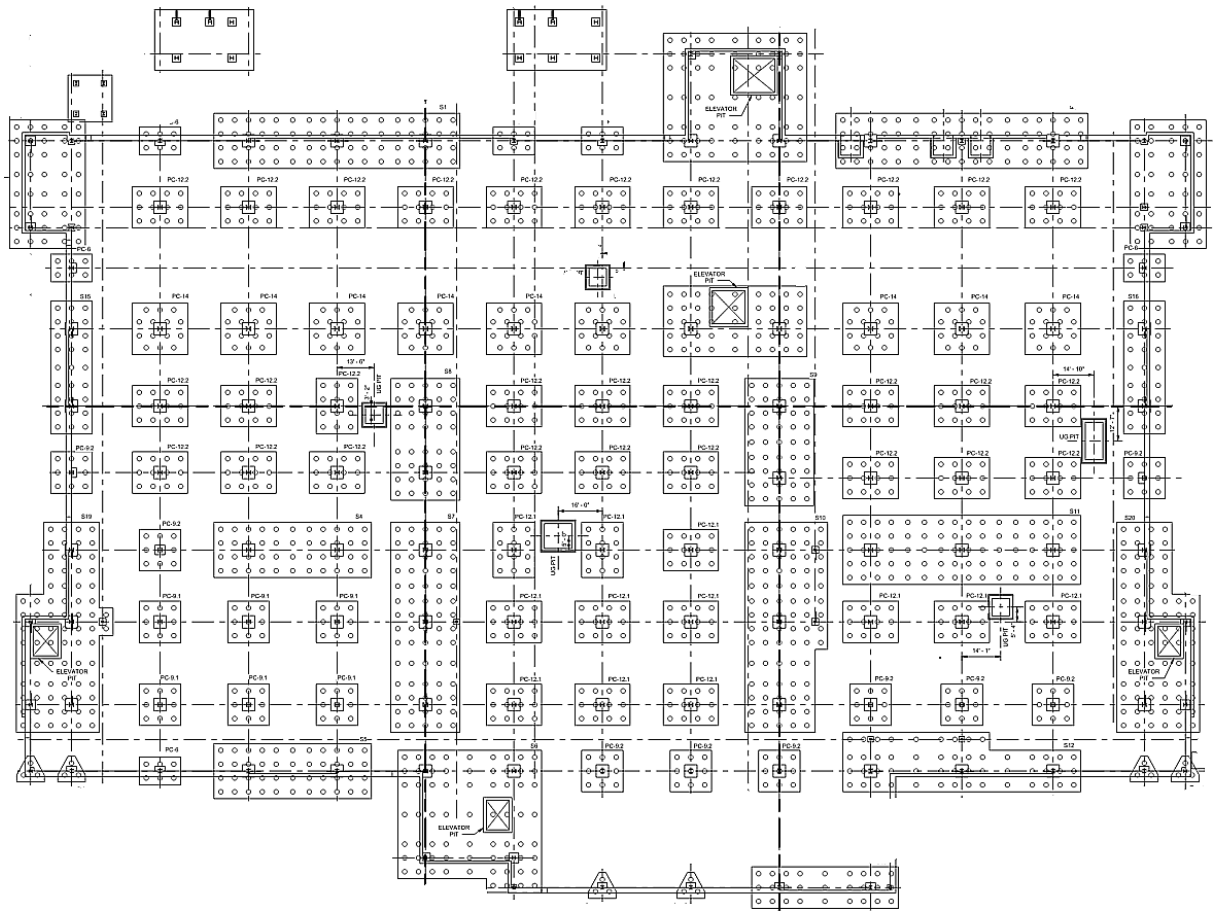


Fig. 2. Peptide 1 Facility Pile Caps and Floor

ENGINEERING/DESIGN

Axial Resistance of Piles and Rigid Inclusions

General

The design of compressive resistance for both ACIP RIs and piles involved application of recognized methodologies from geotechnical literature. Two principal approaches guided the design process:

- The methodology developed by Bustamante and Gianeselli (1982), which utilizes static penetrometer (CPT) data to predict pile bearing capacity through empirically validated correlations

 © Deep Foundations Institute 2025

- The evaluation framework outlined by Coleman and Arcement (2002), specifically developed for auger cast piles in heterogeneous soil conditions similar to those encountered at the site

These methods were refined using a proprietary database of performance of ACIP piles and RIs in comparable geologic settings, with particular attention to fine-grained till soil behavior. This calibration process ensured that theoretical predictions were adjusted to reflect actual field performance in similar conditions.

The designers applied these analytical approaches to both the boring data from the geotechnical report and the CPT data supplied separately. This analysis yielded a representative design profile for the RIs, providing a reliable basis for subsequent detailed design work across the various facility locations.

CUB Facility Rigid Inclusions

Figure 3 presents a representative axial capacity calculation for an individual foundation RI. An important design consideration was that while the soil profile documentation begins at elevation +920 ft, zero capacity was assumed from that level down to elevation +915 ft, representing the lowest anticipated top-of-RI elevation.

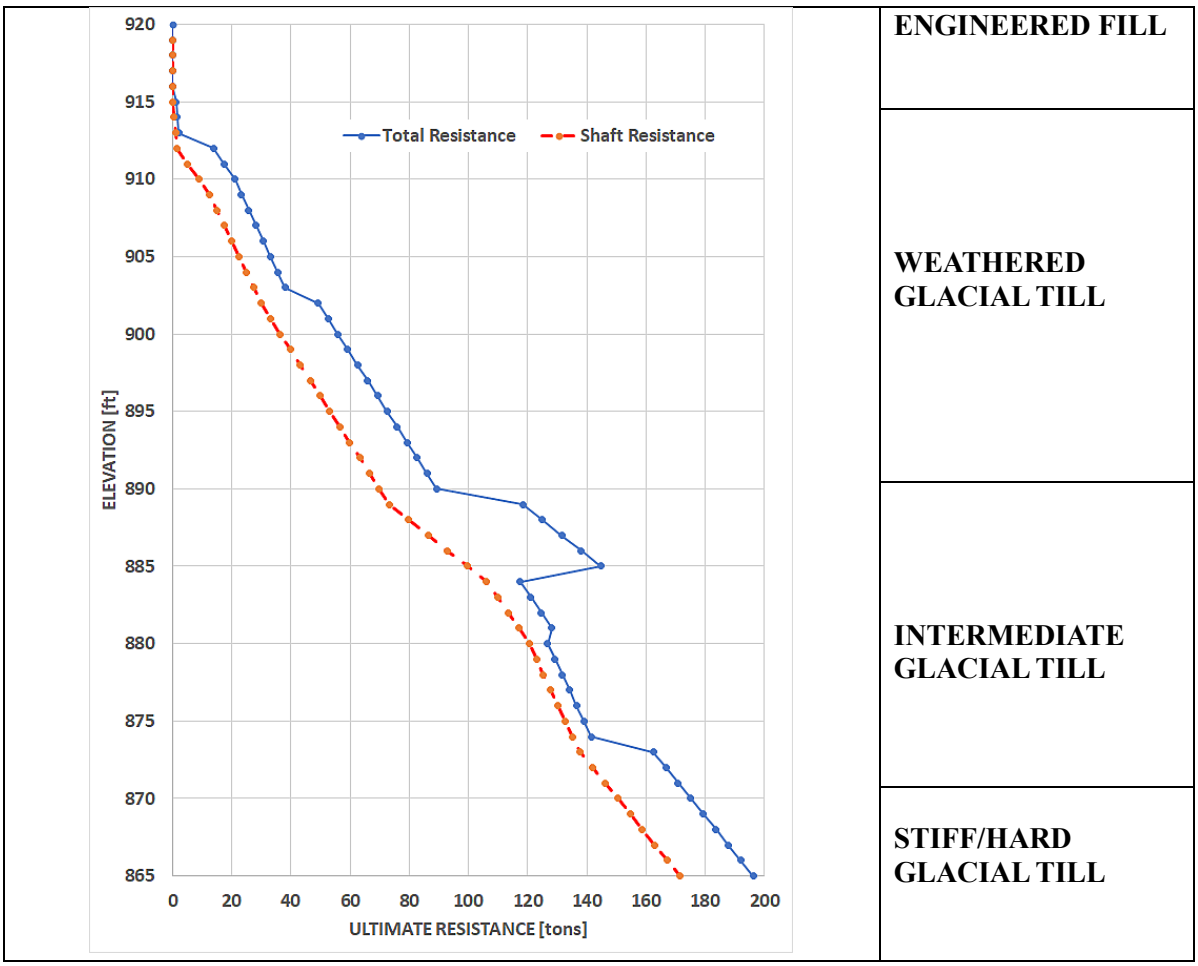


Fig. 3. Example Capacity Estimate 14-in Diameter Augered RI – CUB Facility

 © Deep Foundations Institute 2025

The final design specified 14-inch diameter ACIP RIs extending to toe elevation +865 ft, positioned according to the RI layout plan. This configuration was determined to adequately support the design bearing pressures for the spread footings. Rather than implementing a uniform grid, the design team strategically positioned RIs to address both bearing capacity concerns and settlement limitations as outlined in the project requirements. This non-uniform arrangement optimized material usage while ensuring performance criteria were met. Individual RI axial loading was capped at 95 tons to maintain appropriate safety factors.

For floor support within the CUB facility, the design incorporated 14-inch diameter ACIP RIs arranged in an approximate 10-ft by 10-ft square grid pattern. In areas with design floor pressures up to 450 psf, RIs extended to elevation +888 ft. For zones with higher design pressures (between 450 psf and 1900 psf), RIs reached deeper, to elevation +865 ft, to provide greater allowable bearing pressures.

Peptide 1 Facility ACIP Piles and Rigid Inclusions

An example calculation for axial capacity of a 20-inch ACIP pile is provided in Fig. 4. With the lowest top-of-pile elevation established at approximately +914 ft, the design specified that 20-inch diameter piles extend to elevation +841 ft to achieve the required axial resistance. Production pile lengths were standardized based on reaching this uniform toe elevation, regardless of variations in pile-head elevation (provided these remained above +914 ft). This approach maintained consistent performance characteristics while accommodating final structure levels.

The floor support system for the Peptide 1 facility employed two distinct configurations based on loading requirements. For areas with design pressures up to 4000 psf, 14-inch diameter RIs installed to elevation +876 ft on a relatively tight 7-ft by 7-ft grid were specified. In zones with lighter loading (up to 1000 psf), 14-inch RIs reaching elevation +885 ft on a wider 10-ft by 10-ft grid provided adequate support. The RI layout was carefully engineered to limit floor settlement within project tolerances rather than providing uniform bearing pressure. The design acknowledged that modifications to floor loading configurations might necessitate corresponding adjustments to RI quantity and placement. Under the specified spacing and loading conditions, individual RI axial loads would not exceed 100 tons for the 4000 psf zones or 50 tons for the 1000 psf zones.

Considerations for Underground Utilities

As previously noted, the final equipment layout and associated utility routes were not fully determined at the time of foundation support system design and installation. Furthermore, excavations for utilities were scheduled to take place after installation of the RI support system for building floors. To maximize system flexibility, RIs were installed in potential utility corridors with RI tops positioned below anticipated utility levels.

The project team incorporated a structural mat for the facility floors, and utility excavations were backfilled using the same engineered fill initially employed for building pad construction (see Site Specific Profile). Figure 5 illustrates an example of this configuration.

 © Deep Foundations Institute 2025

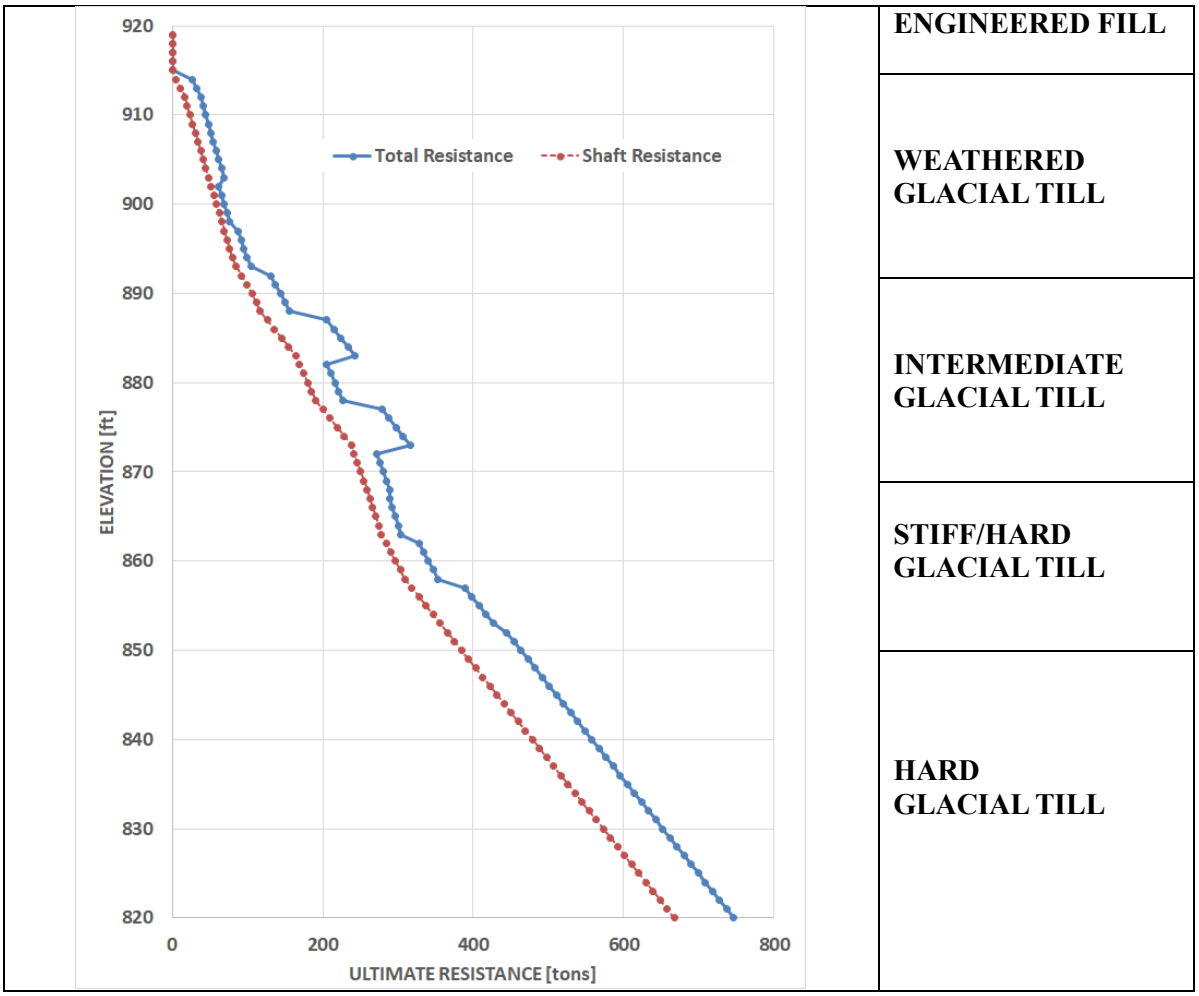


Fig. 4. Example Capacity Estimate 20-in Diameter ACIP Pile – Peptide 1 Facility

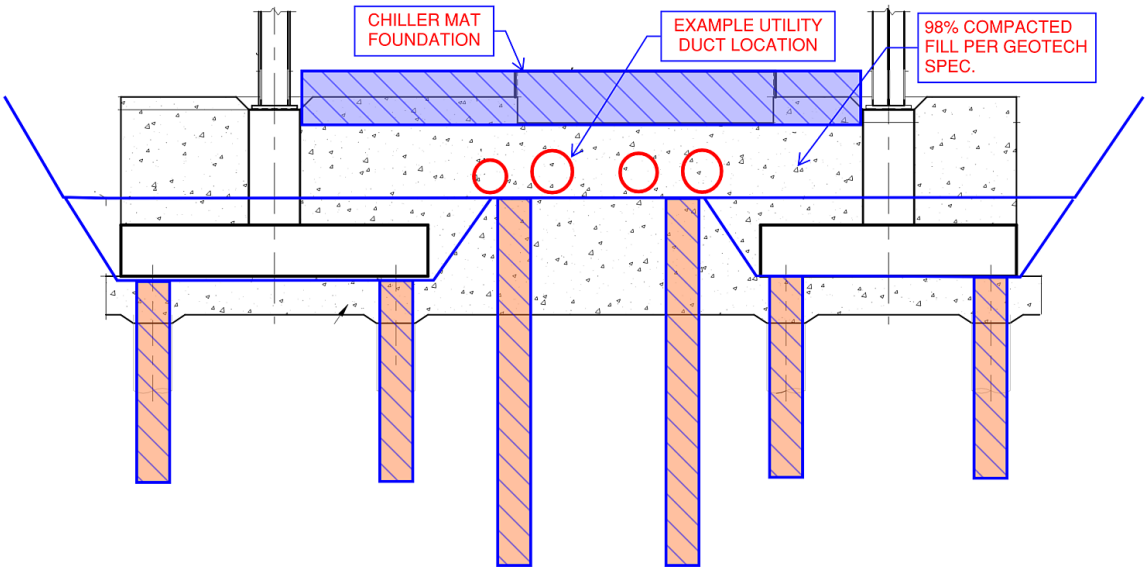


Fig. 5. Example Utility Corridor with Lower RI Levels and Additional Engineered Backfill

 © Deep Foundations Institute 2025

Lateral Resistance of Piles in Peptide 1 Facility

The evaluation of lateral resistance characteristics for the 20-inch diameter ACIP piles employed the industry-standard computational platform LPile 2022 (Ensoft, Inc.). The International Building Code (IBC) defines geotechnical allowable lateral load as one-half of the load that produces 1 inch of deflection under free-head conditions. Computational modeling for a single isolated pile indicated that a lateral load of 139 kips would generate 1-inch deflection, establishing the maximum geotechnical allowable lateral load at 69.5 kips per pile.

However, *the practical lateral load capability of ACIP piles is typically governed by structural considerations*, particularly the bending moments that develop within the pile shaft when subjected to lateral forces. The quantity and arrangement of the reinforcing steel extending from the piles to their caps was considered to produce fixed to semi-fixed conditions for the pile-heads. The structural analysis incorporated both fixed-head and free-head boundary conditions to bracket the range of potential pile behavior. Group effects were particularly significant for this project, as some configurations included more than five rows of piles at relatively close spacing (3 diameters center-to-center). To account for this pile-soil-pile interaction, a p-modifier of 0.3 was applied in the analytical model, representing the reduced efficiency of closely spaced piles in resisting lateral loads. The evaluation determined that the 20-inch diameter ACIP piles could reliably resist service lateral loads up to 22 kips while maintaining acceptable deflection characteristics and structural integrity. Figure 6 presents example analysis results which account for production pile arrangement and variations in top-of-pile elevation.

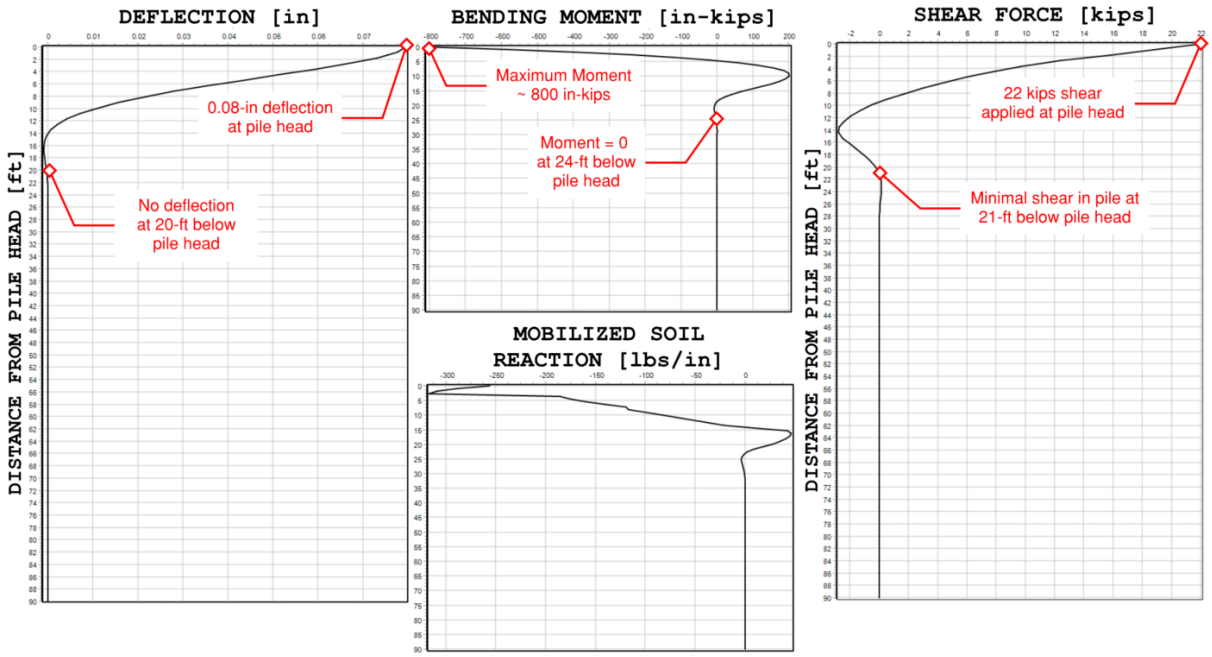


Fig. 6. Example Lateral Analysis Results for 20-in diameter ACIP Piles – Peptide 1 Facility

Settlement Analysis

Equipment manufacturer specifications necessitated limiting total structural settlement to 3/4-inch. The project team initially anticipated that the very stiff till (detailed in the Site-Specific Profile) would provide sufficient resistance to maintain settlements within this limit. However, the large area loads required for floor support, combined with interactions between adjacent columns and specified floor loads, presented significant design challenges.

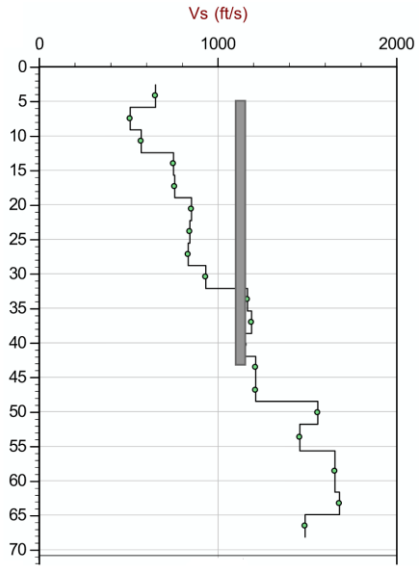
 © Deep Foundations Institute 2025

Initial soil stiffness and compressibility parameters were derived from correlations with SPT and CPT results along with laboratory test data. Settlement estimates based on these preliminary parameters exceeded the project limits. During this assessment period, Seismic CPTs were conducted at several proposed facility locations to enhance the initial site characterization. Stiffness parameters calculated from the shear wave velocities obtained through these tests were significantly higher than those indicated by correlations with CPT tip resistance, SPT N-values, or available laboratory data.

Settlement analyses using these enhanced parameters yielded values well below the 3/4-inch threshold. The load test program (discussed in Performance Verification) provided additional insights. While not directly applicable for structure settlement predictions, the test results demonstrated higher resistance values in the till than those estimated from CPT and SPT-based methodologies.

Young's modulus was also estimated from the axial load test results through a radial shear attenuation analysis (1978) which strongly favored the values estimated from shear wave velocities. The final soil stiffness parameters were implemented in various analytical models to verify compliance with project settlement requirements. Figure 7 presents a comparative example of Elastic Moduli estimated from SPT N-value (q_c) (Coduto, 2001) and those derived from shear wave velocities for the CUB facility, along with a schematic of the RIs in profile to their target depth with corresponding shear wave velocities. The difference in estimated moduli is approximately an order of magnitude.

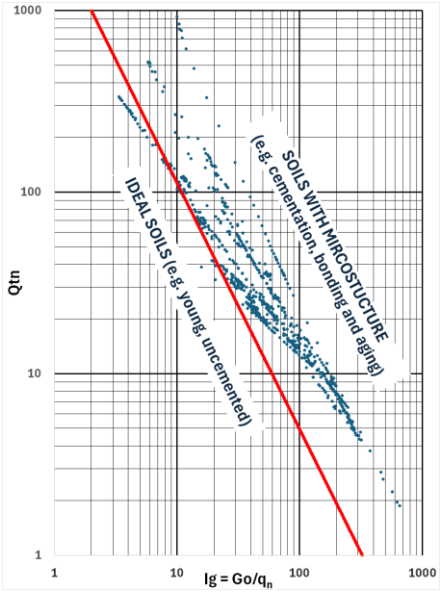
Additionally, soil microstructure was evaluated as described by Robertson (2016). The comparison of tip resistance data and Rigidity Index is also presented in Fig. 7 and further suggests age and bonding effects that would lead to an underprediction of soil stiffness using CPT tip resistance (and particularly SPT N-values). Although the Seismic CPTs were originally conducted to aid in Seismic Site Class determination and subsequent Seismic Design Category assignment, the shear wave velocity data proved invaluable in assuring the project team that total structural settlement would remain within acceptable limits.



(a)

	E' [psf]	
EL [ft]	Vs	SPT N60
919	1,568,131	401,067
911	1,568,131	401,067
910	1,615,647	103,619
905	1,615,647	103,619
904	2,384,332	205,576
895	2,384,332	205,576
894	2,930,909	301,333
888	2,930,909	301,333
887	5,328,253	721,778
882	5,328,253	721,778
881	5,152,125	473,600
872	5,152,125	473,600
871	9,237,119	876,445
865	9,237,119	876,445
864	9,472,450	1,020,121
855	9,472,450	1,020,121
854	11,331,788	1,041,778
820	11,331,788	1,041,778

(b)



(c)

Fig. 7. (a) Schematic of ACIP RI in Shear Wave Velocity Profile

(b) Comparison of Estimated Modulus, E', from Shear Wave Velocity and SPT results

(c) Evaluation of soil microstructure (Robertson, 2016)

 © Deep Foundations Institute 2025

PERFORMANCE VERIFICATION
Compression Test Results
CUB Facility Rigid Inclusions

To verify design assumptions and validate performance characteristics, a test RI was installed from ground surface elevation +924 ft to approximately 59 ft below grade (terminating at elevation +865 ft). Testing followed the procedures of ASTM D-1143-07 for static axial compressive load testing of deep foundations. The loading sequence consisted of approximately 8-ton increments applied at 5-minute intervals until reaching a maximum test load of approximately 200 tons. Unloading proceeded in five nearly uniform decrements, also at 5-minute intervals.

Figure 8 presents the load-displacement relationship observed during testing, including a hyperbolic curve-fitting analysis based on the method developed by Chin (1970). This hyperbolic projection provides an estimate of the ultimate load capacity beyond the maximum applied test load, offering additional insight into foundation performance at higher loading levels.

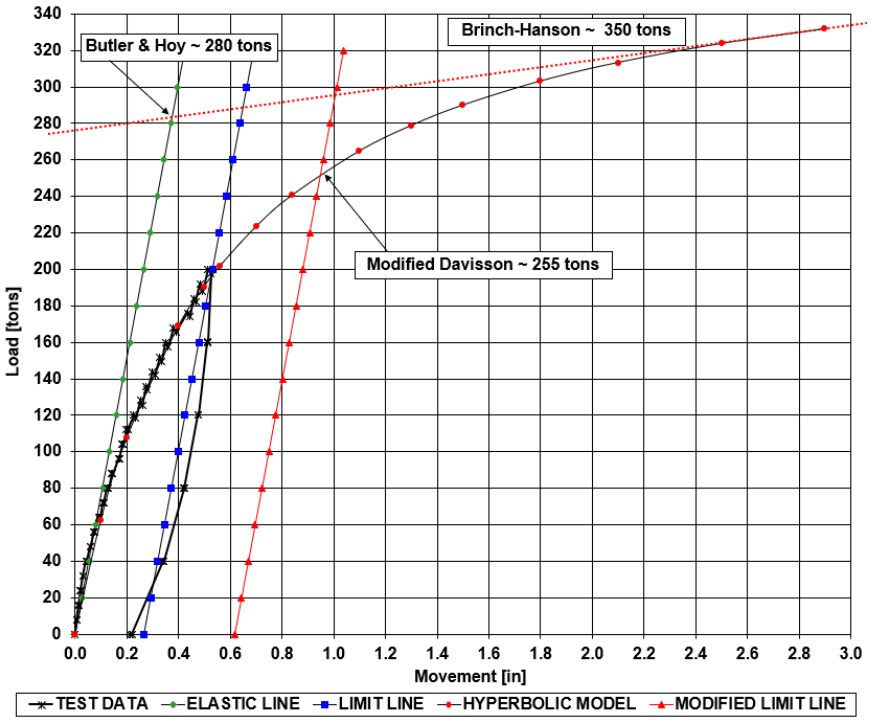


Fig. 8. Geotechnical Capacity Estimate of 14-in Diameter RI – CUB Facility

Ultimate load estimates were determined according to criteria specified in the applicable building code. The Davisson Offset Limit (DOL) approach was employed with a modifier of 4, consistent with Davisson's 1993 recommendations for cast-in-place pile systems.

Further refinements to the analysis included adjustments to the elastic line following methodologies proposed by Kulhawy and Chen (2005) and NeSmith and Siegel (2009). For ACIP piles not loaded to geotechnical failure, Studlein et al. (2014) recommend the Butler-Hoy method for ultimate load estimation. Based on these analytical approaches, the ultimate load of the test RI was established at 280 tons.

 © Deep Foundations Institute 2025

The load transfer mechanism along the RI shaft was evaluated through strain gauge instrumentation at various depths. Figure 9 illustrates the distribution of load with depth for each increment of the loading sequence up to maximum test load.

Peptide 1 Facility ACIP Piles

The Peptide 1 facility testing program included two dedicated test piles, designated CTP-PT and LTP-PT, both installed from surface elevation +924 ft to a depth of approximately 83 ft (reaching elevation +841 ft). Pile CTP-PT underwent compression testing following ASTM D-1143-07, with load applied in approximately 21-ton increments at 5-minute intervals. The test progressed to a maximum load of approximately 504 tons.

While attempting to increase the load to 525 tons, an apparent structural failure occurred within the test pile. This event was characterized by a sudden decrease in the sustainable load (dropping to approximately 370 tons) accompanied by excessive pile head movement. Following this event, the pile was unloaded in five nearly uniform decrements at 5-minute intervals. Figure 10 presents the load-displacement relationship recorded during testing, including a hyperbolic analysis following Chin's method (1970) to estimate ultimate capacity.

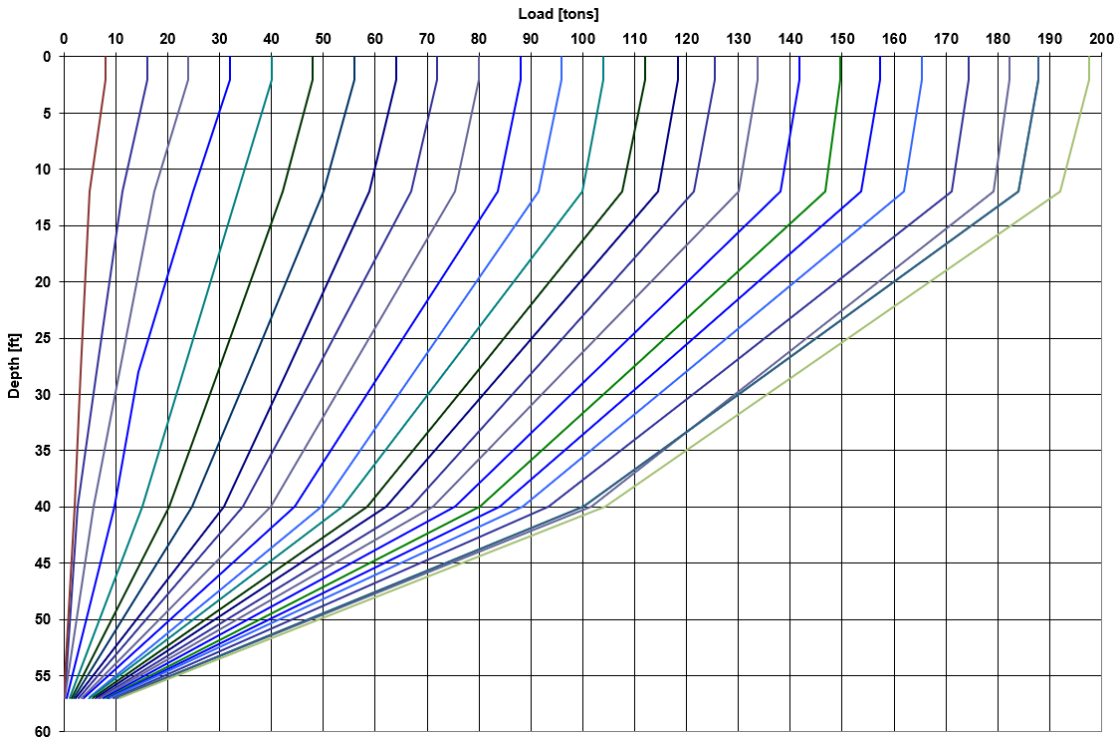


Fig. 9. Load Transfer with Depth – 14-in Diameter RI – CUB Facility

 © Deep Foundations Institute 2025

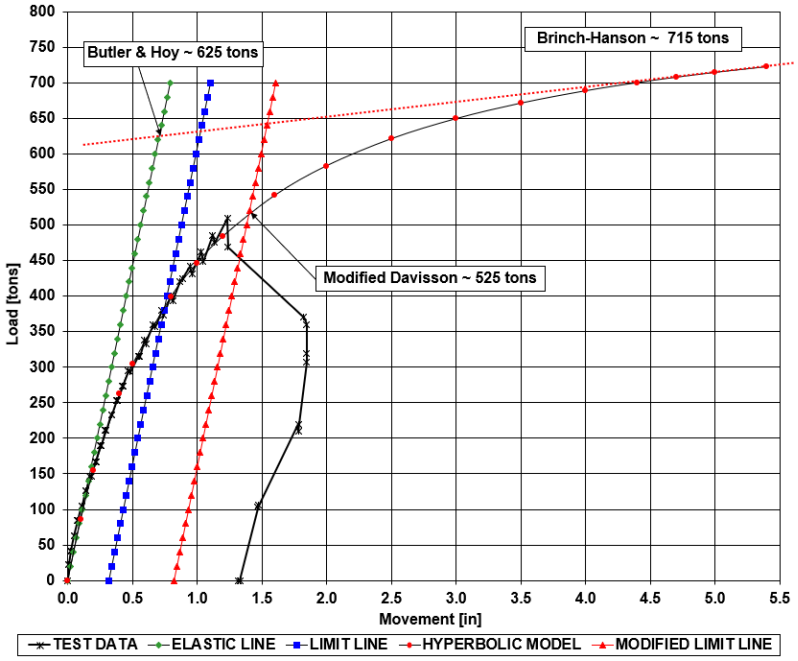


Fig. 10. Geotechnical Capacity Estimate of 20-in Diameter ACIP Pile – Peptide 1 Facility

The ultimate load analysis employed the same methodological approach described for the CUB facility testing, incorporating the Davisson Offset Limit with appropriate modifications, elastic line adjustments per Kulhawy and Chen (2005) and NeSmith and Siegel (2009), and consideration of the Butler-Hoy method as recommended by Studlein et al. (2014). Through this comprehensive analytical framework, the ultimate load capacity of test pile CTP-PT was determined to be 625 tons. Figure 11 depicts the load distribution with depth for the various loading increments. This was derived from strain gauge instrumentation using the analytical approach previously described.

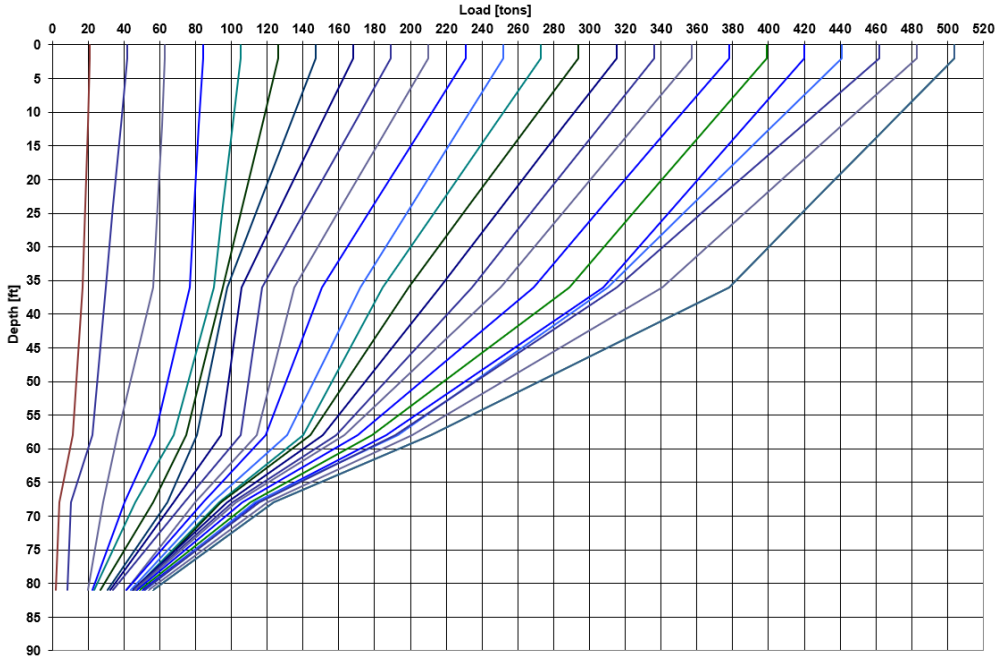


Fig. 11. Load Transfer with Depth – 20-in Diameter ACIP Pile – Peptide 1 Facility

 © Deep Foundations Institute 2025

Lateral Load Test Results Peptide 1 Facility

Lateral load testing was conducted on pile LTP-PT in accordance with ASTM D3966-07 standard procedures. The initial testing sequence involved loading the pile to a maximum lateral load of 22 tons while monitoring pile head displacement. These results are presented graphically in Figure 12. At the request of the design team, a supplementary loading sequence was performed on the same test pile, this time targeting a maximum pile head deflection of 1 inch rather than a predetermined load level. This approach directly assessed the pile's behavior at the deflection threshold specified in building code provisions for determining allowable lateral loads.

The load-displacement relationship from this supplementary test is illustrated in Figure 13. Analysis of the test data indicates that a lateral load of approximately 38 tons (76 kips) produced the benchmark 1-inch pile head deflection, validating the design assumptions employed in the analytical modeling.

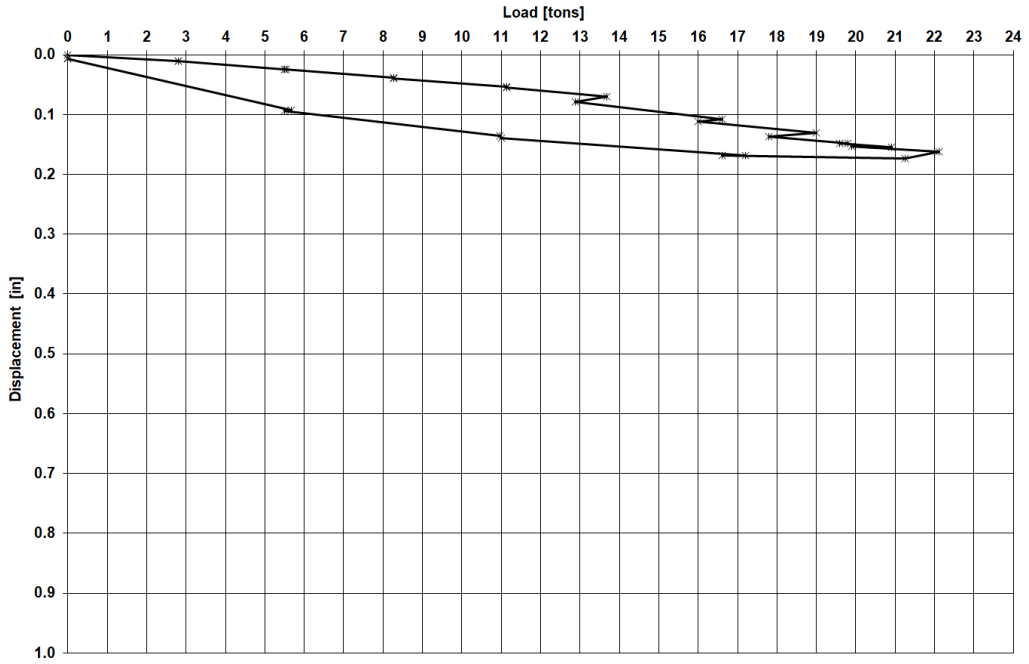


Fig. 12. Lateral Deflection with Load Applied – 20-in Diameter ACIP Pile – Peptide 1 Facility

 © Deep Foundations Institute 2025

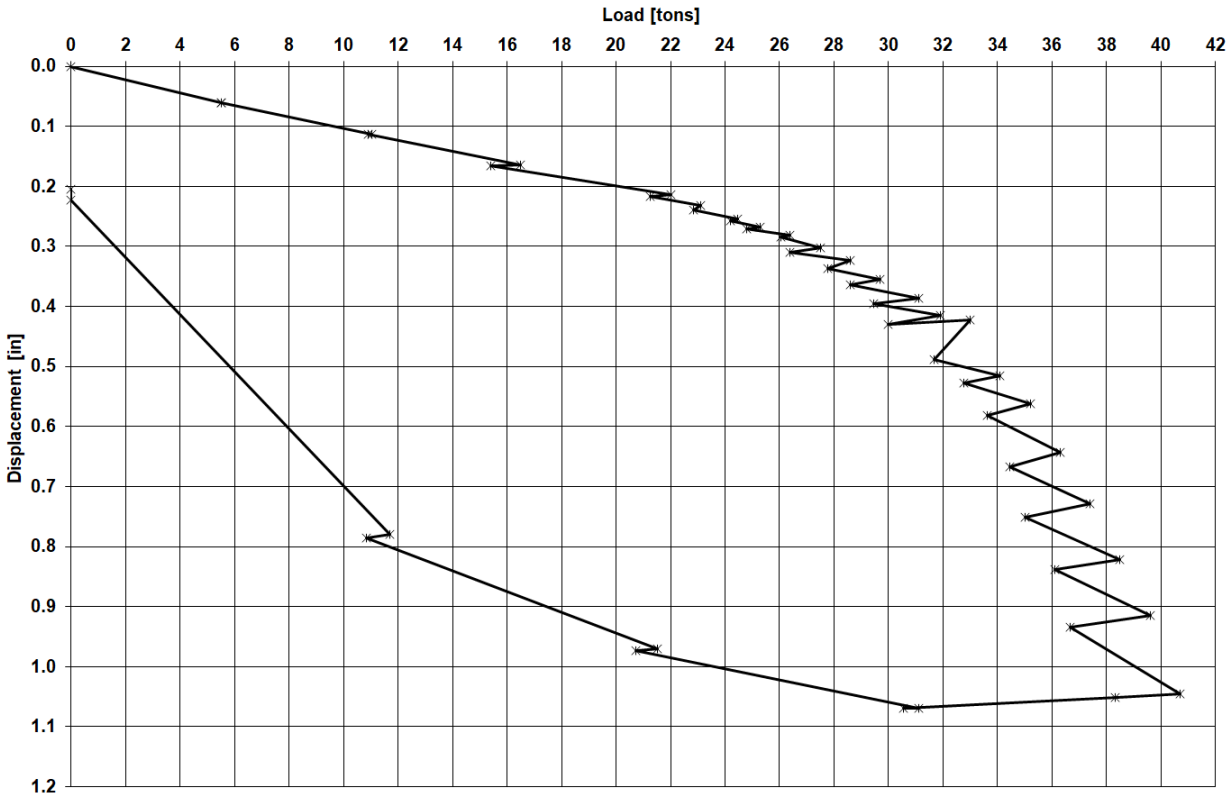


Fig. 13. Lateral Deflection with Load Applied to 1-inch Total Deflection – Peptide 1 Facility

FIELD COORDINATION AND DESIGN EXECUTION

General

Successful execution of the foundation support for the Lilly Medicine Foundry in Lebanon relied heavily on close coordination between field operations, engineering teams, and the construction manager, Fluor. From the outset, the field team had to navigate the unique challenge of beginning pile installation prior to the building being 100% designed. This meant that field operations were carried out based only on the approved-for-construction RIs of the design, while simultaneously staying agile and responsive to design updates as they became available.

Communication between the field and engineering was essential to maintaining schedule without sacrificing quality or safety. The team ensured that pile caps not yet cleared for construction were clearly identified and placed on hold until designs were finalized. This approach allowed work to progress efficiently in the areas that were ready, while maintaining flexibility for the remaining portions of the project.

Engineering also had to remain responsive to unexpected conditions encountered in the field. One such condition was refusal—where the drill rig could not penetrate further to reach the design toe elevation. When this occurred, the engineering team worked quickly to assess the load-carrying capacity of the achieved pile and, if necessary, identify a new location for a replacement pile to meet structural requirements. This dynamic collaboration between field personnel and engineering allowed for real-time problem solving and kept production moving without delay.

 © Deep Foundations Institute 2025

Constructability Challenges

Pile chipping proved to be one of the more logistically demanding phases of the project due to the depth of some pile cutoffs, which in certain caps exceeded 10 feet below working grade. Because these deep cutoffs could not be dipped to elevation at the time of installation, they were left long and required chipping down to final elevation after excavation (Fig. 14).

The chipping process involved multiple layers of coordination. After excavation and mud mat installation, surveyors would lay out the pile cutoff elevations and center bar locations. In cases where piles needed to be chipped multiple feet, a hydraulic pile crusher suspended from a track-mounted crane was employed. The crusher, composed of a donut-shaped frame equipped with hydraulic pistons, compresses the pile from all sides until the concrete fractures and breaks away. The concrete spoils are then collected in a skip pan and removed from the excavation area by crane.

Once piles were chipped and bars were trimmed to design levels, the pile cap construction could begin. The site works contractor would then form and pour the pile caps. This sequence required careful planning to ensure safety and efficiency, particularly given the number of trades and equipment operating in confined excavation zones.



Fig. 14. Excavated Piles to be Chipped to Final Cut-off Levels

Sequencing and Coordination Between Structures

The sequence of installation varied across the site. For example, in Peptide 1, most rigid inclusions (RIs) were installed prior to excavation. This allowed for installation of ACIP piles and RIs from the same working surface but introduced challenges later during excavation, as crews had to dig around already-installed rigid inclusions.

In contrast, at the Small Molecule 1 structure, approximately half the ACIP piles were installed, excavation began on the far west side of the building where there was sufficient separation from active drilling operations. This allowed excavation, pile chipping and pile-cap construction to run concurrently

 © Deep Foundations Institute 2025

with pile installation. After pile caps were completed, drilling crews returned to install the 14-in diameter rigid inclusions in the backfilled zones between caps. Executing this safely and efficiently required careful coordination among all contractors involved, and the project team did an excellent job of maintaining clear communication and collaboration throughout.

Each execution strategy presented distinct advantages and challenges. The approach used at the Peptide 1 building (installing both ACIP piles and rigid inclusions prior to excavation) allowed for earlier completion of the foundation scope and reduced potential conflicts with other contractors during later phases. This method promoted schedule certainty and minimized remobilizations. However, it introduced logistical complications for the excavation contractor, particularly working around numerous rigid inclusions embedded within the building footprint, potentially slowing progress and requiring additional care during earthwork operations.

Conversely, the sequencing at the Small Molecule 1 structure, with delayed installation of rigid inclusions until after pile caps were completed and backfill operations concluded, allowed excavation and cap construction to proceed more rapidly without obstructions. While this phased approach offered advantages in terms of excavation efficiency, it introduced challenges for pile installation, including the need for re-establishing access, preparing stable working surfaces, and coordinating work in tighter spaces. In some instances, RI installation outpaced the availability of work areas, leading to idle time and reduced productivity.

From the authors' perspective, completing all deep foundation elements ahead of excavation remains the preferred strategy, as it allows the foundation contractor to operate continuously and exit the site prior to structural activities. However, the decision must be made with consideration for the overall project sequencing, site conditions, and trade coordination to ensure the safest and most efficient outcome for all stakeholders.

REFERENCES

- Chin, F.K., (1970), "Estimation of Unit Load on Piles not Carried to Failure", Proc. 2nd Southeast Asia Conference on Soil Engineering, 81-90.
- Coduto, D.P. (2001) Foundation Design: Principle and Practices. 2nd Edition, Prentice Hall, Upper Saddle River.
- Davisson, M.T. (1972) "High-capacity piles". Proceedings of the Lecture Series *Innovations in Foundation Construction*, ASCE, Illinois Section, 52 pp.
- Davisson, M.T. (1993) "Negative skin friction in piles and design decisions" *Proceedings*, Third International Conference on Case Histories in Geotechnical Engineering, St. Louis, 1793-1801.
- Kulhawy, F.H. and Chen, J-R. (2005) "Axial compression behavior of augered cast-in-place piles in cohesionless soils" *Advances in Deep Foundations, GSP* 132, ASCE.
- NeSmith, W.M. and Siegel, T. (2009). Shortcomings of the Davisson Offset Limit Applied to Axial Compressive Load Tests on Cast-in-Place Piles**.** *Contemporary Topics in Deep Foundations*. Selected Papers from the 2009 IFCEE. GSP 185**,** pp. 568 – 574. Orlando FL, 15 – 19 March 2009.
- Randolph, M. F. and Wroth, C. P. (1978) "Analysis of Deformation of Vertically Loaded Piles", Journal of the Geotechnical Engineering Division, ASCE, 104(12), 1465-1488.
- Robertson, P.K. (2016). "Cone penetration test (CPT)-based soil behaviour type (SBT) classification system — an update". Canadian Geotechnical Journal, 53, 1910-1927.
- Studlein, A.W., Reddy, S.C., Evans, T.M. (2014). "Interpretation of Augered Cast in Place Pile Capacity Using Static Loading Tests." The Journal of the Deep Foundations Institute. Vol 8, No. 1, pp. 39 – 47. 09 June 2014.

 © Deep Foundations Institute 2025

CASE STUDY - STATISTICAL ANALYSIS OF HELICAL PILE TESTS IN A POWER TRANSMISSION LINE PROJECT IN BRAZIL

Policastro D. Author, Baltimore, MD, USA, dpolicastro@me.com
Lima F. Contributor, Federal University of Minas Gerais, Guarulhos, São Paulo, Brazil, filipe.lima@incotep.com.br
Starling M. Contributor, Federal University of Minas Gerais, São Paulo, São Paulo, Brazil, marcelo.starling@incotep.com.br

ABSTRACT

This article presents a case study of a foundation project for transmission line towers in Brazil, wherein helical piles were employed as the foundation system due to their recognized technical and operational benefits, the primary objective of the study is to evaluate the geotechnical performance of the foundations through a statistical analysis of data obtained from tension and compression load tests conducted throughout the project.

Descriptive statistical methods—including measures such as the mean, standard deviation, and coefficient of variation—were utilized to analyze pile displacements under various loading conditions, taking into account the inherent variability of soil properties along the transmission line corridor. The statistical evaluation enabled the identification of performance trends and the assessment of load-bearing consistency, even in the presence of heterogeneous subsurface conditions.

The findings indicate a high degree of uniformity in the load-bearing capacity of the helical piles, underscoring the reliability of in situ testing as a good practice for verifying foundation performance. The study concludes that the application of above tests and statistical analysis, significantly enhances the reliability and safety of foundation projects. Furthermore, the results reaffirm the suitability of helical piles as an effective and robust solution for transmission line foundations.

Keywords: foundation, towers, helical pile, load capacity, tests, foundation performance

1. INTRODUCTION

The increasing demand for agile, efficient, and reliable foundation systems in infrastructure development has contributed to the growing adoption of helical piles in the construction of power transmission lines. Owing to their installation flexibility and adaptability, helical piles offer distinct advantages in areas characterized by limited accessibility or pronounced geotechnical heterogeneity—conditions frequently encountered across the diverse terrains of Brazil.

Given Brazil's extensive land area and the consequently long transmission line corridors, foundation systems must be capable of accommodating a broad spectrum of geotechnical conditions. Moreover, transmission towers are often situated in remote regions, distant from major logistical centers and infrastructure, where access is commonly restricted by unpaved roads whose usability is highly susceptible to weather fluctuations. These logistical complexities present significant challenges to the implementation of transmission line projects and directly influence the selection, design, and feasibility of foundation solutions.

While helical piles have increasingly emerged as a practical and efficient alternative, traditional foundation methods such as drilled shafts (caissons), spread footings, micropiles, precast blocks, and rock

 © Deep Foundations Institute 2025

anchors continue to be widely employed. Each technique presents specific advantages and limitations that must be carefully evaluated in relation to subsurface conditions, anticipated structural loads, and site accessibility. The appropriate selection of foundation type is critical to ensuring the structural integrity, longevity, and economic viability of the installed system.

Within this context, the present study presents a case analysis incorporating a statistical evaluation of tensile and compressive load test results obtained from helical piles employed in a Brazilian transmission line project under construction at the time of this writing. The objective is to characterize the foundations' geotechnical behavior in response to natural soil variability, identify performance trends, and emphasize the role of statistical methodologies in enhancing design safety and optimization. The findings confirm the effectiveness of the selected solution and offer valuable technical insights for the design and execution of future projects under similar conditions.

2. METHODOLOGY

To achieve the objectives of this study, data obtained during the execution of tension and compression tests on helical piles installed in a Power Transmission Line project in the southeastern region of Brazil were analyzed. Other details, such as the project name, construction company, and transmission operator, will be kept confidential.

The statistical approach adopted in this study was based on the use of simple descriptive statistics — such as mean, standard deviation, minimum, and maximum values — aimed at evaluating the behavior of the displacements recorded during the tension and compression tests.

The data were organized and analyzed using Microsoft Excel, allowing for the identification of patterns and the quantification of result dispersion due to the different geotechnical conditions observed.

2.1 Project Characterization

The transmission line project under study consists of two 500 kV circuits, with a total length of approximately 592 km, crossing regions with varying geotechnical conditions, including lateritic clay soils—typical of tropical climates—sandy soils, and some areas with rock outcrops.

Located in a strategic region of the country, the project aims to expand the power grid to meet the growing demand for electricity.

Table 1 – Number of towers

Project	Number of towers	Types of structures	Transmission line extension
Circuit 1	630	11	296 km
Circuit 2	612		296 km

For both circuits (C1 and C2), the project includes the use of cross-rope and self-supporting structures—both suspension and anchor types. The selection of the tower type follows design criteria that take into account the span lengths, the loads acting on the cables and conductors, as well as the geotechnical and topographical conditions of the various terrain types.

 © Deep Foundations Institute 2025

2.2 Geotechnical Investigation

The geotechnical conditions along the route were determined through investigations conducted during the pre-design phase of both circuits of the line, including SPT-type boreholes – in accordance with NBR 6484, and soil resistivity tests. The survey provided consolidated data to support the selection of the most appropriate foundation solutions for the specific conditions of each section of the line.

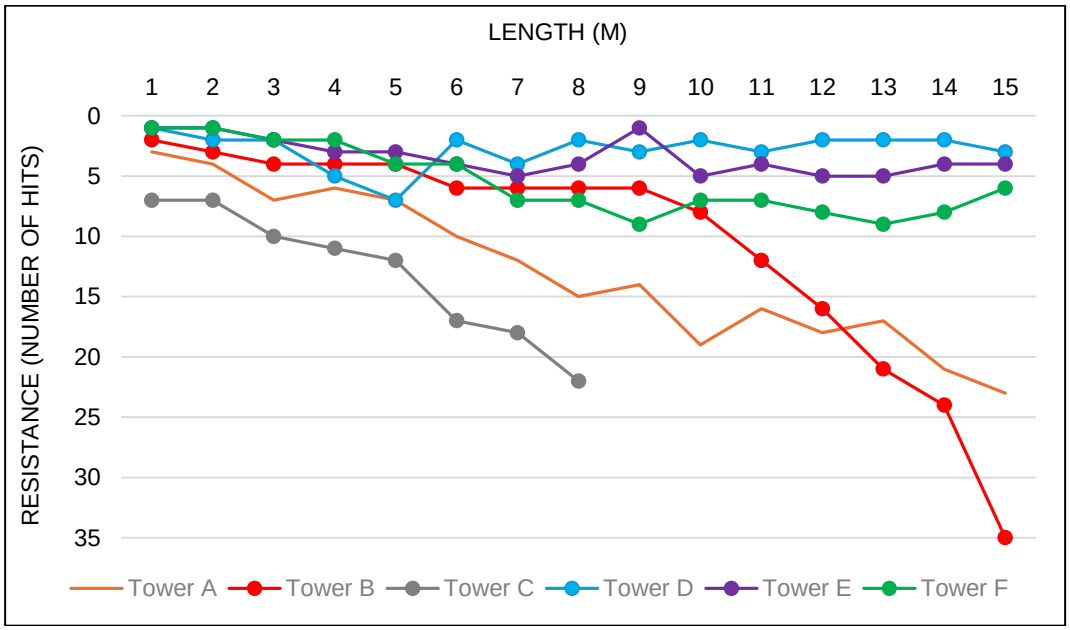


Fig. 1. Survey (SPT-N blows per foot) performed on each tower

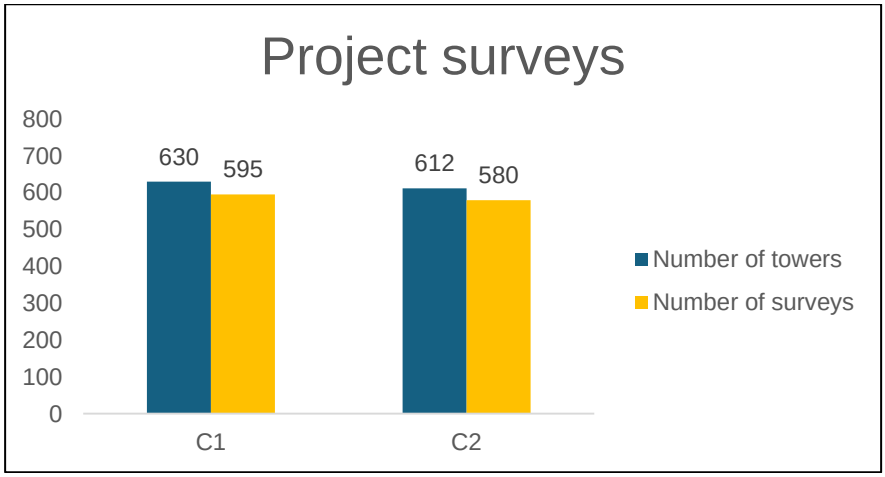


Fig. 2. Relationship between the number of towers and surveys carried out in the project

In Brazil, due to the costs associated with the number of towers, it is common to carry out soil investigations at only one point per structure — a practice that was also adopted in this project. In the not-so-distant past, investigations were conducted in an even more limited manner, based on sampling, which significantly increased the degree of uncertainty

 © Deep Foundations Institute 2025

Based on the results obtained, an analysis of the soil resistance was conducted, considering the averages by structure type and along the entire route of the line. Using this information, a technical and financial feasibility study was carried out for the adoption of conventional foundations, such as drilled shafts, micropiles, and spread footings.

For special situations, such as sections with difficult access and soils with low resistance, classified as type IV and V soils, specific alternatives were analyzed, among which helical piles stood out due to the various technical and operational advantages they offer.

Table 2 – Soil type classification

Soil	Type	SPT
High resistance soils	I or IS	≥ 20 blows per foot
Resistant soils	II or IIS	15 < 19 blows per foot
Medium soils	III or IIIS	10 < 14 blows per foot
Low resistance soils	IV or IVS	5 < 9 blows per foot
Very weak soils	V	< 4 blows per foot

As an initial strategy defined by the construction company responsible for the civil works, the use of helical piles was directed exclusively to the foundations of the central mast and stays of the cross-rope type structures. It is worth noting that, at the time of writing this article, a specific study is also underway to assess the feasibility of using helical piles for the foundations of self-supporting suspension structures.

This decision took into account the specific characteristics of the structures and the constructive advantages of helical piles, such as faster installation, lower environmental impact, and the ability to adapt to different soil conditions. In this way, the goal was to optimize the construction schedule and reduce execution costs in specific sections of the transmission line route.

2.3 Geotechnical Design of the Helical Pile

Based on the concepts presented by Perko (2009), the load-bearing capacity of helical piles can be obtained through two theoretical methods, both grounded in the principles of soil mechanics.

The first method considers the individual contribution of each helix to the pile's load-bearing capacity and is applicable when the spacing between helices is sufficiently large for them to act independently.

During the installation of the pile, there is interaction between the helices and different geotechnical characteristics along the depth, with each helix contributing independently to the overall load-bearing capacity of the foundation.

As the helices advance in the installation process, they pass through soil layers with distinct mechanical properties, and this sequence of interactions determines the final load capacity of the helical pile.

$$Q_{global} = \sum_{h=1}^{n} Q_{hélice} \quad [1]$$

Based on classical theories of load-bearing capacity, with Terzaghi's approach being the most widely recognized, we have:

$$Q_{helix} = A_{helix} . (c . N_c + \gamma . H . N_q) \quad [2]$$

Q_{helix}: load resistance capacity of each individual helix;
A_{helix}: net area of the helix;
c: soil cohesion;
N_c: load resistance factor for cohesive soils (according to specialized literature on helical piles, the value of 9 is conventionally adopted);;
$\boldsymbol{\gamma}$: nit weight of the soil;
H: vertical positioning of the helix in the soil;
N_q: load resistance factor for non-cohesive soils;

In the second method of analysis, adopted when the spacing between the helices is reduced, a soil cylinder is formed between them, causing them to act together. In this case, the load capacity consists of the resistance of the upper helix, in the case of tension, or the lower helix, for compression, plus the resistance mobilized along the shear surface of the formed cylinder.

The method, known as the "shear cylinder," considers the mobilization of the volume of soil located between the helices, where, at the moment of rupture, a cylindrical surface is established between the soil and the helices. Therefore, the load capacity is determined by the sum of the resistance of the helix plus the resistance mobilized on the surface of this shear cylinder. (CARVALHO, 2007)

The expression used to calculate the load capacity according to this methodology can be represented by the following equation:

$$Q_u = Q_p . + Q_f + Q_s \quad [3]$$

Q_u = load capacity of the pile
Q_p = resistance of the upper or lower helix
Q_f = resistance due to the shear cylinder
Q_s = resistance due to the shaft

For the project that is the subject of this study, the individual load capacity method was adopted for the design of the helical piles.

2.4 Tests Conducted

Still in the pre-design phase, with the aim of supporting the preliminary geotechnical design, a validation test was conducted with a focus on validating and adjusting the design assumptions, reducing uncertainties regarding soil behavior, and consequently allowing for a more accurate geotechnical design, installation torque, and especially average depth.

The primary purpose of these tests is to confirm whether the basic data used in the design, such as soil borings (SPT-N), estimated installation torque, and the average depths predicted for the helical piles, adequately reflect field conditions.

For this project, given the extensive implementation area and soil heterogeneity along the route, 6 towers were selected. The choice considered the different types of soil identified to ensure adequate geotechnical representativity.

 © Deep Foundations Institute 2025

For this project, given the extensive implementation area and soil heterogeneity along the route, 6 towers were selected. The choice considered the different types of soil identified to ensure adequate geotechnical representativeness.

The installation of the piles followed the standard currently adopted by the designers, in which three piles are installed in parallel, with a minimum distance of 1.5 meters. All piles are installed according to parameters defined in the preliminary design. The central pile is designated for the compression load test, while the piles at the ends are designed as reaction piles.

At the end of the first test, one of the reaction piles (pile 1 or pile 2) is selected for the tension test, usually the one with the shallower installation depth or the greater torque fluctuation during installation

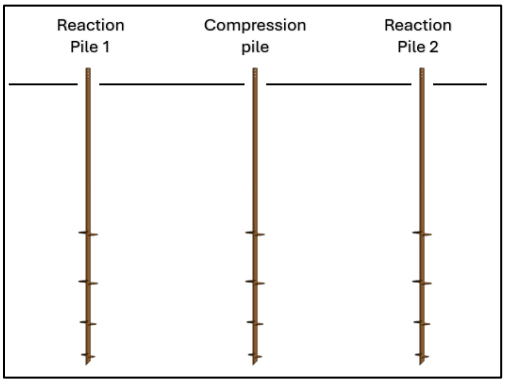


Fig. 3. Representation of piles for tensile and compression tests (Source: authors' elaboration)

In projects involving different types of structures with light and/or heavy loads, it is common for the supply of helical piles to be standardized by the manufacturer or designer, using a pile sized to meet the load and torque parameters of the most demanding structure.

However, in this specific project, this practice was not followed, as the client did not have the financial capacity to exclusively adopt the larger pile, whose cost would be approximately 36% higher than the total cost of the piles actually used. Therefore, three distinct helical piles were specified, each intended for a different type of stay, keeping the outer diameter the same and varying only the thickness of the tubes.

For the central mast structures, since the maximum load allowed per pile was the same for all cases, it was possible to standardize the use of a single pile configuration.

A total of 12 static load tests were performed on the helical piles, with six tests under tensile loads and six under compressive loads. The tests followed the guidelines established by the Brazilian standard NBR 16903 – Soils – Static load test on deep foundations, aiming to determine the allowable load capacity and the behavior of vertical displacements under loading.

Table 3 – Helical Pile design

Tower	Estructura	Outside diameter (mm)	Design wall gauge (mm)	Torque Installation (kN.m)
A	Stay	101,6	8,1	26,44
	Center mast	101,6	7,1	18,58
B	Stay	101,6	7,1	24,41
	Center mast	101,6	7,1	18,58
C	Stay	101,6	7,1	24,41
	Center mast	101,6	7,1	18,58
D	Stay	101,6	8,1	26,44
	Center mast	101,6	7,1	18,58
E	Stay	101,6	8,8	30,12
	Center mast	101,6	7,1	18,58
F	Stay	101,6	8,1	26,44
	Center mast	101,6	7,1	18,58

Table 4 – Validation test parameters

Tower	Circuit	Soil	Type of test	Test load (tf)
A	C2	VS	Tension	50
			Compression	35
B	C1	VS	Tension	46
			Compression	35
C	C1	V	Tension	46
			Compression	35
D	C1	V	Tension	57
			Compression	35
E	C1	IV	Tension	46
			Compression	35
F	C1	III	Tension	50
			Compression	35

* The identification of the towers has been preserved, and for the development of the article, they will be referred to as A, B, C, D, and F

Each test, consisting of two cycles, involved the application of progressive loads while monitoring the displacements in relation to the load increments. The equipment used included a testing table, hydraulic pump, and cylinder, as well as calibrated dial gauges to ensure the accuracy of the results.

 © Deep Foundations Institute 2025

To expand the analysis, the applied loads in the tensile and compression tests were strategically increased by up to 120%. In some cases, this increase was not feasible due to the maximum capacity of essential testing components, such as the hydraulic jack and the reaction frame.

The calculation of elastic displacement for helical piles, according to Das (2014), considers three components: pile elongation (disregarded for helical piles), mobilization of the critical helix, and shaft friction. Therefore, only the displacement needed to mobilize the helix is relevant.

Thus, for the validation test, criteria for admissible displacements were established, which could be adjusted if necessary for the executive project

- Tension Test:
  - 1st cycle: Maximum admissible displacement of 40mm at 100% of the load
  - 2nd cycle: Maximum displacement at 100% of the load, added to the residual value from the 1st cycle, not exceeding 50mm.

- Compression Test:
  - 1st cycle: Maximum admissible displacement of 35mm at 100% of the load.
  - 2nd cycle: Maximum displacement at 100% of the load, added to the residual value from the 1st cycle, not exceeding 40mm.

Theoretically, in the first loading cycle of the pile, it is expected that the displacement achieved at maximum load will be greater than in the second cycle due to the soil's settlement and the need for initial adjustments in the testing system to eliminate play in the threaded connections between the pile sections and to adjust the coupling between the pile's termination and the loading device, in this case, the testing beam. With the soil more compacted and the system stabilized, the displacements tend to be smaller in the second cycle.

Additionally, even after the complete unloading of the load, it is common to observe a residual displacement, which represents the permanent deformation of the system. The presence of this residual displacement, even if of small magnitude, indicates that the soil underwent internal reconfiguration and exhibited a partially plastic behavior during the test, without complete recovery of its initial structure.

Despite the theoretical expectation of a reduction in displacements during the second loading cycle, the results indicated the opposite behavior: the maximum displacement recorded in the second cycle was higher than in the first for all the tested towers.

Even considering that the displacement in the second cycle includes the residual displacement from the first— with the average across all tests being 5.46 mm— the observed behavior can mainly be attributed to the characteristics of the local soils, classified as types III, IV, V, and VS, especially those with extremely low penetration resistance (less than 4 blows/30 cm in the SPT test).

Soils with these characteristics exhibit high compressibility and low confinement, promoting progressive deformations even after successive loading cycles. Unlike denser soils, where initial settlement is more effective, these soils do not provide enough stiffness to stabilize the system after the first cycle, resulting in cumulative displacements.

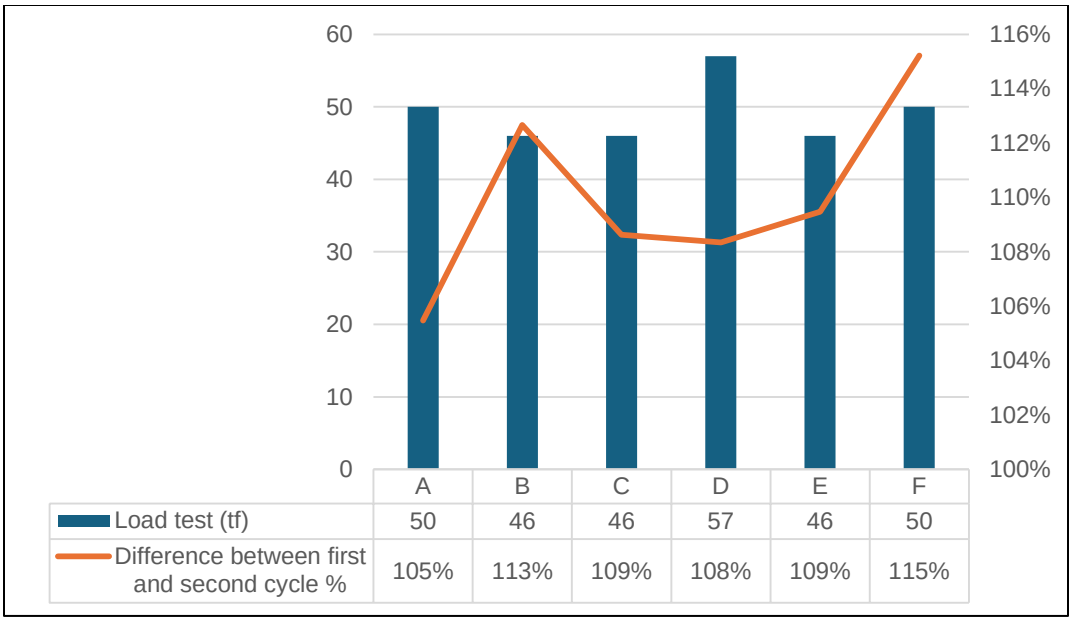


Fig. 4. Relationship between the applied load and the variation in displacement between the 1st and 2nd cycle of the tension test

To numerically represent the difference between the loading cycles, the percentage variation index between the maximum displacements of the 1nd and 2st cycles was calculated. This ratio, shown in the graph as "difference between first and second cycle (%)" indicates how much greater or smaller the displacement in the second cycle was compared to the first. Values above 100% represent an increase in displacement in the second cycle, while values below 100% indicate a reduction, which would be the expected behavior under ideal conditions.

For this project, considering the predominant soil types in the towers defined with the helicoidal pile solution — types III, IV, and V — the maximum load allowed for each pile installed in a concrete block, subjected to compression forces, was limited to 35 tons-force.

This limit, applicable to both the central mast structures and the self-supporting towers, was established based on the pile load-bearing capacity and the overall structural system safety. The goal was to keep the forces transmitted to the soil within acceptable parameters, avoiding failures, excessive displacements, and especially the occurrence of buckling in sections with soils of low geotechnical resistance — characterized by SPT blow counts below 5.

As observed in the tension tests, the compression tests — with the exception of Tower A — showed similar behavior, with displacements in the second cycle, for 100% of the load, being higher than those recorded in the first cycle. This can be attributed to the characteristics of the local soils, which have low resistance and high compressibility, making it difficult to stabilize the system after the first loading cycle, resulting in higher displacements.

 © Deep Foundations Institute 2025

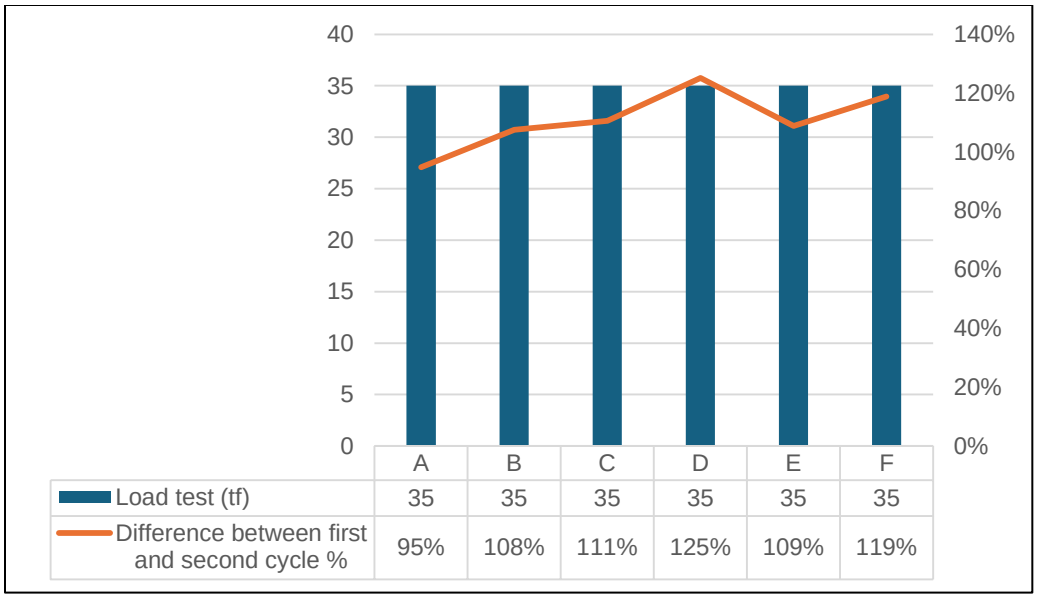


Fig. 5. Relationship between the applied load and the variation in displacement between the 1st and 2nd cycle of the compression test

In both tests (tension and compression), the maximum displacements allowed in the pre-design were found to be adequate, as they stayed within the limits established to ensure the safety and functionality of the system, even under the presented soil conditions.

For the continuation of the final design, based on the data obtained in the validation test, especially the admissible displacements, it was possible to maintain the parameters initially adopted, ensuring the continuity of the project within the safety and performance criteria established.

During the development of this article, the executive design is ongoing, with a total of 1,595 foundations installed so far, representing 22% of the total foundations planned for the project. Of this total, approximately 75% have already been subjected to routine tests, presenting satisfactory results that align with the acceptance criteria defined in the project.

3. ANALYSIS AND DISCUSSION

In this project, the tension and compression tests conducted on the helical piles allowed for the evaluation of both the soil and foundation system behavior under the applied loads. It was observed that, for the most part, the displacements recorded during the tests, even considering the distinct behavior between the first and second loading cycles, remained within the admissible limits established in the pre-design.

 © Deep Foundations Institute 2025

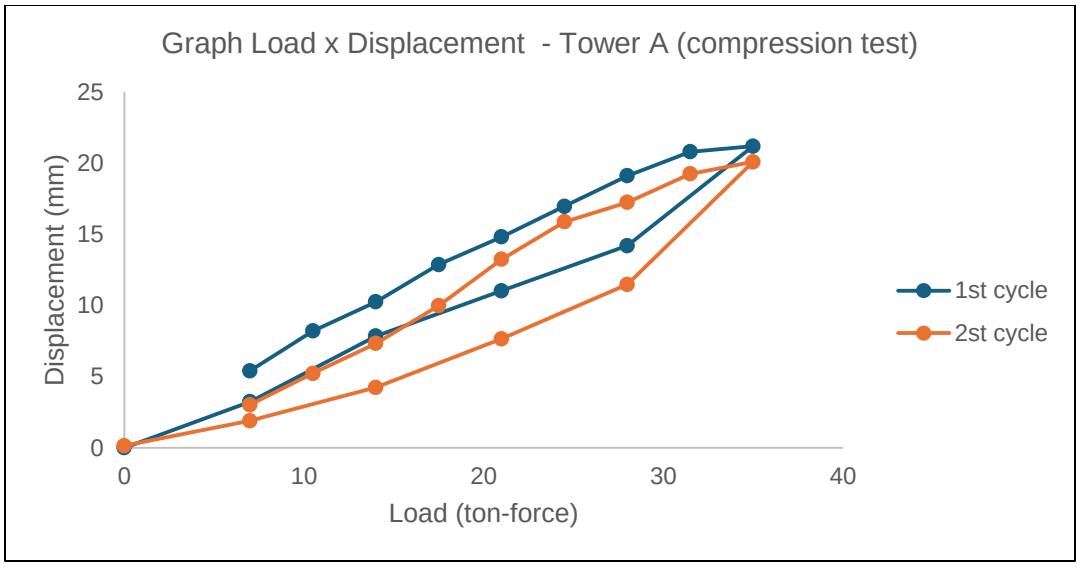


Fig. 6. Load x Displacement – Tower A (compression test)

The comparison between the cycles revealed that, due to the characteristics of the local soil—predominantly of low penetration resistance (SPT < 4 blows)—there was a tendency for displacement increments in the second cycle, a behavior attributed to the high compressibility and low stiffness of the analyzed soils.

To verify the alignment between the preliminary design and the field results, a comparison was made between the admissible loads estimated in the design phase and the load capacities obtained from the tests, based on the maximum observed displacements. For towers A, D, and F, the 20% increase in maximum load was not applied due to the limitation of the hydraulic jack used in the project, which had a maximum mechanical capacity for tests up to 65 tons-force.

Table 5 – Validation test parameters

Tower	Circuit	Soil	Allowable design load (tf)	Load obtained in the test (tf)	Variation (%)
A	C2	VS	50	60	20
			35	42	20
B	C1	VS	46	55	19,6
			35	42	20
C	C1	V	46	55	19,6
			35	42	20
D	C1	V	57	60	5,3
			35	42	20
E	C1	IV	46	55	19,6
			35	42	20
F	C1	III	50	60	20
			35	42	20

The values showed positive variations ranging from approximately 5% to 20%, indicating that the loads obtained in the tests were higher than the admissible design loads, demonstrating a good safety margin and consistency between the design assumptions and the actual performance of the helical piles under different soil conditions.

Within the scope of the executive design, the validation of the parameters used was made possible thanks to the good alignment between the estimated values and the results obtained in the field. Thus, the results achieved reinforce the good performance of the helical piles, validating the design criteria adopted and enabling the continuation of the installations and tests.

4. CONCLUSION

This study underscores the critical role of detailed analyses in the evaluation of foundation systems for transmission lines, contributing to enhanced project reliability, safety, and operational efficiency.

The data from the presented case study confirmed the favorable performance of helical piles, even when installed in low-strength soils characterized by high compressibility and limited confinement. All recorded displacements during load testing remained within the prescribed limits—50 mm for tensile loads and 40 mm for compressive loads—thereby validating the adequacy of the adopted foundation solution and supporting the continuation of the execution phase without necessitating revisions to the design parameters.

In addition, displacement behavior across loading cycles during compression testing was examined. The results generally indicated an increase in displacement during the second cycle, a response attributed to the low stiffness and high deformability of the local soils—predominantly corresponding to soil types III, IV, V, and VS as classified in the geotechnical investigations.

Moreover, the results obtained thus far during project execution highlight the effectiveness of helical piles as a foundation solution for transmission line infrastructure. Their ease of installation, consistent performance under load testing, and adaptability to varying soil conditions establish helical piles as a technically robust, economically viable, and environmentally favorable alternative to more conventional foundation techniques.

Finally, the findings support the broader adoption of helical piles in future transmission line projects and emphasize the importance of continued research to further elucidate their behavior under diverse geotechnical and structural conditions.

5. ACKNOWLEDGMENTS

The authors would like to thank Incotep – Sistemas de Ancoragem for their crucial support in the completion of this work. The company’s involvement in the supply projects was fundamental, providing access to relevant data and practical experiences that directly contributed to the analysis of the methodologies adopted.

6. REFERENCES

ABNT (Associação Brasileira de Normas Técnicas). NBR 16903: Solos – Prova de carga estática em fundação profunda. Rio de Janeiro: ABNT, 2021.

ABNT (Associação Brasileira de Normas Técnicas). NBR 6484: Sondagens de simples reconhecimento com SPT. Rio de Janeiro: ABNT, 2020.

ASTM D1143/D1143M. Standard Test Methods for Deep Foundation Elements Under Static Axial Compressive Load. 2020.

ASTM D3689/D3689M. Standard Test Methods for Deep Foundation Elements Under Static Axial Tensile Load. 2022.

CARVALHO, Igor P. Estudo teórico e experimental da capacidade de carga à tração e compressão de estacas metálicas helicoidais. 205 p. Dissertação (Mestrado em Engenharia) – Departamento de Estruturas, Universidade Federal de Minas Gerais, Belo Horizonte, 2007.

Das, Braja M. Principles of Foundation Engineering. 8th ed. Stamford: Cengage Learning, 2014.

CIGRÈ BRAZIL. Technical Recommendations for Design, Manufacturing, Installation and Maintenance of Helical Piles in Transmission and Distribution Lines. 1st ed. 2019.

DEEP FOUNDATIONS INSTITUTE. Helical Pile Foundation Design Guide. 1st ed. Hawthorne: DFI, 2019.

PERKO, Howard A. Helical Piles: A Practical Guide to Design and Installation. Hoboken: John Wiley & Sons, 2009.

 © Deep Foundations Institute 2025

AN OPTIMIZED APPROACH FOR MANAGING OVERHEAD TRANSMISSION LINE FOUNDATION DESIGN AND CONSTRUCTION RISK

James P. Adams, Salt River Project, Phoenix. AZ, USA, 602-236-8601 James.Adams@srpnet.com
Mariah Paz, Salt River Project, Phoenix. AZ, USA, 602-236-8066 Mariah.Paz@srpnet.com
Daniel Rosenbalm, MasTec Power Delivery – Major Projects (formerly DiGioia Gray & Asso.), Mesa, AZ, USA 480-334-0674 Daniel.Rosenbalm@mastec.com
Peter Kandaris, retired (formerly DiGioia Gray & Asso.), Chandler, AZ, USA, 480-273-9445 petebroncos65@gmail.com

ABSTRACT

A new 20-mile, high voltage transmission line was recently designed and constructed by the Salt River Project (SRP) in Central Arizona. Drilled shaft reinforced concrete foundations were used to support the predominantly laterally loaded monopole structures that cross several geologic regimes. SRP and their geotechnical consultants elected to optimize foundation design by following a rational approach in terms of construction schedule, total installed cost, and reliability. The process involved management of foundation data during both design and construction to minimize schedule and cost risk from unanticipated conditions that were likely to be encountered during foundation construction. This paper details the engineering approach that involved (a) a geological desktop study to select representative locations for subsurface sampling and testing, (b) a statistical approach to estimate characteristic geotechnical design properties along with development of idealized design profiles, and (c) an enhanced foundation inspection program that included detailed logs of soil conditions at each structure site. This process allowed for rapid real-time design changes during construction to account for encountered conditions that differed from design assumptions. To facilitate ease of application and use by the utility and their geotechnical consultants, documentation and management of foundation data was performed using spreadsheets in lieu of typical construction management software. The paper also presents a comparative assessment of the optimized program with other typical approaches used in the industry. The optimized program required design verification/additional analysis for 2.5% of the foundations to determine as-constructed conditions met and exceeded the initial design capacity due to variation in the subsurface profile. The optimized approach was equal to or less costly than the other alternatives while providing a high level of knowledge on foundation and subsurface conditions for improved system reliability.

Keywords: transmission line, foundation design, foundation quality control, inspection

INTRODUCTION

SRP recently completed a new 20-mile, double circuit, 230/69 kV transmission line in the southeast region of the Greater Phoenix Metropolitan Area, beginning at a new Ball Substation site within the Town of Queen Creek and extending through unincorporated parts of Pinal County to the existing Abel 230kV Substation (hereafter referred to as the APB Project). A site map is provided in Fig. 1. The project required installation of 161 reinforced concrete drilled shafts with diameters ranging from 6 to 12 feet and embedment depths ranging from 16 to 38 feet. These piers support predominantly laterally loaded steel monopole structures using an anchor bolt base plate connection. Foundation construction was performed on an expedited schedule encompassing 23 work weeks to meet line in-service needs.

The expedited construction schedule motivated SRP to optimize the investigation and foundation design processes to complete APB Project foundation design as quickly as possible but not sacrifice foundation cost and quality. To better manage risk from unknown conditions that could be encountered between boring locations, a rational approach along with a detailed foundation construction inspection program

 © Deep Foundations Institute 2025

was instituted. Subsurface data would be obtained at locations along the alignment to characterize the various strata anticipated to be encountered during foundation excavation. The inspection program would provide sufficient information during construction to either validate design profile assumptions or modify the profile to match as-found conditions with under-designed foundation embedment depths revised.

SRP managed the geotechnical studies performed in support of foundation design. Studies included review of existing subsurface investigations performed for nearby projects, performing a geological reconnaissance desktop study to delineate likely subsurface conditions and geologic hazards along the alignment and to assist in the selection of optimal locations for geotechnical investigations, and subsurface exploratory drilling program that included sampling and laboratory testing of select test specimens. The goal was to obtain characteristic geotechnical design properties and subsurface profiles representative of the subsurface conditions at all foundation locations along the alignment. Geologic studies and data assessment were performed by SRP's engineering consultant DiGioia Gray and Associates (DiGioia Gray). The subsurface investigation (drilling and sampling) and laboratory testing of samples were conducted by Wood (WSP) with oversight from SRP.



Fig. 1. ABP Project Site Location Map.

SUBSURFACE ASSESSMENT

Geological & Geotechnical Studies

The geotechnical studies were comprised of a desktop study of geologic and geotechnical conditions from existing data sources, geologic field reconnaissance to assess the validity of desktop information, development of the field and laboratory testing program, and performance of field sampling and testing. This information was combined to develop idealized profiles at each pole location that includes characteristic geotechnical properties for foundation design.

The desktop study consisted of collecting and compiling pertinent geological/geotechnical information from SRP, Arizona Department of Water Resources (ADWR), Arizona Geological Survey (AZGS), United States Geological Survey (USGS), NRCS Web Soil Survey, and FEMA flood hazard maps. SRP provided eight geotechnical reports that consisted of five substations and three transmission line projects adjacent to the alignment. Surficial geologic mapping and geohazards (earth fissures, land subsidence features) information was collected from AZGS. Aerial mapping was also reviewed to determine presence of irrigation canals/sloping ground topography and ephemeral stream channels that also can pose as a geohazard. Groundwater depth and water well installation information along the alignment was collected from ADWR interactive database. For design, the alignment was separated into the four geologic zones derived from the published geological mapping of surface and near subsurface depositional characteristics (Fig. 2). Table 1 describes geological characteristics of the zones and Fig. 3 shows their distribution along the alignment.

Geological field reconnaissance site visits were performed to ground truth the published geologic map and to verify geohazards identified in the desktop study. During the reconnaissance, flood potential (foundation proximity to drainage features), sloping ground topography, and potential ground loss due to man-made features (i.e., irrigation canals, drainage basins, etc.) were cataloged along the alignment. Additionally, surficial soils were observed and logged in areas of exposed soil banks/road cuts/fills.

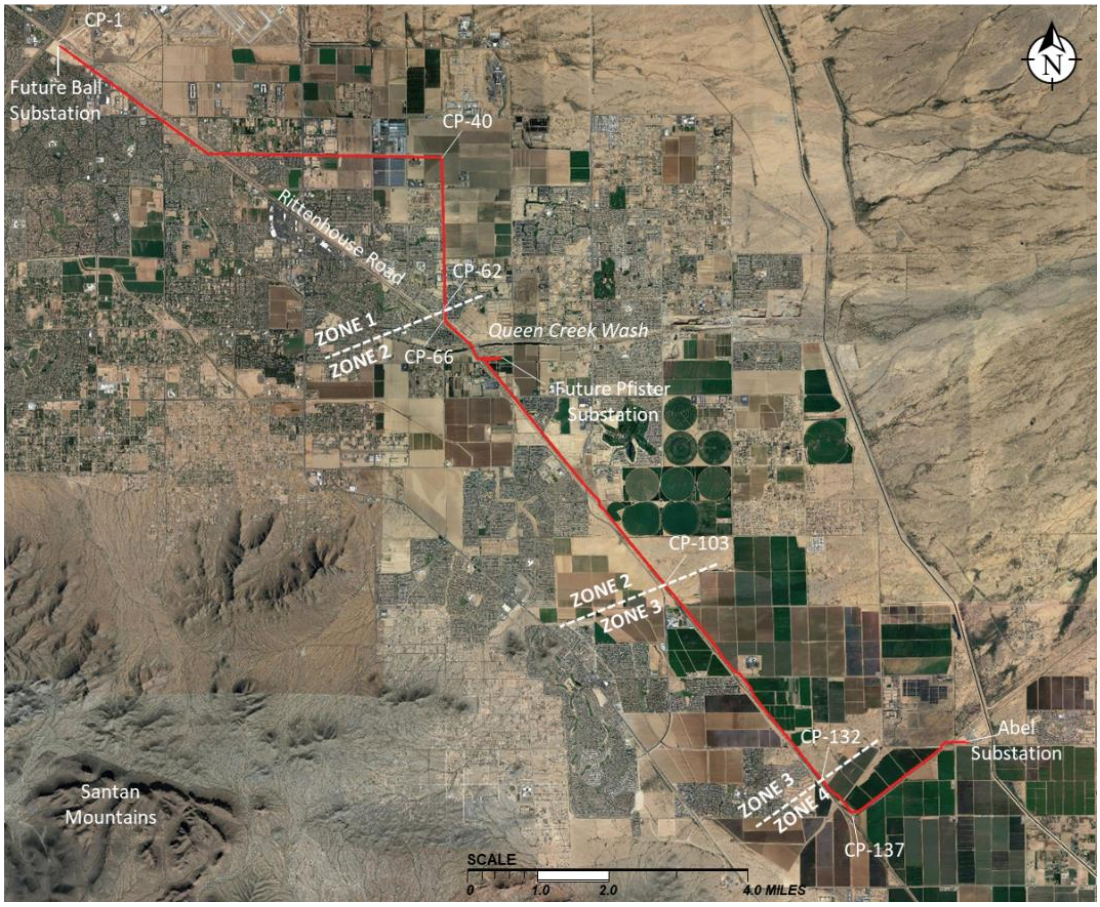


Fig. 2. Overview map with geologic zone designations.

Table 1. Geologic zones encountered along the alignment (see Figs. 2 & 3).

Geologic Zone		Description
1	Young alluvium (Qyc, Qyf)	Non-cemented sands and clay-rich material with surface materials underlain by old, cemented and clay-rich basin fill deposits comprising of material that was eroded from the Superstition and San Tan Mountains.
2	Young alluvium (Qyc) over Intermediate-aged alluvial gravel (Qi)	Same surficial materials as Zone 1; however, underlain by intermediate-aged alluvial gravel deposits that are non-cemented and associated with the sedimentation from Queen Creek. Younger deposits are more prevalent north and south from Queen Creek while older alluvial fan deposits interlayer the subsurface near the channel.
3	Young alluvium Qlyf, Qyc over Old alluvial fans (Qfo)	Dense, weakly cemented sandy clay and clayey sand. The deeper soils in this zone transitions to dense, weakly cemented clay to sandy clay associated with older alluvial fan deposits that predate Queen Creek.
4		Same surficial materials as Zone 3; however, the underlying older alluvium is strongly cemented clay with high plasticity.

The desktop and field reconnaissance information were used to develop the investigation program following the owner's subsurface investigation methodology. The goal of the program was to select field test sites that represented the various subsurface conditions predicted by the prior investigation work and new reconnaissance. Exploration locations were determined by following approach (ranked by order of importance):

- At all dead-end and heavy angle structure locations.
- At or near geologic transitions.
- At least one exploration within each mile of the alignment.

No new access was to be provided for the investigation, so all locations required sites to allow standard two-wheel drive drill rig travel. An additional discussion detailing the utility owner's investigation methodology is outlined later in the paper.

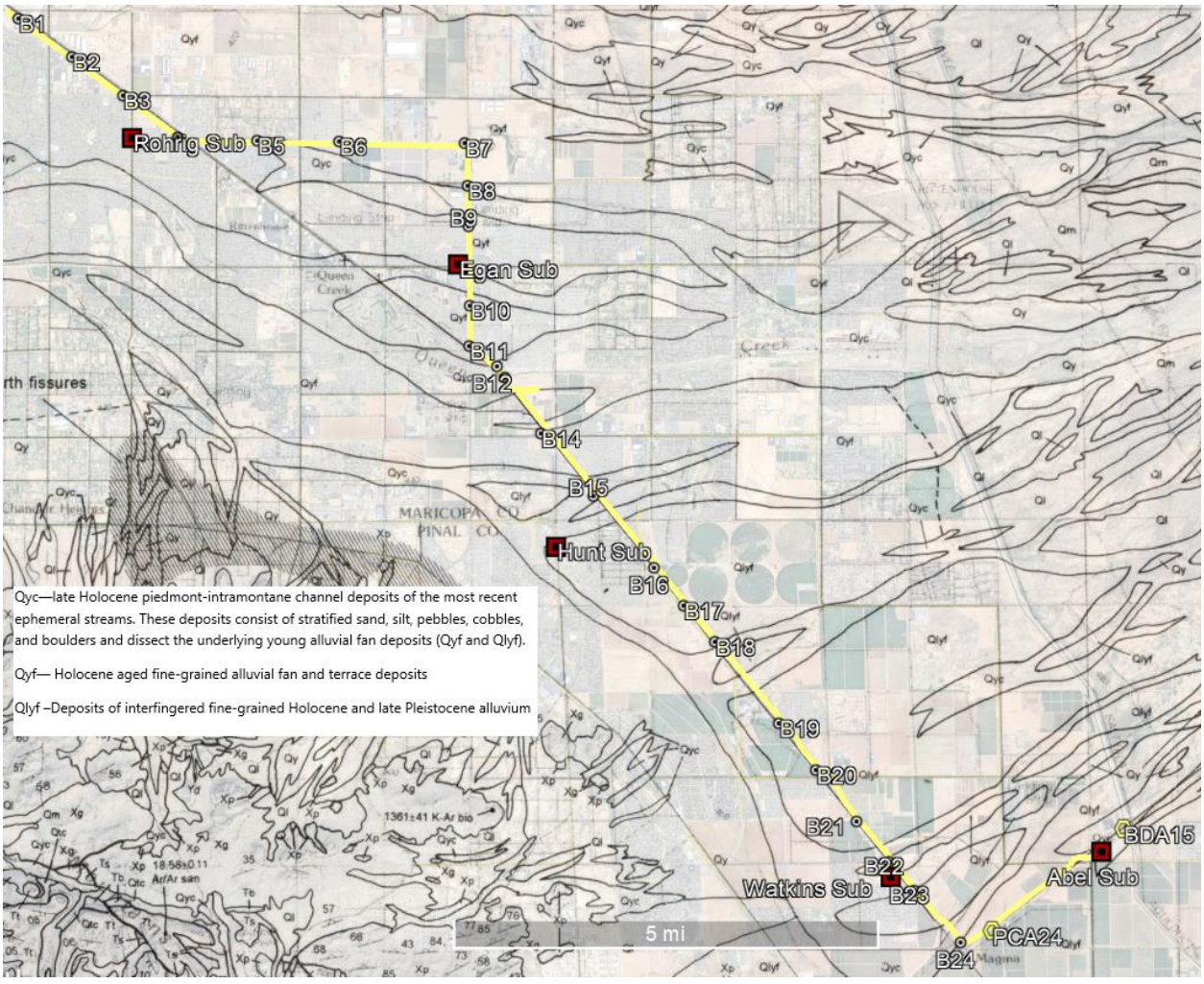


Fig. 3. Geologic overview map with new and previous exploration locations (adapted from Spencer et al. 1996).

Borings were planned to be approximately equal to 2/3rds of the project miles, or for this project 24 new sites along with data from 6 existing substation or transmission line investigations performed for other SRP projects adjacent to the new line (the utility gave the design team permission to use this prior data).

 © Deep Foundations Institute 2025

Bore locations were adjusted to ensure that all anticipated soil deposits within all geologic zones were represented, with special focus on foundations at or adjacent to drainage features or in expected weak ground conditions. This process resulted in one boring for every 5.4 structures, with a distribution of borings approximately 6 to 10 structures apart or 0.6 to 1.0 miles apart. Figure 2 and Figure 3 identify the transmission line alignment, geologic mapping, and new and previous explorations. Table 1 identifies the geologic zones and description along the project alignment.

WSP performed the field investigation using a truck mounted CME 75 drill rig equipped with nominal 7-inch OD, segmented flight, hollow stem auger. Samples of the subsurface and blow counts required to obtain the samples were obtained at a depth of 2.5 feet and every 2.5 feet thereafter to 10 feet, then at 5-foot intervals to the full depth of each boring (typically 35 feet). Relatively undisturbed samples were obtained using a 2.42-inch ID drive ring sampler equipped with 1-inch high brass rings (ASTM D3550). Where ring samples were not practical, disturbed samples and SPT measurements were obtained using a nominal 2-inch O.D. split spoon sampler (ASTM D1586). Both sampler types were advanced using a standard penetration test, 140-pound hammer with a 30-inch free fall raised by auto-hammer method. All samples were stored in the Wood Phoenix laboratory with selected samples tested within the same facility. Laboratory testing on the relatively undisturbed ring samples consisted of moisture and density, direct shear, consolidation, and index properties (sieve analysis and Atterberg limits). All obtained disturbed samples were tested for moisture content with selected disturbed samples tested for index properties and corrosion potential.

Data Evaluation

Characteristic properties and design parameters with idealized layering were primarily derived using a statistical assessment of the blow count data obtained from both the undisturbed and disturbed sampling and accepted soil property-blow count correlations and adjusted by review of laboratory test results. Blow counts were corrected based on sampler type, sampler size, hammer system, and input energy to determine SPT-N values. Characteristic SPT-N for each geotechnical layer were derived by combining the data sets across the alignment for geologically similar materials. The statistical approach defines characteristic properties (including SPT-N values) as the lower bound of a 5% exclusion limit (LEL) of the data mean (assuming a normal data distribution), but no less than the lowest value measured.

Following this approach, nine characteristic geotechnical layers for the full alignment were idealized with corresponding design properties. The nine layers were developed by grouping SPT-N values of similar materials (cohesive/granular/cemented) within the four geologic design zones. A mean and standard deviation was calculated for each layer and outliers were excluded (i.e., refusal blow count). If the coefficient of variation (COV) of the analyzed layer exceeded 35 percent, the data was re-evaluated to determine if outliers existed or if the subdivided data grouping required additional subdivision. A 35 percent COV was utilized based on recommendations identified by Heim (2014). Data manipulation/organization was limited to prevent unwarranted layer subdivision/data exclusions to maintain sufficient data points to develop the lower bound of the LEL and maintain a COV lower than 35 percent. The characteristic value was then derived as previously discussed. Engineering property correlated to SPT-N values were then applied to the grouped dataset. Engineering correlations for unit weight and shear strength (friction and cohesion) were augmented with laboratory test results for the selection of the design property. Likewise, engineering correlations developed by DiGioia Gray specific to Arizona were utilized to develop the characteristic deformation modulus value.

The final step for characterizing the subsurface required development of idealized subsurface soil profiles for pole structure locations. Ground elevation changes were ignored as the relative change from site to site was minimal, so the ground surface was considered the same for all sites. As such, horizontal delineations were assumed between geotechnical layers with depth. The initial layer boundaries were set

based on the location of the nine layers previously discussed. Subsequent changes to the layer boundaries and their vertical occurrence along the alignment were based on the geologic site reconnaissance, mapped geologic unit, and the NRCS web soil survey soil changes. A total of 22 unique idealized soil profiles were developed for foundation design. An example of one of the profile maps is presented as Fig. 4.

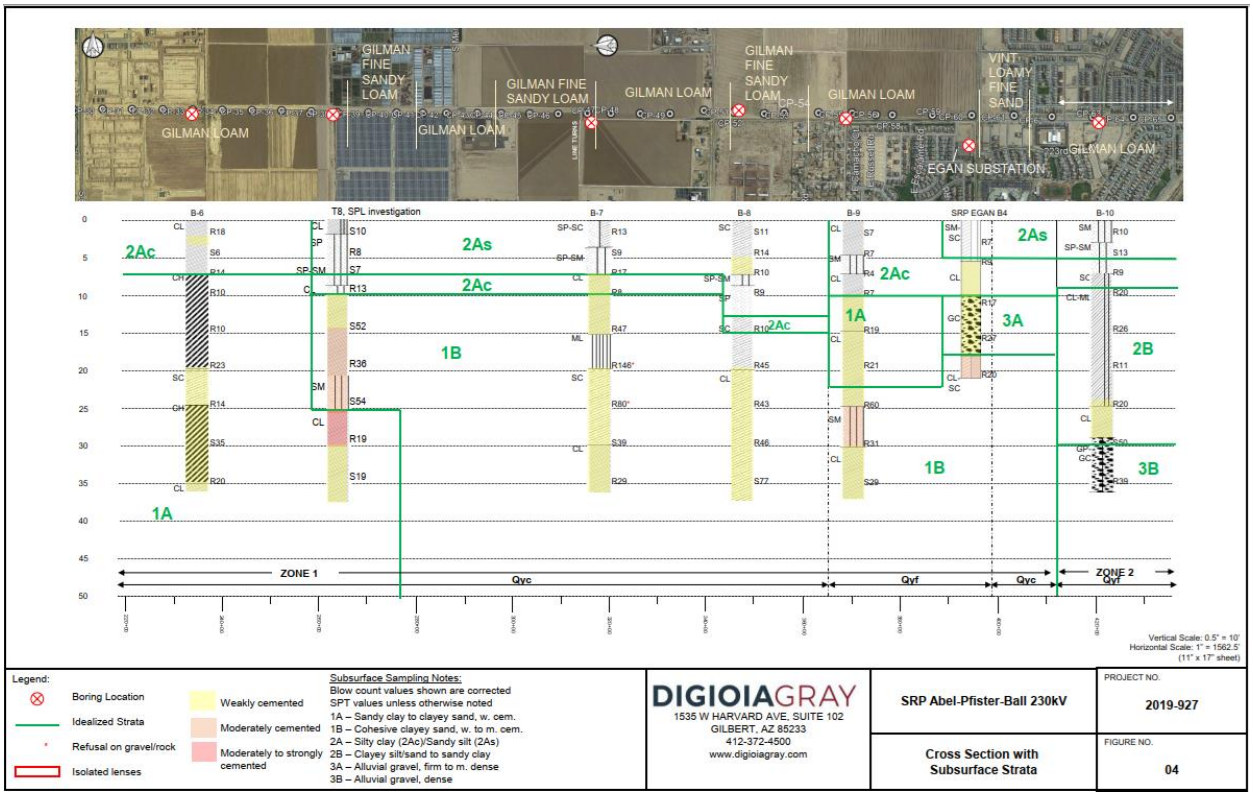


Fig. 4. Example profile (cross section) with subsurface data.

FOUNDATION DESIGN

Design loads for transmission line structure foundations most often derive from the National Electrical Safety Code cases (NESC) on the structures for combined ice and wind based on geographic locations (districts) in the US (NESC Section 250B) or extreme wind (NESC Section 250C) (DFI 2025). From review of structural load calculations, groundline reactions result from either the extreme wind case with a load factor of 1.0, or the NESC "Light" district case with load factors of 2.5 for lateral wind forces at 59.3 mph and 1.65 for initial lateral design tension on the conductors. The NESC is a safety code for safeguarding the public, utility workers, utility facilities and electric supply and communication equipment. Load combinations are based on variable weather events and utilize load factors which model a reliability-based design approach. The power industry commonly accepts that the ground line reactions developed from these load combinations can be used for the foundation design (DFI 2025).

Foundation design was performed using the Electric Power Research Institute's (EPRI) Foundation and Analysis Design (FAD) methodology and computer software (FADTools Version 5.2) in Reliability-Based Design (RBD) mode. This approach requires the use of characteristic subsurface properties in conjunction with factored applied lateral loads. The EPRI model incorporates a 0.63 strength reduction factor for the lateral load model to account for variances in model results from full scale load tests. A load condition factor was applied to the ground line reactions provided by the steel pole manufacturer to

ensure equal to or greater foundation strength than the pole structure strength. The FADTools MFAD module in drilled shaft mode was employed. Other foundation design assumptions included:

- The foundation diameter was a function of the structure's base plate anchor bolt circle diameter, with at minimum concrete cover of 4 or 5 inches (depending on final foundation diameter) and varied in ½-foot increments.
- Standard top of foundation reveal above level ground was 2 feet and adjusted to a higher reveal to account for irregular ground within 2.5 foundation diameters.
- Reduced unit weight, soil strength and lateral soil modulus were applied to the upper 4 feet of the subsurface to account for construction disturbance effects and minor variations in ground conditions.
- Minimum foundation embedment was set at two foundation diameters for non-cemented soils and 1.5 foundation diameters for moderately to strongly cemented soils.
- Performance thresholds at the top of the foundation were used to limit movement of the foundation at maximum design loads, with lateral deflection limited to 4% of the foundation diameter and top of foundation rotation limited to 1 degree. The MFAD program allows for assigning a value for non-recoverable movement. For this project, non-recoverable values were set at 50% of threshold limits.
- Where the concrete cover exceeded 8 inches, a secondary reinforcing cage was added in the reveal section to mitigate temperature induced cracking.
- The anchor bolt cage was used as foundation reinforcement, with lateral stirrups installed at regular intervals in accordance with the concrete design module of the MFAD program.
- Full-length anchor bolts were used as vertical reinforcement, with every other bar terminated at 12 feet below the top of the foundation in accordance with the overturning moment demand of the foundation as given by the concrete design module of the MFAD program.

A sensitivity analysis was performed on foundations that terminated with less than 1-pier diameter of embedment into a stronger layer to address the inherent soil variability that can occur within the design profile. This analysis determined if the foundation would still have sufficient ground line capacity and meet the required foundation performance by extending the weaker layer an additional half-pier diameter below the foundation design depth. For foundations that did not have sufficient capacity with the extended weaker layer, the design embedment was increased until capacity and performance were met.

Foundation embedment optimization was performed to limit the number of unique foundation reinforcing cages/length options. This effort grouped similar foundation types together (same anchor bolt circle diameter and quantity) with a limited number of foundation lengths. Typically, foundations were grouped in 2-foot intervals (i.e., grouping 21-foot with 22-foot foundation lengths).

FOUNDATION & SUBSURFACE INSPECTION

The foundation inspection program was performed by DiGioia Gray and included detailed logs of soil conditions at each structure site, allowing real-time design changes during construction to accommodate foundations where conditions were determined undercapacity assumed in design. Strength testing of cured concrete samples includes early testing to allow a proactive approach to modifying the project design mix and provide continual improvement.

The foundation inspection and testing program was developed to provide three major functions; a) monitor and verify that the foundations being installed and the materials for construction were in accordance with the project plans and specifications, b) provide immediate feedback to the foundation design team and the project owner where non-conformance was identified so that practices could be adopted for ongoing construction., and c) develop as constructed foundation geometry to validate

foundation capacity in real time. This effort required highly qualified field inspection staff who understood soil engineering, concrete materials, and foundation design. DiGioia Gray, as the foundation Engineer of Record (EOR), supplied the field staff to document foundation construction. The composition of the field team included experienced concrete materials technicians, geologists, and geotechnical engineers.

Foundation construction was performed by a contractor as a conventional design-bid-build project, where field monitoring staff reported to SRP and SRP's field construction representative. In this case, monitoring of the construction process is done to ensure that necessary records can be made, and to provide timely information to the foundation EOR and/or the owner's field construction representative concerning unanticipated conditions or deviations from the drawings or specifications. The staff performing this work were able to communicate and compare observations with the contractor but did not direct the construction process.

Typical Drilled Shaft Construction Sequence

The contractor verified construction staking, positioned the drill rig (Fig. 5) with appropriate tooling, and advanced the shaft excavation to the specified depth. Depending on the shaft diameter, the contractor would advance the excavation using either tooling matching the specified diameter or use smaller tooling (pre-drill/pilot hole) and then complete the excavation by attaching reamers to the tooling to achieve the specified diameter. All 161 foundations were constructed in the dry. In instances where noticeable cave-ins (sidewall voids larger than 2 ft) were observed, the contractor filled the excavation with 2-sack cement per cubic yard controlled low strength material (CLSM) to 2 feet above the cave-in depth per the project specifications. During the next shift (typically next day), the contractor continued the excavation to the required depth, excavation through the CLSM material. Upon excavation completion, the contractor set the full-length anchor bolt cage (Fig. 6) with the appropriate support system and formwork (Fig. 7), verified its location, placed the project specified concrete, and finished the exposed shaft per the project specifications.

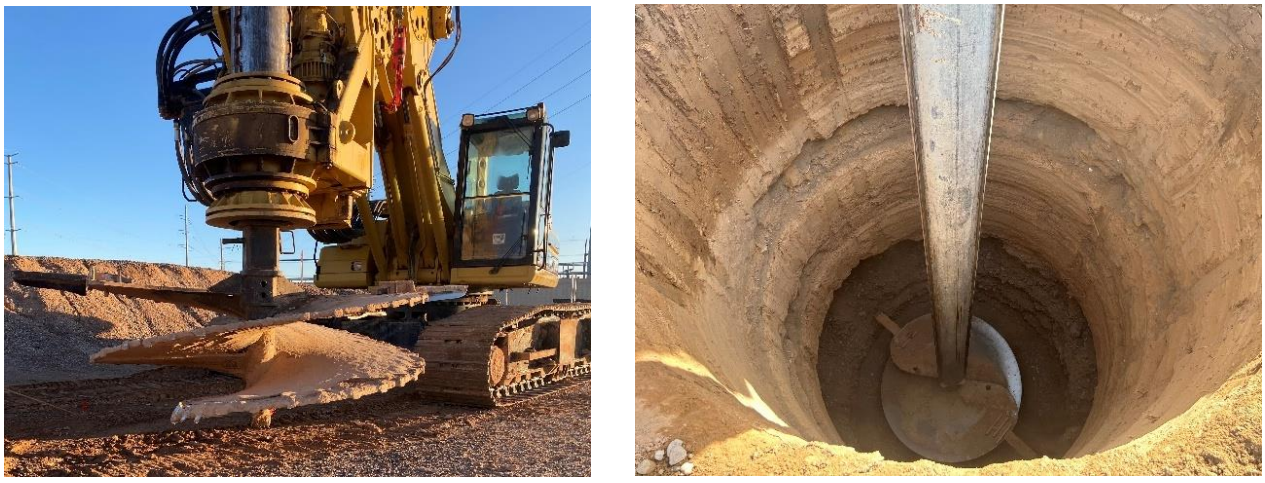


Fig. 5. Shaft excavation.

 © Deep Foundations Institute 2025



Fig. 6. Typical anchor bolt cage.



Fig. 7. Concrete placement.

Field Foundation Construction Monitoring

The foundation design team developed a field inspection manual with monitoring/inspection forms to be used for documentation of foundation installation. The forms were developed using common word processing software with data input tables. Information recorded included:

- Foundation location, type of foundation, and type of structure to be installed.
- Survey completion verification.
- Log of soil layer descriptions obtained from foundation auger cuttings at time of excavation. The log also identified the soil zone corresponding to foundation design.
- Shaft stabilization method and materials (if used), including sketches.
- Fabricated anchor bolt reinforcement cage measurements.
- Shaft drilling: drill type and tooling, shaft geometry including caved locations (with sketches), depth of casing (if used), moisture conditions of shafts drilled in the dry.
- Installed anchor bolt reinforcement cage geometry: clearance to shaft excavation sidewalls, centering or off-set of anchor bolt cage within shaft excavation, anchor bolt orientation, and anchor bolt projection above top of concrete
- Placement geometry of formwork (above and below grade).
- Verification of concrete mix delivered.

SHEET 1 OF 2

ABEL-PFISTER-BALL 230/69KV TRANSMISSION PROJECT
ANCHOR BOLT FOUNDATIONS - PLACEMENT

DRILLED PIER INSTALLATION LOG FOR STRUCTURE NO.: CP-75

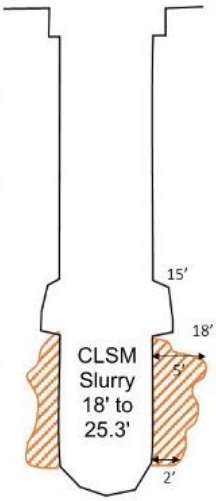
CONTRACTOR: [redacted] DATE: 3/22/23

FIELD REP: [redacted] STRUCTURE TYPE: Tangent FDN TYPE: Drilled Shaft

FNDN DWG: T1952486 – 21.4 AB DWG 22 – 502972 - 411 TEMPLATE NO. 22 – 502972 - 411

RIG TYPE: IMT AF 180 TOOL TYPE: 7' Open Auger w reamers (6" each side)

WEATHER: Cloudy, windy/gusty (50s)

GRND WTR	DEPTH	CROSS SECTION	DIA	USCS	DESCRIPTION AND REMARKS
N/A	GRADE		8'	CL	Silty clay, trace sand & gravel, soft, friable, angular coarse-grained gravel, moderate PI, moist, brown
	5 FT			ML/SM	(7') Sandy silt, trace clay, soft, poorly graded/fine-grained, low PI, sl. moist, brown
	10 FT		7'	SM/SC	Note: clay grades out below 9', becoming well-graded coarse-grained silty sand (SM) (12') Silty/clayey sand, trace gravel, m. dense, sand (75%) well graded, gravel f-c grained and subrounded, weakly/mod.
	15 FT			GM/SM	cemented coarse grained clasts, low-no PI, sl. moist, brown (15') Gravelly sand, trace silt & cobble, sand well graded, gravel subrounded/subangular & coarse-grained, no PI, moist, tan-brown
	20 FT				Note: silt grades out, dense, and more fine-grained from 18' to 22' (GW/SW)
	25 FT				

ARE THE SUBSURFACE CONDITIONS EQUALTO OR BETTER THAN GIVEN IN THE GEOTECH REPORT ASSUMPTIONS? ☑ Yes ☐ No SOIL ZONE 2.4

IF NO, EXPLAIN:,

FOUNDATION DRILLING

DRILL START DATE: 3/22/23 TIME: 0730 EXCAVATION RATE: 3.6 min/ft

DRILL COMPLETE DATE: 3/22/23 TIME: 0900 EXCAVATION TIME: 1.5 hrs

AVG DIAMETER: 84 in. DESIGN DEPTH: 25 ft ACTUAL DEPTH: 25.3 ft

ANCHOR BOLT CAGE

ANCHOR BOLTS SIZE: 18J LENGTH: 334.5 in NO: 12 AB CIRCLE DIA: 68.25 in

CUTOFFS LENGTH: 164 in NO: 12 OUTSIDE CAGE DIA: 72.15 in

T1 TIES SIZE: 6 SPACING: 5 – 6 in NO: 4 LAP LENGTH: 37 in

T2 TIES SIZE: 6 SPACING: 24 in NO: 9 LAP LENGTH: 38 in

T3 TIES SIZE: 6 SPACING: 12-13 in NO: 7 LAP LENGTH: 37 in

(CHECK FOUNDATION DRAWINGS TO VERIFY MINIMUM VALUES ARE MET)

Fig. 8. Example excavation inspection form.

 © Deep Foundations Institute 2025

SHEET 2 OF 2

ABEL-PFISTER-BALL 230/69KV TRANSMISSION PROJECT
CONCRETE PLACEMENT

CONCRETE PLACEMENT FOR STRUCTURE NO.: CP - 75

CONTRACTOR: [redacted] DATE: 3/23/2023
FIELD REP: [redacted] STRUCTURE TYPE: Tangent 84-27 FDN TYPE: Drilled Shaft
CONC MIX DESIGN: 401110 STRENGTH: 4,000 PSI DESIGN SLUMP 3" – 5"
CONC SUPPLIER: AZMM PLANT LOCATION: Queen Creek, AZ
PLACEMENT METHOD (CHECK ONE): END DUMP X PUMP TRUCK
WEATHER: Cleaar, Sunny AIR TEMP: 50s

FORMS / CAGE FINAL INSPECTION

REVEAL HT: 2 ft DIAMETER: 84 in AB PROJECTION (minus cover) 14 1/8 in.
MIN CLEARANCE SIDES: 4 - 5 in. BOTTOM: N/V in. FORM BELOW GRADE: 2 ft
CURING METHOD (CHECK ONE) COMPOUND X POLY SHEET OTHER
TOP OF CONCRETE: SLOPED TO DRAIN? (Y) N) TYPE OF FINISH Trowel and Broom
INSPECTOR TO VERIFY ANCHOR BOLT ORIENTATION & TOLERANCES ARE PER DESIGN DRAWING ☑ Yes

CONCRETE PLACEMENT POUR DATE: 3/23/2023

LOAD TICKET NO: 155478 CU YDS PLACED: 10.5 RISE IN SHAFT: 7.9 ft
CONCRETE TIMES: BATCH: 0824 START PLACEMENT: 0858 END PLACEMENT: 0907
FIELD ADDITIVES: WATER? (Y (N) IF SO, GALLONS: 0 OTHER ADDITIVES Retardent
SLUMP: 4.50 V in CONC TEMP: 80 Deg. F % AIR ENTRAIN: [redacted] BREAK SAMPLE? (Y (N)

LOAD TICKET NO: 155480 CU YDS PLACED: 10.5 RISE IN SHAFT: 5.5 ft
CONCRETE TIMES: BATCH: 0834 START PLACEMENT: 0910 END PLACEMENT: 0922
FIELD ADDITIVES: WATER? (Y (N) IF SO, GALLONS: 0 OTHER ADDITIVES Retardant
SLUMP: 5.00 in CONC TEMP: 76 Deg. F % AIR ENTRAIN: [redacted] BREAK SAMPLE? ((Y) N)

LOAD TICKET NO: 155485 CU YDS PLACED: 10.5 RISE IN SHAFT: 9.2 ft
CONCRETE TIMES: BATCH: 0859 START PLACEMENT: 0924 END PLACEMENT: 0940
FIELD ADDITIVES: WATER? (Y (N) IF SO, GALLONS: 0 OTHER ADDITIVES Retardant
SLUMP: 4.00 V in CONC TEMP: 76 Deg. F % AIR ENTRAIN: [redacted] BREAK SAMPLE? (Y (N)

LOAD TICKET NO: 155487 CU YDS PLACED: ≈ 7.7 RISE IN SHAFT: 5.4 ft
CONCRETE TIMES: BATCH: 0912 START PLACEMENT: 0948 END PLACEMENT: 0958
FIELD ADDITIVES: WATER? (Y (N) IF SO, GALLONS: 0 OTHER ADDITIVES Retardant
SLUMP: 4.50 in CONC TEMP: 74 Deg. F % AIR ENTRAIN: [redacted] BREAK SAMPLE? (Y (N)

(Note: attach lab test reports to log) (V = visual slump check) (N/V = not visible)

INSPECTOR: [redacted] DATE: 3/23/2023

Fig. 9. Example foundation concrete placement inspection form.

 © Deep Foundations Institute 2025

- Concrete placement for each transit truck: delivery ticket number, batch time, fresh concrete quality (temperature, slump, appearance), measurements of concrete rise in the shaft for each load, concrete volume placed per load, placement of concrete per specification, monitor of temperature through full discharge of each load, and length of time for placing each load.
- Verification that ground wires and connectors were installed per specification.
- Top of concrete finish and curing methods, including appearance.

The field team also took photographs of each phase of the field work to provide better clarity on the foundation installation process. Example completed forms are shown in Fig. 8 and Fig. 9. As part of the monitoring process, the field team reviewed the completed excavation log with the contractor to reach agreement on subsurface conditions.

Items out of tolerance from the project specifications were corrected prior to concrete placement. Checklists were developed that referenced excavation and reinforcement tolerances that the field team used for each foundation to help ensure consistency and completeness in the inspection process. The foundation EOR was immediately contacted if subsurface conditions via this qualitative assessment were found to be weaker than was anticipated in design. This process allowed time for real time re-analysis of foundation capacity and modification (if needed) of the shaft geometry or reinforcement prior to concrete placement that typically was done the next morning. When required, the foundation EOR would recalculate capacity.

During construction, it is important to ensure advanced notice for inspections is maintained for all parties involved. The enhanced foundation inspection was not performed at two foundation locations during construction. Foundation inspection was scheduled for these two; however, inclement weather was predicted for the following day or improper notice was provided (i.e., less than 24 hours). For the inclement weather case, the contractor notified the inspection team, a day prior, no activities were going to transpire for the following day. About mid-morning the inclement weather passed, and drilling commenced. The assigned inspectors had been reassigned and they were unable to observe/log drilling and reinforcing steel placement.

The field team provided coordination with the contractor's concrete laboratory testing firm for field sampling and testing to ensure compliance with the project specifications. The field team notified the owner's field representative and the contractor if concrete was out of compliance with the project specifications prior to placement in the shaft.

During concrete placement, the field team plotted the rise of concrete in the shaft for each transit truck load. This plot included the predetermined neat line value assuming the shaft was excavated to the design geometry. This plot, along with visual observations, help mitigate caving concerns during concrete placement. Concrete placement could be halted and the anchor bolt reinforcement cage removed if caving was indicated. Once the field work was completed, concrete placement data along with shaft geometry was provided to the Engineer of Record for final assessment. The data was plotted on a spreadsheet to assess concrete clearance, compare the actual foundation geometry to the design geometry, and identify as-constructed conditions. Figure 10 shows an example of the final form provided by the foundation EOR to SRP.

Structure	CP-75		**Date**	3/23/2023											
Socket Diameter=	40.00	in													
Cage Diameter =	72.15	in	Reveal Height =	2.0	ft			Form Depth =	2.0	ft					
Shaft Diameter =	84.00	in	Embedment Depth =	25.3	ft										
Form Diameter =	84.00	in	Socket Depth=	0.7	ft										

Ticket	Times				Height of Concrete (ft)		Concrete Rise (ft)	Concrete Volume (cy)		Shaft Avg. Diameter (inches)		Neat Line Volume	Shaft Avg. Cover (inches)	
	Batch	Start	Empty	Dur	Load Start	Load Finish		Per Truck	Cumulative	by volume	nominal		by volume	nominal
						28.00			0.0					
155478	8:24	8:58	9:07	0:43	28.00	20.10	7.90	10.5	10.5	81.11	80.10	9.6	4.48	3.98
155480	8:34	9:10	9:22	0:48	20.10	14.60	5.50	10.5	21.0	97.21	84.00	7.8	12.53	5.93
155485	8:59	9:24	9:40	0:41	14.60	5.40	9.20	10.5	31.5	75.17	84.00	13.1	1.51	5.93
155487	9:12	9:48	9:58	0:46	5.40	0.00	5.40	7.7	39.2	84.02	84.00	7.7	5.93	5.93
						Total reported volume (cy)		39.2		2.6% excess of neat line			7.70	
						Neat line volume (cy)		38.2						

Observations: Gray shading denotes caving observed in log

Caving reported above slurry section (17'-20' below top of form) prior during drilling. Overage observed in concrete volume measures.

Differences from expected rises due to 1st, 2nd, and 3rd loads likely due to contractor's inability to accurately measure concrete rise. Cover visually checked.

ASBUILT DIMENSIONS	
diameter	83.7 ft
depth	25.3 ft
length	27.3 ft
Shaft Vol	39.0 cy

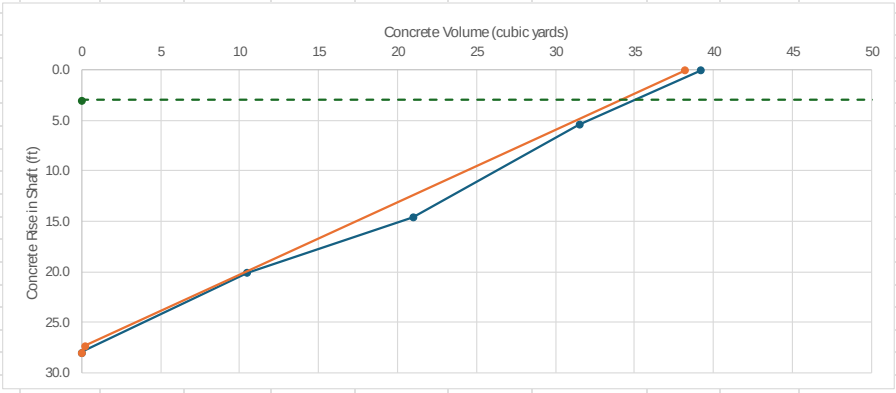


Fig. 10. Example foundation placement inspection form (orange = neat line; blue = measured).

Concrete Materials Review

Table 2 summarizes estimated and actual concrete materials testing quantities evaluated during construction. In addition to evaluating fresh concrete on each transit truck for consistency (slump), six (6) concrete cylinder samples were obtained for strength testing, with two tested at 7 days after placement, three tested at 28 days after placement, and one cylinder held in reserve for potential testing at 56 days after placement or to replace a mis fabricated 28-day test cylinder. Frequency of strength test sampling was done at least once per day, once for every 50 cubic yards, at every dead-end structure, when there was a change in concrete consistency, or as directed by the inspector.

Table 2. APB Project concrete quantities.

Concrete Volume (cubic yards)		Concrete Cylinder Sets	
Estimated	Actual	Estimated	Actual
9,200 (1)	8,870	200	226

(1) Neat line plus 10%

Contractor payment was based on samples achieving a 28-day strength of at least the specified value (4,000 psi). 7-day testing was done to aid in determining if the foundations had achieved sufficient strength to install pole structures. Wire installation and tensioning was permitted once the concrete reached full strength, but no less than 7 days after placement. The 7-day tests also allowed tracking of the foundation concrete to flag potential low strength concrete. History of similar SRP standard concrete mixes showed that, on average, 70% of the final strength was reached at the 7-day mark. Tests analysis of the concrete samples showed this practice to be valid, with the average 7-day strength equal to 68.9%

(±21%) of the average 28-day strength. Statistical analysis of the full data set showed the lower 5% exclusion limit of the data set to be at 68.2% of the average 28-day strength.

Spreadsheets were used to track and monitor concrete strength test results. Figure 11 presents the 7-day strength test results as the project progressed. Data during the first two weeks of placement indicated that some samples may not reach the required 28-day strength level. The concrete supplier modified the mix, which resulted in an increase in strength where nearly all future 7-day tests met the required minimum threshold. Figure 12 presents all strength test data for the project.

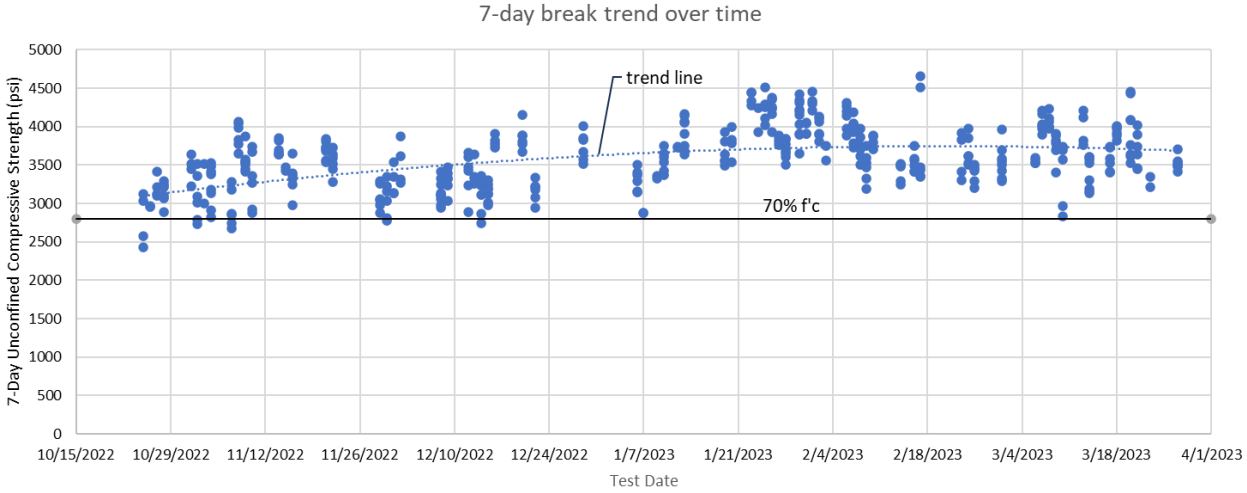


Fig. 11. Plot of all 7-day concrete unconfined compressive strength tests for project.

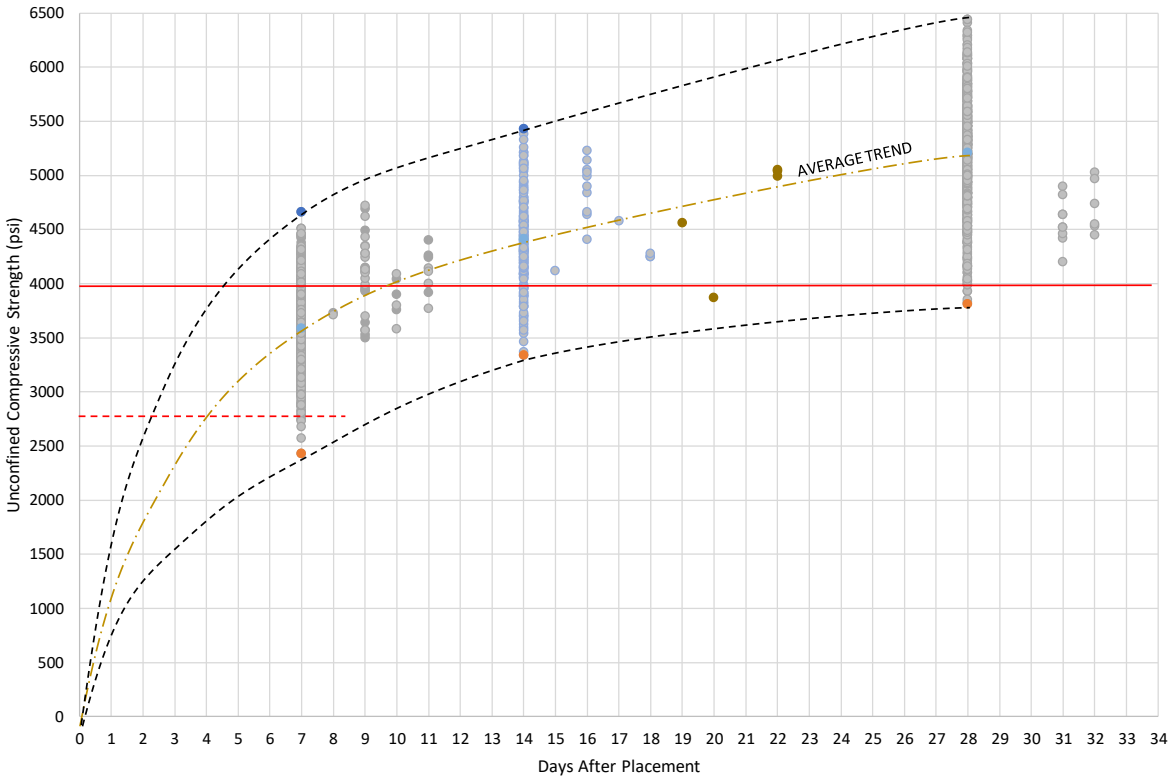


Fig. 12. Plot of unconfined compressive test results of all cylinders for the project by age.

COMPARATIVE ASSESSMENT OF INVESTIGATION APPROACHES

The number of boreholes and boring depths required for a thorough geotechnical investigation of a given project are affected by many factors such as purpose of the investigation, time allocated for investigations, cost, the structure layout/loads, site access, availability of boring/testing equipment, anticipated subsurface conditions/variability, local knowledge, and experience of the geotechnical engineer (DFI 2025). Therefore, the investigation program for an electric transmission line project requires planning to optimize foundation analysis and design. Several general methods summarized in the literature and are presented herein.

A 2014 survey was conducted by the Electric Power Systems Foundations (EPSF) Committee of the Deep Foundations Institute to define the state of practice for transmission structure foundation design. The survey results found that the utility industry typically utilizes three different methodologies to define the subsurface test frequency for subsurface properties determination. The three methodologies consist of tailoring the investigation to focus on structure type, line mileage, or geologic regime (Kandaris and Davidow, 2015).

Structure based subsurface testing consists of either sampling at all locations or site explorations based on criticality of the structure loading (dead-end vs. angle vs tangent). In the EPSF committee survey, 35% of respondents sample at every site and 24% of respondents site explorations at critical structures (dead-end, angle structures) (Kandaris and Davidow, 2015). In an Electric Power Research Institute (EPRI) survey conducted in 2012, identified 79% of the respondence (utility owners) perform borings at all or selected angle or dead-end structure locations, while only 21% responded that they perform borings at every structure location (DiGioia 2012).

Line mile based subsurface testing approach assigns borings per line mile. The EPRI survey also identified 74% of the respondents conduct explorations every mile, 22% of the respondents conduct explorations every two miles, and the remaining 4% of respondents' answers varied (DiGioia, 2012).

In both structure-based and line mileage-based approaches, subsurface data gaps will happen between explorations. Subsurface data gaps contribute to uncertainty in characterizing geotechnical design properties. In the instance of low confidence, engineers will typically select low bound properties instead of developing characteristic properties. Data gaps occur when limited explorations are spaced through the alignment and explorations are not sited where mapped soil/bedrock transitions occur, in areas of known geohazards (i.e., landslides, karsts, faults, etc.), surface and groundwater fluctuation due to topographic relief, and/or areas prone to flooding/inundation.

As was incorporated into the APB Project optimized program, the geologic based subsurface testing approach consists of performing representative explorations in mapped geologic units. Typically, geologic mapping is obtained either from the USGS or a state specific geologic survey. A desktop study is typically performed in conjunction with the review of geologic mapping to identify other features of interest that may warrant additional subsurface testing/investigation (i.e., geologic hazards, flooding/inundation areas). The EPSF committee survey indicated that 19% of the respondents used geologic mapping to determine site exploration locations.

Optimized Approach

Optimizing geotechnical investigations, foundation design, and foundation construction inspection should result in good quality foundations constructed within a reasonable time and at acceptable costs. An assessment of these measures can be made due to the well-documented inspection program. Quality can

be measured in terms of several factors such as change orders, concrete volume above pre-construction estimates, and deviations in foundation geometry due to changed conditions. Table 3 presents several as-constructed foundation quality measurements cataloged for the APB Project during construction.

Table 3. APB Project foundation quality measurements.

Profile at Structure Different and Weaker than Predicted		Subsurface Not Meeting Minimum Required Resistance		Foundation Analysis Performed to Confirm Resistance		Foundation Volume Exceeding Neat Line plus 10%	
Number	Percent	Number	Percent	Number	Percent	Number	Percent
25	15.5%	4	2.5%	11	6.8%	25	15.5%

The overall accuracy in estimating subsurface profiles using the optimized investigation approach was 84.5%. Profile estimate variance sources included:

- Thinner, thicker, or unanticipated gravel and sand lenses (10 structures),
- Weaker profile layers encountered during excavation (15 structures).

Eleven (11) of the foundations were reanalyzed due to under-capacity concerns by the foundation EOR, while the remainder were compared to similar foundations designed in the as-encountered conditions. Of these, four (4) foundations indicated insufficient performance using the design depth and diameter. But all were found to provide sufficient performance when analyzed using the as-constructed foundation geometry since most of the cases were in soils that caved during drilling (increasing the effective foundation diameters) and/or were overdrilled beyond design depth by the contractor.

The misidentification of soil profiles occurred between test bore locations where engineering judgment was used to decide where a zone or layer ended and the next began. This was observed most often at both the north and south boundaries of Zone 2. This zone is heavily influenced by Queen Creek Wash, where unanticipated sand and gravel lenses were observed at varying depths and randomly outside of the predicted limits.

Total concrete volume can be used to assess the cost of the optimized approach. Although concrete volume in 25 individual shafts were more than 10% in excess of neat line values, the total concrete placed in all 161 shafts only exceeded the total project neat line volume by 5.8%. This excess volume is well within the preconstruction budget estimate of 10%. No significant foundation geometry design change was required during the construction.

Schedule was a driving factor in expediting the investigation and construction. Foundation construction began on October 25, 2022, and was completed on March 29, 2023, a 23-week period. There was a general slowdown in activities during the Thanksgiving/Christmas/New Year holidays. Additionally, unusually heavy rains slowed work during November through January. The actual schedule met the owner's requirements.

Total installed foundation cost can be presented in terms of neat-line foundation unit volume. The optimized program design neat line volume was 8,380 cubic yards and the as-installed concrete volume was 8,870 cubic yards. The optimized program costs prior to construction (geotechnical studies, field investigations, foundation design and optimization) was $19 per cubic yard. Construction engineering costs, including concrete materials testing, owner's engineering support, and the enhanced construction inspection (plus reports and as-installed records) was $79 per cubic yard. The foundation construction cost (labor, equipment and materials) averaged $785 per cubic yard. The estimated total cost of the

foundation component of the APB Project (includes geotechnical investigation, construction engineering, and foundation construction) was about $7,800,000.

Investigation Approach Comparisons

Two structure-based alternative investigation and foundation design approaches are used for transmission line projects. The first option (Alternative A) involves conducting site-specific testing and sampling at each structure location, followed by foundation design based on the encountered subsurface conditions. This approach often correlates SPT-N values to geotechnical properties in lieu of extensive laboratory testing of samples. The second approach (Alternative B) uses a limited number of borings as was done for the APB project, then applies the soil profile to foundation design at structure sites nearest to the boring. Geotechnical properties for the borings can either be the average values for each soil layer or the low-bound values where multiple data points are obtained for a layer. The APB Project provided sufficient cost and subsurface data, which were utilized to estimate the comparative costs of implementing each alternative. See the prior discussion in this paper section describing these alternative assessment approaches.

For the purpose of cost comparison, assumptions related to Alternative A are as follows:

- Investigation costs assume an additional 131 standard borings to 35 feet with SPT sampling and a limited amount of additional laboratory work. No pre-investigation reconnaissance is performed since all sites will be tested.
- Soil profile prediction accuracy by this approach will be 100%.
- Installed foundation volumes will reduce by 2.5% from the as-installed amount, based on the revision rate experienced from the optimized program.
- Neat line foundations volumes determined from the reduced as-installed amount plus 3.3% (5.8% excess volume – 2.5% under-design from Optimized Program) to account for changed conditions will be used to determine the alternative approach construction cost.
- Standard quality control of foundation materials and one site inspector to monitor adherence to owner specifications (no enhanced documentation).

Alternative B uses an investigation and design process often seen in the power utility industry. For the purpose of cost comparison, the project foundations were redesigned and based on the following assumptions:

- Borings will be taken at or near major dead-end and angle structures (16 sites), with one boring per 10 (145 remaining structures, 14 sites) minus 6 borings from prior investigations. Limited pre-investigation reconnaissance is performed since borings are based on structure type.
- In a consultant lead design project, there is a likelihood consultants may not rely on explorations performed by others due to legal liabilities and/or data ownership. If the six borings had to be performed as part of this alternative it would increase the preconstruction costs by $2/cy.
- Profiles for foundation design will be modified and based on proximity to borings.
- Low-bound geotechnical design properties from the geotechnical investigation will be used for design since no enhanced inspection will be performed. Redesign resulted in a 12% increase in neat line foundation concrete volumes as compared to the optimized program.
- Neat line foundations volumes determined from the redesign plus 3.3% to account for changed conditions will be used to determine the alternative approach construction cost.
- Standard foundation materials quality control and one site inspector to monitor adherence to owner specifications (no enhanced documentation).

Alternative A provides the most information for foundation design and requires the least interpretation of subsurface conditions to assess variance between borings. Foundation construction costs due to

 © Deep Foundations Institute 2025

foundation size are also expected to drop approximately at the error rate seen in the optimized program. There would also be no need for an enhanced inspection program saving approximately $115,000. But there would be an approximate $353,000 increase in the cost of the investigation program and design effort and 2 months added to the design schedule for performing the field work and interpreting the larger data set. Due to the lower inspection and foundation costs, the total cost of foundations is expected to be equal to or slightly greater than the optimized program.

The standard investigation and design program outlined in Alternative B results in the lowest design and construction engineering cost at approximately $141,000 less than the optimized approach and $379,000 less than Alternative A. But this reduced engineering effort comes at a price for foundation construction. Simplifying engineering and obtaining borings at locations related primarily to the structure type increases the total cost of foundations by nearly $507,000 above the optimized program and $443,000 above the Alternative A approach, or an average 6% increase to the total installed foundation cost.

CONCLUSIONS

This paper presents a case history documenting the design and construction of 161 drilled shaft reinforced concrete foundations for a new Salt River Project 20-mile-long high voltage transmission line in Central Arizona. The project owner and their geotechnical consultants optimized foundation design by following a rational approach in terms of construction schedule, total installed cost, and reliability. An enhanced construction monitoring and inspection program allowed the opportunity to perform a detailed assessment of the process and quantify cost and schedule savings from the approach. Typical documentation developed as part of design engineering and construction inspection are also presented.

Extensive design and construction data generated by this optimized program allowed its comparison with other typical approaches used for transmission line projects via the data generated during construction and the authors' experience with such approaches. In addition to the optimized program, costs and quantities were generated for two alternate approaches.

- Alternative A: Perform a subsurface investigation at each structure location, and
- Alternative B: Perform a subsurface investigation at each deadend and large angle structure site, along with one boring spaced at 10 structure intervals.

Table 4 summarizes the comparison of these alternative approaches. The optimization approach has a comparable cost to Alternative A. However, the optimization program was found to have the following advantages over Alternative A:

- Incorporating a geological reconnaissance program prior to mobilizing field sampling activities can be done in the same time frame as a traditional transmission line investigation but allows borings to be selected at locations that optimize the foundation design process.
- This process, combined with a statistical approach to determining characteristic geotechnical properties for foundation design, results in an acceptably accurate assessment of subsurface conditions without sampling every site.
- An enhanced foundation construction inspection and monitoring program, although higher in cost, provides a rapid means to address changes in field conditions without slowing construction. This approach gives an enhanced understanding of as-installed foundation conditions.

Testing at all sites would have resulted in the lowest foundation construction cost and provided equivalent foundation quality, but would have extended time to design with minimal improvement in understanding subsurface conditions. The highest cost option (Alternative B) provided the least information going into construction and minimal knowledge of the actual subsurface conditions encountered during construction.

Misidentification of soil profiles observed as part of the optimized program mostly occurred within or adjacent to geological zones with less consistent stratification, pointing out that all geological zones should not be considered the same when developing a testing program. More frequent sampling should increase the predicted accuracy of subsurface profile estimates in geological zones with greater variability. Anomalous conditions observed during geological reconnaissance visits should also be tested.

Table 4. Comparison of optimized program with alternative approaches.

Program Element	Optimized Approach	Alternative A	Alternative B
Description	Perform significant pre-exploration survey to strategically locate subsurface investigation locations	Subsurface investigation at each structure site	Subsurface investigation at each large type structure & every 10 small type structures
No. of Geotech Test Sites	30	161	30
Soil Profile Accuracy	84.5%	100%	Not measured
Geotech Characteristic Value	5% LEL	Average	Low Bound
Design Concrete Vol (cy)	8380 (actual)	8363 (estimated)	9368 (estimated)
Installed Concrete Vol (cy)	8870 (actual)	8648 (estimated)	9595 (estimated)
% Concrete Above Neat-line	5.9	3.3	3.3
Quality Control Approach	Enhanced	Standard	Standard
Pre-Construction Engineering Unit Cost (per inst cy conc)	$19/cy	$61/cy	$15/cy
Installed Unit Cost (per cy conc)	$785/cy		
Quality Control Unit Cost (per cy inst conc)	$79/cy	$67/cy	$60/cy
Foundation Cost			
Total Cost	$7.83M	$7.90M	$8.34M
Unit Cost (per inst cy conc)	$883/cy	$913/cy	$860/cy
Unit Cost (per foundation)	$48,653/fndn	$49,051/fndn	$51,802/fndn
Schedule Impact (added time, in months)	Base	2 months	0 months

REFERENCES

DiGioia, A. Jr. 2012. *Transmission Structure Foundation Design Guide.* Technical Report 1024138. Palo Alto, CA: Electrical Power Research Institute.

DFI (Deep Foundations Institute), Electric Power Systems Foundations Committee. 2025. *Design and construction of deep foundations to support electric system transmission lines*, State of the practice committee report. Hawthorne, NJ: DFI.

FADTools, 2018. FAD 5.2 User's Guide. http://www.fadtools.com/TechnicalKnowledge/index.html

Heim, Z., 2014. Probabilistic Based Assessment of the Influence of Nonlinear Soil Behavior and Stratification on the Performance of Laterally Loaded Drilled Pier Foundations. Master Thesis. Arizona State University.

Kandaris, P.M. and Davidow, S., 2015. Study of Electric Transmission Line Deep Foundation Design. In Electrical Transmission and Substation Structures 2015 (pp. 577-587).

 © Deep Foundations Institute 2025

Spencer, J.E., Reynolds, S.J., and Pearthree, P.A., 1996, Geologic Map of the Mesa 30’ x 60’ Quadrangle, East-Central Arizona. Arizona Geological Survey Open File Report, OFR 96-23, 1 map sheet, map scale 1:100,000.

 © Deep Foundations Institute 2025

FROM DATA TO ACTION: USING TESTING TO ADDRESS MWD-IDENTIFIED DEVIATIONS IN RIGID INCLUSION INSTALLATION

Chelsea Riddle, Design Engineer, Keller North America, Budd Lake, NJ, Chelsea.Riddle@keller-na.com
Kenneth T. Kniss, Chief Engineer – Ground Improvement, Keller North America, Charlotte, NC, ktkniss@keller-na.com

ABSTRACT

The demand for Rigid Inclusion (RI) systems as a cost-effective solution to support buildings and infrastructure development has grown substantially in North America over the past decade. With this growth, efforts to standardize RI design have become more prevalent. With much of the available literature focusing on design, there is a notable gap in addressing quality control, construction considerations, and use of quality testing during execution.

Recently, industry has increasingly focused attention on Measurement While Drilling (MWD) data as a tool for quality control of RI installation. While MWD data provides valuable insights into potential non-conformance, not all deviations from expected parameters are indicative of performance issues.

To assess whether non-conformance identified by MWD will impact performance, RI specialty contractors can leverage a variety of available tools, including additional geotechnical exploration, field observations, ASIRI Quality Tests (AQTs), and Thermal Integrity Profiling (TIP) tests. By utilizing this expanded toolbox during installation, practitioners can more effectively evaluate the impact of observed non-conformances in the MWD data, potentially reducing the need for rework of previously installed elements. A project in Bethlehem, Pennsylvania serves as an example of these tools in action.

Key Words: Quality Control, Construction Considerations, Ground Improvement, Rigid Inclusions, Testing, ASIRI, Measure While Drilling, MWD

INTRODUCTION

Rigid Inclusion (RI) systems are increasingly used across North America as a cost-effective solution for supporting structures on soft or variable soils. While RI design practices have received a lot of attention in the industry, and the use of Measure While Drilling (MWD) has gained traction in the field of subsurface exploration, less attention has been given in the literature to RI construction quality control and real-time data interpretation. Recent papers such as Rigid Inclusion Quality Control and Performance Verification Using Drilling Parameters: A Streamlined Approach (Nodine, et al. 2024) identify the value of monitoring drill rig installation parameters, specifically, energy, as an indicator of the geotechnical capacity of a single element. Another paper by Kniss and Riddle (2024) provided a broad framework for quality programs specific to RI systems including, but not limited to, the value of MWD for quality control of the RI elements.

For contractors, MWD offers valuable insights into the consistency of means and methods. Considering the inherent variability of construction in soil, assuring consistent drilling parameters creates context for the inevitable non-conformance within the MWD indicators.

 © Deep Foundations Institute 2025

Consequently, indicators of quality need to be tested for site specific conditions (drill rig, operator, soil profile, tooling, etc). Furthermore, deviations from expected values do not always signal performance concerns. Verification testing of RI systems, specifically single element load tests, are discussed in detail by Kniss & Riddle (2024). Additional verification testing options are addressed by Smith et al (2023). The focus of this paper is supplemental verification testing designed to assess non-conformance in MWD data. By supplementing traditional verification testing programs with tools such as ASIRI Quality Tests (AQTs), Thermal Integrity Profiling (TIP), and site-specific observations, RI practitioners can add context to MWD indicators which potentially reduce non-conformances requiring rework and associated costs and schedule delays.

A RI project in Bethlehem, Pennsylvania highlights how these supplemental testing and site-specific observations were applied to evaluate MWD indicators and reduce unnecessary rework.

MEASUREMENT WHILE DRILLING (MWD) INTERPRETATION AND COMMONLY IDENTIFIED NON-CONFORMANCES

MWD systems also known as data acquisition (DAQ) systems are among the available tools that play a central role in evaluating real time consistency and quality during RI installation. These tools have been consistently utilized in the geotechnical construction industry since the early 2000s. Quality programs that use MWD systems in combination with a calibration program can provide insight to the geotechnical profile at each individual element location, and provide relationships between drilling parameters, soil conditions, and element capacity (NeSmith and NeSmith 2012). Common indicators of the soil conditions are penetration rate, crowd force, torque or rotary head pressure, or any other value or derivative value that will show a marked difference through the stratigraphic changes.

The data collected, in combination with a calibration program may be used to establish the acceptance criteria for the termination depth, grouting/concreting procedure and the approximate geotechnical conditions at a given location. The calibration program includes installing either sacrificial or low-risk production RIs at locations with a known subsurface exploration, typically a soil boring or CPT sounding. Kniss and Riddle (2024) state *the purpose of the calibration program is to ensure the soil conditions match expectations, and the appropriate tooling, equipment, and processes are implemented to meet the design requirements*. This work should be performed prior to load testing to adequately assign the acceptance criteria.

Individual logs generated by the MWD systems can be used to identify non-conformances relative to the acceptance criteria established and verified during the calibration and test programs. Examples of typical non-conformances include higher than anticipated penetration rate in the soils near the bottom of the RI, loss of concrete pressure during grouting, and deviations from the established grouting procedure. Higher than anticipated penetration rates in drill rig response near the bottom of the RI indicates the soil conditions don't match the test location and brings to question if the bearing capacity meets project requirements. Loss of concrete pressure and deviations in grouting/concreting procedures may indicate issues with RI geometry and associated compromised structural integrity. Figure 1 shows some MWD logs with these common deviations.

In these cases, the RI designer needs to address the non-conformance. In many cases, installing additional RIs is the most practical and cost-effective approach to remediate the non-conformance. Alternatively, the RI designer may elect to reduce the capacity of the element,

 © Deep Foundations Institute 2025

recommend a repair or re-evaluate specific design cases with non-conforming elements to determine if remediation is required.

Although the installation data in Fig. 1 shows non-conformance from the established acceptance criteria, these non-conformances may not yield performance issues or reductions in geometry for the installed RIs. Accordingly, the RI designer may elect to test the performance of production elements showing a non-conformance. The static axial single-element load test is the most common form of testing on RIs and is typically performed shortly after the RI contractor has mobilized to the site. In the following section, a modified load schedule, specific to production elements, is discussed.

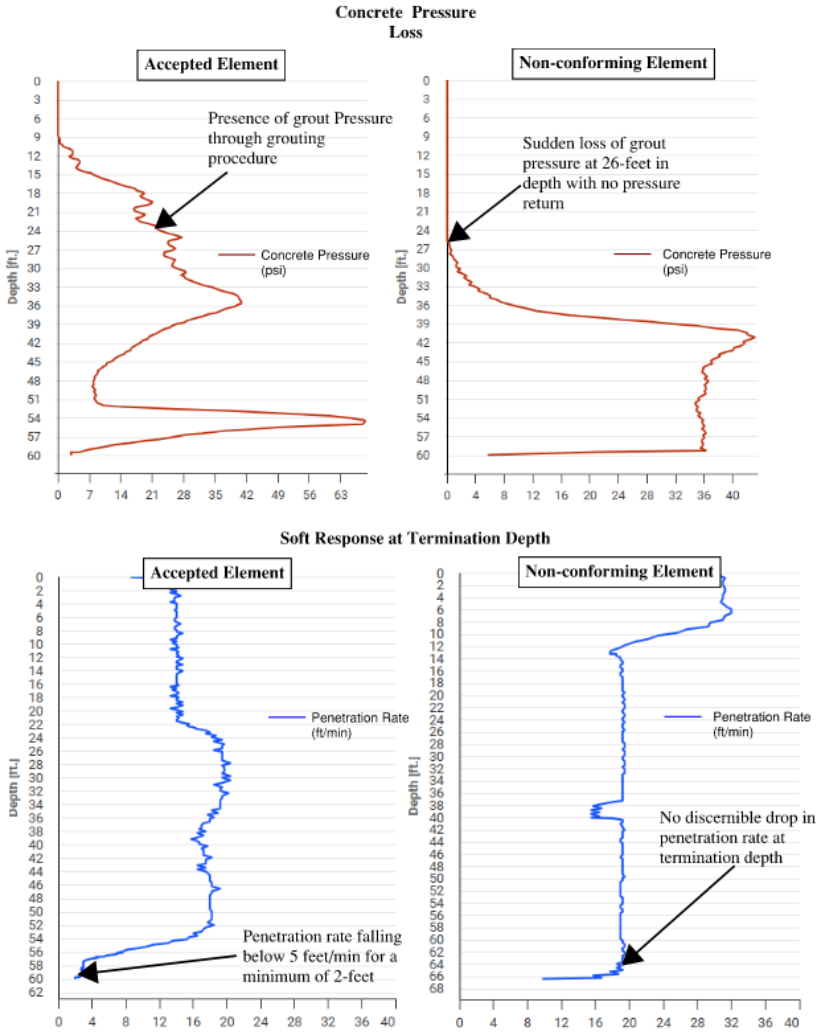


Fig. 1 - MWD logs showing installation data with common non-conformances from established acceptance criteria.

ASIRI QUALITY TESTS (AQTS)

ASIRI refers to the French national research initiative Institut pour la Recherche et l'Expérimentation en Génie civil (IREX, 2012) that produced recommendations for the design, construction and control of rigid inclusion ground improvements. ASIRI Quality Tests (AQTs) are a subset of static axial loading tests on an isolated Rigid Inclusion in compression. ASIRI

 © Deep Foundations Institute 2025

states the Quality Test is specific to rigid inclusions solely serving to reduce settlement and recommends a maximum test load equal to the load inside the rigid inclusion at the neutral plane. Unlike static axial single-element load tests with load schedules intended to verify the geotechnical bearing capacity of the RI, AQT load schedules are intended to verify the performance of rigid inclusions (RIs) that may be integrated into the RI system, i.e. not sacrificial

In the AQT, a load is applied vertically to the head of an individual RI, typically using a jack and reaction frame setup, or utilizing the weight of a piece of equipment (Fig. 2) to act as the reaction frame. The test is conducted incrementally, and displacement is measured at each load step to generate a load-settlement curve, which is then compared to load test data obtained previously. Consequently, AQTs provide a direct, performance-based means to evaluate whether non-conformances identified by installation data effect the load-deflection behavior of the production element in question.



Fig. 2 - Example load test set up for static axial single-element load test.

As a result, the RI designer can incorporate the AQT into the quality plan as a tool to evaluate the quality of RI installation without relying solely on MWD indicators. For example, if a RI terminates shallower than expected or exhibits lower drill pressure at depth, but the AQT confirms adequate performance, the non-conformance may be cleared, and the element may be accepted with confidence. Conversely, if the AQT results are not acceptable, corrective actions and/or replacement of the RI element can be planned and executed before releasing a portion of the site for follow on trades to begin excavation for foundations and installation of the Load Transfer Platform (LTP).

Kniss and Riddle (2024) emphasized the practicality of AQTs through a case history where AQTs were part of a broader quality control program. They noted that while a load test to 150% or 200% of design load provides more data, load schedules requiring test loads beyond the design load can be time-consuming and cost-prohibitive on active construction sites. AQTs offers a more efficient alternative that still yields highly relevant performance data, especially when used to investigate outliers flagged during installation. Furthermore, where a pattern of non-conformance is identified, the RI designer may extrapolate the AQT results from one element as representative of other production elements with a similar non-conformance. For example, if AQT results are acceptable for an element showing loss of grout pressure through a soft soil zone, then the non-conformance of other elements with similar installation data can be cleared without further remediation or testing.

THERMAL INTEGRITY PROFILING (TIP) TESTING

Thermal Integrity Profiling (TIP) is a non-destructive, quick, relatively cost-effective testing method used to evaluate the shape, continuity, and potential defects in cementitious ground improvement elements, such as rigid inclusions. The technique relies on the principle that cement hydration generates heat. By measuring the temperature distribution along the length of the inclusion shortly after installation, TIP can identify variations in RI cross-section and detect

anomalies such as soil contamination, necking, or bulging. TIP is commonly used in quality control programs for deep foundations.

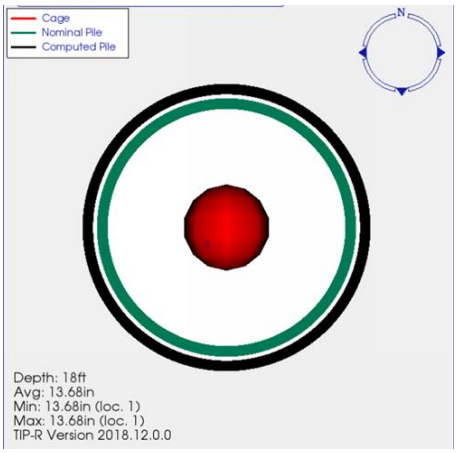


Fig. 3 - TIP results showing central reinforcing bar (Cage), nominal element diameter (green circle) and interpreted element diameter (black circle)

In a typical TIP test (ASTM D7949-14), thermal wires or probes are installed within the RI—either embedded in the reinforcement (if used) or attached to access tubes positioned near the center (Fig. 3). Temperature data is collected over time as the concrete cures, generating a thermal profile that can be compared to the expected shape based on design geometry, material properties and volumes.

TIP is particularly valuable when used in combination with installation data and a calibration program. While installation data may highlight a non-conformance in the grouting procedure or loss of grout pressure during installation, TIP provides post-installation verification that the RI geometry is adequate for the design. For example, a loss in grout pressure in a concentrated length of the element indicates potential necking or unexpected geometry issue caused by the soil conditions. However, if TIP results show consistent temperature profiles and no change in geometry at the depth of concrete pressure loss, the results indicate that the element was successfully constructed despite the non-conformance.

Because TIP wires must be installed while the grout is still fluid, and requires procurement of materials and equipment, using this tool requires more planning than other non-destructive testing methods like Low Strain Integrity Testing. However, the RI designer is likely able to identify sites exhibiting a challenging profile, such as debris within the fill, extremely soft soils, or variable stratigraphy that may complicate installation. In these cases, incorporating TIP into the quality program is an opportunity for early identification of potential quality concerns and provides greater flexibility in evaluating element performance during construction.

CASE STUDY: RIGID INCLUSION PROJECT IN BETHLEHEM, PENNSYLVANIA

Project Overview

The Bethlehem, Pennsylvania RI project was developed to support the construction of a new, cold storage facility adjacent to an existing structure. The proposed cold storage warehouse is approximately 100,000 square feet, including an insulated loading dock occupying about 20,000 square feet. The remaining 80,000 square feet is designed to house a high-density Automated Storage and Racking System (ASRS) reaching heights up to 120 feet.

The ASRS is supported by a 2-foot-thick mat slab designed to distribute significant structural loads. Isolated column foundations in the loading dock were required to achieve a bearing capacity of 4,000 psf, with a live load of 1,650 psf imposed on the mat slab. Site grading was minimal, with little earthwork needed to reach the finished floor elevation.

The project site is located in an area of Pennsylvania known for karst stratigraphy. The general soil profile consisted of an uncontrolled silty sand fill containing slag, concrete, and steel

 © Deep Foundations Institute 2025

obstructions, overlying an approximately 13-feet thick layer of medium to soft clay (Average N value = 5). A medium to stiff silt and medium dense silty sand are present below the soft clay (Average N value = 14). A layer consisting of weathered limestone exists below the silt and sand. Competent rock was not encountered in the subsurface exploration of the site. Due to the karst stratigraphy, groundwater was also not encountered. A soil cross-section interpolated from the subsurface explorations is presented in Fig. 4.

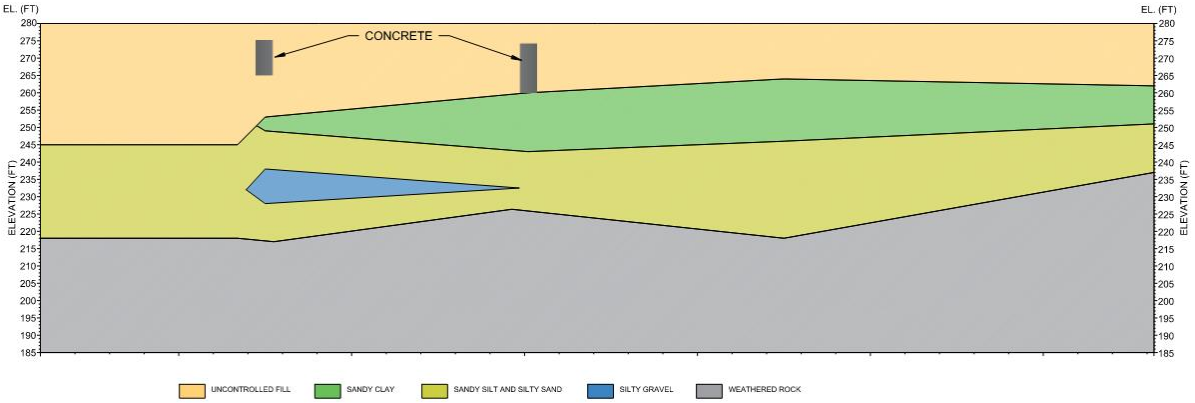


Fig. 4 - Soil Cross-Section for site in Bethlehem, Pennsylvania

Considering the large area load and inherent variability of the uncontrolled fill and soil profile, project settlements were anticipated to exceed the specified project settlement tolerances of 1-inch total settlement, and ½-inch differential settlement. To mitigate settlement, the specialty contractor proposed an RI system consisting of approximately 1,100 elements to support isolated column foundations at the loading dock, exterior wall foundations, and mat slab.

Site challenges

The project site is located on the grounds of a former steel mill that ceased operations in the early 1990s. The facility was demolished in the early 2000s, and the site had remained vacant for over 20 years, with other adjacent cold storage facilities beginning construction in the mid-2000s. Because of the previous site history, obstructions were a major concern for construction and were repeatedly identified in the geotechnical report. The primary obstructions of concern identified within the uncontrolled fill included slag, raw steel and concrete. In addition to the obstructions, remnant voids created by old building structures and poorly placed demolition debris were identified during the site investigation.

Predrilling and Calibration Program

To ensure the RIs would be able to advance through the fill, a rigorous pre-drilling program was implemented. Every individual RI was pre-drilled to a depth of approximately 30-feet with a downhole hammer, prior to mobilization of the RI equipment. Where the predrilling was not able to penetrate the fill, the design called for two replacement RIs offset equally from the planned location – the geometry of which was decided before mobilization to site.

Because of the numerous and widespread obstructions within the fill, the pre-drilling and calibration program had to be rigorously planned prior to mobilization to site. Working with the field crew and superintendent was extremely important, as they could observe the site conditions, and give feedback on where the sacrificial calibration elements should be located successfully.

 © Deep Foundations Institute 2025

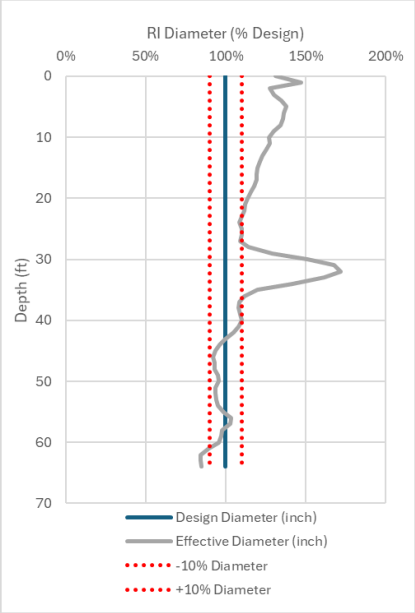


Fig. 5 - TIP test results

During the predrilling program, detailed logs of materials encountered within the fill during the drilling were kept by the field engineer, encompassing site-specific observations. The logs were then reviewed by the RI designer and integrated into the calibration program. For example, large amounts of nested brick were present in one area of the site. The presence of the nested brick introduced the potential for grout loss into void space and, consequently, RI geometry issues. To verify the means and methods were adequate, a TIP wire was installed in a production element located within the area of question to confirm the RI diameter. Concrete pressure and grout volume for the element indicated the geometry was satisfactory. TIP results for this element are shown in Fig. 5.

The back-calculated grout overbreak from the TIP data was in general agreement with the overbreak measured in the field (approximately 30% above neat volume). In the upper 35-feet of the element, TIP data suggests the means and methods produced a larger diameter than neat volume. The increase in diameter generally coincides with the pre-drill depth for this element and the spike in diameter at approximately 30-feet indicates a potential loose zone within the fill (possibly the nested brick). Below 35-feet the interpreted diameter is generally aligned with the design diameter (+/-) 10%. Note: the interpreted diameter dips below 10% of the design diameter near the bottom of the element. This is a typical limitation of the TIP method caused by a larger than average gradient for heat dissipation near the bottom of the element because heat dissipates both radially (horizontally) and vertically (below) the element. Because the installation data showed an adequate volume of grout was pumped in the bottom 4-5 feet of the element, the reduction in the interpreted diameter at the base of the element could safely be ignored.

Non-Conformances Observed During Production

After the predrilling and calibration programs were completed, the RI installer went into production. During production, the RI installer observed non-conformances in some of the installation data. One common non-conformance was the loss of grout pressure at the termination depth of the pre-drill program, and the second was a faster than expected penetration rate in the weathered rock. Examples of MWD logs exhibiting non-conformance are shown in Figs. 3 and 4 below.

During the quality program, each element that exhibited a loss in concrete pressure was individually evaluated to determine potential causes, such as excessive pull speed during grouting, localized soft soil conditions, or the presence of subsurface voids. As part of the quality program, grout return at the ground surface was visually confirmed for each element. The total grout volume was verified using both the MWD log and manual pump records. The target pull speed, calculated based on the pump calibration, was compared to the executed pull speed recorded in the MWD log to ensure it was at or below the target value. Additionally, each element was checked to confirm a minimum overbreak of 10%, meaning the actual grout volume placed was at least 110% of the neat theoretical volume. If any element failed to meet one or more of these criteria, it was replaced with approval

 © Deep Foundations Institute 2025

While MWD logs and site observations suggested elements like the one shown in Figs. 6 had an adequate amount of grout, additional verification was warranted given the subsurface challenges. Although replacement elements could have been used to mitigate non-conformance identified in elements with grout pressure loss, the additional costs and risks associated with pre-drilling, or removing, obstructions to install additional elements were higher than projects without these challenges. As a result, the RI contractor elected to perform AQTs.

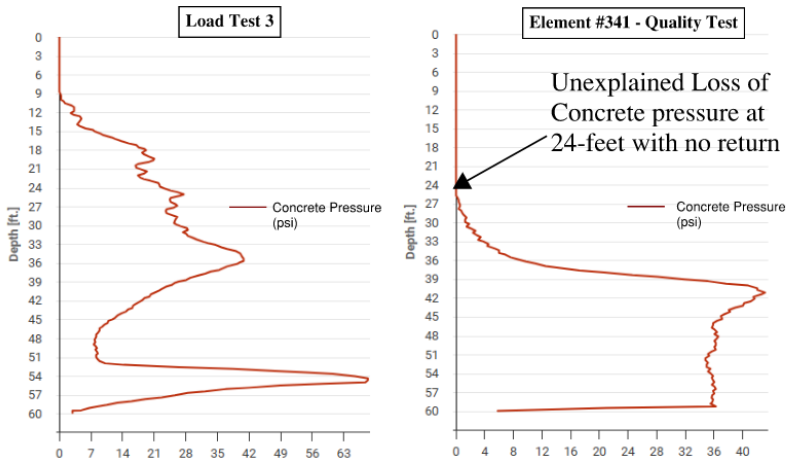


Fig. 6 - MWD log for element #341, showing concrete pressure loss at bottom of pre-drill hole.

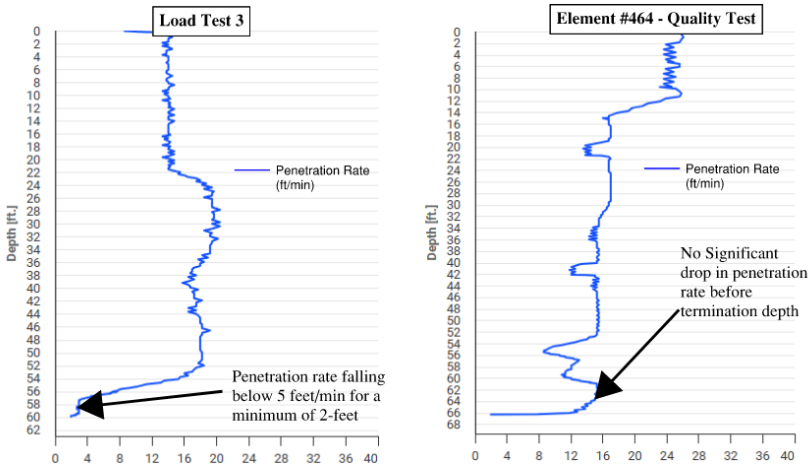


Fig. 7 - MWD log for element #464, showing a penetration rate deviation at termination depth.

AQTs Performed During Production

Element 341 was selected because of the sudden loss in concrete pressure, with no evidence of subsequent concrete pressure above a depth of 24-feet. The maximum test load for the AQT was equal to 109% of the design load. Results of the test in comparison to the single-element load test are displayed below in Fig. 8.

 © Deep Foundations Institute 2025

In addition, for MWD logs indicating higher than expected penetration rate response in the weathered rock, the RI designer wanted to verify the performance of rigid inclusions. Because the purpose of RIs supporting the mat slab are "solely to reduce settlement", the AQT was selected as the best option to clear the non-conformances. The project team selected Element 464 which had the highest penetration rate response of the elements in question (Fig. 7). Element 464 was tested to 100% of the design load.

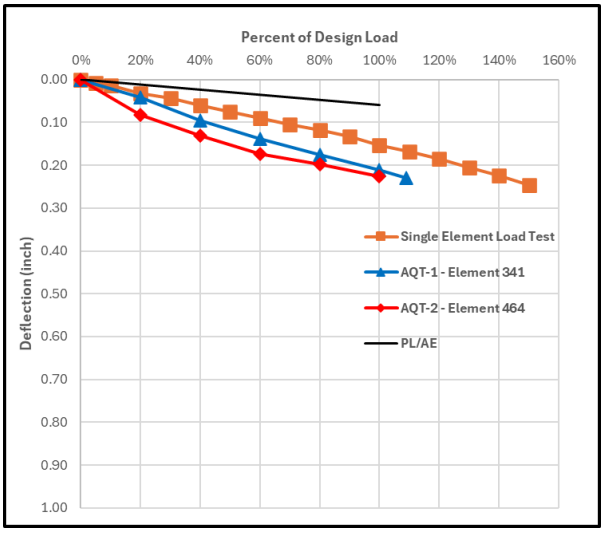


Fig. 8 - Asiri Quality Tests for Element 341 and Element 464 compared to a single-element load test from the test program.

The results of the AQTs are plotted in Fig. 8 along with the calculated elastic deflection of the element (PL/AE) and the results of a representative single-element load test. Each AQT confirmed the elements in question could effectively support the 100% design load without excessive deflection. By selecting the element with the most sudden loss of concrete pressure over the greatest length and the highest penetration rate response within the weathered rock layer, the RI designer was able to extrapolate the test results to other elements with similar installation logs and conclude the non-conformances could be cleared without further remediation or testing. While MWD data indicated non-conformance from the acceptance criteria for these elements, the AQT results confirmed that the non-conformances observed in the installation data did not reflect a meaningful reduction in performance compared to the test element.

By properly planning and executing a calibration program for site specific challenges and performing AQTs on production elements to test MWD identified non-conformances, the project was completed with minimal rework for the contractor and reduced change orders for the client.

SUMMARY AND CONCLUSIONS

As Rigid Inclusion (RI) systems continue to be an effective foundation solution in North America, verifying performance through effective quality control measures has become increasingly important. While Measurement While Drilling (MWD) data offers valuable real-time insight during installation, deviations from acceptance criteria do not inherently indicate compromised performance. This paper highlights how supplemental tools—such as ASIRI Quality Tests (AQTs) and Thermal Integrity Profiling (TIP)—can be used in conjunction with MWD data to assess RI performance more accurately and reduce unnecessary rework.

 © Deep Foundations Institute 2025

The Bethlehem, Pennsylvania project demonstrates how a proactive quality program that includes a site specific calibration program, and strategic quality testing during production can address construction challenges in complex or uncertain subsurface conditions. By leveraging AQTs and TIP, the project team confirmed that non-conformances observed in MWD logs did not yield meaningful changes in the performance of individual elements. As a result, the RI contractor used the additional information to reduce rework, ultimately saving time and money.

The proactive approach to quality control presented herein emphasizes the importance of interpreting MWD data within the broader context of site conditions and available testing methods. As owners and consultants push the use of RI systems into more challenging site conditions, adopting a toolbox mentality toward quality programs—rather than relying on a single data stream—will enhance the reliability, efficiency, and resilience of future ground improvement projects.

ACKNOWLEDGEMENTS

The Bethlehem project was successfully completed through the efforts of Keller North America, Inc., and Primus Builders, Inc. Special thanks go to the Keller field crews, field supervision, field engineers, design engineers, and project management team for their dedication, collaboration and attention to detail in the completion of a safe and successful job.

The authors would also like to express their appreciation to Emily Dean and Drew Deterling of Keller North America for their assistance in the preparation of this paper.

REFERENCES

ASTM International. (2014). ASTM D7949 – Standard test methods for thermal integrity profiling of concrete deep foundations (Withdrawn 2023). ASTM International.

IREX (Institut pour la Recherche et l'Expérimentation en Génie civil). (2012). Recommendations of the French national project on rigid inclusions ASIRI. Operation of the Civil and Urban Engineering Network, France.

Kniss, K., & Riddle, C. (2024, November). Quality programs for rigid inclusions and load transfer platforms. In Proceedings of the 34th Central Pennsylvania Geotechnical Conference.

NeSmith, W. M. (2006, February). Anatomy of a data acquisition system for drilled displacement piles. In Proceedings of GeoCongress 2006: Geotechnical Engineering in the Information Technology Age, Atlanta, GA. American Society of Civil Engineers.

Nodine, M., Englert, C., Gómez, J., & Mallon, A. (2024, October). Rigid inclusion quality control and performance verification using drilling parameters: A streamlined approach. In Proceedings of the 49th Deep Foundations Institute Annual Conference on Deep Foundations, Aurora, CO.

 © Deep Foundations Institute 2025

FOUNDATION DESIGN AND OSTERBERG CELL PILE LOAD TESTING IN BRISBANE, AUSTRALIA

David Cunliffe, EDG Consulting Pty Ltd, Brisbane, QLD, Australia, david.cunliffe@edgconsult.com.au
Daniel Schutt, A-Squared Studio Engineers Pty Ltd, Brisbane, QLD, Australia, daniel.schutt@a2-studio.com

ABSTRACT

As part of Dexus's Waterfront Brisbane project, two new high-rise towers and a deep underground basement are to be constructed. The towers are 234m (49 stories) and 208m (43 stories) above ground. The project site is located in the central business district of Brisbane, Australia, and is situated immediately at the riverbank of the Brisbane River. The basement will be supported by a reinforced concrete diaphragm wall, propped by the permanent basement slabs, and the building will be supported by barrettes and bored piles.

The site is located predominantly within soft Quaternary age fine grained Alluvium, underlain by weathered rock of the Devonian age, Neranleigh Fernvale Beds. The Neranleigh Fernvale Beds predominantly comprise Phyllite and Greywacke and are typically of high to very high strength (UCS = 30MPa to 60MPa or approximately 4,500 to 9,000 Psi) beyond approximately 5m to 10m below the top of the unit.

EDG Consulting was engaged by Principal Contractor John Holland to carry out geotechnical analysis of the diaphragm wall and foundations to inform detailed design as well as being engaged to provide construction phase services. Foundation design parameters were initially selected based on our interpretation of the site geotechnical conditions and consideration of several empirically based methods available in the literature, however, were verified via interpretation of an Osterberg cell load test carried out on site.

This paper presents a case study that describes the adopted foundation design methods along with the interpretation of the Osterberg cell test. Details are presented on the development of the Engineering Geological Model, the interpretation of geotechnical parameters, pile design, 3D finite element modelling of the full construction sequence, details of pile installation and a summary of predicted pile performance compared with Osterberg cell test data. The results from the Osterberg cell test verified the design parameters and typically agreed well with empirically derived relationships for pile shaft and end bearing performance.

Keywords: Osterberg Cell, Foundations, Diaphragm Wall.

INTRODUCTION

Dexus's Waterfront Brisbane project is located in Brisbane's Central Business District (CBD) adjacent to the Brisbane River. The project involves construction of a shared three-level underground basement, two high rise towers and podium structure. The basement design incorporates a permanent under-drainage system in-lieu of a deep hydrostatic slab. The retention system comprises a diaphragm wall terminating into the underlying rock mass to support groundwater cut-off requirements. The super-structure is supported by a combination of barrettes and large diameter piles socketed into rock.

EDG Consulting was engaged by John Holland to provide geotechnical services to help inform design of the basement retention system and building foundations, which included development of an Engineering Geological Model (EGM), geotechnical analyses relating to seepage, foundations and retention system, as

 © Deep Foundations Institute 2025

well as construction phase services. The project site is located on the eastern edge of Brisbane CBD, immediately adjacent to Brisbane River. The site location is shown in Fig. 1.

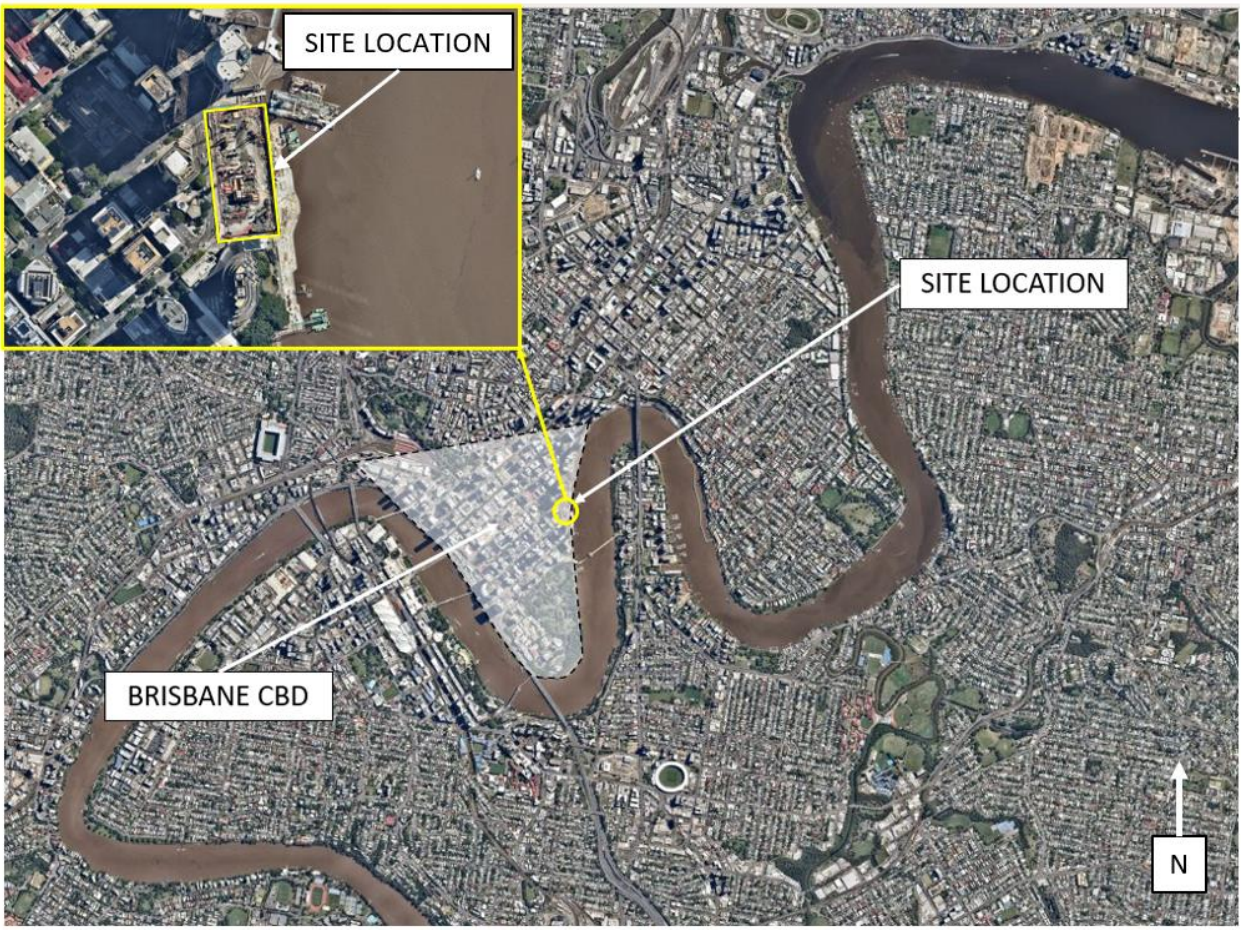


Fig. 1 – Site Location

THE DEVELOPMENT AND CONSTRUCTION SEQUENCE

The near surface geotechnical conditions generally comprised low strength soils, which were unsuitable to support heavy construction equipment including piling rigs, hydrofraise cutters and cranes. Therefore, significant ground improvement works comprising mass soil mixing and deep soil mixing were performed as part of the enabling works to improve the strength and stiffness characteristics of the superficial deposits and create a stable temporary working platform.

The proposed towers are 234m (49 stories) and 208m (43 stories) above ground. Construction of the north tower adopted a '*top-down bottom-up'* sequence whereby installation of the north tower foundations was carried out from ground level, to allow construction of the north tower core to progress concurrently with the basement excavation. The south tower adopted a conventional bottom-up sequence whereby the south tower core foundations were completed following completion of excavation of the basement and prior to advancing the core structure above.

The construction sequence is summarised below:

 © Deep Foundations Institute 2025

- **Pre-existing Condition:** A three-level building existed on the site prior to commencement of the works, including a single-level basement extending down approximately 2m below ground level.
- **Demolition:** Demolition of the pre-existing building is carried out both from the land and from barges positioned in the Brisbane River. The site level following demolition is at approximate RL +2mAHD.
- **Installation of temporary works:** A steel "*Combi-wall*" is driven until refusal into the ground along the river side (eastern side) of the site and approximately halfway along the northern and southern sides. The existing ground is then improved via Mass Soil Mixing (MSM) that extends to 6m depth. In addition to the MSM, Deep Soil Mixing (DSM) columns of 2.2m in diameter are installed adjacent to the Combi-wall. A geogrid reinforced piling platform comprising 300mm of pavement base quality coarse grained fill is constructed over the full area of the site.
- **Installation of D-wall and barrettes:** The diaphragm wall and barrette panels are installed using a combination of grab excavators (within the soil strength materials) and hydrofraise cutters (within the rock strength materials). The excavations are supported with a polymer support fluid.
- **Establish Jump Form and advance north tower:** Following completion of the barrettes that support the north core, the jump form is established allowing the north core to progress from ground level (i.e. in advance of the basement
- **Piling:** Piles are installed to support the tower and basement columns as well as the south tower core. The south tower core piles are tied together via a pile cap constructed below the lowest basement level and therefore those piles are only reinforced below the lowest basement level.
- **Excavate basement:** The basement is excavated in stages with lateral support applied to the diaphragm wall from the permanent building slabs (i.e. the permanent basement slabs are installed as the excavation progresses). A temporary access hole exists adjacent to the western wall, which is required for removal of excavation spoil and therefore requires the installation of two rows of temporary pre-stressed anchors to provide lateral wall support until the permanent slabs are installed in the access hole and the temporary anchors are de-stressed.
- **Advance South tower and construct podium levels:** Following completion of the excavation works, a pile cap is constructed to connect all south tower core piles, which allows the south tower to progress and the basement and podium levels to be completed.

ENGINEERING GEOLOGICAL MODEL

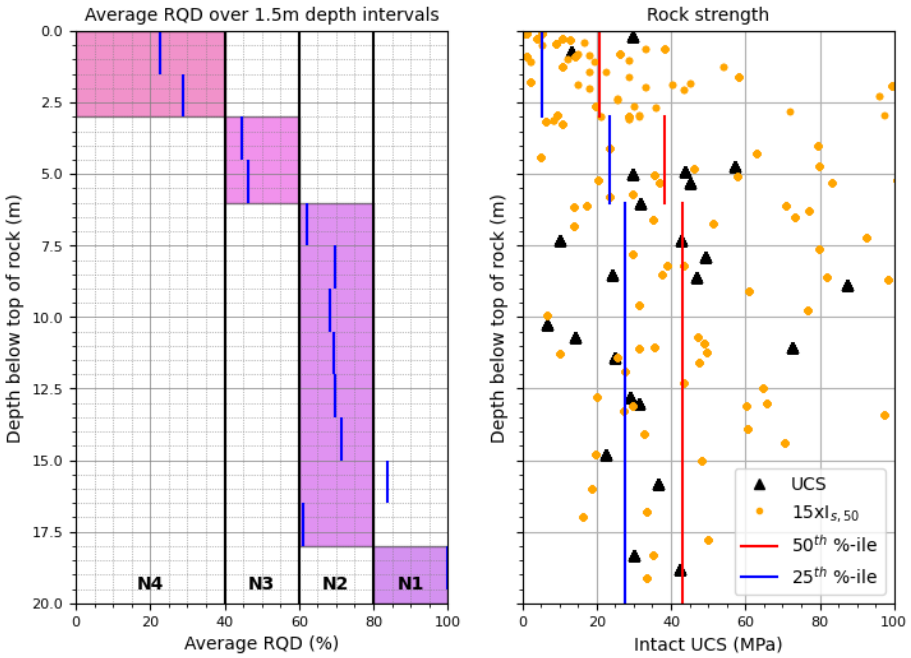
An Engineering Geological Model (EGM) was developed for the project, which was informed by historical and recent boreholes and CPTs, along with topographical and bathymetric surveys. The EGM identified several soil and rock material units and assessed their distribution. The EGM was supported by the development of a 3D geological model of the site. The 3D ground model was provided to the client and incorporated into project wide BIM infrastructure for coordination purposes. The 3D ground model was also used to infer the founding levels of foundations and retention elements in advance of construction, and to inform various geotechnical and hydrogeological analyses.

The site is underlain by rock of the Neranleigh-Fernvale Beds (NFB), which is overlain by Pleistocene age alluvium and in turn Holocene age alluvium. The NFB rock units comprise Phyllite and Greywacke and were formed approximately 360 million years ago due to deposition of sediments off the edge of a broad continental shelf. Over tens of millions of years, the materials were lithified, then folded, faulted, recrystallised and uplifted to form much of the coastal land surface of south-east Queensland. Over time, various stress fields developed within the rocks underlying Brisbane through episodic volcanism and mild compression, leading to the formation of a foliation as the distinct fabric within the rock, and well-developed sets of joints. The rock material units are distinctly foliated which generally dips between approximately 30° and 70° sub-horizontal, towards the northeast.

 © Deep Foundations Institute 2025

The NFB materials were sub-divided into four main units, N4 to N1, which represent increasing rock mass quality. Figure 2 shows the distribution of the average value of the rock quality designation (RQD) and uniaxial compressive strength (UCS) with depth below the rock surface. UCS has been established from laboratory testing and from point load index tests, on the basis that the UCS is approximately equal to the point load strength index (Is50) multiplied by a factor of 15 (UCS ≈ 15 x Is50). Figure 2 indicates that the average RQD and UCS increases with depth, and it is expected that the rock mass properties with regards to strength and stiffness reflect this trend. Table 1 summarises the typical descriptions and key characteristics of the NFB subunits.

The geotechnical design of critical foundations (e.g., barrettes and large diameter single piles supporting heavily loaded tower cores and columns) targeted the N2 (or better) rock mass for rock socketing and termination. The characteristics of the N2 rock mass, including relatively high strength and stiffness, widely spaced defects and observed consistency of the rock core were consistent with an appropriate founding stratum for heavily loaded foundations. For minor foundations (e.g., piles supporting basement columns) the N3 (or better) rock mass materials were considered to be suitable for termination.



Note – RQD ranges are shown in purple. Average RQD is shown in blue.

Fig. 2 – Rock Unit Strength and RQD Summary

Table 1. Rock Unit Summary

Sub-unit	RQD (%)	Typical Intact Compressive Strength MPa (Psi)	Typical Description
N4	<40	0.6 to 6 (87 to 870)	Defect spacing typically 30 - 50mm. Defects are observed to affect a wide range of rock substance strengths, which indicates that the presence of defects may be due to stress relief. Poor rock mass properties.
N3	40-60	10 to 20 (1,450 to 2,900)	Defect spacing ranging typically between 50 – 100mm.
N2	60-80	20 to 60 (2,900 to 8,702)	Medium to high strength, defects typically spaced >100mm.
N1	>80	20 to 60 (2,900 to 29,000)	High to very high strength phyllite. Defects typically spaced > 300mm.

 © Deep Foundations Institute 2025

Soil units identified at the site comprised Fill, Holocene age alluvium, Pleistocene age alluvium and Residual Soil derived from weathered NFB rock. Fill was encountered at most onshore locations with a typical thickness of 1 to 3m, composed of firm to stiff clay or loose to medium dense sand and gravel. The River Mud (RM) consists of very soft clay with interbedded loose sands, thickening from west to east to over 6m near the eastern diaphragm wall.

Holocene alluvium (QHa), primarily comprising high plasticity clay with interbedded sand, ranges from 10m to 15m thick. A desiccated crust was evident above Reduced Level (RL) 0m, while deeper clays remain soft to firm. The sandy subunit QHs is prevalent between 6m to 12m depth, typically loose to medium dense and thicker to the south.

Pleistocene alluvium (QPa) underlies the QHa and thickens to 12m in the southern portion of the site. This unit is generally composed of stiff to very stiff brown clay with occasional sand lenses.

Due to the generally poor consistency of the soil deposits and the magnitude of the structural loads, soils were not suitable as a founding medium. Their impact on the geotechnical requirements of the project primarily related to their effect on the design of the temporary working platform, permanent retention and groundwater seepage conditions. A 2D cross section showing the typical distribution of the project geotechnical units is shown on Fig. 3.

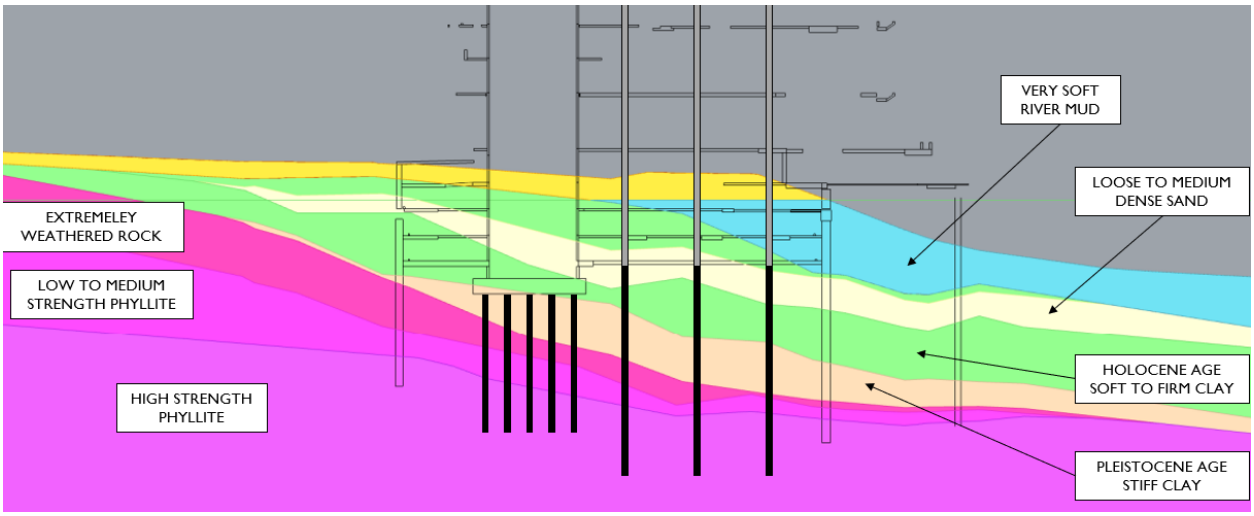


Fig. 3 – Typical Geological Cross Section

SEEPAGE ANALYSIS

EDG carried out a detailed steady-state seepage assessment using MODFLOW6 to inform the design of the diaphragm wall and drainage system. The analysis developed a 3D groundwater flow model, which was based on the distribution of soil and rock units as per the EGM.

Material hydraulic conductivities were selected for each of the material units based on our interpretation of the available in-situ permeability (Packer) tests, along with a comparison against available data from nearby similar projects.

Six model runs were developed, including a base case and five sensitivity models, which varied hydraulic conductivity, presence of shear zones, and D-wall embedment depth. The model boundary conditions

 © Deep Foundations Institute 2025

were adjusted to promote either inflow or drawdown by either allowing groundwater recharge on all four sides of the excavation (i.e. to promote inflow), or by limiting groundwater recharge to the side of the excavation adjacent to the Brisbane River only (i.e. to promote drawdown). In all models, the base of the model was closed to flow. Fig. 4 shows the 3D seepage model and a 2D cross section showing the mesh discretisation.

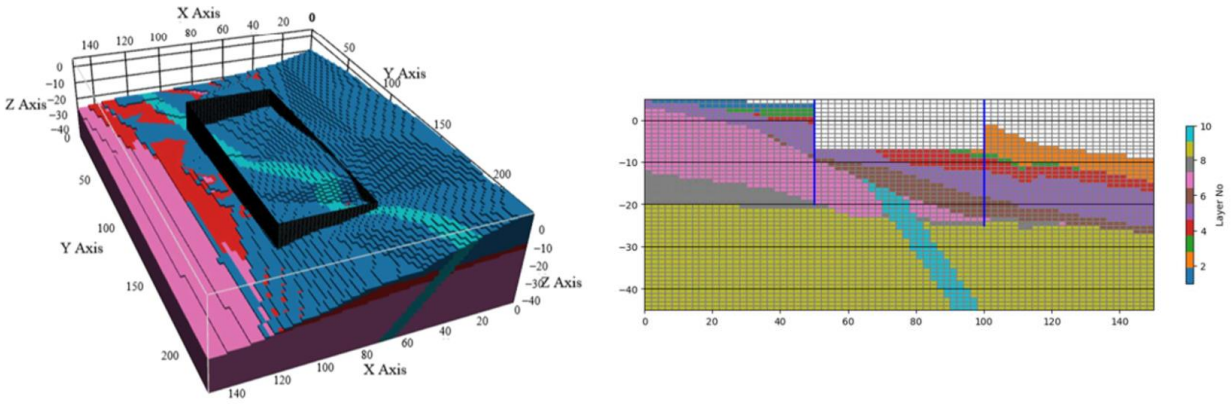


Fig. 4 – Seepage Model

FOUNDATIONS AND RETENTION SYSTEM

Piled Foundations

Pile foundations were selected to support both individual tower and basement columns, as well as the South Tower Core group. Bored pile diameters ranging between 1,200mm and 2,700mm were designed, based on the required geotechnical capacities (lateral and vertical) and the structural capacity.

Ultimate geotechnical resistance under axial load was assessed in accordance with AS2159:2009 using shaft and base resistance parameters developed for each geological unit. The foundation design was based on the piling contractor achieving clean, rough interfaces free from smear or debris, on the basis that the contractor would roughen the pile sidewalls with drilling buckets with teeth that protrude outwards towards the side wall, as well as using cleaning buckets at the pile base. Concrete would be placed via Tremie, which assisted to displace debris from the pile base. Geotechnical reduction factors (φ_g) were selected in accordance with AS2159:2009 of 0.56 to 0.64 depending on pile redundancy.

Pile settlement predictions were conducted using the commercially available software packages Group, developed by Ensoft, and Plaxis 3D. The calculations estimated tower column settlements to be between 20mm and 30mm under working loads. For the south tower pile group settlements were calculated to be up to 20mm and pile cap rotation was assessed to be within serviceability limits.

Spring stiffnesses for structural models were assessed from the predicted axial and lateral performance of the piles. Axial spring stiffness ranged from 1500 MN/m for 1200mm piles to 2000 MN/m for 1500mm piles. Lateral spring stiffnesses were adjusted using reduction factors to account for pile interaction effects. Under Ultimate Limit State (ULS) conditions the analysis demonstrated that the individual piles and the piles within south tower pile group were within their ultimate capacities in all cases.

Barrette Foundations

Barrette foundations were selected to support the north tower core. Barrettes were desired over pile foundations due to the "*top-down bottom-up"* construction approach, which allowed the north tower to progress in advance of the basement excavation.

 © Deep Foundations Institute 2025

The barrette panels were either 800mm and 1000mm wide with typical lengths of either 2.5m (one-bite) or up to 6.2m (three-bite). The barrettes are tied together at ground level by a deep capping beam element, which promotes load distribution and redundancy. Individual barrettes are subjected to a complex loading comprising significant axial, moment and shear forces. Detailed 3D numerical analyses of the north tower core barrettes were carried out using Plaxis 3D to assess their performance under service and ultimate load cases.

Diaphragm Wall

The Diaphragm walls (D-wall) that support the excavation and basement in the permanent case were modelled under staged construction primarily using Plaxis 3D, supported by some additional calculations using Plaxis 2D and Wallap, developed by Geosolve, for verification purposes. In the Plaxis 3D model, each D-wall panel was explicitly modelled to allow assessment of actions within each panel and to provide an allowance for construction joints longitudinally along the wall.

Structural actions and wall deflections were extracted from the model that related to the full construction staging, including a Q100 flood condition. The outcomes were relied upon by the structural engineer in the permanent design.

Holistic Substructure Analyses

A key outcome of the analysis of the foundations and retention system was to assess the interaction effects relating to the barrettes, piles and diaphragm wall panels. A particular focus was on the interaction between lateral loading of the retention system and the north tower core foundations. To facilitate this, a full substructure model was developed in Plaxis 3D which considered the holistic interaction between the retention system, barrette core and piled foundations and basement slabs.

The model considered the complete staged construction of the two towers from enabling works through to the final permanent condition. Pile foundations were modelled as embedded beam elements, whilst barrette cores and diaphragm walls were modelled using plates with interface elements to capture interaction with soil and rock units (Fig. 5).

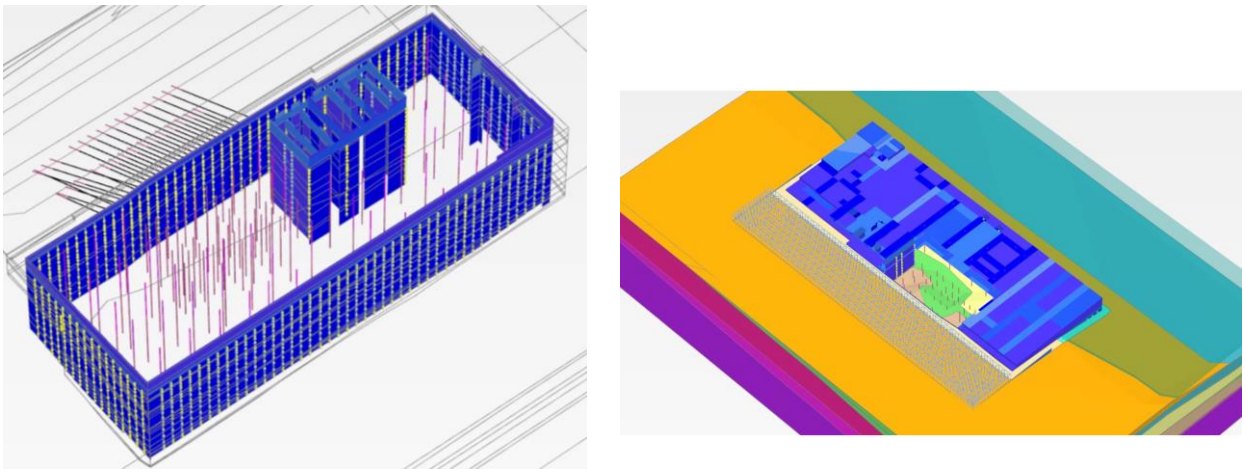


Fig. 5 – Holistic Sub-structure Model

The holistic 3D substructure model enabled identification of performance outcomes that arose due to interaction between various elements, which would have been difficult to conceptualize from the

 © Deep Foundations Institute 2025

assessment of individual components or sub-systems alone. In addition, it provided a means to assess the effect of interactions on structural actions, to inform the structural design of the foundation and retention elements.

OSTERBERG CELL TEST

A 1,200mm diameter bored pile was constructed and tested using the Osterberg Cell (O-Cell) method to assess pile design parameters and performance. The test pile was constructed under polymer slurry to a toe elevation of approximate RL -27m Australian Height Datum (AHD), therefore being approximately 29m long. The arrangement of the O-Cell comprised five 430mm diameter cells, which were placed approximately 600mm above the pile toe as shown in Fig. 6.

The test was conducted by Fugro Australia from 17 to 19 October 2024. The gross load applied reached 32.37MN in both the upward and downward directions, which was at the limit of the O-Cell test configuration. The maximum axial displacements at the top and bottom of the O-Cell were 25.17 mm and 11.51 mm, respectively. Instrumentation included vibrating wire strain gauges at nine levels, extensometers, toe displacement gauges, and digital survey monitoring of pile head movement. Data was recorded at 60-second intervals and processed to generate strain, displacement, and equivalent top load curves.



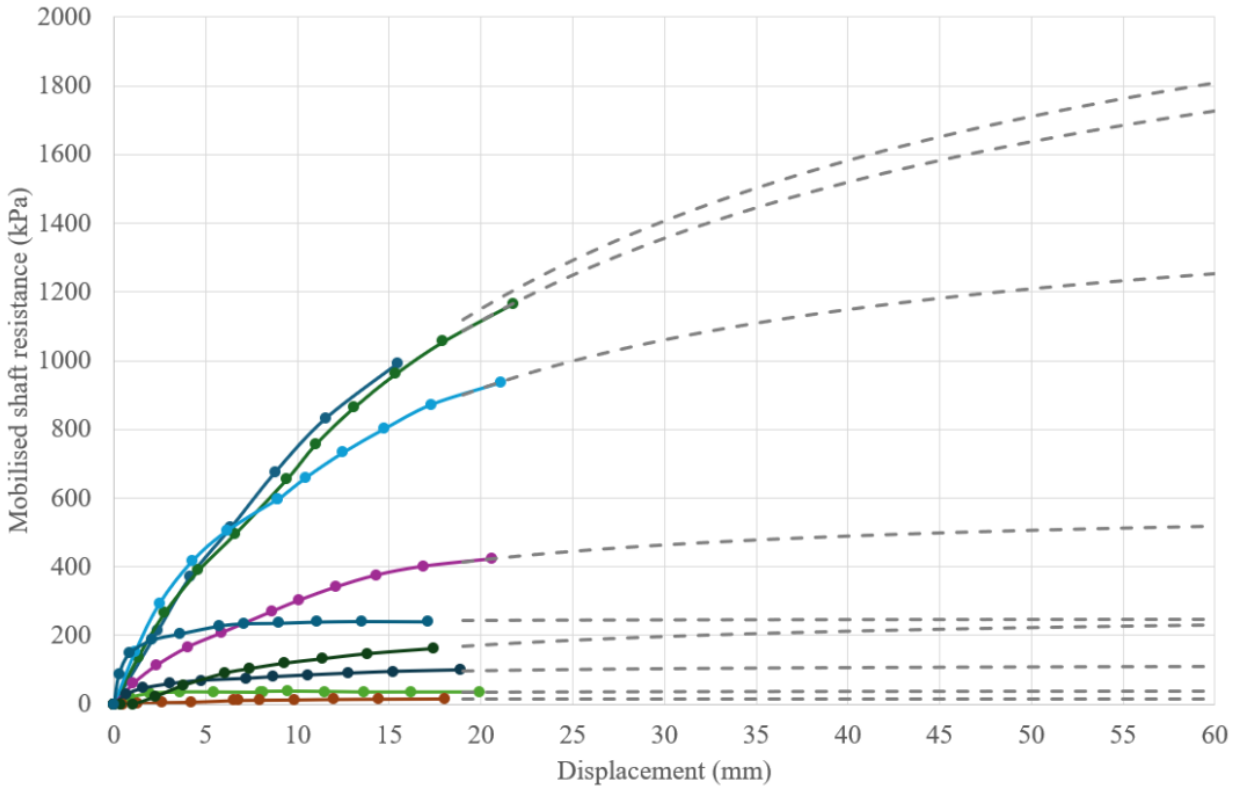
Fig. 6 – O-Cell Instrumentation

Interpretation of the strain gauge data allowed a detailed assessment of mobilized shaft and base resistance. Four strain gauges were positioned at each nominated level within the pile cage. It was noted the strain gauges at each level did not always record uniform strains, which therefore required careful judgement to interpret the representative strain at each level. The mobilized skin friction on the upper shaft reached the limiting test value of approximately 32MN with average mobilized unit side shear up to approximately 1.2MPa. The mobilized end bearing was observed to reach a peak of approximately 30MN, with an interpreted mobilized end bearing base pressure of approximately 27MPa at 11mm displacement.

Ultimate values of skin friction for the project material units described previously were assessed via an extrapolation based on fitting a hyperbolic function to the test data. The extrapolated ultimate shaft

 © Deep Foundations Institute 2025

resistance values are shown in Fig. 7, and are generally consistent with those estimated from typical empirical approaches, when using a lower-quartile estimate of the UCS of the Neranleigh-Fernvale Beds.



Strain Gauge	TOE-SG2	SG 2-3	SG 3-4	SG 4-5	SG 5-6	SG 6-7	SG 7-8	SG 8-9	SG 9-HEAD
Material Unit	N2	N2	N3	N4	QPc	Fill	QHc	MSM	MSM
Interpreted Ultimate Skin Friction (kPa)	1,800	1,725	1,250	500	40	100	20	230	250
Interpreted Ultimate Skin Friction (Psi)	261	250	181	72	6	15	3	33	36

Notes: QPc and QHc refer to Pleistocene and Holocene Age Clay, respectively. MSM refers to Mass Soil Mixing. Fill refers to a flowable cementitious fill that was placed to maintain hole stability following pile sidewall instability.

Fig. 7 – Interpreted Ultimate Skin Friction

Figure 8 shows the recorded pile response below the O-Cell compared with the predicted pile end bearing response using the simplified semi-empirical pile socket analysis approach proposed by Williams, Johnston & Donald (after Johnston, 2020). The simplified method defines the pile base response based on selected ultimate shaft resistance (refer Fig. 7), and rock mass stiffness of the socket.

From the backfit of the pile base response, the ultimate end-bearing resistance was estimated to be approximately 65MPa, which is consistent with the range of values suggested by Pells (1999), and was in excess of the value of ultimate pile end bearing adopted in the design. A rock mass stiffness of 5GPa was estimated from the backfitting process, which is consistent with the range of rock mass stiffness estimated from recent tunnel convergence data in the Neranleigh-Fernvale beds (Buchanan, 2022).

 © Deep Foundations Institute 2025

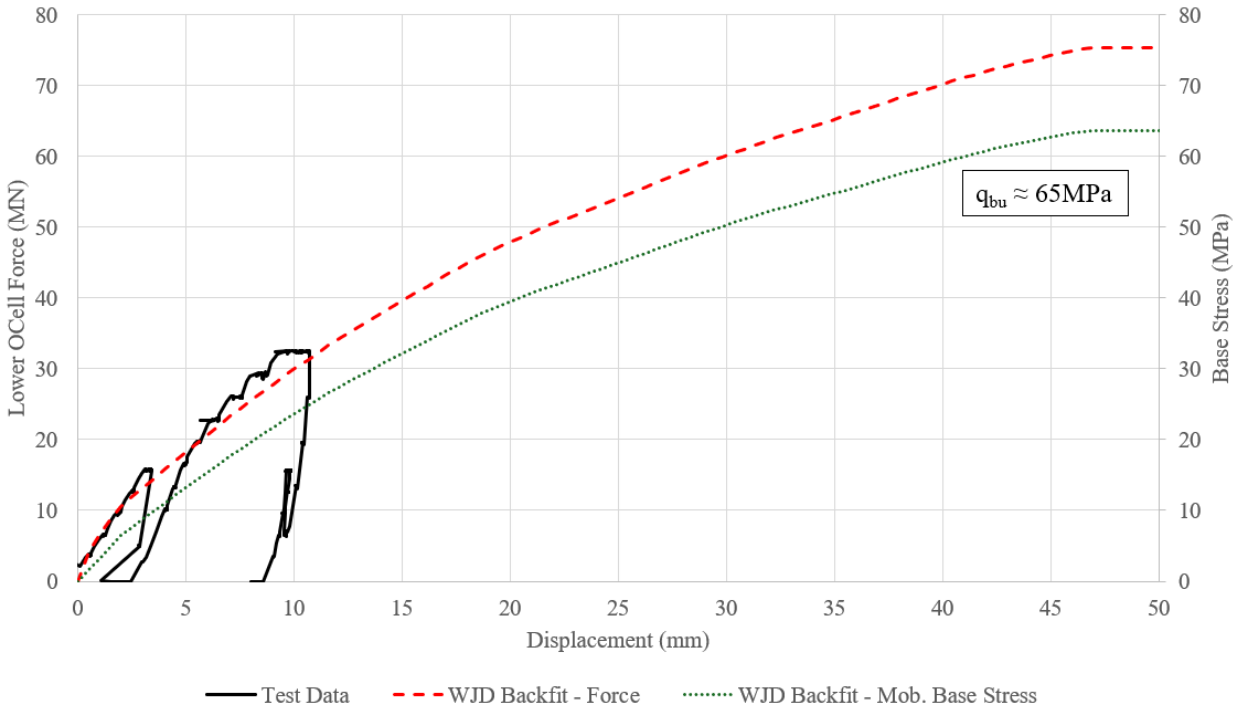


Fig. 8 – Comparison of Pile Base Response Against Empirical Methods

CONCLUSION

This paper has presented a case study describing the design and construction of a deep basement supported by a diaphragm wall and deep foundations comprising barrettes and piles. Geotechnical design parameters were verified on-site via an Osterberg cell test.

It is noted that the O-Cell test was unable to reach ultimate values of skin friction at every strain gauge level and therefore the recorded data was extrapolated to interpret ultimate values. The values of pile skin friction and end bearing interpreted from the O-Cell test gave good agreement with our selected design parameters and therefore helped to verify the foundation designs.

Based on our experience, even with a lot of instrumentation and redundancy, interpretation of O-Cell test data may not be a simple process and assessment of key pile response parameters may not be unique. We therefore recommend that O-Cell tests, particularly those in complex ground conditions, are performed well in advance of production to enable adequate time to synthesize and interpret the data.

REFERENCES

Buchanan, H., 2022. Back-analysis of rock mass modulus and horizontal stress ratio at Roma Street Station, Brisbane, Australia. *Journal of the Australian & New Zealand Tunnelling Societies*, pp.25-35.

Johnston, I.W., 2020. Revisiting methods for the design of rock socketed piles. *Journal of Geotechnical and Geoenvironmental Engineering*, *146*(12), p.04020144.

Pells, P.J.N., 1999, January. State of practice for the design of socketed piles in rock. In *Proc., 8th Australia New Zealand Conf. on Geomechanics, Australian Geomechanics Society, Barton, ACT, Australia* (pp. 307-327).

 © Deep Foundations Institute 2025

INVESTIGATION OF LIMIT EQUILIBRIUM AND FINITE ELEMENT METHODS FOR GROUND-ANCHORED SLOPES

Farnyuh Menq, Ensoft Inc., Austin, TX, USA, (512) 244-6464, f.menq@ensoftinc.com
Daqing Xu, Ensoft Inc., Austin, TX, USA, (512) 244-6464, daqing@ensoftinc.com
Luis Vasquez, Ensoft Inc., Austin, TX, USA, (512) 244-6464, gonzalo@ensoftinc.com
Shin-Tower Wang, Ensoft Inc., Austin, TX, USA, (512) 244-6464, stw@ensoftinc.com

ABSTRACT

Ground anchors are commonly used to stabilize natural slopes. The Limit Equilibrium Method (LEM) is often employed to evaluate the safety factors of the slope before and after the addition of ground anchors. However, applying a large concentrated load on the surface of the slope can cause convergence issues in the rigorous methods and cause erroneous results in simplified methods. To address these issues, Carpenter (1986) developed the Load Distribution Method. This method distributes the force throughout the potential slip surface based on Flamant's (1886) stress distribution model in a semi-infinite elastic half-space. Using the Strength Reduction Finite Element Method (SRFEM), we can evaluate the accuracy of the Load Distribution Method. A hypothetical slope with one row of ground anchors is analyzed using both LEM with the Load Distribution Method and SRFEM. Results from the modeled slope show that safety factors obtained from SRFEM are close to those obtained from LEM when a slip surface is well developed in the slope. Hence, the Load Distribution Method can provide a good approximation under those conditions. However, LEM can't model soil-structure interactions. SRFEM is needed in determining the maximum tieback force limited by a failure surface developed from soil-structure interactions.

Keywords: Limit Equilibrium Method (LEM), load distribution method, Strength Reduction Finite Element Method (SRFEM), ground anchor, tieback, slope stability

INTRODUCTION

Ground anchors (tiebacks) are commonly used for landslide stabilization and support in ground excavations. Compared to piles, constructions of ground anchors generally require smaller machines; hence, ground anchors are more cost-effective and easier to build (Lee et al., 2010). Where failure surfaces are steep, the loading demands of ground anchors are often determined from apparent earth pressure diagrams. However, loading demands of ground anchors calculated from the apparent earth pressure diagrams can underestimate the required force to stabilize a slope to reach a target Safety Factor (SF). Limit Equilibrium Method (LEM) analyses are recommended to evaluate ground anchor and wall loads for anchored slopes and landslide stabilization systems (FHWA-IF-99-015).

Applying a large concentrated tieback force on a slope surface can cause convergence issues in the rigorous slice methods (e.g., Spencer's method) and can cause erroneous results in simplified slice methods (e.g., the Simplified Bishop method). Carpenter (1985) developed the Load Distribution Method to mitigate these issues. This method distributes the force on the potential slip surface based on Flamant's (1886) stress distribution model in a semi-infinite elastic half-space. According to Flamant (1886), for a semi-infinite mass subjected to a concentrated load, P, the distribution of stresses in the radial direction can be calculated as:

$$\sigma_r = \frac{2\,P\cos(\theta)}{\pi\,R} \qquad [1]$$

where: σ_r = radial stress at a point of interest, P = concentrated load applied to an elastic half-space, R = distance to the point of interest, θ = angle formed by the line of action of the concentrated load and the

 © Deep Foundations Institute 2025

line connecting the point of application of the load on the boundary surface and the point of interest. If the trial slip surface intersects the tendon portion of a row of tiebacks, the tieback force is converted into distributed normal stress on the trial failure surface, as shown in **Fig. 1**. This method is first implemented in the computer programs STABL4 and PCSTABL4 by Carpenter (Carpenter 1985 and Carpenter 2017).

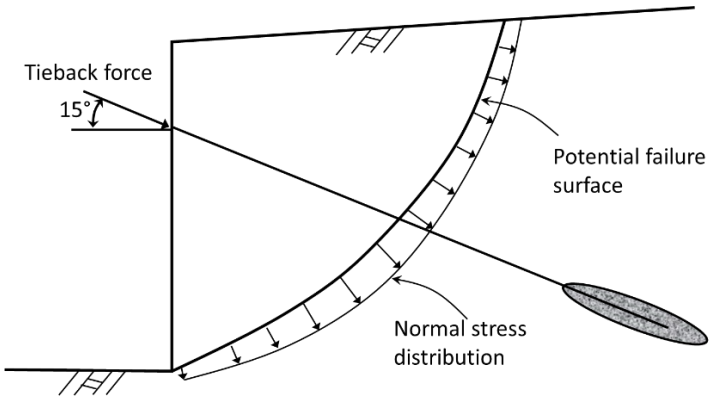


Fig. 1. Distribution of normal stress to the potential failure surface

Using the strength reduction algorithm, finite element analyses can provide a safety factor in slope stability analyses. The main benefit of the Strength Reduction Finite Element Method (SRFEM) for slope stability analyses is that the critical slip surface is formed naturally as soil strength reduces at each step (Griffiths and Lane, 1999). The use of finite element analysis in routine geotechnical practice can be harder to justify, due to the significant amount of time needed to construct the model. However, there are several user-friendly SRFEM packages for slope stability analyses available in both open-source and commercial software (e.g., ABAQUS, ADONIS, EnFEM, MIDAS, OpenSees, OptumG2, Plaxis, and RS2). In addition, some Finite Element Method software provides integrated environments or import functions to facilitate SRFEM analyses from models built for LEM (e.g., MIDAS, EnFEM, and RS2). These new developments reduce the time and labor needed for SRFEM analyses.

This study utilized a commercial program, EnFEM, to examine the accuracy of the Load Distribution Method of a hypothetical slope with one row of ground anchors. Results from LEM analyses are conducted using EnSlope, formerly STABLPro, which utilizes the methodologies from Carpenter (1985 and 2017).

STRENGTH REDUCTION FINITE ELEMENT METHOD (SRFEM) FOR SLOPE STABILITY ANALYSES

Safety factors can be defined by load capacity or by strength capacity in finite element analyses. To define safety factors by load capacity, loadings (e.g., gravity, surface loads) are increased by steps until failure occurs to determine the loading capacity. Safety factors are defined as the ratio between the loading capacity and the loading demand. This is commonly used in bearing capacity analyses. On the other hand, safety factors are defined by strength capacity in slope stability analyses (Griffiths and Lane, 1999). The strengths of soils are reduced in steps until failure is reached; hence, it is named the Strength Reduction Finite Element Method (SRFEM). Safety factors, SF, in SRFEM are defined as:

$$\begin{aligned} SF &= \text{Available strength / Strength at Failure} \\ &= \tan \phi' / \tan \phi'_{mobilized} \\ &= c' / c'_{mobilized} \end{aligned} \quad [2]$$

 © Deep Foundations Institute 2025

There are two stages in an SRFEM analysis. In the first stage, loadings (e.g., gravity force, surcharges) are applied in steps to the slope. In the second stage, the strength of the soil is reduced in steps until a convergence can't be obtained. In practice, users define the range of safety factors to be analyzed. Loadings are applied to the slope with soil strength calculated from the lowest safety factor entered for the analyses. The lowest safety factor should be lower than the actual safety factor of the slope. Otherwise, a solution can't be found in the first stage, and the analysis will stop without an output of the safety factor. After completion of the first stage, the strength of the soil is reduced in steps in the second stage. Failure is defined as the algorithm cannot converge within an iteration ceiling, and/or as displacements rapidly increase in the mesh. This criterion is commonly adopted in the literature (Griffiths and Lane 1999, Griffiths and Marquez, 2007, Cheng et al., 2007, Tschuchnigg et al., 2015a & 2015b, and Theinat et al., 2024). However, the iteration ceiling and the limit of nodal displacements are not well defined. The linear elastic-perfectly plastic constitutive model with a Mohr-Coulomb failure criterion is the commonly utilized failure criterion in SRFEM. Advanced constitutive models (e.g., hardening soil, hardening soil small strain, and soft soil models) can better model soil behaviors. However, these advanced models are not available in LEM. For better comparisons between SRFEM and LEM, the Mohr-Coulomb model is used in this study.

Input parameters

The Mohr-Coulomb model is defined by six parameters. These parameters are: (1) friction angle, ϕ', (2) cohesion, c', (3) unit weight, γ, (4) Young's modulus, E, (5) Poisson's ratio, υ, and (6) dilation angle, ψ. Only the first three parameters (friction angle, cohesion, and unit weight) are required in LEM. In finite element analyses, Young's modulus and Poisson's ratio define the deformations in the linear range, and the dilation angle defines the flow rate of the soil element after yielding. Influences of the values of Young's modulus, Poisson's ratio, dilation angle, and element size on SRFEM are discussed below.

Young's modulus and Poisson's ratio

The selected Young's modulus and Poisson's ratio affect the computed deformations before failure. These two parameters have limited influence on the calculated safety factor once all elements along the slip surface have yielded. Cheng et al. (2007) investigate the influence of the soil elastic modulus with four different geometry settings. In each setting, a slope of uniform strength is separated into two regions of two different stiffnesses. The stiffness in the stiffer zone (soil 1) is assumed to be 1.4×10^5 kPa, and the stiffness in the less stiff zone (soil 2) is 1.4×10^2 kPa. The elastic moduli of soils 1 and 2 are then interchanged to determine the effect of Young's modulus. The resulting safety factors before and after the interchange of the stiffness vary by less than 2.5%. It is interesting to note that the safety factor is determined at the critical state when a slip surface has formed. All elements along the slip surface have yielded, and Young's modulus typically has minimal influence. However, as demonstrated later in this article, if tiebacks are added to the model, soil stiffness can alter the resulting tension requirements of the tiebacks. The nominal values of Young's modulus (10^5 kPa) and Poisson's ratios (0.3) suggested by Griffiths and Lane (1999) are adopted in this study.

Dilation Angle

The dilation angle (ψ) defines plastic deformations of soil elements after yielding. If the dilation angle (ψ) is equal to the friction angle (ϕ'), the flow rule is associated. If $\psi \neq \phi'$, the flow rule is non-associated. Failure mechanisms generated by finite elements with the associated flow rule are expected to be closer to critical slip surfaces predicted by LEM than those from non-associated flow rules (Griffiths and Lane, 1999, and Tschuchnigg et al., 2015a). However, the dilation angle also defines the volume changes of the yielded elements. A positive dilation angle will be accompanied by a volume increase. Similarly, a negative dilation angle will be accompanied by a volume decrease. For most soils with a friction angle

greater than 0, the volume changes are much smaller than those calculated from the associated flow rule assumption. The associated volume changes can increase the strength of an element if the element is confined. Slope stability analysis is relatively unconfined, so the choice of dilation angle is less critical than that in a bearing capacity analysis; hence, Griffiths and Lane (1999) suggested using a compromised value of $\psi = 0$.

Although a smaller dilatancy angle can better model the volume change of soil elements, it can result in numerical instability with no clear indication of the failure mechanism. The solution of the governing equations is not unique for a non-associated flow rule. (Tschuchnigg et al., 2015a & 2015b, Nordal, 2008, Krabbenhoft et al., 2012). Using the Plaxis program, Tschuchnigg et al. (2015a) demonstrate the failure mechanisms of a 45° slope of a uniform soil ($\phi' = 45°$ and $c' = 6$ kPa) oscillate with increasing steps of calculation when ψ is selected to be equal to or less than 10°. This oscillation is not observed when ψ is selected to be equal to or greater than 15°. Results from Tschuchnigg et al. (2015a and 2015b) also show that oscillations do not occur if a coarser element size is used, and oscillations are more pronounced if smaller element sizes are utilized. The resulting safety factors from the associated flow rule are higher than those from the non-associated flow rule. Cheng et al. (2007) also show that safety factors from the associate flow rule are higher. **Fig. 2** shows a comparison between safety factors from these two studies. Both studies utilized the Morgenstern-Price method in LEM analyses. As shown in the figure, results from SRFEM are close to those from LEM, and safety factors from the associated flow rule ($\psi = \phi'$) are higher than those from the non-associated flow rule ($\psi = 0$).

Comparison between LEM and SRFEM is better shown as the difference between safety factors obtained from SRFEM and safety factors obtained from LEM, as shown in **Fig. 3**. The differences between the safety factors from LEM and SRFEM range from – 0.2 to + 0.2. This range is relatively wide for slope stability analyses. Comparisons from other studies, including a special case with a thin weak layer presented by Cheng et al. (2007) and results presented by Griffiths and Lane (1999) and Burman et al. (2015), are added in **Fig. 3**. The special case presented by Cheng et al. (2007) contains a thin weak layer ($\phi' = 25°$ and $c' = 0$). Due to this thin-

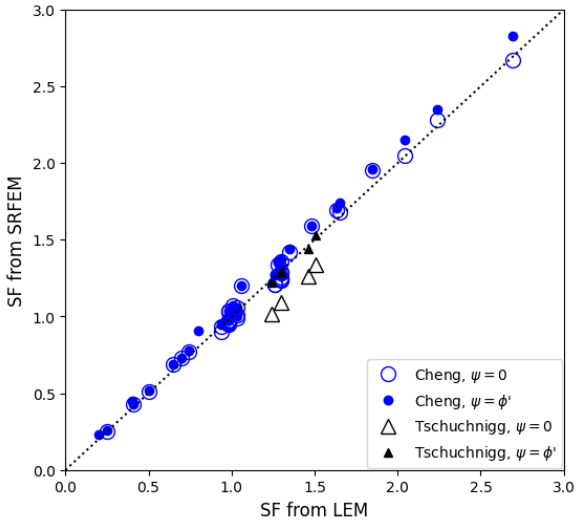


Fig. 2. SF from SRFEM vs. SF from LEM

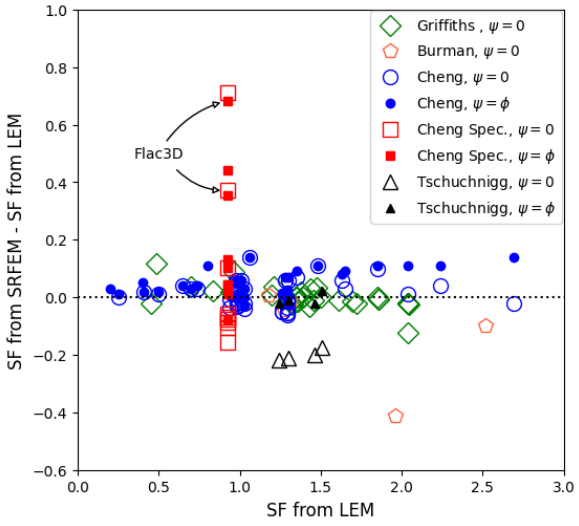


Fig. 3. Difference between SF from SRFEM and SF from LEM vs. SF from LEM

weak layer, the resulting safety factors show much more variation; hence, 3 different commercial programs are utilized by Cheng et al. (2007) to determine the factors of safety. The range of the safety factor increased in this special case to be between -0.4 and 0.8. It should be noted that in the results from

 © Deep Foundations Institute 2025

Flac3D, safety factors from the associated flow rule are lower than those from the non-associated flow rule ($\psi = 0$). Cheng et al. (2007) did not discuss the cause of this reverse trend. Both Griffiths and Lane (1999) and Burman et al. (2015) only presented results for $\psi = 0$. It is interesting to note that the differences between the safety factors from LEM and SRFEM from Griffiths and Lane (1999) are smaller. This might be due to the relatively larger size elements used in their study. Overall, the differences between the safety factors from LEM and SRFEM are mostly within -0.2 and +0.2.

Element size

Ashford and Sitar (2001) show that an element height of H/10 (H: slope height) commonly used in FEM analyses of embankment slopes is adequate. However, they also indicate that an element height of H/32 is necessary to accurately determine tensile stresses within the vicinity of the slope. Theinat et al. (2004) utilize element sizes as small as 5 times the median particle size (~H/700) for soil elements in contact with the retaining wall. Tschuchnigg et al. (2015a) conducted sensitivity studies on element size and showed that an element size of H/25 provides an adequate solution. **Fig. 4** shows the results of four element sizes from a hypothetical 45° slope of a uniform soil layer modeled in this study. The color gradients shown in the figure represent the equivalent magnitude of plastic strain. Parameters of the soil layer are listed as Model A in **Table 1**. The element widths of the four element sizes are 1.0 m, 0.6 m, 0.3 m, and 0.1 m, which are approximately H/11, H/19, H/38, and H/113, respectively. The quadratic triangular element with six nodes and three straight edges (T6) available in EnFEM is utilized in this study. It should be noted that a slightly larger element size is used in regions away from the slip surface in the model with the small-size element to reduce computational time. As shown in **Fig. 4**, the slip surface is more refined using a smaller element size. The resulting safety factor reduces from 0.993 for the extra-large size elements to 0.967 for the small-size elements.

Table 1. Soil and tieback parameters utilized in SRFEM

	Tieback		Soil					
Model	Diameter (inch/cm)	Prestress (kN)	c' (kN)	ϕ' (°)	γ (kN/m^3)	E (kPa)	υ	Ψ (°)
A	None	N/A	4.79	28	19.63	1.0E+05	0.3	28
B	1.0/2.54	0	4.79	28	19.63	1.0E+05	0.3	28
C	1.0/2.54	0	4.79	28	19.63	1.0E+05	0.3	0
D	1.0/2.54	450	4.79	28	19.63	1.0E+05	0.3	28
E	1.0/2.54	0	4.79	28	19.63	1.0E+04	0.3	28
F	2.5/6.35	0	4.79	28	19.63	1.0E+05	0.3	28

The safety factors from the simplified Bishop method and Spencer's method are 0.974 and 0.969, respectively. Both the simplified Bishop method and Spencer's method yield the same critical slip surface. As shown in **Fig. 4**, the difference between the results from the regular-size elements and those from the small-size elements is negligible. The regular-size elements are used in the remainder of this study.

If the non-associated flow rule ($\psi = 0$) is used, convergence issues are encountered in all four element sizes. The safety factor from the last converged step ranges between 0.913 and 0.806 from an element size of 1 m and 0.1m, respectively. Results show no fully developed slip surface from element sizes of 0.6 m, 0.3 m, and 0.1 m at the last converged step. These safety factors from the non-associated flow rule can't be considered as the safety factor of the slope. These results illustrate the difficulty of determining the safety factor based on the last converged step.

 © Deep Foundations Institute 2025

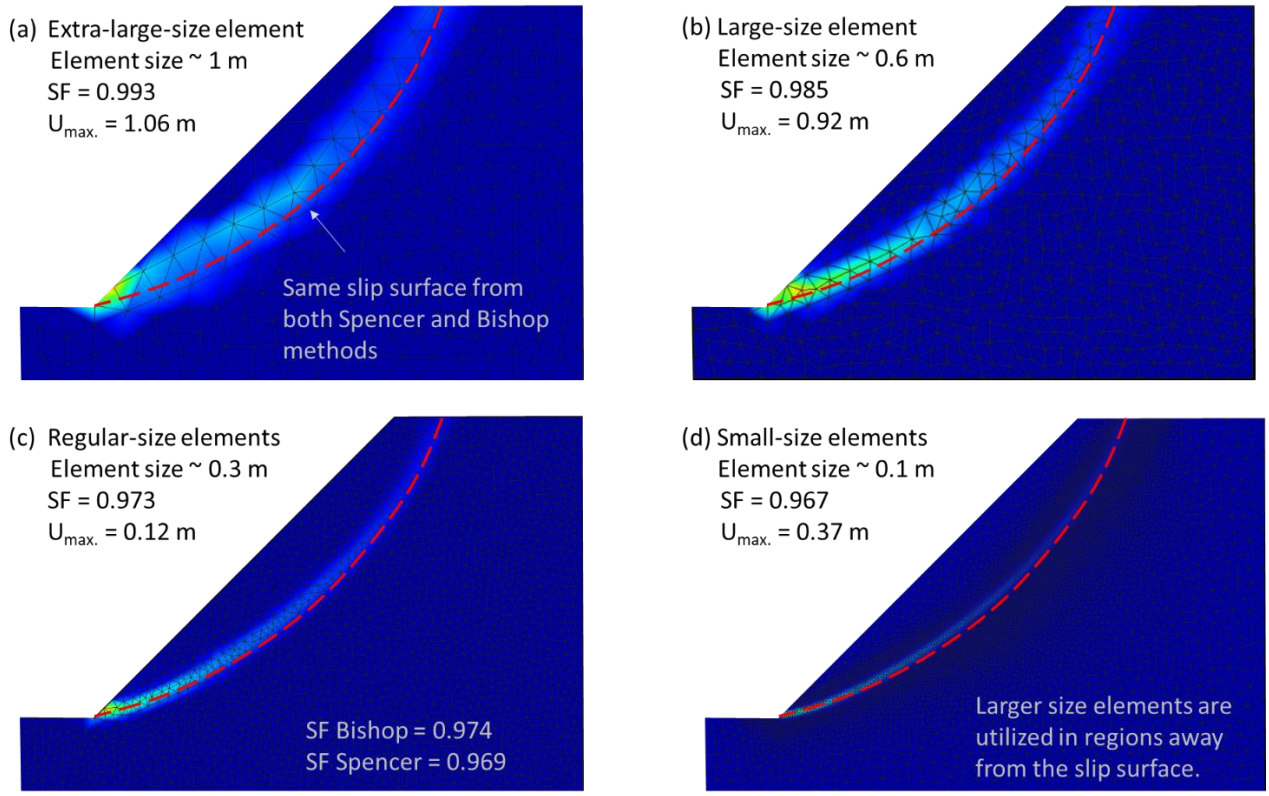


Fig. 4. Results from different element sizes (Model A)

SRFEM SLOPE STABILITY ANALYSES OF A TIEBACK SLOPE

A single row of tiebacks is added to the mid-height of the model slope in the previous example, as shown in **Fig. 5**. The tiebacks have a spacing of 10 m and a 15° inclination. The unbonded length of the tieback is 12 m with a 5 m long anchor. A relatively longer anchor length is selected to avoid pull-out failure of the tieback anchor. A 1-inch (2.54 cm) diameter steel bar with an ultimate strength of 567 kN and a 2.5-inch (6.35cm) diameter with an ultimate strength of 3,457 kN are modeled in this study. The Young's modulus of the tieback is 200 GPa. A concrete facing is added to the surface of the slope using 0.2 m thick beam elements. Young's modulus of the concrete facing is 25 GPa. Tie (fixed) connections are used between soil elements and wall elements, and between soil elements and the tieback anchor.

Five different settings of the soil and tieback parameters are modeled in this study. These 5 settings are listed as Model B to Model F in **Table 1**. In all five settings, the range of the safety factor search is set to be between 1.0 and 2.0 for the strength reduction stage of the SRFEM analyses, and soil strength at a safety factor of 1 is used in stage 1. The gravity load is applied to the soil mass in stage 1. Structure elements, including the wall, the tieback, and the tieback anchor, are activated in the first stage. However, if a prestress is applied to the tieback, a pair of point loads (representing the tension force) is applied to the endpoints of the tieback on the concrete facing and on the anchor. The tieback element is connected after stage 1 is completed. In the second stage, the strength parameters of the soil are reduced by steps until the algorithm cannot converge.

 © Deep Foundations Institute 2025

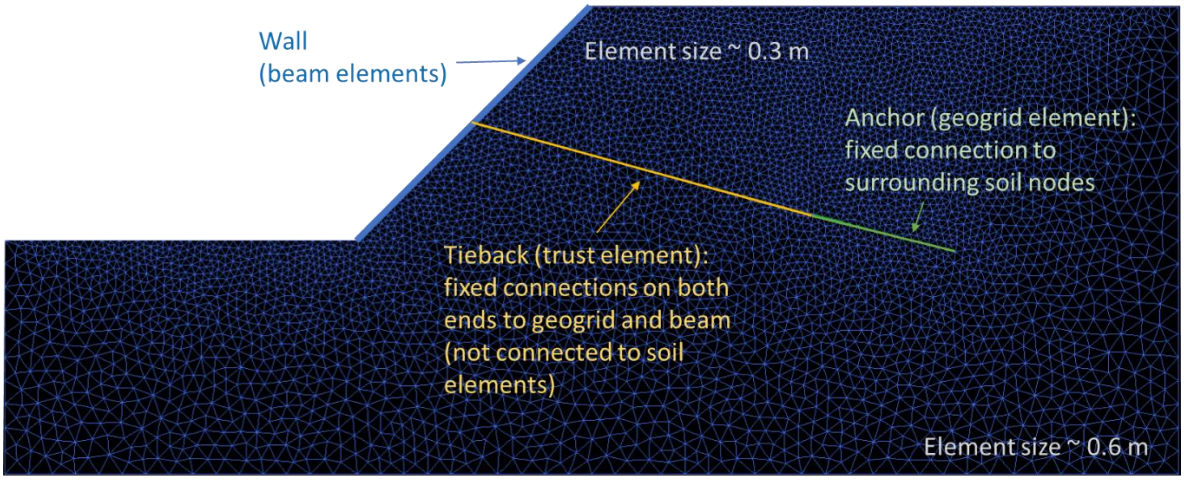


Fig. 5. Mesh plot of the slope with a single row of tiebacks

Stage 2 SRFEM analyses of the anchored slope from Model B contain 72 steps. The equivalent magnitudes of plastic strains from two of these 72 steps are presented in **Fig. 6**. There is no prestress in the tieback. **Fig. 6a** shows the resulting equivalent magnitude of plastic strain at a safety factor of 1.192. In this step, shear strength has been reduced by a factor of 1.192. Since the model slope without the tieback has a safety factor of less than 1.0 (~0.97), tension in the tieback is needed to maintain stability. The resulting tension calculated from EnFEM is 472 kN. Similarly, **Fig. 6b** shows the resulting equivalent magnitude of plastic strain at a safety factor of 1.604. In this step, the resulting tension is 1,554 kN. Applying tension values of 472 and 1,554 kN in EnSlope (a LEM program), the resulting safety factors from the Simplified Bishop method are 1.175 and 1.591, respectively, which are very close to those from SRFEM. It is interesting to note in **Fig. 6** that the volume of the sliding mass increases with decreasing soil strength as the safety factor increases.

Figure 7 shows the safety factors versus the resulting tension in the tieback from SRFEM. The calculated safety factors using both the Simplified Bishop method and Spencer's method are shown in the figure. Results from SRFEM using the non-associated flow rule (Model C) are also presented in **Fig. 7**. The difficulty associated with the non-associated flow rule reported by Tschuchnigg et al. (2015a) is again encountered in this study. The resulting tension of the last converged solution is 1,554 kN from Model B ($\psi = \phi'$) versus 1,261 kN from Model C ($\psi = 0$). However, converged results from both models are close to each other and are slightly higher than those from the Simplified Bishop method. The resulting safety factors from Spencer's method are generally lower than those from the Simplified Bishop method. It should be noted that the ultimate strength of a 1-inch (2.54 cm) steel bar is 567 kN. Data points with a tieback force greater than 567 kN have no physical meaning. However, these data points are shown in the figure to showcase how close the resulting safety factors from LEM and SRFEM are. For ease of discussion, the safety factor versus tieback force curve from the Simplified Bishop method is referred to as the Bishop curve hereafter.

Comparisons between safety factors are better presented by the difference between the two methods. As shown in **Fig. 8**, safety factors obtained from the SRFEM (Model B, $\psi = \phi'$) are only 0.004 to 0.021 higher than those from the Simplified Bishop method. The differences are comparable to the difference between Spencer's method and the Simplified Bishop method, which varies between -0.027 and +0.014. These differences are about 10 times smaller than those from slopes without tiebacks shown in **Fig. 3**. This is due to the differences in how safety factors are defined between an unreinforced slope and a tieback-reinforced slope. During the strength reduction stage of the SRFEM analyses, soil strengths reduce as safety factors increase in each incremental step. For an unreinforced slope, deformations

 © Deep Foundations Institute 2025

increase until a converged solution is found in each step. Soil strengths are further reduced in the following step until the algorithm cannot converge. The safety factor associated with the last converged step or the safety factor associated with a given deformation is defined as the safety factor of the unreinforced slope. As discussed before, it can be difficult to determine the safety factor based on the last converged step. On the other hand, for a slope reinforced with tiebacks, both deformations and the tieback force increase as safety factors increase in each step. The resulting tieback force is the force required for stability at each given safety factor. This process is reversed in LEM, where the safety factor from a trial slip surface is calculated with a given tieback force. The good agreement between results from SRFEM and LEM shows that the Load Distribution Method provides good accuracy in determining safety factors for Model B.

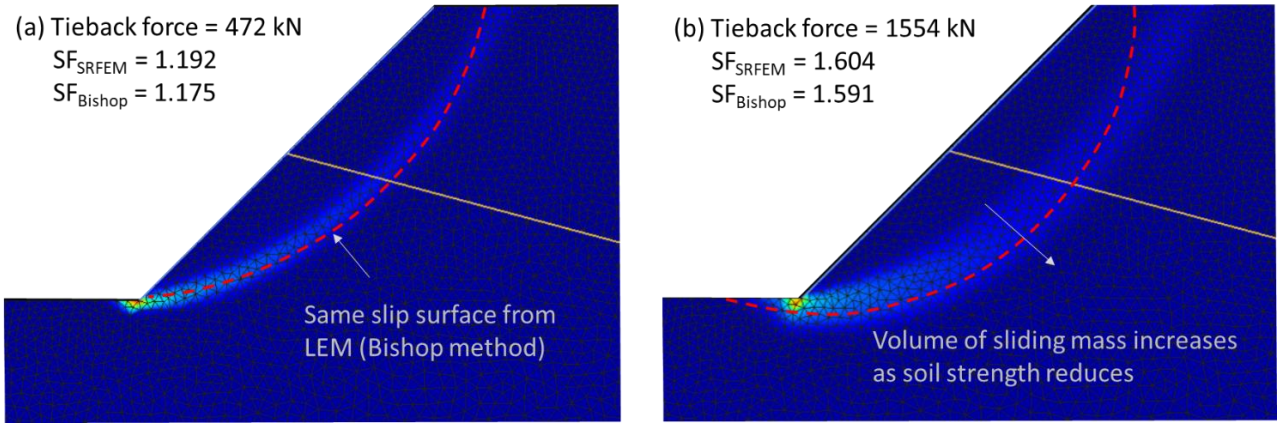


Fig. 6. Tieback force and SF from two different steps in Stage 2 SRFEM analyses (Model B)

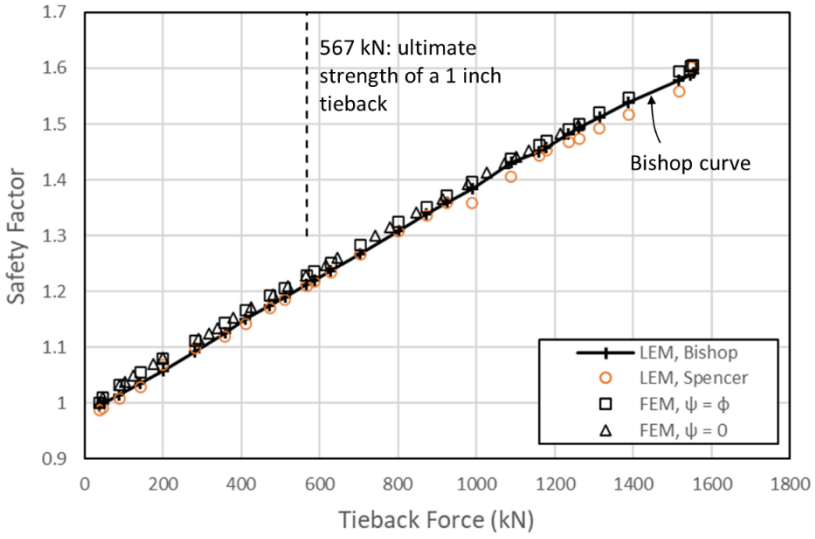


Fig. 7. Safety factors versus resulting tension from Model B

 © Deep Foundations Institute 2025

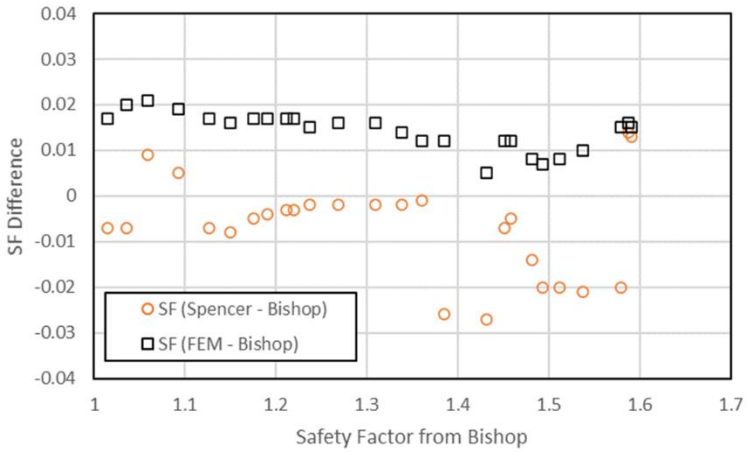


Fig. 8. Safety factor difference between LEM and SRFEM from Model B

Results from Models D and E are presented in **Fig. 9**. A prestress of 450 kN is added to the tieback in Model D, and soil stiffness is reduced to 10% from 10^5 kPa to 10^4 kPa in Model E. As shown in the figure, results from Model D are generally close to the Bishop curve, except those points circled in a red dashed line. In Model D, a prestress of 450 kN is applied during the first stage; hence, the tieback force at SF = 1 is 450 kN. As soil strength reduces with increasing safety factors, no additional force from the tieback is needed to maintain stability until the safety factor rises close to the Bishop curve. Once a slip surface is developed, the safety factor versus tieback force relationship follows the Bishop curve. **Fig. 10a** and **Fig. 10b** show the equivalent magnitude of plastic strain from the second step of stage 2 from Models B and D, respectively. As shown in the figure, a well-developed slip surface is shown in the result from Model B but not in that from Model D. Similarly, due to the relatively lower stiffness of soil in Model E, there is a prestress incurred in the tiebacks during the first stage of the analyses. The resulting tieback force at SF = 1.0 in Model E is 216 kN versus 38 kN in Model B. As soil strength reduces, the SF versus tieback force relationship is close to the Bishop curve.

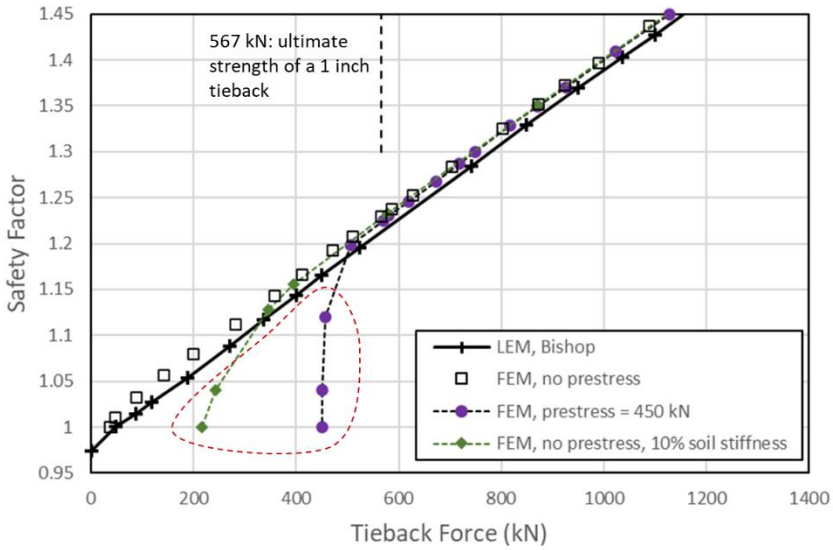


Fig. 9. Effects of prestress and soil stiffness

 © Deep Foundations Institute 2025

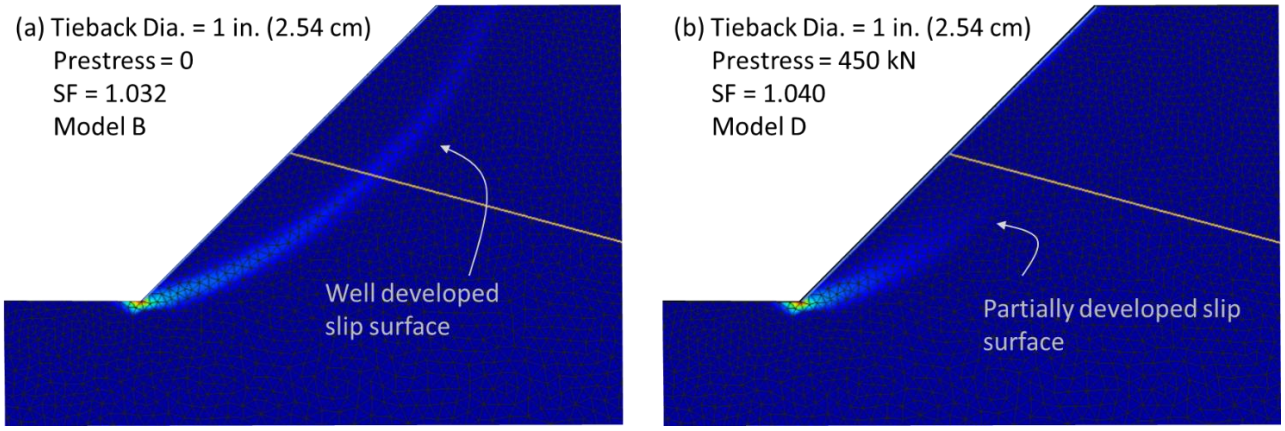


Fig. 10 Equivalent magnitude of plastic strain from the 2nd step of stage 2 from Models B and D

Results from Model F with a larger diameter tieback are shown in **Fig. 11**. Results from Model F are generally close to the Bishop curve. However, noticeable differences can be seen in the lower and upper regions of the curve. Similar to Model E, in the region of lower safety factor, there is a prestress incurred in the tieback during the first stage of the analysis. The resulting tieback force at SF = 1.0 is 153 kN. As soil strength reduces, the SF versus tieback force relationship is close to the Bishop curve. It is interesting to note that when SF increases above 1.790, the resulting tieback force decreases with increasing SF and deviates from the Bishop curve. **Fig. 12** shows the resulting equivalent magnitude of plastic strain at a safety factor of 1.801. As shown in the figure, a clear slip surface is formed between the soil and the wall elements. At this stage, the soil is sliding away from the wall structure as the wall is held relatively in place by the tiebacks. The assumption of the wall moving with the sliding soil mass made in the LEM does not agree with the findings from SRFEM. LEM can't consider the failure mechanism developed by soil-structure interactions.

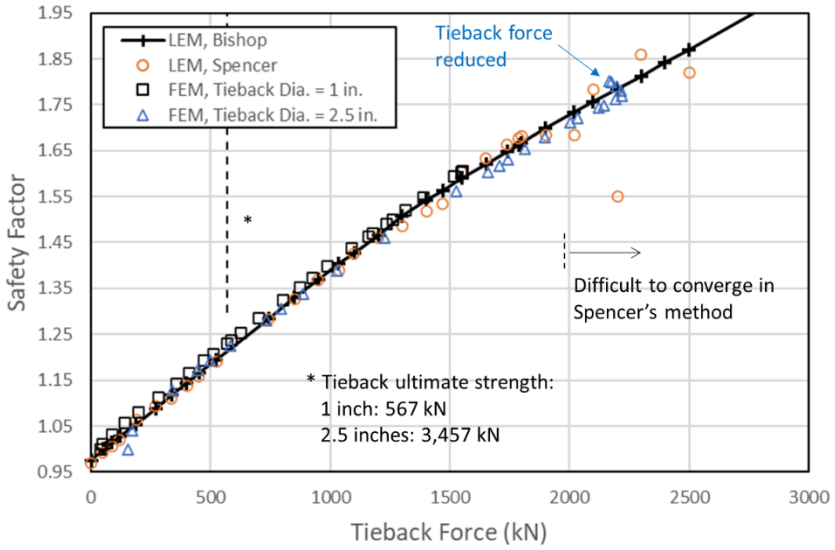


Fig. 11 Effects of the size of the tieback diameter

The final converged step from the SRFEM is at SF = 1.801 and a tieback force of 2,172 kN. The ultimate strength of a 2.5-inch (6.35 cm) diameter steel bar is 3,457 kN. Applying the Load Distribution Method in the Simplified Bishop method, we can continue to calculate the safety factor for the tieback force up to 3,457 kN. However, as shown in **Fig. 11**, safety factors calculated from tieback forces greater than 2,200

 © Deep Foundations Institute 2025

kN using Simplified Bishop method may not be valid. It is interesting to note that using the Load Distribution Method, results from Spencer's method show converging issues for tieback forces greater than 2,000 kN. For example, at a tieback force of 2,200 kN, only 591 out of the 5,000 trial surfaces provide converged solutions. The number is down to 46 out of 5,000 at a tieback force of 2,400 kN. Although Spencer's method is more rigorous, it can have issues of convergence for some slip surfaces. In some cases, safety factors might not be considered for the most critical slip surface. It is a good engineering practice to verify results from Spencer's method with another slope stability analysis method.

Upon close inspection of **Fig. 11**, one will find the resulting safety factors from Model F are slightly lower than those from Model B in the range of safety factors between 1.05 and 1.6. This indicates that, at the given soil strength, a tieback with a larger diameter will carry more load than a tieback with a smaller diameter. This shows that the results of a tieback-reinforced slope are influenced by the sizes of the tiebacks. However, LEM can't consider the effect of tieback diameters.

In addition to the tieback force, SRFEM can also calculate the resulting moment and shear in the concrete facing wall. **Fig. 13** shows the moment outputs from 3 selected steps in Model F with a 2.5-inch (6.35 cm) diameter steel bar. The safety factors of the three steps are 1.0, 1.62, and 1.801. The corresponding tieback forces are 153kN, 1,710kN, and 2,172kN, respectively. As shown in the figure, the moment demands increase with increasing tieback forces. These outputs are needed for the structure designs of the tieback system.

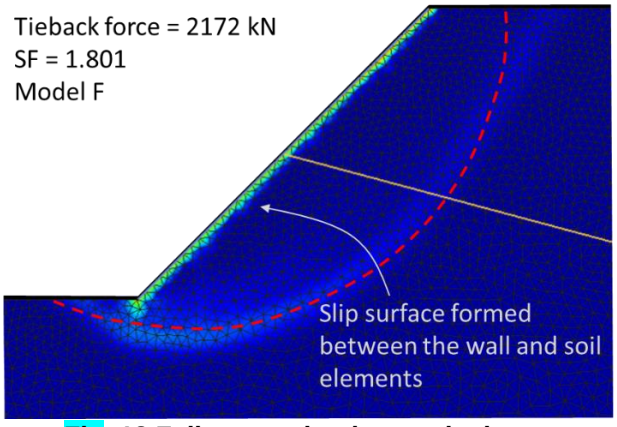


Fig. 12 Failure mechanism at the last converged step of the SRFEM

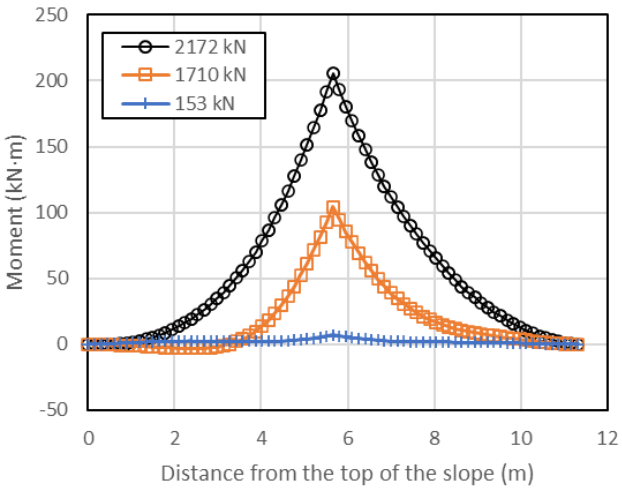


Fig. 13 Moment outputs from Model F

CONCLUSIONS

This study utilized the Strength Reduction Finite Element Method (SRFEM) to examine the accuracy of the Load Distribution Method utilized in the Limit Equilibrium Method (LEM). Results from a hypothetical 45° slope of a uniform soil layer show that safety factors obtained from SRFEM are generally close to those obtained from LEM when a slip surface is well developed in the soil mass. In these cases, the Load Distribution Method can provide a good approximation for analyzing a tieback-reinforced slope. However, LEM can't model soil-structure interactions, and LEM can't determine the maximum tieback force limited by the failure mechanism developed from soil-structure interactions. The findings from this study are summarized below.

1. Safety factors obtained from SRFEM are close to those obtained from LEM using the Load Distribution Method when a slip surface is well developed in the soil mass. The Load Distribution Method provides a good approximation for analyzing a tieback-reinforced slope in these cases.

 © Deep Foundations Institute 2025

2. Increasing the size of the tieback can have an influence on the resulting safety factor as more loads are carried by the tieback. The phenomenon can't be observed in LEM analyses.
3. SRFEM shows there is a limit to applying the tieback force. For a slope with a 2.5-inch (6.35 cm) diameter steel bar, a slip surface between the wall and the soil mass developed at a tieback force of around 2,200 kN. The assumption of the wall moving with the sliding soil mass made in LEM is not valid. The safety factor calculated from LEM with a tieback force higher than 2,200 kN may not be valid.
4. Although Spencer's method is more rigorous, it can have issues of convergence for some slip surfaces, and no safety factor can be obtained for those surfaces. As a result, the resulting safety factor might not include the most critical slip surface. It is a good engineering practice to verify results with multiple methods.
5. In addition to the tieback force, SRFEM can also calculate the moment and shear demands in the concrete facing wall, which are beneficial for structure designs.

It should be noted that these conclusions are based on a hypothetical slope of a single soil type. Additional studies are needed to verify the findings for slopes of different geometries and soil types.

REFERENCES

1. Burman, A., Acharya, S. P., Sahay, R. R., Maity, D., 2015. A comparative study of slope stability analysis using traditional limit equilibrium method and finite element method. Asin Journal of Civil Engineering Vol. 16-4, pp. 467-492.
2. Carpenter J. R., 1985. PCSTABL4 User Manual. Joint Highway Research Project JHRP-85-7, School of Civil Engineering, Purdue University, West Lafayette, In.
3. Carpenter, J. R., 2017. Analysis of Tieback Slopes and Walls Using STABL5 and PCSTABL5. Transportation Research Record.
4. Cheng, Y. M., Lansivaara, T., and Wei., W. B., 2007. Two-dimensional slope stability analysis by limit equilibrium and strength reduction methods. Comput. Geotech. 34 (3), pp.137–150.
5. Flamant A., 1886. Stabilite des constructions: resistance des materiaux. Paris, France.
6. Griffiths, D., Lane, P., 1999. Slope Stability Analysis by Finite Elements. Géotechnique 51, pp. 653–654.
7. Griffiths, D. V., and Marquez. R. M., 2007. Three-dimensional slope stability analysis by elasto-plastic finite elements. Géotechnique 57 (6), pp. 537–546.
8. Krabbenhoft K., Karim M.R., Lyamin A.V., Sloan S.W., 2012. Associated computational plasticity schemes for nonassociated frictional material. Int J Numer Method Eng, 90:1089–117.
9. Lee, D. H.; Cunningham, C. E.; Geraci, K. E.; Lee, D. E., 2010. Using Tieback Anchors to Stabilize an Active Landslide in San Juan Capistrano, California. In Earth Retention Conference 3. American Society of Civil Engineers: Bellevue, Washington, United States, pp. 910–919.
10. Nordal S., 2008. Can we trust numerical collapse load simulations using nonassociated flow rules? In: Singh, editor, Proceedings of 12th International Conference of the International Association of Computer Methods and Advances in Geomechanics (IACMAG), Goa, India, pp. 755–762.
11. Sabatini et al., 1999. FHWA-IF-99-15 Ground Anchors and Anchored Systems
12. Theinat, A., Salgado, R., Prezzi, M., Sakleshpur, V. A., 2024. Stability and Factor of Safety of Gravity-Retaining Structures Using the Strength Reduction Method. Journal of Geotechnical and Geoenvironmental Engineering, 150 (12), 04024118.
13. Tschuchnigg, F., Schweiger, F., Sloan, W., 2015. Slope Stability Analysis by Means of Finite Element Limit Analysis and Finite Element Strength Reduction Techniques. Part I: Numerical Studies Considering Non-Associated Plasticity. Computers and Geotechnics 70, 169–177.
14. Tschuchnigg, F., Schweiger, F., Sloan, W., 2015. Slope Stability Analysis by Means of Finite Element Limit Analysis and Finite Element Strength Reduction Techniques. Part II: Back Analyses of a Case History. Computers and Geotechnics 2015, 70, 178–189.

 © Deep Foundations Institute 2025

IMPROVING THE RELIABILITY OF PILE DRIVABILITY STUDIES BY EXPLICITLY SIMULATING GROUND DISTURBANCE

Edward J. Smith, The University of Queensland, Brisbane, Queensland, Australia,
edward.smith1@student.uq.edu.au

ABSTRACT

Pile drivability studies are often undertaken on projects involving the installation of driven piles to estimate the founding level and therefore the total pile length, predict the required hammer size, and ensure stresses induced in the pile section are within allowable limits. The models typically used to estimate the ground resistance acting on a pile in these studies are highly empirical and may not reliably consider how the ground behavior may vary due to pile installation and the effects of time after installation. This empiricism increases uncertainty in both the estimated driving performance and predictions of how the pile capacity may vary with time after installation. Failure to reliably predict these effects can lead to unexpected project delays or inefficient pile design. In this study, an approach is proposed to couple conventional stress wave theory used in drivability studies with numerical models designed to simulate the ground resistance. These ground resistance models may account for how shaft resistance evolves during pile installation and with time after installation. Opportunities to extend the modeling approach to predict a range of factors and mechanisms which contribute to soil/pile set-up are discussed.

Keywords: pile drivability, stress wave theory, soil/pile set-up, installation effects, temporal effects

INTRODUCTION

Driven piles are one of many foundation solutions available to geotechnical engineers wanting to support the loads imposed by structures from the built environment (Fleming et al., 2008). An important factor affecting the adoption of a driven pile foundation is the ability to select and procure an appropriately sized hammer to install the pile. With the advent of improved computing power and the application of stress wave theory by Smith (1960) to simulate the pile installation process, engineers were able to more systematically predict pile driving performance due to explicit consideration of the driving system, pile type and geometry, and the static and dynamic response from the ground. In the proceeding years, with the increased accessibility to computational resources and the development of specific drivability programs such as GRLWEAP (Pile Dynamics Inc., 2022) and IMPACT (Geocalcs, 2021), pile drivability studies have become common practice.

A current and significant difficulty when undertaking these studies relates to estimating the effect of pile installation on the ground resistance to pile loading, and how this resistance might evolve with time following installation. These factors, if considered at all, are typically incorporated through empirical correlations as a function of distance behind the pile toe or time following installation (Geocalcs, 2021; Rausche, 2020a, 2020b). However, it is difficult for these empirical correlations to describe installation and temporal effects in a broadly applicable manner, often relying on an engineer's experience in particular ground conditions to select appropriate coefficients and achieve meaningful insights. In this paper, a framework is described to reduce the empiricism in these predictions by simulating the interaction between pile installation and the ground, and the ground response following installation. The framework is designed with practical application in mind, allowing for important aspects of the ground behavior to be captured whilst avoiding the considerable computational expense of full 3D dynamic numerical simulations. The work described in this paper does not in itself reduce empiricism in the prediction of installation and temporal effects, but provides a basis which can be extended through appropriate simulation of the pile toe arriving at a given soil horizon (e.g., cavity expansion, strain path

 © Deep Foundations Institute 2025

method), advanced constitutive models (to describe important soil behaviors including consolidation, soil destructuration, particle breakage, and creep) and mechanism specific adjustments to the boundary conditions (e.g., due to corrosion) to better predict these effects. By applying the appropriate extensions the proposed framework could be applied to a range of pile types and ground conditions, although the description in this paper is limited to closed-ended piles. The proposed framework is focused on the improved prediction of shaft resistance, with temporal variations in end bearing resistance not considered.

BACKGROUND

Pile Drivability

Pile drivability studies are based on simulating the stress wave introduced to the pile by the hammer and how this stress wave subsequently interacts with the ground. As the hammer impacts the pile head, a compressional stress wave propagates towards the pile toe (direction z) at speed $c = \sqrt{E_p/\rho_p}$, where E_p is the Young's modulus and ρ_p the density of the pile material (Holloway, 1975). The propagation of the stress wave can be modelled using the wave equation (Equation **Error! Reference source not found.**), where A_p is the pile cross-sectional area, $R(z,t)$ are any forces mobilized to resist the pile penetration per unit length of pile, and $u(z,t)$ is the displacement of the pile in the z direction (along the pile) with time t (Holloway, 1975).

$$c^2 \frac{\partial^2 u}{\partial z^2} - \frac{R}{A_p \rho_p} = \frac{\partial^2 u}{\partial t^2} \quad [1]$$

Smith (1960) proposed a ground model which separates the ground resistance developed along the pile shaft and at the pile toe into static and dynamic components (Equation **Error! Reference source not found.** and **Error! Reference source not found.**, **Error! Reference source not found.**). The static resistance is modelled using a spring with stiffness (K_s, K_b) controlled by an empirical quake parameter (Q_s, Q_b) and a plastic slider activated when the static resistance reaches a limiting value (f_s, f_b). Dynamic effects are modelled using a viscous dashpot controlled by the mobilized static resistance and empirical dashpot coefficients ($J_{vs}, J_{vb}, N_{vs}, N_{vb}$). In the model proposed by Smith (1960) $N_{vs} = N_{vb} = 1$, however this can be extended to include velocity dependence of the viscous coefficients as demonstrated by Gibson and Coyle (1968) by using values not equal to unity ($N_{vs} = 0.2$ is typical (Randolph, 1991), with appropriate modification to J_{vs}).

$$R_s = \min\left(\min\left(\underbrace{K_s u_{s,p}}_{Spring}, \underbrace{f_s}_{Limiting\ static\ resistance}\right)\left(1 + \underbrace{J_{vs}\left(\frac{v_{s,p}}{v_{ref}}\right)^{N_{vs}}}_{Viscous\ dashpot}\right)\right) A_s \quad [2]$$

$$R_b = \left(\min\left(\underbrace{K_b u_{b,p}}_{Spring}, \underbrace{f_b}_{Limiting\ static\ resistance}\right)\left(1 + \underbrace{J_{vb}\left(\frac{v_{b,p}}{v_{ref}}\right)^{N_{vb}}}_{Viscous\ dashpot}\right)\right) A_b \quad [3]$$

Where A_b and A_s are pile base and shaft areas, f_b and f_s are limiting static end bearing and shaft resistances, J_{vb} and J_{vs} are viscous dashpot coefficients, $K_b = \frac{f_b}{Q_b}$, $K_s = \frac{f_s}{Q_s}$, N_{vs} and N_{vb} are viscosity velocity dependence exponents, Q_b and Q_s are base and shaft quake, R_b and R_s are base and shaft resistance in units of force, $u_{b,p}$ and $u_{s,p}$ are the pile base and shaft displacements, $v_{b,p}$ and $v_{s,p}$ are the

 © Deep Foundations Institute 2025

pile base and shaft velocities, v_{ref} equal to 1m/s is used for clarity of units. Whilst not captured for the sake of clarity, care is required for negative velocities/displacements to ensure that the pile toe does not support tension and that $\left(v_{s,p}/v_{ref}\right)^{N_{vs}}$ remains defined.

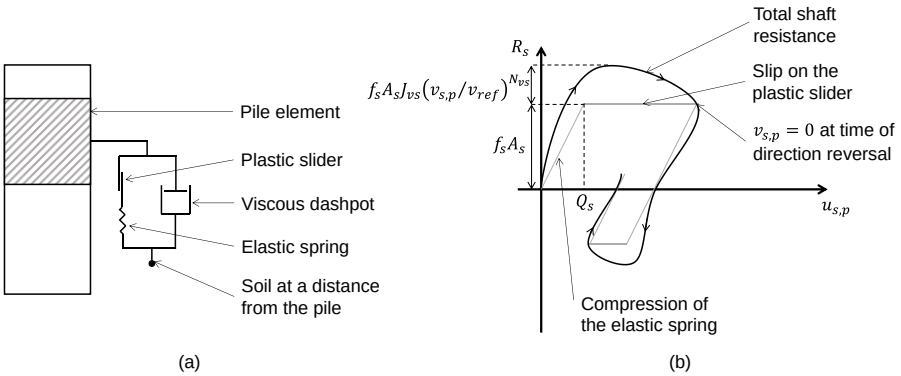


Fig. 1: Shaft resistance model adopted in the Smith (1960) model (after Holloway (1975)) (a) Rheological model (b) Load deformation behavior.

Simons and Randolph (1984) developed the continuum model with the aim of reducing the empiricism required to model the ground resistance, separating the energy dissipation mechanisms into the energy radiated into the far field (radiation damping) and the energy dissipated due to slip between the pile and ground (viscous damping) (**Error! Reference source not found.**). Equation **Error! Reference source not found.** describes the resistance that is mobilized on the shaft, with the spring and inertial dashpot acting until the demand exceeds the static resistance that can be developed at the shaft and slip occurs (pile shaft velocity $v_{s,p}$ not equal to ground velocity $v_{s,g}$). The ground movement (displacement $u_{s,g}$, velocity $v_{s,g}$) during slip is calculated by setting the demand from radiation damping equal to the available resistance from viscous effects. Equation **Error! Reference source not found.** describes the resistance that is mobilized at the base, with viscous effects not included but compensated for by allowing inertial damping to continue unaffected after the static base resistance is exceeded and slip starts to occur (Randolph, 1991). The development of the continuum model was an important advancement as it allowed for the spring and inertial dash pot constants to be derived from soil mechanics principles and enabled the explicit calculation of the interface slip and the amount of deformation that the ground is subject to.

$$R_s = \min\left(\underbrace{K_s u_{s,g}}_{Spring} + \underbrace{C_s v_{s,g}}_{Inertial\ dashpot}\ ,\ \underbrace{f_s}_{Limiting\ static\ resistance} + \underbrace{f_s J_{vs}\left(\frac{\left|v_{s,p} - v_{s,g}\right|}{v_{ref}}\right)^{N_{vs}}}_{Viscous\ dashpot}\right) A_s \qquad [4]$$

$$R_b = \left(\min\left(\underbrace{K_b u_{b,p}}_{Spring},\ \underbrace{f_b}_{Limiting\ static\ resistance}\right) + \underbrace{C_b v_{b,p}}_{Inertial\ dashpot}\right) A_b \qquad [5]$$

Where $C_b = 3.4\sqrt{G_g \rho_g}/\pi(1-\nu_g)$, $C_s = 6.28\sqrt{G_g \rho_g}/2\pi$, G_g is the ground shear modulus, $K_b = 4G_g/\pi r_0(1-\nu_g)$, $K_s = 2.75G_g/2\pi r_0$, r_0 is pile radius, ν_g is the ground Poisson's ratio, ρ_g is the ground density. The direction of the shaft resistance is given by the spring and inertial dashpot terms. Whilst not captured for the sake of clarity, care is required for negative velocities/displacements to ensure the pile toe does not support tension.

 © Deep Foundations Institute 2025

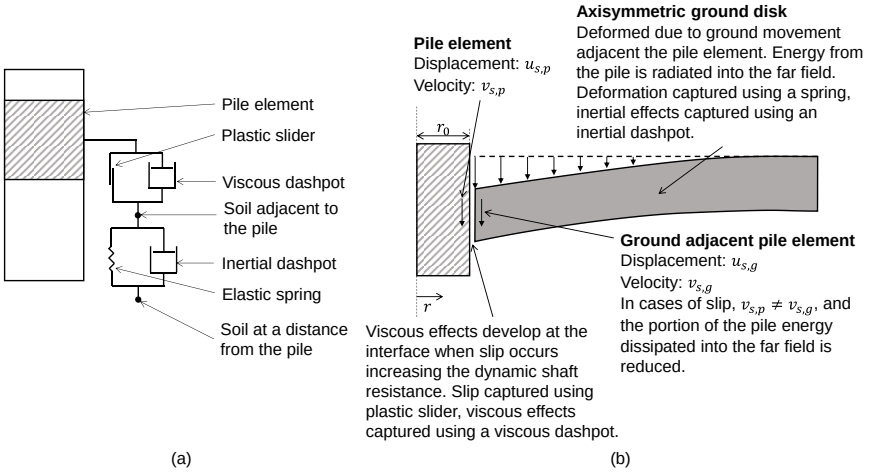


Fig. 2: Pile shaft resistance continuum model as proposed by Simons and Randolph (1984) (a) Rheological model (b) Conceptual illustration.

Due to the displacement and velocity dependence of the ground resistance, numerical techniques are often employed to solve the wave equation (Equation **Error! Reference source not found.**) including the finite difference method (Holloway, 1975), the method of characteristics (Randolph, 1991), and the finite element method. These solutions allow assessment of the pile penetration and stresses developed in the pile, which can be used to inform the selection of the driving system including hammers, helmets, and cushions.

Installation Effects and Soil/Pile Set-up

The ground resistance parameters adopted during a drivability study are known to vary during installation and with time after installation due to a range of complex and concurrent mechanisms. Where the pile capacity increases with time after installation, this phenomenon is referred to as soil/pile set-up, and is most often associated with increases in shaft resistance. The mechanisms which contribute to soil/pile set-up include the accumulation and dissipation of excess pore pressures, soil structure alteration, migration of the shear failure surface into the soil, relaxation of arching stresses, enhanced constrained dilation, as well as a range of factors associated with the pile material, size, installation method and testing sequence (Jardine, 2023; Komurka et al., 2003). Given the range of contributing mechanisms, and possible permutations which may be realized on a particular site, installation and temporal effects are highly variable and difficult to predict.

If they are to be considered, current practice is to incorporate these effects into drivability simulations using empirical correlations. For example, the method proposed by Alm and Hamre (2001) may be used to estimate the reduction in shaft resistance with distance behind the pile toe (Equation **Error! Reference source not found.**), whilst the increase in shaft resistance with time is often estimated using an expression inspired by the work of Skov and Denver (1988) (Equation **Error! Reference source not found.**). Whilst some guidance may be available, parameter selection for these correlations remains difficult as the underlying mechanics vary due to a range of factors relating to ground conditions, pile type, installation method and testing sequence. By explicitly simulating the mechanisms which lead to installation and temporal effects, the empiricism required in parameter determination can be transformed into more clearly defined soil mechanics principles, improving the applicability and reliability of predictions.

$$f_s(p) = f_{s,res} + \left(f_{s,i} - f_{s,res}\right)e^{k(d-p)} \quad [6]$$

Where d is the depth to the layer of interest, $f_s(p)$ is the static shaft resistance to adopt at depth d for a given pile toe penetration p, $f_{s,i}$ is the initial static shaft resistance, $f_{s,res}$ is the residual static shaft resistance, k is an empirical coefficient controlling the rate of degradation with distance behind the pile toe.

$$f_s(t) = f_{s,t_0}\left(A \log_{10}\left(\frac{t}{t_0}\right) + 1\right) \quad [7]$$

Where A is the rate of static shaft resistance increase per log cycle, $f_s(t)$ is the static shaft resistance to adopt at time t, f_{s,t_0} is the static shaft resistance at time t_0, t_0 is the time from which the set-up trend becomes linear with log time.

MODEL DESCRIPTION

Model Features

The modeling approach discussed in this paper provides a means to simulate the effects of pile installation on the adjacent ground and then allow this simulation to provide the inputs for subsequent stress wave simulations. The approach is based on the following key features,

- Stress wave theory using the continuum model is adopted to simulate the interaction between the pile and the ground, allowing for the determination of the amount of interface slip and ground displacement. The one-dimensional wave equation (Equation **Error! Reference source not found.**) is solved using the finite element method with the Bathe time-stepping technique (Bathe, 2016).
- A series of ground nodes are used to simulate the ground resistance, with the resistance to be applied to each pile node determined using interpolation from the ground nodes (**Error! Reference source not found.**). Separating the ground nodes from the pile nodes allows for large pile displacements, and for the ongoing simulation of installation/temporal effects at each ground node.
- Each ground node is associated with an independent axisymmetric finite element model. Before a given stress wave simulation, the stiffness and strength of the ground is predicted by applying fictitious displacements (approximately consistent with the displacements arising from the subsequent stress wave simulation) to the ground node finite element models and extracting the ground response in terms of interface stress mobilization and far field ground stiffness.
- During each time step of the stress wave simulation, pile movements are transferred to the ground nodes allowing for the stiffness and mobilized resistance to be calculated (extracted from the stiffness and resistance response curves) and transferred back to the pile nodes.
- Following a given stress wave simulation the calculated interface slip and ground displacement are applied to each ground node finite element model to simulate the installation effects.
- The axisymmetric finite element models at each ground node can also be programmed to simulate temporal effects between stress wave simulations (such as soil consolidation, creep, and corrosion).

A range of controls have also been implemented into the modelling software to enhance robustness and reduce the required computational effort without unduly compromising the predictive abilities of the program. A discussion on these controls is beyond the scope of this paper.

 © Deep Foundations Institute 2025

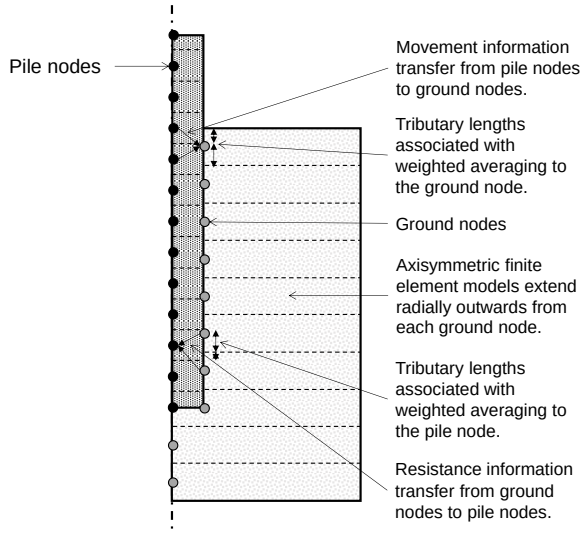


Fig. 3: Axisymmetric illustration demonstrating the arrangement of pile nodes and ground nodes and information transfer between the nodes.

Finite Element Models to Simulate Shaft Resistance

The finite element models used to simulate the shaft resistance at each ground node are illustrated in **Error! Reference source not found.**. The model features an interface element (closest to the pile) which captures the effects of slip between the pile and the ground (describing the ground resistance), with the elements beyond the interface used to capture the far field ground response (describing the ground stiffness). All vertically aligned nodes have their horizontal and vertical displacements tied together to create a simple shear condition which captures the restraint provided by the ground above/below the node at a sufficient distance from the ground surface/pile toe without explicit simulation. This approach has also been adopted by Basu et al. (2011), with the decoupling of the ground nodes reducing the computational cost of simulation whilst also allowing the finite element simulations at multiple ground nodes to be run in parallel. 8 node full-integration elements are used with an Updated Lagrangian formulation as described by Chen and Mizuno (1990).

This paper is focused on demonstrating that stress wave simulations can be coupled with explicit simulations of ground disturbance. For demonstration purposes, the constitutive model adopted is a linearly elastic model with von Mises failure criterion. The yield surface is given by Equation **Error! Reference source not found.**.

$$f\left(\boldsymbol{\sigma}, \kappa, \sigma_y, \sigma_{y,ult}, H\right) = \sqrt{3J_2} - \left(\sigma_y + H \min\left(\kappa, \frac{\sigma_{y,ult} - \sigma_y}{H}\right)\right) \quad [8]$$

$$\kappa = \int d\kappa = \int \sqrt{\frac{2}{3}\boldsymbol{d\epsilon^p} : \boldsymbol{d\epsilon^p}} \quad [9]$$

Where H is a parameter which controls the rate of hardening/softening, J_2 is the second deviatoric stress invariant, $\boldsymbol{\epsilon^p}$ is the plastic strain tensor, κ is the equivalent plastic strain, $\boldsymbol{\sigma}$ is the stress tensor, σ_y is the peak material yield stress, $\sigma_{y,ult}$ is the ultimate material yield stress.

The model can simulate perfect plasticity (i.e., $H = 0$) which allows for the simulation of a constant limiting static shaft resistance. Since the failure mode at the pile-soil interface is closer to pure shear than

 © Deep Foundations Institute 2025

triaxial compression/extension, σ_y should be given by Equation **Error! Reference source not found.** to replicate the shaft resistance corresponding to f_s (Chen & Mizuno, 1990; Potts & Zdravkovic, 1999). The potential to simulate the accumulation of installation effects such as friction fatigue can also be demonstrated by simulating softening of the yield surface with accumulating plastic shear strain (i.e., $H < 0$). To more explicitly capture the mechanisms associated with installation and temporal effects, a more advanced constitutive model would be required. This is beyond the scope of this paper, but a focus of ongoing research.

$$\sigma_y = \sqrt{3} f_s \quad [10]$$

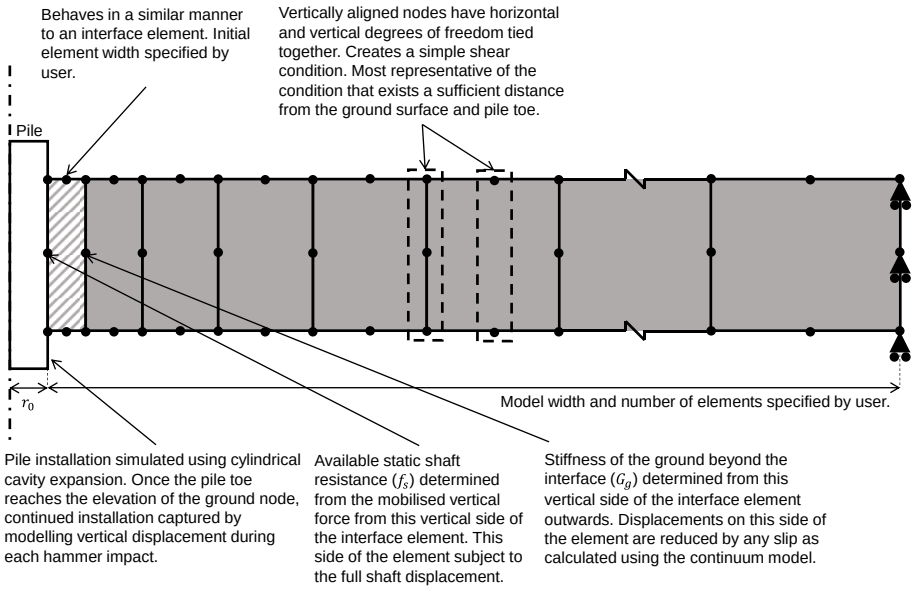


Fig. 4: Illustration of the axisymmetric finite element model used to simulate installation and temporal effects on shaft resistance.

Establishing Shaft Stiffness and Resistance

Prior to each stress wave simulation, the shaft resistance and stiffness are established for each ground node. This is achieved as follows,

1. Apply a user-defined displacement, $u_{s,s}$ (s,s refers to shaft, stiffness), to both sides of the interface element in an upwards direction over a user defined number of steps, n_s. For each step, calculate an equivalent shear modulus for all elements beyond the interface element (described below), the vertical force supported by the ground just beyond the interface element, and the displacement at the outside of the interface. Reset the model to the initial condition.
2. Apply a user-defined displacement, $u_{s,r}$ (s,r refers to shaft, resistance), to the pile side of the interface element (fixing the outside of the interface element in the vertical direction) in an upwards direction over a user defined number of steps, n_r. For each step extract the vertical force on the pile side of the interface element and the corresponding relative vertical displacement (i.e., the slip) across the interface element. Reset the model to the initial condition.
3. Repeat step 1 in the downwards direction.
4. Repeat step 2 in the downwards direction.

 © Deep Foundations Institute 2025

The shear modulus at each vertical element side across the finite element model is calculated as described in **Error! Reference source not found.**. For the purposes of this exercise, Simpson's rule is given by Equation **Error! Reference source not found.**. The equivalent shear modulus for all elements beyond the interface element is then calculated as per Equation **Error! Reference source not found.** (Kraft et al., 1981). Use of this shear modulus means that the change in resistance developed at the outside of the interface for a given change in vertical displacement will match the result of the finite element model. It is important that shear modulus contributions from the interface element are not used in calculating the shear modulus at the outside of the interface, else yielding of the interface will erroneously reduce the equivalent shear modulus.

Combining the results from steps 1 and 3 allows for the ground stiffness curve (GSC) to be established as illustrated in **Error! Reference source not found.**. During the subsequent stress wave analysis, the shear modulus to use in Equation **Error! Reference source not found.** can be determined by referencing the GSC for the given ground displacement (from the point of zero ground load).

Combining the results from steps 2 and 4 allows for the ground resistance curve (GRC) to be established as illustrated in **Error! Reference source not found.**. During the subsequent stress wave analysis, the static shaft resistance to use in Equation **Error! Reference source not found.** can be determined by referencing the GRC for the given interface slip.

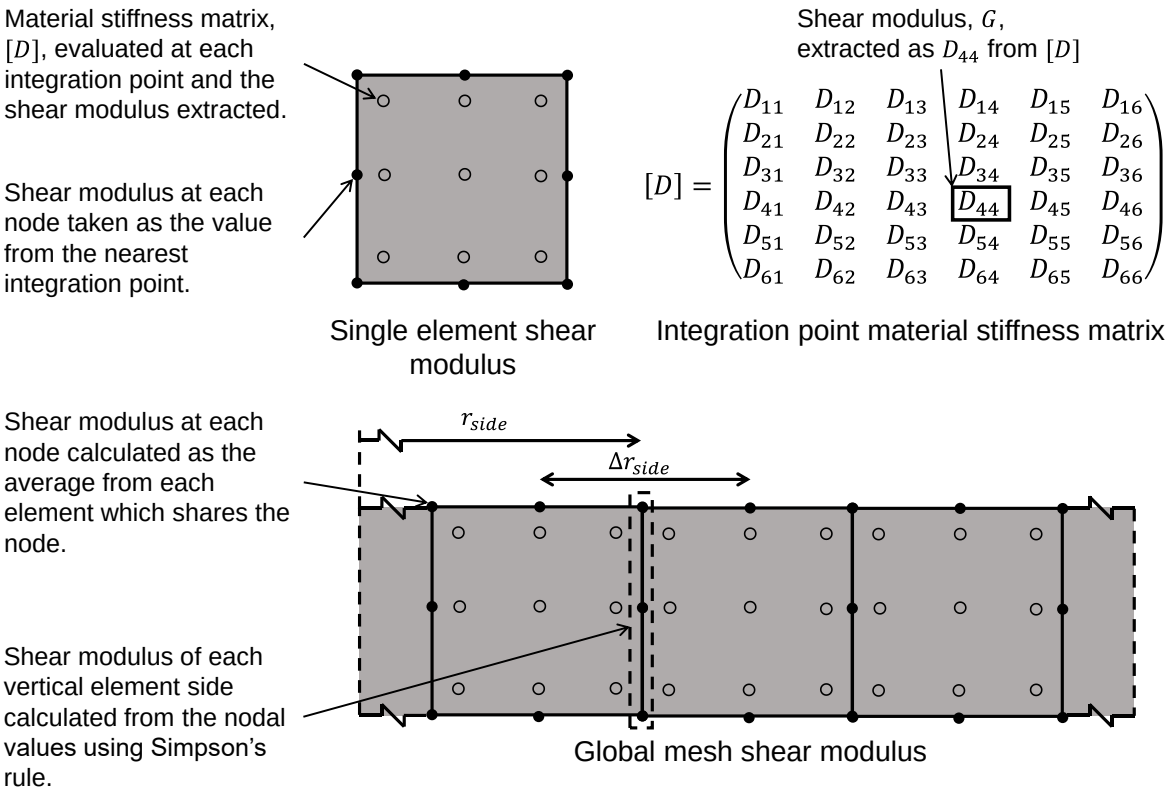


Fig. 5: Illustration demonstrating the calculation of the shear modulus at each vertical element side in the global mesh.

$$G_{side} = \frac{\left(G_{top} + 2G_{mid} + G_{bottom}\right)}{4} \quad [11]$$

[12]

 © Deep Foundations Institute 2025

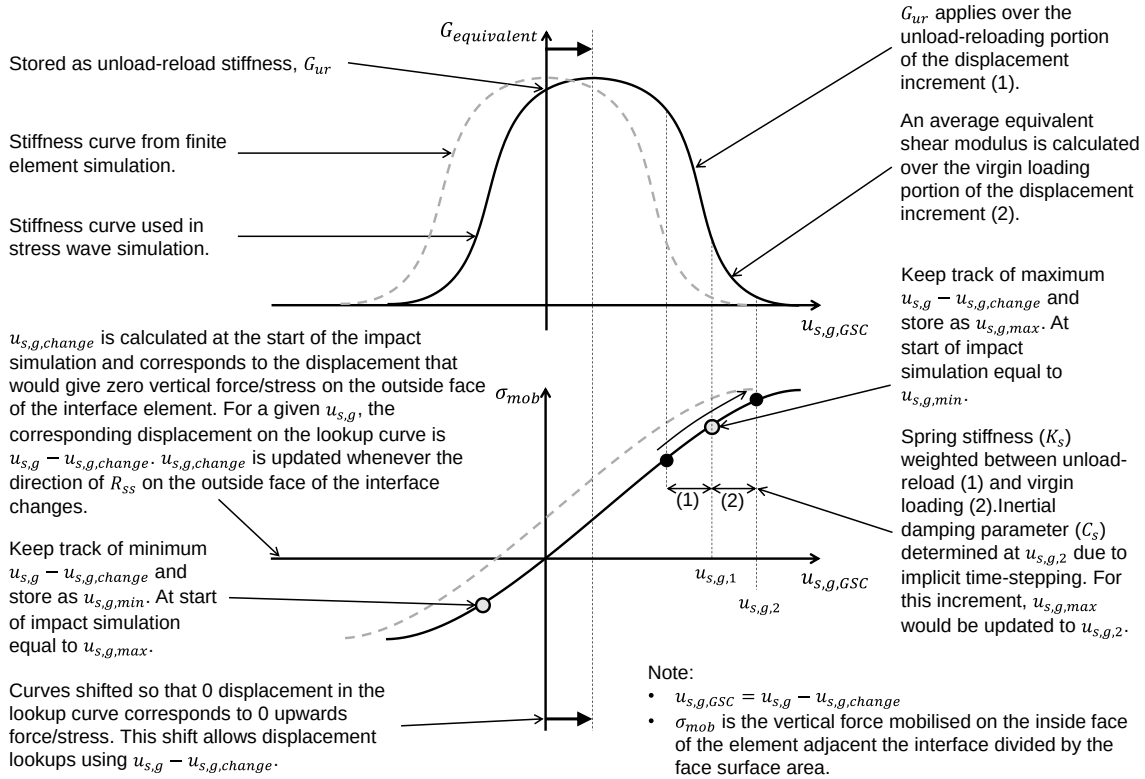
$$G_{equivalent} = \frac{\int_{r_{outer\ interface}}^{r_{boundary}} \frac{dr}{r}}{\int_{r_{outer\ interface}}^{r_{boundary}} \frac{dr}{Gr}} \approx \frac{\sum_{sides} \frac{\Delta r_{side}}{r_{side}}}{\sum_{sides} \frac{\Delta r_{side}}{G_{side} r_{side}}}$$

Simulating Ground Disturbance along the Pile Shaft

Disturbance to the ground during pile installation is caused by a combination of the pile toe arriving at a given ground horizon, and the ongoing shearing at that ground horizon as the pile embedment increases. To minimize complexity, the work in this paper simulates pile arrival at a ground node using cylindrical cavity expansion (Carter et al. (1979), with an initial radius $r_0/10$), although more advanced methods such as the strain path method (Baligh, 1985) are available and will be discussed in later works.

Following the arrival of the pile at a ground node, each subsequent stress wave simulation stores the maximum (downward or upward) vertical displacement during the simulation and the static resistance mobilized at the ground node at the end of the simulation. Following the completion of the stress wave simulation these displacements are applied to the ground node finite element model as follows,

1. Apply the maximum displacement from the outside of the interface (i.e., away from pile, $\Delta u_{s,g}$) to both sides of the interface (i.e., no slip).
2. Apply the maximum interface slip (i.e., $\Delta u_{s,p} - \Delta u_{s,g}$) to the pile side of the interface with vertical movement of the other side (i.e., away from pile) of the interface fixed.
3. Apply the static resistance mobilized at the end of the stress wave simulation to both sides of the interface element so that the load on the finite element model matches that at the end of the stress wave simulation.



 © Deep Foundations Institute 2025

Fig. 6: Illustration demonstrating the ground stiffness curve (GSC) established from ground node finite element simulations.

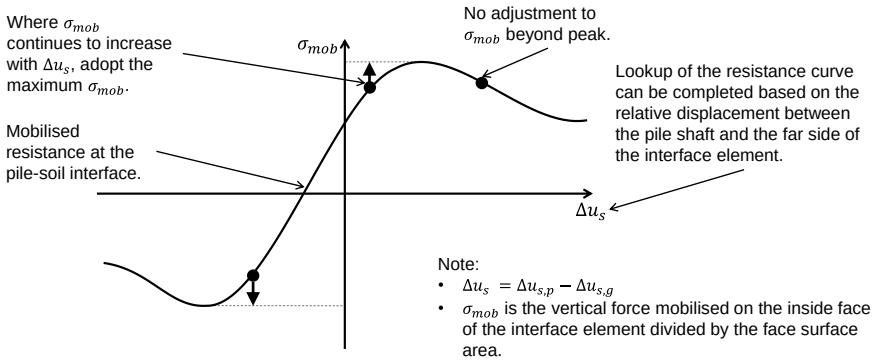


Fig. 7: Illustration demonstrating the ground resistance response curve (GRC) established from finite element simulations.

Modeling End Bearing Resistance

Increases in pile capacity with time are most often associated with increases in shaft resistance (Axelsson, 1998; Chow et al., 1998; Jardine et al., 2005). For this reason, the simulation of installation and temporal effects for end bearing are not considered in the proposed modeling approach, and end bearing is simulated using Equation **Error! Reference source not found.**. The reduction in end bearing resistance with time has been documented in certain conditions (Komurka et al., 2003), and would need to be accounted for in other ways.

APPLICATION OF THE MODELING APPROACHS

Matching the Conventional Continuum Model

This series of simulations is designed to demonstrate that the resistance and stiffness parameters determined using the ground finite element models are able to, at a minimum, replicate the response of the shaft resistance and shear modulus typically specified when using Equation **Error! Reference source not found.**. The ground, pile and hammer parameters adopted are summarized in **Error! Reference source not found.** and have been selected for demonstration purposes, without being associated with any particular ground conditions or footing installation. The case simulated involves striking the pile at the noted embedment with no initial residual stress in the pile other than self-weight.

The GRC and GSC used in the stress wave simulation based on explicit ground reaction curves are presented in **Error! Reference source not found.**. The calculated resistance and shear modulus are generally consistent with those that are adopted in the conventional continuum model without explicit ground reaction simulations. At larger displacements, the shear modulus adopted does tend to soften in the explicit GSC as the system beyond the interface approaches yield. Since yielding due to vertical loading during any particular hammer impact is to be largely concentrated within the interface shear zone, it is of little interest to generate considerable softening of the shear modulus when producing the GSC.

 © Deep Foundations Institute 2025

Table 1: Parameters adopted for comparison of conventional continuum model simulation with the method proposed in this paper.

Ground conditions	General	10 m thick layer, ρ = 1800 kg/m^3, E = 30 MPa, ν = 0.5
	Shaft	f_s = 50 kPa, J_{vs} = 1.5, N_{vs} = 0.2, H = 0 kPa
	End bearing	f_b = 900 kPa
	Finite element models	40 no. ground nodes, initial model width = 4 m, initial internal radius = 0.015 m, initial interface element width = 0.05 m (reducing to 0.01-0.015 m on cavity expansion), 15 no. elements with width increasing geometrically.
Pile parameters	Length	10 m embedded 9 m, 40 no. elements
	Section	Diameter = 0.3 m, perimeter = 0.9425 m, area = 0.0707 m^2
	Material	Concrete, ρ = 2400 kg/m^3, E = 40 GPa
Hammer parameters	Energy	Drop height = 1.0 m, 100% efficiency, gravitational acceleration = 9.81 m/s^2
	Ram	Length = 3 m, mass = 3000 kg, ρ = 8000 kg/m^3, E = 210 GPa, 3 no. elements
	Cushion	Thickness = 0.1 m, mass = 5.65 kg (resting on pile head), ρ = 800 kg/m^3, E = 500 MPa, 1 no. element

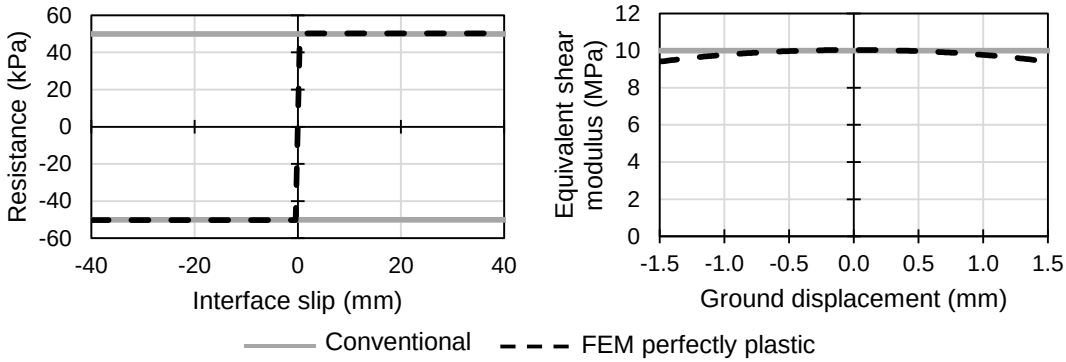


Fig. 8: Ground resistance and stiffness curves (GRC left and GSC right) adopted in stress wave simulations to match the conventional continuum model.

The stress wave response calculated at the top of the pile for both modeling approaches are compared in **Error! Reference source not found.**, demonstrating acceptable agreement. These results demonstrate that the use of explicit ground reaction simulations can, at a minimum, replicate the results of the conventional continuum model stress wave simulations.

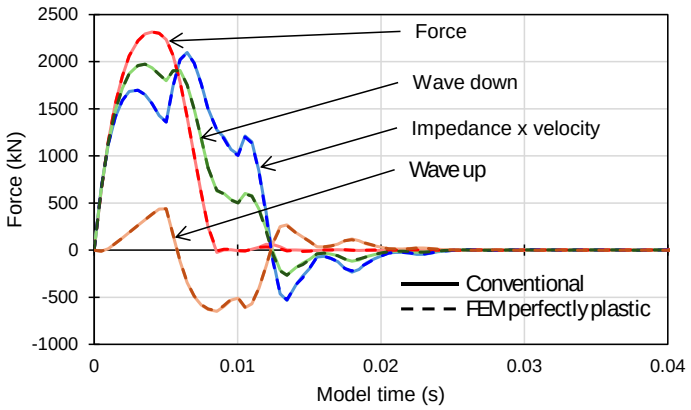


Fig. 9: Stress wave response at pile head comparing conventional continuum model and the approach described in this paper.

Demonstrating the Simulation of Installation Effects

As a demonstration of the opportunities made available through the modeling approach documented in this paper, a ground model is considered involving softening of the shaft resistance with accumulating plastic strain (H = -0.5 kPa, $f_{s,ult}$ = 25 kPa). The value of *H* is adopted for demonstration purposes only and is not intended to simulate any particular soil. Additional simulations were performed to compare this softening ground model with the perfectly plastic ground model (H = 0 kPa) after driving the pile from 2 m to 9 m embedment.

The simulation using the perfectly plastic ground model required approximately 220 hammer blows to achieve the required embedment, whilst the softening ground model required approximately 130 hammer blows. **Error! Reference source not found.** compares the maximum static shaft resistance from the ground resistance curves, and the stress wave response at the pile head. The softening of the shaft resistance due to ongoing installation is apparent and demonstrates the potential benefits of using finite element simulations to explicitly simulate the disturbance from pile installation. With the implementation of more advanced constitutive models into the proposed modeling framework, many of the mechanisms associated with pile installation and temporal effects could be explicitly simulated and implicitly weighted without having to resort to wholistic friction fatigue parameters (e.g., Equation **Error! Reference source not found.**) or indeed softening moduli (e.g., H in Equation **Error! Reference source not found.**).

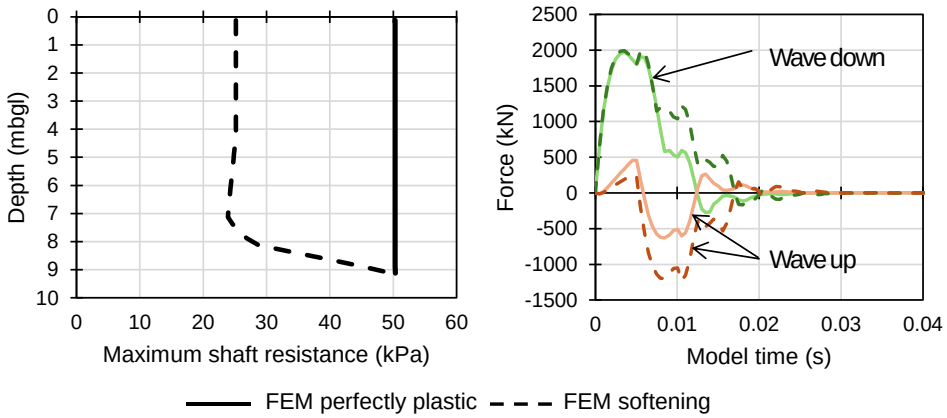


Fig. 10: Maximum available shaft resistance (left) and stress wave response at pile head (right) for perfectly plastic and strain softening simulations.

 © Deep Foundations Institute 2025

OPPORTUNITIES FOR FURTHER DEVELOPMENT

Whilst the modeling approach described in this paper creates the opportunity for significant enhancement of pile drivability studies to better consider installation and temporal effects, there are several opportunities for development to realize the potential of the approach. These opportunities include,

- The adoption of a more advanced constitutive model able to simulate the mechanisms often associated with installation and temporal effects for displacement piles including hardening on plastic volumetric straining, destructuration, anisotropy, particle breakage, cyclic degradation, and creep.
- The strain paths associated with the arrival of the pile toe at a given soil horizon could be described using the strain path method (Baligh, 1985) or even the shallow strain path method (Sagaseta, 1987; Sagaseta et al., 1997), which better account for the two-dimensional nature of pile installation.
- The introduction of an interface coefficient which reduces the shaft resistance that can be mobilized at the pile-soil interface. The pile roughness could also evolve as a function of time, for example due to corrosion.
- The simulation of waiting periods between pile installation and testing to allow temporal effects such as excess pore pressure dissipation and creep. Simulation of cavity expansion during pile waiting periods could be used to capture the increased pile volume associated with the formation of corrosion products (Jardine, 2023).

In addition to these opportunities, additional work is required to confirm the validity of the proposed modeling approach. A non-exhaustive list of items to be considered during this validation process includes,

- Confirming that static simulations can adequately capture the ground disturbance imposed by dynamic loading.
- Confirming that the ground node finite element models can continue to provide adequate predictions of ground response as large deformations develop.
- Understanding the ground node finite element model width, mesh density and interface element thickness to adopt, and how these may vary as a function of the ground conditions, pile type, and installation method.

SUMMARY AND CONCLUSIONS

Pile installation and temporal effects are caused by the complex interaction of several mechanisms which vary as a function of various factors including the ground conditions, pile type, installation method and testing sequence. Given the range of contributing mechanisms, and possible permutations which may be realized on a particular site, installation and temporal effects are highly variable and difficult to predict. The current approach to simulate these effects relies on establishing the values of empirical coefficients, at best based on experience in similar conditions (if available for the specific permutation), and at worst, with little basis at all resulting in considerable uncertainty. The modeling approach proposed in this work creates the opportunity to explicitly simulate the effect of pile installation on the ground and then feed the response of the disturbed ground into subsequent stress wave simulations. In doing so, the establishment of model parameters can be transformed into an exercise based on laboratory testing and more clearly defined soil mechanics principles, improving the applicability and reliability of predictions.

ACKNOWLEDGMENTS

The author prepared this manuscript during their studies at The University of Queensland which are supported by the Australian Government Research Training Program Scholarship and the National Industry PhD Program. The author acknowledges David Williams of The University of Queensland for his guidance and for supporting the attendance of the author at the Deep Foundations Institute 50th Anniversary Conference. The author would also like to thank staff at FSG Geotechnics and Foundations for their feedback on the manuscript prior to submission.

REFERENCES

Alm, T., & Hamre, L. (2001). Soil model for pile driveability predictions based on CPT interpretations. International Conference on Soil Mechanics and Geotechnical Engineering, Istanbul, Turkey.

Axelsson, G. (1998). Long-term increase in shaft capacity of driven piles in sand. Fourth International Conference on Case Histories in Geotechnical Engineering St Louis, Missouri, USA.

Baligh, M. M. (1985). Strain Path Method. *Journal of Geotechnical Engineering*, *111*(9), 1108-1136. https://doi.org/10.1061/(ASCE)0733-9410(1985)111:9(1108)

Basu, P., Loukidis, D., Prezzi, M., & Salgado, R. (2011). Analysis of shaft resistance of jacked piles in sands. *International journal for numerical and analytical methods in geomechanics*, *35*(15), 1605-1635. https://doi.org/10.1002/nag.968

Bathe, K.-J. (2016). *Finite Element Procedures* (2nd ed.). Prentice Hall.

Carter, J. P., Randolph, M. F., & Wroth, C. P. (1979). Stress and Pore Pressure Changes in Clay during and after the Expansion of a Cylindrical Cavity. *International journal for numerical and analytical methods in geomechanics*, *3*(4), 305-322. https://doi.org/10.1002/nag.1610030402

Chen, W. F., & Mizuno, E. (1990). *Nonlinear Analysis in Soil Mechanics*. Elsevier.

Chow, F. C., Jardine, R. J., Brucy, F., & Nauroy, J. F. (1998). Effects of time on capacity of pipe piles in dense marine sand. *Journal of Geotechnical and Geoenvironmental Engineering*, *124*(3), 254-264. https://doi.org/10.1061/(Asce)1090-0241(1998)124:3(254)

Fleming, K., Weltman, A., Randolph, M., & Elson, K. (2008). *Piling engineering*. CRC press. https://doi.org/10.1201/b22272

Geocalcs. (2021). *IMPACT - Pile Driving Analysis* https://www.geocalcs.com/impact

Gibson, G. C., & Coyle, H. M. (1968). *Soil damping constants related to common soil properties in sands and clays* (Report No. 125-1). Texas Transportation Institute - Texas Highway Department.

Holloway, D. H. (1975). *Wave Equation Analyses of Pile Driving* (Report No. S-75-5). Soils and Pavements Laboratory - U.S. Army Engineer Waterways Experiment Station.

Jardine, R. (2023). The 6th ISSMGE McClelland Lecture: Time-dependent vertical bearing behaviour of shallow foundations and driven piles. 9th International Offshore Site Investigation Geotechnics Conference - Innovative Geotechnologies for Energy Transition,

 © Deep Foundations Institute 2025

Jardine, R., Chow, F., Overy, R., & Standing, J. (2005). *ICP Design Methods for Driven Piles in Sands and Clays*. Thomas Telford Publishing. https://doi.org/10.1680/idmfdpisac.32729

Komurka, V. E., Wagner, A. B., & Edil, T. B. (2003). *Estimating Soil/Pile Set-Up* (Report No. 03-05). (Wisconsin Highway Research Program, Contract No. 0092-00-14).

Kraft, L. M., Ray, R. P., & Kagawa, T. (1981). Theoretical T-Z Curves. *Journal of the Geotechnical Engineering Division*, *107*(11), 1543-1561. https://doi.org/10.1061/AJGEB6.0001207

Pile Dynamics Inc. (2022). *GRLWEAP 14 - Wave Equation Analysis of Pile Driving* (Version 14.1.20.1)

Potts, D., & Zdravkovic, L. (1999). *Finite Element Analysis in Geotechnical Engineering Theory* (Vol. 1).

Thomas Telford.

Randolph, M. (1991). Analysis of the dynamics of pile driving. In P. K. Banerjee & R. Butterfield (Eds.), *Advanced Geotechnical Analyses* (1st ed.). CRC Press.

Rausche, F. (2020a). *GRLWEAP Static Analysis and Driveability*. Pile Dynamics Inc.

Rausche, F. (2020b). *GRLWEAP Webinar Day 4 - Large pipe and offshore pile driving problems and analysis concerns*. Pile Dynamics Inc.

Sagaseta, C. (1987). Analysis of Undrained Soil Deformation Due to Ground Loss. *Géotechnique*, *37*(3), 301-320. https://doi.org/10.1680/geot.1987.37.3.301

Sagaseta, C., Whittle, A. J., & Santagata, M. (1997). Deformation and analysis of shallow penetration in clay. *International journal for numerical and analytical methods in geomechanics*, *21*(10), 687-719. https://doi.org/10.1002/(Sici)1096-9853(199710)21:10<687::Aid-Nag897>3.0.Co;2-3

Simons, H. A., & Randolph, M. F. (1984). *New Approach to One Dimensional Pile Driving Analysis* (CUED/D-Soils TR 159). University of Cambridge.

Skov, R., & Denver, H. (1988). Time-dependence of bearing capacity of piles. Proceedings 3rd International Conference on the Application of Stress-Wave Theory to Piles, Ottawa, Ontario, Canada.

Smith, E. A. L. (1960). Pile-Driving Analysis by the Wave Equation. *Journal of the Soil Mechanics and Foundations Division*, *86*(4), 35-61. https://doi.org/10.1061/jsfeaq.0000281

 © Deep Foundations Institute 2025

MODERN VIEW OF IN-SITU WALL PREDICTION AND MOVEMENT

Enrique Farfan, PE, PhD, HDR, Lexington, Kentucky, USA, Enrique.Farfan@hdrinc.com
Adam Hacker, PE, HDR, Louisville, Kentucky, USA, Adam.Hacker1@hdrinc.com
Tom Pace, PE, PhD, HDR, Lexington, Kentucky, USA, Tom.Pace@hdrinc.com

ABSTRACT

A 3.94-ft-thick diaphragm-wall cofferdam socketed into shale was designed for Louisville's Paddy's Run Flood Pump Station capacity upgrade. Global soil–structure effects were captured initially in PLAXIS 3D and refined PLAXIS 2D cross-sections; the resulting shear-moment envelopes were converted to statically equivalent lateral-pressure loads that the structural engineer could apply directly in a 3D STAAD model, avoiding the need for STAAD's limited soil-interaction springs. This collaboration allowed STAAD to focus on the concrete panel and joint behavior—modeled with selective plate releases—while PLAXIS handled ground response. The hybrid workflow predicted wall deflections below 0.15% of the excavation height , and in-place inclinometers later confirmed only 0.09 % of the excavation height, validating the approach and underscoring the value of joint-level modeling and coordinated geotechnical–structural analysis for complex deep excavations.

INTRODUCTION

The Louisville Metro Levee System plays a critical role in protecting Louisville, Kentucky, from flooding. Originally built by the U.S. Army Corps of Engineers (USACE), the levee system is currently managed by the Louisville and Jefferson County Metropolitan Sewer District (MSD). It stretches over 26.1 miles and includes concrete floodwalls, earthen levees, and sixteen flood pump stations.

One key component of this system is the Paddy's Run Flood Pump Station, located in western Louisville. Constructed in the 1950s, both the levee and the flood pump station were designed by USACE to shield Louisville's western metropolitan area from flooding by the Ohio River. After the levee was built, stormwater was diverted beneath the levee through the Southwestern Outfall by gravity which flows directly into the Ohio River. However, when river levels rise, gravity drainage is no longer possible, and stormwater must be pumped over the levee by the Paddy's Run Flood Pump Station, which collects water in its wet well and ponding area before pumping it into the river.

MSD has proposed upgrading the Paddy's Run Flood Pump Station to accommodate an increased stormwater capacity. This upgrade aims to handle storm events equivalent to a projected 10-year, 24-hour storm within a 20-year planning timeframe. To meet this demand, the station's pumping capacity needs to be elevated significantly, from the current 875 million gallons per day (MGD) to 1,900 MGD. Given this substantial increase and the existing facility's condition, MSD concluded that a completely new flood pump station was required.

DESIGN SOLUTION

The new Paddy's Run Flood Pump Station requires careful excavation support due to challenging site conditions, including deep alluvial sands, gravels, and groundwater issues. The design team identified three key objectives: managing groundwater during excavation, addressing potential seepage risks affecting levee safety, and maintaining levee stability during normal, flooding, and seismic conditions. To achieve these objectives, the team selected a diaphragm wall (D-Wall) system keyed into bedrock (see Fig. 1), eliminating the need for active dewatering, providing a permanent seepage barrier, and serving

 © Deep Foundations Institute 2025

both temporary construction and permanent structural purposes. Extensive use of Finite Element Analysis (FEA) was made in preparation of the design.

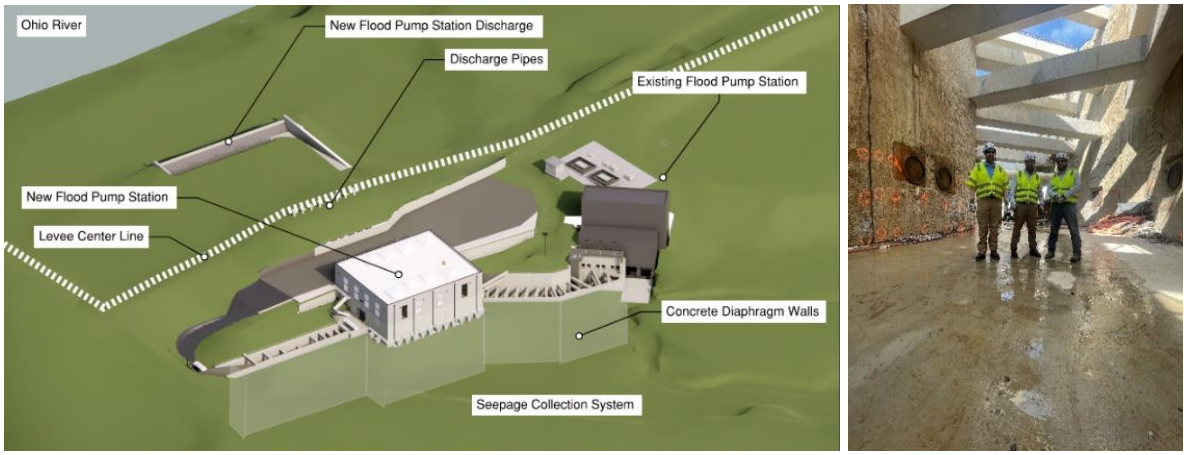


Fig. 1. Paddy's Run Flood Pump Station Capacity Upgrade Project (Isometric View, Authors Inside Channel Structure)

IDEALIZED SOIL PROFILE

The levee embankment is approximately 45 feet in height, with a crest elevation of 460.0 feet. It is composed of compacted lean clay over a native clay blanket layer. The embankment slopes vary from 2H:1V to 4H:1V, reaching the ponding area at El. 412.0 feet and the river side at El. 425.0 feet. A land side bench at El. 450.0 feet provides access to the Paddy's Run Flood Pump Station. The height of the embankment and thickness of the clay blanket varies due to the original drainage valley. The clay blanket consists mainly of medium stiff to very stiff lean clay with some silt and sand, though softer zones were noted near the levee toe. Beneath the clay blanket, an alluvial sand zone, composed of glacial outwash sands and gravels, extends to the bedrock, which consists of a hard shale. This outwash is divided into an upper layer of medium dense, poorly graded sands with silt (with some loose zones) and a lower, denser, coarser sand layer (Hacker et al, 2024). These subsurface conditions and the flood pump station's location are illustrated in Fig. 2.

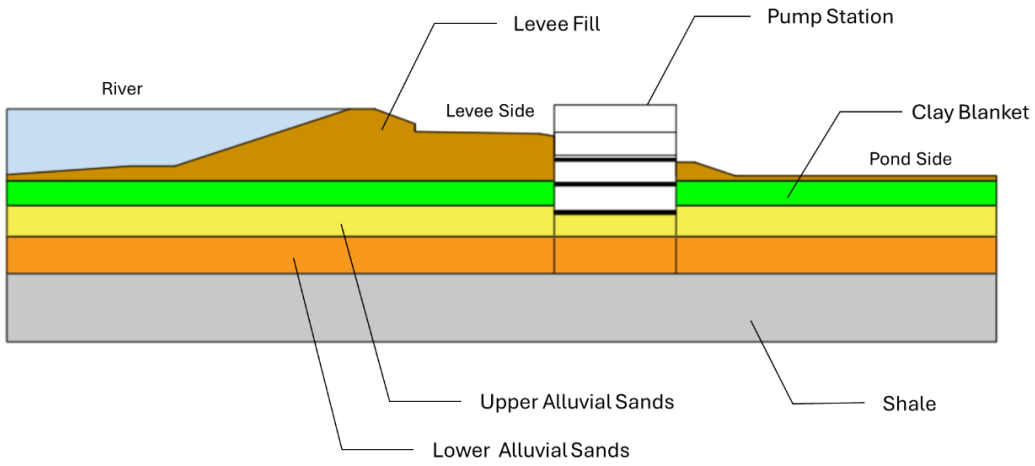


Fig. 2. Cross Section across Pumpstation showing idealized soil layering.

 © Deep Foundations Institute 2025

An evaluation of the field investigation data including disturbed and undisturbed soil samples coupled with laboratory testing, cone penetration testing with seismic testing, and shear wave velocity were done to further understand the soil properties needed for the analysis to support the design. Table 1 summarizes the soil layers properties that were used to design the diaphragm walls.

Table 1. Summary of Soil Properties

Material	Unit Weight		Drained Strength		Undrained Strength		Elastic Material Properties		
	γ_{dry} (pcf)	γ_{moist} (pcf)	ϕ' (deg)	c' (psf)	ϕ (deg)	c (psf)	E_{50} & E_{oed} ref (ksf)	E_{ur} ref (ksf)	m
Levee Fill	106	125	28	0	0	1460	1,000	3,000	0
Clay Blanket	95	120	28	0	0	1000	1,000	3,000	0
Upper Alluvial Sands	100	119	30	0	30	0	1,900	5,700	0
Lower Alluvial Sands	109	126	32	0	32	0	3,000	9,000	0

Mixed soil conditions, with alternating layers of different soil types like clay and sand, introduce complexities in predicting deflections. FEM studies have explored the sensitivity of wall deflection to specific soil parameters. An increase in the soil's elastic modulus reduces lateral deformation, underscoring the role of soil stiffness in controlling displacement. Similarly, higher soil cohesion tends to decrease deflection. However, an increase in the friction angle can, in some cases, lead to greater deformation (Boonyarak et al., 2024).

THE PUMP STATION STRUCTURE

The project support of excavation consists of three main components: the Influent Channel, the new Flood Pump Station, and the Access Ramp. The D-Wall design considers variations in soil profiles, seasonal water levels, excavation depths, and lateral loading conditions, requiring a complex bracing system. The D-Walls, 3.94 feet thick and extending 95 feet below the El. 430 feet platform, provide structural support with reinforced panels. The Influent Channel connects the existing and new pump stations with a sinuous open-braced cut, while the Pump Station excavation, measuring 125 by 96 feet, requires a stiffer support system to limit horizontal movement; a berm on the land side of the D-Wall mitigates any potential displacement. The Access Ramp, running parallel to the levee, includes a sloped subgrade and varying excavation depths. The D-Wall bracing system incorporates concrete and temporary steel struts, with permanent support provided by a concrete base slab and drainage system. Various reinforcement strategies ensure structural stability throughout construction and operation.

 © Deep Foundations Institute 2025

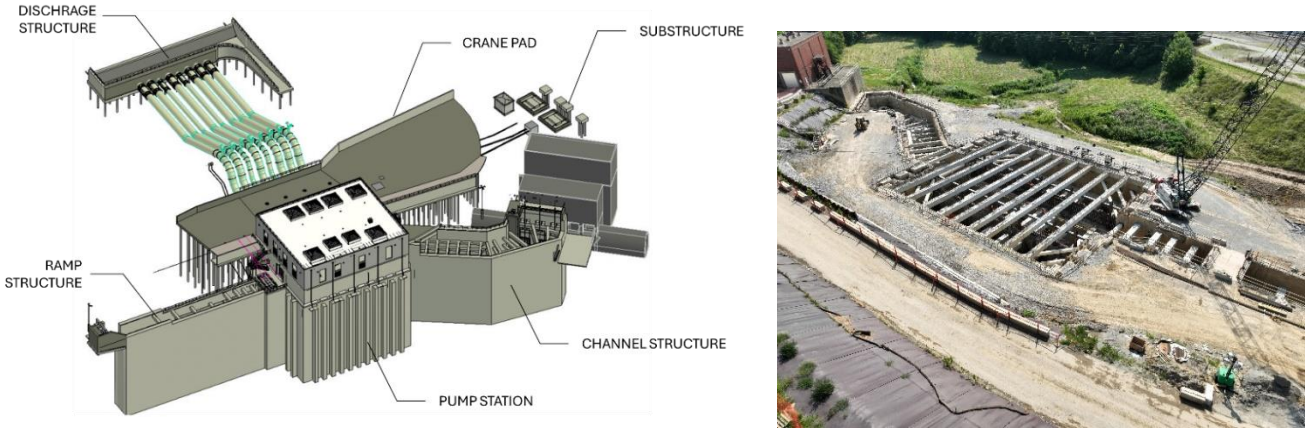


Fig. 3. Isometric View of Pump Station from Ponding Side (Embankment and foundation soil not shown for clarity); Aerial view of the Pump Station, Channel Structure (left) and Ramp Structure (right) from Levee Side during construction.

Struts and other support systems play a crucial role in limiting diaphragm wall deflections in deep excavations. These systems provide lateral support, counteracting the inward movement caused by lateral earth pressures.

SELECTED SOIL MODEL

Several soil constitutive models are used in FEA for diaphragm wall analysis. The Mohr-Coulomb model, a linear-elastic perfectly plastic model, is commonly used but has limitations in capturing non-linear behavior (Teparaksa and Teparaksa, 2019). The Hardening Soil Model accounts for non-linear stress-strain behavior, stress-dependent stiffness, and hardening, offering advantages over Mohr-Coulomb (Dwarampudi et al, 2022, Phien-Wej et al 2012).

The choice of soil model is critical for accurate FEA predictions. Advanced models like Hardening Soil Model (HS Model) capture complex behavior better but require more detailed data and calibration. Obtaining accurate parameters for advanced models can be challenging, often relying on empirical correlations

The soil-structure interaction analysis for the D-Walls was conducted using PLAXIS 2D (Version 21) based on the Finite Element Method (FEM). The simulation accounted for staged construction, lateral support bracing, and precise stress conditions, requiring close coordination between the geotechnical engineer and the D-Wall contractor (Hacker et al, 2024). The modeling process began under drained conditions before transitioning to undrained behavior for D-Wall installation. Due to limited soil stiffness data, an "Undrained B" drainage type was used to prevent overestimating soil strength and underestimating internal wall stress. The HS Model was selected over the Mohr-Coulomb Model for its ability to capture non-linear soil responses, simulating stiffness variations during loading and unloading. Stress paths during excavation were analyzed at different soil points: below the excavation (unloading), behind the retaining wall (unloading and reloading), and laterally to the excavation (lateral unloading). The HS model provided more accurate deformation predictions than traditional models, ensuring a realistic understanding of soil behavior and improving excavation planning and safety.

FROM 3D to 2D, AND BACK

FEA can provide good agreement with measured data when appropriate models and parameters are used, but discrepancies can occur due to the idealization of complex soil behavior and the difficulty in obtaining

 © Deep Foundations Institute 2025

accurate soil parameters (Yeh et al, 2022). Simplified models might not fully capture the effects of the construction sequence, and accurately modeling the soil-wall interface can be challenging (Dong, 2024, Hsieh et al, 2016). Standard FEA software might not directly model concrete cracking, which can affect wall stiffness or the panel joint interaction that can influence the development of the internal forces in the panel (Kumar, 2024).

For the project, a PLAXIS 3D FE model was generated to evaluate the interaction between the complex grading with varied slopes and changes in elevation and the nonlinear channel structure alignment. A limitation of the FE model was the representation of the interface (joint) between panels. PLAXIS 3D only provides two options: fully released (allowing free movement) or fully fixed (preventing any movement), which may not accurately capture the joint behavior.

For the structural analysis, the structure was modeled using the computer program STAAD (Structural Analysis and Design), a finite element analysis and design software developed by Bentley Systems for 2D and 3D structural modeling. STAAD supports multiple materials and international design codes. But the program has limitations with respect to soil-structure interaction. Although soil can be modeled using nonlinear springs (or p-y curves), this would require a large amount of data input at each node in the model. The 3D STAAD model provided a framework for the structural evaluation of the internal forces developed in the structure considering different stiffness for the joints between panels, as well as other aspects of the structural design.

A series of PLAXIS 2D models at various cross sections along the structure were used to translate the soil-structure interaction into the 3D STAAD model. However, the resultant forces obtained from the PLAXIS 2D models cannot be directly applied in 3D STAAD. This is because achieving force equilibrium in the 3D STAAD model requires structural supports, which influence load distribution and consequently alter the internal force results.

An advantage of the PLAXIS 2D model over the PLAXIS 3D model was the ease of applying different soil conditions in the same model, from undrained to drained. This made it possible to simulate the long-term conditions of the structure. In contrast, the PLAXIS 3D model failed to converge due to the complexity of the mesh. In addition, the translation of the resultant forces from the PLAXIS 3D model to the 3D STAAD model is more complicated since the forces to apply in the structural model need to refer to the particular nodes in 3D STAAD. A disadvantage of the PLAXIS 2D model is that it cannot model those locations where a more irregular arrangement is required for the positions of the struts, such as near the existing pump station.

To preserve the internal forces on the panels calculated in the PLAXIS 2D, the resultant moments and shears from the PLAXIS 2D model were transformed to equivalent loads.

INFLUENT CHANNEL STRUCTURE ANALYSIS

PLAXIS 3D (Initial Model)

An initial analysis was conducted using a 3D model to account for the complex topographic variations and the asymmetric geometry of the channel structure. This model was utilized to evaluate global structural behavior and the distribution of stress along various sections of the structure. In the PLAXIS 3D model, changes in grading associated with the construction

 © Deep Foundations Institute 2025

sequence were only approximately represented to mitigate numerical instabilities. Figure 4 depicts the overall view of the mesh in the 3D model and the channel structure highlighted in an isometric view. Results of wall displacements were normalized to the excavation height for different construction stages. According to the PLAXIS 3D model the maximum lateral wall displacement normalized to the excavation height (δ_{max}/He) of the structure remained under 0.27% for all construction stages.

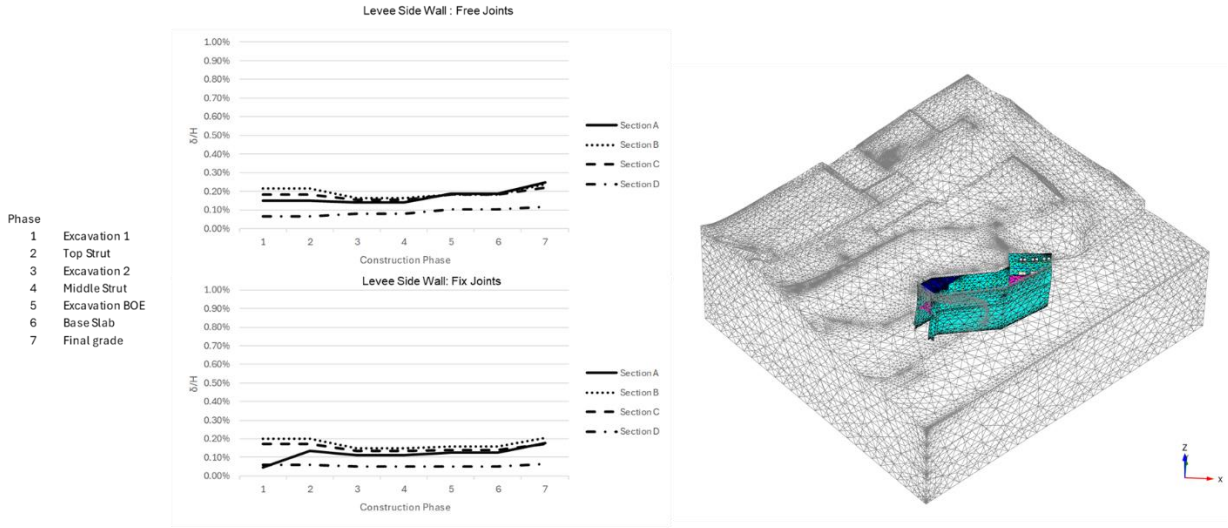


Fig. 4. PLAXIS 3D Analysis Chanel Structure

PLAXIS 2D (Refined Model)

The diaphragm walls were modeled in the PLAXIS 2D analyses as plate elements, as was the base slab. These plate elements were shown as lines in the 2D model, with their structural properties defined per foot of wall in the out-of-plane direction. The struts providing lateral support to the walls were also modeled using plate elements in most cases. However, in certain sections, a top strut was observed to experience tension during the final stages of excavation. To avoid relying on tension in these struts, they were replaced with node-to-node anchors. These anchors allowed the input of a maximum tension value, which was set to zero. Unlike plate elements, properties for node-to-node anchors were defined per individual strut along with their spacing, and PLAXIS 2D internally converted this input to per-foot values in the out-of-plane direction. Figure 5 depicts the mesh in the PLAXIS 2D model, and the maximum lateral wall displacement results normalized to depth of excavation for different construction stages. The normalized maximum lateral wall displacement (δ_{max}/He) of the structure remained under 0.27% for most cross sections and construction phases.

 © Deep Foundations Institute 2025

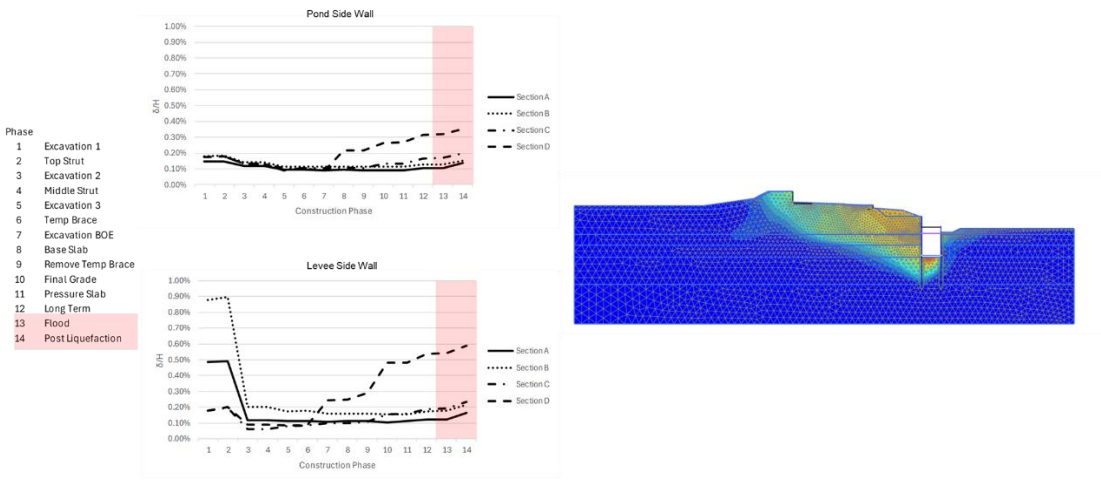


Fig. 5. PLAXIS 2D analysis Chanel Structure

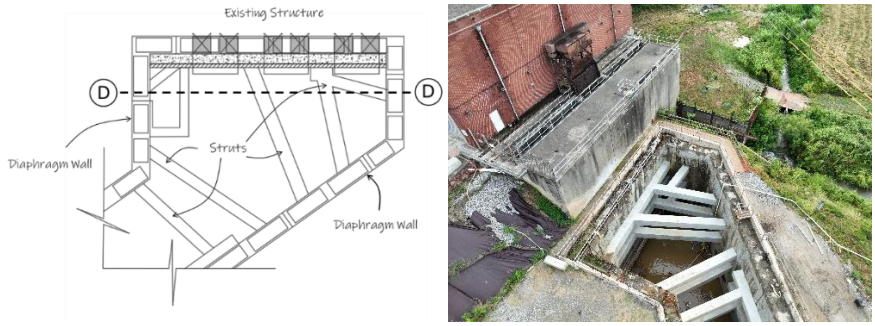


Fig. 6. Section D (Plan View) and aerial view

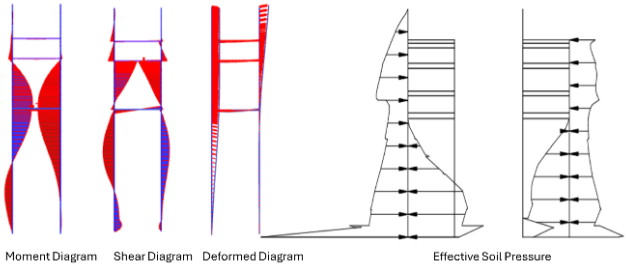


Fig. 7. Resultant forces diagrams from PLAXIS 2D Chanel Structure

To determine the appropriate lateral pressures for the 3D STAAD model, the effects of braces were first removed from the PLAXIS shear and moment diagrams. A statically equivalent lateral pressure diagram was then developed to replicate the results from PLAXIS 2D. The shear and moment diagrams from PLAXIS 2D were interpolated to match the specific points required by the 3D STAAD model. For each 3D STAAD segment, two lateral pressures were computed: one to match the shear diagram and another to match the moment diagram from PLAXIS 2D. A weighted linear combination of these two pressures was used to define the final pressure values. Finally, STAAD commands were generated to apply the

computed lateral pressures to the model. The objective is to apply a lateral pressure over the given segment that will result in shear and moment matching the values interpolated from the PLAXIS 2D results.

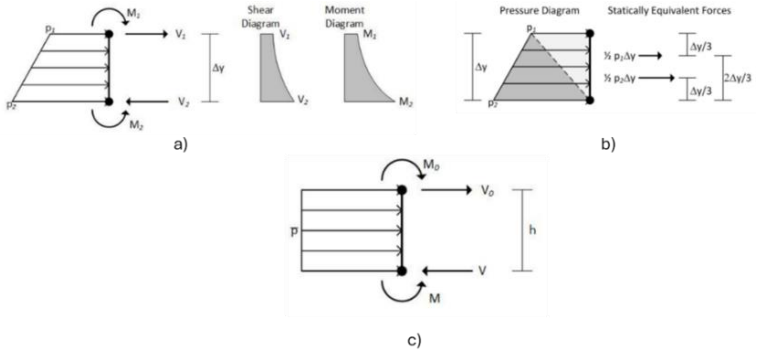


Fig. 8. Equivalent Pressure derivation from PLAXIS 2D for 3D STAAD a) Calculate the equivalent pressures from Moment and Shear diagrams b) Calculate the statically equivalent forces c) Equivalent load at given 3D STAAD nodes.

Since it is not possible to exactly match both the shear and moment diagrams from PLAXIS 2D, a weighted average of the corresponding pressures was used to approximate them. Trial calculations showed that matching the shear diagram alone provided a reasonable approximation of the moment diagram, while matching the moment alone resulted in unstable, oscillatory pressures. As a result, the weighted average was designed to place more emphasis on matching the shear diagram, which produced the most balanced and representative results.

Section D

A limitation of 2D models is the selection of a cross section that adequately represents the three-dimensional characteristics of the structure within a two-dimensional profile. This constraint becomes particularly evident when modeling the portion of the channel structure near the existing flood pump station. The results shown in Fig. 5 illustrate that the response of Section D, as modeled in PLAXIS 2D, is more flexible compared to the response obtained from the PLAXIS 3D model. This discrepancy is primarily due to the inability of PLAXIS 2D to fully represent the multiple struts that support this section.

3D STAAD (Structural Model)

The supports for the structure were modeled as pinned connections in both horizontal directions and as compression springs in the vertical direction. An iterative process was used to define the spring value to replicate the PLAXIS 2D vertical deflections. The wall base supports were assigned as a compression only spring to prevent any tension from developing at the bottom of the wall.

The panel connections act like pinned joints, allowing some lateral force transfer but no moment transfer. In the model, this is shown using plate releases at the two nodes next to each joint (see Fig. 9). These releases are placed along the full height of the wall at each joint. Since vertical joints can't carry tension, the horizontal force is also released at joints where there is net horizontal tension.

 © Deep Foundations Institute 2025

The equivalent geotechnical loads from PLAXIS 2D were applied in 3D STAAD as plate pressures for each construction phase. These loads, which account for soil, groundwater, and flood conditions, were combined using superposition to track residual stresses. In 3D STAAD, soil loads are defined as "Reference Load Definitions" and divided into four sections (A–D), considering different excavation and construction stages. Initially, base slabs and struts are deactivated, then progressively activated as construction advances. Skin friction on the excavation side above the base slab is ignored due to disturbance, but resistance below the slab is included.

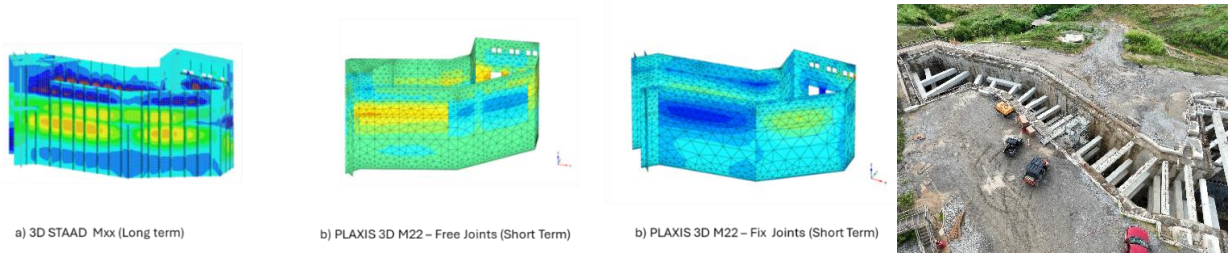


Fig. 9. Isometric view 3D STAAD and initial PLAXIS 3D Models Chanel Structure, and aerial view

MONITORING MOVEMENTS

Monitoring diaphragm wall deflections is crucial for verifying design assumptions, ensuring safety, and detecting potential issues early (Castelli and Lentini, 2016). More frequent measurements are needed during construction, and instruments should be placed strategically. Data interpretation involves comparing measurements with predictions, and automated alerts can help in timely intervention. Detailed documentation of monitoring data is important.

Monitoring provides crucial feedback on wall performance and allows for adjustments if needed. Integrating monitoring data with FEA can improve the accuracy of numerical models.

The project included an Instrumentation Monitoring Plan, which included the installation of several slope inclinometers and vibration monitoring points. Also, the monitoring plan included the installation strain gages at strategic points.



Fig. 10. Instrumentation a) Inclinometer casing b) In-Place Inclinometer sensor c) Strain gage installation

 © Deep Foundations Institute 2025

REALITY VS. DESIGN

Real-world examples provide valuable data on the range and patterns of wall deflection observed in practice. A comprehensive study encompassing 60 deep excavation projects supported by rigid diaphragm walls revealed maximum lateral displacements (δ_{max}) normalized by excavation depth (He) ranging from 0.10% to 0.27% for the top-down construction method, and from 0.20% to 0.50% for the bottom-up method (Boonyarak et al, 2024). However, with the bottom-up method and a wall thickness of 1.0 m (3.3 ft), longer excavation times can lead to displacements as high as 0.60%He. Another study in Shanghai's soft soil reported mean values of 0.27%He for top-down and 0.4%He for bottom-up methods.

Masuda et al. (1994) compiled and analyzed a database of 52 deep excavation case histories, ranging from 10 to 42 meters in depth. They simplified each case and developed a first-stage procedure to estimate the maximum lateral deflection of concrete diaphragm walls. The dominant parameters—soil stiffness above and below the excavation, wall flexural rigidity, embedment length, strut number/spacing, and construction measures such as strut pre-loading, top-down sequencing, and soil improvement—were consolidated into an "excavation-system stiffness" coefficient, R. When the measured deflection ratios ($\delta = \delta_max / He$) were plotted against R on log–log axes, a correlation expressed as $\delta = A (R / R_I)^{½}$ was obtained, with A values of approximately 0.012 for sand, 0.030 for mixed ground, and 0.035 for clay. The correlation can be employed to size walls, select strut layouts, and quantify the benefits of mitigation options—such as closer strut spacing, pre-loading, deeper embedment, or ground treatment—during preliminary design, while well-controlled projects are indicated to limit δ to about 0.05–0.5% He.

The lateral displacement readings from one string of in-place inclinometers are compared to PLAXIS 2D model predictions in Fig. 11. Both results are from a diaphragm wall panel in the new pump station section on the levee side. The maximum displacement predicted in the PLAXIS 2D model was 0.15% He. The maximum displacement measured in the in-place inclinometer was 0.09% He. Three-dimensional effects not represented in the 2D model are the most likely reason why the model predictions were larger than the actual measured values.

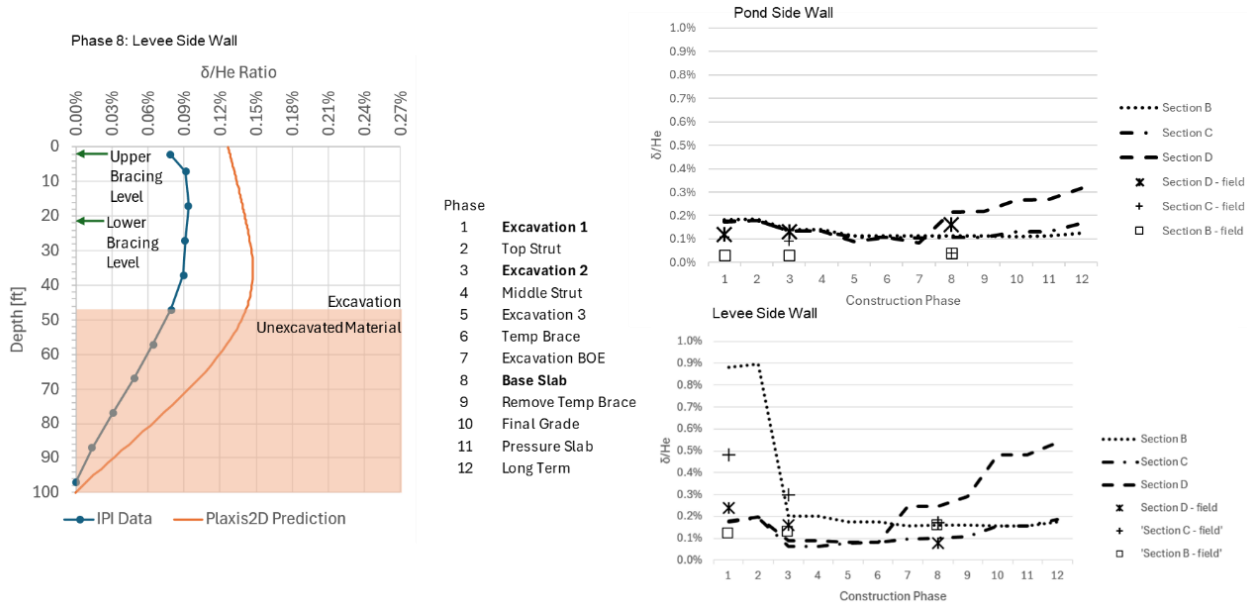


Fig. 11. Comparison of Field-Measured Displacements and Plaxis2D Model Predictions

 © Deep Foundations Institute 2025

CONCLUSIONS

A two-stage workflow was adopted: 2D PLAXIS generated detailed shear-moment envelopes for each construction phase, which were converted into statically equivalent lateral pressures and imported as reference loads in a 3D STAAD model that focused on panel-joint flexibility and reinforcement. This hand-off captured soil–structure interaction without burdening the structural team with ground modeling, yet required only routine PLAXIS and STAAD skills—far less effort than mastering fully coupled codes such as LS-DYNA or ABAQUS. Field inclinometers later showed wall movements of 0.09% He, comfortably below the 0.15% He predicted in PLAXIS and well under the 0.5% He industry benchmark, confirming both the accuracy and cost-efficiency of the procedure.

This project illustrates the benefits to be gained from the use of finite element modeling in design. Despite the complex geometry and varying subsurface materials, the design currently appears to be performing even better than expected. The use of advanced modeling provided cost savings and functional benefits to the project owner.

REFERENCES

Dong, Y.P.., 2024. Effect of diaphragm wall construction process on the performance of braced excavation. 10.1201/9781003413790-20.

Boonyarak, Thayanan & Aung, Aye & Kamchoom, Viroon & Aye, Zaw., 2024. Diaphragm wall lateral movement in deep excavations in Bangkok clays: impacts and influencing factors. Canadian Geotechnical Journal. 62. 1-16. 10.1139/cgj-2024-0058.

Castelli, Francesco & Lentini, Valentina., 2016. Monitoring of Full Scale Diaphragm Wall for a Deep Excavation. 1st IMEKO TC-4 International Workshop on Metrology for Geotechnics. Benevento, Italy, March 17-18.

Dwarampudi, Lavanya & Teo, Peiling., 2022. A study on the deflection behaviour of diaphragm walls supported laterally by cross walls in deep excavations.

Hacker, Adam & Farfan, Enrique & Pace, Tom & Giacometti, Benjamin., 2024. Complex Geotechnical Engineering for a Levee Project. 49th Deep Foundation Institute Conference. October 7-10. Aurora.

Hsieh, Pio-Go & Ou, Chang-Yu & Hsieh, Wei-Han., 2016. Efficiency of excavations with buttress walls in reducing the deflection of the diaphragm wall. Acta Geotechnica. 11. 10.1007/s11440-015-0416-6.

Kumar, Sanjie Dutt & Dela Cruz, Orlean., 2024. Using Finite Element Method in Seismic Analysis: A Literature Review on Diaphragm Wall. IOP Conference Series Earth and Environmental Science. 1326. 012003. 10.1088/1755-1315/1326/1/012003.

Masuda, T., Einstein, H. H., & Mitachi, T. 1994. Prediction of lateral deflection of diaphragm wall in deep excavations. Journal of Geotechnical Engineering, (505/I-29), 19–29.

Phien-Wej, N. & Humza, Muhammad & Aye, Zaw., 2012. Numerical modeling of diaphragm wall behavior in Bangkok soil using hardening soil model. 715-722. 10.1201/b12748-95.

 © Deep Foundations Institute 2025

Teparaksa, Wanchai & Teparaksa, Jirat., 2019. Comparison of Diaphragm Wall Movement Prediction and Field Performance for Different Construction Techniques. Underground Space. 4. 10.1016/j.undsp.2019.01.001.

Yeh, Tzu-Yuan & Ou, Chang-Yu & Lim, Aswin., 2022. A case study of strut-free excavation retaining system. Acta Geotechnica. 17. 10.1007/s11440-022-01526-4.

 © Deep Foundations Institute 2025

CASE HISTORY: HARBOR POINT BALTIMORE EVOLUTION OF DEEP FOUNDATIONS OVER 40 YEARS

Adam M. Dyer, PE, Senior Associate: Mueser Rutledge Consulting Engineers, PLLC, New York, New York, United States, (917) 339-9460, adyer@mrce.com
Srinivas Yenamandra, PE, Associate Principal: Mueser Rutledge Consulting Engineers, PLLC, New York, New York, United States, (917) 339-9399, syenamandra@mrce.com

ABSTRACT

Harbor Point in Baltimore, Maryland has undergone a transformation from industrial hub to environmental cleanup site to a commercial office space hub over the span of the last 40 years from 1985 to present day. This evolution has spanned a myriad of advancements in deep foundations, waterfront revetment, underground barrier technology, groundwater modeling and maintenance, and re-development. Site development included stabilization of the shoreline with an engineered embankment, dismantlement of the industrial plant, early use of groundwater computer modeling using MODFLOW to assess various environmental remedies, application of geosynthetics and hydraulic barriers to contain contaminants and control groundwater flow, and design and approval of driven piles through geosynthetics to meet environmental controls and support high-rise structures. Together, these various aspects of groundwater control and deep foundation design have maintained efficacy of the in-place environmental remedy, facilitated revitalization of the waterfront, and development of an entirely new neighborhood for the city. With one parcel remaining for re-development, current plans contemplate the re-use of existing abandoned foundations to act as improved ground, developing pile designs to support cantilevered floors and compatibility with aggressive groundwater chemistry.

Keywords: case history, brownfield site, embankments, slurry walls, multimedia cap, driven piles

Note from the Authors

The site described herein has been subject to many significant environmental impacts. The focus of the paper is limited to soil mechanics and foundations. For information regarding environmental aspects, see Baltimore Chromium Residue Cleanup website: http://baltimorechromiumresiduecleanup.com/

INTRODUCTION

In the late 1970s, the Harbor Point peninsula in Baltimore, Maryland was an industrial hub for manufacturing and chrome ore processing. At about the same time, the United States Environmental Protection Agency (USEPA) and Maryland Department of the Environment (MDE) were beginning to combat groundwater pollution from such industrial centers. As part of that process for the cleanup of the Harbor Point Site, see **Error! Reference source not found.**, Mueser Rutledge Consulting Engineers (MRCE) became involved in 1987. This paper provides an overview of the geotechnical work performed at the site, highlights analysis, decision making, and construction practice at the time.

 © Deep Foundations Institute 2025

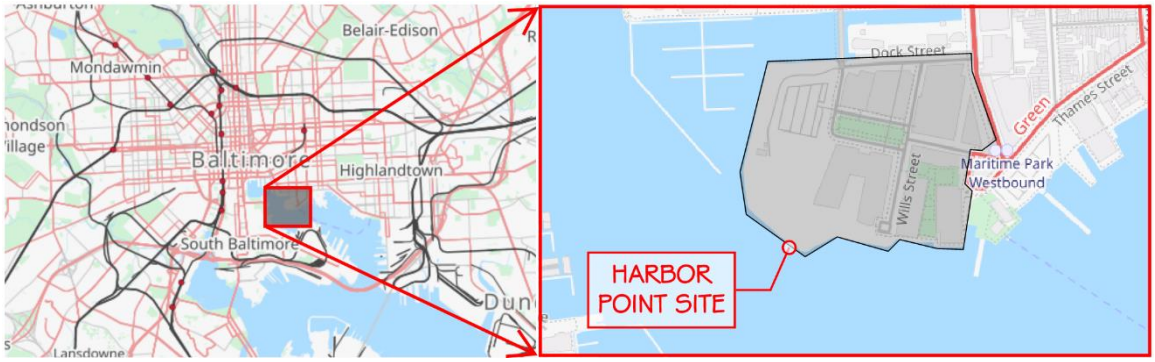


Fig. 1 – Site Location

SITE GEOLOGY

Harbor Point is a natural peninsula which extends into the northwest branch of the Patapsco River, to become part of the eastern shoreline of today's Baltimore Inner Harbor. The original peninsula was a mound of Coastal Plain sediments consisting of Pleistocene and Cretaceous deposits, see **Error! Reference source not found.**. The Cretaceous strata range from hard clays to compact sand and gravel. The underlying rock, a gneiss, exhibits a profile of advanced weathering and generally transitions to less weathered rock with depth. The rock surface slopes down to the southeast. The peninsula was enlarged by filling beyond the original shoreline. The fill overlies gray organic clay and sand outboard of the original shoreline.

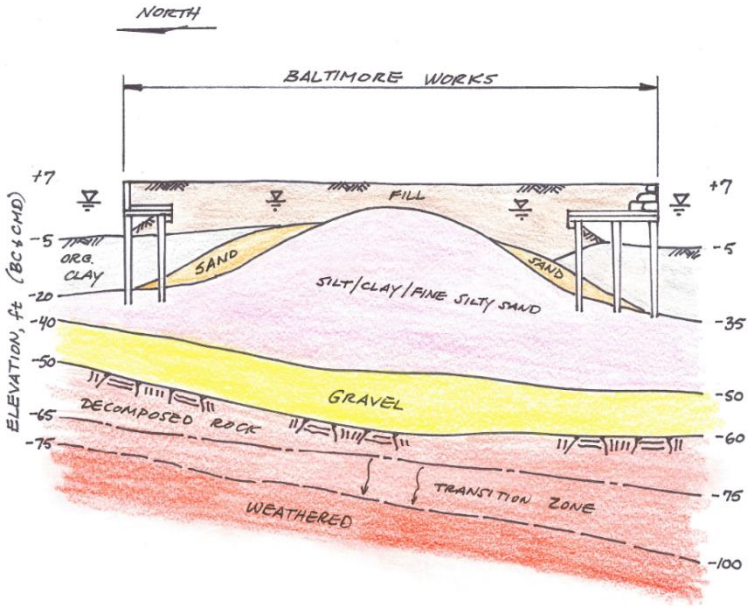


Fig. 2 – Generalized Site Geology (Not to Scale)

INDUSTRIAL DEVELOPMENT (PRIOR TO 1985)

Summaries presented herein are based on research material available at the Fells Point Historical Society and historical files from Allied Chemical.

 © Deep Foundations Institute 2025

Trading and Tall Ship Building

In the 1700s European settlement of the Harbor Point Peninsula included shops and services for merchant ship crews and harbor workers. Historically, the center of the peninsula was the highest and the eastern end where it connects to the mainland would routinely flood and turn the peninsula into an island. As was common of such areas at the time, fast land was made by pushing debris into the marsh land to raise grade and develop the land. In the late 1700s and early 1800s, much of the peninsula was used as tall ship building yards for merchant and military ships made from timber.

Chrome Ore Processing

From the mid-1800s until 1985 the Mutual Chemical Company and later Allied Chemical owned and operated a chrome ore processing facility throughout most of the peninsula. The facility included over 30 structures which were used for storage, chemical washing, mechanical grinding, firing, treating, and packaging the chrome ore and its' byproduct which contained hexavalent chromium (Cr+6). Many of the facilities utilized deep foundations including:

- Timber Relieving Platforms – constructed at low tide over open water consisting of two alternating layers of timbers resting on timber piles with timber and granite block bulkheads.
- Steel Sheet Pile Cofferdams – interlocked steel sheets about 45 feet in diameter for moorings.
- Raymond Stepped Taper Piles – driven steel piles consisting of male to female connections.

PLANT CLOSURE AND CLEANUP (1985 TO 1999)

Summaries presented for this section are based on review of historical files from MRCE, an interview with former MRCE Principal and Engineer of Record Mr. Peter W. Deming, PE.

Environmental Cleanup/Containment

Operations throughout the plant's lifetime led to contamination of groundwater at the site and in 1989 Allied Chemical entered into a Consent Decree with USEPA and MDE requiring an environmental remedy which contained potentially hazardous contamination within the site, eliminated human and animal contact with contamination, and prevented further contamination of surrounding groundwater. The final Environmental Remedy System (ERS) consisted of a stone embankment along the waterside perimeter to provide lateral confinement of a soil bentonite hydraulic barrier, groundwater monitoring and head maintenance system (HMS), and multimedia cap (MMC). The ERS acts to maintain a water level inside the site below that outside the site and reduce overall flow into the site ("Inward Gradient"). Over the course of a period of 13 years, the ERS was constructed in three phases from 1989 to 2002.

Geotechnical Investigations

Throughout each phase of the cleanup, a separate geotechnical subsurface investigation was conducted to supplement available historic borings (239 borings) throughout the 26 acre site and provide more detailed stratification and physical samples to inform the design. Boring, sampling, and laboratory testing methods were performed in general conformance with ASTM standards, however some of the work was performed prior to issuance of the standard and included some variation. Methods employed included, Split Spoon sampling by Standard Penetration Test (ASTM D1586), hydraulically actuated or fixed piston type undisturbed sampling (ASTM D6519), and double-tube rock coring (ASTM D2113). All borings were advanced using mud rotary drilling (ASTM D5783) and casing with positive head during installation and removal of tooling. Investigations by MRCE included (159 borings):

- Along site perimeter to evaluate hydraulic cutoff (1988, 1992-1993);

- Paired borings onshore and offshore to evaluate stability of bulkheads to accommodate dredging and embankment construction (1989-1990);
- Interior of the site to develop feasibility studies for re-development (1991, 1994);

Laboratory testing included Oedometer (ASTM D2435), undrained shear strength (ASTM D2850), consolidated undrained shear strength (ASTM D4767), Atterberg Limits (ASTM D4318), grain size analysis (ASTM D421 and D422), and hydraulic conductivity or reconstituted samples (ASTM D5084). Sitewide review of laboratory testing indicated predictable variability of parameters such that extrapolation to areas of the site in between laboratory testing locations could be performed with reasonable certainty. For example, void ratio (e_0) and coefficient of consolidation (C_c) of the organic clay exhibited a strong correlation with water content (w), see **Error! Reference source not found.**. This correlation was able to reduce or eliminate the need for costly additional soil sampling and laboratory testing which would require significant environmental review and subsequent engineering controls to obtain.

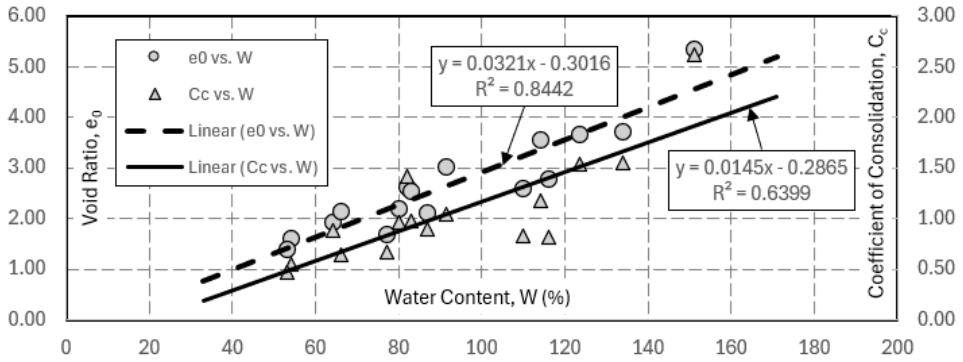


Fig. 3 – Sample Void Ratio as a function of Water Content correlation

Phase I: Outboard Embankment (1989 to 1993)

The Consent Decree required a contaminant source perimeter that was proximal to the existing bulkheads. Given the proximity of the existing bulkheads, stabilization of the waterside perimeter was required and was to be provided by a stone embankment. The stone embankment design required dredging of soft marine sediments to a depth of up to about 30 feet below Mean Low Water (MLW) and placement of stone of specific gradation in a tightly sequenced manner. To facilitate construction of the embankment an evaluation of global and local stability of the waterside perimeter was required.

Condition Survey of Existing Bulkheads

An in-depth condition survey of the existing bulkheads was conducted to evaluate local stability of the perimeter to facilitate embankment construction. The condition survey included extensive reviews of historical documentation, photo, test pit, and measurement survey of the existing bulkheads. This review indicated 15 distinct bulkhead types in conditions varying from collapsed to intact and in usable condition. See **Error! Reference source not found.** below for an example bulkhead schematic.

 © Deep Foundations Institute 2025

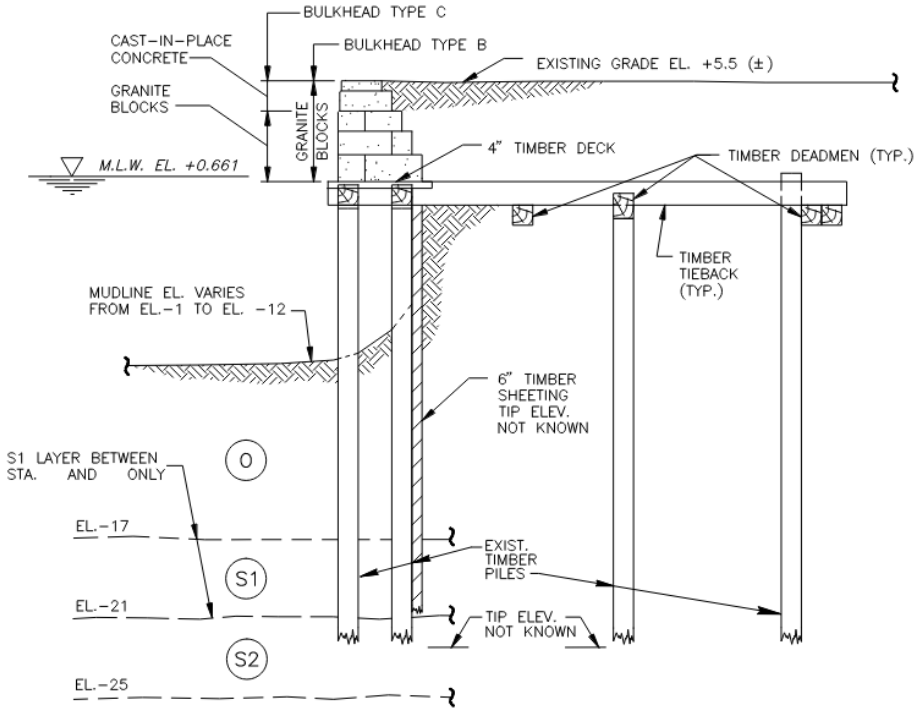


Fig. 4 – Example bulkhead along north side of the site with granite stone headwall

Local Stability

Two-dimensional limit equilibrium analyses were performed to assess the existing loading conditions and temporary loading conditions throughout construction of the embankment using hand methods. Analyses concluded that temporary stabilization measures were required to facilitate dredging. These stabilization measures included: (i) temporary battered and vertical steel H-piles and wale along the bulkhead to provide support during dredging; (ii) removal and or abandonment of piles and abandonment portions of existing piers; and (iii) filling and surcharge of an existing slip.

Global Stability

Two-dimensional limit equilibrium analyses were performed to assess the final configuration of the stone embankment and fill placement for grades using the program "PC-Slope" by GEO-Slope Programming, Ltd., a pre-cursor to the commonly used current day Slope/W. Analyses demonstrated that the existing marine clays in front of the bulkheads needed to be dredged out and would be stable (Factor of Safety > 1.25) during the dredging process.

Construction

Work was performed from 1990 to 1992 to stabilize the existing bulkheads, dredge the river bottom around the site perimeter, and then place the various stone strata. For typical embankment section, see **Error! Reference source not found.**. The embankment was constructed by dredging the river bottom and placing stone from barge mounted equipment until the embankment reached about Mean High Water (MHW). The remainder of the fill was placed by dump truck and graded from land.

A monitoring program was employed to verify stability of existing bulkheads including surface monitoring points and inclinometers. Surface settlement and inclinometer readings indicated less than ½ inch settlement and translation, except at a 70-foot long section of timber platform which collapsed.

 © Deep Foundations Institute 2025

While dredging along a timber low platform, the bearing surface was found to be about five feet deeper than expected and did not consist of the medium compact sand that was expected to help support the existing timber piles in the area. The affected structure was removed and debris was dredged and subsequently the final stone embankment was constructed to the originally planned extents and fill was placed in the collapsed section. During dredging and fill placement a robust quality assurance / quality control (QA/QC) program was employed which surveyed the river bottom prior to and immediately upon completion of dredging, stone placement by layer along the site perimeter.

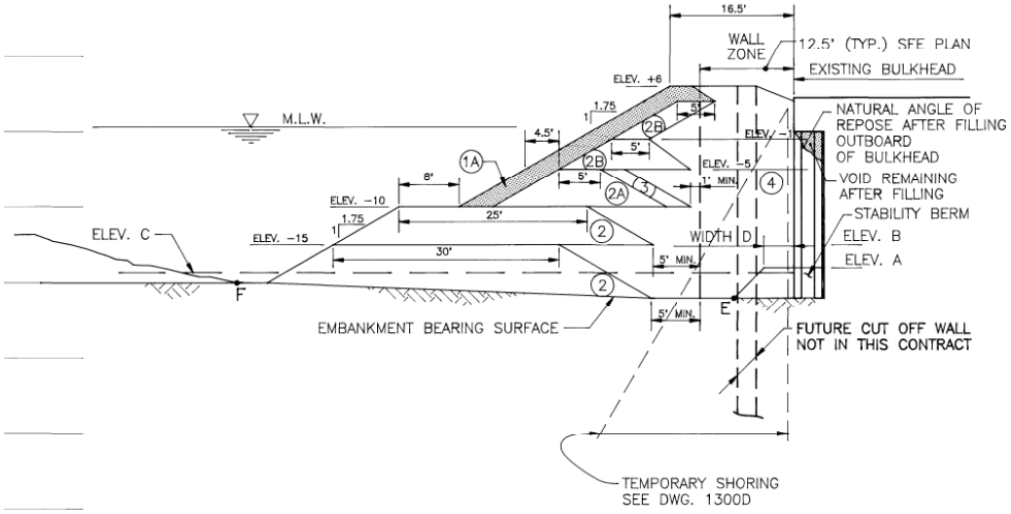


Fig. 5 – Typical Embankment Design Section. Note that numerical callouts refer to the various gradations required to be placed for the embankment construction, e.g. Material 1A was specified as "Maryland DOT Class II Rip Rap"

Phase II: Soil-Bentonite Hydraulic Barrier (HB)

The Consent Decree required that the contaminant source be restricted from spreading and expanding the existing contaminant plume. Based on a review of the known geology in the area, a site-specific aquifer testing program was performed to evaluate the potential solutions. Design and construction are briefly summarized below, for more in-depth description, see Deming (1997).

Aquifer Testing

Aquifer testing was performed to evaluate the anticipated quantity of effluent required to maintain the Inward Gradient by assessing the storage and flow within the aquifers. Testing was performed by installing pumping wells and stress testing in select locations onsite with monitoring provided by a series of piezometers at set distances away from the pumping wells, developing hydraulic conductivity parameters and evaluating flow for various pumping conditions by utilizing the Modular Three-Dimensional Finite Difference Groundwater Flow Model (MODFLOW). The testing and analysis confirmed that maintaining a cost-effective Inward Gradient at the site would require a low permeability hydraulic barrier keyed into bedrock at about 85 feet below grade.

Hydraulic Barrier Design

Utilizing the information from the geotechnical investigation and aquifer testing, the alignment of the HB was selected with a requirement to key into the decomposed rock a minimum of 3 feet. A series of bench scale tests were performed utilizing a mixture of onsite soil and groundwater anticipated to be encountered within the HB section and different types of bentonite. The resultant backfill was required to

 © Deep Foundations Institute 2025

be well graded sand and gravel with at least 20% fines including WyoBen SW-101 bentonite 3% dry weight addition and mixed with slurry.

Construction

Work was performed from 1994 to 1996 to excavate, mix, and place soil-bentonite in a trench up to 85 feet deep and about 3 feet wide along a perimeter about 2,800 feet long. For example photos of trench excavation and progress, see **Error! Reference source not found.** and **Error! Reference source not found.**.





Fig. 6 (left) – Slurry trench preparing to receive backfill

Fig. 7 (right) – Slurry trench in the process of QA/QC, bridge over trench visible at right side for engineers to measure trench bottom

During construction, a robust QA/QC program was implemented which monitored the slurry mix and soil-bentonite backfill for viscosity by marsh funnel, for specific gravity by mud balance, and for hydraulic conductivity by wet grab samples and laboratory permeability testing. Typical hydraulic conductivity of the backfill was about 4×10^{-9} cm/sec, well below the specification requirement.A portion of the trench was measured for width and verticality along the embankment to demonstrate stability of the slurry trench. To accomplish this, a device dubbed a “hexometer” was developed to measure the width of the trench in the upper 25 feet. The device was capable of measuring the width of the trench by lowering a tool incrementally into the slurry and expanding it to the width of the wall with a screw jack. Measurements demonstrated that the trench remained open within the stone embankment.

Phase III: Multimedia Cap (MMC) and Head Maintenance System (HMS)

As the final phase of ERS work, the manufacturing facility was to be dismantled and the site was to be graded to facilitate placement of the MMC that would provide passive drainage out to the waterside perimeter and integral with the MMC, the HMS serves to monitor, collect, and store groundwater pumped from the site to be transferred to trucks and disposed of offsite. To accomplish this, fill would need to be placed over compressible deposits and a high point created in the center of the peninsula to provide positive drainage off of the MMC with 3 to 8 feet of fill.

A geotechnical subsurface investigation was conducted to evaluate the depth and extent of compressible deposits throughout the interior of the site. The investigation included test pits in select locations of foundations to be abandoned, survey of foundations to be abandoned, borings to bedrock with fixed piston sampling and a laboratory testing program including oedometer, strength, and Atterberg Limits testing to evaluate the soil properties of the compressible deposits.

Settlement and Bearing Capacity

To facilitate raised grades, vault structures, and pumping Transfer Station in areas overlying abandoned foundations and soft compressible organic clay deposits, evaluations of settlement and allowable bearing were performed. From the subsurface investigations, the extents and thickness of the compressible deposits were well established and known to be up to 25 feet thick and from the condition surveys the existing bulkheads along the alignment were capable of supporting vaults and some regular weight fill placement.

However, review of the interior of the site indicated that, where compressible deposits were present, surcharge fill was required to reduce settlement concerns at (i) the filled-in "South Slip", (ii) the "Foot of Wills Street", and (iii) in the area of the Transfer Station. For schedule reasons, wick drains were utilized to speed up consolidation at the Transfer Station building bad.

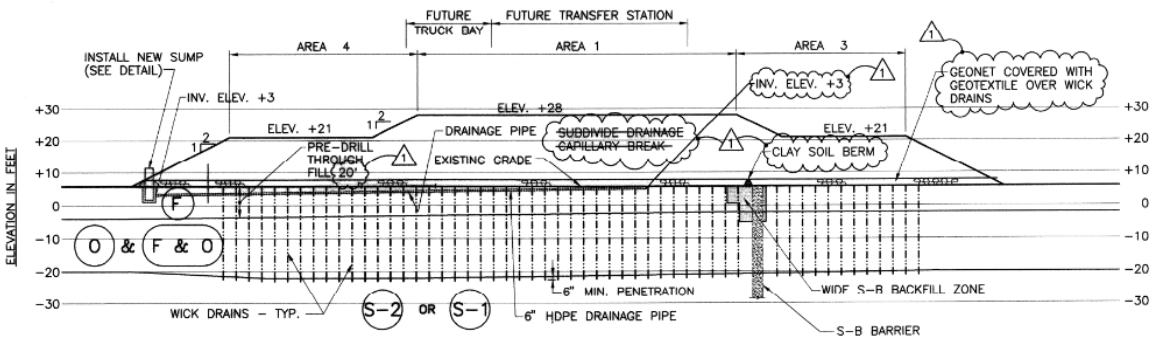


Fig. 8 – Example Surcharge Section at Transfer Station with Wick Drains and Surcharge Pile where "F" is Granular Fill, "O" is Organic Clay, and "S-1" / "S-2" is a Fine to Medium Sand

Construction

Work was performed from 1996 to 1999 to place surcharge, dismantle the remaining manufacturing facilities, install the HMS and MMC, and construct the Transfer Station. The final phase of the ERS consisted of six subprojects: (i) Surcharge Placement, (ii) Dismantlement, (iii) HMS Installation, (iv) MMC Construction, (v) Soil Cap, (vi) Transfer Station.

Surcharge Placement

Surcharge placement at the South Slip and Foot of Wills Street locations consisted of a compacted fill of generally known density and observation of settlement. Surcharge for the Transfer Station location required an accelerated schedule and was supplemented by wick drains. In some areas, the surcharge placement was in close proximity to the recently completed HB. In these areas, inclinometers were utilized to verify lateral displacement of the HB was within acceptable limits.

Dismantlement

The remaining structures on the site were demolished to about Elev. +7. Asphalt was placed to reduce stormwater infiltration within the HB perimeter until the MMC could be placed.

Head Maintenance System (HMS)

A series of piezometers were installed in twelve pairs roughly evenly placed around the perimeter of the size to monitor groundwater elevation on the inside and the outside of the HB. These pairs communicate with the Transfer Station to signal adjacent pumping wells located at the midpoints between each piezometer pair. Together the piezometers, pumping system, and Transfer Station work to maintain a hydraulic gradient which flows from outside the barrier to inside the barrier.

 © Deep Foundations Institute 2025

Multimedia Cap (MMC)

In the area within the HB, a multimedia cap was constructed consisting of a layer cake of soil and synthetic materials which together act as double-protection to reduce capillary rise and surface water infiltration, as well as promote stormwater runoff to the waterside perimeter. For a schematic of MMC components see **Error! Reference source not found.**.

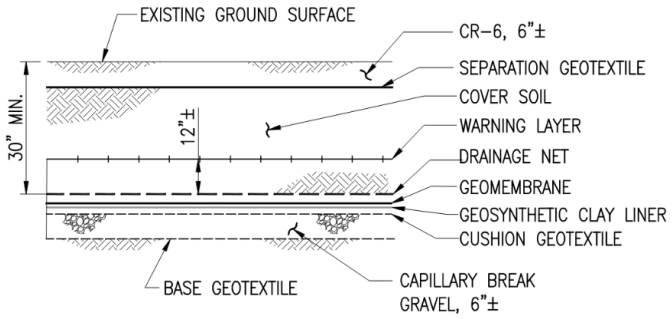


Fig. 9 – Multimedia Cap Layering

Transfer Station

The Transfer Station consisted of a two-story office building with mechanical pumping and electronic data acquisition systems. The building was steel framed and founded on shallow foundations bearing within the MMC.

RE-DEVELOPMENT (2005 TO PRESENT)

While the ERS was being constructed, Honeywell engaged in consultation with area residents, city and state regulators, and private developers and developed a Planned Urban Development (PUD). The PUD consists of five mixed-use development parcels, public parking, a 7-acre public park, and extension of the city street and utility grids into a new neighborhood for Baltimore, now known as Harbor Point, see **Error! Reference source not found.**. The following is a discussion of the design of deep foundations for sites located within the HB.

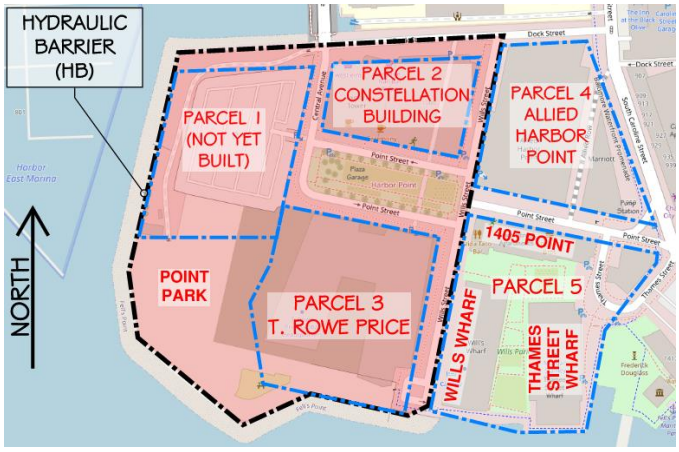


Fig. 10 – Approximate extents of development projects to date

 © Deep Foundations Institute 2025

Optimizing Foundations "On Cap"

In general, foundation selection is driven by the lowest cost solution which provides foundations of sufficient capacity and performance for a particular project. This site is no exception to that rule. However, for "On Cap" projects the ordinary relevance of various parameters becomes heavily skewed with the required environmental controls at the site. For instance, consider the cost of groundwater control on contaminated sites in current prices, groundwater contaminated with NAPL or similar costs on the order of $0.02/gal to treat and discharge, whereas contaminated groundwater at the site costs on the order of $1.00/gal to treat and dispose offsite (note that onsite treatment and discharge would be even more!).

Every action below the MMC costs more. More controls, more unique conditions, more review, more documentation, more oversight, etc. The name of this game is to find where the total cost considering capacity and constructive effort reside with a heavy emphasis on the process. Early in the development process, a general contractor and specialty environmental excavation contractor were brought on to the team to assist with evaluating the intricate sequence of opening the MMC to allow for construction of foundations at the site.

Given the presence and depth of uncontrolled fill throughout the site, nearly every area of the site and structure required for re-development was recommended to bear on deep foundations.

Deep Foundation Design

During the design phase of the first "On Cap" project, the project design and construction teams worked closely to evaluate the cost implications of driven versus drilled foundations. Weighing the costs of drill spoils containment, stormwater management, environmental controls, installation duration, and pile replacement ratio (i.e. – Pile Type A has a capacity of 2 times that of Pile Type B). These cost studies indicated that driven piles were optimal for the project and it was decided that a design phase pile load testing program would be performed to optimize pile capacity.

As a starting point, the driven pile type used for the Thames Street Wharf projects was reviewed. This review indicated that 16-inch diameter driven pipe piles with an allowable load of 200 tons were utilized. Upon review of the production pile load tests and pile driving records, it was noted that surplus capacity may be available on the selected piles. Therefore, a load test program which evaluated the actual failure point of the piles was designed.

Pile Load Testing Program

Since the USEPA and MDE had not yet approved work to occur within or below the MMC ("Intrusive Activities"), a design pile load testing program was performed from the lot adjacent to the east of the Constellation Building project within Parcel 4. The load testing program consisted of:

- Two test locations, with one inboard (Area 1) and one outboard (Area 2) of the historic shoreline
- Testing consisted of:
    - Pile Driving Analyzer (PDA, ASTM D4945) testing on 16-inch and 18-inch diameter conical tip pipe piles filled with 4,000 psi concrete, HP14x117, and HP18x135 piles;
    - Static axial compressive load tests in accordance with ASTM D1143-07 Maintained (Procedure B) and Excess (Procedure C) load tests; and
    - Static lateral load tests in accordance with ASTM D3966-07.

Prior to assembly of load test frame pile driving records for each of the pile types were compared to select which pile type would be load tested. See **Error! Reference source not found.** below for comparison of installation results. Based on the comparison below, it was decided that the pipe piles would be more economical and load testing was advanced on that type.

 © Deep Foundations Institute 2025

Table 1 – Summary of Test Pile Installation

Pile Type	PDA Ultimate Capacity, tons	Drive Time, minutes	Length of Pile, feet	Weight of Steel per Pile, tons	Splice Required
16-inch Pipe	500	40	50	2.1	No
18-inch Pipe	575	40	50	2.4	No
HP14x117	600	60	90	5.3	Yes
HP18x135	650	60	90	6.1	Yes

Example Load Test Results

On the 16-inch diameter pipe pile, a maintained load test was performed by loading the pile in increments of 25% of a design load of 300 tons up to 450 tons whereupon one additional load increment was attempted to 500 tons, 168% of design load. At this point, a hold period was initiated and after 9 hours was backed off to 400 tons, 133% of design load, and reloaded again to 450 tons, 150% of design load then held for 48 hours. At the end of the hold period, it was observed that the pile crept less than 0.01 inches per hour with a maximum pile top movement of less than 1 inch and settlement of about 0.3 inch and providing an allowable load of 200 tons. See **Error! Reference source not found.** (left) for results.

Upon removal and full rebound of the maintained test, an excess test was performed by loading the pile in increments of 50% of the maintained test allowable load of 225 tons to 450 tons, 200% of the maintained test allowable load. From there, additional load was applied in 10% increments until reaching a load of 600 tons whereupon rapid progressive movement of the pile was observed. See **Error! Reference source not found.** (right) for results.

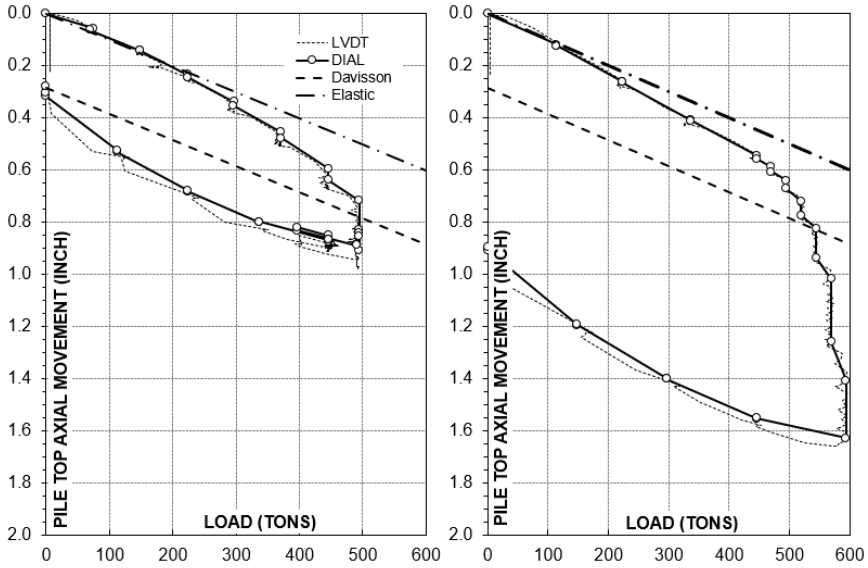


Fig. 11 – 16-inch Diameter Pipe Pile Maintained (Left) and Excess (Right) Load Test Results

Recommended Allowable Load

Based on these load tests, it was verified that additional capacity was available and allowable load for the 16-inch diameter pipe piles was recommend at 250 tons. Similar testing was also performed for the 18-inch diameter pipe piles and provided a recommended allowable load of 287 tons. It was decided to carry

 © Deep Foundations Institute 2025

the design forward using the two test pipe pile sizes. By performing the Excess Test, an extra 25% allowable capacity was able to be proven out and saving a corresponding percentage of required piles.

Lessons Learned

While constructing foundations for projects located within the HB, the excavation sequence has evolved. The lessons learned predominantly revolved around reducing stormwater infiltration to below the MMC as much as possible such that the water could be deemed as "non-contact" (meaning that the water did not come into contact with site contamination and was eligible to be tested and treated as such). These lessons included, but are not limited to: modifications to slope setbacks for temporary work to reduce stormwater catchment areas; usage of sump pumps and storage tanks to collect stormwater from excavations and minimize drainage into subgrade to prevent the accumulation of "contact" water; where long gaps in stages were required, the geosynthetics were temporarily restored to minimize the accumulation of "contact" water.

Developments to Come

As of the writing of this paper, one development site in the northwest corner remains. The final site includes some of the most densely populated abandoned foundations and harsh groundwater chemistry conditions with pH ranging from 3 to 12 in a distance of less than 50 feet. Abandoned foundations include several tank foundations, dense driven pile caps, thick concrete mat foundations, steel rails, stone foundations, abandoned timber relieving platforms, among other miscellaneous foundations.

CLOSING

The Harbor Point site has been a challenging site to remediate and re-develop. Investigations, analysis, and solutions at the site have continued to grow and evolve as the industry has grown and evolved over the past 40 years. The site has been around to witness the full life cycle evolution of commonly used digital tools such as Slope/W, MODFLOW, and AutoCAD. As work continues, the site serves as a reminder of an evolving industry and understanding of the state of practice and makes one take notice of the potential for beneficial adaptation and inclusion of the available potential solutions based on the observational method.

ACKNOWLEDGEMENTS

MRCE would like to acknowledge the USEPA, MDE, and the entire Harbor Point team in providing the leadership, expertise, development, and implementation of numerous concepts to a complex site. Including, but not limited to: Honeywell International, Beatty Development Group, Jacobs, Beatty Harvey Coco Architects, iO Studio, Armada Hoffler Construction, Environmental Waste Minimization, Wagman, Hallaton, Environmental Resources Management, Morris Ritchie Associates, Tadjer Cohen Associates, Hillis Carnes Associates, Black and Veatch, Weeks Marine, Conti Environmental, Greenhorne and O'Mara, Gerraghty and Miller (a.k.a. Arcadis) and the many other consultants, designers, and contractors who have helped make the re-development of the site an ongoing success.

Lastly to our dear friend and former Principal, the late David R. Good, PE we extend our gratitude for his dedication to his work, the detail of field documentation and innovation to complete the environmental remedy at the site and assist with the re-development of the site.

REFERENCES

Deming, P. W., 1997. Design and Construction of a Deep Slurry Trench Barrier, Proceedings of the International Containment Technology Conference.

 © Deep Foundations Institute 2025

SUSTAINABLE SOLUTIONS FOR RCC FOUNDATION DURABILITY: CASE STUDIES IN AGGRESSIVE SUBSOIL AND GROUNDWATER CONDITIONS

Geethanjali Koppolu, Engineers India Limited, New Delhi, India, 9250928456, geethanjali.k@eil.co.in
Sampat Raj, Engineers India Limited, New Delhi, India, sampat.raj@eil.co.in
Sanjoy Bhowmik, Engineers India Limited, New Delhi, India, sanjoy.bhowmik@eil.co.in
VK Panwar, Engineers India Limited, New Delhi, India, vk.panwar@eil.co.in

ABSTRACT

The durability of structures in aggressive environmental conditions significantly influences their performance and design life. For underground structures and foundations, current practices often prioritize strength over durability, relying on concrete's inherent corrosion protection. However, corrosion can occur when the protective oxide film on embedded reinforcement is compromised by aggressive substances, leading to severe structural deterioration.

This paper presents case studies highlighting the challenges and protective measures adopted for shallow and deep foundations in diverse geological conditions with high sulphate, chloride, and acidic content in subsoil and groundwater. In one case, highly acidic soil conditions (pH 3–4) necessitated measures like Sacrificial Anode Cathodic Protection (SACP) using zinc anodes, tanking systems, increased cover, and composite cement. Whereas the other case involved extremely high chloride contents (8,400–108,000 mg/l) in groundwater, requiring dense, impermeable concrete through optimized mix design, superplasticizers, ultrafine additives, and enhanced cover. Additionally, waterproofing systems, including SBS membranes and HDPE liners, were implemented to prevent the intrusion of aggressive substances.

This paper discusses the findings from chemical analyses of soil and groundwater and the protective measures implemented to make concrete dense and impermeable, ensuring that it performs satisfactorily throughout its design life. It also covers secondary protective measures like the SACP system and the permanent liner adopted for the reinforced concrete piles.

Keywords: durability, aggressive environmental conditions, reinforced concrete piles, corrosion protection, and structural performance

INTRODUCTION

High chloride and sulfate levels in soil and groundwater are detrimental to reinforced concrete. These case studies show how unusually high concentrations of both were mitigated in the design of deep and shallow foundations. The embedment of steel in concrete enhances its applicability widely however, it is vulnerable to corrosion under aggressive environment and impairs the durability of reinforced cement concrete (RCC).

Corrosion in steel is an electrochemical process that requires three elements viz. anode, cathode, and electrolyte. Due to the difference in electrical potential along the steel in concrete the anodic and cathodic regions are formed. The free water present in the concrete act as an electrolyte. In the electrochemical reactions, the positively charged ferrous ions (Fe^{++}) at anode regions pass into the solution and negatively charged free electrons (e^-) pass through the steel into the cathode where they combine with water and oxygen to form hydroxyl ions (OH^-). The reaction at the cathode is called a reduction reaction and thus to maintain electrical neutrality, the ferrous ions move through the pore water present in concrete towards the cathodic region and combine with hydroxyl ions to form ferric oxide $Fe(OH)_2$ which further react with free oxygen ions and make hydrated ferric oxide which is known as rust. The volume of the rust is approximately six times higher than the base material due to which it exerted an outward pressure on the

 © Deep Foundations Institute 2025

concrete resulting in spalling and cracking of the concrete. Figure 1 shows the spalling concrete and corroded reinforcing bars. Corrosion in the concrete reduces the intended design life of the structure.



Fig. 1. Spalling concrete and corroded reinforcing bars

Corrosion in RCC mainly occurs due to carbonation or by the ingress of soluble chlorides. Carbonation is a process in which carbon dioxide from the environment reacts with calcium hydroxide in the concrete and makes calcium carbonate. This reaction reduces the pH of the concrete below 8.5 which makes the passive layer unstable. The carbonation process is very slow and generally less destructive for subsurface concrete due to inadequate carbon dioxide. For subsurface concrete, the main reason for corrosion in steel is chloride ions which penetrate through the pores of the concrete and break the passive layer and makes reinforced concrete vulnerable to corrosion.

In additions to the chlorides, high sulphate concentrations in soil or groundwater can also severely damage RCC structures by reacting with cement compounds to form expansive products like ettringite and gypsum. This leads to internal stresses, cracking, spalling, and loss of strength. The resulting cracks increase permeability, allowing further ingress of aggressive agents, which accelerates the corrosion of reinforcement. Over time, this compromises the durability and serviceability of the structure. To mitigate these effects, sulphate-resistant materials and dense, impermeable concrete must be used along with additional protective measures.

Corrosion in the reinforced concrete reduces the cross-sectional area of the structure, which may impart loss of strength and sometimes make it unserviceable. Therefore, it is essential to keep reinforced concrete free from corrosion throughout its intended design life to make it durable and serviceable. The primary cause of the corrosion is the ingress of deleterious substances through the pores of the concrete. Therefore, to reduce the intrusion of these deleterious substances, the concrete should be made dense and impermeable. The concrete can be made impermeable by using a suitable cement type, optimum cement content, low water-cement ratio, high clear cover, etc. For making the concrete dense and highly workable, admixtures and supplementary cementitious materials are also added.

When the concrete is exposed to highly aggressive conditions, the first line of defence is provided by using high quality concrete with maximum chemical resistance. This is further enhanced by the application of protective treatment on the concrete surface using epoxy coating, bituminous coating, HDPE membrane, etc.

This paper presents two case studies of the protective measures adopted for RCC foundations located in extremely aggressive ground conditions. In the first case study, chemical test results indicate that high chloride content along with high sulphate concentrations along with very acidic environment. In the second case study the chemical test results reveals higher chloride content and higher sulphate concentrations.

The high concentration of chloride content that existed in groundwater would corrode the concrete if suitable protection measures are not adopted. In addition to chloride-induced corrosion, high sulphate concentrations in subsoil and groundwater pose a serious threat to RCC durability. For the proposed site the environmental exposure condition falls under the very severe category according to IS 456 (2000) and appropriate values of minimum cement content, maximum water-cement ratio, clear cover, and grade of concrete were adopted to make concrete durable. Further, based on the sulphate concentrations the site falls beyond the class-V specified in IS 456 (2000). These levels are so extreme that standard approaches are not viable and necessitated creative alternatives and accordingly a novel protection scheme was formulated. The scheme comprises the protection of concrete by making it dense and impermeable as well as encapsulating it with a completely waterproof barrier.

The details of various protective measures adopted to prevent the corrosion of RCC foundations are discussed in the paper. These measures would be useful for the practicing engineers as well as research fellows for guidance and future development for structures resting in similar types of aggressive conditions.

CASE STUDY-1

Site Information

An existing refinery in southern part of India, is being expanded to nearly double its current capacity. A new plot of land was acquired from the adjacent fertilizer plant for accommodating some of the refinery's facilities. The newly acquired land was previously used for fertilizer plant operations, gypsum dumping, and industrial waste disposal. Figure 2 shows the Gypsum dumping yard.



(a) **(b)**

Fig. 2. (a) Gypsum dump yard; (b) Acidic groundwater

Aggressiveness of Subsoil and Groundwater

Gypsum is corrosive to concrete foundations, and traces of gypsum were most likely left in the subsoil even after grading work was completed. A detailed soil investigation was carried out to determine the subsoil profile and their engineering properties. The chemical tests were conducted on subsoil and groundwater samples to determine the concentration of sulphates and chlorides. For the tests, groundwater was collected from boreholes and soil samples were collected at various depths along the boreholes. According to chemical test results, the maximum chloride content in groundwater ranges from 8400 to 24100mg/l, which was higher than the chloride content in sea water (17000-18000 mg/l). The chloride content of soils ranges from 0.52% to 0.74%. The maximum sulphate concentrations in soil samples and groundwater were 0.88% and 5360mg/l respectively. Groundwater and soil samples had pH values ranging from 2.98 to 3.90 (min.). The pH values indicated a very acidic environment.

Considering the prevailing subsoil strata i.e. soft marine clay is underlain by rock strata and high groundwater in this proposed area, all major foundations are supported on Bored cast-in-situ RCC pile socketed into rock. A permanent mild steel liner was initially considered to protect the pile foundation; however, metal is highly vulnerable to corrosive in an acidic environment, hence, this option was ruled out following receipt of the chemical test results.

Mouallif et al. (2013) demonstrated that polymer-based casings, particularly High-Density Polyethylene (HDPE), offer superior resistance to acidic environments compared to conventional materials. Based on these findings, a mock test pile was constructed on-site using HDPE casing enwrapped around the reinforcement cage and included spacers to ensure adequate cover. However, due to collapsible soil conditions, the HDPE casing could not be properly inserted into the bored hole, and the scheme was subsequently rejected.

Holloway et al. (2012) demonstrated that Cathodic Protection (CP) is an effective technique for preventing the corrosion of metal surfaces. Based on their findings, a SACP system was implemented to protect reinforcing bars from corrosion. This paper presents the key features of the SACP system adopted for piles, along with other protective measures employed for RCC foundations in aggressive ground conditions.

Protection Measures Adopted for Concrete

Several studies for this type of extremely aggressive subsoil and groundwater conditions have been carried out and the corresponding protective measures against sulphate attack on concrete and chloride attack on reinforcement along low pH are summarised below:

Sulphate Attack on Concrete

Concrete for piles, pile caps, and shallow foundations was protected against the presence of high concentrations of sulphates (along with high concentrations of chlorides) and low pH, by implementing suitable measures to achieve the following:

a) Enhancement of concrete durability
b) Use of composite cement
c) Additional protective measures

Chloride Attack on Reinforcement

Protection of reinforcement in concrete against high concentrations of chlorides and low pH conditions was achieved through the implementation of the following measures:

a) Utilization of dense, low-permeability concrete
b) Increase in concrete cover to reinforcement
c) Incorporation of suitable admixtures to enhance concrete durability
d) Application of additional protective measures

It was determined that protective measures could be implemented in two distinct stages, primary and secondary, to ensure that the RCC substructure performs satisfactorily throughout their intended design life:

- Primary protection to RCC by making it dense and impermeable concrete so that the deleterious ions will not penetrate into the concrete.

- Secondary protection to RCC piles by providing SACP system and for pile caps/shallow foundation encapsulating all RCC surfaces exposed to aggressive environment, by polyethylene membrane (i.e., Tanking).

Primary protection measures

Primary protection measures are essential for all substructure concreting works, including piles, pile caps, and shallow foundations, where the concrete is exposed to aggressive environmental conditions. In this context, dense and low-permeability concrete is crucial to prevent the penetration of deleterious substances such as chlorides, sulfates, and pH, which can compromise the durability of reinforced concrete structures. For this purpose, M40 grade concrete with a low permeability is adopted, ensuring that the concrete remains durable even under harsh environmental conditions.

The use of Composite Cement (CC) is a key aspect of the primary protection strategy. CC, as per IS 16415, includes Ordinary Portland Cement (OPC) combined with Ground Granulated Blast Furnace Slag (GGBS), Fly Ash (FA), and Silica Fume (SF). GGBS (40-60%) and FA (20-30%) are both Supplementary Cementitious Materials (SCM), while SF (5-7%) acts as a mineral admixture. These components are known to significantly reduce the permeability of the concrete, enhancing its resistance to chemical attack and improving its long-term durability in aggressive environments. The GGBS improves the concrete's resistance to sulfate attacks, while fly ash helps reduce the risk of alkali-silica reaction and improves workability. Additionally, silica fume contributes to a denser concrete matrix, further reducing the chances of chloride ingress, which can accelerate reinforcement corrosion.

A maximum water-cement ratio of 0.40 is maintained (Start, 1989) to achieve low-permeability. Fe500D corrosion-resistant reinforcement and a minimum 100 mm concrete cover further enhance durability by protecting against aggressive environmental exposure (Mouallif et al., 2013).

To improve protection, specialized admixtures are incorporated. A Permeability Reducing Admixture for Hydrostatic Conditions (PRAH), as per ACI 212.3, acts as an integral crystalline waterproofing agent, crucial for substructures exposed to variable water tables. A bipolar corrosion-inhibiting admixture reduces electrical conductivity, delaying corrosion initiation. Additionally, a PCE-based superplasticizer enhances workability and lowers water content, improving density and durability in aggressive environments.

Secondary Protection Measures

When the concrete is exposed to highly aggressive conditions, the first line of defence is provided by using high quality concrete with maximum chemical resistance. This is further enhanced by the application of protective treatment on the concrete surface using epoxy coating, HDPE membrane, bituminous coating and so on. Therefore, the following additional protective measures were implemented.

Sacrificial Anode Cathodic Protection (SACP) system for Piles

To mitigate the risk of reinforcement corrosion in piles exposed to aggressive, chloride-laden environments, SACP system was adopted. Figure 3 shows sacrificial galvanic anodes attached to the reinforcement bars, conforming to ASTM B418 Type II standards. The selected anodes, with a minimum zinc mass of 40 grams per anode, were installed at 0.5 m centers in both directions, providing a distribution density of one anode per 0.25 m² of reinforcement surface area.

 © Deep Foundations Institute 2025

The anode spacing and mass were determined based on critical parameters such as steel density ratio, chloride concentration levels within the concrete, and the need to ensure a minimum trouble-free service life of 10 years, in line with performance-based durability requirements. This design approach was guided by current industry practice and manufacturer recommendations, and verified using Faraday's Law to ensure that the total anode capacity meets or exceeds the estimated charge demand over the service life. This approach ensures that the sacrificial anodes corrode preferentially, protecting the embedded steel by maintaining it in a cathodic state, thus extending the service life of the piles even in harsh substructure conditions (Holloway et al., 2012).



Fig. 3. Installation of Sacrificial Anodes

Tanking System for Pile caps and Shallow foundation

Tanking was provided to prevent the ingress of groundwater to the reinforced concrete. A Polyethylene sheet of 1mm thickness was used to encapsulate the shallow foundation and pile caps as shown in figure 4(a). Chemically resistant high build coal-tar epoxy-based coating having minimum Dry Film Thickness (DFT) of 400-500 microns in two coats (200 to 250 microns per coat) was applied as shown in Fig. 4(b) on external concrete surfaces of pile-caps and shallow foundations.



(a) **(b)**

Fig. 4. (a) Laying of HDPE membrane (b) Applying coal-tar epoxy

CASE STUDY-2
Site Information

This case study presents the protective measures adopted for the RCC foundations at a refinery site in western Rajasthan. Previously, the site was used for salt mining. Because of the site's geographical conditions, groundwater from the catchment area flows from the upper gradient to the lower gradient and accumulates at the proposed site location. Groundwater is extremely saline in nature, and it is converted to salt through a chemical process. Several salt ponds having approximate sizes of 100 m width, 30 m

length, and 3m to 4m depth existed within the proposed site area. Figure 5 shows a typical salt ponds that existed in and around the refinery site. These salt ponds were filled using the locally available soil during general site grading works.



Fig. 5. Salt pond (© Google Earth)

Aggressiveness of Subsoil and Groundwater

A detailed soil investigation was carried out to determine the subsoil profile and the aggressiveness of subsoil and groundwater. The stratigraphy may be broadly classified into three strata. The top stratum, with a maximum thickness of about 4 meters, comprises loose to medium dense filled-up soil, primarily silty sand and sand. This is underlain by a 5 to 6 meter thick layer of loose to dense silty sand/sand, followed by a very stiff to hard clay layer extending up to the termination depth of the borehole, i.e., 25.0 meters below ground level. The groundwater table was encountered at a depth of 1 to 3 meters below ground level. Chemical tests were conducted on subsoil and groundwater samples to determine the concentration of sulfate and chlorides. According to the test results, the soil contains 0.01 – 0.97 % chloride contents and groundwater contains 8400-108000 mg/l of chloride contents. The test results showed that the subsoil and groundwater were extremely aggressive, and concrete requires adequate protection measures to ensure its durability.

The limiting values for the categorization of exposure classes corresponding to chlorides present in the external environment are not documented yet. However, the exposure classes are classified into various categories based on the environmental conditions to which the concrete will subject. The subsurface concrete would be in contact with aggressive sub-soil and groundwater. Thus, the proposed site falls under the very severe category as per the exposure conditions indicated in IS 456 (2000).

Protection Measures Adopted for Concrete

Due to the extremely aggressive subsoil and groundwater conditions, the following protection measures were taken to ensure that the RCC substructure performs satisfactorily during its design life:

- Primary protection to RCC by making it dense and impermeable concrete.
- Secondary protection to RCC by encapsulating all RCC surfaces exposed to aggressive environment, by self-adhesive membranes.

Primary Protection Measures

Various measures were taken to make concrete dense and impermeable so that the deleterious chloride ions will not penetrate into the concrete. The optimal values of maximum water-cement ratio and the cement content play an important role in making durable concrete. The maximum water-cement ratio of 0.40 or less (Start, 1989) lowers the corrosion activity. The maximum water-cement ratio and minimum cement content used for making concrete were 0.38 and 375 kg/m^3. The type of cement used was Portland slag cement. The concrete's design grade was M35.

Self-compacting concrete was used to make concrete dense due to its higher workability, filling, and passing ability in congested areas. The aggregates used for making concrete were less than 20 mm in size, with the majority being 10-12 mm in size. The aggregates were round and chemically inert.

Alccofine was used as an ultrafine supplementary cementitious material (SCM) to achieve a low w/c ratio and to improve the packing density of the paste component. Alccofine accounted for 6% of the total cementitious materials. This results in lowering water demand, admixture dosage and hence improving the strength and durability parameters of concrete. Poly-Carboxylated Ether based super-plasticizer was used as a water reducer and to increase the workability of concrete. The dosage of superplasticizer was 0.9 to 1% by weight of cementitious materials. Bi-polar concrete penetrating corrosion inhibiting admixture was also used to reduce corrosion.

Clear cover provided for substructure concrete was 65 mm, while for pile foundation was 75 mm. The nominal cover specified in IS 456 for very severe exposure conditions is 50 mm. However, increases in cover for reinforcement delay the ingress of corrosive chemicals. Therefore, the concrete cover was increased over the normal covers specified in IS 456 (2000).

Secondary Protection Measures

A protective coating system was installed all around the surface of foundation concrete to prevent the ingress of deleterious substances through aggressive water and to increase its durability. The arrangement of the protective coating system is shown in Fig. 6 which includes a vapor barrier provided beneath the PCC. Polyethylene of 1000 gauge (0.25mm) thick was used as a vapor barrier. A HDPE membrane of 1.2mm thickness was installed above the PCC of the foundation base to enclose the foundation concrete from the bottom up and to project by 250 mm on all sides of the concrete structures from the PCC top level. A layer of minimum 1.5 mm thick self-adhesive rubber/bitumen waterproof membrane (SBS membrane), which is made of cross-laminated high-density polyethylene, has been placed on the vertical sides of the foundation member. Lapping of minimum 150 mm was provided between the HDPE and SBS membrane, which have been bonded using a single sided HDPE tape. Aluminum flashing has been used to fix the SBS membrane to concrete structures at grade level, and polysulphide sealant has been used to plug the top gap between the membrane and the surrounding earth.

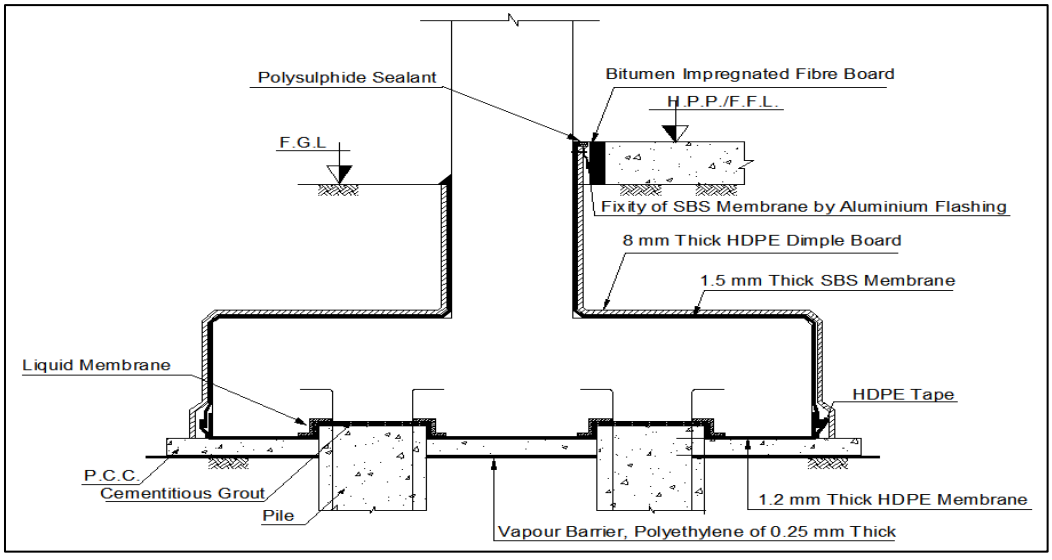


Fig. 6. Protective coating system

 © Deep Foundations Institute 2025

The HDPE membrane that makes up the water-proofing system is susceptible to damage during construction, so the entire system was enclosed in 8 mm thick HDPE dimple board with a minimum density of 85 kg/m3 and a hardness of 20 (Shore-A) as shown in Fig. 7.



Fig. 7. Installation of HDPE membrane and dimple board

For the protection of bored cast-in-situ reinforced concrete piles a permanent mild steel liner of a minimum 6 mm thickness was provided. This liner will serve as a sacrificial member and the thickness of it was decided by considering the rate of corrosion of steel in aggressive environment and the intended working life of the structures. The loss of thickness for steel members due to corrosion in marine conditions is 0.02 mm per year as per EN1993-5. Therefore, for 100-year working life, the total estimated decrease in liner thickness would be around 2 mm. The length of the liner varies from 6 to 7m below the cutoff level of the pile. The liner's length was chosen with consideration for the soil type, embedding in hard clayey layers, and probable fluctuation in the groundwater table. In Case Study-1, the steel liner was not adopted due to highly acidic subsoil conditions. However, in Case Study-2, where the subsoil and groundwater were found to be non-acidic, the liner was provided.

The pile head was waterproofed by applying 30 mm thick (minimum) free flow premix type non-shrink cementitious grout having 28 days compressive strength not less than 40 N/m^2 on top & side of the pile head, including the application of a two-component polyurethane liquid membrane with consumption of 1.5 kg/m^2 (1.5 mm thick) over the cementitious grout. The indicative protective coating system provided at the pile head is shown in Fig. 8.

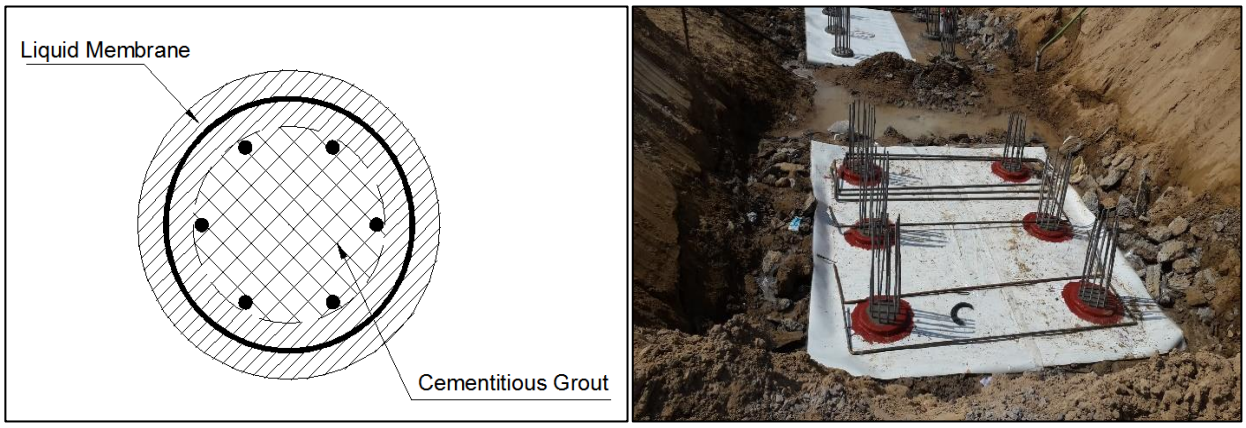


Fig. 8. Indicative protective coating system at the pile head

 © Deep Foundations Institute 2025

TEST ON CONCRETE

For both the case studies Rapid Chloride Permeability Test (RCPT) and water permeability tests were carried out on the concrete samples to check the resistance of concrete against the penetration of chloride ions. A rapid chloride permeability test was performed on various samples in accordance with ASTM C1202, and the results were compared to the RCPT ratings listed in Table 1.

Table 1. RCPT ratings (per ASTM C1202)

Charge Passed (Coulombs)	Chloride Ion Penetrability
> 4,000	High
2,000-4,000	Moderate
1,000-2,000	Low
100-1,000	Very Low
<100	Negligible

According to the test results, the total charge passed was <1000 coulombs, indicating that the chloride ion penetrability was very low and that the concrete would provide adequate resistance to chloride ion penetration. Water permeability tests were performed in accordance with the provisions of DIN 1048, and the test results show that the maximum depth of water penetration was 4-8 mm, which was well within the permissible limit of 10 mm.

The concrete samples were also tested to determine the acid soluble chlorides in accordance with the provisions of IS 14959, and the test results show that the acid soluble chlorides were 0.26 to 0.30 kg/m^3, which was well within the permissible limit of 0.6 kg/m^3.

SUMMARY & CONCLUSIONS

The two case studies presented in this paper illustrate different strategies for addressing similar durability challenges posed by aggressive subsoil and groundwater conditions. While both sites exhibited extremely high concentrations of chlorides and sulfates, the severity, soil types, and constructability constraints necessitated customized protection approaches.

Case Study 1 involved a refinery expansion on reclaimed industrial land with acidic, chloride and sulfate-rich groundwater. The site's acidic level made conventional liners impractical. Therefore, the primary protection focused on dense, impermeable concrete using composite cement, corrosion-resistant reinforcement, and admixtures. A Sacrificial Anode Cathodic Protection (SACP) system was implemented for pile foundations, along with a tanking system for shallow foundations using polyethylene membranes and epoxy coatings.

Case Study 2, located at western Rajasthan, was characterized by extremely saline groundwater. The protection strategy included the use of self-compacting concrete with Portland slag cement and ultrafine additives like Alccofine. A sacrificial steel liner was provided for piles, and an extensive multi-layer waterproofing system was used for shallow foundations including HDPE membranes, SBS membranes, and dimple boards to shield against mechanical damage.

 © Deep Foundations Institute 2025

While both cases followed the principle of combining dense concrete with barriers, the implementation methods were tailored to local conditions, highlighting the importance of site-specific durability design. These examples demonstrate that thoughtful integration of material selection, protective systems, and constructability considerations is essential for ensuring long-term performance of RCC foundations in highly aggressive environments.

To maintain performance throughout the intended design life, the concrete must be dense and impermeable. This was achieved through limiting the water-cement ratio to 0.40 or less, selecting suitable cement types, and incorporating superplasticizers and ultrafine additives. Material selection was verified using tests such as acid-soluble chloride test, and durability was validated using RCPT and water permeability tests, confirming low permeability and chloride resistance.

The use of HDPE membranes, epoxy coatings, SACP systems, and sacrificial steel liners provided an added layer of protection, customized to site conditions. These case histories offer a practical reference for engineers and practitioners involved in the design and construction of RCC foundations in chemically aggressive environments, reinforcing the need for site-adapted, multi-layered durability strategies.

ACKNOWLEDGEMENTS

The authors express their gratitude to the management of Engineers India Limited for granting permission to publish this paper.

REFERENCES

1 ACI 212.3. Chemical Admixtures for Concrete- American Concrete Institute.

2 ASTM B418. Standard Specification for Cast and Wrought Galvanic Zinc Anodes.

ASTM C1202. Standard Test Method for Electrical Indication of Concrete's Ability to Resist Chloride Ion Penetration, (ASTM C1202-94) 1994 Annual Book of ASTM Standards V 04.02, ASTM, Philadelphia, pg. 620-5.
DIN 1048 Part-5. Testing of Hardened Concrete.

3 EN 1993-5. Design of steel structures – Part 5: Piling.

4 Holloway, L., Green, W., Karajayli, P., and Birbilis, N., 2012. A review of sacrificial anode and hybrid cathodic protection systems for the mitigation of concrete reinforcement corrosion. Corrosion Engineering, Science and Technology, 47(4), 267–285.

5 IS 456, 2000. Plain and Reinforced Concrete -Code of Practice. Bureau of Indian Standards.

6 IS 14959 (Part 2), 2001. Determination of Water Soluble and Acid Soluble Chlorides in Mortar and Concrete — Method of Test.

7 IS 16415, 2015. Composite Cement-Specification. Bureau of Indian Standards.

8 Mouallif, M., Benzerzour, M., and Jalham, I., 2013. Resistance of different materials used in sewer systems (Polyvinyl chloride (PVC), polypropylene (PP), and High-density polyethylene (HDPE)) to sulfuric acid and sodium sulfate attack. International Journal of Environmental Science and Development, 4(5), 551-555.

 © Deep Foundations Institute 2025

9 Stark D., 1989. Influence of Design and Materials on Corrosion Resistance of Steel in Concrete. RD098, Portland Cement Association, Skokie, Illionis.

 © Deep Foundations Institute 2025

CONCEPTUAL AXIAL STRESS-STRAIN BEHAVIOR OF DRILLED DISPLACEMENT PILES USING FULL-SCALE LOAD TESTS DATABASE

Abolfazl Eslami, Professor in Geotechnical Engineering, Department of Civil and Environmental Engineering, Amirkabir University of Technology (AUT) (Tehran Polytechnic), Tehran, Iran, afeslami@aut.ac.ir
Arshiya Mehrazma, M.Sc. in Geotechnical Engineering, Department of Civil and Environmental Engineering, Amirkabir University of Technology (AUT) (Tehran Polytechnic), Tehran, Iran, arshiya8m@gmail.com
Amirhossein Ebrahimipour, Ph.D. Candidate in Geotechnical Engineering, Department of Civil and Environmental Engineering, Amirkabir University of Technology (AUT) (Tehran Polytechnic), Tehran, Iran, a.ebrahimipoor151273@gmail.com

ABSTRACT

Drilled displacement (DD) piles have gained widespread implementation as foundation elements, recognized as an efficient alternative for medium driven piles and drilled shafts, owing to their practical and environmental advantages. Load-displacement records substantially reflect bearing capacity, settlement, and the interactions between superstructures and substructures. A database has been compiled comprising 40 full-scale load tests on drilled displacement piles, embracing various types, such as Fundex, De Waal, Olivier, Berkel D, Omega, and Atlas. The database covers diameters ranging from 350 to 650 mm, with embedment depths varying from 7 to 19.5 m, installed in cohesive, granular, and mixed deposits. Load-displacement records are presented as projected force, recognized as pressure, versus the ratio of displacement to diameter, namely relative displacement, for unitless results interpretation. Accordingly, a new approach is being developed for stress-strain behavior appraisal. Dominant factors were scrutinized, including embedment depth, breadth, and surrounding soil type. Furthermore, the energy conserved through stress and strain integration is realized as toughness. The comparative analysis of different factors clearly distinguishes between various groups. Low-diameter, longer DD piles installed in more competent deposits are preferred. Hence, the proposed approach for stress-strain appraisal advances insights into optimum foundation design.

Keywords: Drilled Displacement Piles, Load-Displacement, Database, Stress-Strain, Toughness

1-INTRODUCTION

Data-centric geotechnics is a developing field that equips geotechnical engineering for the digital era. Emphasizing data utilization enables broader and more in-depth applications of information to support decision-making across all stages of project lifecycles and various aspects of practice (Phoon et al., 2022). A database is an organized collection of data that enables easy access and retrieval. It serves as a valuable tool for saving time and reducing costs, allowing for the development of more efficient designs.

Bearing capacity, settlement, and soil-structure interaction are critical considerations in foundation design and analysis, requiring an integrated approach that accounts for the relationship between the superstructure, the foundation as an intermediary element, and the underlying soil (Eslami et al., 2025). These factors are reflected in load-displacement records, which provide valuable insights into foundation behavior (Eslami & Ebrahimipour, 2024). Utilizing load-displacement data from full-scale load tests is one of the most accurate methods for determining bearing capacity. A lower safety factor can be applied by significantly reducing uncertainties, leading to a higher allowable load and greater reliability, ultimately optimizing foundation geometry and quantity. Predicting settlement remains a complex challenge due to numerous assumptions and simplifications. However, load-displacement records help

 © Deep Foundations Institute 2025

address this issue by accommodating ultimate and serviceability limit states. Beyond bearing capacity and settlement, axial stiffness, linked to the equivalent spring stiffness used in structural analysis and design, can also be accurately derived from these records.

Drilled displacement piles offer several advantages and applications. In addition to being efficient and cost-effective, these piles possess several other beneficial characteristics. During the construction, the soil is primarily displaced radially rather than excavated, as seen in bored piles. This process enhances the properties of the surrounding soil, resulting in higher bearing capacity compared to a drilled shaft or a continuous flight auger (CFA) pile of similar geometry (Brown 2005; Prezzi and Basu 2005). With minimal spoil generation, these piles are an ideal option in cases where soil contamination is a concern or where reducing spoil is preferred (Brown 2005). The other potential application is where environmental concerns, such as possible damage to nearby structures or ground loss, are important considerations (Moshfeghi and Eslami, 2018). Also, these piles are recommended for areas where the feasibility of constructing drilled shafts or CFA piles is uncertain, such as sites with a weak layer overlying medium-dense sands at a moderate depth (approximately 20–25 meters or less).

Drilled Displacement (DD) piles have emerged as an effective and environmentally favorable alternative to medium driven piles and drilled shafts. A database of 40 full-scale load tests covering various pile types, diameters (350–650 mm), and depths (7–19.5 m) in diverse soil conditions was compiled to analyze load-displacement behavior. The data, presented as normalized pressure-relative displacement curves, support the development of a new stress-strain evaluation method. Key factors such as depth, diameter, and soil type were examined through the toughness concept, enabling clear differentiation. Results offer insights for optimizing foundation design.

2-DATABASE OF LOAD-DISPLACEMENT RECORDS

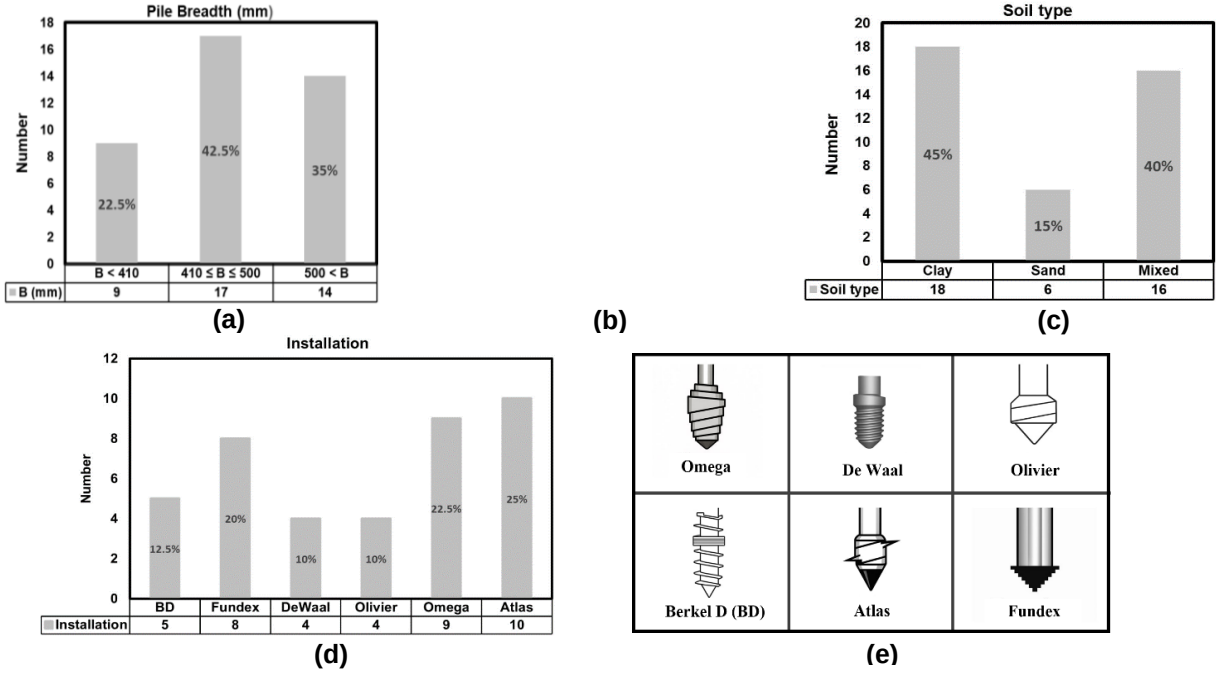


Fig. 1. Graphical distribution of compiled records characteristics: a) breadth, b) embedment depth, c) surrounding soil type, d) DD piles type, e) Included DD piles configuration

The compiled database comprises full-scale static load tests (SLT) for 40 DD piles across various soil types: 40% mixed, 15% sand, and 45% clay. The piles embedment depth ranges from 7 to 19.5 meters,

 © Deep Foundations Institute 2025

and the diameters vary from 356 to 650 mm. Six categories of DD piles are incorporated: 5 Berkel D, 8 Fundex, 4 De Waal, 4 Olivier, 9 Omega, and 10 Atlas. The database represents data from 5 countries across two continents. Table 1 summarizes the case records, while Fig. 1 visually displays the distribution of DD pile types, embedment depth, diameter, and soil type, along with the schematic view of different included types. Based on the maximum measured load, the records are divided into up to 1500 kN, between 1500 and 2500 kN, and over 2500 kN. Figures 2.a to 2.c show the corresponding load-displacement curves for each category.

Table 1. Summary of case records

Case No.	Reference	Location	Pile Data				Deposit	Maximum Measurement	
			Installation	D_{SN} (mm)	D_{BN} (mm)	D_f (m)		Load (kN)	Disp. (mm)
01	Holeyman et al. (2000a, b)	Belgium	Fundex	380	400	11.5	Clay	2000	15
02			De Waal	410	410	11.73	Clay	1800	18
03			Olivier	510	510	11.68	Clay	1900	20
04			Atlas	510	510	11.76	Clay	2100	22
05	De Cock (2001)	Belgium	Atlas	360	460	13.1	Clay	1765	35.5
06		Belgium	Atlas	360	460	13.1	Sand	2763	46.6
07		Belgium	Atlas	460	460	13.5	Sand	3000	66
08		Germany	Atlas	410	510	9.5	Mixed	2300	25.8
09		Germany	Atlas	410	510	7	Mixed	1710	29.8
10		Belgium	Atlas	360	500	13	Clay	1950	24.1
11		Belgium	Atlas	510	650	13.2	Clay	2487	64.9
12		Belgium	Atlas	360	500	13	Clay	2055	26
13		Netherlands	Fundex	450	560	11	Sand	3000	35.8
14		Germany	Fundex	420	560	14	Mixed	3000	31.4
15		Germany	Fundex	440	560	8.5	Sand	1752	28.2
16		Belgium	Fundex	380	450	13	Mixed	2400	45.6
17		Belgium	Fundex	380	450	13	Mixed	2063	42.1
18		Belgium	Omega	410	410	8.2	Sand	1900	55.9
19		Belgium	Omega	360	360	14.5	Clay	1200	46.2
20		Belgium	Omega	360	360	14.5	Clay	1350	46.6
21		Belgium	Omega	360	600	11	Clay	1500	42.9
22		Belgium	Omega	360	600	11	Clay	1800	42.5
23	Holeyman & Charue (2003)	Belgium	Fundex	390	450	9.5	Clay	3012	69
24			Olivier	550	550	9.2	Clay	3368	31.5
25			Omega	410	410	9.5	Clay	2826	54
26			DeWaal	410	410	9.5	Clay	2441	66
27			Olivier	550	550	9.1	Clay	2910	30
28			DeWaal	410	410	9.5	Clay	2267	86.5
29	NeSmith & NeSmith (2007)	USA	BD	406.4	406.4	18.3	Sand	3430	38.1
30	Park et al. (2012)	USA	BD	356	356	15.3	Mixed	3350	46
31			BD	356	356	19.5	Mixed	3000	30.5
32			BD	406	406	17.4	Mixed	3400	31
33			BD	356	356	15.2	Mixed	3200	32
34	Moshfeghi & Eslami (2018); Charue (2002)	Belgium	Atlas	510	510	9.6	Mixed	3603	65.5
35			DeWaal	410	410	9.5	Mixed	2653	63
36			Fundex	390	450	9.6	Mixed	3129	69.5
37			Omega	410	410	9.5	Mixed	3206	100
38			Olivier	550	550	9.5	Mixed	3062	31.5
39	Krasiński (2021)	Poland	Omega	400	400	12.6	Mixed	890	44.5
40	Krasiński (2023)	Poland	Omega	300	500	11	Mixed	993	40

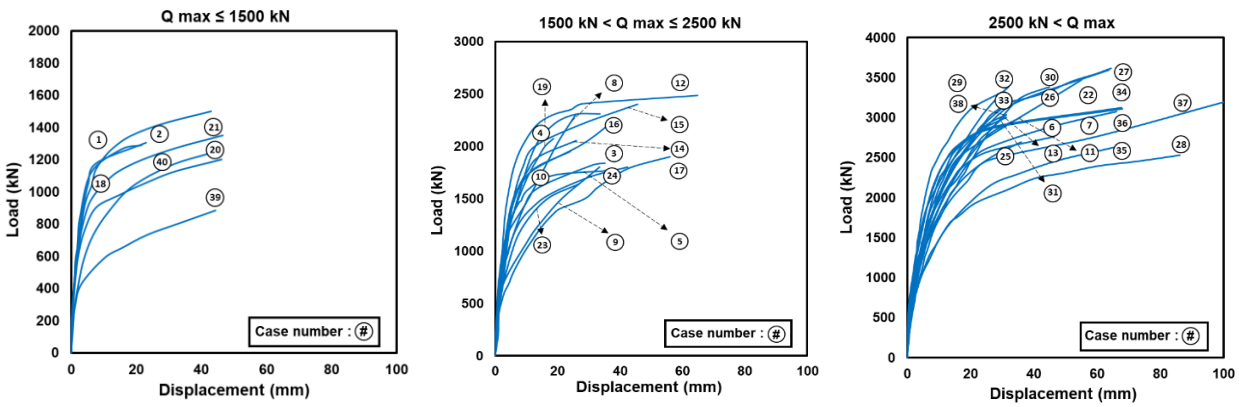


Fig. 2. Load-displacement diagrams for all compiled cases: a) Q_{max} ≤ 1500kN, b) 1500kN < Q_{max} ≤ 2500kN, c) 2500kN < Q_{max}

3-ANALYSIS OF ULTIMATE PRESSURE

Several methods are used to determine the ultimate load, such as Hansen Brinch (Hansen, 1963), Davisson offset limit (Davisson, 1972), and Decourt (Decourt, 1999). For further details and discussions on these methods, references such as Fellenius (1980) provide comprehensive insights. In addition to these established methods, the displacement ratio, defined as the ratio of displacement to foundation breadth, is widely used in engineering practice to determine the ultimate load. While the 10% B criterion is the most applied, 5% to 15% B values are also used, depending on the foundation type.

All analyzed cases have been assessed for ultimate pressure, determined through the 10% B criterion, the 5% B criterion, and the Brinch-Hansen 80% method. The 5% and 10% B criteria are extensively used in engineering practice due to their simplicity. The Brinch-Hansen 80% method is a practical engineering approach in geotechnical applications. The results for all cases, along with the maximum reported pressure, are presented in Fig. 3a.

For each type of drilled displacement (DD) pile, the average ultimate pressure was calculated based on the Brinch-Hansen 80% criterion. Among the evaluated types, the APGD pile exhibited the highest average ultimate pressure, reaching approximately 38.2 MPa, while the Omega pile recorded the lowest, at around 11.3 MPa. These findings, illustrated in Fig. 3b, underscore the variability in bearing performance associated with different DD pile types and emphasize the impact of installation techniques and geometry on load transfer efficiency.

4-APPRAISAL OF DOMINANT FACTORS

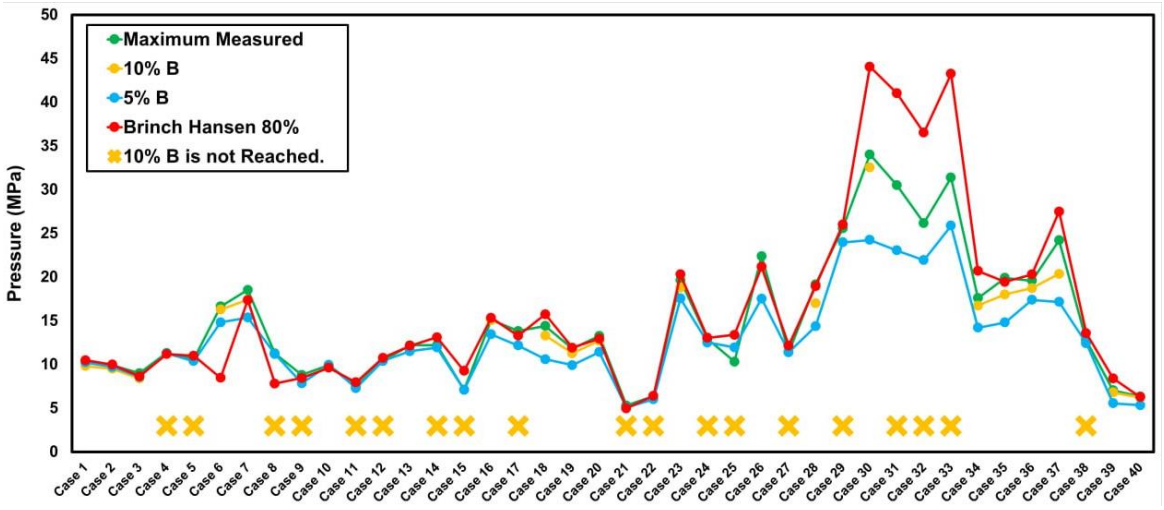
The piles were categorized into three subgroups and were evaluated based on embedded depth, breadth, and soil type separately. For each group, pressure-relative displacement curves were presented. The upper and lower bounds of the initial modulus are given. The pressure values corresponding to relative displacements of 5% were also examined. Displacement corresponding to a relative displacement of 0.5% has been considered the limit for linear behavior.

4-1 Embedment Depth (D_f)

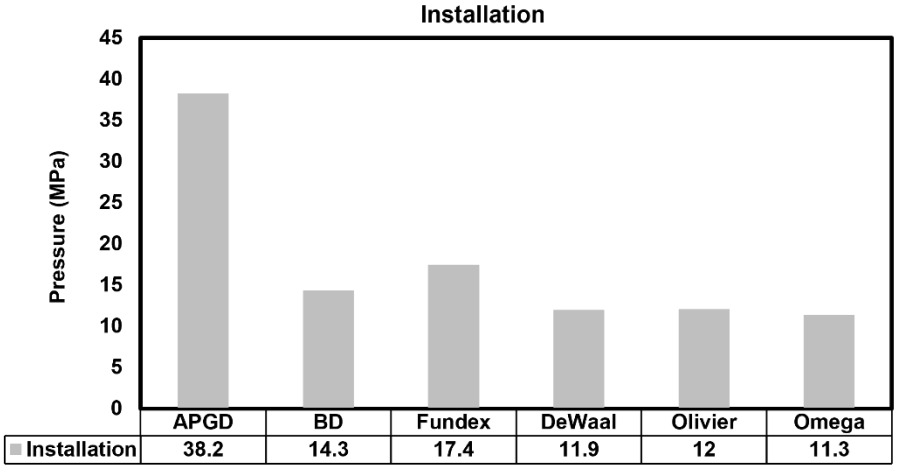
The depth at which a foundation is embedded plays a crucial role in determining its geotechnical behavior, particularly concerning bearing capacity, settlement, and overall structural stability. This

 © Deep Foundations Institute 2025

influence stems from the added surcharge loads and increased confining stresses that modify the failure mechanisms involved. Embedment depths vary from 7 meters to 19.5 meters in the dataset. For a more precise analysis, the cases have been grouped into three categories based on embedment length: short piles (up to 10 meters), medium piles (between 10 and 13 meters), and long piles (longer than 13 meters).



(a)



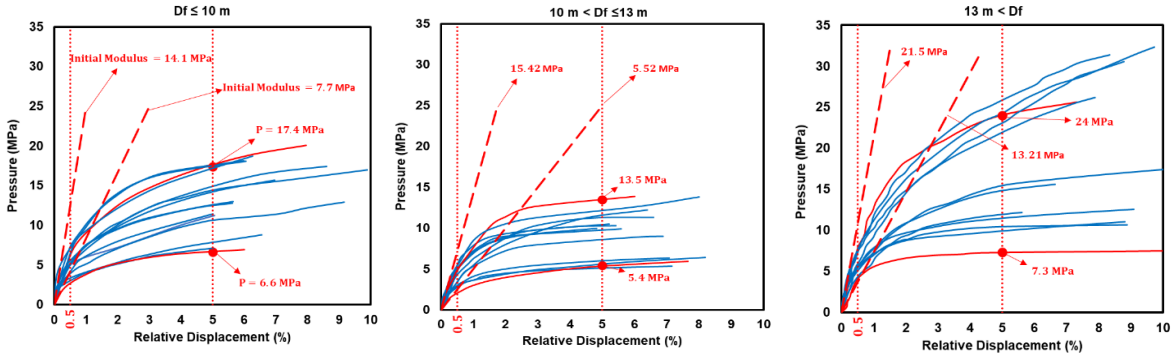
(b)

Fig. 3. a) Comparison of records by analyzing ultimate pressure through different criteria, b) Comparison of database records by analyzing ultimate pressure of different DD pile types using Brinch-Hansen 80% criterion

The calculated initial modulus for each group reveals meaningful trends. For short piles, the lower bound value is 7.7 MPa. The upper bound increased to 14.1 MPa. In the case of medium piles, the value at the lower bound is 5.5 MPa and rises to 15.4 MPa at the upper bound. The lower bound value for long piles is 13.2 MPa, increasing to 21.5 MPa at the upper bound. The relative displacement–pressure behavior for each category is depicted in Figures 4.a to 4.c, emphasizing the influence of embedment on load-bearing performance. The pressure corresponding to relative displacements of 5% further illustrates this effect. For short piles, the pressure is in the range of 6.6 and 17.4 MPa. For medium piles, they are 5.4 MPa and 13.5 MPa; for long piles, the values increase to 7.3 MPa and 24 MPa. These observations

 © Deep Foundations Institute 2025

underscore the significant impact that embedment depth has on the load-displacement behavior of foundations, highlighting deeper embedment as a key factor in enhancing geotechnical performance.



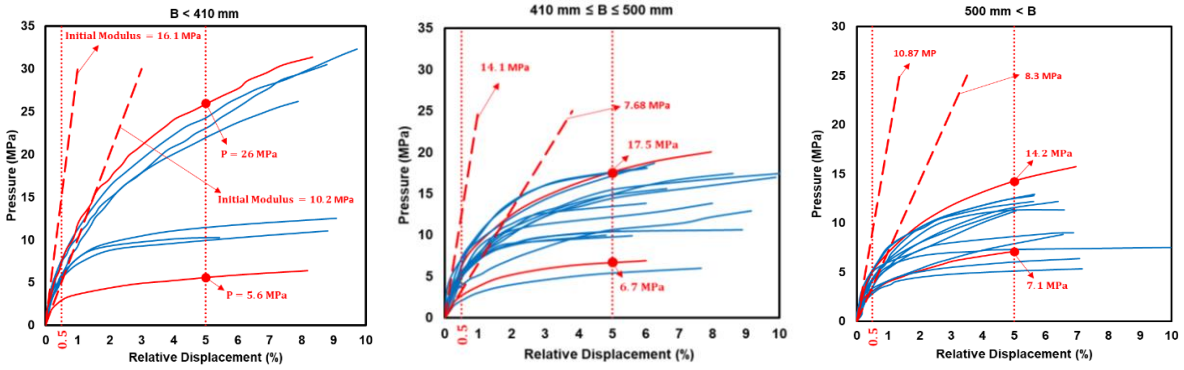
(a) (b) (c)

Fig. 4. Pressure-relative displacement behavior realizing embedment depth: a) $D_f \leq 10$ m, b) 10 m < $D_f \leq 13$ m, c) 13 m < D_f

4-2 Breadth

In addition to embedment depth, the breadth of a foundation is a critical factor influencing its technical performance, particularly in deep foundations, where it directly impacts both shaft and toe resistance through changes in the effective shaft and toe areas. The dataset analyzed includes pile breadths ranging from 356 mm to 650 mm, and for clarity in evaluation, are categorized into: piles with a breadth up to 410 mm, those between 410 mm and 500 mm, and the ones greater than 500 mm. For the first group, piles with a breadth up to 410 mm, Fig. 5a shows that the initial modulus for the lower bound is 10.2 MPa. This value shifts to 16.1 MPa at the upper bound. In the second group, with pile breadths ranging from 410 mm to 500 mm, the lower bound is 7.7 MPa. The upper bound value is 14.1 MPa, as depicted in Fig. 5.b. For the third group, which includes piles with a breadth exceeding 500 mm, the lower bound is 8.3 MPa. At the upper bound, the value is 10.9 MPa, as shown in Fig. 5c.

Figures 5.a through 5.c illustrate the pressure-relative displacement curves for each breadth category. The pressure level corresponding to relative displacements of 5% highlights notable differences across the three categories. For piles with a breadth up to 410 mm, the respective pressure is between 5.6 and 26 MPa. For piles between 410 mm and 500 mm, the values are 6.7 MPa and 17.5 MPa, and for piles with a breadth greater than 500 mm, the corresponding pressure ranges from 7.1 MPa to 14.2 MPa. These results demonstrate that the pressure associated with a given relative displacement tends to decrease as foundation breadth increases, underscoring the pivotal role of breadth.



(a) (b) (c)

Fig. 5. Pressure-relative displacement behavior based on pile breadth: a) B < 410 mm, b) 410 mm ≤ B ≤ 500 mm, c) 500 mm < B

 © Deep Foundations Institute 2025

4-3 Surrounding Soil Type

The type of soil surrounding a foundation plays a critical role in its geotechnical behavior (Ebrahimipour & Eslami, 2024) and strongly influences the resulting load-displacement response observed during loading tests. For instance, when comparing two identical piles, those installed in granular soils are typically expected to exhibit higher initial stiffness and greater ultimate load capacity than those embedded in cohesive soils. Figure 6.a presents the initial modulus for piles installed in clayey soils. At the lower bound, the value is 5.5 MPa. The upper bound value rises to 14.1 MPa. For sandy soils, as shown in Fig. 6.b, the lower bound is 8.7 MPa, while the upper bound value is 11.8 MPa. For cases installed in mixed deposits, the lower bound value is 10.9 MPa, and the upper bound value is 16.1 MPa. The pressures corresponding to a relative displacement of 5% demonstrate distinct variations across soil types. The pressure values for piles embedded in clay are between 5.2 and 17.4 MPa. In sandy soil, these values increase to 11.5 MPa and 15.5 MPa. The highest pressures are recorded in mixed soils, with corresponding values of 14.2 MPa and 25.8 MPa.

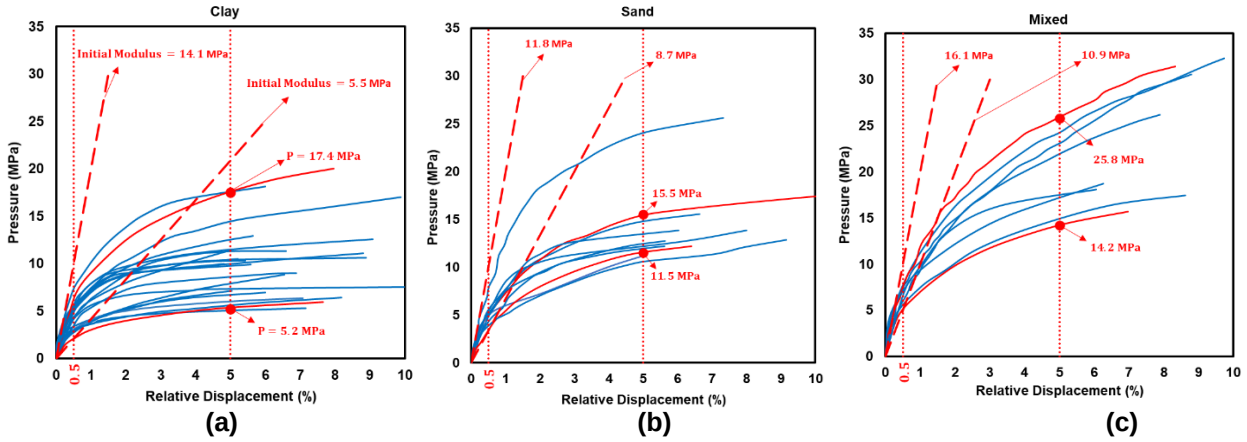


Fig. 6. Pressure-relative displacement behavior considering soil type: a) Clay, b) Sand, c) Mixed

4-4 Remarkable Points

Overall, a comparison of the initial tangent modulus in the linear part of the load-displacement curve shows that piles with an embedment depth of less than 10 meters exhibit, on average, a 3.9% higher initial tangent modulus than those with embedment depths between 10 and 13 meters. For piles embedded deeper than 13 meters, the initial tangent modulus shows a 65.7% increase relative to the 10–13 meter category. Notably, the variation in ultimate (limit) load at the yield point across these three embedment depth groups is more significant than the variation in stiffness. The average stiffness ratio of medium to short piles is 0.96, i.e., medium piles have 96% of the stiffness of short piles, while the average stiffness ratio of long to medium piles is 1.66, i.e., long piles are 1.66 times stiffer than medium piles.

Regarding foundation breadth, the initial tangent modulus increases by an average of 17.2% for piles with a breadth less than 410 mm compared to those in the 410–500 mm range. However, for piles wider than 500 mm, there is a 12% decrease in this modulus relative to the medium breadth group. The stiffness ratio between low- and medium-breadth piles is 0.83; between medium- and high-breadth piles, it is 0.88. Regarding soil type, the highest initial tangent modulus and ultimate load are observed in piles installed in Mixed soils, while the lowest values are recorded in clay. Sandy soil yields intermediate performance levels. On average, the initial tangent modulus in clay conditions is 4.6% lower than in sandy conditions, while mixed deposits show a 31.7% increase relative to sand. The average ratio of ultimate load between clay and sand is 1.05, and between sand and mixed soils, it is 1.32.

 © Deep Foundations Institute 2025

5-STRESS-STRAIN APPROACH FOR TOUGHNESS EVALUATION

In geotechnical engineering, toughness refers to the ability of a material or system to absorb energy and undergo plastic deformation prior to failure. This property reflects the capacity of the material to withstand high levels of stress and strain under loading conditions and is particularly important under dynamic loads such as seismic events or pile driving. In a study by Crockford and Little (1994), experimental and analytical methods were introduced to determine the fracture toughness of cohesive soils using the ring test. This research examined fracture toughness to measure soil resistance to crack propagation. The results showed that the fracture toughness of cohesive soils is significantly influenced by the type of material and its moisture content at the time of failure. The study emphasized that fracture toughness can serve as a critical index in assessing the geotechnical performance of soils, especially under dynamic loading conditions.

Toughness can be determined by integrating the stress-strain curve. It is the energy of mechanical deformation per unit volume prior to fracture. As stated by Soboyejo (2003), based on the following equation:

$$\frac{energy}{volume} = \int_0^{\varepsilon} \sigma \, d\varepsilon \qquad [1]$$

Where

ε = Strain,

σ = Stress

In the present study, the area under the pressure–relative displacement curve (as depicted in Fig. 7) was used to calculate the toughness for each pile, which was determined at a displacement equal to 1 inch, as shown in Fig. 8. The displacement of 1 inch is regarded as the allowable settlement in many codes and references, as mentioned in Coduto et al. (2016), commonly applied for serviceability limit state analyses as reviewed by Ebrahimipour and Eslami (2025). The adopted method enables the evaluation of the energy absorption characteristics of DD piles under axial loading and offers a deeper insight into their mechanical resistance. Selecting the 1-inch displacement criterion facilitates a consistent and meaningful comparison across different categories of embedment depth, pile diameter, and soil type. Since toughness fundamentally represents the energy absorbed or dissipated per unit area, it directly relates to deformation energy and provides a mechanical interpretation beyond conventional load-bearing capacity assessments.

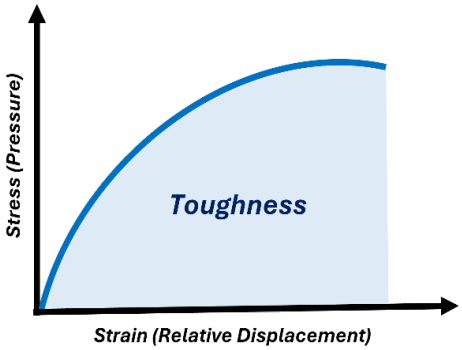


Fig. 7. Toughness Concept

 © Deep Foundations Institute 2025

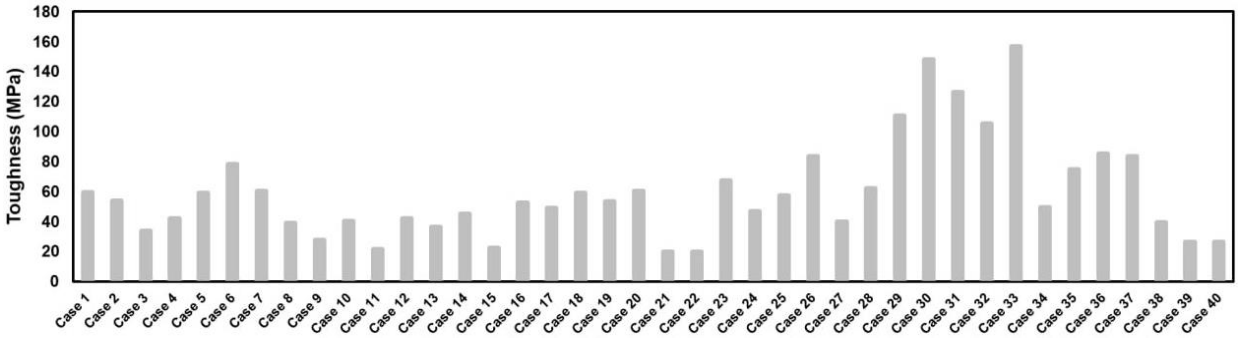
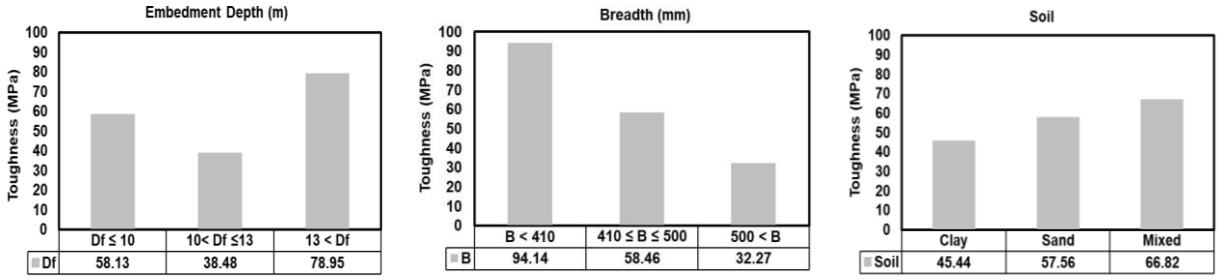


Fig. 8. Comparison of calculated toughness for all the compiled cases

Figure 9.a to 9.c presents a comparative analysis of the average toughness values for the previously defined pile categories. Regarding embedment depth, piles with depths greater than 13 meters exhibited the highest toughness values, followed by those with embedment depths of less than 10 meters, and finally by piles between 10 and 13 meters. Regarding pile breadth, the highest average toughness was observed in piles with a diameter of less than 410 mm, followed by those with diameters in the range of 410-500 mm, and finally by piles with a diameter larger than 500 mm. For soil type, mixed soils yielded the highest average toughness, with sandy and clayey soils ranking second and third, respectively. These trends suggest that both geometric parameters and confining soil characteristics significantly influence the energy absorption capacity of piles under axial loading.



(a) **(b)** **(c)**

Fig. 9. Average toughness values: a) Embedment depth, b) Breadth, c) Surrounding soil type

6- CONCLUSIONS

The current research addresses the load-displacement behavior of Drilled Displacement (DD) piles using a robust database of 40 full-scale static load tests. The evaluation incorporated various DD pile categories, soil types and geometrical configurations, enabling a broad and in-depth understanding of their geotechnical performance. By expressing load-displacement results in a unitless format through pressure-relative displacement records, the research offered a standardized approach for cross-comparative analysis, contributing to a general interpretation of pile behavior.

The study analyzed the influence of dominant factors, including embedment depth, pile breadth, and surrounding soil type, on the initial modulus and ultimate pressure of DD piles. The stress-strain framework also enabled the estimation of toughness.

Key findings revealed that deeper embedment significantly enhances initial modulus and ultimate pressure, while narrower pile breadths often yield higher initial modulus, likely due to stress concentration effects. Soil type emerged as a dominant factor, with piles in mixed soils performing better than those in clay or sandy soils. The pressure values associated with relative displacements of

5% across different categories highlighted clear behavioral distinctions and reinforced the reliability of relative displacement as a dimensionless metric for comparative design and analysis.

Results lie in the quantification of toughness, the area under the pressure-relative displacement curve, which provides an integrated measure of the pile-soil system ability to absorb energy prior to failure. This energy-based parameter captured the pile-soil system strength and ductility characteristics, offering additional insight into performance evaluation. The toughness metric effectively differentiates pile behavior across soil types and geometrical configurations and has the potential to be used for optimizing the design for applications requiring enhanced energy dissipation, such as seismic zones or dynamic loading environments. It was observed that the highest average toughness corresponded to piles with greater embedment depth, narrower breadth, and implemented in mixed deposits.

7- REFERENCES

Basu, P., Prezzi, M., & Salgado, R. (2014). Modeling of installation and quantification of shaft resistance of drilled-displacement piles in sand. International Journal of Geomechanics, 14(2), 214–229. https://doi.org/10.1061/(ASCE)GM.1943-5622.0000303

Brown, D.A. (2005). Practical considerations in the selection and use of continuous flight auger and drilled displacement piles. In Advances in Designing and Testing Deep Foundations (pp. 251–261). Geotechnical Special Publication No. 129, ASCE.

Charue, N. (2002). Results of an international pile load testing prediction event. Proceedings of Deep Foundations Institute Conference, 67–76. http://www.onemine.org/document/abstract.cfm?docid=186756&title=Results-Of-An-International-Pile-Load-Testing-Prediction-Event

Coduto, D.P., Kitch, W.A., & Yeung, M.R. (2016). Foundation design principles and practices (3rd ed.). Upper Saddle River, NJ: Prentice Hall, Inc.

Davisson, M.T. (1972). High capacity piles. Proceedings of Lecture Series on Innovations in Foundation Construction, American Society of Civil Engineers, ASCE, Illinois Section, Chicago, March 22, pp. 81–112.

De Cock. (2001). A database approach to overview pile loading tests on displacement screw piles in Western Europe – 1970-2000. Holeyman (ed.), Screw Piles - Installation and Design in Stiff Clay, Swets & Zeitlinger

Decourt, L. (1999). Behavior of foundations under working load conditions. Proceedings of the 11th Pan-American Conference on Soil Mechanics and Geotechnical Engineering, Foz DoIguassu, Brazil, August 1999, Vol. 4, pp. 453–488.

Ebrahimipour, A., & Eslami, A. (2024). Analytical study of piles behavior for marine challenging substructures. Ocean Engineering. 292, https://doi.org/10.1016/j.oceaneng.2023.116514

Ebrahimipour, A., & Eslami, A. (2025). Raft Foundations Under Combined Vertical-Moment-Horizontal Loading: A Numerical Study on Design-Adaptive Serviceability. Transportation Infrastructure Geotechnology, https://doi.org/10.1007/s40515-024-00528-x

Eslami, A., & Ebrahimipour, A. (2024). Load-displacement appraisal and analysis for driven piles; a data-centric approach. Computers and Geotechnics, 171, 106377.

Eslami, A., Ebrahimipour, A., Imani, M., Imam, R. and Mo, P.Q. (2025). Form and Load Transfer Aspects of Foundation Systems; Case-Based Implementation and Adaptation for Buildings, Deep Underground Science and Engineering, DOI:10.1002/dug2.12146

Fellenius, B.H. (1980). The analysis of results from routine pile loading tests. Ground Engineering, Foundation Publishing Ltd., 13(6), 19–31.

Hannigan, P.J., Goble, G.G., Likins, G.E., & Rausche, F. (2006). Design and construction of driven pile foundation, Vol. I. US Department of Transportation, Federal Highway Administration, Publication No. FHWA NHI-05-042.

 © Deep Foundations Institute 2025

Hansen, J.B. (1963). Discussion on hyperbolic stress-strain response. Cohesive soils. ASCE Journal of Soil Mechanics and Foundation Engineering, 89, 241–242. SM4.
Hardin, B.O., & Mahboub, K.C. (1994). Fracture toughness of compacted cohesive soils using ring test. Journal of Geotechnical Engineering, 120(5), 872–891. https://doi.org/10.1061/(ASCE)0733-9410(1994)120:5(872)
Holeyman, A., Maertens, I., Huybrechts, N., & Legrand, C. (2000a). Preparation of an international pile dynamic testing prediction event. In S. Niyama & J. Beim (Eds.), Application of Stress-Wave Theory to Piles (pp. 733–739). Balkema. ISBN: 90-5809-150-3.
Holeyman, A., Maertens, I., Huybrechts, N., & Legrand, C. (2000b). Results of an international pile dynamic testing prediction event. In S. Niyama & J. Beim (Eds.), Application of Stress-Wave Theory to Piles (pp. 725–732). Balkema. ISBN: 90-5809-150-3.
Holeyman, A., & Charue, N. (2003). Observations on pile capacity prediction event at Limelette. In J. Maertens & N. Huybrechts (Eds.), Belgian Screw Pile Technology – Design and Recent Developments (pp. 215–234). Swets & Zeitlinger. ISBN: 90-5809-578-9.
Krsiński, A., & Wiszniewski, M. (2021). Identification of residual force in static load tests on instrumented screw displacement piles. Studia Geotechnica et Mechanica, 43(4); 438–451. https://doi.org/ http://dx.doi.org/10.2478/sgem-2021-0025.
Krasiński, A. (2023). Estimation of screw displacement pile-bearing capacity based on drilling resistances. Studia Geotechnica et Mechanica, 45(s1); 282–292, https://doi.org/10.2478/sgem-2023-0014
Moshfeghi, S., & Eslami, A. (2018). Reliability-based assessment of drilled displacement piles bearing capacity using CPT records. Marine Georesources & Geotechnology, 36(5), 550–561. https://doi.org/10.1080/1064119X.2018.1448493
NeSmith, W.M., & NeSmith, W.M. (2007). Quality control of drilled displacement piles through an integrated automatic data acquisition system, GSP 158 Contemporary Issues in Deep Foundations
Park, S., Roberts, L.A. & Misra, A. (2012). Design Methodology for Axially Loaded Auger Cast-in-Place and Drilled Displacement Piles. Journal of Geotechnical and Geoenvironmental Engineering, 138(12), pp.1431–1441. doi:https://doi.org/10.1061/(asce)gt.1943-5606.0000727.
Phoon, K., Ching, J., & Cao, Z. (2022). Unpacking data-centric geotechnics. Underground Space, 7(6), 967–989. https://doi.org/10.1016/j.undsp.2022.04.001
Prezzi, M., & Basu, P. (2005). Overview of construction and design of auger cast-in-place and drilled displacement piles. Proceedings of DFI's 30th Annual Conference on Deep Foundations, Chicago, United States, 497–512.
Soboyejo, W. O. (2003). Toughness and fracture process zone. In Mechanical properties of engineered materials. Marcel Dekker.

IT'S NOT DELIVERY, IT'S DYNAMIC COMPACTION

Noah Miner PE, Malcolm Drilling, Milwaukee, WI, nminer@malcolmdrilling.com
Lisheng Shao, Ph.D, PE, GE, Malcolm Drilling, San Francisco, CA, lshao@malcolmdrilling.com
Jim Glider, Malcolm Drilling, Milwaukee, WI, jglider@malcolmdrilling.com

ABSTRACT

If you live in the Midwest, chances are you've tasted a frozen pizza from Palermo's. Even if you haven't had the pleasure of feasting on a "Screamin' Sicilian" you can appreciate that making pizzas, or anything, at scale takes a significant facility. When Palermo's purchased a plot of land on the outskirts of metropolitan Milwaukee, they knew that the screamin' deal they got came at a price. The new Palermo's site was previously an industrial malt development consisting of several structures across the site. The structures were razed, the rubble left in place and the lot stayed vacant for decades. The concrete and miscellaneous rubble extended to 25 feet below ground surface. Below the rubble fill was lean clay that is typical for the great lakes basin.

These subsurface conditions provide unique challenges for providing building support. If left untreated, the void space in the rubble will lead to significant differential settlements over the long term. The nature of the rubble fill precludes the use of deep foundations supporting structural loads as a driven or drilled pile solution would inevitably meet refusal. To accommodate the obstructions in the rubble and provide the most cost effective ground improvement, Malcolm Drilling applied Deep Dynamic Compaction (DDC) by dropping thirty (30) ton tamper over 50 ft height. The high energy impacts densify the rubble, increasing the bearing capacity of the site while mitigating the potential for differential settlements over the 350,000 square foot building footprint. By recording the DDC generated crater depths and analysis their distributions as a quality control procedure, the Engineer can identify the soft spots and apply additional treatment.

Using a heavy weight to make the ground suitable for construction is the oldest known form of foundation construction in the world. In the modern world Deep Dynamic Compaction (DDC) is often used on landfill sites and remote areas since the high energy wave propagation can be unpleasant for those nearby and may even damage more fragile proximal structures. Malcolm was able to perform high energy drops in a dense urban setting through careful planning and various innovative techniques protecting houses as close as 100 feet from the construction site.

Since no new materials are used in DDC, it is likely the most sustainable foundation technique available, with minimum carbon footprint. The concrete rubble layer that was seen as a scourge to the site, is ultimately a great building material. Instead of spending more resources and energy trying to remove or penetrate the layer, Malcolm used it to provide a cost effective and resilient end product.

Keywords: DDC, Densification, Workpad Stability, Sustainability

INTRODUCTION

In 1822 Solomon Juneau built the first log cabin in Milwaukee and two years later, the first frame building. Between 1835 and 1850, Milwaukee's population grew from a handful of fur traders to more than 20,000 settlers. Between 1846 and 1854, a wave of German immigrants arrived, bringing with them expert industrial skills. Milwaukee soon became a center of foundry, machinery, and metal-working industries, as well as a center for brewing and grain trading. World War Two demanded huge amounts of factory goods between 1941 and 1945, and the city saw a boom in manufacturing. Since 1970,

 © Deep Foundations Institute 2025

manufacturing has ceased to dominate Milwaukee's economy, although traditional industries such as heavy machinery, tools, engines and brewing survive.

Remnants of this boom are still evident in the landscape of the city. Across the metro Milwaukee, there are parcels of land with abandoned monuments to the productivity of the past. Once such parcel lay just inside the city proper on Grant Street. For years, the pile of concrete rubble visible from the street was the only indication that the site used to be part of the manufacturing boom of the 20th century. The industrial malt development had long since been abandoned at the time of site exploration. The razed concrete buildings had been demolished and the concrete rubble left in place for years. Some of the industrial rubble was used as fill to grade the site, and the remainder that was not needed was left in piles across the parcel.

The location of the subject site provided unique benefits and challenges to potential developers. The centralized location in the city makes the site advantageous to industrial producers looking for a site with proximity to transportation hubs. While the presence of concrete rubble limited the feasibility of development, it also reduced the property value. This provides an opportunity for development if a creative solution could be found.

The planned industrial building would be a single-story steel-framed structure with precast walls. The total footprint of edifice was over three hundred thousand (300,000) square feet, as shown in Fig. 1. Foundation loading was designed as seven thousand (7,000) pounds per linear foot for walls and five hundred thousand (500,000) pounds per column. No basement was planned, and the at-grade floor loading was assumed to be one hundred and twenty-five (125) pounds per square foot.



Fig. 1: Overall Site and Surrounding Area

 © Deep Foundations Institute 2025

SOIL PROFILE

The subject site had between ten (10) and twenty five (25) feet of non-cohesive fill material overlying natural clay deposits, that are typical of the Milwaukee area. The fill exhibited highly-variable strength characteristics with N-values ranging from single digits to refusal. The fill material predominantly consisted of gravelly silty sand and silty sand. Foundry material, slag, concrete rubble, wood debris, and cobbles were encountered within the fill material, and were often accompanied with higher N-values. The lower clay exhibited medium stiff to hard comparative consistency. Groundwater ranged in depth between ten (10) and twenty (20) feet below ground. A typical boring log at the planned building footprint is provided in Fig. 2.

The presence of the foundry materials within the fill precluded the use of deep foundations as both driven and drilled solutions would inevitably experience refusal. Spread footings would have to be implemented, but the fill showed such variability and given the nature of uncontrolled deposition of foundry materials, the potential for voids heightened concerns of differential settlements. Removal and replacement of all the foundry materials across the site would have been cost prohibitive.

DEEP DYNAMIC COMPACTION PROGRAM

The geotechnical engineer of record (GEOR) investigated potential ground improvement methods, such as aggregate pier, soil mixing, and rigid inclusion, which all have difficulties to penetrate the uncontrolled fill. Although jet grouting is capable to drill through the fill/rubble material, the cost of jet grouting to treat the 300,000 square feet building site will be prohibitively higher than the construction budget.

GEOR was aware of Malcolm's previous successful use of Deep Dynamic Compaction (DDC) to remediate an industrial landfill site with similar conditions and demands. Malcolm teamed with the developer and the GEOR to develop the DDC solution. Dynamic compaction was chosen to improve the site because it allowed the foundry materials to remain in place, while eliminating the potential for differential settlements.

A primary fifteen (15) foot square patterned grid was overlayed on to the area of improvement. A secondary split spaced grid was utilized to ensure full treatment of the area. The design utilized Malcolm's thirty (30) ton, high energy tampers, dropping from a height of sixty (60) feet. Based on FHWA-SA-95-037 Dynamic Compaction Guidelines, the impact intensity of 1800 ton*ft, will reach the densification depth of 29.3 ft, assuming in the intermediate soil deposit. This combination was anticipated to provide enough energy to densify material within the fill layer. After the primary pass in 15 ft by 15 ft square grids, the earth work contractor would fill in the craters with suitable fill and the secondary pass at the middle of the grids would be tamped. A typical DDC layout is shown in Fig. 3.

 © Deep Foundations Institute 2025

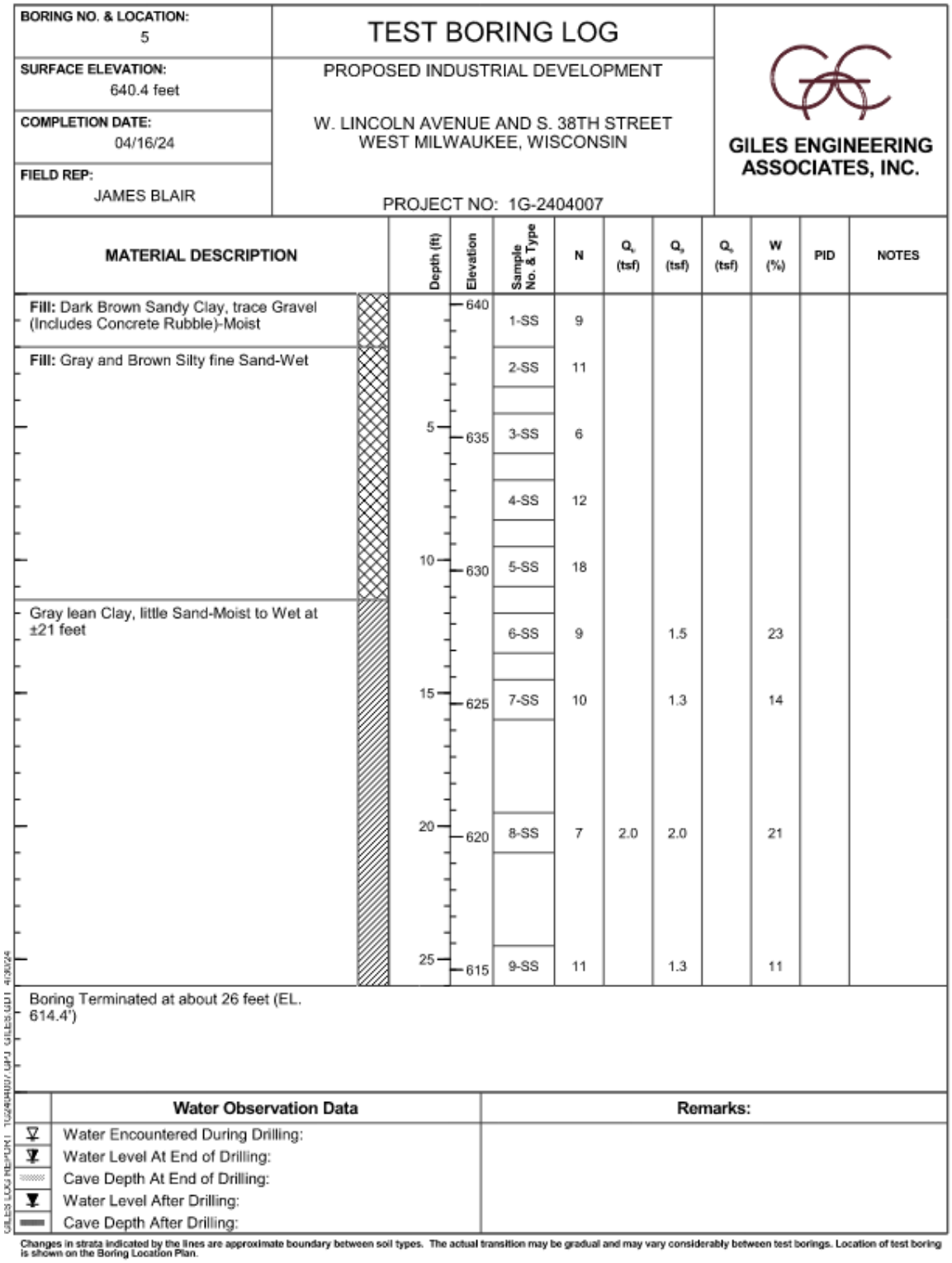


Fig. 2: Typical SPT Boring Log Under the Planned Building Footprint.

After the filling of the secondary craters, a final ironing pass with a ten (10) ton tamper would ensure that all the material in the craters were densified.

 © Deep Foundations Institute 2025

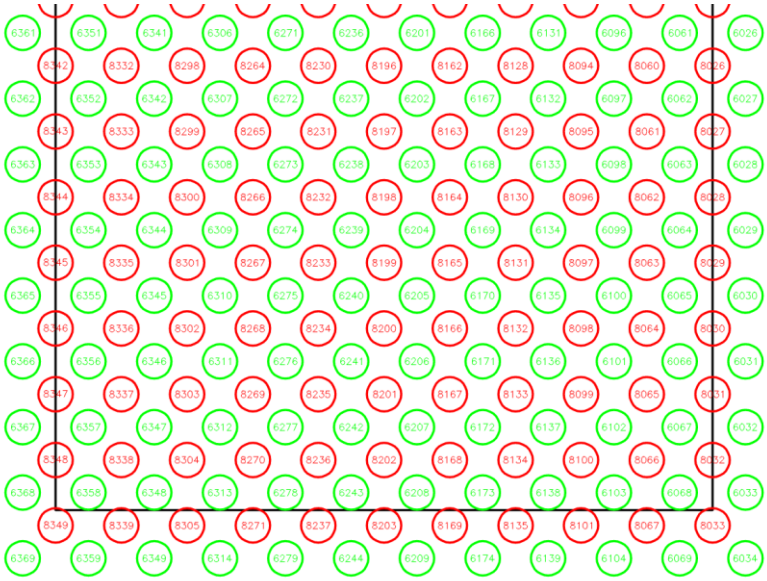


Fig. 3: Typical DDC layout in a primary/secondary locations on 15 ft by 15 ft square grids

The final challenge to improving the site was the proximity to existing utilities, industrial and most importantly, residential structures. With plans to drop as close as two hundred (200) feet, the calculated peak particle velocity would approach the cutoff limit of 0.7 inches per second for damage to drywall. The contractor analyzed the DDC induced vibration curve based on FHWA-SA-95-037 Dynamic Compaction Guidelines, and plotted in Fig. 4.

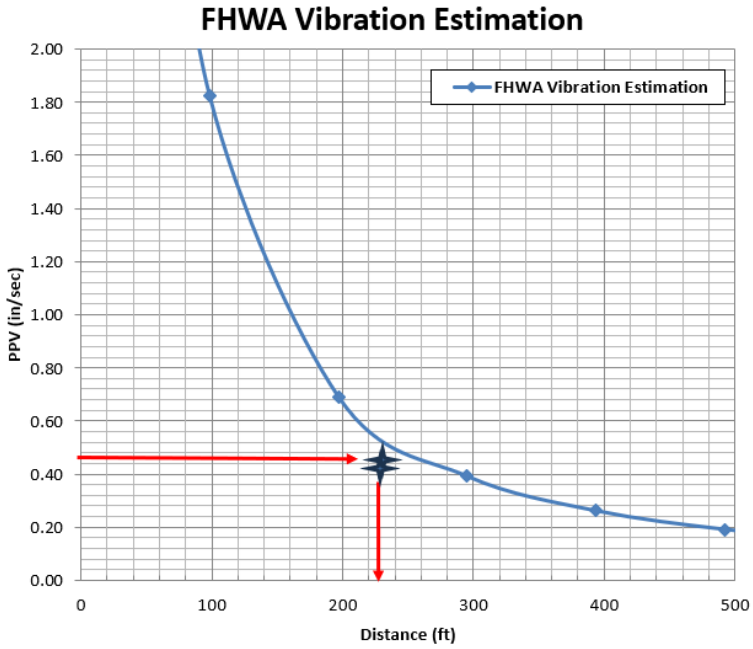


Fig. 4: DDC induced vibration attenuation curve based on FHWA-SA-95-037 Dynamic Compaction Guidelines and compared with the filed measurements.

 © Deep Foundations Institute 2025

Malcolm worked with the project team to develop a robust vibration mitigation program to protect the nearby structures and allow the work to proceed. The developer hired a vibration monitoring company to install seismographs next to the structures of highest concern. Malcolm worked with the earthwork contractor to cut a vibration mitigation trench along the property line abutting the closest structures (Fig. 5). Finally, a reduced energy regime was developed if the seismographs caught peak particle velocities approaching the cutoff limits. These limits were approached, and the reduced energy regime was instituted in 10% of the project area, but the work was completed without exceeding the vibration limits.



Fig. 5: Vibration Mitigation Trench Protecting Nearby Structures

QA/QC

The DDC work was completed and proved out with a series of twelve (12) modulus tests on a 30 inch diameter steel plate. An allowable ground bearing pressure of three thousand (3,000) pounds per square foot was assumed for the building spread footings. Eleven (11) of the twelve (12) plate load tests successfully supported twice the design load with less than a quarter inch of movement at design load. The only non-conforming test was performed at the top of the vibration mitigation trench slope and was unduly affected by the lack of confinement on one side of the supporting material. A typical load test result is shown in Fig. 6.

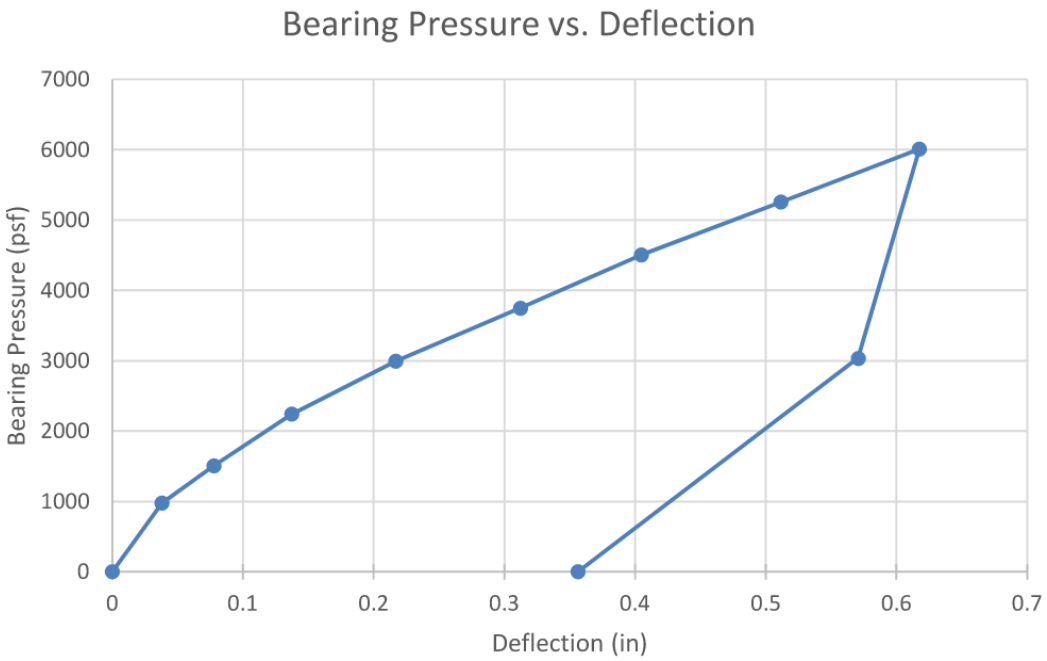


Fig. 6: Typical Modulus Test on a 30-inch Diameter plate.

CONCLUSION

Deep dynamic compaction has proven to be an effective tool for reclaiming land made unsuitable by uncontrolled fill (Fig. 7). The lack of need for new building material needed makes it one of the most sustainable foundation tools. Previously the technique was relegated to municipal landfills and other land outside of cosmopolitan zones. The ability to renew abandoned lots in urban zones provides significant opportunities for forgotten industrial areas that would otherwise be overlooked as unbuildable. Although care and creativity are needed, Malcolm has proven that even the most stubborn areas of industrial zones can be rejuvenated with the use of DDC.

 © Deep Foundations Institute 2025



Fig. 7: DDC Work in Progress

REFERENCE

FHWA (Federal Highway Administration). (1995). Geotechnical Engineering Circular No. 1, Dynamic Compaction, Publication No. FHWA-SA-95-037. FHWA, Washington, DC.

Giles Engineering Associates, Inc. Geotechnical Engineering Exploration and Analysis - Proposed Industrial Development 3830 W. Grant Street West Milwaukee, Wisconsin (2024)

 © Deep Foundations Institute 2025

SUSTAINABLE SHORING: PRE-CONSTRUCTION CARBON SAVINGS

Chelsea N. Miller, United Rentals Trench Safety Engineering, Seattle, WA, USA, (206) 947-6393, cmiller12@ur.com

ABSTRACT

For decades now, sustainable efforts have been researched and implemented to reduce the building industry's carbon footprint and environmental impact, which presently account for around 40% of energy-related carbon emissions globally. A target reduction of 20% structural embodied carbon has a potential impact to save over 200,000 kg CO_2e per year, which is significantly higher than the potential impact of many other prescribed lifestyle reductions (driving, flying, diet changes, etc). However, little thought or engineering analysis has been made to lower the environmental impact from pre-construction stages, including the design and construction of temporary works like excavation support systems, which currently account for approximately 55% of a building's total CO_2e emissions.

This study investigates the environmental impact of modular hydraulic bracing and slide rail systems compared to conventional shoring systems for temporary works in construction. Life Cycle Assessment (LCA) methodology and carbon emission calculators were employed to assess the environmental burdens associated with material extraction, manufacturing, transportation, construction, and end-of-life disposal (A1-A5 modules). Key findings demonstrate that modular hydraulic bracing and slide rail systems, when used as alternative options to conventional steel braced shoring systems, offer significant environmental advantages. These systems provide modular designs with high strength-to-weight ratios which minimize material usage, reducing embodied carbon emissions. Furthermore, these systems reusability and ease of transportation contribute to lower operational emissions and reduced waste. By quantifying these environmental benefits and reduction in total embodied carbon, this study provides valuable insights for construction professionals seeking to minimize their carbon footprint and promote sustainable construction practices. This is the first known comparative LCA of temporary works shoring systems.

Keywords: carbon, pre-construction, sustainable, shoring, support, excavation

INTRODUCTION

This paper demonstrates the potential for substantial embodied carbon reductions through the use of reusable shoring systems as an alternative to traditional steel shoring in deep foundation construction. The built environment is responsible for around 40% of all global emissions. Many advancements in technology and evolving building regulations have successfully reduced operational CO_2 in the built environment. However, as operational carbon has fallen over the past two decades, embodied carbon, or the estimate of greenhouse gas (GHG) emissions associated with stages of a building's life cycle, has risen to approximately two-thirds of a building's carbon costs. The importance of calculating the embodied carbon (or carbon footprint) of buildings has increased and exploring different ways to reduce this number is highly desirable. To reduce embodied carbon we must look to minimize the use of new materials as far as possible. When assessing a building's lifecycle and evaluating its embodied carbon, the products used and the construction of the building are the key contributors, accounting for up to 50% of a building's entire embodied carbon.

By quantifying the embodied carbon at different phases in the construction phases and isolating different material's net effects on embodied carbon, allows for environmental impact assessments in the planning and design stages, making it possible to design alternatives based on environmental friendliness of methods and materials and move toward more sustainable practices in the construction industry. Most

 © Deep Foundations Institute 2025

research has focused on the total carbon of final building materials but yet there is significant embodied carbon that results from support of excavation for structures of all sizes. How do we quantify the carbon relating to these construction stages and is there a way to reduce this carbon?

The options for sustainable efforts in the pre-construction stages of a building are extremely limited and thus, have not been researched in great depth. Pre-construction carbon costs are generally accounted for in material manufacturing, transport to site, and installation process. Reusable modular shoring solutions like hydraulic bracing and slide rail solutions offer significant advantages over traditional single-use structural steel, primarily through their design for multiple reuses across various projects. This reusability not only enhances efficiency but also significantly reduces the total embodied carbon per project, making these system a more sustainable option for temporary shoring.

LIFE CYCLE ASSESSMENT

Embodied carbon assessment is a subset of a broader discipline called Life Cycle Assessment (LCA). LCA was first developed in the 1960s and has since become the most widely used and highly regarded tool for quantifying the environmental impacts of products and services. To quantify embodied carbon, designers use Life Cycle Assessment (LCA) tools which analyze each material's carbon footprint from extraction to manufacturing and transportation. Per BS EN 15978[1], a widely-used European Standard for sustainability of construction works, a building's LCA is divided into four stages, A, B, C and D, with each stage encompassing specific phases (A1, A2, etc) and processes relevant to that stage. For shoring projects, the focus is on Stage A which covers all phases before the building's completion and active use. Phases A1 through A3 cover the manufacture and acquisition of building materials and products necessary for the construction phases, while phases A4 and A5 cover the actual construction process, starting with the transportation of ready-for-use materials. The following sections outlines these phases in more detail.

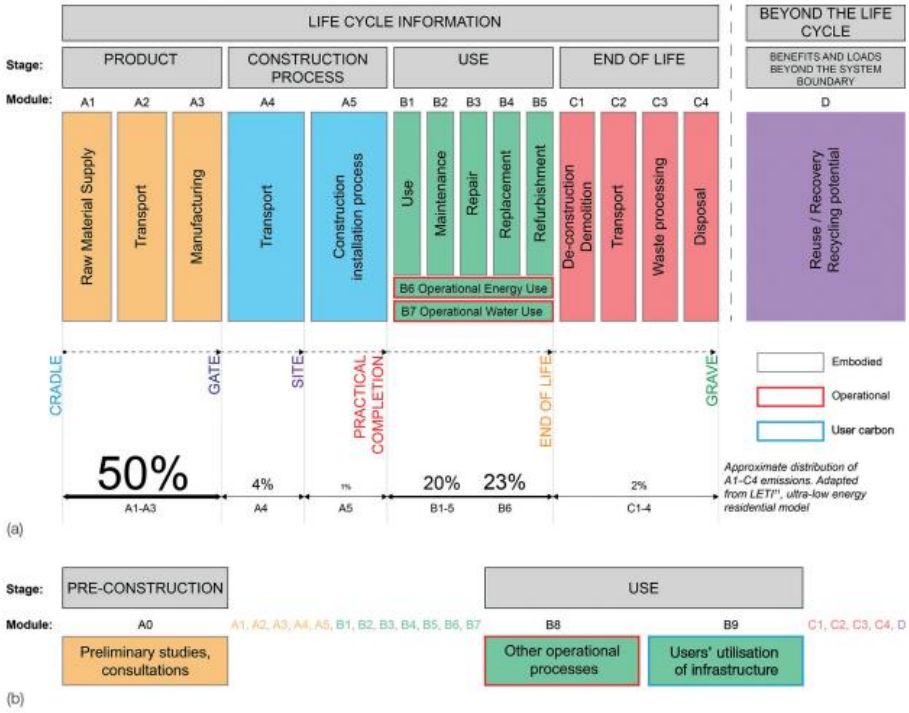


Fig. 1. BS EN 15978 Life cycle stages

 © Deep Foundations Institute 2025

Product Stage (A1-A3)

These stages encompass the extraction of raw materials (A1), transportation of these materials to manufacturing sites (A2), and the manufacturing process itself (A3). For temporary shoring, this means calculating the embodied carbon based on the material and the weight of each item. This calculation will be bifurcated into two distinct outputs: the embodied carbon of creating the item (to be used when selling the product) and the embodied carbon per week on hire (to be used when hiring out the product).

Transportation (A4)

Stage A4 addresses the transportation of equipment to and from the construction site. This stage is project-specific and involves calculating the emissions associated with transporting the equipment over the required distances. Factors such as the type of transportation used, fuel consumption, and distance travelled will be taken into account to ensure an accurate calculation.

Construction and Installation Process (A5)

Stage A5 covers the installation of the equipment on-site. This includes emissions from on-site activities such as assembly, installation, and any machinery used during the process.

Process of Assessment

The fundamental principle of performing embodied carbon calculations is to multiply the quantity of each material by a carbon factor for the life cycle modules being considered:

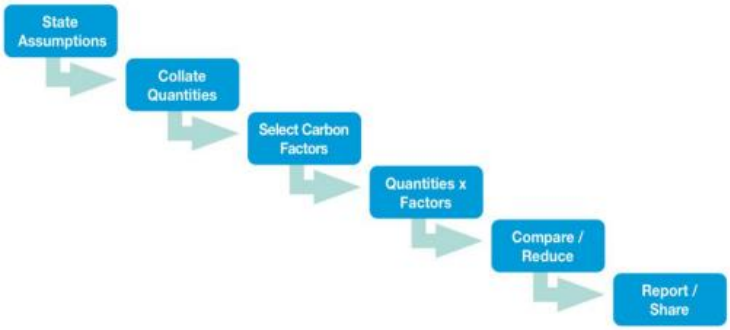


Fig. 2. Temporary Works Carbon Estimate Process

Material quantity (kg) x carbon factor ($kgCO_2e/kg$) = embodied carbon ($kgCO_2e$)

At a minimum, the life cycle scope of embodied carbon assessments for structural elements should include life cycle Modules A1-A5, cradle to gate to site. The reason behind this is that these are the quantities that we currently have the most certainty over, that make up the majority of the embodied carbon of structures, and will be the emissions that will be released before 2050 and thus are the most urgent to both understand and minimize. When analyzing supportive excavation systems on a project, these are the Modules that nearly comprise the entirety of the system's life cycle.

Assumptions are important factors to be included in the assessment process. Assumptions are generally made as to the average distance materials must be transported both from their source to fabrication and from fabrication to the site. The assessment assumes a typical life span for certain materials that will be

 © Deep Foundations Institute 2025

reused and how much of the materials will end up as waste or will be recycled. The analysis does not take into consideration any maintenance or repair of products. The end result is reported in units of $kgCO_2e$ or ton CO_2e, often referred to as 'carbon' for short. This measure considers other greenhouse gas emissions (GHGs) in addition to carbon dioxide (CO_2), expressing them in terms of CO_2 normalized by their global warming potential (GWP).

End Goal of Assessment

By performing a LCA on a building, the engineers, architects, and contractors can work collectively to reduce the embodied carbon footprint of that building. This assessment allows the building's team to estimate the amount of carbon in different parts of the design. The assessment can identify carbon hotspots and opportunities to target for material reduction. The assessment can allow for understanding of rough differences between different shoring options. The assessment can help each individual to communicate decision-making impacts with the rest of the design team. The earlier that the assessment is performed and reported to stakeholders the more opportunity there is to capture reductions in the net embodied carbon on a project.

EMBODIED CARBON ASSESSMENT IN SUPPORT OF EXCAVATION

The embodied carbon assessment is performed using the EEFC DFI Carbon Calculator Tool[2]. Launched in 2012 by EFFC, DFI, and Carbone 4, this tool remains a leading excavation-focused embodied carbon tool and the one used in the comparative analysis for this paper. This tool calculates the primary source of embodied carbon, that encompassed in the source and manufacturing of the material, along with all secondary sources of embodied carbon that include emissions from site activities, worker transport to and from the site, delivery transport of the materials, waste disposal, water use and treatment, etc.

Product Stage (A1-A3) Calculations

For this stage, the EEFC DFI Carbon Calculator Tool uses the material properties and their associated carbon factors, duration of use on the project, and the quantities of materials to be used to calculate the primary source of embodied carbon.

The total material usage of the steel on the project was determined based on the total volume of the steel required and the density of the steel of 7,850 kg/m^3.

A shown in Table 1, the carbon factor for steel ranges from 1.8 to 2.4 $kgCO_2e/kg$, based on the carbon factors sourced from Ecoinvent v3.9[3]. The carbon factor is dependent on the shape of the steel section.

Using the embodied carbon factors, the embodied carbon of each element, is determined from the equation:

$$EC_{A13} = \sum_{i=1}^{n} [Q_i (ECF_{A13,i}) \quad [1]$$

EC_{A13} = total embodied carbon for life cycle Modules A1-A3 ($kgCO_2e$)
Q_i = quantity of i^{th} material (kg)
$ECF_{A13,i}$ = Modules A1-A3 embodied carbon factor for i^{th} material ($kgCO_2e/kg$)

 © Deep Foundations Institute 2025

Table 1. Carbon Factors for Steel Materials

Steel Product	Unit	Emission Factor (kg CO_2e / t)	Source
Steel sheets	t	1,861.0	Ecoinvent v3.9[3]
Steel rebars	t	1,838.0	Ecoinvent v3.9
Steel tubes	t	2,332.0	Ecoinvent v3.9
Steel wires	t	2,259.0	Ecoinvent v3.9

Transport Stage (A4) Calculations

The embodied carbon due to transportation of the steel from source to the site were included as secondary sources of embodied carbon. The transport emission factors (TEF_{mode}) were obtained from EEFC DFI Carbon Calculator Tool and are shown in Table 2. The table provides respective conversion factors for all major greenhouse gases for a wide range of vehicles. An averagely laden delivery vehicle was assumed with the distance from the hub to project site set to 40 miles (80 miles is used for delivery trip and empty return trip). The Module A4, embodied carbon for transport, was calculated using the following equation:

$$ECF_{A4,i} = \sum(TD_{mode} x TEF_{mode}) \quad [2]$$

$ECF_{A4,i}$ = embodied carbon factor for transport for the i^{th} material Modules A4
TD_{mode} = transport distance
TEF_{mode} = transport emission factor

Table 2. Carbon Factors for Transportation

Mode / Vehicle Type	Unit	Emission Factor (kg CO_2e)	Source
Diesel	liter	3.20	Defra 2022 (v2)[4]
Road – Rigid >3.5–7.5t	vkm	0.61	Defra 2022 (v2)
Road – Rigid >7.5–17t	vkm	0.74	Defra 2022 (v2)
Road – Rigid >17t	vkm	1.21	Defra 2022 (v2)
Road – Articulated >3.5–33t	vkm	0.95	Defra 2022 (v2)
Road – Articulated >33t	vkm	1.13	Defra 2022 (v2)
Maritime – General cargo	tkm	0.02	Defra 2022 (v2)
Maritime – Container	tkm	0.02	Defra 2022 (v2)

vkm = vehicle-kilometer (emissions per km traveled by vehicle)
tkm = tonne-kilometer (emissions per ton of freight per km)

Construction Stage (A5) Calculations

This stage in an embodied carbon analysis accounts for pre-construction demolition (Module A5.1), construction activities (Module A5.2), waste and waste management (Module A5.3), and worker transport (Module A5.4). All emissions associated with A5 are included as secondary emissions.

Pre-construction demolition is applicable whenever an existing building asset requires demolition. For the consideration of this analysis and with most respects to temporary support of excavation services, this is considered zero.

 © Deep Foundations Institute 2025

Construction activities module encompass any site services, temporary works, ground works, onsite assembly of products, installation and removal of formwork, energy and water usage in construction activities, etc. The EEFC DFI Carbon Calculator Tool assumes default values based on industry averages.

The carbon factor associated with waste and waste management of materials used in temporary shoring is calculated by multiplying a waste factor by the sum of the carbon factors associated with Module A1-A3 for that material. The waste factor is dependent on the waste rate and is calculated by:

$$WF_{i} = \frac{1}{1-WR_i} - 1 \quad [3]$$

For steel frame members, the waste rate is 1% and the corresponding waste factor is 0.010. The embodied carbon factor for Module A5.3 is calculated by:

$$ECF_{A5.3,i} = WF_i x (ECF_{A13,i} + ECF_{A4,i}) \quad [4]$$

$ECF_{A5.3,i}$ = embodied carbon factor for waste for the i[th] material Modules A5.3
WF_i = waste factor for i[th] material
$ECF_{A13,i}$ = embodied carbon factor for A1-A3 for the i[th] material
$ECF_{4,i}$ = embodied carbon factor for A4 for the i[th] material

Comparison between conventional bracing and hydraulic bracing and slide rail

Results of the upfront carbon, CO_2e for the project, resulting from Modules A1-A5 for both hydraulic bracing, the modular slide rail system, and the conventional counterpart are reported to compare and analyze the differences in the calculated net carbon and realize potential CO_2e savings by using one system over another. The resulting equation for the total upfront carbon is given as:

$$EC_{A15} = EC_{A13} + \sum[Q_i(ECF_{A4} + ECF_{A5.3})] + EC_{A5.2} \quad [5]$$

One key contributor factored into the carbon calculations for both the hydraulic bracing system and the slide rail system is the reusability of these systems. The total embodied carbon for reusable shoring systems assumes an average lifespan of the system components at roughly 10 years, based on industry averages. However, the total embodied carbon also takes into account a 50% utilization rate of these systems over that lifespan. The rate of embodied carbon costs for the hydraulic bracing and slide rail systems are calculated based on quantity of weeks of hire.

ALTERNATIVE SUPPORTS FOR TEMPORARY EXCAVATIONS

Hydraulic Bracing Systems

An alternative approach to conventional steel welded walers and struts is the use of high load capacity modular hydraulic bracing. A typical hydraulic bracing system includes hydraulic struts (rams) which are telescoping or fixed steel tubes preloaded with hydraulic pressure to provide outward force, walers or horizontal steel beams that distribute the strut force along the excavation wall, corner brackets and joints that use modular connectors that secure struts to walers or to other struts, and a pump and gauge system, which is used to preload and monitor the hydraulic pressure in the struts.

These systems work by installing the rams and extension members on the inside of the excavation along opposing walls and then applying hydraulic pressure to the struts, which brace the walls by pushing

outward. As excavation progresses, additional levels of struts can be added. Struts can be repositioned or removed during backfill.

These systems allow for use in a variety of configurations, both short and small. The joints and corners offer quick assembly on site without the need for welded connections. The system can be used for non-rectangular or tight excavations and the high load capacity and option to use internal hydraulic struts to form a continuous heavy duty waling beam means that excavations requiring large clear spans or long lengths are easily achievable. The modular format of the system also allows for installation using relatively light duty lifting equipment.

Slide Rail System

Slide rail systems are a durable, modular, low-vibration shoring solution that allows the users to push the system in place while digging the excavation to depth. Slide rail systems are a pre-engineered system composed of vertical rails and horizontal steel panels (or plates) that "slide" into place as the excavation progresses. A slide rail system includes vertical corner posts or rails, steel panels (shoring plates) and sometimes struts or crossbars for longer excavated spans.

These systems work by installing the vertical corner posts at the corners of the excavation and then the steel panels are guided between the track in the rails and slid down into place to resist the lateral loads as soil is subsequently removed. Cross struts are added to brace the system as needed. The system is fully removed by reversing the installation sequence during backfill.

Slide rail systems are advantageous compared to alternative shoring methods because they can provide sufficient clearance, they minimize site restoration cost, enables the use of smaller excavators, and decreases the overall installation and removal time of the system with no welding or cutting on site. The applicability of slide rail shoring systems is extensive over a wide range of projects from tank installations to pump stations, bore pits, linear pipeline runs, as well as areas that have poor soil conditions, are near vibration sensitive areas or railroads with tight movement tolerances.

Shared Sustainability Features

Both the hydraulic bracing and slide rail systems are favorable options in temporary shoring when the goal is to reduce the embodied carbon cost for a project. As opposed to other temporary shoring systems (cast-in-place retaining walls, secant pile walls, soldier pile beams and plates, soil nails and tieback anchors, sheeting with static steel walers, etc.) these systems are modular, reusable, and install and dismantles quickly on site.

Furthermore, the applicability of use of both systems on a wide range of projects means that their reusability is very high. Having the option to use either of these systems on many projects does also mean that transportation costs can be minimized by being able to source pieces from local suppliers and transportation costs from manufacturing or to waste processing or disposal are nearly irrelevant.

The faster installation time of both shoring systems results in less time using excavators, cranes and other heavy equipment that runs on fuel emitting CO_2. Additionally, both systems are designed for tight spaces and minimal over-digging which results in less soil removal. Less soil being removed means fewer truckloads and less fuel burned in hauling and disposal. Additionally, these systems are pre-engineered and delivered in modular form, reducing on-site fabrication.

 © Deep Foundations Institute 2025

Finally, without the need for welding connections, the need for an individual with welding certifications and the length of time it takes to install steel with welded connections is no longer a factor when installing temporary shoring.

CASE STUDY: SHIP CANAL WATER QUALITY PROJECT BORING AND RECEIVING PITS

The combined sewer overflows (CSOs) in the Seattle neighborhoods of Ballard, Fremont, Queen Anne, and Wallingford must be limited to one overflow per year on average for each affected outfall. The current average is 130 overflows annually, equating to 80 million gallons (MG) (303 ML) of polluted water in the Seattle waterways. In 2018, 84% of the city's overflows came from combined sewers from these Seattle neighborhoods.

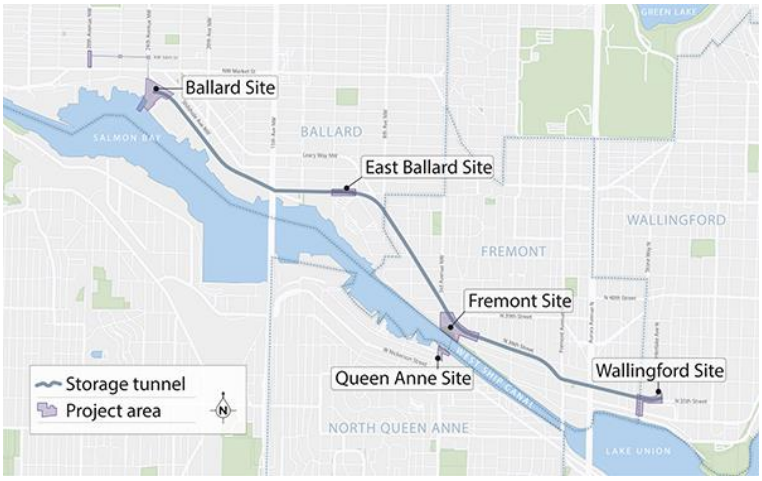


Fig. 3. Project Site Plan for Ship Canal Water Quality Project (SCWQP)

The 14,000-foot-long (4,267 m) Tunnel Storage project is the program's central feature and is anticipated to improve the water quality in the area by keeping more than 75 million gallons of polluted stormwater (from rain) and sewage from flowing into the Lake Washington Ship Canal, Salmon Bay, and Lake Union on average each year. The boring and receiving pits are for the launching and retrieving of the tunnel boring machine employed to bore this new CSO. The boring pit is 14' wide, 28' long, and 22' deep and the receiving pit is 12' wide, 16' long, and 24' deep, each located in medium dense silty sand. The boring pit is located within 5' from an existing diversion structure with its foundation extending below base of excavation.

The size and depth of each pit allows for several different options when exploring the temporary bracing of the excavations. For this analysis, the carbon emissions from three very applicable designs have been explored and calculated; soldier pile beams with steel plate lagging and braced with welded walers, a slide rail system, and sheeting braced with a hydraulic bracing system.

Carbon emissions from soldier piles with steel plate lagging and welded steel walers

For the conventional approach to temporary shoring, using structural steel soldier piles with steel plate lagging and braced with welded steel walers, each material was quantified and given an embodied carbon factor based on the material. For both the receiving pit and boring pit, ASTM A992 W14x120 steel beams were used at 8' spacing, 1-1/2" ASTM A36 steel plates were used for the full height of the excavation for lagging, and ASTM A992 W24x192 and W32x256 beams were used as welded walers.

 © Deep Foundations Institute 2025

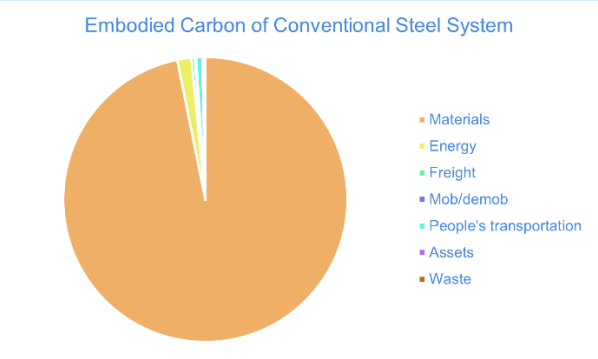


Fig. 4. Original Design Embodied Carbon

Carbon emissions from slide rail

The slide rail system is composed of four components; linear posts, corner posts, strut carts with structural steel beam extensions, and slide rail inner and outer panels. Similar to the conventional steel shoring system stated above, the slide rail system is also made from all steel parts.

However, unlike conventional steel sections used in welded waler systems, the slide rail equipment has a long lifespan, assumed at 10 years. The reusability of the slide rail components means that the equipment can be used over and over again reducing the amount of embodied carbon that would otherwise be created due to waste and disposal of used steel and fabrication of new steel. As equipment hires tend to be in weekly increments, we modified the 10-year lifespan to 520 weeks. In order to ascertain the usable life of the slide rail, the utilization rates were calculated and apportioned out the embodied CO2e over the products' useable life. The assumed product utilization rate of 50% would have a usable life of 260 weeks (520 x 50%). The calculated embodied carbon of the slide rail system was then calculated by:

$$EC_{A13} = \frac{ECF_{A13,i}}{520xUt} \quad [6]$$

Ut = Utilization rate of equipment, assumed at 50%

Transportation of the slide rail equipment to the hub was factored into the calculations. It was assumed that one vehicle was able to carry all of the equipment from production to the hub, where it is then distributed to project sites. For slide rail, the travel distance from manufacturer to the region's hub in Tacoma, WA is 2,250 miles.

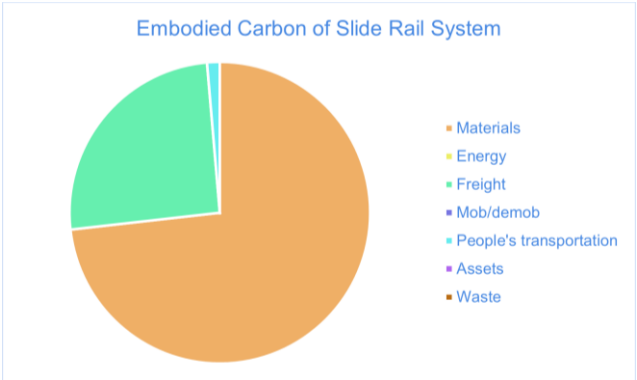


Fig. 5. Substituted Design Slide Rail Embodied Carbon

 © Deep Foundations Institute 2025

Carbon emissions from sheeting with hydraulic bracing

The analysis of sheeting braced with hydraulic bracing is performed much similar to that of the slide rail system in that the utilization rate of 50% of the system is assumed with a lifespan of 10 years or 520 weeks and the embodied carbon from transport from the manufacturer in the UK to the region's hub in Tacoma, WA (an average laden general cargo ship and average laden truck cross country) is accounted for in the total carbon. The embodied carbon from the sheeting is also added to the total embodied carbon.

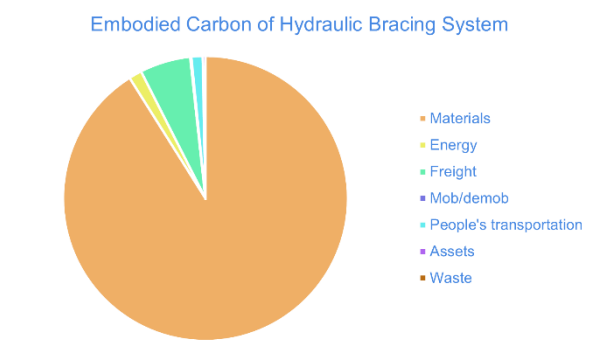


Fig. 6. Substituted Design Hydraulic Bracing Embodied Carbon

SUMMARY AND CONCLUSIONS

Through the embodied carbon life cycle assessment performed for the three systems the resulting totals of embodied carbon resulting from Modules A1-A5 (cradle to site) are presented in Fig. 7. Unsurprisingly, the system utilizing conventional steel piles, plates and bracing resulted in the highest total embodied carbon, followed by the system using steel sheeting with hydraulic bracing and with the slide rail system yielding the least net carbon.

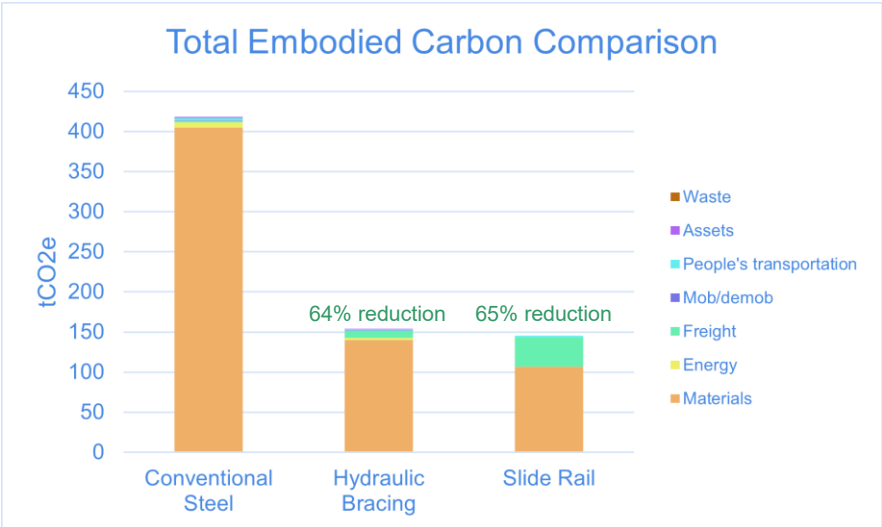


Fig. 7. Total CO_2e Comparison by System

With slide rail producing only about 35% of the embodied carbon of its conventional counterpart, the projected carbon savings from moving from an all-steel support of excavation system to slide rail is

 © Deep Foundations Institute 2025

substantial and proves that these alternative systems should be worth considering on every project requiring temporary shoring.

As the world and the construction industry continue to look at ways to reduce our carbon footprint, the approach to temporary shoring can and should be considered. The reusability of temporary shoring systems is in use worldwide but is not currently considered on every project. The substantial reduction in CO_2 through the use of these systems may hopefully persuade a deeper dive into the pre-construction methodologies of every project.

REFERENCES

[1] BS EN 15978:2011, *Sustainability of construction works – Assessment of environmental performance of buildings – Calculation method*, BSI, London, UK, 2011.

[2] EFFC/DFI Carbon Calculator Task Group. (2022). EFFC/DFI Carbon Calculator: Foundation & geotechnical CO_2 emissions assessment tool [Excel-based software]. Developed by European Federation of Foundation Contractors (EFFC) & Deep Foundations Institute (DFI). Tool certified to ISO 14067, GHG Protocol and PAS 2050.

[3] Ecoinvent Centre. (2022). Ecoinvent database v3.9 [Data set]. Swiss Centre for Life Cycle Inventories, Zürich, Switzerland. Available at: https://www.ecoinvent.org

[4] HM Government, "Greenhouse gas reporting: conversion factors 2021 (2nd edition)," 24 Jan 2022. [Online]. Available: https://www.gov.uk/government/publications/greenhouse-gas-reporting-conversion-factors-2021. [Accessed March 2025].

[5] RICS, "Elemental Standard Form of Cost Analysis (4th edition)," 2012. [Online]. Available: https://carbon.tips/bcis. [Accessed March 2025].

 © Deep Foundations Institute 2025

A NEW GEOMATERIAL FOR ROADS BASED ON MINING WASTE FOR SUSTAINABILITY AND RESILIENCY

M.V. Morais, GeoBioTec, Civil Engineering and Architecture Department, University of Beira Interior, Covilhã, Castelo Branco, Portugal, vitoria.morais@ubi.pt
L. Marchiori, GeoBioTec, Civil Engineering and Architecture Department, University of Beira Interior, Covilhã, Castelo Branco, Portugal, leonardo.marchiori@ubi.pt
L. Andrade Pais, GeoBioTec, Civil Engineering and Architecture Department, University of Beira Interior, Covilhã, Castelo Branco, Portugal, ljap@ubi.pt
A. Albuquerque, GeoBioTec, Civil Engineering and Architecture Department, University of Beira Interior, Covilhã, Castelo Branco, Portugal, antonio.albuquerque@ubi.pt
V. Cavaleiro, GeoBioTec, Civil Engineering and Architecture Department, University of Beira Interior, Covilhã, Castelo Branco, Portugal, victorc@ubi.pt

ABSTRACT

Mining operations produce substantial waste, often referred to as tailings, which are traditionally viewed as unusable by-products. However, innovative strategies in the construction industry are exploring the reuse of these materials, promoting sustainability and reducing environmental impact. This article investigates the potential of granite mining waste (MW) as a component in granular road materials, specifically in large-grained crushed aggregate (ABGE) or tout-venant (TV). By incorporating varying proportions of waste (0%, 25%, 50%, 100%) and analyzing different particle sizes (>0.063 mm, >0.400 mm), this study aims to provide a sustainable alternative for traditional construction materials. Chemical, physical, and mechanical analyses were conducted to evaluate the properties of the mixtures and pure materials. Mixtures have met plasticity limits and granulometric criteria for sub-bases, exhibited optimal performance in oedometric testing, and surpassed the required California Bearing Ratio threshold. Materials with higher fines content also demonstrated reduced permeability, making them suitable for liners, regularization, and berm filling layers. The findings highlight 25% introduction of MW sieved through 0.063mm as a viable granular sub-base material, contributing to sustainable infrastructure development and aligning with goals for economic and environmental balance. By identifying practical applications for mining waste in road construction, this research supports the principles of the circular economy, offering a pathway to repurpose industrial by-products while conserving natural resources. This approach demonstrates how innovative material reuse can drive resiliency and sustainability in the construction industry, fostering a more sustainable future.

Keywords: granite mining waste; *tout-venant*; geotechnical characterization; granular sub-base; circular economy

INTRODUCTION

Mining activities bring economic benefits, however, requires processing to enable the commercialization of the extracted ore (Huang et al. 2025). Those processes generate several products, including rock powder, sludge, soil, and chemicals, representing potential environmental risks (Marchiori et al. 2025). These by-products, often generated in large quantities, pose significant challenges in terms of management and disposal. While some materials have limited potential for reuse due to their composition or economic constraints, others present viable opportunities for application in different industries (Weiksnar et al. 2024).

Considering this situation, it is necessary to develop effective methods for reusing disposed materials (Marchiori et al. 2022). One approach is to verify and quantify the hypothesis of chemical contamination and then use these mining by-products as components in road materials (Malaoui et al. 2024; Chlahbi et

 © Deep Foundations Institute 2025

al. 2024; Inabi et al. 2025), representing a sustainable and innovative strategy for the construction industry (Chandra and Sinha 2024). Waste from granite is mainly composed of granite rock fragments, which seem to have mechanical properties and durability that make them suitable for use as aggregates in pavements (Alhomaidat et al. 2025). Furthermore, the mineralogical composition of granite waste may include minerals such as quartz, feldspar, and mica (biotite and muscovite), which contribute to the strength and stability of roads (Chlahbi et al. 2024).

Given the significant volumes of waste generated, its integration into construction materials presents an opportunity to reduce environmental impacts while promoting sustainable resource management. From a practical perspective, utilizing this waste can enhance sustainability in the mining sector, mitigate disposal-related issues, and contribute to the development of eco-efficient engineering solutions. This research aims to incorporate granitic mining waste, or mining waste (MW), as filler in road granular layers, from a mine, which is recognized as an extractive unit for granite rocks in the region of Guarda (Portugal).

Furthermore, this approach aligns with global sustainability strategies, particularly the Sustainable Development Goals (SDGs), including SDG 9 (Industry, Innovation, and Infrastructure) and SDG 12 (Sustainable Consumption and Production), which emphasize the importance of sustainable industrial practices and responsible resource use. By fostering innovation in material reuse, this study contributes to the circular economy and advances sustainable engineering practices. Besides, this approach not only addresses the responsible environmental management of mining waste disposal but also seeks to promote sustainability in the construction of road infrastructure, thus contributing to more eco-efficient practices in the sector.

MATERIALS AND METHODS

Two materials were used for the research: *tout-venant* and granite mining waste. *Tout-venant* is typically commercialized and obtained from crushing and screening natural rocks such as granite, basalt and limestone. It is normally characterized by its variable particle size, which includes a mixture of fine to coarse particles and has high resistance due to the presence of hard minerals such as quartz. TV used in all mixtures was from the same batch, ensuring consistency in grain size. The mining waste mud from a granitic quarry is a fine-grained by-product generated during the cutting, crushing, or washing processes of granite extraction. It typically consists of suspended particles of granite minerals such as quartz, feldspar, and mica, and is often stored in sedimentation basins or deposited as slurry. The granite mining waste used is from a quarry called “Pedreira da Devesa”, located in Santana de Azinha, Guarda (Portugal).

Mixtures with different percentages of residue and variations in particle size were defined, the materials were organized into six groups of samples, as shown in Table 1. They were characterized to evaluate their geotechnical characteristics following standards in Table 2. In addition, chemical and mineralogical composition and compatibility were analyzed by (Marchiori, et al., 2023). In Fig. 1, mixtures as well as pure materials are shown side by side. In Fig. 1a is the TV100% material, Fig. 1b it is the MW25% (0.063), Fig. 1c is the MW50% (0.063), Fig. 1d is the MW50% (0.063), Fig. 1e is the MW50% (0.400), and in Fig. 1f it is MW100%. Both materials were sieved prior to the mixtures’ development to capture the finer portions from the by-product, mining waste, and to analyze the behavior of the composites according to different introduction ratios. All geotechnical tests were conducted using samples compacted at their respective optimum moisture content (OMC) and maximum dry density (MDD) as determined by the Normal Proctor test. For the CBR, specimens were compacted in molds at the MDD, soaked for 96 hours in water prior to testing, and then tested under saturated conditions. The hydraulic conductivity (k) was determined using the falling head method, with compacted specimens placed in permeameter cells

and saturated under back pressure prior to initiating flow. All tests were performed in triplicate to ensure repeatability, and average values are reported

Table 1. Materials and mixtures developed and tested in the research

Samples	Nomenclature
(100% *tout-venant*)	TV100%
(75% *tout-venant*) + (25% of mining waste passed through a sieve <0.063)	MW25% (0.063)
(75% *tout-venant*) + (25% of mining waste passed through a sieve <0.400)	MW25% (0.400)
(50% *tout-venant*) + (50% of mining waste passed through a sieve <0.063)	MW50% (0.063)
(50% *tout-venant*) + (50% of mining waste passed through a sieve <0.400)	MW50% (0.400)
(100% mining waste)	MW100%

Table 2. Testing program standards

Tests	Specific Gravity	Particle Size	Atterberg Limits	Normal Proctor	Oedometric	CBR	Hydraulic Conductivity
Parameters	Gs	Curve	PI W_L W_P	OMC MDD	Cc Cr Cs	CBR Swelling	k
Standards	ISO17892-2 2014	ISO17892-4 2016	ISO17892-12 2018	BS1377-4 1990	ISO17892-5 2017	AASHTO T193 1999	ISO17982-11 2019



(a) (b) (c) (d) (e) (f)

Fig. 1. Samples, mixtures and pure materials

RESULTS AND DISCUSSION

Chemical Compatibility

The mineralogical composition of MW100% and TV100% revealed the presence of Quartz, Kaolinite and Muscovite. The identification of quartz, one of the most abundant and hardest minerals, suggests that the residue has potential for applications in civil construction, as aggregate in concrete and pavements, due to its strength and durability. Kaolinite, a clay with high plasticity and adsorption capacity, can be used to improve the cohesion of sandy soils, increasing the stability of foundations and support structures, and in road cuts it can be applied to reduce soil erodibility, preventing landslides, and ensuring the safety of infrastructures. The presence of muscovite may reduce interparticle bonding due to its smooth surface and cleavage properties, potentially influencing the compaction behavior and

 © Deep Foundations Institute 2025

increasing deformability of the mixtures. In addition to this, the heterogeneous structure of minerals generates greater resistance (Marchiori et al. 2023).

The results for pH values indicate an average value of 6.8 for MW100% and 6.0 for TV100%. Soils with a pH between 6.0 and 6.5 are classified as slightly acidic to neutral (Pessoa 2004). Both soils are within a favorable range for most paving applications. MW100% with pH 6.8 is ideal as it offers a neutral condition that minimizes adverse chemical reactivity with stabilizing materials, facilitating the stabilization and durability of the pavement. When mixed, it should ensure better stabilization of the slightly acidic pH of TV100%. The results are consistent with what is presented in the literature (Campanha 2011; Galhardo 2015; Malaoui 2023; Marchiori et al. 2023). It is understood that the mixtures would present variations in values within the limits of values found between MW and TV, and it is not necessary to carry out this analysis for the mixtures.

Heavy metals leaching of the residue are in accordance with EPA SW-846 (Method 1313) and meet all limits set by Council Decision 2003/33/EC (E.P. 2014), which is the applicable legislation in Portugal, and would be acceptable in the majority of countries throughout the world. This compliance with the waste acceptance criteria demonstrates that granite mining waste is safe for use in paving, posing no significant risk to human health or the environment. Compliance ensures that potential leachate components will not leach into the soil or groundwater, preventing contamination.

Physical Characterization

The particle size distributions of the analyzed material are shown in Fig. 1, and physical parameters are summarized in Table 3. As expected, the mixtures have well-graded curves, varying only the proportions of fines. The granulometric curves of the mixtures are within the ranges recommended by the CETO from EP LNEC E 196 (E.P. 2014), for use in granular subbases where the percentage of material that passes sieve No. 200 ASTM maximum is 15%, excluding MW100% and MW 50% (0.400) due to higher fine portions.

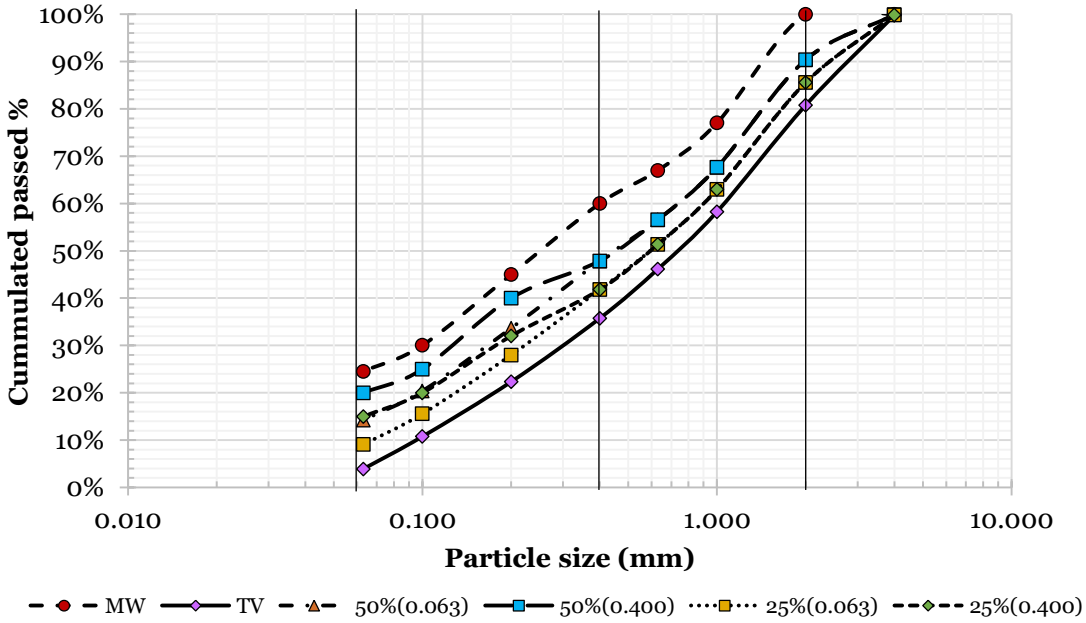


Fig. 2. Results of granulometric curves for pure materials and mixtures

 © Deep Foundations Institute 2025

According to the Atterberg limits, MW100% has high plasticity; and finally, TV100% during the test did not present plastic characteristics for its execution, being classified as non-plastic. Furthermore, MW25% (0.063) and MW50% (0.400) can be classified as having low plasticity; and the mixtures MW25% (0.400) and MW50% (0.063) with medium plasticity. This occurs due to the different introductions of finer material, smaller particles usually present higher plasticity. The highest index is MW100%, as expected.

Table 3. Physical parameters of the tested materials

Parameter	Gs	WL	WP	PI	OMC	MDD	k
Units	-	%	%	%	%	g/cm^3	m/s
MW100%	2.50	33.90	11.90	22.00	21.60	1.50	6.9×10^{-9}
MW25% (0.063)	2.58	23.50	19.00	4.50	9.85	2.00	2.7×10^{-8}
MW25% (0.400)	2.63	29.70	21.20	8.50	10.51	1.73	5.2×10^{-8}
MW50% (0.063)	2.56	29.70	19.40	10.30	10.40	1.93	1.7×10^{-8}
MW50% (0.400)	2.59	29.70	27.60	2.10	10.67	1.79	3.9×10^{-8}
TV100%	2.70	18.50	NP	NP	10.00	2.03	6.3×10^{-8}

The MW25% (0.063) mixture had an OMC of 9.85%, while the MW25% (0.400) had a slightly higher OMC of 10.51%. The usual behavior, that the finer material retains more moisture compared to the coarse material, and for those mixtures, given due to the quantity of introduced residue, the 0.400 incorporation uses more fine material than the 0.063, corroborating with the usual behavior. When increasing the mixing ratio to 50%, MW50% (0.063) had a moisture content of 10.40%, and MW50% (0.400) had the highest moisture content of 10.67% among mixtures. These results indicate that, at larger proportions, the coarser material continues to retain more moisture than the finer material. This may be due to the greater ability of thicker materials to create interstitial spaces that retain water, thus increasing optimal humidity. Furthermore, the mixtures do not show significant modification of OMC related to TV100%, which seems a consistent procedure to be utilized regarding compaction.

As expected, MDD is decreasing with the residue introduction, corroborating with lower values of specific gravity (Gs), this is a good behavior for lowering the costs in transportation and lower content of materials utilization (Marchiori, Albuquerque, & Cavaleiro, Granitic Mining Waste Feasibility for Liner Material Production, 2022), but the strength must be analyzed. Hydraulic conductivity also followed the expected, decreasing while higher finer content is present, the values did not reached the outlined for bottom liner, however could be used as top layers in liner facilities (Marchiori et al. 2022), as typical requirements for hydraulic conductivity for liner materials are lower than 10^{-9} m/s, ensuring low permeability to prevent fluid migration.

Mechanical Behavior

Geotechnical parameters are summarized in Table 4. MW100% has a relatively higher compression coefficient (Cc) than the other samples, but not significantly, indicating low compressibility under normal consolidation loads. This suggests that the mixtures can be suitable for use in road granular layers as it can lead to lower settlements over time. For the MW25% sample (0.063), Cc decreases, making it less compressible and more stable, while recompression coefficient (Cr) remains constant, suggesting that the structure recovery capacity is not affected by the addition of fine material. For MW50% (0.063) and MW25% (0.400), the Cc is the same, while the MW50% (0.400) mixture presents the worst value among mixtures, but still stable. Analyzing the table, the MW25% (0.063) mixture is one of the best options, with a very low Cc and swelling coefficient (Cs). Considering that the compressibility index is dependent on the density and initial void index, Andrade Pais [22] classifies the

 © Deep Foundations Institute 2025

type of soil according to values found for Cc. The results found in this research classify all samples as sand.

Table 4. Consolidation, swelling, and bearing capacity parameters of the tested materials

Parameters	Cc	Cr	Cs	CBR	Swelling
Units	-	-	-	%	%
MW100%	0.109	0.030	0.020	2.4%	0.39
MW25% (0.063)	0.045	0.030	0.012	22.1%	-0.13
MW25% (0.400)	0.058	0.011	0.019	2.9%	0.22
MW50% (0.063)	0.058	0.013	0.015	14.7%	0.03
MW50% (0.400)	0.078	0.008	0.011	5.9%	0.23
TV100%	0.100	0.033	0.009	24.6%	0.23

MW100% presents the highest expansion of the materials studied, 0.39%, but still very low expansion. The MW25% (0.063) and MW50% (0.063) mixtures present almost zero expansion, slight contraction, due to the introduction of a low quantity of silty clay material which could fill the voids, suggesting a stable material, which may indicate an improvement in volumetric stability when compared to other mixtures with particle size 0.400. Samples with 50% mixture show interesting results, MW50% (0.063) has an almost neutral expansion, indicating that the increase in the amount of fine material continues to reduce the expansion, while at MW50% (0.400) maintains an expansion of 0.23%, like TV100%. MW25% (0.400) presents an expansion of 0.22%, which is lower than that of the pure residue. These results suggest that adding finer material to soil or waste can reduce expansibility, improving material stability. The expansion limit established by E.P. (2014) is 1.5% for sub-base layers, and there are no required expansibility values for regularization and berm filling layers.

MW100% presented a CBR value, of 2.4%, while TV100% presented 24.6%. Lower CBR values were found in mixtures with a particle size of 0.400, reinforcing the idea of expansion values. The mixtures with 0.063, with a greater presence of clay-silty material, presented higher CBR values, especially the mixture with 25%. For the sub-base layer, the E.P. (2014) requires a minimum of 20% for the CBR value, with the MW25% (0.063) mixture being the only one that meets this parameter. For regularization and filling layers there are no minimum values required, and all mixtures can be applicable.

The notably higher CBR value observed for the MW25% (0.063) mixture, compared to the other compositions, may be attributed to an optimal combination of fine particles and overall gradation. The inclusion of 25% of mining waste passing through the 0.063 mm sieve appears to enhance the packing density of the matrix, promoting a denser and more interlocked structure after compaction. Finer particles can effectively fill the voids between larger aggregate grains, thereby improving the load distribution and inter-particle friction, which is critical under load-bearing conditions. Furthermore, under soaked conditions, this gradation likely minimized water-induced softening effects by reducing permeability and limiting water retention in the voids. This leads to greater structural stability after saturation, enhancing resistance against deformation and justifying the superior bearing capacity observed. These findings suggest that a well-balanced mix of coarse and fine fractions can substantially improve mechanical performance, particularly for sub-base layers subjected to moisture variations.

SUMMARY AND CONCLUSIONS

The findings of this study highlight the potential use of granite mining waste as a sustainable alternative material for geotechnical applications, particularly in foundation engineering. The laboratory analyses

demonstrated that incorporating mining waste into *tout-venant* mixtures can enhance certain geotechnical properties, making them suitable for use in sub-base layers, leveling layers, and berm fillings. Among the tested compositions, the MW25% (0.063) mixture showed the most promising results, meeting the technical specifications required for granular sub-base applications, while other mixtures presented viable alternatives for secondary applications.

From a foundation engineering perspective, the mechanical behavior of these materials suggests potential applications in road base layers and as compacted fill in shallow foundation systems. The presence of quartz, a highly resistant mineral, contributes to the overall stability of the material, ensuring durability and load-bearing capacity. Additionally, the low compressibility observed in the oedometer tests, along with favorable CBR values in certain mixtures, indicates that granite mining waste can contribute to the improvement of foundation support conditions, reducing settlement risks in infrastructure projects. Beyond the technical performance, this research underscores the environmental benefits of utilizing granite mining waste. By integrating this by-product into construction materials, the study contributes to circular economy principles, reducing the need for natural aggregate extraction and minimizing landfill disposal. This aligns sustainable construction practices and reinforces the role of geotechnical engineering in promoting eco-friendly solutions in infrastructure development.

Future research should explore the long-term behavior of these materials under field conditions, particularly their performance under cyclic loading and different environmental exposures. The potential for stabilization techniques or chemical treatments to enhance the mechanical properties of the material should also be investigated to expand its applications in foundation engineering. In conclusion, this study presents a viable and environmentally responsible approach to incorporating mining waste into geotechnical works. The promising results encourage further research and pilot-scale applications to validate its full potential in real-world construction scenarios, particularly in foundation engineering where cost-effective and sustainable materials are increasingly in demand

REFERENCES

AASHTO T193, 1999. Standard Method of Test for The California Bearing Ratio.

Andrade Pais, L.J., 2007. Comportamento Mecânico do Solo Residual Granítico da Covilhã com Efeito de Contaminantes. Covilhã.

Alhomaidat, F., Al-Kheetan, M. and Alosifat, S., 2025. Recycling phosphate mine waste rocks in asphalt mixtures to fully replace natural aggregate: A preliminary study. Results in Engineering, 25, pp. 104324.

BS 1377-4, 1990. Methods of test for Soils for civil engineering purposes - Part 4: Compaction-related tests. British Standards Institution.

Campanha, A., 2011. Caracterização de Rejeitos de Minerio de Ferro para uso em Pavimentação. Viçosa.

Chandra, S. and Sinha, S. 2024. Strength Assessment of Cement Treated Coal Mine Overburden Material in Subbase and Base Layers. SSRG International Journal of Civil Engineering, 11(6), pp. 24-30.

E.P., 2014. Caderno de Encargos Tipo Obra: Pavimentação - Caracteristica dos Materiais. Estradas de Portugal.

 © Deep Foundations Institute 2025

Galhardo, D.C., 2015. Estudo sobre a viabilidade tecnica da utilização de rejeitos de mineração de ferro em camadas de pavimentos rodoviários. Rio de Janeiro.

Inabi, O., Khalil, A., Benzaazoua, M. and Taha, Y. 2025. Toward Sustainable Mining: Repurposing Benguerir's Phosphate Mine Waste Rock for Road Subgrade Construction. E3S Web of Conferences, 601, pp. 10.

ISO 17892-2, 2014. Geotechnical investigation and testing - Laboratory testing of soil - Part 2: Determination of bulk density.

ISO 17892-4, 2016. Geotechnical investigation and testing - Laboratory testing of soil - Part 4: Determination of particle size distribution.

ISO 17892-5, 2017. Geotechnical investigation and testing - Laboratory testing of soil - Part 5: Incremental loading oedometer test.

ISO 17892-11, 2019. Geotechnical investigation and testing - Laboratory testing of soil - Part 11: Permeability tests.

ISO 17892-12, 2018. Geotechnical investigation and testing - Laboratory testing of soil - Part 12: Determination of liquid and plastic limits.

Malaoui, R., Harkati, E., Soltani, M., Djellali, A., Soukeur, A. and Kechiched, R., 2023. Geotechnical Characterization of Phosphate Mining Waste Materials for Use in Pavement Construction. Engineering, Technology & Applied Science Research, 13(1), pp. 10005-10013.

Marchiori, L., Albuquerque, A. and Cavaleiro, V., 2022. Granitic Mining Waste Feasibility for Liner Material Production. Proceedings of the 7th World Congress on Civil, Structural, and Environmental Engineering (CSEE'22), Virtual Conference, 2022.

Marchiori, L., Studart, A., Morais, M.V., Albuquerque, A., Andrade Pais, L. and Cavaleiro, V., 2023. Environmental-chemical compatibility of granitic-mining waste for liner material. WASTES: Solutions, Treatments and Opportunities IV, vol. 1, C. Vilarinho, F. Castro e M. Quina, Coimbra, CRC Press.

Marchiori, L., Albuquerque, A., Andrade Pais, L., Boscov, M.E.G. and Cavaleiro, V., 2025. Geoenvironmental Engineered Structures for Water Protection: Challenges and Perspectives for Sustainable Liners. Sustainability, 17, pp. 1850.

Pessoa, F.H.C., 2004. Análise dos solos de Urucu para fins de uso rodoviário. Distrito Federal.

Weiksnar, K., Ferraro, C., Kari, R., Mayer, N. and Townsend, T., 2024. Opportunities and challenges with implementing a recycling program for municipal solid waste incineration (MSWI) bottom ash as a construction aggregate: A programmatic review. Journal of the Air & Waste Management Association, 74(10), pp. 699-713.

 © Deep Foundations Institute 2025

DUCTILE IRON PILES USED AS RIGID INCLUSIONS FOR THE ACCELERATED CONSTRUCTION OF THE RAILWAY BRIDGE OVER THE MAIN ROAD B25 IN DONAUWÖRTH (GERMANY)

Freddy Lopez, Tiroler Rohre GmbH, Hall in Tirol, AUSTRIA, +4915140796868, freddy.lopez@trm.at
Erich Steinlechner, Tiroler Rohre GmbH, Hall in Tirol, AUSTRIA, erich.steinlechner@trm.at

ABSTRACT

In late January 2024, a new 28 m (89 ft.) - long railway bridge over the main road B25 nearby Donauwörth (southern Germany) was placed on its final position using the lateral bridge slide (LBS) procedure, to replace a 92-year-old structure, which was still fully operational. The main challenge of the design and construction approach was to limit the disruption of the railway operations to a minimum. In this context, the new structure was built next to the existing one. After finishing the construction of the new structure, the contractors had a track possession period of only 10 days to demolish the existing bridge, move the new bridge to the position of the old one, rebuild the track and reestablish the railway operations. The existing ground conditions (presence of soft soils) added complexity to the execution works. A ground improvement solution, using rigid inclusions was adopted for the foundation of both the (temporary) thrust beds and the (permanent) bridge abutments. Ductile iron piles (DIP) were used as rigid inclusions, to provide the immediate load transfer to the ground during the sliding procedure. The fast, simple, and safe installation of the DIPs was carried out within a very limited period of time (60 hours) and allowed for the successful execution of the sliding procedure. This technical paper presents an overview of the adopted solution, focusing on the design and execution of the ground improvement.

Keywords: Bridge foundations, ductile iron piles, design and construction, ground improvement

SI CONVERSION FACTORS

Table 1. Approximate conversions from SI Units

Dimension	Symbol	When you know	Multiply by	To Find	Symbol
Length	cm	centimeters	0.394	inches	in
	m	meters	3.281	feet	ft
Force	kN	kilonewtons	224.81	poundforce	lbf
	MN	meganewtons	224.81	kilopoundforce	kip
Stresses	kPa (kN/m^2)	kilopascals	0.145	Poundforce / square inch	psi
	MPa (MN/m^2)	megapascals	145	Poundforce / square inch	psi

PROJECT DESCRIPTION

As part of a comprehensive infrastructure project, the German Railways (*Deutsche Bahn*) executed an intervention to modernize a railway overpass, built in 1931 along the railway tracks 5310 (Donauwörth - Treuchtlingen) over the main road B25, located at the outskirts of the Bavarian city of Donauwörth (Fig. 1). This important traffic artery, which last underwent renovation works on the superstructure in 1977, required extensive repairs of the abutments, with the corresponding line closure. In coordination with the State Construction Office of Augsburg, the German Railways used the opportunity to modernize the entire bridge and to resolve traffic flow problems along the main road B25 in the long term. The intervention project was divided into two parts, with the first phase being completed with the construction of the new railway bridge by the German Railways in February 2024. This phase of the project marked an important milestone and ensured that the rail infrastructure meets current standards and accommodates the growing demands of rail traffic. The second part of the project, which covers the upgrade (widening) of the main road B25 was carried out by the State Construction Office of Augsburg during 2024. This

 © Deep Foundations Institute 2025

section of the project focuses on improving the road infrastructure and optimizing traffic flow to eliminate bottlenecks and increase road safety.

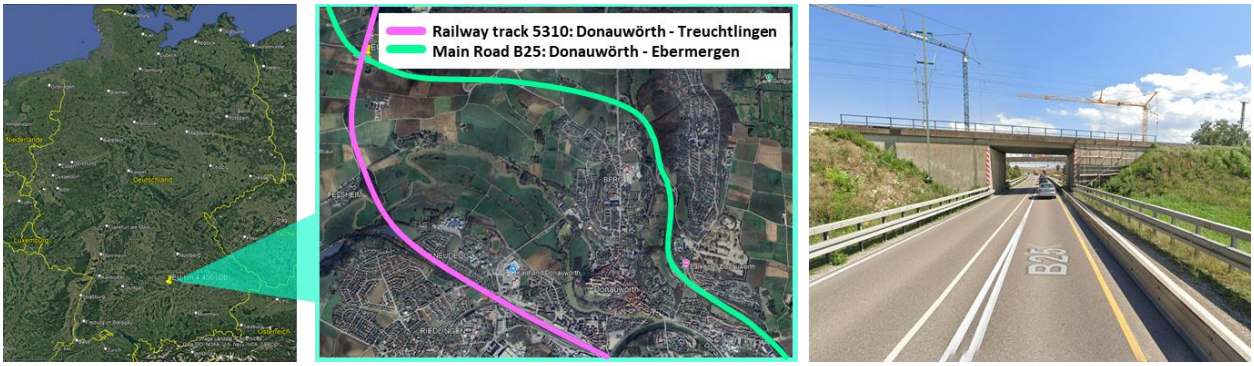


Fig. 1. Geographic location of the project (left), intersection of the railway track 5310 and the main road B25 (center) and view of the old railway overpass (right)

Both the railway tracks 5310 and the main road B25 are integral parts of the regional transport network, hence the main challenge of the design and construction approach for the intervention was to limit the disruption of the railway and road operations to the barest minimum. In this context, a constructive method was adopted, which involved building the new bridge structure next to the existing one (Fig. 2) and moving it to its final position using the lateral bridge slide (LBS) procedure, once the old bridge structure was demolished.



Fig. 2. Views of the new bridge structure, built next to the railway track 5310 (old overpass) (RBM, 2024)

During the construction of the new bridge (September 2023 – January 2024), the main road B25 was closed only twice: one week in August 2023 (installation of the steel girders and a safety scaffolding) and one week in November 2023 (installation of the formwork for the deck), while the railway track was fully operational.

After finishing the construction of the new bridge structure, the contractors had a track possession period of only 10 days (January 22 – February 1, 2024) to demolish the existing bridge, move the new bridge to the position of the old one, rebuild the track and reestablish the railway operations (Fig. 4). The main road B25 was also closed during the lateral bridge sliding process and for posterior widening works (earthworks and paving). It was reopened to traffic on February 9, 2024 (Fig. 3).



Fig. 3. Railway track 5310 (left) and main road B25 (right) open back to traffic (RBM, 2024)

SUBSOIL CONDITIONS

According to LfU-Bayern (2023), the subsoil conditions in the project area are characterized by the presence of a geological unit called **colorful breccia** (*bunte Breccie, miXb*), a mixture of sediments (mostly silts/clays and limestone, from small fragments to blocks) that was ejected from the *Ries meteorite crater*, an impact structure of 26 km diameter in southern Germany (Hörz et al, 1983).

The highly heterogeneous soils (silty/clayey matrix of the colorful breccia) are partially sensitive to water and frost, presenting variable mechanical properties (soft to stiff consistency). A shallow foundation placed directly on these soils usually results in differential settlements, hence special measures are often recommended. This layer extends up to depths between 4 m – 8m below ground level in the specific area of the project (LfU-Bayern, 2025). The colorful breccia is underlain by stiff to semi-solid silty clays of the geological unit called **upper freshwater molasses** (*obere Süßwassermolasse, OSMu,F*) - extending up to depths between 11.5 m – 15.5 m - followed by the dense to very dense silty fine sands of the geological unit called **upper marine molasses** (*obere Meeresmolasse, OMMo,S*), which extend to depths of at least 23 m below ground level (LfU-Bayern, 2025).

The subsoil profile at the project area is schematically presented in Fig. 4 and the geotechnical properties of the identified soil units are summarized in Table 2

Table 2. Geotechnical parameters of the soil units

Layer	Thickness (m)	ϕ' (°)	c' (kN/m^2)	c_u (kN/m^2)	γ / γ' (kN/m^3)	E_s (MN/m^2)
Colorful Breccia (miXb)	4.5 – 6.0	22.5 - 25	10 - 15	20 - 60	19 / 9	12 - 18
Upper freshwater molasses (OSMu,F)	2.0 – 8.0	25 – 27.5	5 - 15	100 - 150	20 / 10	20 – 40
Upper marine molasses (OMMo,S)	undefined	32 - 36	0 - 3	-	21 / 11	40 – 60

The use of shallow abutment foundations on the colorful Breccia (*miXb*) was discarded, due to the aforementioned risk of differential settlements. In this context, the preliminary assessment for the new bridge structure required the transfer of the loads from the abutments (axis 10 and 20, Fig. 5) to the more competent strata, preferably to the upper marine molasses (*OMMo,S*).

 © Deep Foundations Institute 2025

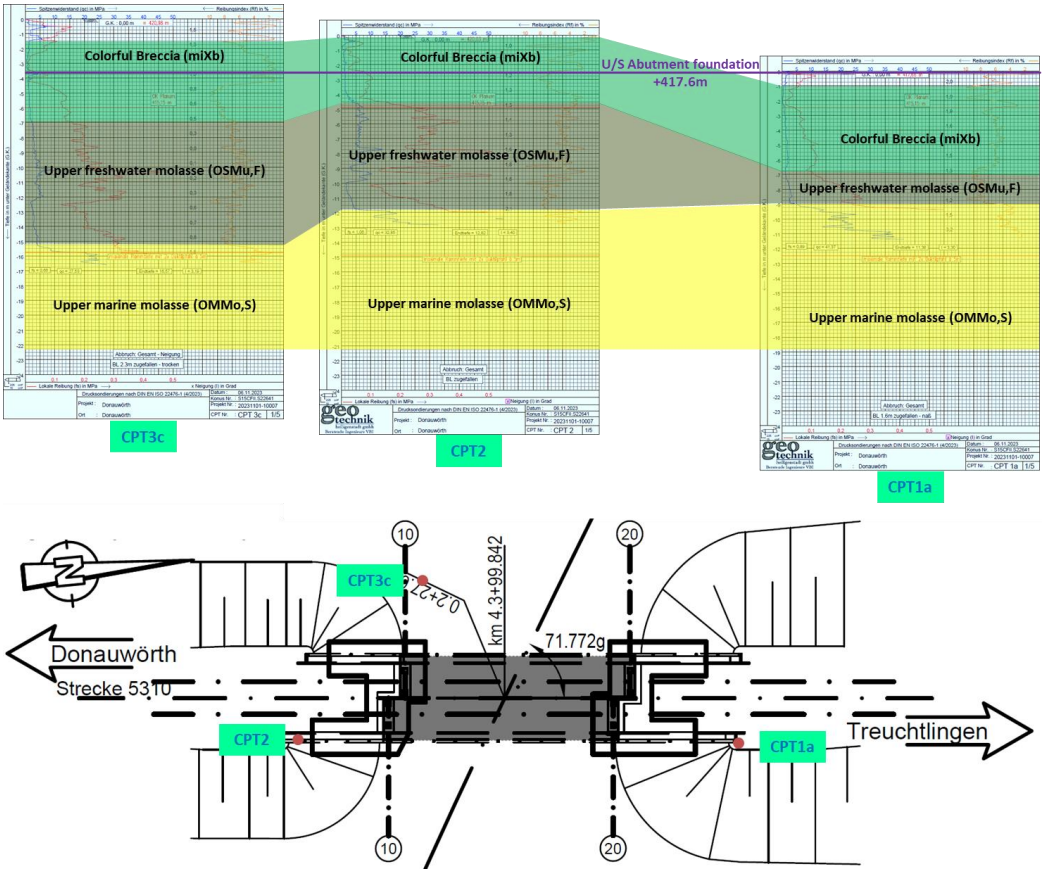


Fig. 4. Subsoil profile at the project area (modified after Max Bögl, 2023)

LATERAL BRIDGE SLIDING (LBS) PROCEDURE

The adopted lateral bridge sliding (LBS) procedure is an accelerated bridge construction (ABC) technique, in which the new bridge structure was constructed and then moved laterally into its final position (TRB, 2015). The new superstructure – with a self-weight of about 4,000 metric Tons - was built on temporary supports, equipped with tracks and rollers/slide bearings. Once the construction of the new bridge and the demolition of the old one were complete, the lateral slide was executed by moving the new structure on low-friction bearing pads or rollers using hydraulic jacks to push the structure (Fig. 5).

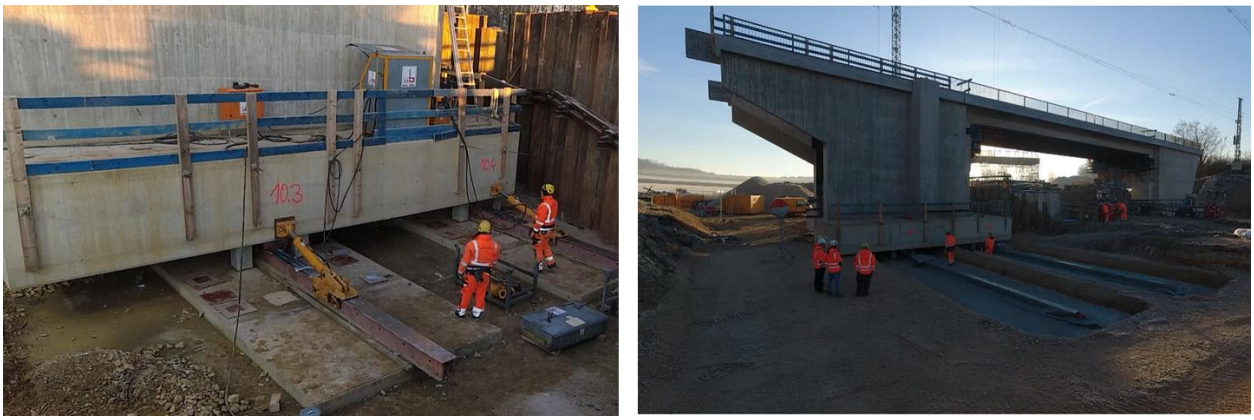


Fig. 5. Hydraulic jacks (left) and bearing pads with low-friction tracks (right) (RBM, 2024)

 © Deep Foundations Institute 2025

The lateral slide operation requires maintaining deviations from the overall alignment (longitudinal, transversal, and vertical) within tight tolerances, usually ≤ 7mm or ¼ inch (TRB, 2015). In the specific case of the project, special attention had to be paid to the coordination of the pushing works, since four simultaneously acting hydraulic jacks (two jacks/abutment, Fig. 5) were considered for the sliding process.

GROUND REINFORCEMENT

Due to the heterogeneous ground conditions present in the project area (Fig. 5), which could lead to differential settlements during the lateral slide operation, it was decided to carry out ground reinforcement with rigid inclusions (RI) to transfer the loads to the deeper layer of marine molasses (*OMMo,S*) and to reduce the settlements to 10 mm or less.

Rigid inclusion elements are defined as stiff, columnar, slender, vertical, discrete elements typically installed in regularly spaced groups. The term rigid inclusion applies to a variety of materials, but unreinforced, cementitious, cast-in-place elements are the most widely used (Smith et al, 2023).

Adopted solution

Due to the very tight time schedule (10 days of track possession), the rigid inclusions needed to be installed within 60 hours. Under these conditions, the most suitable, fast and cost-effective solution was provided by non-grouted ductile iron piles (DIPs), due to the flexibility, large adaptability and installation speed. In addition, the non-grouted piles can be fully loaded immediately after the pile driving works are completed.

DIPs are low vibration, driven, full-displacement piles, installed using a medium-sized excavator and a hydraulic breaker hammer with a modified shank that seats into the pile socket (bell) for driving, using the hammer's percussive energy. The hydraulic hammers typically range from 1,200 kg to 2,500 kg and operate at frequencies ranging from 250 to 500 blows per minute, delivering much higher frequency than traditional high-impact, low-frequency driven piling systems (Lopez and Steinlechner, 2023). DIPs are used to transfer loads from the superstructure into the lower soil layers and/or to limit deformations according to the principles of executing geotechnical works and have the flexibility to be installed to transfer the loads developing skin friction and/or end-bearing capacity (Lopez and Steinlechner, 2023).

For the project, end-bearing non-grouted ductile iron piles (DIP) were adopted and their execution is schematically presented in Fig. 6. After driving the piles, the inner core is filled with cement mortar/grout.

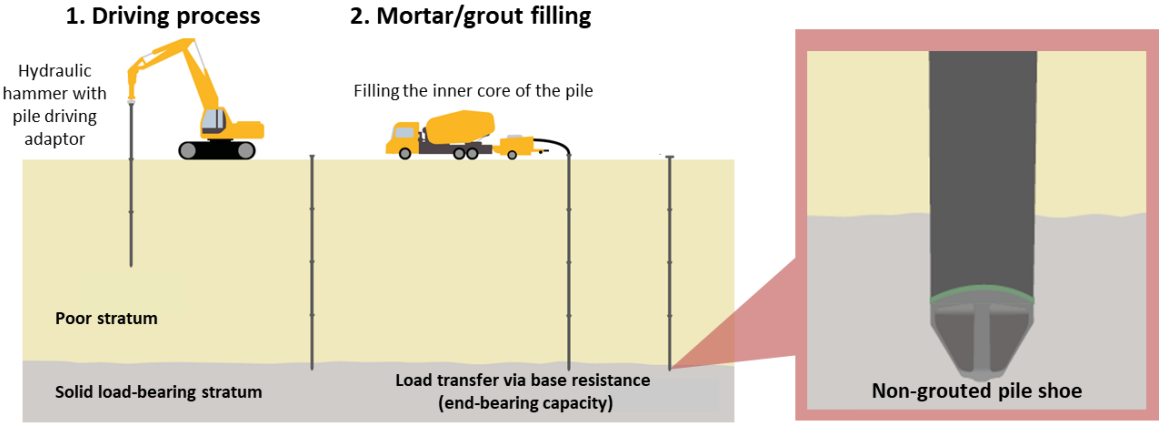


Fig. 6. Execution of end-bearing (non-grouted) ductile iron piles (after Lopez and Steinlechner, 2023)

 © Deep Foundations Institute 2025

Design considerations

Three constructions stages were considered for the design of the ground reinforcement:

- **Temporary: lateral sliding process** ➔ self-weight of the new bridge structure (reinforced concrete only: about 4,000 metric tons), distributed over four reinforced concrete thrust beds
- **Temporary: construction of the new overpass** ➔ self-weight of the new bridge structure, including the backfilling of the abutments as well as the new track (ballast, sleepers and rails) and the dynamic effects from compaction
- **Permanent: service life of the bridge (100 years)** (Holst and Holst, 2013) ➔ self-weight of the new bridge structure, including the backfilling of the abutments as well as the new track (ballast, sleepers and rails). Longitudinal vertical traffic loads for a design speed of 160 km/hour (load models LM 71 and HSLM A1-10). Longitudinal horizontal traffic loads (start-up and breaking loads) and transversal horizontal traffic loads (lateral impact)

The relevant longitudinal soil profiles (subsoil model) adopted for the design of the reinforcement are presented on Figs. 7 and 8. A granular load transfer platform (LTP) with a uniform thickness of 1.3m and reinforced with a geogrid was considered for the efficient load transfer onto the inclusions via arching effect. Steel plates (400mm x 400mm x 30mm) were used at the top of the pile to aid in the effective load transfer from the LTP to the pile. The rigid inclusions needed to reach the dense to very dense upper marine molasses (*OMMo,S*) in order to minimize the settlements, resulting in an average length of 10 m.

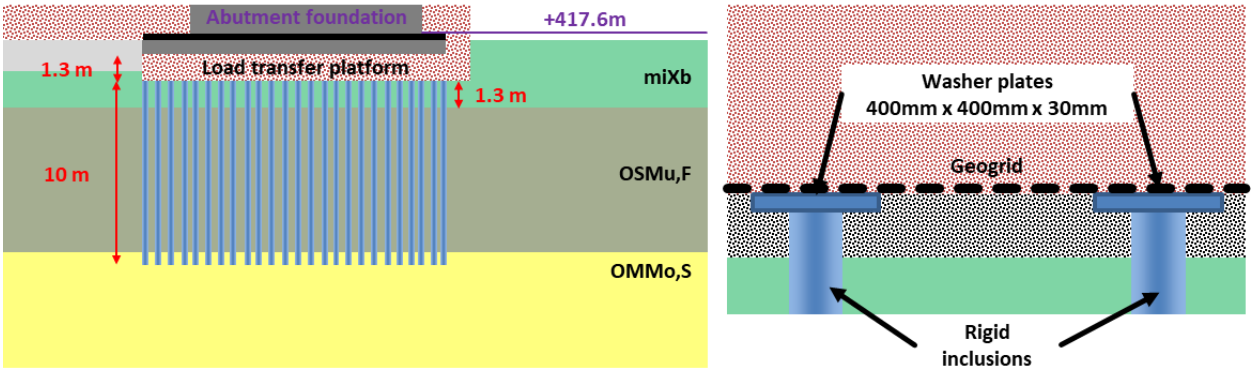


Fig. 7. Relevant subsoil model for the design of the ground reinforcement (Axis 10) and detail of the pile head

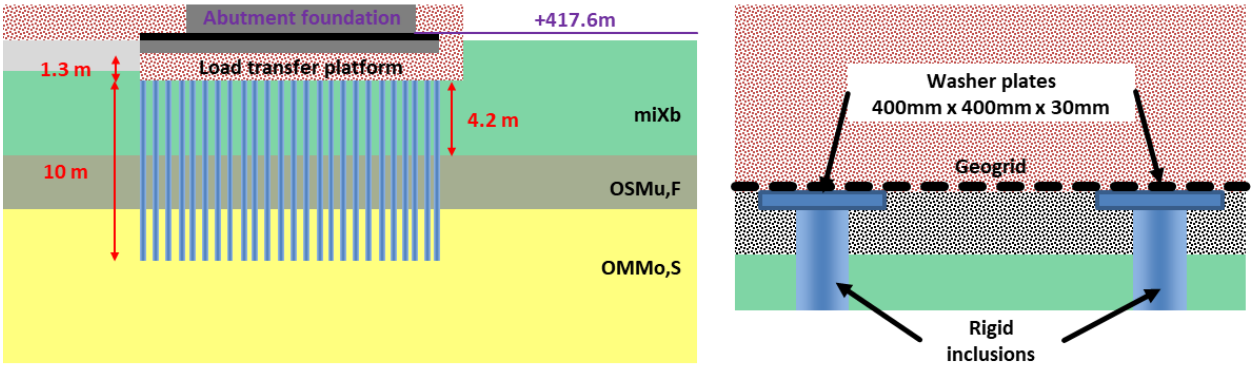


Fig. 8. Relevant subsoil models for the design of the ground reinforcement (Axis 20) and detail of the pile head

 © Deep Foundations Institute 2025

The abutments have an asymmetrical shape, leading to a variable distribution of the rigid inclusions along the temporary thrust beds. The thrust beds beneath the girder supports (bearing plates) have the largest concentration of elements (Figs. 9 and 10).

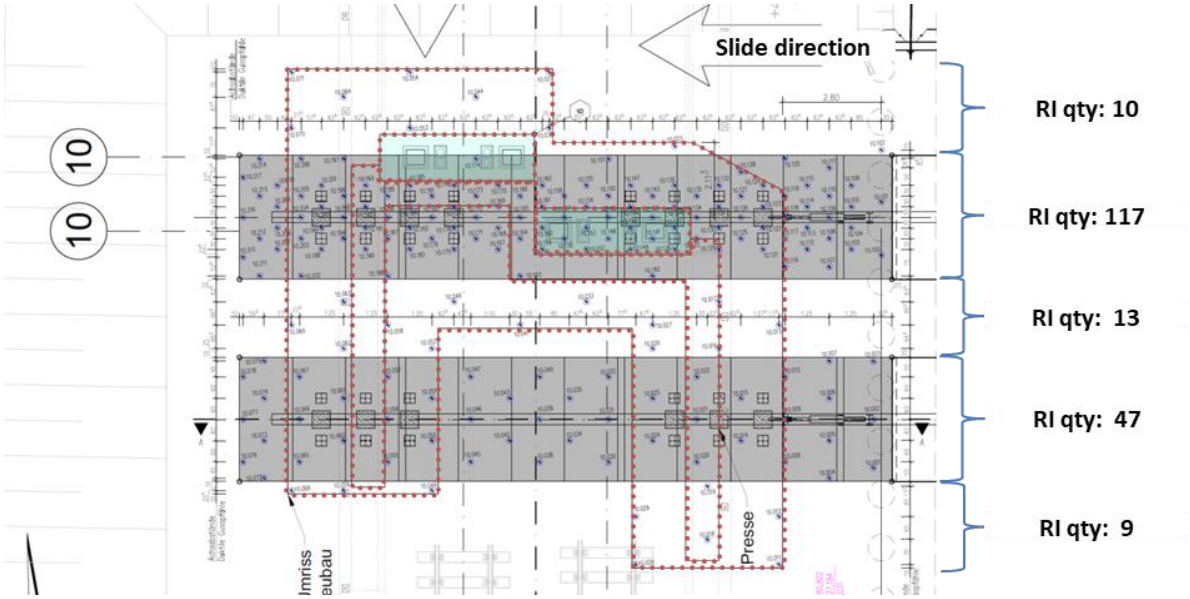


Fig. 9. Plan view with the distribution of RIs for the south abutment (modified after Max Bögl, 2023)

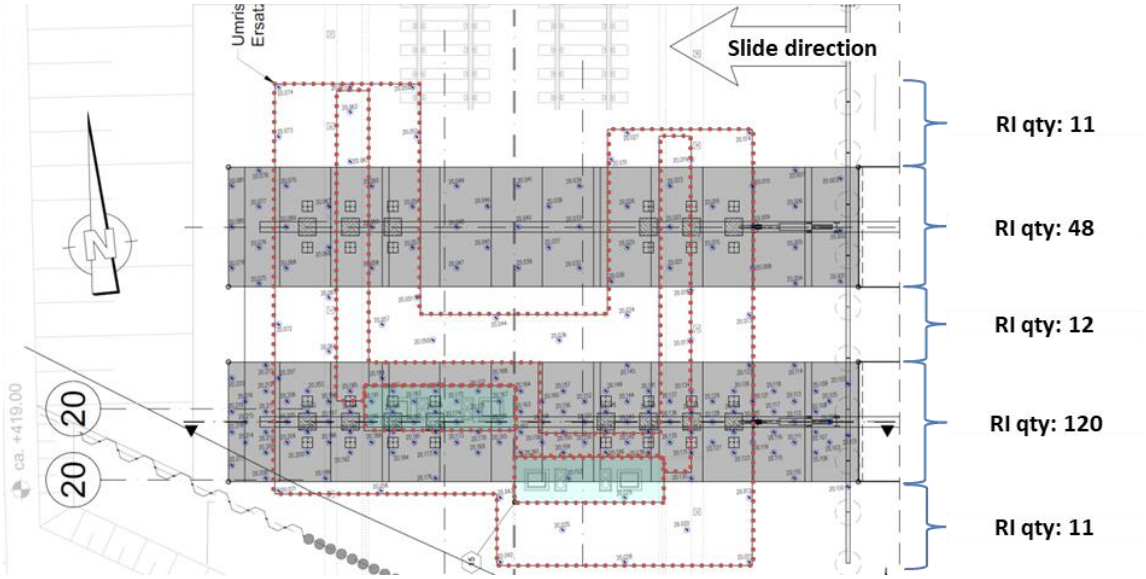


Fig. 10. Plan view with the distribution of RIs for the north abutment (modified after Max Bögl, 2023)

Typically, the ground improvement with rigid inclusions would be designed to allow for load sharing with the surrounding soil. However, following a conservative approach, it was adopted that the ductile iron piles (DIP) would receive 100% of the resulting loads acting on the abutments' foundations.

External load bearing capacity of the rigid inclusions

As previously mentioned, the piles needed to reach the dense to very dense sandy upper marine molasses (*OMMo,S*), where they were expected to develop the required geotechnical capacity to minimize the

 © Deep Foundations Institute 2025

settlements of the new bridge structure. Based on experience in the local subsoil conditions, it was expected that the load transfer would occur mainly in end-bearing. The mobilization of the end-bearing capacity of DIPs is usually reached when the pile head deflection is less than 30 mm during a continuous driving time of 60 seconds (TRM, 2022), provided that the hydraulic hammer is working at full performance.

Internal load bearing capacity of the rigid inclusions

After finishing the pile driving works, the internal core of the ductile iron pile pipe was filled with neat grout (resistance class C20/25). For the temporary cases, the internal load bearing capacity of the pile elements was conservatively defined only by the mechanical and geometrical properties of the ductile iron pipe itself (cross-section: with an effective diameter D_{eff} and an effective wall thickness t_{eff}), without considering the contribution of the grouted core (Fig. 11). For the permanent case, the composite cross-section including both the ductile iron pipe and the grout were considered, including the corrosion loss of the ductile iron pipe´s "outer skin" (r_o) (Fig. 11). The values for D_{eff} and t_{eff} correspond to the nominal values for the diameter and wall thickness (D and t), informed in DIBt (2022).

Under the existing subsoil conditions, the internal load bearing capacity of the DIPs is defined by their buckling resistance. Conservatively, the DIPs were analyzed as Euler-bars (Fig. 11), without lateral support (bedding). For the analysis, a critical length (L_{crit}), equal to the maximum observed thickness of the soft colorful Breccia (*miXb*) (Fig. 8) was adopted. The required reinforcement is presented in Table 3.

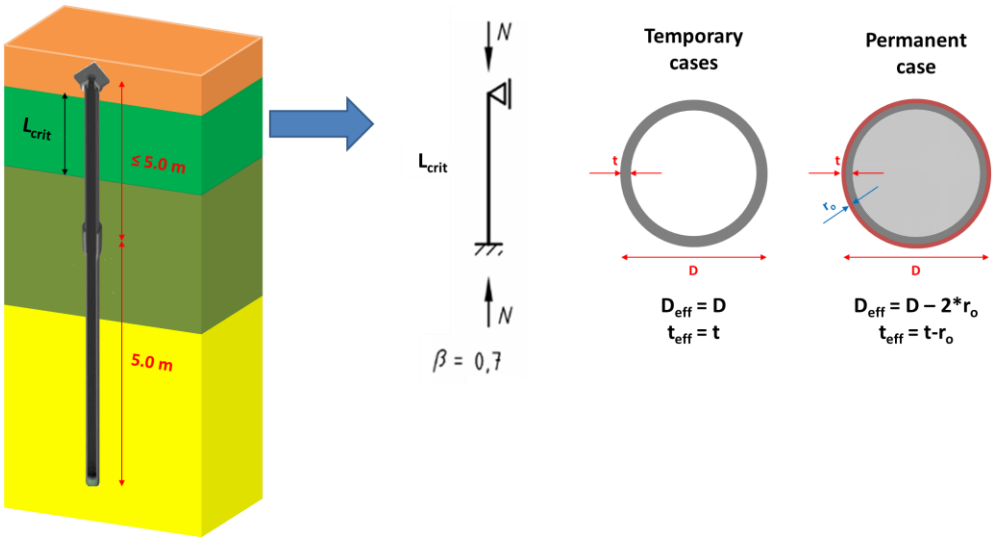


Fig. 11. Buckling and cross-section considerations for the temporary and permanent cases

Table 3. Internal load-bearing capacity of the rigid inclusions

Abutment	Pile type	Number of piles	Length (m)	L_{crit} (m)	Internal load bearing capacity (design) (kN)	
					Temporary cases	Permanent case [1)]
Axis 10	TRM 170 | 10.6	196	10	4.2	995	860
Axis 20	TRM 170 | 10.6	202	10	4.2	995	860

[1)] Considering a corrosion loss of r_o = 2 mm (outer skin) for a service life of 100 years

 © Deep Foundations Institute 2025

Execution

The contractors had a track possession period of only 10 days (January 22 – February 1, 2024) to demolish the existing bridge, move the new bridge to the position of the old one, rebuild the track and reestablish the railway operations. A total of 398 DIPs (total length of around 4,000 lineal meters) for the ground reinforcement were successfully installed by the German company Carl Heuchel GmbH & Co. KG on schedule from January 25 to 27, 2024 (60 hours). Fig. 12 shows some impressions from the pile driving works.

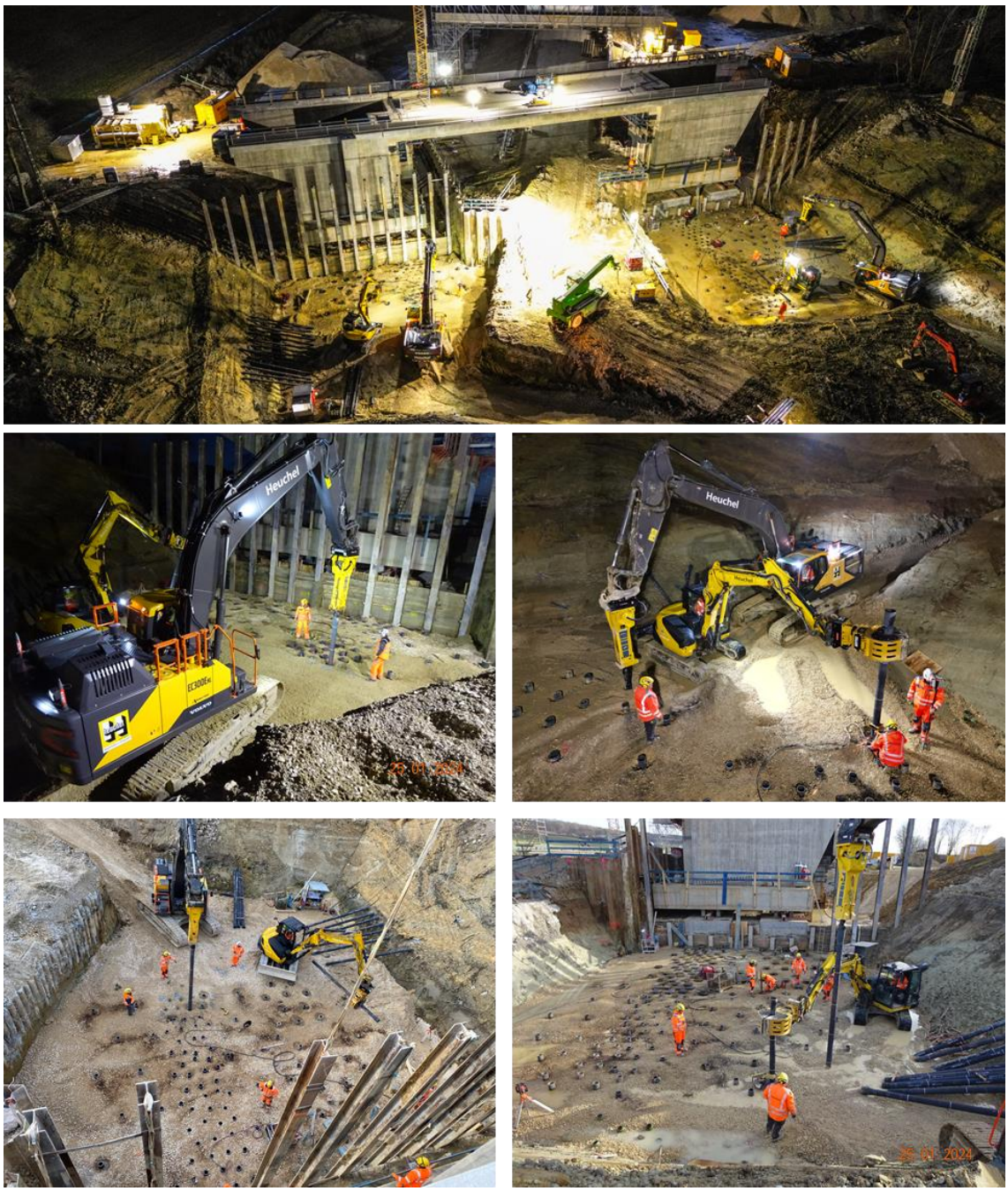


Fig. 12 Installation of the DIPs for the ground improvement (courtesy of Carl Heuchel GmbH & Co. KG)

 © Deep Foundations Institute 2025

After installing the last DIP and placing the head plates, the load transfer platform (LTP) was installed on January 27, followed by the construction of the temporary reinforced concrete thrust beds with the sliding rails. The lateral sliding procedure took place on January 28, lasting 3 hours. Once the new bridge structure reached its final position, the backfilling of the abutments and the construction of the new tracks commenced and were finished on January 31. With an estimated investment of 12,000,000 €, the new railway overpass over the main road B25 in Donauwörth (Bavaria) was reopened to traffic on February 1, 2024.

REFERENCES

Bayerisches Landesamt für Umwelt (LfU-Bayern), 2023. *Digitale Geologische Karte von Bayern 1:25000. Blatt 7230 Donauwörth*

Bayerisches Landesamt für Umwelt (LfU-Bayern), 2025. *Standortauskunft Baugrund und Bohrungen . 7230BG015682 und Bohrungen_7230BG015683 (Donauwörth).* *https://www.umweltatlas.bayern.de/mapapps/resources/apps/umweltatlas/index*. Accessed 04/02/2025.

Deutsches Institut für Bautechnik (DIBt), 2022. National Technical Approval / General Construction Technique Permit Z-34.25-230

Holst, R. and Holst, K.H., 2013. *Brücken aus Stahlbeton und Spannbeton. Entwurf, Konstruktion und Berechnung*. 6. Auflage. Ernst & Sohn.

Hörz, F., Ostertag, R. and Rainey, D. A., 1983. Bunte Breccia of the Ries: Continuous deposits of large impact craters. Reviews of Geophysics: 47(8), pp. 1667–1725. doi: 10.1029/RG021i008p01667.

Lopez, F. and Steinlechner, E., 2023. A new approach for the calculation of the external load-bearing capacity of ductile iron piles. Proceedings of the 18th Portuguese National Congress of Geotechnical Engineering (18CNG), Évora (Portugal), May 14-17 (unpubl.)

Lopez, F., Steinlechner, E. and Maier. G., 2023. The foundations of the Rhine bridge Fussach-Hard (Austria). Proceedings of the 48th Annual Conference on Deep Foundations, Seattle, Washington (USA), October 31 – November 11.

Max Bögl Bauservice GmbH & Co. KG, 2023. *EÜ km 4,406. Bodenverbesserung / Verdübelung mit duktilen Gussrammpfählen – Achsen 10 und 20. Ausführungsplanung* (Detailed design and execution drawings, German, unpubl.)

Ratisbona Media Documentation Services (RBM), 2024. *Neubau Eisenbahnüberführung (EÜ) Donauwörth, B25*. https://dokumentationsdienst.com/2024/02/11/neubau-eisenbahnueberfuehrung-eue-donauwoerth-b25/. Accessed 04/07/2025.

Smith, M., Bishop, J., Collin, J., Gallant, A., Hudson, M., Johnsen, L., Kniss, Kenneth, Pockoski, M., Swift, S., Warren, S., Wissmann, K., and Siegel, T., 2023. Part I: Selection and Design of Rigid Inclusions. DFI Journal 17 (2). DOI: 10.37308/DFIJnl.20230303.279

TRM Piling Systems (TRM), 2022. *Verfahrensanweisungen für den Duktilrammpfahl* (Method statement for the execution of .ductile iron piles, German, unpubl.)

Transportation Research Board of the National Academy of Sciences (TRB), 2015. SHRP 2 Renewal Project R04. ABC Standard concepts: the lateral slide addendum report.

 © Deep Foundations Institute 2025

LARGE DRILLED SHAFT FOUNDATIONS AND BI-DIRECTIONAL TEST PROGRAM FOR THE WEST SEATTLE LINK EXTENSION PROJECT

Dirk Bakker, Sound Transit, Seattle, WA, USA, 206-370-5661, dirk.bakker@soundtransit.org
Yang Jiang, HNTB Corporation, Seattle, WA, USA, 425-455-3555, yjiang@hntb.com

ABSTRACT

As part of the Final Environmental Phase, Sound Transit has completed the preliminary engineering for 2.8 miles of elevated guideway structures for the West Seattle Link Extension Project. Following an extensive bridge type study and evaluation, Sound Transit advanced the preliminary engineering for the guideways that consists of three structural systems: a cable-stayed bridge over the West Duwamish Waterway, segmentally constructed concrete box girders for long-span guideways, and prestressed girders for typical span guideways. The cable-stayed Duwamish Crossing will be the longest cable-stayed bridge carrying light rail in the United States and the first designed to withstand a 2,500-year return period seismic event in a high-risk seismic zone.

Given the complex geotechnical conditions—characterized by liquefiable soils and the depth of the glacial till layer as far down as 270 feet—the piers on the east and west shores of the Duwamish Waterway would experience significant lateral spreading forces in addition to inertial loads during seismic events. Consequently, the foundation systems were carefully selected and analyzed to optimize structural efficiency and cost-effectiveness. The adopted foundation systems at each of the long-span piers consist of multiple drilled shafts with a shaft cap. These foundations are designed to accommodate substantial vertical service loads and lateral seismic loads, making them well-suited for the heavy segmental box girder spans and the cable-stayed bridge. Other critical loading conditions, such as downdrag and the combined effects of seismic inertial and lateral spreading loads, were rigorously considered during the preliminary design phase.

To enhance design reliability, validate end bearing and side friction capacities, and refine installation methods, two full-scale bi-directional load tests are planned near the cable-stayed bridge foundation sites. These tests will be conducted prior to the start of final design of the foundation to ensure optimized design and constructability.

Keywords: foundation design, seismic design, lateral spreading, full scale load tests, bi-directional tests, O-cell tests, liquefaction, downdrag

INTRODUCTION

Sound Transit has completed the preliminary engineering for the West Seattle Link Extension (WSLE) Project as part of the Final Environmental Phase. This 4.7-mile extension will connect the SODO area of Seattle to the Alaska Junction neighborhood in West Seattle. The project includes 2.8 miles of elevated guideway, with the remainder being at-grade or in a tunnel.

Due to the challenging geotechnical conditions—such as liquefiable soils and glacial till reaching depths of up to 270 feet—the piers on both the east and west shores of the Duwamish Waterway must withstand significant lateral spreading forces and inertial loads during seismic events. As a result, the foundation systems were carefully selected and analyzed to maximize both structural efficiency and cost-effectiveness. The chosen foundation solution for the typical spans that are less than 200 feet is the single drilled shaft with ground improvement for single column piers, but for the long-span piers, the foundations are consisted of multiple drilled shafts capped with a shaft cap. The multiple drilled shaft foundations are designed to support substantial vertical service loads and lateral seismic forces, making

 © Deep Foundations Institute 2025

them ideal for the heavy segmental box girder spans and cable-stayed bridge. Other critical load factors, such as downdrag and the combined effects of seismic inertial and lateral spreading forces, were thoroughly considered during the preliminary design phase.

Two full-scale bi-directional load tests are planned near the cable-stayed bridge foundations to improve design reliability, confirm end bearing and side friction capacities, and refine installation methods. These tests will be conducted before finalizing the foundation design to ensure optimal design and constructability.

ALIGNMENT AND BRIDGE TYPES

The overall WSLE project alignment is shown in Fig. 1. Figs. 2 through 4 show the bridge types and layouts that are used along different segments of the alignment.

Alignment

The WSLE (Fig. 1) would begin south of South Holgate Street and include a new SODO Station that would allow for transfers with the existing SODO Station on the existing Link light rail line [1]. The WSLE would travel south from the SODO Station across South Lander Street at-grade and continue south from South Lander Street towards South Spokane Street on an elevated guideway. In the vicinity of South Spokane Street, it would turn west on an elevated guideway on the south side of the West Seattle Bridge, where it would cross the Duwamish Waterway on a light-rail only, high-level fixed bridge structure. On the west side of the Duwamish Waterway, the guideway would remain mostly elevated to the west side of the Delridge valley. In the West Seattle Junction area, the guideway could be elevated or below ground. Three stations would be constructed in West Seattle: Delridge, Avalon, and Alaska Junction. The Delridge Station would be elevated, and the Avalon and Alaska Junction stations could be elevated or below ground.



Fig. 1. West Seattle Link Extension Alignment

 © Deep Foundations Institute 2025

The height of the guideway will range from a retained cut to approximately 170 feet above ground, with its peak height reached when crossing the West Duwamish Waterway, matching the elevation of the West Seattle High Bridge (WSHB). West of the Duwamish Waterway, the alignment will cross the northern edge of Pigeon Point, transitioning between elevated guideway and retained-cut and fill sections, before turning southwest onto an elevated guideway that follows Delridge Way Southwest.

Bridge Type and Foundation Types

Following an extensive bridge type study and evaluation, Sound Transit advanced the preliminary engineering for the WSLE guideways that consists of three structural systems: prestressed girders for typical span guideways, segmentally constructed concrete box girders for long-span guideways, and a cable-stayed bridge over the West Duwamish Waterway. Figure 2 shows a sample stretch of the typical span aerial guideways, which are the spans with a precast, prestressed girder superstructure or cast-in-place (CIP) girders with span lengths less than 150 feet. This encompasses the superstructure and substructure of the elevated guideways in the SODO area.

The foundations will be single drilled shaft with ground improvement supporting single column piers due to the reduced strength associated with excess pore pressure in liquefiable soils. The ground improvement will mitigate against liquefaction and increase the lateral resistance and reduce column deflections of the guideway. The ground improvements considered include deep soil mixing, jet grouting, and vibro-compaction/stone columns. Depending on the methods, which are corresponding varying replacement ratios, the ground improvements range from 70 to 80 feet in diameter and 35 to 50 feet in depth. Drill shafts are expected to be installed after the ground improvement is completed. The improved soil properties are used in the design of the drilled shafts.

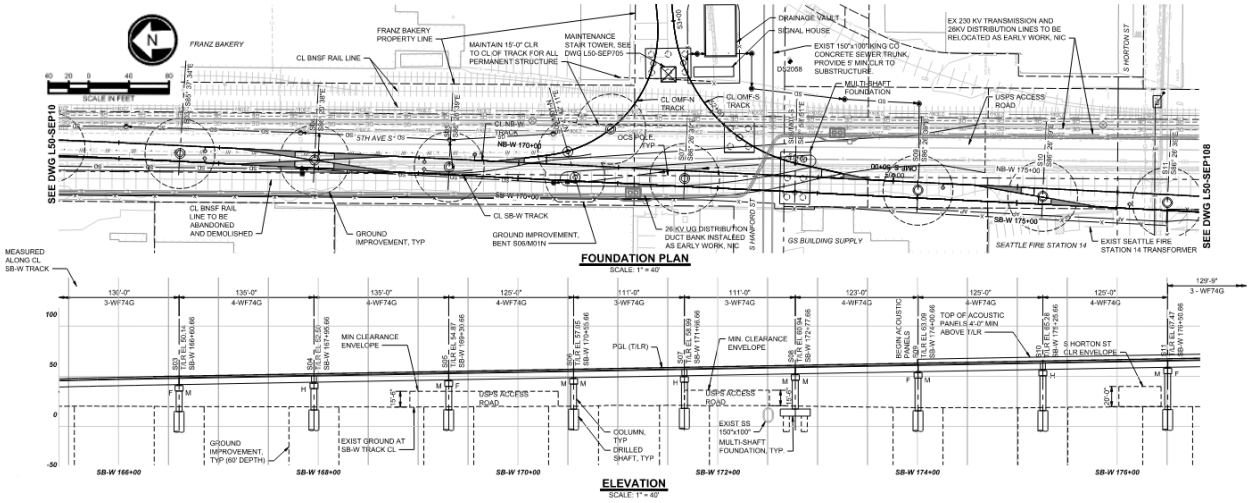


Fig. 2. Partial Typical Gateway and Foundation Layout

The long-span elevated guideway begins north of the West Seattle Bridge/Spokane Street viaduct, then continues to the west on the south side of the West Seattle Bridge, with several long-span structure units due to the various constraints. Figure 3 shows the bridge and foundation layout near the east Duwamish Waterway. The long-span guideway units are concrete segmental box structures, which are assumed to be constructed using the cast-in-place (CIP) balanced cantilever method. Short portions of each end span are expected to be cast on falsework. Cantilever piers utilize twin leaf columns integrally connected to the superstructure for stability during construction. High load multi-rotational disc bearings are proposed at

the abutment and expansion piers between units due to the expected structure movements and loading. The foundations will be mostly four 10-ft drilled shafts with shaft caps supporting single double-leaf or single mast piers.

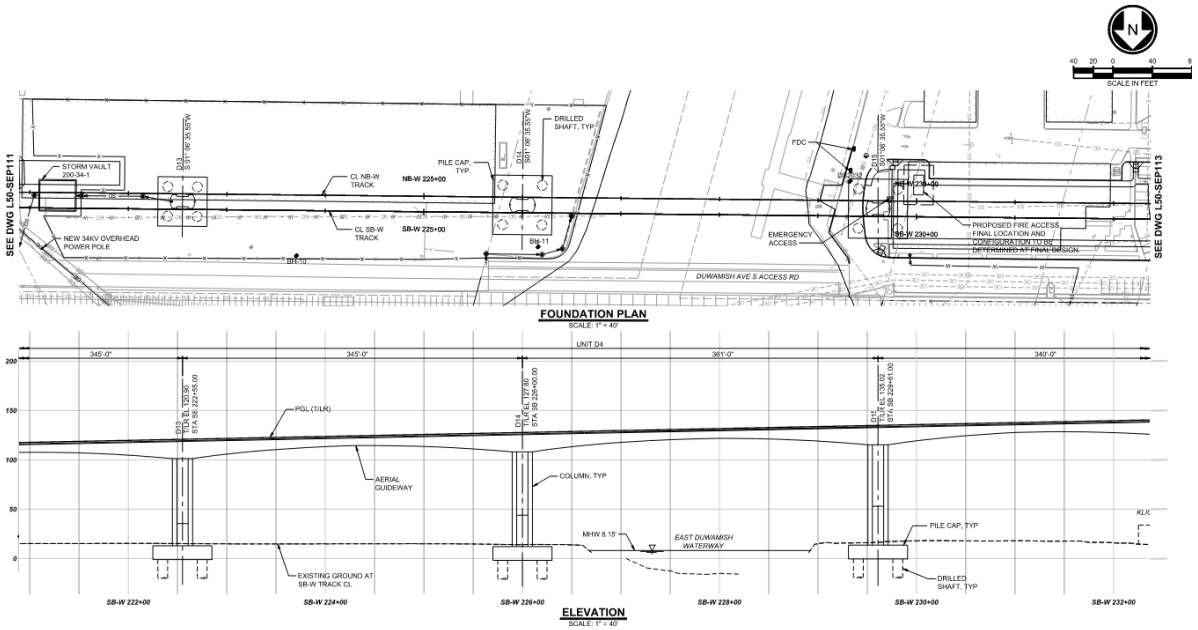


Fig. 3. Partial Long-Span Guideway and Foundation Layout

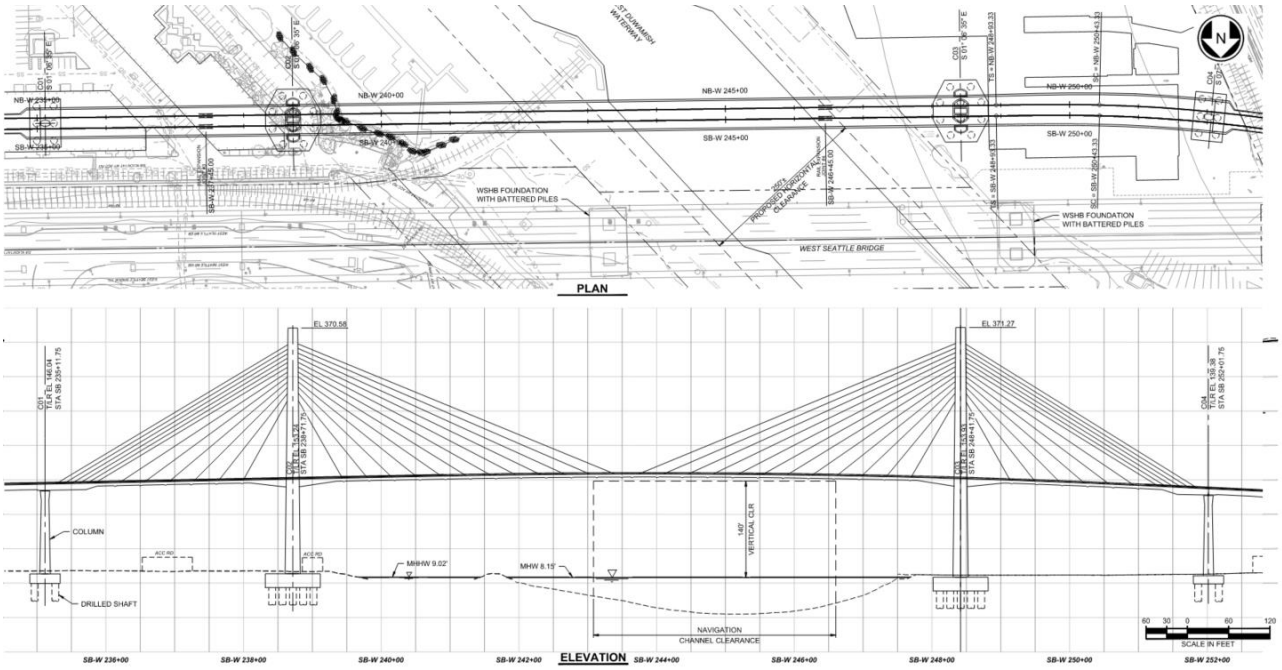


Fig. 4. Duwamish Crossing Structure and Foundation Layout

Figure 4 shows the Duwamish Crossing, which will be a cable-stayed bridge that has a span arrangement of 360’-970’-360’. The main pylons were designed as a diamond shape, made with reinforced concrete. The bridge deck has been designed as an open deck system with two concrete edge girders and concrete deck slab and floor beams in between with two slanted cable planes. The one exception to the open deck

 © Deep Foundations Institute 2025

is at pier tables where the project architect prefers a closed deck through the addition of a concrete soffit slab. The foundations will be four 10-ft drilled shafts with shaft caps at the end piers and nine 10-ft drilled shafts with shaft caps at the main piers in accordance with preliminary engineering.

The typical and long-span guideway section is 27’-11” wide, and the typical section for the cable-stayed varies from 45’-0” to 48’-7”, to accommodates two tracks with emergency walkway and OCS poles located between the tracks.

SUBSURFACE CONDITIONS

Figure 5 illustrates the geotechnical profile for a portion of the alignment near the west Duwamish Waterway. The alignment passes through the former tide flat at the mouth of the Duwamish Waterway, most of it is situated on fill deposits. The fill, which can reach a thickness of up to 25 feet, primarily consists of sand to gravelly sand, with varying amounts of silt, along with layers of cohesive silt and clay. Beneath the fill, the underlying soils are composed of recent granular deposits as well as recent clay and silt layers, which are often interbedded. The granular soils typically consist of clean to silty, fine to medium sand, with multiple seams and layers of cohesive to non-cohesive fine sandy silt. These granular soils are usually medium dense, but their density can range from loose to dense.

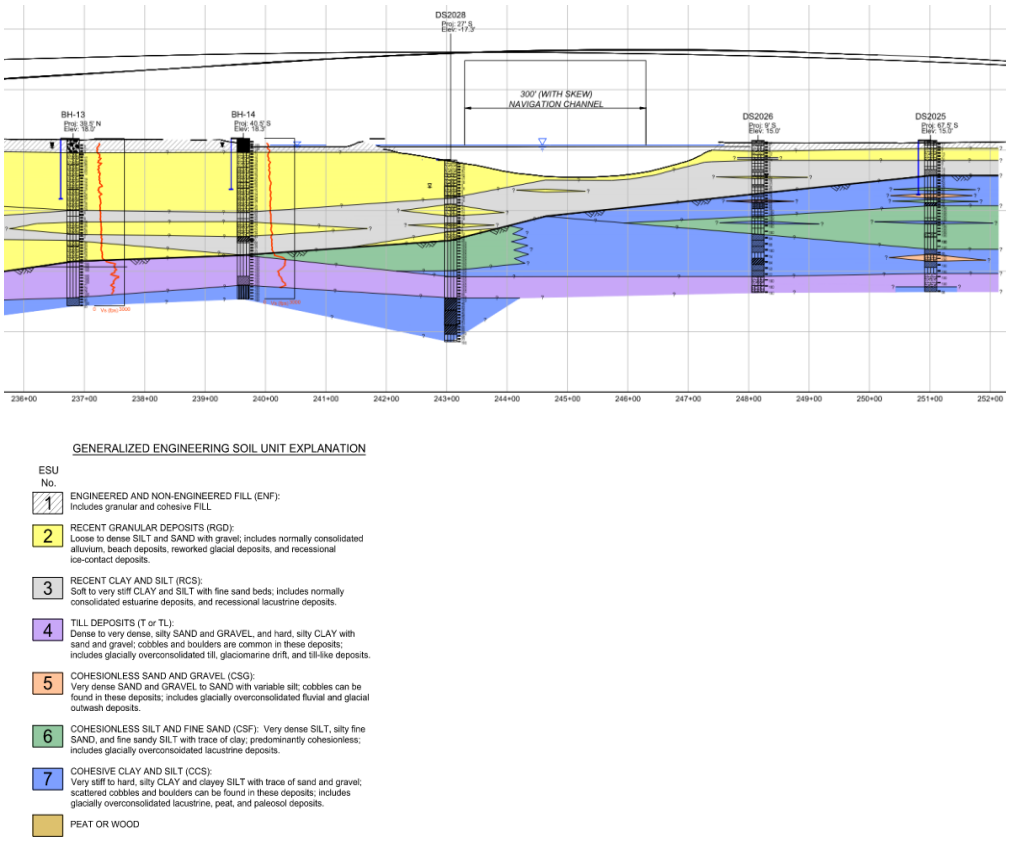


Fig. 5. Partial Geotechnical Profile

The recent clay and silt deposits are finer-grained compared to the recent granular deposits. They consist of very loose to loose or very soft to soft fine sandy silt to slightly sandy, clayey silt, with abundant shell fragments and fine organic materials. These soils generally exhibit some cohesion but are typically of low or very low plasticity. The recent clay and silt soils often appear as seams or layers, usually less than 5 to

 © Deep Foundations Institute 2025

10 feet thick, within the sandier granular deposits. However, a thicker, more cohesive layer of recent clay and silt soils is commonly found just above the glacially overridden soils, typically at depths of about 100 to 160 feet. These deeper clay and silt deposits are very soft to very stiff, clayey silt to silty clay, and may reach thicknesses of up to 50 feet. The glacially overridden soils mainly consist of hard clay and silt, with varying amounts of sand and gravel, and are present beneath most of the alignment. The depth to the top of the glacially overridden soils varies, ranging from about 17 feet at the west end of the Duwamish Crossing to approximately 270 feet at the east end of the crossing.

SEISMIC HAZARDS

The WSLE is in an area with a history of numerous small to moderate earthquakes, along with occasional strong earthquakes. Most of this seismic activity is driven by the ongoing movement and collision of the tectonic plates beneath North America and the Pacific Ocean. These tectonic plates include the Juan de Fuca Plate and the North American Plate, with their intersection known as the Cascadia Subduction Zone (CSZ). As the plates collide, the Juan de Fuca Plate is being subducted beneath the North American Plate to the northeast. Geologic evidence from the 1990s suggests that geophysical lineaments in western Washington can produce earthquakes with magnitudes up to 7.5. The project adopted 2018 USGS NSHMP as base for the site-specific ground response, which considered near fault effect and basin amplifications as requited by Sound Transit Design Requirements Manual [2].

GEOTECHNICAL SITE INVESTIGATION, ANALYSIS, AND DESIGN

An extensive field exploration program was carried out for the project, consisted of drilling the soil borings, collecting soil and water samples, and performing field and laboratory testing. Drilling and sampling were performed by mud rotary and sonic drilling methods. For mud-rotary borings, truck-mounted drill rigs were equipped with automatic hammers. Standard penetration tests (SPTs) and split-barrel sample collection were conducted as appropriate for ground conditions encountered, generally at 5-foot intervals. Shelby tube samples were collected at select representative locations when cohesive soil layers were encountered. Sonic borings were advanced by truck-mounted drill rigs using vibratory motion, down pressure, and rotation to obtain nearly continuous soil core samples extruded into flexible plastic sleeves. Downhole suspension logging was performed in selected borings to estimate the shear and compression wave velocity over the depth of the boring for use in determining seismic site class and site response analysis.

CHOICE OF FOUNDATIONS

The selection of foundation types for the elevated guideways is influenced by the presence of soft, compressible sediments extending 17 to 270 feet deep, the potential for significant seismic-induced settlements along the alignment, and the proximity of critical infrastructure. Given these factors, deep foundations were recommended to support the bridge structures, with drilled shafts identified as the preferred foundation type. These shafts may be founded in glacially overridden deposits. Although driven piles could be considered, their installation may generate vibrations and induce settlement that could adversely affect nearby infrastructure.

Each pier for the long-span elevated guideway and the cable-stayed Duwamish Crossing will be supported by a group of 10-ft in diameter drilled shafts, with the number of shafts varying per pier. The drilled shaft foundations are designed according to AASHTO BDS [3] and WSDOT GDM [5] using the LRFD method. The foundations are proportioned so that the factored axial resistance of the soil meets or exceeds the factored axial load applied for the Service, Strength, and Extreme Event Limit States. The foundations were also designed to resist lateral loads from for Strength and Extreme Event Limit States.

Axial Resistance

Drilled shaft axial resistances were determined based on subsurface conditions encountered in the borings nearest to each pier. These assessments considered the relative densities and consistencies of the subsoils, as indicated by SPT N-values, laboratory test results, and experience with similar soil and project conditions. Factored axial resistances were estimated for the service, strength, and extreme event limit states. For the extreme event limit, the estimated liquefaction thickness was derived from nonlinear effective stress site response analyses.

To mitigate risks associated with installing large-diameter deep foundations, the design considered both cased and uncased drilled shafts. Permanent casing may be required in certain conditions. In accordance with AASHTO BDS Section 10.8.1.2 [3], group effects were considered when the center-to-center spacing of drilled shafts was less than three diameters. These group effects reduce the effective stresses on both the shaft sides and base, resulting in lower axial capacity for shaft groups compared to individual shafts. Recommended reduction factors for group effects are provided in WSDOT Bridge Design Manual Table 7.8.1-1 [6]. According to the WSDOT GDM [5], resistance factors must be applied to nominal axial resistance to determine the factored resistance. The resistance factors for side and base resistance are based on the analytical methods used to develop factored axial resistance plots. For drilled shafts at the Duwamish Crossing, the resistance factors have not yet been increased to account for the AASHTO code-allowed resistance factor increase, as the bi-directional load test at the main river bridge is still pending.

In accordance with AASHTO BDS Section 10.8.1.2 [3], group effects were considered when the drilled shafts center to center spacing is less than three diameters. Group effects will reduce the effective stresses against both the side and base of the existing shaft, thus leading to lower resistances of axial capacity for groups than for individual shafts. The project used the recommended reduction factors for group effects as presented in the WSDOT Bridge Design Manual Table 7.8.1-1 [3].

Lateral Resistance

Lateral loads on the structure are resisted by the lateral soil resistance of the drilled shafts. Analyses of laterally loaded shafts were conducted using LPILE [7] and/or GROUP [8]. The recommended input parameters for lateral resistance analysis incorporate post-seismic adjustments for potentially liquefiable layers, accounting for excess pore pressures generated during nonlinear effective stress site response analyses. These parameters were developed for both the Operational Design Earthquake (ODE) and Maximum Design Earthquake (MDE) ground motions. Where applicable, p-multipliers were used to account for group effects based on specific shaft configurations. The p-multipliers were computed using AASHTO (2017) and Reese and Van Impe [9] assuming shafts constructed in a group configuration provided by structural engineers.

Drag Load Considerations and Settlement

The neutral plane method [10] was used to evaluate liquefaction-induced settlement and associated drag loads on the deep foundations. This method concurrently analyzes three key design considerations:
The axial resistance of the drilled shaft (geotechnical strength limit),

- The structural resistance of the drilled shaft (structural strength limit), and
- The settlement of the drilled shaft (geotechnical and structural service limit).

Drag load is considered alongside dead load in evaluating the structural limit state of the drilled shaft. It serves as a settlement consideration in the geotechnical service limit state and as a structural consideration in the drilled shaft structural limit state. Drag loads do not develop during porewater pressure buildup but

 © Deep Foundations Institute 2025

instead occur after porewater pressure dissipates following an earthquake, consistent with FHWA NHI-16-009 [11]. Since drag loads do not affect geotechnical strength, they were not treated as additional loads requiring support from the drilled shaft. In the neutral plane analyses, embedment depth was determined based on anticipated design loads and a two-shaft diameter embedment into glacial soil was assumed.

Liquefaction and Lateral Spreading

A 2D nonlinear effective stress site response analysis was performed for the Duwamish Crossing segment. The nonlinear effective stress analyses site response models consider pore pressure development and provide estimates of soil strength reduction in soils susceptible to liquefaction during seismic loading based on the PM4SAND constitutive model. The PM4SAND constitutive model is a stress-ratio controlled, critical state compatible, bounding surface plasticity model for sand and other purely non-plastic granular soils that has been implemented for use with the FLAC. The sample results for D11 foundation in the longitudinal direction with earthquake records considered are shown in Fig. 6.

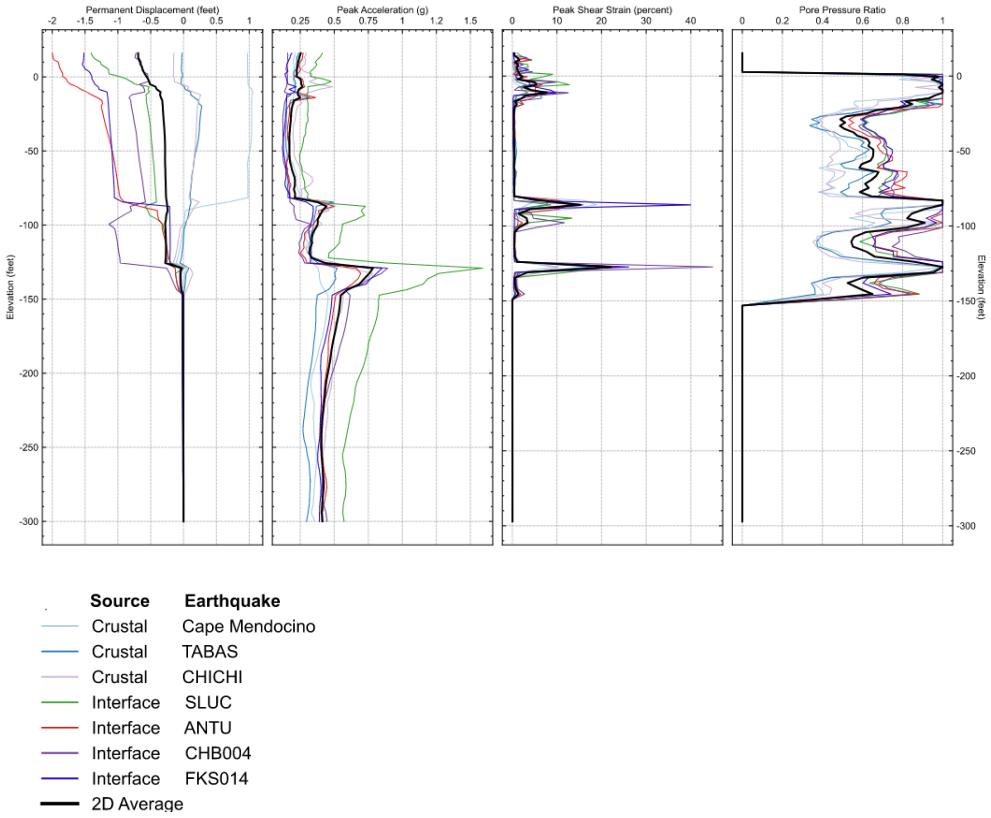


Fig. 6. Sample Longitudinal Effective Stress Analysis Results for MDE

Along with the existing ground slope and soil conditions, lateral spreading toward the east and west Duwamish Crossing channels may occur during the MDE design ground motion. The analysis provided estimates of permanent ground displacement and an alternative estimate of lateral spreading impact using a force-based approach. While the force-based method is not tied to a specific ground motion return period, it is suitable for preliminary design. A displacement-based method may be considered in subsequent design phases.

For preliminary design, the force-based method outlined in WSDOT GDM [5] was used to estimate lateral spreading-induced loads on foundations for piers adjacent to the east and west Duwamish Waterways. The

model includes a non-liquefiable crust overlying a liquefiable layer. In evaluating lateral spreading forces, soil layers contributing to lateral displacement below the non-liquefiable crust were assumed to extend to a maximum depth of 80 feet during the MDE design ground motion. A sample lateral spreading loading diagram is shown in Fig. 7.

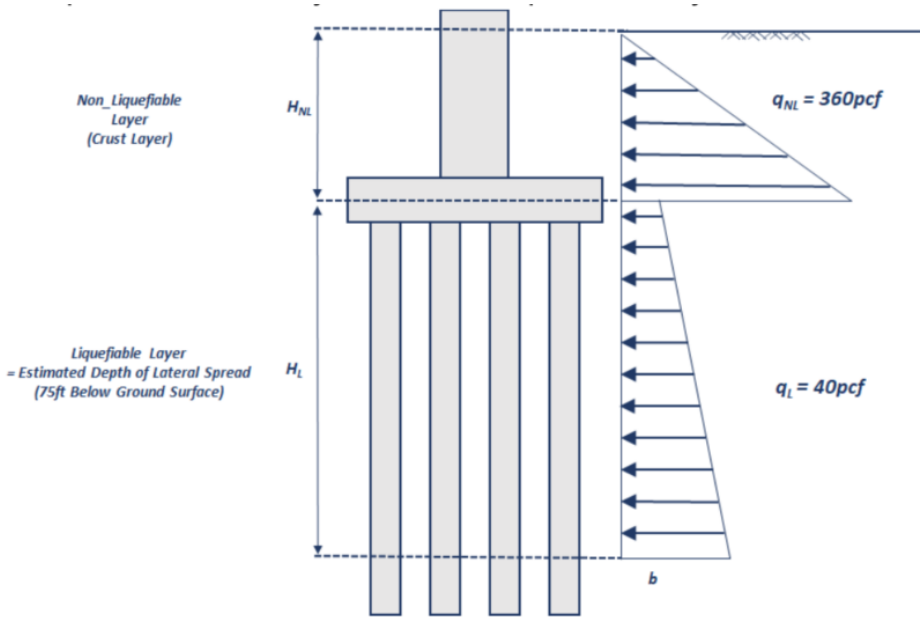


Fig. 7. Lateral Spread Load Application

FUTURE DESIGN ENHANCEMENT

In accordance with WSDOT GDM [5], the preliminary foundation design assumes the combination of inertial and lateral spreading loads. This approach is used because more than 20% of the hazard contributing to peak ground acceleration at the project sites originates from earthquakes with a magnitude of 7.5 or greater. While it is generally recognized that seismic acceleration and the onset of liquefaction may not occur simultaneously, there is no consensus on how to address this timing difference. This topic is the focus of a recent FHWA-funded research project. Findings from this research, along with advanced methods such as nonlinear effective stress analysis—which accounts for pore-water pressure buildup and soil stiffness/strength degradation in liquefiable layers—may be incorporated in later design phases to achieve a more economical solution.

Sound Transit Requirements Manual [2] permits in-ground plastic hinging under the special MDE load case that includes liquefaction-induced lateral spreading. However, the preliminary design has assumed no in-ground plastic hinging due to incomplete geotechnical exploration data and the necessary conservatism at this stage. In subsequent design phases, in-ground plastic hinging may be considered, if displacement ductility demands do not exceed 4. Additionally, strain limits for confined concrete and reinforcing steel must comply with the requirements outlined in AASHTO Articles 8.4.2 and 8.4.4 [3]. The lengths of in-ground plastic hinges must be determined in accordance with AASHTO SGS Article 4.11.6 [4] and specified on a project-specific basis, considering the site's soil properties and stratigraphy.

BI-DIRECTIONAL TESTS

Two bi-directional load tests are planned for the project, with one test near each of the main pylons of the cable-stayed bridge foundations. The load test program is designed to represent the sizes, depths, and

 © Deep Foundations Institute 2025

geologic conditions of the drilled shaft foundations for the Duwamish Crossing. The testing will be performed on designated, sacrificial test shafts that will not be incorporated into the final foundation footprint. This approach allows for full mobilization of soil resistance without concerns about long-term shaft performance.

As shown in Fig. 8, the test shaft will be located at least 20 feet away from the edge of the pylon foundations based on the preliminary design. The use of designated, sacrificial test shafts enables maximum mobilization of soil resistance without concern for long term shaft performance. Test shaft dimensions and bi-directional loads were selected to mobilize nominal soil resistance. The proposed test shaft lengths are 225 feet at Site 2 and 125 feet at Site 3 (Fig. 7).

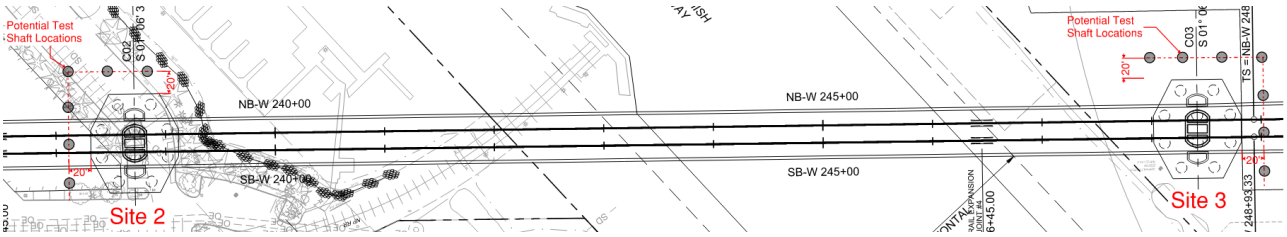


Fig. 8. Potential Test Shaft Locations

The tests will assess the nominal side resistance of surrounding soil layers and the nominal base resistance at the bottom of each test shaft. The resistance parameters obtained from these tests will be used to validate and, if appropriate, refine the design parameters. Successful completion of the load test program may allow for increased resistance factors in accordance with AASHTO LRFD Bridge Design Specifications. AASHTO permits a resistance factor of 0.7 when supported by load testing, which could potentially reduce the number of shafts or the shafts' dimensions.

In addition to refining design parameters, the tests will provide valuable insights into constructability, including excavation techniques, clean-out methods, concrete placement, and the potential use of permanent casing.

Subsurface Conditions

As previously discussed, the overall subsurface conditions have been characterized. At test Sites 2 and 3, subsurface conditions consist of varying thicknesses of fill, alluvial sand and silt, and estuarine silt and clay deposits, all of which overlie very dense and hard glacially overridden materials.

At Site 2, the fill layer is approximately 20 feet thick, underlain by medium-dense to dense alluvial silty sands and loose to medium-dense estuarine sandy silts, extending to a depth of about 200 feet. Beneath this, hard glacially overridden glaciomarine silt and glacial till deposits are present. The test shaft at Site 2 will be founded in the glacial soil.

At Site 3, the fill layer is also about 20 feet thick, followed by approximately 15 feet of loose alluvial sand. Below this, loose to medium-dense lacustrine silt extends to a depth of 90 feet. The deeper strata consist of hard glacially overridden glaciolacustrine silty sand, glaciomarine lean clay, and non-fluvial lacustrine silts. The test shaft at Site 3 will be founded in the non-fluvial lacustrine silt.

Drilled Shaft Construction

Based on subsurface conditions encountered during explorations, a review of planned shaft dimensions, and contractor input, drilled shafts will be installed using a temporary casing and the wet construction

 © Deep Foundations Institute 2025

method. The temporary casing is expected to be advanced using an oscillator, with soil excavation performed using a spherical grab and digging crane. The casing is intended to be extracted following shaft installation. If the contractor identifies casing extraction as a potential risk, the temporary casing may be left in place up to the top of the glacially overridden soil.

Prior to reinforcement cage and concrete placement, the shaft base will be cleaned. A downhole camera inspection will be conducted to confirm proper cleanout. Concrete will be placed using a tremie pipe. Upward movement of each test shaft will be measured using a pair of digital survey levels in accordance with ASTM D1143. Shaft compression, from the top of the shaft to the top plate of the load cell assembly, will be measured using two pairs (four total) of diametrically opposed telltales.

Bi-Directional Load Cell Assembly

The bi-directional load cell assembly will be installed as an integral part of the shaft's steel reinforcing cage. Its placement and configuration are designed to achieve force balance above and below the cells, ensuring mobilization of resistance. The bi-directional jack capacity will be selected to fully engage the nominal side and base resistance of the test shaft. It was recommended that the load cell assembly include a minimum of three bi-directional jacks installed between two steel bearing plates. The final number and configuration of jacks will be determined by the load testing subcontractor to ensure even load distribution and uniform jack expansion. The steel bearing plates have a minimum thickness of 2 inches and be sufficiently thick to distribute loads into the concrete without bending.

Test Shaft Instrumentation and Test Performance

A test shaft instrumentation system as shown in Fig. 9 will be in place to measure movement of the top of the shaft, shaft compression, expansion of the bi-directional cells, and strain along the length of the shaft. The instrumentation systems are redundant and use multiple instruments to provide data if a single unit fails or becomes unusable. The instrumentation is positioned to allow for determination of shaft side and base resistances. Load testing will be conducted in general accordance with ASTM D8169-18: Standard Test Methods for Deep Foundations Under Bi-Directional Static Axial Compressive Load. The test shaft will be loaded in a minimum of ten equal increments, with each increment not exceeding 5% of the minimum bi-directional capacity. Each load increment will be maintained for 8 minutes. Loading will continue until one of the following conditions is met:

- The minimum bi-directional cell capacity is reached,
- Shaft head displacement exceeds 6 inches, or
- The jack assembly can no longer maintain load under relatively constant displacement.

The maximum test load will be held for up to 60 minutes. Unloading will occur in steps of 75%, 50%, 25%, 12.5%, 6%, and 0% of the failure load, with each decrement held for 4 minutes. Shaft instrumentation readings will be recorded using an automatic data acquisition system, capturing time, bi-directional cell pressure, strain, and displacement at 1-, 2-, 4-, and 8-minute intervals after load application. Digital survey data will be collected at the same time intervals.

Data Interpretation and Application of Results

Upon completion of each load test, the load test contractor will provide a report that meets the applicable ASTM standards. The report will include a table summarizing key test data, such as the start and finish times, load increments, bi-directional cell readings, LVDT measurements, telltale LVDT movements, digital survey displacements, strain gauge readings, and the average load at each measurement point along the pile.

The test results will be analyzed to determine the concrete modulus and estimate the side and base resistance of each soil layer. The report will also include an Equivalent Top of Shaft Load-Settlement plot, as well as creep plots for side and base resistance. In addition to the contractor's report, independent analyses will be conducted to verify the load test results. These results will be used to validate and, if necessary, refine the drilled shaft axial resistance values. Based on the findings, the Design Team may adjust shaft diameters, lengths, or the number of shafts per group. The final load test report will be made available for use in future design phases.

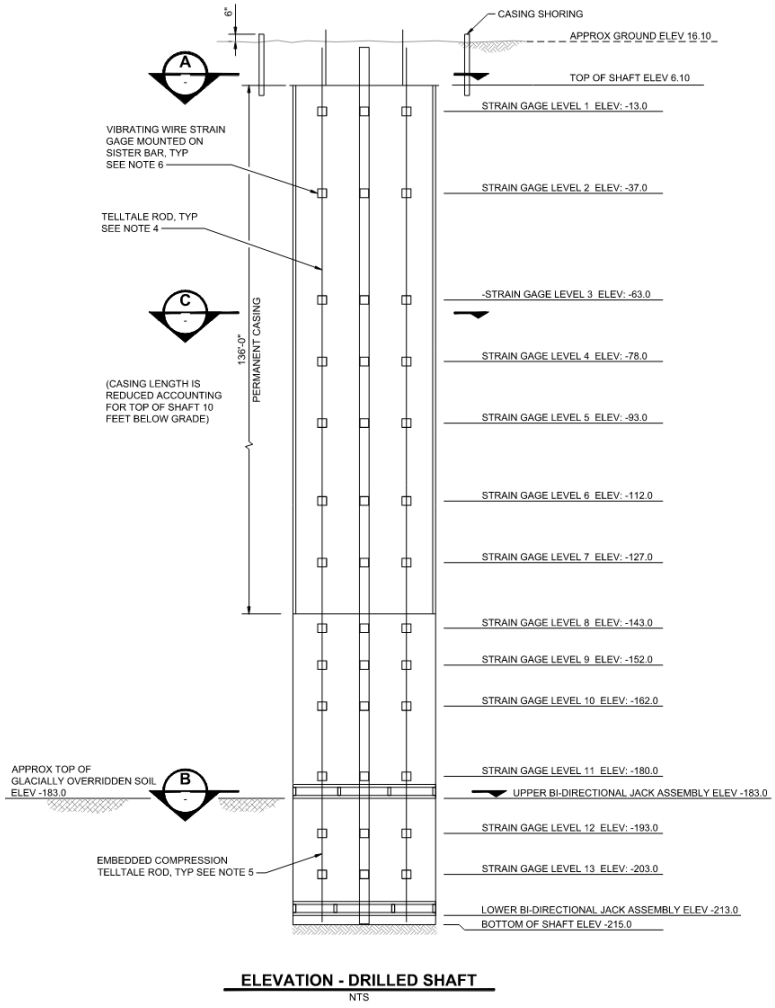


Fig. 9. Test Drilled Shaft Instrumentation

SUMMARY

This paper discusses the elevated guideways and their foundations for Sound Transit's West Seattle Link Extension project at the preliminary design phase. The selection of foundation types was primarily influenced by the presence of soft, compressible sediments ranging from 17 to 270 feet deep, the potential for significant seismic-induced settlements along the alignment, and the proximity of critical infrastructure. Given these challenges, deep foundations were recommended to support the bridge and guideway structures, with drilled shafts identified as the preferred type. To further optimize the design, a bi-directional load test program is being planned. Additionally, this paper explores potential design enhancements for subsequent phases of the project.

REFERENCES

1. Sound Transit (2024) “West Seattle Link Extension Final Environmental Impact Statement (EIS)”.
2. Sound Transit (2023) “ST Requirements Manual – Revision 0”.
3. American Association of State Highway and Transportation Officials (AASHTO) (2020) “AASHTO LRFD Bridge Design Specifications 9th Edition”.
4. American Association of State Highway and Transportation Officials (AASHTO) (2011) AASHTO Guide Specifications for LRFD Seismic Bridge Design 2nd Edition.
5. Washington Department of Transportation (WSDOT) (2019) “Geotechnical Design Manual M46-03.12”.
6. Washington Department of Transportation (WSDOT) (2024) “Bridge Design Manual (LRFD) M23-50.23”.
7. Ensoft Inc. (2022) LPILE
8. Ensoft Inc. (2022) GROUP
9. Reese, LC, W. Van Impe (2001) “Single Piles and Pile Groups under Lateral Loading”, 2nd Edition.
10. Fellenius, BH (2004) “Unified Design of Piled Foundations with Emphasis on Settlement Analysis”.
11. Federal Highway Administration (FHWA) (2016) “NHI-16-009 “Design and Construction of Driven Pile Foundations”.

ACKNOWLEDGEMENT

The authors extend their gratitude to Reda Mikhail and Joe Hachey of Jacobs Engineering Group, Bob Mitchell and Kathryn Petek of Shannon & Wilson, Inc., and Conrad Felice of C.W. Felice, LLC for their invaluable contributions and expertise in geotechnical and seismic engineering throughout various phases of the project.

ASTM D8505 COMPLIANT MULTI-BAR GFRP TIEBACKS FOR TEMPORARY AND LONG-TERM APPLICATION

Mike Porco, P.Eng., Grounded Engineering, Toronto, Ontario
Naji Shbaklo, P.Eng., M.Eng., Grounded Engineering, Toronto, Ontario, Canada
Alireza Asadian, PhD, MST Rebar Inc., GTA, Ontario, Canada
Rick V. Dozzi, P.Eng., CANADIAN BBR INC., Scarbrough, ON, Canada
Borna Hajimiragha, M.Eng. MST Rebar Inc., GTA, Ontario, Canada

ABSTRACT

ASTM D8505 compliant multi-bar GFRP tiebacks, made from Glass Fiber Reinforced Polymer (GFRP), offer an innovative solution for both temporary and long-term anchoring applications, providing advantages over traditional steel tiebacks. A key feature of multi-bar GFRP tiebacks is their low relaxation, improved creep behavior, and very high bond strength, ensuring that the bonded zone remains in-place under cyclic loading. These features make them highly effective in retaining structures under demanding conditions. Additionally, their lightweight and corrosion-resistant properties contribute to a reduced carbon footprint compared to steel alternatives. For both short- and long-term applications, GFRP tiebacks are lighter to transport and easier to install, reducing cost and logistics during construction.

For short-term applications, multi-bar GFRP tiebacks offer the added benefit of being easy to cut, a feature particularly useful in urban projects where future expansions may require additional excavation. This feature also minimizes the risk of tunnel boring machines getting stuck on traditional steel tiebacks left behind from previous construction projects, especially when clear blueprints are unavailable. Steel tiebacks are harder to cut, posing challenges during infrastructure expansion.

This study presents the results of extensive field testing, which validates the performance of multi-bar GFRP tiebacks. Long-term monitoring of creep and relaxation behavior under different load conditions demonstrated exceptional stability and reliable load retention. multi-bar GFRP tiebacks, with their enhanced load capacity and eco-friendly characteristics, represent a sustainable and high-performance alternative to steel for a wide range of construction and infrastructure projects.

Keywords: Multi-bar GFRP tiebacks, corrosion resistance, load capacity, creep behavior, relaxation behavior, sustainable construction, urban infrastructure, temporary anchoring, long-term anchoring.

INTRODUCTION

Glass Fiber Reinforced Polymer (GFRP) has emerged as a high-performance alternative to traditional steel reinforcement in civil engineering applications, particularly in environments where corrosion resistance, weight reduction, and long-term durability are critical. Unlike steel, GFRP does not rust or corrode, even in aggressive environments. This inherent corrosion resistance significantly extends the service life of structures where GFRP is employed, thereby reducing maintenance requirements and lifecycle costs (ACI 440.1R-15). One notable application is in tieback systems used for retaining walls and slope stabilization, where GFRP offers several advantages over conventional materials. Moreover, its

 © Deep Foundations Institute 2025

extended durability minimizes the need for rehabilitation or replacement, further conserving resources over time. Additionally, the Corrosion resistance offer cost savings for longer service life applications where corrosion protection for steel can be costly.

The key benefits of GFRP tiebacks for short- and long-term applications include their lightweight nature, which facilitates easier handling, transportation, and installation, especially in remote or logistically constrained sites (ACI 440.1R-15).

In addition to performance advantages, GFRP also contributes to sustainability goals by lowering the environmental footprint of infrastructure projects. Its production and application typically result in reduced carbon emissions compared to traditional steel. Although the Environmental Product Declarations (EPDs) for both GFRP and steel bars vary depending on factors such as raw material sources, manufacturing techniques, and energy use, the global warming potential (GWP) for the GFRP bars used in these anchors is 1.5 kg CO_2e/kg (modules A1–A3). When comparing GWP values between GFRP and steel, it is important to consider the significant difference in material density, 2,100 kg/m³ for GFRP versus 7,850 kg/m³ for steel. To enable a direct comparison for bars of the same nominal size, the GWP value for GFRP should be divided by the density ratio of 3.74 (7,850 ÷ 2,100), resulting in an equivalent GWP of approximately 0.4 kg CO_2e/kg. Depending on the type of steel used for comparison, this represents a reduction in GWP of approximately 100% to 500%.

Another practical benefit is that GFRP can be more easily cut than steel, a feature particularly advantageous in installations near electrical infrastructure where precise adjustments may be required. This characteristic also proves beneficial when temporary tieback systems are installed in areas earmarked for future construction or expansion, as it enables easier modification or removal during excavation activities. This feature also minimizes the risk of tunnel boring machines getting stuck on traditional steel tiebacks left behind from previous construction projects, especially when clear blueprints are unavailable. Steel tiebacks are harder to cut, posing challenges during infrastructure expansion.

The bars used in ASTM D8505 compliant multi-bar GFRP tiebacks is a high-performance glass GFRP bar. It is manufactured to exceed the stringent global standards, including ASTM D8505, ASTM D7957, and CSA S807 and is widely used by various Transportation Authorities across the United States and Canada as well as several industrial and residential applications.

However, despite these advantages, the use of GFRP in tieback systems introduces a unique set of challenges. A primary concern is its creep behavior under sustained loads, which can affect the long-term performance and reliability of anchored systems. Additionally, the bond performance of GFRP within anchoring systems, critical for effective load transfer from the tieback bar to the surrounding ground or grout—remains a key design consideration.

The table below summarizes the key differences in material properties between ASTM D8505 compliant multi-bar GFRP bars, grade 350W structural steel (CSA G40.21), and DYWIDAG seven-wire, low-relaxation, 270 ksi strands commonly used in tieback applications by local shoring trades.

Table 1 – Material properties between ASTM D8505 compliant GFRP bars, grade 350W structural steel, and DYWIDAG steel strands

	Unit Weight, γ (kN/m^3)	Modulus of Elasticity, E (GPa)	Yield Tensile Strength, f_y (MPa)	Ultimate Tensile Strength, f_u (MPa)	Ultimate Transverse Shear Strength, τ_u (MPa)
Structural Steel (350W)	77	200	350	450	231
DYWIDAG Steel Strand			1670	1860	1102
ASTM D8005 GFRP BAR	21	60	N/A	1000	220

As highlighted in the table above, ASTM D8505 compliant GFRP bars are four times lighter than steel, which benefits handling and logistics. They exhibit a relatively low modulus of elasticity and an ultimate tensile strength approximately half that of high-strength steel strands, though still markedly higher than that of structural steel. Notably, the ultimate tensile strength of GFRP bars is significantly higher than their transverse shear strength of approximately 231 MPa.

On face value, the primary concern with these GFRP bars is their low modulus of elasticity, which would lead to excessive elongations if used as passive anchors. Additionally, they are elastic until failure, with no distinct yield point. This results in a brittle failure mechanism, which is perceived to be undesirable as it provides no warning signs of failure, whereas steel would yield and experience significant elongation prior to rupturing. However, this feature needs to be addressed in design by implementing safety factors.

What can be easily overlooked, if this material is not studied carefully, is its susceptibility to creep failure. Under sustained loading, the bars could rupture given enough time (also known as endurance time). In contrast, steel does not exhibit creep rupture.

Although the current body of literature offers insights into the mechanical properties of GFRP, there remains a notable gap in long-term performance data, particularly regarding creep and stress relaxation behavior under sustained high loads in real-world conditions. This lack of comprehensive data has resulted in conservative design standards and ongoing hesitation regarding the broader adoption of GFRP in permanent anchoring systems.

Due to the lack of design codes and standards on the short-term application of GFRP bars, design practitioners typically rely on CSA S806:12 (R21), CSA S6:19, ACI code-440.11-22, and AASHTO LRFD guidelines for GFRP. Although these codes are intended for permanent applications, they are commonly applied to temporary SOE (Support of Excavation) systems, which generally have design service lives of less than five years, with one to two years being most common. This practice results in conservative and inherently safe designs. Given the temporary nature of SOE walls, future applications may allow for a more optimized design approach. There is a distinct possibility to take advantage of GFRP material properties for short-term temporary systems if future iterations of design codes were to tabulate creep safety factors for specified design service life.

This study seeks to address these knowledge gaps by analyzing both laboratory and field data on the performance of a commercially available GFRP bar compliant with ASTM D8505. The research investigates the mechanical behavior of GFRP under sustained stress, evaluates its bond characteristics

within anchorage zones, and presents findings from a real-world application—Kipling Station Condos—as a case study. Through this comprehensive assessment, the study aims to offer critical insights into the feasibility, performance, and design considerations of GFRP tiebacks in short-term civil infrastructure applications.

BEHAVIOUR OF GFRP BARS UNDER CREEP

Creep behavior is a critical performance parameter for Glass Fiber Reinforced Polymer (GFRP) bars, particularly in structural applications where the bars are subjected to sustained loads over extended periods, as is the case with tieback systems. In this study, the deformation characteristics of the #3 ASTM D8505 compliant GFRP bars, were investigated under long-term loading to evaluate both creep strain development and creep rupture resistance at elevated stress levels.

During the long-term creep tests, five GFRP specimens were subjected to a constant load corresponding to 45% of their average ultimate tensile strength (UTS) over a period of 1,780 hours. The results demonstrated limited and gradually decreasing creep strain over time. As presented in Table 2, the additional strain observed after 1,000 hours ranged between 2.1% and 5.8% of the initial strain, with negligible deformation beyond that point (ranging from 0.2% to 1% increase in strain from 1000 hours to 1780 hours). These findings indicate a stable long-term performance of GFRP bar under sustained loading conditions. The increase in strain was calculated as the ratio of the increase in strain over time to the initial strain.

Table 2 – relaxation test results (45% UTS) for #3 Grade III GFRP bar.

Nominal Applied Load	Specimen	Initial strain (με)	Creep strain (strain increase) (με) after initial strain								$\frac{Creep\ strain}{Initial\ Strain}$ (% of initial strain)
			24 hrs	48 hrs	144 hrs	288 hrs	528 hrs	1000 hrs	1560 hrs	1780 hrs	1000 hrs
45% UTS	1	9174	161	224	285	322	359	405	462	480	4.4
	2	9430	120	155	227	284	338	409	489	509	4.4
	3	9376	Rejected (The bar slippage from steel tube)								
	4†	9304	54	72	101	123	147	2193	229		2.1
	5	9665	444	484	520	544	551	569	593	604	5.8

Note: † The results obtained during the first week after reinstalling the bar.

In the creep rupture strength phase of the study, 24 GFRP samples were tested under sustained load levels ranging from 65% to 90% of their ultimate tensile strength (UTS). A creep rupture test involves applying a constant tensile stress to specimens over an extended period and recording the time to failure at each stress level (ASTM D7337/D7337M and CSA S806, Annex H). By conducting tests across multiple stress levels, a time-to-rupture curve can be developed, which is then extrapolated to estimate the material's long-term rupture strength over extended service durations.

In this study, all specimens loaded at 90%, 85%, and 80% of UTS failed within a few hours, illustrating the upper stress limit for sustained loading. In contrast, specimens tested at 75% and 70% demonstrated significant durability, with some surviving for over 5,000 hours. Notably, samples loaded at 65% of UTS did not fail even after 8,000 hours of continuous loading, as presented in Table 3.

 © Deep Foundations Institute 2025

Using the recorded time-to-failure data and applying extrapolation techniques, the projected creep rupture strength of ASTM D8505 compliant GFRP bars at 1 million hours (approximately 114 years) is estimated to be around 62% of its UTS. This finding highlights the bar's excellent long-term performance and supports its use in critical applications where resistance to sustained loading over decades is essential.

Table 3 – Applied sustained stress and rupture time of the samples

Applied Tensile Load (% UTL)	Specimen No.	Applied Sustained Tensile Load (kN)	Rupture Time (hours)
90	1	102.2	0.07
	2		0.03
	3		0.02
	4		0.05
85	1	96.5	0.25
	2		0.06
	3		0.03
	4		0.2
80	1	90.8	1.83
	2		0.66
	3		6.03
	4		1.77
75	1	85.2	550
	2		210
	3		408
	4		595
70	1	79.5	3120
	2		4002
	3		3300-No bar failure
	4		3005-No bar failure
65	1	73.8	5000-No bar failure
	2		Runout Test stopped (after 8000hrs)
	3		Runout Test stopped (after 8000hrs)
	4		Runout Test stopped (after 8000hrs)

CASE STUDY: KIPLING STATION CONDOS

Located in Toronto, Ontario, Kipling Station Condos is a new 50-storey residential tower under construction by CentreCourt (“Developer”), one of the largest high-rise developers in Canada. The site is bordered by Dundas Street West to the north, Auckland Road to the east, Hydro One lands to the west containing a nearby steel lattice transmission tower, and a surface parking lot to the south owned by Toronto Transit Commission (TTC) for the Kipling Subway Station – see Fig. 1.

The regulatory constraints imposed by Hydro One and TTC directly led to the selection of GFRP material for the tieback anchors on the south and west frontages. Hydro One maintained a line of steel lattice transmission towers in proximity to the development and were concerned about the electrical conductivity potential between steel tiebacks and the foundations of the transmission towers due to tight installation clearances. The TTC parking lot contained a mechanically stabilized retaining wall supporting the higher grading of the development site and were concerned about potential difficulties removing steel tiebacks should they ever redevelop their parking lot site in future and/or rebuild the retaining wall.

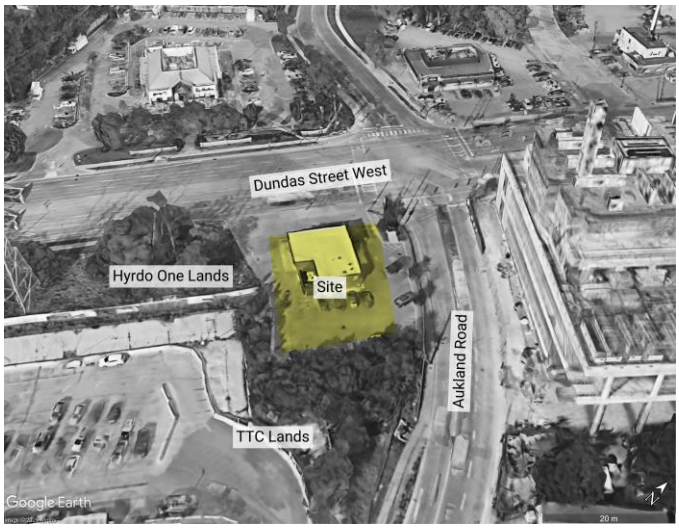


Fig. 1 - Aerial view of development site

To model the west and south SOE walls, the engineering team analyzed the soldier piles as two-dimensional continuous beams subjected to transverse static loads, including earth pressure and construction surcharge. Axial load effects were superimposed, treating the piles as beam-columns. Lateral support was provided by the GFRP-reinforced tiebacks.

STRUCTURAL DESIGN AND MODELING

Since the temporary SOE walls primarily retain dense to very dense cohesionless soils, the design adopted Terzaghi and Peck's rectangular apparent earth pressure envelope ("AEPE") for idealized sands, with an intensity of $0.65k_a\gamma H$. The active earth pressure coefficient (k_a) was set at 0.28, as recommended by the project geotechnical engineer. To maintain conservatism, the effect of wall friction on k_a (per Coulomb earth pressure theory) was neglected. The tieback design loads obtained from the model were adjusted based on the SOE engineer's experience and discretion. This approach considered the arching behavior of the retained soils and the resulting load redistribution to the tieback anchors, fostering an anchor loading regime that minimizes SOE wall displacement. The maximum anticipated pile displacement into the site was estimated as approximately 11 mm.

While the AEPE used in the design aids in estimating tieback loads, it does not reflect the actual earth pressure distribution behind the SOE wall. Instead, it serves as a conservative tool to ensure that estimated tieback loads are unlikely to be exceeded. Accordingly, it was assumed that the maximum sustained loads experienced by the GFRP anchors would correspond to the design pre-stressing loads.

The retained shoring contractor opted for a 152 mm (6") diameter drill hole for the tiebacks, extending from the face of the SOE wall to the tip of the tieback, with the temporary casing extending 3 meters into bedrock. This approach deviated from the standard practice of terminating the temporary casing at the top of sound bedrock and advancing the drill bit beyond that point along the bond zone.

This modification was necessary to provide enough room for up to four #8 ASTM D8505 compliant GFRP bars, while maintaining sufficient grout cover along the bond zone. In collaboration with GFRP tie-back supplier and the retained shoring contractor opted, the engineering teams also opted for multiple smaller-diameter bars instead of a single larger reinforcement bar. This decision was aimed at enhancing stress distribution across the entire bar cross-section by minimizing stress variability across the bar fibres, improving overall load transfer efficiency, and optimizing performance.

It is noteworthy that since this project represents one of the first applications of Multi-bar Tiebacks in excavations of this scale in Toronto, adhering to the available codes for permanent applications serves as a prudent measure to mitigate unforeseen risks.

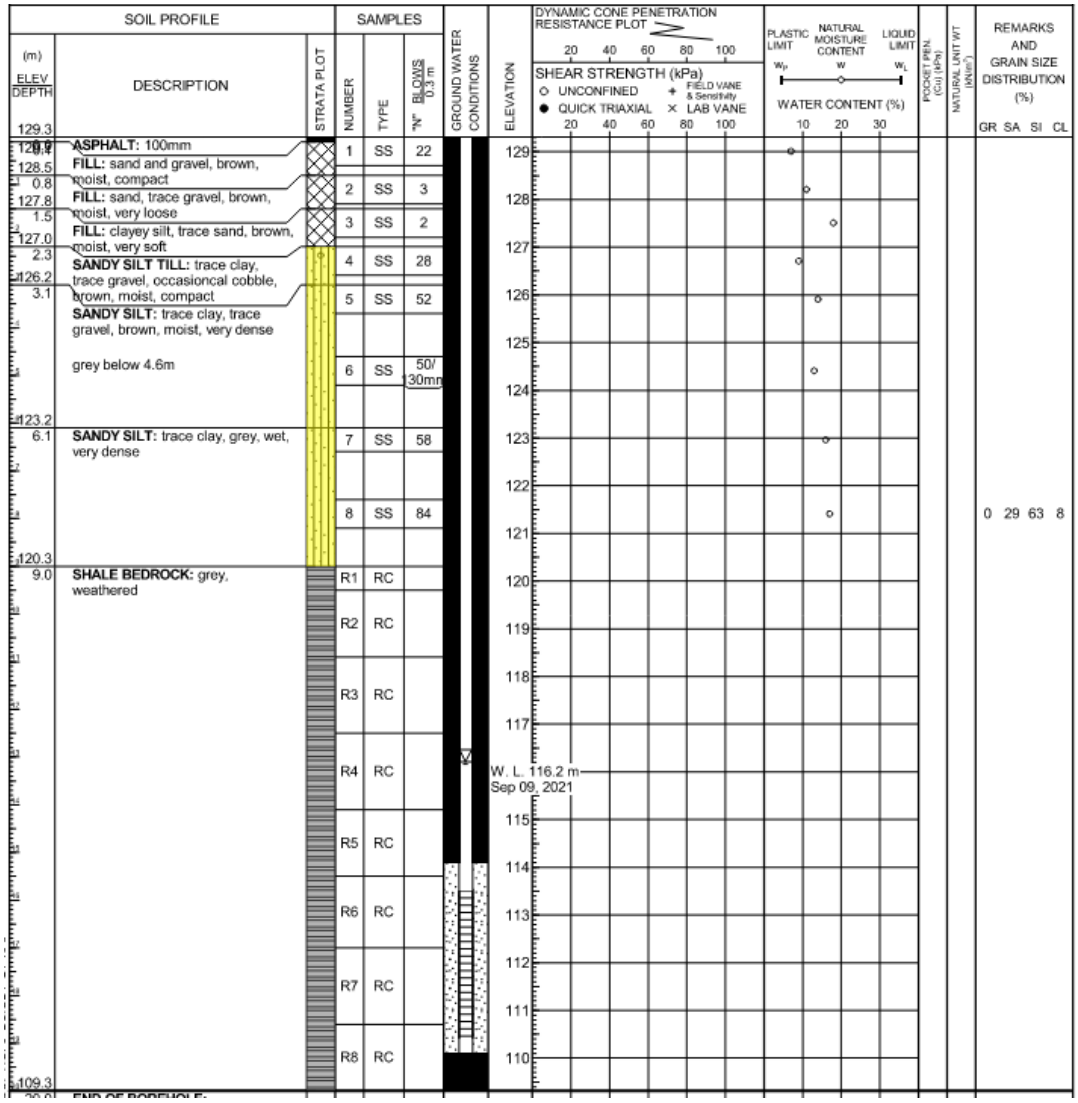


Fig. 2 - Typical soil profile

To maintain SOE wall displacements within 0.2% of the excavation height, the engineering team opted to actively pre-stress the tieback anchors—an uncommon approach for GFRP-reinforced anchors. The following key design considerations were derived from the applicable codes:

 © Deep Foundations Institute 2025

1. The maximum stress during pre-stressing should be limited to 30% of the ultimate tensile strength (1000 MPa).
2. The maximum stress at lock-off/transfer should be limited to 25% of the ultimate tensile strength, in recognition of the GFRP reinforcement's susceptibility to time-dependent (i.e., creep) rupture. The 25% stress limit is a conservative design decision adopted from CSA S806-12, primarily intended for permanent applications. However, given the temporary nature of SOE walls, future projects may benefit from more optimized design approaches based on product-specific test data on their creep behaviour over time, particularly as more targeted standards are developed.

In contrast to the single level of steel-reinforced tieback anchors used for the north and east walls, which support similar excavation depths, the design for the west and south SOE walls required three levels of tieback anchors, strategically placed at elevations that facilitate tieback de-stressing and eliminate the need for formwork penetrations at the tieback connections. The piles at the west and south SOE walls were spaced 2.45 meters (8') apart, and the load demand per tieback level was close to 350 kN at a declination angle of 45°. To meet the code requirements outlined in the previous section, the following calculations were made to determine the number of GFRP bars (n) to be employed, based on the assumption that #8 GFRP bars will be used and bundled together, with a pre-stressing load of 350 kN:

1. During tieback proof-testing to 133% of the design load (DL):

$$\sigma_{max} \leq 0.3 f_u$$

$$\frac{1.33DL}{nA_{\#8}} \leq 0.3 f_u$$

$$n \geq \frac{1.33DL}{0.3 f_u A_{\#8}}$$

$$n \geq \frac{1.33 \times 350kN}{0.3 \times 1000MPa \times 507mm^2}$$

$$n \geq 3.1$$

2. During tieback lock-off (at transfer):

$$\sigma_{max} \leq 0.25 f_u$$

$$\frac{DL}{nA_{\#8}} \leq 0.25 f_u$$

$$n \geq \frac{DL}{0.25 f_u A_{\#8}}$$

$$n \geq \frac{350kN}{0.25 \times 1000MPa \times 507mm^2}$$

$$n \geq 2.8$$

Following the considerations above, four #8 GFRP bars are required per tieback anchor. Based on the recommendations of the geotechnical report, local practice standards, and past project experience, a working gravity-grouted adhesion of 620 kPa was selected for tiebacks bonded in sound bedrock. This

 © Deep Foundations Institute 2025

value was used for design purposes, but would ultimately be verified by a field performance testing program. Based on 620 kPa, the required bond zone length based purely on grout-to-rock adhesion is approximately 1.2 meters. A minimum bond zone length of 3 meters was selected to ensure sufficient development length in the grouted hole.

PRE-PRODUCTION TIEBACK TESTING PROGRAM

Though it is acknowledged that the declination angle of the tiebacks is 45 degrees, for practical reasons, three sacrificial vertical tieback pre-production tests were carried out at the site prior to the shoring works, as summarized in the table below:

Table 4 – Pre-production tests were carried out at the site prior to the shoring works

Test #	Reinforcement	Design Load, DL (kN)	Maximum Load (% of DL)	Bond Zone Length (m)
1	7 steel strands	650	198	3.0
2	4-#8 MST-BAR	350	300	3.0
3	4-#8 MST-BAR	675	133	4.2

Test #1 was intended as a control test to confirm a factor of safety of 2.0 for the design gravity-grouted adhesion of 620 kPa in sound bedrock. Tests #2 and #3, on the other hand, were conducted using GFRP reinforcement to evaluate the adequacy of the grout-bar adhesion, assess the capability of the collar stressing assembly to sustain high loads, and gain insight into short-term field loading in excess of 30% fu for future applications.

Test #2 stressed the bars up to 45% fu, with a 60-minute loading period at 200% DL (0.71 mm of measured creep) and 10 minutes at 300% DL (0.57 mm of measured creep). Test #3 stressed the bars up to 52% fu with a 10-minute holding period (2.92 mm of measured creep). The bars did not fail, and the stressing program was successfully completed.



Fig. 3. - Multi-bar GFRP Tiebacks

 © Deep Foundations Institute 2025

The displacement monitoring program included reflective monitoring targets placed at the top of piles and all anchor points, as well as an inclinometer installed at the west SOE wall, where the excavation was the deepest. Displacement monitoring data were collected starting immediately before bulk excavation until the below-grade construction reached street level. The data from the reflective targets and inclinometer indicated pile displacements ranging between 7–12 mm, which aligned closely with the theoretical estimate of 11 mm. The west and south SOE walls performed as expected, with no issues raised during excavation. The inclinometer data presented in Fig. 4 below summarizes the SOE system performance:

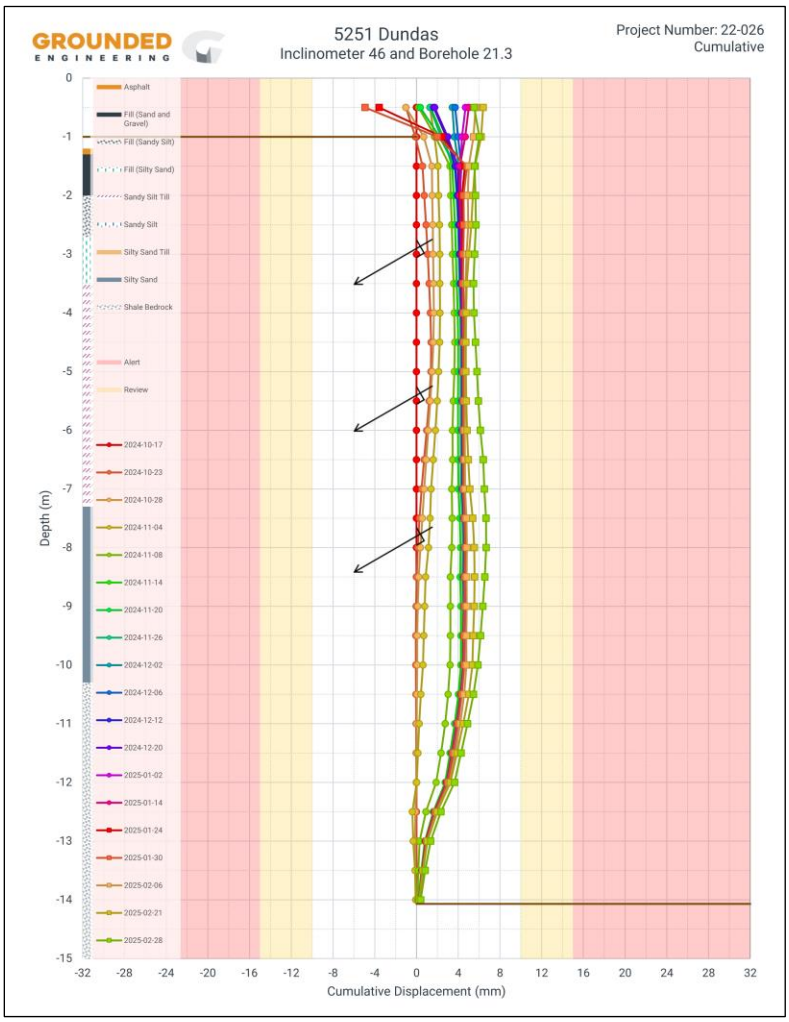


Fig. 4 - Inclinometer data on the SOE system performance

SUMMARY AND CONCLUSIONS

This study presents a comprehensive evaluation of the long-term performance of ASTM D8505-compliant GFRP bars, with a focus on relaxation and creep rupture strength through tastings done in accordance with ASTM D7337/D7337M and CSA S806, Annex H. The results demonstrate that GFRP exhibits stable behavior under sustained loading, with low creep strain accumulation and high creep rupture thresholds—particularly at stress levels up to 65% of the ultimate tensile strength (UTS).

 © Deep Foundations Institute 2025

A real-world application of this technology is showcased in the Kipling Station Condos project in Toronto, Ontario—a 50-storey residential tower currently under construction by CentreCourt, one of Canada's largest high-rise developers. The site's excavation utilized GFRP's Multi-bar Tieback system, marking one of the first implementations of this technology on such a large scale in Toronto. In this context, adherence to existing design codes for permanent applications, such as CSA S806:12 (R21), CSA S6:19, ACI 440.11-22, and AASHTO LRFD guidelines, served as a prudent approach to mitigate unforeseen risks, despite the temporary nature of the support of excavation (SOE) system.

Although these codes are primarily intended for permanent applications, they are commonly applied to temporary SOE structures, which generally have design service lives of less than five years, with one to two years being most common. This conservative practice results in inherently safe designs. However, given the temporary role of SOE walls, future projects may benefit from more optimized design approaches as the industry evolves and develops more targeted standards. There is a distinct possibility to take advantage of GFRP material properties for short-term temporary systems if future iterations of design codes were to tabulate creep safety factors for specified design service life.

Overall, both the experimental results and field application confirm that ASTM D8505 compliant multi-bar GFRP tieback is a durable and reliable solution for structural reinforcement, with significant potential for broader implementation in both temporary and permanent excavation systems. It is important to note that the results presented in this study are specific to the ASTM D8505-compliant multi-bar GFRP tiebacks used herein.

REFERENCES

American Association of State Highway and Transportation Officials (AASHTO). (2018). *AASHTO GFRP-2B: LRFD Bridge Design Guide Specifications for GFRP-Reinforced Concrete, 2nd Edition*. Washington, DC: AASHTO.

American Concrete Institute (ACI) (2015). ACI Committee 440.1R-15, Guide for the Design and Construction of Structural Concrete Reinforced with Fiber-Reinforced Polymer (FRP) Bars. American Concrete Institute, Farmington Hills, MI, 2015.

American Concrete Institute (ACI). (2022). *ACI CODE-440.11-22: Building Code Requirements for Structural Concrete Reinforced with Glass Fiber-Reinforced Polymer (GFRP) Bars—Code and Commentary*. Farmington Hills, MI: ACI.

ASTM International. (2023). *ASTM D8505/D8505M-23: Standard Specification for Basalt and Glass Fiber Reinforced Polymer (FRP) Bars for Concrete Reinforcement*. West Conshohocken, PA: ASTM International.

ASTM International. (2022). *ASTM D7957/D7957M-22: Standard Specification for Solid Round Glass Fiber Reinforced Polymer Bars for Concrete Reinforcement*. West Conshohocken, PA: ASTM International.

ASTM International. (2019). *ASTM 7337/D7337M-12: Standard Test Method for Tensile Creep Rupture of Fiber Reinforced Polymer Matrix Composite Bars.* West Conshohocken, PA: ASTM International.

 © Deep Foundations Institute 2025

Canadian Standards Association (CSA). (2019). *CSA S807:19: Specification for Fibre-Reinforced Polymers*. Mississauga, ON: CSA Group.

Canadian Standards Association (CSA). (2013). *CSA G40.20-13/G40.21-13 (R2023): General Requirements for Rolled or Welded Structural Quality Steel/Structural Quality Steel*. Mississauga, ON: CSA Group.

Canadian Standards Association (CSA). (2012, reaffirmed 2021). *CSA S806:12 (R2021): Design and Construction of Building Components with Fibre-Reinforced Polymers*. Mississauga, ON: CSA Group.

Canadian Standards Association (CSA). (2019, reaffirmed 2024). *CSA S6:19 (R2024): Canadian Highway Bridge Design Code*. Mississauga, ON: CSA Group.

EPD [Online]: https://epd-australasia.com/epd/mst-bar-fiberglass-rebar/

MST Rebar. [Online]. https://www.mstrebar.com.

 © Deep Foundations Institute 2025

COMPLEX LOGISTICAL CONSTRAINTS AND THEIR TECHNICAL IMPACT ON A DEEP EXCAVATION DESIGN, OTTAWA, ONTARIO, CANADA

A.M. Crockford, Brierley Associates, Denver, CO, USA, acrockford@brierleyassociates.com
C.A. Luxford, Brierley Associates, Austin, TX, USA, cluxford@brierleyassociates.com
H. Batenipour, Kiewit Engineering Group Canada ULC, Toronto, ON, Canada, Hamid.Batenipour@Kiewit.com
K.P. Burnham, Brierley Associates, Syracuse, NY, USA, kburnham@brierleyassociates.com
C.E. Valle, Brierley Associates, Austin, TX, USA, cvalle@brierleyassociates.com

ABSTRACT

The Kiewit Eurovia Vinci (KEV) Partnership are completing construction on the Confederation Line Extension (Ottawa Stage 2) LRT Project. The project includes up to 3.4 km of cut and cover tunnels within the urban center. Brierley Associates provided temporary Support of Excavation (SOE) system designs for various segments of the open-cut trench excavation through soil and rock. This paper will focus on the Parkway Zone 12 and Zone 13a segments of the project where the open-cut trench extends up to 12 m below grade through glacial till, sands and clay. Due to complex logistical constraints for this segment of the open cut excavation, the Designer and Contractor collaborated and provided a unique design solution to meet the project needs. Logistical constraints for this segment included tight temporary and permanent ROW restrictions, accommodations for existing and proposed utilities (with several crossing the excavation at high skew angles), and traffic sequencing. The SOE system needed to account for stringent hydraulic cutoff requirements, utility crossings, and limited bracing options due to tight ROW limits.

Keywords: Case Study, Heavy Civil, Braced Excavation, Secant Piles, Utility Crossing

INTRODUCTION

The Kiewit Eurovia Vinci (KEV) Partnership are currently completing the Confederation Line Extension (Ottawa Stage 2) Light Rail Project, which was developed using the Design-Build-Finance contract model. The project was awarded in April 2019, to expand the City of Ottawa's transit system East and West from Canada's Capital City's downtown core, as shown in Fig. 1 and 2. The project includes a new 27 km LRT extension of the Confederation Line (West Extension 14.5 km, East Extension 12.5 km) with 16 new stations (11 West Extension Stations, 5 East Extension Stations), and a Light Maintenance and Storage Facility (LMSF). Within the extension scope, the project includes 3.4 km of cut and cover tunnels. KEV subcontracted various design firms, including Brierley Associates, to provide temporary Support of Excavation (SOE) system design for various segments of the open-cut trench excavation through soils and rock.

This paper focuses on a Cut and Cover portion of the West Extension, and in particular a segment of the Parkway Cut-and-Cover tunnel. The topic segment is located where the tunnel alignment transitions from running along Richmond Rd and Byron Linear Park to running along the Kichi Zibi Mikan Parkway and the adjacent Ottawa River (Fig. 2). As the Cut-and-Cover excavation passes from Richmond Road to the Kichi Zibi Mikan Parkway, the contract added limitations to groundwater drawdown outside of the excavation, which led to a transition from free draining SOE systems to watertight SOE systems. From Sherbourne Station, the tunnel descends to the east through several construction "zones": Zone 11 runs along Byron Linear Park, and then passes through Zone 12 and 13a to reach Zone 13b thru 13e which run along the Kichi Zibi Mikan Parkway and connect to Kìchì Zìbì Station. Zone 11 and 12 SOE were designed as free draining, internally braced soldier pile and lagging walls. Zone 13a was designed as a watertight secant pile wall system with a combination of internal and external bracing systems to account for various site constraints and unbalanced loading. The Zone 12 and 13a designs will be the focus of this paper.

 © Deep Foundations Institute 2025



Fig. 1. Project location (image courtesy of KEV).

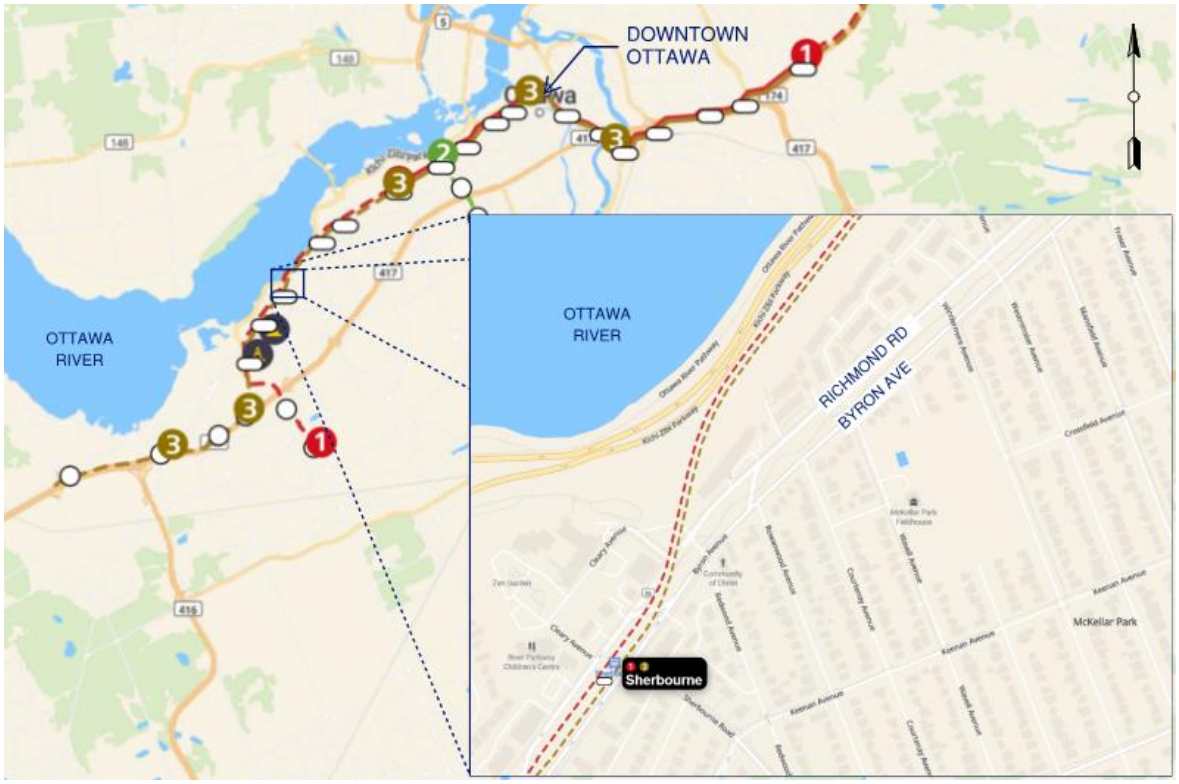


Fig. 2. O-Train Extension map (dashed Line 1 and 3). Enlarged inset map provided for the topic Cut-and-Cover segment (after the OCTranspo online Interactive System Map https://www.octranspo.com/en/interactive-map).

SITE CONDITIONS

The Parkway Cut-and-Cover tunnel within Zone 12 and Zone 13a presented unique site constraints and challenges which needed to be accounted for in the SOE designs. Site constraints included: tight

 © Deep Foundations Institute 2025

temporary and permanent right-of-way (ROW) restrictions, existing and proposed utilities to be accommodated (with several crossing the excavation at high skew angles), and traffic sequencing.

The tunnel extended up to 12 m below existing grade at this location and was up to 13 m wide. The tunnel alignment in this area was bounded by City roadway ROWs, and two adjacent private condominium properties. Zone 12 limits were defined by the extent of the alignment which crossed Richmond Road from the Byron Linear Park. As Richmond Road is a busy local roadway with heavy traffic, Zone 12 was sequenced to be built following the Zone 13a segment to limit traffic disturbance to only occur during the construction of Zone 12, which meant that no ROW encroachment was allowed for the construction of Zone 13a. In addition, two utilities passed under Richmond Rd and the adjacent sidewalk, which were necessary to protect and support in place during installation of the Light Rail Tunnel. Figure 3 shows the approximate alignment of Zone 12 & 13a, as well as the alignment of the water, electric and gas line that were to be protected, and are of note for this paper. Additional utilities and utility relocations were associated with both segments of the alignment but are not outlined here given the focus of the paper.

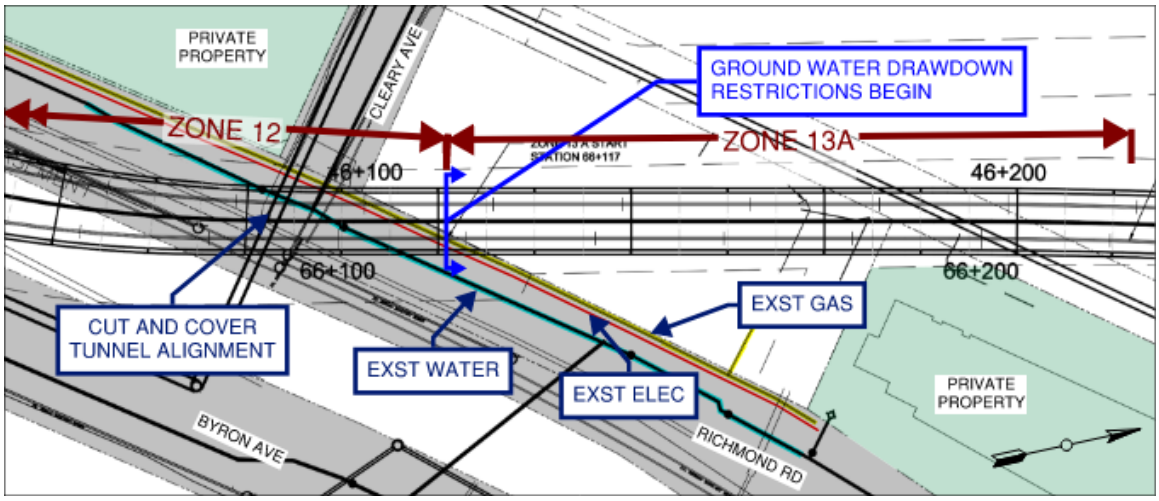


Fig. 3. Zone 12 and Zone 13a site contraints

Zone 12 geology consisted of urban fills, medium-dense to dense sands, and dense glacial tills. Urban fill materials had SPT blow counts ranging from 4 to 78 blows per foot and varied in thickness from 1.25m to 3.5m thick. Dense glacial till was encountered as shallow as 3.5m below ground surface to the north near Zone 13a. The glacial till had SPT blow counts ranging from 8 blows per foot to refusal, and typically classified as dense to very dense. Near the Zone 12/Zone 13a interface a clay crust was encountered below the urban fill. The clay crust varied in thickness up to 3m along the Zone 13a alignment and had SPT blow counts ranging from 4 to 84 blows per foot. The clay crust was encountered above the glacial till for the southern half of Zone 13a and above a very soft to soft silty clay layer for the northern half. The silty clay varied in thickness up to 4m thick at the northern end of Zone 13a and had SPT blow counts between weight of hammer and 7 blows per foot. The silty clay unit is known to potentially exhibit “sensitive” clay behavior when disturbed or internal water pressures are altered. Groundwater in Zone 13a was up 8m above the bottom of excavation, at El. 57 m, for design.

This paper focuses on the installation of SOE systems at the south end of Zone 13a and north end of Zone 12. As a result, the potentially sensitive clays are not encountered within the footprint of the SOE discussed herein, but were mentioned here as they drove the limits of the water-tight SOE system requirements defined by the Owner.

 © Deep Foundations Institute 2025

SUPPORT OF EXCAVATION DESIGN

As noted above, the contract for this area of the project limited groundwater drawdown outside the excavation to prevent water drawdown in surrounding sensitive clay soil layers. Secant piles were selected to allow for a stable water-tight SOE system that could be installed into the underlying till unit. However, secant piles could not be installed where the utilities conflicted with the wall layout, so an alternate design was required in the utility area to maintain stability and reduce groundwater drawdown. As the utilities run at an oblique angle to the excavation, the utility conflict zone is large and results in a very wide opening in the SOE system. Additional restrictions to the development of the SOE system design were the presence of the watermain to the South of the electric lines (see Fig. 3), and the proximity to Richmond Rd which could not be closed to traffic during the installation of the Zone 13a SOE system.

The main SOE for Zone 13a consisted of secant piles with two levels of internal braced steel frames for the southern half of the excavation, adjacent to Zone 12, and external bracing along the northern half. The internal steel braced frame designs consisted of WF wales and HSS pipe struts for Level 1 and Level 2 (strut levels numbered from top to bottom, in order of installation, e.g. Level 1 representing the topmost level). At the bulkhead, a "U" shape brace frame was designed to absorb the lateral loads from the bulkhead and transfer the loads to the adjacent secant pile walls (see Fig. 4). Beyond the bulkhead frame, typical "H" frames were designed to resist the lateral loads from the track-parallel secant pile walls.

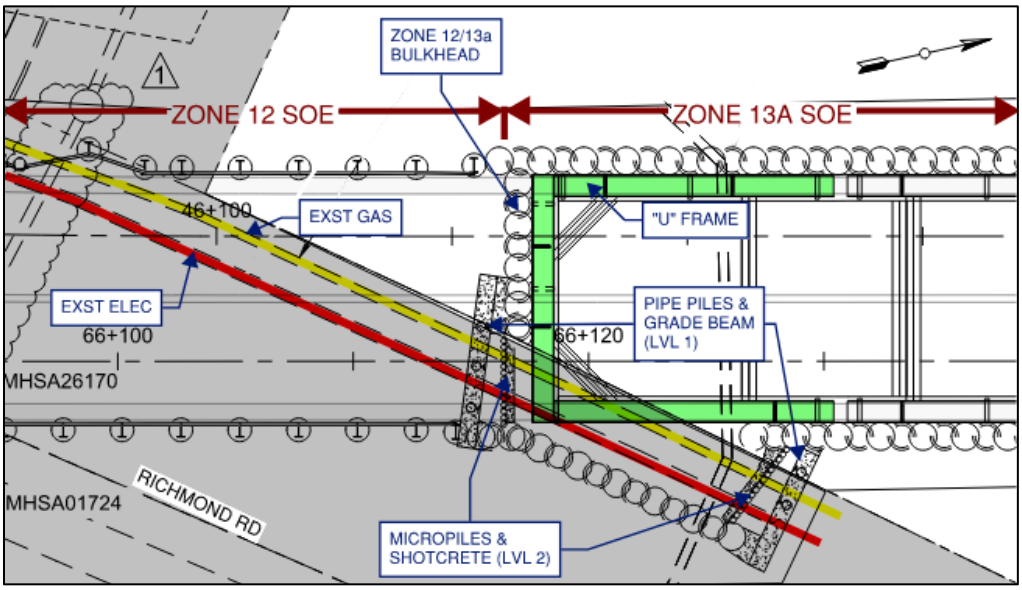


Fig. 4. Zone 12 and Zone 13a bulkhead and utility configuration

Zone 13a – Utility Accommodations

The utilities entered and exited the excavation zone between Sta. 66+115 and 66+130, for a span of approximately 15m, as shown in Fig. 4. This configuration and depth of utilities presented significant challenges to the Design-Build team. Through multiple meetings, the Designers and Contractors worked to brainstorm constructable alternatives that adequately protected the utilities in place, provided a stable SOE system, maintained a water-tight system and did not encroach on the Richmond Rd ROW. The Design-Build team ultimately selected a combination pile system using secants, micropiles and pipe piles. The alignment of the secant wall at the south east end of the Zone 13a excavation was shifted to parallel to the utility lines starting at approximately Sta. 66+115, with a gap left in the Zone 12/13a bulkhead (Fig.

 © Deep Foundations Institute 2025

4). The utility-parallel wall extended from just beyond the planned bulkhead wall at the south to past the first secant piles beyond the utility conflict parallel to the tunnel at the north. A combination of micropiles and pipe piles were designed to connect the utility-parallel secant wall to the rest of the secant system at the north and south end of the utility crossing. This configuration resulted in a near-triangular-shaped recess in the SOE system in the southeast corner and a roughly rectangular recess at the bulkhead, both of which presented a lateral load transfer challenge for the "U" frames. To address the load transfer concerns, reinforced concrete diaphragm slabs were designed for each bracing level. The concrete diaphragm slabs provided a connected rigid system, which supported a portion of the "U" frame while allowing the lateral forces to be transferred and pass back to the exterior secant pile wall for resistance.

Pipe piles and lagging were designed to support the ground above the design water level at the connection of the utility-parallel secant to the main secant system. To support the pipe piles, a concrete grade beam was required, to allow the pipe piles to span vertically and install lagging as the excavation progressed. Once the excavation had progressed to the design groundwater depth, micropiles were planned to be installed below the utilities with low clearance equipment. The micropiles were designed to be tangent piles. The Level 1 concrete diaphragm slabs were designed to be installed following the installation of the micropiles, and extended from the front face of the pipe piles and lagging to the "U" frame. The Level 2 concrete diaphragm slabs extended from front face of the micropiles to the "U" frame. At each level, the concrete was designed to be allowed to reach sufficient strength prior to excavating below.

The diaphragm slab designs were secured to the adjacent piles using dowels in the secondary piles (Level 1 & Level 2) and headed studs welded to the micropiles (Level 2). Knee braces were installed at every secondary pile along the utility-parallel wall for both concrete diaphragms to provide vertical support. To prevent ponding from occurring at the surface, the slabs were designed to be graded to drain and included PVC blockouts for use during the backfilling process. The free ends and edges were fitted with embed plates having HRC headed rebar. These embed plates were cast-in-place, and were designed to transfer load from the internal braced frames to the diaphragm slab. Once the slab reached adequate strength, the internal brace frames could be installed and the connections provided vertical support and shear load transfer. Configurations of the Level 1 slabs are shown Fig. 5 below for reference.

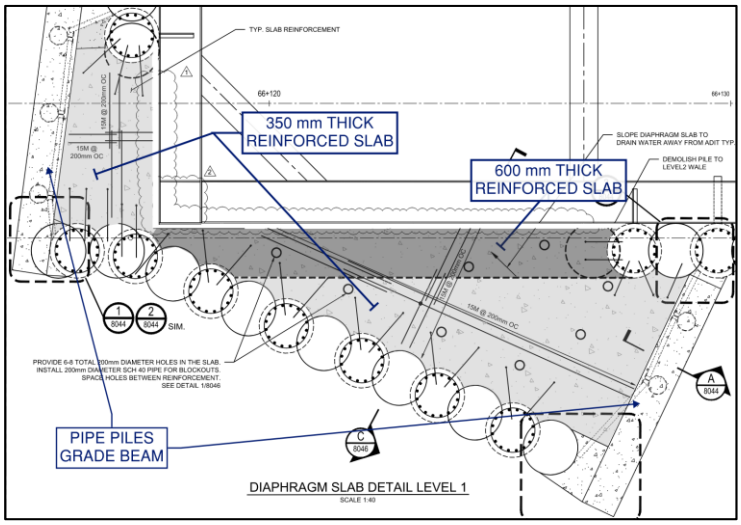


Fig. 5. Level 1 diaphragm slab configurations, cast-in-place to the face of the SOE systems.

A utility support system was integrated with the SOE design and included cap and carrier beams with diaphragms designed to span the length of the utility crossing, anchoring into secant piles as shown in Fig. 6. Strapping was required to connect the utilities to the overlying support beams.

 © Deep Foundations Institute 2025

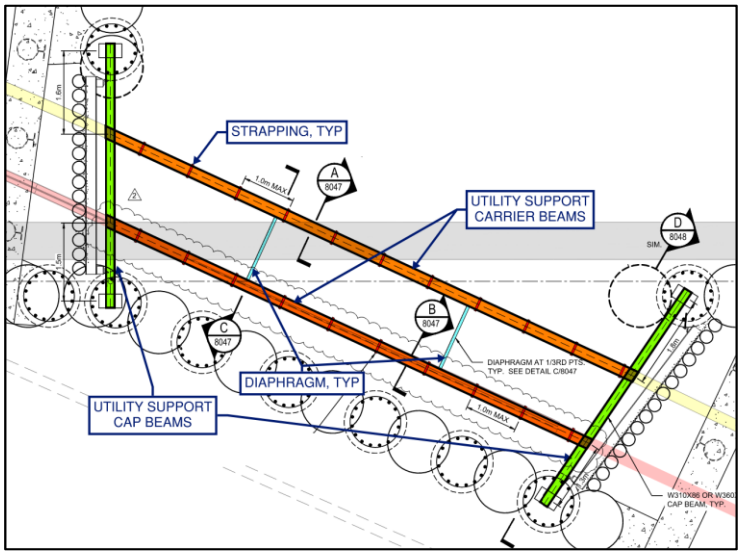


Fig. 6. Zone 13a utility support beam configuration.

Zone 12/13A Bulkhead Wall Removal

Zone 12 SOE was designed during the Zone 13a construction phase and was constructed after most of the work was completed in Zone 13a. In order to tie-in Zone 12 and Zone 13a, careful consideration had to be taken for the removal and demolition of the bulkhead separating the two zones.

The Zone 13a permanent structure was planned to be completed to within 1m of the face of the bulkhead prior to the excavation of Zone 12 and the removal of the bulkhead. The Zone 13a Level 1 "U" frame internal bracing frame was to be left in place to provide support for the gap between the bulkhead and the permanent structure. Lock blocks were installed on top of the completed tunnel structure, near the end of the tunnel heading, to act as retaining walls allowing backfill to be placed above the completed structure and keeping the tunnel heading free of backfill. Flowable fill was placed between the invert slab of the permanent tunnel and the bulkhead to reduce the span of the bulkhead as shown in Fig. 7.

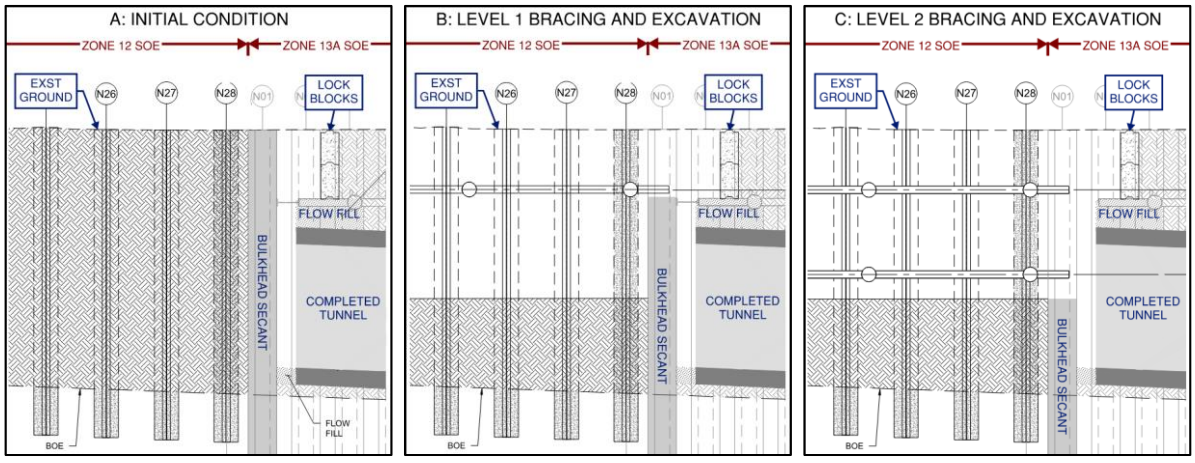


Fig. 7. Zone 12/13a bulkhead removal sequence

 © Deep Foundations Institute 2025

The Zone 12 Level 1 internal bracing was designed to be slightly higher than the existing Zone 13a Level 1 internal bracing, which allowed for the installation of the Zone 12 bracing while the existing Zone 13a bracing remained in place. The bulkhead was planned to be excavated and demolished concurrently with the excavation of Zone 12 mass excavation, up to 1m below the centerline of the Zone 12 Level 1 frame. The Zone 12 Level 1 frame was then installed extending into the bulkhead alignment to provide support for the remaining open span in front of the permanent structure. After installation of the Zone 12 Level 1 bracing, the remaining Zone 13a bracing could be removed. A similar construction sequence was followed to install the Zone 12 Level 2 bracing frame. Once both bracing frames were installed, the remaining portions of the bulkhead could be demolished to the bottom of the excavation. Select stages of the excavation sequence are shown in Fig. 7.

Prior to the demolition of the bulkhead, however, the Zone 13a utility support cap beam supporting the carrier beams at the south end of the Zone 13a utility crossing needed to be removed. This cap beam was supported on one end by a secant pile required to be removed as part of the bulkhead demolition. A new carrier beam was installed over the full width of the completed Zone 13a excavation to which the beams supporting the utilities could then be braced (Fig. 8). As the support load was transferred from the original cap beam to the new carrier beam, continuous monitoring of the support beams and utility straps was required to monitor for any signs of excessive tension or slack and movement of utilities.

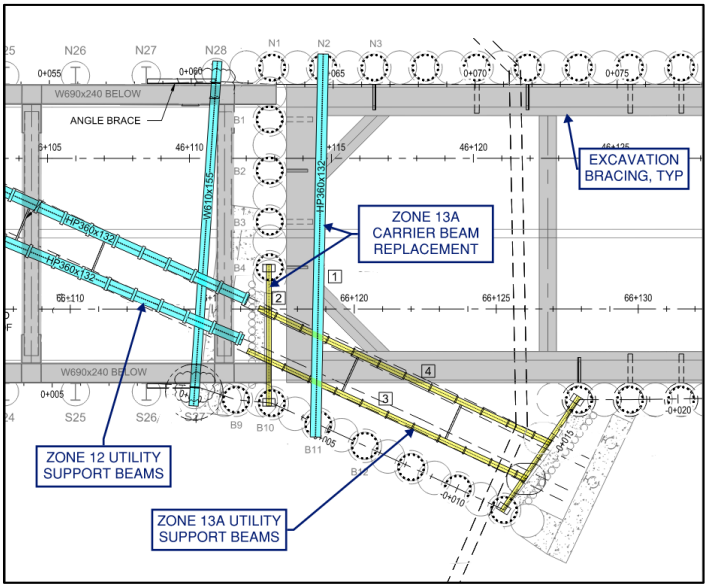


Fig. 8. Zone 12/13a utility support beam configuration and replacement (beams in yellow installed during Zone 13a work, beams in blue installed for Zone 12 work and the removal of the bulkhead).

CONSTRUCTION

Due to stringent schedule requirements, installation of the Zone 13a secant piles initiated prior to the issuance of the final design package. As a result, Contractor-driven adjustments to the design were common at the site and were integrated directly into the final design package. Refinements to the design included substituting member sizes based on Contractor supplies, adjustment to diaphragm slab configurations and 3-dimensional geometries, adjustment of sequencing based on logistical considerations, etc.

Overall, the construction of the utility zone for Zone 13a was successful with no visible water infiltration and no damage to the overlying utilities. The sequencing of the excavation and SOE installation was

 © Deep Foundations Institute 2025

paramount in the vicinity of the utilities, to ensure that utilities were properly protected and supported in place, and that the SOE systems were not overloaded during installation:

- The utilities were exposed using vacuum excavation methods prior to the installation of pipe piles and micropiles from surface, in order to reduce the risk of contact with the utilities. The pipe piles were all installed from surface once the utilities were visible and a physical barrier was installed to protect them from inadvertent damage. The tangent micropiles, which were not in conflict with the utilities, were also drilled from surface to allow for less low-clearance drilling.
- Upon daylighting, the electrical conduit was determined to be a cluster of five individual conduits, which were encased in a timber box structure to keep the electric bundle contained and reduce risk of damage to the lines. The electric and gas lines were then supported with straps to overlying carrier beams (as shown in Fig. 9).
- Once utilities were secure, excavation proceeded below the utilities to a depth identified by the design team to allow for clearance of the micropile equipment and installation of the Level 1 concrete diaphragm slab. The remaining micropiles were installed where utilities had previously impeded installation from the surface. During excavation, it was determined that the micropiles were not perfectly tangent, and a shotcrete facing was designed to ensure water-tight conditions between the micropiles. The shotcrete was designed to withstand groundwater pressures and seal gaps between piles.
- The Level 1 slab was poured prior to the installation of the internal frame, which then required significant shimming to ensure the required contact for load transfer. Based on the challenges on Level 1 installation, the Level 2 sequence was updated to have the bracing frame in place prior to the diaphragm slab pour, such that full contact was ensured.

Select construction photos are provided for the Zone 13a utility accommodation area (Figs. 9-11).



Fig. 9. Zone 13a utility accommodation area, during installation of utility support system, looking southeast in February 2022 (photo courtesy of KEV).

 © Deep Foundations Institute 2025



Fig. 10. Zone 13a utility accommodation area, during installation of the level 2 "U frame" with Level 1 and 2 diaphragm slabs installed, looking south in April 2022 (photo courtesy of Brierley).



Fig. 11. Zone 13a utility accommodation area, with Level 1 and 2 bracing and diaphragm slabs installed, looking southeast in May 2022 (photo courtesy of KEV).

During excavation below the design water table, it was determined that the water table in the vicinity of the bulkhead was lower than designed, and watertight components were able to be reduced. As the excavation of Zone 13a proceeded in advance of Zone 12, information gathered from the work on Zone 13a was able to be incorporated into the Zone 12 design. Most notably, observations of the ground conditions from the Zone 13a excavation allowed for the Zone 12 SOE to be optimized for better-than-anticipated soil conditions and a lower design groundwater table.

 © Deep Foundations Institute 2025

The removal of the Zone 12/13a bulkhead was successful through the ongoing collaboration between the Designers and Contractors. As noted above, the sequencing of the excavation and SOE installation was paramount in the vicinity of the utilities, to ensure that utilities were properly protected and supported in place, and that the SOE systems were not overloaded during excavation and strut installation. The utility support load was successfully transferred to the replacement carrier beam prior to removal of the bulkhead piles.



Fig. 12. Zone 13a utility accommodation area, during installation of the tunnel base slab, looking east in June 2022 (photo courtesy of KEV).

As of the date of publication, the installation of the permanent structure in Zones 12 & 13a has been completed and backfilled. The OLRT West Expansion is anticipated to be opened to the public in 2027.

SUMMARY AND CONCLUSIONS

This paper particularly focuses on the challenges encountered and solutions developed during the design and construction of a segment of the Parkway Cut-and-Cover tunnel, specifically Zones 12 and 13a. These zones presented unique site constraints including existing utilities, traffic sequencing, and soil conditions. The support of excavation (SOE) design for these zones had to consider the transition from free draining to watertight systems, and the accommodation of the existing utilities in the design was critical. The construction process involved iterative adjustments to the design based on site conditions and logistical considerations. Contractor-driven modifications were integrated into the final design, ensuring the successful execution of the project. Despite the complexities involved, the construction proceeded smoothly with minimal disruption, and the SOE systems effectively protected the surrounding environment and utilities.

Key lessons learned for the SOE design at this section of the project included: 1) tight logistical constraints on a site can drive the SOE design more than technical limits of the SOE and are critical to understand as early in a project or pursuit phase as possible, and 2) the importance of continual communication between the designer and Contractor to ensure that all components of the system were constructable and stable.

ACKNOWLEDGMENTS

The Kiewit-Eurovia-Vinci (KEV) team and Brierley would like to acknowledge the contributions of the SOE subcontractors for the two sites: Preco-MSE and Marathon Underground. The success of the project is due in large part to the strong communication channels established by KEV on the project, and the collaborative nature of the project team.

 © Deep Foundations Institute 2025

HIGHWAY 417 BRIDGE REPLACEMENTS REUSE OF EXISTING PILES STUDY

Tony Sangiuliano, P.Eng., MTO, Toronto, ON, Canada, 647-330-3743, Tony.J.Sangiuliano@ontario.ca
Nathan Bakker, P.Eng., Stantec, Ottawa, ON, Canada, 613-703-5104, Nathan.Bakker@stantec.com
Susan Ould-Brahim, Stantec, Ottawa, ON, Canada, 613-704-7293, Susan.Ould-Brahim@stantec.com
Gregory Louisy, P.Eng., Stantec, Ottawa, ON, Canada, 613-703-5982, Gregory.Louisy@stantec.com
Paul Carnaffan, P.Eng., Thurber, Ottawa, ON, Canada, 343-803-7738, pcarnaffan@thurber.ca

ABSTRACT

The Ministry of Transportation Ontario (MTO) is exploring reuse of existing piles to enhance traffic mobility, sustainability, and cost-effectiveness. Five bridges on Highway 417 in Ottawa, constructed between 1960–1968, are scheduled for replacement using rapid bridge replacement (RBR) techniques. This includes salvaging existing abutments and deep foundation elements where possible. A corrosion assessment was conducted involving soil sampling, in-situ investigations, and ultrasonic testing to evaluate the condition and longevity of steel H piles. Pile section loss and soil corrosivity were analyzed at the Richmond Road and Woodroffe Avenue sites. Based on the findings, site-specific corrosion rates were determined—0.015 mm/yr at Woodroffe and 0.007 mm/yr at Richmond—allowing for structural capacity validation and avoidance of unnecessary pile replacement. This paper demonstrates how supplementary corrosion testing can justify reuse of deep foundations and contribute to reduced costs, lower emissions, and shorter construction timelines.

Keywords: corrosion, pile reuse, foundation durability, bridge replacement, MTO, steel piles, ultrasonic testing

INTRODUCTION

Highway 417 Overpasses at Woodroffe Avenue, Maitland Avenue, Richmond Road and Pinecrest Avenue in the City of Ottawa, Ontario are scheduled for construction between 2026 and 2029. At all bridge locations, the existing superstructures and piers are to be replaced, utilizing rapid bridge replacement (RBR) techniques, while the abutments are to be rehabilitated.

The bridges were constructed between 1960 and 1968 and have a similar 2-span configuration, supported on perched abutments and a central pier. This paper describes the investigation procedure and engineering analysis to assess the feasibility of the reuse of existing piles at Woodroffe Avenue and Richmond Rd.

At Woodroffe Avenue and the NBL Richmond Rd, the reinforced concrete abutments are founded on two rows of BP14x73 (HP14x73/HP360x108) steel piles. The SBL Richmond Rd structure is founded on smaller BP12x53 (HP12x53/HP310x79) steel piles. The pier at Woodroffe is founded on spread footings. The piers at the NBL and SBL Richmond Rd structures are supported on three rows of BP14x73 steel piles (HP14x73/HP360x108) and BP12x53 steel piles (HP12x53/HP310x79), respectively. Widening of the Woodroffe structure is required and will consist of adding piles with extension of the reinforced concrete footings and abutments.

A comprehensive investigation, engineering and analyses were carried out to assess the capacity, integrity, durability, and service life of the existing piles. The investigation included chemical analyses of the soil and groundwater to determine the aggressivity of the subsurface conditions. Supplemental site investigations at Richmond Rd and Woodroffe Ave included exposing piles at the abutments to determine a corrosion rate to be utilized for the existing substructure deep foundation elements. A corrosion specialist was retained to conduct a visual inspection and to determine pile section losses.

 © Deep Foundations Institute 2025

BACKGROUND

Each of the bridges will be replaced using RBR with a two-span reinforced concrete slab-on-steel plate girder structure with an integral pier and semi-integral abutments. The new structures will maintain the existing overall span configuration, span lengths and skew. A reinforced concrete slab on steel plate girders is the proposed superstructure for both sites.

Subsurface Conditions

The subsurface conditions at each site were investigated using a phased approach. The first phase of the investigation included a detailed review of historical borehole data from investigations completed for the original bridge construction and nearby related facilities (e.g. sign supports structures and retaining walls) as well as the preliminary design phase of the current project. The second phase of the investigation consisted of a supplemental field investigation completed in summer 2023. The supplemental investigation included:

- Boreholes advanced into bedrock at select locations.
- Chemical analyses of soil samples for corrosivity parameters at regular depth intervals from boreholes adjacent to the existing piles (8 samples at Woodroffe Ave and 17 samples at Richmond Rd).
- Downhole geophysical (borehole magnetometer and vertical seismic profiling) testing to help assess pile length and the stratum at the pile tips at Richmond Road piers.

Richmond Road

The subsurface conditions at the Richmond Rd structure generally consist of embankment fill over interlayered clay, silt and sand deposits over limestone bedrock. Cobbles were noted within the overburden just above the bedrock in several boreholes. The bedrock surface elevation varies by over 20 m across the site.

The existing abutments are perched within approach embankments. The fill within the upper 2.3 to 5.3 m consists of the Richmond Rd pavement structure and granular fill consisting predominantly of sand to silty sand with varying amounts of gravel. The lower fill, extending to depths ranging from 6.9 to 9.9 m was variable and ranged from sand with silt to clayey silt.

Groundwater was measured in a piezometer behind the north abutment approximately 3 m below the top of Highway 417.

The results of analytical testing on 17 soil samples from the site are summarized in Table 1. Although the pH indicates a neutral to alkaline condition, the resistivity and chloride results indicate a moderately corrosive to very corrosive subsurface environment.

Table 1. Analytical Test Results – Richmond Rd

Site	Range	Median
pH	7.4 to 8.5	7.8
Resistivity (Ω·cm)	170 to 1460	450
Chloride (µg/g)	337 to 3540	1200

Woodroffe Avenue

The subsurface conditions at the Woodroffe Ave structure generally consist of fill overlying relatively thin clay and glacial till deposits which are underlain by limestone bedrock. Bedrock was proven by

 © Deep Foundations Institute 2025

coring at ten borehole locations and consisted of strong limestone. The bedrock is approximately 3.7 m below the top of pavement on Hwy 417 and 10 m below the top of pavement of Woodroffe Avenue.

Groundwater was measured in a piezometer to be approximately at the bedrock surface.

The existing abutments are perched within approach embankments. The fill within the upper 2.6 to 4.5 m consists of the Woodroffe Ave pavement structure and granular fill consisting predominantly of sand to silty sand with varying amounts of gravel. The lower fill, extending to depths ranging from 6.1 m to greater than 10 m was variable and ranged from sand with clay to sandy silty clay. Concrete debris was encountered within the lower fill in two boreholes. Where the fill extends deeper than about 7 m, it is likely associated with an abandoned sewer trench.

The results of analytical testing on 9 soil samples from the site are summarized in Table 2. Although the pH indicates a neutral to alkaline condition, the resistivity and chloride results typically indicate a moderately to very corrosive subsurface environment.

Table 2. Analytical Test Results – Woodroffe Ave

Site	Range	Median
pH	7.4 to 7.8	7.6
Resistivity (Ω·cm)	570 to 1950	1025
Chloride (µg/g)	210 to 1050	468

Downhole Geophysical Testing

Downhole geophysical (borehole magnetometer and vertical seismic profiling) testing was carried out in PVC casings installed within boreholes advanced adjacent to piles supporting the piers of the Richmond Rd structure to help assess pile length and the stratum at the pile tips. The casings were installed to a depth of approximately 5 m into bedrock within boreholes adjacent to the end piles on the east and west sides of the middle pier. Both borehole magnetometer testing and seismic down-hole testing were carried out in both casings. In both boreholes, the resolution was not high enough to determine if the piles reached the bedrock surface. Table 3 summarizes the depths below ground surface to the bedrock surface based on the borehole data and the estimated pile length based on the magnetometer testing. In both cases, the estimated pile length is 800 to 900 mm above the bedrock surface, suggesting that the piles reached refusal within cobbles above the bedrock surface.

Table 3. Bedrock Depth and Estimated Pile Length

Borehole	Bedrock Surface	Pile Depth
39-23-01	19.8 m	18.9 m
39-23-02	24.6 m	23.8 m

Downhole geophysical testing was not conducted at Woodroffe Avenue as there are no deep foundation elements at the pier and there was less concern of achieving the design pile length with relatively shallow bedrock depths and loose to compact overburden.

CORROSION ANALYSIS AND IMPACTS ALTERNATIVES

Initial Recommended Corrosion Rates

Based on the groundwater levels measured at the bridge sites, most of the length of the existing abutment piles are above the water table. Due to the low resistivity and high chloride content, there can be an expectation of section loss above the groundwater level. CALTRANs suggests a section loss rate per side

of pile of 0.025 mm/year is appropriate for piles in potentially corrosive soils whereas Eurocode and BS8002-1994 recommends a rate of 0.015 mm/year. This corrosion rate range (0.015 mm/yr to 0.025 mm/yr) was used for design and evaluation of the piles.

Pile Capacity

The reuse of existing piles needs to consider both the geotechnical and structural capacity of the piles. A structural and seismic evaluation of the existing piles at Woodroffe Ave under the proposed replacement bridge superstructure was performed according to the Canadian Highway Bridge Design Code CAN/CSA S6-19 (CHBDC) and Commentary CSA S6-19.1 (evaluations for the Richmond Rd structures have not yet been conducted). The objective of the evaluation was to determine whether the existing abutment piles have sufficient capacity to resist maximum loading from the new bridge superstructure for a 75-year service life.

Factored Structural Capacity

The structural capacity is significantly impacted by section loss due to corrosion. The impact of the section loss on pile capacity was assessed for the previous 65 years and the future 75 years following the bridge replacement. It was found that the performance criteria from Section 4 of the CHBDC could not be met with the existing piles at all sites for corrosion rates in excess of 0.015 mm/yr.

For a corrosion rate of 0.015 mm/yr, the factored structural resistance for each pile applying the resistance factor from section 6.11.4.4 of the CHBDC is shown in Table 4, assuming steel strength of 230 MPa.

Table 4. Structural Capacity of Piles using 0.015 mm/yr Corrosion Rate

Level of Corrosion	Factored Pile Resistance [kN]	
	HP360x108	HP310x79
No pile corrosion/section loss (1960 construction)	1585	1110
15% section loss (2024: 64 years of age)	1345	895
33% section loss (2101: 75-year design life)	1060	665

Geotechnical Capacity

The original drawings for the Woodroffe Avenue structure indicate that the piles were to be driven “into sound limestone bedrock to provide a minimum design load capacity of 60 tons” (600 kN).

The original drawings for the Richmond Road structure indicate that the piles were “to be driven to refusal in bedrock as directed by the engineer”. The original geotechnical report from 1966 recommended that “the bridge piers and abutments be supported on end-bearing piles driven to bedrock” and indicated that 14 BP 74 (HP 360x108) may be designed for 90 tons per pile (approximately 900 kN).

The factored geotechnical resistances of the existing piles at both sites are shown in Table 5. The factored geotechnical resistance for the piles at Richmond Road account for the potential that the piles did not reach the bedrock surface, as indicated by the downhole geophysical testing.

 © Deep Foundations Institute 2025

The geotechnical resistances for piles driven to bedrock provided in the original geotechnical reports are conservative compared to the factored axial geotechnical resistance at ultimate limit states (ULS) provided by current design methods. The geotechnical axial resistance is not impacted by corrosion of the piles**.** For piles end-bearing on hard, strong to very strong bedrock, the factored axial geotechnical resistance will generally be greater than the structural capacity of the pile.

Table 5. Factored Geotechnical Resistance of Existing Piles

Site	Pile Size	Pile Length	Factored Axial Geotechnical Resistance	
		[m]	ULS [kN]	SLS [kN]
Woodroffe	HP 360x108	7.3 to 8.5	1,600	> 1,600
Richmond	HP 360x108	<20	1,000	800
		≥20	1,400	1,200
	HP 310x79	<20	1,000	800
		≥20	1,200	1,000

PILE CORROSION INVESTIGATION

Based on the outcome of the pile evaluation, a corrosion rate greater than 0.015 mm/yr would necessitate the addition of supplemental deep foundation elements. Feasible alternatives included localized widening of the abutments involving the addition of approximately 4 to 6 piles on each side of the abutment (assuming a corrosion rate less than 0.025mm/yr). A supplemental site investigation was conducted at both Woodroffe Ave and Richmond Rd to determine site specific corrosion rates that could be utilized for further refinement of the anticipated structural capacity of the piles.

Excavation and Exposure of Piles

The MTO retained a contractor to complete the localized excavation and pile exposure at the investigation sites. The work included localized removal of vegetation and tree clearing, excavation along the wingwalls in conjunction with a trench box installation, hydrovac exposure of the piles, abrasive blast cleaning of the piles, placement of unshrinkable fill following completion of pile inspection, backfill and site restoration.

Three piles were partially exposed at each site, under the southwest wingwall at Woodroffe Ave and under the southeast wingwall at Richmond Rd. The wingwall locations were selected due to site access considerations, to minimize required traffic control and minimize restoration requirements. The depth of the excavation below the pile cap was limited to 1.5 m and the front face and sides of the piles were exposed, to minimize undermining of the pile cap and not impact the integrity of the abutment and roadway fills. The work commenced on October 21, 2024, with pile inspection undertaken on October 30, and site restoration was completed by November 21, 2024. The Richmond Rd. excavation is shown in Fig. 1.

Due to tight space restrictions and spacing of the piles, some faces of the exposed pile were difficult to access and clean. The faces that were exposed and sand blasted are highlighted in red in Fig. 2.

 © Deep Foundations Institute 2025



Fig. 1. Richmond Road pile excavation and trench box

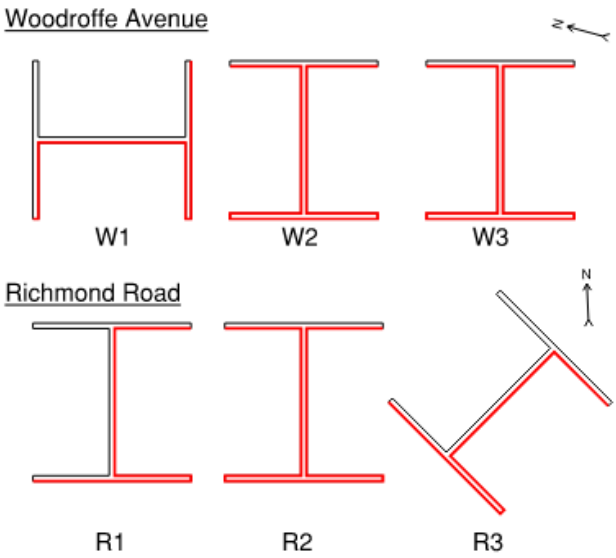


Fig. 2. Pile faces available for inspection

Visual Observations

Before abrasive blast cleaning, black and red-orange corrosion byproducts were observed with intact mill scale observed at several locations. Photos of Pile W3 before and after abrasive blast cleaning are shown in Fig. 3.

From visual observation, the type of corrosion observed on the piles can be classified as pitting corrosion. There are portions of the exposed piles at both sites where minimal corrosion was observed, however there are widespread areas on both the flanges and webs where pitting corrosion was noted. Some areas of localized severe section loss at the edges of the flanges (“flange thinning”) were observed at both sites.

 © Deep Foundations Institute 2025

Pitting Corrosion

Once the piles were exposed and cleaned, a corrosion specialist conducted visual and ultrasonic testing of the exposed steel piles. The inspection purpose was to determine the nominal thickness and damage to the piles over time due to corrosion.



Fig. 3. Pre-blasting and post-blasting photographs of pile W3 at Woodroffe site

Nominal Thickness and Pitting Depths

Pitting depth measurements were taken utilizing ultrasonic testing (UT) in addition to an external pit gauge. A portable grinder was used to prepare the steel for testing in some locations where abrasive blast cleaning could not reach to allow for more accurate UT readings. On each section of a pile (web and each flange), the depth of the deepest pit was measured using a caliper. UT testing was performed to measure the nominal thickness and the lowest thickness that could be found on a 'best effort' basis. Table 6 summarizes the data obtained during their investigation.

Table 6. Average Deepest Pits

Site	Pile	Average Deepest Pit [mm]
Woodroffe	W1	8.21
	W2	6.54
	W3	5.82
Richmond	R1	4.36
	R2	5.58
	R3	4.09

For Woodroffe Ave, the worst pit depths ranged from 25.6% to 99.8% of the overall web or flange thickness. For Richmond Rd, the worst pit depths ranged from 28.8% to 41.1% of the overall web or flange thickness. There were no full penetration holes at either site, but Pile W1 had one pit that was nearly the full depth of the web thickness (representing approximately 10% of the web area). Only pile W2 at Woodroffe Ave had full-penetration flange loss with a width of 12.7 mm.

Pitting Rates

The calculated corrosion rates are within the areas of pitting corrosion. For both locations, pitting corrosion rates were developed using the averages for the deepest corrosion pitting for each pile and the

 © Deep Foundations Institute 2025

age of the piles, assuming a constant corrosion rate. At the Woodroffe site, the calculated pitting corrosion rates range from 0.09 mm/yr to 0.13 mm/yr with an average of 0.11 mm/yr. At the Richmond site, the pitting corrosion rate ranged from 0.06 mm/yr to 0.09 mm/yr with an average of 0.07 mm/yr. Table 7 summarizes the pitting corrosion rate calculations.

Table 7. Pitting Corrosion Rates

Site	Pile	Pitting Corrosion Rate [mm/yr]	Average Pitting Corrosion Rate [mm/yr]
Woodroffe	W1	0.13	0.11
	W2	0.10	
	W3	0.09	
Richmond	R1	0.07	0.07
	R2	0.09	
	R3	0.06	

Soil Grab Samples

Soil samples were taken at each of the exposed pile locations: 3 at Woodroffe Ave. and 3 at Richmond Rd. Similar to the borehole samples, the samples were tested for pH, soil resistivity and chloride content. The results are presented in Table 8.

Table 8. Analytical Test Results

Site	Parameter	Range	Median
Woodroffe	pH	7.5 to 8.1	7.8
	Resistivity (Ω cm)	150 to 1480	653
	Chloride (µg/g)	66 to 2000	1285
Richmond	pH	7.5 to 8.1	7.7
	Resistivity (Ω cm)	750 to 1720	1150
	Chloride (µg/g)	164 to 267	218

The analytical test results from the grab samples taken from immediately adjacent to the exposed piles were similar to the results from the samples from the boreholes. Although the pH indicates a neutral to alkaline condition, the resistivity and chloride results indicate a mildly corrosive to very corrosive subsurface environment at both sites.

SECTION LOSS ANALYSIS

Currently, there is no widely accepted method of predicting pile corrosion. Most research previously performed on metal corrosion in soil has focused on the degradation of buried pipelines or tanks for which pitting corrosion would represent a functional failure if perforation (or excessive localized thinning) in a wall were to occur. For steel piles, the principal concern is the loss of material (cross-sectional area) presenting a structural risk: compromising the pile's ability to resist axial, shear, and bending loads (Romanoff 1957).

Deterioration Mapping

To estimate the cross-sectional area loss of the piles due to the pits and the flange thinning, qualitative observations and photographs from the inspection were used to determine an appropriate surface area upon which pits are occurring. Photographs of each pile were studied, and an estimate of the intensity (number of pits per square metre) and the average surface area of each pit were determined for regions of

 © Deep Foundations Institute 2025

varying severity of pits on each pile. This information was consolidated into a deterioration map for each exposed face of the piles, as presented in Fig. 4.

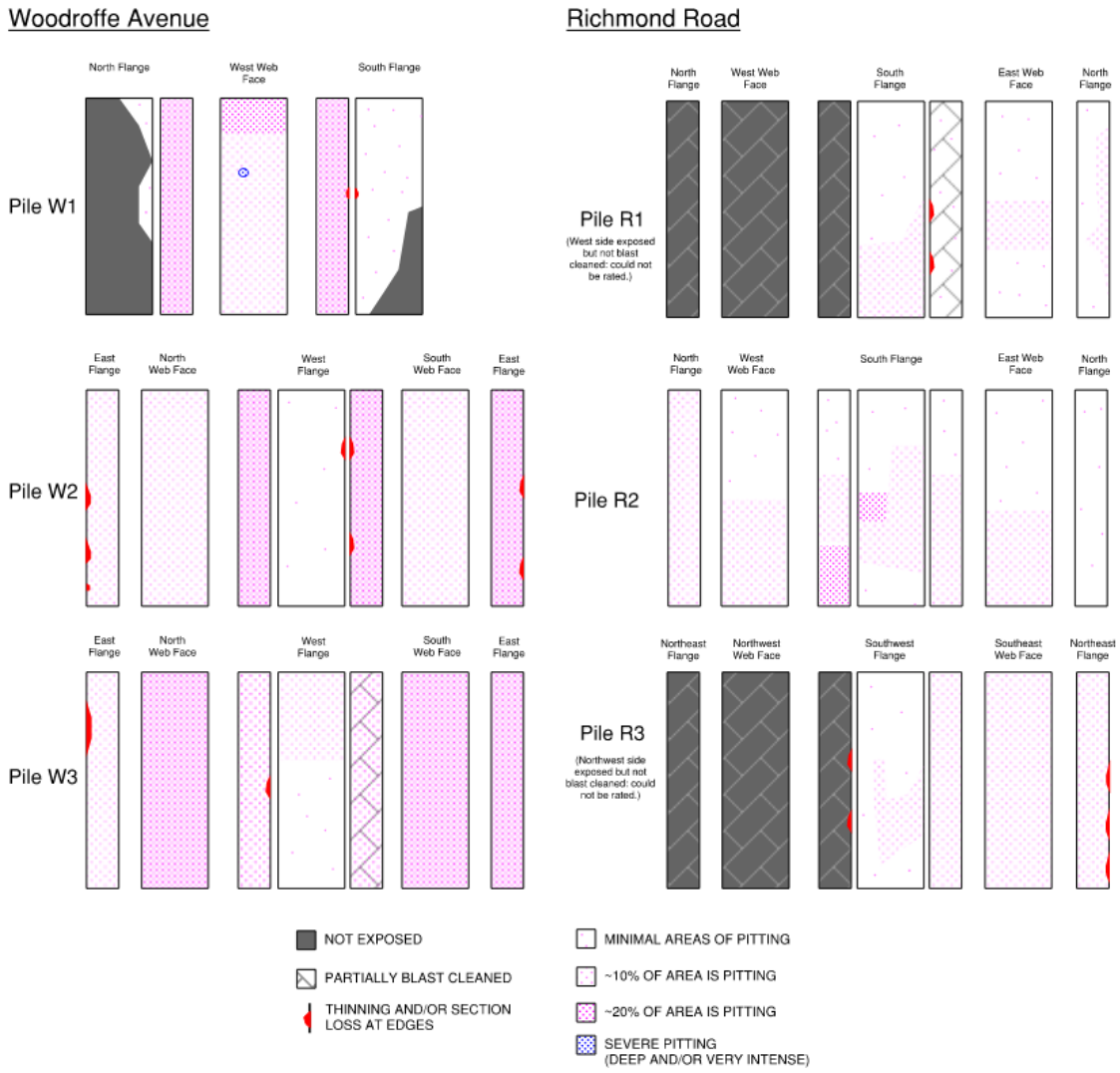


Fig. 4 Deterioration mapping for exposed faces of piles

Cross-Sectional Area Loss

Using the deterioration mapping, a conservative estimate of the percent area of the exposed pile experiencing pitting corrosion was determined using Equation 1,

$$\frac{SA_{pitting}}{SA_{total}} = \sum I_{pit,i} \cdot \overline{SA}_{pit,i} \cdot \frac{SA_i}{SA_{total}} , \quad [1]$$

where $SA_{pitting}$ is the total area experiencing pitting corrosion, SA_{total} is the total surface area of the pile, $I_{pit,i}$ is the intensity of pits in the region under study, $\overline{SA}_{pit,i}$ is the average surface area of one pit in the region under study, and SA_i is the total surface area of the region under study.

 © Deep Foundations Institute 2025

To estimate the total section loss due to the flange thinning, it was conservatively assumed that the width of each flange was reduced by the full 1 inch (12.7 mm) observed on the Woodroffe W2 pile. The total cross-sectional area loss for each pile was then calculated using Equation 2,

$$A_{combined} = \frac{SA_{pitting}}{SA_{total}} \cdot \bar{d} \cdot P_{pile} + 2t_f \cdot b_{loss} \, , \qquad [2]$$

where $A_{combined}$ is the total cross-sectional area loss for each pile, $\bar{d}$ is the average of the three deepest pits as measured by the corrosion specialist, P_{pile} is the theoretical pile perimeter, t_f is the flange thickness, and b_{loss} is the flange width loss due to corrosion.

Average Site Corrosion Rate

The average site corrosion rate for each of the two sites (Woodroffe and Richmond) was then calculated considering the age of the piles at the time of the investigation (in years) using Equation 3,

$$\bar{r}_{site} = \frac{1}{3} \sum \frac{A_{combined,i}}{N \cdot P_{pile,i}} \, , \qquad [3]$$

where $\bar{r}_{site}$ is the average site corrosion rate, $A_{combined,i}$ is the total cross-sectional area loss for each pile at the site, N is the age of each pile in years, and P_{pile} is the theoretical pile perimeter for each pile at the site. Table 9 summarizes the average site corrosion rates.

Table 9. Section Loss Analysis

Site	Pile	Percent area of pitting corrosion [%]	Cross-Sectional Area Loss [mm^2]	Average Site Corrosion Rate [mm/yr]
Woodroffe	W1	10%	2131	0.015
	W2	11%	1841	
	W3	15%	2149	
Richmond	R1	5%	793	0.007
	R2	5%	948	
	R3	10%	1203	

The corrosion rates above were calculated assuming a uniform rate since the time of construction (i.e. a linear relationship between thickness and time). Research suggests, however, that corrosion is generally nonlinear, and the rate decreases over time due to the depletion of oxygen and the build-up of corrosion products that form a protective layer. Corrosion measurements over a 14-year period on bare steel piling supporting a bridge deck pier showed an initial corrosion rate of approximately 0.010 mm/yr decreased to 0.001 mm/yr after 14 years (Escalante 1990). Romanoff (1957) also noted that in well-aerated soils, the rate of pitting corrosion falls off rapidly from initial rates and postulated a nonlinear law for localized pitting corrosion. Therefore, a linear rate represents a conservative prediction for future corrosion.

Current Condition

The average cross-sectional area loss was further used to provide insight into the present condition of the piles. Using the nominal area for HP360x108 and a calculated cross-sectional area for Woodroffe pile W1 (which is larger than what was presented on the design drawings), the percent area loss for each site was determined. Table 10 summarizes the present conditions of the piles.

 © Deep Foundations Institute 2025

Table 10. Present Condition of Piles

Site	Pile	Nominal Cross-Sectional Area of Pile [mm^2]	Cross-Sectional Area Loss of Pile [mm^2]	Site Cross-Sectional Area Loss [%]
Woodroffe	W1	14414	2131	14.6
	W2	13800	1841	
	W3	13800	2149	
Richmond	R1	13800	793	7.11
	R2	13800	948	
	R3	13800	1203	

Benefit Cost of Supplementary Corrosion Assessment

The costs for completion of the supplementary corrosion assessment was approximately $400,000, which included the costs for exposure of the piles at both sites, site restoration, in addition to the engineering fees associated with the site measurements, corrosion assessment, field sampling and testing and associated reporting.

The projected construction cost savings as a direct result of the outcome of the supplementary corrosion assessment, is conservatively estimated at $1.65M. This value represents the anticipated costs for the addition of supplementary piles at the abutments in addition to required abutment modifications. These costs do not include costs associated with construction staging nor does it factor in the additional costs associated with increased construction duration.

CONCLUSIONS

The type of corrosion observed on the piles is classified as pitting corrosion. A novel method was developed and utilized to calculate an average site corrosion rate for the existing H-piles of 0.015 mm/yr and 0.007 mm/yr at Woodroffe Avenue and Richmond Road, respectively.

The use of a corrosion rate of 0.015mm/yr per pile surface is therefore deemed appropriate for use at the bridge sites included in this assignment. Although pile exposure was not conducted at the Pinecrest Avenue and Maitland Avenue sites, there are many similarities between the structures, including subsurface conditions, soil corrosivity results and environmental exposures; it is reasonable that the design team can anticipate similar pile performance at all sites. The selected corrosion rate of 0.015 mm/yr represents a conservative estimate. The results of the investigation correlate well with the lower bound corrosion rates identified within published literature.

From the results of the soil testing, it is evident that there is variability in the soil corrosivity results; however, in general, the soils can be classified as ‘moderately corrosive to very corrosive environment’ at Woodroffe and a ‘very corrosive environment’ at Richmond Road. The observed corrosion at Woodroffe would suggest that the soil conditions are more corrosive at that site, but the extent of corrosion could be due to other factors, including the limits of disturbance of soils within the upper regions of the pile and associated presence of oxygen. In general terms, the results of the soil testing correlate well with the observed condition.

As a direct result of the in-situ corrosion investigations, the design team was able to validate the predicted service life of the structure, with an anticipated additional 75 years of service of the deep foundation

elements. This allows the Ministry to salvage the abutments and deep foundation resulting in several benefits such as significant cost savings of more than $1.25M, lower impacts to public with reduced construction duration and reduced carbon emissions.

This project is demonstrative of the Ministry's commitment to strategic investments for overall net benefit to public, in addition to continued desire to exploring new approaches to encourage the reuse of existing foundations.

REFERENCES

Decker, J.B., Rollins, K.M. and Ellsworth J.C. 2008. Corrosion Rate Evaluation and Prediction for Piles Based on Long-Term Field Performance, *Journal of Geotechnical and Geoenvironmental Engineering*, ASCE, 134(3), 341-351.

Escalante, E. 1990. Measuring the Corrosion of Metals in Soil, *Corrosion Testing and Evaluation: Silver Anniversary Volume, ASTM STP 1000*, American Society for Testing and Materials, Philadelphia, USA: 112-124.

Romanoff, M. 1957. *Underground Corrosion*, National Bureau of Standards Circular 579, Washington D.C., USA: 9-14.

 © Deep Foundations Institute 2025

EVALUATION OF PILES' ULTIMATE CAPACITY UTILIZING DIRECT CPT METHODS CONSIDERING CONSOLIDATION AND AGING SETUP

Murad Y. Abu-Farsakh, Ph.D., P.E., F.ASCE, Research Professor, Louisiana Transportation Research Center, Louisiana State University, Baton Rouge, Louisiana, USA, Email: cefars@lsu.edu
Isam A. Khasib, Ph.D. Student, Department of Civil and Environmental Engineering, Louisiana State University, Baton Rouge, Louisiana, USA.

ABSTRACT

The work described herein estimates the axial pile capacity subjected to consolidation setup and aging. Two models were developed for clay and sand to estimate aging setup based on the data collected from the literature where piles have been tested at different times after the excess pore pressure dissipation. One model for clay was developed based on Louisiana database comprising 10 instrumented piles to quantify the consolidation setup. A separation before and after excess pore water pressure indicates that aging takes place after the excess pore water pressure. The best 8 direct CPT methods evaluated by previous researchers were used in this study. The results indicate that the CPT methods were capable of estimating side capacity considering consolidation setup (more than or less than 14 days) without any modification. Regarding Aging, the results show that all pile CPT methods evaluated underestimate the pile capacity and the accuracy of these methods increases by applying the aging databases for both sand and clays.

Keywords: Consolidation setup, Aging, Cone penetration test (CPT), Pile resistance, Direct CPT methods.

INTRODUCTION

Piles driven into soils typically experience an increase in resistance over time, known as pile "setup" or "freeze," primarily affecting side resistance. Researchers have developed models to predict pile resistance at specific time intervals post-driving and integrate setup effects into design. Komurka et al. (2003) classify pile setup into three phases: logarithmic nonlinear, logarithmic linear, and aging (Fig. 1). Initially, due to soil disturbance, excess pore water pressure (PWP) dissipation follows a nonlinear log-time pattern, influenced by soil properties and pile characteristics. Over time, PWP dissipation transitions to a linear log-time rate, aligning with pile setup rate. The point at which this shift occurs is termed of initial time, t_0, in empirical models. The third phase of pile setup, aging, occurs independently of effective stresses and involves time-dependent changes in soil properties under constant stress. Factors such as thixotropy, secondary compression, particle interference, and clay dispersion contribute to this phenomenon. Schmertmann (1991) noted that aging is more pronounced in soils with high organic content due to secondary compression. During this phase, the surrounding soil's shear strength, stiffness, and interface friction angle with the pile increases, while soil compressibility decreases.

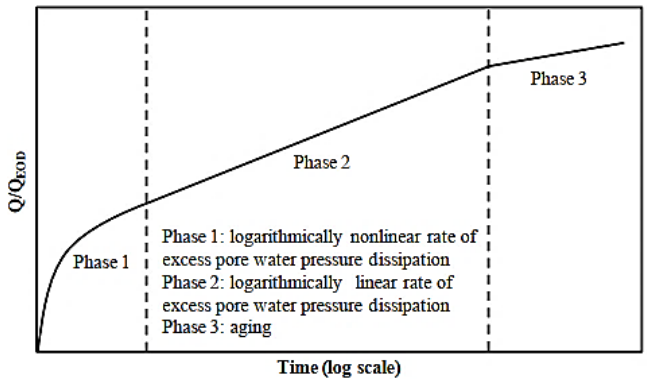


Fig. 1. Three phases of pile setup (Haque 2015)

 © Deep Foundations Institute 2025

In Louisiana, pile design typically relies on load tests conducted 14 days after installation, disregarding long-term setup effects, resulting in conservative designs. However, consolidation and aging related resistance gains are expected to extend the service life of superstructures and enable the reuse of existing pile foundations. A key challenge is accurately estimating the additional resistance mobilized over decades. Since pile evaluation long after installation is necessary, the 14-day testing standard may not be ideal. This study focuses on aging effects, where pile resistance continues to increase beyond the consolidation phase after excess pore water dissipation.

Tavenas and Audy (1972) provided the first well-documented case of aging in cohesionless soils. Initially, setup effects were attributed to both tip and shaft resistance, but recent studies suggest that only shaft resistance contributes significantly, with minimal impact on the tip (Attar and Fakharian 2013). While consolidation and aging setups may occur concurrently, they are distinct processes. During reconsolidation, excess pore water pressure dissipation primarily governs strength recovery, making aging effects negligible. In contrast, aging setup becomes dominant once reconsolidation is complete. To simplify analysis, researchers, including Gong et al. (2020), assume that aging occurs only after consolidation setup.

Most of the previous studies on pile setup have proposed the following correlation between pile/soil setup effect and the elapsed time, t, for the linear logarithmic phase 2:

$$\frac{Q}{Q_0} = A \times \log\left(\frac{t}{t_0}\right) + 1 \quad (1)$$

where Q/Q_0 = ratio of pile resistance at time t to pile resistance at initial reference time, t_0; t/t_0 = ratio of elapsed time to the initial reference time from the end of drive; and A = setup parameter.

The logarithmic setup parameter (A) in Equation 1 varies based on factors such as soil type, pile type, material, size, and overall pile resistance. Skov and Denver (1988) recommended values of $A = 0.2$ for sand and $A = 0.6$ for clay, with reference times, $t_0 = 0.5$ days for sand *1* day for clay.

This study evaluates the increase in axial pile resistance due to consolidation and aging effects. To achieve this, data from 10 instrumented test piles for consolidation setup and 26 test piles for long-term aging were collected from literature. Models were developed to assess resistance changes over time for each effect. The study utilizes the top eight pile-CPT methods from a previous study to estimate pile resistance at 14 days post-driving as a reference. The developed models were then applied to extrapolate/interpolate resistance at the end of consolidation and for long-term aging. The estimated values were compared with field-measured resistance for validation.

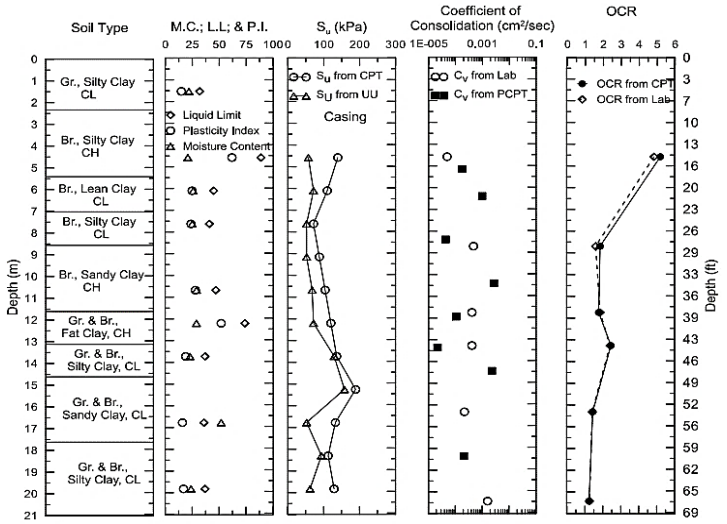
COLLECTED DATABASE FOR SETUP IN LOUISIANA

Abu-Farsakh et al. (2016) conducted a comprehensive study to estimate the magnitude of setup and setup parameter (A) by analyzing the increase in side resistance across individual soil layers. The study focused on four project sites in Louisiana, Bayou Lacassine, Bayou Boeuf, Bayou Zourie, and LA-1, using 10 fully instrumented precast concrete test piles (Table 1). Of these, six piles were tested at the LA-1 site, two at Bayou Lacassine, one at Bayou Zourie, and one at Bayou Boeuf. The piles were equipped with strain gauges, pressure cells, and piezometers to monitor resistance changes, with additional multilevel piezometers installed in the surrounding soil.

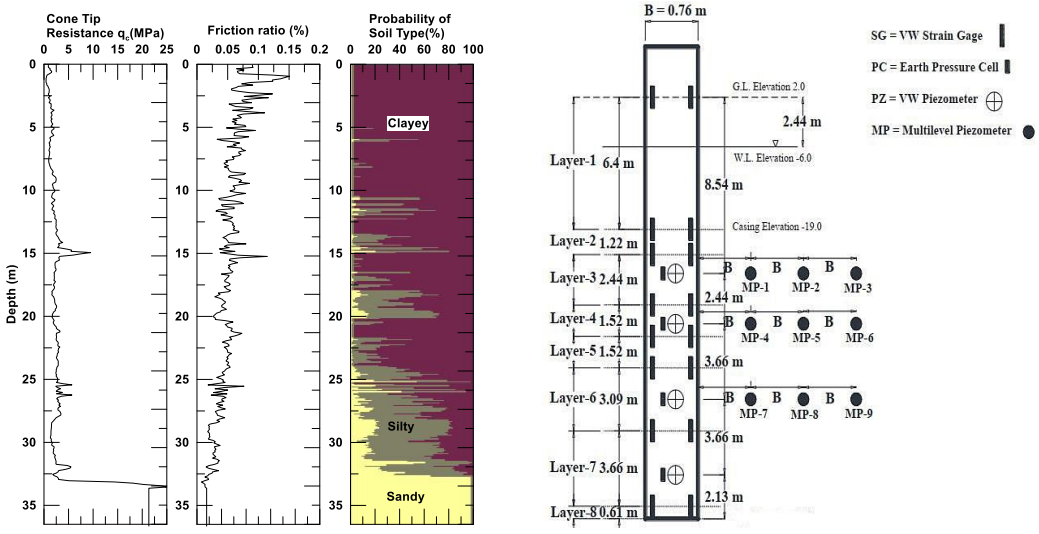
The subsurface conditions at the four Louisiana sites were evaluated through extensive laboratory and in-situ testing. Laboratory tests on 3-inch (76 mm) Shelby tube samples included Atterberg limits, soil classification, water content, unit weight, UU triaxial, and one-dimensional consolidation tests. In-situ testing involved SPT during soil boring and CPT near test piles. Figure 2a presents an example of soil profile and properties for the Bayou Lacassine BL3 test pile. The CPT results, including cone tip resistance (q_c) and friction ratio (R_x), along with probabilistic CPT soil classification, are shown in Fig. 2b. The instrumentation plan (Fig. 2c) featured strain gauges, earth pressure cells, and piezometers on the pile face and surrounding soil. The unit side resistance for BL3 was calculated across seven soil layers using strain gauge data.

Table 1. Database of the 10 instrumented test piles

Project Name	Pile ID	Width, in (mm)	Embedded length, ft. (m)	Scour elevation, ft. (m)
Bayou Lacassine	BL-1	30 (762)	67 (20.4)	21 (6.4)
	BL-3	30 (762)	67 (20.4)	21 (6.4)
Bayou Zourie	BZ	24 (610)	51 (15.5)	20 (6.1)
Bayou Boeuf	BB3	30 (762)	130 (39.6)	6 (1.8)
LA-1	LA1-2	16 (406)	120 (36.6)	-
	LA1-3	30 (762)	180 (54.9)	70 (21.3)
	LA1-4a	24 (610)	150 (45.7)	-
	LA1-4b	24 (610)	201 (61.3)	-
	LA1-5a	24 (610)	139 (42.4)	-
	LA1-5b	24 (610)	160 (49.7)	-



(a)



(b) **(c)**

Fig. 2. Bayou Lacassine test pile BL3: (a) Soil profile and properties, (b) CPT data and CPT soil classification, and (c) Instrumentation plan

 © Deep Foundations Institute 2025

This study examined setup in both clay and sandy soil layers, with the focus on clay due to its higher setup magnitude. Sandy layers exhibited minimal setup. Piezometers installed on the pile faces and surrounding soils measured excess pore pressure over time, allowing differentiation between consolidation setup, thixotropy, and aging setup. However, pile load test data for different soil layers at Bayou Bouef were unavailable due to the use of the O-Cell test, limiting the study to nine instrumented piles. Side resistance measurements from clay layers were tracked until the completion of excess pore pressure dissipation, defining consolidation setup. Additional resistance beyond this phase was attributed to aging setup. Dissipation times varied, with LA-1 site piles averaging 7 days (13 days for LA1-3), Bayou Zourie reaching 77 days, and Bayou Lacassine piles requiring 13 to 29 days. Using a logarithmic time scale, pile resistances were plotted against time, and the consolidation setup factor (*Ac*) was determined (Fig. 3). Due to the short dissipation time in sandy layers, all setup data for sand were included in the aging database. This separation aimed to quantify the long-term contribution of both consolidation and aging setups to pile side resistance. The normalized resistance values showed a clear trend over time, with an average *Ac* value of 0.53. This correlation is essential for estimating the side resistance increases in clay layers up to the end of consolidation setup.

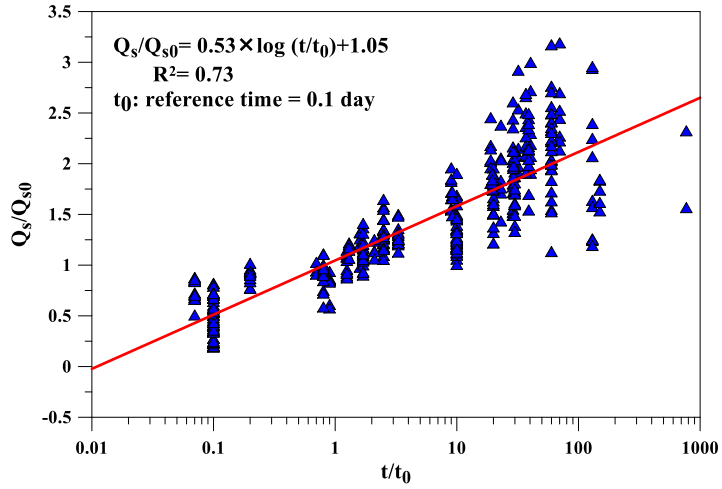


Fig. 3. Louisiana database for consolidation setup

COLLECTED DATABASE FOR AGING SETUP

Research on the increase in pile resistance due to aging effects is limited. This study compiled 17 case studies as shown in Table 2 that examined pile aging in both sand and clay soils. The tested piles varied in material - precast concrete, steel, or wood - with diameters range from 4 to 30 inches and lengths range from 16 to 230 feet. These studies involved multiple load tests on individual piles. To ensure reliability, aging setup data, particularly for clay soils, were collected based on known excess pore water pressure (PWP) values and available pile load test results conducted at or beyond the completion of PWP dissipation.

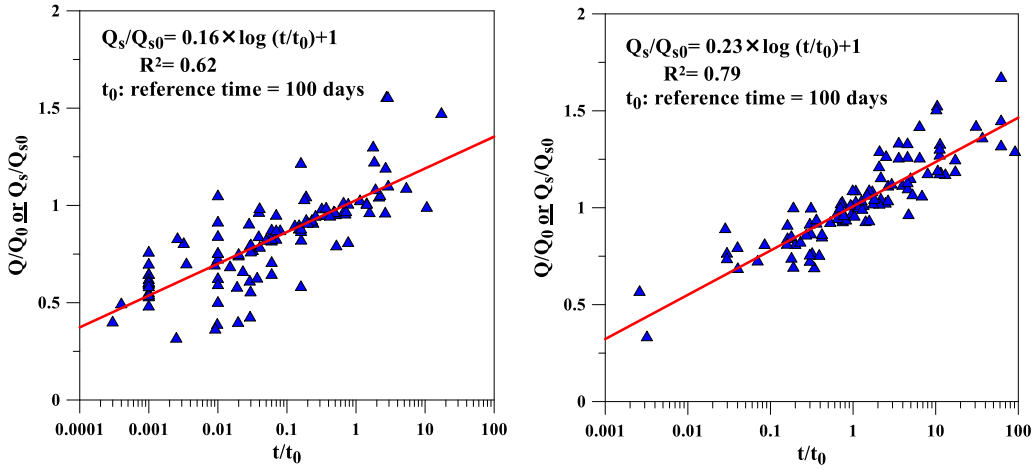
The normalized aging database (Q_s/Q_{s0} or Q/Q_0) was plotted against the logarithmic time ratio (t/t_0), with results shown in Figs. 4a and 4b for clay and sand layers, respectively. Despite variations in loading histories across the 17 case studies, most piles exhibited a similar trend of increasing resistance over time in clay soils (Fig. 4a). An exception was noted in a large-diameter pile at West Delta, Gulf of Mexico, where side resistance decreased by 3.5% after a year due to reduced long-term radial stresses around the shaft (Chan and Birrell, 1998). In sandy soils, pile side resistance followed a logarithmic increase over time, though some cases showed resistance reductions at later stages, resulting in a lower R^2 value (0.62). This decline may be attributed to aging process disturbances in cohesionless particles due to repeated load testing, leading to a reduction in the interface friction angle.

 © Deep Foundations Institute 2025

Table 2 Summary of aging setup database from 17 case studies

Site	Soil type	Pile material	Pile diameter/ width (inch)	# of pile load tests
Cowden	Clay	Steel/open ended	18	4
Canons park	Clay	Steel/closed ended	7	15
Houston	Clay	Steel/closed ended	11	3
Nitsund	Clay	Timber	7	10
Drammen	Clay	Timber	10	3
Ska-Edeby	Clay	Timber	4	17
Belfast	Clay	PPC	10	7
Haga	Clay	Steel/closed ended	6	6
Bothkennar	Clay	PPC	4	2
Buckman Bridge	Sand	PPC	18	4
Aucilla River	Sand & clay	PPC	18	10 clay; 6 sand
Vilano Bridge East	Sand & clay	PPC	18	3 clay; 4 sand
Vilano Bridge West	Sand & clay	PPC	18	6 clay; 4 sand
Seabreeze Bridge	Sand & clay	PPC	18	5 clay; 6 sand
West Delta	Clay	Steel/open ended	30	2
Bayou Zourie	Sand	PPC	24	2
Bayou Lacassine	Clay	PPC	30	9
Bayou Teche	Sand	PPC	24	3
LA-1	Sand	PPC		25
Alberta	Sand	H-Steel	HP (12.20× 3.1)	2
Hamburg	Sand	PPC	14	4
Alborg	Sand	PPC	10	3
Stockholm	Sand	PPC	10	13
New York	Glacial Sand	Steel/monotube	14	30
Victoria	Sand	PPC	18	2
Dunkirk	Sand	Steel/open ended	12	4

A reference time of 100 days was used for both sand and clay soils, consistent with prior research on pile aging effects. This choice aligns with the typical duration of excess pore water pressure dissipation, as measured by various methods, including piezometers. It is important to note that the aging setup parameter (A_g) and initial resistance (Q_0) vary with changes in the reference time. As shown in Fig. 4, the aging factor for sand ($A_g = 0.16$) is lower than for clay ($A_g = 0.23$).



(a) Sand soil (b) Clay soil

Fig. 4. Normalized pile resistance vs. normalized time for aging database in literature

ESTIMATING THE RESISTANCE OF CLAY LAYERS WITHIN CONSOLIDATION SETUP USING PILE-CPT METHODS

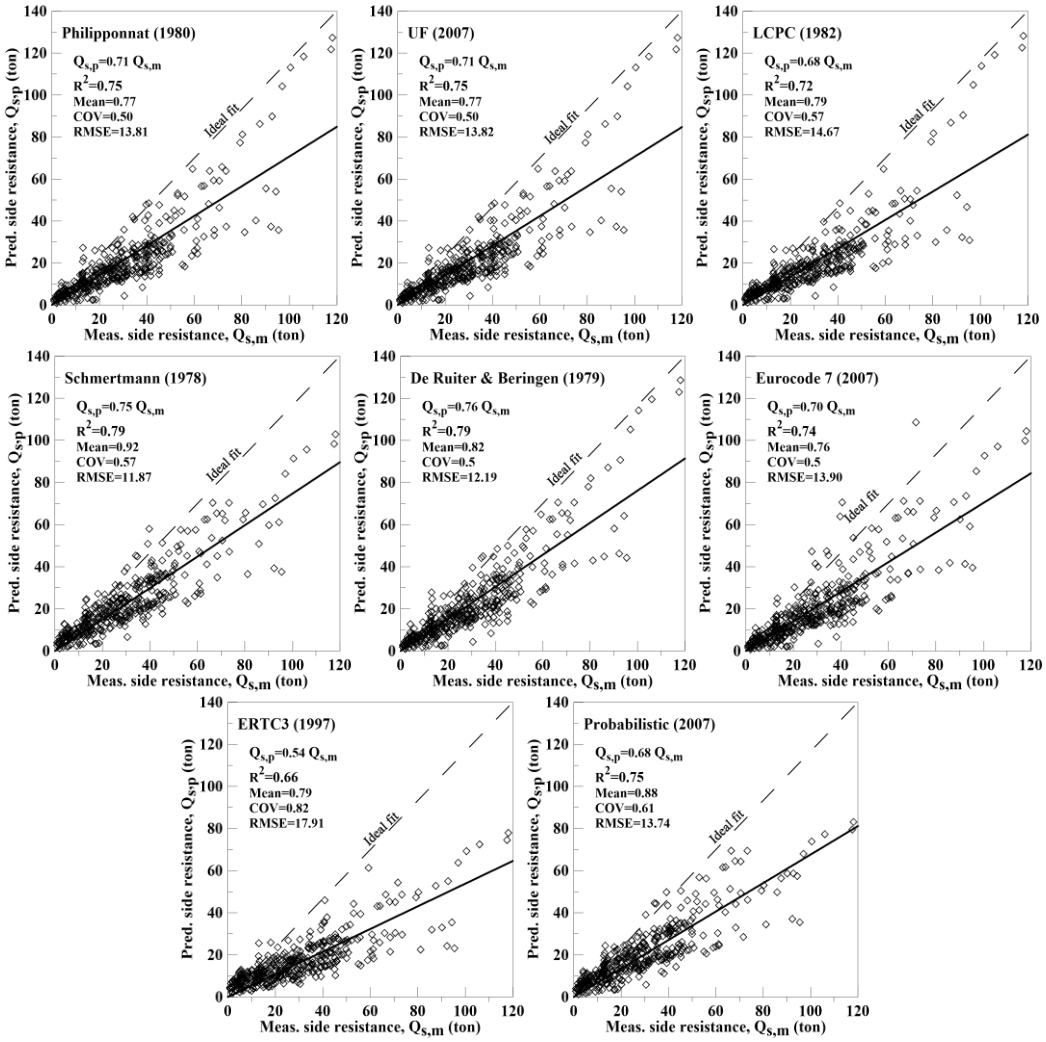


Fig. 5. Measured versus predicted capacities for clay layers considering consolidation setup

 © Deep Foundations Institute 2025

The developed consolidation setup equation was applied to extrapolate (or interpolate) pile resistance estimates derived from the eight best-performing direct pile-CPT methods. These methods were selected based on their closest prediction to actual pile capacity, as determined in a previous study (Amirmojahedi, 2020) using a database of 80 PPC piles driven in Louisiana soils. The direct pile-CPT methods were calibrated using a database of pile load tests conducted 14 days after driving. Consequently, the 14-day pile resistance serves as the reference time in this study. The side resistance of each soil layer was then extrapolated (or interpolated) using the consolidation setup model from Fig. 3 to estimate resistance at the time of complete excess PWP dissipation and the results were compared with the measured resistances from pile load tests as shown in Fig. 5. The comparison shows that the combination of direct pile-CPT methods and consolidation setup model have fair estimations of the measured accumulated side resistance with time.

ESTIMATION OF THE SIDE RESISTANCE CONSIDERING AGING SETUP

This study used the Missouri Department of Transportation (MDOT) study to evaluate the eight pile-CPT methods, and the aging model presented in Fig. 4. The MDOT study assessed the axial resistance of in-place piles from two bridges built in the 1960s and replaced in 2017, the UU Bridge and WW Bridge (Boeckmann et al., 2018). The WW Bridge was supported by driven, closed-end steel pipe piles filled with concrete (CIP piles), while the UU Bridge used octagonal precast concrete piles. Testing began in 2016, nearly 50 years after construction. Five piles (four vertical and one battered) were tested on UU Bridge, and six piles (four battered and one vertical) were tested on WW Bridge. This study focuses on evaluating pile-CPT methods specifically for the precast concrete piles in UU Bridge. The subsurface conditions at the UU Bridge include highly plastic soft clays in the upper 5 to 8 feet, underlain by medium to very dense poorly graded sand extending to a depth of 66 feet. The water table was approximately 20 feet below the surface. Soil boring was conducted on one embankment side, while the CPT test was performed on the opposite side. Figure 6 presents the soil boring and CPT data, showing similar soil profiles despite a 65-foot separation between test locations, indicating low site variability.

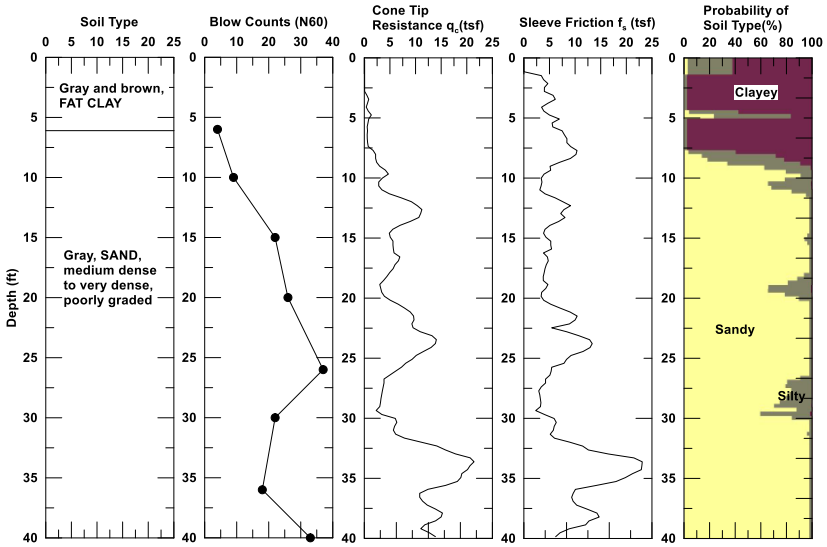


Fig. 6. Soil profile and CPT data at UU Bridge

The eight direct pile-CPT methods were used to estimate the axial resistance at 14 days, followed by extrapolation to 50 years using the aging model from Fig. 4. The CPT profile showed an 8-ft clay layer overlying sand, requiring consolidation setup estimation for pore pressure dissipation before applying aging effects. Due to the lack of pore pressure data above the 20-ft water table, only the aging model was used. Side resistance for clay and sand layers was first calculated at 14 days, then adjusted using aging

 © Deep Foundations Institute 2025

models, with end-bearing resistance added for total capacity. Figure 7 presents results for pile #1 (embedment depth = 21.3 ft.).

The side and total resistances for all tested piles at the UU Bridge were calculated using eight pile-CPT methods and aging models (Fig. 5, applied only to side resistance). Statistical analysis of predicted-to-measured resistance ratios ($Q_s,p/Q_s,m$ and Q_p/Q_m) was performed, with results presented in Table 6. The mean (μ) of $Q_s,p/Q_s,m$ ranged from 0.76 (De Ruiter) to 1.29 (LCPC), with a COV of 0.16 (De Ruiter) to 0.29 (Eurocode 7). For Q_p/Q_m, μ ranged from 0.85 (De Ruiter) to 1.20 (LCPC), with a COV of 0.09 (De Ruiter) to 0.21 (LCPC). Most pile-CPT methods (except De Ruiter, ERTC3, and Probabilistic) overestimated end-bearing resistance ($\mu > 1.0$). However, incorporating end-bearing resistance with side resistance (including aging) improved accuracy by reducing COV. Overall, the Philipponnat and UF methods provided the most accurate estimations among all pile-CPT methods.

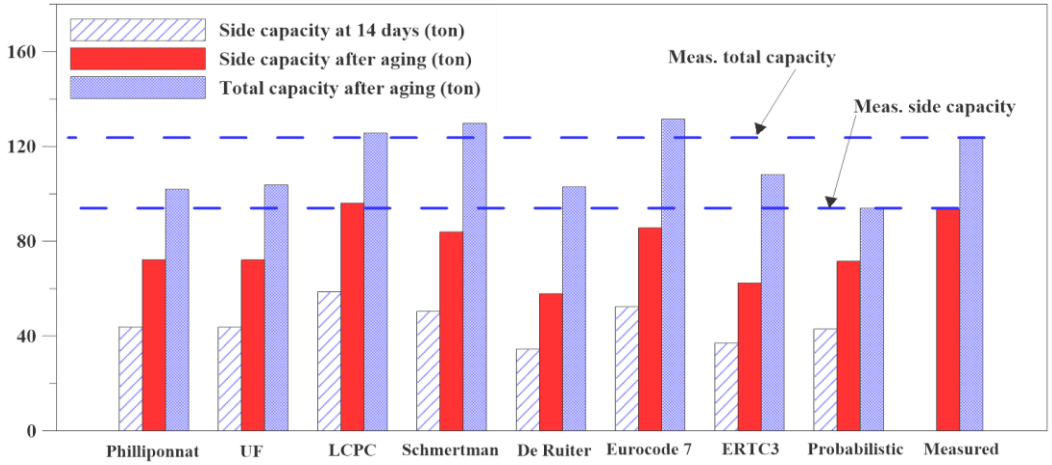


Fig. 7. Predicted resistance of pile #1 based on the 8 direct-CPT methods

Table 6. Statistical analyses of predicted versus measured capacities

CPT method+ Aging model	$Q_{s,p}/Q_{s,m}$			Q_p/Q_m		
	μ	COV	RMSE	μ	COV	RMSE
Philipponnat	1.01	0.24	17.72	0.97	0.13	15.09
UF	1.01	0.24	17.61	0.98	0.12	13.59
LCPC	1.29	0.28	31.87	1.20	0.21	30.29
Schmertman	1.12	0.26	19.71	1.12	0.15	19.44
De Ruiter	0.76	0.16	30.72	0.85	0.09	25.84
Eurocode 7	1.22	0.29	27.01	1.19	0.16	27.89
ERTC3	0.84	0.20	25.08	0.91	0.11	19.65
Probabilistic	0.95	0.21	17.66	0.89	0.13	21.76

 © Deep Foundations Institute 2025

CONCLUSIONS

The findings of this study can be summarized as follows:

- In clay, the consolidation setup parameter (A_c) was 0.53, and the aging setup parameter (A_g) was 0.23; in sand, A_g was 0.16.
- All eight pile-CPT methods underestimated unit side resistance in clay, with predicted/measured (μ) values ranging from 0.71 to 0.85, with Schmertmann showing the highest (μ = 0.85).
- Combining pile-CPT methods with the consolidation model also underestimated side resistance in clay. De Ruiter and Beringen performed best ($Q_{s,p} = 0.76Q_{s,m}$), while ERTC3 had the lowest accuracy ($Q_{s,p} = 0.54Q_{s,m}$).
- Significant aging effects were observed beyond consolidation setup.
- The predicted/measured side resistance ($Q_{s,p}/Q_{s,m}$) ranged from 0.76 (De Ruiter) to 1.29 (LCPC), while total resistance (Q_p/Q_m) ranged from 0.85 (De Ruiter) to 1.20 (LCPC). Most methods overestimated end-bearing resistance ($\mu > 1.0$), except De Ruiter, ERTC3, and Probabilistic methods.
- The Philipponnat and UF methods provided the most accurate total resistance estimations.
- Integrating aging models into pile-CPT methods significantly improved the prediction accuracy of pile resistance.

ACKNOWLEDGEMENTS

This research project is funded by the Louisiana Transportation Research Center (LTRC Project No. 22-3ST) and Louisiana Department of Transportation and Development (State Project No. DOTLT1000457). The authors would like to express their thanks to Walid Alaywan and LA DOTD engineers for providing valuable help and support in this study.

REFERENCES

Abu-Farsakh, M. Y., Haque, N., & Chen, Q. (2016). Field instrumentation and testing to study set-up phenomenon of piles driven into Louisiana clayey soils (No. FHWA/LA. 15/562). Louisiana Transportation Research Center.

Amirmojahedi, M., & Abu-Farsakh, M. (2019). Evaluation of 18 direct CPT methods for estimating the ultimate pile capacity of driven piles. Transportation Research Record, 2673(9), 127-141.

Attar, I. H., & Fakharian, K. (2013). Influence of soil setup on shaft resistance variations of driven piles: Case study. International Journal of Civil Engineering, Transaction B: Geotechnical Engineering, 11(2), 4-5.

Boeckmann, A. Z., Rosenblad, B. L., & Bowders, J. J. (2018). Foundation reuse: length, condition, and capacity of existing driven piles (No. cmr 18-008). Missouri. Dept. of Transportation. Construction and Materials Division.

Chan, J. H., & Birrell, N. D. (1998, May). Project Overview and Organization-Tension Pile StudyProject Overview and Organization-Tension Pile Study. In Offshore technology conference (pp. OTC-8762). OTC.

Gong, W., Li, L., Zhang, S., & Li, J. (2020). Long-term setup of a displacement pile in clay: an analytical framework. Ocean Engineering, 218, 108143.

 © Deep Foundations Institute 2025

Haque, M. N. (2015). Field instrumentation and testing to study set-up phenomenon of driven piles and its implementation in LRFD design methodology. Louisiana State University and Agricultural & Mechanical College.

Komurka, V. E., Wagner, A. B., & Edil, T. B. (2003). Estimating soil/pile set-up (No. Report No. 03-05,). Madison, WI, USA: Wisconsin Highway Research Program.

Schmertmann, J. H. (1991). The mechanical aging of soils. Journal of Geotechnical Engineering, 117(9), 1288-1330.

Skov, R., & Denver, H. (1988). Time-dependence of bearing capacity of piles. In Proc. third international conference on the application of stress-wave theory to piles, Ottawa (pp. 25-27).

Tavenas, F., & Audy, R. (1972). Limitations of the driving formulas for predicting the bearing capacities of piles in sand. Canadian Geotechnical Journal, 9(1), 47-62.

 © Deep Foundations Institute 2025

FINITE ELEMENT STUDY ON THE EFFECT OF BARGE IMPACT ON BRIDGES WITH DIFFERENT PILE GROUP CONFIGURATIONS

Murad Y. Abu-Farsakh, Ph.D., P.E., F.ASCE, Research Professor, Louisiana Transportation Research Center, Louisiana State University, Baton Rouge, Louisiana, USA.
Ahmad Souri, Ph.D., P.E, Director of Geotechnical Engineering, WSB, Melissa, Texas, USA.
George Z. Voyiadjis, Ph.D., Boyd Professor, Department of Civil & Environmental Engineering Louisiana State University, Baton Rouge, Louisiana, USA.

ABSTRACT

To assess how barge collisions at varying speeds affect the lateral behavior of three different pile group (PG) arrangements (vertical, battered, and mixed) in terms of peak lateral dis-placement, peak axial reaction, peak shear force, and the contribution of piles and pier columns to the overall resisting force, a dynamic analysis using 3D finite elements was carried out. The vertical PG had the lowest lateral stiffness, according to the data; the battered and mixed PGs, on the other hand, had comparatively higher stiffness, which led to higher impact forces and pile cap displacements in the vertical PGs compared to the other PGs. According to the shear force results, in battered and mixed PGs, the foundation accounted for about 82% of the overall lateral force. The findings indicated that in battered PGs, the load percent-ages were uniformly distributed across the rows, but in vertical PGs, the first row displayed a little higher percentage of lateral force than the remaining rows. For mixed PGs, a different performance was noted. Because of the greater displacement of the pile cap, the bending moments (BMs) of the piles in a vertical PG were much larger than those of the piles in other PGs, according to the data. The BM ratio was higher in the piles located on the outer (edge) column of each PG, with the leading row (L) having the highest BM ratio (69–72%) of any PG.

Keywords: Finite element analysis, Barge impact, Lateral displacement, Shear force, Bending moment.

INTRODUCTION

The growing number of inland vessels crossing waterways beneath bridges has made boat-bridge collisions a significant problem, particularly in light of a number of tragic incidents that have occurred since the 1960s. The 1980 Sunshine Skyway Bridge collapse in Florida, which happened when a freighter hit one of the bridge's piers, is an example of a catastrophic event (Consolazio et al., 2006). Every bridge element in a navigable river must be built to withstand vessel collisions, according to the American Association of State Highway and Transportation Officials' (AASHTO) current bridge design guidelines (AASHTO, 2012). The size, kinds, and frequency of vessels that pass through, the bridge and channel configuration, the water depth, the speed and direction of the vessels, and the bridge's structural response are all important considerations when evaluating the forces resulting from vessel-bridge accidents (Larsen, 1993). Kinetic energy (KE) and the crush depth of the barge's bow (a_B) are taken into account in empirical equations that calculate the AASHTO design impact force (equivalent static force) produced by a barge.

$$KE = \frac{C_H W_B V_B^2}{29.2} \tag{1}$$

$$a_B = 10.2\left(\sqrt{1 + \frac{KE}{5672}} - 1\right) \tag{2}$$

$$P_B = \begin{cases} 4112 a_B\,, & \text{for } a_B < 0.34 \\ 1349 + 110 a_B\,, & \text{for } a_B \geq 0.34 \end{cases} \tag{3}$$

 © Deep Foundations Institute 2025

where KE is the kinetic energy (kip-ft.), C_H is the hydrodynamic coefficient (= 1.05 for draft ≥ 0.5 ft., 1.25 for draft ≤ 0.1 ft.), W_B is the barge weight (ton), V_B is the barge speed (ft./s), a_B is the bow crush depth (ft.), and P_B is the equivalent static impact force (kips).

The impact load generated by barges and the variables that affect it, including speed, pier column width and shape, vessel weight, and bow stiffness, have been the subject of a large number of numerical and experimental investigations over the last 20 years (e.g., Consolazio and Cowan, 2003; Yuan and Harik, 2010; Sha and Hao, 2012; Kantrales et al., 2016; Zhang et al., 2016). Proposing and validating a simplified model for determining the extent of impact load was the primary objective of these studies. The most adaptable studies were conducted by the University of Florida study team, who used numerical and experimental techniques to examine and test the predictive models for the barge impact problem (Consolazio et al., 2009; Consolazio and Cowan, 2003). According to their findings, the existing AASHTO equivalent static force model tends to overestimate impact force magnitudes for high energy impacts while underestimating them for low to moderate energy impacts. Additionally, they discovered that the maximum impact force is highly influenced by the geometry of the impacted pier (Consolazio et al., 2009).

The lateral reaction of piling groups impacted by a barge was investigated in this study using finite element numerical models, with a focus on the case of pier M19 of the I-10 Twin Span Bridge in Louisiana. For the vertical, battered, and mixed pile group situations, these models comprised the soil mass, superstructure, and pile group foundation.

FINITE ELEMENT MODELING

Three types of pile group foundations (vertical, battered, and mixed) subjected to barge impacts at varying speeds - two knots (3.37 ft/s), four knots (6.75 ft/s), and six knots (10.12 ft/s) - were the subjects of this investigation. According to AASHTO (2012), these velocities represent barges' slow to moderate navigation speeds. The weight of the barge was kept constant at 1873 tons in each instance. Based on the average water level for the M19 pile group foundation, the barge was positioned in the FE models to strike the middle of the pile cap (Fig. 1). According to the AASHTO barge design rules, a fully laden barge has a draft of 8.7 feet. The barge's centerline axis and the cap's central axis were parallel in the horizontal plane.

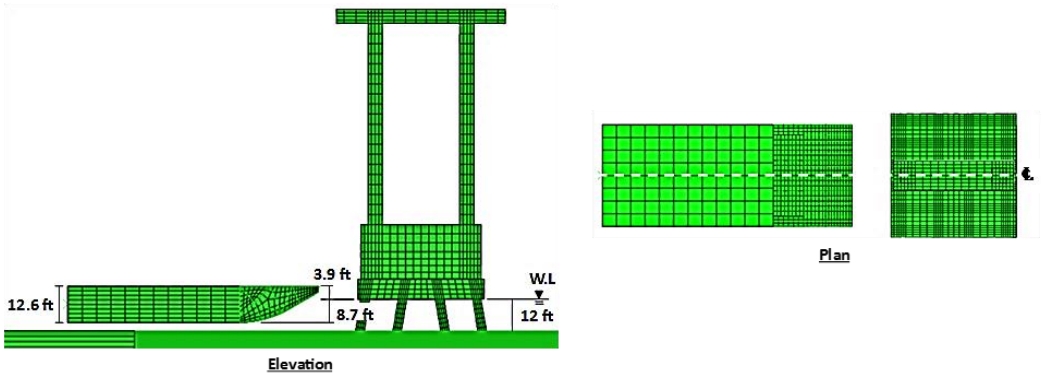


Fig. 1. Positioning of the barge and impact point.

FE Model of Barge

The usual Jumbo Hopper (JH) barge characteristics were utilized in this investigation in accordance with AASHTO criteria (AASHTO, 2024). The barge is 195 feet long and 35 feet wide. W times 12 feet. D, and the total weight of a fully loaded barge is 1873 tons. The two main structural elements of the JH barge are the cargo space and the bow rake (Fig. 2). The entire JH barge is constructed with steel panels and trusses. The bow rake model in this study was created using three-dimensional beam and shell components. The exterior steel plating was represented by shell elements, and the inside truss frames were replicated by

 © Deep Foundations Institute 2025

beam components. The freight room was constructed as a single, solid block of A36 steel and weighed a total of 1873 tons. The components utilized were the 3-D solid continuum elements (C3D8R), which included approximately 500 elements overall. The bow rake and cargo compartment were numerically connected by constraints so they could operate as a single unit.

FE Model of Pile Group and Bridge Pier

The base of the M19 pier for the I-10 Twin Span Bridge was inspected in order to assess the lateral reaction of the three PGs struck by a barge. The three main components of the FE model are the pier superstructure, bridge deck and girders, and PG foundation. The upper structure of the concrete pier was made up of the columns, the protective wall, and the beam that held up the girders. The pier's superstructure was modeled using a 3-D solid continuum element (C3D8R). Twelve girders and two concrete slabs made up the pier's substructure. The girders were made of LG-78 concrete types, had a span length of 200 feet, and were spaced 10.75 feet apart. To reduce the section detail for LG-78 girders, the FE model employed an approximate I-section based on cross-sectional area and second moment of area. The concrete decks were modeled as 8-inch-thick solid slabs using 3-D shell elements (S4R). After that, tie constraints were used to secure them to the girders.

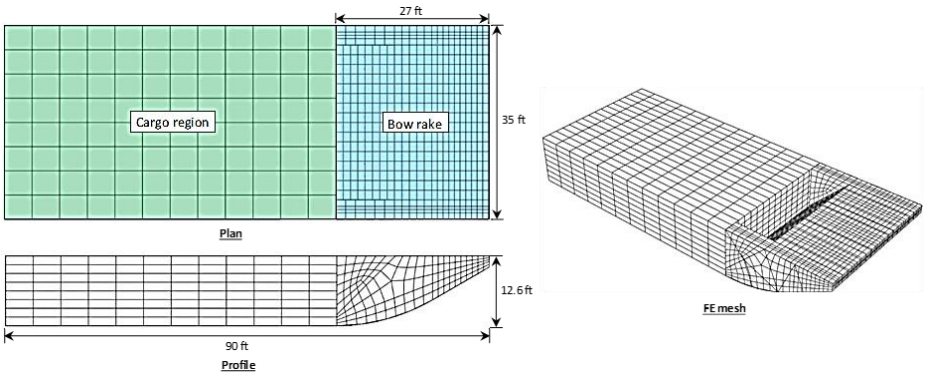


Fig. 2. FE model for the Jumbo Hopper barge.

To evaluate the lateral reaction of the three PGs impacted by a barge, the base of the M19 pier for the I-10 Twin Span Bridge was examined. The pier superstructure, bridge deck and girders, and PG foundation are the three primary parts of the FE model. The protective wall, columns, and the beam supporting the girders comprised the concrete pier's upper construction. A 3-D solid continuum element was used to model the superstructure of the pier (C3D8R). The superstructure of the pier was made out of two concrete slabs and twelve girders. The concrete and girders conformed to the LG-78 design, having a span length of 200 feet, a 10.75-foot spacing. An approximate I-section based on cross-sectional area and second moment of area was used in the FE model to simplify the section detail for girders. Using 3-D shell elements (S4R), the concrete decks were modeled as solid slabs that were 8 inches thick. They were then attached to the girders using tie restrictions.

This study made use of the soil profile from the M19 area, which was two sand layers and six clay layers. Two types of components were used to create the soil layer mesh: infinite elements (CIN3D8) and standard 3-D solid continuum elements (C3D8R). The Drucker Prager model (DP) was used to describe the behavior of the sand material, while the Modified Cam Clay (MCC) model was used to illustrate the behavior of the clay material. The findings of the site's statnamic test validated the soil model parameters utilized in the barge effect analysis. The two-parameter Rayleigh damping method was used to apply the damping for the soil material.

 © Deep Foundations Institute 2025

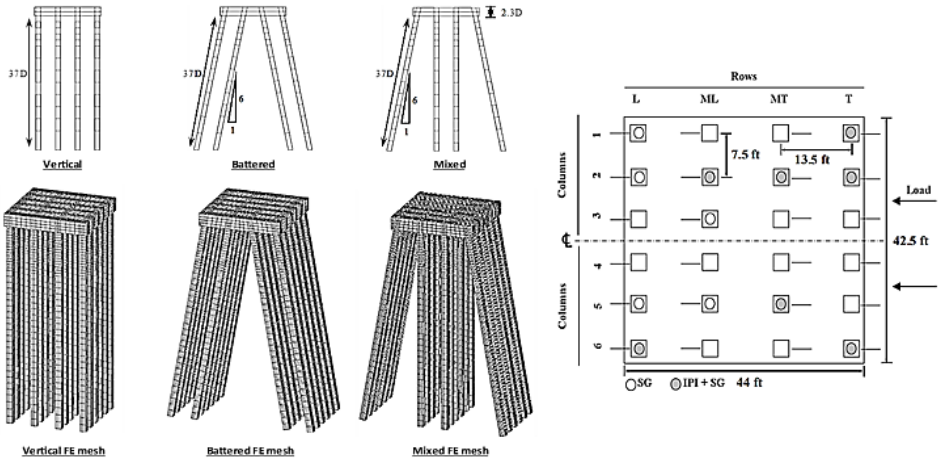


Fig. 3. Geometry of PGs and FE models (D is pile width = 3 ft.)

The ABAQUS contact model, which mimics the two primary mechanisms—normal (to surface) behavior and tangential behavior—was used to define the interface between the pile and soil. "Hard contact" refers to the typical behavior, which acknowledges either separation or interpenetration. The interaction occurring parallel to the pile-soil interface is referred to as tangential behavior, and it can exhibit either sticking or sliding. Without any movement between the pile and the soil, the tangential motion in adhesion mode transfers the shear stress to the soil. The Coulomb friction requirements, which are defined by the friction coefficient (μ) and the peak friction stress (τ_{max}), limit the shear stress transmitted in sliding mode to a maximum threshold value (τ_{lim}).

Barge Impact Load

Gravity and damping were two of the forces at play in the barge collision scenario. The soil mass, deck, girders, pier superstructure, and PG were all subject to the force of gravity. Establishing an initial velocity in a horizontal direction created barge momentum, which in turn produced the effect of the load from the barge. In order to prevent os-cillations caused by gravity acceleration from affecting the model's response during the barge impact, damping loads were used to remove them from the model once the oscillations stopped. Two two-second stages were used to model the barge collision: the equilibrium stage and the impact stage. By letting the soil achieve geostatic stress balance and eliminating the oscillations brought on by gravitational acceleration, stage 1 nearly stabilizes the model. Based on the barge's velocity and a two-second stage time, the barge is positioned at a range that guarantees the collision happens after completing, stage 1. The impact is imminent at the end of stage 1, and the barge's bow is only making contact with the pile cap. The barge's influence lasts until the momentum diminishes in stage 2, at which point it bounces back from the PG.

DISCUSSION OF RESULTS

Lateral Displacement

The lateral displacements of the pile caps and pier caps of each type of pile configuration as a result of barge collisions at different speeds is displayed in Fig. 4. The displacement chart shows a prominent peak in the initial 0.2–0.4 seconds caused by the impact force, followed by smaller peaks that show the structure's inherent oscillations. After two seconds, the dis-placement stopped for the mixed and battered PGs, but for the vertical PG, it returned to a non-zero value. This observation can be linked to the substantial damage to the piles for the vertical PG and the development of voids in the surface soil. In all impact situations, the battered and mixed PGs displayed no damage. In the vertical PG, the maximum displacement at the pile cap was significantly greater (2.0–8.4 inches); in the battered and mixed PGs, it was constant at 2.0–2.5 inches for all barge speeds. The impact force, which is reliant on the rigidity of the barge bow and the lateral PG

 © Deep Foundations Institute 2025

stiffness, was the primary factor in determining the degree of peak displacement. Two methods were used to account for the absorption of the barge's impact energy during the collision: (1) PG displacement and (2) barge bow deformation. Compared to battered and mixed PGs, vertical PGs have less side stiffness. As a result, the generated effect increased the lateral force and the pile cap's displacement for vertical PG.

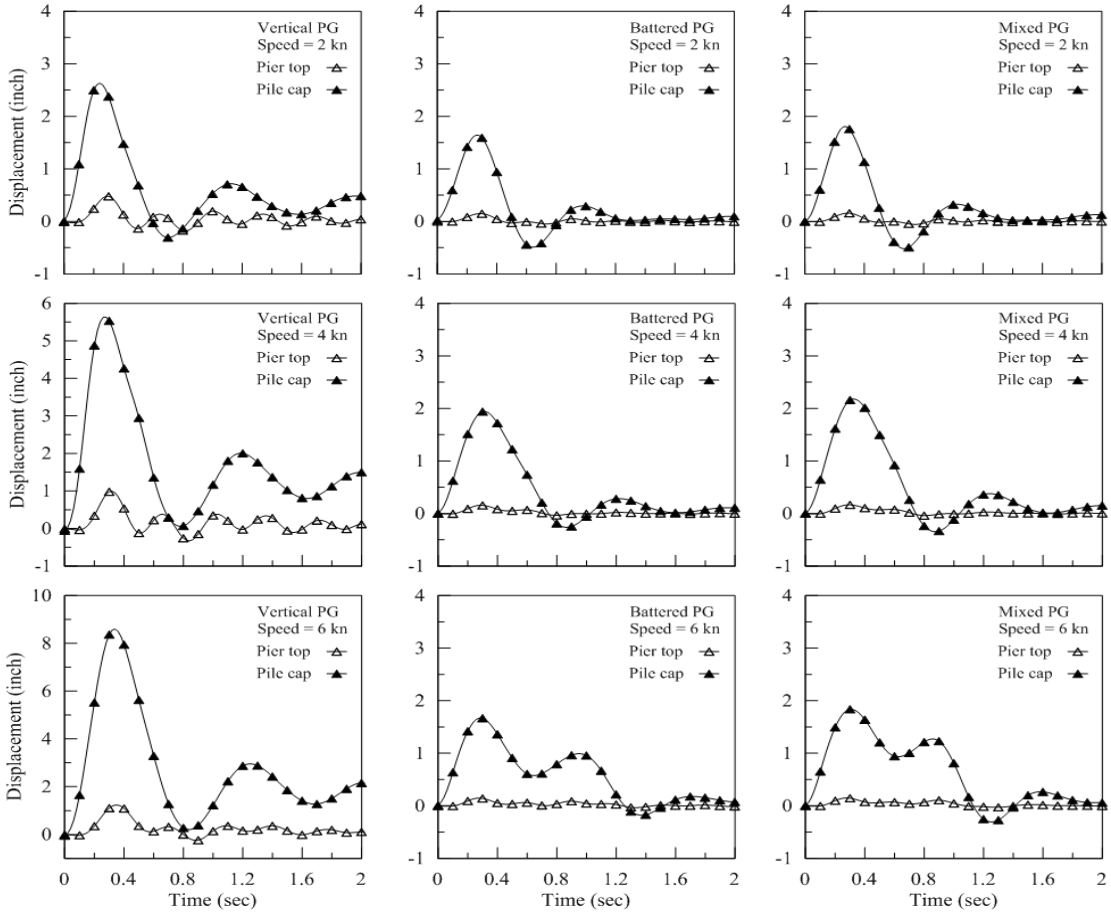


Fig. 4. Lateral displacement with time

Shear Forces and Impact Forces

Figure 5 shows the results of the shear force timeline calculation for each pile and the two pier columns. The combined effect force is shown by the total shear forces. In contrast to the battered and mixed PGs, the vertical PG scenario showed a significantly higher impact force. By using more kinetic energy, the vertical PG increased the lateral force from the im-pact. Greater lateral displacement and more severe damage levels in the piles were made possible by the reduced rigidity of vertical PG. However, because of their increased stiffness, the battered and mixed PGs absorbed less kinetic energy, which caused the barge bow to bend significantly and absorb a significant quantity of kinetic energy. The force as a function of time after impact shows that the vertical PGs sustain a higher rate of force increase than the other PGs. It has been observed that after the impact, the forces in the vertical PG piles become negative, primarily as a result of the damage the piles have experienced. An overall positive shear in the pier columns counterbalanced the damaging shear in the negative pile. Bow distortion caused the initial peak to last longer in the battered and mixed PGs. The force data for both PGs indicates two consecutive force maxima at a barge speed of 6 knots, suggesting that the collision was extremely inelastic.

The peak shear force in the pier columns and piles with respect to the barge's speed is shown in Fig. 6. The findings indicate that in the vertical PG, the peak force rose linearly with barge speed, whereas in the battered and mixed PGs, it stayed relatively constant. The findings indicate that in the battered and mixed

 © Deep Foundations Institute 2025

PGs, the ratio of force carried by the piles compared to total force remained constant at 82%; however, in the vertical PG, as barge speed increased, the force ratio dropped from 75% to 65%. This is mostly because the piles were damaged, which made them less sturdy in the vertical PG.

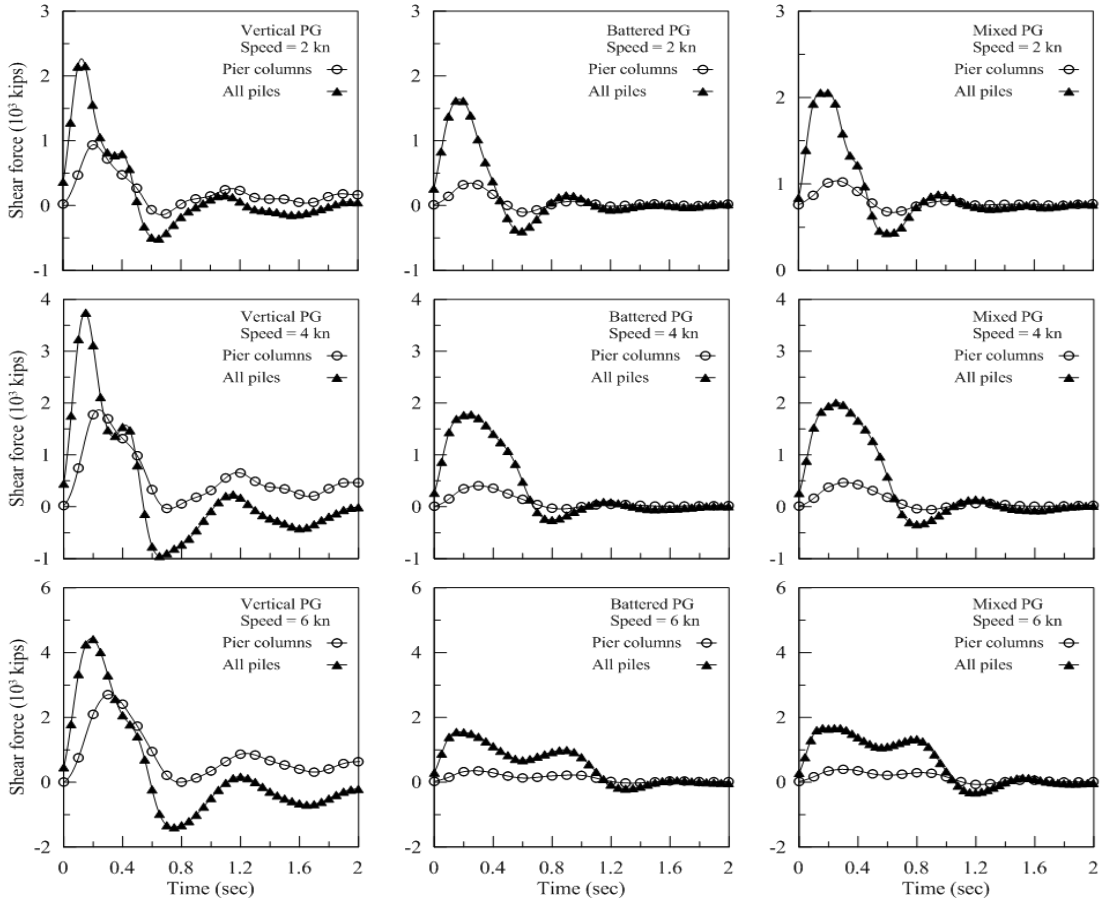


Fig. 5. Shear force with time

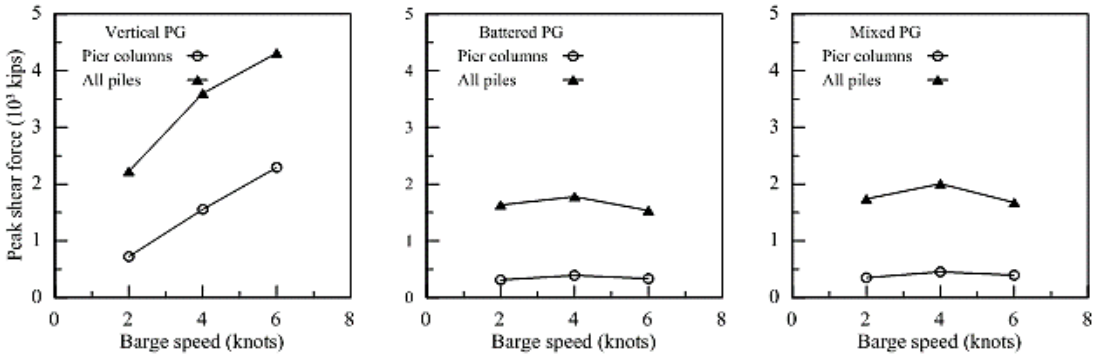


Fig. 6. Peak shear versus barge speed

The leading row (L) for the vertical PG had the most contribution (27%), closely followed by the end row (T) (25%), while both rows ML and MT each contributed 24%, according to an analysis of the effects of each pile row (L, ML, MT, and T) on the overall shear force. Compared to the distribution obtained from the static analysis, the impacted PG rows showed similar percentages of roughly 25% (Souri et al., 2011). But at 28% in rows L and T and 22% in rows ML and MT, the mixed PG showed the biggest diversity across the rows.

 © Deep Foundations Institute 2025

Bending Moment

Figure 7 displays the results of calculating the bending moment (BM) for the piles at the height of the pile cap at a barge speed of 4 knots. Although the degrees varied, a similar pattern in the results was observed for barge speeds of 2 and 6 mph. Every pile in the PGs exhibits surprisingly similar reactions and contributions, as shown by the BM history data. Because of the significant movement of the pile cap, the piles in the vertical PG had significantly higher peak BM than those in the other PGs. By normalizing the maximum BM of each pile with the PG shear (VPG), the pile length (L=110 ft.), and the number of piles in the PG (n=24), the BM ratio was determined. The maximum BM for each pile was computed. The findings imply that in all PGs, the piles located in the outer (edge) column (col. 1) displayed a greater BM ratio. In the vertical PG, 2.3% in the battered PG, and 2.2% in the mixed PG, the BM difference between the inner columns and the outer (edge) column was 1.3%.

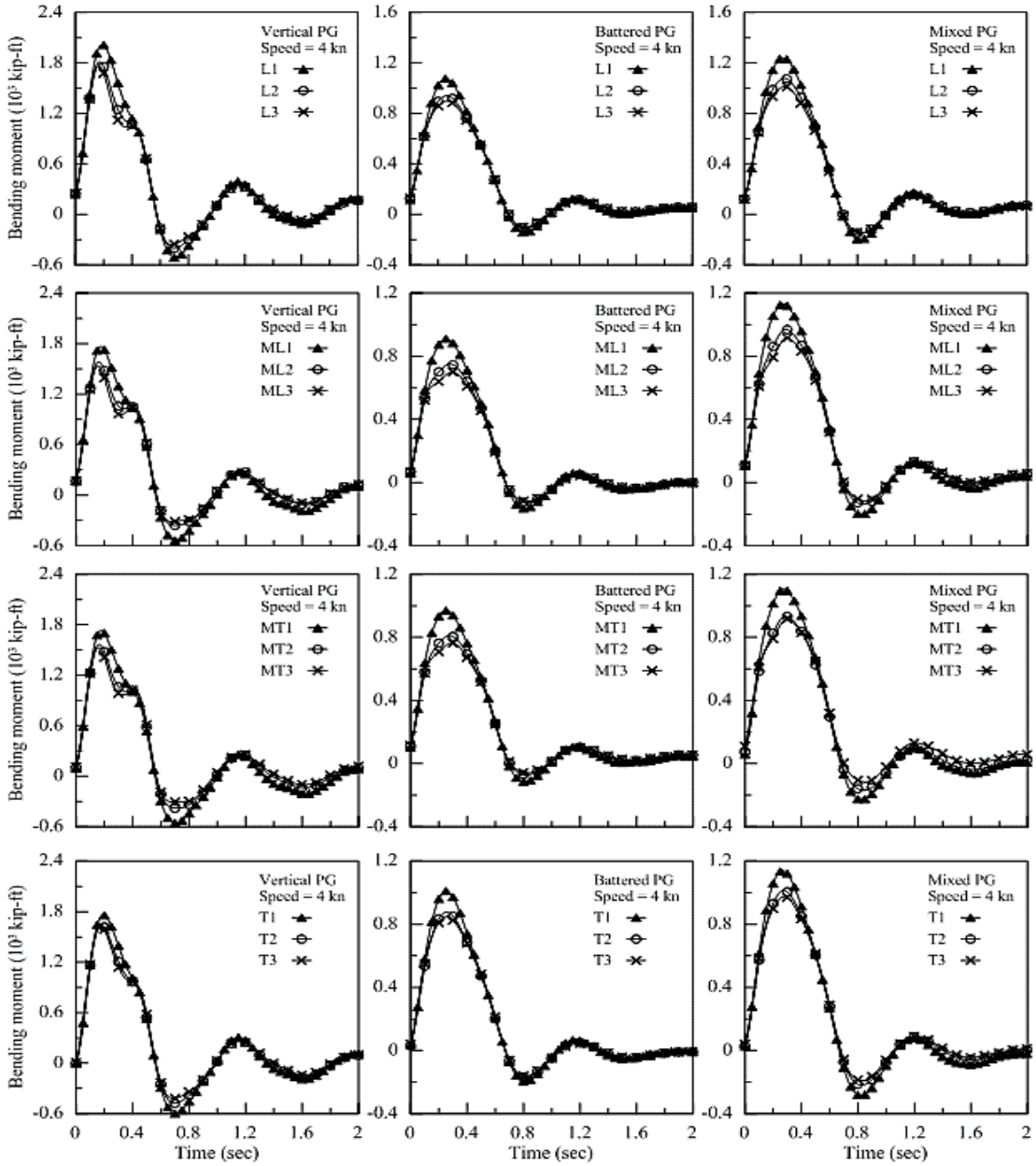


Fig. 7. Bending moment history results at barge speed = 4 knots

 © Deep Foundations Institute 2025

Figure 8 provides information on the distribution of BM among the rows (L, ML, MT, and T) by displaying the BM ratio for each row. According to the diagram, out of all the PGs, the top row (L) had the greatest BM ratio (69–72%). The BM ratio for rows ML, MT, and T in vertical PG was quite comparable (58–61%). The BM ratios for rows L, ML, MT, and T in the battered PG were 71, 57, 61, and 67%, respectively. The BM ratios for rows L, ML, MT, and T in mixed PG were 72%, 65%, 62%, and 68%, respectively.

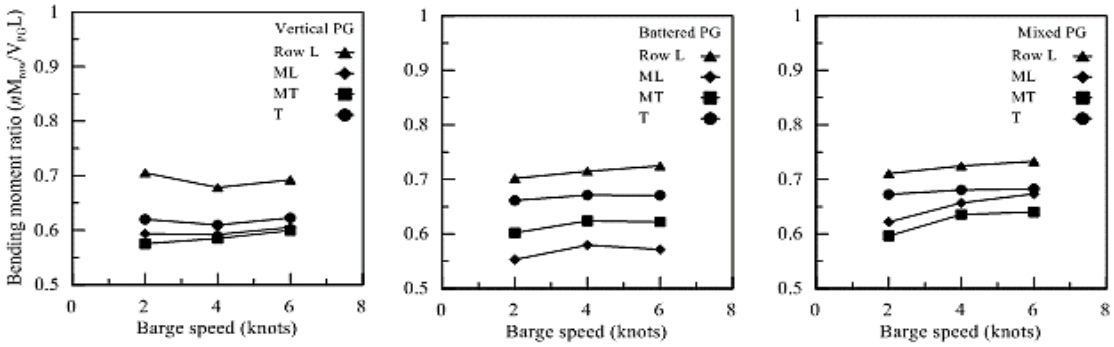


Fig. 8. Summary of bending moment ratio per row

CONCLUSIONS

- The impact force and pile cap displacement were larger in the vertical PG than in the other PGs because it had the lowest lateral stiffness, whereas the battered and mixed PGs had almost the same stiffness.
- According to the shear force results, the foundation was responsible for up to 82% of the total lateral force. The foundation received 65-75% of the load distribution in the vertical PG, whereas the pier columns received 24-35%. The force distribution in the foundation and pier columns of the battered and mixed PGs was 82% and 18%, respectively.
- The first row in vertical PG had a comparatively greater percentage (27%) than the subsequent rows, which exhibited comparable percentages (24–25%), according to the lateral force distribution. The load percentage in the battered PG was 25%, which was split equally among the rows. In the mixed PG, there was a noticeable variance in the %. There was 28% in the first and fourth rows and 22% in the second and third rows.
- Because of an increase in pile cap displacement, the total contribution from all of the piles in the vertical PG demonstrated noticeably higher BM than the piles in other PGs. The outer (edge) column piles had a greater BM ratio for all PGs, according to the peak BM contribution for each pile. The findings also revealed that, out of all the PGs, the front row (L) had the greatest BM ratio (69–72%). The BM ratio (58–61%) in vertical PG remained comparatively constant over rows ML, MT, and T. The BM ratios for rows L, ML, MT, and T in the battered PG were 71, 57, 61, and 67%, respectively. Rows L, ML, MT, and T in mixed PG had BM ratios of 72%, 65%, 62%, and 68%, respectively.

ACKNOWLEDGEMENTS

This research project is funded by the Louisiana Transportation Research Center (LTRC Project No. 13-3GT) and Louisiana Department of Transportation and Development (State Project No. DOTLT1000103).

 © Deep Foundations Institute 2025

REFERENCES

AASHTO, 2024. AASHTO LRFD Bridge Design Specifications. American Association of State Highway and Transportation Officials, Washington, D.C.

Consolazio, G., Cook, R., McVay, M., Cowan, D., Biggs, A., and Bui, L. 2006. Barge Impact Testing of the St. George Island Causeway Bridge. Phase III: Physical Testing and Data Interpretation, University of Florida, Gainesville.

Larsen, O. 1993. Ship collision with bridges: the interaction between vessel traffic and bridge structures. International Association for Bridge and Structural Engineering, International Association for Bridge and Structural Engineering, Zürich, Switzerland.

Consolazio, G., and Cowan, D. 2003. Nonlinear analysis of barge crush behavior and its relationship to impact resistant bridge design. Computers & Structures, K.J Bathe 60th Anniversary Issue, Vol. 81, No. 8-11, pp. 547–557.

Yuan, P., and Harik, I., 2010. Equivalent barge and flotilla impact forces on bridge piers. Journal of Bridge Engineering, Vol. 15, No. 5, pp. 523–532.

Sha, Y., and Hao, H., 2012. Nonlinear finite element analysis of barge collision with a single bridge pier. Engineering Structures, vol. 41, pp. 63–76.

Kantrales, G., Consolazio, G., Wagner, D., and Fallaha, S., 2016. Experimental and analytical study of high-level barge deformation for barge–bridge collision design. Journal of Bridge Engineering, Vol. 21, No. 2.

Zhang, J., Chen, X., Liu, D., and Li, X., 2016. Analysis of bridge response to barge collision: refined impact force models and some new insights. Advances in Structural Engineering, Vol. 19, No. 8, pp. 1224–1244.

Consolazio, G., Davidson, M., and Cowan, D., 2009. Barge Bow Force-Deformation Relationships for Barge-Bridge Collision Analysis. Transportation Research Record, Vol. 2131, No. 3-14, pp. 1-12.

Souri, A., Abu-Farsakh, M., and Voyiadjis, G., 2011. Evaluating the effect of pile spacing and configuration on the lateral resistance of pile groups. Marine Georesources & Geotechnology, Vol. 39, No. 2, pp. 150–162.

 © Deep Foundations Institute 2025

DEEP FOUNDATION DESIGN AND CONSTRUCTION CHALLENGES AT HUNTS POINT ACCESS IMPROVEMENT PROJECT IN BRONX, NEW YORK

Alireza Ayoubian, P.E.,[1] Paul B. Pizzimenti, P.E.,[2] Jean Louis Locsin[2], P.E., and Alfredas Daugiala, P.E.,[3]

[1]Parsons Corporation, 100 Broadway, New York, NY 10005; e-mail: alireza.ayoubian@parsons.com
[2]Haley & Aldrich of New York, 213 West 35th Street, New York, NY 10001; email: ppizzimenti@haleyaldrich.com, jlocsin@haleyaldrich.com
[3]Underpinning and Foundation Skanska, 46-36 54th Road, Maspeth, NY 11378; e-mail: alfredas.daugiala@skanska.com

ABSTRACT

Contract 3 was the third and final contract in NYSDOT's $1.7B Hunts Point Access Improvement Project to provide improved vehicular access between the wholesale commercial businesses on the Hunts Point Peninsula and the Sheridan and Bruckner Expressways. Contract 3 required complex temporary traffic staging to construct new ramps and interconnections of active roadways between the prior improvements made in Contracts 1 and 2 and a replacement pedestrian bridge over Bruckner Boulevard. The ramps were nestled between a more than 100-year-old underground MTA NYCT tunnel and through the fill of a large gravity retaining wall bordering a sunken Amtrak corridor. The ground conditions included Fill and Glacial Soils overlying decomposed and competent Schistose bedrock. Depth to bedrock varied between 20 and 43 feet (ft) below grade. New foundation elements to support the ramps were not allowed to exert additional stresses on either structure. The selected foundation systems consisted of rock-socketed 36-inch, 72-inch, and 84-inch diameter drilled shafts and 18-inch diameter micropiles. The drilled shaft foundations were used within the influence zone of the NYCT tunnels and were encased in isolation sleeves to prevent the transmission of lateral stresses onto the tunnels. Beyond the influence of the tunnel, micropiles were installed in a congested, low-headroom site. Micropiles were also used within the limits of influence of the Amtrak retaining walls, which were analyzed under revised surface loading conditions to maintain stresses on retaining structures to below pre-existing conditions. All rock sockets were visually observed by the designer, and both drilled shafts and micropiles were load tested axially to confirm the nominal bond stresses used in design.

Keywords: foundations, tunnels, bridges

BACKGROUND

Hunts Point Interstate Access Improvement Contract 3 was the third and final phase of a transportation improvement project undertaken by the New York State Department of Transportation (NYSDOT) with the primary purpose of facilitating access to Hunts Point Food Distribution Center, which supplies New York City with over 12 percent of its daily food. In addition, the project will reduce congestion by removing trucks from local streets, improve air quality as a result of decreased truck traffic, enhance safety for pedestrians and bicyclists, improve public access to the Bronx River waterfront, create two new parks with pedestrian access, and improve livability within the Hunts Point community. Each contract was executed in a mostly sequential fashion to maintain traffic flows and is briefly described as:

- Contract 1 was completed in October 2022 and included the reconstruction of a nine-span overpass and three bridges above Amtrak/CSX train tracks, and the construction of two new ramps connecting Hunts Point Peninsula with the Bruckner Expressway and Sheridan Boulevard.

 © Deep Foundations Institute 2025

- Contract 2 involved improvements to the Bruckner Expressway between 141st Street and Barretto Street. The scope of work included widening the roadway and providing new entrance and exit ramps that connect the Bruckner Expressway to Leggett Avenue.
- Contract 3 re-aligned the interchanges between the Bruckner Expressway, Bruckner Boulevard, and Sheridan Boulevard to create a mainline thru-flow of traffic for the Expressway with logically flowing exit and entrance ramps to the Sheridan. A modernized and accessible pedestrian ramp was reconstructed over the Bruckner Boulevard to allow for community access to the peninsula. A plan view of the contract arrangements and Contract 3 is presented in Fig. 1.

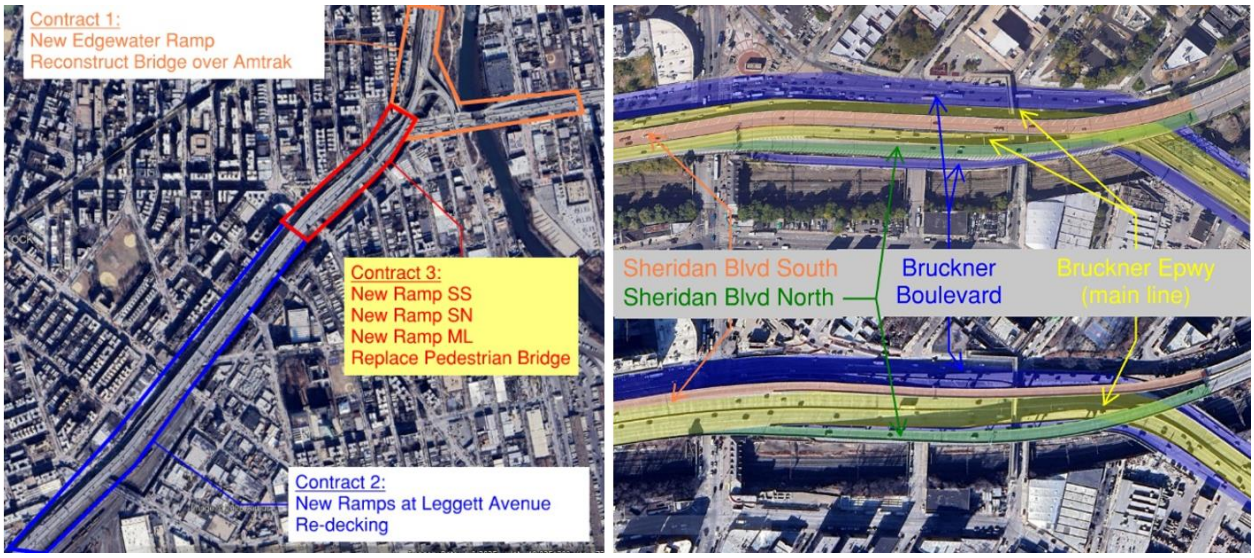


Fig. 1. Hunts Point Interchange Access improvement contract limits (left), and Contract 3 Re-alignment of Interconnections (right) with original and final configurations shown above and below, respectively.

PROPOSED STRUCTURES

The Contract 3 Project includes new exit and entrance ramps connecting the north- and south-bound Sheridan Boulevard into the Bruckner Expressway. The Bruckner Expressway will be re-oriented into a centralized Mainline Corridor from Longfellow Avenue to Hunts Point Avenue (Fig. 1). The new Sheridan Boulevard ramps will flank the mainline Bruckner Expressway. The existing pedestrian bridge at Bryant Avenue will be replaced.

Mainline Corridor Piers and Ramp

The Mainline Corridor work included replacing and widening the deck of the existing Bruckner Expressway over nine spans and completing structure replacement over 23 spans. Four new Mainline Corridor pier sub-structures, 143A through 146A, and the Mainline Abutment were supported using micropile foundations. Substructures 142 and below were modified but reused the existing foundations.

The re-orientation of the Mainline Corridor included the construction of a new earth-filled ramp with pre-fabricated modular retaining walls (T-walls) supported on grade to contain the new fill behind the new ML Abutment. The ramp was approximately 450 ft long, 95 ft wide, and reached a maximum new fill height of approximately 15 ft.

 © Deep Foundations Institute 2025

Pedestrian Bridge and Ramp

The pedestrian bridge replacement included the construction of a new earth-filled ramp with retaining walls supported on shallow foundations, located on the north sidewalk of Bruckner Boulevard, a new micropile supported abutment (End Abutment), a new drilled shaft supported pier constructed under the present-day southbound Sheridan Boulevard (Pier 4), and a new micropile supported pier under the present-day eastbound Bruckner Expressway (Pier 3). The new pedestrian bridge spans over the existing New York City Transit (NYCT) tunnel located under the westbound Bruckner Boulevard over which the pedestrian bridge passes.

Ramp SN

The Sheridan Boulevard North Ramp SN work included the construction of a new independent and elevated right-hand exit ramp structure connecting east-bound Bruckner Expressway onto north-bound Sheridan Boulevard. New straddle-bent substructures consisted of two concrete columns connected by a concrete cap beam supporting the roadway. The Ramp SN pier substructures were supported using micropile foundations within the fill of an existing NYSDOT retaining wall bordering the Amtrak railroad corridor.

Ramp SS

The Sheridan Boulevard South Ramp SS work included the construction of a new independent elevated right-hand exit ramp structure connecting south-bound Sheridan Boulevard onto south-bound Bruckner Expressway. New pier substructures consisted of single concrete columns with a concrete hammerhead cap beam supporting the roadway. The Ramp SS pier substructures were supported using single drilled shafts or micropile-supported pile caps. The new columns and foundations were located adjacent and parallel to the NYCT subway structure. Drilled shaft foundations with oversized outer isolation casings were used at substructures within the influence zone of NYCT. Isolation casings were intended to prevent transmitting lateral loads toward the NYCT structure.

GEOTECHNICAL CONDITIONS

The geotechnical and foundation design was based on the interpretation of the factual subsurface data obtained from a subsurface exploration program completed by NYSDOT for the Hunts Point Interstate Access Improvement – Contract 3 (existing borings) provided to the bidders as reference documents, and a supplemental subsurface exploration program completed specifically for the contract and tailored to the planned designs.

Supplemental and Existing Test Boring Data

A total of approximately 51 test borings were available based on the combined results of the supplemental and existing subsurface exploration programs. Geotechnical laboratory tests were performed on select soil and rock samples. The results of the subsurface explorations, including boring logs, groundwater level measurements, and geotechnical laboratory test results, were accumulated into geotechnical data reports for the project record.

Soil and Bedrock

Generalized subsurface conditions encountered during the supplemental subsurface exploration program and the existing subsurface exploration logs and rock core evaluation logs are described below in order

 © Deep Foundations Institute 2025

of increasing depth below ground surface (bgs). A typical soil profile along Ramp SN is provided in Fig. 2.

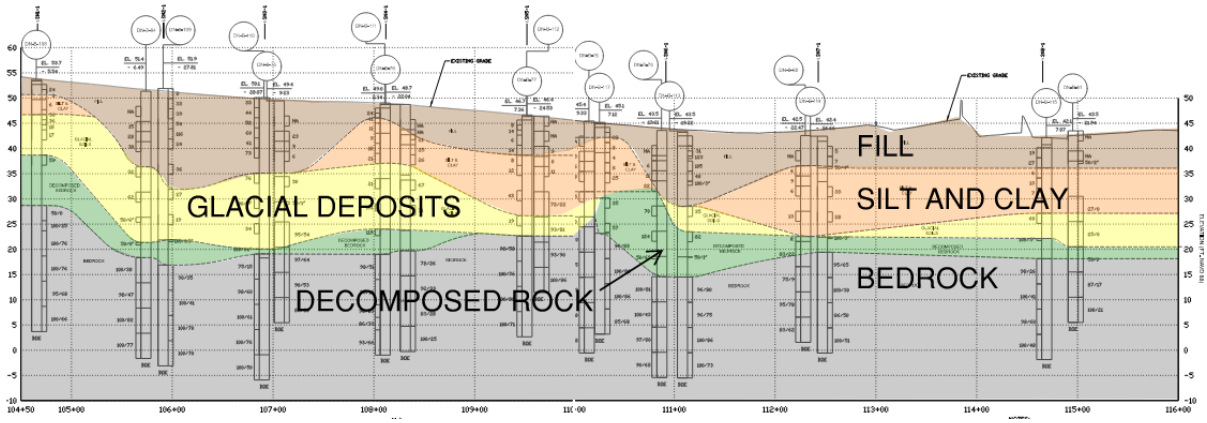


Fig. 2. Typical geologic profile along Ramp SN.

Overburden Soils

The overburden soil and rock strata were encountered in the following order:

- **Surface Cover:** A surface cover of approximately 1 ft to 1.5 ft consisting of asphalt, concrete, and sub-base was encountered at most locations throughout the urban site.
- **Fill:** Fill Stratum was encountered in every test boring and ranged between 4 ft to 28.5 ft in thickness below the ground surface. The Fill was typically silty and gravelly SAND with varying amounts of gravel, and gravelly SILT with varying amounts of SAND, and occasional traces of clay and mica. Asphalt, concrete, and red brick pieces were present in various samples encountered. Typically, looser soils were encountered near the ground surface.
- **Silt and Clay:** SILT and CLAY Stratum was generally encountered throughout the site and ranged between 0 ft and 13 ft thick. The soils encountered near these structures were generally silty CLAY, sandy CLAY, and Sandy SILT with varying amounts of gravel.
- **Glacial Deposits:** Glacial Deposits were typically encountered below either the Fill or the SILT and CLAY and ranged between 4 ft and 24 ft in thickness. They were generally described as gravelly SAND with varying amounts of SILT and sandy SILT with varying amounts of gravel.
- **Decomposed Bedrock:** Decomposed Bedrock was encountered in most test borings. The Decomposed Bedrock ranged from 1 ft to 30 ft in thickness. Decomposed Bedrock was generally described as GNEISS with varying amounts of silt, clay, and Mica.

Bedrock

The project limits lie entirely within the Hartland Formation bedrock (Baskerville 1992) of the Middle Ordovician to Lower Cambrian period and is mapped predominantly as schist and granite. The nearest thrust fault is located less than a mile to the south of the project. Soft to very hard, fresh to highly weathered Gneiss and medium to hard, fresh to highly weathered Schist were encountered within the borings. The rock quality designation (RQD) values of 0 to 95 percent were observed, typically concentrated between 50 and 80 percent.

Groundwater

The groundwater levels were approximately 9 to 27.0 ft below existing site grades which generally corresponded to El +20 to +30ft..

 © Deep Foundations Institute 2025

FOUNDATIONS

This project required the design of various deep foundation types to address the geotechnical challenges and meet the load demands across the different sections: Mainline Corridor (ML), Pedestrian Bridge (PB), SN Ramp (SN), and SS Ramp (SS). The deep foundation types designed for this project included:

1. **Drilled Micropiles (Rock-Socketed):**
    - 18-inch diameter drilled micropiles at ML Corridor, SN, and SS Ramps.
    - 9.625-inch diameter drilled micropiles at the Pedestrian Bridge abutment and one pier.
    - These were used in areas with limited access or where minimal disturbance to existing structures was necessary.

2. **Drilled Shafts (Rock-Socketed):**
    - 3-ft diameter drilled shafts at one Pedestrian Bridge pier.
    - 6-ft diameter drilled shafts at SS Ramp.
    - 7-ft diameter drilled shafts at SS Ramp.
    - These larger diameter shafts were employed to provide substantial load-bearing capacity and stability, particularly in areas with significant lateral forces and nearby sensitive existing structures.

Each foundation type was selected based on site-specific conditions.

Drilled Micropiles
Design

Drilled micropile deep foundations, as shown in Fig. 3, were composed of 18-inch diameter micropiles with casing thicknesses of 0.5 inches and 0.625 inches, depending on structural load demands to support structures at the ML Ramp and Abutment, SN Ramp, and select piers of SS Ramp. At the PB Ramp, 9.25-inch diameter micropiles with casing thickness of approximately 0.5 inches were used. All micropiles were drilled and socketed into bedrock. Axial resistance was designed based on rock socket bond stresses only. Lateral resistance was determined based on soil and pile stiffness.

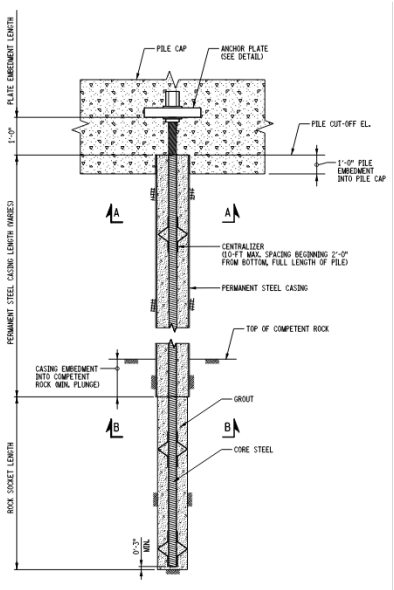


Fig. 3. Schematic View of Typical Micropiles.

The 18-inch diameter micropile was introduced to NYSDOT on the Hunts Point Access project, starting with Contract 1. This pile has all attributes of the typical micropile, including 5- to 10-ft casing sections joined with the flush joint type thread through overburden materials, seated into rock, an open-hole rock socket, a steel core, and a tremie-grouted casing. The only difference is the larger-than-customary size.

Design Challenges
Micropiles in Retaining Wall Backfill

The new foundations at some ML and SN piers were located within the backfill behind the existing NYSDOT Retaining Wall bordering the Amtrak Right of Way (ROW). Lateral pile resistance was

 © Deep Foundations Institute 2025

provided by the lateral stiffness of the backfill behind the retaining walls. The impacts of lateral pressure on the NYSDOT retaining wall were estimated from soil reactions in the FBMPier by the Bridge Software Institute soil-structure interaction model and applied to the existing wall.

As-built drawings from the 1960s indicate that the columns of the existing expressway bear on footings shared with the wall, and the expressway columns were structurally connected to the wall stems. Therefore, the wall was subject to both lateral earth pressures and direct lateral and vertical loads from the expressway structure. By estimating the applied loads on the wall from the existing structure and comparing them against the calculated pressures exerted on the wall by the new foundations, we determined that the applied lateral earth loads were equal to or less than the existing loads acting on the wall. A view of a proposed ML Pier close to the existing NYSDOT wall is shown in Fig. 4.



Fig. 4. Proximity of new column footings to retaining wall (right).

SN Ramp Asymmetric Embankment Loads

The SN section involved the design of 18-inch diameter micropiles for 16 substructures, with additional loads on some piles due to a 20-ft-high embankment adjacent to the mainline ramp. Figure 4 presents a schematic view of the proposed micropiles for the SN Ramp.

Select SN pile caps were located next to the nearly 20-ft-high mainline earth-filled ramp and were installed before constructing the mainline embankment. These piles were subjected to additional vertical and lateral loads and overturning moments from the mainline embankment surcharge. Additional factored lateral loads and overturning moments on the side of pile caps due to adjacent embankment self-weight and 250 pounds per square foot (psf) of live load surcharge were included in the FB-MultiPier analyses.

Construction Challenges

One of the construction challenges was installing foundations with adequate structural stiffness under the existing structures, where the limited headroom conditions dictate the foundation system selection. The use of micropiles facilitated the ability to install in low-headroom, and the large diameter casing sections provided the stiffness needed to support the highway structure loads.

To account for required casing embedment into competent rock, to resolve the flexural load demands and limit the differential settlement within the pile group, the piles were installed through overburden using a ring bit hammer assembly with an internal air flush method. The ring bit system offers the ability to drill through natural obstructions, advancing the casing and hammer bit as one unit, with no need to stop drilling and change tooling. The hammer delivers impact energy at the casing tip and uses internal air flush to bring the cuttings to the surface. The same system offers the ability to advance the casing to the required depth into bedrock formation to resolve flexural loads.

To verify the pile load axial capacity and rock socket peripheral shear resistance values, an Osterberg Cell (O-Cell) test was performed in micropiles. The load tests were designed to mobilize the required bond resistance, and not necessarily a fixed total load. In order to test the bond resistance, the O-Cell was located mid-length of the bond zone, and a compressible end bearing device was installed at the bottom of the socket. It was a challenge to fit the 10-inch diameter O-Cell assembly within a 16-inch diameter rock socket, then encapsulate the assembly with sanded grout placed via tremie line.

The test location was deliberately selected to represent the lowest rock quality setting to conservatively represent all rock-socketed micropiles on this project. Video inspections of the rock sockets were performed for the test micropile and 100 percent of production micropile locations. Video inspections were performed to confirm that the quality of the rock sockets was equal to or greater than that of the test location. Figure 5 shows the installation of the O-Cell and a typical video observation of the rock socket quality.



Fig. 5. O-Cell testing of 18-inch diameter micropiles (left) and typical video inspection observation of rock sockets (right).

Drilled Shafts
Design

Drilled shaft foundations were composed of single 36-, 72-, and 84-inch diameter drilled shafts with telescoped outer isolation casings approximately 6 inches larger in diameter than the interior shaft as shown in Fig. 6. Drilled shafts were used to support structures at select piers of the SS Ramp and Pedestrian Bridge. All shafts were drilled and socketed into bedrock. Axial resistance was designed based on rock socket bond stresses only. Lateral resistance was determined based on soil and shaft stiffness, except where isolation casings were used, in which case no lateral soil stiffness was considered.

The design of drilled shafts that were located within the 1H:1V influence of the buried NYCT tunnel was controlled by a design requirement that no new loads can be placed on the buried tunnel structure. This requirement prevents consideration of lateral soil resistance within the depth of the influence zone along the length of the shaft. In order to practically meet this design assumption, an oversized isolation casing was installed into the ground at the shaft location that extended to the depth of the influence zone, cleared of soil, and the permanent shaft was installed centered into the casing. The size of the isolation casing was determined based on the maximum predicted lateral deflection of the drilled shaft.

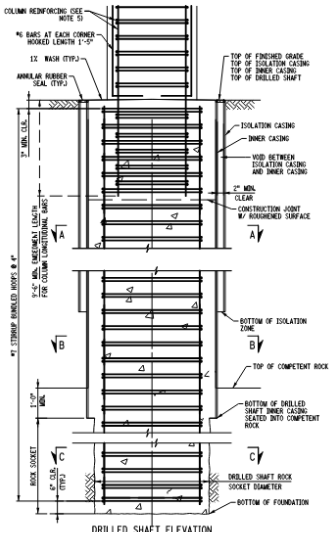


Fig. 6. Schematic of drilled shaft with isolation casing.

 © Deep Foundations Institute 2025

Design Challenges

An impact assessment on the adjacent NYCT tunnel was performed. The new Pedestrian Bridge foundations at Pier 4 and Abutment 2 were located on either side of the buried tunnel. New shallow foundations for the Pedestrian Bridge ramp were situated further from the tunnel than the Abutment 2 piles and were bearing at least 4 ft below grade. Pier 4 foundations were within the tunnel's influence zone, and the analysis and design of the foundations and substructure included isolation casings extending to the influence line at the point of intersection with the outer limit of the shaft. The intersection point was estimated to be approximately 9 ft bgs and was confirmed based on a tunnel survey. This design ensured that the new shafts would not exert lateral and vertical pressures on the tunnel structure. Axial loads were resisted by drilled rock sockets located below the influence zone.



Fig. 7. Drilled shaft rig located within confined work zone between active traffic and existing highway.

Since the new Pedestrian Bridge was in the same location as the existing one, and the new drilled shafts could not be installed in low headroom, a dual shaft straddle bent arrangement was chosen for constructability, allowing foundations to be installed off to the sides of the existing bridge before demolition and reconstruction.

Drilled shafts for the SS Ramp included single 72- or 84-inch diameter drilled shafts with isolation casing. O-Cell tests verified load-carrying capacity, and an impact assessment on the NYCT tunnel was conducted. The design of foundations for the SS Ramp accounted for loads from the adjacent ML embankment for SS-3 to SS-5 and addressed uplift forces in rock. Isolation casings were a minimum of 6 inches larger in diameter than the drilled shaft to be isolated and extended at least to the depth of intersection of the NYCT influence line with the theoretical outer limit of the drilled shaft. The nearest shaft was located with a clear distance of approximately 13.3 ft from the east limit of the tunnel, as shown in Fig. 8. The inside of the subway structure was surveyed by the contractor nearest each proposed Ramp SS substructure, and sections were cut to determine the influence relationship and corresponding isolation depths.

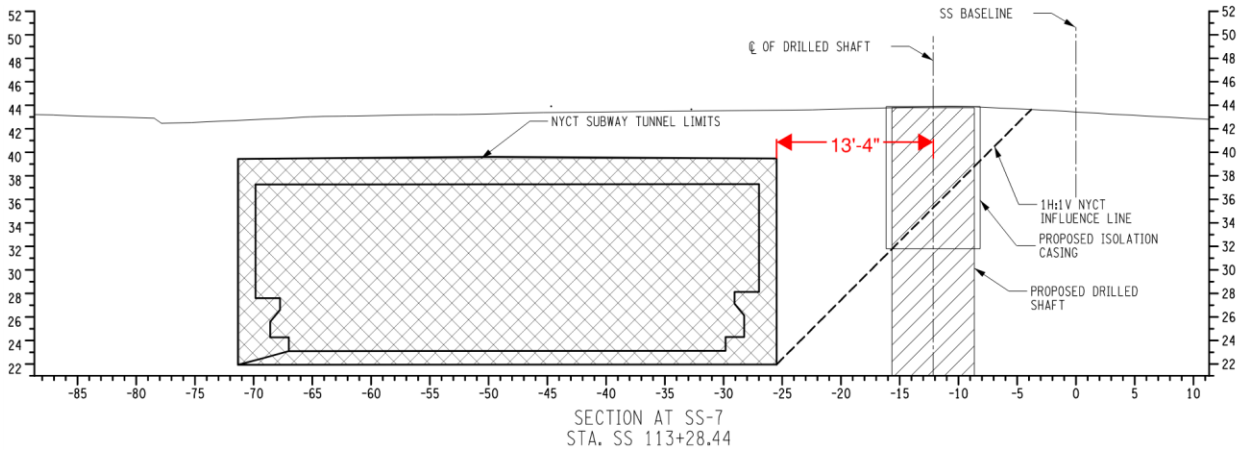


Fig. 8. Typical cross-section of NYCT tunnel (left) relative to drilled shaft (right).

 © Deep Foundations Institute 2025

At Piers SS-3 to SS-5, drilled shafts with an outside diameter of 72 inches surrounded by an isolation casing extending to the influence line at the point of intersection with the outer limit of the shaft were selected for the design. At SS-6 and SS-7, the drilled shafts will be 84 inches in diameter with isolation casings. This design ensured that the new shafts would not exert lateral and vertical pressures on the tunnel structure. Axial loads were resisted by drilled rock sockets located below the influence zone. Fig. 9 illustrates the confined work area between the SS Piers and the existing roadway, under which was the NYCT tunnel.



Fig. 9. Completed SS Ramp columns adjacent to Bruckner Boulevard (right).

Construction Challenges

The construction of drilled shafts was challenged by the urban setting in which they were installed, including the constrained site and laydown space and the proximity of the shafts to existing underground subway tunnels.

The NYC Building Code requires the Owner or the Contractor to obtain a determination of no impact from NYCT when working near a tunnel after demonstrating that the construction equipment, installation process, and foundation permanent load transfer response will pose no detrimental effects on existing structures. The use of large-diameter drilled shafts allowed the designer to use a single isolation casing, as previously discussed, to resolve load transfer. However, this required the use of large equipment on confined city streets. Furthermore, the load of the rig could not be placed over the buried tunnel. The drilled shafts were comprised of a telescoping casing solution where the outer casing was used to provide the lateral load isolation gap within the influence depth, while the inner casing was designed to deliver the function of flexural resistance. The great challenge to installation was to provide a reliably high level of shaft position and verticality to ensure that the casings were concentric and in the correct location. Typically, this tolerance is met by over-sizing the shaft; however, given the close proximity to the tunnel, increasing the shaft diameter had major implications on design and drilling equipment size. To solve the tolerance requirements, a drilled shaft guide-collar guide was used and offered superior position control and drill rig rigidity to maintain the required verticality. Figures 10 and 11 show examples of the guide collar, the rebar cage with O-Cell attached, and the top of a shaft with isolation casing as load testing was taking place.



Fig. 10. Concrete guide collar to control drilled shaft location tolerances.

 © Deep Foundations Institute 2025



Fig. 11. Drilled shaft rebar cage and Osterberg Load Cell (left) and load test on completed test shaft (right).

CONCLUSIONS

Hunts Point Interstate Access Improvement Project – Contract 3 presented many geotechnical design and construction challenges. The proposed structures and foundations had to be constructed in a densely populated urban setting with limited above and underground spaces, with the goal of minimizing or eliminating impact to the existing structures, which included an NYCT tunnel and an NYSDOT retaining wall. The design and construction of the proposed foundations were tailored to meet these requirements, accommodating an aggressive project schedule.

REFERENCES

Baskerville, C.A., “Bedrock and engineering geologic maps of Bronx County and parts of New York and Queens Counties, New York”, US. Geological Survey, 1992.

 © Deep Foundations Institute 2025

RELIABILITY ANALYSIS OF DRILLED SHAFT RESISTANCE – A CASE STUDY OF THE CIRCUNVALACION NORTE VIADUCT PROJECT

Bernardo Jiménez, Research Affiliate, Dept. of Civil Eng., University of São Paulo, Brazil, b.jimenez.geotech@gmail.com
Adrián Torrico Siacara, Associate Professor, Dept. of Civil Eng., University of São Paulo, Brazil, adrian.torrico@usp.br

ABSTRACT

This paper presents a method for estimating drilled shaft resistance using both random variable (RV) and random field (RF) approaches to account to soil variability, and compares the results with a deterministic case. The study is focused on Circunvalacion Norte viaduct project in Costa Rica, which includes 426 drilled shafts and 58 piles caps. Soil characterization is based with an extensive database of 138 pressuremeter (PMT) tests. Simple Monte Carlo Simulation (SMCS) is then used for performing reliability analysis. The spatial variability of the soil is modeled through the RF approach with Karhunen–Loève expansion. A comparison of deterministic and probabilistic analyses reveals significant discrepancies between the two approaches. The deterministic calculations, which are commonly used, indicates that the suggested drilled length may be sufficient, however, the results from the probabilistic methods such as RV and RF models predict a higher risk, in some cases with an unacceptable probability of failure under variable terrain conditions. The paper also investigates the sensitivity of RF models to correlation length variations, and shows how this parameter influences the calculated shaft resistance. These findings underscore the importance of considering soil variability and the inherent uncertainties in geotechnical design. This paper highlights the necessity of implementing a probabilistic approach to better consider uncertainties of soil properties. By applying reliability analysis, the study provides a more robust framework for evaluating drilled shaft performance, leading to safer and more resilient geotechnical designs.

Keywords: drilled shaft, random variable, random field shaft, reliability, probability of failure

INTRODUCTION

The design of deep foundations, including drilled shafts, plays a crucial role in ensuring the stability and safety of infrastructure projects. Traditional geotechnical design methodologies often rely on deterministic approaches, using single-point estimates of soil properties such as the mean undrained shear strength (S_u). While these methods are widely applied in practice, they fail to account for the inherent spatial variability of soil properties (Baecher & Christian, 2005), which can lead to an underestimation of risk and, consequently, an increased probability of failure.

Geotechnical materials exhibit natural heterogeneity due to complex geological processes. Even within the same geological unit, soil properties can vary significantly (Baecher, 2023). In cases where such variability is substantial, probabilistic approaches provide a more robust framework for design (Fenton & Griffiths, 2008). Reliability analysis allows engineers to quantify the probability of failure (P_f), offering a more comprehensive assessment of foundation performance under uncertain conditions.

 © Deep Foundations Institute 2025

The Circunvalacion Norte project represents the final segment of an urban peripheral highway encircling San José, the capital city of Costa Rica. It features the longest viaduct in the country (see **Error! R eference source not found.**), spanning 4 km, and is supported by 426 drilled shafts distributed across 58 pile caps. Given the project's scale-as the largest viaduct in the country with drilled shafts depts up to 42.0 m- and the geotechnical challenges associated with its foundation design, ensuring the reliability of the drilled shafts is of paramount importance.

This study aims to compare deterministic and probabilistic methods for evaluating the axial resistance of drilled shafts. Specifically, it contrasts conventional deterministic approaches with probabilistic methods incorporating random variables (RV) and random fields (RF), which are described in this paper, to assess their impact on design reliability.



a) b)

Fig. 1. Circunvalacion Norte Viaduct a) drilled shaft construction b) completed structure.

PROBLEM DEFINITION

The accurate calculation of drilled shaft resistance is directly linked to a realistic representation of soil resistance. For the Circunvalacion Norte project, silty and silty clay soils with medium to low plasticity were encountered. Soil resistance was determined through pressuremeter (PMT) tests, with 138 tests conducted across the viaduct. The test results yielded a mean value of the effective pressure limit (P_L*) of 3657 kPa and a standard deviation of 1732 kPa, Fig 2 shows the probability density function (PDF) of the performed tests which justifies an assuming a log-normal distribution. The P_L* obtained from these tests is used to compute drilled shaft resistance based on the following equations:

$$S_u = P_a \times 0.21 \times (\frac{P_L^*}{P_a})^{0.75} \quad [1]$$

$$R_T = R_{side} + R_{base} \quad [2]$$

$$R_{side} = \pi B \Delta z \alpha S_u \quad [3]$$

$$R_{base} = N_C^* S_u \quad [4]$$

 © Deep Foundations Institute 2025

Where S_u is the undrained shear strength; P_a is the atmospheric pressure; R_T is the total drilled shaft resistance; R_{side} is the side resistance; R_{base} is the base resistance; B is the drilled shaft diameter; Δz is the the thickness of the layer; α is the coefficient relating unit side resistance to undrained shear strength; Nc*is the bearing capacity factor

The Eq. 1 is obtained from Briaud (2019), while Eq. 2 through Eq 4 are obtained from FHWA GEC-10 (Brown et. al, 2018). As seen in these equations, drilled shaft resistance is directly related to the undrained shear strength (S_u), which can be treated either as a deterministic constant (typically using the mean value) or as a random variable to capture inherent soil variability.

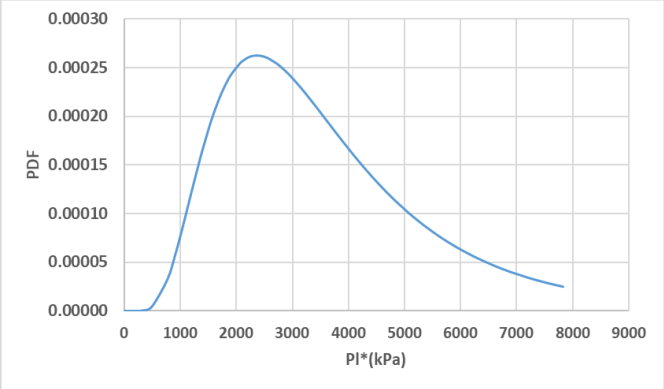


Fig. 2. Probability density function (PDF) of the 138 PMT tests.

METHODS

In this study, two approaches are used to account for soil spatial variability: the random variable approach (RV) and the random field approach (RF). For both methods, a Simplified Monte Carlo Simulation (SMCS) is performed to estimate the probability of failure (P_f) and the associated reliability index (β). The results obtained from these probabilistic analyses are compared with a deterministic method, where drilled shaft resistance is calculated using the mean value of the soil's undrained shear strength.

Random Variable Approach

The random variable approach (Fenton & Griffiths, 2008) provides a straightforward method to account for uncertainty in soil properties by treating them as statistically independent variables rather than spatially correlated fields. In this study, soil resistance parameters are modeled as lognormal random variables, preserving the inherent variability observed in field measurements while ensuring positive values for geotechnical properties.

A random variable X is characterized by its mean μ_X and standard deviation σ_X, with its probabilistic distribution defined as:

$$f(X) = \frac{1}{X\sigma_X\sqrt{2\pi}} \exp\left(-\frac{(\ln X - \mu_X)^2}{2{\sigma_X}^2}\right) \quad [5]$$

 © Deep Foundations Institute 2025

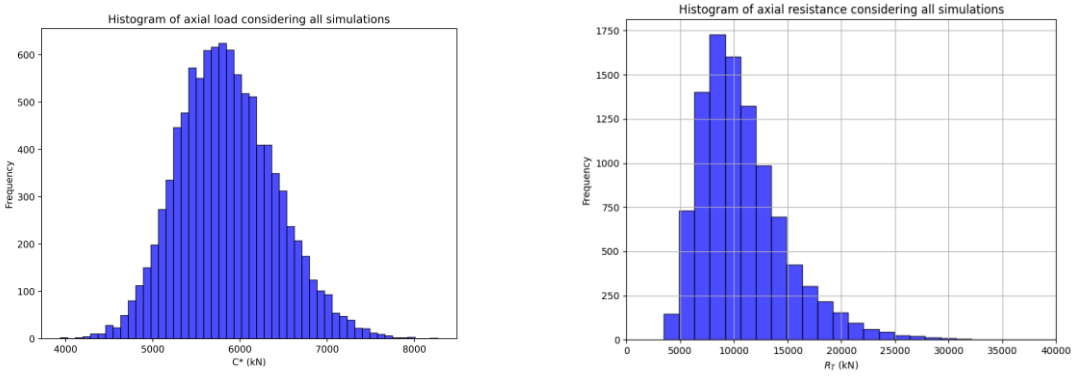
where X represents a given soil parameter (e.g., drilled shaft resistance), and μ_X and σ_X are obtained from the statistical analysis of pressuremeter test (PMT) results.

For this study, the coefficient of variation (*CoV*) is used to quantify the uncertainty in soil properties:

$$CoV = \frac{\sigma_X}{\mu_X} \quad [6]$$

Previous geotechnical studies suggest that many soil resistance properties (e.g., PMT limit pressure, undrained shear strength, friction angle) often have *CoV* values between 10-50%, depending on soil type and test method (Duncan, 2000; Baecher & Christian, 2005; Phoon, 2008). For this study, a *CoV* of 47% is used, derived from the mean and standard deviation of 138 PMT tests conducted on site. This value influences directly on the number of simulations required for the Monte Carlo analysis, as will be discussed later in the document.

In this study, both axial loads (defined as C^*) and soil resistance (previously defined as R_T) are treated as random variables. From the structural model, the mean value of the axial load acting in the drilled shafts correspond to 5825 kN with and a standard deviation of 105 kN. For RV approach, the drilled shaft is characterized by a random value of S_u along its entire length and tip. **Error! Reference source not found.** illustrates the statistical distributions of both parameters, considering their respective probability density functions and an example case of a drilled shaft of 1.0 m diameter, a length of 25.0 m and 10,000 simulations.



a) **b)**

Fig. 3. Distribution of a) loads b) resistance.

Random Field Approach

The random field approach (Vanmarcke, 2010) provides a rigorous tool to characterize and model the spatial variability of soil properties. In this study, the Karhunen–Loève Expansion (KLE) is used to efficiently represent the random field while preserving the key statistical characteristics of the soil. KLE is a powerful mathematical technique for modeling stochastic processes, expressing them as an infinite series of deterministic functions weighted by uncorrelated random variables (Zhang et. al, 2023).

A second-order stochastic process X(s) (e.g., the soil's effective limit pressure from PMT tests) with mean μ_x and covariance function $C_X(x,x')$ can be describes as:

$$X_s = \mu_X + \sum_{n=1}^{N} \sqrt{\lambda_N}\xi_n \Phi_n(s) \quad [7]$$

Where λn is the eigenvalues of the covariance function $C_X(s,s')$; Φ_n (s) the corresponding eigenfunctions; ξn the uncorrelated standard normal random variables; N the number of terms retained in the expansion.

The eigenvalues and eigenfunctions are obtain by solving the Fredholm integral equation:

$$\int_D C_X(x,x')\Phi_n(x')dx' = \lambda_N \Phi_n(x) \quad [8]$$

$$C_X(x,x') = \sigma_X^2\left(\frac{|x-x'|}{dx} - \frac{|y-y'|}{dy}\right) \quad [9]$$

The correlation lengths (*dx*-*dy*) appear in the covariance function $C_X(s,s')$, which determines the spatial structure of the random field. Large values of *dx* or *dy* indicates smoother, slow varying fields, small values of *dx* or *dy* indicates highly fluctuating fields. For this study, random fields are generated using Python code and three combinations of correlation lengths are tested (*dx* = 20, *dy* = 3), (*dx* = 10, *dy* = 3), and (*dx* = 3, *dy* = 3) to evaluated its impact on the reliability index. **Error! Reference source not found.** s hows the example of random fields for one simulation of each of the three correlations lengths tested. The red line indicates the position and depth of the simulated drilled shaft. This element with a *L* length is computed in the center of the field, then the drilled shaft is discretized with *Δl* values of 1,0 m and each mean P_L* value is computed for the corresponding *Δl*.

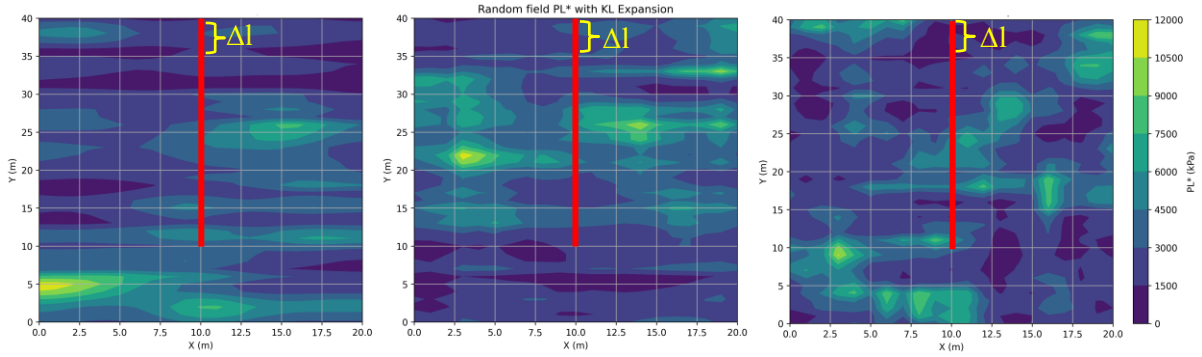


Fig. 4. Example of random field generated for P_L*a) *dx*=20 *dy*=3 b) *dx*=10 *dy*=3 c) *dx*=3 *dy*=3.

Simple Monte Carlo Simulation (SMCS)

Simulation methods are based on the generation of a large set of deterministic samples and the evaluation of the performance of each sample. For this study a Simple Monte Carlo Simulation (SMCS) approach is used. In SMCS, each simulation is independent and uses standard random sampling, providing provides a straightforward and transparent approach to quantify the effects of uncertainty in geotechnical parameters.

Since each simulation involves generating a correlated spatial field, SMCS works more efficiently than other sampling methods like Latin Hypercube (LHS). The probability of failure P_f in SMCS is computed as:

$$P_f = \frac{N_F}{N} \quad [10]$$

Where N_F is the number of samples where failure was observed and N is the total number of samples. The corresponding generalized reliability index β_{SMCS} can be defined as:

$$\beta_{SMCS} = -\Phi^{-1}(P_f) \quad [11]$$

In this study, three reliability indices are analyzed: β=2.33, β=3.09, and β=3.72, which correspond to probability of failure values of P_f=0.01, P_f =0.001, and P_f =0.0001, respectively. These values are classified as moderate, high, and very high reliability levels (Ditlevsen & Madsen, 1996). CALTRANS (2019) indicate that for drilled shafts, past geotechnical design practice has resulted in an effective reliability index, β, of 3.0, or an approximate probability of a failure of 1 in 1,000, for foundations in general, and for highly redundant systems, such as pile groups, since that redundant group effect exists, it is not necessary to use such a high beta value for design, an approximate reliability index, β, of 2.3 is used, with an approximate probability of failure of 1 in 100. This classification helps in assessing the risk associated with different design scenarios and understanding the impact of soil variability on drilled shaft performance. As defined by Paikowsky (2004), a redundant pile system is defined as 5 or more piles per pile cap, 4 or fewer piles per pile cap is defined as nonredundant.

A key metric for assessing the convergence of a SMCS is given by the coefficient of variation *CoV* defined as:

$$CoV = \sqrt{\frac{1 - P_f}{NP_f}} \quad [12]$$

As seen in Eq. 12, for the P_f values used in this study (0.01, 0.001, and 0.0001), 9900, 99900, and 999900 simulations, respectively, are required to ensure a *CoV* of 10%. This *CoV* value measures the uncertainty of the simulation, and it independent of the materials statistics. Additionally, as shown in **Error! Reference s ource not found.**, increasing the number of simulations reduces the uncertainty in the drilled shaft resistance value, considering a 95% confidence interval *CI*. Simulations greater than 1,000 already ensure stable resistance values.

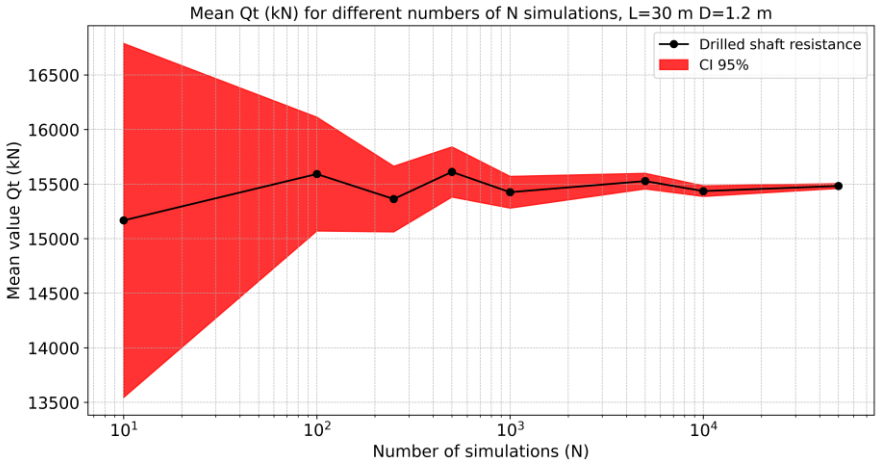


Fig. 5. Impact on the converge of drilled shaft resistance with the increase of N simulations.

RESULTS

The following presents the results obtained from the reliability analysis for the piles using the deterministic, random variable, and random field approaches. For the deterministic case, the pile resistance was computed using the mean value of P_L*. A comparison of the probability of failure for each combination of pile length and diameter is made, with a more in-depth analysis conducted for the random variable and random field cases.

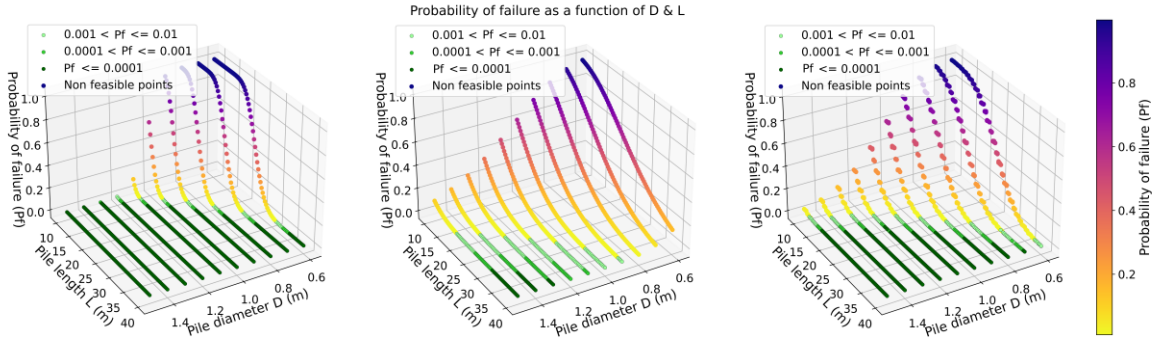
Comparison of Deterministic and Probabilistic Analyses

The results of the failure probability are presented in **Error! Reference source not found.**. These results h ave been discretized according to the target P_f values (0.01, 0.001, and 0.0001), with those having a probability of failure (P_f) greater than 0.01 considered unfeasible for design. **Error! Reference source n ot found.** a) shows the results for the deterministic case, where it can be observed that all diameters ranging from 1.5 m to 1.2 m have P_f values lower than 0.001. It is also observed that even for the smallest diameter of 0.6 m, pile lengths starting from 30 m indicate a P_f lower than 0.01. **Error! Reference source n ot found.** 1b) shows the P_f results for the random variable approach, where fewer feasible combinations are observed compared to the deterministic approach. Even for the largest diameter of 1.5 m, not all combinations yield results with a P_f lower than 0.01. In this case, no combination for diameters between 0.6 m and 0.8 m indicates an adequate design, with P_f values greater than 0.01. **Error! Reference source n ot found.** c) shows the results for the random field approach. Fewer feasible combinations are observed compared to the deterministic case but more than the random variable case.

Overall, the comparison of these methods highlights that, deterministic analyses, which have been more commonly used, may lead to risky designs if the nature phenomena involved in the problem is not considered. This is because both the loads and soil resistance should not be treated as a single value, as they inherently have variability. A 15 m pile with a diameter of 1.0 m, according to the deterministic case, would indicate a P_f of 0.004, considered adequate. However, under the random variable approach, the same pile has a P_f of 0.33, and under the random field approach, a P_f of 0.19, values associated with pile collapse.

 © Deep Foundations Institute 2025

According to CALTRANS (2019) criteria, if the foundation is classified as a highly redundant system, a target P_f of 0.01 is acceptable, and piles with diameters from 0.9 m can be considered in the RV approach. The Random Field (RF) approach is less stringent; for the same redundant foundation, feasible designs exist with piles as small as 0.6 m in diameter. For more general systems, a reliability index β of 3.0 (or a target P_f of 0.001) is required, which limits the RV approach to piles with diameters of 1.1 m or larger, and the RF approach to piles of 0.7 m or larger.



a) b) c)

Fig. 6. Probability of failure ext not clear in Figs. 3 and 4 for a) deterministic b) random variables c) random field.

Probability of Failure (Pf) Analysis

The **Error! Reference source not found.** represents the curves relating the pile diameter-to-length ratio (*B/L*) and the probability of failure P_f. Results are presented for the deterministic, random variable, and random field approaches. The figures exhibit a blank area on the right-hand side, which corresponds to an infeasible construction zone due to the assumed limitation that the kelly bar of the drill rig cannot exceed a depth of 40.0 m.

It can be observed that for the case with the lowest calculated P_f values (deterministic), the curves are relatively well-separated. For the random field case (with higher P_f values), the curves start to cluster more closely together. For the random variable case, the curves converge even more and tend toward a *B/L* ratio of approximately 0.04. This indicates that, under the random variable approach, the optimal design—associated with the lowest P_f values—corresponds to *B/L* combinations near 0.04. Specifically, P_f values lower than 0.0001 are found for *B/L* ratios between 0.035 and 0.045. Additionally, under the random variable approach, no *B/L* combination greater than 0.08 achieves P_f values below 0.01.

 © Deep Foundations Institute 2025

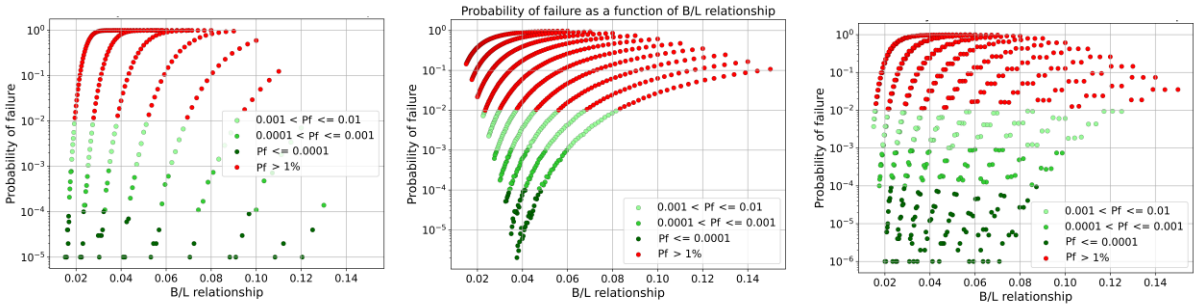


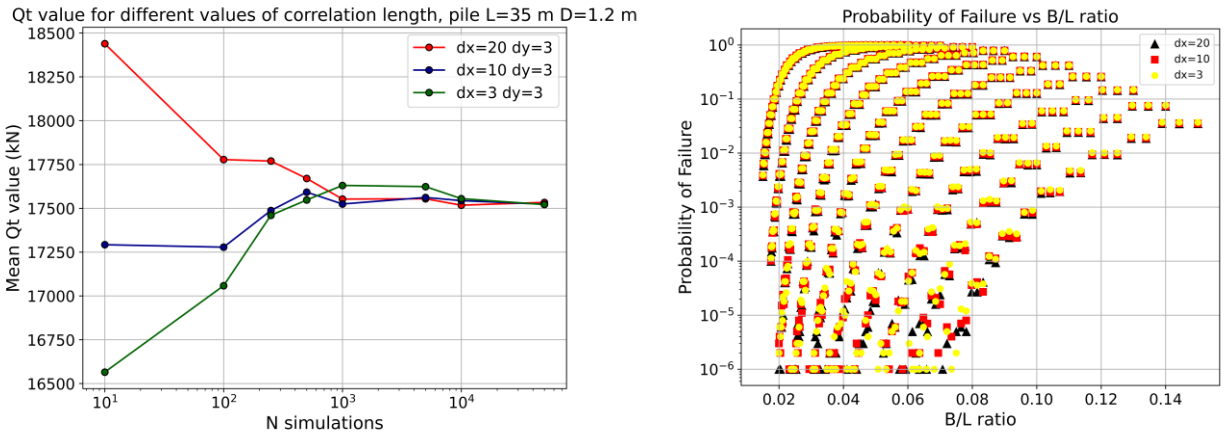
Fig. 7. Probability of failure as a function of B/L relationship a) deterministic b) random variable c) random field.

As previously observed, these relationships reinforce the risk of relying solely on deterministic approaches in pile design. As shown in **Error! Reference source not found.** a), deterministic results s uggest that *B/L* values greater than 0.12 can lead to P_f values below 0.01, which contradicts the results obtained from both the random variable and random field methods.

Sensitivity Analysis of Correlation Lengths

For this study, within the random field framework, analyses were conducted using three different correlation length combinations (*dx=20–dy=3*, *dx=10–dy=3*, and *dx=3–dy=3*). **Error! Reference source n ot found.** examines the influence of these spatial correlation structures on the results. **Error! Reference source not found.** a) presents the variation of the average axial resistance as a function of the number of simulations for each correlation length. It is observed that for *dx*=20, higher initial values of axial resistance (Qt) are obtained, particularly when the number of simulations is below 500. The case with *dx*=10 shows intermediate Qt values, while *dx*=3 yields the lowest. However, this behavior dissipates as the number of simulations increases, and around 10,000 simulations, the three correlation length cases converge to a similar mean value. This suggests that, within the random field framework, provided that a sufficiently large number of simulations is used, the influence of the correlation length on the mean response becomes negligible. Fenton & Griffiths (2008) indicate that the mean response from random field simulations will converge to the expected value of the system as the number of simulations increases. The variability may persist, but the central tendency is stable.

A comparison between the levels of P_f obtained for different correlation lengths is presented in **Error! R eference source not found.** b). The results indicate that the case with *dx=20* yields the lowest P_f values, suggesting more resistant pile behavior. However, the differences between the results for *dx=20* and *dx=3* are relatively small, with variations around 5%. This behavior can be explained by the spatial characteristics imposed by the correlation structure: larger values of *dx*, while maintaining *dy*, represent soil properties that vary gradually in the horizontal direction, leading to smoother transitions and lower P_f values. In contrast, smaller *dx* values imply that soil properties fluctuate strongly in both directions, increasing the local variability and leading to higher P_f levels (Fenton & Griffiths, 2008).



a) b)

Fig. 8. Sensitive of correlation length dx a) number of simulations b) Probability of failure

Furthermore, when the correlation length becomes large relative to the size of the pile or the domain, the RF tends to become nearly constant approaching the RV analysis. As the scale of fluctuation increases relative to the system size, the spatial field approaches perfect correlation—effectively behaving as a constant random variable (Vanmarcke, 2010).

Comparison of Random Variable and Random Field

Based on the results shown in the previous sections, it is evident that RV calculates fewer feasible points for all P_f objectives (0.01, 0.001, 0.0001), indicating higher P_f values compared to the RF method. The **Error! Reference source not found.** shows the results for each combination of pile diameter (B) and l ength (L), as well as the difference between the values obtained by RF and RV. Positive values in this figure indicate that RF calculated higher P_f values, while negative values indicate that RV calculated higher P_f values. As shown in the figure, most of the results are negative, suggesting that RV values are greater than RF values. However, there are a few exceptions, such as some points for piles with diameters between 0.6 and 1.0 m, but for larger piles, all P_f values calculated using RV are higher.

This behavior can be explained by the inherent characteristics of each method. RV assumes a constant value for the undrained shear strength (S_u) of the pile, treating it as a random variable, but it can produce more "extreme" samples because each simulation uses a single random value, without the cancellation of extremes (Fenton & Griffiths, 2008). This approach does not capture spatial variability but only global uncertainty. On the other hand, RF discretizes the Su values along the pile, smoothing the spatial variability and leaving the mean with less variation (Phoon & Kulhawy, 1999).

Both methods are suitable for reliability analysis, as they account for the inherent variability of the soil. However, Random Field is considered a more realistic representation of a geotechnical model, with the possibility of presence of softer or harder material that do not fully envelop the pile, with stratigraphy that can be better adjusted to field observations, leading to more accurate reliability assessments in geotechnical engineering (Siacara, Beck & Ji, 2024).

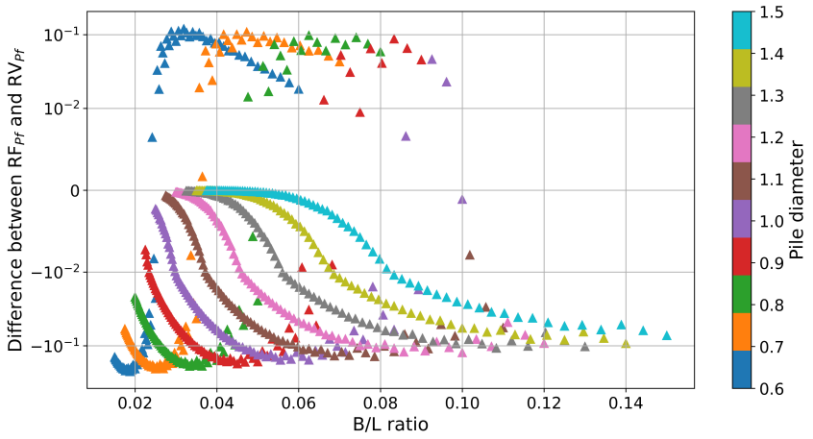


Fig. 9. Comparisson between RV & RF

CONCLUSIONS

This study presents a reliability-based framework for evaluating drilled shaft resistance, applied to the Circunvalacion Norte viaduct project in Costa Rica, which comprises 58 piles caps and 426 drilled shafts, with lengths up to 42.0 m. Soil variability was characterized using an extensive geotechnical database of 138 pressuremeter (PMT) tests. The analysis compared deterministic design methods with two probabilistic approaches: random variable (RV) and random field (RF). Simple Monte Carlo Simulation (SMCS) was used for reliability quantification, and spatial variability in the RF method was modeled via the Karhunen–Loève expansion.

The results reveal clear differences between the approaches. Deterministic analyses, although commonly used in practice, consistently underestimate the P_f. This method assumes fixed soil parameters, which may lead to unconservative designs, particularly when soil variability is high. For example, a 15 m long, 1.0 m diameter pile yields a P_f of 0.004 under deterministic assumptions, yet rises to 0.33 under RV and 0.19 under RF—both suggesting potential failure.

When comparing the probabilistic methods, RV consistently calculated higher P_f values than RF. This is due to its nature: RV models assume a single value for soil strength per simulation, allowing extreme realizations to dominate and fail to account for spatial trends. On the other hand, RF models discretize the soil profile and incorporate spatial correlation, leading to smoother variability and, consequently, lower P_f s. As the simulations progress, the mean responses of RF models converge to stable values, as suggested by Fenton & Griffiths (2008), highlighting the method's robustness.

A sensitivity analysis of spatial correlation lengths (dx = 3, 10, and 20) within the RF framework revealed that increasing the horizontal correlation (dx) leads to slightly lower P_f values. When dx is large (e.g., dx = 20), soil properties vary gradually in the horizontal direction, producing smoother resistance profiles along the pile and reducing the occurrence of weak spots. Conversely, smaller dx values introduce more local heterogeneity, increasing P_f. However, the variation between P_f results for dx = 20 and dx = 3 was moderate (~5%), and all correlation length cases converged to similar mean resistances after 10,000 simulations. Notably, when the correlation length exceeds the pile or domain size, the RF model approaches a perfectly correlated field, behaving similarly to a constant random variable

 © Deep Foundations Institute 2025

Overall, although both RV and RF are valid for reliability analysis, RF is more representative of geotechnical reality. It captures complex subsurface behaviors such as the presence of weak zones, stratigraphic layering, and pockets of contrasting material—conditions often observed in the field but missed in simpler models. As demonstrated by Siacara, Beck & Ji (2024), random field simulations lead to more accurate reliability estimations and help mitigate unsafe designs.

REFERENCES

Baecher, G. B., & Christian, J. T. (2005). *Reliability and statistics in geotechnical engineering*. John Wiley & Sons.

Baecher, G. B. (2023). 2021 Terzaghi lecture: Geotechnical systems, uncertainty, and risk. *Journal of Geotechnical and Geoenvironmental Engineering*, *149*(3), 03023001.

Briaud, J. L. (2019). *The pressuremeter*. Routledge.

Brown, D. A., Turner, J. P., Castelli, R. J., & Loehr, E. (2018). *Drilled shafts: Construction procedures and design methods* (No. FHWA-NHI-18-024). National Highway Institute (US).

Caltrans (2019). *California Amendments to the AASHTO LRFD Bridge Design Specifications (2017 Eighth Edition)*. California Department of Transportation

Ditlevsen, O., & Madsen, H. O. (1996). *Structural reliability methods* (Vol. 178). New York: Wiley.

Duncan, J. M. (2000). Factors of safety and reliability in geotechnical engineering. *Journal of geotechnical and geoenvironmental engineering*, *126*(4), 307-316.

Fenton, G. A., & Griffiths, D. V. (2003). Bearing-capacity prediction of spatially random c φ soils. *Canadian geotechnical journal*, *40*(1), 54-65.

Fenton, G. A., & Griffiths, D. V. (2008). *Risk assessment in geotechnical engineering* (Vol. 461). New York: John Wiley & Sons.

Paikowsky, S. G. (2004). *Load and resistance factor design (LRFD) for deep foundations* (Vol. 507). Transportation Research Board.

Phoon, K. K., & Kulhawy, F. H. (1999). *Characterization of geotechnical variability*. Canadian Geotechnical Journal.

Phoon, K. K. (Ed.). (2008). *Reliability-based design in geotechnical engineering: computations and applications*. CRC Press.

 © Deep Foundations Institute 2025

Siacara, A. T., Beck, A. T., & Ji, J. (2024). Impact of random field simulations on FEM-based earth slope reliability. *Geotechnical and Geological Engineering*, *42*(8), 7873-7891.

Vanmarcke, E. (2010). *Random fields: analysis and synthesis*.

Zhang, J., Xiao, T., Ji, J., Zeng, P., & Cao, Z. (2023). Bayesian methods. In *Geotechnical Reliability Analysis: Theories, Methods and Algorithms* (pp. 265-307). Singapore: Springer Nature Singapore.

 © Deep Foundations Institute 2025

NORTH EAST LINK PROJECT, MELBOURNE, AUSTRALIA
LOWER PLENTY ROAD INTERCHANGE DIAPHRAGM WALL WORKS

Z. El Hajj[1] , MEng. and T. Khin[2], BE Hons. MIEAust NER.

[1]Project Manager, Trevi Australia, Melbourne, VIC, Australia, email: zelhajj@trevispa.com
[2]Production Manager, Wagstaff Piling, Melbourne, VIC, Australia, email: t.khin@wagstaffpiling.com.au

ABSTRACT

The Lower Plenty Road Interchange for the North East Link project in Melbourne requires the use of a specialist foundation technique known as a diaphragm wall. The diaphragm wall was selected as a robust and economical solution that is structurally stable and watertight and allows for the cut and cover tunnel excavation method to be undertaken once the diaphragm walls are installed. The specialist ground engineering contractor Trevi Australia Wagstaff Piling Joint Venture (TAWP JV) has mobilised four Hydromill cutters to the project which is the first instance of its kind in Australian history. These cutters install diaphragm walls up to 45m in depth in individual interlocking panels up to 6.7m long and 1.2m in width using a bentonite slurry as support fluid. There are 471 of these individual diaphragm wall elements referred to as 'panels' on this project spread over 900 lineal metres which encompasses significantly varying and challenging ground strata. One such significant challenge has been the presence of major geotechnical fault lines characterised with steeply dipping bedding planes with a relatively high strike to the diaphragm wall trench. These sharply dipping bedding planes have interacted with other joints and defects within the rock mass which has led to block wedge failure of the wall and collapse of the trench. Post collapse remedial works and the use of preventative design and construction measures including reducing panel geometry, adjustments to bentonite mix properties and performance, soil nailing, pressure grouting and increasing the pressure head differential between natural ground water and the bentonite support fluid were implemented by the project.

Keywords: collapse, diaphragm, bentonite, stability, hydromill, fault

1 INTRODUCTION

This paper presents a case study of the geotechnical and construction challenges involved in the diaphragm wall installation at the North East Link Lower Plenty Interchange. Amongst the challenges are the presence of fault zones, trench stability, highly variable strata, challenging site layout and the ongoing management of four (4) hydromill cutters to maintain a safe and productive environment.

2 DESIGN AND GROUND CONDITIONS

2.1 Construction Methodology

The diaphragm wall at the Lower Plenty Interchange site is being constructed as a permanently reinforced concrete structure that's 1.2m thick and over 3km in length with panels extending

 © Deep Foundations Institute 2025

45m below existing ground level. The purpose of the diaphragm wall is to behave as a water retaining structure for a cut and cover box with tunnel portals at each end to allow the safe launching and retrieval of a tunnel boring machine to build the twin North East Link tunnels.

The diaphragm wall is constructed using specialist foundation piling equipment called a hydromill cutter. This heavy foundation machine excavates soil with a suspended cutting module that weighs 44T and advances through a combination of its self weight and high torque delivered to a set of independently rotating cutting wheels. The cutter module excavates the rock and soil and mixes it with a bentonite clay support fluid and pumps it back into a desanding plant which filters the bentonite and soil so the fluid can be sent back to the panel and re-used. This process is undertaken for the entire length and depth of the panel until the excavation is complete and the panel is fully supported by the bentonite fluid. The role of the bentonite support fluid is to provide hydrostatic support and pressure against the soil and rock excavation face as the unit weight of bentonite will be higher than that of water. The bentonite support fluid also applies a thin film on the side walls called filter cake which helps to stop fluid loss from the excavation providing further benefits to panel stability. As rock and soil is removed from the panel, more bentonite is added to maintain a fluid level as close to guide wall level as possible. The bentonite used for excavation is called “Working slurry” and will typically not be within project specification parameters for casting.

At the completion of panel excavation the fluid inside the panel undergoes a cleaning and desanding process to restore it to a near fresh state called “casting slurry”. The bentonite parameters in this state aim to meet an optimum criteria for specific gravity, sand content and fluid viscosity to allow the best possible quality for the panel when placing reinforcement and concrete. The parameters are determined using slurry test methods known as the mud balance test, the sand screen test and marsh cone funnel test. The bentonite specification for support fluids in their different states are shown in Table 1. As the concrete is required to displace the bentonite fluid during the casting operation, a lower weight slurry with less fines and sand content will lead to a better quality finish with a lower likelihood of bentonite caking and forming on the reinforcement or the side wall of the excavation. If the fluid was heavy and the sand content was high then as the panel was excavated and exposed there may be potential issues with quality.

During excavation, the working slurry continuously undergoes a desanding process at the specialised slurry treatment plant. Through this desanding process the excavated soil and working slurry is separated through a series of vibrating screens, shakers, hydro cyclones and desilters. The typical particle size the desanding plant utilised by the project can filter down to is about 150 microns, however the profile of the Silurian siltstone produces a lot of micro fines during the excavation process which cannot be filtered out. These particles remain in the bentonite and are not removed through the desanders and do not appear in the sand content testing results. They instead build and accumulate in the slurry as micro fines.

A sand content result may show less than 0.25% however the unit weight could be as high as 1.40 grams per millilitre which is enormously significant. During bentonite rejuvenation the working slurry in the panel is exchanged for clean and fresh casting slurry which is required to be less than 1.15 grams per millilitre. This is a significant reduction in fluid density and subsequent reduction

in net hydrostatic pressure being exerted on the excavation face. This process of pre-pour bentonite slurry rejuvenation known as a “clean and exchange” has been the preceding activity in each instance of trench instability indicating that net hydrostatic pressure plays a significant role in overall trench stability. Thus a project decision was made to implement a bentonite pre-pour fluid density as close to the maximum allowable limits in the specification as possible.

Table 1. Bentonite Support Fluid Parameters

Property to be measured	Units	Test method and apparatus	Compliance values measured at 20°C		
			Freshly mixed	Ready for re-use	Sample from excavation prior to concreting
Density	g/ml	Mud balance	<1.10	<1.25	<1.15
Fluid loss (30-minute test)	ml	Low-temperature test fluid loss	<30	<50	N/A
Filter cake thickness	mm	Low-temperature test fluid loss	<3	<6	N/A
Viscosity	s	Marsh cone	32 to 50	32 to 60	32 to 50
Sand content – refer note 1	%	Sand screen set	N/A	N/A	<4
pH	N/A	Electrical pH meter; range pH 7 to 14	7 to 11	7 to 12	N/A

2.2 Overall Geotechnical Profile

The geology of the Lower Plenty Interchange cut and cover site consists predominantly of Silurian age sedimentary rocks overlain by Quaternary alluvium associated with the Banyule Creek. The rock is primarily composed of Melbourne Formation and Anderson’s Creek Formation. The degree of weathering and strength of the rock typically improves with depth with some cases of reverse weathering evident. The alluvium overlying the rock is predominantly cohesive with minor lenses and channels of granular material however the proportions of clay and silt vast outweigh the discontinuous layers of sand. The residual clay and silt soils above the bedrock are derived from in-situ weathering and typically range between 1m and 5m in thickness. The Silurian rock consists of siltstone, sandstone and interbedded siltstone and sandstone layers with the bulk of the rock mass being primarily siltstone. The rock is classified into different rock classes (S1 to S4) which correspond with the distinct weathering grades.

The UCS of the various units ranges from 20 MPa to 60 MPa based on the UCS samples and test results. The rock mass itself however is highly anisotropic and defines by its various bedding planes, joints and other defects in the rock mass including the aforementioned fault and sheared zones. The box itself sits in an anticline with the bedding planes dipping towards each respective wall alignment with the strike of the fault lines almost perpendicular to the longitudinal section of wall. This means that large steeply dipping rock wedges can form on the face of the

 © Deep Foundations Institute 2025

excavation, causing the panel to sit in a precarious situation due to these defects. The bedding planes typically dip between 50 and 75 degrees at the wall intersect. In the below figure the inferred fault lines (dashed red lines) and general bedding trends (dashed black lines) can be seen intersecting each other. The next picture below it is a cross section of the anticline hinge and the general representation of the likely orientation of major bedding plane discontinuities.

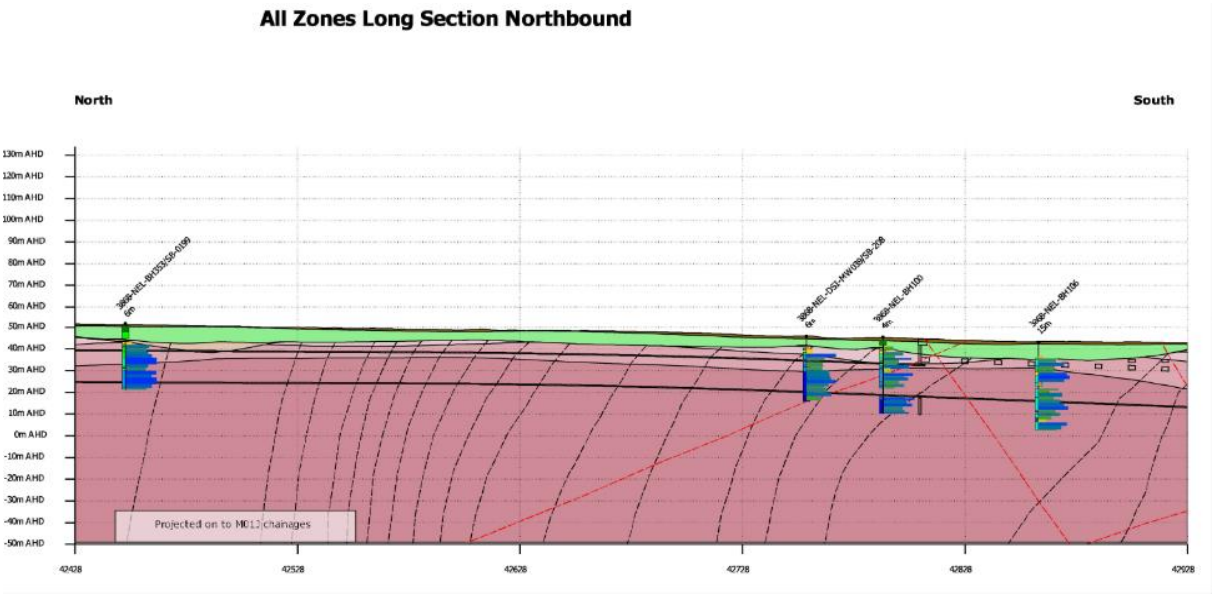


Fig. 1: Geotechnical Long Section – Apparent Fault Lines in Red, Bedding Planes in Black

The large anticline structure present causes the changes in the rock mass orientation across the Lower Plenty Interchange. The dip and dip direction are both affected as a result of this. This further develops the potential of a large scale sliding rock wedge appearing at an open trench, such as a diaphragm wall panel. Whilst these rock wedges can be accounted and designed for in the structural design of the diaphram wall using additional reinforcement, increasing concrete strength, additional and staged propping etc, they are often unaccounted for in the temporary open trench condition.

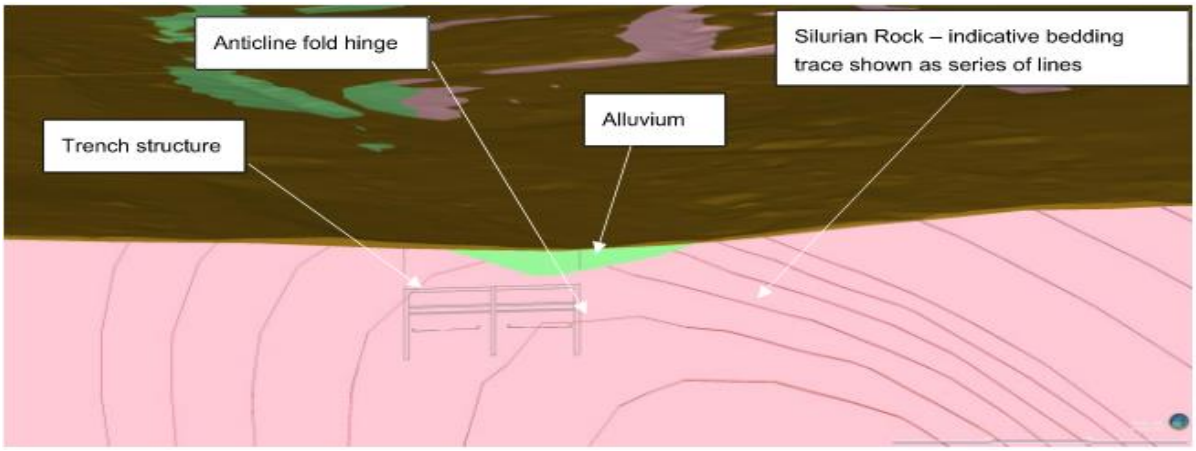


Fig. 2: Anticline Fold Structure – General Simplified Structural Features

 © Deep Foundations Institute 2025

2.3 Trench Stability Analysis

As part of the diaphragm wall panel layout design, trench stability analysis is undertaken prior to final design of platforms, guide walls, working levels, panel lengths and geometries. All these parameters can affect the overall trench stability of the panel so a careful geotechnical assessment must be undertaken. The general calculation method for this is as per the European standard DIN 4126 Deutsche Norm "Cast in situ diaphragm walls design and construction" which assesses soil stratigraphy and geotechnical parameters, bentonite support fluid properties, geometry of the panel and surcharges and loads applied near the trench such as weight and pressure of the piling rig tracks. For the purposes of the trench stability assessment a series of "worst case" assumptions were assumed for the calculation.

The TAWP JV report consisted of the following trench stability assumptions:

- Panel geometry: 7m in length, 1.2m width
- Maximum panel depth: 45m
- Groundwater table: 1.5m below platform
- Track load: 235kPa, 3m from trench
- Bentonite level: 0.2m below platform
- Bentonite weight: 10.3kN/m³

In addition, the below geotechnical parameters and stratigraphy was assumed:

SOIL STRATIGRAPHY & GEOTECHNICAL PARAMETERS								Number of Layers		5
Layer (-)	Soil Type	Z,str (m)	γ_{nat} (kN/m³)	γ_{sat} (kN/m³)	Gs (kN/m³)	C_K (kPa)	φ'_K (°)	K_0 (-)	D_{10} (mm)	I_{s0} (kN/m³)
1	Cohesive	3.00	16.0	17.0	26.5	25.0	0.0	0.600	0.0010	20000
2	Cohesive	6.00	18.0	19.0	26.5	70.0	0.0	0.700	0.0010	20000
3	Cohesive	12.00	23.0	23.0	26.5	40.0	35.0	1.000	0.2000	100
4	Cohesive	23.00	24.0	24.0	26.5	75.0	41.0	1.000	0.2000	100
5	Cohesive	55.00	26.0	26.0	26.5	200.0	46.0	1.000	0.2000	100

Fig. 1: Geotechnical Design Parameters:

A general assessment of the stability of the excavated panel does not present a concern through the rock profile as evidenced in the below graph. The figure presents the design resistance of the support fluid (Rd) versus design action loads due to earth pressure (Ed) along with Factor of Safety (FoS).

 © Deep Foundations Institute 2025

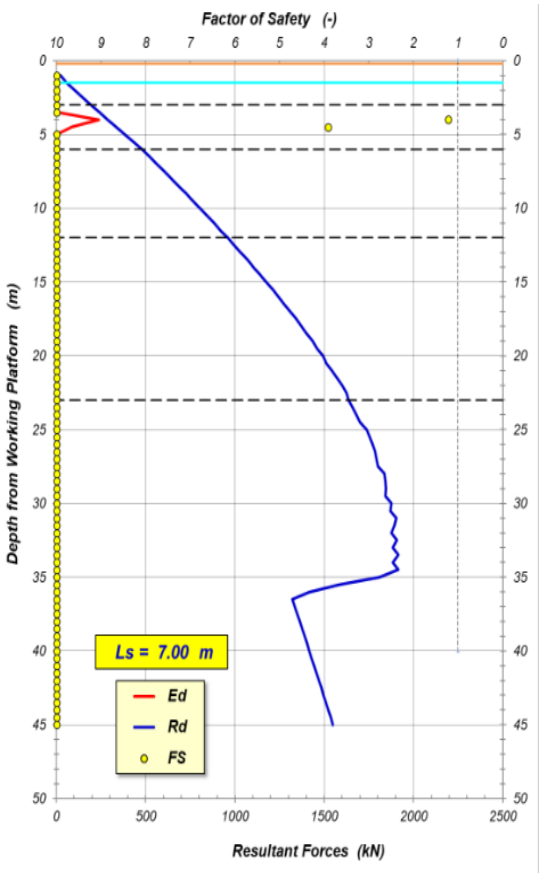


Fig. 3: Rd, Ed, FoS plotted against depth

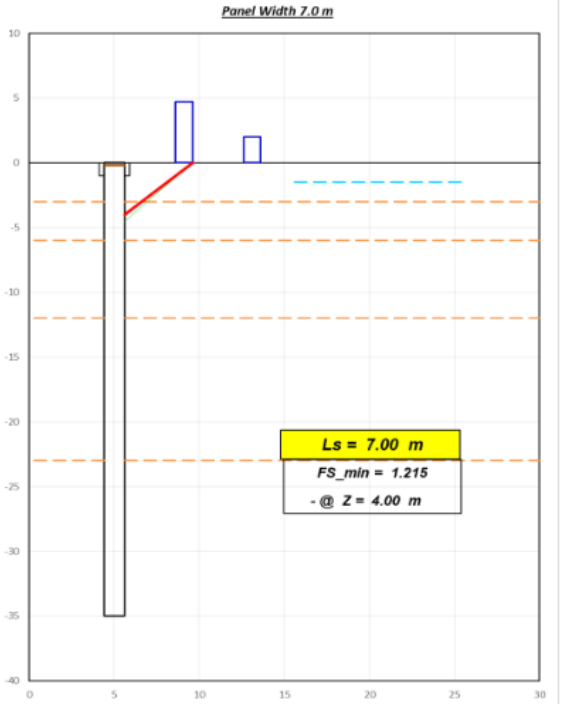


Fig. 2: Panel section and critical depth with minimum FoS

The results of the analysis indicate a critical depth at 4m in the alluvium cohesive layer which is modelled as soft-firm. The minimum FoS reaches 1.215. This result is acceptable for an analysis using the design parameters.

The trench stability analysis is revisited after a series of trench collapses which occur in panels near the fault lines. The analysis is undertaken using values derived from direct shear testing performed on defect samples in the rock mass.

The above characteristic design values displayed in Fig. 4 differ significantly for the rock mass. The defect rock mass parameters attained are c' = 0 kPa and Ø' = 23°.

This has a profound effect on the re-analysis undertaken for trench stability with a newly assessed 6.7m long panel failing to achieve stability. Figs. 4 and 5 analyses with the revised rock mass parameters are shown below.

 © Deep Foundations Institute 2025

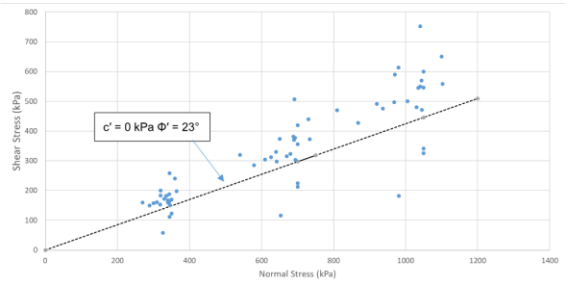


Fig. 4: Direct shear testing undertaken on defects on the project. Characteristic design values for cohesion and phi shown.

SOIL STRATIGRAPHY & GEOTECHNICAL PARAMETERS										Number of Layers	5
Layer	Soil	Z,str	γ_{nat}	γ_{sat}	Gs	C_K	φ'_K	K_0	D_{10}	f_{s0}
(-)	Type	(m)	(kN/m³)	(kN/m³)	(kN/m³)	(kPa)	(°)	(-)	(mm)	(kN/m³)
1	Cohesive	3.00	16.0	17.0	26.5	25.0	0.0	0.600	0.0010	20000
2	Cohesive	6.00	18.0	19.0	26.5	70.0	0.0	0.700	0.0010	20000
3	Cohesionless	12.00	21.0	21.0	26.5	0.0	23.0	0.609	0.2000	100
4	Cohesionless	23.00	21.0	21.0	26.5	0.0	23.0	0.609	0.2000	100
5	Cohesionless	45.00	21.0	21.0	26.5	0.0	23.0	0.609	0.2000	100

Fig. 5: Geotechnical Design Parameters - Defected Rock

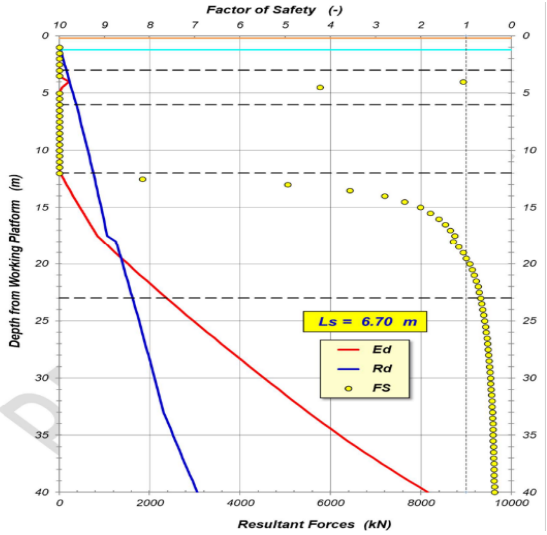


Fig. 6: Rd, Ed, FoS plotted against depth - defected rock (6.7m long panel)

As the above plots indicate, the achieved FoS using defect zone rock mass parameters is 0.374 at the toe of the panel and the FoS drops below 1 at approximately 20m below guide wall.

2.4 Trench Collapse

As previously mentioned, several diaphragm wall panels have undergone collapse in the rock layers during the installation process. Each collapse occurred immediately after the bentonite "clean and exchange" process which swaps out the working slurry for a lighter and within specification casting slurry. A summary of the below collapsed panels occurs in the table below:

 © Deep Foundations Institute 2025

Panel	Date of Collaps	Volume of Collaps	Immediate Action
W2-2	3/04/2023	130	Backfill lean concrete
W1-2	2/05/2023	35	Grab out material and Continue Pour
W3-12	19/06/2023	70	Backfill lean concrete
W3-7	7/10/2023	30	Grab out material and Continue Pour
NRW4-18	26/10/2023	10	Grab out material and Continue Pour
W3-13	2/11/2023	30	Grab out material and Continue Pour
W3-14	15/11/2023	25	Grab out material and Continue Pour
SRE5-04	8/02/2024	20	Grab out material and Continue Pour
SRW5-04	22/02/2024	35	Grab out material and Continue Pour
SRW5-06	9/04/2024	35	Grab out material and Continue Pour
SRE5-08	12/04/2024	25	Grab out material and Continue Pour

Fig. 7: Sumary of collapsed panels with immediate rectification and collapsed volumes

The first panel to collapse, W2-2, was quite major and comprised over half the neat excavation volume of the panel. As it was the first collapse, a conservative approach was taken. The excavated panel depth was 35m from top of guide wall and the panel dipped between 12m and 19m below top of guide wall post collapse. The collapsed rock material was excavated carefully with the clamshell grab and a Koden Ultrasonic drilling monitor which maps the side wall of the excavation using ultrasonic echo sensing methods was used to investigate the collapsed panel profile with examples shown below.



Fig. 8: Collapsed rock material in panel W2-2

After careful consideration of the Koden mapping and the quantum of collapsed material, the decision was made to backfill the panel with lean concrete immediately. As the collapse was propagating upwards on the excavation face underneath where the hydromill and cranes would sit, there was risk of undermining the platform and instability for plant and equipment that needed to be urgently addressed.

The panel collapses were mostly occurring in areas where the rock profile was shallower and significantly more fractured. When mapping it against the inferred fault lines it was found that there was a higher propensity for collapse in these areas. As such, after the first few lean concrete backfilled panels, it was decided to implement remedial measures.

 © Deep Foundations Institute 2025

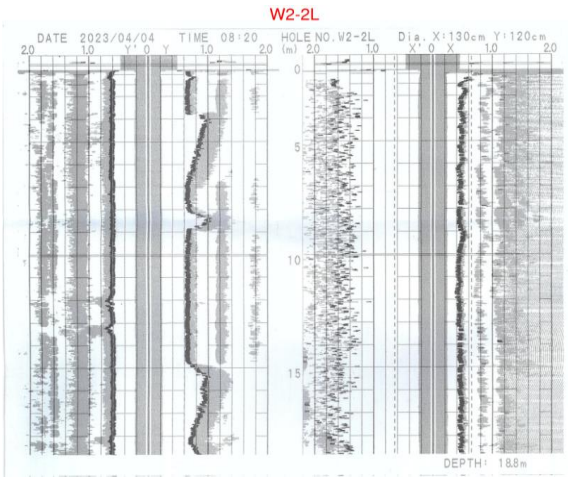


Fig. 9: Koden Profile of W2-2 South Bite. Y' = Soil Face. Y = Excavation Face.

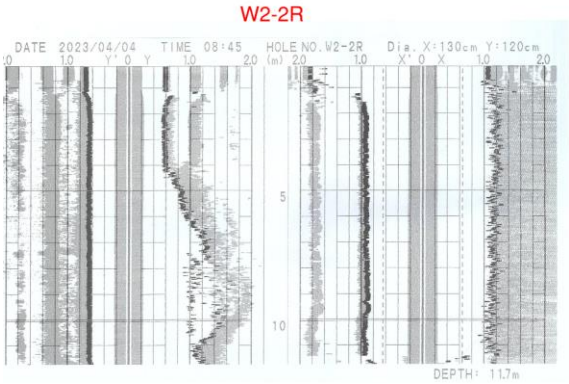


Fig. 10: Koden Profile of W2-2 North Bite. Y' = Soil Face. Y = Excavation Face

Several remedial measures were implemented for the safe re-excavation of these panels:

- Heavier Casting Slurry: The weight of the casting slurry was increased by blending it with working slurry to the project specification limit of 1.15g/ml
- Grouting: The collapsed material at the base of the excavated panels were pressure grouted to fill any voids.
- Soil Nails: Vertical reinforcement bars was anchored on the collapsing face to pin the lean concrete wedge that formed from backfilling with 20MPa lean mix. This is to stop the wedge falling on the cutter during re-excavation and potentially trapping the cutter module below ground.
- Panel geometry: To limit large scale sliding blocks, the panels in these collapse zones were reduced in length from 6.7m to as small as 2.8m.
- Raising platform and guide wall: In areas where the natural groundwater table was close to platform level, the guide wall and subsequent working level were increased for additional head pressure in the panels.

The above measures were implemented immediately where possible and whilst trench collapses still occurred, they were far more minor with less material collapsing into the excavation. A

 © Deep Foundations Institute 2025

series of minor collapses occurred around fault lines in other panels however an informed decision was made to excavate out the material using mechanical grab and mechanically clean and re-test the bentonite parameters. Once this was complete, cage installation and casting was to resume on these panels and any overbreak in the concrete curve was closely monitored for any further collapses. A further analysis of the trench stability was undertaken using smaller panels using the defected rock mass parameters and stability against sliding was achieved with a FoS of 1.216. This suggests that panel geometry influences the stability of open trenches significantly.

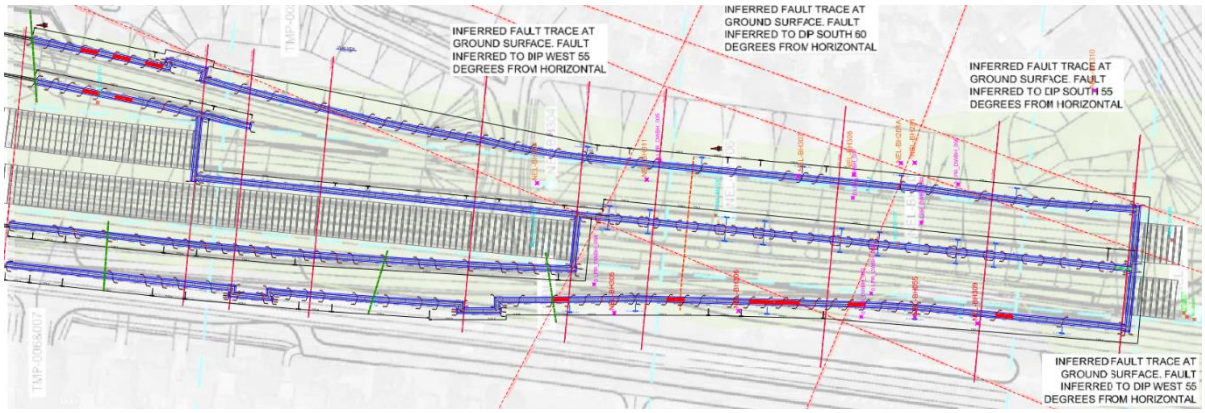


Fig. 11: Inferred fault lines (red) against panel layout. Solid Red hatched panels are trench collapses.

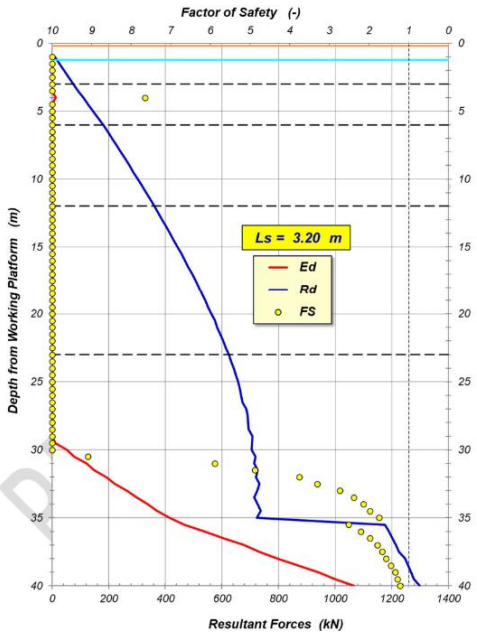


Fig. 12: Rd, ED, SF plotted against depth – defected rock (3.2m long panel)

The revised panelling in the collapsed zones required significant rework and cage modifications as they were already fabricated, plan shown.

 © Deep Foundations Institute 2025

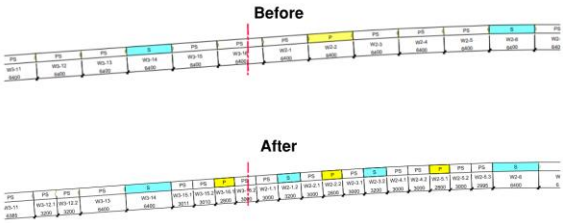


Fig. 13: Panel modification for panels in the collapse zone

The intention of the grouting and nailing as preventative measures are to stabilise the collapsed rock and material sitting in the base of the panel and pin any concrete wedges that have formed in place of the void when the panel was backfilled. The risk of the concrete rock wedge and the collapsible material is loss of the hydromill cutter module which would have catastrophic impacts to the project for safety, cost, program and the environment. The remedial measures implemented were successful as all panels in the collapsed areas were successfully excavated and cast without any further incident.

3 CONCLUSION

The installation of diaphragm wall panels at the Lower Plenty Interchange site has been extremely challenging in part to the unique and difficult geotechnical conditions present. The collapse of diaphragm wall trenches is a major problem which can affect the quality of the panel, the project program and the safety of the platform and operations. Utilising the collective experience of all parties involved, the design remedial measures implemented allowed for a successful excavation in the most challenging and risky ground conditions.

4 ACKNOWLEDGEMENTS

The authors wish to thank Trevi Australia and Wagstaff Piling for assistance in writing this paper. Thanks also to the client for the project, SPARK D&C Joint Venture, for providing the opportunity to perform these works for them.

 © Deep Foundations Institute 2025

DESIGN AND GEOTECHNICAL STUDIES OF DEEP FOUNDATIONS FOR BRIDGES IN THE PERUVIAN LOWLAND RAINFOREST

Jorge E. Alva, Universidad Nacional de Ingeniería, Lima, Perú, 051 952088403, jalvah@uni.edu.pe
Miriam R. Escalaya, Universidad Ricardo Palma, Lima, Perú, 051 951529442, miriam.escalaya@urp.edu.pe
Alvaro J. Pérez, Universidad Peruana de Ciencias Aplicadas, Lima, Perú, 051 992546224, pccialpe@upc.edu.pe

ABSTRACT

This paper summarizes the geotechnical studies carried out in the 1990s by the Centro de Investigaciones Sísmicas y Mitigación de Desastres (CISMID) of the Universidad Nacional de Ingeniería, for the design of deep foundations of five single-span bridges (25–60 m) located in the Amazonian lowlands of Madre de Dios, Peru, as part of the Southern Interoceanic Highway. Standard Penetration Tests (SPT) were performed to define stratigraphy and soil mechanical properties. Based on this data, the axial bearing capacity of steel driven piles was estimated using empirical and analytical methods, incorporating group efficiency and safety factors to define allowable loads. Settlement predictions for single piles and groups confirmed compliance with international displacement criteria. Steel piles were selected due to regional logistical constraints, including difficult access, lack of aggregates, and equipment transport limitations. Additionally, the construction of protective works was proposed to isolate the foundations from the effects of river erosion. To verify the load capacity and settlements of the piles determined in the designs, load tests were suggested in areas with previously known and more unfavorable profiles. The importance of conducting pile driving tests was also emphasized to ensure the success of the design and construction.

Keywords: deep foundations, bridges, geotechnical studies

1. INTRODUCTION

Bridge construction in the Peruvian Amazon presents significant technical challenges due to the region's unique geological, logistical, and environmental conditions. This paper documents the geotechnical studies conducted for the foundation design of five bridges located in the Madre de Dios department, along the Puerto Maldonado–Iberia–Iñapari section of the Southern Interoceanic Highway Corridor which connects Peru with Brazil. All bridges are single-span structures ranging from 25 to 60 meters in length.

The studies were conducted in the 1990s by the Centro de Investigaciones Sísmicas y Mitigación de Desastres (CISMID) of the Universidad Nacional de Ingeniería (UNI), Peru, under the commission of the Proyecto Especial Madre de Dios (PEMD). The field campaigns included detailed investigations at the Yaverija, Primavera, Noaya, María Cristina, and Alerta bridges, all located in the Tahuamanu Province. The primary technical objective was to develop safe and efficient deep foundation solutions tailored to the complex geotechnical conditions of the Amazonian lowlands.

This paper systematizes the methodology applied and the results obtained in the analysis and design of deep foundations using driven piles, based on a detailed geotechnical characterization of the study area. Figure 1 shows the general location of the analyzed bridges, situated in southeastern Peru near the tri-border region with Bolivia and Brazil, underlining their importance for regional road integration. The inset highlights the relative position of the region within the national territory.

 © Deep Foundations Institute 2025

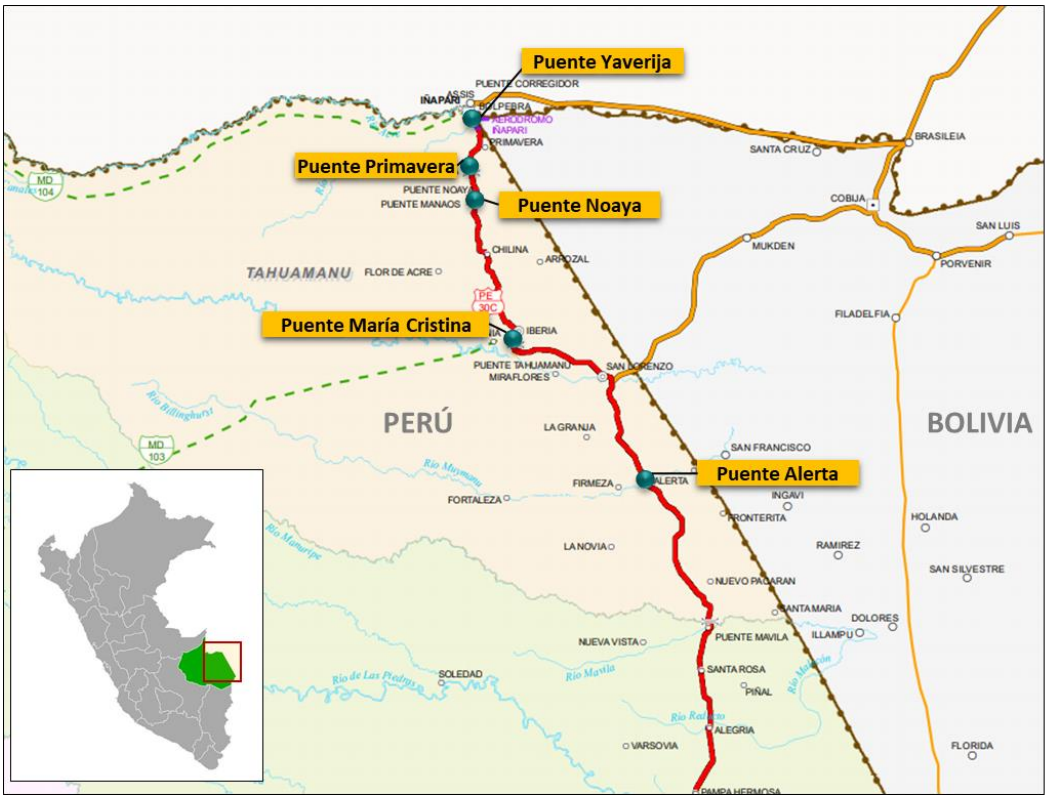


Fig. 1. General location of the Yaverija, Primavera, Noaya, María Cristina, and Alerta bridges in the department of Madre de Dios, Peru.

Geology of the Area

The study area is located within a tectonically formed sedimentary basin, situated between the Brazilian Shield and the Sub-Andean Zone. This depression is characterized by gently undulating topography, consisting of Quaternary deposits overlaying older formations, where thick sedimentary sequences with low-intensity folding have accumulated.

Lithologically, the area is dominated by sedimentary rocks of the Capas Rojas Group, composed of red and white sandstones, gray shales, reddish-brown clayey sandstones with clay interbeds, unconsolidated mudstones, and reddish-brown limonites, as well as feldspathic sands of varying grain size.

Additionally, ancient Quaternary sediments have been identified, including beds of whitish-yellow silica sands, gray claystones, and friable sandstones containing paleontological remains, along with more recent deposits of sands, clays, and silts exhibiting pseudostratification.

Although no igneous outcrops have been observed, fragments of volcanic material such as tuffites and volcanic glass have been recorded. This lithological assemblage suggests a complex sedimentary environment with fluvial and possibly lacustrine influences, as evidenced by the textural features and the presence of organic remains.

2. RESEARCH METHODOLOGY

The geotechnical investigation conducted for the five bridges involved a combination of field exploration, laboratory testing, and computational analysis aimed at the design of deep foundations.

The field campaigns included the execution of mechanical borings with Standard Penetration Tests (SPT) performed at 1.0 m depth intervals, as well as test pits and trenches for visual observation and soil classification. Piezometers were installed, and in-situ permeability tests were carried out. These activities enabled the definition of stratigraphic profiles and hydrogeotechnical conditions at each site. The collected samples were tested in the laboratory to determine index properties and strength parameters. Grain size distribution analyses, Atterberg limits, specific gravity, and moisture content were measured. In addition, direct shear tests, one-dimensional consolidation tests, and unconsolidated-undrained (UU) triaxial tests were performed, depending on the nature of the materials. Chemical analyses of the soils were also conducted.

The results were integrated into bearing resistance and settlement models using specialized software, allowing the selection of the most suitable foundation solutions according to ground conditions, structural loads, and logistical constraints of the environment.

3. FOUNDATION ANALYSIS

The analysis of deep foundations was carried out considering the characteristics of the stratigraphic profile and the loads transmitted by the proposed structures, using both empirical and analytical methods. Since SPT testing is the most widely used geotechnical investigation method in Peru, empirical formulas based on N-SPT values were applied to estimate the bearing resistance of piles. Specifically, the methods of Aoki-Velloso (1975), Decourt-Quaresma (1978), P.P. Velloso (1982), and Meyerhof (1976) were used, with and without N-SPT value corrections. These calculations were processed using the FEPC software developed by Bertolucci et al. (1988) and modified by Guillén (1993).

In parallel, analytical methods were applied using the SPTSP software (based on Schmertmann, 1967) for the Yaverija, Primavera, and María Cristina bridges, and the SPILE program (which incorporates the methodologies of Nordlund (1963), Tomlinson (1980, 1985), and FHWA (1993)) for the Noaya and Alerta bridges.

Settlement calculations included the evaluation of single piles using both the semi-empirical (Vesic, 1977) and the empirical (Vesic, 1970) methods, as well as group pile analysis based on the approaches of Vesic (1977) and Skempton (1951). Additionally, group efficiency was assessed in accordance with the AASHTO Bridge Design Specifications using the Converse-Labarre equation.

The selection of driven open-ended steel piles as the foundation solution was based on their construction practicality under remote site conditions, supported by the results of bearing resistance and settlement performance analyses.

4. EVALUATED BRIDGES

The following sections detail the investigations conducted for each of the analyzed bridges. In all cases, the use of open-ended steel piles with a diameter of 0.30 m was recommended.

Yaverija Bridge

Located over the Yaverija River in the district of Iñapari, Tahuamanu Province, the Yaverija Bridge spans 60 m. The fieldwork was carried out in 1998 and included two boreholes reaching depths of up to 30.45 m, with Standard Penetration Tests (SPT) conducted at 1.0 m intervals, one test pit, permeability tests performed within the boreholes, and the installation of piezometers. The stratigraphy revealed high- and low-plasticity clay soils interbedded with sandy layers, as shown in Fig. 2.

 © Deep Foundations Institute 2025

The recommended foundation solution consisted of driven steel piles, 10 m long and 0.30 m in diameter, with allowable capacities of 350 kN and a group efficiency factor of approximately 0.90. Settlement calculations were conducted for both individual piles and pile groups, yielding values of 5.0 mm for individual piles and 21.4 mm and 35.0 mm for the group. It was recommended that at least one pile load test be conducted at each abutment of the bridge foundation.

In 2003, static load tests were conducted on both abutments, following the guidelines established in ASTM D 1143 Standard. The results yielded allowable capacities of 637 kN for the right abutment and 701.18 kN for the left abutment, values that exceeded those considered in the initial design. The corresponding pile lengths were 11.60 m and 8.90 m, respectively. The ENR (Engineering News Record) driving formula was used during pile driving to determine the refusal. To determine the ultimate capacity in the load tests, Davisson's (1972) graphical method was applied.

As an additional measure against scour, in 2005, riverbank protection works were implemented using geocells filled with concrete over geotextile layers.

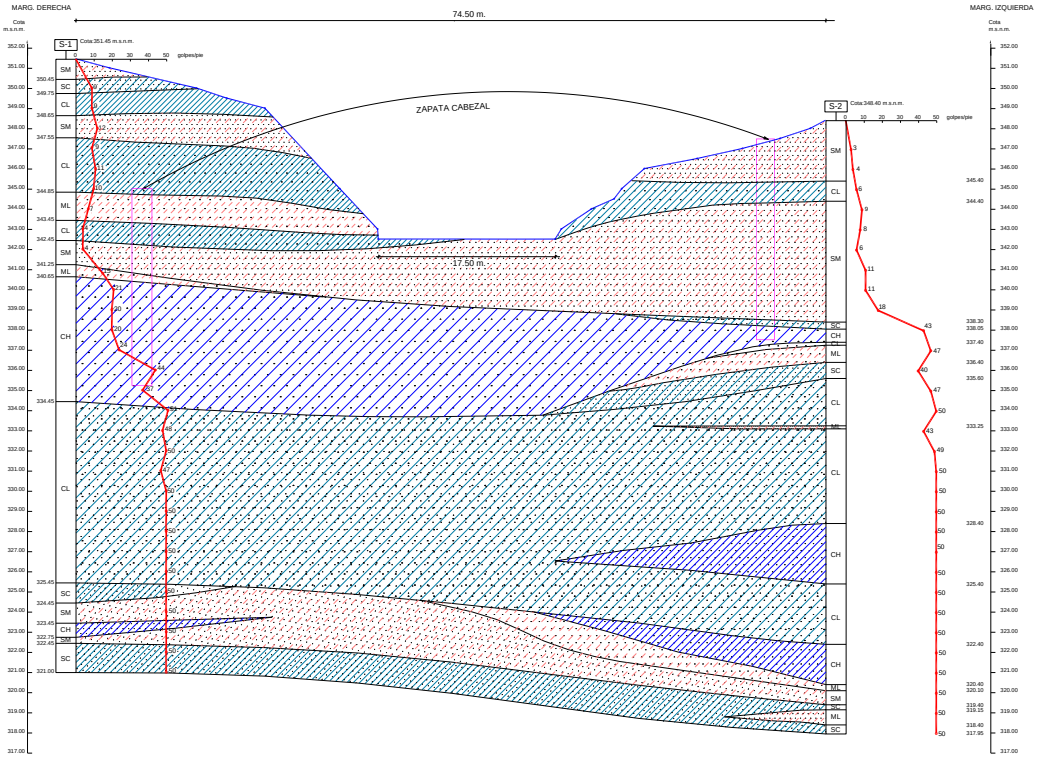


Fig. 2. Stratigraphic profile of the area where the Yaverija Bridge is located

Primavera Bridge

Located over the Primavera River, approximately 10 km from the city of Iñapari, this bridge has a length of 55 m. Field investigations were conducted in July 1999 and included two boreholes reaching depths of 20.45 m, with SPTs performed at 1.0 m intervals, one test pit, one trench, in situ permeability tests within the boreholes, and piezometer installation. The stratigraphic profile revealed predominantly clayey soils with interbedded silty sands, as shown in Fig. 3. The proposed foundation consisted of steel piles with a diameter of 0.30 m and lengths ranging from 8 to 10 m. The allowable load capacity was determined to be

 © Deep Foundations Institute 2025

350 kN, with a group efficiency of 0.85. The calculated settlements were approximately 5.3 mm for individual piles and between 20.1 mm and 22.3 mm for the pile group.

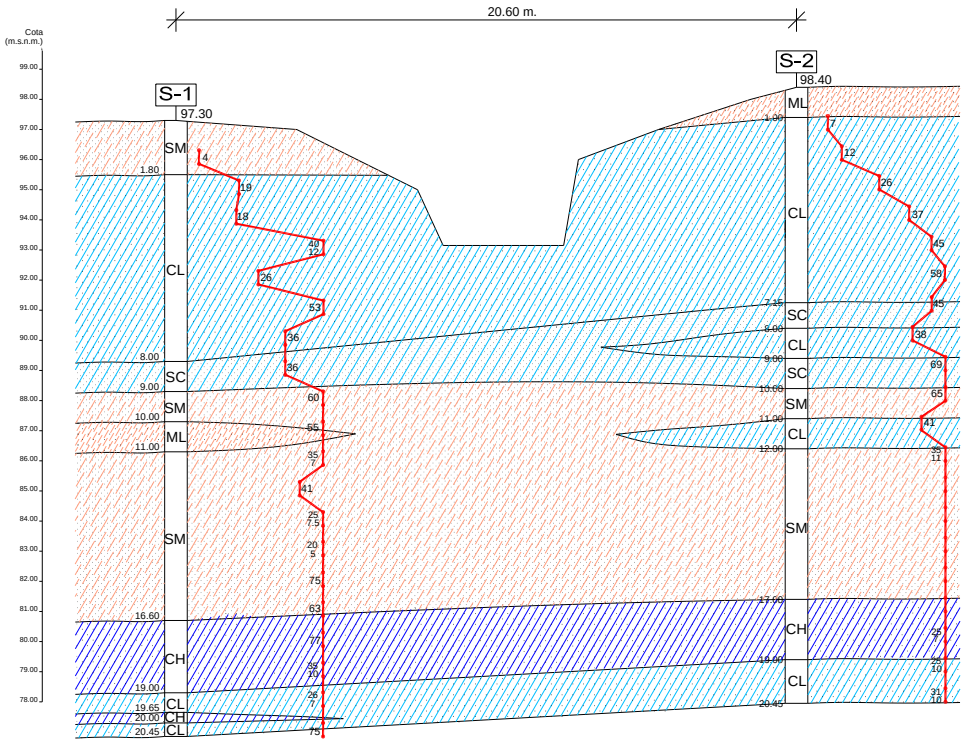


Fig. 3. Stratigraphic profile of the area where the Primavera Bridge is located

Noaya Bridge

Situated over the Noaya River, approximately 30 km from Iñapari, this bridge has a length of 35.0 m. Fieldwork was carried out in August 1999 and consisted of two boreholes up to 25.45 m deep, with SPTs performed every meter, one test pit, one trench, permeability tests within the boreholes, and piezometer installation. The stratigraphy showed high- and low-plasticity clays in the upper layers, followed by sandy soils, as illustrated in Fig. 4. The recommended foundation system comprised driven steel piles 9 m in length and 0.30 m in diameter. The allowable capacity was 300 kN, with a group efficiency of 0.85. Settlements ranged from 5.3 to 5.6 mm for individual piles and up to 23.1 mm for the group. Drainage works were recommended to protect the wall edges from erosion and scour caused by rainwater runoff and river flow.

 © Deep Foundations Institute 2025

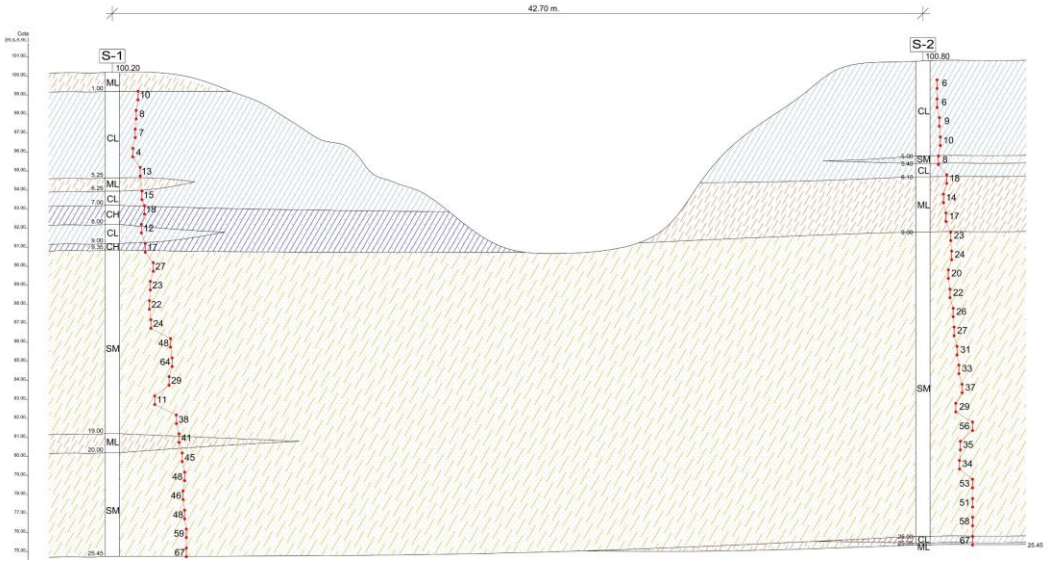


Fig. 4. Stratigraphic profile of the area where the Noaya Bridge is located

María Cristina Bridge

Located at kilometer 162 of the Puerto Maldonado – Iberia road, this bridge spans 30 m. In April 1994, four geotechnical boreholes were performed to depths between 11.45 and 14.45 m, as two alternative locations were evaluated: the existing bridge site and another 80 m upstream. The stratigraphic profile consisted mainly of sandy soils, as shown in Fig. 5. The recommended foundation solution included driven steel piles 8 m in length, with both 0.25 m and 0.30 m diameters evaluated. Allowable capacities ranged from 300 to 330 kN at the left abutment and from 410 to 510 kN at the right abutment, with a group efficiency of 1. Settlements for individual piles ranged from 2.7 to 3.3 mm, and up to 19.6 mm for the group.

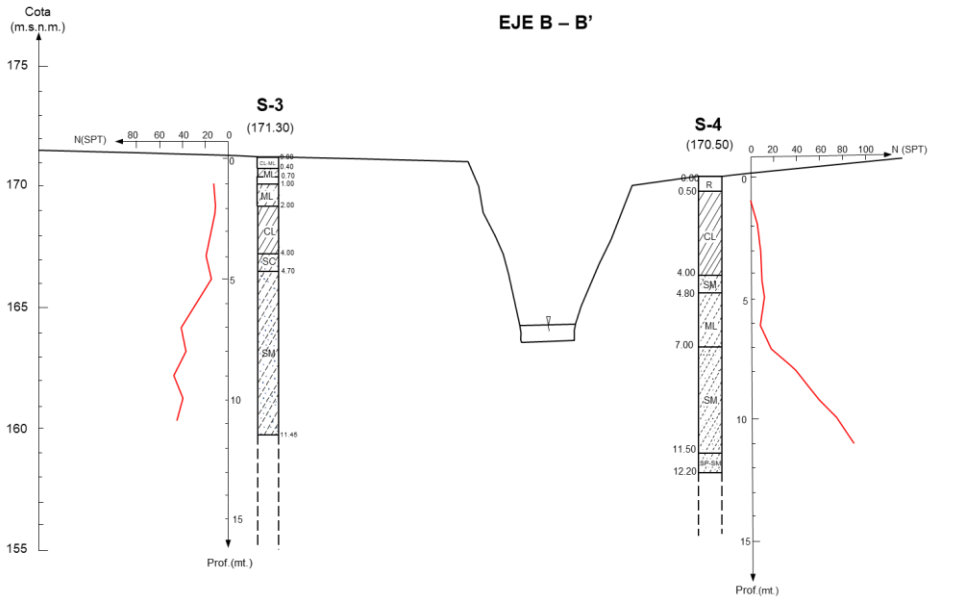


Fig. 5. Stratigraphic profile of the area where the María Cristina is located

 © Deep Foundations Institute 2025

The design included recommendations for implementing necessary protective measures along the ravine to isolate the foundation area from potential river scouring effects. These measures were complemented by drainage structures designed to safeguard the riverbanks against erosion caused by rainwater runoff.

Alerta Bridge

Located in the town of Alerta, this bridge spans 25 m. Field investigations were carried out in August 1999 and included two boreholes (17.45 m and 15.45 m in depth), one trench, in situ permeability tests, and piezometer installation. The predominant soils were low- and high-plasticity clays, along with silty sands, as shown in Fig. 6. The foundation design included driven steel piles 10 m in length and 0.30 m in diameter, with an allowable capacity of 300 kN and an estimated group efficiency of 0.85. Estimated settlements ranged from 4.6 to 5.0 mm for individual piles and up to 19.8 mm for the group. At least one pile load test was recommended, along with protective works on both riverbanks to shield the foundation area from potential scour.

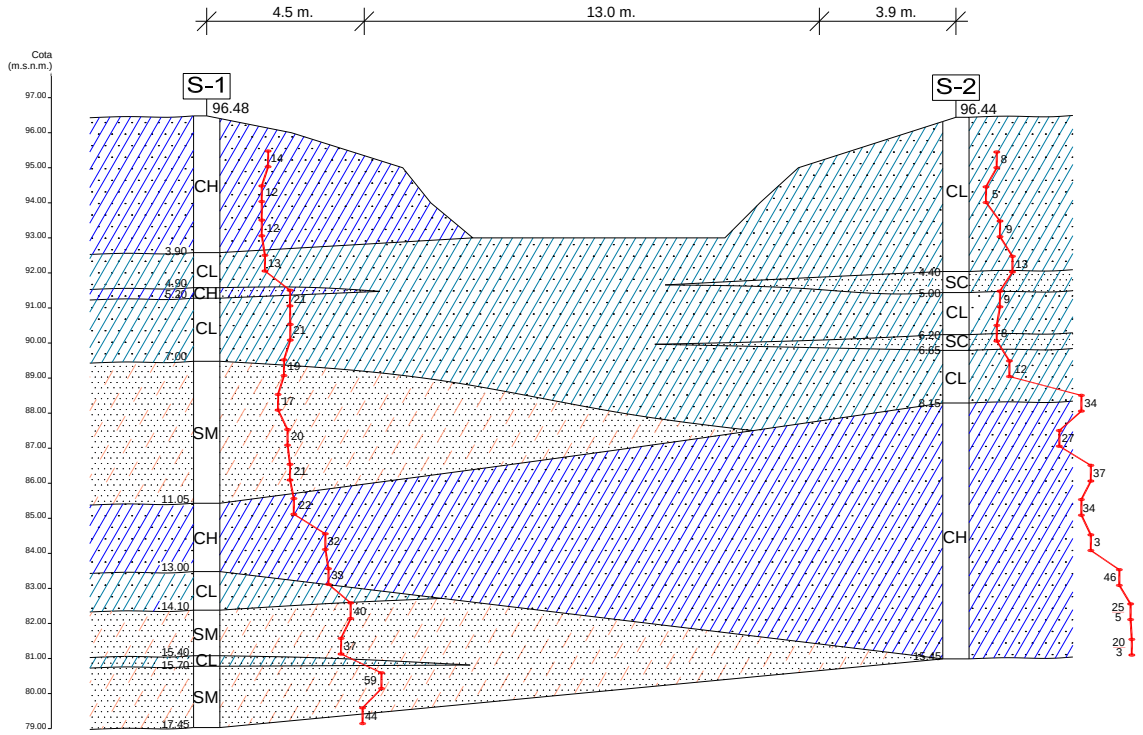


Fig. 6. Stratigraphic profile of the area where the Alerta Bridge is located

5. SUMMARY AND CONCLUSIONS

Table 1 presents a comparative summary of the load-bearing capacities obtained using different methods for the evaluated bridges. Table 2 shows the final allowable capacities considered for the driven open-ended steel piles with 0.30 m diameter and lengths between 8 and 10 m, which were found to be suitable for the site conditions. Final allowable capacities were selected conservatively, prioritizing methods validated by local experience.

 © Deep Foundations Institute 2025

Table 1. Allowable load capacity of evaluated bridges determined by different methods

bridge	side	pile length (m)	Empirical Methods					Analytical Method (kN)
			Aoki-Velloso (kN)	Decourt-Quaresma (kN)	Pedro P. Velloso (kN)	Meyerhof s/c (kN)	Meyerhof c/c (kN)	
Yaverija	right	10	350	524	768	304	304	570
	left	10	360	606	760	438	438	
Primavera	right	8	409	707	729	532	532	313
	left	8	446	700	738	379	379	338
Noaya	right	9	374	463	532	275	275	345
	left	9	428	492	598	305	305	370
María Cristina	right	8	836	876	1179	635	635	519
	left	8	807	654	862	337	337	420
Alerta	right	10	339	685	749	500	500	340
	left	10	427	599	720	451	451	267

Table 2. Final allowable load capacities

Bridge	side	pile length (m)	diameter (m)	q_{all} (kN)
Yaverija	right	10.0	0.3	350
	left	10.0	0.3	360
Primavera	right	8.0	0.3	350
	left	8.0	0.3	350
Noaya	right	9.0	0.3	300
	left	9.0	0.3	300
María Cristina	right	8.0	0.3	510
	left	8.0	0.3	330
Alerta	right	10.0	0.3	300
	left	10.0	0.3	300

- This study has documented the geotechnical characterization, analysis, and design of deep foundations for five single-span bridges located in the Madre de Dios region, within the Peruvian Amazon, as part of the Southern Interoceanic Highway Corridor. Field investigations included standard penetration tests (SPT), test pits, piezometer installation, and permeability testing, supplemented by laboratory tests for classification and strength. The data collected enabled the characterization of stratigraphic profiles composed of clayey and silty soils, highly saturated and of low bearing capacity.
- The bearing capacity of the driven steel piles was estimated using empirical methods (Aoki-Velloso, Decourt-Quaresma, P.P. Velloso, and Meyerhof) and analytical methods (SPTSP and SPILE), applying safety factors of 2.5 and group efficiency factors ranging from 0.85 to 1.00. Final allowable capacities ranged from 300 to 510 kN and, in some cases, were confirmed by static load tests.
- The calculated settlements for individual piles (2.7 to 5.6 mm) and pile groups (up to 35.0 mm) were within acceptable limits for bridge structures. Additionally, the need for riverbank protection works against scour was identified, and such measures were implemented to ensure the long-term stability of the foundations.
- The selection of steel piles for bridges in the Madre de Dios rainforest was based on two key factors: first, the need to penetrate deep, dense soil strata that could damage concrete piles during driving; and second, the logistical challenges of transporting heavy equipment to the area. It is concluded that

driven steel piles represent a viable, efficient, and constructionally appropriate foundation solution for the geotechnical and logistical conditions of the Peruvian lowland rainforest.

- For improved geotechnical evaluation of the study area, it is currently recommended to include geophysical surveys as part of the field investigations, particularly using the Multichannel Analysis of Surface Waves (MASW) method. This will allow for the development of a seismic profile based on S-wave propagation velocities, inference of soil compaction states, and determination of elastic parameters that may be used in foundation analysis.

6. REFERENCES

Aoki, N., and Velloso, D. A., 1975. An approximate method to estimate the bearing capacity of piles. Proceedings of the 5th Pan-American Conference on Soil Mechanics and Foundation Engineering, Buenos Aires, Argentina, pp. 367-376.

Bertolucci A.A., Albiero J.H. and Gonzaga S.C., 1988. Programa para cálculo de capacidade de carga em estacas fórmulas empiricas, Simposio sobre Aplicaciones de Microcomputadores en Geotecnia, Microgeo 88, Brasil.

Davisson M.T., 1972. High Capacity Piles. Proceedings, Lecture Series, Innovations in Foundation Construction, ASCE, Illinois, Section, 52 pp.

Decourt, L. and Quaresma, A. R., 1978. Capacidad de carga de pilotes a partir de valores de SPT. In Proceedings of the 6to Brazilian Symposium on Soil Mechanics and Foundation Engineering, Rio de Janeiro.

FHWA, 1993. SPILE a microcomputer program for determining ultimate vertical static pile capacity-user's manual. U.S. Department of Transportation, Federal Highway Administration, USA

Guillén N.,1994. Capacidad ultima de carga de pilotes en carga axial. Tesis de Grado, Facultad de Ingeniería Civil, Universidad Nacional de Ingeniería, Lima, Perú.

Meyerhof G.G., 1976. Bearing capacity and settlement of pile foundation. Eleventh Terzaghi Lecture, Journal of the Soil Mechanics and Foundations Division, ASCE, GT3, pp. 195-228.

Nordlund R.L., 1963. Bearing capacity of piles in cohesionless soils. ASCE, SM&F Journal SM-3

Schmertmann, J., 1967. Guidelines for use in the soil investigation and design of foundation for bridge structures in the state of Florida. Florida Department of Transportation, Research Bulletin 121.

Skempton, A.W., 1951. The bearing capacity of clays. Building Research Congress, London, 1951, 1, 180-189

Tomlinson M.J., 1980. Foundation design and construction. Pitman Advanced Publishing, Boston, MA, 4th edition.

Tomlinson M.J., 1985. Foundation design and construction. Longman Scientific and Technical, Essex, England

Velloso P.P.C., 1982. Cimentaciones – Aspectos Geotécnicos, Vol.3, Pontificia Universidade Católica, Río de Janeiro.

Vesic, A., 1970., Tests on instrumented piles, Ogeeche River Site. J. Soil Mechanics and Foundation Div., ASCE, Vol.96, No.SM2, pp.561-584.

Vesic A.S., 1977. Design of Pile Foundations. National Cooperative Highway Research Program, Synthesis of Highway Practice, Transportation Research Board, Washington, D.C

 © Deep Foundations Institute 2025

DESIGN AND EXECUTION OF LONGEST BORED CAST-IN-SITU RCC RAKER /BATTER PILE IN THE WORLD

Naveen Govindaraju[1a], Udai V. Singh[2a], Vikas C. Rane[3a], Ramesh K. Shrivastava[4a]
[1] *Asst. General Manager, Design Department, +91 9500137198, naveen.govindaraju@afcons.com,*
[2] *Exec. Vice President, Operations, +91 9116365147, udaiveer@afcons.com,*
[3] *Dy. General Manager, Design Department, +91 9820378287, vikas.rane@afcons.com,*
[4] *Jt. General Manager, Design Department, +91 7893217244, ramesh.shrivastava@afcons.com*
[a] *AFCONS Infrastructure Ltd, Mumbai, India*

ABSTRACT

This paper intends to detail few of the key challenges faced by author's firm during the design and execution of this volta bridge with raker/batter pile type of foundation system, which is one such unique system in the country of Ghana, and Authors' firm have designed and executed this longest *Bored Cast-In-Situ RCC Raker/Batter Pile* in the world. Volta River located at Ghana, this resrvoirs area of 8,502 square kilometers is one of the *largest man-made waterbody* in terms of area, in the world. *Volta lake*, being man-made, the variation in overburden sand was significant.

The design and construction of this 300m long single standard gauge railway bridge was a challenging task. Volta bridge was designed as 5-span simply supported structures between the abutments with a span length of 60m each. Initially, *2.0m diameter concrete vertical piles* were planned for foundations, given the fact that the peak ground acceleration (PGA) was 0.16g. Due to revision in Ghana Building Code, PGA value was revised from 0.16g to 0.35g in this revision, hence, piling philosophies had to undergo a complete revamping to mitigate such large seismic lateral forces, R*aker/Batter pile* option was found to be optimal. For this *deep gorge* of Volta River, with a maximum *water depth of 31m*, liner length requirement for the *longest pile was 65m* till the rock top levels. The maximum length of pile constructed was 76.5m including its length of socketing into hard rock.

Keywords: Raker Pile, Deepest Pile, Volta

INTRODUCTION

Table 1. Structure Details of Completed Bridge:

Bridge Elements	Description		
Total length	300 m (5 x 60m)		
Span arrangement	5 spans each 60.0m length		
Structural system	Simply supported system		
Superstructure	Structural steel plate girder with RCC deck slab		
Substructure	Superstructure resting on pile caps over and bearings pedestals		
Foundation	The foundation consists of group of vertical and raked piles topped in rock at both abutments and pier locations.		
	Location	***Type***	***Nos. of Piles/Pile Configuration***
	Abutments – A1 and A2	*Vertical Piles*	*6 Piles (2 x 3)*
	Piers – P1, P3 and P4	*Raked Piles*	*4 Piles (2 x 2)*
	Pier – P2	*Raked Piles*	*6 Piles (2 x 3)*

 © Deep Foundations Institute 2025

The Volta bridge is part of one of the most important infrastructure projects in Ghana. This challenging link of the railway project is set to improve transportation sector of the country. The socio-economic impact of the project is massive with a potential to change the face of the region, and, the nation at large. The present Volta river flows from the outlets of the dam's powerhouse and spillways to the Atlantic Ocean in southern Ghana. Lake Volta is the largest artificial reservoir in the world based on surface area (8,502 Km^2). It is situated behind the Akosombo Dam which generates a substantial amount of Ghana's electricity.

DESIGN APPROACH

The bridge is designed in accordance to European standards (EURO) and specifications with various loads and load combinations. Different loads considered are tabulated and presented below in Table 2.

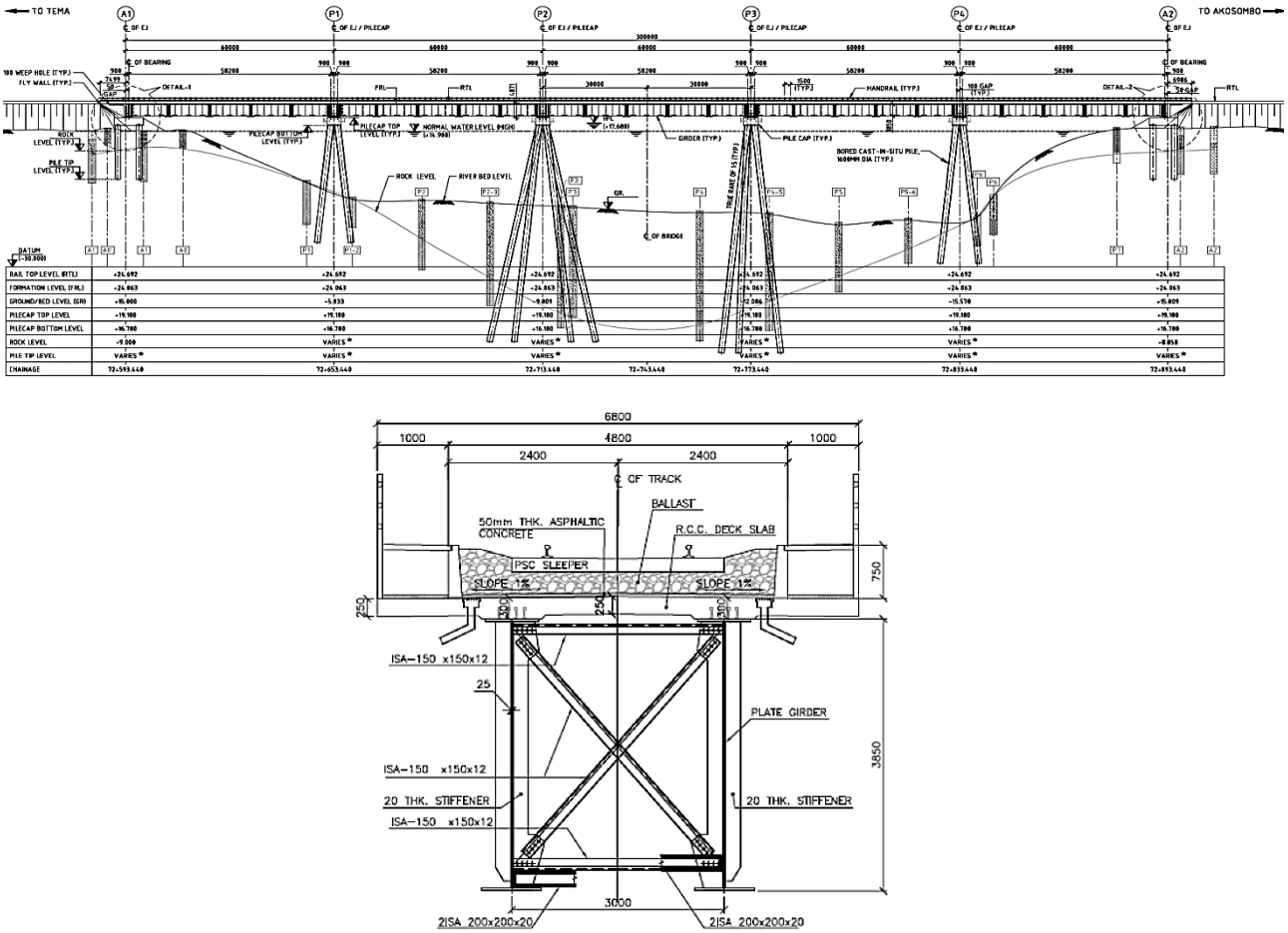


Fig. 1. General Arrangement and Typical deck cross section of the bridge

Table 2. Design Loads and Load Combinations:

Parameters	Description
Design Loads / Forces	• Self-weight of the structure / Dead load of the structure • Super-Imposed Dead Loads (SIDL) like loads due to Handrails, Ballast retainer, Footpath slab, Rails, Sleepers, Ballast and Utilities • Pedestrian live loads over footpath slab • Live Loads (including dynamic factor, longitudinal forces, centrifugal forces, nosing loads) • Forces due to use of Long welded rails (LWR) / Continuous welded rails (CWR) to take up Rail Structure Interaction (RSI) analysis, Derailment Loads, jacking conditions for bearing replacement • Earth Pressure, Water Current Forces, Wind Loads, Temperature Effects, Creep and Shrinkage effects, Seismic Loads, Buoyancy Loads.
Load Combinations	The loads and forces as mentioned above are combined to have worst effects on the structure and its components

With all above said loads with their combinations, the bridge was modelled and analyzed using advanced software tools.

GOVERNING DESIGN PARAMETERS

Apart from the loads and load combinations, the design of this bridge across volta lake, one of the largest man-made channel was governed by following parameters:

1. Peak ground acceleration coefficient
2. Type of Pile foundation (Vertical / Raker)
3. Rock Touch Levels

In following sections below, we will be discussing how these parameters govern the entire design and construction of this bridge.

Peak Ground Acceleration Coefficient (PGA)

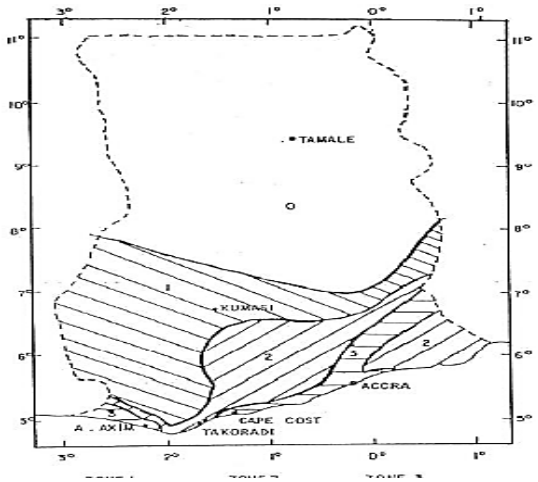


Figure 2-2 Seismic risk map of Ghana (extracted from "Ghana Building Code")

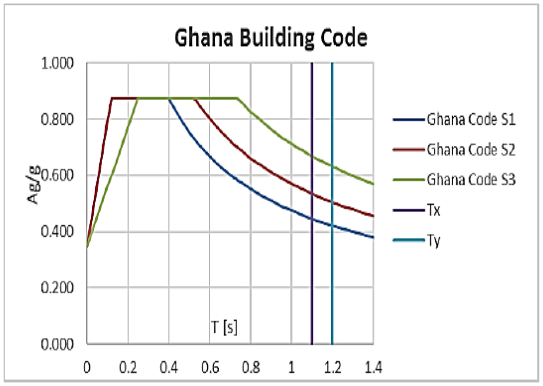


Figure 2-3 Graph for Type Elastic Response Spectra from Ghana Building Code

Fig. 2. Seismic Risk Map of Ghana *Ref. No .2*

 © Deep Foundations Institute 2025

The Project stretch was categorized under Seismic Zone-3 as per the Ghana Building Code. The PGA coefficient was 0.16g. when the contract was awarded. Subsequently, the Ghana Building Code was revised in the year 2018, where, even for Zone-3, the PGA coefficient was revised to 0.35g, nearing twice the value that the structure was designed for originally. Due to this increase, seismic forces became governing case for the design of foundations resulting to a significant increase in the pile numbers, pile diameter and pile reinforcements.

Type of Pile foundation (Vertical / Raker)

The initial designs of vertical piles under abutments and piers were carried out with pile foundation having a diameter of 2.0m each. The Peak ground acceleration (PGA) was 0.16g and the same was considered for design of vertical Piles.

Due to increase in PGA value, it was quite evident that increase in the number of piles and its diameter would attract more forces compared to initial proposal. Several other pile design options were explored to reduce the horizontal seismic forces in the pile group system.

Considering this, raker / batter pile system seemed to be a feasible option to reduce the vertical and horizontal forces in the piles. Raker piles are subjected to all three demand actions concurrently.
However, to understand the Raker pile behaviour against vertical piles, the Fig. 3 below shows the forces *P (vertical) and M (overturning)* acting on the foundation system. Normally, the axial load from overturning usually exceeds the dead and live gravity loads, resulting the pile in tension.

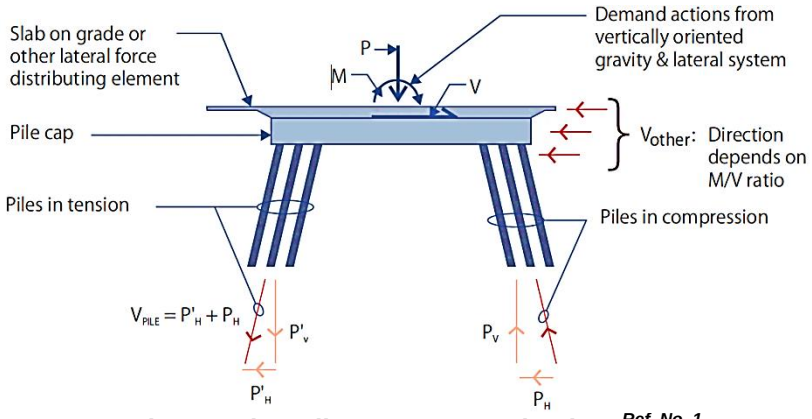


Fig. 3. Raker Piles – Force Mechanism ***Ref. No .1***

For simplicity, these loads are represented as a single force vector at each end of the pile cap. Due to inclination in Raker pile, a horizontal component to the pile axial force is developed as a resisting force, which opposes the applied load and is dependent on the pile inclination. There is greater resistance to the horizontal component in raked piles than in normal vertical piles. Hence, by adjusting the pile angle, *shear demand (V)* induced by the seismic event could be reduced.

The design was finalized with Raker pile system and it was virtue of arrangement that, forces reduced considerably on the piles. The pile diameter had also reduced from 2.0m to 1.6m with total pile numbers reduced too. This raker pile system was feasible option to reduce the larger seismic forces and an optimal solution. The Pile group under piers P2 and P3 had the longest piles of about 76.5m and constructability issues were anticipated during the design stage. In order to minimize further construction delays in the future with Raker pile configuration for longer piles, a backup of an alternate design proposal (vertical pile system) was also kept ready with prior approvals.

 © Deep Foundations Institute 2025

Apart from design, construction of raker pile for length of more than 60.0m in the river with uneven bed rock profile was also great challenges for project team. Initially vertical piles at abutments (A1 and A2) and raker piles for all intermediate piers (P1, P2, P3, P4) were planned. The rake in pile system was kept 1:5 as flat as possible to avoid drivability issues during construction. A dedicated team of AFCONS devised the construction scheme for these challenging operations of Raker Pile system. Special guide frame for liner pitching using guide rollers and special tie back arrangment to maintain the rake position of piles were devised and installed. A brief on construction methodology is further mentioned under separate section on construciton methodology.

Rock Touch Levels (RTL)

Geotechnical Investigations was also one of the critical parameters for designing the entire foundation. As the Volta river is an artificial channel, ascertaining the exact rock touch levels was very important. Being the largest man-made channel, the rock profile in the river bed varied every metre along the bridge length. Also, the designed system was complex and quite challenging. The in-house Geotechnical team had devised a mechanism to get exact rock touch levels for the proposed raker pile foundation based on available confirmatory boreholes.

During piling activity, actual rock touch levels against confirmatory bore holes variation was enormous and it required a re-check of the existing pile foundation design and pile group system. During the construction of first raker pile in piers, the variation in rock touch levels noticed was significant. These variations were all along the channel and became one of the critical design parameters.

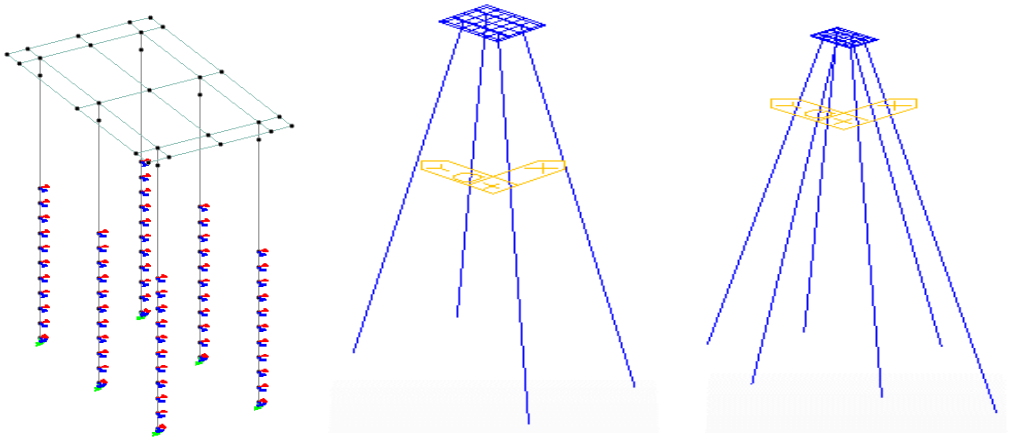


Fig. 4. Analysis of Piles under each Foundation during the construction.

When the assumed RTL varied within a pile group, the design of pile foundations also must be reviewed. This was one of the parallel activities throughout the completion of all the piles under each pier. Frequent monitoring of RTL variation under each pile was done to ensure the design forces are within permissible limits. The site team was asked to share the RTL for each pile boring, and the design team kept checking the adequacy of the proposed pile strength based on the recorded RTL. This co-ordination between the design and site team was followed throughout the piling construction process.

CONSTRUCTION METHODOLOGY OF RAKER/BATTER PILES

In the present world, piling activity are very common, and the methodology of construction of vertical piles are well known to all. In this topic, the construction challenges faced during Raker pile is mainly

 © Deep Foundations Institute 2025

emphasized. A special type of construction methodology was devised in-house by the expert team, details are discussed below:

Brief method of construction:

- Drive temporary piles using crane mounted on barge with the help of vibro hammer,
- Erect temporary platform over temporary piles along with guide frames for pitching the permanent liner of raker pile.
- Drive liners by vibro hammer up to refusal.
- Erect the RCD rig on liner and perform the boring up to design pile tip level.
- Remove the RCD rig upon completion of boring.
- Lower the reinforcement cages into the liner.
- Lower the tremie pipe for concreting.
- Pour the design mix of concrete with the help of pump and pipeline arrangement.
- After concreting cut the liner at pile cap bottom level

Survey and positioning of barge

Crane barge was equipped with 260 MT capacity crane, power pack, compressor, vibro hammer. Detailed survey was done to fix the temporary pile co-ordinates and anchor the position of crane barge. After thorough surveying, anchor was placed at the planned positions using total station. Then, the crane barge was shifted and positioned to drive the temporary piles

Driving of temporary piles

Guide frame fixed with base frame was fixed to the barge for driving of temporary pile. Temporary pile was lifted using crane from material barge and pitch it through guide frame. Vibro hammer was lifted by crane and attached to temporary pile and pile driven upto refusal. After the driving of temporary piles, the vibro hammer was detached and placed in the crane barge.



Fig. 5. Driving of Temporary Piles

Erection of base frame and guide frame

All the temporary piles were braced together and main girders, secondary girders and base frame was fixed on to temporary piles using crane on barge. Temporary platform was fixed over this and 2-level guide frame was fixed on the base frame.

 © Deep Foundations Institute 2025



Fig. 6. Temporary Piles, Guide frame set-up and Installation of Raker Pile Platform

Driving of liner

The fabricated liner of designed lengths was transported using barge to pile location. Liner was lifted by crane mounted on barge at the lifting point in 1:5 rake and pitch through the guide frame. Once again, survey was done to ensure the designed position and inclination of liner. Liner could penetrate in ground by its self-weight and then vibro hammer was lifted by crane and fixed on top of liner.

Liner was driven upto a level such that, approx.500mm of liner is above the guide frame to facilitate welding of next liner piece, if required. While driving of liner, the proposed rake of 1:5 was continuously monitored so that, the rake is maintained throughout. Once the liner is driven upto refusal, then vibro hammer will be detached from liner and placed on the barge.

Before driving the liner fully, a window of 250mm x 250mm will be cut such that it is below low water level after driving, for water flushing inside the liner.

 © Deep Foundations Institute 2025



Fig. 7. Transportation of Liner and Driving of Liner for raker pile

Installation of RCD rig over casing

Once driving of liner was completed, RCD rig with all accessories was brought to the pile location using crane barge and the RCD rig was lifted and fixed on the top of line and clamped. After that, Compressor hoses and power pack hoses are connected to RCD rig. Later, the drill string, drill bit, stabilizer units was lowered inside the liner.



Fig. 8. Reverse Circulation Drill (RCD) Installation

Boring / Socket Drilling

RCD cutter was operated, and its torque was controlled by operator for continuous drilling activity. All the crushed materials mixed with water was drained out using suction pipe. Boring / Drilling was stopped after achieving designed depth and the samples were collected at regular intervals to check the solid characteristics.

A simple basket/net arrangement was provided at the discharge point for collecting these samples. Once the drilling is completed upto founding level, drill string along with drill bits was removed from RCD rig and the opening kept for water flushing was closed before concreting.

 © Deep Foundations Institute 2025



Fig. 9. Boring / Socket Drilling

Reinforcement cage lowering

Reverse circulation method was adopted in this process of rake pile driving, so there was no need to do air flushing. All the fabricated pile reinforcement cages were brought to the pile location using material barge. First the cage was lowered in the liner and locked at the liner top such that approx., 1.0 m length of the cage is left over. The second cage was lifted with the crane and positioned over the bottom cage and coupled with the first cage. Similar procedure was done upto the designed length of pile (max. length of pile was 76m). Cover blocks of 75mm diameter, 4 nos. every 3m vertical intervals throughout the pile length was fixed to the reinforcement cage itself.



Fig. 10. Reinforcement Cage Lowering

Tremie lowering and Pile concreting

All the pipe joints of tremie pipes was doubly checked and cleaned from rust and deleterious material. Joints was made waterproof by applying bituminous compound. Tremie pipes of 1 to 1.5m length pieces was joined on ground at site itself for the maximum length and it was thoroughly cleaned using wire brush. After complete joining and cleaning, it was lifted with crane and lowered inside the liner. The tremie was lowered upto 300mm above founding level by subsequently adding tremie pipes. At the top, concrete funnel was attached for pouring of concrete into the pile.

The design mix concrete was brought to the pile location by pump and pipeline arrangement. Concrete was poured into the funnel attached to the tremie pipe. Initially, funnel bottom must be closed with removal plate (plug) to avoid segregation of concrete. Once, the funnel is filled up with concrete, the plug was removed, and full load of concrete was poured in a single pour. After concreting upto the pile cap bottom level, the liner was cut.



Fig. 11. Tremie pipe assembly, lowering and Pile concreting

CONCLUSIONS

With all these difficulties right from planning stage to design and construction stage, the project team completed the execution of total 30 nos. of pile foundations for the railway bridge crossing the largest artificial lake in the world. The continuous challenges in both design and execution were challenging yet resolved by the design team on this important Ghana project.

The Volta bridge now stands completed in the year 2024 and is an epitome of design and execution challenges and how they were overcome. Authors firm has constructed several railway bridges on water bodies in the past. However, bridge across Volta River has been like no other due to the unexpected geological conditions.

Contents of the proposed paper is planned to provide a background of the project and factors that lead to Raked/battered foundation design. The paper discusses analyses of the raked/battered pile foundation, construction methodologies and how critical bottlenecks during their execution were overcome.

- Any mega foundations involve challenges, particularly when there is no known history of execution in similar situations. Marine works involve different logistics for temporary structures, piling, concreting and Temporary platforms.
- Raked / Battered piles at Volta bridge was one such unique achievement. Apart from construction, analysis and design of such structure always has challenges during execution. At Volta Lake, being one of the largest Man-Made / Artificial River, the variation in rock top levels (RTL's) were significant.
- Design validation had to be done during construction of at every pile in a group (raked pile group) before concreting. Any design modifications required were timely conveyed to construction team and implemented.

- Confirmatory of the works done were demonstrated by conducting successful lateral load test using Cross Hole Sonic Logging (CHSL) Method. Spring stiffness were validated with this test as per our design considerations

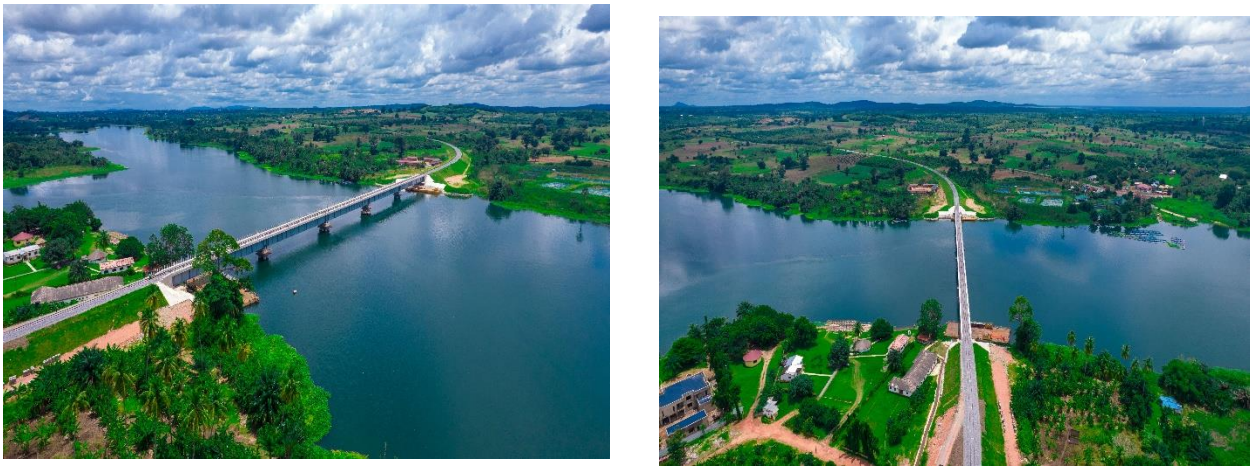


Fig. 12. Completed Bridge

REFERENCES

1. Article "*Raked Piles Battered and Misunderstood"*, Mark A. Morre, STRUCTURE magazine, December 2005 edition, 49-53.
2. GS 1207 : 2018, *Ghana Building Code (GhBC)*, Ghana Standards Authority (GSA)
3. *EN 1990*, Eurocode 0, "*Basis of Structural Design"*, European Commission.
4. *EN 1991*, Eurocode 1, "*Actions on Structures - General Actions (Part 1-1:2002, Part 1-2:2002, Part 1-4:2005, Part 1-5:2003, Part 1-6:2005, Part 1-7:2006 and Part 2:2003)"*, European Commission.
5. *EN 1992*, Eurocode 2, "*Design of Concrete Structures (Part 1-1:2004 and Part 2:2005)"*, European Commission.
6. *EN 1993*, Eurocode 3, "*Design of Steel Structures (Part 1-1:2005 and Part 2:2006)"*, European Commission.
7. *EN 1994*, Eurocode 4, "*Design of composite steel and concrete structures (Part 1-1:2004, Part-2: 2005)"*, European Commission.
8. *EN 1997*, Eurocode 7, "*Geotechnical Design (Part 1:2004 and Part 2:2007)"*, European Commission.
9. *EN 1998*, Eurocode 8, "*Design of structures for Earthquake Resistance (Part 1:2004, Part 2:2005 and Part 5:2004)"*, European Commission.
10. *UIC 776 2R: "Design requirements for rail bridges based on interaction phenomena between Train, track and bridge", 2009,* International Union of Railways, Paris, France.
11. *UIC 776 3R: "Deformation of Bridges",* International Union of Railways, Paris, France.
12. IRS (Indian Railway Standards) Code, "*Code of Practice for The Design of Sub-Structures and Foundations of Bridges".*

 © Deep Foundations Institute 2025

CONSTRUCTION OF A RETAINING STRUCTURE WITHIN COMPLEX SITE CONDITIONS

Clayton Price, Wagstaff Piling Pty Ltd, Melbourne, Victoria, Australia, +61468546799, clayton.price@wagstaffpiling.com.au

ABSTRACT

A case study of the construction of a diaphragm wall situated within complex site conditions to form the tunnel access shaft retention structure as part of Melbourne, Australia's most ambitious rail infrastructure project. The diaphragm wall structure consisted of 57 each 1000mm reinforced concrete panels with excavated depths ranging from 24m to 31m with 38 of the total panels being constructed within uncontrolled fill. The location of the site is approximately 27km South-East of Melbourne's CBD and was a former sand quarry that had been backfilled with uncontrolled fill to a depth of approximately 13m with underlying dense sands and a high-water table. All fill material was determined to be contaminated with non-friable asbestos. The site conditions presented significant risk to the project both commercially and from a constructability perspective. The documented history of the fill used to backfill the quarry was limited which provided uncertainty for the presence of inground obstructions, the stability of the fill, and management of the bentonite support fluid. The presence of asbestos required the workforce to conduct the works under strict conditions. The panels were all constructed using diaphragm wall hydraulic grabs under bentonite support fluid. The ground conditions required the placement of concrete to be executed as soon as possible once excavations were completed which posed as a problem due to the asbestos working conditions. To accelerate this process, stop-end lengths were reduced, and reinforcement cages were installed in single lengths up to 24.5m. While several problems became present during the works and needed to be carefully managed, the structure was completed on time and within budget.

Keywords: Diaphragm Wall, Landfill, Asbestos, Bentonite

INTRODUCTION

In 2023 Wagstaff Piling were awarded a subcontract to construct the tunnel access shaft retention structure with works commencing and coming to completion in 2024. The works formed part of Melbourne, Australia's most ambitious rail infrastructure project at a site that is approximately 27km South-East of Melbourne's CBD and had previously been used as a landfill site. It was initially recommended to the client that based on the geological conditions that a bored secant pile wall utilising segmental casing would be the most suitable solution for the works, however it was insisted that the existing specification could not be deviated from, and the structure was to be constructed as a diaphragm wall. The scope of works under the subcontract was construct only and included the supply of all labour & machinery as well as the supply and installation of all materials. The diaphragm wall structure consisted of 57 each 1000mm reinforced concrete panels with excavated depths ranging from 24m to 31m with 38. of the total installed panels being constructed within uncontrolled fill which had been deemed to be contaminated with non-friable asbestos. Due to the significant difference in working requirements for the panels contaminated with non-friable asbestos, it was decided that the 19 panels that were not contaminated were to be constructed prior to any works commencing on the contaminated panels.

CASE STUDY

Site History & Geology

The Diaphragm Wall was to be constructed inside a former sand quarry that has been backfilled with uncontrolled fill to an approximate depth of 14m with underlying natural sands and a high-water table

 © Deep Foundations Institute 2025

which was deemed to be 3.1m below the working platform level. The documented history of the fill used to backfill the quarry was limited which provided uncertainty for the presence of inground obstructions, the stability of the fill, and management of the bentonite support fluid. Historical aerial imaging was relied upon to obtain an understanding of the site history which indicated that sand quarrying operations were commenced in 1995 and ceased sometime between 2000 to 2007, and the filling of the site being undertaken up until as late as 2012. No records of the filling history of the site were available. An overlay of the Diaphragm Wall layout over a historic image of the site from 2006 is shown below in Fig. 1.



Fig. 1 - Diaphragm Wall Layout Over Historical Image (2006)

The project geotechnical consultant conducted a site investigation which consisted of a combination of boreholes and Cone Penetration Test's (CPT's) which reported that the fill used for quarry backfilling activities was variable in composition and contains inert waste including brick and brick fragments, timber and steel. The material generally ranges from firm, stiff and very stiff clay and silty clay to loose and medium dense silty sand and sand. Given the variability in the origin and placement of fill materials, the consistency of the unit varies both laterally and vertically. CPT tip resistances vary significantly with depth and location, typically ranging between about 1.5 MPa and 10 MPa with occasional bands of higher resistance and some instances of CPT refusal on inferred obstructions. Fill depths in the centre of the backfilled quarry footprint range between about 13m and 14m and reduce towards the perimeter, presumably along the former side slopes of the quarry.

The underlying materials typically consisted of natural sands with 50mm to 100mm cemented layers occurring throughout the site. Refer Fig. 2 below.

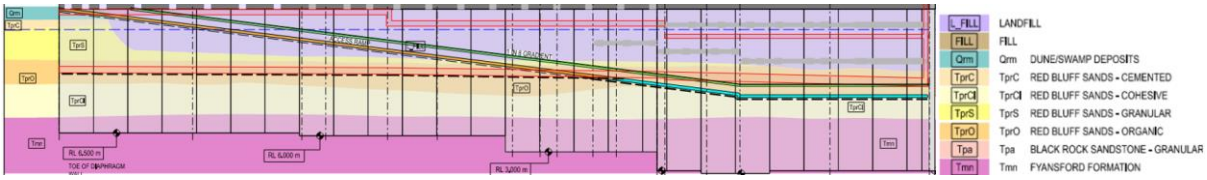


Fig. 2 - Site Geological Long Section

Site Requirements and Mobilisation

To construct the wall, two track mounted rigs each fitted with diaphragm wall hydraulic grabs were utilised for the excavations. Both of the hydraulic grabs had an open bucket width of 2.5m, thickness of 1m, and were fitted to three stage kelly bars rather than ropes. Lifting activities utlised a 180T and 100T track mounted lattice boom cranes for major lifts such as reinforcement cages and stop-ends. A 40T track mounted hydraulic boom crane was also used to perform various lifts to service the works. In addition to these cranes, an additional heavy duty 100T crane was mobilised specifically to complete all chiseling works. To batch, store and maintain support fluid required for the works, an on-site batch plant was established which included a high-speed shear mixing dosing unit for batching the bentonite, 660,000

 © Deep Foundations Institute 2025

liters of storage units made up with a combination of silos and rectangular tanks were required and for desanding of the bentonite, two desanding units were set up over 30,000L tanks. Due to the high traces of silt encountered that were too fine to capture with the desanders, a desilting unit was also mobilised to site halfway through the works. Images of the site arrangement can be seen below in Fig. 3.



Fig. 3 - Batch Plant, Site Arrangement, Hydraulic Diaphragm Wall Grab

The working platform was provided by the client prior to mobilising to site and was constructed with cement treated material at a uniform working level of 29.800 Australian Height Datum (AHD). The site was located within the flight paths of a nearby general aviation airport mainly for light aircrafts but also receives commercial airline services from time to time. Working within the vicinity of the airport meant that strict height restrictions outlined within the aviation authorities permit needed to be always adhered to. These restrictions included no cranes or piling rigs to exceed a height of 58.0AHD (28.2m above working platform level) outside of daylight hours and 63.5AHD (33.7m above working platform level) cannot be exceeded at any time which governed the allowable boom lengths configured on the crawler cranes.

Due to the presence of asbestos within the landfill, the majority of the works were required to be performed under strict asbestos working conditions which meant that the entire work zone including the batch plant would be considered contaminated with asbestos and all personnel who enter the work zone would need be fitted with a P2 rated particulate respirator, wear other mandatory PPE such as disposable hazmat suits, boots and gloves and would need to fully decontaminate prior to leaving the work zone for breaks or changes of shifts which involved installing designated decontamination facilities. All personnel also needed to be trained and qualified in Asbestos Containing Material (ACM) removal which also included any maintenance personnel that were required to repair or service machinery from time to time. To manage fatigue associated with wearing the required PPE, the workforce were required to take a mandatory 1-hour break after every 3 hours worked, which required resources to be allocated on staggered shifts to avoid a loss of efficiency for excavation works and also provide constant coverage for longer activities such as reinforcement cage installations and concrete pours.

Excavation Process

All panels were designed to be constructed as 6.4m wide panels with the exceptions of the two z-panels where the tunnel access shaft widens, the two corner panels at the Eastern end, and the center panel along the headwall which was constructed as a single bite primary panel. The panel arrangements utilised were a combination of primary, secondary, and closing panels. “Primary” panels were constructed as the initial panel in a sequence and included cast-in stop-ends at both ends of the panel. “Secondary” panels which

were constructed in succession to a previously constructed adjacent panel, these panels require both the removal of the already cast-in stop-end from the adjacent panel as well as the installation of a new stop-end on the virgin end. To complete sequences “closing” panels are constructed between two already constructed panels on each side, these panels require already cast-in stop-ends to be removed from both sides and do not require any new stop-ends to be cast-in. When determining the panel layout and construction sequencing, the risks associated with excavating within landfill were front-of-mind and it was decided to utilize a total of nine primary panels spread out across the site which would allow machinery to relocate to alternate locations and maintain efficiency in the event that any major issues were encountered which could bring productive works to cease.

The excavation width of the hydraulic grab buckets was 2500mm and panels were each constructed in three sections with the first being on the virgin-end (the side furthest away from the previously constructed panel), the second section is excavated on the opposite end, hard up against the already cast-in stop-end, and the final section is removing the remaining material in the center of the panel.

Several foreign objects were identified and recorded during the excavation of panels such as bricks, concrete boulders, timbers, metals, and decayed tree stumps (Fig. 4). These identified items raised concerns for the overall finish quality of the face of the diaphragm wall, however no obstructions were encountered which couldn’t be removed and would have caused excavation works to cease.



Fig. 4 - Site Images of Excavated Landfill

Stop-End Installation & Removal

At the completion of a panel excavation, the stop-end is removed from the previously cast adjacent panel and another stop-end is installed at the opposite end of the panel to be cast into the concrete. The stop-end is to act as temporary formwork for the ends of the panels and is specifically shaped to create a key joint between the panels which includes a continuous PVC water-stop blade that is inserted into a central slot of the stop-end and is left behind in the concrete when a stop-end is removed and creates a barrier to prevent leaks between the joints of two panels. The general arrangement of the stop-ends utilised are shown below in Fig. 5.

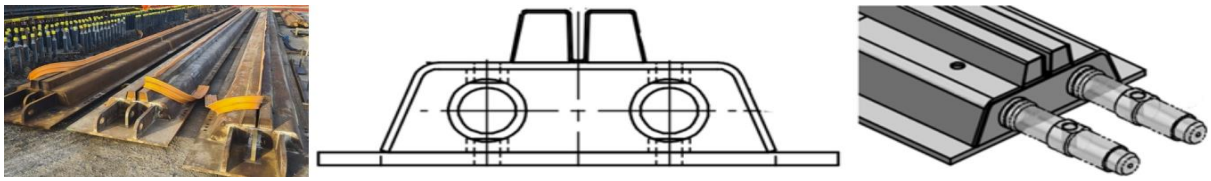


Fig. 5 - Stop-End/Water-Stop Image, Stop-End Cross Section, Stop-End Pin Connections

One area that was agreed to deviate from the original design specification was for the length of the stop-ends to go all the way to the design toe of each panel which would have resulted in stop-end lengths of

 © Deep Foundations Institute 2025

approximately 30.3m at the deepest section of the works and 24.3m at the shallowest section. A risk that was identified prior to works commencing was the potential difficulty removing stop-ends due to excessive concrete overbreak's occurring with the uncontrolled fill and the underlying sands which would result in excessive chiseling work being required and overall delays to the works program. To mitigate this risk, it was decided that all stop-ends would be installed to a uniform depth of 21m below the working platform level for all panels which also meant that the toe of the stop-ends would all be at least 4m deeper than the final bulk excavation level. An added benefit to having a uniform depth for stop-ends was that all stop-ends were able to be 22.5m in length made up of a 11.5m top sections and an 11m bottom sections and assembled at the commencement of the works and remained as singular sections for the entire works as the total lengths of 22.5m were able to be pitched from horizontal to vertical as singular sections via a dual lift with two 100T cranes which eliminated any requirement to disconnect and reconnect sections over the excavation which increased productivity and made coordinating the asbestos working roster times more manageable. To remove stop-ends, a purpose-built chisel is run down the flat side of the stop-end for the full depth to remove any excess concrete that may have made its way around the stop-end during the concrete pour, this is executed by placing the chisel over the stop-end with the main line of the crane positioning the vertical guides down the sides of the stop-end and continually lifting and dropping the chisel in free fall at approximately 300mm to 600mm drop height increments while the auxiliary line is attached to the top of the stop-end. When the stop-end has become free, it is removed from the excavation leaving behind the PVC waterstop. Once the panels in the undisturbed natural material were completed and the works in the uncontrolled fill commenced, there was a noticeable increase in concrete overbreak's occurring around the stop-ends which was evident by the amount of concrete being removed from the panel at completion of the chiseling works and the chisel itself sustaining significantly more damage after each use which resulted in the chisel needing to be sent off site for repairs usually after two to three uses. Generally, the chiseling works on the project were efficient with all stop-ends each being removed within one to four hours with the exception of one stop-end which required almost three full days of chiseling to remove all the concrete overbreak which had trapped the stop-end. Images of the chiseling works undertaken are shown below in Fig. 6.



Fig. 6 - Chisel, Concrete Overbreak, Damaged Chisel Blade, Damaged Chisel Guide

Support Fluid

During the excavation of each panel, excavations were constantly filled with a bentonite drilling fluid to a minimum of 500mm below the working platform to maintain a positive head pressure 3.6m above the ground water table. The bentonite product utilised recommended a mixing ratio of 30kg to 50 kilograms per 1000 liters of water for stable ground conditions, however the dosage rate was increased to approximately 65kg per 1000 liters to provide additional stability. Testing of the bentonite was undertaken daily to monitor the properties and performance of the recycled fluid, and all panels were tested prior to concreting. The specification adopted for the project is shown below in Table 1.

 © Deep Foundations Institute 2025

Table 1 - Bentonite Testing Specification

Test	Method	Recycled Fluid	Pre-Pour
Viscosity	Marsh Cone	30s - 60s	30s - 60s
Density	Mud Balance	1.02 - 1.08	< 1.15
pH	Digital pH Meter	7 - 11	7 - 11
Filter Loss	Filter Press	< 30mm	< 50mm
Filter Cake	Filter Press	< 3mm	< 5mm

A false assumption made prior to commencing the project was that significant fluid loss within the uncontrolled fill was going to be an ongoing problem, however this did not eventuate, and it would turn out that retaining too much fluid over the course of the works would become a problem as the storage tanks on site were usually at capacity with bentonite that was continually being recycled which limited the opportunities to batch fresh bentonite as the works progressed to manage the properties and performance of the fluid. Not being able to rely upon gradual fluid loss over the course of the works to be able to replenish the bentonite supply resulted in fluid needing to be continuously removed from the storage tanks on site via vacuum trucks and disposed of at a licensed off-site facility which proved to be challenging due to the contamination within the landfill. During the construction of the first 19 panels within the "clean" undisturbed natural material, the bentonite was more easily managed but changed noticeably once works within the "dirty" uncontrolled fill material commenced. The two properties of bentonite which required the most attention were density and viscosity. The material that was being excavated contained high traces of silt which was too fine to be captured during the desanding process and continually accumulated within the recycled bentonite which resulted in density values being at the upper end of the pre-pour limit even when the sand content had been reduced to 0.5%. Once the impact that silts were having on the bentonite was identified, a desilting unit was mobilised which managed to bring the specific gravity down to an approximate average of 1.10. With respect to the viscosity of the bentonite, the Marsh cone values were consistently falling towards the lower limit of the specification. During the works in the "clean" material, the addition of cellulosic polymers was enough to achieve Marsh cone values above 35 seconds; However once works commenced in the "dirty" material the presence of organic material was noticed and caused a further decrease in the viscosity causing the Marsh cone values to decline towards 30 seconds. Refer Fig. 7 below.

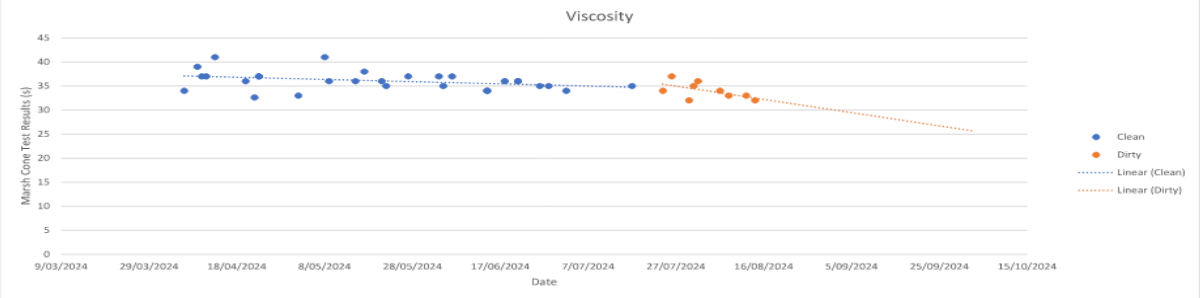


Fig. 7 - Viscosity Values in Clean V Dirty

To increase the viscosity of the bentonite in circulation, a combination of adding cellulosic polymers to combat the effects of the organic material as well as disposing of stored recycled fluid and replacing it with fresh fluid with high dosages of bentonite was used. While this combination had some success, the constant disposal of bentonite was not cost effective. In an attempt to reduce the amount of bentonite needing disposal, the use of sulfamic acid was trialed on samples to combat the effects that the organic material was having on the fluid's viscosity. The first trial was conducted in a 14L bucket on a sample that

had a Marsh cone time of 29.71 seconds. By adding only 1 gram of sulfamic acid and mixing using a drill with a paint mixer, the Marsh cone increased by almost 5 seconds over a 2-hour period and eventually achieved a Marsh cone time of 40.16 seconds with a total of 3 grams of sulfamic acid after 42 hours. The trial was then reconducted on a larger sample size inside a 1000L container and again using a drill with a paint mixer to mix. With an equivalent dosing of sulfamic acid, the 1000L test viscosity increased similarly to the 14L test and achieved a Marsh cone time of 36.21 seconds over 40 hours. A summary of these results is shown below in Fig. 8.

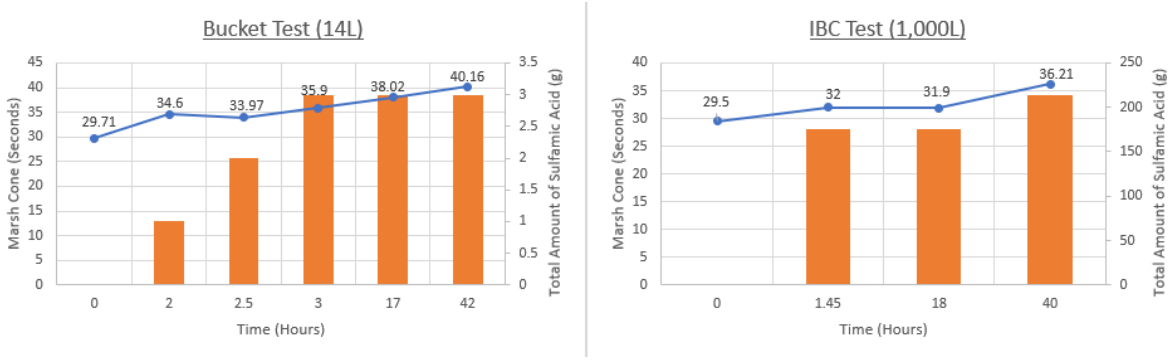


Fig. 8 - 14L Bucket Marsh Cone Test, 1000L Container Marsh Cone Test

A key observation from the 1000L test which raised concerns was that even though a desired increase in viscosity was achieved, introducing sulfamic acid resulted in obvious clotting occurring all throughout the sample with the clots appearing more like a paste rather than a liquid. This lead us to believe that the excessive amounts of bentonite within the recycled support fluid were not actually being broken down by the presence of organics, but it was instead only being masked by the presence of the organics. This meant that once the sulfamic acid was introduced and the effects of the organics were removed, all the bentonite in the system that was previously masked became active again all at once which produced a fluid with far too much bentonite in the system. Considering the major effects that minor doses were having on the test samples, it was decided that it would be too greater risk to introduce sulfamic acid to the bentonite in storage and instead elected to persist with adding cellulosic polymers and replenishing the bentonite as required to manage the viscosity.

Reinforcement

As a contingency measure adopted by the clients' designer, the diaphragm wall structure was designed to allow for one row of the external strutting system to fail during the bulk excavation works which resulted in the reinforcement cages being heavily congested. Each 6.4m wide panel was made up of two cages each 2750mm x 850mm to allow for 75mm concrete cover on both the excavation and soil faces with plastic wheel spacers being used to position the cage. All vertical bars were 40mm diameter with up to 48 vertical bars per cage (96 bars per panel) and all ligatures and tie bars were all 16mm diameter at spacings ranging from 150mm to 300mm with complete cages weighing up to 27T (54T total within the panel). All cages were fabricated off-site and delivered to site for installation. Another key risk identified prior to the works commencing was the cage splicing process being undertaken with the limitations caused by the asbestos working conditions including the limited working windows and PPE restricting the ability for the workforce to communicate effectively. To accommodate for these conditions, cages up to 24.5m in total length were fabricated and spliced together off-site and delivered as complete cages using oversized transport arrangements and permits. This allowed 26 panels (52 cages) to be completed without requiring any cage splicing to be done over the panel excavation. While there were additional costs associated with

 © Deep Foundations Institute 2025

the off-site fabrication and the oversized transport, the benefits of the efficiency gained on site far outweighed these costs with cages not requiring splicing being able to be installed in around 30 minutes compared to cages that required splicing on site taking two to three hours to install. However, due to the height restrictions from the local airport being enforced, 24.5m was the largest size that could fit under the fixed ceiling height which meant that all cages larger than 24.5m would require on site splicing over the panel excavation. All cages were pitched from horizontal to vertical using a dual lift technique with the 180T crane being the lead crane lifting from the top of the cage and the 100T being the tailing crane and utilising an equalising running sheave and detaching once the cage was vertical leaving the 180T to lower the cage into the panel excavation. The four panels along the head wall of the tunnel access shaft were constructed using a combination of steel reinforcement and glass fiber reinforcement to create the "soft eye" for each of the two tunnel boring machine breakthrough locations. These sections of wall were 9.4m diameter zones that could not include any steel but were still required to be fully reinforced which led to the design of these panels utilising three section cages that included top and bottom steel cages, and a center cage made from only glass fiber. The glass fiber bars were manufactured in Thailand and the cages were assembled in Melbourne at an off-site location. To lift the glass fiber reinforcement cages from horizontal to vertical, cages were laid into a purpose built steel frame which was lifted by the 100T crane until it reached a pitched angle of 75 degrees, at this point the 180T crane would take the full weight of the glass fiber cage and remove it from the frame while it was in a vertical position, the cage is then able to be tracked over to the panel and installed. Site images of the reinforcement installation process are shown below in Fig. 9.



Fig. 9 – 24.5m Cage Dual Lift, Cage Splicing Over Excavation, Lifting GFRP Cage via Pitching Frame

Concrete Specification & Placement

The concrete specified for the works was a 50 MPa strength self-consolidating concrete mix which needed to meet strict durability requirements and contain a minimum of 66% Supplementary Cementitious Materials (SCMs) which was achieved by the supplier utilising fly ash. The mix included 20mm aggregate and had a design slump flow of 650mm plus or minus 100mm. Due to the large width of the panels at 6.4m, the concrete was pumped through twin 5-inch "stiff legs" rather than the tremie method with each stiff leg placed in the center of each reinforcement cage. The concrete volume of each panel ranged from 150m^3 to 210m^3. The mix proved to be extremely temperamental with on-site testing results varying greatly which resulted in several loads being deemed unusable throughout the works. To manage the inconsistency of the quality of the concrete being delivered, the testing requirements were increased so that every load that was delivered to site would need to be slump flow tested and satisfy the

design specification rather than just the initial four deliveries as required by the Australian Standards. Refer Fig. 10 below.

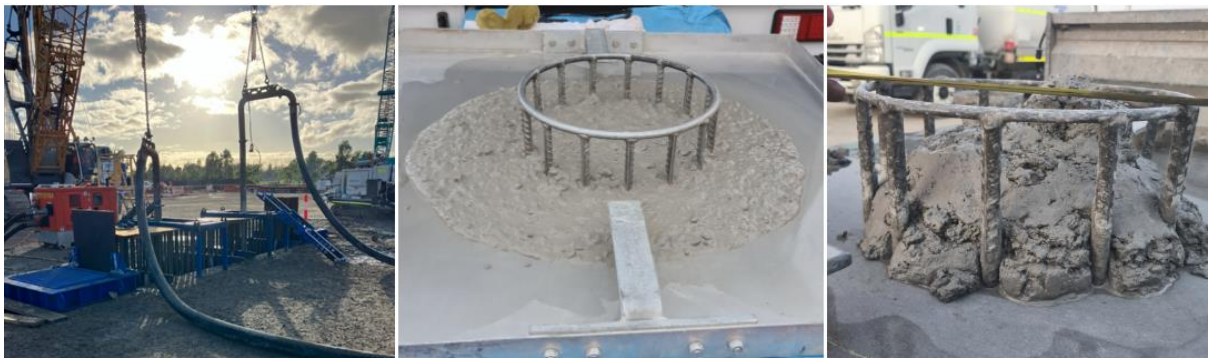


Fig. 10 - Stiff Leg Arrangement, Compliant Slump/Flow Test, Failed Slump/Flow Test

DISCUSSION

During the course of the project, the three main complex issues that impacted the works involved dealing with uncontrolled fill, the presence of asbestos, and the working height restrictions which all imposed several limitations on how the works were to be conducted. The diaphragm wall was completed within program and the works were ultimately considered a success as a result of thorough planning and collaboration with a proactive client.

At the time of writing this paper, the bulk excavation of the tunnel access structure had commenced and exposed approximately 5 meters of the diaphragm walls excavation face showing a stark contrast of the finish of the panels constructed in the undisturbed natural ground compared to the panels constructed within the uncontrolled fill. The panels constructed in the natural ground show the type of finish that is to be expected for panels cast in granular material and no surface irregularities outside of the design tolerance. The panels constructed within the uncontrolled fill, however, have several surface irregularities and large bulges which indicate that voids were present within the uncontrolled fill or minor collapses occurred during the panel excavations. Figure 11 below shows a site image of the exposed diaphragm wall with the panels on the right-hand side of the image being the panels cast in the natural ground conditions and the panels directly in front and on the left-hand side the panels cast in the uncontrolled fill.



Fig. 11 - Exposed Diaphragm Wall

 © Deep Foundations Institute 2025

BRIDGING CHALLENGES: CREATIVE SOLUTIONS FOR THE I-81 BRIDGE FOUNDATION DESIGN

Ram K., P.E., KC Engineering and Land Surveying P.C., New York, New York, United States, (646) 975-5289, rkasturi@kcepc.com
Kamal R., P.E., KC Engineering and Land Surveying P.C., New York, New York, United States, (646) 795-5070, kregmi@kcepc.com

ABSTRACT

The project involves an Alternative Technical Concept that realigns East Brighton Avenue in Syracuse, NY. As part of this realignment, a new bridge east of the existing East Brighton Avenue bridge over Existing I-481 ramps from existing I-81SB and existing I-81NB will be constructed. The new bridge is a 133 ft long, single-span superstructure on integral abutments. Based on the proposed profile of realigned East Brighton Avenue and the roadway underneath, the bridge height was over 42 ft. A tall abutment adjacent to an existing bridge posed construction and schedule challenges, and potential quality control issues due to large volume of mass concrete. Additionally, New York State Department of Transportation (NYSDOT) Bridge Manual's standard integral abutment designs are limited to a maximum height of 15 ft. and require complicated finite element analysis for taller abutments. To address these challenges, anchored soldier pile and lagging walls were designed in front of abutments to reduce the abutment heights. Due to the site constraints, the bridge piles were re-designed using larger size H-piles with increased spacing to accommodate the anchors in between the piles. A 3D model was developed to more accurately layout the piles and avoid conflict with crisscrossing soldier pile anchors.

Keywords: Integral Abutment, Soldier Pile, Deadman Anchor

INTRODUCTION

Although the concept of Integral abutments bridges isn't new and was first used in the United States in the early 1900s, they have gained widespread use only in the recent years (Hassiotis et al. 2006). Integral abutment bridges have the superstructure cast integrally with the substructure. The superstructure thermal movement is accommodated by the movement of the abutment and flexible pile foundation, eliminating the need for conventional expansion joints. Eliminating expansion joints and bearings simplifies construction and reduces bridge maintenance costs. Over recent years, many bridges with expansion joints have exhibited deterioration of the bridge joint and bearing components, primarily due to the water leakage through the joints. By eliminating expansion joints, the costs and efforts required for bridge maintenance are reduced. In recent years, integral abutments are preferred by many State Department of Transportation (DOT) agencies.

Integral abutments have been conventionally used as stub abutments. With recent advancement in finite element modeling capabilities like improved constitutive models, connection models, and super structure interaction (SS) capabilities, similar to NYSDOT practice for integral abutment design, DOT agencies allow the use of taller integral abutments if detailed analysis is performed. The NYSDOT Bridge Manual provides standard integral abutment designs for abutments up to 15 ft. in height (New York State Department of Transportation 2025), and abutments taller than 15 ft. require creation of a finite element model. The finite element model includes all bridge components including soil springs to evaluate soil-structure interactions.

As part of the I-81 Viaduct Project - Phase 1, Contract 2, Design-Build contract, a new bridge with integral abutments was proposed as part of an Alternative Technical Concept for reconstruction of East

 © Deep Foundations Institute 2025

Brighton Avenue in Syracuse, NY. See Fig. 1 for an aerial view of the project area and Fig. 2 for the bridge site location.



Fig. 1. Project Aerial View

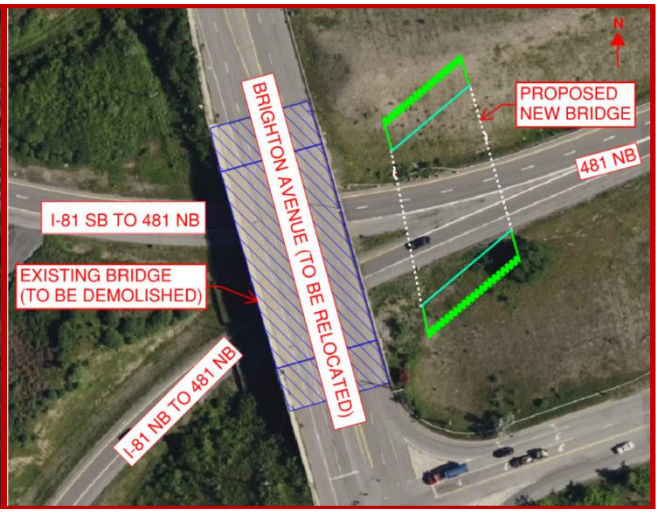


Fig. 2. Bridge Site Location

PRELIMINARY DESIGN:

As part of the Request for Proposals (RFP) documents, NYSDOT provided a preliminary design for a new East Brighton Avenue over New I-81 bridge with a 282 ft long, two-span superstructure on integral abutments and a 25-degree skew. This preliminary bridge was along the existing alignment of East Brighton Avenue and within the vicinity of the existing bridge. See Fig. 3A and Fig. 3B for the plan and elevation of the preliminary bridge design.

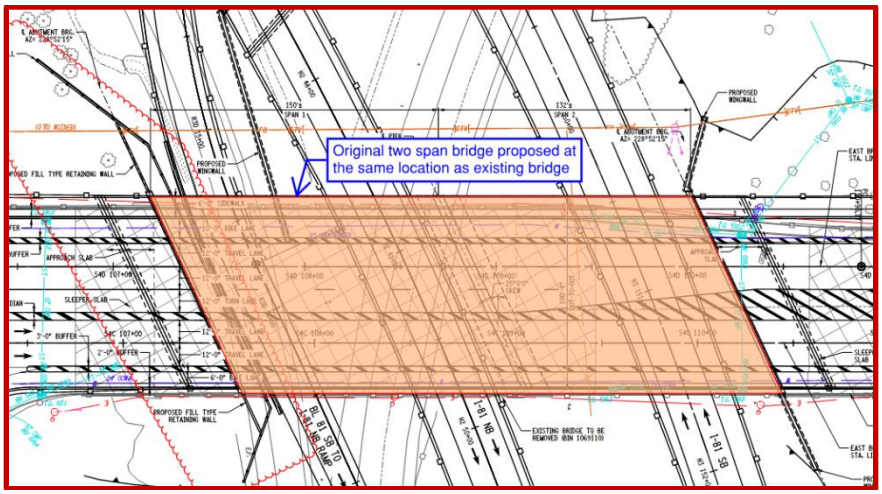


Fig. 3A. Preliminary Bridge Design (Plan)

 © Deep Foundations Institute 2025

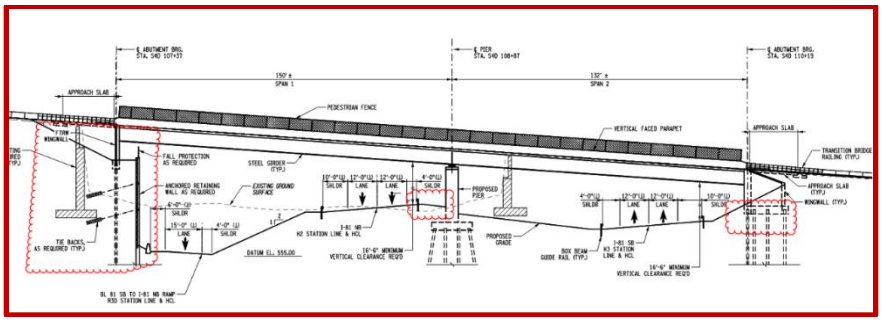


Fig. 3B. Preliminary Bridge Design (Elevation)

The construction of this bridge at the existing East Brighton Avenue alignment would require staged construction of the bridge with many traffic shifts, and temporary relocation of two large watermains to keep it operational during construction. To mitigate these construction challenges, our team proposed a creative alternative design and construction approach through Alternative Technical Concept for the project.

ALTERNATE DESIGN:

As part of Alternative Technical Concepts for the project, our team shifted the alignment of East Brighton Avenue to the east, realigned the proposed roadway crossings under East Brighton Avenue, and designed two single span bridges supported by integrals abutments instead of one two-span bridge. These changes eliminated the need for staged construction on the existing East Brighton Avenue alignment, reduced impacts to traffic on East Brighton Avenue, eliminated the need for temporary waterline relocations during construction, and simplified construction. In addition, splitting the originally proposed bridge into two structures (Bridge 7S; 133 ft. long and Bridge 7N; 106 ft. long) helped reduce the overall bridge area, therefore reducing construction and future maintenance costs. See Fig. 4A for the alternate bridge design plan. This paper discusses the design and construction challenges related to Bridge 7S.

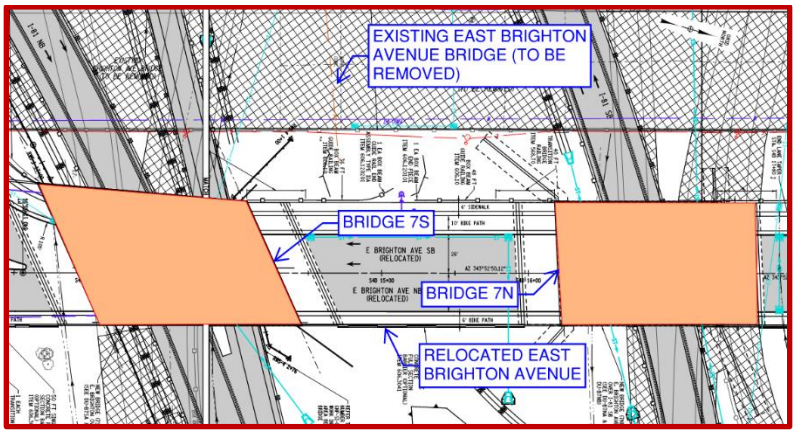


Fig. 4A. Alternate Bridge Design

The maximum height of proposed Bridge 7S was initially 42 ft. measured from the top of bridge deck to the roadway below. A tall integral abutment would require a very wide section to sufficiently withstand the passive pressure from the backfill behind the abutment. Placement of heavy volume of concrete to a height of more than 40 ft. could lead to potential construction and quality control challenges. Also, abutments taller than 15 ft. would require creating a finite element model that includes all the bridge

 © Deep Foundations Institute 2025

components including soil springs to evaluate soil-structure interactions. To mitigate these geotechnical and structural challenges related to a skewed bridge with tall integral abutments, an alternate and innovative foundation design approach was developed. To reduce the abutment height to be within the allowable NYSDOT standard design limits and simplify the design process, retaining walls were introduced in front of the abutments, similar to the preliminary design. See Fig. 4B and 4C for plan and elevation of Bridge 7S.

Due to the limited space between the abutments and the adjacent roadway with active traffic, the solution required construction of retaining walls with minimum footprint. Accordingly, the proposed retained walls were designed as anchored soldier pile and concrete lagging walls.

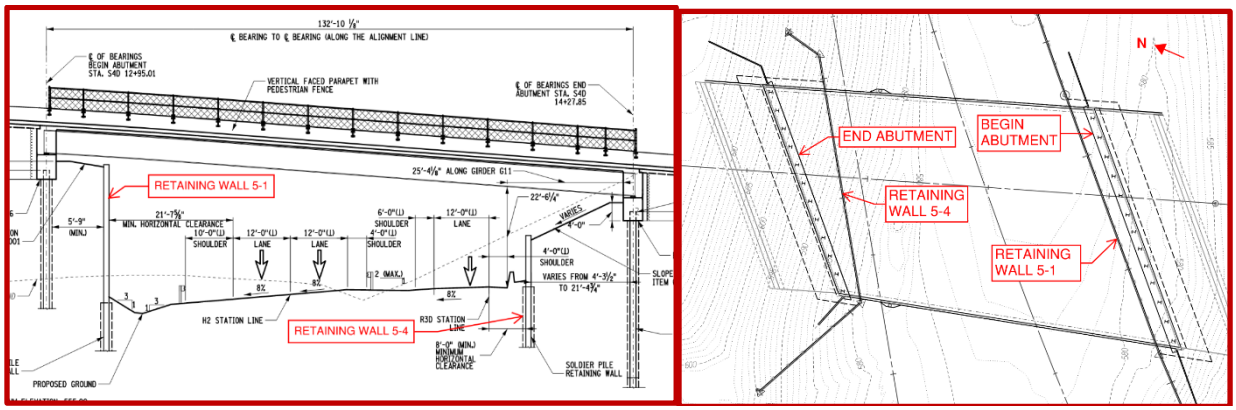


Fig. 4B and 4C. Bridge 7S Abutment and Soldier Pile Wall Plan and Elevation

This alternate design has its own design and construction challenges. Due to the close proximity between the abutments and the retaining walls (See Fig. 4C), additional loading on the retaining walls due to the thermal movements of the abutment was analyzed.

Initial design of the bridge piles consisted of HP 14x117 with a spacing of 3 ft. o/c. As part of this alternate design effort, the bridge piles were redesigned with larger size piles (HP16X162) and with increased spacing of 8 ft. o/c to accommodate the tieback anchors in between the bridge abutment piles. See Fig. 7 and 8 for the tieback arrangement between the bridge piles. With the wingwalls wrapping around the abutment, the anchors crisscross at some locations. This required the development of a detailed 3D layout for the bridge piles, retaining wall soldier piles, and crisscrossing tieback anchors to avoid conflicts during construction. As part of this design alternate, detailed installation and construction procedures were also developed.

Figure 5 shows construction in progress. The construction of the retaining walls in front of the abutment is near completion. Due to the variation in retained soil height, the tieback anchor locations were carefully selected to provide a uniform pattern to the extent possible.

 © Deep Foundations Institute 2025



Fig. 5. Bridge construction in progress

SOLDIER PILE RETAINING WALL:

The soldier pile retaining wall height varied from 1 ft to 42 ft along the wall. The design varied from cantilever soldier pile wall at the wall sections with less retained soil height to the anchored soldier pile wall at the higher retained soil height sections, with up to four (4) levels of anchors at the maximum height. Two types of anchors were utilized for the retaining wall RW5-1. Grouted tiebacks were used in the excavation area and Deadman anchors were utilized in the embankment area.

The grouted anchors varied considerably in length due to the variations in the rock profile and presence of voids at localized areas. A detailed anchor testing program was implemented including performance testing and proof testing to verify the anchor capacity and adjust the bonded length of the anchor. The total length of the grouted anchors varied from 22 ft. to 100 ft. with a bond length of up to 60 ft. The maximum installed capacity of the anchor rods is up to 210 kips. All the components of the grouted anchors were verified for all pertinent limit states to account for the maximum loading conditions. Additional construction measures were implemented including the use of grout socks at void locations to ensure proper grouting within the bonding zone.

DEADMAN ANCHORS

All the anchors for retaining wall RW5-4 were designed as Deadman anchors. Due to the presence of shallow bedrock, anticipated difficult driving conditions, and to minimize excessive vibration and impact to the existing bridge, all the soldier piles were designed to be installed in augured holes.

The Deadman system derives its resistance through the passive pressure acting on the Deadman element positioned behind the wall. The Deadman anchor system on this project consisted of a steel sheet pile (SCZ12) installed behind the wall and connected to the soldier pile with a steel tie. The steel ties were encapsulated along their entire length with concrete for corrosion protection. Corrosion protection with concrete encapsulation was also provided at the anchor heads. The distance between the sheet pile and the soldier pile was determined based on the NAVFAC DM 7.2 (US Department of the Navy 1984).

 © Deep Foundations Institute 2025

The length of the Deadman anchor rod varied from 20 ft to 55 ft. Bracing of soldier piles with wales was avoided to improve the aesthetic appearance of the retaining wall. The Deadman anchors and grouted tieback anchors were installed at each soldier pile location by creating an opening in the soldier pile. See Fig. 6 for a typical section of the Deadman system. Additional design checks were performed for the soldier pile with reduced section at the anchor locations to verify flexural strength. Steel stiffener plates were used to improve the strength based on the maximum anchor loading.

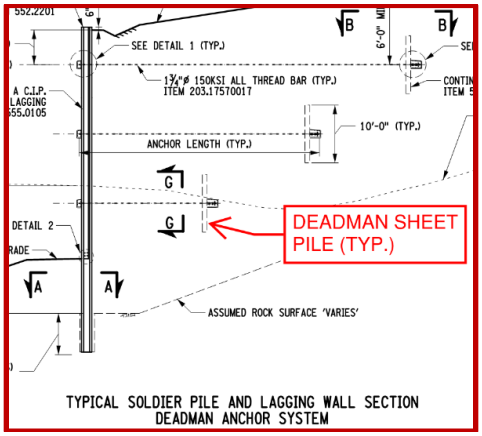


Fig. 6. Deadman Anchor System

SITE CONSTRAINTS

The proximity of the soldier pile walls to the bridge abutment piles posed design and construction challenges. Additionally, the tieback anchors, spaced at 8' c/c, were required to be accommodated between the bridge abutment piles, which further complicated the design and construction. The abutment piles were carefully placed in between the tieback anchors to avoid the conflict using a 3D CAD model. To provide sufficient room for the installation of tieback anchors between the bridge piles, the design of the bridge piles was revised using large size H-Piles (HP16x162) with increased pile spacing. The alignment of anchors and the 24-degree skew angle of the bridge was also considered in developing the layout of the foundation system. Deadman anchor rods between the bridge piles can be seen in Fig. 7.



Fig. 7. Deadman Anchors between the Bridge Piles

 © Deep Foundations Institute 2025

The alignment of soldier pile wall RW5-4 wraps around the north bridge abutment, resulting in crisscrossing of the anchors and conflicts at many of the Deadman sheet pile locations. The 3D CAD model was utilized to identify the area of conflicts. To resolve the issue, the design was modified by locating some anchors further back to resolve the conflict and developed construction staging. See Fig. 8 for the crisscrossing anchors.

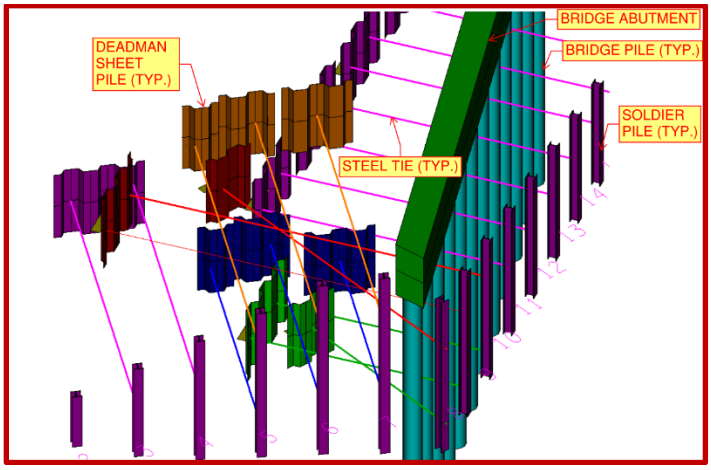


Fig. 8. Criss crossing of Deadman Anchors at Retaining Wall 5-4

Effect of Integral Abutment and Pile Movement

Because of the rigid connection between the bridge girders and abutments in an integral abutment bridge, the abutment and its supporting piles move together as the girders expand and contract with temperature changes. According to NYSDOT design guidelines, this movement must be accounted for in the retaining wall analysis—unless the abutment is located at least 15 feet away from the wall. In this case, since the soldier pile wall is within 15 feet of the abutment, the additional lateral forces caused by the movement of the abutment and piles were included in the analysis of the soldier piles that fall within the zone of influence. Figure 9 shows a typical section highlighting the proximity of the soldier pile wall to the bridge piles. The distance between the bridge piles and the retaining wall piles ranges from approximately 4 feet to 21 feet.

Following NYSDOT LRFD Bridge Design Specifications, a temperature range of -30°F to 120°F was applied to the girders to estimate the resulting abutment movement. The depth of influence for the abutment piles was defined as the point where lateral displacement becomes negligible. Lateral loads were calculated by considering the passive soil pressure between the abutment structure/piles and the soldier pile wall. Based on the minimum spacing between the abutment and the soldier piles, the design lateral load was prorated in accordance with NYSDOT Bridge Manual guidelines, with the assumption that no influence occurs when the separation is 15 feet or more.

 © Deep Foundations Institute 2025

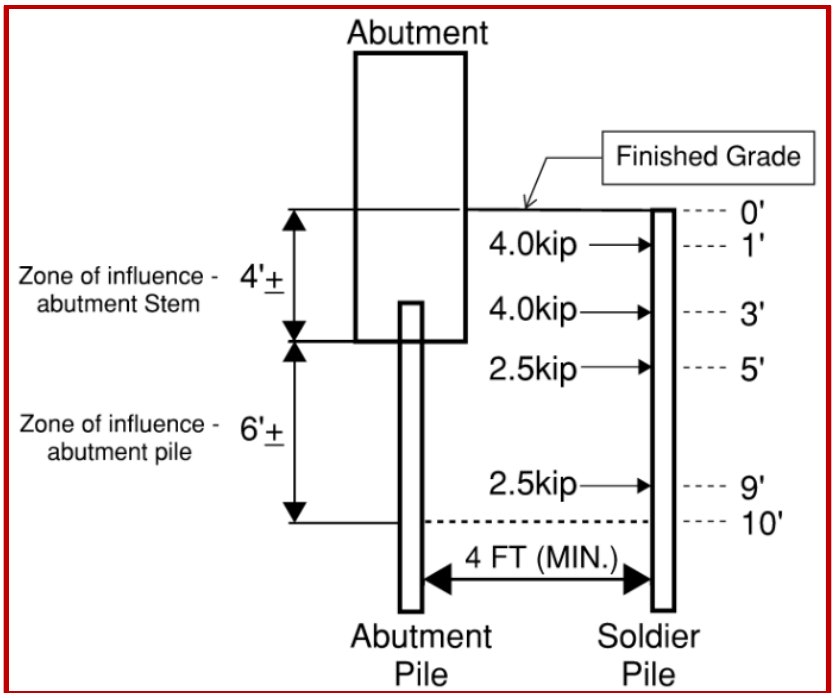


Fig. 9. Additional Lateral Load on Soldier Pile

Bridge Pile Installation

The proposed bridge site is within an area with possible karst formations at some of the localized locations. Borings taken at the bridge abutments during the design phase revealed an erratic rock profile and the presence of rock voids. See Fig. 10A for subsurface profile indicating dense soil layers underlain by shale rock at a depth of approximately 30 ft. below bottom elevation of the pile abutment stem. A geophysical survey (see Fig. 10B) was also conducted to further assess the extent of these formations. The geophysical rock profile indicated no major voids below the tip elevation of the piles. The piles were designed with the tip elevation below the weathered shale rock layer to ensure that the piles have required bearing resistance.

To avoid hard pile driving within the hard rock layers and to minimize any impact to the existing bridge structure due to excessive vibrations, all the piles were installed within augured holes. PDA tests were performed to verify the capacity of the installed piles and to ensure proper seating of the piles on a sound rock within the augured holes. To engage pile shafts to the sidewall of augered holes, upper portion of augered holes was backfilled with loose sand up to the depth of fixity to accommodate the superstructure thermal movements underlain by stone backfill at the lower portion.

 © Deep Foundations Institute 2025

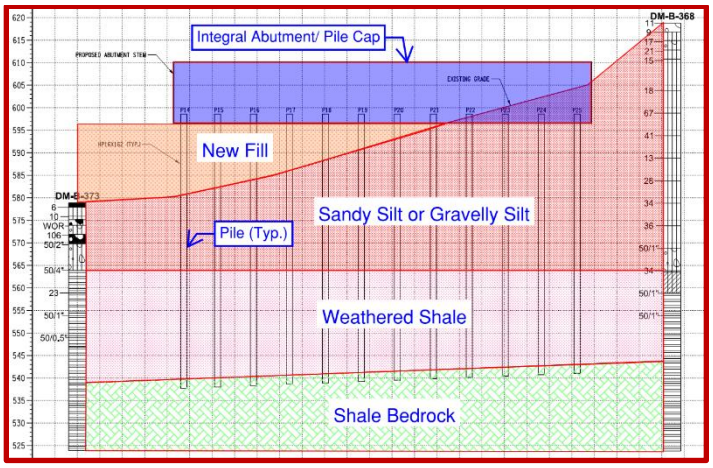


Fig. 10A. Typical Subsurface Soil/Rock Profile (End Abutment)

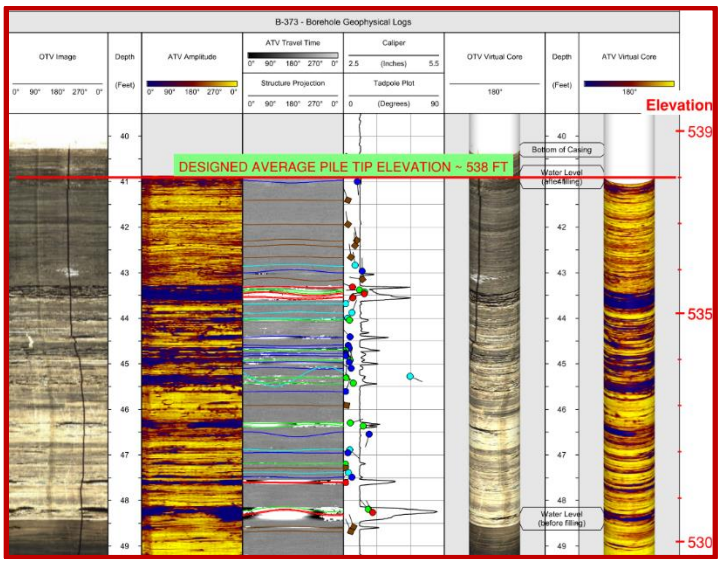


Fig. 10B. Geophysical Survey Rock Profile

Based on the field-testing data, the pile lengths were adjusted during construction to account for the localized weak spots. Due to variation in rock profile, some of the piles extended almost 14 ft deeper than the adjacent piles. Some piles deviated from their designed plan location by as much as 11 inches due to possible presence of localized hard rock formation. The piles with excessive deviations were pulled out and reinstalled at the intended location within allowable limits.

One of the extracted piles indicated pile tip damage due to possible excessive driving in the processes of meeting the required pile tip elevation. See Fig. 11 for the damaged pile. Even with augured hole installation option, pile installation was a challenge due to the erratic existing subsurface rock profile.

 © Deep Foundations Institute 2025



Fig. 11. Bent Bridge Pile

CONCLUSION

Integral abutment bridges are the preferred choice for many of the State DOT agencies due to lower construction cost and less maintenance issues over the life span of the bridge. Construction of long-span bridges is becoming feasible with the availability of higher strength materials.

Integral abutment design is more complex compared to traditional bridge design and requires detailed analysis of soil-structure interaction and thermal forces. However, subject to feasibility of construction, the long-term benefits outweigh the complexities of design. This paper describes the innovative construction and design methodologies utilized for the new bridge on realigned East Brighton Avenue over New I-81 in Syracuse, NY, and demonstrates how design modifications can be made to resolve complex geotechnical and structural analysis requirements for a tall integral abutment. Based on the site constraints and construction feasibility issues, a soldier pile retaining wall with multi-level tieback support was incorporated into the design. This solution required bridge pile foundation and layout modifications to accommodate all elements of the proposed retaining wall within the available footprint area. In addition, careful planning and development of detailed construction procedures eased the complexities of construction and ensured smooth quality construction adjacent to an existing bridge with live traffic.

REFERENCES

Hassiotis, S., Khodair, Y., Roman, E., & Dehne, Y. 2006. *Evaluation of integral abutments* (No. FHWA-NJ-2005-025).

New York State Department of Transportation 2025. *Bridge Manual*

US Department of the Navy 1984. *Foundations and Earth Structures (NAVFAC DM7.2).*

 © Deep Foundations Institute 2025

PROBABILISTIC ANALYSIS OF LATERALLY LOADED PILES USING COMMERCIAL FINITE DIFFERENCE SOFTWARE

Adam Hassan, Geo/Structural Services Group, LLC, Nashville, TN, USA, adam.hassan@geossg.com
Ahmed Mahgoub, Geo/Structural Services Group, LLC, Nashville, TN, USA, ahmed.mahgoub@geossg.com
Don Dotson, Geo/Structural Services Group, LLC, Nashville, TN, USA, don.dotson@geossg.com
D.V. Griffiths, Colorado School of Mines, Golden, CO, USA, d.v.griffiths@mines.edu

ABSTRACT

Laterally loaded piles are commonly analyzed using either a finite element continuum or a beam-on-Winkler foundation approach. The beam-on-Winkler foundation approach employs finite difference techniques to analyze pile and soil responses using established p-y curves. This method is widely favored over a continuum approach by many practitioners for its computational efficiency, as it provides similar results for most scenarios. Both approaches generally assume deterministic soil properties and neglect the uncertainty of material properties in many soils. Research has demonstrated that accounting for this uncertainty through probabilistic analysis methods can lead to reliable safety assessments for pile foundations. Despite this, commercial finite difference software, such as L-Pile and AllPile, do not support probabilistic analyses with randomly varying soil properties. This paper introduces a computer application, called AllPile Randomizer, that was developed to account for uncertainties in soil layer corrected SPT numbers and water table elevations by assigning random values commercial software. The application is freely available on GitHub (https://github.com/Geo-Structural-Services-Group-LLC/AllPile-Randomizer) for use by practitioners and researchers. A parametric study was conducted to determine the effect of randomly varying corrected SPT numbers and water table depth on the probability of failure. An example involving the reliability-based calibration of pile deflection limits is also presented in the paper. Analysis results from the parametric study proved that varying the randomness in corrected SPT numbers has a greater influence on the probability of failure than varying the randomness in the water table.

Keywords: laterally loaded piles, probabilistic analysis, finite difference, computer application

INTRODUCTION

The analysis of laterally loaded piles typically involves the use of one of two common numerical approaches to determine the response of piles in a soil media. The first consists of a continuum approach, where both a pile and surrounding soil are explicitly modeled using finite element software packages like PLAXIS and DIANA. Although this method can be highly accurate, it is computationally expensive and time-consuming, which makes it impractical to implement in routine engineering practice. The second approach, the beam-on-Winkler foundation method, does not require explicit modelling of soil media and employs finite difference software, such as LPILE (Wang et al. 2022) and AllPile (2021), to analyze pile and soil responses based on linear or nonlinear springs placed along the length of an elastic beam. The behavior of nonlinear springs in finite difference software is governed by p-y curves that were established through empirical approaches for a variety of soils (Matlock 1970; Reese et al. 1974; Reese and Welch 1975). The beam-on-Winkler foundation method has proven to provide results comparable to continuum approaches for most scenarios (Brown and Shie 1991; Rollins et al. 2005). For both continuum and beam-on-Winkler foundation approaches, deterministic material properties are assumed to be constant for soil media being modelled.

In practice, soil properties exhibit a high degree of uncertainty, which remains a principal reason behind the use of large safety factors in conventional geotechnical design (Lumb 1966; Duncan 2000). Beyond

 © Deep Foundations Institute 2025

general uncertainty, soils exhibit a high degree of spatial variation in strength and stiffness parameters that vary both laterally and with depth. This spatial variation is generally caused by a variation in deposition and environmental factors (Griffiths et al. 2002; Vanmarcke 1977; Phoon and Kulhawy 1999). To capture the spatial variability of soil properties, random field theory has been widely researched and has proven effective for representing soil parameters as spatially correlated random processes. The implementation of random fields in practice remains challenging due to the large number of layers required to discretize a stochastic mesh with sufficient accuracy. In particular, finite difference software programs, including LPILE and AllPile, impose limitations on the maximum number of soil layers that can be defined in a simulation file, which constrains the practical application of random field modeling. Instead, these programs perform deterministic analyses that often rely on conservative assumptions that may lead to economically inefficient or unsafe designs. Researchers such as Haldar and Babu (2008), and Zhang and Ng (2005), applied probabilistic methods to pile foundation analysis to more accurately capture the influence of soil variability and to better assess the associated design risks. Their work demonstrated that incorporating the spatial variability of soil properties results in a more realistic evaluation of pile behavior under both lateral and axial loads compared to traditional deterministic methods. Paiboon (2008) used similar methods for lateral pile analysis which was expanded by Griffiths et al. (2013). By providing a direct measure of reliability, probabilistic approaches enable engineers to move beyond overly conservative assumptions and enable designs to be optimized for both safety and economy.

The objective of this paper is to present a computer application, called AllPile Randomizer, that was developed to introduce a probabilistic approach to the lateral load analysis of piles in AllPile using Monte Carlo simulation. Monte Carlo simulation is a widely used probabilistic method that estimates the probability of failure by repeatedly sampling random variables and evaluating performance criteria based on several simulations. The computer application parses a base AllPile input file as a template (containing pile geometry, loads, material properties, etc.) to create AllPile input files with randomly varying corrected SPT numbers and water table elevations. Due to the limitation on the maximum number of layers in AllPile and the need for a fine stochastic mesh to discretize random fields for soil, a random variable approach was implemented in the application. This still provides an improvement to the existing deterministic functionality of AllPile and provides functionality to conduct probabilistic analyses of laterally loaded piles in soil. Currently, the Python application is limited to input files with one layer of sand, however the functionality will be expanded in future versions to files with more than one layer and for different types of soil. The computer application was applied to 1) conduct a parametric study on a laterally loaded pile embedded in dense sand to observe the influence of varying the layer's corrected SPT numbers and the water table, and 2) calibrate pile head deflection limits utilizing a reliability-based approach to demonstrate the value of probabilistic analysis for laterally loaded piles.

PROBLEM DESCRIPTION

The pile considered in the parametric study consisted of a 50-foot long 1-foot diameter auger-cast concrete pile embedded in a layer of dense sand with a water table elevation that averages five feet below ground. The concrete was assumed to have a 28-day compressive strength, f'_c, of 4,000 psi and an elastic modulus, E, of 3,605 ksi. A lateral load, P, was applied at the pile head at the ground level. For the parametric study, P was kept constant as 19.5 kip based on a deterministic analysis where the pile head deflected one-inch. After conducting parametric study, the pile head deflection limits were calibrated, where different values of P were assigned to the base input file to achieve pile head deflections equal to the deflection limits that were considered.

 © Deep Foundations Institute 2025

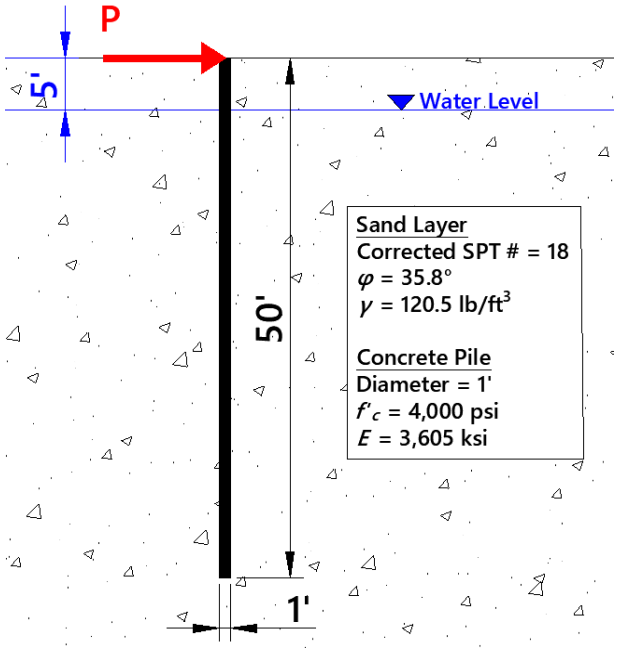


Fig. 1. Schematic of considered pile and surrounding soil

METHODOLGY

The methodology for creating the computer application, conducting the parametric study, and calibrating the deflection limits mainly involved the following tasks:

- Construct AllPile input file using AllPile graphical user interface (GUI) to act as a base input file for random simulations.
- Determine what lines represent in base AllPile input file and how lines can be modified to randomize soil material properties.
- Create Python script to conduct preliminary analysis and determine viability of running Monte Carlo simulation using all6.exe (AllPile solver).
- Code computer application and verify the application modifies input files correctly and all output results are correct.
- Identify common ranges of variation in corrected SPT numbers and water table.
- Conduct parametric study to analyze the sensitivity of varying corrected SPT number and water table on the probability of failure.
- Calibrate deflection limits based on a selected target reliability using random parameters selected from parametric study results and literature.

FUNCTIONALITY OF COMPUTER APPLICATION

Application Description

AllPile Randomizer was developed, using Python, to have a user-friendly graphical user interface (GUI) that enables engineers to easily define input parameters. The GUI and an example of random parameter definition is showcased in Fig. 1. The following steps must be followed to successfully conduct Monte Carlo simulations using the application:

 © Deep Foundations Institute 2025

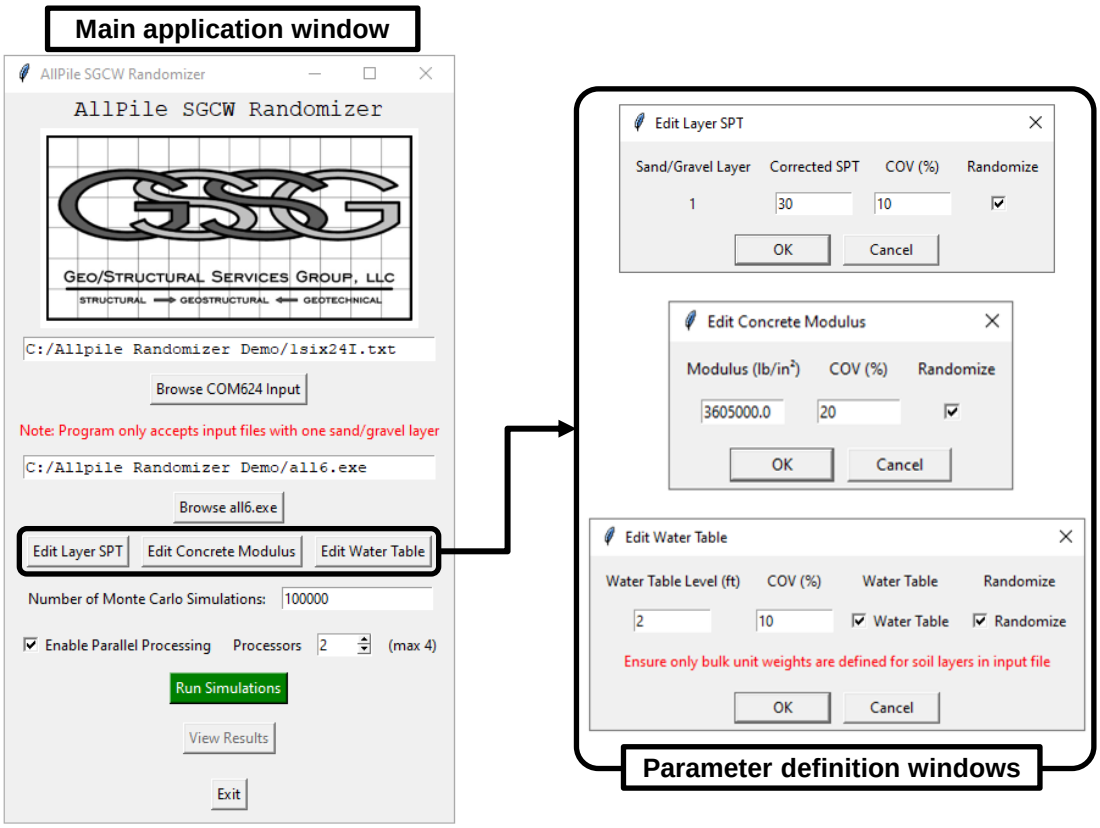


Fig. 2. AllPile Randomizer graphical user interface with random parameter definition

1. **Define COM624 input file and all6.exe paths** – the user must extract the COM624 input file that is created when a lateral analysis is conducted using AllPile. This input file is parsed, copied and modified by AllPile Randomizer to assign random or deterministic numbers to key lines that define properties in the input file. The input file is usually located in the same folder as the AllPile executable and should be named "1six24I.txt". The path to all6.exe is also required to solve the modified input files. The all6.exe file is the main executable, originally based on the well-known COM624 program, that AllPile GUI utilizes to solve for the response of piles subjected to lateral and vertical loads. To run, a licensed copy of the AllPile software must be purchased from Civiltech Software.
2. **Define random or deterministic parameters** – the user must specify randomness in a layer's corrected SPT number, concrete elastic modulus, and/or the water table depth below ground level. Deterministic definitions ignore the default COV values whereas random definitions require the "Randomize" checkbox to be enabled. In AllPile, a layer with a water table must be split into two layers, one with the original bulk unit weight above the water table, and one with the effective unit weight which is the difference between the bulk unit weight and water unit weight (62.4 lb/ft^3). The application first assigns random unit weights and then splits the layer into two layers; one layer with the random unit weight above the water table and the effective unit weight based on the assigned random unit weight below the water table.
3. **Specify number of Monte Carlo simulations and number of processors** – the user must specify the number of desired Monte Carlo simulations and the number of processors in case parallel processing is enabled. The number of Monte Carlo simulations should be strategically selected based on expected probabilities of failure. A low number of Monte Carlo simulations will result in a low confidence interval associated with the computed probabilities of failure.

When parallel processing is enabled, the application performs asynchronous function calls to reduce the computational time required for many Monte Carlo simulations.

4. **Run simulations and compute probability of failure or reliability index** – after defining all parameters Monte Carlo simulations are conducted and the application has a "View Results" button which plots histograms of the generated variables and output results such as pile moment, shear, and head deflection in a separate window. The probability of failure and associated reliability index can be computed directly in the window based on an input deflection limit. Output csv files are also saved in the same folder where the defined COM624 file is stored for further post-processing in Microsoft Excel if desired.

Parametric Study

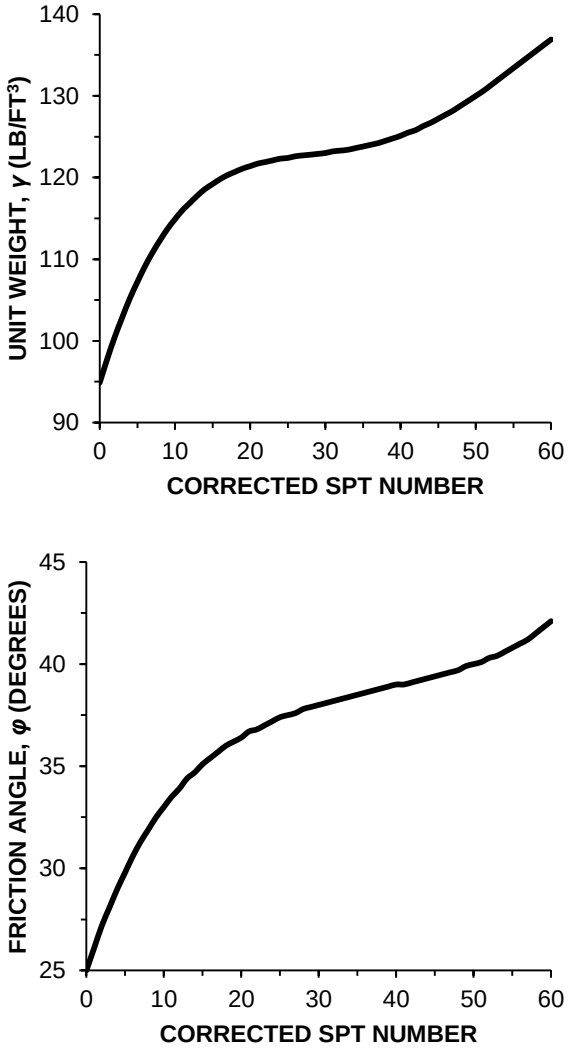


Fig. 3. Mapped unit weights and friction angles vs. corrected SPT numbers

For the lateral response of piles in sand, two main parameters influence the lateral resistance: unit weight and friction angle (Wang and Reese 1993). The AllPile GUI automatically maps corrected SPT numbers to sand unit weights and friction angles. For the range of corrected SPT numbers from 0 to 60, unit weight and friction angles as determined in the AllPile GUI are presented in Fig. 3. The purpose of the

 © Deep Foundations Institute 2025

study was to determine the influence of randomly varying the layer's corrected SPT number and water table on the response of the pile and the probability that the pile does satisfy predefined response limits. For this study, the limit that governed failure was set to be a pile head deflection of more than one-inch. This is a common limit that is set based on serviceability considerations where excessive deflections can compromise structural integrity and aesthetics of supported structures (Higgins et al. 2013; Abouziad and El Naggar 2023).

Random and deterministic parameters

The pile length, concrete elastic modulus, and lateral load were kept deterministic in the parametric study. The corrected SPT number varied and followed a lognormal distribution with a mean of 18 and coefficient of variation (COV) values ranging from 2.5% to 50%. Using the randomly sampled corrected SPT numbers, corresponding friction angles and unit weights were interpolated using cubic spline interpolation based on the relationships presented in Fig. 3 above. The water table was kept constant as 5 feet below ground level when the corrected SPT number was varied. Histograms of generated corrected SPT number samples are presented below in Fig. 4. 10,000 trials were conducted for parametric study for each COV considered.

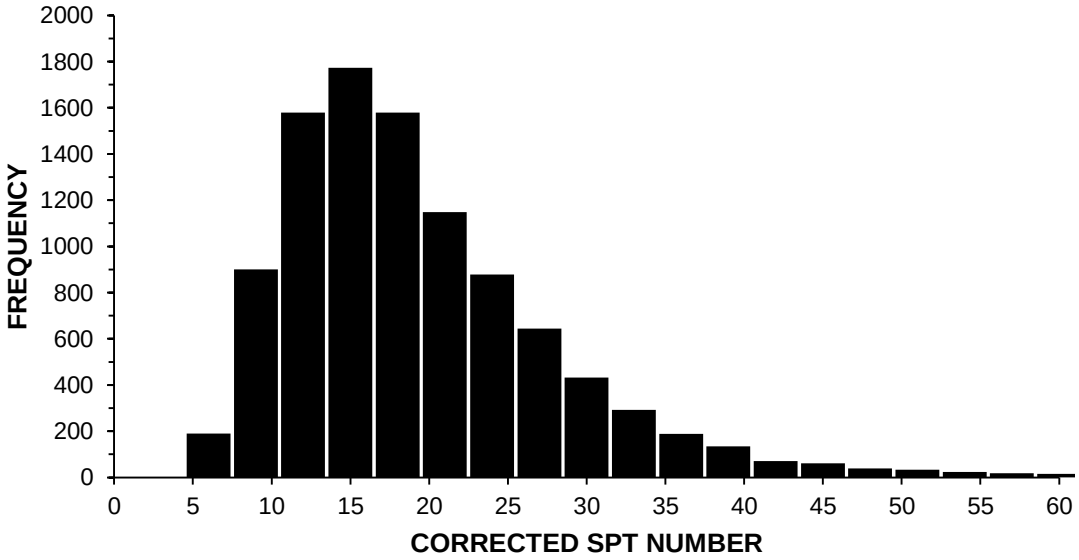


Fig. 4. Histogram of corrected SPT number for COV of 50%

Variance in the water table was introduced by modelling the depth of the water table below ground as a random variable that was lognormally distributed with a mean of 5 feet and COV values ranging from 2.5% to 50%. In simulations where the water table was varied, the corrected SPT number was kept constant as 18. A sample histogram of water table depth below ground is presented in Fig. 5.

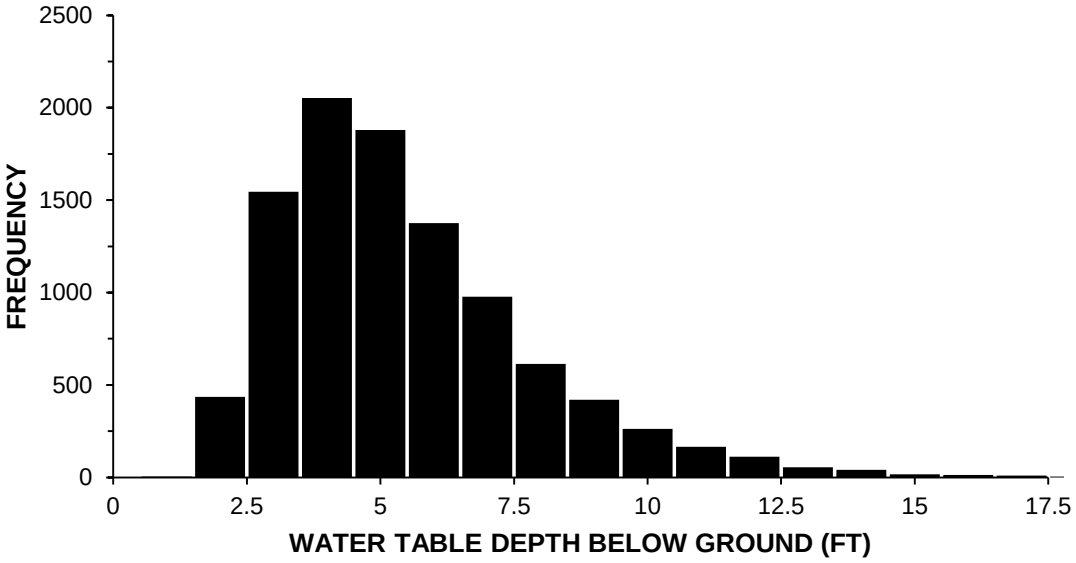


Fig. 5. Histogram of water table depth below ground for COV of 50%

Results

For each specified coefficient of variation of the corrected SPT number and water table depth, the probability of failure was computed using Equation 1, where failure is classified as the pile head deflection exceeding one-inch.

$$P_f = \frac{N_{fail}}{N} \quad [1]$$

Where N_{fail} = number of simulations where pile head deflection exceeded one-inch, and N = total number of trials.

The results presented in Figs. 6 and 7 demonstrate that variability in corrected SPT values has a significantly greater influence on pile performance than variability in water table elevation. As shown in Fig. 7, increasing the COV of the water table depth leads to a gradual and relatively linear increase in the probability of failure, where the probability rises from approximately 0.45 at a COV of 2.5% to about 0.59 at a COV of 50%. In contrast, Fig. 6 shows that the probability of failure is initially highly sensitive to increases in corrected SPT COV values but begins to plateau as COV values exceed approximately 30%. At low COV values for the corrected SPT number, the probability of failure sharply increases from 0.07 at a COV of 2.5% to approximately 0.37 at a COV of 10%. The probability of failure is very close to zero at a COV of 2.5%, and a probability of zero is expected when the COV is exactly zero (i.e., a deterministic analysis). In the deterministic case, the pile tip deflection is exactly equal to one-inch which matches the deflection limit used in the parametric study. These results highlight that the response of laterally loaded piles in sand is more sensitive to uncertainties in soil strength than to fluctuations in the water table depth.

 © Deep Foundations Institute 2025

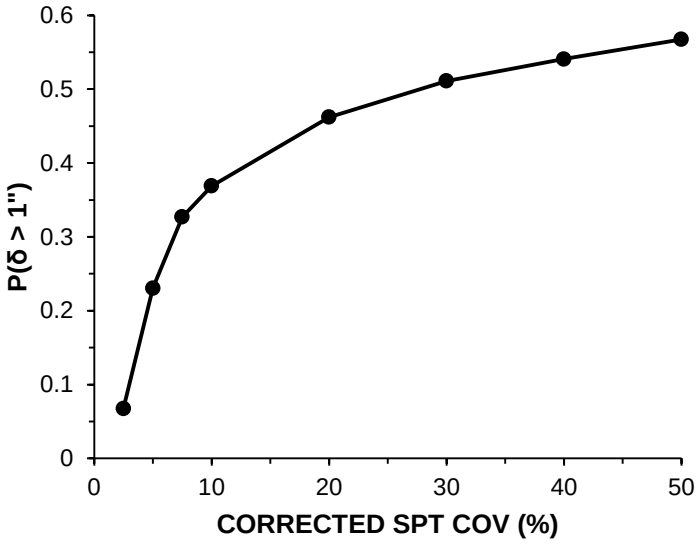


Fig. 6. Probability of pile tip deflection exceeding 1" vs. corrected SPT COV (%)

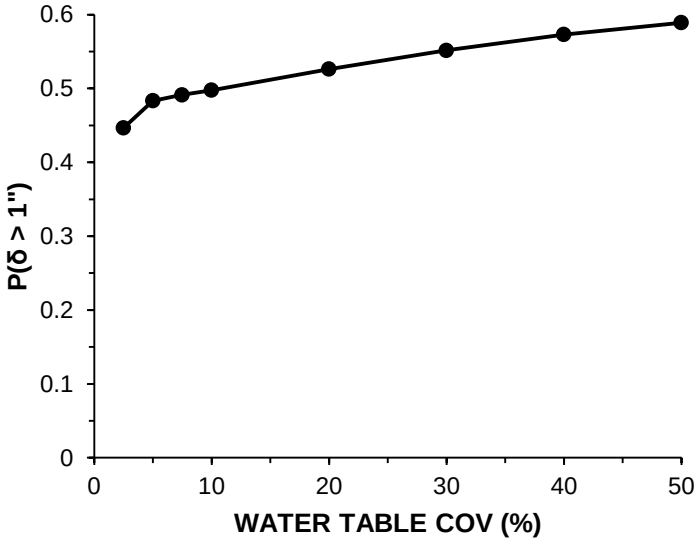


Fig. 7. Probability of pile tip deflection exceeding 1" vs. water table COV (%)

Deflection limit calibration

Based on the results obtained in the parametric study, a practical example involving the reliability-based calibration of allowable pile tip deflection was conducted. This can be applicable in a real-world scenario wherein probabilistic limits that meet acceptable levels of safety are required. Using the same pile previously presented, the mean and COV corrected SPT number for the sand layer and the mean and COV for the water table depth below ground were set as 18, 40%, 5 feet, and 30%, respectively. The selected COV values were selected based on the values where the probability of failure generally plateaued for the corrected SPT number COV and water table depth COV. The values are also consistent with variability observed in experimental field data (Zhang et al. 2004; Briaud and Tucker 1984). The range of allowable deflections considered was 0.4 inches to 0.8 inches with increments of 0.1 inches. The considered deflections represent a range of geotechnical safety factors ranging from 1.25 to 2.5 based on

 © Deep Foundations Institute 2025

an ultimate deflection of one-inch. For each deflection limit, a COM624 input file was created by varying the applied load at the pile head to achieve the desired deflection. The deflections and corresponding applied loads are presented in Table 1.

Table 1. Deflection limits with corresponding applied loads at pile head

Deflection (in)	Applied load at pile head, *P* (kip)
0.4	10.6
0.5	12.3
0.6	13.9
0.7	15.4
0.8	16.8

Using the generated COM624 input files, AllPile Randomizer was used to conduct Monte Carlo simulation with 100,000 trials for each deflection limit. The corresponding reliability index, β, was computed as the negative value of the inverse of a standardized normal cumulative distribution function with a probability equal to the probability of failure, as presented in Equation 2. Similar to the parametric study, the probability of failure was defined as the probability that the head deflection exceeded the ultimate limit of one-inch.

$$\beta = -\Phi^{-1}(P_f) \quad [2]$$

Where $\Phi^{-1}(x)$ = inverse standard normal cumulative distribution function.

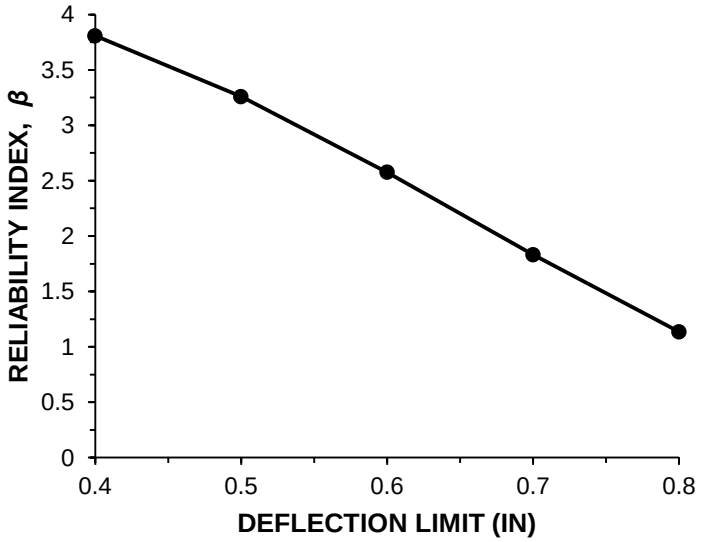


Fig. 8. Generated reliability index vs. deflection limit chart

A chart showing the reliability indices corresponding to the considered deflection limits is presented in Fig. 4. As the deflection limit is increased from 0.4 inches to 0.8 inches, the reliability index linearly decreases from 3.8 to 1.1. The chart can be a valuable tool for practicing engineers to determine allowable deflection limits for pile design, especially for high-importance projects that require optimization (i.e., hospitals, post-disaster facilities, etc.). A target reliability can be determined using risk

 © Deep Foundations Institute 2025

assessment methods that determine acceptable levels of safety or probabilities of failure based on the consequences of failure and associated costs or liabilities (Fenton and Griffiths 2008). For simplicity, the acceptable probability of failure is assumed to be 1/10,000, which corresponds to a target reliability index of 3.7. Based on the target reliability, a deflection of 0.42 inches was obtained. This limit is specific to the pile being considered and may be a generic limit that can be applied to a pile with different material properties or embedded in other types of soil. Further studies should be conducted to calibrate deflection limits for piles in different types of soil with more than one layer to investigate if a generic deflection limit can be proposed.

SUMMARY AND CONCLUSION

A computer application, called AllPile Randomizer, was developed to randomize soil properties in AllPile input files and to conduct Monte Carlo simulations using AllPile. Due to limitations on the maximum number of layers that can be defined in AllPile, and the resulting inability to discretize an adequate stochastic mesh for random field modeling, a random variable approach was adopted. To better capture the spatial variability of soil properties in future analyses, it is recommended that commercial finite difference software for laterally loaded piles allow for a greater number of layers to be specified.

The application was used in a parametric study to investigate the effects of varying corrected SPT number and water table elevation. It was observed that variability in the corrected SPT number had a greater influence on the probability of exceeding a deflection limit of one-inch compared to variability in the water table elevation. Based on the results of the parametric study, an example involving the calibration of a deflection limit was carried out to present the practical utility of the computer application and the need for functionality to conduct probabilistic analysis for laterally loaded piles. The parametric study and example confirmed that probabilistic approaches allow for a more detailed evaluation of how soil variability affects pile performance and how more optimized designs can be achieved when probabilistic approaches are incorporated.

REFERENCES

Abouziad, A., and El Naggar, M.H., 2023. Experimental and numerical analysis of laterally loaded single- and double-paddled h-piles in clay. Geotechnics, 3(4), pp. 1324-1345.

AllPile Version 7, 2021. User's manual volume 1 and 2. CivilTech Software, USA.

Briaud, J.L., and Tucker, L., 1984. Coefficient of variation of in situ tests in sand. Proc. Probabilistic Characterization of Soil Properties: Bridge Between Theory and Practice, Atlanta, GA, pp. 119-139.

Brown, D.A., and Shie, C.-F., 1991. Some numerical experiments with a three dimensional finite element model of a laterally loaded pile. Computers and Geotechnics, 12(2), pp. 149-162.

Duncan, J.M., 2000. Factors of safety and reliability in geotechnical engineering. American Society of Civil Engineers, ASCE Journal of Geotechnical and Geoenvironmental Engineering, 126(4), pp. 307-316.

Fenton, G.A., and Griffiths, D.V., 2008. Risk assessment in geotechnical engineering. John Wiley & Sons, Inc., pp. 239-262.

Griffiths, D.V., Fenton, G.A., and Lemons, C.B., 2002. Probabilistic analysis of underground pillar stability. International Journal for Numerical and Analytical Methods in Geomechanics, 26(8), pp. 775-791.

 © Deep Foundations Institute 2025

Griffiths, D.V., J. Paiboon, J. Huang, and G.A. Fenton. 2013. Reliability analysis of beams on random elastic foundations. Géotechnique, 63(2), pp. 180-188.

Haldar, S., and Babu, G.L.S., 2008. Reliability measures for pile foundations based on cone penetration test data. Canadian Geotechnical Journal, 45(12), pp. 1699-1714.

Higgins, W., Vasquez, C., Basu, D., and Griffiths, D.V., 2013. Elastic solutions for laterally loaded piles. ASCE Journal of Geotechnical and Geoenvironmental Engineering, 139(7), pp. 1096-1103.

Lumb, P., 1966. The variability of natural soils. Canadian Geotechnical Journal, 3(2), pp. 74-97.

Matlock, H., 1970. Correlations for design of laterally loaded piles in soft clay. Proc. 2nd Offshore Technol. Conf., Houston, TX 1, pp. 577–594.

Paiboon, J. 2008. Probabilistic analysis of laterally loaded piles. Master's Thesis. Division of Engineering. Colorado School of Mines.

Phoon, K.-K. and Kulhawy, F.H., 1999. Characterization of geotechnical variability. Canadian Geotechnical Journal, 36(4), pp. 612-624.

Reese, L.C., Cox, W.R., and Koop, F.D., 1974. Analysis of laterally loaded piles in sand. Proc. 6th Offshore Technol. Conf., Houston, TX 2, pp. 473–483.

Reese, L.C., and Welch, R.C., 1975. Lateral loading of deep foundations in stiff clay. American Society of Civil Engineers, ASCE Journal of the Geotechnical Engineering Division, 101(7), pp. 633-649.

Rollins, K.M., et al., 2005. Lateral resistance of a full-scale pile group in liquefied sand. American Society of Civil Engineers, ASCE Journal of Geotechnical and Geoenvironmental Engineering, 131(1), pp. 115-125.

Vanmarcke, E.H., 1977. Probabilistic modeling of soil profiles. American Society of Civil Engineers, ASCE Journal of Geotechnical Engineering Division, 103(11), pp. 1227-1246.

Wang, S.-T., and Reese, L. C., 1993. COM624P – Laterally loaded pile analysis program for microcomputer, version 2.0, Report No. FHWA-SA-91-048.

Wang, S.-T., et al., 2022. LPILE v2022 user's manual. Ensoft Inc., Austin, TX, USA.

Zhang, L., and Ng, C.W.W., 2005. Probabilistic analysis of lateral pile response using response surface methodology. Canadian Geotechnical Journal, 45(12), pp. 1735-1746.

 © Deep Foundations Institute 2025

CONSTRUCTION CHALLENGES OF THE PORT EVERGLADES BYPASS ROAD ON HIGHLY COMPRESSIBLE SOILS IN BROWARD COUNTY, FLORIDA

Gustavo J. Hernandez, P.E., Langan, Miami, Florida, 305-302-7934, ghernandez@langan.com
Rafael M. Pina, P.E., BC.GE, Langan, Miami, Florida, rpina@langan.com
Matthew Meyer, P.E., BC.GE, Langan, Miami, Florida, mmeyer@langan.com

ABSTRACT

This paper will present the design and construction challenges of the Port Everglades Bypass Road project located in Fort Lauderdale, Florida. The project has been designed to relieve vehicle traffic at the intersection of US-1 (SR 5) and SE 17th Street, and along SE 17th Street, and includes an approximately 1,317-feet-long highway bridge crossing several existing and proposed surface roadways.

The project alignment is in an industrial area with multiple fuel, petroleum and chemical storage tanks and support facilities. There are multiple underground utilities along the alignment, including petroleum, fuel and gas pipelines, water and sewer lines, electric and fiber optic communication lines, and stormwater drainage lines.

The bridge consists of an elevated roadway on pre-stressed concrete Florida I-Beams supported by 12 individual piers and 2 end-bents. Highly compressible organic silt and peat are present along the bridge alignment, including at the approach embankments at both ends of the bridge. Because of the numerous existing underground utilities and fuel lines at the approach embankment locations and because subsurface materials in the area potentially impacted by petroleum, removal/replacement or in-situ improvement of the organic silt and peat to construct the approach embankments using conventional earth fills and retaining walls bearing at grade was neither practical nor cost effective. Supporting the bridge required the implementation of a deep foundation system that would limit construction vibrations that would potentially impact the multiple underground utilities and petroleum pipelines in the area.

This paper/presentation will discuss in detail the analysis and design of the Auger Cast Pile (ACP) system selected for support of the bridge, which, because of the site's unique subsurface conditions, necessitated developing a project-specific correlation between SPT N_{60} data and ultimate design side-shear resistance, similar to the industry-accepted correlations by the Florida Department of Transportation (FDOT). The developed design side-shear values were validated via an extensive load test program, including multiple embedded bi-directional load tests and proof testing performed via High Strain Dynamic Testing at each bridge pier. The paper/presentation will also discuss anomalies and atypical conditions documented by non-destructive test techniques and how these were assessed and remediated during construction.

Keywords: Florida Department of Transportation (FDOT), Standard Penetration Test (SPT), Auger Cast Pile (ACP), Soils and Foundation Handbook (SFH), Thermal Integrity Profiling (TIP)

PROJECT BACKGROUND

The Port Everglades Bypass Road project is located in Fort Lauderdale, Florida. The project has been designed to relieve vehicle traffic at the intersection of US-1 (SR 5) and SE 17th Street, and along SE 17th Street by allowing vehicles to access the new A1A Bypass Road. The project connects Eisenhower Boulevard south of SE 17th Street to Spangler Boulevard (SR 84) via new surface roads and an elevated roadway bridge. The bridge component of the project consists of an approximately 1,317-feet-long, approximately 39-feet-wide elevated two-lane roadway bridge structure in the east-west direction of SR84 and crosses several existing and proposed roadways. The project site location is shown in Fig. 1 below.

 © Deep Foundations Institute 2025



Site grades along the project alignment are between about elevation el +5 and el +6 feet, North American Vertical Datum of 1988 (NAVD88).

Based upon the review of historic aerial photographs (1950's and 1960's), the areas surrounding and in proximity to the roadway and bridge alignment were undergoing land reclamation. Due to the resolution as well as the available information, it is difficult to confirm if the roadway and bridge alignment were reclaimed; however, there are numerous low-lying tidal areas, waterways, and documented land reclamation in proximity to the roadway and bridge alignment.

GEOTECHNICAL INVESTIGATION AND SUBSURFACE CONDTIONS

The design phase geotechnical investigation for the bridge component portion of the project included twenty-one (21) Standard Penetration Test (SPT) borings and rock core borings to depths between 73 feet to 130 feet. Laboratory tests were performed on selected soil samples recovered from the field investigation and included: grain-size analysis, natural moisture content, organic content, and corrosion tests (i.e., pH, chloride content, sulfate content and resistivity). Unconfined compression tests and split tensile tests were performed on selected rock core samples.

Based on the subsurface conditions encountered in the SPT borings drilled along the bridge alignment, the subsurface conditions were summarized into five separate strata as shown in Table 1 below.

Groundwater levels encountered at each boring location at the time of drilling were between 4 and 5 feet below ground surface, corresponding to groundwater levels between about el -0.5 ft and el +2.2 ft. In the coastal areas of Broward County, groundwater levels are influenced by tidal fluctuations and seasonal rainfall variation.

Table 1. Summary of Subsurface Strata

Strata No.	Description	Average Top of Stratum Elevation (ft, NAVD)
1	Fill (sand and limerock gravel)	5.2
2	Muck (Organic silt and peat)	-2.1
3	Limestone (Oolitic limestone of the Miami Formation)	-8.6
4	Sand/Silty Sand (with occasional limestone fragments of the Fort Thompson Formation)	-17.6
5	Limestone with sand (Fort Thompson Formation)	-44.3

 © Deep Foundations Institute 2025

Table 2 below provides the geotechnical parameters that were used in the geotechnical analysis of the piles and bridge foundations.

Table 2. Geotechnical Parameters used in the Geotechnical Analysis

Strata No.	Soil Type	SPT N_{60} (bpf)	Total Unit Weight (pcf)	Undrained Shear Strength (psf)	Young's Modulus of Elasticity (ksf)
1	Cohesionless	25	125	N/A	500
2	Organic	0	100	250	60
3	Cohesionless (Limestone N_{60} < 25 bpf)	17	120	N/A	510
4	Cohesionless	9	110	N/A	180
5	Limestone	25	125	12,400	750

ENGINEERING EVALUATIONS

The relatively low shear strength and high compressibility of the upper four strata shown in Table 2 above, required deep foundations as support of the bridge. In addition, because of the difficulties of removing/replacing or performing in-situ improvement of the compressible organic materials to construct the approach embankments using conventional earth fills and retaining walls bearing at grade, the project team decided to support the approach embankments and retaining walls on a reliving platform (i.e., approach slab) also supported on deep foundations.

Auger Cast Piles (ACP), also known augered cast-in-place (ACIP) piles or continuous flight auger (CFA) piles are the most commonly used deep foundation system in South Florida for supporting buildings. Their use in transportation structures has been limited until recently. ACP were successfully used in the late 1980's and early 1990's for supporting sections of the Metrorail and Metromover guideways in Miami-Dade County. ACP are currently being used to support several of the bridges associated with the I-395/SR-836 reconstruction, including the large cable-stayed bridge over Biscayne Boulevard (US-1/SR 5). At prior Port Developments within the overall Port Everglades Complex, auger cast piles have been utilized extensively. Like drilled shafts, ACP can attain relatively high side-shear resistances against the sedimentary rocks present throughout the area; however, because their installation does not require the use of drilling fluids, they have the potential for developing even higher unit side-shear resistances. Additional ACP advantages are their rapid rate of installation, negligible vibration levels, and relatively low noise levels (desirable for urban foundation installation applications). Recent improvement in drilling equipment have led to ACP diameters of up to 36 inches and ability to install them to depths of up to 175 feet. Other ACP technology improvements include the use of automated monitoring equipment (AME) during installation and thermal integrity profile (TIP) testing for improved quality control.

The borings performed revealed the presence of highly organic silt and peat (Stratum 2 / Muck) that could result in relatively large consolidation settlement, and thereby downdrag forces on deep foundations, if subjected to loads associated with placing fills for raising or adjusting site grades. The project included construction of new surface roadways or reconstruction of existing roadways that needed placement of fill directly adjacent to the bridge piers and potentially resulting in compression of the upper Stratum 1 and Stratum 2 and create negative skin friction (downdrag) along the pile shafts.

The Stratum 3 of Oolitic Limestone for the Miami Formation and Strata 4 and 5 materials of the Fort Thompson Formation can be relied upon for support of the ACP foundation elements. These materials have been utilized as the bearing stratum for buildings and bridge structures supported on deep foundations in Broward and Miami-Dade County.

The design capacity of ACP was evaluated based on side-shear resistance only; end-bearing resistance was neglected because of the relatively large displacements required to mobilize end bearing, in accordance with local practice and FDOT guidelines.

According to the FDOT Soils and Foundation Handbook (SFH), the ultimate side-shear resistance of limestone can be determined by either of the following methods:

- FDOT SFH – Appendix A: McVay's method for "Determination of Design Side-Shear Resistance Test Data to Design Parameters for Drilled Shaft & Auger Cast Piles Socketed in Florida Limestone". The ultimate side-shear resistance for the portion of the drilled shaft or ACP socketed into the limestone is expressed as:

$$f_{su} = \frac{1}{2} * \sqrt{q_u} * \sqrt{q_t} \quad [1]$$

Where q_u = the unconfined compression strength of rock core and q_t = the split tensile strength of rock core.

To consider the spatial variations of the rock qualities, McVay's method applies the average percent recovery expressed as decimal (REC) to the ultimate side shear resistance, f_{su}, and the product is used as the design ultimate side shear resistance:

$$(f_{su})_{DESIGN} = REC * f_{su} \quad [2]$$

To obtain representative q_u, q_t and REC values, a statistical data reduction method based on the above McVay's method was performed to calculate the design side-shear resistance for Stratum 5.

The field geotechnical investigation and laboratory testing data from the borings performed for this project were evaluated using the above method. However, based on the analysis performed, it was determined that the data set resulting from viable cores available for testing resulted in a conservative interpretation of the available ultimate side-shear resistance values for the design of the piles. Considering the Appendix A approach of the FDOT SFH, the results indicated that the design ultimate side shear resistance values in Stratum 5, were between 2.1 tons per square foot (lower bound) and 3.7 tons per square foot (upper bound). The respective lower bound and upper bound design ultimate side shear resistance values were assigned equivalent safety hammer energy SPT N-Values of 22 blows per foot and 50 blows per foot in accordance with the procedures outlined in Appendix A of the FDOT SFH.

- FDOT SFH – Appendix B: When rock cores and laboratory testing is not available, the design ultimate side shear resistance of limestone with SPT N-Values greater or equal to 25 blows per foot (bpf) can be evaluated using SPT N-Value data as follows:

$$f_{su} = 0.1\ N\ (tsf) \leq 5.0\ tsf\ (tons\ per\ square\ foot) \quad [3]$$

Where f_{su} = design ultimate side shear resistance of limestone and N = equivalent safety-hammer energy values adjusted for use of automatic hammer.

Based on the range of corrected SPT N-Values (i.e., 60% equivalent hammer energy) recorded in the borings within the anticipated rock socket zone in Stratum 5, the calculated ultimate side shear resistance for calculating the ACP capacity is between 2.5 tsf and 5.0 tsf. Table 3 below shows the design ultimate side shear resistance of limestone per FDOT SFH – Appendix B for a construction phase boring at Pier 3.

 © Deep Foundations Institute 2025

Table 3. Design Ultimate Side Shear Resistance of Limestone for SPT Boring at Pier 3

Stata No.	Elevation (ft, NAVD)	Depth (ft)	SPT N-Value	Corrected SPT N-Value	Unit Side Shear per FDOT 0.1N (tsf)
	5.7	0			
1 - Fill	4.7	1	92	50	
	2.7	3	40	50	
	0.7	5	57	50	
	-1.3	7	17	21	
2 - Muck	-3.3	9	2	2	
	-6.3	12	3	4	
3 - Limestone	-8.3	14	17	21	
	-11.3	17	18	22	
	-13.3	19	4	5	
	-16.3	22	4	5	
4 - Sand	-18.3	24	2	2	
	-21.3	27	2	2	
	-23.3	29	5	6	
	-26.3	32	6	7	
	-28.3	34	14	17	
	-31.3	37	8	10	
	-33.3	39	13	16	
	-36.3	42	17	21	
	-38.3	44	12	15	
5 - Limestone	-41.3	47	14	17	0.0
	-43.3	49	27	33	3.3
	-46.3	52	49	50	5.0
	-48.3	54	44	50	5.0
	-51.3	57	100	50	5.0
	-53.3	59	31	38	3.8
	-56.3	62	21	26	2.6
	-58.3	64	100	50	5.0
	-61.3	67	63	50	5.0
	-63.3	69	100	50	5.0
	-66.3	72	100	50	5.0
	-68.3	74	34	42	4.2
	-71.3	77	16	20	0.0
	-73.3	79	31	38	3.8
	-76.3	82	49	50	5.0
	-78.3	84	8	10	0.0
	-81.3	87	12	15	0.0
	-83.3	89	32	40	4.0

 © Deep Foundations Institute 2025

The axial capacity was calculated for 18-inch-diameter, 24-inch-diameter and 36-inch-diameter ACP using this method based on the SPT N-Values from the respective boring closest to the location of the respective end bent, pier or approach slab.

The design ultimate side-shear resistance and pile capacity were subject to confirmation by full-scale field load testing; however, it should be noted that bi-directional pile load tests with embedded hydraulic load cells in Stratum 5 materials in the vicinity of the project, have shown that mobilized unit side shear resistance for limestone materials with SPT N-Values of about 20 bpf is on the order of 2.2 tsf, and the mobilized unit side shear resistance for limestone materials with SPT N-Values averaging about 34 bpf is on the order of 6 tsf. This nearby full-scale load testing experience correlated with site specific and nearby boring data substantiates that FDOT's procedures as suggested in their SFH – Appendix B provide a conservative methodology for calculation of ACP's ultimate side shear resistance (for the Fort Thompson Limestone) typical to the Port Everglades area. Comparison of design methodologies that have been utilized at the Port Everglades complex for successful design of ACP's since the late 1990's resulted in the same conclusion and affirmed the use of Appendix B procedure of the SFH as a conservative methodology for establishing the design ultimate side shear resistance for ACP piles at this project.

In calculating the nominal resistance of the ACP's, the subsurface materials of Stratums 3 and 4 were modeled in the FB-Deep computer program presuming the material consists of clean sand having the respective SPT N-Values and available side shear resistance for drilled shafts. This available resistance, which is deemed to be a conservative approach, was added to the nominal resistance obtained from within Stratum 5 to determine the required tip elevations. It should be noted that full-scale load testing of ACP's embedded through Stratums 3, 4, and 5 has shown the above-mentioned approach to be conservative and combining side shear resistances from Stratum 3, 4, and 5 as indicated above is deemed viable and conservative. It should also be noted that Stratum 3 consists of limestone of the Miami Formation and was conservatively modelled as a clean sand material in accordance with FDOT procedures.

Downdrag Load

Downdrag for piles used on this project was calculated in accordance with Appendix C of the FDOT SFH. The calculated downdragload is the negative skin friction along the pile shaft from settlement cause by the new fill below existing grade. The portion of the piles subjected to downdrag was determined to be located from the ground surface to about the top of Stratum 3. The recommended downdrag load values used for the design of the pile foundations for support of the bridge are summarized in Table 4 below.

Table 4. Downdrag Load on Piles

Pile Type	Downdrag Load
18-inch-diameter ACP	15 tons
24-inch-diameter ACP	20 tons
36-inch-diameter ACP	30 tons

ACP RECOMMENDATIONS

Per FDOT, installation of the ACP shall be performed in accordance with FDOT's Developmental Specification Dev455ACP as indicated in Section 3.5.20 of the FDOT Structures Design Guidelines (SDG).

The required nominal bearing resistance for auger cast piles is calculated as follows:

$$Nominal\ Bearing\ Resistance\ \geq \frac{Factored\ Design\ Load + Downdrag\ Load}{phi\ factor}$$

The minimum pile tip elevations were calculated based on:

(1) A design ultimate side shear resistance between 2.5 tsf and 5.0 tsf for limestone in Stratum 5 with SPT N-Values of 25 bpf or higher and a conservative modeling approach for Stratum 3 and Stratum 4 as indicated in the previous section;
(2) The factored design loads provided by the structural engineer per end bent and pier;
(3) Available Load Resistance Factor Design (LRFD) resistance (phi) factors specified in Section 3.5.20 of the FDOT SDG. The available design resistance factors are presented in Table 5 below.

Table 5. Resistance Factors for ACP Bridge Foundations (2025 FDOT SDG Section 3.5.20)

Loading	Quality Control Method	Resistance Factor (phi)
Compression	Static Load Test	0.6
Uplift	Static Load Test	0.5
Lateral	Lateral Load Test	1.0

Twenty-four (24) inch-diameter ACP were selected for support of the bridge end bents and 36-inch-diameter ACP were selected for support of the bridge piers.

Settlement

The settlement of the end bent, and pier foundations supported on pile groups was evaluated using the Federal Highway Administration (FHWA) Soils and Foundations Reference Manual – Volume II (Publication No. FHWA NHI-06-089) recommended methodology, and experience with settlement of structures on deep foundations in South Florida. Evaluation of the available subsurface information together with the loading information provided by the structural engineer indicated that the settlement of the bridge supports founded on pile groups bearing in Stratum 5 was calculated to be on the order of 1 inch or less, with differential settlement between adjacent piers or bents about ¼ inch and ½ inch.

Construction Phase Pilot Borings

Changes in the proposed bridge pier locations following completion of the geotechnical design phase investigation resulted in several of the completed borings offset from the proposed bridge pier, end bent or approach slab locations. For those areas where the completed borings were located 25-feet or more away from the foundation construction phase pilot borings were required at those specific foundation element locations to satisfy the requirements of the FDOT SFH.

LOAD TEST PROGRAM

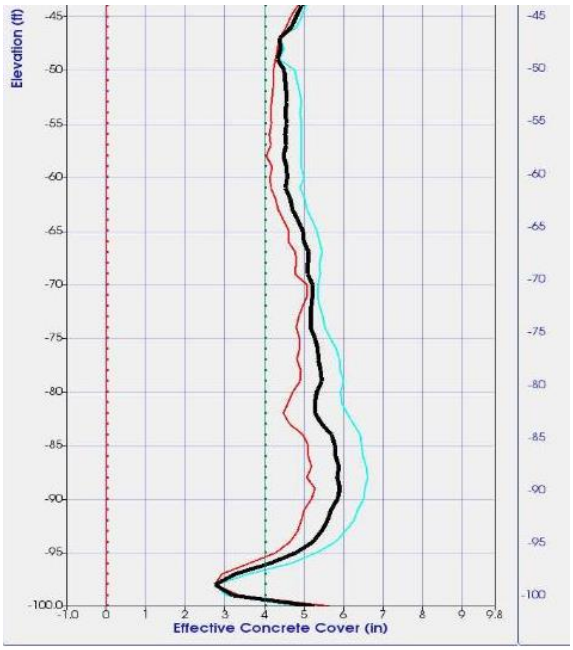
Based on the subsurface conditions present at the site, the pile factored design loads, calculated required nominal bearing resistances and calculated pile tip elevations, three full-scale instrumented bi-directional embedded jack load tests were recommended and performed for the project. Before test pile installation, a supplemental boring was drilled at each test pile location to confirm the subsurface conditions at the specific location and the tip elevation of the test pile was determined based on the specific subsurface

 © Deep Foundations Institute 2025

conditions at the selected test pile location. A demonstration pile or method pile was also installed for each pile diameter prior to the installation of the test piles. All test piles and demonstration piles were instrumented with five thermal integrity wires attached to the reinforcing steel cage and evaluated using embedded thermal sensors per ASTM D 7949 Method B. Thermal Integrity Profiling (TIP) reports were prepared by the specialty consultant retained by the piling contractor.

Test Pile Installation for 36-inch-diameter piles

Demonstration Pile 1 was installed to a tip elevation of el -94 ft with and FDOT approved mix. The TIP report for this demonstration pile showed that the pile did not meet the temperature requirements per Dev455ACP as the core temperature exceeded 160º F for about the full length of the pile. The report also indicated that the calculated pile diameters for all wires at el -90 ft to el -94 ft did not meet the specified design criteria for grout coverage. An alternative FDOT mix was approved, and the contractor installed a trial 20-foot-long 36-inch-diameter demonstration pile (Demonstration Pile 2), which was successful and complied with the temperature requirements per Dev455ACP. The piling contractor installed a third 36-inch-diameter demonstration pile (Demonstration Pile 3) to a tip elevation of el -100 ft (the same tip elevation as the deepest production pile indicated in the contract plans) using the alternative approved grout mix. The TIP report for Demonstration Pile 3 showed that the pile generally met the temperature requirements (i.e., maximum permissible temperature of 160 degrees Fahrenheit and differential temperature per FDOT Dev455ACP), except between elevation el +4 ft to el +1 ft, which are above the pile cutoff elevation. TIP report indicated the calculated in-place pile diameters exceeded the nominal 36-inch auger diameter and provided the required minimum grout cover of 4 inches over the reinforcing steel, except for the zone below el -96 ft to the tip of the pile, where the TIP report indicated reduced pile diameter and grout coverage. See Fig. 2 for zone below el -96 ft.

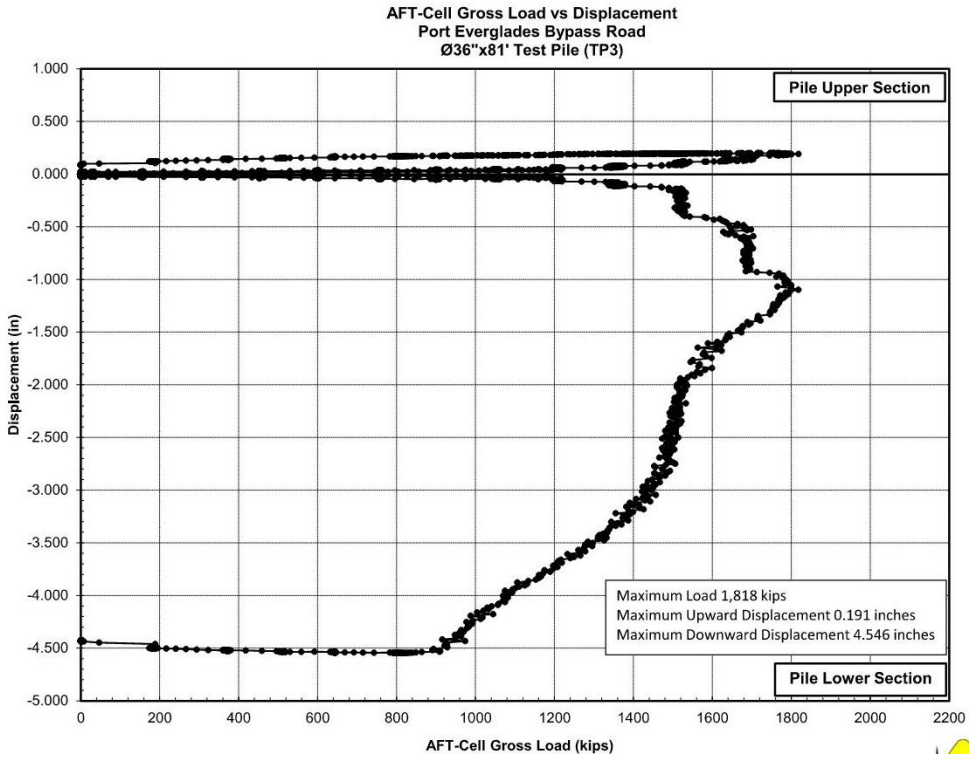


□□□

direction) capacity (3,000-ton approximate equivalent top load (ETL) capacity) embedded jack within the test pile with its fracture plane at el -56 ft. The test pile was instrumented with two displacement transducers embedded within the pile, and eleven pairs of vibrating wire strain gauges fastened to the reinforcing cage assembly. Figure 3 shows the reinforcing cage assemblies for the test piles.



□□□



□□□□□□□□□□□□□□□□□□sus Displacement Plot for 36-inch-diameter pile

For the evaluation of the load test results, an analysis was performed using the procedure discussed in FDOT SFH – Appendix B. The axial capacity was calculated using this method based on SPT N-Values within Stratum 5 from the boring drilled at the test pile location including the resistance from an equivalent sand material per FB-Deep between the top of Stratum 3 and the top of Stratum 5. The calculation showed that the capacity determined from the load test exceeded the predicted capacity utilizing the pilot boring data at the test pile location by a factor of 1.2 indicating the site specific, design, ultimate side shear capacity calculations underestimate the available pile capacity. If the load carrying capacity from the material present above Stratum 3 is removed and the material present at Stratum 3 and Stratum 4 is modeled as sand from a side shear resistance perspective, the load test still verified that the site specific, design, ultimate side shear capacity calculations underestimate the available capacity by a factor of 1.1. It was noted that the predicted ultimate side shear resistance from FB-Deep was about 40% of the mobilized side shear resistance documented in the completed load test based upon strain gauge measurements from the top of Stratum 3 to the top of Stratum 5. Thus, indicating a conservative underprediction of available side shear resistance, when considering this material to be an equivalent sand per FB-Deep, by a factor of 2.5. A comparison between the SPT N-Values obtained from the boring drilled at the test pile location and the mobilized and ultimate side shear resistances obtained from the load test confirmed that the results show a higher multiplier than the 0.1 multiplier per FDOT SHF – Appendix B. Table 6 below shows the average corrected SPT N-Values from the boring and the peak side shear resistances obtained from the load test at depths above and below the cell. The peak side shear resistance was limited to values at the calculated average creep limit below the cell and to peak values above the cell as the creep limit was not reached above the cell. Dividing the side shear resistances by the averaged corrected SPT N-Values, a higher multiplier than 0.1 (from the FDOT SFH Appendix B design methodology) was obtained. Thus, validating the recommended site-specific, design procedure.

Table 6. Averaged Corrected SPT N-Values from Test Pile Boring and Peak Side Shear Resistances from Load Test – 36-inch test pile

Depth (feet)	Averaged Corrected SPT N-Values from Test Pile Boring	Peak Side Shear Resistance (tsf) from Load Test	Calculated Multiplier
50.25 to 56.5	26	3.5	0.13
56.5 to 62	48	7.4	0.15
62 to 81	39	3.8	0.10

Test Pile Installation for 24-inch-diameter piles

The 24-inch-diameter demonstration pile was installed to a tip elevation of el -95 ft, the 24-inch-diameter test pile near Pier 3 (TP-1) was installed to a tip elevation of el -95 ft, and the 24-inch-diameter test pile near the east approach slab (TP-2) was installed to a tip elevation of el -75 ft. The two test piles were configured for testing using the embedded bi-directional jack procedure in accordance with the same procedures previously described for the 36-inch-diameter test pile.

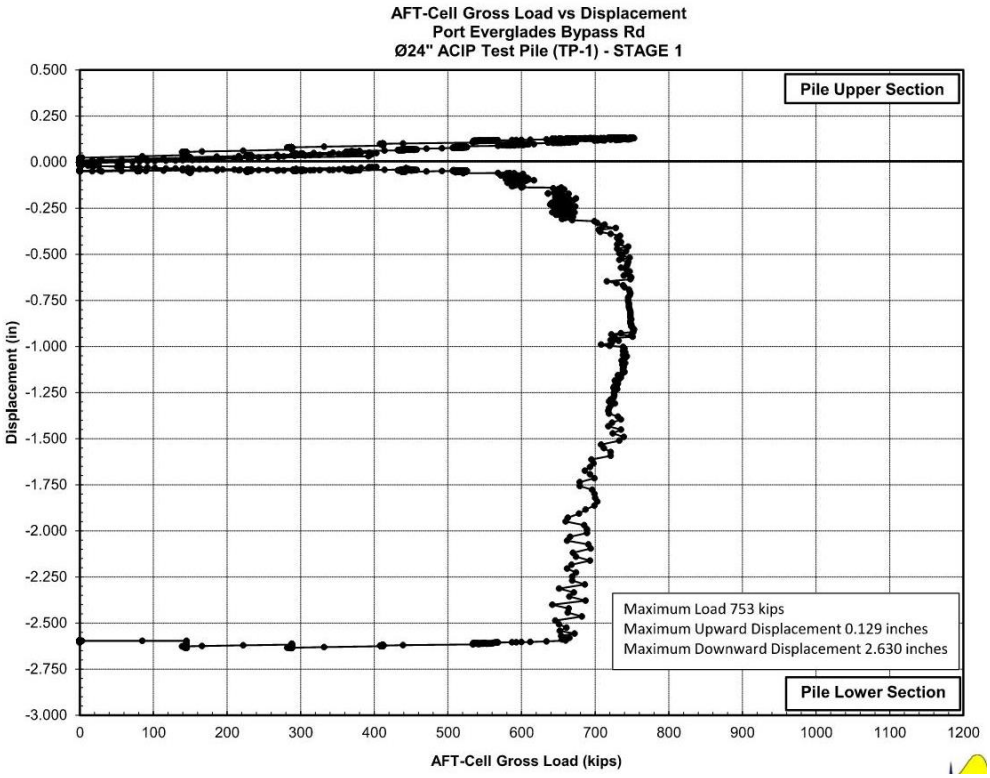
The loading assembly within TP-1 consisted of two 18-inch-diameter hydraulic jacks with a 750-ton bi-directional capacity (1,500-ton approximate equivalent top load (ETL) individual jack capacity) embedded within the test pile with its fracture planes at el -67.5 ft and el -83 ft. The test pile was instrumented with two displacement transducers embedded within the pile and twelve strain gauges fastened to the reinforcing cage assembly.

The loading assembly within TP-2 consisted of one 18-inch-diameter hydraulic jack with a 1,500-kip bi-directional embedded within the test pile with its fracture plane at el -59 ft. The test pile was instrumented with two displacement transducers embedded within the pile and ten strain gauges fastened to the reinforcing cage assembly.

The intent of the bi-directional load tests on the 24-inch-diameter test piles was to confirm the nominal, axial compressive capacity of the 24-inch-diameter piles by testing the pile to the nominal axial compressive capacity (i.e., 705 tons for TP-1 and 570 tons for TP-2) or twice the maximum factored design (i.e., 2xFDL= 806 tons for TP-1 and 680 tons for TP-2) axial compressive load (i.e., whichever is greater) and to confirm the design ultimate side shear resistance within the bearing layer or stratum.

Figure 5 below shows the load versus displacement plot for the pile upper section (above the cell) and pile lower section (below the cell) for the 24-inch-diameter test pile TP-1.

 © Deep Foundations Institute 2025


AFT-Cell Gross Load vs Displacement
Port Everglades Bypass Rd
Ø24" ACIP Test Pile (TP-1) - STAGE 1
Pile Upper Section
Pile Lower Section
Maximum Load 753 kips
Maximum Upward Displacement 0.129 inches
Maximum Downward Displacement 2.630 inches
Displacement (in)
AFT-Cell Gross Load (kips)
0.500
0.250
0.000
-0.250
-0.500
-0.750
-1.000
-1.250
-1.500
-1.750
-2.000
-2.250
-2.500
-2.750
-3.000
0
100
200
300
400
500
600
700
800
900
1000
1100
1200

□□□

Table 8. Averaged Corrected SPT N-Values from Test Pile Boring and Peak Side Shear Resistances from Load Test – TP-2

Depth (feet)	Averaged Corrected SPT N-Values from Test Pile Boring	Peak Side Shear Resistance (tsf) from Load Test	Calculated Multiplier
43 to 50	28 to 32	1.5 to 2	0.05
50 to 65	36	2.8	0.08
65 to 78.6	47	6.5 to 7.4	0.14 to 0.16

Assessment and Calculation of Load Test Determined Multipliers

Based on the three load tests performed for the project, an analysis was performed to calculate the average, weighted multipliers at different tip elevations. The calculated multipliers are average values at the specified tip elevations considering the load test back-calculated multipliers over the respective depth intervals documented in the load tests. These values are valid to use from the top of Stratum 5 to the designated tip elevations in the table below; however, when the calculated multiplier exceeds 0.1, the value for the design was limited to a maximum of 0.1 consistent with the SFH – Appendix B.

Table 9. Calculated Multipliers at different Pile Tip Elevations from the Load Tests performed at the Project Site

Pile Tip Elevation (feet, NAVD)	36-inch Load Test	24-inch Load Test, TP-2	24-inch Load Test, TP-1
-70	0.12	0.10	0.09
-75	0.12	0.10	0.10
-80	N/A	N/A	0.11
-85	N/A	N/A	0.11
-90	N/A	N/A	0.11
-95	N/A	N/A	0.11
-100	N/A	N/A	0.10

THERMAL INTEGRITY PROFILING (TIP) TESTING

The TIP reports for the demonstration and test piles indicated that the maximum permissible core temperature of 160º F was not exceeded (see discussion for Demonstration Pile 1 in Test Pile Installation for 36-inch-diameter piles) and the differential temperatures did not exceed 35º F as required per FDOT's DEV455ACP. However, TIP data for the piles show a reduction in diameter in the last 4 feet of the pile shafts near the pile tips which did not meet the requirements per Section 455-44 of DEV455ACP. The reduction in diameter measured by the TIP is the result of the temperature "roll off" effect that is typical of the TIP testing in ACP. The piling contractor suggested over drilling the piles and discounting a specified lower portion of the pile and all production pile tip elevations included a non-load carrying capacity zone of 4-feet to account for the reduction in diameter.

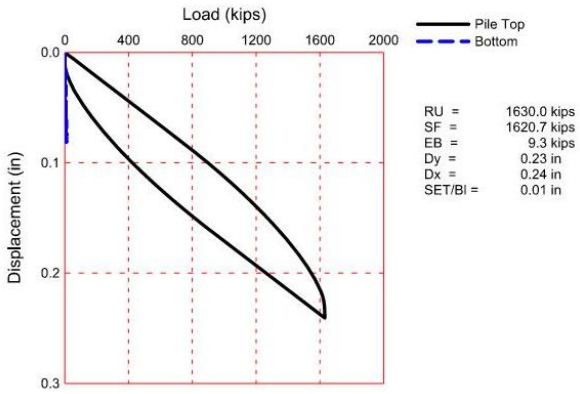
PRODUCTION PILE INSTALLATION AND DYNAMIC PROOF TEST RESULTS

All production piles were installed using the same procedures implemented for the successfully installed and load tested piles and in accordance with the recommendation contained in pile authorization letters,

 © Deep Foundations Institute 2025

load test reports, DEV455ACP, projects drawings and geotechnical report. All production piles for the end bents and bridge piers, 25% of the production piles for the west approach slab, and 50% of the piles for the east approach slab were instrumented with four thermal wires attached to the reinforcing steel cage.

One pile at every pier and bent was proof tested to at least the factored design load plus the downdrag load via High Strain Dynamic Testing. Proof testing performed on the piles confirmed the structural integrity of the piles, mobilized capacity exceeded the required load test and equivalent top load versus displacement showed relatively low displacements (less than 0.5 inch) indicating no failure on the piles. Figure 6 shows the load versus displacement curve for the proof tested pile at Pier 10.



□□□□□6□ Load versus Displacement Curve for Proof Tested Pile

Pile Certification Packages for each end bent and pier were prepared and submitted by the Construction Engineering and Inspection (CEI) consultant which included pile installation records, results of compressive strength testing on grout samples, TIP reports, and a proof test performed for one pile at every end bent or pier.

CONCLUSION

From the evaluation of the load test data obtained from the load tests, the design approach utilizing the design unit ultimate side shear resistance relationship and values presented above are valid for properly constructed ACP piles installed into Stratum 5.

Based on the site subsurface conditions, the results of the pile load test program, the pile installation records, the results of compressive strength testing on grout samples, TIP reports and proof testing, the production piles were satisfactorily installed in accordance with the project drawings, the project specifications, approved submittals and geotechnical report. The installed piles can sustain their respective design capacities with the appropriate factors of safety verified during the load test program.

REFERENCES

ASTM Standard D7949-14, 2014. “Standard Test Methods for Thermal Integrity Profiling of Concrete Deep Foundations”. ASTM International, West Conshohocken, PA, 2003, DOI: 10.1520/D7949-14.

ASTM Standard D8169-18, 2018. “Standard Test Methods for Deep Foundations Under Bi-Directional Static Axial Compressive Load”. ASTM International, West Conshohocken, PA, 2003, DOI: 10.1520/D8169_D8169M-18.

 © Deep Foundations Institute 2025

Developmental Specification DEV455ACP, 4-25-2023. “Auger Cast Piles”. Florida Department of Transportation, Tallahassee, Florida, USA.

FHWA, 2006. “Soils and Foundation Reference Manual – Volume II”, Report No. FHWA NHI-06-089. Authors Naresh C. Samtani, PE, PhD and Edward A. Nowatzki, PE, PhD, Federal Highway Administration, U.S. Department of Transportation.

Soils and Foundation Handbook, 2024. Florida Department of Transportation, Tallahassee, Florida, USA.

 © Deep Foundations Institute 2025

SUBSURFACE EXPLORATION FOR I-40 RECONSTRUCTION IN THE PIGEON RIVER GORGE POST HURRICANE HELENE

Christopher J. Ramsey, PE, Schnabel Engineering, LLC, Nashville, Tennessee, United States, 629-257-6520, cramsey@schnabel-eng.com
Michael Senior, PE, Schnabel Engineering, LLC, Seattle, Washington, United States, 206-573-5190, msenior@schnabel-eng.com

ABSTRACT

Following devastation caused by Hurricane Helene throughout the western North Carolina region in September 2024, North Carolina Department of Transportation (NCDOT) reached out to the engineering community for the rebuilding process under an emergency condition. As part of the RK&K design team for the reconstruction of Interstate 40 (I-40), Schnabel Engineering developed an expedited geotechnical subsurface exploration program for the first 5-miles (8 km) in North Carolina. I-40 experienced numerous failures along the five-mile corridor which is adjacent to the Pigeon River. In order develop repair concepts and ultimately to design the permanent repairs, a subsurface exploration program was established that included desktop review of historic geotechnical data, rock probes by air track drilling, rock probes by soil nail drilling, rock core sampling with standard coring methods, optical televiewer logging, and geophysical investigations using MASW methods. A suite of laboratory testing was performed to characterize engineering properties of the subsurface soils and rock.

A large amount of data was gathered, and the need was recognized to keep the records in an organized fashion to streamline data review and meet the needs of an emergency response project where the design team and contractor's team under an alternative delivery contract are working in unison. An internally developed database system (Mortar) that integrates different applications and services was deployed. Using Mortar, data mapping and integration is possible, facilitating a more informed design process.

INTRODUCTION

The initial 5-mile (6.4 km) stretch of Interstate 40 (I-40) within North Carolina near the Tennessee border was planned in the early 1950's. The route lies within the Pigeon River Gorge adjacent to tall, steeply dipping exposed bedrock faces. I-40 was originally constructed through the Pigeon River Gorge in the 1960's by blasting the bedrock on the north side of the river. Various NCDOT geologic reports acknowledge the repercussions of the blasting – exacerbating existing joints in the rock and creating new discontinuities. Due to upslope rock slope instability, in the 1980's the NCDOT shifted the roadway closer to the Pigeon River with an embankment. The embankment was made up of primarily silty sand with gravel, cobbles, and boulders and has an average height of 50 feet (15.2 m) above the river channel bed. Since its placement, the embankment has had a documented history of scour due to flood events, with notable failures in 2004 following Hurricane Ivan that led to the installation of numerous retaining walls to rebuild the roadway.

In September 2024, Hurricane Helene devastated western North Carolina. Rainfall totals were significant and intense, with a range of 13-inches (330 mm) to approximately 30 inches (762 mm) of rainfall between September 25 and September 28, 2024. This led to a peak flow through the Pigeon River Gorge estimated to be 62,000 cubic feet per second (cfs) (1,755 m^3/s), equivalent to a 500-year return period storm event. Due to high velocity flows and sharp curvatures of the gorge, the flow caused numerous embankment failures adjacent to I-40 eastbound (EB) lanes, where approximately 40 % of the project corridor was impassable via EB lanes. Additionally, the storm event destroyed the service road that NCDOT maintenance crews use around the twin tunnels at MM 4.0, cutting-off access. A typical failure section of EB lanes is shown in Fig. 1.

 © Deep Foundations Institute 2025



Fig. 1 - Typical slope failure

NCDOT responded to the extensive damage throughout the region by utilizing emergency on-call and alternative delivery contracts. Schnabel Engineering was selected as part of the RK&K design team for the I-40 reconstruction. Geotechnical subsurface exploration efforts were planned in three phases, the first two of which were executed November 2024 through February 2025. NCDOT separately selected a contractor for the reconstruction, through the Construction Manager General Contractor (CMGC) alternative delivery process.

SUBSURFACE EXPLORATION PLANNING

Typically, a 5-mile (8 km) stretch of highway includes infrequent borings for minor structures, such as sound walls and high mast lighting, and concentrated locations of borings for structures such as bridges and retaining walls. However, in the Pigeon River gorge, the reconstruction effort will require continuous installation of geo-structural systems to repair and rebuild embankments along the corridor. Design and installation of geo-structural solutions are highly dependent on subsurface exploration data. The design team formulated a plan that obtained information quickly, covering as much of the project corridor as practicable. The subsurface exploration was performed in three phases. Phase I occurred within the existing westbound (WB) lanes of I-40 while the road was entirely closed to public traffic in December 2024. Phase II activities occurred in the existing EB lanes where it was safe to do so given the failures. Phase III required close coordination with the CMGC contractor in order that ramps were constructed to enable access to the bottom of the gorge at the toe of what remains of the existing embankment immediately adjacent to the water. Due to the overall mountainous terrain of the project location and steeply dipping nature of the bedrock towards the river it was deemed critical by the design team to collect data in the north-south direction across the highway, as well as east-west along the highway alignment.

 © Deep Foundations Institute 2025

Previous explorations had been conducted throughout the corridor, for other landslide and rockslide related projects over the years. The prior explorations used standard penetration test (SPT) borings, geophysical investigations, and rock coring. These data were provided from the NCDOT records for use by the design team and dated from the 1970's onwards. The SPT vales from these prior borings through the embankment fill were wide ranging due to the frequent presence of cobbles and boulders. The rock core information from the prior explorations was informative, providing characteristics of the bedrock surface and discontinuities.

Based on exposed scarps within the embankment and material observed within the river at the toe of the embankment, the overburden generally consists of 'shot rock' with varying sizes of cobbles and boulders within a silty sand matrix and is shown in Fig. 2. Boulders were noted to be large, with maximum diameters reaching over 10 feet (3 m). This observation was key in developing the approach to define the bedrock surface at the project site. Additionally, the previous explorations helped to inform anticipated depths to bedrock that was particularly helpful in the early formulation of design concepts shortly after award of the project.



Fig. 2 - Typical shot rock embankment

The subsurface exploration (Phases I through III) deployed a variety of tools and approaches to gather data. Initially, emergency on-call contractors for NCDOT were on site to install temporary stabilization measures, implementing soil nail walls to stabilize what remained of the EB lanes and to arrest subsequent failures from encroaching on the WB lanes. The design team mobilized personnel to observe representative portions of the soil nail drilling operations. This was done to gain a rapid insight into the top of rock in the extents where new borings were not possible due to conflicts with the soil nails, and/or access and safety limitations arising from the failures. Much of the soil nail installation was done using roped access techniques. The next step included the use of geophysical investigations through multichannel analysis of surface waves (MASW) methods and rock probes using air track drilling. Within the CMGC project delivery method, the contractor provided subcontract drilling crews and equipment to operate air track rock probes to help expedite the data collection. The air track drilling crews were deployed throughout the project corridor to help define the top of the bedrock surface. These data were obtained rapidly, and were insightful in calibrating the MASW data. Traditional geotechnical borings were planned to follow-on behind the geophysics, to core and sample bedrock and to enable down-the-hole (DTH) optical televiewer scanning of the rock cored holes.

The use of multiple operations to gather subsurface exploration data required the use and coordination of concurrent crews. Design team staff observed soil nail installation by monitoring rate of penetration and total installation depths into the embankment. During the observation of rate of penetration, response by the DTH equipment to material that was encountered within the embankment was noted. This provided a general understanding of the variable nature of the bedrock surface and confirmed the presence of boulders within the embankment. Observing drilling of soil nails for the temporary stabilization provided a form of rock probe subsurface exploration data, as depicted in Fig. 3.



Fig. 3 - Temporary soil nail drilling

Geophysical investigations were conducted throughout approximately the first four miles (6.4 km) of the project. Generally, three transect alignments were used to conduct the study, one in the WB uphill shoulder, a complimentary one near the roadway centerline and a final line within the bottom of the gorge and is near the toe of the proposed stabilization system. The parallel alignments were used to compare rock surface uphill to downhill. In total, the geophysical program consisted of about 15 miles (24.1 km) of MASW data. The lines of MASW data within the limits of the existing roadway were collected in only 12 days by utilizing three concurrent crews from three different firms to meet the urgent timeline, commensurate with the emergency nature of the project. The program included review of historical MASW data collected by the authors' firm in 2004 following Hurricane Ivan. Data collection was concurrent with on-going construction of temporary stabilization efforts which necessitated an extra level of field coordination and an almost continuous 24-hour per day data collection program. Data processing in the office was conducted concurrently with field data collection to minimize the timeframe from project award to final geophysical deliverable. As the designed progressed, additional MASW lines were added into the Phase III program to collect data as close to wall alignment as safely possible.

Air track drilling crews were mobilized and used to expedite subsurface exploration efforts. As noted, the design team, through observations of existing scarps and observing temporary soil nail installation, were able to discern the composition of the existing shot rock embankment. The air track rock probes were deployed to rapidly advance through the shot rock overburden and identify the top of bedrock surfaces. Air track probes were drilled at approximately 200 feet on center in areas where the EB travel lanes had failed, and approximately 500 feet on center between failed sections.

Following air track drilling of rock probes, traditional geotechnical rock cores were drilled at a spacing of approximately 500 feet along the alignment in areas of failed embankment. The borings were advanced through the overburden by either predrilling using micropile DTH methods or using a casing advancer on the geotechnical drilling rig. Once it was determined that bedrock rock was encountered, coring with HQ sized conventional double-barrel wireline methods was performed. The HQ core size was selected to provide better clearances when deploying televiewer probes in the cored holes.

SUBSURFACE EXPLORATION FINDINGS

The approach to determine the bedrock surface, and to advance through the shot rock fill, was to drill continuously to a depth of 30 feet (9.1 m) in rock or greater. This would mitigate terminating borings prematurely on large boulders within the fill. The exploration team used this approach when drilling air track rock probes and traditional geotechnical coring. Since observation of soil nail installation and geophysical investigations were performed first, the results from these explorations were used to guide defining the depth to rock in the air track probes and core borings. The actual top of rock encountered in drilling was then used to calibrate the MASW results. The geophysical mapping indicated a highly variable rock surface along the alignment as shown in Fig. 4. Top of bedrock was delineated based on assigning a shear wave velocity of 1,500 ft/s (457 m/s) to 2,000 ft/s (609 m/s).

 © Deep Foundations Institute 2025

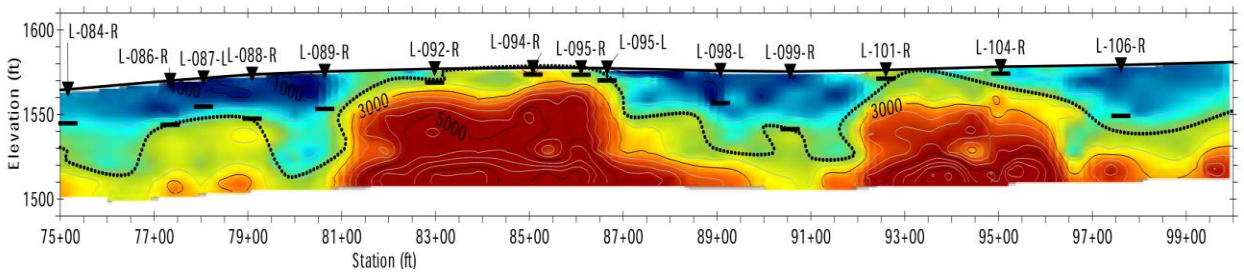


Fig. 4 - MASW results (2,500 linear feet (762 m) shown); triangle symbol indicates boring location, dash indicates top of rock in the boring

The air track rock probes advanced through the shot rock embankment with mostly minimal difficulty. Rock probe depth was limited by the ability of the equipment to produce air return and move cuttings. The probes with drilling difficulty were concentrated in areas where valleys traverse downslope. When rock was encountered, the air track drilling experienced a noticeable decrease in rate of penetration accompanied with a change in the drill cuttings. The cuttings changed in color, from brown to gray, and the size of the cuttings were similar to dust within the bedrock layers.

Initially, the traditional rock coring began by using a casing advancer through the shot rock. This was a slow operation and significant loss of drilling fluids was experienced. Ultimately, this approach was abandoned, and alternatively borings were advanced through the shot rock fill using micropile DTH drilling methods. When the micropile casings reached assumed top of bedrock, drilling was discontinued, and a PVC casing was left in the hole to facilitate the coring operation and subsequent televiewer logging to commence from the top of bedrock.

The process for traditional geotechnical rock coring was refined during the Phase III exploration, to mitigate some the drilling challenges experienced during Phases I and II. As noted above, a micropile rig was used to set casing to top of rock, although this process could not determine if the casing depth encountered a boulder or bedrock and some iterative drilling was needed in Phases I and II to increase casing depth to confirm top of bedrock. During Phase III, the process was evaluated for better efficiency to have the air track equipment advance a rock probe to determine depth to bedrock and permit the micropile equipment to set a casing to a predetermined depth confirmed by the air track rock probe.

Based on historical data and desktop studies, bedrock geology was anticipated to represent four formations, progressing from west to east along the alignment as the Pigeon Siltstone, Roaring Fork Sandstone, Longarm Quartzite, and Wading Branch Graywacke. The project team encountered the four various formations as identified in rock cores and observed that in many locations the metasiltstone, metasandstone, and quartzite were layered. Through geologic processes, the bedrock surfaces are dipping steeply to the south, and generally towards the Pigeon River; an adverse dip for stability of the existing embankment and a key consideration in subsequent design of the permanent reconstruction. NCDOT noted in past geologic reports that there was a trend of upslope rock failures (wedge failure) near or at the four mapped formations. See Fig. 5 for photo documentation of previous rock slides within this corridor.

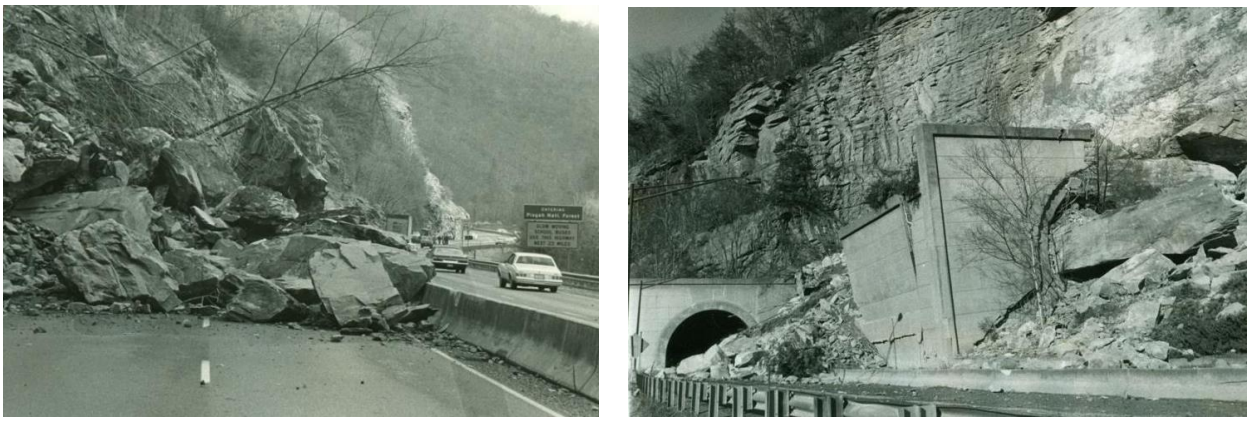


Fig. 5 - Historical photos of rock slides near MM1.0 (left) and east portals of tunnels (right) at MM4.0 (photos courtesy of The Mountaineer)

Information gathered from the televiewer logs of rock cores were used as part of kinematic analyses. Overall, the design team shared concerns with the steeply dipping bedrock and potential rock planes daylighting within exposed rock surfaces as part of the EB roadway embankment. The televiewer logs were used to identify critical locations where potential planar sliding and wedge sliding may need to be considered within the overall design.

The rock in the WB lanes was expected to be relatively shallow considering the steeply dipping nature of the rock and it ranged in depth from about 4 feet (1.2 m) to approximately 54 feet (16.4 m) with most of the alignment within the 5 to 10 feet (1.5-3.05 m) range. The deeper values are likely the bottom extent of the 1960's fill placement over blasted rock. Some deeper sections are in line with the natural mountain valleys, infilled with colluvium deposits.

The thickness of embankment in the EB lanes was expected to be larger based on the steeply dipping nature of the rock and history of the 1980's roadway expansion towards the river with embankment fill. The depth to rock ranged from about 10 feet (3.04 m) to approximately 70 feet (21.3 m). An excerpt from the data management system Mortar, discussed in the next section, is shown below in Fig. 6 and illustrates the variability in top of rock across the alignment and towards the river. The legend coding shown in the figure is based on data type (i.e. soil nail, boring, air track, etc.) and depth from road surface to top of rock, namely:

Data Type:

- Star: Soil Nail
- Circle: Air Track Rock Probe
- Square: Rock Core and Televiewer
- Boring Symbol: Historic Boring
- Triangle: MASW

Depth to Rock:

- Green: D < 10 feet (3.04 m)
- Yellow: 10 feet (3.04 m) < D < 20 feet (6.1 m)
- Orange: 20 feet (6.1 m) < D < 30 feet (9.1 m)
- Red: D > 30 feet (9.1 m)

 © Deep Foundations Institute 2025

The design team denoted red as the flag for notable depth to rock based on experience with anchored retaining walls and similar geo-structural solutions in the corridor following Hurricane Ivan in 2004. At deeper rock sections the number of anchors and/or large structural elements would be needed.

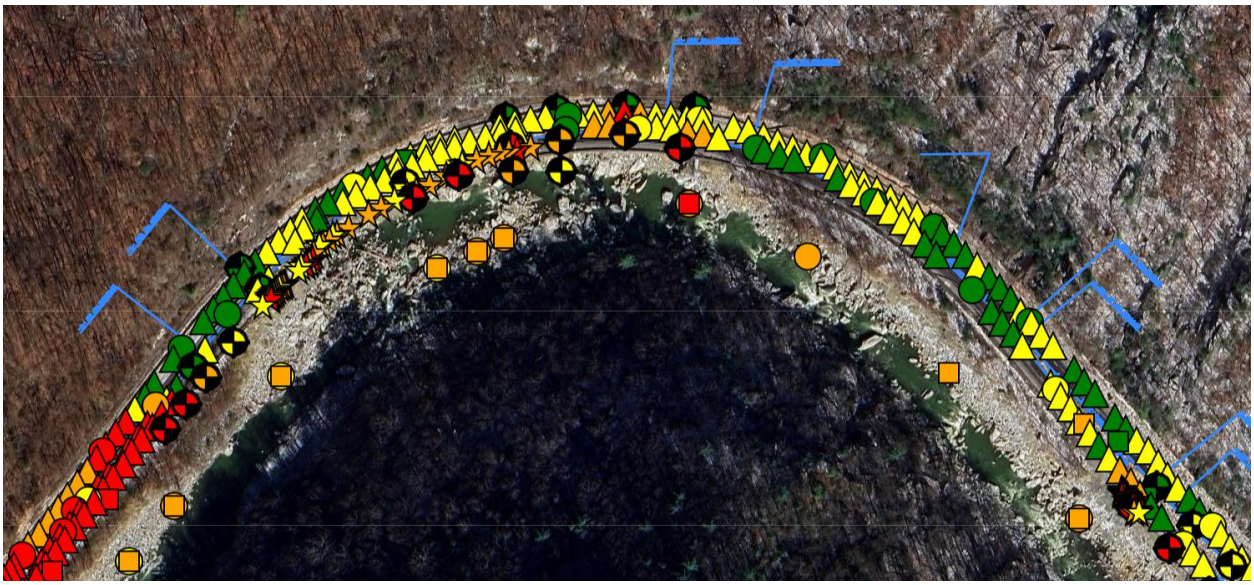


Fig. 6 - Excerpt from Mortar database

Top of rock data collected in Phase III was informative in relation to the estimated depth of scour that could be anticipated in the next 500-year flood event, removing passive soil from in front of the geostructural repair.

LABORATORY TESTING

Select samples collected during the explorations were submitted to certified laboratories. The laboratory tests conducted primarily consisted of:

- Unit weight of rock (ASTM D7012)
- Ultimate compressive strength (UCS) of rock cores (ASTM D7012 Method C)
- Elastic moduli in uniaxial compression (ASTM D7012 Method D)
- Point load index (ASTM D5731)
- Direct shear sliding friction (ASTM D5607)
- Slake durability (ASTM D4644)
- Acid producing rock (ASTM D5744)

In total, approximately 300 samples were tested and the results received were cataloged. Laboratory test results are being used to develop design parameters for the selected design concepts in the various geologic formations.

In general, UCS for rock cores ranged from approximately 7,500 psi to 44,000 psi with mean values ranging from 11,000 psi to 25,000 psi according to bedrock type. Additionally, acid producing rock was checked due to proximity to a region identified to contain bedrock with this property. Acid producing rock test results were negative indicating these materials are not anticipated within the project limits.

 © Deep Foundations Institute 2025

DATA MANAGEMENT

The three phases of subsurface exploration comprised logging of 473 soil nails, 308 air track rock probes, 166 traditional geotechnical coring locations with televiewer and approximately 15 miles (24.1 km) of MASW geophysical investigation. This large volume of data necessitated an organized data management system to be implemented.

The authors' firm deployed an internally developed database tool (Mortar) that is a platform for subsurface exploration data management. Mortar is an interactive web visualization platform that connects multiple data sources. Some of the data sources utilized were aerial drone video, geologic maps, historical data, field logs generated using electronic tablets, laboratory data and televiewer logs. It was also used as a tool for the various companies and staff involved in the data collection to track progress and quality control of the program

Mortar includes tools with customizable analysis for the data sources which are geo-located across an aerial image of the project site. Data points can be coordinated by shape or color to represent different properties of the investigation such as method of investigation (soil nail, geophysics, air track probe, etc.) or depth to rock. The rock depth can be overlain with surface topography using three-dimensional imagery, providing advanced visualization throughout the project corridor. Project progress was communicated to all stakeholders with access, showing what information had been obtained and what additional information was planned to be acquired. Project critical decisions were made using the visualization of the near real-time data uploaded from the field team. This communication allowed collaboration and efficient data delivery.

DESIGN CONCEPTS

Design concepts were evaluated prior to and throughout the subsurface exploration program, to meet a long-term resiliency goal for the project. Several options were rejected, including tunnels and viaducts, for a variety of schedule, cost, right of way, maintenance, and other logistical considerations. At the time of writing this paper (July 2025) two repair options have been selected; roller compacted concrete (RCC) embankment buttressing, and continuous pile walls. The RCC, a no slump concrete, will be used primarily to re-establish a stable embankment adjacent to and supporting the EB travel lane. RCC has been selected for its track record in high velocity flow applications in dams, hydraulic structures, and river bank protection works. River velocity is on the order of 35 ft/s (10.7 m/s) for the majority of the corridor and will be imposed on the repairs around the meanders and bends of the gorge. It also lends itself to rapid placement and compaction using conventional heavy earthwork means and methods. In areas where the existing river alignment is too close, thereby placing limiting the construction of a stable embankment, continuous pile walls will be installed using bottom-up construction methods. Additionally, continuous pile walls are considered for areas where flood damage during Hurricane Helene was limited to a small portion of the existing embankment, and bedrock was determined to be relatively shallow and above the design flood elevations. In these areas the construction of the walls will be from roadway grade and utilize top-down construction methods.

CONCLUSIONS

The subsurface explorations for the I-40 reconstruction project are extensive and atypical. Although there was some historic data available to inform an initial understanding of anticipated subsurface conditions, the data coverage was not adequate throughout the corridor. This dictated the need to collect a substantial amount of new data in a short time frame. Coordination between the design team, NCDOT, the CMGC contractor, and the emergency response contractor was vital to meet the needs of the exploration program. A key factor in enabling the data to be collected was closure of I-40 to public traffic at the start of the

program. Although the site was congested with construction traffic, the exploration team did not have to work in a typical Maintenance of Traffic (MoT) pattern.

The history of the project corridor with rockslides and landslides also necessitated the need to be thorough in the data collection with rock coring and DTH televiewer to better understand the rock mass characteristics. The exploration program was designed to balance volume of data needed to inform design of the permanent reconstruction, requiring adequate coverage both along the corridor and with depth, and the expedited schedule needs of this emergency reconstruction project.

The organization and geo-referencing of the data, and speed of the project and decision making processes, was paramount. Use of the Mortar data management system enabled the design team to present findings to NCDOT and the CMGC team in a timely manner and it enabled the design process to start earlier than using a traditional approach to data collection and reporting. Mortar has been a cornerstone in the facilitation of project workshops, used to brainstorm access, design solutions, and to inform constructability issues.

ACKNOWLEDGEMENTS

The authors would like to acknowledge the following organizations who were involved with the project and whose collaboration was invaluable throughout exploration and design to date: NCDOT Division 14; design team members RK&K, LLP and WSP; F&ME Consultants, Inc. and S&ME, Inc. who supplemented the geophysical investigation field resources, and performed televiewer logging. East Coast Drilling & Blasting, Inc. performed the air track rock probe drilling under subcontract to the CMGC contractor Ames Construction. Wright Brothers Construction Company and their sub-contractors GeoStabilization International/Access Limited are acknowledged for their cooperation during the emergency access and temporary stabilization works that was instrumental in enabling an expedited subsurface exploration program through the corridor.

REFERENCES

NCDOT (2024) Brief history of geotechnical issues with I-40 through Pigeon River Gorge, Tennessee Line to Mile Marker 5.0, North Carolina Department of Transportation Raleigh, October 25, 2024.

 © Deep Foundations Institute 2025

USE OF NONDESTRUCTIVE TESTING TO ESTABLISH INSTALLATION DISTURBANCE ZONE CRITERIA FOR ADJACENT CONTINUOUS FLIGHT AUGER PILE INSTALLATION ON DESIGN BUILD PROJECT

Saad Rehmatullah, EIT[1], Alfredas Daugiala, PE, M.ASCE[2], Les R. Chernauskas, PE[3], William D. Oder, PE[4]

[1]Student, Dept. of Civil and Environmental Engineering, New Jersey Institute of Technology, Newark, NJ; formerly, Underpinning and Foundation Skanska Inc., Maspeth, NY
[2]Chief Engineer, Underpinning and Foundation Skanska Inc., Maspeth, NY
[3]President, GTR Engineering of NY, Armonk, NY.
[4]Technical Manager, GTR Engineering of NY, Armonk, NY

ABSTRACT

Concerns regarding defects in cast-in-place deep foundations are amplified for piles constructed closely together as the geotechnical and structural capacity of the pile could be compromised. Defects such as pile necking (i.e. reduction in cross section diameter) can occur when drilling nearby an adjacent foundation element undergoing curing processes with increasing lateral earth pressures and disturbances experienced by the freshly poured foundation element. The final design of the Metropolitan Transit Authority (MTA) Jamaica Bus Depot Expansion Phase I included approximately one-thousand, 24 in (0.6 m) diameter continuous flight auger (CFA) piles. The project design criteria limited pile installation within 15 ft (4.6 m) of grouted piles to a waiting period of twenty-four hours. This project presented challenges relating to establishing project site-specific disturbance zone criteria for uncased CFA piles. The Design-Build team devised an innovative approach to propose nondestructive testing during installation to quantify site-specific disturbance zone criteria for adjacent foundation construction and prove an acceptable and more efficient construction sequence for approximately one-thousand production piles. Results from Thermal Integrity Profiling (TIP) and Sonic Echo (SE) tests completed at three different locations during the test program showed no detected effect on the pile integrity from adjacent drilling. The study successfully demonstrated a reduced drilling distance of 12 ft (3.7 m) adjacent to freshly grouted piles as acceptable, as well as a distance of 6 ft (1.8 m) adjacent to piles which had cured for approximately sixteen hours. The Design-Build team achieved a favorable outcome for an increased production schedule as a result of this innovative use of TIP testing, which served benefit to all stakeholders.

Keywords: Auger Cast-In-Place, Grout, Thermal Integrity Profiling, Sonic Echo

INTRODUCTION

The Metropolitan Transit Authority (MTA) Jamaica Bus Depot Expansion is a $480 million project to construct a new bus depot, parking lot, and administrative building located in Jamaica, Queens, New York replacing the almost ninety-year-old current facility, for an electric fleet of buses servicing the borough of Queens in New York City. The new bus depot is expected to open in the year 2026 and feature 272 battery electric buses (BEBs) by the year 2030 as part of the MTA's zero-emissions bus plan. The MTA Capital Construction and Development Company (client) in its document Project Requirements and Design Criteria (PRDC) mandates not to install piles within 15 ft (4.6 m) of grouted piles that are less than twenty-four hours old. This requirement applies for all grouted or cast-in-place piles, including drilled displacement piles and auger cast-in-place piles. A later section of this paper will review and compare existing national codes pertaining to disturbance zones for auger cast-in-place pile installation. The Design-Build team selected continuous flight auger (CFA) piles, an auger cast-in-place system where the auger is attached to a drill rig and grout is pumped through a hollow stem auger in a single pass, as the

 © Deep Foundations Institute 2025

foundation type for this project. The final design of the Jamaica Bus Depot Expansion Phase I includes approximately one-thousand, 24 in, or 2 ft (0.6 m) diameter CFA piles approximately 48 feet (14.6 m) in length. The apparent advantages with CFA piles are the ability to meet stringent noise constraints, reduced steel material and associated cost, minimal vibrations, and their speed of installation due to their aforementioned single pass nature. This project requirement imposed by the client on all cast-in-place deep foundations presented a challenge to make use of the speed and efficiency of CFA piles' single-pass system. Design-build procurement allows the engineer and contractor to work with one another during the early stages and throughout a project. The Design-Build team, during the test pile program, installed the CFA piles within a shorter distance and time than in the original project requirements and proposed nondestructive testing on these piles to establish an acceptable and more efficient construction sequence for approximately one-thousand production piles.

On a project of this magnitude and demanding schedule, and where geotechnical scope is on the critical path, such a requirement would increase significantly the schedule, or likely require mobilizing additional drill rigs, which require additional qualified personnel and manpower – overall reducing the economic advantage with this type of foundation solution. Other conventional options for auger cast-in-place pile installation include adjusting pile sequencing or using temporary casings; however, each of these options increase cost and schedule and decrease production per shift. The use of temporary casing can permit piles to be drilled in a shorter distance, although it includes an additional bid item and connected operation which significantly increases the cost per pile. Accordingly, it is in the best interest of the project stakeholders to construct the CFA piles without the use of casing and in the most safe and efficient pile sequence possible.

State of The Industry

This section will provide review of New York City Building Code and deep foundation industry guidelines for installation criteria of auger cast-in-place pile construction in comparison with the PRDC. The 2022 New York City Building Code (NYCBC) is based on the International Building Code and is the most recent version published; the NYCBC also has local jurisdiction on the project located in the New York City borough of Queens. The NYCBC offers a section on cast-in-place piles, including CFA piles. The code states:

> *Augered cast-in-place piles shall not be installed within a distance equivalent to the center-to-center spacing equivalent to six times the diameter of a drilled pile filled with concrete or grout less than 12 hours old, unless approved by the engineer* (1812.3.3 Installation).

This minimum drilling distance prescribed by the NYCBC is six diameters spacing center-to-center within twelve hours, therefore, the adjacent drilling distance is dependent on the pile design. For a pile diameter of 24 in (0.6 m) the acceptable distance for adjacent drilling within twelve hours should be equivalent to 12 ft (3.7 m). Further, the code provides inference that a responsible geotechnical engineer can shorten the required distance (conceivably in very dense geomaterial). Guidelines provided by the Deep Foundations Institute (DFI) in the Augered Cast-In-Place Pile Manual, Third Edition provide similar agreement that adjacent piles installed within twelve hours of one another should have a center to center distance of six pile diameters (2025).

While the fixed distance may be suitable and on par with industry standard for larger auger cast-in-place piles (i.e. thirty-inch diameter), or for some drilled displacement piles, the minimum adjacent center-to-center drilling distance required should be six times the diameter which is equivalent to 12 ft (3.7 m) for 24 in (0.6 m) CFA piles, as for the piles on the Jamaica Bus Depot Expansion project. Furthermore, the NYCBC and the DFI's Augered Cast-In-Place Pile Manual both offer a reduced drilling distance after twelve hours of grout hardening, whereas the PRDC allows reduction after twenty-four hours after installation, double the time required by these widely accepted codes and guidelines.

MATERIALS AND METHODS

The Design-Build team employed an innovative approach to establish a more efficient construction sequence with CFA piles, which involved drilling within a shorter distance and within a shorter time from adjacent piles than specified in the PRDC and conducting additional deep foundation testing during the pile installation test program. The Design-Build team installed the CFA piles at a 12 ft (3.7 m), six diameter, center-to-center distance between freshly poured piles in the same day and working shift. Additionally, the team installed CFA piles at a 6 ft (1.8 m), three diameter, center-to-center distance on the next day from piles which had cured for approximately sixteen hours. The inspector documented the non-conformance report (NCR) to the team for violating the PRDC during the pile installation test program.

The deep foundation test methods proposed would demonstrate whether the shortened drilling distance and installation time would impact the pile foundation integrity for adjacent potentially disturbed piles, and include:

1. Thermal Integrity Profile (TIP) testing
2. Sonic Echo (SE) testing
3. Field observation and construction records

An example pile cap construction sequence is shown in Fig. 1. It is important to note that this pile cap is proposed to be completed in four working days, whereas, it would take six working days spread across twelve working shifts, with half of them being downtime, to install a six pile group as shown below following the PRDC's wait times between each pile installation. The testing program took place similar to the arrangement shown in Fig. 1 at three different locations on the project site.

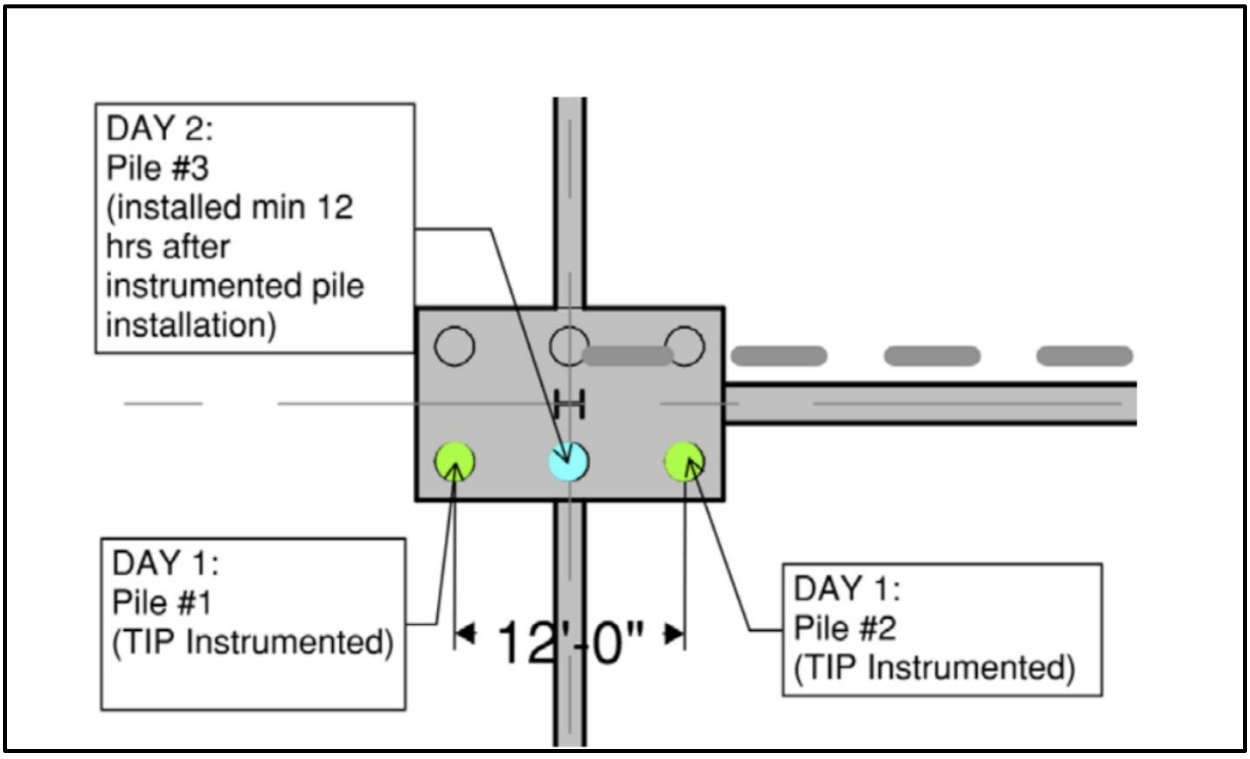


Fig. 1. Example of Generic layout of Test Pile Test Location (TL)

 © Deep Foundations Institute 2025

Thermal Integrity Profiling is a nondestructive testing method for testing the integrity of concrete shafts patented in 2004 (Mullins and Kranc, 2004). TIP testing is able to represent the shape of the entire shaft cross section by monitoring the temperature profile generated by the exothermic heat of hydration reaction as concrete cures and comparing it to the concrete's signature thermal profile (ASTM, 2014). For instance, low temperature zones represent anomalies which should be further evaluated to confirm flaws or defects. A defect is distinguished from a flaw because it has an adverse effect on the performance of the foundation (Sellountou et al., 2019).

Thermal Integrity Profiling is a popular industry standard quality assurance test method for cast-in-place deep foundations where blind concreting processes are common. TIP testing was selected rather than other nondestructive deep foundation testing methods on this project because it takes continuous measurement as opposed to a manual test, offering temperature data versus time that allows for analysis of potential impact of site activities (such as adjacent drilling) during curing. TIP offers assessment of the entire concrete cross section which is particularly useful for uncased piles with soil interface, and where soil caving is a potential problem on this project.

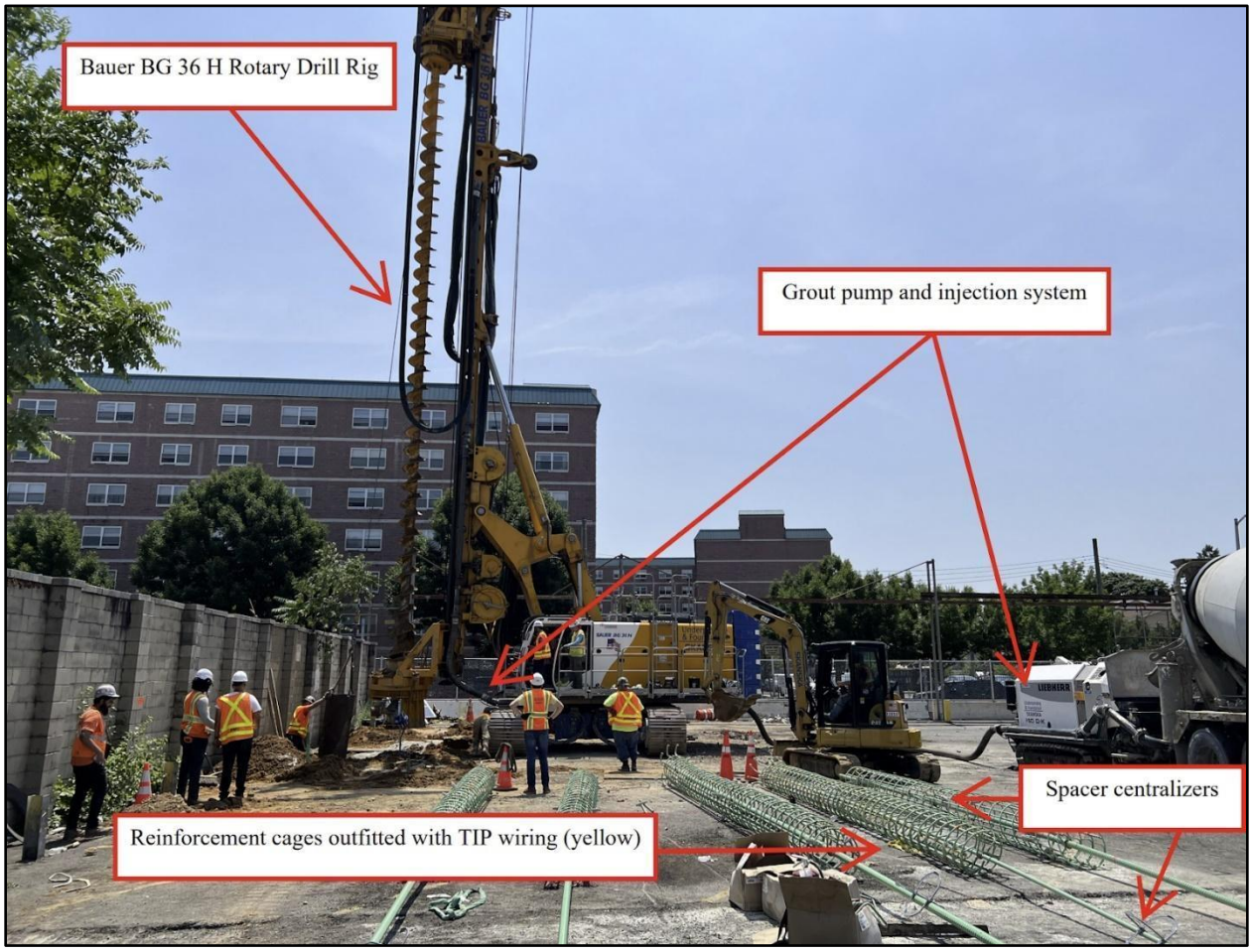


Fig. 2. Installing CFA Test Pile at Jamaica Bus Depot Expansion Phase 1

The auger cast-in-place piles were drilled using a Bauer BG 36 H rotary drilling rig with continuous flight auger drilling, depicted in Fig. 2 photo. The pile was drilled to the target depth then grouted in one pass using a hollow stem auger as the auger was raised to the surface. The reinforcement cage was then placed in wet grout. The reinforcement cages were outfitted with TIP wires at three, six, nine, and twelve o'clock orientations for the full length of the 27 ft (8.2 m) rebar cage and then converged at the number 18 center

reinforcement bar extending to 48 ft (14.6 m) below cutoff. Four TIP wires were used in each test pile to mitigate the risk of damage to wires during installation and prevent loss of all data. Centralizing wheels attached to the rebar cage and spacers on the center reinforcement bar below the cage were placed at 10 ft (3 m) vertical spacing. The Design-Build contractor drilled the adjacent pile at a distance of 12 ft (3.6 m) in the same work shift. The third pile (Pile #3 in Fig. 1 above) was installed at an adjacent distance of 6 ft (1.8 m) in the next shift at a time of about sixteen hours after grouting the previous pile. It is worth noting that the drill rig is positioned away from the other piles in the test group to reduce surcharge imposed by the drill rig on piles undergoing curing.

The second and third methods employed to evaluate pile integrity include Low Strain Impact Integrity Testing (also known as Sonic Echo (SE) testing) as well as field observation. SE testing was the original quality assurance method required on this project before introducing the pile disturbance evaluation. The SE method is referred to as a surface reflection technique. A hand held hammer is used to strike the top surface of the pile instrumented with an accelerometer that records the compression waves generated by the hammer strikes. The data is integrated with time to obtain velocity (ASTM, 2016). Reflections in the velocity can represent increases or decreases in pile impedance, which is mainly affected by changes in cross sectional area. SE testing also offers test repeatability as it is an external integrity test, and thus an anomalous area of the shaft can be tested at any time after grout hardening (unlike TIP testing which is an internal integrity test with a time window limited by grout curing).

Construction observation and monitoring for CFA piles includes spoil inspection, rotational and axial drilling speed, grouting pressure and grout volume, among other parameters. During auger withdrawal, spoil coming out of the ground is observed to confirm expected subsurface conditions and inspect for signs of communication between adjacent piles. Observation of change in grout head from a datum can be caused by grout permeating through soil as a result of disturbance indicating communication between shafts. Visual inspection of pile diameter and top of pile offer an additional verification to more robust testing methods, especially advantageous as one of SE testing's disadvantages is detecting defects at the top of pile. Pile grouting data can be produced automatically with advancements in drill rig technology like the Bauer B-Tronic used on this project; actual grout volumes are compared to theoretical grout volumes to model necking or bulging. These records maintain a critical role in the overall quality control process. Further, Measure While Drilling (MWD) capabilities on the drill rig (Bauer, Liebherr, Casagrande, etc.) measure various parameters while drilling, such as drilling speed, pull speed, grout pressure, and torque for quality control purposes.

Grout Mix Design

The pile grout mix design is an important factor for the success of the Design-Build team in this consequential application where the pile integrity is evaluated. Grout was pumped through the hollow stem auger as the auger was extracted (see Fig. 2 above). The pile resistance, designed as a friction pile, comes from the interface friction developed between the grout and soil. While grout admixtures can be used to achieve hardening earlier, challenges can arise in setting the rebar cage in wet grout. Therefore, the grout mix design included both a hydration stabilizer (retardant) as well as a water retention admixture. The hydration stabilizer, SikaTard 440, slows the heat of hydration reaction process and was important for the wet placement of the reinforcement cage in grout. Meanwhile the water retention admixture, Specrete Intrusion-Aid-Max, is used in augercast pile foundation construction which also exhibits fluidifying, water reduction and resistance to bleed properties of sanded grout mix. Due to the retardant, TIP recording began several hours after placement of the reinforcement cage.

RESULTS AND DISCUSSION

The test program was performed to demonstrate that the integrity of the grouted foundation elements would remain undisturbed during adjacent foundation element installation at a 12 ft (3.7 m) distance in

the same shift, and 6 ft (1.8 m) distance after a practical curing time of sixteen hours. Out of nine piles tested during the pile installation test program for Phase 1 of the Jamaica Bus Depot Expansion, two piles,

Pile 497 and Pile S-0, had anomalies. As previously stated, anomalies are areas which need to be further analyzed to determine if it is a flaw or defect which can be detrimental to the structural integrity of the pile foundation. These anomalies were not a result of the installation sequencing from nearby piles, but instead occurred during installation.

Three piles were installed in each of three test locations (TL). The generic layout of the piles were installed as shown in Fig. 1. The pertinent information is summarized below in Table 1. For TL1, Pile S-1, which was sacrificial, was installed first on the left. Pile 498 was installed 12 ft (3.7 m) away (on the right) around 68 minutes after Pile S-1 was completed. Pile 497 was installed in the middle between the two piles on the next day around 19 hours after Pile S-1 and 18 hours after Pile 498 were completed. The piles in the other two TL were installed similarly as shown in Table 1.

Table 1. TL1 CFA Pile Construction Details

CFA Pile No.	Grout Placement Date/Time Completed	Hydration Start time and Start of Test	CFA Pile Diameter (inches)	Center Bar Size/Dia. (Inches)	Total CFA Pile Grout Length (Feet)	Tested Length of Grout (Feet)	Theoretical vs. Installed Grout Vol. (yd^3)
PILE S-0	6-25-2024 / 2:28 PM	6-25-2024 / 7:45 PM	24	18/2.25	37	37	4.31 / 5.11
PILE 681	6-25-2024 / 2:47 PM	6-25-2024 / 7:55 PM	24	18/2.25	48	48	5.58 / 5.86
PILE 679	6-26-2024 / 7:52 AM	6-26-2024 / 1:10 PM	24	18/2.25	48	48	5.58 / 6.39

Table 2. TL2 CFA Pile Construction Details

CFA Pile No.	Grout Placement Date/Time Completed	Hydration Start time and Start of Test	CFA Pile Diameter (inches)	Center Bar Size/Dia. (Inches)	Total CFA Pile Grout Length (Feet)	Tested Length of Grout (Feet)	Theoretical vs. Installed Grout Vol. (yd^3)
PILE 80	9-9-2024 / 2:17 PM	9-9-2024 / 11:31 PM	24	18/2.25	39	38	4.53 / 5.43
PILE 81	9-10-2024 / 8:54 AM	9-10-2024 / 4:19 PM	24	18/2.25	39	38.5	4.53 / 5.37
PILE 82	9-9-2024 / 1:59 PM	9-9-2024 / 10:27 PM	24	18/2.25	39	38.5	4.53 / 5.45

Table 3. TL3 CFA Pile Construction Details

CFA Pile No.	Grout Placement Date/Time Completed	Hydration Start time and Start of Test	CFA Pile Diameter (inches)	Center Bar Size/Dia. (Inches)	Total CFA Pile Grout Length (Feet)	Tested Length of Grout (Feet)	Theoretical vs. Installed Grout Vol. (yd^3)
PILE S-1	6-17-2024 / 3:03 PM	6-17-2024 / 9:11 PM	24	18/2.25	48	47	5.58 / 6.17
PILE 498	6-17-2024 / 4:11 PM	6-17-2024 / 10:57 PM	24	18/2.25	48	38	5.58 / 6.24
PILE 497	6-18-2024 / 10:26 AM	6-18-2024 / 2:30 PM	24	18/2.25	48	48	5.58 / 6.45

Figures 3-4 present the relationships of the average temperature with time measured by the TIP wires for each of the three piles in two example TLs. Test Location 1 was similar. The times when grouting for each pile was completed is also shown on the figures to compare grouting completion times to the curing times of the piles. In each of the TLs, the second pile was grouted prior to the reinforcing bars being inserted in the first two piles, therefore the temperature time histories for the first two piles start shortly after the completion of grouting of the second pile. The third pile was installed around the peak temperature times of the first two piles. The maximum average temperature typically ranged between 140 to 160 degrees Fahrenheit and the time of maximum average temperature was typically between 15 to 25 h after grouting. As mentioned earlier, the retarders in the grout mix typically delayed the start of hydration; four to eight hours after grout placement for piles in test locations TL1 and TL2 and around eight to twelve hours in TL3.

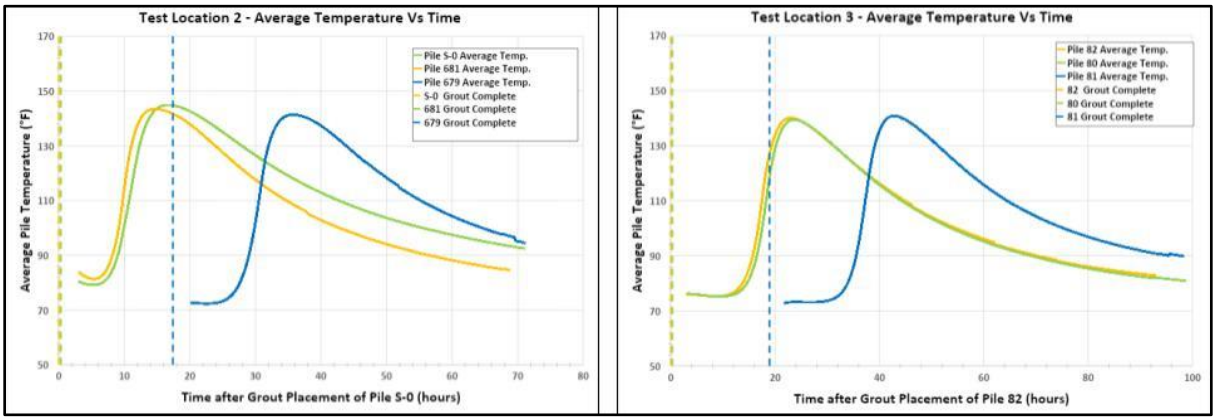


Fig. 3 (left) Temp vs Time TL2.

Fig. 4 (right) Temp vs Time TL3

In all TLs, the installation of subsequent piles did not create anomalies (or defects) in earlier installed piles. Practically, the average temperature with time for each pile is not sensitive enough to detect the effects of nearby pile installation, unless the disturbance was very large (e.g. large neck). However, the TIP testing, SE testing, and construction records confirmed that the adjacent piles did not disturb the earlier installed piles. A more precise way to evaluate the effects of the adjacent pile installation is by reviewing the temperature with depth at various times (as opposed to average). An example of this is presented in Fig. 5 for Pile 82 (first pile installed in TL3). The red line is the earliest reading taken around 3 h after Pile 82 was grouted and around 2.5 h after Pile 80 was subsequently grouted. The dark blue line and purple line are before and after, respectively, when Pile 81 was installed on the next day. The peak temperature is represented as the purple line and the dashed red line is after peak, thus lower temperatures. All of the plots show the temperature with no significant temperature reductions along the depth of the pile at each stage.

 © Deep Foundations Institute 2025

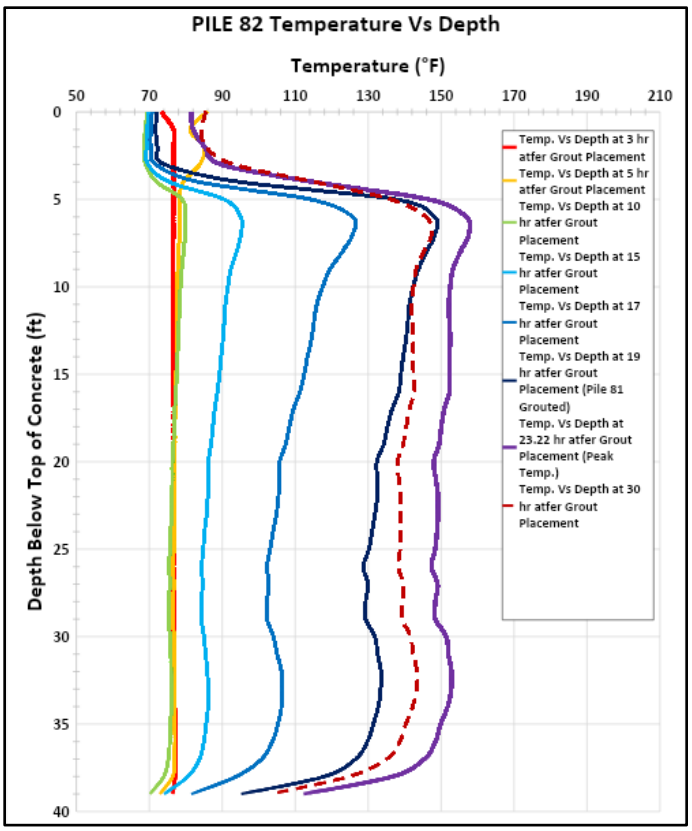
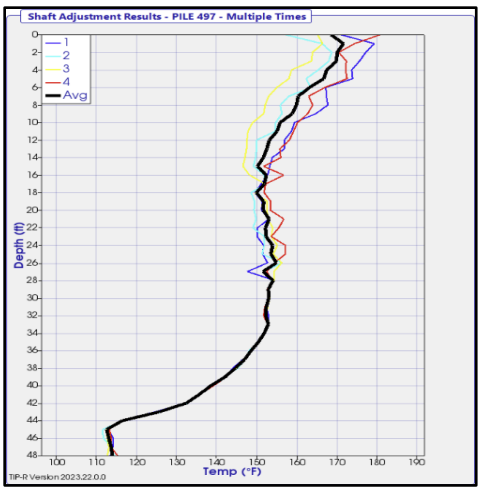


Fig. 5. Temp vs Depth for Pile 82 in TL3 at various times

As stated earlier, Pile 497 and Pile S-0 exhibited significant anomalies. The TIP results for Pile 497 are presented in Figs. 6-7. Figure 6 shows the average relationship of temperature vs time. The overall temperature with time is shown as the black line, while the temperature with time in the mid portion of the pile, 28 ft (8.5 m) to 35 ft (10.7 m), is the purple line. The peak average temperature of 152 degrees Fahrenheit occurs around 13 h after grouting. There is an anomalous zone from 36 ft (11 m) to 48 ft (14.6 m) in which the temperature decreases, as can be seen in Fig. 7 temperature with depth (the solid black line in Fig. 7 is the average temperature of all of the wires with depth). The solid blue line in Fig. 6 represents the temperature with time for a short segment at the bottom of the anomalous zone from 45 ft (13.7 m) to 47 ft (14.3 m), where the maximum average temperature within this zone only reaches 113 degrees Fahrenheit, compared to 152 degrees for the mid portion of the shaft. The 39 degree Fahrenheit difference or change in temperature from this zone at 45 ft (13.7 m) to 47 ft (14.3 m) compared to the nominal zone from 28 ft (8.5 m) to 35 ft (10.7 m) is represented by the dashed blue line in Fig. 7. This drop off in temperature represents an anomaly that should be further investigated.

 © Deep Foundations Institute 2025



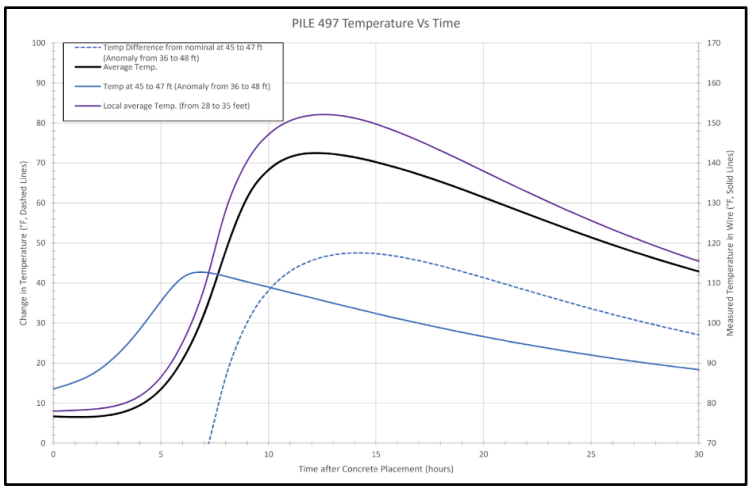


Fig. 6 (left) Temperature vs Time for Pile 497.

Fig. 7 (right) Temperature vs Depth for Pile 497

The individual wire temperatures with depth presented in Fig. 7 converge at the end of the rebar cage at a depth of approximately 27 ft (8.2 m), and continue for the remaining full length of the reinforcement bar to the bottom of the pile. Interestingly, there is a seemingly consistent approximate 10 degree Fahrenheit difference between wire 1 (blue) and wire 3 (yellow) along the top portion of the reinforcement. Therefore, it is likely that the reinforcement cage is closer to the edge of the shaft near wire 3 due to the lower temperature.

The gradual reduction in temperature from 36 ft (11 m) to 48 ft (14.6 m) is most likely due to a slight out-of-plumbness of the reinforcement resulting in decreased grout cover on the TIP wires (which are tied to the reinforcement) as the depth progresses to the bottom of the pile. As the grout cover decreases, the wires on the bar detect the gradual cooler temperatures closer to the soil rather than the full grout heat of hydration reaction. Thus, it is determined that the gradual reduction in temperature representing the anomaly is caused by the deviation in verticality in which the TIP wiring is increasingly affected by the soil at ambient temperature. The Sonic Echo (SE) testing nor the pile installation logs did not corroborate any necking in this zone.

The SE results for Pile 497 shown in Fig. 8 indicates a downward tip reflection near the recorded tip depth, confirming that the pile cross-sectional area and grout integrity remains consistent to the planned design depth with no necking between 36 ft (11 m) to 48 ft (14.6 m). The anomaly, therefore, can only be attributed to the bar angle rather than necking. In order to rectify this, increased focus and attention was directed to the proper placement and use of rebar centralizing wheels during production installation. Pile 497 was installed on the second day after the other two piles were installed in this testing location, thus there is no adjacent pile installation disturbance on this pile and the cage shift is a result of initial pile cage placement. The grout mix design was refined during the testing program with increased retardant to support the reinforcement cage placement in wet grout and achieving plumbness. Furthermore, Pile 497 underwent a successful load test.

 © Deep Foundations Institute 2025

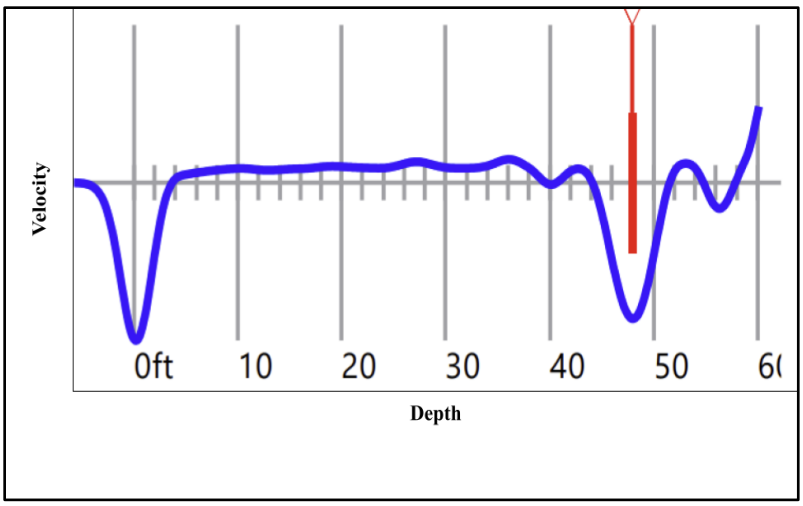


Fig. 8. Sonic Echo (SE) Results for Pile 497

The anomaly detected in Pile S-0 by the TIP results was between 28 ft (8.5 m) to 34 ft (10.4 m) below top of pile, immediately below the rebar cage where the single reinforcement bar is located. Figure 9 shows a three-dimensional pile shape interpretation of the shaft based on a recorded grout volume of 5.11 yd^3 (3.9 m^3). The pile bulges within the upper 14 ft (4.3 m), however, there is a reduced diameter at the depth of 28 ft (8.5 m) to 34 ft (10.4 m). Temperature with depth is presented in Fig. 10 (note that wire 2 was damaged and data could not be collected). The anomaly is represented by a large reduction in temperature between 28 ft (8.5 m) and 34 ft (10.4 m). The anomaly is further confirmed through SE test results shown in Fig. 11, which corroborate the TIP results showing that there is an anomaly at 28 ft (8.5 m). The downward reflection at approximately 28 ft (8.5 m) depth shows a lower impedance (based on smaller pile area).

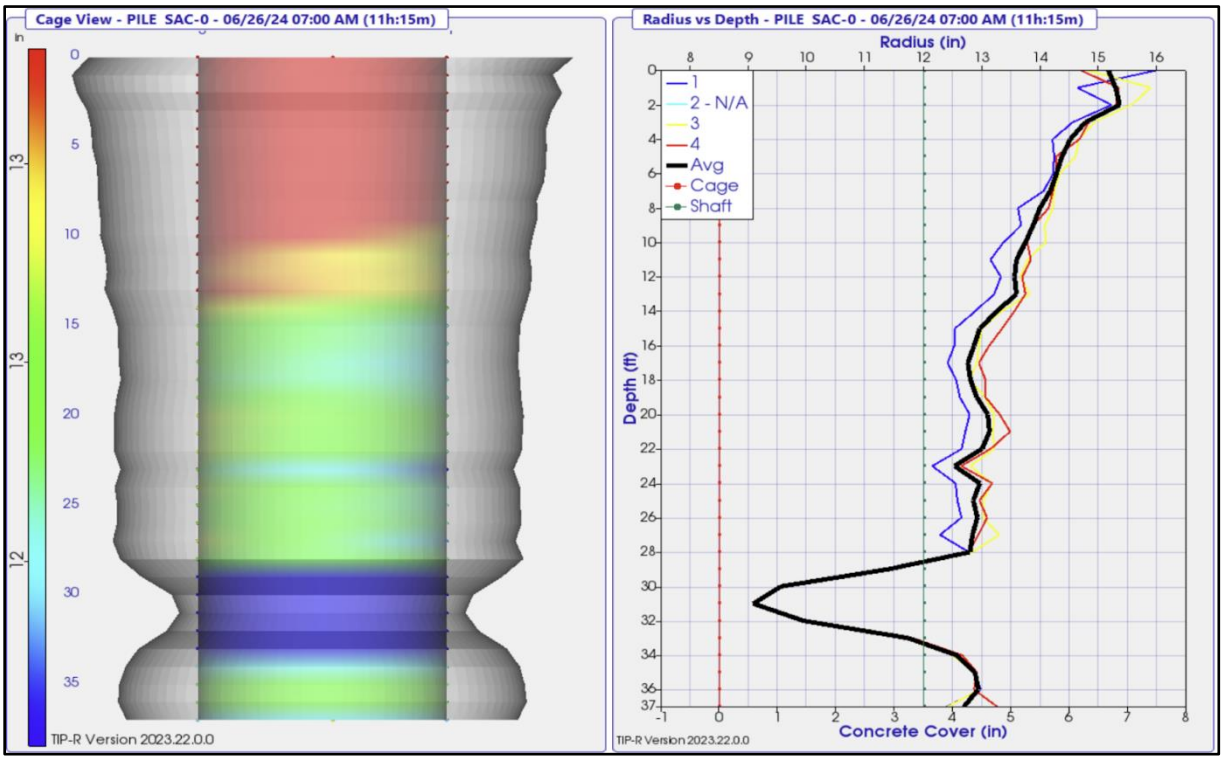


Fig. 9 (Left) TIP Pile Shape for Pile S-0.
Fig. 10 (right) Temperature vs Depth for Pile S-0

 © Deep Foundations Institute 2025

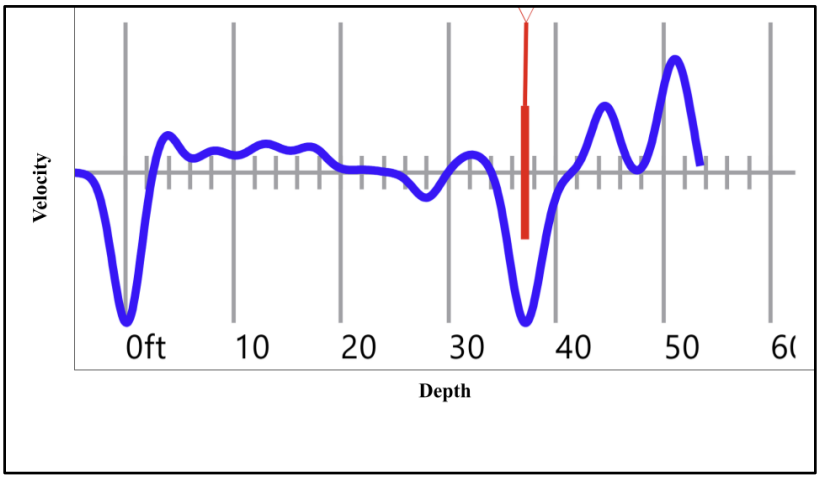


Fig. 11. Sonic Echo (SE) Results for Pile S-0

Pile installation logs in Fig. 12 demonstrate the perspective that the defect is due to initial pile construction, rather than adjacent construction. Installation logs for Pile S-0 show a reduction of grout volume and very low pull speeds through the length of the anomaly from 28 ft (8.5 m) to 34 ft (10.4 m) of about 4 ft/min (1.2 m/min), which increase by more than double then remain steady at approximately 11 ft/min (3.4 m/min) for the remainder of the shaft as the auger is extracted and the column is simultaneously grouted. The area of low pull speed (high withdrawal resistance) and reduced grout volume coincide with the necking determined from TIP and SE results. On the contrary,

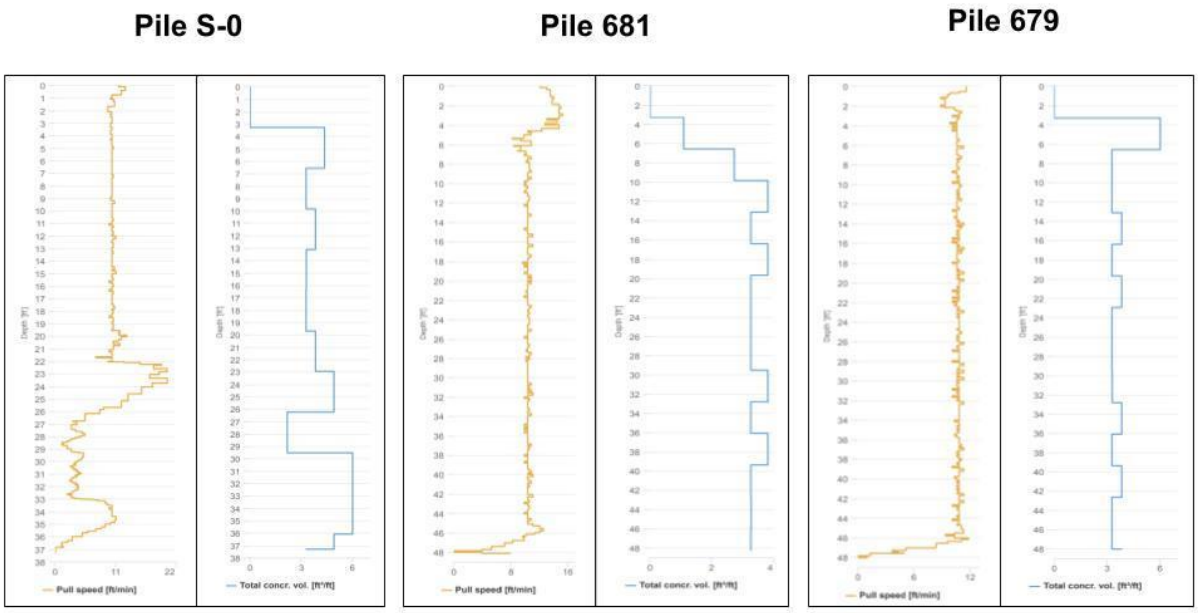


Fig 12. Pull Speed vs Depth and Grout Volume vs Depth for Piles in TL2

pile installation logs for the other two piles at this testing location, Pile 681 and Pile 679 remain uniform for the entire length of the pile. While there is a defect in Pile S-0, it is neither caused by drilling Pile 681 in the same shift at a distance of 12 ft (3.7 m), nor by drilling Pile 679 in the next shift 6 ft (1.8 m) away,

 © Deep Foundations Institute 2025

but rather occurred during initial pile construction due to increased withdrawal resistance experienced and effective grout volume placement fluctuation as a result of resistance to auger withdrawal. Pile S-0 was a sacrificial pile used as a reaction pile for the successful load test of Pile 679, therefore, no corrective action is required.

SUMMARY AND CONCLUSIONS

The Design-Build team proposed and installed around one-thousand CFA piles on the Jamaica Bus Depot Phase I project. Industry standard practice for CFA piles denotes a minimum six diameter drilling distance between piles that have not been sufficiently cured. However, the Owner's PRDC specified a 15 ft (4.6 m) fixed distance between installation of grouted piles that are less than twenty-four hours old. While this may be suitable and on par with industry standard for larger auger-cast piles (i.e. thirty-inch diameter), or for some drilled displacement piles, it was understood to be overly-conservative and the installation distance proposed by the client in its PRDC could be shortened for this project. In order to take full advantage of speed of CFA pile installation, the Design-Build team drilled 12 ft (3.7 m) adjacent to freshly grouted piles as well as 6 ft (1.8 m) adjacent to piles that had cured for approximately sixteen hours, and completed deep foundation testing to prove an acceptable and more efficient construction sequence. Results from the testing completed during the pile test program at three different locations within the project site demonstrate that drilling 12 ft (3.7 m), or six diameters, from adjacent freshly grouted piles does not impact the integrity of the pile. Additionally, drilling 6 ft (1.8 m), or three diameters, from adjacent piles in the next shift after a curing time of approximately sixteen hours also does not impact the integrity of the pile. This work corroborates the accuracy of NYCBC and deep foundation industry guidelines related to CFA pile installation.

The use of TIP testing with time added another level of confidence in evaluating the pile installation sequence, as well as Sonic Echo (SE) testing, and visual inspection/construction records. This project was aided by advanced rig technologies and automated data acquisition tools that were used to determine actual grout volumes which are required for accurate TIP testing results and analysis. Further the design build procurement allowed the foundation contractor and engineer to collaborate at an early stage and be able to devise a testing program capable of showcasing a more efficient pile sequence as acceptable to the client. The project continued with the new and proven drilling distances with the original five percent SE testing requirement on production piles and no defects were detected. All stakeholders benefited with this innovation; the MTA benefitted with increased schedule and the Design-Build team accomplished their goal of completing the project at a lower cost.

Future research should further explore the impact of adjacent disturbance on curing grout columns in different soils, at different spacing, diameters and times.

ACKNOWLEDGMENT

I express my sincere gratitude to the entire team at Underpinning and Foundation Skanska for the summer experience and learning on important and challenging projects (in addition to the project data used in this paper), many of the underlying themes in this paper are from what I have learned during my summer internship. Thank you to Andy Burns, P.E. for teaching me that a great engineer can confidently challenge ideas. The authors acknowledge Geosciences Testing and Research (GTR, Inc.) as the deep foundation testing engineer and STV as the Design-Build partner to Skanska on this project. Special thanks to Dwarika Mallick, P.E. and MTA C&D for permission to publish this paper for the purpose of technical knowledge sharing.

REFERENCES

ASTM. (2014). “Standard Test Methods for Thermal Integrity Profiling of Concrete Deep Foundations (Withdrawn 2023)” ASTM Standard ASTM D7949-14, ASTM International, West Conshohocken, PA. https://doi.org//10.1520/D7949-14.

ASTM (2016), “Standard Test Method for Low Strain Integrity Testing of Piles” ASTM Standard ASTM D5882-16, ASTM International, West Conshohocken, PA. https://doi.org//10.1520/D5882-16.

Daugiala A. "MTA CD CONTACT C-40355 JAMAICA BUS DEPOT QUEENS, NY – 24-in Augercast Pile TIP (ASTM D7949) Pile Disturbance Zone Evaluation" Underpinning and Foundation Skanska Inc., Maspeth, NY, September 27, 2024.

Deep Foundations Institute. (2025). “Augered Cast-In-Place Piles Manual,” 3rd ed, Deep Foundations Institute, Hawthorne, NJ.

Mullins, A. G. and Kranc, S. C. (2004). U.S. Patent No 6,783,273. Washington DC: U.S. Patent and Trademark Office.

New York City Buildings. 2022. *Chapter 18: Soils and Foundations, Section BC 1812: Cast-In-Place Concrete Piles.* New York City Building Code, 2022. https://www.nyc.gov/assets/buildings/apps/pdf_viewer/viewer.html?file=2022BC_Chapter18_SoilsFoundationsWBwm.pdf&section=conscode_2022.

Sellountou, E. A., Amir, J., Canivan, G., Chernauskas, L., Hertlein., B., Kandaris, P., Kavacs, T., Likins, G. (2019). “Terminology and Evaluation Criteria of Crosshole Sonic Logging (CSL) as Applied to Deep Foundations.” 2018 Deep Foundations Institute.

 © Deep Foundations Institute 2025

NAVIGATING COMPLEXITY: ENGINEERING SOLUTIONS FOR A 15-SPAN CSX RAILYARD BRIDGE EXPANSION

Ram Kasturi, P.E, KC Engineering and Land Surveying, P.C, New York, NY, United States
phone: +1 (203) 521-0971; email: rkasturi@kcecpc.com
Eshana Kolli, KC Engineering and Land Surveying, P.C, New York, NY, United States
phone: +1 (765) 404-6298; email: ekolli@kcepc.com

ABSTRACT

The rehabilitation and widening of a 2100 ft long, 15-span I-481 northbound and southbound bridges over the CSX railyard in Syracuse represents a critical infrastructure initiative aimed at improving accessibility and mobility across the region. This paper explores the engineering challenges and solutions associated with the foundation design and construction of this complex project. Key constraints included the close proximity of active rail lines, the need to schedule construction around rail yard operations, and limited space for widening towards the median. Additionally, subsurface conditions posed difficulties due to the presence of wetlands and thick layers of soft soils, necessitating innovative foundation strategies. To support the bridge widening—from two to three lanes in each direction, designs had to integrate seamlessly with the existing structures. Extended foundations utilized similar pile layouts and types to match existing foundations, with a combination of independent and combined pier foundations determined by the required pier fixity. Combined pier foundations were designed using the ASD method, similar to the original design approach, while independent footings followed LRFD principles to meet current design standards. The project serves as a model for complex urban bridge rehabilitation efforts and contributes significantly to infrastructure resilience and performance.

Keywords: pile design, bridge rehabilitation, bridge widening, construction challenges, soft clayey soils

INTRODUCTION

The I-481 Northbound and Southbound bridges span the CSX railyard and adjacent wetland areas, forming a vital part of the Eastern Corridor in Syracuse, New York as shown in Fig. 1. The bridge widening project, driven by the New York State Department of Transportation (NYSDOT), aims to improve mobility, safety, and regional economic vitality. Given the high commercial traffic volume through the railyard, the project was executed with minimal interference to ongoing rail operations and to the live traffic on the existing bridges.

Rather than opting for full bridge replacement, the NYSDOT design team proposed widening the existing structures while retaining their foundations. A thorough structural evaluation confirmed the feasibility of this approach, though the foundations and superstructures required selective strengthening and reconstruction to support the widened bridge configuration.

The total length of each proposed 15 span bridge is 2100 ft. With three lanes in each direction, the total width of each bridge including shoulders is 54 ft.

Superstructure for the widened bridge consisted of a link slab system with fewer joints as compared to the separate individual spans of the existing bridge. This design change required analysis of the structure using a refined analysis method of the superstructure and a detailed analysis of the existing foundation system to verify conformance with the applicable current loading requirements.

 © Deep Foundations Institute 2025

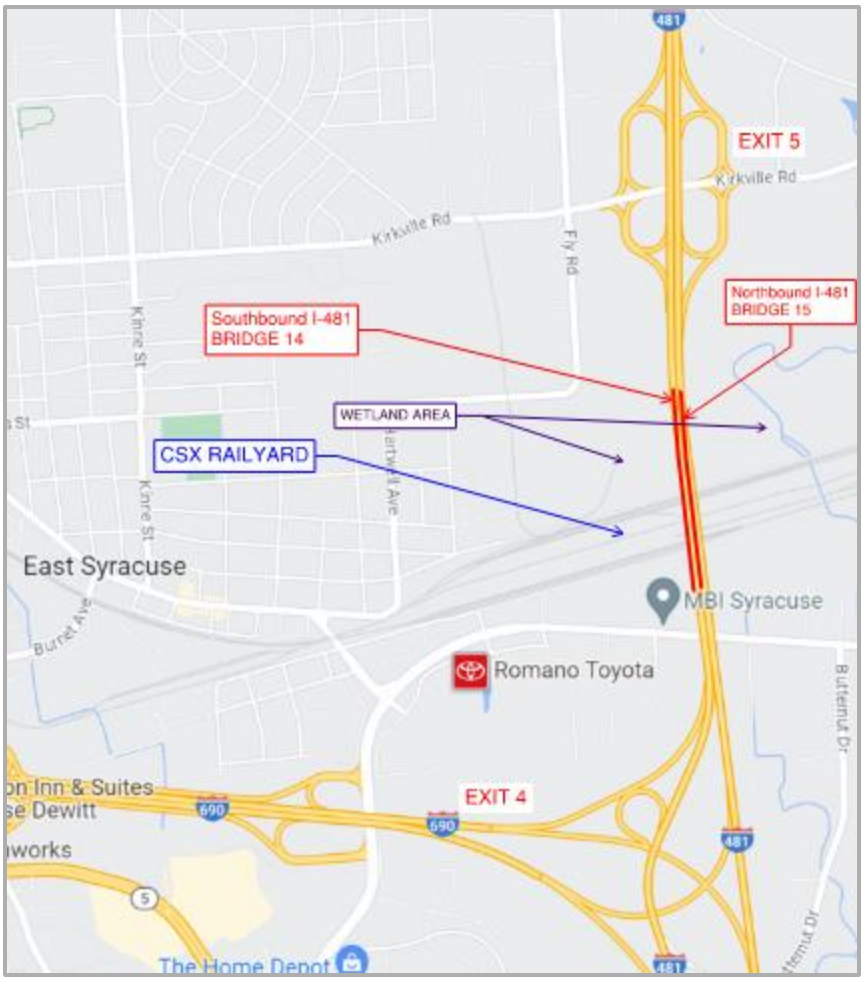


Fig. 1. Location of Bridge and Project Layout

DESIGN CHALLENGES AND SITE CONSTRAINTS

Rehabilitation of any bridge is a challenge by itself due to the many unknowns and lack of sufficient information in the record plans. Key challenges influencing design and construction included:

- Limited access and overhead clearance in the railyard
- Presence of wetlands around the site and restricted work area
- Required minimum 15 ft separation between the pier columns of NB and SB bridges
- Shallow groundwater levels and thick, soft clay layers across the site
- Determination of existing pile capacity with limited information
- Evaluation of pile loading with existing cast-in-place (CIP) piles and proposed steel pipe piles
- Requirement of a refined analysis for the proposed link slab system
- Strict limitations on pile driving tolerance and construction schedules

These constraints required refined analysis and coordination between structural engineers and geotechnical engineers. Iterative analysis was conducted by changing the location of fixed bearings among the piers to develop an optimum design solution. Site constraints required careful planning and sequencing of the construction schedule, while addressing environmental and operational considerations. Figure 2 shows the existing bridges and adjacent wetland area.

 © Deep Foundations Institute 2025



Fig. 2. I-481 Northbound and Southbound over CSX Railyard and Wetland Area

Project RFP drawings indicated widening of the SB bridge towards the outer shoulder and the NB bridge towards the median. After careful evaluation, the design team developed an alternate solution and the widening for the SB bridge was also moved to the median side. This alternate solution minimized impact on the wetlands and facilitated erection of the girders using gantry cranes, thereby expediting the construction schedule. However, there was a limit to how far the foundation could be extended due to the required 15 ft. clear spacing between pier columns of the NB and SB bridges. Due to the limited overhead clearance, increased loading would require installation of new micropiles along the pier. This option was not considered since it would have added more construction challenges and complicated the design with an additional type of supporting pile.

To overcome these issues, the design team opted to extend the pile cap only in one direction away from the existing deck and developed a pile group layout sufficient to satisfy the increased loading requirements. At the abutments, a pile supported retaining wall was introduced to combine the northbound and southbound bridge abutments to increase the stability and capacity of the foundation, eliminating the need for expanding the substructure and foundation at these locations.

ORIGINAL STRUCTURE

Constructed in the 1970s, both the bridges were designed as a 15-span structure supported by 14 multi-column piers. The bridges carried two 12 ft travel lanes with 5 ft to 6.5 ft wide shoulders. Expansion and fixed bearings were installed at each pier location. With this configuration, the load at each pier was limited and within the allowable capacity of the piles. Piers 1 to 6 are located within the CSX railyard, while piers 7 to 14 are located north of the railyard in wetland area.

Based on the available record plans, the length of the existing piles varied from 55 ft to 80 ft. The pile layout also varied by pier, with the number of piles per pier ranging from 24 to 56. The outer rows of piles are battered at a 6:1 ratio (vertical to horizontal). The existing foundation comprised of 12 inch-diameter cast-in-place concrete piles with steel casings. Each pile is embedded 6 inches into the pile cap, with reinforcement consisting of six #6 rebars extending into the pile cap to ensure an adequate pile connection. No data was available on the thickness of the steel casing. Based on localized inspection on-site, the steel casing indicated signs of severe corrosion due to the shallow groundwater.

PROPOSED WIDENED STRUCTURE

For the new widened bridge super structure, link slabs were introduced in place of the existing expansion and fixed joints to minimize the joints in the superstructure and to reduce maintenance over the long term.

 © Deep Foundations Institute 2025

Figure 3 shows a rough deck joint layout with the deck joints existing at three pier locations – Piers 4, 7 and 11. This figure also indicates superstructure fixity with fixed bearing at Piers 2, 5, 9 and 13 and schematic outline of each of the pier footings.

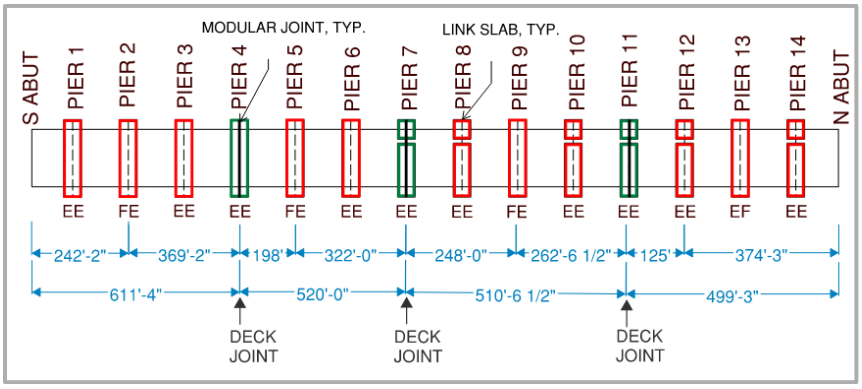
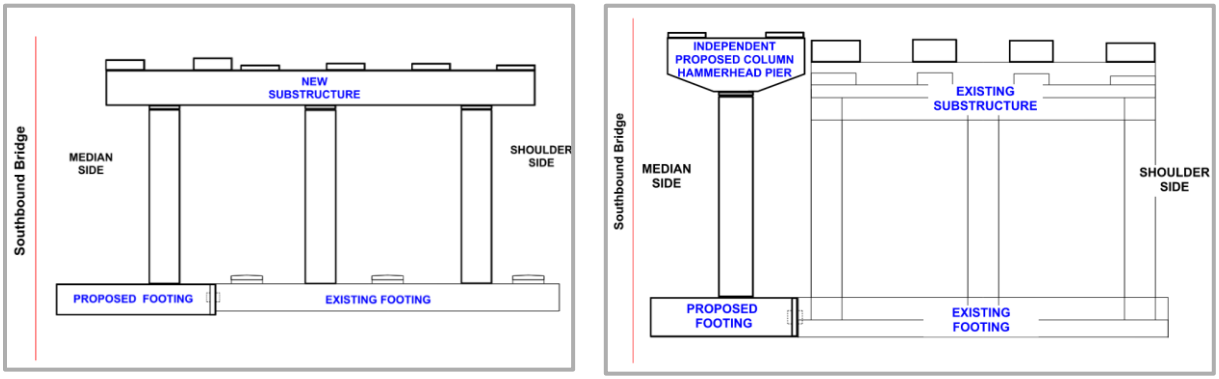


Fig. 3. Deck Joint Layout and Pier Fixity

Existing piers 1 to 5 were removed down to the top of the footings and rebuilt as three-column piers with a pier cap. The footings were also widened towards the median to accommodate the expansion. Figure 4 (a) shows the general elevation and configuration of the piers with the modified substructure. Due to the proximity of the tracks, piers 1 to 5 were fully reconstructed from the columns upward to prevent future disruptions to rail yard operations in the event of possible future bridge repairs. Pier 6 is in the railyard, but being away from the track, a different design was used.



(a) (b)

Fig. 4. (a) Pier 1-5 Elevation View, (b) Pier 6, 9 & 13 Elevation View (Elevation view is of the northbound bridge looking north)

Piers 6, 9 and 13 have a new single column hammerhead pier constructed to the median side of the existing pier to support the widened superstructure. Figure 4 (b) shows general elevation of the configuration of the piers with a modified substructure. Footings are integrally connected to the existing footing due to the higher loading requirement at these piers.

Piers 2 to 6 are provided with crash walls based on AREMA code requirements and the additional deadload was considered as part of the analysis.

 © Deep Foundations Institute 2025

Piers 7, 8, 10, 11, 12 and 14 are similar to Piers 6, 9 and 13 except that the foundation for the new single column hammerhead widened portion is not connected to the existing footing. Figure 5 shows general elevation of the configuration of these piers with an added new substructure.

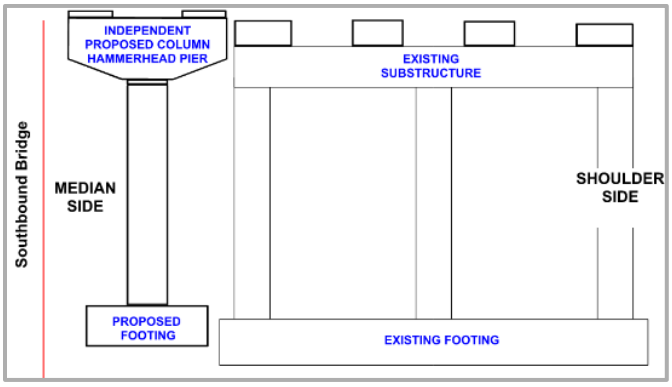


Fig. 5 Elevation View - Pier 7, 8, 10, 11, 12 and 14
(Elevation view is of the northbound bridge looking north)

SUBSURFACE INVESTIGATION

As part of geotechnical subsurface investigation and to evaluate the design soil parameters for the foundation design and analysis, SPT (Standard Penetration Test) and CPT (Cone Penetration Test) borings were conducted along the length of the bridges. The SPT borings indicated that the top layer consists of stiff silt or clay (ML or CH), followed by a soft clay (CL) layer approximately 30 ft to 50 ft thick, underlain by a medium dense sand (SP/SM) followed by a hard silt (ML) layer resembling glacial till. Historical borings in the area confirmed a similar soil profile, suggesting that the subsurface conditions were relatively uniform throughout the site. Figure 6 shows a generalized soil profile of the existing subsurface conditions.

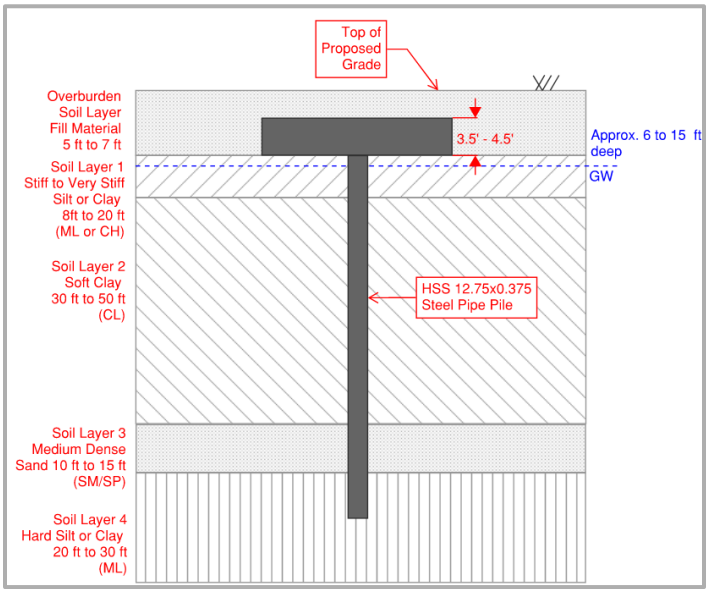
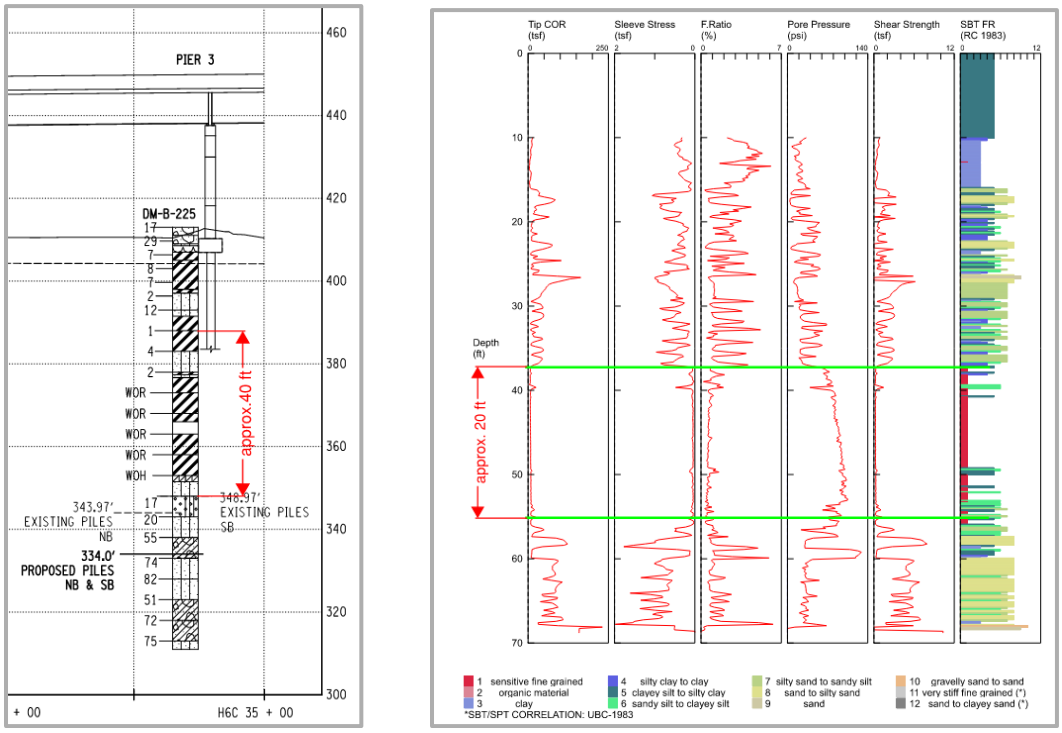


Fig. 6. Generalized Subsurface Soil Profile

 © Deep Foundations Institute 2025

The CPT borings, which provided a more accurate estimate of the soft soil layer thickness, indicated a thickness of 10 ft to 15 ft less than the nearest SPT boring. Figure 7 shows the difference between the soil profile obtained from a SPT boring and a CPT boring performed approximately 120 ft away. The thickness of the soft soil layer reduces towards the north abutment. To account for potential variations in the soil profile, a conservative approach was taken in estimating the proposed pile length, ensuring that the pile tip would extend past the soft soil layer and rest in a competent bearing material.



(a) (b)

Fig. 7. Comparison of SPT and CPT logs. (a) SPT log at Pier 3 (b) CPT log at Pier 2

PROPOSED PILE FOUNDATION

The proposed piles for the expanded foundation consist of 12.75 inch-diameter steel pipe piles with a casing thickness of 0.375 inches, filled with concrete to the full length of the pile. The piles follow the same layout as the existing piles with the outer row of piles battered 6:1 ratio (vertical to horizontal). Piles are embedded 2 ft into the pile cap at piers 1, 5, 6, 9, and 13 to ensure fixed head condition for the piles. Due to the conflict with pier columns, a 2 ft pile embedment was not feasible at the other pier locations. To provide the required moment resistance, the steel casing was embedded 6 inches into the pile cap and provided with required reinforcement (varying from #7 bars to #11 bars) from the piles into the pile cap.

STRUCTURAL ANALYSIS APPROACH – PILE LOADING

As per the project specifications, both the existing and modified substructures can be designed in accordance with the NYSDOT LRFD Bridge Design Specifications (LRFD) or the NYSDOT Standard Specifications for Highway Bridges (ASD or LFD). The new substructure, however, should be designed in accordance with Load and Resistance Factor Design (LRFD). Table 1 summarizes the design criteria applied at each pier.

Initially, an envelope approach was considered, using both LRFD and Allowable Stress Design (ASD) design methods.2 LRFD design methods require higher braking and thermal lateral loads compared to ASD. This resulted in a more conservative analysis, where the existing piles were overstressed by approximately 10 to 15%. Therefore, the analysis was updated to apply ASD for the existing and modified piers, and LRFD for the piers with a new substructure.

Table 1. Design Criteria and Grouping of Piers

Pier	Pile Evaluation & Design
Piers 1, 2, 3, 4, 5, 6, 9, 13 (Modified substructure) Existing Pier 7, 8, 10, 11, 12, 14 (Existing substructure)	ASD
Proposed Piers 7,8, 10, 11, 12, 14 (New substructure)	LRFD

The incorporation of link slabs at several pier locations required the design team to perform a refined analysis to assess the structure's global behavior and determine foundation design loads. Replacing traditional deck expansion joints with link slabs creates a contiguous superstructure segment. Under vertical loads, the superstructure behaves as simply supported at the link slab locations but responds similarly to a continuous multi-span system when experiencing horizontal forces and thermal movements. To capture this complex behavior, structural models were developed that accounted for all forces acting on the substructures and foundations, including the influence of link slabs, bearings, and other relevant modifications. These forces were determined through a relative stiffness analysis, which distributes lateral loads based on the multi-directional stiffness characteristics of the superstructure, bearings, and substructures. This refined analysis reduced overstress on the existing piles at the fixed pier locations, bringing them within allowable limits and ensuring compliance with project requirements.

To further minimize the loading on the piles, the existing fill on top of some of the pile caps was replaced with lightweight fill to reduce the deadload. At Pier 1, the height of the fill was approximately 11 ft. Replacing it with a lightweight fill greatly helped reduce the loading on the piles.

The proposed steel pipe piles were analyzed using the GROUP software. A sample model of the pile group layout is shown in Fig.8. As per the NYSDOT Bridge Manual, an envelope approach is required to determine the controlling forces the entire foundation structure may experience. The piles are required to be designed for fixed head condition and pinned head condition.

Two sets of loads were considered to account for the effects of wind loading from different longitudinal directions, Northwest and Northeast. The change in wind direction influenced the distribution of axial loads. The Northwest wind loading resulted in higher axial loads on the new piles, while the Northeast wind loading caused higher axial loads on the existing piles, as shown in Fig. 9. However, in terms of moment distribution, both wind directions resulted in higher moments on the proposed piles, as seen in Fig. 10. This is due to the increased rigidity of the new piles, which have thicker steel casing and stronger pile connections, leading to a higher moment transfer.

 © Deep Foundations Institute 2025

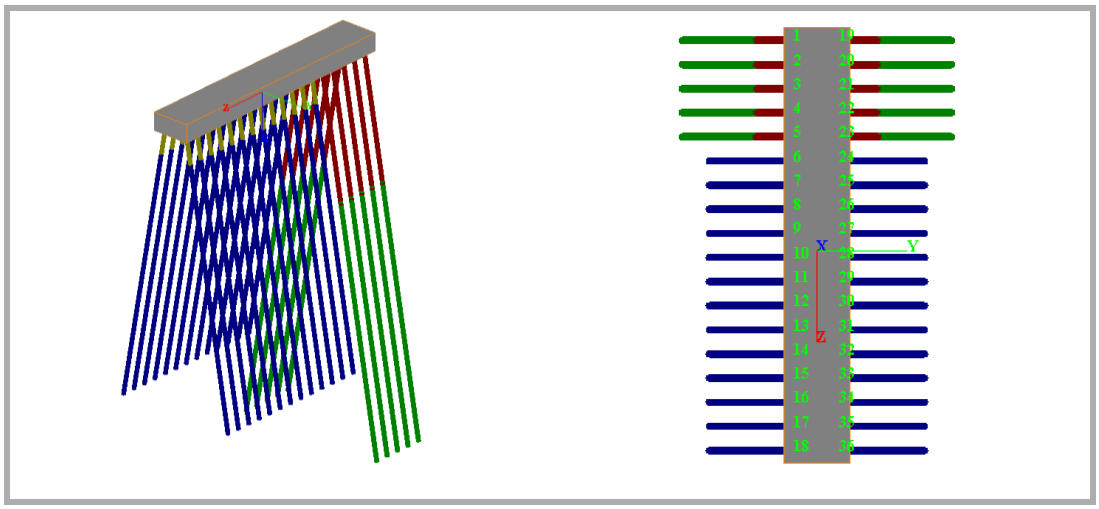
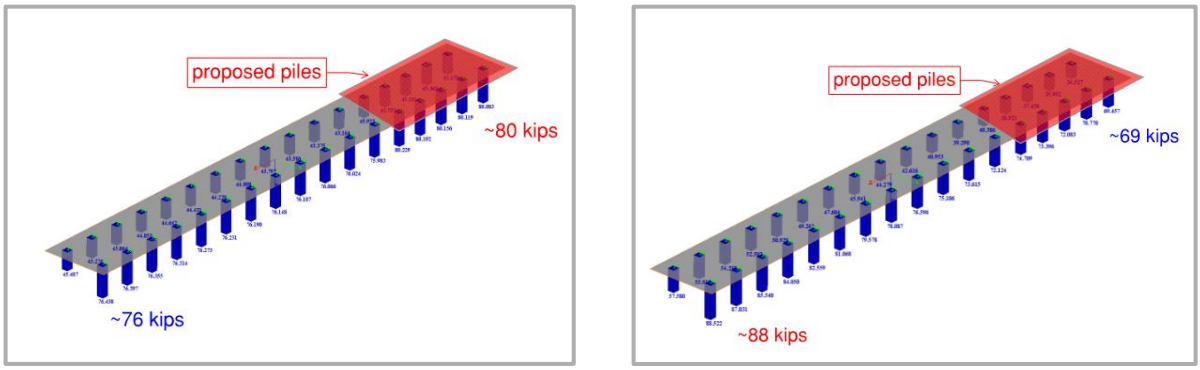
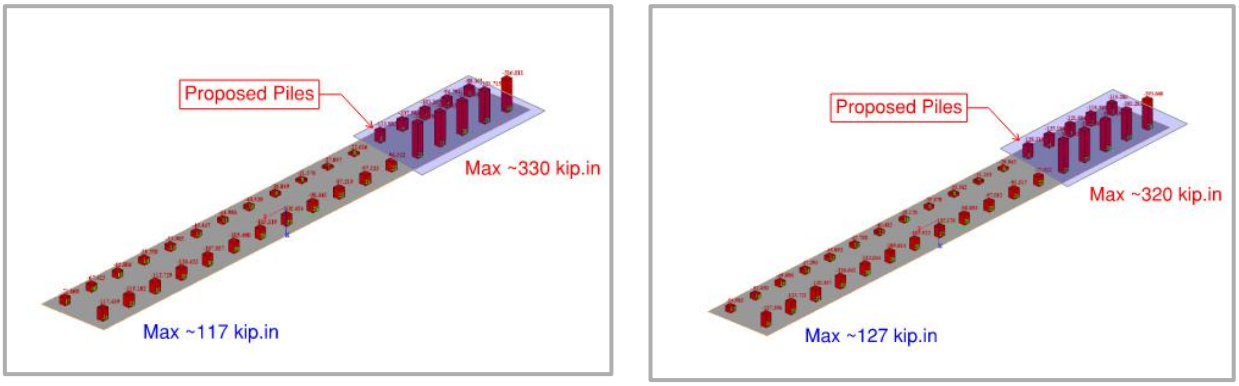


Fig. 8. Sample Pile layout and GROUP model



(a) (b)

Fig. 9. Axial forces in pile group. (a) Wind from NW (b) Wind from NE



(a) (b)

Fig. 10. Transverse moment in the pile group. (a) Wind from NW (b) Wind from NE

 © Deep Foundations Institute 2025

PILE FOUNDATION ANALYSIS

The existing bridge, constructed approximately 50 years ago, was originally designed using the ASD method. According to the bridge's record plans, the allowable capacity of the piles was 35 tons (70 kips). Based on the pile loading analysis, some existing piles at fixed bearing piers were overstressed, mainly due to the proposed link slab system and change in fixity conditions at the piers compared with the original design. Since ASD method of analysis is considered conservative, a design exception was granted to allow a maximum of 5% overstress on the existing piles. Proposed piles were designed with no overstressing. Due to excessive corrosion of the steel casing of the existing piles, these piles were modeled without casing.

For the modified substructures, the piles were checked for both geotechnical and structural capacity using ASD design methods. ASD design method allows the piles to be analyzed for increased overstress of 25% to 50%, depending on the load combinations in Table 3.22.1A - Table of Coefficients γ and β (AASHTO Standard Specifications for Highway Bridges, 17th Edition., 2002). This same overstress factor was applied to the existing pile capacity, which resulted in an allowable capacity range of 78.5 kips to 98 kips depending on the load combination instead of the allowable capacity of 70 kips based on the record plans. For the piles at the new substructures, the geotechnical and structural design was done following procedures outlined in the AASHTO LRFD Bridge Specifications Manual.

CONSTRUCTION CHALLENGES

The installation of long piles was a challenge due to the presence of a thick, soft soil layer. With no resistance from the soft soils, it was difficult to keep the initial pile section to the required alignment for both vertical and battered piles. During the pile-driving process, the top of the piles was not allowed to vary from the planned location by more than three inches. In several instances, the offsets exceeded the three-inch limit. Dynamic pile load testing (PDA) and Case Pile Wave Analysis (CAPWAP) were conducted at each pier foundation to assess the driving resistance. Based on the PDA test results, the piles achieved the required capacity at a shorter depth compared to the design pile lengths. A revised as-built foundation analysis was performed to validate the design with the actual pile locations.

Shallow groundwater conditions posed additional challenges during the placement of concrete for the pile caps. Proper dewatering measures had to be implemented to ensure the subgrade soil was dry before placing the formwork and the concrete.

Some of the new proposed piles were within 3 ft. of the existing piles and required careful maneuvering of the equipment in installing those piles. The piles were driven carefully to the required batter to avoid conflict with the existing piles. Coordinating the work with the railyard schedule also presented scheduling issues. There was only one access road to the pier locations beyond the rail yard, and space for construction equipment was limited.

SUMMARY and CONCLUSION

The widening of the Southbound and Northbound I-481 over the CSX railyard will greatly improve accessibility and mobility along the eastern corridor, fostering economic growth in Syracuse. Bridge expansion and rehabilitation are inherently complex, requiring seamless integration of new structures with existing ones. This project's location posed additional challenges due to soil conditions and project constraints, further complicating both design and execution.

Rehabilitation and modification of any bridge structure presents itself many challenges. With lack of sufficient data for the existing piles and the requirement of utilizing those piles within a new structure requires careful planning and analysis. The complexity of design increased further with the proposed

change in the super structure to link slab system and due to increased loading requirements as per the latest code requirements.

Design of pile foundation required iterative analysis in coordination with the structural engineering team to optimize the loading conditions and to develop an efficient pile layout suitable for constrained site conditions. Combining the new proposed pile cap with the existing pile cap resulted in keeping the pile loading within the allowable capacity of the existing piles. Use of ASD and LRFD methods based on the foundation configuration also helped in minimizing the number of piles required to carry the loads. As part of the refinement of the analysis, existing fill on top of the pile cap was replaced with lightweight fill to reduce the deadload sufficiently enough to keep the overall pile loading within limits.

REFERENCES

New York State Department of Transportation. (2025). *Bridge Manual*.

American Association of State Highway and Transportation Officials, (10th Edition, 2024) *LRFD Bridge Design Specifications.*

American Association of State Highway and Transportation Officials, (2002), *Highway Design Manual.*

American Railway Engineering and Maintenance-of-Way Association (2019), *AREMA Manual for Railway Engineering.*

ACKNOWLEGMENTS

The authors would like to acknowledge the use of ChatGPT (developed by OpenAI) to assist with improving the clarity, grammar, and overall readability of the manuscript. All content and conclusions presented in the paper are the sole responsibility of the authors.

 © Deep Foundations Institute 2025

APPLICATION OF DIVERSE GROUND IMPROVEMENT TECHNIQUES FOR THE STABILIZATION OF REINFORCED EARTH WALL APPROACH RAMPS

Vijaya Bhushan Rao, Author, BAUER Spezialtiefbau GmbH (Dubai Branch), United Arab Emirates, +971 (56) 545 0821, vijay.bhushan@baueruae.ae
Jason Redgers, Contributor, BAUER Spezialtiefbau GmbH (Dubai Branch), United Arab Emirates, +971 (56) 996 0403, Jason.Redgers@baueruae.ae

ABSTRACT

As part of the Kingdom of Saudi Arabia's drive to create a pre-eminent destination, an Elevated Iconic Steel structure supporting a section of elevated road way is being built connecting to lower-level area. The structure has length of 635m, and it projects 60 to 70m above existing ground levels and is supported by multiple columns. The approach ramps towards the structure connecting the piled abutments on both sides are proposed via a Reinforced Earth Wall with heights ranging from 3m to 26m. The sub soil conditions comprising of silty sands and gravels in the top layers were shown to be of collapse potential by inundation due to water ingress., as evident from tests carried out in accordance with the BREA Infiltration test and Plate Load Tests, PLT as per Saudi Building Code SBC 303:2018. Therefore treatment is required to mitigate such issues and ground improvement was proposed to increase the stiffness and shear strength of the underlying ground to be able to withstand overburden loads and limit post construction settlements on the road surface to ensure smooth traffic flow and transition between the piled structure and treated approach ramps. The specifications allowed for various measures to the consultant's satisfaction, Deep Soil Mixing technique in the areas where maximum heights of the reinforced earth walls are located and an average target unconfined compressive strength, UCS of 1.5 MPa and a minimum ground stiffness of 200 MPa requirements are specified. For the areas with lower heights of reinforced earth walls, minimal treatment comprising of vibro-replacement-stone columns for deep treatment supplemented by further surface compaction techniques for near surface treatment using Rapid Impact Compaction, RIC, and High Energy Impact Compaction, HEIC are applied. Quality assurance testing consisting of Wet Grab Sampling, Zone Load Tests, ZLT and Cone Penetration Tests, CPT were carried out for verification of ground improvement.

Keywords: Approach Ramp, Reinforced Earth Walls, Soil Mixing, Unconfined Compressive Strength, UCS

INTRODUCTION

The project comprises of an elevated steel structure supporting a section of elevated high-speed road. It is envisaged to be an iconic structure. The proposed structure has length of 635m, and it projects 60-70m above existing surrounding ground levels and shall be supported by multiple columns (V structures).

The approach ramps towards the structure are proposed Mechanically Stabilized Earth Walls (MSE walls) or Reinforced Earth walls on the North and South sides connected to the piled Abutments and heights ranging from minimum 3m to maximum of 26 m, where the MSE wall connects to the Abutment. The scope of work consists of improving the soil conditions beneath the MSE ramps by increasing its stiffness and shear strength to withstand loads and limit post construction settlements on the surface to avoid any roadblocks and ensure smooth traffic flow and transition between the structure and approach ramps.

The main scope of works consists of construction of approach ramps 1 and 2 hereafter considered as north and south ramps towards the steel structure using Mechanically stabilized earth walls, MSE walls.

 © Deep Foundations Institute 2025

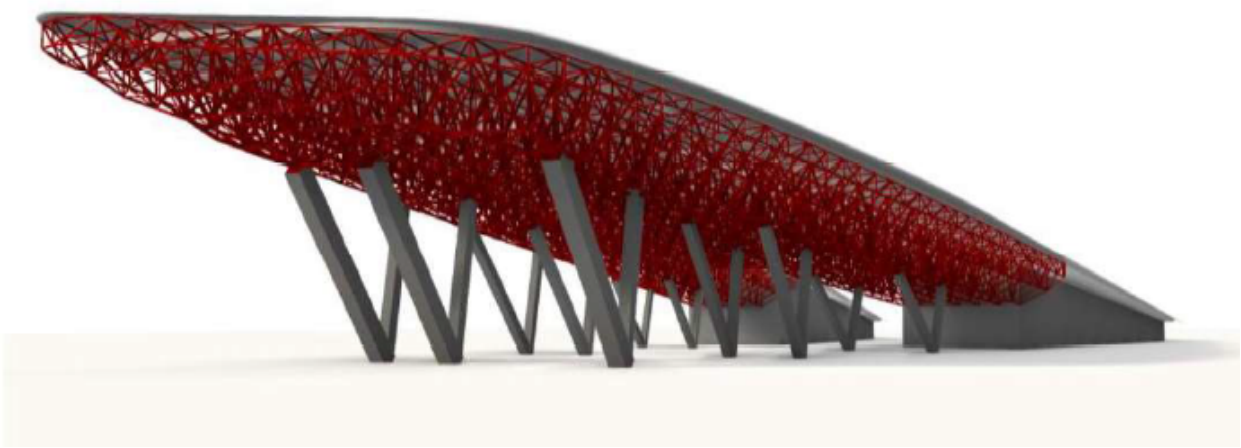


Fig. 1. Perspective view of the structure

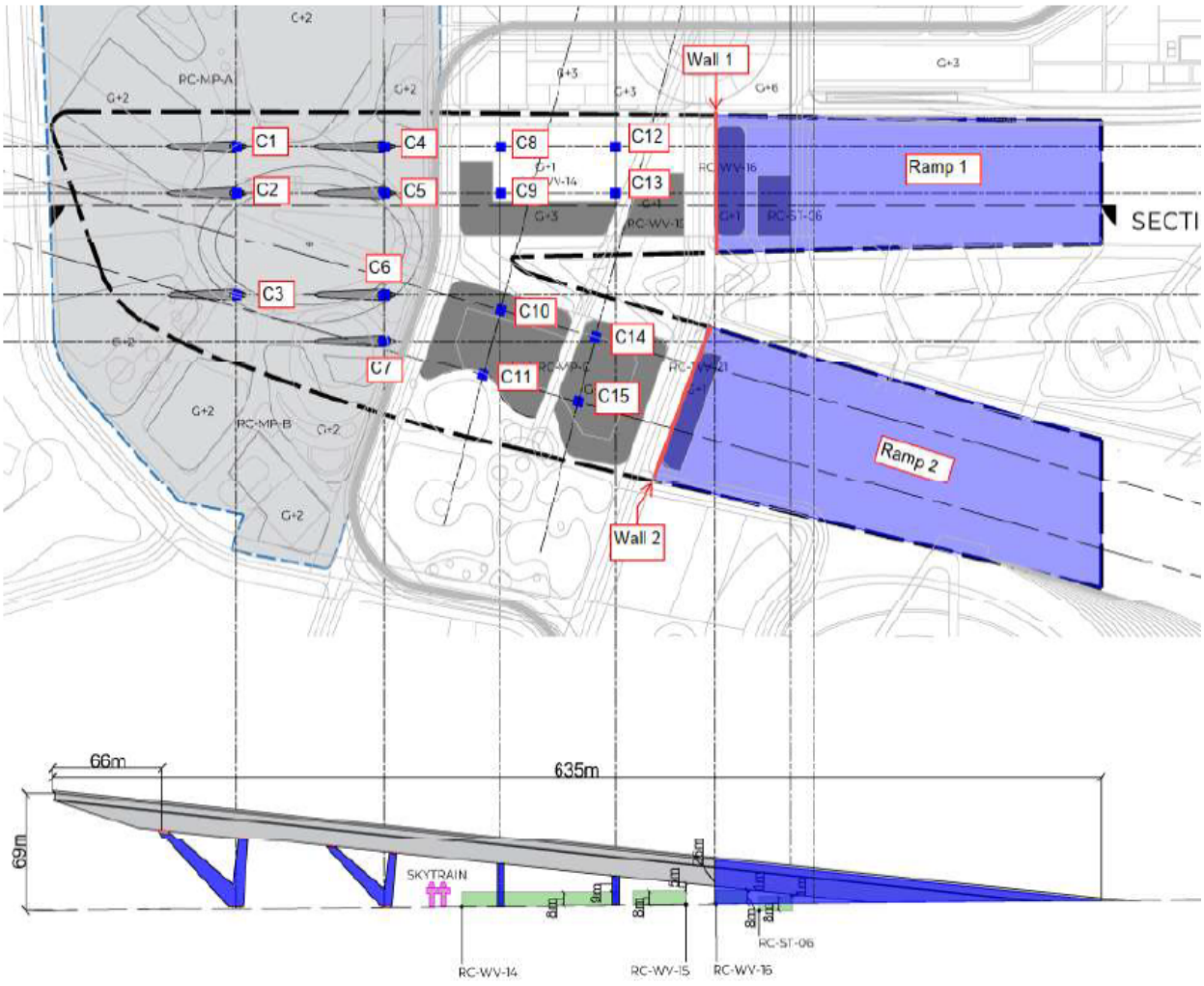


Fig. 2. Layout of North and South Approach Ramps towards the structure

 © Deep Foundations Institute 2025

The areas under the ramps are further divided into Zones 1 to 5 as follows with Zone 1 and Zone 4 located in the maximum MSE wall height locations where the MSE wall connects to Abutments.

North Ramp:

- Zone 1 (MSE Height 26 ~ 16m)
- Zone 2 (MSE Height 16 ~ 8m)
- Zone 3 (MSE Height 8 ~ 4m)

South Ramp:

- Zone 4 (MSE Height 26 ~ 16.5m)
- Zone 5 (MSE Height 16.5 ~ 9.0m)

The existing soil conditions in these zones to be treated accordingly to withstand the anticipated loads from the respective reinforced fill heights of MSE walls and reduce settlements to allowable limits

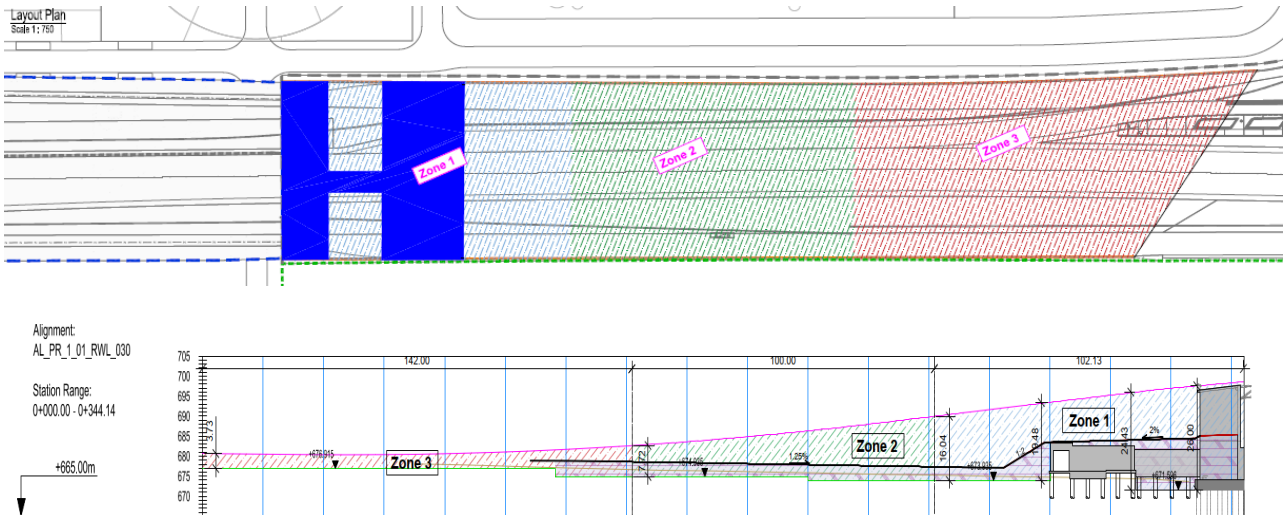
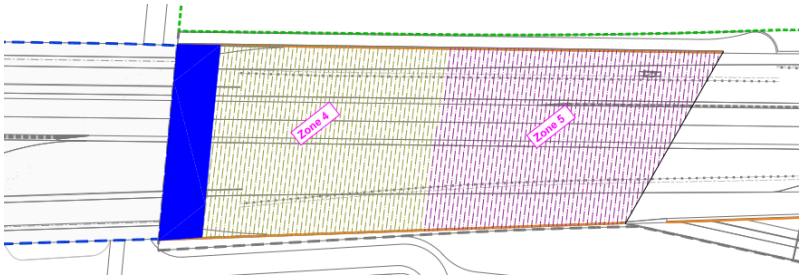


Fig. 1. Layout and Longitudinal Section of North Ramp



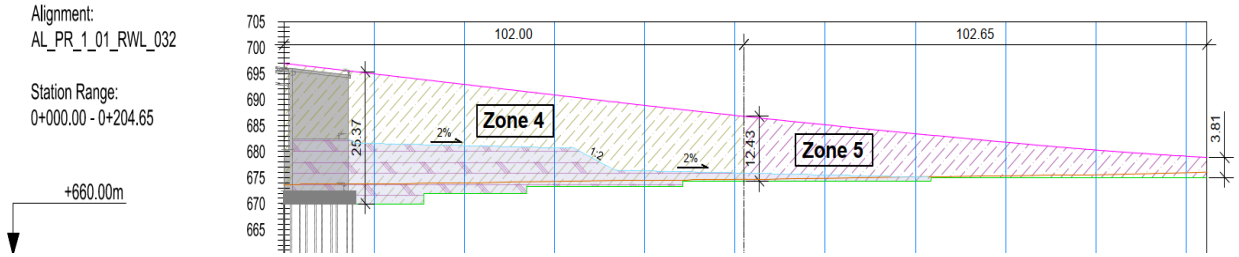


Fig. 4. Layout and Longitudinal Section of South Ramp

 © Deep Foundations Institute 2025

SOIL CONDITIONS

The representative boreholes in the North ramp are BH 18 and BH 20 and for the South ramp are BH 19 and BH 21 as shown in the Borehole layout below.

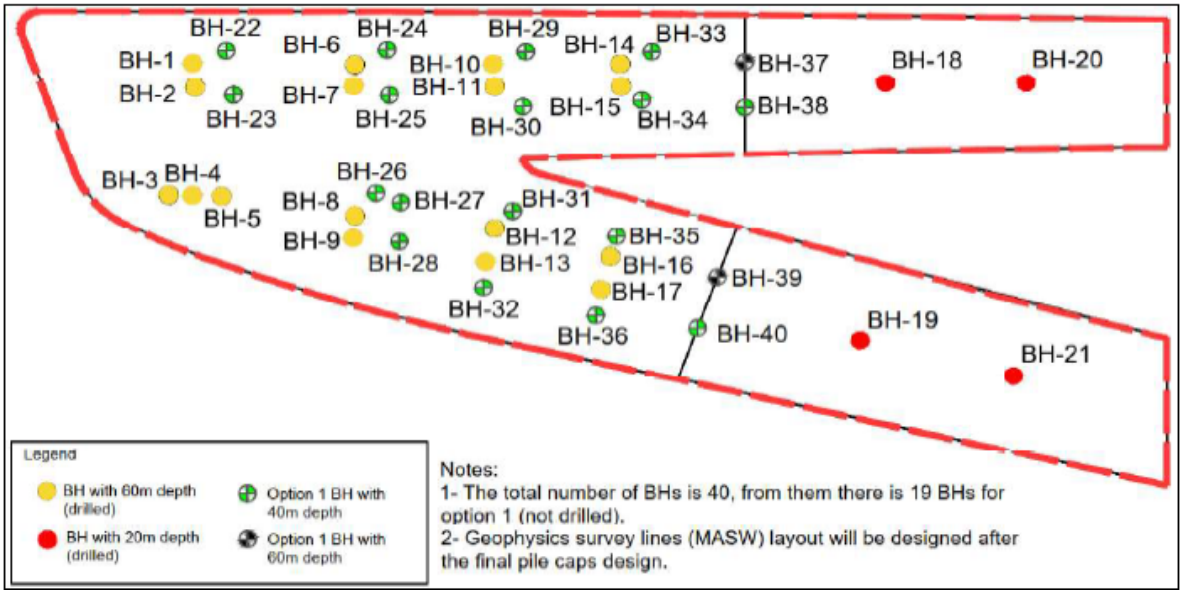


Fig. 5. Borehole Layout

The SPT N vs Fines Content vs Elevation of the Boreholes BH 18 & BH 20 at the North Ramp and of the boreholes BH 19 & BH 21 at the South Ramp as shown below:

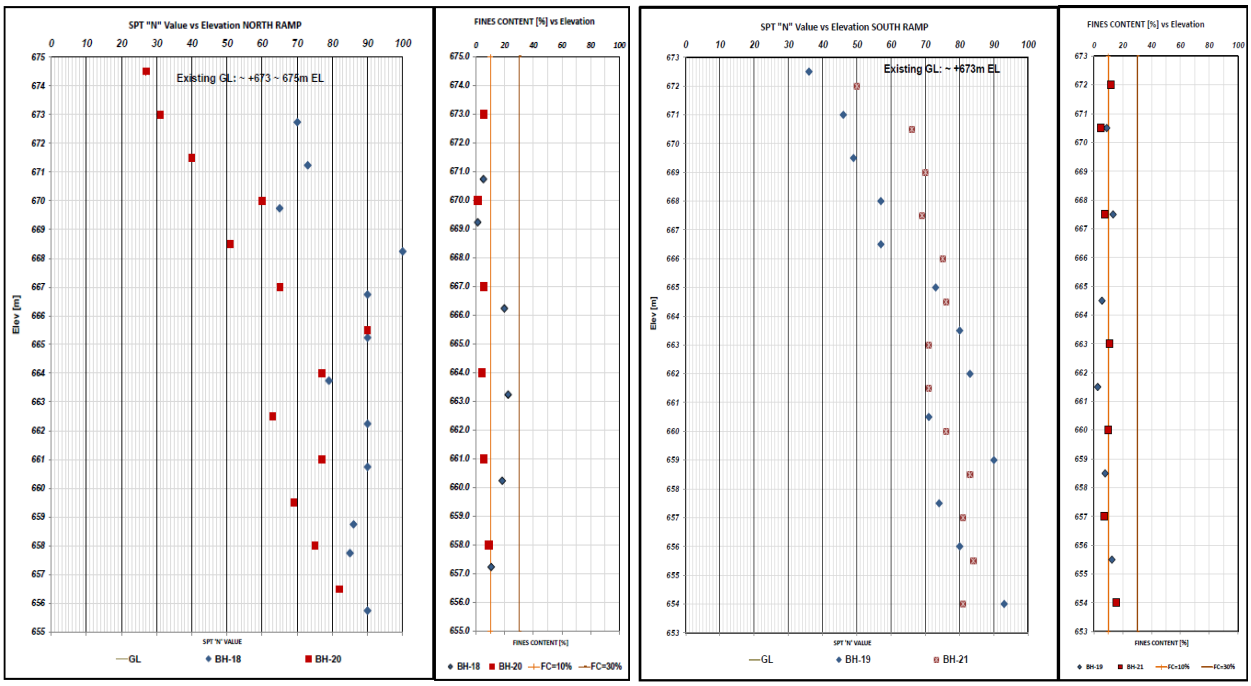


Fig. 6. SPT N vs Fines Content vs Elevation at North and South Ramps

 © Deep Foundations Institute 2025

The factual report describes this formation as Dense to very dense, medium to coarse grained Silty SAND and Gravels, and Gravel sheets formation. SPT N values range from 27 to 100 with average 80. The soil is classified as mainly silty to very gravely fine to medium SAND, with the percentage of Gravel ranging from 20.5 to 44.5 % in the uppermost 6m and reducing with depth. The soil is mostly non-plastic.

Additional Geotechnical Investigation (GI) has been carried out to assess the collapse potential of the Superficial Soil under the proposed MSE Wall locations. The tests were carried out in accordance with the BREA Infiltration Test and Plate Load Test specified in the Saudi Building Code SBC 303:2018 clause 10.3.2.1.3. A total of twenty (20No.) tests were performed on a staggered grid pattern along the proposed alignment of the MSE Walls as shown below. It should be noted that all the tests were undertaken at the foundation level of the proposed MSE wall inside the trial pits.

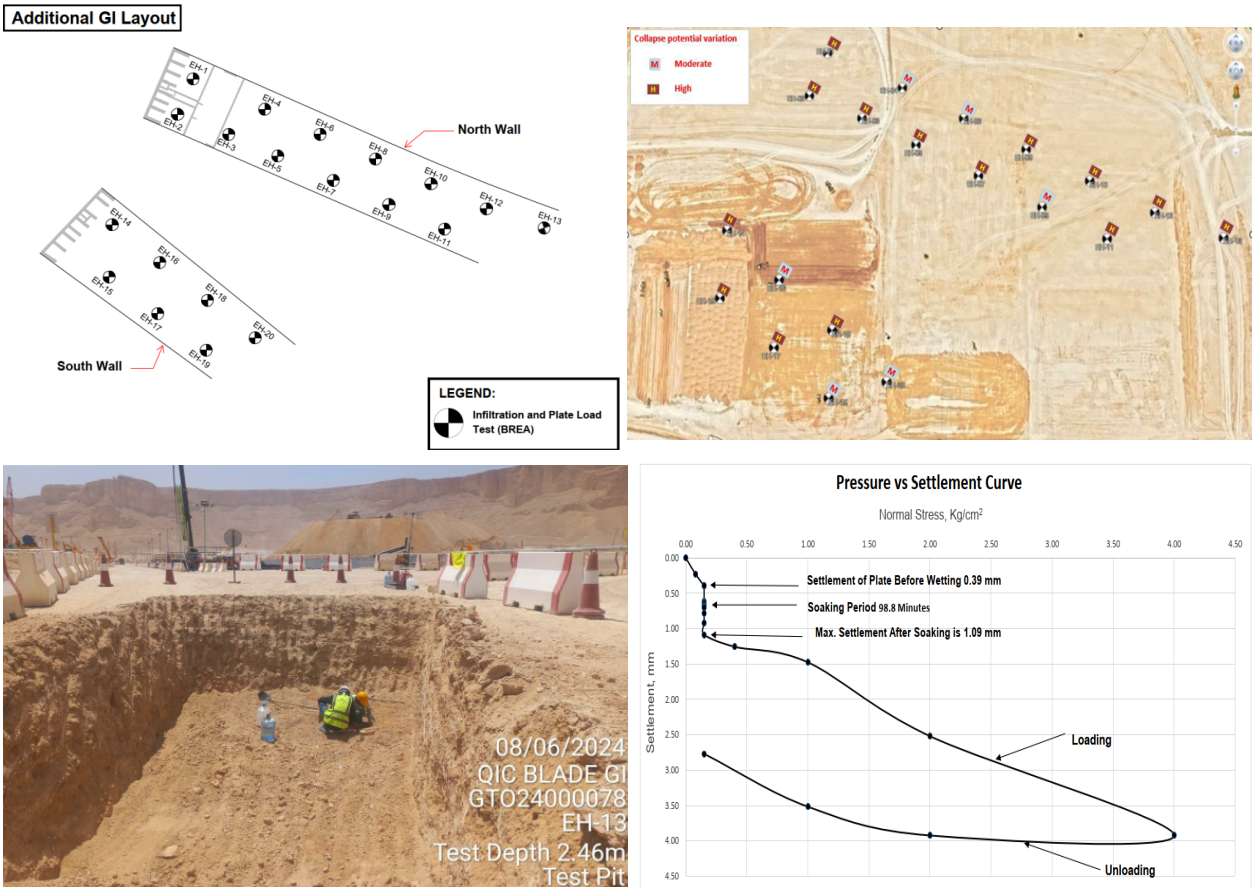


Fig. 7. BREA Infiltration and Plate Load Test locations and Results

The results of the tests indicated that the Superficial Soils exhibited 70% of the samples characterized as having high collapse potential and 30% of the samples testing has moderate collapse potential. The analysis of the Plate Load Tests, PLT results indicated a 60% of reduction in soil stiffness (Young's) modulus after wetting, which will result in potential excessive settlement of the proposed MSE Wall structures if not mitigated.

The very dense soil profile encountered at depth has a relatively low permeability compared to the overlying soil profile. Therefore, the very dense soil profile is not expected to exhibit significant collapse potential on wetting.

As such, ground treatment has been specified in the upper soils encountered above the very dense soil horizon. Based on the above findings, although the required treatment depth below the foundation level varied from 3 to 7.5m, to maintain the consistency and provide a homogeneous treatment, a general treatment depth of 7.0m was proposed to be undertaken within the footprint of MSE walls.

GROUND IMPROVEMENT DESIGN

Taking into consideration of these soil conditions, as a first measure of improvement, is to collapse the soils as they could be considered dry of optimum moisture content. This can be done by first pre-boring the ground on a defined grid to loosen the subsoils and undertake the necessary forms of ground improvement as required in each zone elaborated as below:

ZONE 1 AND ZONE 4

As the maximum height MSE walls are in Zone 1 and Zone 4 and connected to Abutments that are supported on piles, so pursuant to ground improvement specifications, the average unconfined compressive strength, UCS of the selected working columns shall be a minimum of 1.5 MPa and a minimum stiffness of 200 MPa shall be required to meet the embankment settlement tolerance. Therefore, to achieve the above specified criteria, the proposed ground improvement technique shall be implemented in Zone 1 and Zone 4.

- Pre-boring using 660mm Dia ϕ tool on 2.25 x 2.25m Triangular grid
- Soil Mixing Columns, SCM with 2000mm Dia on 2.25 x 2.25 Triangular grid
  (In this case, the in-situ soils are mixed with an injected cement slurry to generate the stiff composite material to carry the proposed imposed loads and control settlements)

ZONE 2, ZONE 3 AND ZONE 4

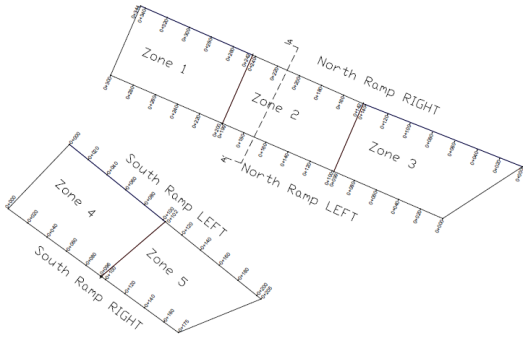
As the relatively lower height MSE walls located in Zone 2, Zone 3 and Zone 5, minimal treatment of the ground is required to increase the stiffness of ground sufficiently enough to be able to withstand loads from MSE wall heights and limit post construction settlements on the surface. As such the following sequence of ground improvement works are proposed and shall be implemented in Zone 2, Zone 3 and Zone 5.

- Pre-boring using 660mm Dia ϕ tool on 2.5 x 2.5m Triangular grid.
- Vibro replacement/ Stone Column with 900mm Dia on 2.5 x 2.5m Triangular grid (in the pre-bored locations) for deep treatment to increase the composite stiffness of ground.
- Surface Compaction Techniques using Rapid Impact Compaction, RIC on 3.0 x 3.0m Triangular grid and High Energy Impact Compaction, HEIC techniques for near surface treatment of ground.
  (In this case, granular columns are installed on a defined grid pattern for 7m depth for deeper treatment and near surface soils are compacted using surface compaction techniques. The resulting composite ground in combination with compacted surface provides the necessary stiffness for the ground to carry the imposed loads and control settlements)

ZONE 1 AND ZONE 4 – DEEP SOIL MIXING, DSM

In Zone 1 and Zone 4, to meet these heavy requirements of achieving UCS of 1.5 MPa and a minimum stiffness of 200 MPa, ground treatment using Deep Soil Mixing, DSM technique is specified. As the maximum height of MSE walls in the order of 26m located in Zone 1 and Zone 4, and for the specified unit weight of reinforced fill = 21.5 kN/m3 and proposed surcharge of 20 kN/m2, higher loads in the order of 79 kN/m2 are anticipated in these areas. DSM requires the use of a slurry pump and specially designed mixing auger to combine the in-situ soils with the cement slurry to provide a homogeneous mixed material.

The DSM design methodology is in accordance to specified FHWA manual - Federal Highway Administration Design Manual: Deep Mixing for Embankment and Foundation Support Publication No. FHWA-HRT-13-046, which follows the typical design configuration and layout of DSM columns under the embankment loads as shown in the figure below.



The overall dimensions, grid spacing, diameter and location of the DSM columns has been selected to satisfy settlements, stability requirements and ensure the structural capacity of the DSM column.

Isolated columns are the most common configuration for withstanding loads and reducing settlements below infrastructure embankments. As there are no side slopes and treatment is only required under the vertical sections for the MSE wall, a cost-effective combination based on isolated DSM columns has been considered in the design to withstand the specified loads and reduce settlements to tolerable limits.

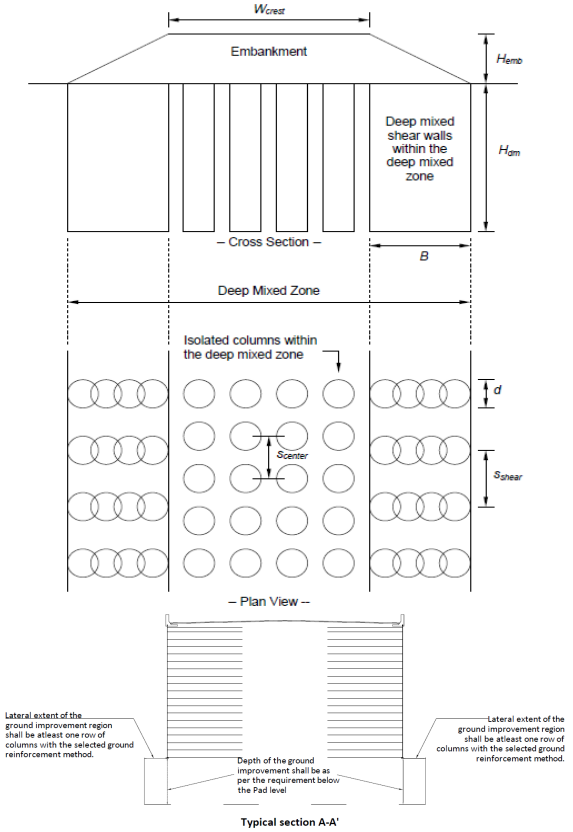


Fig. 8. Specification requirements of treatment

Design Criteria: Deep Soil Mixing, DSM

- Target Design strength (unconfined compressive strength) UCS, qdm = 1.5 MPa
- Stiffness/Modulus of DSM column considered, Edm = 300 qdm (for wet mixing, FHWA manual) = 300x1.5 ~ 450 MPa
- Design Diameter of DSM column, Ø = 2.0m; Average Stiffness of soil = 30 MPa

Based on approach embankment/MSE wall heights and loads imposed to the ground, the following design criteria have been implemented:

Required Area Replacement Ratio, ARR [%]

$$a_{s,center} \geq F_{cc} \frac{q}{2 s_{dm} f_v}$$

Fcc = Factor of safety against crushing of the center isolated columns
Sdm = Shear strength of deep mixed ground

$$s_{dm} = \frac{1}{2} f_r f_c q_{dm,spec}$$

qdm = Unconfined Compressive Strength, UCS

Vertical Stress [kPa]	579
Required ARR [%] @ centre using UCS = 1.5 MPa	66.2%
Provided ARR [%]	71.7%
Proposed Grid Spacing , Triangular [m x m]	2.25 x 2.25
Composite Modulus, Dc [MPa]	330.4

 © Deep Foundations Institute 2025

Based on the design guidelines following FHWA manual, design value for the undrained shear strength of the deep mixed ground (Sdm) is estimated from the specified (qdm = UCS) which is essentially considered commonly as half of the UCS value and corrected for fc = curing factor and fr

fc = curing factor, which is the ratio of UCS at time "t' to the unconfined compressive strength, UCS at 28 days, t = curing days. The fc is determined using the estimated time, t between mixing and application of 75% of the proposed embankment height from the equation fc = 0.187 ln (t) + 0.375

As such curing factor, fc can be used from 28 to 365 days between mixing and application of 75% of the proposed embankment height. The fc value ranges from 1.00 for 28 days to 1.48 for 365 days i.e., 1 year. Assuming curing time, t = 28 days between mixing and application of 75% of the proposed embankment height, the fc value considered is 1.0.

fr = factor considered to account for the differences between unconfined peak and confined large strain strengths and typically range from 0.65 to 0.9, and a value of fr equal to 0.8 is recommended for application to transportation embankments. The factor fv accounts for the probability that the actual deep mixed strength exceeds the specified deep mixed strength and following FHWA guidelines a value of 0.95 considered in design.

Then the required/necessary ARR (%) which is defined as the ratio of the column area to the tributary soil area surrounding the column, and if the columns are arranged in a square array, then considered as the area of square based on grid spacing between the columns determined. Based on the estimated value of shear strength and the loads, which is q, vertical stress imposed on the ground, allowing for possible crushing below the centre of an isolated column as well as a variation in strength considering a recommended factor of safety, Fcc of 1.3 against crushing of the center isolated columns.

Thus, from the studies and calculations as above, an Area Replacement Ratio (ARR [%]) of 66.2% is required to prevent the possible crushing below the center of an isolated column considering a recommended factor of safety of 1.3 against crushing. The provided Area Replacement Ratio ARR [%] considering a 2.0m Diameter ϕ column on a grid spacing of 2.25 x 2.25m Square is in the order of 71.7% resulting in an overall composite ground stiffness > specified 200 MPa.

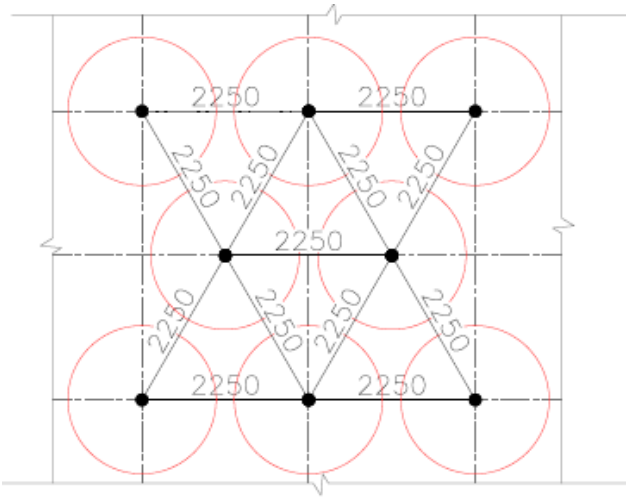


Fig. 9. Typical 2.25 x 2.25m c/c Triangular grid configuration of Soil Mixed Columns 2.0m Dia ϕ

The proposed Area Replacement Ratio, ARR [%] are exceeding than the required values and all the anticipated settlements shall occur during the construction stage with the negligible post construction settlements occurring from the surcharge loads. The concern with soil mixing is ensuring the mix quality and also the mix chemical composition to samples and trial mixes are essential to fine tune the additives and cement content and to ensure the long-term quality. The mix design shall be established in two stages. First, defining the slurry quantity required for the adequate liquefaction of the soil, in dependence of the moisture content of the soil, its granulometry and cohesive content. Based on the slurry quantity required for liquefaction, the cement factor required for the achievement of the specified mechanical properties of the final DSM material - average Unconfined Compressive Strength of min.1.5 MPa and a Modulus of Elasticity not below 200 MPa – is established as an envelope. In the second stage those mixes shall be verified by trial columns on site.

 © Deep Foundations Institute 2025

The technique chosen for this project is single column mixing (SCM) whereby in situ soils are mixed with a binder in a process involving rotation of a single mixing tool (paddle with auger starter) into the soil while simultaneously injecting the binder. The mixing tool is drilled into the ground at a continuous rotation speed. The soil is cut by the auger which contains two blades equipped with drill bits and a central pilot (stinger). At the same time, grout is pumped through a flexible hose to the nozzles located at the lower blade of the mixing tool. Here the soil is mixed with the slurry as part of the cutting process. The grout injection rate will be controlled by the rig operator in compliance with the minimum cement content stipulated in the DSM design. After reaching the design depth, the mixing tool will be withdrawn. Slurry can still be added during the withdrawal process in line with DSM design requirements.



Fig. 10. Details of Single Column Mixing Installation Technique and Procedures

 © Deep Foundations Institute 2025

ZONES 2, 3 AND 5 – DEEP TREATMENT AND SURFACE COMPACTION TECHNIQUES

As explained in the ground improvement design section, after pre-drilling -Vibroreplacement / stone columns carried out in the prebored locations on a 2.50 x 2.50m triangular grid essentially performed to liquefy and collapse the ground by mechanically induced vibrations from the vibrators, the void or annulus thus formed is maintained by means of water flushing. This method then involves the introduction of backfill material – stone gravel into a void in the ground made by penetrating the vibroflot to the design depth as needed. The backfill is then compacted in increments by successive withdrawal and re-penetration of the vibroflot to form a column throughout the treated soil layers and therefore rearranging the particles into a denser state ensuring the void closure due to vibration and wetting. As the supplementary techniques to vibroreplacement / stone columns, surface compaction methods using Rapid Impact Compaction, RIC and High Energy Impact Compaction, HEIC methods followed to ensure the near surface top 3 to 4m thick ground layer is well compacted to maximum density and all voids are closed. Brief description of these methods are as follows:

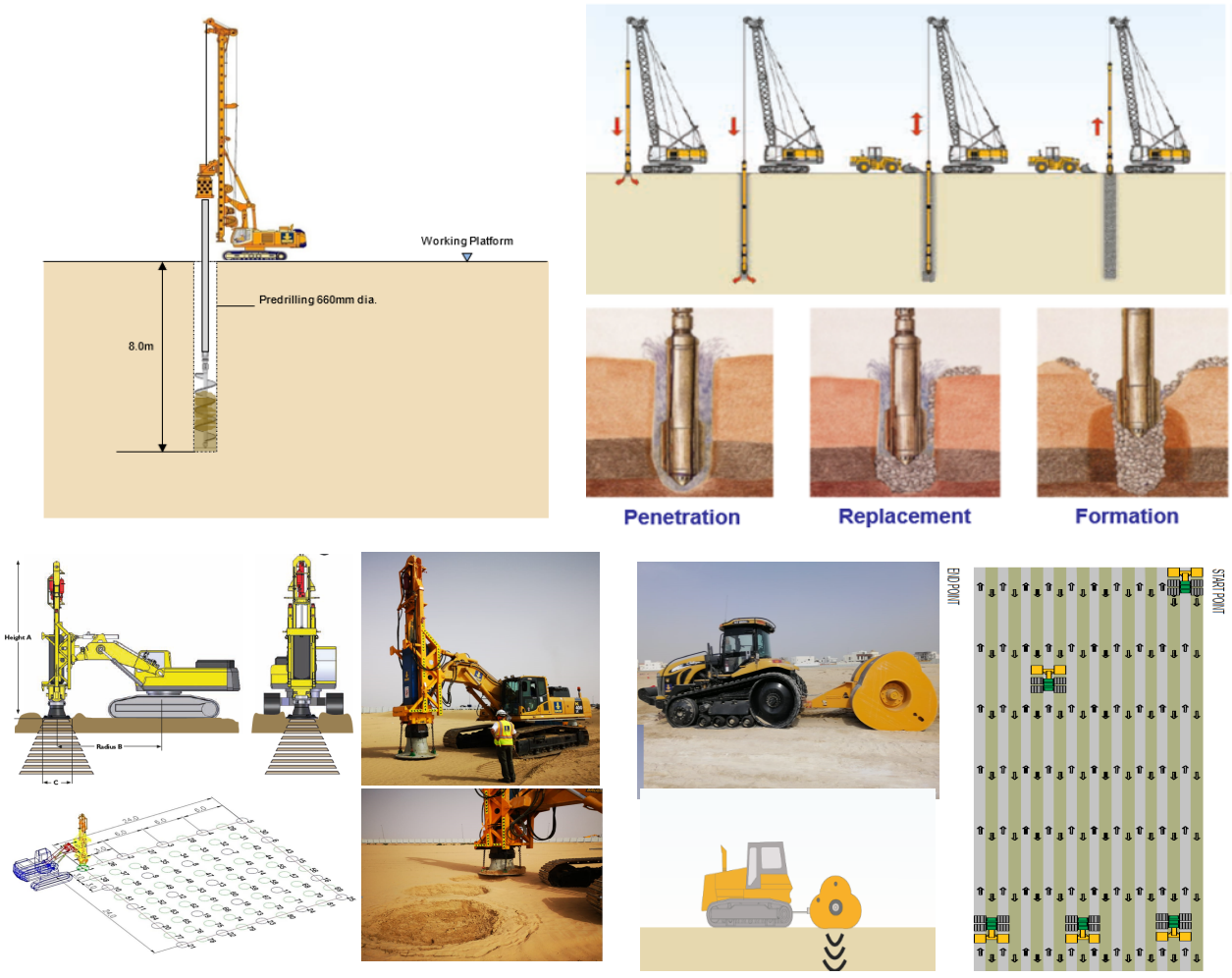


Fig. 11. Preboring, Stone Columns, RIC and HEIC Techniques implemented in Zones 2,3 & 5

Rapid impact compaction (RIC) is a soil densification method whereby a hydraulic hammer (9 tonnes) is raised up to 120cm and repeated strikes on to a 1.5m diameter foot in contact with the ground. The RIC technique is typically suitable for soils with less than 15% of fines content (i.e. passing the 63-micron sieve).

 © Deep Foundations Institute 2025

The energy due to the hammer is transferred to the underlying soil and rearranges the soil particles into a denser state, which means an increased density of soil, angle of friction and overall stiffness.

High Energy Impact Compaction, HEIC technique involves the dual drum – 3 or 5 sided Triangular 25 kJ High Energy Impact Compactor, towed by a crawler-based hauler of sufficient engine power and of sufficient capacity to maintain an optimal compactor towing speed (7.5 – 9 mi/h 12-15 km/h) on a maximum uphill gradient of 5%. The impact compactor compacts the area in tracks or lanes. The treatment area is divided in the 3m wide tracks as per equipment dimension. The roller is passed from each lane 30 – 40 times to achieve the sufficient compaction.

VERIFICATION TESTING

In the areas of Zone 1 and Zone 4, where soil mixing was proposed, Zone Load Test, ZLT carried out on soil mix columns for the working load/stress of 575 kPa and maximum load/stress of 200% working load applied over 3m x 3m i.e., 9 m2 area. As per the specs, the final settlement corresponding to the working load shall not exceed 12.5mm i.e., a subgrade modulus of at-least 46MPa/m shall be achieved.

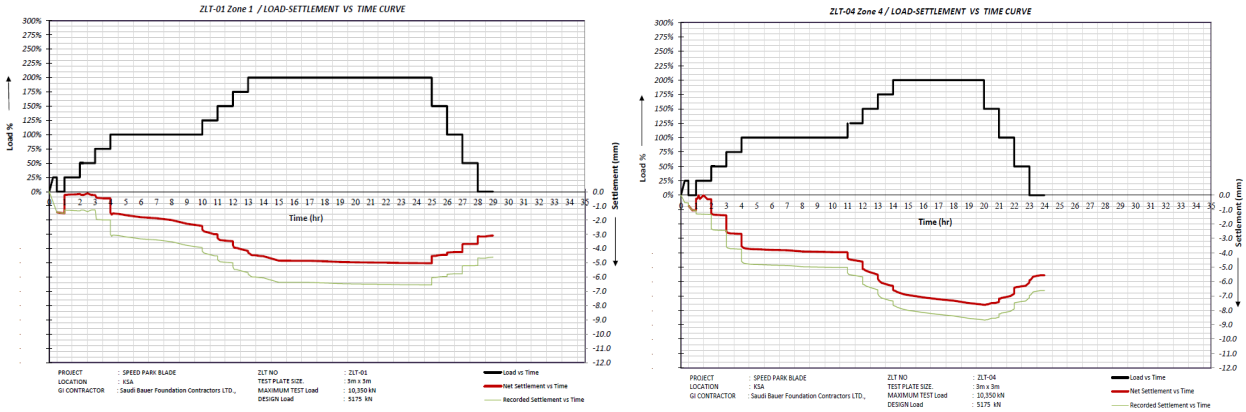


Fig. 12. Trial Zone Load Test, ZLT results in Zone 1 and Zone 4

However, the actual settlements measured in Trial Zone Load Test, ZLT results in Zone 1 and Zone 4 are much lower in the order of 3 to 5mm at the working load and 5 to 8mm even at the maximum load i.e., 200% of working load, still lower than the specified target settlement of 12.5mm at the working load. Further wet grab sampling carried out from the freshly produced soil mix columns for testing of UCS strength and stiffness. Total 360 Compressive Strength Tests were performed at various depths and results verified after 7 days and 28 days respectively.

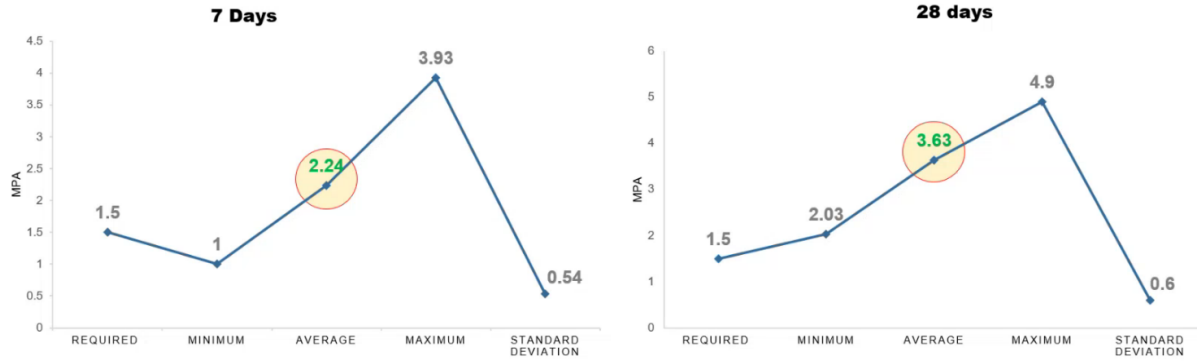


Fig. 13. Deep Soil Mixing Compressive Strength Testing Results

 © Deep Foundations Institute 2025

In the areas of Zone 2, Zone 3 and Zone 5, Field verification testing comprising of Cone Penetration Tests, CPTs were carried out post improvement and all the PostCPTs encountered early refusals within the top 1 to 1.5m depth ensuring the increase in the stiffness of ground. Further Tests were preferred to carry out in these Zones as these are not critical for the project performance.

RESULTS AND CONCLUSIONS

Understanding the soil conditions and more importantly the collapse potential in the upper layers, specific project performance requirements and sensitivity to settlements at the maximum height of Reinforced Earth Wall locations, where they are connected to piled abutments, more robust technique of Deep Soil Mixing, DSM is applied. Whereas in the areas of lower height of Reinforced Earth Walls, cost effective treatment techniques applied to treat for the minimum requirements of bearing capacity and settlements. Verification tests results are satisfactory. However, it should still be noted that Reinforced Earth wall is built in layers (20 – 80cm layers typically) and that this will mean the load is added to the treated ground in approximately by 20 kPa intervals, and majority of settlements expected to occur during the construction stage and negligible settlement at the road surface after construction is completed.

REFERENCES

Federal Highway Administration. 2013. Federal Highway Administration Design Manual: Deep Mixing for Embankment and Foundation Support. Publication No. FHWA-HRT-13-046

The Saudi Building Code Structural Requirements for Soil and Foundations - BREA Infiltration Test and Plate Load Test. Publication No. SBC 303:2018

 © Deep Foundations Institute 2025

MULTIOBJECTIVE OPTIMIZATION OF DRILLED SHAFTS IN THE CIRCUNVALACIÓN NORTE VIADUCT USING PARETO-FRONT ANALYSIS

Bernardo Jiménez, Research Affiliate, Dept. of Civil Eng., University of São Paulo, Brazil, b.jimenez.geotech@gmail.com
Adrián Torrico Siacara, Associate Professor, Dept. of Civil Eng., University of São Paulo, Brazil, adrian.torrico@usp.br

ABSTRACT

This study focuses on the multiobjective optimization of drilled shafts for the Circunvalación Norte viaduct project in Costa Rica, utilizing the Pareto-Front method. The viaduct is supported by 58 piles, consisting of 426 drilled shafts, and an efficient design must balance the minimization of shaft length or quantity with maximizing their resistance to ensure structural safety. Both Deterministic Design Optimization (DDO) and Reliability-Based Design Optimization (RBDO) are applied, with the resistance of each drilled shaft modeled using random variables (RVs) to account for the inherent variability in soil conditions and material properties. The Pareto-Front method addresses these conflicting objectives by identifying optimal solutions that offer a trade-off between the two criteria. The optimization process involves calculating the total drilled shaft length for each pile and its corresponding resistance, then applying the Pareto-Front technique to determine the best compromise. These configurations are considered Pareto-optimal, as no improvement can be made in one objective without worsening the other. This approach not only enhances the design efficiency of the Circunvalación Norte viaduct but also demonstrates the effectiveness of the Pareto-Front method in large-scale civil engineering projects. By integrating multiobjective optimization, the project effectively balances economic and safety goals, establishing a benchmark for future infrastructure developments.

Keywords: Pareto-front, multi objective optimization, drilled shaft, random variable, data science

INTRODUCTION

Optimizing drilled shaft design is crucial for large-scale infrastructure projects, where balancing safety, cost, and performance is essential. Drilled shafts, used in complex subsurface conditions, must be designed to support significant axial loads while ensuring long-term stability. Efficient optimization ensures the judicious use of resources while meeting stringent safety standards. This is especially important in urban projects, where space constraints and variable geotechnical conditions present unique challenges to engineers.

The Circunvalacion Norte viaduct in Costa Rica exemplifies these challenges. Spanning 4 kilometers, and connecting critical areas around the capital city of San José, the viaduct's foundation comprises 426 drilled shafts and 58 pile caps, each designed to carry substantial loads. Optimizing these designs is vital not only for safety but also to control construction costs. The project underscores the need for an efficient design process that combines structural safety and cost-effectiveness while accounting for the variability in the soil conditions.

 © Deep Foundations Institute 2025



Fig 1. Circunvalacion Norte Viaduct.

Balancing safety and cost in drilled shaft design is challenging due to the inherent variability of geotechnical properties. Traditional methods, such as Deterministic Design Optimization (DDO), rely on fixed values for soil properties, which may result in overly conservative or unsafe designs. Reliability-Based Design Optimization (RBDO) accounts for uncertainties but requires extensive computational resources.

This study leverages multiobjective optimization using the NSGA-II algorithm and Pareto-Front analysis to explore optimal trade-offs between cost and safety. The approach integrates both deterministic and probabilistic methods to efficiently estimate safety factors and failure probabilities. The goal is to develop an optimized design framework for drilled shafts, applicable to the Circunvalacion Norte viaduct and other large-scale infrastructure projects.

METHODOLOGY

The optimization of drilled shafts for the Circunvalacion Norte viaduct involves a multiobjective framework that integrates deterministic and probabilistic approaches within an NSGA-II-based optimization process. The design variables—shaft diameter and length—are selected to balance structural safety and cost efficiency. The deterministic approach ensures a fixed Factor of Safety (FS) of 3.0, while the probabilistic method incorporates soil variability using random variables (RVs) to achieve a Probability of Failure (PF) of 0.001. The Pareto-front analysis is applied to identify optimal trade-offs between cost and safety, ensuring an efficient and robust design for the drilled shafts. All results were calculated using implementation of Python code on IDE Jupyter Notebook.

Deterministic vs. Probabilistic Approaches

The design of drilled shafts can follow either a deterministic or a probabilistic approach, each offering distinct perspectives on safety and performance. In the Deterministic Design Optimization (DDO), the objective is to ensure a Factor of Safety (FS) of 3.0, meaning that the computed resistance is at least three times the applied load. This method relies on single-point estimates of soil and material properties, typically using mean values, without accounting for spatial variability. While widely used in practice, it may underestimate the true risk of failure in heterogeneous soil conditions.

 © Deep Foundations Institute 2025

In contrast, Reliability-Based Design Optimization (RBDO) explicitly incorporates the uncertainty in geotechnical properties by treating resistance parameters as random variables (RVs). This approach aligns with methodologies proposed by Fan & Liang (2013), where soil properties such as soil strength parameters are modeled as random variables. A random variable X is characterized by its mean μ_X and standard deviation σ_X, with its probabilistic distribution defined as:

$$f(X) = \frac{1}{X\sigma_X\sqrt{2\pi}} \exp\left(-\frac{(\ln X - \mu_X)^2}{2\sigma_X{}^2}\right) \quad [1]$$

where X represents a given soil parameter (e.g., drilled shaft resistance), and μ_X and σ_X are obtained from the statistical analysis of pressuremeter test (PMT) results and transformed to undrained shear strength *Su* by:

$$S_u = P_a \times 0.21 \times \left(\frac{P_L^*}{P_a}\right)^{0.75} \quad [2]$$

Instead of enforcing a fixed FS, RBDO seeks to limit the Probability of Failure (PF) to 0.001, ensuring a reliability level of 99.9%. By integrating statistical distributions of soil strength and variability, RBDO provides a more robust framework for assessing safety while optimizing material use. This approach is particularly beneficial in complex subsurface conditions where deterministic methods may lead to overly conservative or unsafe designs.

The determination of the undrained shear strength (S_u) values, both for the deterministic and random variable cases, was carried out using data from 138 pressuremeter tests distributed along the viaduct. For the deterministic case, the distribution of S_u follows Eq. 3. For the random variable case, a mean value of the effective pressure limit (P_L*) of 3203 kPa and a standard deviation of 1732 kPa were used.

$$S_u(kPa) = 52.2 + log\big(D_f(m)\big) \times 80.4 \quad [3]$$

For the determination of the probability of failure, P_f, 99,900 simulations are generated for each combination of shaft diameter (B) and shaft length (D_f). (equivalent to a coefficient of variation lower than 10% for a P_f of 0.001), using different values of S_u. The number of scenarios in which the resistance R is lower than the applied load Q is then counted as the value of P_f.

A load test can be incorporated to calibrate and validate the numerical resistance models employed in both the deterministic and probabilistic frameworks. However, this approach must be treated with caution, as assuming that a single or limited number of tests can represent the full spatial variability of the subsurface may lead to misinterpretation due to the *law of small numbers*, as discussed by Baecher (2021).

Optimization Framework

The optimization process for drilled shafts in the Circunvalacion Norte viaduct is structured around two key design variables: shaft diameter (B) and shaft length (D_f). The diameter ranges from 0.3 m to 3.0 m in increments of 0.1 m, while the length varies between 10.0 m and 45.0 m with 0.5 m increments. These

 © Deep Foundations Institute 2025

variables define the design space within which optimal solutions are sought. A deeper drilled shaft was not feasible due to restrictions of the kelly bar in the drill rig.

The optimization follows a bi-objective approach, aiming to balance cost efficiency with structural safety. The first objective is to minimize the total cost, which is primarily a function of the total drilled shaft volume and reinforcement requirements. The cost function can be approximated as a function of diameter and length, where larger shafts lead to higher material and construction expenses. Based on internal calculations, the drilled shaft cost is estimated from the equation:

$$cost\ (\$) = 244 \times e^{1.1214\,B} \times Df \quad [4]$$

The second objective focuses on maximizing structural resistance, which is evaluated differently depending on the design approach. In the deterministic case, the optimization seeks to achieve a target factor of safety (FS=3.0), minimizing deviations from this value. In the probabilistic case, the optimization ensures a maximum probability of failure (PF≤0.001), capturing soil variability through random variables. The Pareto-front analysis is used to identify optimal solutions, where no improvement in one objective is possible without negatively impacting the other.

The optimization process is subject to both structural and geotechnical constraints to ensure the feasibility of the selected designs. Structurally, the shaft resistance must always exceed the applied axial load (Q=2500 kN) , incorporating the required safety factor or failure probability. From a geotechnical perspective, the tip and shaft resistance must meet soil-bearing capacity requirements, preventing punching failure or excessive settlement. Furthermore, a minimum embedment depth (10,0 m) is enforced to ensure proper load transfer.

By integrating these constraints, the optimization framework ensures that the selected drilled shaft configurations are not only cost-effective but also structurally and geotechnically viable. The use of multiobjective optimization provides engineers with a range of Pareto-optimal solutions, allowing them to select the most appropriate design based on project-specific trade-offs between cost and safety.

Sensitivity index (*SI*) is a dimensionless metric used to quantify how sensitive a design's performance is to variations in its input parameters. In foundation engineering, it typically measures how changes in soil or design parameters (e.g., undrained shear strength, diameter, or depth) affect the factor of safety or bearing capacity. A high SI value means a more risky or sensitive design and a low SI value means more robust and stable design. The general equation for SI is:

$$SI = \sqrt{J^2} = |J| \quad [5]$$

$$J = \frac{R}{R-(Q+W)} \quad [6]$$

Where is a normalized gradient vector; R is the total resistance (tip + shaft); Q is the structural load; W is the weight of the pile. Drilled shaft resistance was determined using equations from GEC-10 FHWA (Brown et. al, 2018). The *SI* is a non-dimensional measure, and it becomes large when $R \approx Q+W$, i.e., when the design is close to failure.

Implementation of NSGA-II Algorithm

The Non-dominated Sorting Genetic Algorithm II (NSGA-II) (Deb et.al, 2002) is a widely used evolutionary algorithm for solving multiobjective optimization problems. It efficiently identifies a set of Pareto-optimal solutions, where no objective can be improved without worsening another. In this study, NSGA-II is applied to balance two conflicting objectives in drilled shaft design:

1. Minimizing construction cost, represented by total drilled shaft length.
2. Ensuring structural safety, defined by either a target factor of safety (FS = 3.0) in the deterministic case or a probability of failure (PF ≤ 0.001) in the reliability-based case.

The design variables considered in the optimization are:

- B: Shaft diameter ($0.3 \leq B \leq 3.0$ m).
- D_f: Shaft length ($10.0 \text{ m} \leq Df \leq 45$ m).

Each candidate solution is represented as a chromosome in the genetic algorithm, encoded as:

$$x = (B, Df) \quad [7]$$

The fitness functions used to evaluate solutions depend on the design approach:

- Deterministic Design Optimization (DDO):

$$f_1(x) = total\ shaft\ length_{min}\ f_2(x) = \left|\frac{FS}{3.0} - 1\right|_{min} \quad [8]$$

- Reliability-Based Design Optimization (RBDO):

$$f_1(x) = total\ shaft\ length_{min}\ f_2(x) = |P_F - 0.001|_{min} \quad [9]$$

where f_1 minimizes cost and f_2 ensures compliance with safety constraints.

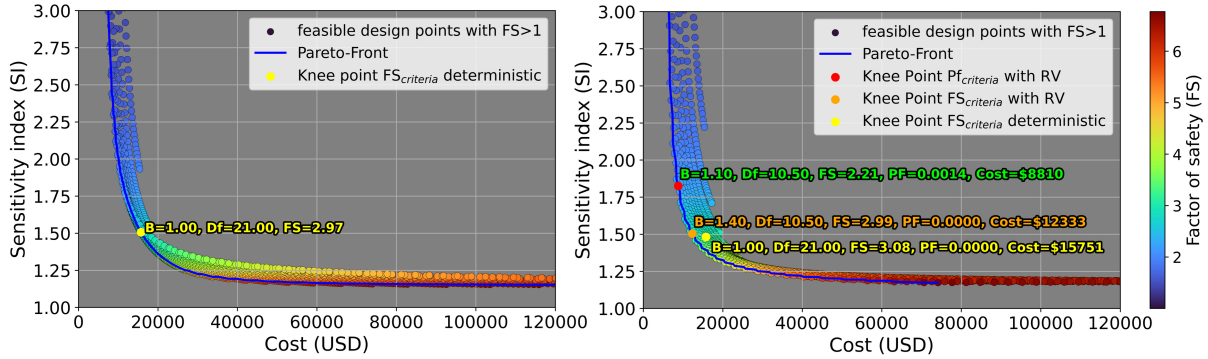
RESULTS AND DISCUSSION

Optimization Results and Trade-Off Analysis

The difference between the deterministic approach and the random variable approach lies in how S_u is calculated. **Error! Reference source not found.** shows the results of the Sensitivity Index (SI) as a function of drilled shaft cost. Due to the difference in S_u methodologies, the results vary slightly between the two approaches. The multi-objective optimization begins with the construction of the Pareto front. This process involves selecting, for each diameter, the point with the lowest cost and the highest safety. Connecting these points results in the Pareto-Front frontier (PF). To determine the optimal point—known as the *knee point*—within the PF, the point with safety closest to the target value is selected: FS = 3 for the deterministic

 © Deep Foundations Institute 2025

approach, and Pf = 0.001 for the random variable approach. The resulting point satisfies the safety target, and no other available design offers a similar level of safety at a lower cost.



a) b)

Fig 2. Pareto Front analysis for the a) deterministic and b) random variable approaches.

The **Error! Reference source not found.** a) shows in the DDO analysis that for an axial load of 2500 kN, the *knee point* corresponds to a pile with a diameter of 1.0 m and a length of 21.0 m. As expected, this point lies on the PF frontier and is referred to as *FS deterministic*. **Error! Reference source not found.** b) presents the results for the RV approach in the RBDO analysis, which, due to the inherent variability of the soil, represents a more realistic scenario. In this case, the *knee point*—identified as the closest point to P_f = 0.001 with the lowest cost, for the same 2500 kN load—corresponds to a pile with a diameter of 1.1 m and a length of 10.5 m. This point is referred to as *Pf with RV*. Interestingly, if we also search for a *knee point* within the RV approach using a safety factor target of FS = 3, it does not coincide with the point found in the deterministic approach. Instead, the new optimal design corresponds to a diameter of 1.4 m and an embedded length of 10.5 m, which we call *FS with RV*. It is also observed that the optimal point from the deterministic approach is not as efficient under the RV approach. In this case, its safety factor increases to 3.08. This leads to a broader discussion on suitable solutions. For instance, the *Pf with RV* point has the P_f closest to the target, but an FS of 2.21. From a resource optimization perspective, this is desirable, as overly conservative designs with very low P_f values result in higher costs. Moreover, due to geotechnical variability, P_f is often more representative of safety than FS. There is no issue with having a pile with an FS slightly below the target if the P_f is within acceptable limits. Additionally, among the three *knee points* discussed, *Pf with RV* is the most cost-effective, with a cost of $8,810. The other points, due to their unnecessarily low P_f values, lead to increased costs of $12,333 and $15,751, respectively, with cost rising as FS increases.

 © Deep Foundations Institute 2025

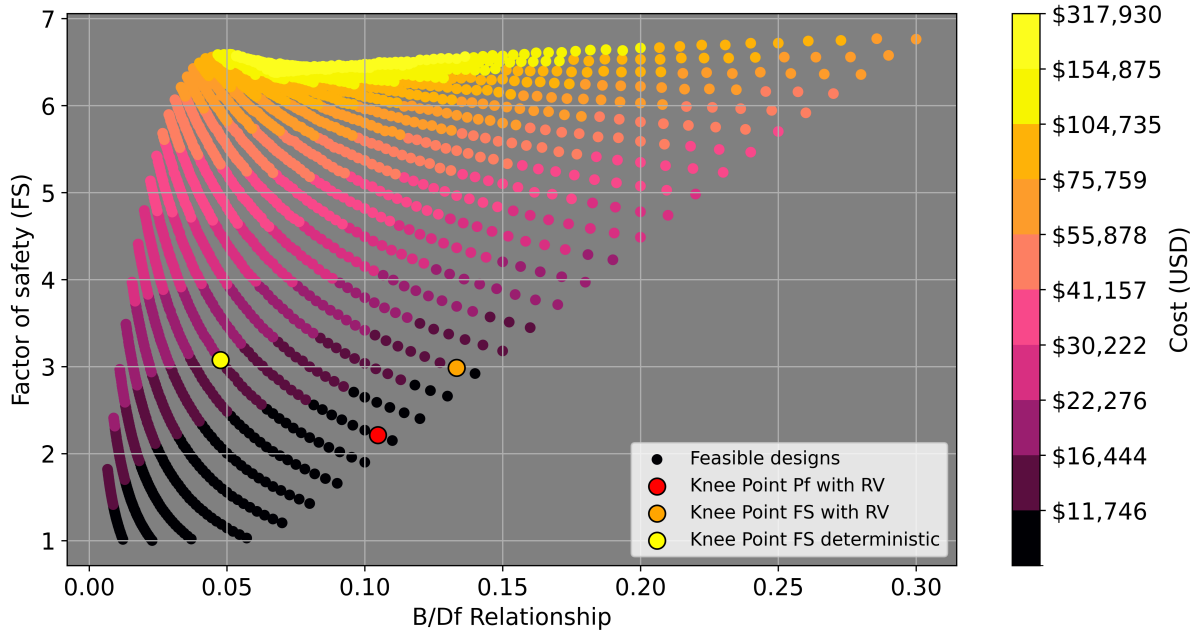


Fig 3. Relationship between B/Df ratio with different levels of cost and factor of safety.

Another way to interpret the optimization results is through **Error! Reference source not found.**, which shows the relationship between B/D_f and the associated cost and factor of safety levels. Each curve represents a pile diameter, with the 0.3 m diameter being the lowest curve and the 3.0 m diameter the highest. Each color scale represents a cost percentile, with each band corresponding to 10% of the dataset. It can be observed that piles with a safety factor (FS) close to 3.0 fall within the 2nd to 3rd cost percentiles—that is, between $11,746 and $22,276—and have a B/Df ratio no greater than 0.15. Piles with costs above the 4th percentile (greater than $30,222) exhibit excessively high FS values, often greater than 4.0. The optimal points found in the analyses are displayed on the figure. In the RBDO analysis, optimal points—whether based on P_f or FS—show B/Df ratios between 0.11 and 0.14 and fall within the 1st percentile of cost. Meanwhile, the optimal point from the DDO analysis has a B/D_f of 0.05, but its cost is higher, falling between the 2nd and 3rd percentiles. This indicates that DDO analysis may yield less optimal solutions when compared to the RV approach.

 © Deep Foundations Institute 2025

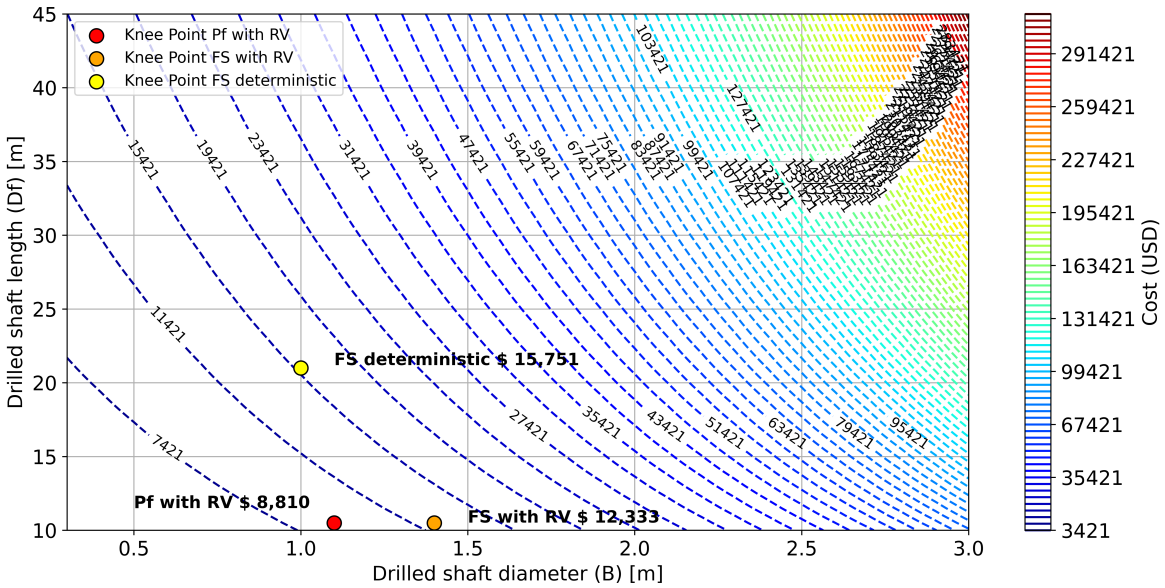


Fig 4. Cost isocurves.

Using the results from all combinations, the costs can be grouped to create cost isocurves, as shown in **Error! Reference source not found.**. In this figure, it can be observed that as the diameter increases, the concentration of curves also increases, indicating that the cost grows nonlinearly with diameter. The point labeled *Pf with RV* lies close to the first cost isocurve, confirming the efficiency of the cost optimization. The other points filtered by FS from the DDO and RBDO analyses fall on higher-cost curves. Both RBDO (random variable approach) solutions correspond to piles with shorter lengths but larger diameters when compared to the solution obtained through the DDO analysis. For example, when the drill rig cannot bore a certain diameter or depth, this graph becomes useful for selecting a new diameter or depth while maintaining the same cost.

 © Deep Foundations Institute 2025

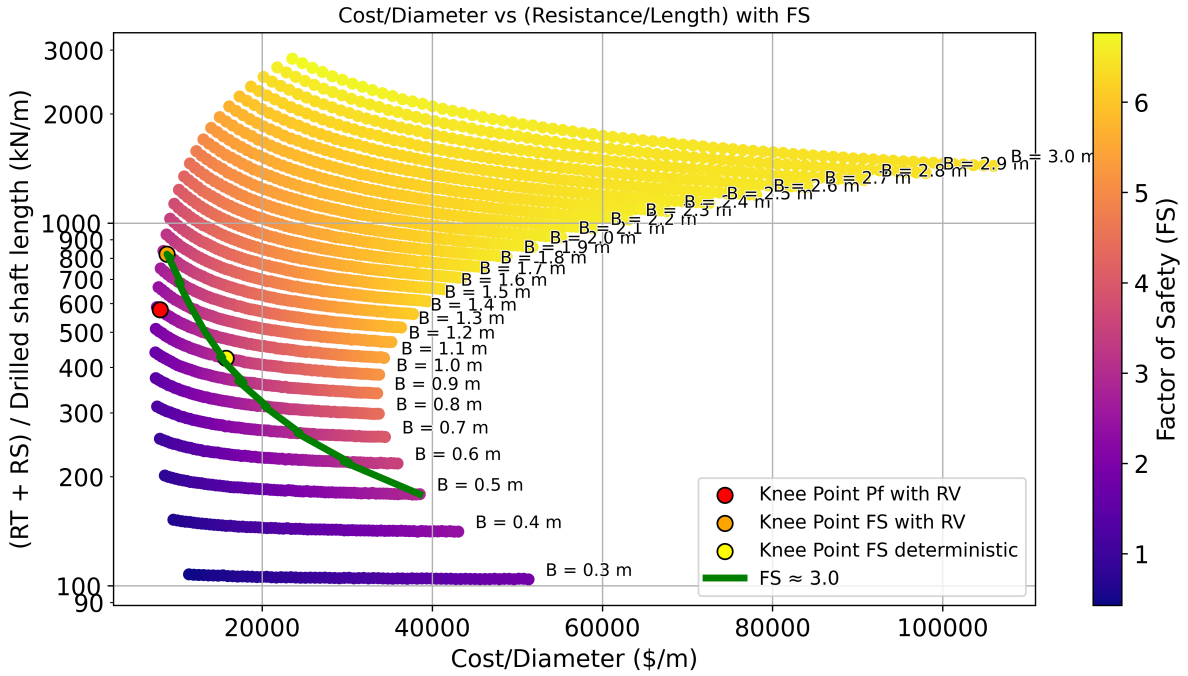


Fig 5. Normalized resistance as a function of normalized cost.

Error! Reference source not found. shows the normalized resistance and normalized cost for each diameter combination. It can be observed that for small diameters, increasing the length—and therefore the cost—has little effect on the normalized resistance. For larger diameters, an increase in pile length actually decreases the normalized resistance. A line is drawn on the figure representing combinations with a FS = 3, demonstrating that some combinations are overly conservative in terms of safety, as they already have FS values above this line from the beginning. For the RBDO optimal point filtered by P_f, the normalized resistance is 600 kN/m. The *FS with RV* point shows a higher normalized resistance but also a higher cost, while the *FS deterministic* point is less efficient, as it has a lower normalized resistance and a higher cost.

Correlation Analysis of Key Design Factors

When analyzing a problem from a data science perspective, it is important to understand how the variables relate to one another. One method for doing this is by creating the correlation matrix between the variables. **Error! Reference source not found.** shows the correlation matrix between pile resistance and the variables FS and P_f. In this matrix, positive values indicate a direct correlation—when one increases, so does the other. Negative values indicate an inverse correlation—when one increases, the other decreases. High magnitude values (close to 1 or -1) suggest a strong correlation, while low magnitude values (close to 0) imply that there is no clear linear relationship between the two variables; in other words, knowing the value of one variable does not help much in predicting the value of the other. These relationships indicate whether strong correlations exist, but only in terms of linear relationships—nonlinear patterns cannot be identified through this method.

 © Deep Foundations Institute 2025

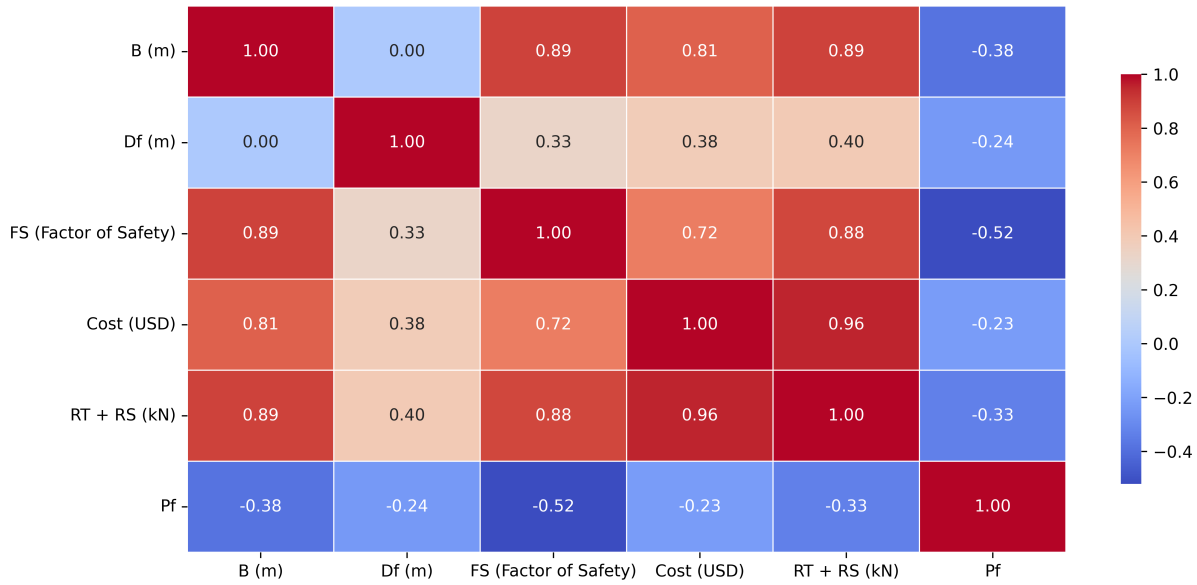


Fig 6. Correlation matrix of the pile resistance variables

The correlation plot is useful in optimization because it helps determine which variables to modify by showing which ones have the greatest influence on the outcome. It also provides insight into the constraints of each variable. It is observed that B is more influential in describing cost, factor of safety (FS), and resistance (RT+RS) compared to D_f. The variable D_f shows its highest correlation with resistance at 0.4; however, among the variables influencing resistance, D_f has the lowest correlation, while the others show stronger relationships. For cost, the most important variable is resistance, with a correlation of 0.96—indicating that as pile resistance increases, so does the cost. As expected, the probability of failure (P_f) shows negative correlations with the other variables: more resistant, more expensive, larger diameter, or deeper piles tend to have lower P_f values.

Clustering-Based Risk and Cost Classification

When working with large datasets, it is useful to apply clustering methods to classify the data into subgroups, where each centroid represents a specific behavioral pattern. In this case, the k-means method (Jain, 2010) was used to generate the clusters, and classification parameters were defined based on FS and P_f values to identify risky, optimal, and excessively costly design zones. For the FS-based classification, an optimal design zone was defined as having values between 2.5 and 3.5. For the P_f-based classification, the criteria established by CALTRANS (2019) were considered. This document, which serves as an annex to the AASHTO bridge design specifications, deems it acceptable to have piles with a P_f of 0.01 for highly redundant systems, and a P_f of 0.001 for other cases (Paikowsky, 2004), thus defining an appropriate design zone.

 © Deep Foundations Institute 2025

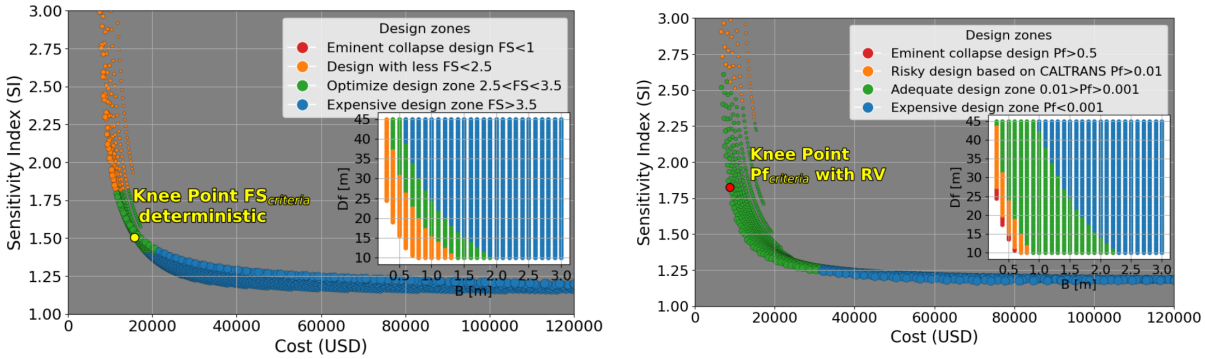


Fig 7. Clustering of design zones for the approach: a) deterministic b) random variable.

The definition of these clusters establishes zones that, in the context of pile optimization, can be interpreted as decision boundary points. **Error! Reference source not found.** a) presents the results of the DDO analysis, where the optimal zone is defined by SI values lower than 2 and costs below $20,000. As expected, the point identified as optimal in this analysis lies within this region. In this figure, the size of the markers represents the diameter of the piles. **Error! Reference source not found.** b) shows the results of the RBDO analysis, where the optimal zone includes piles with SI values lower than 2.6 and costs below $30,000. The optimal point from this analysis also falls within this region. Points with SI values exceeding the optimal region threshold are considered risky, as a high SI indicates scenarios where R is very close to $Q+W$, indicating a proximity to failure. Points located to the right of this optimal zone represent excessively expensive solutions that lack the technical justification for their high safety levels.

In both plots on **Error! Reference source not found.**, an inset displays the combinations of B and D_f corresponding to each assigned cluster. It can be observed that the adequate design zone, when using the probability of failure criterion (P_f), is broader compared to the zone defined by the factor of safety criterion (FS). Some of these additional points are associated with FS values below 2.5, yet they exhibit a satisfactory failure probability of $P_f < 0.01$. Therefore, by adopting the P_f -based criterion, pile configurations that are both structurally adequate and more cost-effective are validated for design purposes.

The decision of which of the two results to use as the selection criterion depends on the chosen approach to the problem. However, it must be clearly stated that, first, the use of a random variable better captures the inherent variability of S_u, and second, the determination of P_f is a more appropriate safety parameter than FS.

CONCLUSIONS

This study demonstrated the effectiveness of multiobjective optimization, particularly using the NSGA-II algorithm and Pareto-Front analysis, in achieving cost-efficient and structurally sound designs for drilled shafts in large-scale infrastructure projects. By comparing Deterministic Design Optimization (DDO) and Reliability-Based Design Optimization (RBDO), it became evident that accounting for geotechnical variability through random variables yielded more realistic and more efficient designs.

Several graphs for optimization decision making were presented. The deterministic approach, while simple and widely used, led to overly conservative or suboptimal solutions when considering a random variable approach (RV). In contrast, RBDO integrated statistical variability in undrained shear strength (S_u), enabling the identification of designs that met reliability criteria ($P_f \leq 0.001$) while potentially reducing material use and construction costs. This was clearly observed in the case study: the optimal deterministic design (B = 1.0 m, D_f = 21.0 m) was significantly more expensive than the reliability-based solution (B = 1.1 m, D_f = 10.5 m), which still satisfied the target probability of failure.

The correlation matrix analysis provided insights into the linear relationships between variables in the dataset. It showed that B had a greater influence on cost, factor of safety (FS), and resistance (RT+RS) than Df. Additionally, probability of failure (P_f) demonstrated negative correlations with other variables: as resistance, cost, pile diameter, and depth increased, the probability of failure decreased.

The clustering analysis revealed distinct zones that served as decision boundaries in pile optimization. In the DDO analysis, the optimal zone was characterized by SI values below 2 and costs below $20,000. Similarly, the RBDO analysis defined an optimal zone with SI values below 2.6 and costs below $30,000. Points outside the optimal range—either with higher SI values or excessive costs—were considered risky or inefficient.

Although both the FS and P_f criteria can be used for design evaluation, the P_f based criterion better captures the inherent variability of the soil. It enables the identification of configurations with lower FS values that still exhibit structurally adequate performance, leading to more cost-effective solutions without compromising reliability.

Ultimately, the integration of RBDO and multiobjective optimization into the drilled shaft design process represents a significant advancement in foundation engineering. It aligns with the broader goals of modern geotechnical practice—efficiency, safety, and adaptability—and serves as a valuable reference for similar future infrastructure projects.

REFERENCES

Baecher, G. B. (2023). 2021 Terzaghi lecture: Geotechnical systems, uncertainty, and risk. *Journal of Geotechnical and Geoenvironmental Engineering*, *149*(3), 03023001.

Brown, D. A., Turner, J. P., Castelli, R. J., & Loehr, E. (2018). *Drilled shafts: Construction procedures and design methods* (No. FHWA-NHI-18-024). National Highway Institute (US).

Caltrans (2019). *California Amendments to the AASHTO LRFD Bridge Design Specifications (2017 Eighth Edition)*. California Department of Transportation

Deb, K., Pratap, A., Agarwal, S., & Meyarivan, T. A. M. T. (2002). A fast and elitist multiobjective genetic algorithm: NSGA-II. *IEEE transactions on evolutionary computation*, *6*(2), 182-197.

 © Deep Foundations Institute 2025

Fan, H., & Liang, R. (2013). Reliability-based design of axially loaded drilled shafts using Monte Carlo method. *International Journal for Numerical and Analytical Methods in Geomechanics*, *37*(14), 2223-2238.

Jain, A. K. (2010). Data clustering: 50 years beyond K-means. *Pattern recognition letters*, *31*(8), 651-666.

Paikowsky, S. G. (2004). *Load and resistance factor design (LRFD) for deep foundations* (Vol. 507). Transportation Research Board.

Phoon, K. K., & Kulhawy, F. H. (1999). Characterization of geotechnical variability. *Canadian geotechnical journal*, *36*(4), 612-624.

 © Deep Foundations Institute 2025

SACRAMENTO RIVER EAST LEVEE CONTRACT 4 – CONSTRUCTION OF SEEPAGE CUTOFF WALL

Pablo Bassola, Treviicos Corporation, Charlestown, MA, USA, +1 857-260-2063, pbassola@treviicos.com
Scott Gordon, Treviicos Corporation, Charlestown, MA, USA, +1 617-275-3250, sgordon@treviicos.com
Maurizio Siepi, Consultant, Cesena (FC), Italy, +39 348-145-0274, maurizio.siepi@outlook.com
Chris Hamilton, United States Army Corps of Engineers, Sacramento, CA, USA, +1 916-557-7612 Christopher.E.Hamilton2@usace.army.mil

ABSTRACT

The Sacramento River East Levee Contract 4 was the fourth contract of the American Common Features (ARCF) 2016 project. The United States Army Corps of Engineers (USACE) developed a program to improve the seepage and stability conditions along the Sacramento River East Levee (SREL). This contract included construction of a cutoff wall utilizing jet grouting or deep mixing method to adjoin existing cutoff walls from previously completed contracts. TREVIICOS Corporation (TIC) was selected by the General Contractor, Maloney-Odin A Joint Venture (MOAJV) to be the Jet Grouting Contractor and complete the jet grout cutoff wall portion of the contract.

The scope of work outlined for the Jet Grout contractor involved installation of a Jet Grout Cutoff Wall (JGCOW) connecting to previously installed Deep Mixing Method (DMM) Cutoff Walls. The project consisted of constructing a JGCOW at multiple locations with controlled strength and permeability properties. The project presented unique challenges for installing the cutoff wall, such as varying geology at each specific location, significant depths reaching up to 145+ feet, limited real estate near the active public and sensitive structures, active discharge pipes from a pump station, and an active pressurized gas line.

To circumnavigate these unique challenges, as required by the contract specifications, TIC installed 8 foot or 10.5 foot diameter triple fluid jet grout columns utilizing air, water, and grout at high pressures. In addition to triple fluid, TIC also implemented some single fluid high pressure grout columns reaching diameters of 3 to 4 foot to mitigate previously unknown challenges that arose during the construction of the jet grout cutoff wall. This paper details the unique challenges encountered, and the solutions implemented to successfully install the jet grout cutoff wall.

INTRODUCTION

The Sacramento, California area has often been denoted as relatively high at-risk region for major flooding. The American River Common Features 2016 Project, a collaboration between the USACE, the California Department of Water Resources (DWR), the Central Valley Flood Protection Board (CVFPB), and the Sacramento Area Flood Control Agency (SAFCA), is a combination of multiple projects to help improve the system of levees and other flood control features. Sacramento River East Levee Contract 4 (SREL4) was the fourth installment of features along the eastern levee (left bank) of the Sacramento River. In previous contracts, cutoff walls were constructed in several areas along the Sacramento River. SREL4 utilized two separate methodologies of cutoff wall, Deep Mixing Method (DMM) Cutoff Walls and Jet Grout Cutoff Walls (JGCOW) to adjoin and connect with the existing cutoff walls installed in the other contracts. The Jet Grout technology was selected in part due to the logistical constraints where DMM was not feasible due to proximity to sensitive structures and utilities.

 © Deep Foundations Institute 2025

The contract required the installation of a total of 99 jet grouting columns of 8ft and 10.5 ft diameter, to a maximum depth of 145 ft, to obtain a target unconfined compressive strength of 200 psi on core samples and a mean laboratory permeability of 5 x 10^{-7} cm/s on core samples. Every column was surveyed for verticality, to assure the JGCOW has a minimum thickness of 36 inches.

JET GROUT CUTOFF WALL

TREVIICOS was selected as the Jet Grout Cutoff Wall Contractor by MOAJV for the SREL4 contract. TIC was initially tasked with installation of four separate cutoff wall segments in four separate locations within the Sacramento area along the Sacramento River left bank. The four locations were labeled as Sump 132 Pump Station, Westin Hotel, the Marina, and Broadway. However, the Marina was later removed from the Jet Grout scope in favor of the DMM method due to possible schedule constraints and value engineering.



Fig. 1: Project Site Locations

There are typically three main forms for Jet Grouting based on the number of fluids to be applied: single, double, and triple fluid jet grouting. For this contract, triple fluid jet grouting was the primary installation technique, which included water, air and grout. The grout utilized was a cement-water mixture outlined by the contract specifications. Figure 2 below shows the triple fluid technology.

 © Deep Foundations Institute 2025

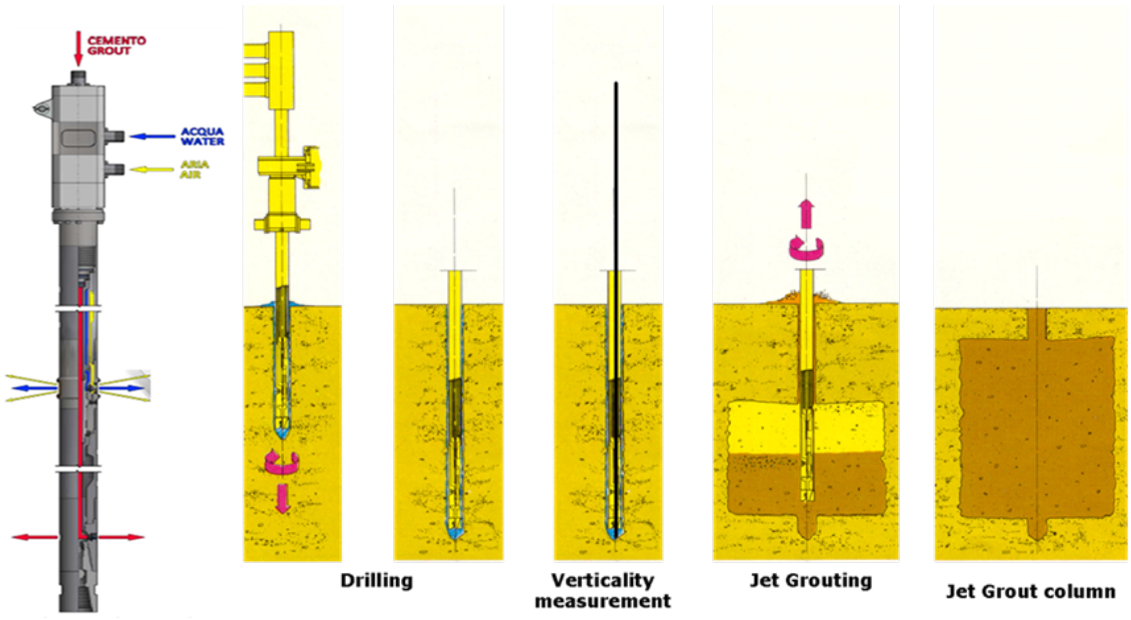


Fig. 2: From Left to Right, Triple Fluid Jet Grout Equipment; Triple Fluid Jet Grout Injection Process

Prior to beginning jet grout work, two phases of demonstration were required. First, TIC was required to perform a batch plant certification which would allow the client, USACE, to verify the equipment brought to perform the work was capable of meeting specific guidelines such as flow rate and pressures. Additionally, the devices to be used to monitor and record these parameters in real time were tested and verified. Tests were performed with specific flow rates and pressures with each high-pressure pump with both grout and water separately. A 10,000-liter agitator tank was at the end of the pipeline, to receive the fluids pumped during the tests. A sight tube was attached to the agitator to measure the level and calculate the volume of the pumped fluid to verify the device's abilities to properly record. Two separate plant certifications were successfully performed before each test section at the Sump 132 and Westin Hotel. A batch plant installed at the Westin Hotel location is shown below in Fig. 3.



Fig. 3: Jet Grout Batching Plant

 © Deep Foundations Institute 2025

Once the equipment was verified to be able to perform the high-pressure injections, TIC was next required to construct two test sections in the native soil at Sump 132 and Westin Hotel to ensure the proposed injection parameters could meet the expected element diameters and the specified acceptance criteria. TIC jet grout technical consultant assisted in developing set parameters based on contractual documents of the native lithology expected in each area.

For the selection of the testing parameters, TIC used the approach of volumetric specific energy, using a range between 30 and 55 MJ/cu.m. for the 8-ft without air, 8-ft with air, 10.5 ft with air. For the calculation of the Volumetric specific energy, only the water and air parameters were used with the criteria suggested by Tornaghi & Pettinaroli, 2004. In the same paper, it is explained how the Volumetric Specific Energy for single fluid (as used for the 8-ft without air) is in the range of 20-30 MJ/cu.m for medium loose silty sand, whereas in the same soil type the double and triple fluid systems require just a fraction (10-20 MJ/cu.m).

Prior to the contractual required test sections, TIC implemented its own internal test where it performed three sacrificial elements outside the footprint of the cutoff wall to better fine-tune these parameters.

The first element was installed regularly with initial set parameters to ensure all equipment was functioning properly. The next two sacrificial elements utilized three (3) 20 ft long rebars painted white that were installed at three separate distances away from the center of the sacrificial element into the ground. The following day, TIC installed the sacrificial element and then removed the rebars to determine if the grout had reached them, indicating the true diameter of the column. Based on these two element test observations, TIC fine-tuned its parameters to perform its 8 ft and 10.5 ft diameter elements by adjusting the rotation and dwell time at each incremental step during its withdrawal. An example of the installation and evaluation of the rebar is shown in Fig. 4.



Fig. 4: From Left to Right, Installation of Rebar into Borehole; Evaluation of Rebar After Test

The same set of parameters was utilized at both test locations; however, the 10.5 ft diameter was primarily only used at Sump 132.

Pump Station Sump 132

The Sump 132 test section consisted of three sets of paired elements for a total of six elements. One set was 8 ft diameter with triple fluid including high pressure air, one set was an 8 ft diameter element with no air, and the final set was 10.5 ft diameter element with triple fluid and high-pressure air.

 © Deep Foundations Institute 2025

During the installation of these elements, TIC ran into some challenges, specifically unexpected massive quantities of wood and a very dense permeable sand and gravel layer (N_{60} greater than 50) that is assumed to also contain cobble. These findings forced TIC to change its initial approach of just drilling with a regular drill bit and water. Instead, a Wassara Hammer, as shown below in Fig. 5, was attached to the rods and used to assist in hammering through potential wood obstructions and along with the dense gravel layer. Due to the significant permeable gravel layer, a polymer water drilling fluid was used to assist in keeping consistent flow return and stabilizing the borehole to prevent collapse. Samples were collected and tested to assure cement-polymer compatibility.

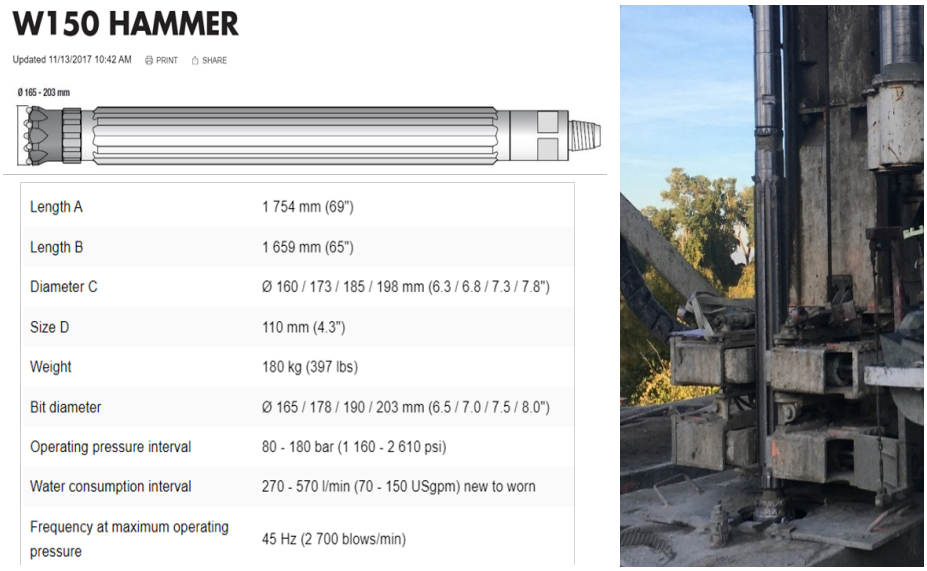


Fig. 5. Wassara Hammer

Each set of two (2) columns were cored and tested for permeability and strength for a total of three. The verification drilling and testing was accepted allowing TIC to proceed with the production cutoff wall.

After successful completion of the test section, the Sump 132 area presented its own unique challenge of installation of elements between large (42-inch and 66-inch diameter) active discharge pipes from the pump station. Specifications had a restriction on drilling being at minimum 1 foot away from the outer edge of the discharge pipes. This restriction led to the development of the 10.5 ft diameter elements. During the execution of the second phase at Sump 132, multiple challenges were encountered that required a team effort in coordination with TREVIICOS, MOAJV, and USACE to ensure a successful completion of the wall.

At the initial start of phase two, bubbles were observed within the river during the installation of a few columns. This was not entirely unexpected (especially with the use of triple fluid), however due to the vulnerability of the levee and the potential for environmental disturbance, it required close monitoring to ensure grout was not escaping into the river. After the first observation of bubbles, work was initially stopped and meetings with all pertinent parties were completed to determine a plan of action. Consistent monitoring and turbidity testing were performed during the remaining portion of work to ensure that only air was escaping into the river, and a plan of action was put in place in case more seeping was detected. There was no grout or turbidity detected within the river.

 © Deep Foundations Institute 2025

Another significant challenge was to install elements at depths of 145 ft while ensuring the active discharge 56-inch diameter pipes were not impacted or damaged. Prior to the start of the work an extensive potholing campaign was performed to determine location and confirm diameters of the discharge pipes. Once known, TIC developed its parameters for 10.5 ft diameter elements and located each element to ensure the design overlap was maintained underneath the discharge pipes.

The most significant challenge that impacted drill rates was the unexpected enormous quantities of wood, both fresh and charred within the embankment and the hard, permeable gravel layer. Due to the gravel layer and wood obstructions found, TIC used the Wassara Hammer to punch through, which added additional redrills of the same element due to retrieval of hammer and replacing with the jet grout monitor. Large collections of wood that were displaced during injection are shown below in Fig. 6.



Fig. 6: Wood and Debris Found During Injection of Jet Grout Element

Due to the limited space available, all the return spoil had to be pumped 2000 feet away, to a separation plant, where it was desanded and dewatered before being hauled to the approved disposal area. There was a large volume of pumping required (up to 400 GPM) which caused some overflows, which in turn required stoppage of jetting to allow the plant to keep up. However, excellent coordination between the two operations was able to fine-tune an optimized rate to mitigate overflows as much as possible.

After installation of all the columns in the area, four (4) coring locations were selected by USACE for testing of the production cutoff wall. In-situ water testing and laboratory tests were generally compliant with specifications, and only 6 partial columns had to be performed to repair defects within the borehole. These defects were likely attributed to the significant amount of wood found within the soil creating small shadow effects.

Westin Hotel

Similarly to the Pump Station Sump 132, TIC was required to perform an additional pre-production test section at the Westin Hotel. This area presents its own challenges both with native soil and the extremely close proximity to the public and the hotel itself. Due to the being so close to the public, a noise barrier was erected to help mitigate the construction sites and sounds that would impact and disturb the local public at this location. Noise Barrier between the drill rig and Westin Hotel is illustrated below in Fig. 7.



Fig. 7: Noise Barrier and Westin Hotel

In this area, known as Edwards Break, the levee was breached during the historic flood of 1904, and an emergency backfilling was done here with unknown materials and procedures. It was anticipated to encounter cobbles and boulders and for this reason the Specifications required the Contractor to have available a water-powered hammer to drill through obstructions.

Based on information that was obtained during the first test section, the same parameters were selected to be utilized for the second test section. The same requirements of 3 sets of paired elements were required with 2 being triple fluid with air and 1 triple fluid without air. There was one additional stipulation that one of the test elements be within the Edwards Break area. As described previously, this area represented one of the significant challenges for installation of the cutoff wall in this area due to unknowns of the soil that were below. Wood, cobbles, etc. were placed into this zone from that previous event, with assumed little to no compaction and great potential for voids.

During the execution of the test section, TIC was presented with another significant challenge in that sink hole formation, as shown in Fig. 8, occurring during injection of elements. Although at the time of the installation of the cutoff wall it was not fully determined, it's believed that the significant amount of debris including small gravel and wood were removed during the injection which caused the upper loose sand layer to collapse. During the initial ex

 © Deep Foundations Institute 2025



Fig. 8: Sinkhole Formation During Jet Grout Injection

For the test section, the team moved away from areas of the sinkholes and backfilled with grout at low pressure to initially stabilize the area.

In order to mitigate this issue posed to the adjacent buildings and site safety, a stabilization program was developed by TREVICOS and presented to the MOAJV and USACE. After further discussion, it was determined that single fluid jet grout would be utilized for the top 20 feet in 2 rows as shown below. After a section of these 3 ft and 4 ft diameter elements were installed, TIC returned to install the 8 ft diameter triple fluid element. The layout below in Fig. 9 illustrates how the 8 ft diameter triple fluid elements would overlap with the 3 ft and 4 ft diameter single fluid stabilization elements.

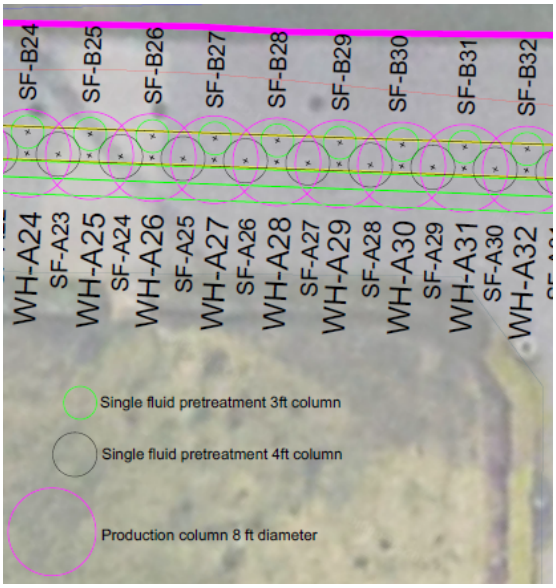


Fig. 9: Snapshot of Stabilization Element Layout

TIC believes this implementation was successful in assisting with protecting the Hotel Side foundation from sink holes, however, due to the lack of a protective row on the lower river side, sink holes continued to form. Along with the sink holes in varying locations, TIC observed grout loss and spoil return loss in the Edward's Break area.

Due to the ongoing sink holes and spoil return loss observed, another coordination effort with all parties was required. In addition to continuing the stabilization program, TIC developed a hybrid element with both single fluid and triple fluid injection completed one after the other.

An initial 4 ft diameter single fluid element was installed for the top 49 ft to bridge and stabilize the upper loose sand layer and the void-prone breach fill. Then immediately following its completion, the element was drilled while still fresh with grout to full depth and immediately started triple fluid injection. Once the triple fluid injection reached 20 ft depth (the depth of the adjacent stabilizing single fluid columns), the water and air were shut off to perform a second single fluid injection in the same depths as the previous single fluid injection, to further stabilize the upper layer of loose sand.

Utilizing this newly developed hybrid methodology, TREVIICOS was able to successfully complete the jet grout cutoff wall at the Westin Hotel.

A total of 12 coring locations were selected: three (3) for the test section and nine (9) for the production cutoff wall. Ten (10) partial columns were required to remove some small defects in the wall however this was attributed to the many unknown objects and voids likely found within the Edwards Breach area. The area was completed and accepted to the satisfaction of the USACE.

Broadway

The final jet grout cutoff wall required from the SREL4 project was a location located next to the street named Broadway. This presented its own unique challenge with the installation of a jet grout cutoff wall directly above an active 24-inch high-pressure gas line.



Fig. 10: Jet Grout Installation Close Proximity to Overpass and Active Gas Line

This area was left open from a previous contract due to the active line, which required coordination with the local authorities and the utility owner. Due to the sensitive nature of this gas line, there was a strict buffer zone of 10 feet required for how deep drilling could proceed. However, due to the nature of how triple fluid technology works as shown below, the drill bit would encroach into the buffer zone. To combat this, USACE and TREVIICOS developed a single fluid design to cover the area above where the gas line was located. The single fluid monitor and drill bit were several feet shorter than the triple fluid monitor. In

 © Deep Foundations Institute 2025

a coordination effort with the local gas company, it was agreed to adjust the buffer zone for the single fluid monitor. This monitor would stop just shy of an adjusted 8-foot clearance above the gas line. During installation of elements in the vicinity of the gas line, a representative was onsite and in constant communication with personnel.

TREVIICOS was able to complete both the single fluid and triple fluid jet grout installation at Broadway without causing any impact to the active gas line.

Due to the short length of cutoff wall at this location, only one (1) location was selected for verification drilling and testing. Both the UCS and permeability results were satisfactory for acceptance.

VERIFICATION DRILLING AND TESTING

Verification drilling and testing were required at each location to ensure compliance with contract requirements. This involved an unconfined compressive strength of 200 psi on core samples and a mean laboratory permeability of 5 x 10^{-7} cm/s on core samples. Additionally, there were 2 stages of in-situ permeability testing that required to be less than 1 x 10^{-6} cm/s. The first stage was performed within 1 ft of the water table with a 3-hour constant head test and 5 hour falling head test. The second stage rising head permeability test was performed after completion of the drilling to the final depth of the verification borehole which was within 5 ft of the bottom of the wall. A total of 20 verification core holes were selected for drilling and testing by the USACE.

For the drilling and testing, a CME85 Drill rig was used performing triple barrel wireline coring. Core runs were completed in 5 ft intervals with a borehole logger documenting the characteristics of the core samples immediately after retrieval. A five (5) foot core run from the Pump Station Sump 132 is shown below in Fig. 11.

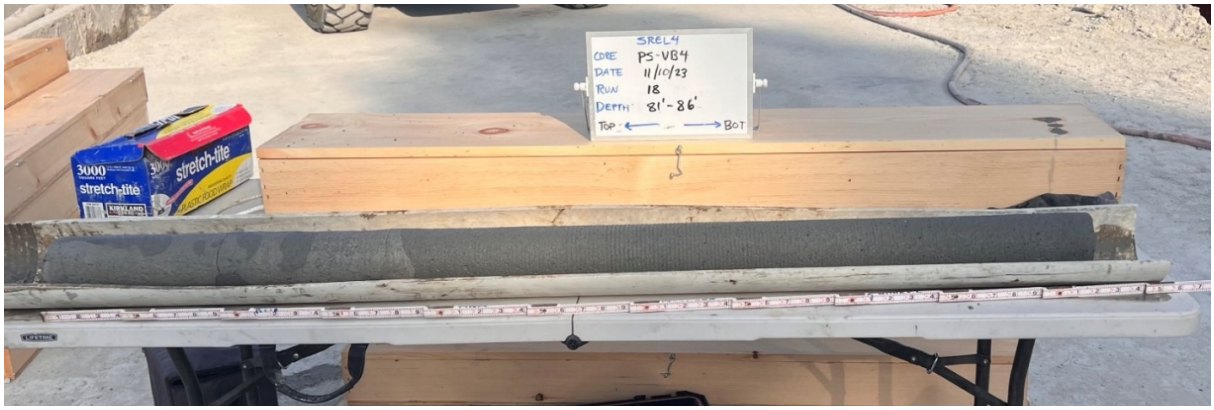


Fig. 11: Verification Core Run of 5 feet

After completion of the coring, water was pumped out of the borehole to allow a Closed Circuit Television (CCTV) recording of the inside of the borehole.

CONCLUSIONS

The SREL4 project presented some extremely difficult and unique challenges to the team. Working on a levee with limited space, fluctuating water levels to install large diameter columns was already a significant challenge, with a potential risk of causing piping. Additionally, during the installation of the columns, TIC encountered some unexpected conditions such as excessive wood debris, sinkholes, active gas lines and

 © Deep Foundations Institute 2025

discharge pipes. However, in a strong coordination effort with TREVIICOS, MOAJV, and USACE, the jet grout cutoff wall was successfully completed as intended in each of the required areas to the satisfaction of the Owner.

ACKNOWLEDGMENTS

The authors want to acknowledge the contribution of all the people involved in the project including but not limited to the operational crews, management teams, suppliers, contractors, subcontractors, and the Owner. We express our sincerest gratitude for all that made this project a success and instrumental in the production of this paper.

REFERENCES

Tornaghi, R., and Pettinaroli, A. (2004). “Design and control criteria of jet grouting treatments.” Proceedings of ASEP–GI international symposium sur l’ame´lioration des sols en place, vol.1, pp. 1–24. Paris, France: Ecole Nationale des Ponts et Chausse´es.

 © Deep Foundations Institute 2025

SPEEDY REBUILDING OF EARTHQUAKE-DAMAGED HIGHWAY EMBANKMENT WITH PRESSED-IN PIPE PILE WALL

Takefumi Takuma, Giken America Corp., Orlando, FL, U.S.A., Phone: 407-380-3232, ttakuma@gikenamerica.com
Shinya Kubo, Giken Ltd., Tokyo, Japan, E-mail: kubo@giken.com

ABSTRACT

An arterial expressway running in the Noto peninsula of Japan was closed due to landslides and slope failures at multiple locations caused by a very strong earthquake which occurred in January 2024. One of the abutments of a viaduct was threatened and a half width of its approach section of the roadway embankment was lost due to a local landslide. For its reconstruction, a pressed-in pipe pile wall was built as the primary earth retaining structure because the construction access was limited and the slope next to the abutment was unstable. Thirty-four 800mm diameter, 23.5m long pipe piles were pressed into the slope with a rotary press-in piling machine. A special crane was utilized along with the piling machine; both of which moved forward and backward safely on top of already installed piles without building a large construction staging area, contributing to the fast full reopening of the expressway.

Keywords: landslide, press-in piling, earth retaining wall, rotary press-in piling, pipe pile

BACKGROUND

The M7.6 earthquake that occurred in the Noto peninsula in Japan (Fig. 1) on New Year's Day of 2024 severely destroyed many buildings and infrastructure in the area in addition to casualties of more than 400. Included was a part of the Noto-Satoyama Kaido Expressway's embankment as shown in Fig. 2.

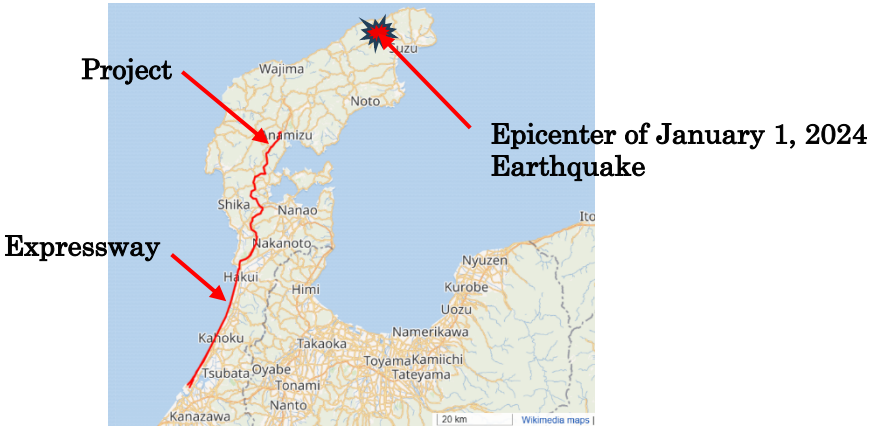


Fig. 1. Noto Peninsula in Japan

 © Deep Foundations Institute 2025



Fig. 2. Collapsed Embankment next to Viaduct after Emergency Repair

Only one lane of the expressway was open to traffic after emergency repair was complete. Safe and expedient opening of its full two lanes was urgently needed for recovery of the hard-hit areas in the region. Figure 3 shows the plan view of the pipe pile earth retaining wall that was built to accomplish this goal.

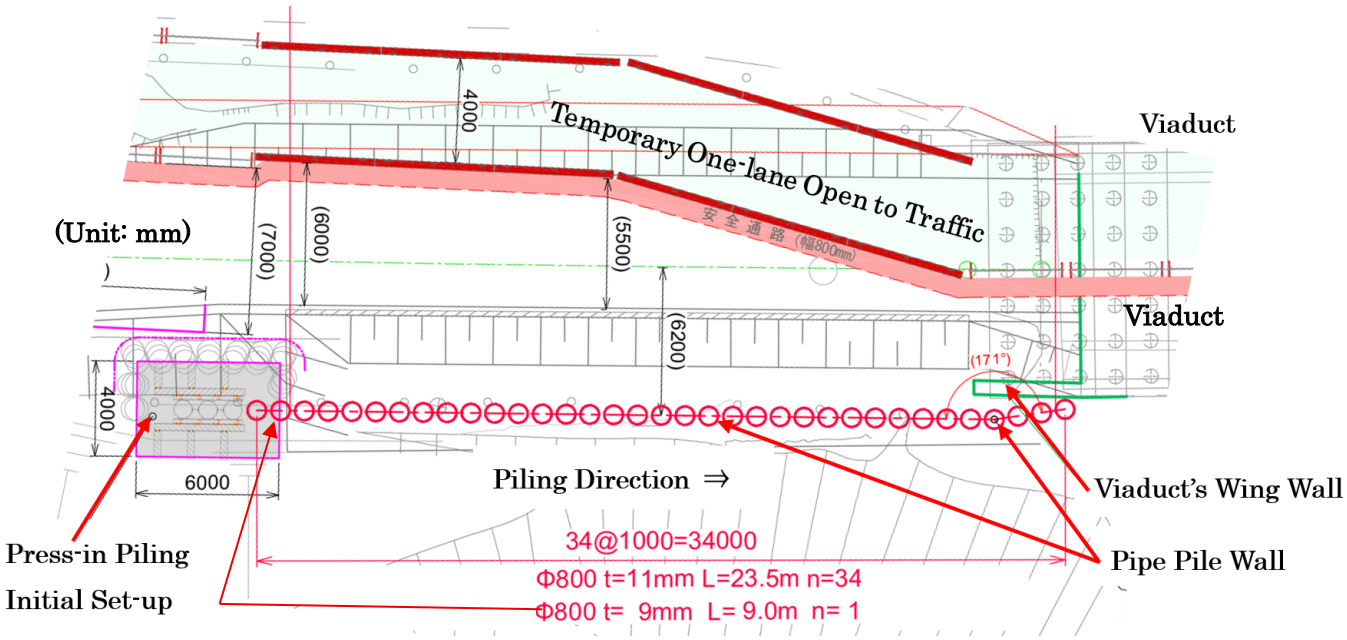


Fig. 3. Plan View of Pressed-in Pipe Pile Wall and One-lane Expressway during Construction

 © Deep Foundations Institute 2025

The pressed-in pipe pile wall was selected as the primary earth retaining structure for the following reasons:

1. The foundation of the viaduct's abutment was threatened due to a landslide caused by the earthquake.
2. A part of the embankment of the roadway's approach section collapsed during the earthquake, making only one lane of the expressway available for traffic even after emergency repair.
3. The partially slid-off slope was unstable and sensitive and a further landslide was feared with vibration during construction.
4. The available construction staging area was small and the access to the earth retaining wall construction was very narrow because one lane of the expressway had to be kept open to traffic.
5. Boulders were expected in the slope. Rotary press-in piling is capable of installing pipe piles through a boulder layer as described in the next section.
6. The Press-in Piling Method had been successfully utilized for the prompt and reliable recovery of eroded highway embankment on other projects.

Figure 4 shows the concept of the pressed-in pipe pile wall to be directly installed into the partially collapsed slope. Figure 5 shows typical soil conditions with the planned vertical pile location on the right. It was constructed on a design-build basis by the general contractor, Kajima Corp.

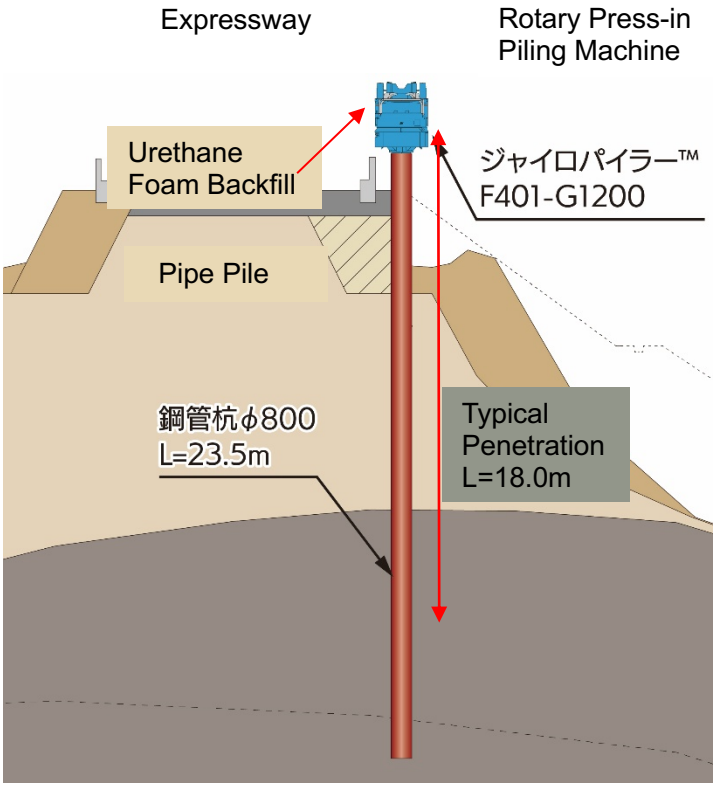


Fig. 4. Conceptual Cross Section of Earth Retaining Wall with Pressed-in Pipe Piles

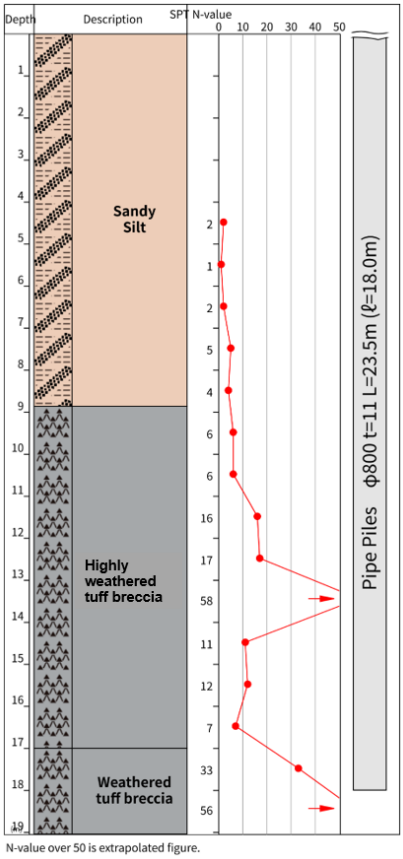


Fig. 5. Typical Soil Conditions and Pipe Pile Location

 © Deep Foundations Institute 2025

PRESS-IN PILING METHOD

So, what is a pressed-in pile and the press-in piling method?

The press-in piling method utilizes hydraulic force to push piles into the ground with minimal noise and vibration compared with other piling methods (White et al. 2002). The reaction force needed for press-in piling typically comes from the interlock resistance between already installed piles and the skin friction from the soil surrounding them plus the weight of the machine and the pile to be installed. There are a few variations in obtaining the reaction force. However, the type described above is most widely used. It is suited for horizontally continuous piles such as sheet piles and pipe piles which are either connected together or placed close to each other. Speaking of pipe pile installation, they can be installed either with press-in force only (piles can have interlocks and connected with each other, Takuma et al. 2017) or by rotating and simultaneously pressing them in (without interlocks). Figure 6 shows the schema of the latter type, which was utilized for the subject project. In this case, a cutting shoe was welded at the toe of each pile for a faster pile installation even into hard soil, rock, boulders, or existing concrete structures, if necessary (Takuma et al. 2013). The piling machine does not require a service crane to move forward or backward from one pile installation to another as shown as the self-walking sequence in Fig. 7. This capability becomes critical when the access to the piling location is limited such as the subject project. The rotating cutting shoe with a small amount of water reduces press-in resistance without loosening the soil. See Fig. 8 for different types of cutting shoes for a wide range of soil conditions. In addition, this pile installation does not generate spoil. Applying the method to discrete piles placed at further than 2.5 times the pile's diameter on center is not currently practical due to the capability of the equipment available.

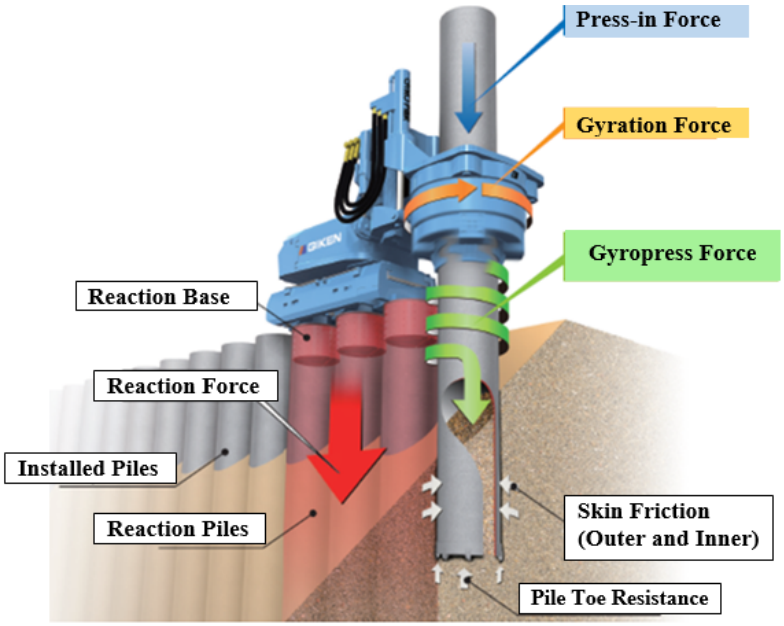


Fig. 6. Concept of Rotary Press-in of Pipe Piles

 © Deep Foundations Institute 2025

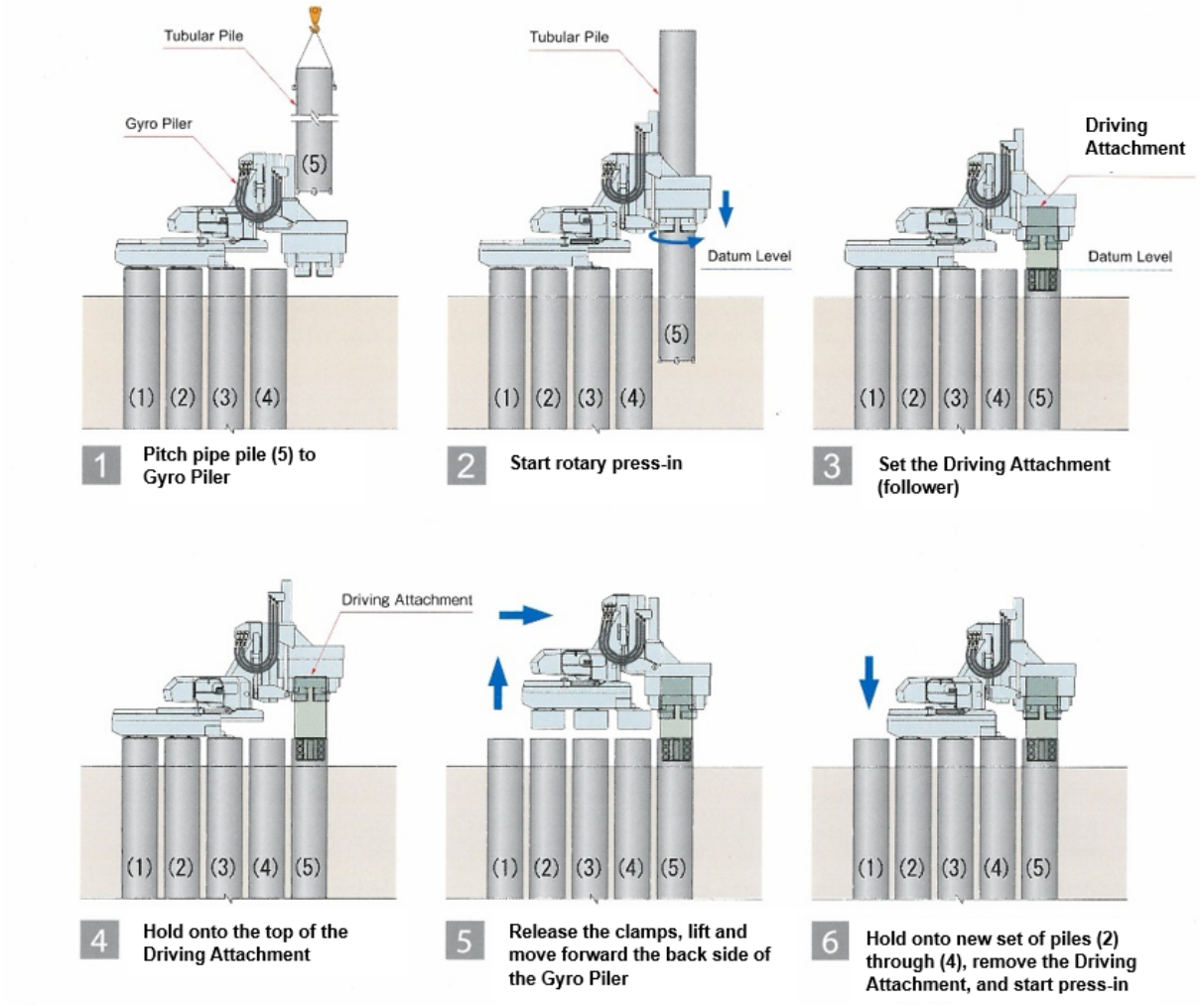


Fig. 7. Self-walking Sequence of Pipe Pile Press-in Piling



Fig. 8. Different Cutting Shoes (From left to right, Light-, Medium- and Heavy-duty)

Figure 9 shows the concept of the proprietary Giken Reaction Base System involving a rotary press-in piling machine with its power unit on a special truck, a CLAMP CRANE™, and a PILE RUNNER™; all

 © Deep Foundations Institute 2025

working and moving on top of already installed piles by using the line of the installed piles as a construction staging area as well as an access path. The PILE RUNNER hauls piles from a faraway access point by travelling on the piles to the CLAMP CRANE, which picks up one of the piles and hoists it to the piling machine. Once these pile sections are fully unloaded, the PILE RUNNER goes back to the access point for the next batch of piles. This system can reduce temporary staging areas and makes pile installation possible even where construction access is extremely difficult to secure; although the subject project utilized only the CLAMP CRANE without the PILE RUNNER because of the short piling distance. The details will be discussed in the following Construction section of this paper.

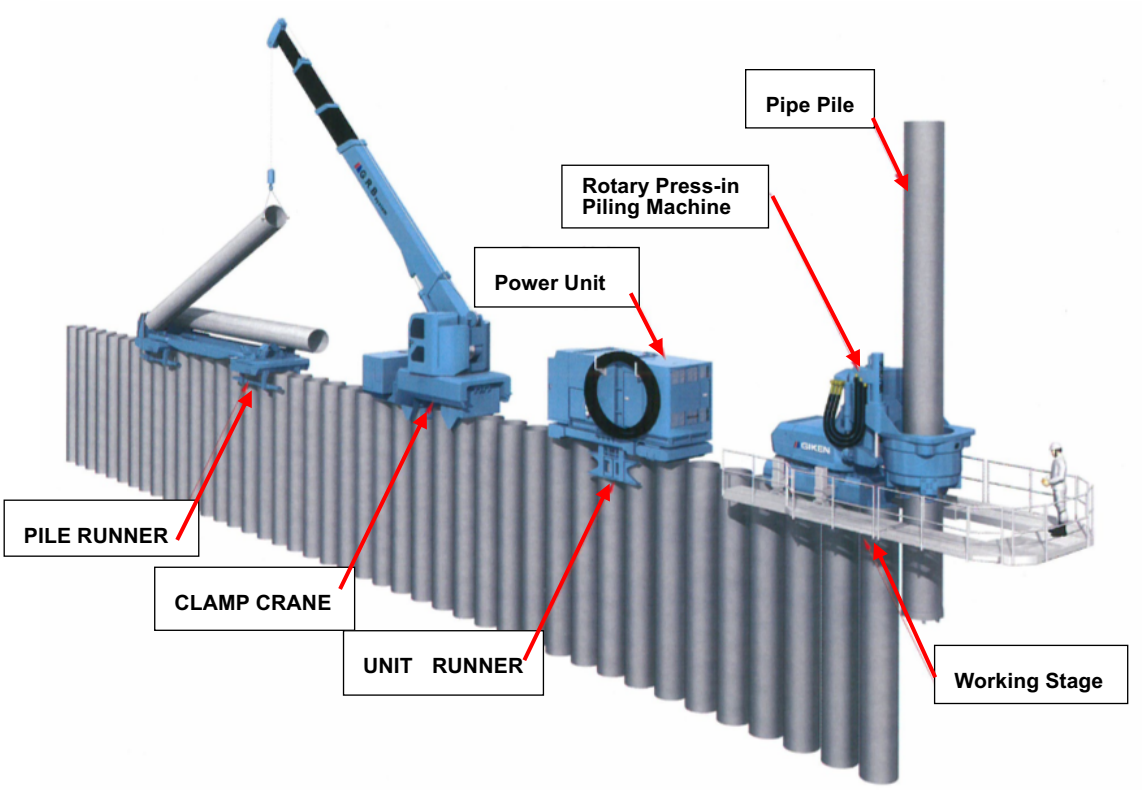


Fig. 9. Concept of GRB (GIKEN Reaction Base) System

CONSTRUCTION

An embankment in the size of 4.0m times 6.0m was first constructed at the starting point of piling where the piling machine was assembled and started pile installation with counter weight. See Fig. 10. A 70-ton capacity crawler crane with a 30.5m long boom was used for putting the rotary press-in piling machine together and pitching the pipe piles to the piling machine thereafter up to production pile number 14. Then, a 10-ton capacity CLAMP CRANE was assembled on the installed piles and started to hoist the rest of the piles to the piling machine since the crawler crane was not able to reach the piling machine as shown in Fig.

 © Deep Foundations Institute 2025

11. Each pile was spliced once to make it be 23.5m long. Typical penetration was 18.0m with exposed height of 5.5m. The total wall length was 34.0m with 34 piles installed in 9 working days with double shifts.

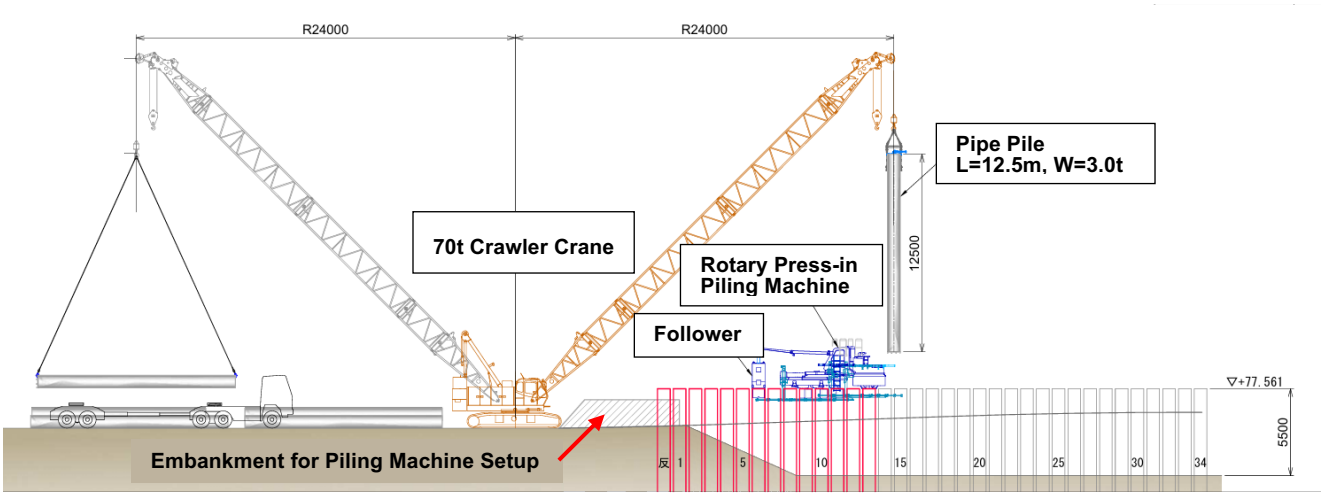


Fig. 10. Profile of Pile Installation for the First 14 Piles

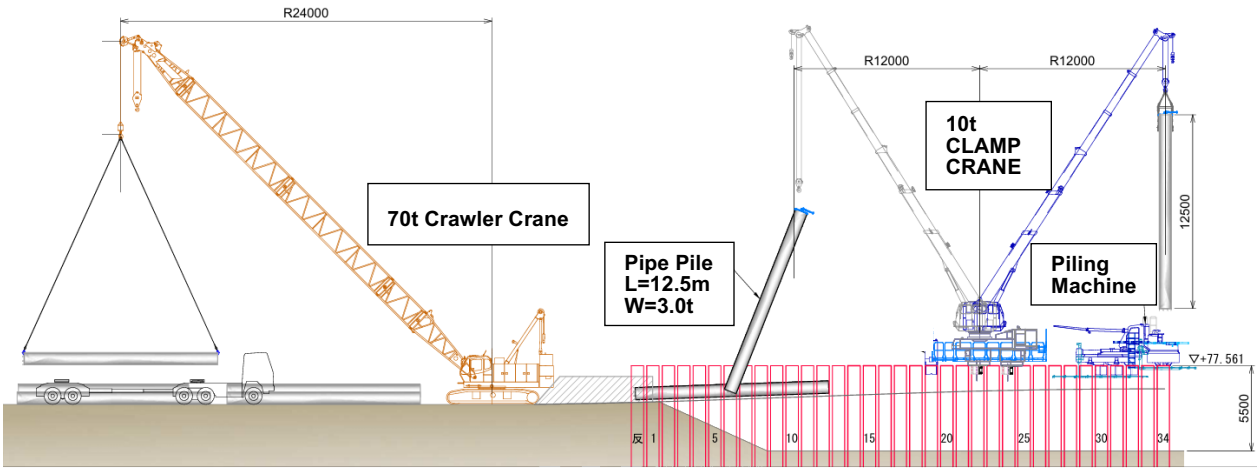


Fig. 11. Profile of Pile Installation for the Pile Nos. 15 through 34

The piles were 800mm in diameter and 11mm in wall thickness. They were installed with 250mm gaps as shown in Fig. 12. They were connected with each other via a pair of pile top connector plates (350mm wide and 250mm long) and a gap filler plate (250mm wide and 5.5m long) for preventing back fill materials from escaping through the gaps. These plates were welded to the piles onsite as the piling progressed.

 © Deep Foundations Institute 2025

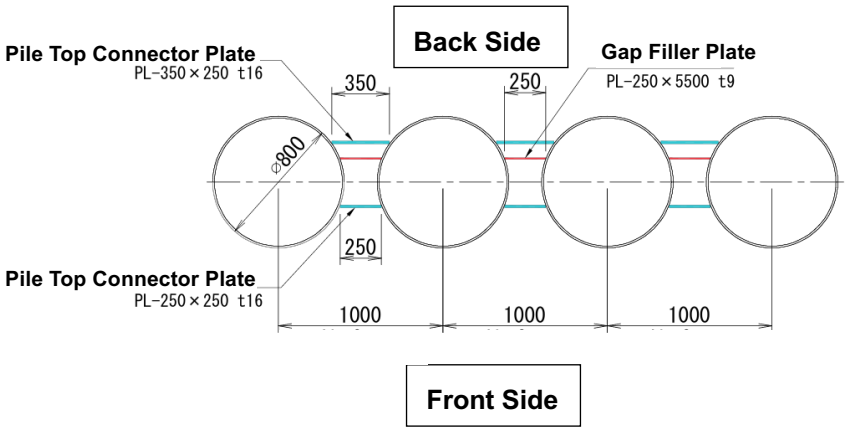


Fig. 12. Typical Plan View of Pile Arrangement

Figure 13 shows the CLAMP CRANE hoisting a new pile over to the rotary press-in piling machine with the crawler crane on the left. The embankment prepared for the piling machine setup is seen on the slope side of the crawler crane. The pile was rotated and simultaneously pressed through relatively loose sandy silt and highly weathered breccia layers and finally socketed into a less weathered tuff-breccia base rock. After the piling work, urethane foams were placed as primary backfill materials to lighten the earth pressure on the wall (0.4t/m^3 in comparison to approximately 2.0t/m^3 in the case of soil backfill).



Fig. 13. Rotary Press-in Piling with CLAMP CRANE

 © Deep Foundations Institute 2025

Figure 14 shows the completed earth retaining wall with roadway reconstruction at its final stage. Figure 15 shows the complete project with both lanes open to traffic with the Noto Ohashi viaduct as its backdrop. Roadway embankments are often damaged with erosion and/or landslides such as the case of the subject project. Their reconstruction with pressed-in piles has shown its advantages in speed, safety, and overall construction cost, once again on another project (Takuma et al 2024).



Fig. 14. Roadway Reconstruction with Completed Pressed-in Pipe Pile Wall



Fig. 15. Fully Reopened Expressway Leading to Noto Ohashi Viaduct

 © Deep Foundations Institute 2025

CONCLUSIONS

A pipe pile earth retaining wall was built with the rotary press-in piling method for reconstruction of an expressway embankment, which had been severely damaged by a strong earthquake. The pile installation was completed in a minimal footprint with the rotary press-in piling machine and CLAMP CRANE to allow one lane of expressway open during the construction. The project was completed within a relatively short period of time without building a construction access road or a temporary working platform. The method's low vibration feature assured a safe pile installation near the sensitive bridge abutment. An eroded or collapsed roadway embankment can be safely and expediently reconstructed with pressed-in pipe pile walls.

ACKNOWLEDGMENT

The authors appreciate the support provided by Kajima Corporation (General Contractor), Giken Seko Co. Ltd. (Piling Contractor) and Ian Vaz of Giken America Corp.

REFERENCES

Takuma, T., Nishimura, H., Kambe, S. (2013). "Low noise and low vibration tube pile installation by the press-in piling method", *Proceedings of 2013 Annual Conference of Deep Foundations Institute.*

Takuma, T., Nishimura, H., Vaz, I., and Nagano, M. (2017). "Deep Pipe Pile Cell Foundations Built in Rivers for Expressway Viaduct Widening", *Proceedings of 2017 International Bridge Conference*, Engineers' Society of Western Pennsylvania.

Takuma, T., Nagano, M., Kubo, S., (2024), "Emergency Repair of Severely Eroded Highway Embankment with Pressed-in Pipe Piles", *Proceedings of 2024 International Foundation Congress and Equipment Expo",* International Association of Foundation Drilling, Deep Foundations Institute, Geo-Institute of the American Society of Civil Engineers, and Pile Driving Contractors Association.

White, D., Finlay, T., Bolton, M., and Bearss, G., 2002. Press-in Piling: Ground Vibration and Noise during Piling Installation, *Proceedings of the International Deep Foundation Congress*, ASCE Special Publication 116.

 © Deep Foundations Institute 2025

INNOVATIVE BRIDGE PIER INSTALLATION USING THE SUPER REACH ATTACHMENT SYSTEM: INSIGHTS FROM THE DESIGN-BUILD JIMMIE DAVIS BRIDGE REPLACEMENT PROJECT

Jewels Stover, Bauer Equipment, Denver, CO, USA 303.746.1072, jewels.stover@bauer-equipment.com
Sean Pruet, R.R. Cassidy Inc. Prairieville, LA, USA 404.539.1092 sean.pruet@rrcassidy.com

ABSTRACT

The $360 million Jimmie Davis Bridge Replacement project in Shreveport, Louisiana is a design-build initiative consisting of aa new four-lane bridge construction, alongside essential roadway enhancements, just north of the existing two-lane structure spanning the Red River. A key focus of this case history is the installation of the bridge piers utilizing the innovative Super Reach Attachment (SRA), a new-to-market leader system mounted to a duty-cycle foundation crane. This equipment enables an extended drilling axis, facilitating the installation of 45 drilled shafts, each with a diameter of 58.5 in (1486 mm), at depths ranging from 100-150 ft (30.48 – 45.72 m) into the riverbed, ensuring robust support for the new bridge structure.

INTRODUCTION

Completed in 1968, the two-lane Jimmie Davis Bridge stretches 1.1-mile (1.8 km) between Shreveport and Bossier City, Louisiana. to. The original, metal truss bridge was constructed on land owned by former Louisiana Governor Jimmie H. Davis and is notable for its impressive 300 ft (91.44 m) spans across the Bayou State's Red River. The bridge's piers were seen by some as monuments to the former Governor's administration, with construction commencing just two weeks before the end of Davis's final term in office and 2.5 years prior to the start of superstructure construction and. Designed with a 50-year lifespan – standard for the era – the bridge has now exceed its tenure by several years and is due for replacement by a modern river crossing, which are typically built to last between 70 and 100 years.



Fig. 1. Jimmie Davis Bridge

 © Deep Foundations Institute 2025

In 2024, construction began on the design-build contract for the new four-lane bridge adjacent to the existing structure, as shown in Fig. 2. According to the Louisiana DOT, the new bridge will significantly improve traffic flow, reduce congestion, and support economic development by doubling the vehicle capacity of the current river crossing. The project is expected to be completed in 2027, at which point the original, two-lane bridge will be repurposed as a pedestrian- and bike friendly route that preserves the historically significant, original structure while also providing a safe alternative route for non-motorized transportation.



Fig. 2. Location and Plans for New Bridge

SCOPE OF WORK AND CONSTRUCTION SEQUENCE

R.R. Cassidy Inc was selected to support the construction of the 3 new bridge piers by installing 45 deep-drilled shafts in the bed of the Red River. The scope of work includes15 drilled shafts per pier, arranged in 3 rows of 5 piles each. All drilled shafts will be installed from a floating barge platform within the river channel.

With depths ranging from 100 ft (30.48 m) to approximately 150 ft (45.72 m), the drilled shafts have a nonstandard diameter of 58.5 in (1486 mm) is and require the use of custom-fabricated drill tools. Installation of each drilled shaft begins with the placement of a 96 in (2438 mm) inside diameter (ID) surface casing, 35 ft (10.7 m) in length. This casing is installed using a crane-suspended, free-hanging vibrator as shown in fig. 3. The surface casing functions as a cofferdam, preventing river water intrusion and maintaining the integrity of the seal at the split casing formwork as shown in fig. 5.

Following the installation of the surface casing, a 'sacrificial' permanent casing of approximately 61 ft (18.6 m) in length, is driven inside the surface casing using an impact hammer, as shown in fig. 4, because vibratory methods are prohibited below the scour depth. The 60 in (1524 mm) ID permanent casing provides support for the upper portion of the borehole, which primarily consists of poorly graded, medium-dense sands.

The top of the sacrificial permanent casing terminates at elevation 140.5 ft, placing it approximately 4.5 ft (1.4 m) underwater at normal pool elevation and 1.5 ft (.46 m) below the top of the drilled shaft concrete. A split casing is then bolted to the top of the sacrificial permanent casing to serve as formwork for the final 1.5 ft (.46 m) of the drilled shaft. This configuration also maintains visibility of the shaft excavation for the operator above the waterline, facilitating alignment and drilling efficiency. The split casing is then removed after the pile concrete has achieved initial set.

 © Deep Foundations Institute 2025



Fig. 3. Installation of Surface Casing



Fig. 4. Installation of Sacrificial Permanent Casing



Fig. 4: Installation of Split Casing Formwork



Fig. 6. Belling Bucket used for Over Reaming

 © Deep Foundations Institute 2025

Below the sacrificial permanent casing, the borehole is stabilized using a polymer slurry to the final excavation depth. Specification provisions require that once excavation proceeds below the permanent casing, all subsequent operations – including completion of drilling, bottom cleaning and inspection, including firmness measurements, placement of reinforcement, and concrete placement – must be completed within a 36-hour window. If this time constraint is exceeded, the pile must be over reamed using a belling bucket as, shown in fig. 6, to increase the pile diameter to 63 in (1600 mm). The over-reaming process ensures fresh concrete has contact against a clean sidewall surface. While this type of specification is traditionally associated with bentonite slurry, due to the formation of filter cake on the borehole walls, it remains a requirement for this project despite the use of polymer slurry which does not exhibit the same filter cake behavior.

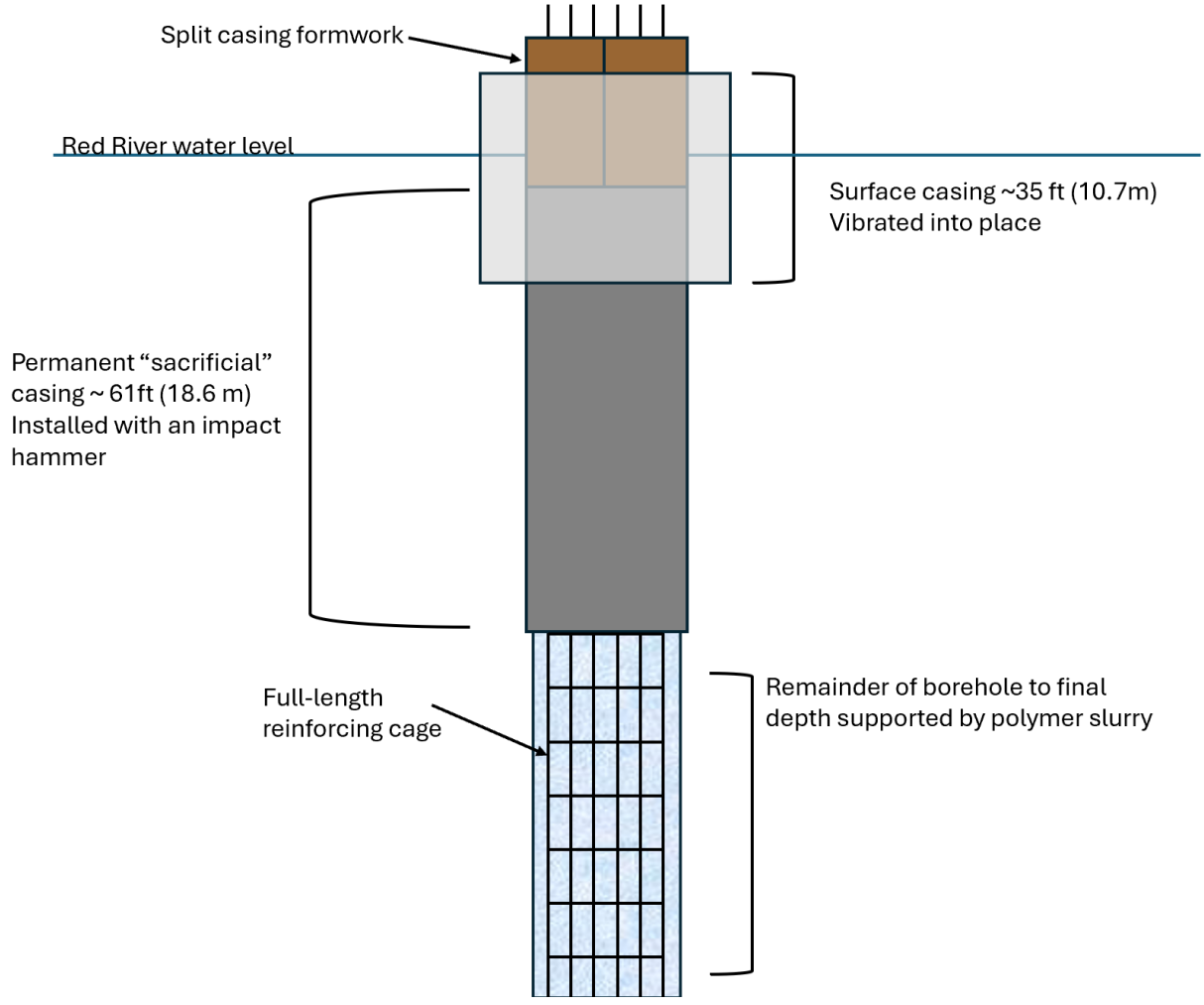


Fig. 7. Cross Section of Pile Design (not to scale)

Through Thermal Integrity Profiling (TIP) and Crosshole Sonic Logging (CSL) of a test shaft, it was determined that an SID (Shaft Inspection Device) camera would be used on all production shafts to verify a firm, sediment-free base prior to concrete placement.

The SID camera is equipped with prongs that allow visual measurement of sediment depth at the bottom of the borehole. As the camera contacts the base, sediment accumulation can be observed against the prongs in the video feed. Measurements are taken at five locations: north, east, south, west, and center as shown in

 © Deep Foundations Institute 2025

fig. 8. To confirm a clean bottom and proceed with shaft installation, sediment must not exceed ½ in (12.7 mm) at any three of the five locations, and no single measurement may exceed 1.5 in (38.2 mm). If these criteria are not met, the borehole must be recleaned and re-evaluated using the SID camera.

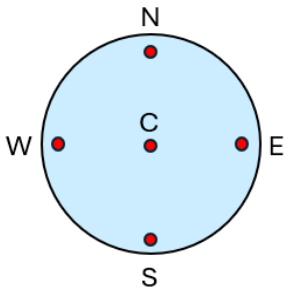


Fig. 8. Locations of Sediment Measurements with SID Camera

Once the borehole is confirmed to have a clean bottom, a full-length reinforcing cage is lowered into the borehole using a utility crane assisted by a specialized tilting device to vertically orient the cage from its horizontal position as depicted in fig. 9.

Using the tremie method, concrete is pumped at 5000 psi (34.5 MPa) from trucks and pumps on the land-based trestle, via delivery lines suspended on floating platforms, to the pile location illustrated in fig. 10. The Concrete is introduced at the base of the borehole via the submerged tremie pipe, displacing the polymer slurry up the shaft. The displaced slurry is collected at the top of the shaft and pumped back to storage tanks on the barge for reuse in subsequent shaft excavations.



Fig. 9. Tilting Device for Picking Rebar Cages



Fig. 10. Floatation Supported Lines for Concrete Delivery

 © Deep Foundations Institute 2025

The polymer slurry maintains borehole stability and promotes settling of sand and fine particles at the bottom of the borehole during excavation. These settled materials are then removed with a flat-bottomed cleanout bucket upon reaching final depth. Due to the self-flocculating nature of the polymer, no additional slurry treatment or cleaning processes are required prior to concrete placement.

The production cycle is limited to one completed pile installation at a time. Given the layout of 5 piles per row, maintaining multiple boreholes or shafts in different stages of construction is not feasible. To minimize the risk of disturbance to recently completed shafts, new boreholes must not be initiated adjacent to completed piles within 24 hours of concrete placement. As a result, installation follows a primary-secondary sequence, as shown in fig. 11, with drilling operations scheduled during the night shift and subsequent activities – borehole cleaning, bottom inspection, reinforcement cage placement, and concrete placement – performed during the day shift.

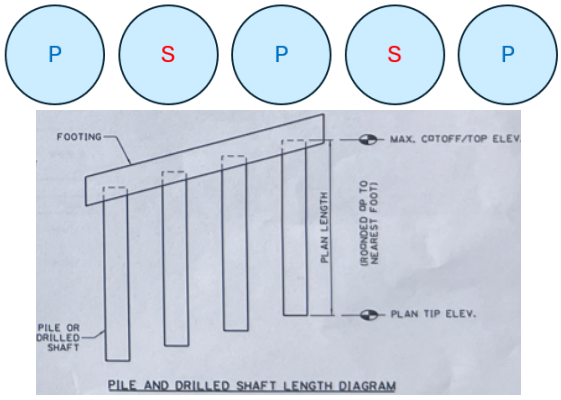


Fig. 11. Pile Sequence and Layout

TECHNICAL CHALLENGES AND DRILLING EQUIPMENT

Working from a floating barge posed significant challenges that required detailed planning. The team carefully analyzed how drilled shaft installation would be carried out from a mid-river platform, focusing closely on the stability of the equipment as it was operating on what is, essentially, a moving surface.

Given the complexity and scale of the project, the team concluded that multiple, smaller barges would provide more flexibility for access and support. These smaller barges could maneuver more easily within the confines of the river, improving coordination and allowing for a more efficient installation process. For the drilling operation, the team selected a140 ft x 55 ft x 8ft (42.7 m x 16.8 m x 2.4m) spud barge to serve as the main work platform.

However, this choice introduced a new challenge in selecting suitable drilling equipment. The use of fixed-mast piling rigs to install drilled shafts is very common, and these types of rigs are capable of installing shafts in the water from a barge, but further evaluation was needed for a rig like this on a relatively small barge.

A third-party engineering review of the original plans for a fixed mast piling rig found a critical issue. To maintain stability, the rig would need to be placed near the center of the smaller barge. In that position, however, the rig would not have enough displacement of the drill axis to reach the required shaft locations.

 © Deep Foundations Institute 2025

A stability analysis, depicted in fig. 12, confirmed this limitation. The combination of the barge dimensions and the rig specifications meant the equipment couldn't safely or effective complete the shaft installation from the position on the barge necessary to maintain stability.

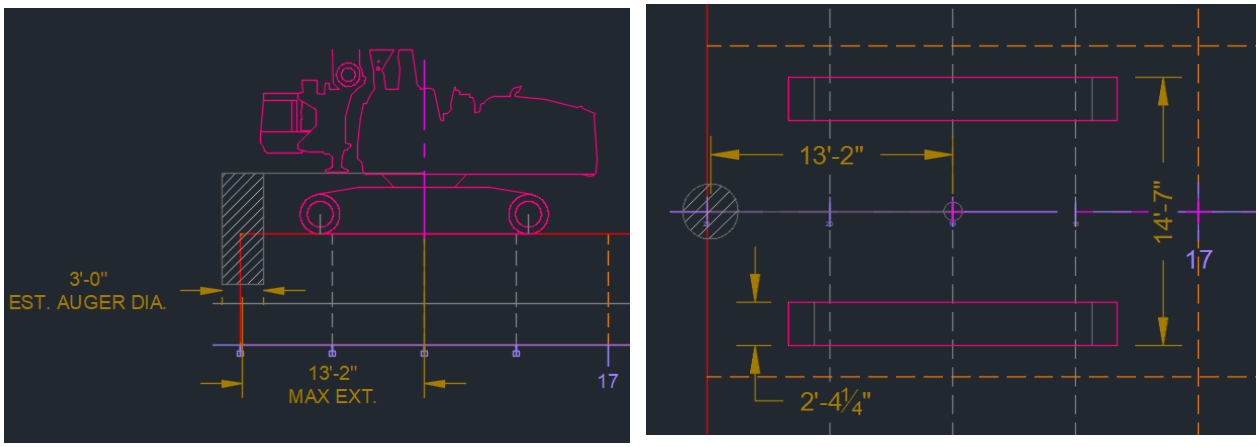


Fig. 12. Stability Evaluation of Fixed Mast Piling Rig

To overcome this challenge, the contractor needed to identify an alternative to the conventional fixed-mast piling rigs. The selected equipment had to ensure barge stability while providing sufficient outreach to access the pile locations in the river.

A potential solution emerged through a post on the professional networking platform LinkedIn, which introduced the contractor to a new-to-market system: a specially adapted Vertical Travel Lead (VTL) Suspended Leader System designed for use with a foundation crane. The system, referred to as the Super Reach Attachment (SRA) shown in fig. 13, integrates the proven performance of rotary drilling tools with the flexible kinematics of a duty-cycle Crane.

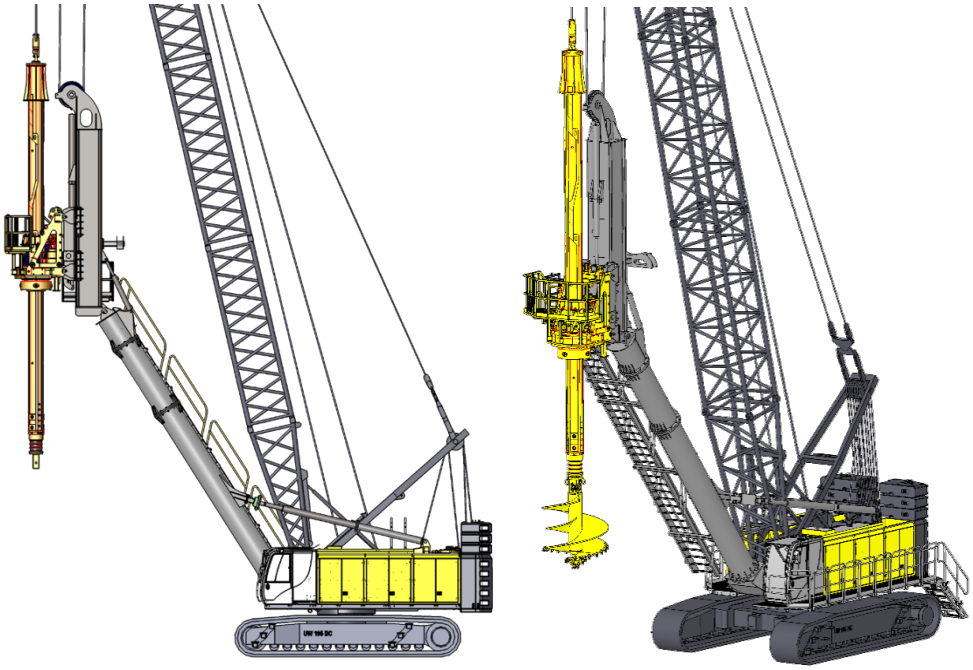


Fig. 13. Duty-Cycle Foundation Crane with SRA Attachment

 © Deep Foundations Institute 2025

The SRA system is configured with both a crowd and auxiliary winch system, providing not only rotational torque but also the significant downforce required for effective drilling. The attachment is fully integrated into the crane's hydraulic and elecrtrical systems, allowing complete control through the onboard computer interface. All hydraulic power needed to operate the SRA is provided from the crane base carrier, ensuring efficient, self-contained operation. This equipment is particularly well-suited for installing large-diameter drilled shafts at extended distances from the base machine, and accessing difficult-to-reach pile locations.

The SRA system supports multiple mast configurations compatible with cranes in the 130-200 ton class, offering a significantly greater working range than standard fixed-mast piling rigs or other crane-mounted attachments. With a mast extension, the SRA system is capable of achieveing a maximum working radius of 42.7 feet (13 meters).

After initial discussions with the equipment manufacturer, the contractor provided the equipment specifications to the thrid-party engineering firm to assess the feasibility and stability of the SRA system. The analysis confirmed that, thanks to the extended reach of the SRA, the crane could be centrally positioned on the barge, ensuring access all required pile locations while maintaing stability. From this position, the crane and SRA achieved a functional working radius of 30 feet (9.1 meters) as shown in fig. 14.

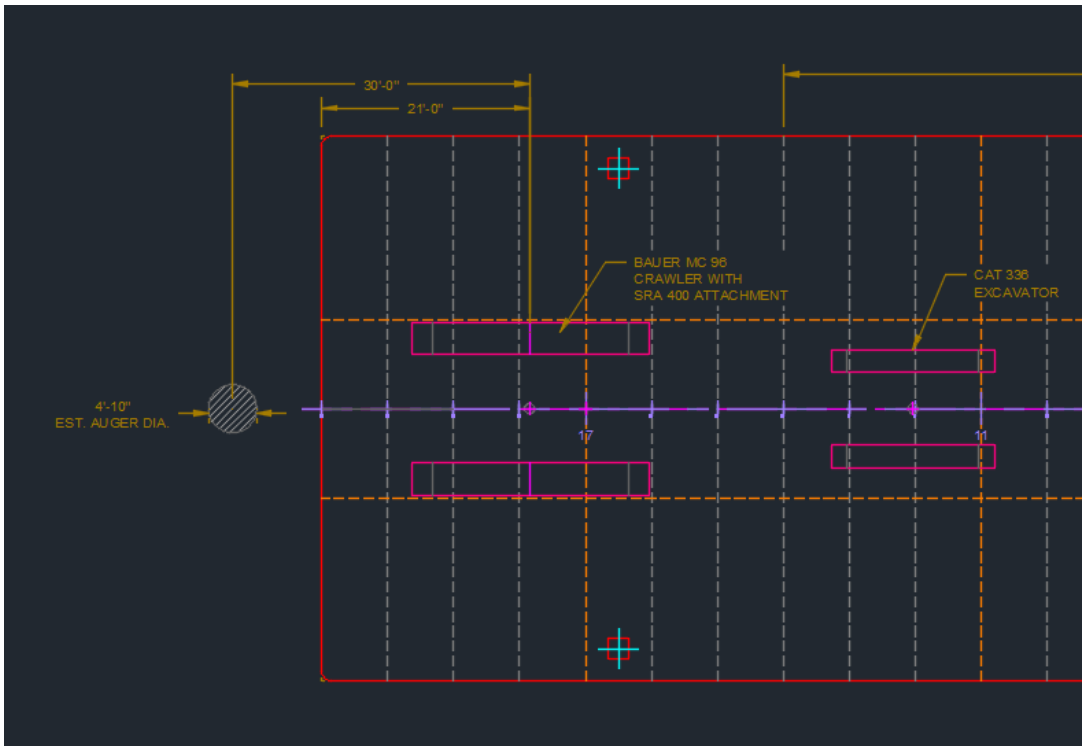


Fig. 14. Evaluation of barge positioning for the Duty-Cycle Foundation Crane with SRA

To safely support the equipment and distribute operational loads, timber crane mats were installed beneath the crane, and the equipment was anchored to the barge deck. This eliminated the need to structurally modify or reinforce the barge, maintaining the intergrity and streamlining set-up of the drilling barge.

The equipment manufacturer also provided valuable support in adapting the system for site-specific conditions, including management of barge listing during spoil deposition, and ensuring proper tool alignment when working from the uneven or shifting platform.

A major advantage of this crane and leader set up was its ability to install drilled shafts in multiple locations without the need to reposition the barge. The extended reach also allowed the excavated material to be offloaded directly on to a separate spoil barge, greatly improving operational efficiency and reducing handling time.

Finally, the SRA system came equipped with automated drilling assistant features. These functions enhanced production quality, reduced wear on the drilling tools and minimized mechanical stress on the equipment – leading to improved consistency and reduced maintenance needs throughout the project.



Fig. 15. Duty-Cycle Foundation Crane with SRA Installing Drilled Shafts from the Barge

CONCLUSION

The challenges of complex construction environments require more than a single tool or standard approach and seasoned professionals understand that successful project delivery often requires innovation, flexibility, and collaboration across disciplines. This project exemplifies how creative thinking and close coordination between designers, engineers, contractors, and equipment manufacturers can lead to effective, custom solutions.

 © Deep Foundations Institute 2025

The strategy implemented on this project, utilizing multiple smaller, more maneuverable barges to increase installation efficiency, demonstrated how solving one operational challenge can often introduce new ones. However, through collaborative problem-solving and the adoption of a new-to-market drilling system, the team successfully developed safe, efficient, and practical solutions to each obstacle encountered. This project highlights the importance of adaptive engineering, integrated construction planning, and thoughtful equipment selection in overcoming even the most demanding project conditions.

 © Deep Foundations Institute 2025

CSO52 - TEMPORARY SUPPORT OF EXCAVATION AND DEEP FOUNDATIONS FOR FLOOD PROTECTION

Garrison Mueller, P.E., Clark Foundations, LLC, McLean, VA USA.
Jake Coibion, Guy F. Atkinson Construction, Austin, TX USA

ABSTRACT

The CSO-52 Storage Tunnel and Pump Station project located in Lynchburg, VA, consist of constructing a new CSO storage Tunnel, two diversion structures, a tunnel dewatering pump station, an electrical building and appurtenant work. The upstream (CSO 52) and downstream (CSO 134) sites containing the diversion structures, pump station and electrical building, are located adjacent to Blackwater Creek. During intense rain events, the sites are exposed to significant flood risk.

This paper focuses in the design and construction of the temporary support of excavation (soil and rock) and groundwater cutoff measures needed to enable the work for the pump shaft (approximately 98 feet deep) and diversion structures, as well as the permanent 4-ft diameter caissons with permanent casing and 12-ft deep rock socket required for foundation support of the Electrical Building designed to resist the 500-yr flood.

Temporary SOE for soil and water at the pump shaft consisted of a circular sheet pile system designed to provide protection for 100-yr flood during construction. Shotcrete and rock bolts were used within the rock strata. A pre-excavation rock grouting program was conducted from the surface to reduce the seepage into the rock shaft excavation during construction.

The paper will describe the design and construction challenges, as well as the various solutions needed for the project's unique conditions such as access constraints, contaminated soils, rock variability, and several unforeseen obstructions in the soil matrix.

PROJECT BACKGROUND

This project also know as LYHBeyond or Blackwater CSO Tunnel Project is ,located in Lynchburg, Virginia. The project consists of constructing a new CSO (combined sewer overflow) storage Tunnel, two diversion structures, a tunnel dewatering pump station, an electrical building and appurtenant work. The upstream (CSO 52) and downstream (CSO 134) sites are located adjacent to Blackwater Creek. The CSO 134 site contains the diversion structures, pump station and electrical building. No construction work has been started at the CSO 52 site by the date this paper was written. Therefore, this paper focuses on the work at the CSO 134 site. An overview of the project site is shown in Fig. 1.

The City of Lynchburg has removed 115 of their 132 CSO locations from 1979 to 2014. Since 2014, the city has implemented a new "Long Term Control Plan" (LYHBeyond) to address the remaining CSO points. The Blackwater CSO Tunnel provides up to 4.7 million gallons of storage for these major storm events to further increase the city's capacity. This project will bring the City to a 95% reduction in CSO overflow since the Program began. The tunnel, drop shaft and pump shaft will serve as a large water reservoir. The

 © Deep Foundations Institute 2025

diversions structures at each location will serve as a way for water to reach a certain elevation within the pipes and then divert into the tunnel. The valve vault and electrical building will house key electrical equipment that will then pump the water from the bottom of the tunnel back into the system to then get treated further downstream once the storm has passed.

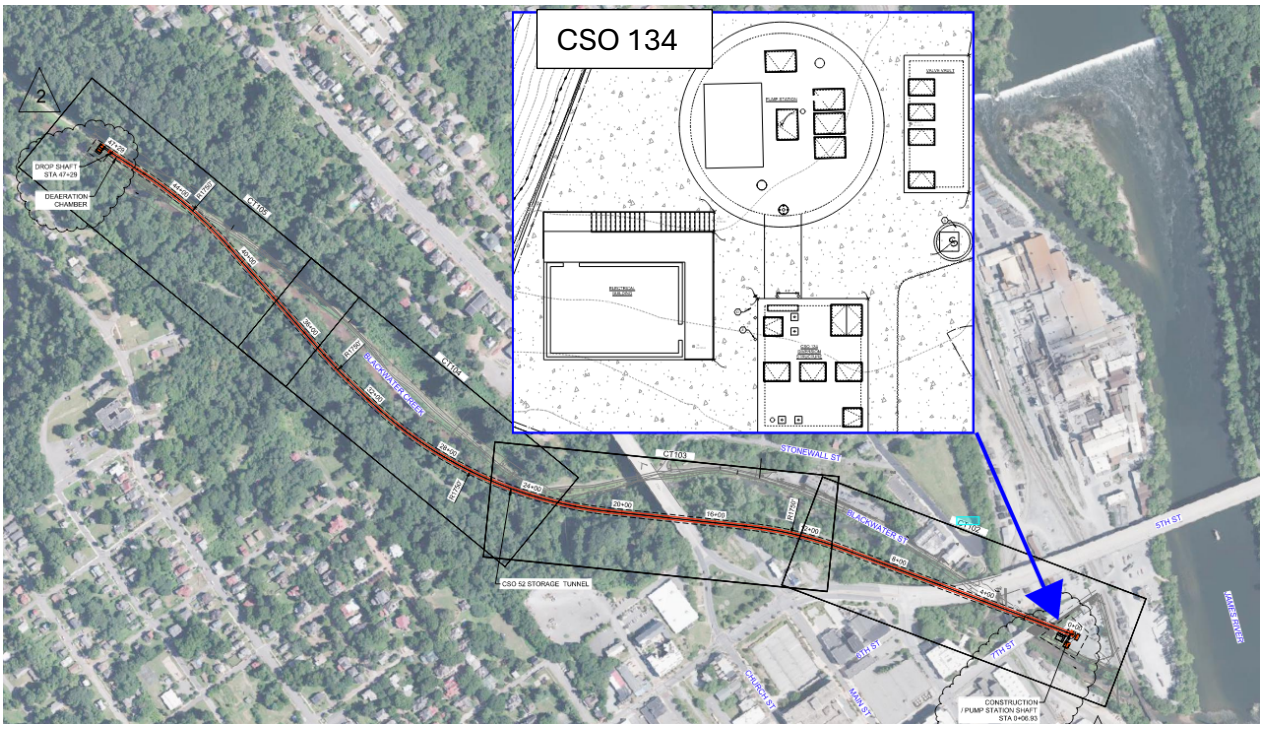


Fig. 1. 134 Overall Project Work Zones.

CSO 134 is located near the conflux of the blackwater creek and James River. The site has experienced flooding that has extended to elevation 529’. The existing grade for the site is elevation 520’. This site contains a pump shaft, diversion structure, valve vault, and an electrical building. This is the origine point for the start of the tunnel.

Improvements at the CSO 134 (Tunnel Pump Station Site) site include:

Pump Station: Dewatering pump station with 38-ft inside diameter shaft and an air vent pipe. The shaft is used for tunnel construction as well as a straight plunge-type drop shaft to receive flow from the James River Interceptor. Total pump shaft depth is about 97 feet.
Electrical Building: Houses electrical and instrumentation equipment that is used to operate the pump station facility.
Diversion Structure: Flow diversion and regulation structure used to discharge flow to the pump station shaft and to ta new CSO outfall pipe and structure at the Blackwater Creek.

 © Deep Foundations Institute 2025

SUPPORT OF EXAVATION AND DEEP FOUNDATON SYSTEMS

Geology and Hazards

The project is within the northwestern portion of the Piedmont Physiographic Province of western Virginia. The site stratigraphy consists of undocumented fill, alluvial and residual soils deposits, weathered rock (transition zone) and rock (Gneiss and Schist). The undocumented fill stems from the historic use of the area which includes industrial use. The residual soils are a result of weathering of saprolite. The weathered saprolite in the area is highly porous, low-density soil that is susceptible to sloughing below the water table and to consolidation when loaded or dewatered. The rock joints act as pathways for groundwater flow.

According to the 2008 Flood Insurance Rate Map (FIRM), the CSO 134 site is within an area subjected to inundation by the 1% annual chance flood (100-year flood). Ground elevation around the shaft is at elevation 520', and the 100-year flood elevation is approximately 527' as shown in Fig. 2. Since the construction of the project starts with the excavation of the pump shaft, it was determined by the project's engineer of record that the shaft and the tunnel construction could be impacted by the 100-year flood event. Therefore, the contract documents specified that the design of the temporary SOE for the pump shaft had to consider this probability of flooding.

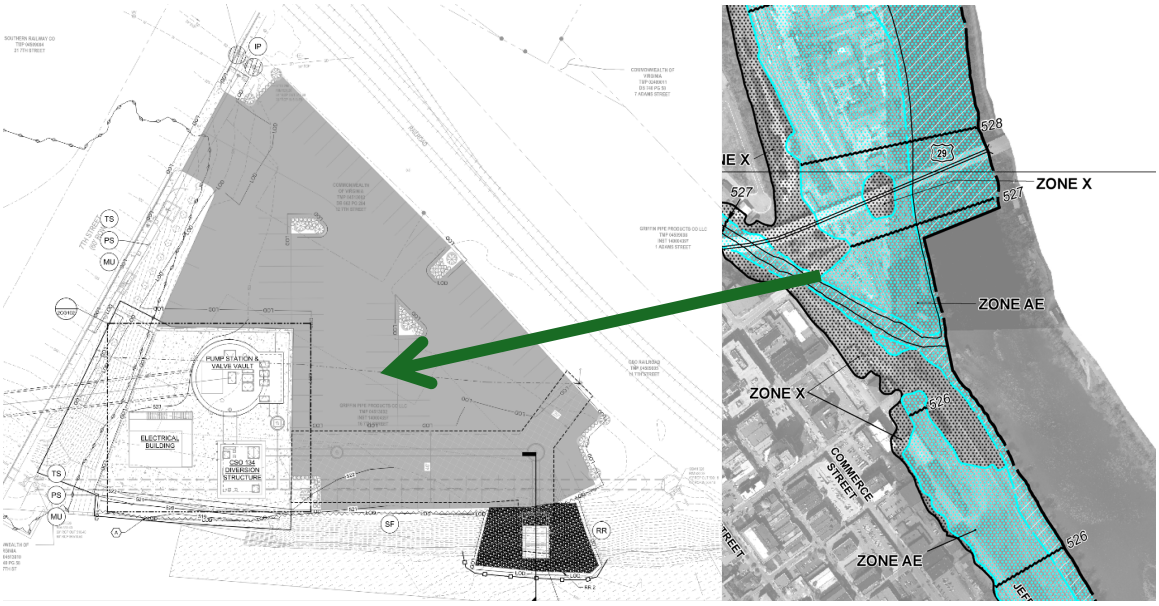


Fig. 2. FEMA 100-year flood at the CSO 134 site

The electrical building that supports the pump shaft is located close to the banks of the Blackwater creek and is subjected to flooding and scouring. Flood risk for this building is different than the temporary design criteria as this is a permanent structure. The flood risk is high as its location may expose it to the 500-year flood event (Design Flood EL 534).

Environmental investigations at the site concluded that all of the overburden soils were contaminated and are not suitable to support the Diversion and Valve Vault structures. These soils had to be removed between

 © Deep Foundations Institute 2025

ground surface and top of rock, and replaced with structural fill or stone. The maximum depth to top of rock was 28 feet.

System Selection

Deep Foundations at the Electrical Building were fully specified by the EOR and consisted of 4-foot diameter caissons with permanent casing and a 3-foot diameter rock socket, with a grid of deep grade beams and pile caps. An isometric view of the electrical building and the deep foundation and grade beams layout is shown in Fig. 3.

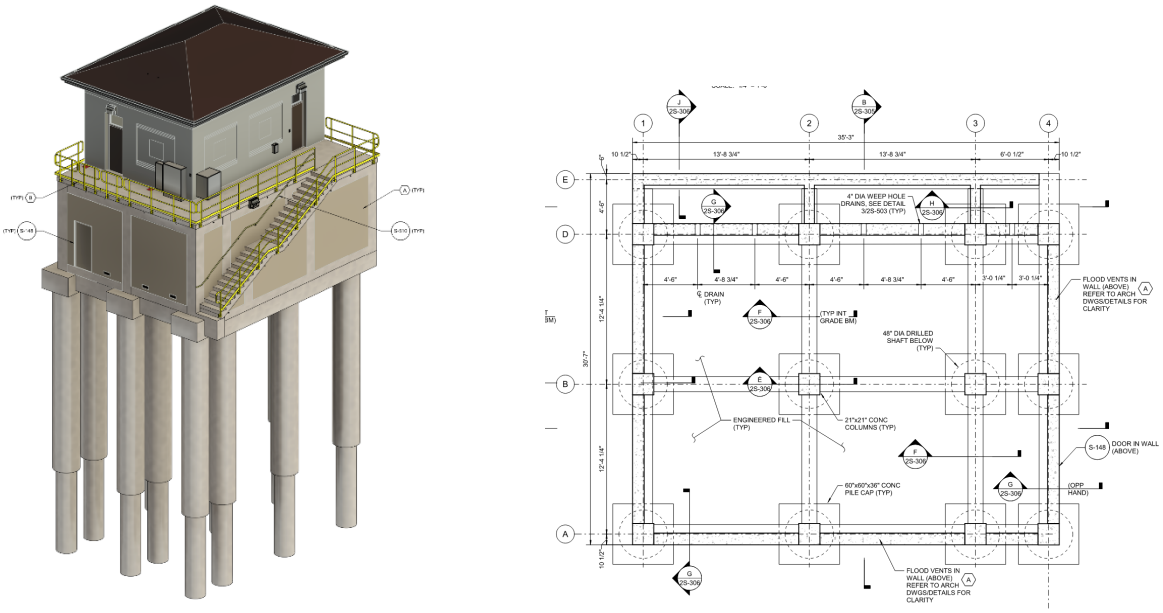


Fig. 3. Electrical Building Deep Foundations.

This robust foundation design for the electrical building was controlled by the 500-year flood extreme event. It was considered that scouring and high water flows would also impact this building.

At the pump shaft, the temporary support of soil and rock system selection and design responsibilities was split. Temporary support within the soil and transition zones were the responsibility of the contractor. Design of the rock support was provided by the EOR and consisted of grouted rock anchors and fiber reinforced shotcrete. A schematic section and an actual photo of the SOE at the pump shaft is provided in Fig. 4.

 © Deep Foundations Institute 2025

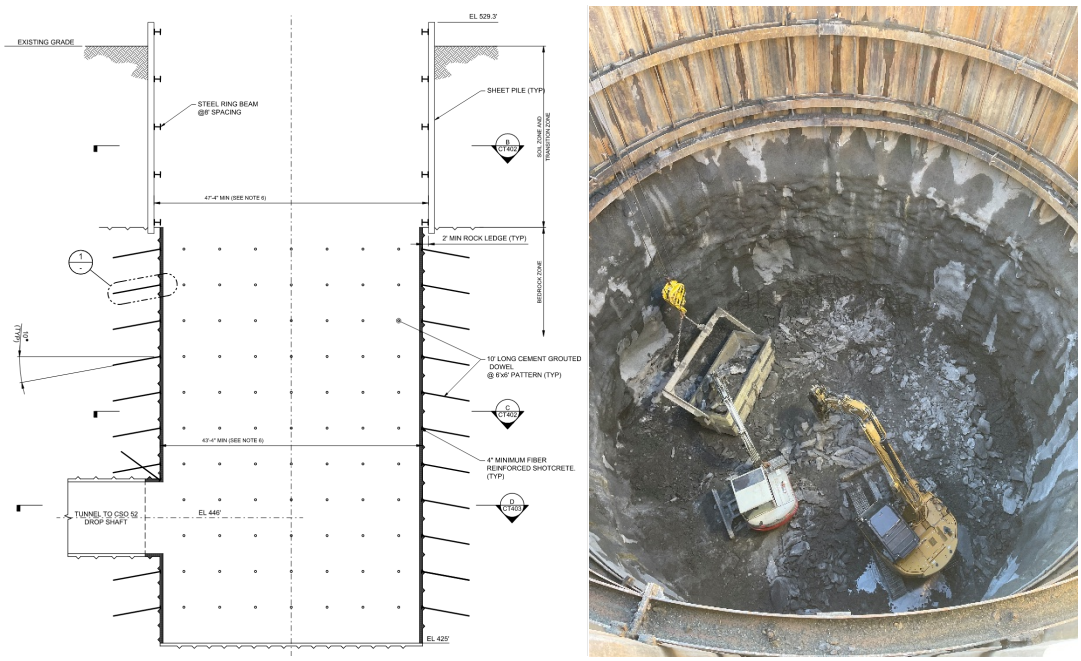


Fig. 4. Schematic (left) and actual photo (right) of the Temporary SOE for the Pump Shaft

The soil temporary SOE was required to be a watertight system capable of providing temporary flood protection during the 100-year flood event. Several systems were considered during the bid phase including rectangular and circular systems. Circular systems are typically preferred for shaft excavations. However, rectangular systems were considered because the original layout of the pump shaft and valve vault included the valve vault partially embedded into the shaft. And, since the overburden soils were required to be fully removed to top of rock within the valve vault, a fully circular SOE would either had to be large enough to fit both structures, or it would require extensive bracing to accommodate the truncated circle.

A couple of iterations included secant piles with walers and corner braces to create the required, unobstructed opening within the center of the pump shaft and installation of plates along the perimeter for flood protection. Another design iteration included soldier beam installation with metal plate lagging and a similar internal bracing scheme.

After the project was awarded, Atkinson (general contractor) proposed to detach the Valve Vault and the pump shaft structures for better constructability. Another value proposition was to support the Valve Vault structure on deep foundations. By doing this, the team was able to reduce the excavation depth and disposal of contaminated soils, since all structures not supported on deep foundations needed to be supported on top of competent rock.

Atkinson and Clark Foundations coordinated this design change for the Valve Vault structure, which made us reconsider the pump station shaft SOE system to a circular shape. The final selected system consisted of sheet piles supported with four levels of circular steel rings. This design did not extend beyond the footprint of the shaft and allowed for a clear and unobstructed entrance into the shaft. Subgrade elevation for design was EL. +496 for soil support with the maximum retained height of 27 feet. Top of sheet piles at the pump shaft is 529.3’ to protect during a 100-year flood event.

 © Deep Foundations Institute 2025

Groundwater infiltration into the excavation through the rock mass was specified to be mitigated by Pre-Excavation Grouting. This program included high mobility grouting outside of the perimeter of the SOE. A schematic plan view and section of the SOE at the pump shaft is provided in Fig. 5.

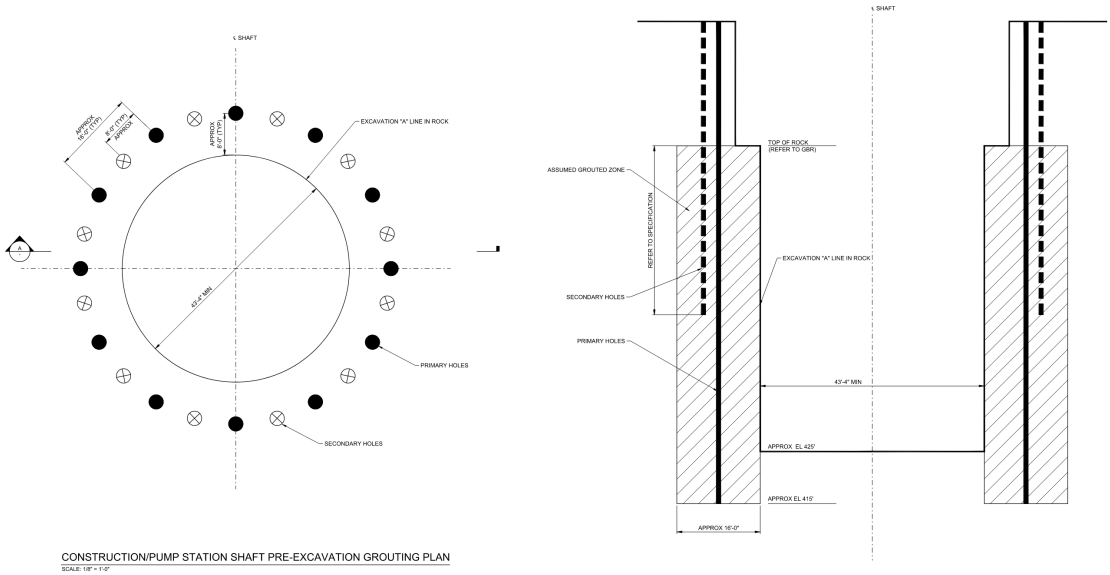


Fig. 5. Schematic Rock Mass Grouting

At the diversion structure and valve vault, there were no specific requirements for the type of SOE and entirely delegated to the Contractor. The SOE at these structures was needed to facilitate excavation to top of rock, however the contractor elected to value engineer the valve vault structure to use caissons to support the structure. Soldier pile and timber lagging with various tiers of internal bracing were chosen for these structures.

ANALYSIS AND DESIGN OF SOE IN SOIL

The design was approached taking into consideration staged construction, service and extreme load cases, as well as time dependency strength characteristics of the soils. Service load case included all expected surcharges, soil and groundwater loading under undrained and drained strength conditions. Surcharge loads were coordinated with Atkinson to better understand the type, magnitude, and location all probable surcharges during construction. These included, a duty cycle 150 TN crane, support cranes, stockpile zone for excavated soils and rock, temporary stockpile of materials, and temporary electrical and mechanical support elements. Extreme load case included the 100-yr flood event at for the Pump Shaft SOE.

Limit equilibrium analyses were performed for the various stages of construction and loading conditions. Also, the maximum and minimum rock elevations from the geotechnical borings were considered. This rock variability was the most important factor when designing the internal bracing for the sheet piles. Since the ring beams act as compression rings, the variability of the rock could result in unbalanced loading within the ring. This becomes more prevalent for the lower tiers closest to the rock.

 © Deep Foundations Institute 2025

The design of the sheet piles and soldier piles also relied on a minimum embedment into the weathered rock to allow for the installation of the lowest tier of bracing.

CONSTRUCTION

By the time that this paper was written, the pump shaft sheet piles and excavation, electrical building piles and soldier pile installation of the diversion structure SOE have been completed. The other elements of the project are yet to be completed.

Pump Shaft and Diversion Structure

The SOE Contractor started the construction of the ninety eight foot deep pump station by vibrating and driving sheet piles around the outer edge circumference of the pump shaft, with an inside diameter of approximately 45 feet. A two-tiered circular template was built above grade to guarantee that the full closure of the circular layout was accomplished, and to maintain the tight tolerances of the project. All of the sheet piles were vibrated to the top of the transition layer and then driven with an impact hammer to practical refusal to top of rock which ranged from twenty-one to twenty-eight feet from existing grade.

Unforeseen obstructions were found during the installation of the sheet piles and soldier piles. The obstructions consisted of buried slabs, columns, concrete footings, concrete retaining walls and bearing walls. It appeared that a building had been located at this site, but there were no records of its existence. Clark Foundations had done its due diligence to try to understand the history of this site during the design phase. No one had any idea that these types of obstructions were present at the site. Installation of the sheet piles and soldier piles were impacted by these obstructions by delaying the operations. Obstructions found within the sheet pile alignment had to be excavated and removed. Obstructions found within the diversion structure soldier piles could not be excavated and removed due to proximity to an existing 60 inch diameter storm sewer. These obstructions and the affected soldier piles had to be drilled.

Detailed information of sheet pile installation including blows per penetration and tip elevation were recorded since the design relied on a minimum embedment into the transition layer and the rock elevation influence the location of the walers. Figure 6 shows the variability of the top of rock along the sheet pile alignment. It can be observed that the top of rock is highly variable considering the size of the shaft. This variability and the actual elevation of the sheet pile toes required a redesign of the bracing elevations.

 © Deep Foundations Institute 2025

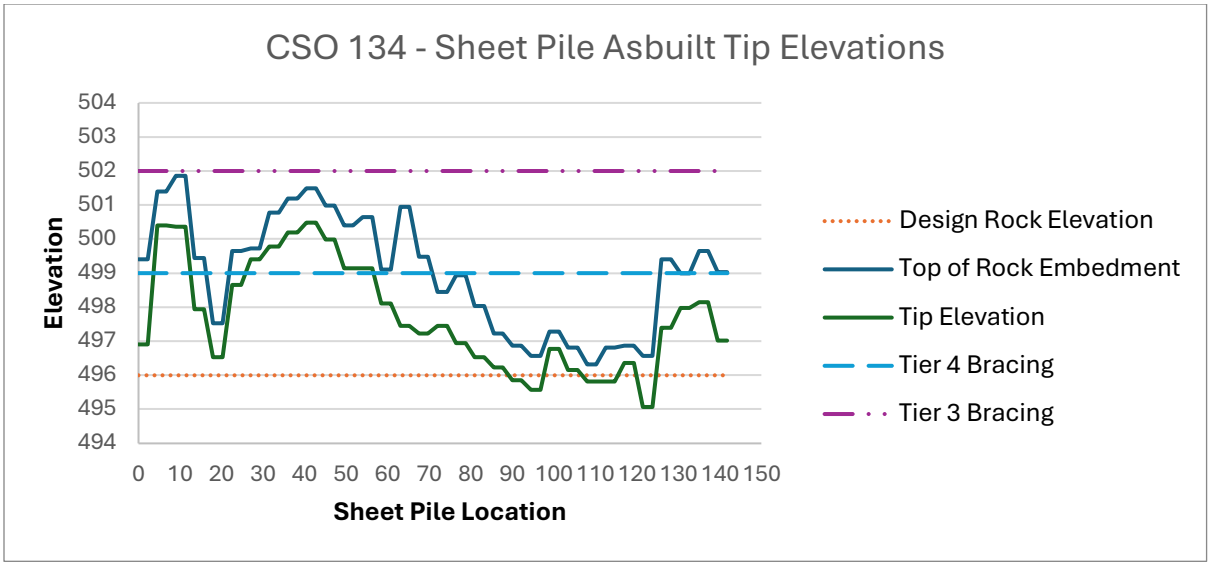


Fig. 6. Pump Shaft sheet pile as built

The design tip/rock elevation was EL 496 during the design phase. The higher and lower tip elevations recorded during sheet pile installation were about EL 500.5 and 495, respectively. By the time that the sheet piles were installed, the ring beams were already under fabrication. Ring beam elevations had to be shifted up to a location that would provide support to the sheet pile system and not be overstressed.

Prior to beginning the excavation within the shaft, the high mobility rock mass grouting program was implemented. The contractor started by drilling the primary holes five feet outside the circumference of the shaft and spanned between to the bottom of the pump shaft to the top of weathered rock. The grouting operations began in an alternating pattern around the circle to reduce any communication between grout locations. Secondary holes were needed to meet the performance criteria of the project.

The Contractor then began excavation of the shaft while installing ring beams at the designed elevation. The installation of the ring beams were more challenging for tiers 3 and 4. The third tier needed to connect to each sheet pile, whereas the fourth tier could only connect to the portion of sheet piles that were driven to deeper rock depths.

Since the sheet piles terminate on top of solid rock, the seal between the sheet and the rock is imperfect and prone to seepage. To mitigate this, the interface was sealed with shotcrete. The combination of the shotcrete and the high mobility grout yielded excellent results as nominal seepage have been observed through this interface. Atkinson then began to drill and blast the competent rock. They provided rock bolts and shotcrete at each excavation lift as designed by the EOR of the project. Figure 7 shows pictures of the excavation when it reached top of rock and after the first lift of blasting into rock.

 © Deep Foundations Institute 2025



Fig. 7. Photos of the excavation progress.

Electrical Building

The electrical building required the installation of a four-foot diameter casing to top of rock followed by a three-foot diameter, twelve-foot-deep rock socket. To account for the rock variability that was observed during the sheet pile installation, the foundations contractor purchased extra length of casing and rebar cages to ensure proper construction of the caissons.

Probe holes were performed at the center of each caisson to assess the quality of the rock up to ten feet beyond the bottom of the rock socket. Once the rock sockets were excavated, the caisson had to be poured within forty-eight hours. This posed some logistical challenges due to the available work area and the time it took to drill the rock sockets.

The available working space was one of the main challenges for this operation. The work area was constrained by the creek, LOD/Embankment, pump station sheet piles, stockpile of materials, and the casings that are temporarily sticking up during installation of the caissons. The size of the rig needed to drill the 3-foot diameter rock sockets was substantial for the amount of space available (Figure 8). The crews had to do thorough planning to be able to be productive.

The first caisson that was installed had to be tested to 200% of the design load capacity through a 72-hour compression load test. The caisson performed within the project's specifications and had settled 0.1690" at 200% design load. Only casing installation could be done until the test results were obtained. Production caissons followed the load test results. Similar obstructions to the ones found during sheet pile and soldier pile installations were found while installing 30% of the caissons. We had planned to drill through obstructions after what was previously observed in the adjacent areas.

 © Deep Foundations Institute 2025



Fig. 8. Caisson installation

SOE PERFORMANCE

The sheet pile SOE was monitored using optical survey points throughout construction. Manual readings were taken twice a week and the readings reviewed and compared with the anticipated movement for the various stages of the excavation and the surcharges. Figure 9 shows the measured horizontal movement along the circumference of the SOE.

 © Deep Foundations Institute 2025

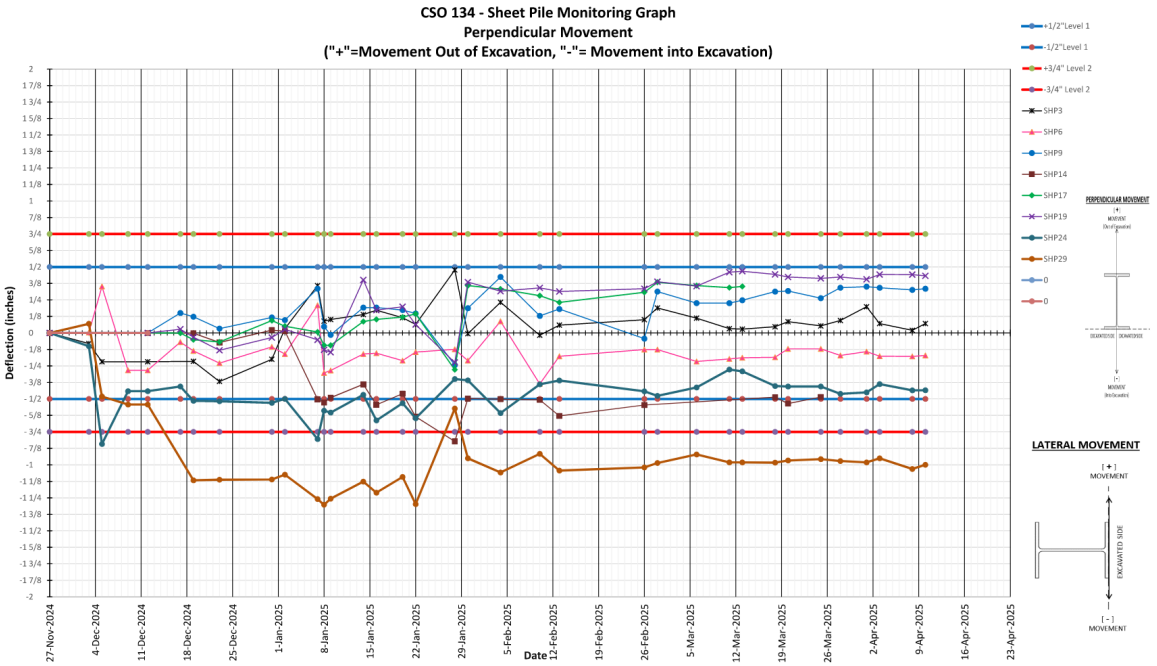


Fig. 9. Measured Horizontal Deformation of Sheet Pile SOE

Anticipated horizontal deformation of the sheet pile was approximately 3/8-inch during soil excavation and 3/4-inch maximum deformation throughout construction. Overall, the performance of the system matched really well with the estimated horizontal deformation at the top of the sheet pile under service loads. The southeast section of the sheet pile that experienced larger deformations than the rest of the system. This was due to a larger surcharge than anticipated from a large temporary stockpile of contaminated soil that was not able to be removed from the site for several weeks. When the team noted this movement, the excavator contractor was directed to redistribute the stockpile to reduce the surcharge into the system.

There hasn't been a flood event at the CSO 134 site by the time that this paper was written.

CONCLUSION

The CSO 52 project presented unique challenges for the design and construction of the temporary support of excavation and deep foundations. Close coordination and collaboration with the general contractor and good planning resulted in a cost-effective SOE solution that met the project requirements. When unforeseen conditions or different site conditions arise (i.e., higher rock elevation than anticipated), a quick response by all the parties involved is needed to maintain schedule and to limit exposure.

 © Deep Foundations Institute 2025

THE ROLE OF MECHANIZED SHAFT SINKING WITH VSM IN INNER-CITY APPLICATIONS

Stefan Frey and Julian Binder
Product Management Business Unit Utility Tunnelling
Herrenknecht AG, Schwanau-Allmannsweier, Baden-Wuerttemberg, Germany
Phone : +49 7824 302 7865, Email: frey.stefan@herrenknecht.com

1 ABSTRACT

Space on the surface is becoming increasingly scarce and expensive. Safe and economic construction of underground infrastructure in steadily increasing depths requires mechanized tunnelling and shaft sinking solutions. Shafts are needed for tunnelling operations, sewer systems, storage or for ventilation and rescue purposes in traffic tunnels.

The Vertical Shaft Sinking technology (VSM) is a mechanized approach developed to overcome challenging mixed-ground conditions with high groundwater tables, and safety or economic limits of conventional methods. Since 2004, far more than 100 circular shafts have been sunk with VSM, to depths of up to 115 meters and an inner shaft diameter range from 4.5 to 12 meters. The VSM is remote-controlled from the surface, thus, it is a completely unmanned sinking procedure without personnel required in the shaft during the sinking process. It meets the key requirements for shaft construction in inner cities: no groundwater lowering, maximum production accuracy and safety, and flexible arrangement of jobsite equipment. Due to the electrified operation of the overall VSM equipment with the possibility to be powered by the local grid, the CO_2 footprint and noise emissions can be considerably reduced compared to conventional construction methods. When using prefabricated concrete segments, shaft sinking with VSM requires up to 40% less concrete for the shaft structure, compared to diaphragm walls and bored pile walls.. This paper presents the VSM technology, with international project references in urban infrastructure projects.

Keywords: Mechanized shaft sinking, VSM, foundation shafts, tunnelling shafts

2 INTRODUCTION

Almost all tunnelling projects require shafts, either as launch and reception shafts for the tunnelling process or for inspection, ventilation, and rescue purposes. Also, a current trend towards infrastructure installations in growing depths can be observed. It is driven, among other things, by deep sewer construction projects that aim to avoid pumping stations as well as the need to build new installations below existing infrastructure.

The Vertical Shaft Sinking Machine (VSM) was developed by Herrenknecht AG. Its original purpose was the mechanized construction of deep launch and reception shafts for microtunneling projects. The goal was to overcome existing challenges in deep vertical shaft construction while enhancing safety and project reliability for all stakeholders. Beginning with design and testing in early 2004, the first VSM equipment was successfully deployed in Kuwait and Saudi Arabia in 2006.

Unlike conventional or competitive technologies, such as diaphragm wall, bored pile walls or open excavation shafts, which require lowering the groundwater table and can cause settlement or structural damage to surrounding areas, the VSM is designed to operate entirely underwater. The slurry system functions exclusively within the water, ensuring stability and minimizing environmental impact. This makes the VSM particularly effective in urban environments and challenging geological conditions where conventional construction methods are impractical or pose significant risks.

 © Deep Foundations Institute 2025

Another key design advantage of the VSM is its adjustable working diameter through the extendable cutting drum, allowing it to cover a range of shaft diameters. This flexibility makes the machine more economical by reducing the need for additional machineary equipment. Additionally, VSM technology offers exceptional accuracy in shaft construction, ensuring precise alignment and minimal deviation.

The machine concept, fully remote-controlled from the surface, as well as its implementation on site proved to be an efficient solution right from the start for the safe and fast construction of shafts especially in difficult, inner-city environments without lowering the groundwater table.

The latest application was the construction of two shafts for the first U-Park® system in Nanjing, China, with on OD of 12.8 m and a depth of 65 m each. U-Park® is an underground car parking system ideal for cities with high-density populations, like London or Paris, where the availability of parking places is limited and therefore expensive. A VSM shaft might even be used as a underground parking space as well as a permanent statical foundation simultaneously, not only for buildings above surface, but also for bridges and other near-shore construction foundations relying on the principle that deeper soil layers are often more stable than surface layers. By excavating the shaft into these stable layers, the structure's weight is evenly distributed, ensuring a stable foundation. Also, the friction between the shaft walls and surrounding soil provides extra support, further reducing stress on the ground and enhancing stability.

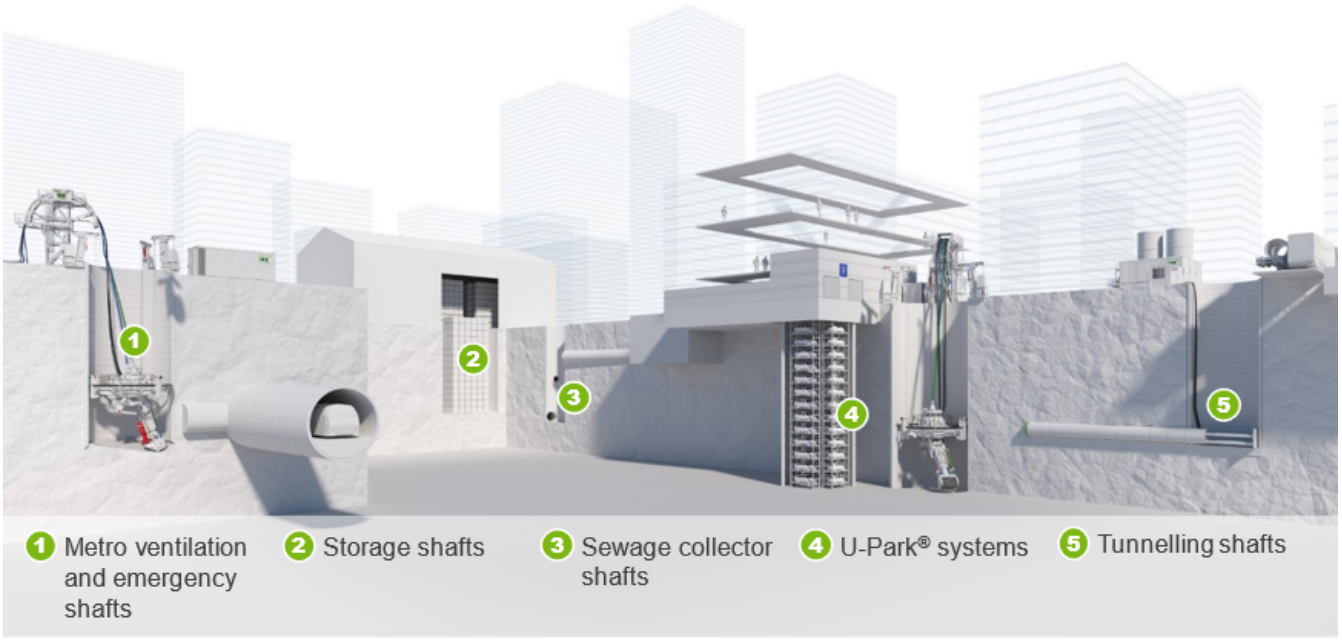


Fig. 1. Overview of VSM application fields in inner-city surroundings

3 MECHANIZED SHAFT SINKING WITH VSM

3.1 Benefits of VSM Technology

The VSM technology overcomes the main challenges associated with shaft sinking: inner-city shaft structures demand safe working conditions for surrounding buildings and the environment, especially regarding potential ground settlement. There is an increased requirement to avoid the lowering of groundwater during the construction of shafts in order to avoid subsequent settlement, which can affect a wide, inner-city area and the surrounding buildings. Deep shaft construction companies often encounter

 © Deep Foundations Institute 2025

difficult geological conditions such as high groundwater pressure combined with layers of hard and soft material. In addition, deep shafts need special attention for the safety of the operating personnel.

3.3.1 Cost and Time Benefits

Simultaneous excavation and ring building facilitate high advance rates and shortened overall project duration. At the same time, continuous performance ensures overall high planning reliability for all stakeholders.

The lining of a VSM shaft consists of either precast segments or cast-in-situ concrete. As the lining installation is completed on the surface, high quality installation can be accomplished, leading to greater accuracy of the shaft structure. In most cases, a secondary, time-consuming lining is not required, resulting in a reduced wall thickness of the shaft and, thus, less soil excavation.

The possibility of combining the two lining methods provides the flexibility of having the best structural and functional configuration at different depths, this characteristic allows for greater efficiency from both the technical and economic point of view of the projects. For the DTSS2 Project in Singapore, the lower portion of the shaft was constructed using in-situ concrete, while the remainder was built with prefabricated segments. This approach enabled a safe TBM launch from the shaft, as the integrated reinforcement in the in-situ section consisted of fiber instead of steel, preventing potential damage to the TBM from metallic components.

Furthermore, each VSM type is very flexible as its excavation diameter can be adjusted within a specific range. A VSM12000 (named after the maximum shaft diameter of 12 meters), for example, can cover an inner shaft diameter range from 7 meters to 12 meters and is, therefore, a one-time investment for multiple use cases.

3.1.1 Construction and Occupational Safety Benefits

As the water level in the shaft is maintained close to the groundwater level outside the shaft, water inflow is prevented which otherwise could cause ground movement and lead to a high risk of settlement. The VSM can be utilized below groundwater with a high hydrostatic pressure and in heterogeneous soil and hard rock with compressive strength up to 140 MPa in intermediate layers.

All installations, including the lining erection, are remotely controlled from the surface. No personnel have to enter the shaft until it has reached the final depth and is fully secured. In general, mechanized shaft sinking requires less personnel and machinery on site, which leads to minimized risk exposure.

3.1.2 Environmental Benefits

Measures for groundwater lowering are not necessary, as the VSM machine concept is designed for operation under groundwater. VSM technology enables highly accurate shaft construction, as the entire shaft structure is continuously supported by the lowering units and guided by an advanced measurement system with a precision of 0.2% or better. This high level of accuracy allows for a minimized shaft lining thickness, reducing the volume of excavated soil and, consequently, lowering construction costs.

3.2 VSM Machine Components

The VSM consists of two main components (Fig. 2): the excavation unit and the lowering unit. The excavation unit systematically cuts and excavates the soil and consists of a cutting drum attached to a telescopic boom that allows excavation of a determined overcut. The lowering unit on the surface stabilizes

the entire shaft construction against uncontrolled sinking by holding the total shaft weight with steel strands and hydraulic jacks. When one excavation cycle is completed, the complete lining can be lowered uniformly and precisely.

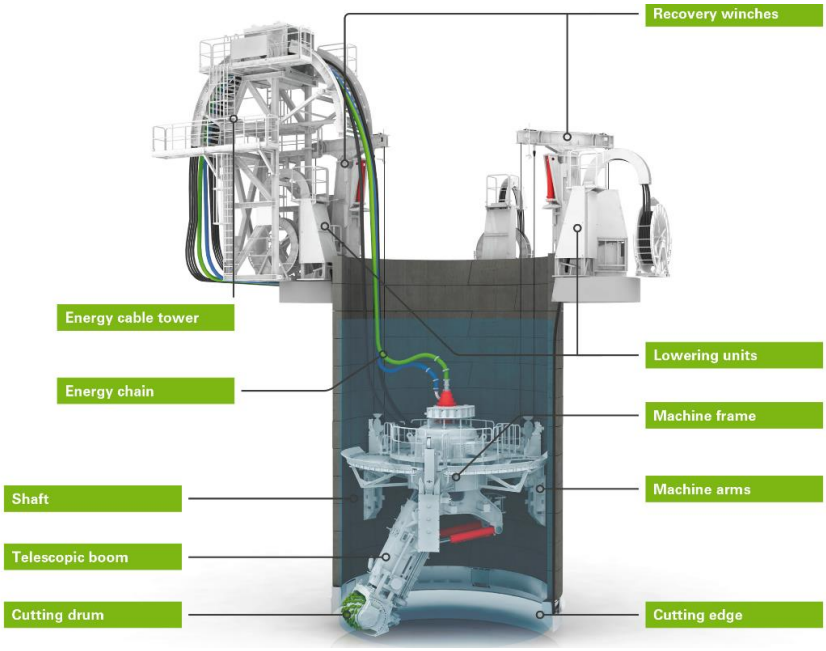


Fig. 2. VSM components of equipment

A slurry discharge system removes the excavated soil and a submerged slurry pump is located directly on the cutting drum casing. It transports the water and soil mixture through a slurry line to a separation plant on the surface. The whole operation takes place from the surface and is controlled by the operator from the control container on the surface. All machine functions are remote-controlled without the necessity to view the shaft bottom or the machine. Power supply for the submerged VSM is secured by the energy chain. After reaching its final depth, the VSM is lifted out of the shaft by the recovery winches and the jobsite crane.

3.3 Jobsite arrangement in inner-city conditions

Depending on the space conditions on site, the VSM components can be positioned flexibly to suit local circumstances (Fig. 3). As most sites are located in heavily built-up urban areas, access for logistics (e.g. trucks, ring segment stock, or soil disposal) is limited. Special concepts to relocate components such as the separation plant already exist for this purpose and can be discussed if required. The advantage of modular and flexible arrangement of the system makes the VSM perfect for urban shaft applications where space is limited.

 © Deep Foundations Institute 2025

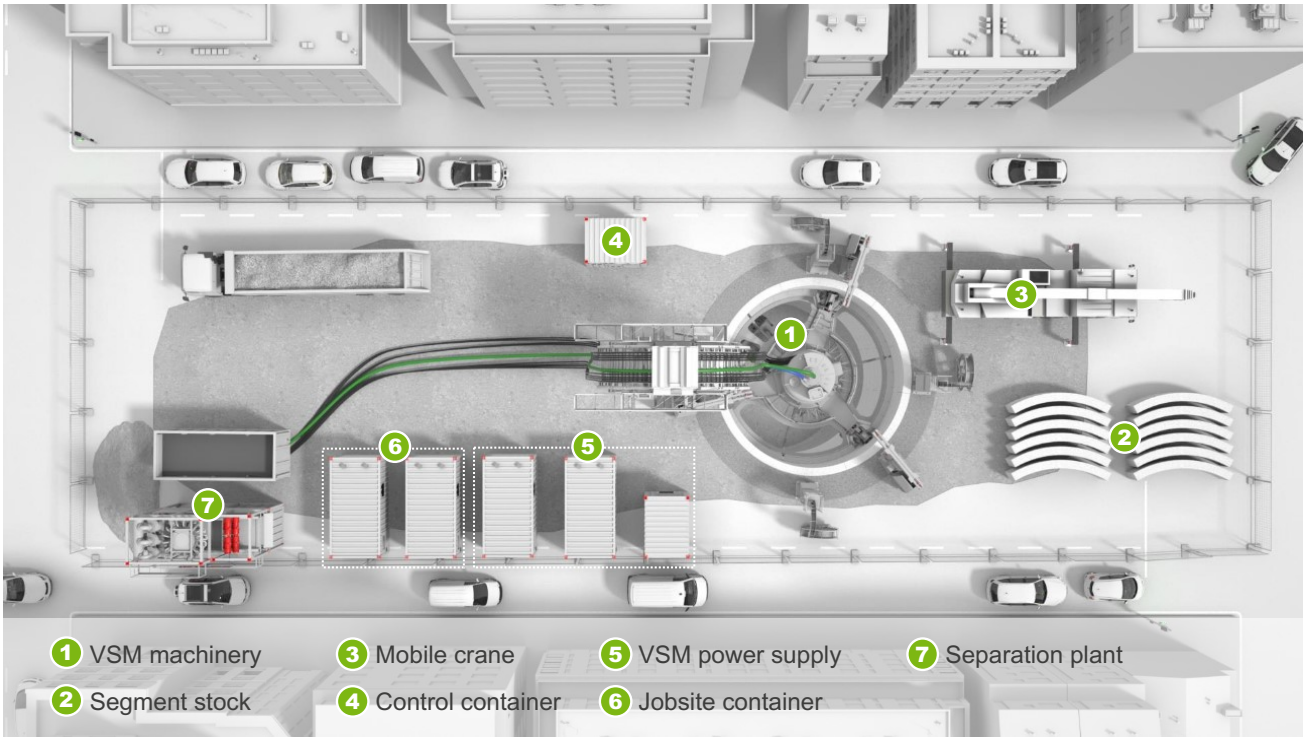


Fig. 3. Layout of a VSM jobsite in dense urban area

3.4 Installation of VSM Equipment

The excavation unit arrives on site in three parts: the telescopic boom with the cutting drum, the machine main body, and the adapter parts to the required shaft internal diameter. The lowering unit consists of the strand jacks and the coiled steel strands on a drum. The number of strands depends on the total predicted weight of the shaft lining including the machine weight and the estimated buoyancy and friction forces. The strand jacks are bolted to the ring foundation by anchor bolts. Coming from the strand drum, the strands are fed through the strand jack, lowered through the outer annulus of the shaft wall, and connected to the cutting edge. When all strand jacks are installed and connected to the cutting edge the strands can be tensioned and carry the loads.

Now, the preassembled excavation unit can be lifted into the start section. The VSM is secured by hydraulically activated locking bolts. When the VSM is in place, the recovery winches are installed and connected to the three arms of the machine. The recovery winches are used to recover the VSM for required maintenance or for final machine recovery.

Next, the energy chain system is installed, and the excavation unit is connected to the hydraulic and electrical supply as well as to the feed and discharge lines. The energy chain tower with its winch has bolted connections for easy assembly. As a final step, all the electrical and hydraulic connections are made, and the equipment is now ready to operate. Before starting the excavation, a calibration of the VSM in reference to the projected alignment of the shaft is required to ensure the accurate action of the cutting boom.

3.5 VSM Operation – Shaft Sinking Procedure

Excavation is remote-controlled from the operator cabin at the surface. Stored data, together with the position of the cutting boom, is shown on a graphic display, giving the operator full control of the excavation and sinking process. The cutting arm moves radially from the center to the outside of the shaft with an

 © Deep Foundations Institute 2025

additional telescopic extension. With a rotation of +/-190° the cutting boom covers the whole cross section of the shaft. The cutting speed and the movement of the boom can be varied to achieve the best excavation rate.

During the excavation and sinking process, the shaft is kept full of water to balance the level of the groundwater table in the surrounding geology. The cutting drum cuts and crushes the material to a granular size that can be handled by the discharge pumps. A slurry circuit transports the excavated material from the shaft to a separation plant on the surface.

The excavation unit can be operated in three different overcut options. The respective annulus should be stabilized by a bentonite-water suspension in soft ground conditions. In addition, each segment can be equipped with bentonite nozzles for lubrication, which can also later be used to grout the annulus. Within the standard installation for shafts up to 50m, bentonite lubrication is only installed in the start section of the shaft.

In contrast to horizontal tunnelling procedure, excavation and ring building are taking place simultaneously. Therefore, the lowering units hold the already assembled shaft structure in place until the subsequent excavation cycle is finished. Then the shaft structure is lowered to the next position and excavation can start again. The stabilization of the annulus by the right use of bentonite, together with the controlled sinking of the shaft by the lowering units, minimizes the risks of settlement.

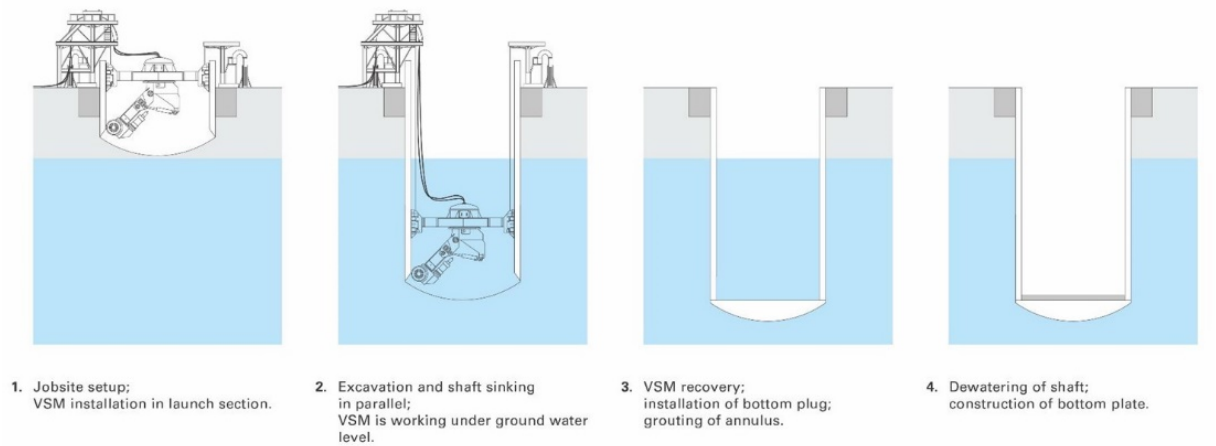


Fig. 4. Installation steps of mechanized shaft sinking with VSM

3.5.1 Shaft lining

In most cases, the shaft lining consists of precast concrete segments installed at the surface. This so-called “ring building” is comparable to segmental lining in tunnelling. The ring is built at the surface by a crane. The number of segments depends on the shaft diameter. Ring building work includes the proper connection of the rings by anchors and bolts, which can be handled from outside the shaft. The excavation process of the VSM is not affected by the ring building process, which increases the shaft sinking performance significantly.

Alternatively, in-situ concrete casting of the shaft walls is another solution, especially for larger shaft diameters where segment handling becomes more difficult. In this case, the progress of shaft construction is slowed down by the necessary time to build the formwork and the setting time of the concrete structure. The benefit of in-situ casing is the "continuous" structure without joints and the possibility to integrate entire entry and exit structures (e.g. for microtunnelling activities in the shaft walls).

 © Deep Foundations Institute 2025

As mentioned previously, there is the possibility of combining the two lining methods, allowing for the best structural and functional configuration at different depths within one shaft.

3.6 Completion of the shaft

After reaching the required shaft depth, the bottom plug must be installed. Usually, the VSM is used to perform the required over-excavation for the bottom plug. When this final excavation is done, the VSM can be disconnected, recovered by the recovery winches, and lifted to the surface and out of the shaft by a crane. The bottom plug is cast with underwater concrete. Following final excavation, the shaft annulus is grouted through the lubrication lines to stabilize and anchor the shaft to the surrounding geological formation(s). Finally, the shaft water can be pumped out and the shaft is completed. Personnel access is now possible.

4 VSM IN INNER-CITY PROJECTS

4.1 Grand Paris Express, France

The Grand Paris Express is currently the largest infrastructure project in Europe with 200 kilometers of track on four new, fully automated subway lines with 68 stations and seven technical centers. The metropolitan area of the French capital is getting an additional network of routes, designed with sustainability in mind, whose main task is connecting the municipalities surrounding the city with each other more efficiently. Since August 2018, a VSM has been in operation for the first time in France on Line 15 Sud (T3C). Until end of November 2019, the VSM12000 had sunk four emergency and ventilation shafts for the Line 15 South tunnels, excavated by a tunnel boring machines. The shafts are up to 48 meters deep with inner diameters between 8.3 to 11.9 meters. So far, the respective outer diameter of 12.8 meters is the largest diameter ever installed by VSM technology with prefabricated concrete segments.

4.1.1 Large-Diameter Shaft Construction

In mechanized construction of large diameter shafts, the flexible use and setup options of all VSM components is a major benefit of the VSM technology. Within a given jobsite surface, in extremely restricted inner-city conditions, all components can be arranged according to the available space conditions, enabling the construction of a large diameter shaft at the same time. Nevertheless, detailed planning of the jobsite logistics and organization of the overall process is mandatory prior to the arrival of the equipment onsite. With growing diameter, the ring arrangement and related number of segments must be adapted. For the large inner diameter of 11.9 meters in Paris, 6 segments have been used for the construction of the shaft lining. The in-time delivery of the large and heavy precast segments required detailed planning and adaptation to the sinking progress during construction. Figure 5 shows the jobsite layout for the first shaft.

4.1.2 Noise Emissions

Furthermore, the client and contractor considered the significantly lower level of noise emissions as a further decisive benefit of the VSM technology compared to conventional shaft construction methods. During shaft construction, the main components of the VSM equipment work underwater and are supplied with electrical power. Instead of using diesel generators, the electrical power for the VSM jobsite was provided by the municipal power grid. Thus, a considerable reduction in noise emissions was achieved.

 © Deep Foundations Institute 2025



Fig. 5. View on shaft sinking jobsite in inner-city conditions, Paris, France

4.1.3 Reduced CO_2 emissions

The VSM machine offers significant environmental advantages, particularly in reducing CO_2 emissions. Its innovative design and efficient construction process help minimize the environmental footprint of construction projects. The VSM enables much faster installation on construction sites due to modularity of the jobsite equipment. By speeding up the process, the machine reduces overall operating time and, consequently, the energy consumption associated with prolonged site activities. This not only improves construction efficiency but also lowers CO_2 emissions. Secondly, the VSM's shaft lining doubles as the permanent shaft lining, eliminating the need for additional concrete work. Concrete production and transportation are major sources of CO_2 emissions in construction, so reducing the amount of concrete required has a direct and significant impact on the overall carbon footprint of the project. Finally, the VSM machine and related equipment (e.g. powerpacks and separation plant) are powered entirely by the public electricity grid, eliminating the need for combustion engines to run the site and reducing greenhouse emissions. In regions where the electrical grid increasingly relies on renewable energy, the environmental benefits are even more pronounced. By integrating faster processes, reducing material consumption, and relying on cleaner energy sources, the VSM machine provides a forward-thinking solution for environmentally friendly construction, aligning efficiency with sustainability.

4.1.4 Mobility

Due to the inner-city locations of the different shaft construction sites, a quick and smooth mobilization and demobilization of all VSM components and detailed logistics planning was required, not only before the construction start of the first shaft, but also for disassembly, transport and installation of the VSM equipment on subsequent locations. After completion of the shaft, disassembly and assembly of the equipment at the next location took place simultaneously, because of the flexibility and compact design of the VSM equipment. A duration of three weeks from the recovery of the machine on one shaft until ready-to-bore on the next location was a remarkable performance of the jobsite and logistics crew.

4.1.5 Soil Conditions

Challenging geological conditions due to changing strata ranging from very cohesive clay to limestone with a compressive strength of up to 100MPa required continuous monitoring, adaptation of excavation parameters, and correction of the shaft position at any time. Due to the swelling clay expected, the overcut around the shaft lining had to be adapted flexibly to avoid getting the shaft structure stuck. The cutting tools were adjusted regularly, according to the ground conditions, to achieve optimal performance rates. Furthermore, a high-pressure nozzle system has been used to clean the cutting drum during excavation in sticky soil conditions in order to maintain production rates. The modular design of the separation equipment provided the ability to adapt to soil and space conditions at each shaft location, and for flexible use of coarse and fine screens, different cyclone stages, and a centrifuge.

4.2 Other tunnelling shafts built with VSM in Europe

4.2.1 Napoli, Italy

Constructing subway tunnels beneath the historic city center of Naples, a UNESCO World Heritage Site, demanded precise planning and cutting-edge technology. A crucial element in this project was the use of the Vertical Shaft Sinking Machine (VSM), which played a central role in ensuring the successful and efficient completion of key infrastructure components.

The VSM was tasked with drilling vertical shafts from the surface down to the tunnel level, for ventilation and to serve as emergency exits. Over the course of the project, the machine drilled ten shafts each with a diameter of 4.5 meters and depths of up to 45 meters. The technology and design of the VSM proved effective, particularly given the narrow streets and limited space in Naples. Its compact footprint made it ideal for urban environments, and the reduced noise disturbance ensured that the surrounding residents were only mildly affected by the work.



Fig. 6. VSM construction for ventilation shaft in Naples

 © Deep Foundations Institute 2025

The VSM offered further advantages with its daily production rates, advancing nearly five meters each day. This speed was possible due to the simultaneous drilling and lining of the shaft, using prefabricated concrete segments to ensure ground stability as the machine advanced. Additionally, the tight construction site conditions required a space-efficient solution, making the VSM the preferred approach over conventional methods. Unlike conventional methods, which demand large work areas and extensive ground preparation measures, the VSM's compact and modular design allowed for efficient operation in a highly constraint urban environment. Once a shaft was completed, the VSM's modular design allowed for quick disassembly and transportation to the next site, further optimizing the workflow.

While two Earth Pressure Balance (EPB) Tunnel Boring Machines (TBMs) were also working underground to bore the twin subway tunnels, the VSM's visible work at the surface was instrumental to the overall optics of the project with the public, showcasing a modern and efficient approach to underground construction in a highly sensitive and historic area.

4.2.2 Barcelona, Spain

With speeds of up to 350 km/h, high-speed trains on the AVE line connect Spain's major cities, Madrid and Barcelona, to the French border. A significant portion of the route runs underground, requiring the installation of escape routes and ventilation shafts. For this purpose, two Vertical Shaft Sinking Machines (VSMs) were deployed to excavate a total of six shafts along the Montcada to Trinitat section of the track, demonstrating the capabilities of VSM technology in challenging environments.

The first shaft was particularly demanding, passing through varying geological conditions, from very soft to extremely hard, down to a depth of 56 meters. The top 15 meters consisted of loose sand and gravel, while the remaining 42 meters required penetrating 200 MPa hard quartz slate rock. This was achieved using the VSM equipped with two specialized cutting wheels designed for the variation in ground conditions. The main challenge in this densely populated area was to avoid ground settlements during shaft construction, a task for which the VSM was designed.

During the construction of the first shaft, a daily progress of 3,5 meters was achieved with a 16-hour, two-shift operation. By simultaneously sinking and lining the shaft with precast concrete segments , the project advanced swiftly and safely, with the first shaft completed on October 2, 2009. A follow-up shaft was completed by mid-2012.

In 2015, a second VSM was deployed to construct an additional shaft for the high-speed rail line. The machine continued its work in 2019, drilling three more shafts for the project, demonstrating continuing reliability and efficiency of the VSM in delivering critical infrastructure for Spain's high-speed rail network.



Fig. 7. VSM construction for ventilation and emergency shaft in Barcelona

VSM technology was chosen specifically due to the dense network of existing underground infrastructure, which required highly accurate shaft installation. The proximity of buildings above ground also demanded a solution that could minimize the risk of settlements to avoid structural damage. Unlike conventional methods, the VSM enabled precise and settlement-free shaft construction, making it the logical choice for this complex urban project.

While tunnel boring machines (TBMs) handled the underground sections, the VSMs installed the necessary safety infrastructure, demonstrating the effectiveness of the method and equipment in large-scale urban projects.

5 CONCLUSION

The current and worldwide trend in inner-city environments is to construct more and more underground infrastructure, which has resulted in a growing demand for the construction of shafts. In challenging ground conditions with high groundwater levels and increasing shaft depths, conventional methods reach their technical and economical limits. The mechanized construction approach with VSM has many benefits in terms of budget, construction time, and occupational safety, which has led to a total of more than 111 VSM projects where shafts have been successfully constructed in dense, urban surroundings. These ongoing technological advancements significantly expand the potential applications of vertical shaft sinking machines, enabling projects at increasing depths and with considerably larger shaft dimensions. For future urban development, underground storage of goods and sustainable energy generation concepts will be major considerations that require safe, economical, and ecological shaft construction approaches. VSM technology has the potential to play a key role in enabling vertical underground applications, such as hydrothermal energy storage, underground food production, or logistical hubs for urban supply chains. By providing highly accurate and space-efficient shaft construction, VSM opens new possibilities for future-proof, sustainable infrastructure in dense metropolitan areas.

 © Deep Foundations Institute 2025

ADAPTING DIAPHRAGM WALL DESIGN FOR POST-DISASTER STRUCTURES ON SOFT GROUND: CHALLENGES UNDER THE 6TH GENERATION SEISMIC CODE

Atieh Shooshpasha, EllisDon, Toronto, Ontario, Canada, (437) 227-6478, ashooshpasha@ellisdon.com
Amir Poshnejad, EllisDon, Toronto, Ontario, Canada, (437) 779-7702, aposhnejad@ellisdon.com

ABSTRACT

This paper is about the challenges of constructing diaphragm walls for post-disaster buildings on soft soils under Canada's 6th-generation seismic code. The study examines a case study in British Columbia, where poor soil conditions, urban restrictions, and pressurized artesian layers create significant design and constructability issues for a permanent diaphragm wall. The significant increase in seismic hazard values from the 5th to 6th generation of seismic codes has added more complexity to the design of geotechnical structures, demanding higher capacity against seismic forces. This study developed a new solution using Finite Element Analysis (FEA) and PLAXIS software to optimize diaphragm wall design, address site-specific challenges, and meet the 6th generation seismic code requirements. The findings indicate that through advanced numerical analysis, material optimization, and adapted construction methodologies, it is possible to achieve both resilience and compliance with the new seismic code. This research highlights how innovative engineering solutions can effectively address geotechnical and urban challenges to ensure the safety and performance of critical infrastructures in seismically active regions.

Keywords: diaphragm wall, 6th generation seismic code, finite element analysis (FEA), PLAXIS

INTRODUCTION

Expanding urban areas, specifically into soft ground conditions, has created significant geotechnical challenges for infrastructure development. In such settings, traditional retaining walls and foundation systems may not provide an ideal solution for extreme seismic events, especially for post-disaster infrastructures where operational continuity is critical. This paper presents a case study to bridge the gap between the new generation of seismic code and practical engineering applications to create a sustainable solution for post-disaster buildings. This study investigated the use of diaphragm walls as a separating retaining system to reduce the seismic demands for post-disaster buildings. These diaphragms isolate the structure from the soil, protecting it from soft clay amplification during earthquakes. Barrettes—deep, rectangular foundation elements constructed using diaphragm wall techniques—were selected as the primary foundation solution for the hospital building presented in this case. These types of deep piles are less common in foundation design. The big advantage of barrettes is their substantial axial and lateral load capacities, making them suitable for supporting heavy structures, especially in soft soils. In this project, the upper 14m of soil consisted of highly sensitive clay with very low strength. Combined with elevated seismic demands introduced by the 6th generation of seismic code, the use of barrettes provided a robust foundation system capable of addressing axial and lateral performance requirements under extreme loading conditions.

THE 6TH GENERATION SEISMIC CODE OVERVIEW

In NBC 2015, nonlinear amplification was according to aggregated probabilistic PGA_{ref} value. The amplified hazard value in NBCC2015 was based on site class C, which is defined by average shear wave velocity in the uppermost 30m, V_{S30} = 450 m/s, as a reference ground condition (Finn et al. (2003)). While NBC2020 uses the sixth-generation hazard model (SHMC-6) the nonlinear amplification is based on the median ground motion intensity in each event scenario considered in the hazard model. In NBCC2020, the amplification is treated internally in the hazard model by using ground motion model (GMM) specific to each tectonic regime. These hazard values are then probabilistically aggregated to generate the Uniform

 © Deep Foundations Institute 2025

Hazard Response Spectra (UHRS), PGA, PGV as a function of V_{S30}. (Kolaj et al. (2019)). As a result, NBCC2020 usually gives higher Response Spectral Ratios (RSR) values compared to 2015, especially in greater PGA values. This shift reflects both an improved understanding of Canada's seismic hazard landscape and the integration of modern GMMs and ground tectonic parameter (GTP) sources.

Impacts on Seismic Foundation Design

The updated ground motion model (GMM) predicts higher seismic hazard values in many locations particularly in eastern Canada. This increase in seismic demand has significant implications for foundation design, especially for post-disaster buildings, which must remain functional immediately after a major seismic event. To accommodate the increased seismic forces and associated displacement demands, foundation systems must be reevaluated and, in many cases, re-engineered to ensure sufficient strength, ductility, and energy dissipation.

Performance-Based Seismic Design (PBSD)

NBCC2020 emphasizes on performance-based seismic design (PBSD) principles, which require structures to meet specific performance objectives under predicted seismic hazards. This approach shifts the design philosophy from satisfying prescriptive code requirements to achieving specific performance objectives tailored to the function and criticality of the building. In post-disaster buildings, this objective can be narrowed down to two main goals:

1. **Life safety:** ensuring occupants can evacuate the building safely during and after a major earthquake.
2. **Operational continuity:** maintaining the building's functionality after the event to support emergency response and recovery operations.

The PBSD allows geotechnical engineers to integrate detailed site-specific seismic analysis into the foundation and structural design. This method typically includes advanced modeling of soil behavior, damping characteristics, and deformation compatibility between soil and structure. The design process is iterative, requiring multiple rounds of analysis, refinement, and validation to confirm that the foundation system will meet both performance targets under varying seismic intensity levels.

PROJECT DESCRIPTION

This project involves the development of an advanced healthcare facility in British Columbia, Canada, offering specialized cancer treatment. The hospital will be a vital infrastructure piece for the region, designed to remain operational during and after major seismic events. The facility consists of 11 stories above ground and two levels of underground parking, encompassing a total gross building area of approximately 70,000 m^2. Excavation for the substructure reaches the depth of 12 meters, and the main hospital building is supported by a deep foundation system. Due to the high seismic hazard and challenging subsurface conditions, including soft, sensitive clay, both the structural and geotechnical designs integrate advanced seismic design strategies consistent with the objectives of post-disaster infrastructure.

 © Deep Foundations Institute 2025

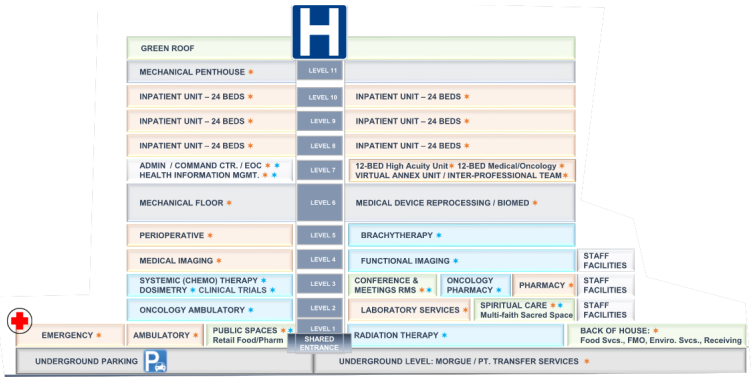


Fig 1. Section view of the hospital building

GEOTECHNICAL CONDITION

The general geology of the region is described as Pleistocene Age Capilano Sediments (Ce) over Vashon Drift Glacial Till, as identified in the Geological Survey of Canada's surficial geology map (Map 1484, 1978). The Ce sediments are mainly marine silt to clay loam with minor sand and silt. Beneath this lies the Vashon Drift Till, composed of glaciofluvial sandy gravel outwash and ice-contact deposits, often with interspersed sand lenses. Quadra Sand, a well-known pre-glacial deposit, is commonly encountered below the dense Vashon Drift layer.

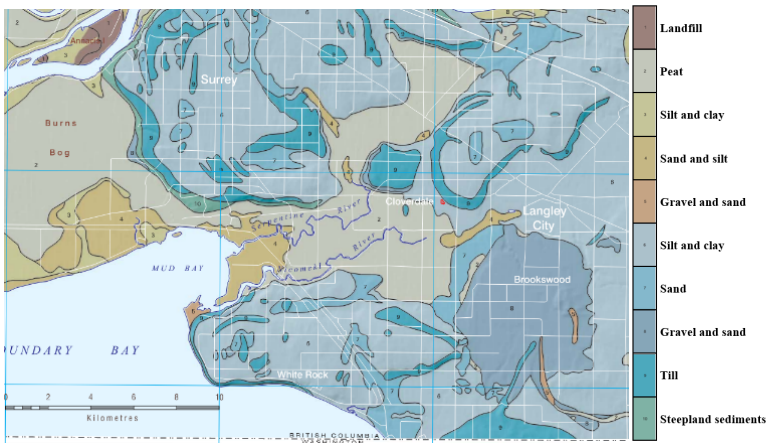


Fig. 2. Geological Map of the Vancouver Metropolitan Area (adopted from Geological Survey of Canada (1998))

Site-Specific Challenges

The site investigation revealed significant geotechnical challenges, primarily due to the presence of weak, highly sensitive soft clay extending to a depth of approximately 16 meters. The shear strength of clay deposits generally ranges between 20 and 50 kPa. Field Vane Shear tests (VST) have shown a sensitivity of clay from 4.6 to 10.3, putting the soil in the category of highly sensitive clay. The Vashon Drift Till, consisting of silty sand with variable gravel, was encountered below the clay between depths of 12m to 19m below grade. According to the Province of British Columbia's online Aquifer Classification Sheet, two aquifer units are present at the site. The shallower aquifer is located about 1.5m below grade, and the second aquifer was observed between 23m and 30m below grade. The results from Slug testing indicate that the Vashon Drift has a highly variable permeability range between 2.4×10^{-8} to 1.1×10^{-5}m/s, and the Sand Aquifer has a relatively high hydraulic conductivity. Figure 3 shows the schematic view of soil stratigraphy in the project area.

 © Deep Foundations Institute 2025

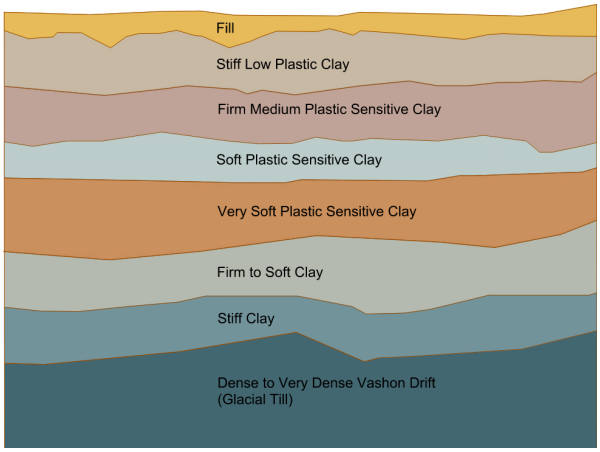


Fig 3. Schematic section of site stratigraphy

These soil and groundwater conditions posed major challenges to the foundation design, especially considering the hospital's classification as a post-disaster structure requiring high stability and resilience against seismic events. The discovery of pressurized groundwater and high-permeability sandy till at deeper levels further complicated excavation and foundation design. To mitigate high groundwater pressure and buoyancy risks, a tanked foundation was designed. This included a diaphragm wall system integrated with a thick structural raft slab and tie-down anchors to resist uplift pressures. During construction and excavation, a dewatering system is needed to depressurize the soil underneath, and based on assessments, the pumping volume was in the range of 750,000 L/day to 1,500,000 L/day. For the permanent condition, the building must be tanked using thick structural raft slabs and tie-downs to resist the uplift water pressure.

Foundation System Evaluation

Given the challenges above, the selection of a suitable foundation and shoring system was the critical part of the design. The presence of soft clay and depth of Vashon Drift made slope excavation impractical. Several alternative systems were evaluated, including conventional drilled shaft, driven steel piles, and combined soil improvement and piling systems. However, the adoption of 6th generation seismic hazad model, as previously discussed, led to a substantial increase in seismic demand. To meet this increase in axial and lateral load demand, more than 900 piles would have been required. This high pile count given the tight space configuration was structurally inefficient and impractical.

Barrettes, by contrast, offered significantly higher moment and axial capacity per element, superior performance under lateral loading, and more efficient use of site space. Additionally, because barrettes can be installed using diaphragm wall construction techniques, they provided an opportunity to integrate the foundation and shoring systems using the same construction equipment. This dual-purpose approach helped using diaphragm walls as both temporary excavation support and part of the permanent foundation system and proved to be highly cost- and schedule-effective. It allowed for rapid construction, minimized material usage, and optimized logistics, making it a highly suitable and innovative solution for the demanding conditions of this post-disaster healthcare facility.

FINITE ELEMENT ANALYSIS

The foundation design of the hospital was carried out through a series of detailed numerical analyses, using both structural and geotechnical finite element modeling tools. A comprehensive workflow was developed to accurately account for site-specific seismicity, soil-structure interaction (SSI), and foundation system

 © Deep Foundations Institute 2025

performance under extreme seismic loading. Figure 4 shows the flowchart of building design process for this study.

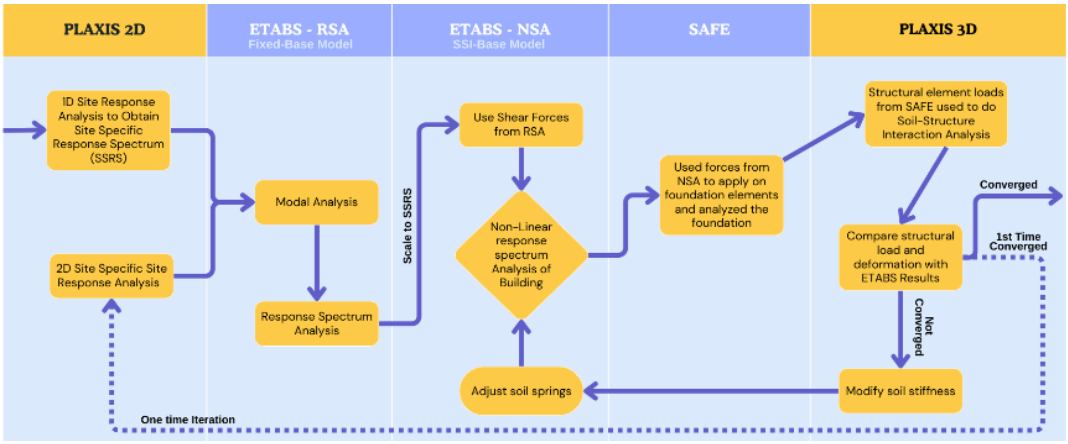


Fig 4. Building Design Process

Site Response Analysis

The design process began with a 1D and 2D site response analysis (SRA) to develop a Site-Specific Response Spectrum (SSRS). Carvajal et al. (2020) verified, using linear, equivalent linear, and nonlinear finite element analyses, that response spectrum-based seismic response analysis provides a reliable approximation of seismic behavior compared to FE simulations. The complex subsurface profile and high seismicity of the region necessitated a 2D SRA using PLAXIS 2D, where the model included the anchored diaphragm wall, building raft slab, and site stratigraphy. A total of 44 ground motions (22 short-period and 22 long-period) were applied to evaluate amplification effects. The constitutive HSsmall model (Benz, 2007) with small strain stiffness was used to capture the strain-dependent stiffness and nonlinear response of the soils under dynamic loading. Soil parameters are shown in Table 1.

Table 1. Soil Properties

Layer	γ (kN/m^3)	e_o	E_{50}^{ref} (kPa)	ν_{ur}	G_o^{ref} (kPa)	C_{ref} (kPa)	ϕ (°)	OCR
Fill	20	0.33	60,000	0.20	128,000	1	42	1.0
Clay 1	19	1.1	5,171	0.20	52,145	230	0	9.0
Clay 2	18	1.1	1,825	0.20	29,580	63.5	0	2.68
Clay 3	18	1.1	980	0.20	19,488	28.5	0	1.33
Clay 4	18	1.1	1,791	0.20	29,982	30.3	0	1.35
Clay 5	18	1.1	3,155	0.20	44,197	43.0	0	1.52
Clay 6	18	1.1	5,462	0.20	68,001	67.5	0	1.89
Glacial Till 1	21	0.38	69,403	0.20	155,771	10	40	5.0
Glacial Till 2	21	0.38	120,777	0.20	271,077	10	40	5.0
Glacial Till 3	21	0.38	189,126	0.20	424,484	10	40	5.0
Glacial Till 4	21	0.38	239,077	0.20	536,595	10	40	5.0
Glacial Till 5	21	0.38	145,244	0.20	325,992	10	40	5.0

ETABS Analysis

A fixed-base structural model was developed in ETABS using the SSRS obtained from site response analysis to conduct modal and response spectrum analyses (RSA). This analysis phase was used to evaluate

 © Deep Foundations Institute 2025

the natural periods, mode shapes, and lateral forces due to seismic loading. A scale factor was calculated for spectral analysis based on NBCC provisions:

$$Scale\ Factor = g * \frac{I_e}{R_d R_0} = 9.8064 * \frac{1.5}{2} = 7.3548\ m/s^2$$

To account for SSI, a refined structural model was developed in ETABS, where the foundation was modeled using nonlinear springs (p-y elements) rather than assuming a fixed base. This technique allowed for a more realistic simulation of the interaction between the superstructure and soil. The nonlinear spring parameters were developed based on an iterative calibration process involving Static load tests, Anchor pullout tests, and O-cell tests, which were performed on-site to obtain representative stiffness and load-deflection behavior. The p-y curves were calibrated with test data through PLAXIS 3D push-over simulations. These calibrated springs were then implemented in ETABS for nonlinear static analysis (NSA).

Nonlinear Static Analysis (NSA)

A series of push-over analyses were conducted in ETABS to assess structural performance beyond the elastic range. These analyses incorporated nonlinear soil springs based on the calibrated p-y curves, plastic hinges at beam and column locations, and lateral load patterns representative of seismic behavior. This method allowed for the identification of failure mechanisms, plastic hinge formation, and the structure's overall deformation capacity under extreme seismic loading. An overview of building model for NSA analysis is shown in fig. 5.A.

Foundation Analysis

After determining the superstructure forces, the foundation was modeled and analyzed in SAFE. Structural loads were then transferred to PLAXIS 3D for a detailed geotechnical analysis using volume elements and advanced constitutive soil models. In PLAXIS 3D, the diaphragm wall and barrettes were modeled using volume and interface elements. Tie-down anchors were modeled using embedded beam and node-to-node anchor elements. The same HSsmall soil models presented in Table 1 were applied to capture soil nonlinearity and stress dependency. A push-over analysis was performed in PLAXIS 3D to evaluate foundation performance under seismic loads, including evaluation of differential movements and wall-soil interaction. Figure 5.B shows an overview of the model in PLAXIS 3D.

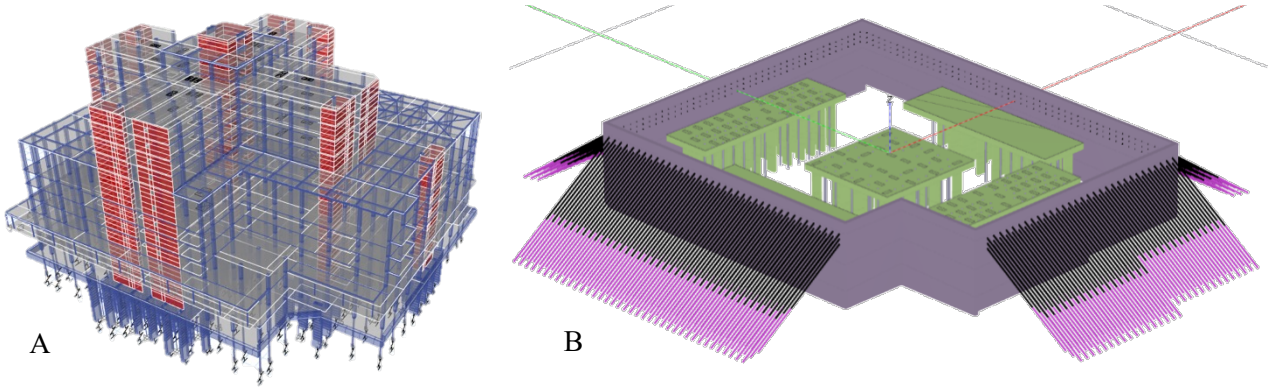


Fig 5. A: Building model overview in ETABS (NSA) B: The foundation and retaining wall model in Plaxis 3D

An iterative process was followed among ETABS, SAFE, and PLAXIS 3D to achieve convergence of structural forces and soil reactions. After each iteration, soil stiffnesses were updated based on observed deformations and foundation response, which led to the redistribution of structural loads. SSI behavior was

 © Deep Foundations Institute 2025

validated against expected performance criteria, and this iterative loop ensured internal consistency between structural and geotechnical models under seismic loading.

Foundation Components

The foundation system of the hospital building comprises multiple elements, each designed to serve specific structural and geotechnical functions.

A. Barrettes
Barrettes in this analysis are the main elements in transferring lateral loads induced from shear walls to the underlying dense till layer. These are rectangular columns 2.8m×1.0m in section and are embedded at least 5 m into the till layer to provide the required fixity to resist bending moments. With all the limitations described in this project, a group of barrettes was used under each shear wall of the building to resist the axial and lateral seismic forces.

B. Raft Slab
The lateral load-resisting system of the superstructure consists of several shear wall cores that are designed to transfer lateral loads from the floor diaphragm to the foundation. These cores along with the concrete columns that account for vertical loads, are arrayed on a raft foundation. Azizkandi et al. (2017) demonstrated in their analysis with shaking table test that a connected raft system can effectively reduce both differential settlement and lateral movements. The raft thickness is considered to be 2.5 m under the shear wall cores and 2.0 m elsewhere in the raft. The 2.5 m thickness is required to account for congested rebar arrangements, large bending moments, and shear forces at these cores. The raft slab is connected to the surrounding diaphragm wall, and to model the interaction with the diaphragm wall, specific measures are considered to calculate the effective stiffness at the raft edge.

C. Steel Piles
Steel piles were installed beneath the raft slab to support vertical loads from concrete columns in areas where the underlying soft clay could not provide adequate bearing resistance. These piles are driven down to bear on the dense till layer, ensuring sufficient vertical capacity. The piles are modeled using frame elements with hinged connections at both ends. The bottom tip of each pile includes a spring element to simulate soil resistance and base stiffness. This simplified yet effective approach captures the piles' axial behavior while accounting for soil-structure interaction.

D. Tie-downs
While some uplift resistance is provided by the skin friction of barrettes, this capacity is limited. Given the presence of pressurized groundwater and high uplift pressures, especially during earthquakes, high-strength tensile anchors were added around barrettes, consisting of 57 mm diameter strands installed into the till layer and prestressed to 1000 kN. The ultimate tensile capacity of each anchor is 2000 kN. Tie-downs were modeled using link elements with nonlinear plastic behavior, allowing simulation of yielding under uplift loads. These elements provide essential restraint against flotation and maintain the stability of the tanked foundation system. Figure 6 presents a plan and 3D view of the foundation model in ETABS, highlighting the integration of all key components.

 © Deep Foundations Institute 2025

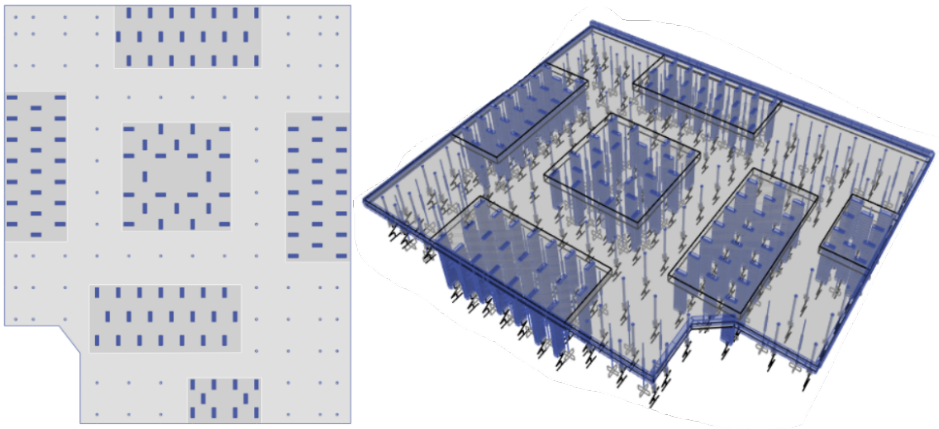


Fig. 6. Overview of building foundation model in ETABS

FEA Model Validation

Many researchers analyzed laterally loaded piles in multi-layer soils. Basu D. (2006) used differential equations to develop nonlinear algorithm for p-y curves for circular piles. In this study, the lateral behavior of barrettes was determined by developing nonlinear P-Y curves specific to the barrette size, depth, and surrounding soil parameters. Since the structural software ETABS is not able to accurately account for soil confining pressure and soil-structure interaction, a comprehensive FEM analysis in PLAXIS 3D was carried out to create modified p-y curves to be used in the ETBAS model. The p-y curves were used to create discrete nonlinear springs and were placed in interval along the length of the barrettes. The stiffness in each horizontal direction was modified based on the aspect ratio of the barrette section. Further, Mohammadi et al. (2023) emphasized the influence of varying shear wave velocity with depth on spectral response, especially in high-PGA regions. The results show that the spectral responses generated by the model may not match the field results. Therefore, a series of springs were modeled to account for the vertical interaction between soil and barrette. The FEM was calibrated using field test results, including O-cell test and anchor pullout tests. Comparison between simulated and measured p-y curves confirmed the model's reliability under both axial and lateral loading. Figure 7 illustrates the 22m long barrette model both in PLAXIS 3D and SAP2000, where the model was validated against o-cell test results with surrounding soil parameters and interface properties calibrated accordingly.

Group Effect and Bearing Capacity Adjustment

In the final phase of the analysis, the group effect of barrettes was analyzed in PLAXIS 3D. Designing the foundation based on developed individual p-y offers a first-order approximation of soil-structure interaction, and they do not capture the interaction between closely spaced group configurations. Given the tight spacing in the foundation system, a significant interaction was observed, requiring refinement of barrette capacity. Barrettes in the proximity, influence one another's mobilized shear stress and displacement. This was especially evident in the barrettes at the edge, where stress distribution was different from interior barrettes. P-multipliers were applied to the axial and lateral soil springs to account for the group effect. This process required iterative analysis, and element loads were redistributed based on changes in the spring stiffness. To ensure consistency between models, p-y curves were recalibrated. The process was repeated until a stable and converged load and deformation were achieved in both ETABS and PLAXIS 3D models. This iterative coupling between the two software ensured a robust representation of the group effect, resulting in a more realistic assessment of load distribution, deformation, and overall group performance under both gravity and seismic loads.

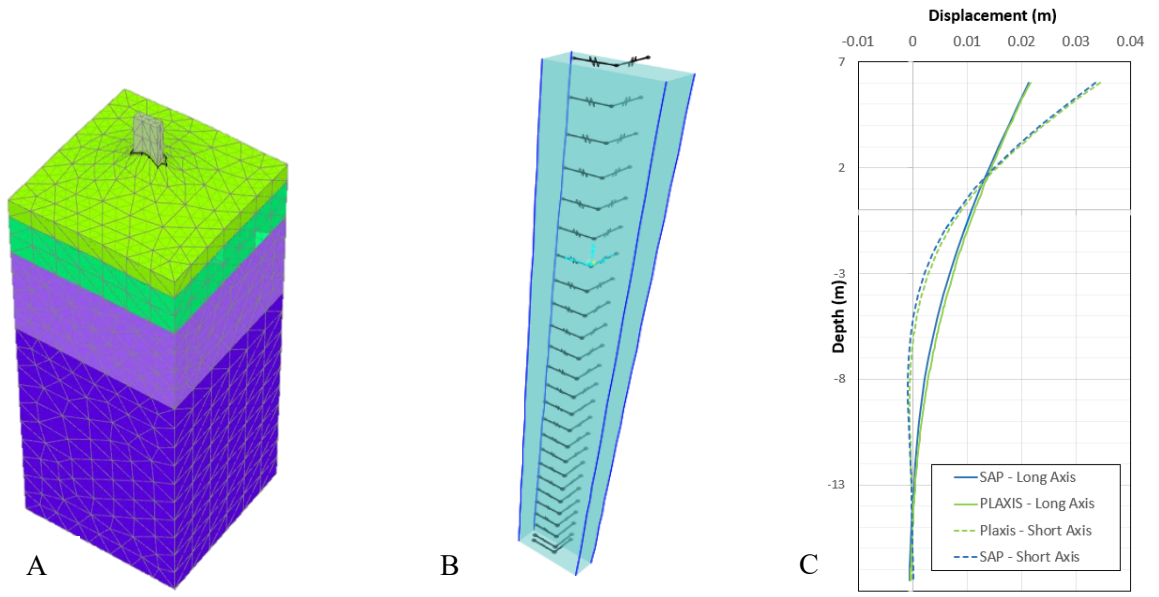


Fig 7. A: Single Barrette Model in PLAXIS 3D B: Barrette model in SAP2000 based on p-y curve development C: Comparison of lateral deflection of barrette models in SAP and PLAXIS 3D under same lateral load

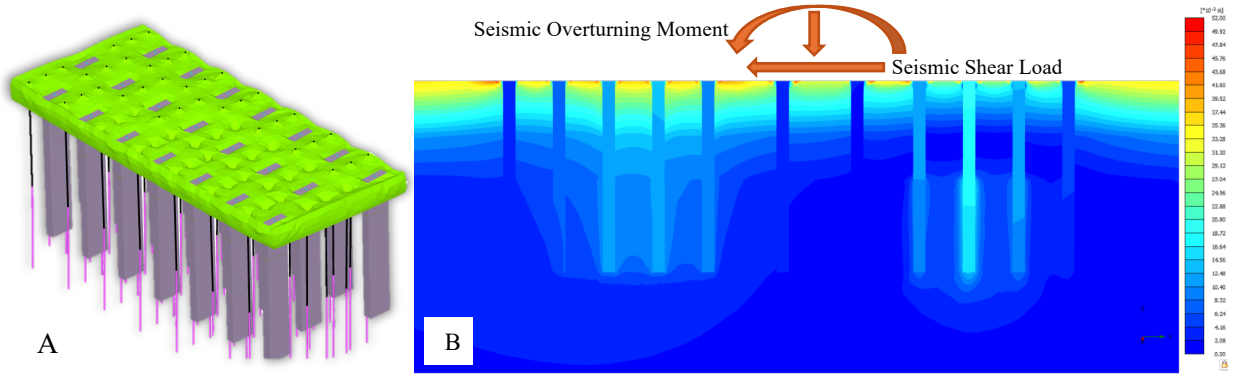


Fig 9. A: Group of barrettes and tie-downs in Plaxis 3D B: Soil deformation contours due to group effect

SUMMARY OF KEY INNOVATIONS

This project presented the first documented use of barrette foundations for a post-disaster hospital in Canada, demonstrating a pioneering application of advanced geotechnical techniques for critical infrastructure. The foundation system was developed in response to two major challenges: adopting the new generation of seismic code and addressing complex ground conditions. An integrated and innovative approach was undertaken to meet these demands, combining advanced 2D site-specific response analysis to develop custom response spectra, performance-based seismic design, and rigorous soil-structure interaction (SSI) modeling. The methodology involved a multi-platform, multi-phase modeling process using ETABS, SAFE, PLAXIS 2D, and PLAXIS 3D, while rigorously calibrating the models with field tests. This ensured reliable representation of SSI and group effects, reducing design uncertainty and risk.

There are very limited resources on developed shear strain wedges for laterally loaded barrettes. Most conventional methods simplify them as circular piles with equivalent diameters. Kumari et al. (2019), for instance, analyzed different pile shapes by applying circular pile theory. Unlike common approaches, this study recognized the inherently anisotropic behavior of barrettes, which have direction-dependent stiffness and capacity. An optimized layout with different orientations was used to balance the developed passive

 © Deep Foundations Institute 2025

resistance and skin friction mobilization, achieving uniform group behavior. The site-specific p–y curves were developed using a comprehensive in-situ testing program (O-cell, static load, and anchor pullout tests) and calibrated in 3D finite element models to reflect true soil-barrette interaction. The group effect of barrettes was explicitly addressed through iterative modeling and the application of reduction factors to accurately capture load distribution and differential settlement. An iterative loop between structural and geotechnical models across multiple software platforms (ETABS, SAFE, PLAXIS 2D, and PLAXIS 3D) was central to achieving a reliable soil-structure interaction and harmonizing geotechnical and structural analysis. These strategies allowed the project to move beyond conventional foundation design, delivering a high capacity, performance-based foundation system tailored to the site seismic condition.

CONCLUSION

This foundation system met all performance criteria required for a post-disaster healthcare facility, including life safety, operational continuity, and seismic resilience. By applying a highly tailored approach with rigorous site-specific data and iterative analysis, the design team successfully addressed the complex seismic demands, poor subsurface conditions, and construction constraints. More importantly, it provides a robust framework for future high-performance foundation design in seismically active regions. The approach demonstrated here is based on a cross-disciplinary integration, calibrated modeling, and iterative analysis, which offers a significant advantage over conventional methods. The success of this integrated design demonstrated the feasibility and benefits of barrette foundations in high seismic zones. The combined system minimized excavation risk, improved schedule significantly, and provided seismic resilience, and is recommended for broader adoption in similar urban projects where poor subsurface condition and seismic demands are critical factors.

ACKNOWLEDGMENTS

The authors wish to acknowledge the support of the broader EllisDon project team for their coordination and contributions to the successful execution of this work. The authors also gratefully acknowledge the collaboration of **Thurber Engineering Ltd.**, in particular for their expertise in the development of constitutive soil models and execution of 2D site response analyses, which formed a critical part of the geotechnical design. The contributions of **Bush, Bohlman & Partners** in the structural modeling and analysis are also acknowledged; their technical input was instrumental to the successful integration of structural and geotechnical components in this design.

Language editing assistance was provided using AI tools (ChatGPT by OpenAI) for grammar refinement and clarity improvements only. No AI tools were used in this analysis, generation of figures, or interpretation of technical results. The authors take full responsibility for the content, conclusions, and originality of this work.

REFERENCES

Adams, J., Allen, T., & Kolaj, M. (2019). Canada's 6th Generation Seismic Hazard Model, as prepared for the 2020 National Building Code of Canada. *Proceedings of the 12th Canadian Conference on Earthquake Engineering*, Quebec City, Canada.

Adams, J., Halchuk, S., Allen, T., & Rogers, G. (2015). Canada's 5th Generation Seismic Hazard Model, as prepared for the 2015 National Building Code of Canada. *Proceedings of the 11th Canadian Conference on Earthquake Engineering*, Victoria, BC, Canada, July 21–24.

 © Deep Foundations Institute 2025

Azizkandi, A. S., Baziar, M. H., & Fallah Yeznabad, A. (2018). 3D dynamic finite element analyses and 1 g shaking table tests on seismic performance of connected and nonconnected piled raft foundations. *KSCE Journal of Civil Engineering*, 22, 1750–1762.

Basu, D. (2006). *Analysis of laterally loaded piles in layered soil* (PhD thesis). Purdue University, West Lafayette, Indiana, USA.

Benz, T. (2007). *Small-strain stiffness of soils and its numerical consequences* (PhD thesis). Geotechnical Institute, University of Stuttgart.

Carvajal, J.C., Finn, W.D.L., and Ventura, C.E. (2020). Response spectrum-based seismic response of bridge embankments. *Can. Geotech. J.*, **57**(11): 1639–1651. https://doi.org/10.1139/cgj-2019-0619

Finn, W. D. L., & Wightman, A. (2003). Ground motion amplification factors for the proposed 2005 edition of the National Building Code of Canada. *Canadian Journal of Civil Engineering*, 30, 272–278. https://doi.org/10.1139/L02-081

Kolaj, M., Allen, T., Mayfield, R., Adams, J., & Halchuk, S. (2019). Ground-motion models for the 6th Generation Seismic Hazard Model of Canada. *Proceedings of the 12th Canadian Conference on Earthquake Engineering*, Quebec City, Canada, Paper 192-hHtH-159, 9 pp.

Kumari, A., Thakare, S. W., & Dhatrak, A. I. (2020). Lateral and uplift capacities of barrette pile in sandy soil. In Latha Gali, M. & Rao, P. R. (Eds.), *Construction in Geotechnical Engineering*, Lecture Notes in Civil Engineering (Vol. 84). Springer, Singapore. https://doi.org/10.1007/978-981-15-6090-3_15

Mohammadi, R., Motamed, R., & Faeli, Z. (2023). Numerical modeling of soil-shaft interaction validated using the instrumented Hayward Bridge in California. *Proceedings of the DFI 48th Annual Conference on Deep Foundations*. https://doi.org/10.5281/zenodo.11026667

Turner, R. J. W., Clague, J. J., Groulx, B. J., & Journeay, J. M. (1998). *GeoMap Vancouver: Geological map of the Vancouver metropolitan area*. Geological Survey of Canada Open File 3511.

Natural Resources Canada. (n.d.). *Seismic hazard maps of Canada*. Retrieved from http://www.earthquakescanada.nrcan.gc.ca/hazard-alea/interpolat/index-en.php

 © Deep Foundations Institute 2025

PRESERVING THE PAST, ENGINEERING THE FUTURE: FAÇADE RETENTION MEETS EARTH RETENTION IN THE UNITED BLDG. PROJECT

Mark Reinders, P.Eng, Green Infrastructure Partners Inc., mreinders@gipi.com
Thomas Fiala, P.Eng, Green Infrastructure Partners Inc., tfiala@gipi.com
Lauren Speakman, Green Infrastructure Partners Inc., lspeakman@gipi.com

ABSTRACT

The United Bldg. is a landmark project located in the crowded downtown core of Toronto. The 50-storey structure occupies a full city block and incorporates two heritage façades: a nine-storey 1928 Beaux-Arts style structure and a ten-storey 1961 Modern Classical style. Both were required to be retained in place during construction (City of Toronto, 2017) (Davpart Inc., n.d.). Before the inception of this project, a façade retention system (FRS) of ten storeys was unprecedented in the industry (Immen, 2019). This led to the development of a sophisticated hybrid support system which integrated the FRS with the support of excavation (SOE) system to meet the project's complex requirements. The preservation of the historic façades combined with the intricacies of urban construction near sensitive infrastructure, presented significant challenges throughout various stages of the project. These included: controlled demolition of the interior structure while preserving the façade, installation of secant piles, king piles, and micropiles for both the SOE and FRS, FRS steel installation and transferring the existing structure's load onto the newly installed piles, and finally, laterally supporting four storeys of underground excavation while navigating the complexities of working around and beneath the FRS. This paper will provide details of the construction of North America's largest FRS and its successful incorporation into the SOE.

Keywords: Support of excavation, façade retention, secant pile, micropile, tieback, waler, GUL cement, shotcrete, demolition, load transfer

INTRODUCTION

The United Bldg., a landmark project by Davpart Inc., is in the crowded downtown core of Toronto, Canada (Fig. 1). The 50-storey structure will encompass a city block and incorporate two heritage façades as a tribute to Maclean Publishing, the original owners. The façades consist of a nine-storey 1928 Beaux-Arts style structure at 210 Dundas Street and a ten-storey 1961 Modern Classical style at 481 University Avenue. Both the 1928 and 1961-era buildings were designated with cultural heritage status by the City of Toronto and the heritage façades were required to be preserved in place through all phases of construction (City of Toronto, 2017). All brick, stone, concrete and steel finishes could not be dismantled and/or reconstructed; they were required to be secured and protected in their original location for the full duration of construction. Before this project, a Façade Retention System (FRS) of ten storeys was unprecedented in the industry. The unique challenge of positioning this record-setting FRS above a four-storey excavation required an innovative approach, which led to the development of a hybrid support system integrating the FRS with the Support of Excavation (SOE).

This paper focuses on the constructability aspects of the project and specifically examines key aspects of the demolition strategy, installation of SOE elements, connection and load transfer between the two retention systems, and finally the lateral excavation support. The project was further challenged by strict deflection criteria (Table 1) as well as a dense urban environment. Bringing success to this project heavily relied on all stakeholders being flexible with designs and workplans, maintaining open channels of communication and establishing tight coordination.

 © Deep Foundations Institute 2025



Fig. 1. Architectural Renderings of The United Bldg. Looking Northwest (Left) & East (Right) (B+H Architects Corp., 2023)

Table 1: Deflection Criteria

Monitoring Data	Review Level	Alert Level
Façade Lateral Deflection (mm)	10	15
Façade Tiltmeter (degrees)	0.09	0.18
Facade Vertical Deflection (mm)	10	15
SOE Lateral Deflection (mm)	10	15
Subway Tunnel Lateral Deflection (mm)	6	8

DEMOLITION OF EXISTING STRUCTURES

Construction began with the complete removal of two low-rise buildings in the northeast corner, followed by the partial deconstruction of 210 Dundas St. and 481 University Ave. The FRS design relied on elements of the existing structures to ensure stability of the façade in place. This required the first interior bay of columns, slabs, and girders to remain in situ and to be integrated with façade retention reinforcement. The interior demolition required a precision approach to mitigate damage to the façade. Small excavators and skid steers were hoisted floor-by-floor to dismantle the columns, slabs, and girders that were not integral to the FRS (Fig. 2). Strategic saw cuts were made at joints to ensure demolition did not propagate vibration into the retained portion of the façade. Drop zones were established within the structure to allow material to be deposited onto the floor below and transferred into bins for disposal. Dropping material posed another vibration risk, therefore vertical form props beneath the drop zones helped to distribute the impact load and absorb the vibration.

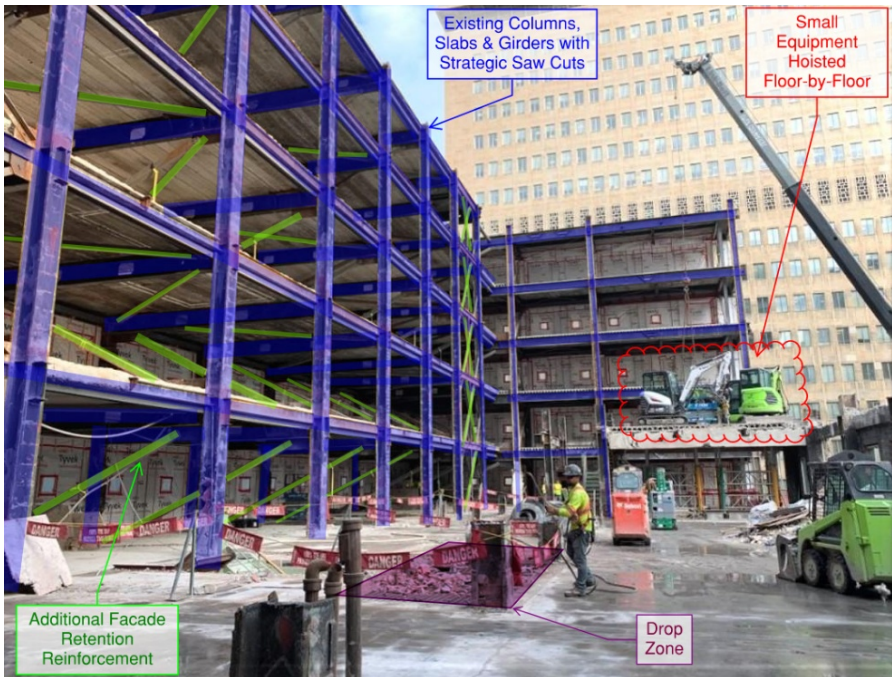


Fig. 2. Demolition of 481 University Ave. on 5th Floor

PILE INSTALLATION FOR SOE AND FRS

The earth retention system for this project was designed to provide both lateral support of excavation and vertical support for the record setting FRS. Drilling techniques took into consideration the geotechnical conditions of the site, where some perched water was evident. The stratigraphy generally consisted of the following with elevations noted in meters above sea level (masl): Fill and Existing Structure (94.3 – 89.0), Clayey Silt (89.0 – 85.0), Silty Sand (85.0 – 81.7), Clay & Silt (81.7 – 78.7) and Shale Bedrock (78.7 onward). There was no considerable groundwater concern.

Secant Pile Installation

The SOE consisted of a secant pile wall, covering two-thirds of the perimeter. The use of one filler for one reinforced pile was required where the FRS was to be supported, due to the SOE's high degree of stiffness. The reinforced piles were 1.0 m (39 in) in diameter, using up to W610 x 217 (W24 x 146) beams and 20 MPa (2900 psi) concrete.

Load bearing piles for supporting FRS elements, were increased in size to 1.3 m (51 in) diameter with steel sections up to W760 x 257 (W30 x 173) and 50 MPa (7250 psi) concrete to accommodate the additional vertical loads. To effectively transfer the forces from the FRS through these higher capacity piles, studs were added along the web of the wide flange to engage the high strength concrete. To install these elements within 400 mm (16 in) of the façades (Fig. 3, Left), a Bauer BG36 rig was used to drill with cased-kelly techniques. Not only did this method support surrounding soils, but also provided verticality control, both of which were critical criteria in mitigating any disturbance to the existing foundations during the ongoing demolition works.

Servicing this operation required careful management. The drill rig's footprint occupied the full 7 metres available, preventing other operations from passing it. The spoils discharged from the auger were stockpiled away from the operation to allow steel and concrete placement to occur from opposite sides of the rig. Concrete was placed within the steel casing via free-fall to a depth of 23 m (75.5 ft). The casing would

 © Deep Foundations Institute 2025

carefully be extracted and crews would monitor the concrete elevation and steel positioning within. This all needed to occur while tri-axles removed the spoil stockpile, demolition debris was hauled offsite, façade retention steel was delivered, and micropile operations were ongoing. Daily site coordination meetings were held to ensure all trades were aware of current and forecasted plans to support each other's work.



Fig. 3. Cased-Kelly Drilling of Secant Piles (Left) & Drilling of Micropiles (Center-Left), King Pile Drilling Near FRS (Center-Right), King Pile Toe (Right)

Micropile Installation

Due to ground bearing load restrictions next to the existing subway infrastructure, as well as overhead and underground utility obstructions that could not be removed or relocated, cased-kelly drilling could not be used in this zone. Instead, micropiles were employed for vertical and lateral supports the remaining third of the SOE. Smaller and highly manoeuvrable equipment was needed, resulting in the KLEMM 806-5G using down-the-hole-hammer to complete the job. The edge of the micropiles were generally within 200 mm (8 in) of the heritage façade and as close as 100 mm (4 in) to the façade protection (Fig. 3, Center-Left). The project team collaborated on finding optimal micropile sizes to eliminate re-tooling and provide consistent construction techniques - exterior micropiles were designed as HSS 406 x 14.6 (HSS 16 x 0.57), while interior micropiles were designed as HSS 346 x 15.9 (HSS 13-5/8 x 0.625). All micropiles had a central bar, ranging from 43 mm (#14) to 90 mm (#28) and were filled with 60 MPa (8700 psi) grout. Spacing between micropiles was between 100 mm and 1200 mm (4 in and 47.25 in), while drill depths in overburden and shale were 15.3m (50.2 ft) and 8.0m (26.25 ft) respectively, maintaining a 4.0 m (13.1 ft) toe below excavation.

At peak activity, four major operations (demolition, FRS steel installation, secant pile drilling, and micropile drilling) had to share the limited site footprint. Material storage was at a premium for items such as wide flange beams, FRS steel, micropile casing, threadbar, grout, and especially drill spoils plus access routes for deliveries (concrete, spoil removal, and steel) had to be maintained. This posed a challenge for grout supply, as the neat volume of grout alone required over 3000 kg (6600 lbs) of cement per micropile. To support both volume and performance demands, a specialized blend of Type GUL (General Use Limestone) cement with water reducers and strength enhancers was developed through advanced trials. Using GUL cement allowed for bulk supply in two 20 MT (44.1 tons) silos, as opposed to 1000 bags or 25 skids, thereby minimizing the footprint of the grouting operation.

King Pile Installation

Almost a year after the completion of the SOE drilling, the partial demolition of 210 Dundas St. and 481 University Ave. had progressed enough to allow for the installation of king piles within the footprint of the

new building. The king piles (temporary caissons reinforced with a wide flange beam) were installed with a Bauer BG28 using cased-kelly drilling techniques (Fig. 3, Center-Right). The equipment was as close as 250 mm (10 in) from overhead FRS elements. The king piles were designed to support the interior component of the FRS and to be cast within the new columns of the permanent structure. To maximize access within the excavation, only 16 king piles were used to support 50% of the weight of the combined structure. This resulted in design loads as high as 6125 kN (690 tons) per king pile, with wide flange sections as large as W360 x 818 (W14 x 550). These were installed within a 1.0 m (39 in) shaft with 2.55 m toe (8.3 ft) below the underside of the permanent footings, in the shale bedrock. Due to the significant load and thickness of the wide flange sections, 108 studs were welded to the web and flanges within 1.75 m (5.75 ft) of the pile toe (Fig. 3, Right). This transferred the vertical load to the 60 MPa (8700 psi) self-consolidating concrete and subsequently into the shale bedrock.

CONNECTING ABOVE AND BELOW GRADE SYSTEMS TOGETHER

The installation of the FRS and tying it to the temporary load-bearing elements was an exceedingly complex process. Multiple designers and drawing iterations were required to analyse potential failure modes and ensure structural stability. The complexity is a challenge to convey in a single image; however, Fig. 4 and subsequent images show how some of the more complex systems were integrated.

As detailed above, the internal structure up to the inner bay of columns, was also retained. Not only did this provide stability for the heritage façade, but also minimized the need for excess temporary façade reinforcement. The existing structure was supplemented with diagonal struts and cross beams secured between the interior and exterior columns, as well as across the existing structural slab. The steel beams were installed on all floors, starting from the top down to the second floor.

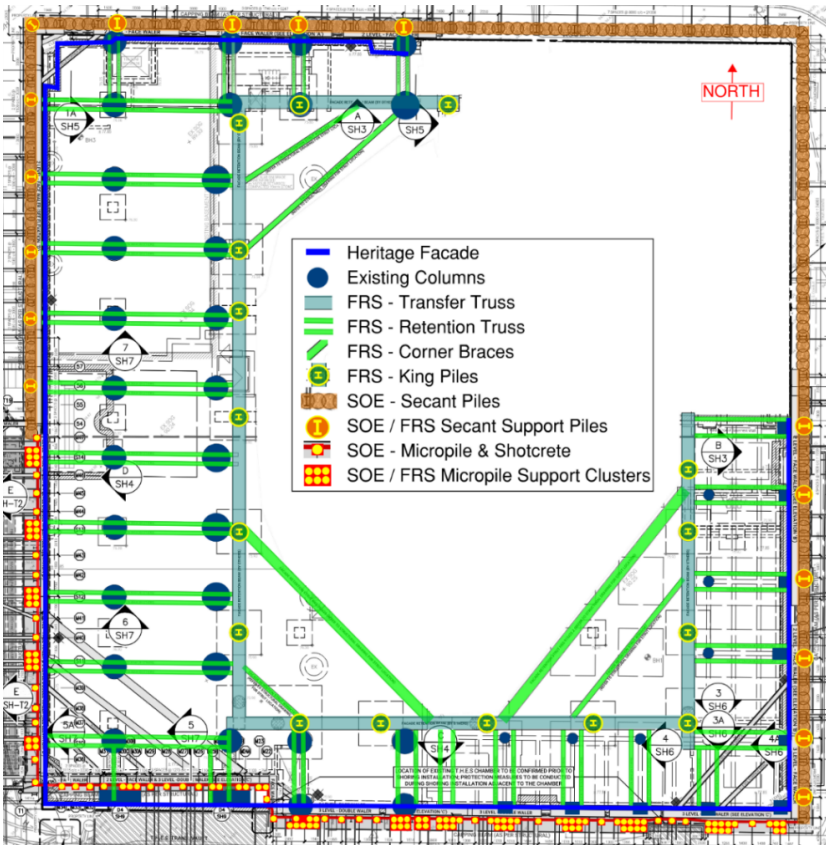


Fig. 4. Visual Representation of the FRS and SOE Connection

 © Deep Foundations Institute 2025

As the FRS steel was being installed inside the interior of the existing structure, the SOE piles were capped and prepared for a concrete cap beam. The pile caps consisted of steel plates as thick as 90 mm (3.5 in) welded to the top of the secant piles and micropiles. The plates had vertical dowels secured to them to allow tie-in with the concrete cap beam. The secant pile caps aligned with the FRS supporting columns required over 50 hours of field welding each, inclusive of pre-heat and post-cooling time (Fig. 5 Left). The clustered micropiles supporting the FRS loads required a survey and template to accurately position the cap plate around the entire cluster (Fig. 5 Right). Upon completion of pile caps, a dense rebar cage was placed on top of the SOE, then formed and poured with 55 MPa (8,000 psi) concrete.

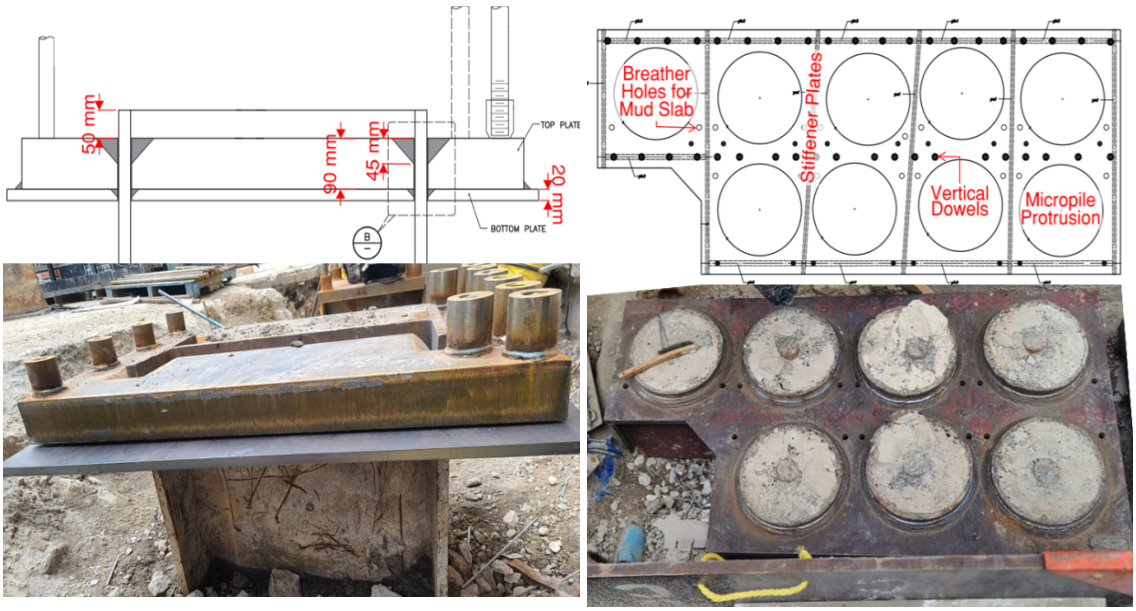


Fig. 5. FRS Loaded Secant Pile Cap (Left) and Micropile Cap (Right)

Truss Installation

After the FRS steel above the second floor and the concrete cap beam were complete, the construction of the at-grade "Retention Truss" began as detailed in Figure 6 and Figure 7.

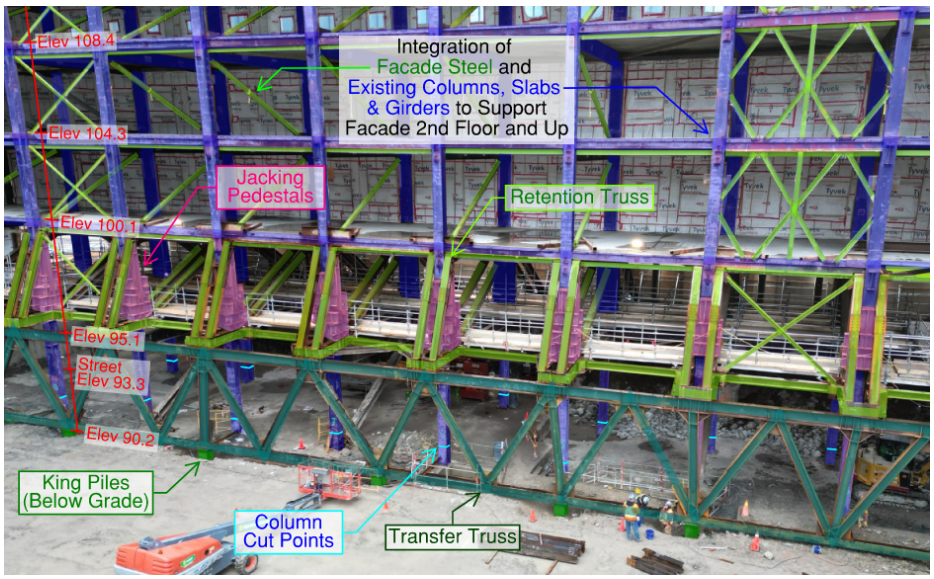


Fig. 6. 481 University Ave. FRS Elevation View

 © Deep Foundations Institute 2025

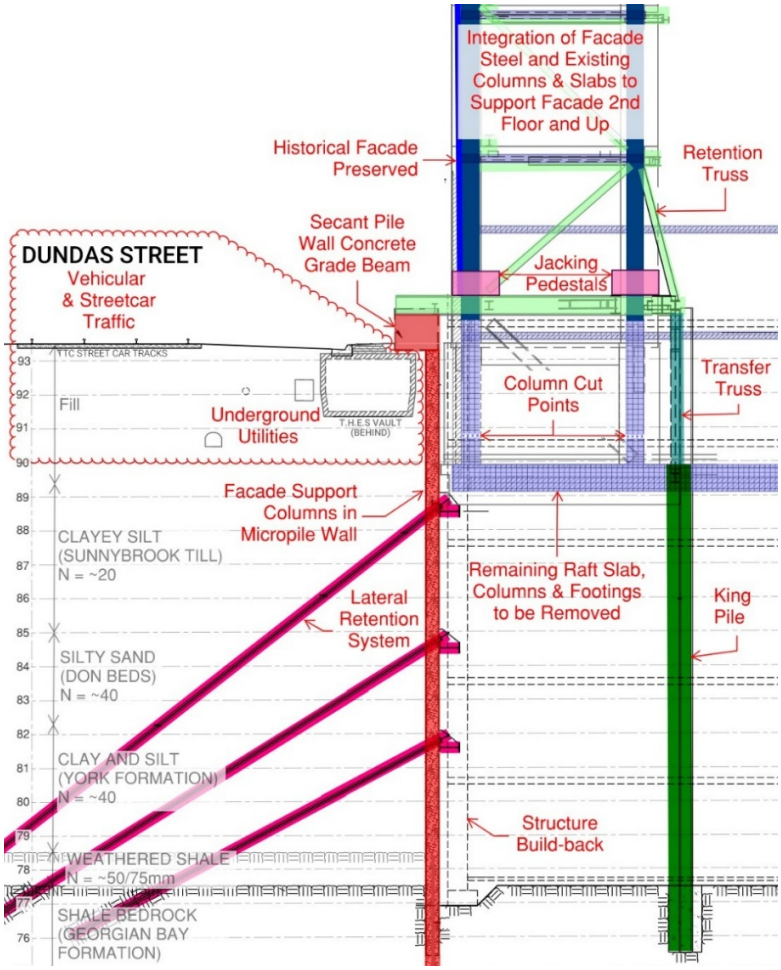


Fig. 7. 210 Dundas St. FRS-SOE Elevation Section View

The retention truss was built around both sides of the retained exterior and interior columns which held jacking pedestals around each of these columns. On the exterior face, the retention truss extended through a pocket in the façade to bear on the concrete cap beam. The interior end of the retention truss terminated in line with the interior columns but contained connections points for future extension. This allowed installation of the king piles as close as possible to the FRS. The tops of the 16 king piles were cut-off at the underside of the existing basement elevation, allowing the installation of the "Transfer Truss" which was approximately 3 m (10 ft) tall and is attached to the top of all king piles. The retention truss then was extended to bear directly on top of the transfer truss, securing these two elements together. To complete the FRS system, six interior corner braces were installed to provide lateral support across the three corners of the FRS.

Load Transfer

Upon final connection of the FRS to the SOE elements, the team prepared to transfer the load from the existing footings to the support system. Determining the load of the retained heritage structure was a sizeable challenge. The intact structure's dead weight was estimated using a combination of 3D finite element modelling as well as detailed hand calculations of each of the columns. In addition to typical live loads (wind, snow, construction), thermal loads on the retention and transfer trusses had to be considered due to their size and constraints. After evaluating these factors, an average load of 400 MT (440 tons) per

column was estimated with a variation of +/- 15%. Across the 50 columns supported, the total anticipated weight was near 20,000 MT (22,200 tons).

Each existing column required multiple 150 MT (165 ton) jacks to support the anticipated loads (Fig. 8). There were 175 jacking positions positioned around the columns and on the retention trusses. The jacking sequence split the structure into eight segments, reducing the number of jacks needed and allowed progressive load transfer. Each segment was jacked independently and monitored by strain gauges mounted to the columns below these lifting points. Measured strain was compared to calculated strain to determine if the existing foundation was being unloaded.



Fig. 8. Jacks Around Existing Columns at 481 University Ave. (Left) & 210 Dundas St. (Right)

Jacking Sequence

The following jacking sequence was completed at all eight segments were completed prior to moving to the next step:

1. Load jacks to 50% of the anticipated load. Record monitoring data. Secure with temporary shims to allow relocation of jacks. Record monitoring data again.
2. Load jacks to 75% of the anticipated load. Record monitoring data. Secure with temporary shims to allow relocation of jacks. Record monitoring data again.
3. Separate columns:
   a. Steel columns (Fig. 9): Torch cut individual flanges and weld compression plates across gap. Torch cut web.
   b. Concrete columns (Fig. 10): 100 mm (4 in) core through centre of column. Wire saw 25mm (1 in) slot across half of column. Place poly-propylene bond-breaker on bottom of cut, then liquid grout on top to fill cut gap. Continue sequence for other half of column. Insert steel bar through central core to act as a shear key for potential lateral shifting.
   c. Place dial indicators accurate to 25 µm (0.001 in) across bearing joint to monitor structure lift-off.
4. Load jacks to 100% of the anticipated load, or:
   a. until dial indicator identifies any movement at column, or

 © Deep Foundations Institute 2025

b. strain gauge indicates no further load is released.

5. Stop jacking and secure column to transfer truss with transfer plates or adjustable shims.

Final jacking loads at all columns fell within the 15% variation expected, while monitoring indicated movement remained below the alert limits. The full jacking sequence took place over the course of six weeks, allowing for the next stage of work to follow immediately after.



Fig. 9. Separation of Existing Steel Columns



Fig. 10. Separation of Existing Concrete Columns

EXCAVATION AND LATERAL SUPPORT

With the façade and FRS secured to the SOE and king piles, the below grade excavation could begin for the basement and permanent foundations on the shale bedrock (Fig. 11). The existing foundations were demolished together with the removal of the existing basement walls, exposing the face of the SOE. The excavation process had to be carefully coordinated with installation of internal bracing supports to ensure lateral loads were balanced and SOE performance remained within tolerance. At the original basement

 © Deep Foundations Institute 2025

elevation, corner braces were primarily used due to headroom constraints and encroachment limitations imposed by neighbouring structures. This was particularly critical in the southwest corner, where the SOE system adjacent to the underground subway station required strict movement limitations.



Fig. 11. Excavation and Lateral Support of 481 University Ave.

Piles immediately under the retention truss supported high vertical FRS loads, therefore tiebacks against them were minimized to limit additional downward force. To provide lateral resistance in these axially loaded piles, a discrete waler spanned across it to the adjacent piles that had minimal vertical load. Tiebacks against these adjacent piles transferred the vertical force into the respective piles, but distributed the lateral force across the waler and into the axially loaded FRS pile. The micropile SOE required three to four rows of continuous walers and the dense micropile spacing limited availability for tieback placement. 30 MPa (4350 psi) shotcrete was applied between the micropiles in 1.5 m (60 in) lifts. The shotcrete ranged from 150 to 200 mm (6 to 8 in) thick and was reinforced with two layers of welded wire mesh. In the northeast corner, the secant wall did not support FRS loads, therefore three rows of tiebacks stabilized the secant piles for a maximum excavation depth of 22 m (72 ft).

Upon detailed review of the design, the construction team determined that the walers and tieback connections were the critical path of the excavation. The client was particularly interested in optimizing the construction sequence to reduce welding and waler installation times. A collaborative effort among stakeholders led to improvements in waler and tieback designs by leveraging in-situ material strengths. For example, the micropile casing was originally designed with 345 MPa (50 ksi) steel and 60 MPa (8,700 psi) grout, but actual material strengths were 550 MPa (80 ksi) and nearly 70 MPa (10,000 psi), respectively. These strength increases allowed reliance on vertical SOE members to redistribute tieback loads, thereby minimizing waler sizes.

 © Deep Foundations Institute 2025

CONCLUSION AND PROJECT COMPLETION INSIGHTS

Early in the planning stages, it became clear that site logistics would be critical to success. Detailed planning was required to stage operations in a manner that used every bit of the site available. Regular coordination meetings between the trades helped with the tight scheduling of deliveries and managing site access points. Multiple staging plans were issued based on a granular sequence of works. Timing of completing one operation to allow another one to start was closely managed, with acceleration efforts implemented in advance to help with managing stages.

The overall completion of the FRS and SOE works were deemed an overwhelming success. The project scope was completed on time and on budget, all while maintaining the highest degree of care for worker health and safety, the public environment and the quality of construction. Furthermore, the success was confirmed by meeting the stringent deflection criteria with monitoring movements over the 24 months the scope spanned. On occasion, alert levels were exceeded. When an alert level was exceeded, the Shoring Engineer would identify the specific details of that monitoring point and the activities at that time to evaluate if the event was of concern. However, it was observed that temperature fluctuations had a considerable impact on the monitoring points and when deflections exceeded the limitations. Figure 12 and Figure 13 illustrate the temperature correlation with the quantity of exceedances over the various scopes of work for both lateral and vertical movements. Based on these considerations, it was generally concluded that ambient temperature impacted the deflection criteria to a greater extent than the construction activities. Table 2 details the peak deflection observed during the respective scope of work.

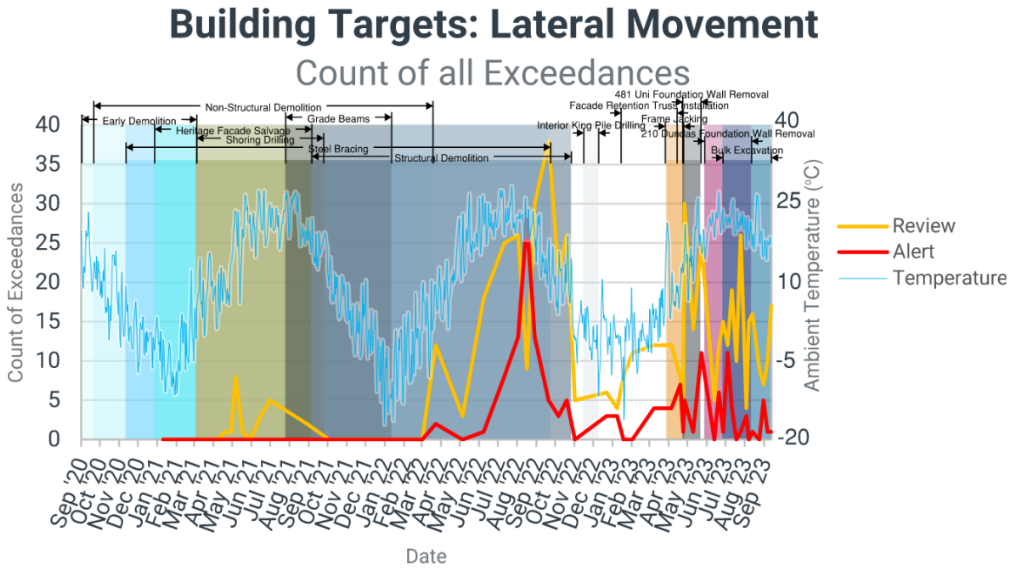


Fig. 12. Quantity of Peak Exceedances for Façade Lateral Movement

 © Deep Foundations Institute 2025

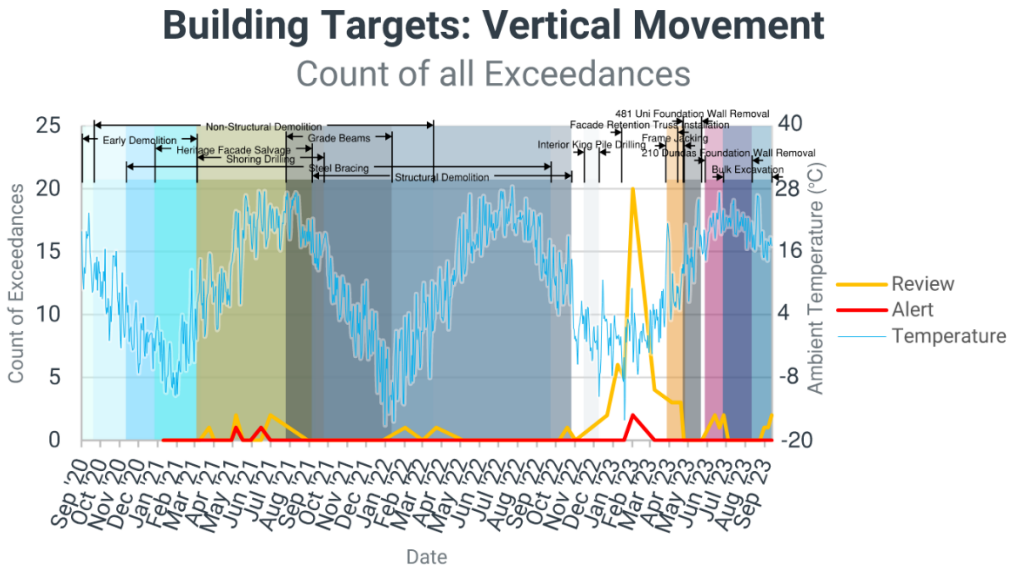


Fig. 13. Quantity of Peak Exceedances for Façade Vertical Movement

Table 2: Peak Deflection Incurred During Works

Monitoring Data	Review Level	Alert Level	Demolition	Drilling	FRS Install	Jacking	Excavation & Bracing	
Façade Lateral Deflection (mm)	10	15	5	10	23	18	15	
Façade Tiltmeter (degrees)	0.09	0.18	0.05	0.05	0.13	0.09	0.05	
Facade Vertical Deflection (mm)	10	15	10	15	14	13	12	
SOE Lateral Deflection (mm)	10	15	n/a				12	
Subway Tunnel Lateral Deflection (mm)	6	8	8	8	6	3	5	

The success of the façade and excavation support were primarily due to extensive planning and detailed review conducted with a team-centric approach. All stakeholders agreed that the achievement of this project could not be attributed to a sole individual or company but required the collaboration of all parties. Experts in their field respected insights and suggestions to improve on both design and construction methods to find the most effective path forward while keeping safety and quality paramount. No singular entity dictated what had to be done. This mutual endeavour for collaboration between the Owner, Architects, Designers, Consultants, Constructors, Inspectors and Vendors should be a model for all future projects that step into unknown territory. This was the key to successfully producing North America's tallest façade retention system.

ACKNOWLEDGEMENTS

- Davpart (Owner)
  - David Zeegen – Director of Development
- ELLISDON Residential (G.C.)
  - Dawn Spironello – Pre-Construction and Risk Manager
  - Kevin Ryan – Superintendent
- Read Jones Christoffersen (RJC) Ltd. (Structural Engineer)

 © Deep Foundations Institute 2025

    - Matthew Swayne, B.A.Sc., P.Eng, LEED AP BD+C, Sr. Project Engineer (now with Mott MacDonald Canada Limited.)
- Grounded Engineering
    - Amanda Li – Associate, Geostructural Engineering Services

REFERENCES

1. City of Toronto. (2017, December 8). *By-law 1393-2017: To designate the property at 481 University Avenue…as being of cultural heritage value or interest.* Retrieved from https://www.toronto.ca/legdocs/bylaws/2017/law1393.pdf

2. Davpart Inc. (n.d.). *History: A pressing back story.* The United Bldg. Retrieved from https://theunitedbldg.com/content/history/

3. Immen, W. (2019, May 1). Residential tower grows… *The Globe and Mail.* Retrieved from https://www.theglobeandmail.com/business/industry-news/property-report/article-residential-tower-grows-out-of-historic-maclean-hunter-buildings/

4. B+H Architects Corp. (2023, June 26). *481 University Ave. Redevelopment.* Issued for Construction Drawings

 © Deep Foundations Institute 2025

MODELING TO MONITORING: EVALUATING ADJACENT STRUCTURES FEET FROM A BOSTON EXCAVATION

Tyler M. Poggiogalle, Haley & Aldrich, Inc., New York, NY, USA, 646.277.5689, tpoggiogalle@haleyaldrich.com
Damian R. Siebert, Haley & Aldrich, Inc., Boston, MA, USA, 617.886.7399, dsiebert@haleyaldrich.com
Wystan Carswell, Haley & Aldrich, Inc., Providence, RI, USA, 617.886.7357, wcarswell@haleyaldrich.com

ABSTRACT

Challenges with protecting adjacent structures require careful consideration during all aspects of excavation support design and construction, including the installation, enabling systems, and the primary support of excavation (SOE). This paper examines a deep excavation in a dense urban environment where a reinforced concrete diaphragm "slurry" wall with internal bracing facilitated below-grade construction to depths of 25 to 45 feet. Proximity to sensitive structures, including a nearby transit tunnel and greater than 100-year-old adjacent masonry buildings, heightened the complexity of the project. Finite element modeling (PLAXIS 2D) was employed to predict excavation-induced movements of both the SOE and adjacent structures, and extensive monitoring documented movement of that adjacent structures remained within specified tolerances. While the primary SOE performed as anticipated, enabling work and wall installation resulted in movements of adjacent structures that were not modeled. This case study underscores the critical importance of integrating enabling and installation-induced effects into design and planning. The paper demonstrates the value of robust analysis, monitoring, and adaptive measures in managing the challenges of urban excavation.

Keywords: support of excavation, instrumentation, monitoring, slurry wall, PLAXIS

PROJECT BACKGROUND

The development, located in Boston, consisted of a new 30+-story tower with a basement footprint of approximately 15,500 square feet. The basement consisted of a parking garage with 2.5 to 3 levels below-grade depending on the location. The below-grade portion of the development covered the entire site, extending to the property lines on all four sides. Existing site grades varied by up to 9 ft and the lowest floor slab resulted in excavation depths ranging from approximately 27 to 43 ft below existing ground surface (25 to 33 ft below site groundwater levels). The primary SOE system (slurry wall with internal bracing) was designed by the engineer retained by the contractor under a design-bid-build contract delivery method. The development included sensitive abutters including a heavily trafficked roadway that runs atop a transit tunnel to the north, a three-story brick building to the east, a 100-year-old four-story theater to the west, and a narrow public alley to the south. Refer to Fig. 1 for a site photo of the below-grade construction.

The transit tunnel varies in distance, ranging from approximately 15 to 22 ft, from the site's north property line beneath a heavily trafficked roadway. Historic drawings and the existing conditions survey plan indicated that the top of the transit tunnel is located at approximately 8 ft below ground surface with the bottom approximately 27 ft below ground surface.

 © Deep Foundations Institute 2025



Fig. 1. Below grade construction

The three-story brick building to the east contains a first-floor restaurant with apartments on the second and third floors. The basement slab is located approximately 8 ft below surrounding grades and was observed to be founded on granite blocks supported on wood piles. Pile design capacity and lengths were not confirmed but it was assumed that the wood piles terminate in the Marine Sand layer. Piecing together available information on the three-story brick building, it was determined that the building was supported on two rows of pile supported granite blocks that were located approximately 2.5 and 23.5 ft from the property line.

The 100-year-old four-story theater to the west is L-shaped and as noted on the 1924 original construction drawings and later confirmed in test pits conducted as part of the subsurface exploration program, is supported on enlarged base concrete caissons. Although the drawings did not indicate the bearing level of stratum of the caissons, based on the bearing capacity of 4 tons per square foot indicated on the drawings, it was assumed that the caissons bear within the Marine Sand layer. From the original construction drawings, it was shown that the two rows of concrete caissons closest to the property line were located approximately 4 and 16 ft from the property line.

The narrow public alley to the south was approximately 16 ft wide and was used to facilitate construction access to keep construction vehicles off the major roadway to the north. The alley was depressed about 8 ft from the major roadway to the north which posed logistical construction challenges. Refer to Fig. 2 for site plan with locations of adjacencies.

 © Deep Foundations Institute 2025

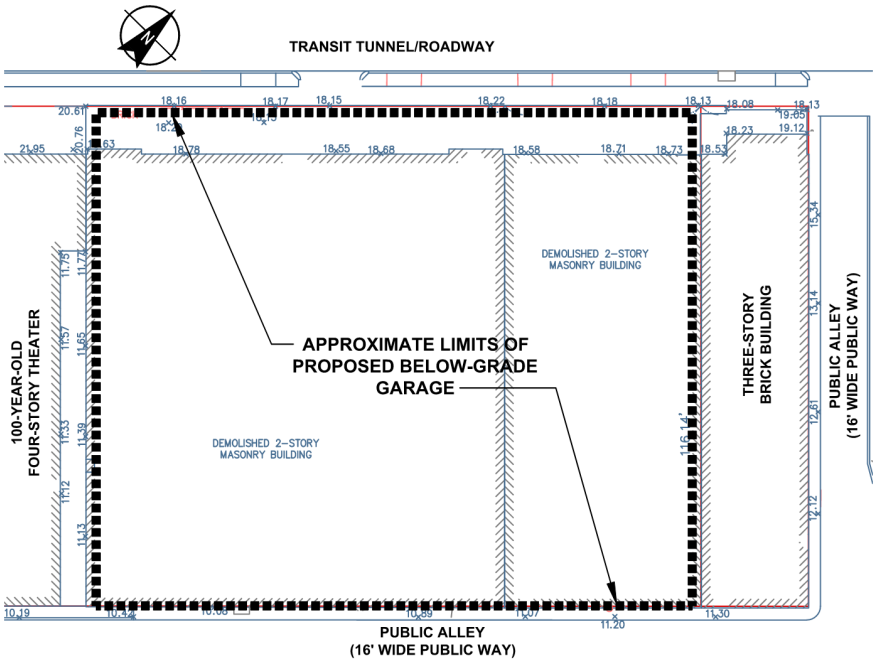


Fig. 2. Site plan

Figure 3 provides a generalized site soil profile for the site. The subsurface conditions consisted of typical urban fill, a granular material containing varying amounts of asphalt, bricks, concrete, and metal. Below the fill is an organic soil deposit up to about 12 ft thick. A marine sand up to 20 ft thick is present below the organic soil followed by a marine clay known locally as the Boston Blue Clay; stiff clay deposits, typically referred to as the clay crust, were encountered in the top 5 to 15 ft of the strata. This clay layer ranges in thickness across the site between approximately 50 and 100 ft. A thin glacial deposit follows the marine clay over bedrock consisting of Cambridge argillite, a sedimentary rock.

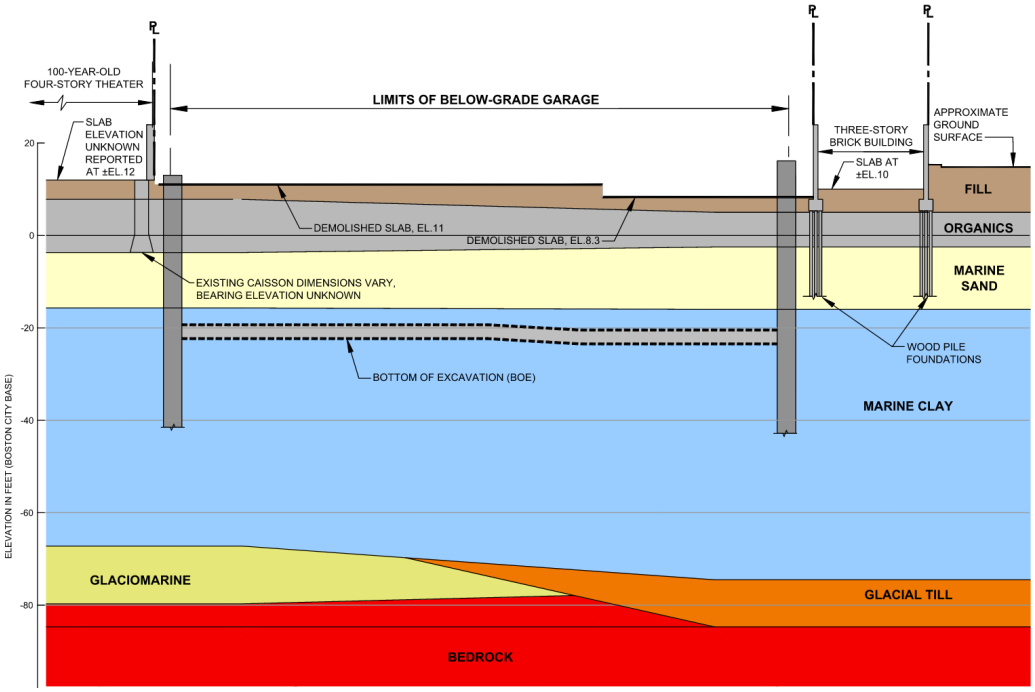


Fig. 3. Generalized site soil profile

 © Deep Foundations Institute 2025

Data obtained from groundwater observation wells at and nearby the site indicated the water table ranged from 2 to 10 ft below ground surface, depending on the ground surface elevation.

SUPPORT OF EXCAVATION SYSTEM

With the significant change in grades across the site and to enable excavation to the top of the slurry wall, an enabling SOE system was necessary prior to the installation of the slurry wall. The enabling SOE system along the north, west, and south sides of the site consisted of drilled micropiles with timber lagging. The portions along the west and south side of the site were cantilevered, while along the north side of the site, where the cut heights were up to 15 ft and allowable movements were limited due the adjacent transit line, rakers extended to temporary reaction micropiles were required. Along the east side of the site, where the site abutted the three-story brick building with one partial level of below grade space, a MSE wall with wrapped face was utilized. The MSE wall reduced the lateral load applied to the rubble foundation wall of the adjacent building and also doubled as the hydromill working platform. The MSE wall was constructed inboard of the slurry wall location and the area between the MSE wall and three-story brick building was filled with controlled low strength concrete in small lifts, to again reduce the pressure on the adjacent building foundation wall.

A diaphragm “slurry” wall system, varying from 3-ft to 4-ft thick, was chosen as the primary SOE system due to the site’s complex geotechnical and structural constraints, settlement sensitive abutters, as well as the need to maximize the buildable area within a dense urban environment. The below grade excavation extended to depths of up to 43 ft, with the basement footprint extending to the property line on all four sides. This condition, coupled with the presence of sensitive adjacent structures, necessitated an excavation support method capable of minimizing ground movement and controlling groundwater effectively. The stiffness and low permeability of the slurry wall made it particularly well-suited to maintain excavation stability while limiting adjacent infrastructure movement. Additionally, the slurry wall was designed to serve as the permanent structural basement walls for the building. This dual functionality eliminated the need for a separate cast-in-place wall system, conserving space, reducing construction time, and improving overall efficiency. Select slurry wall panels also incorporated load-bearing elements (LBE), constructed deeper than the surrounding panels, to transfer vertical building loads directly into the underlying competent glacial soils and bedrock. The integration of LBEs within the slurry wall system allowed the wall to function not only as excavation support and groundwater cutoff, but also as the building’s foundation system. The ability to construct the slurry wall directly along the property line further enabled full utilization of the site footprint, which was essential for meeting the project’s programmatic demands.

Due to the variability in ground surface elevation, top of slurry wall elevation, and the spiraling nature of the parking garage ramp slabs, a complex system of internal bracing was required. The bracing system included two levels of bracing which generally consisted of 36-in. diameter pipe struts and wide flange walers. Many braces sloped to avoid conflicts with the permanent ramp slabs constructed prior to bracing removal. To understand the potential slurry wall movement given the varying geometry, several distinct finite element sections were evaluated. Each section was analyzed independently to capture the unique geometry within the excavation and of the adjacent structures, ensuring accurate representation of the behavior throughout the excavation and construction process. As the building footprint extended to the property line, and there was insufficient space outside the property limits to facilitate mass excavation of the below grade space, an H-pile–supported equipment platform was designed and constructed. Refer to Fig. 4 for SOE plan which includes the extents of enabling SOE, slurry wall alignment, LBE panels, equipment platform location, and the first level of bracing configuration. Slurry wall panels extended approximately 20 feet below the bottom of excavation, with tip elevations ranging from El. -37 to El. -45. LBE panels extended 3 to 13 feet into the top of sound bedrock, with tip elevations ranging from El. -95 to El. -139.

 © Deep Foundations Institute 2025

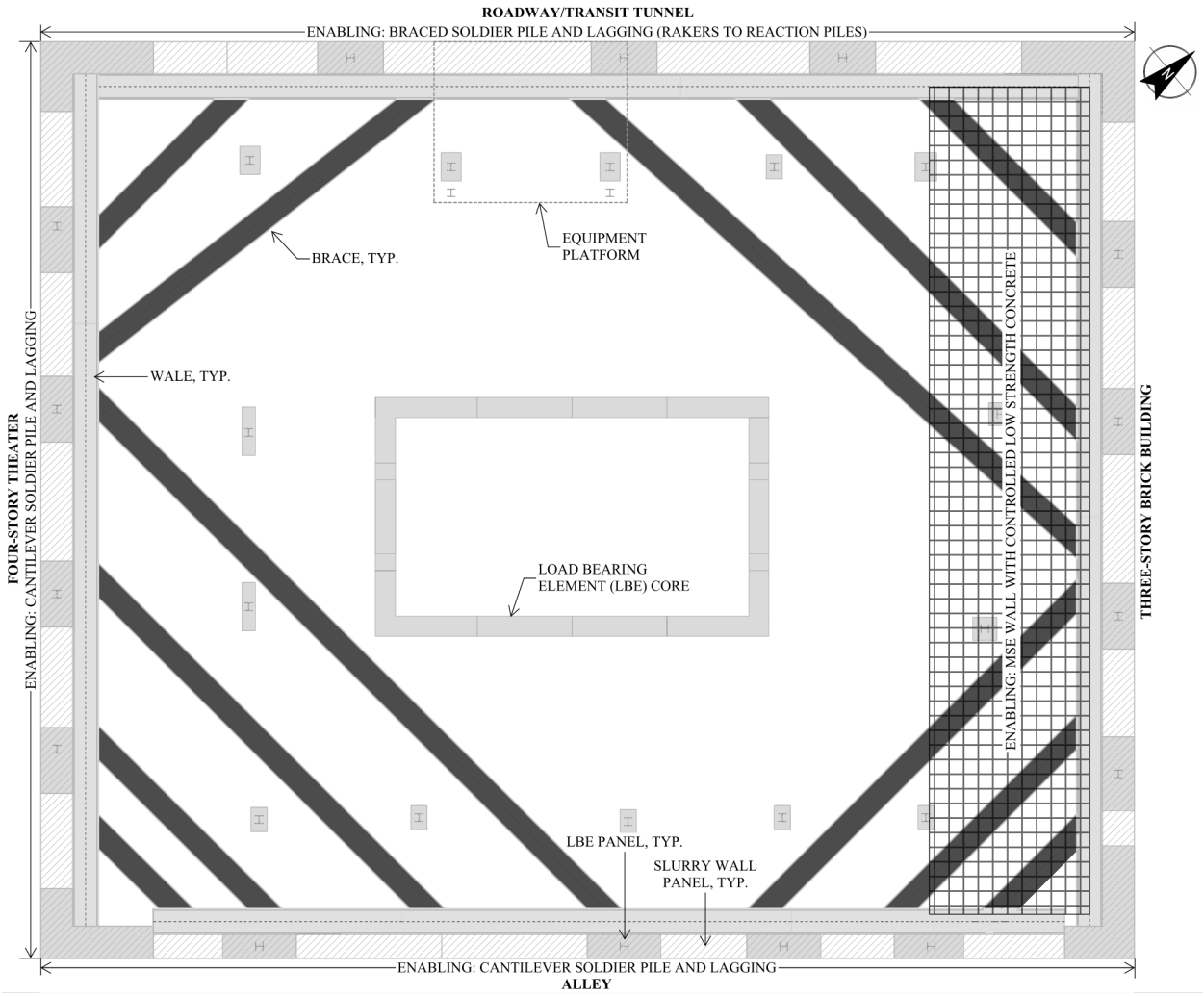


Fig. 4. SOE plan

ENGINEERING ANALYSIS AND MODELING

PLAXIS 2D was selected for modeling due to its robust capabilities in modeling complex soil-structure interaction, ability to model staged construction, and provide estimated movements of adjacent structures throughout each construction stage. The software predicted horizontal and vertical displacements of adjacent structures at each construction stage, providing confidence that movements would remain within allowable limits during construction. The SOE system designed for this site required detailed consideration of varying conditions of ground surface elevation, bottom of excavation, bottom of slurry wall/LBE panels, thickness of slurry wall/LBE panels, internal bracing elevations, permanent ramp slab elevations, and surcharges from construction and adjacent structures.

The PLAXIS 2D analysis used the Hardening Soil (HS) or Hardening Soil with Small Strain (HSS) constitutive soil models for Marine Sand, Marine Clay, and Glacial Soils; HS and HSS are elasto-plastic models formulated to account for stress dependent stiffness and change in stress with unloading and reloading. Fill and Organics used the Mohr-Coulomb constitutive model, where a simpler representation of soil behavior was sufficient. Design soil parameters were developed based on prior project experience in the Boston area, site-specific subsurface investigation and laboratory testing, and empirical correlations.

The Marine Clay stratum was subdivided into Marine Clay Upper, Marine Clay Middle, and Marine Clay Lower based on variations in blow counts from the boring logs and supporting laboratory test data.

It should be noted that actual movements will vary from the model due to variability with in-situ soil stratigraphy, soil parameters, as-built conditions, contractor construction techniques, soil model limitations, and simplified loading and structure assumptions. In addition, PLAXIS 2D assumes two-dimensional, plane strain behavior, which does not consider the benefits of the three-dimensional effects of the site (such as soil arching and corner stiffening). The model did not include the various enabling systems, slurry wall installation, permanent slab shrinkage, or contractor means and methods when evaluating the potential movement of adjacent structures. Designs should recognize and educate stakeholders that the results of the PLAXIS 2D analysis are inherently dependent on the assumptions, input parameters, and modeling decisions made by the designer, and therefore are just "best-estimate" predictions.

A total of twenty (20) representative sections were modeled and analyzed using PLAXIS 2D to account for the varying conditions around the site, as previously described. Figure 5 shows an example PLAXIS 2D section through the north side of the project site. For each section, results were extracted at critical stages of construction to inform both temporary and permanent structural design. The following key results were obtained:

- Brace loads were used to determine the sizes and required capacities of the temporary bracing system;
- Temporary loads on the permanent ramp slabs were provided to the structural engineer to check if the slabs could resist the forces;
- Shear forces, bending moments, and lateral displacement of the slurry wall were used to design slurry wall reinforcement and confirm wall deflections remained within allowable limits;
- Vertical and lateral displacement of adjacent structures were evaluated to verify the movement remained within the limits set for the project.

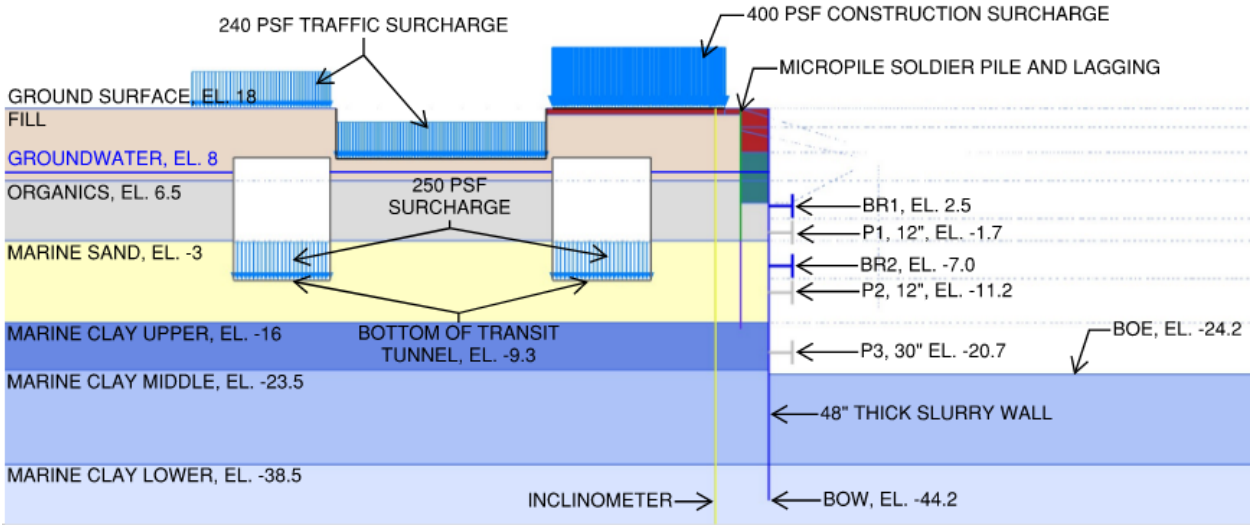


Fig. 5. Example PLAXIS 2D section

MONITORING AND PERFORMANCE ASSESSMENT

Given the sensitivity of the adjacent structures, an extensive instrumentation and monitoring program was implemented to track movements and vibrations throughout construction. The monitoring system consisted of the following:

- Transit tunnel: One vibration monitoring unit, 14 optical monitoring points, nine tilt meters, two crack gauges, and two inclinometers installed in the soil between the property line and the tunnel.
- 100-year-old four-story theater: One vibration monitoring unit, 19 optical monitoring points (8 on lower portion of the face of the theater and 11 on the roof), and four tilt meters.
- Three-story brick building: One vibration monitoring unit, 14 optical monitoring points (6 on lower portion of the face of the building and 8 on the roof), and two tilt meters.
- Slurry wall: Five inclinometers.

Instrumentation monitoring commenced prior to the start of construction activities to establish an accurate baseline. As previously described, prior to mass excavation, enabling work was performed. These activities included the installation of the enabling SOE system, pre-excavation and installation of the guide wall to facilitate slurry wall installation, installation of the slurry wall, and construction of the cap beam (a below grade structural wall that ties the slurry wall panel elements together). During these activities prior to mass excavation, the three-story brick building to the east and the 100-year-old four-story theater to the west settled an average of approximately ¼ in. to ½ in., with a few points indicating larger movement. These movements occurred prior to the commencement of mass excavation and were not accounted for in the PLAXIS model. Instrumentation measured maximum movements of adjacent structures prior to mass excavation are provided in Table 1.

Table 1. Instrumentation measured maximum movements of adjacent structures prior to mass excavation

	Conclusion of Enabling and Pre-Excavation for Slurry Wall Installation		Conclusion of Slurry Wall Installation		Conclusion of Cap Beam Construction	
Structure	Max. Vert.	Max. Horiz.	Max. Vert.	Max. Horiz.	Max. Vert.	Max. Horiz.
	(in.)	(in.)	(in.)	(in.)	(in.)	(in.)
Transit Tunnel	0.1	0.1	0.1	0.2	0.2	0.3
Theater	0.2	0.2	0.4	0.5	0.5	0.5
Brick Building	0.3	0.5	0.6	1.3	0.7	1.4

Given the movement of the buildings prior to any mass excavation, the project stakeholders convened to assess potential mitigation strategies. Several additional measures were taken to reduce the potential movement during mass excavation and limit impact to adjacent structures. The first method was to increase the slurry wall brace preloads from 30 percent to 50 percent. Preloading the braces with a higher force slightly pushes the slurry wall back into the soil and reduces the elastic shortening of the braces as the excavation proceeds, reducing the overall deflection of the system. An observational approach was undertaken next, comparing the actual movements at each stage of excavation to the predicted to understand the performance before other measures would be taken. However, the project team developed a movement mitigation plan if further measures be necessary. Other measures that were included in the movement mitigation plan consisted of additional bracing levels, subgrade struts, accelerated construction schedule, and sequenced slab construction. These other mitigating measures were designed and planned in case they needed to be implemented quickly but were not implemented at this phase of the project.

 © Deep Foundations Institute 2025

As mass excavation progressed, minimal additional movements of the adjacent structures were observed and the slurry wall performed better than expected (PLAXIS 2D predicted movements were less than inclinometer measured movements). However, the critical stage of the excavation was the final cut to subgrade which included removal of some of the stiffer portion of the upper marine clay crust. In addition, the project team was concerned about the potential for creep of the toe of the slurry wall which was situated in the softer clay. Utility and other below slab work required approximately two months between when the time at which the final subgrade was reached and when the lowest level floor slab would be placed raising the concern for time related movement that was not captured in the PLAXIS 2D analysis.

To mitigate potential slurry wall creep and the resulting movement of the adjacent structures, the project team decided to implement parts of the movement mitigation plan including a modified excavation sequence, smaller sections of floor slab placement, and a subgrade strut system. Subgrade struts are structural elements, installed below the bottom of the excavation, to provide additional lateral stability by engaging friction or bracing against other structural components. For this project, the subgrade struts were constructed with an excavator, excavating a 2-foot-wide by 3-foot-deep slot below the final excavation and filling with 1,500 psi unreinforced concrete. These struts extended from the slurry wall to the project's load-bearing element (LBE) core. The subgrade struts were installed from approximately 5 feet above the final excavation depth, with their tops positioned 2 feet below the bottom of the excavation elevation.

Comparisons between PLAXIS 2D predicted slurry wall deflections and actual performance as measured by inclinometers highlighted the efficacy of the implemented mitigative measures as well as the need to account for movement not included in the PLAXIS 2D analysis. Instrumentation measured and PLAXIS 2D analysis predicted slurry wall deflections at the end of below-grade construction are provided in Table 2. The PLAXIS 2D predicted values provided in Table 2 do not include the implemented mitigation strategies.

Table 2. Inclinometer measured and PLAXIS 2D predicted slurry wall deflections at end of below-grade construction

	Slurry Wall Deflection (in.)			
	Alley	Theater	Transit Tunnel	Brick Building
Inclinometer Measured	0.9	0.5	0.9	0.8
PLAXIS 2D Predicted	1.4	1.2	0.9	1.2

Comparisons between PLAXIS 2D predicted movements of adjacent structures and actual performance data obtained from instrumentation highlight the extent of movement that occurred both prior to and during mass excavation, as well as the effectiveness of the mitigation strategies implemented. Table 3 summarizes the predicted and measured movements of the adjacent structures at the completion of below-grade construction, along with the changes in measured movements specifically attributed to mass excavation. Notably, the data in Table 3 shows minimal additional movement of the adjacent structures during mass excavation, suggesting that the implemented mitigative measures (increasing brace preloads modified excavation sequence, smaller sections of floor slab placement, subgrade strut system), were effective in controlling deformation and maintaining structural stability.

Table 3. Instrumentation measured and PLAXIS 2D predicted adjacent structure movements at end of below-grade construction

	Instrumentation Measured				PLAXIS 2D Predicted	
	Conclusion of Below Grade Construction		Change Due to Mass Excavation		Conclusion of Below Grade Construction	
Structure	Max. Vert.	Max. Horiz.	Max. Vert.	Max. Horiz.	Vert.	Horiz.
	(in.)	(in.)	(in.)	(in.)	(in.)	(in.)
Transit Tunnel	0.2	0.3	0.0	0.0	0.5	0.5
Theater	0.7	0.5	0.2	0.0	1.0	0.7
Brick Building	0.8	1.7	0.1	0.3	0.9	0.6

SUMMARY AND CONCLUSIONS

The successful construction of this high-rise residential tower within a tightly constrained urban setting presented significant geotechnical challenges due to the proximity of sensitive structures and infrastructure. A project-specific support of excavation (SOE) system, paired with a comprehensive monitoring program, was essential to navigating these challenges. Early instrumentation data revealed that adjacent structures were experiencing greater-than-anticipated movement during enabling works, prior to mass excavation. In response, the project team implemented targeted mitigation measures, including increased bracing preloads, the addition of subgrade struts, and a strategically adjusted construction sequence. This adaptive and data-driven approach effectively reduced lateral displacements and settlement, safeguarding nearby assets throughout mass excavation.

A key lesson from this project is the importance of anticipating and accounting for movements that may not be fully captured in early-stage analytical models, particularly those associated with enabling works, slurry wall installation, or contractor-specific means and methods. These “unmodeled” movements can have significant implications and should be factored into the SOE design and establishment of threshold and limiting values for movement.

The project also reinforces the importance of a flexible, feedback-informed approach to geotechnical design and construction. Early coordination, real-time monitoring, and iterative model refinement based on observed performance were instrumental in managing risk and responding to evolving site conditions. Ultimately, the experience demonstrates how adaptive design, reliable instrumentation, and responsive decision-making are critical to the successful delivery of complex urban geotechnical projects.

DESIGN, CONSTRUCTION, AND PERFORMANCE OF A SENSITIVE BRACED EXCAVATION IN BOSTON BLUE CLAY

Dylan W. Locke, McPhail Associates LLC, Burlington, MA, USA, 617-868-1420, DLocke@mcphailgeo.com

Collin E. Sweeney, GeoEngineers USA, P.C., Southborough, MA, USA, 317-437-0652, csweeney@geoengineers.com

Jeffrey M. Taylor, TREVIICOS, Charlestown, MA, USA, 617-839-2711 JTaylor@treviicos.com

ABSTRACT

This Boston project involved constructing a 14-story mat-supported building with three below-grade parking levels. The site adjoins a 17-story building founded on micropiles, a 3-story building supported by a structural mat, an 8-story historic brick building, and above-grade portions of the Massachusetts Bay Transit Authority (MBTA) Green Line. Excavations of up to 44 feet (13.4 m) extending into a sensitive clay deposit were required to construct the below-grade levels. To address the proximity of adjacent foundations and sensitivity of the underlying clay, a robust SOE system was required to construct the below-grade levels and mat foundation. A slurry wall system was used to cut off groundwater, provide stiff lateral support, and serve as the building's perimeter foundation. The walls were supported by three levels of internal bracing. Since the excavation terminated below the stiff crust of the Boston Blue Clay, an innovative "subgrade strut" approach was employed to minimize movement of adjacent structures. During and after construction, extensive geotechnical instrumentation was performed to monitor the movement of the slurry wall, adjacent buildings, and MBTA track settlement. Based on data collected during and following construction, the excavation system support met project requirements under complex conditions.

Keywords: braced excavation, slurry wall, subgrade struts, instrumentation, urban construction

INTRODUCTION

An internally braced excavation system was effectively used for this project in the Fenway neighborhood of Boston, Massachusetts, in a constrained urban environment to facilitate below-grade construction, construct building foundations, and protect adjacent structures against movement during construction. The project consisted of the construction of a 14-story tower with three levels of below-grade parking occupying a footprint of 65,000 square feet (6,040 square meters). A rendering of the building is shown in Fig. 1. Below-grade construction was split into two phases to allow for the continuous use of existing loading docks on the property. Phase 1 of the project involved the construction of about 85% of the garage footprint, followed by the construction of the remaining 15% of the building during Phase 2. The overall durations of the below-grade construction of Phase 1 and Phase 2 were about 12 months and 6 months, respectively.
Portions along the southeast side of the project directly abutted existing buildings. In addition, MBTA Green Line light rail tracks run parallel to the project's northwestern boundary, around 50 feet (15.2 m) from the edge of the building. As such, a major consideration for the project was minimizing lateral displacement of the SOE system to reduce vertical and horizontal movement of the adjacent buildings and infrastructure. The selected SOE system consisted of a perimeter slurry wall with three levels of internal bracing. Sheet piles were utilized at the interface separating the Phase 1 and Phase 2 portions of the excavation. The innovative use of unreinforced concrete subgrade struts was used to provide additional stiffness to the SOE system.

 © Deep Foundations Institute 2025



Fig. 1. Rendering of Proposed Building.

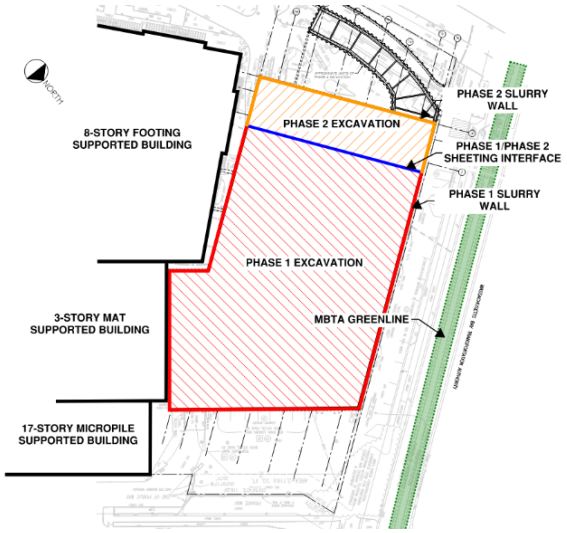


Fig 2. Site Location and Adjacent Structures.

PROJECT SETTING

The project site, shown in Fig. 2, is generally bounded by high-traffic roadways to the southwest and northeast, above-grade portions of the MBTA Green Line to the northwest, and existing buildings to the southeast. The overall subject site occupies a plan area of approximately 383,000 square feet (35,600 square meters) and is occupied by existing buildings, which were originally constructed in 1928 (8-story building) and 1965 (3-story building). The original buildings were renovated in the late 1990s and again in 2018 for use as office/retail and parking garage space. The 3-story building was subsequently expanded starting in 2019 with the construction of the 17-story building. Adjacent foundation structures to the site consisted of the following:

- 8-story concrete-framed building (1928):
  - Founded on spread footings bearing on marine sand at a depth of approximately 16 feet (4.9 m).
  - Single below-grade level.
- 3-story concrete-framed building (1965):
  - Founded on a structural mat bearing on marine sand at a depth of approximately 14 feet (4.3 m).
  - Single below-grade level.
- 17-story steel-framed building (2019):
  - Founded on micropiles bearing in bedrock extending to depths of approximately 240 to 250 feet (73.2 to 76.2 m).
  - No below-grade levels.
- MBTA Green Line Light Rail
  - Founded on a mat foundation bearing on marine clay and marine sand at depths of approximately 6.5 to 20 feet (2 to 6.1 m).
  - Drops below-grade as the tracks move from southeast to northwest.

 © Deep Foundations Institute 2025

SUBSURFACE CONDITIONS

Subsurface soil and bedrock conditions at the site generally consisted of a surficial urban fill layer that was underlain by subsequent organic deposits, marine sand and clay deposits, glacial deposits, and bedrock. The approximate thickness of each of the soil strata is summarized in Table 1 below. Bedrock at the site consisted of a moderate to severely weathered shale-like bedrock deposit locally referred to as Cambridge Argillite. Groundwater was observed within installed observation wells at levels varying from about 8 to 11 feet (2.4 to 3.4 m) below ground surface, with an average measured site groundwater level at an approximate depth of 10 feet (3 m).

Table 1. Generalized Subsurface Conditions

Generalized Subsurface Strata	Approximate Thickness (Feet)
Fill	4 to 21 (1.2 to 6.4 m)
Organics	1 to 18 (0.3 to 5.5 m)
Marine Sand	4 to 16.5 (1.2 to 5 m)
Marine Clay	135 to 173 (41.1 to 52.7 m)
Glacial Deposits / Weathered Bedrock	10 to 18 (3 to 5.5 m)
Bedrock	N/A

Laboratory tests were performed on undisturbed (Shelby tube) samples of the marine clay collected during the boring program to determine the compressibility parameters for use in settlement analyses and to determine design parameters for the SOE system. The laboratory testing performed on the marine clay deposit consisted of Constant Rate of Strain (CRS) consolidation tests. A total of nine cone penetration tests (CPTs) were performed at the site to determine undrained shear strength parameters of the marine clay deposit. The marine clay deposit has a stiff overconsolidated upper crust, generally considered to be the result of desiccation during a period of significantly lower ocean levels in the geologic past. The middle portion of the marine clay deposit consists of a very soft to soft, normally consolidated, silty clay. Within the lower portion of the marine clay deposit, the sand content and stiffness of the marine clay deposit was observed to increase with depth. This marine clay deposit was consistent with Boston Blue Clay, and is henceforth referred to as such.

SITE CONSIDERATIONS

The urban project setting created several site constraints to be considered in the design and construction of the basement excavation. The most critical of these constraints was the close proximity of existing abutting structures, some of which were particularly sensitive, as previously described. Due to the sensitivity of these existing structures to settlement, a stiff SOE system was required. When considered alongside other benefits such as groundwater cutoff, a braced slurry wall system was selected as the most appropriate for SOE.

The existing foundation system for the historic brick building consisted of 12-foot (3.7 m) square-spread footings located approximately 20 feet (6 m) on center, with the nearest edge of footing located approximately 5 feet (1.5 m) away from the proposed slurry wall at its nearest approach. The footings each had a design bearing pressure of 4,200 pounds per square foot (201 KPa). Limiting foundation settlement was particularly important for this structure to limit repairs to the building's sensitive masonry walls.

The MBTA Green Line foundation structure, located along the full length of the northwest project boundary, is a 25 foot (7.6 m) wide concrete structure, with a nearest approach to the slurry wall of approximately 50 feet (15.2 m). The structure consists of a 4 foot thick (1.2 m) concrete slab and two cantilevered retaining

 © Deep Foundations Institute 2025

walls to form a U-shaped lidless tunnel ("boat" structure) as the Green Line track level gradually drops underground to the east. Limiting settlement of the boat structure was important to preserve track serviceability during construction.

SUPPORT OF EXCAVATION DESIGN

The permanent building design called for a basement with three levels of parking, comprised of a foundation mat slab, variably 2-to-5-feet (0.6 to 1.5 m) thick, and two intermediate 1-foot (0.3 m) thick slabs above. To construct the basement, the design employed the "bottom up" method of excavation. The general construction sequence consisted of excavation to a maximum of 2 feet (0.6 m) below each bracing level followed by the installation of internal steel bracing. Once the bottom of the excavation was reached, bracing was removed from the bottom-up following installation of the corresponding slabs at each level.

A 2-dimensional lateral earth analysis was created using the DeepEX software to model the subsurface conditions and determine the temporary loads on the slurry wall at all stages of construction. For each stage of construction, earth pressures and resulting wall moments, shears, and bracing reactions were determined using limit equilibrium methods. Rankine active and passive lateral earth pressure were used for construction stages with one or zero levels of bracing. For stages with two or more levels of bracing, two-step rectangular apparent earth pressure diagrams were used, in accordance with standard practice in Massachusetts; 24*H was used above the design water table and 12*H was used below the water table, where H is the wall cut height. For structural design of the slurry wall and sizing of internal bracing members, the maximum moments, shears, and reactions for all stages were used.

In order to accurately estimate wall deflections and corresponding ground settlements, finite element method (FEM) models, created within DeepEX, were used. Design parameters were determined based on the results of standard penetration testing (SPT) and the undrained shear strength determined by laboratory and field testing. FEM models require determination of elastic modulus for each soil layer. Elastic modulus values were chosen to be approximately 600 times the undrained strength value for cohesive soil layers, and were based on correlations to SPT blow count for cohesionless soil layers. All elastic modulus values were then slightly adjusted based on SPT blow counts and prior experience in the Boston Blue Clay.

SOE design for Phase 1 was split into three parts to expedite the project timeline by allowing design and construction to proceed in parallel. First, the Contract design called for an intermediate sheet pile wall to separate Phase 1 and Phase 2 of the excavation. The sheet pile wall was designed first, independently of the slurry wall SOE. Both limit equilibrium and FEM analyses were performed on this wall to model its performance, maximum loads, and estimated deflection. This first wall design package included design soil parameters that were negotiated with the Geotechnical Engineer, allowing the design team to manage design conservatism and confirm which soil parameters would be used on the remaining wall designs on the project.

For the second part of Phase 1 SOE design, the perimeter slurry wall, four lateral earth analysis design sections were used to model different adjacent surcharge loads. Each model considered two walls to represent the actual width of the excavation and appropriately model any resultant effects on passive earth pressure. The first design section considered only a 600-psf by 20-ft (28.7 KPa by 6 m) construction equipment surcharge for slurry wall panels where no adjacent buildings were located; primarily the west side of the excavation. The second design section considered footing loads to model the adjacent historic building to the east, and the existing boat structure to the west. No footing load was considered for the boat structure due to the distance from the excavation; however, it was included in the model so that settlement estimates could be calculated beneath it. The third design section considered a distributed load to model the adjacent garage building to the southeast. The final design section was a copy of the second, modeling the historic brick building, with a slightly deeper excavation to model a proposed elevator pit in the southeast

portion of the excavation. FEM analyses were performed on each design section to provide accurate estimations of wall deflections and settlements of adjacent structures. Slurry wall reinforcement was designed to resist the maximum wall moment and shear from all construction stages per the lateral earth analyses. Slurry wall panels were limited to a width of 10 feet (3 m) immediately adjacent to the existing building to limit potential footing settlements.

Once the lateral earth analyses were finalized, temporary internal bracing was sized and specified based on the maximum line loads determined by lateral earth analysis. Both external and internal wales were used to provide continuous support of the wall and funnel load into struts. External bracing wales consisted of steel wide flange members erected web-horizontal against the slurry wall. Bracing struts were welded to wales to form a rigid frame system. Along the long, straight, north and west sections of the slurry wall, internal wales consisting of additional horizontal rebar were used to transfer load. Internal wales are a design choice that saves on the cost of procuring and erecting external steel wales by including the required steel for bending and shear in the slurry wall reinforcement cage. Struts consisted of large diameter (generally 3-foot) steel pipe struts; where strut lengths exceeded lateral buckling limits, pairs of pin piles were driven and support structures erected to provide a pinned support and limit pipe size. Struts were located at wall panel joints to provide continuity between panels that utilize internal wales.

SUBGRADE STRUTS

As previously established, limiting settlements of adjacent structures, and therefore SOE wall deflections, was a primary objective of the excavation. The proposed excavation terminated in the soft to very soft portions of the Boston Blue clay, meaning that the largest wall deflections would occur at the wall toe, causing the toe to “kick in” and exceed the allowable deflection criteria. During preliminary design of the SOE system, the Owner expressed concern over wall movements due to the presence of this soft clay at the wall toe. To address this concern, a “subgrade strut” approach was developed by the project team to limit deflections. This approach entailed installation of short slurry wall panels, end to end, in line across the excavation to form compressive struts below the bottom of excavation, in the softest portion of the clay profile.

To provide the best value, subgrade struts were proposed for use only at wall sections adjacent to the historic brick building where initial deflection estimates were the greatest. The struts would span from the east wall to the west wall (i.e. the short dimension of the excavation), directly beneath three parallel cross-lot pipe struts. Subgrade struts in these locations would provide additional wall support beneath the bottom of excavation and limit deflections next to the sensitive building. Preliminary design of the SOE system with subgrade struts was performed using DeepEX lateral earth analysis. A model was developed with a distinct subgrade strut concrete material of increased elastic modulus; this modulus value and the model geometry were adjusted to analyze the effect of variable strut spacings, concrete strengths, and strut panel depths. Options were presented to the Owner and a scope of three subgrade struts spanning the short dimension of the excavation was approved for implementation. The addition of subgrade struts was predicted to lower settlement beneath the adjacent building from 1.3 inches (33 mm) to 0.9 inches (23 mm).

Once subgrade struts were approved for use, the design was finalized and optimized. Along the east wall, subgrade wale panels were installed parallel and directly adjacent to the existing east slurry wall to transfer load evenly from the existing slurry wall to the subgrade struts. These subgrade wales consisted of short slurry wall panels extending along a 57-foot (17.4 m) total tributary length of the south wall. Subgrade panels of varying depth were used to minimize the construction effort while still providing adequate support. For example, a 70-foot (21.3 m) long portion in the center of each strut was shortened to only 10 feet (3 m) deep, from the initial 15-foot (4.6 m) panel depth. Additional optimization was found in the existing steel bracing design. Installation of subgrade struts allowed the third level of cross-lot pipe struts to be omitted, granting further cost and schedule savings. Subgrade struts were studied again for the Phase

 © Deep Foundations Institute 2025

2 excavation. However, they were not deemed cost-effective for the movement reductions that they would provide. Also, due to the narrow excavation geometry of Phase 2, the movement reductions were minimal and would pose additional construction challenges.

For Phase 2 of the excavation, the primary challenge was bracing geometry. Due to the long and narrow shape of the excavation, and that there was no north wall to brace against, the bracing layout would be inefficient due to acute angles. After discussions with the Contractor and Owner, it was decided that bracing members could extend into the previously constructed Phase 1 excavation, in between permanent slabs, to make the bracing more efficient and distribute load more evenly. This posed a construction challenge for the Contractor, but the bracing was installed successfully in between the permanent slabs, connecting to existing Phase 1 panel joints.

SUBGRADE STRUT CONSTRUCTION

As determined during the Support of Excavation Design phase, subgrade struts were added to the system to limit wall deflections in the soft clay at the toe of the wall and limit settlements of adjacent structures. Following completion of the 36-inch (0.91 m) thick perimeter slurry wall of Phase 1, three 30-inch (0.76 m) thick subgrade struts were installed using same slurry wall method in primary and secondary sequencing of panels between the east wall (historic brick building side) to the west wall (MBTA boat structure side) with maximum depth of about 55 feet (16.8 m) below grade. The subgrade strut typical panel length was set at 23 feet (7.0 m). However, during construction, panel lengths were increased to 35 feet (10.7 m) to reduce installation time without any issues with panel stability or effect on quality. Concrete for each subgrade strut panel was placed via the tremie method from the bottom of panel to just below the bottom of excavation, which was about 40 feet (12.2 m) below grade. Following concrete placement, cement grout was added to the bentonite slurry that remained in the panel and mixed in place to create a “C/B” material that once set, provided sufficient panel support up to existing grade and was easily excavatable during the mass excavation work phase.

ENDSTOP CONNECTION BETWEEN PHASE 1/PHASE 2 SLURRY WALL

To maintain access to the existing loading docks during construction, the slurry wall foundation and building construction was completed in two phases. A requirement for the Phase 1 slurry wall was to provide a positive connection for the future Phase 2 slurry wall at the south end of the project. To accomplish this, a W-section end stop beam was installed at the south edge of Panels 1 and 44, which were the southernmost panels at the interface with Phase 2 as shown in Fig 3. The end stop beams included a sheet metal blockout to prevent concrete from filling the end stop “key” on the Phase 2 side. In addition, shear studs were provided on the concrete side of the end stop beam that secured it to the concrete within the Phase 1 panels. During Phase 2 slurry wall construction, the sheet metal blockout was removed by clamshell prior to concrete placement for the secondary (tie-in) panels. A watertight connection between phases was confirmed during mass excavation work.

 © Deep Foundations Institute 2025

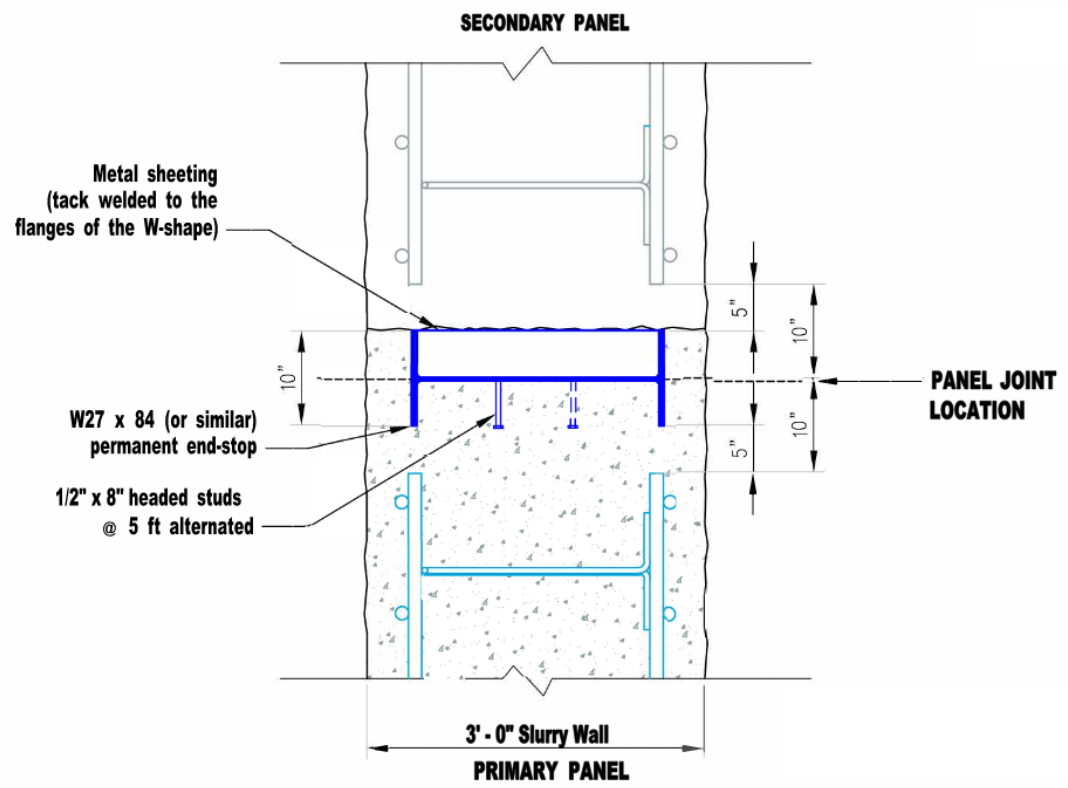


Fig. 3. End Stop Detail

INTERMEDIATE STEEL SHEET PILE WALL

In addition to an end stop connection between Phase 1/Phase 2 slurry walls, an intermediate steel sheet pile wall was installed along the southwest side of the excavation during Phase 1, between the east wall (historic brick building side) and west wall (MBTA boat structure side) as shown in Fig 2. The steel sheet pile elements were the NZ19 section and varied in length from 55 feet (16.8 m) to 60 feet (18.3 m), with 60 feet (18.3 m) lengths being used along a short stretch where a deeper elevator pit excavation had to be performed. Steel sheet pile elements were driven with a crane suspended vibratory hammer along a temporary false work beam to ensure alignment. To provide a seal at the interface of the sheet pile wall and slurry wall to control water and/or soil material ingress, a single cement/bentonite panel element was installed at each location to about 5 ft (1.5 m) into the underlying clay layer prior to steel sheet pile installation. During the mass excavation and bracing work under Phase 1, internal bracing members including W-section waler and corner braces (pipe and W-sections) were fitted between the steel sheet pile wall and slurry wall and successfully preloaded.

BRACING PRELOADING

With the temporary internal bracing transferring loads between corners and opposing slurry walls of the SOE system, a majority of the members required preloading to ensure rigid contact between members and limit wall movements during excavation. Preloading is the process of compressing or jacking the bracing members with tandem hydraulic jacks placed between jacking ears on the bracing members and waler/jacking end as shown in Fig. 4. During preloading, the tandem jacks are pressurized incrementally to apply the specified loading, which tops out at 50% of the design load for this project. Once preloading is complete, the separation between bracing members at the jacking end is shimmed and welded to provide

 © Deep Foundations Institute 2025

rigid contact between members. Once bracing preloading is “locked off” for a level or area, excavation work may commence down to the next level as required.



Fig. 4. Bracing Preloading

INSTRUMENTATION AND PERFORMANCE

The performance of the slurry wall, adjacent facades, building columns, and MBTA tracks was regularly monitored through a series of inclinometers, manual survey points, and automated motorized total station (AMTS) systems. These systems provided a means to assess the performance of these systems and structures during and following the construction of the building.

Lateral Movement of Slurry Wall

A total of ten inclinometers were installed within the Phase 1 slurry wall, and four inclinometers were installed within the Phase 2 slurry wall. Inclinometers were installed to a minimum depth of 2*H below the existing ground surface, where H is the height of the excavation. The inclinometers were terminated within the marine clay deposit, so regular rounds of surveys were performed at the tops of the inclinometers to confirm fixity at the bottom of the inclinometers. A plan indicating the location of inclinometer locations in relation to the subgrade struts is shown in Fig. 5.

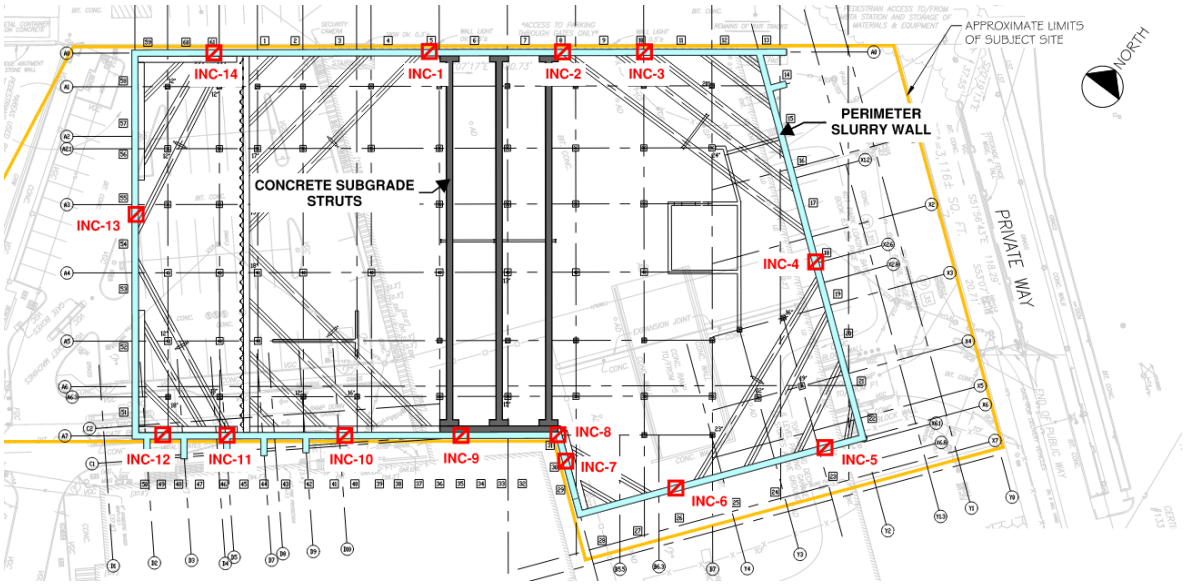


Fig. 5. Inclinometer Location Plan

Maximum lateral displacements of the slurry wall at the end of Phase 1 construction were generally below established project thresholds. Maximum total displacements were observed at inclinometers INC-4, INC-10, and INC-13 where longer spans of the slurry wall were present and not supported by subgrade struts. Maximum lateral displacements at each inclinometer location are shown in Table 2.

Table 2. Summary of Maximum Inclinometer Readings

Inclinometer	Maximum Lateral Displacement from Baseline (Inches)	Corresponding Depth Below Ground Surface (Feet)
INC-1	0.9 (23 mm)	34 (10.4 m)
INC-2	0.6 (15 mm)	28 (8.5 m)
INC-3	0.9 (23 mm)	58 (17.7 m)
INC-4	1.9 (48 mm)	58 (17.7 m)
INC-5	1.2 (30 mm)	58 (17.7 m)
INC-6	1.3 (33 mm)	58 (17.7 m)
INC-7	0.8 (20 mm)	58 (17.7 m)
INC-8	0.8 (20 mm)	58 (17.7 m)
INC-9	0.5 (13 mm)	58 (17.7 m)
INC-10	1.5 (38 mm)	56 (17.1 m)
INC-11	0.5 (13 mm)	56 (17.1 m)
INC-12	0.4 (10 mm)	56 (17.1 m)
INC-13	2.0 (51 mm)	56 (17.1 m)
INC-14	0.4 (10 mm)	56 (17.1 m)

Maximum lateral displacements of the slurry wall were generally observed to be the greatest at the toe of the slurry wall. Toe movement was observed to be reduced at locations where subgrade struts were installed. Typical inclinometer profiles at locations with and without subgrade struts are included below in Fig. 6.

 © Deep Foundations Institute 2025

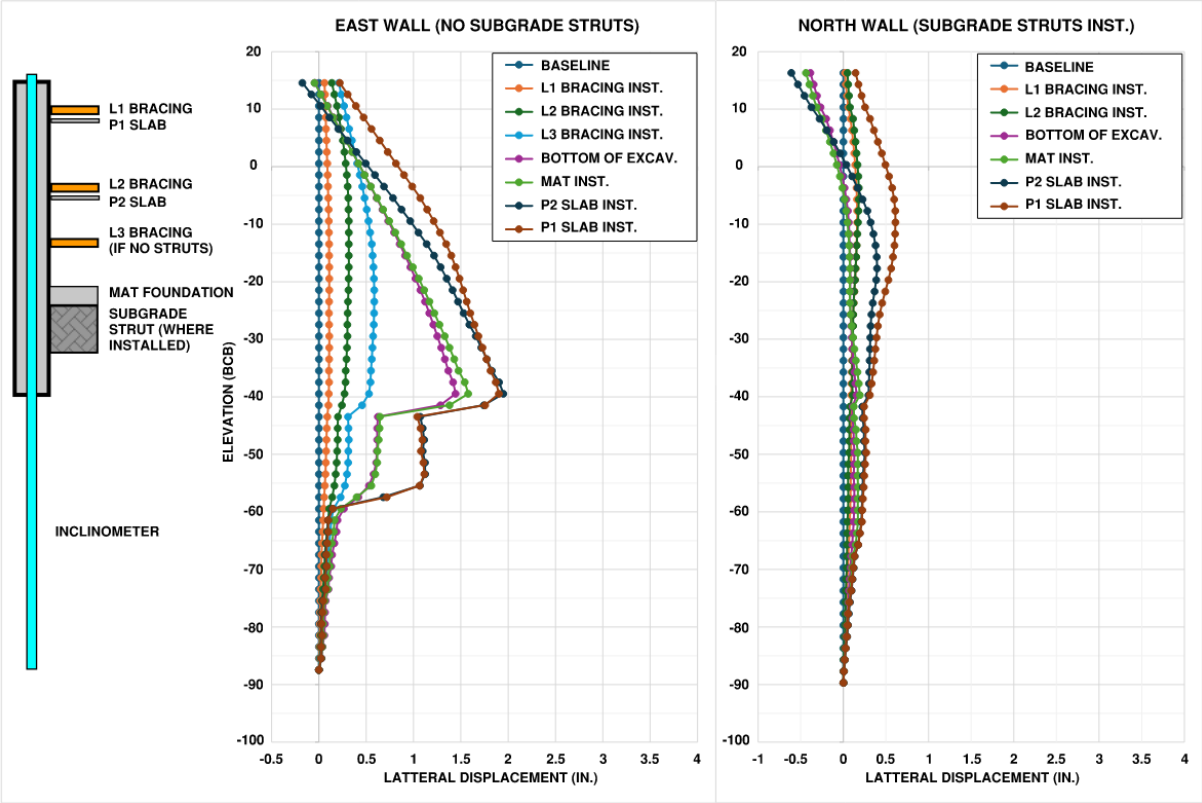


Fig. 6. Inclinometer Measurements at Panels With and Without Subgrade Struts

Vertical Movement of Adjacent Buildings

The facade and building columns of adjacent buildings were monitored for settlement during construction. The largest magnitude of vertical displacement was observed at columns closest to the excavation. Furthermore, total vertical settlement was observed to be reduced where subgrade struts were installed. An elevation plot indicating the settlement profile along the building facades is illustrated on Fig. 7.

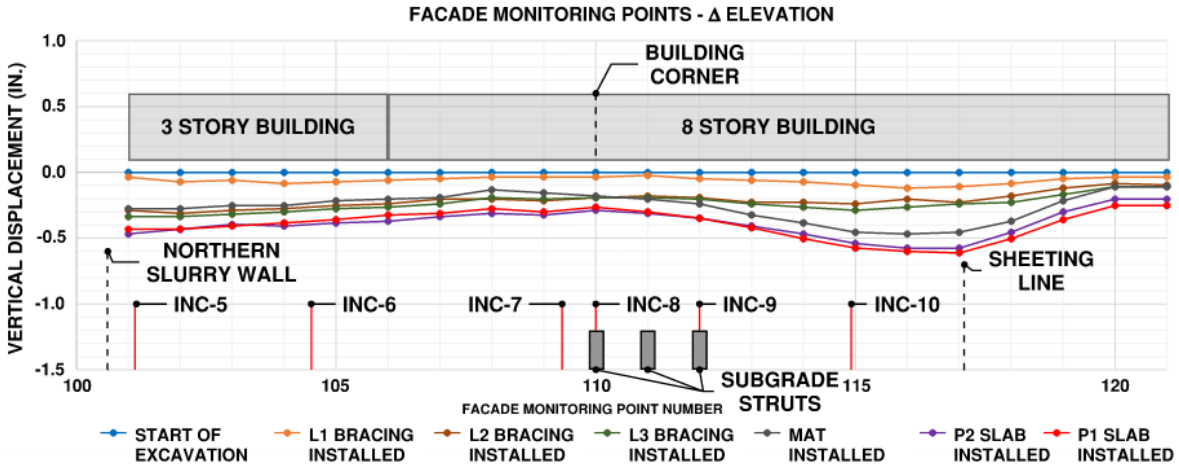


Fig. 7. Adjacent Building Settlement During Phase 1 Construction

 © Deep Foundations Institute 2025

At the completion of the Phase 2 excavation, building settlement was observed to be minimal, with about a tenth of an inch (2.5 mm) of additional building settlement in addition to the Phase 1 settlement shown in Fig. 7 at points adjacent to the Phase 2 excavation.

Vertical and Lateral Movement of MBTA Tracks

The adjacent MBTA tracks were continuously monitored using an AMTS system that surveyed a series of 130 monitoring points along the tracks and boat section. Points were generally spaced at 15-feet (4.6 m) on center. Deflections were measured in the vertical direction, perpendicular to the tracks, and parallel to the tracks. Maximum measured movement at the conclusion of the below-grade work was measured at -0.125 inches (-3.2 mm) in the vertical direction, 0.25 inches (6.4 mm) toward excavation, and 0.25 inches (6.4 mm) parallel to the tracks. Movement parallel to the tracks was measured to fluctuate coincident with fluctuations in temperature as the steel tracks and concrete boat section experience thermal expansion and contraction.

In general, movement was observed to a lesser extent at the majority of points, and the track movements were limited below project criteria established by the MBTA.

SUMMARY AND CONCLUSIONS

A stiff slurry wall SOE system in conjunction with internal steel bracing and unreinforced concrete subgrade struts were successfully used to construct a 3-story below-grade garage adjacent to sensitive buildings and infrastructure. Lateral deflections of the SOE system were minimized with the use of subgrade struts and a stiff slurry wall system in a sensitive Boston Blue Clay deposit to reduce the total settlement of adjacent structures. Adjacent building settlement was reduced in areas where subgrade struts were utilized.

 © Deep Foundations Institute 2025

PERFORMANCE OF ROCK ANCHORS FOR UNDERGROUND CONSTRUCTION IN MANHATTAN SCHIST – INFLUENCE OF GEOLOGICAL FEATURES

Chu E. Ho, WSP USA, Chicago, IL, USA, chu.ho@wsp.com

ABSTRACT

This paper presents the results of tension proof tests on rock anchors for underground excavations in Manhattan Schist at 63rd Street Station and 86th Street Station for the Second Avenue Subway Phase 1 expansion in New York City. A total of 23 tied-back rock anchors, 4 rock dowels and 2 prestressed toe anchors in rock were tested. Back-analysis of the test results was performed to investigate the development of bond resistance in the rock. The results were correlated with rock mass properties characterized by borings located within the vicinity of the excavations, with particular focus on site-specific geological features that may influence anchor performance. Rock mass strength was determined using the relationships proposed by Zhang (2010) and Brown and Hoek (1988) based on rock quality designation (RQD) and rock mass rating (RMR) respectively. The RMR approach, which accounts for RQD, joint properties and water conditions, produced less scatter for rock mass strength than using RQD alone. The equation for grout-rock bond resistance proposed by Horvath and Kenny (1979) for small diameter rock-socketed drilled shafts and anchors is recommended, with modifications for improved quantification of rock mass strength using RMR. This paper highlights the influence of geological features on grout-rock interface bond resistance and provides new insights for rock anchor design.

Keywords: rock anchors, grout-rock bond resistance, rock mass strength, geological features

INTRODUCTION

As part of the Metropolitan Transportation Authority's Second Avenue Subway Phase 1 expansion program in New York City, the existing 63rd Street Station at Lexington Avenue was retrofitted to accommodate an extension of the Q Line via two twin tunnels in rock from 63rd Street to 92nd Street running beneath Second Avenue, with the addition of three new underground stations at 72nd, 86th and 96th Streets. The existing station at 63rd Street and the new stations at 72nd Street and 86th Street were constructed in underground openings in hard rock, whereas the 96th Street Station was constructed using cut-and-cover method in soft ground (Fig. 1).

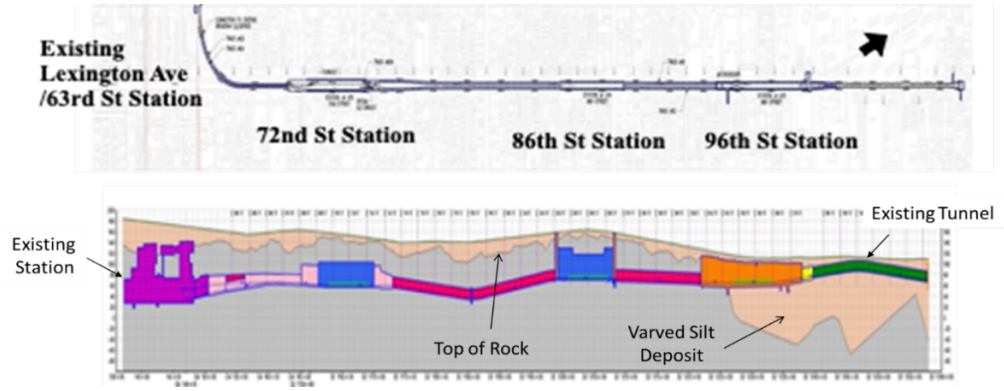


Fig. 1. Underground stations in hard rock for Second Avenue Subway Phase 1

The design and construction of the underground stations in rock caverns have been described by Garavito-Bruhm et al. (2012), Nasri et al. (2013), Kiernan et al. (2014), and Voorwinde et al. (2014, 2015). This paper focuses on the excavation support for construction of a new entrance structure located within an

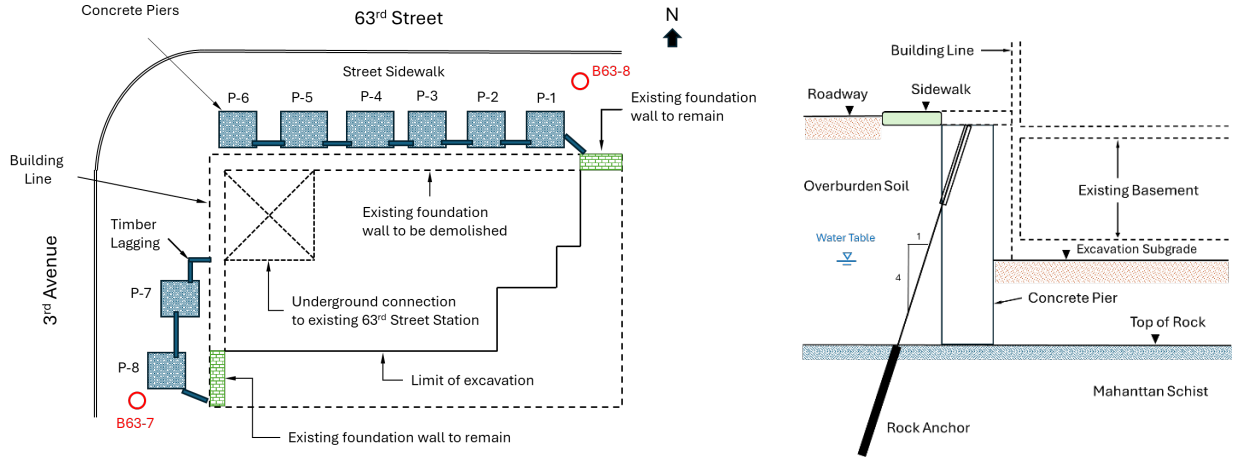
 © Deep Foundations Institute 2025

existing building basement at 63rd Street Station and for construction of an ancillary substructure located underground in rock beneath Second Avenue at 86th Street Station. In both cases, rock supports were installed in the Manhattan Schist. Results from proof load tests on selected rock anchors and rock dowels are reviewed to investigate the development of grout-rock bond resistance and the influence of geological features on rock anchor behavior.

EXCAVATION SUPPORT SYSTEMS

Entrance 1, 63rd Street Station

Entrance 1 at 63rd Street Station was located at the intersection of 63rd Street and 3rd Avenue (Fig. 2a). The new facility was constructed within the basement of an existing seven-story tall residential building to provide an underground link to the 63rd Street Station. The building occupied a corner lot at the southeast sector of the street intersection. The basement comprised a single-level rubble wall with internal columns and walls supported by footings founded directly on dense native sandy soil. Retrofit of the building's first floor and basement structures was necessary to accommodate the new entrance facility. All temporary support framing for the new structure was limited to below the second-floor level and the basement. Construction was carried out while the building remained occupied by tenants. A 12 feet deep open pit was excavated along the edge of the building within the street sidewalk for construction access to the basement interior (Fig. 2b).



(a) Plan (b) Typical Section

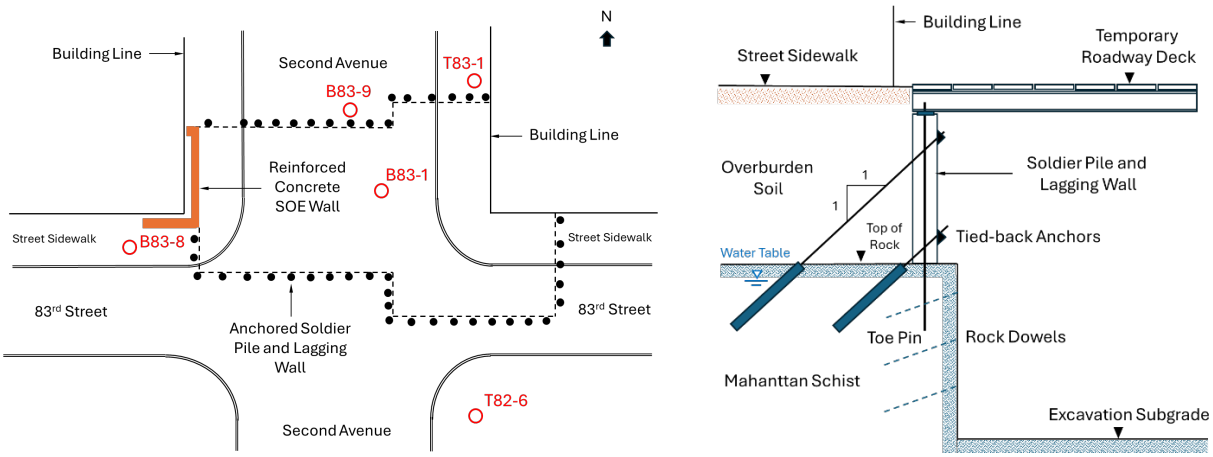
Fig. 2. Excavation support system at Entrance 1 (63rd Street Station)

Eight reinforced concrete piers, 5.5 feet by 5.5 feet or 6 feet by 5 feet in size, were installed spaced 9 to 10 feet apart to provide excavation support. The concrete piers were locally hand-mined within timber sheeting enclosures to reach the top of Class 1d or better bedrock (defined as soft to weathered rock per NYCBC, 2008) or very dense sands, and cast with 5000 psi concrete. The gaps between the concrete piers within the overburden soils were bridged using hand-excavated timber lagging. Inclined tied-back anchors were installed from the top of each pier to provide resistance against active overturning moments from lateral soil pressures behind the piers. The anchor head was located at the center of each pier. A 10 feet long Schedule 40 PVC sleeve pipe approximately 5 inches in diameter was cast into the concrete, inclined at 1 (horizontal) to 4 (vertical) to provide access for anchor installation. Drilling was achieved using 3.0-inch diameter Williams Form B7X Geo-Drill self-drilling rock anchors (net steel area, A_s = 3.88 square inches, ultimate strength, f_u = 105 ksi) fitted with a 5.0-inch diameter Type CC drill bit. The completed holes were

grouted with 5000 psi non-shrink cementitious grout. The upper 10 feet of each anchor within the sleeve pipe was debonded. Groundwater table was located close to the general excavation subgrade.

Ancillary 2, 86th Street Station

At 86th Street Station, a temporary shaft was required for construction of a new underground ancillary structure located at the intersection of 83rd Street and Second Avenue (Fig. 3a). The shaft was approximately 113 feet long, 42 to 63 feet wide and 27 feet deep, and was excavated beneath the existing roadway along Second Avenue. Top of rock varied between 10 to 21 feet below ground surface. Excavation support for the overburden soils involved tied-back soldier pile and lagging walls to top of rock (Fig. 3b). A temporary steel-framed roadway deck was mounted over the soldier piles to allow uninterrupted traffic operation at street level. The shaft was excavated beneath the roadway deck, extending into the street sidewalk and abutting the existing building basements on either side of Second Avenue. On the West excavation face, a localized cast-in-place (CIP) reinforced concrete support of excavation wall had to be installed to the top of rock with vertical pre-tensioned toe anchors to stabilize an existing basement vault where soldier piles could not be installed. Rock excavation was performed using controlled drill-and-blast method. Groundwater table was located just below the top of rock.



(a) Plan (b) Typical Section

Fig. 3. Excavation support system at Ancillary 2 (86th Street Station)

Soldier piles comprised W14 x 68 steel sections (ASTM A572, yield strength f_y = 50 ksi) encased in 2 feet diameter holes filled with flowable fill. The soldier piles were spaced between 5 and 10 feet apart due to localized adjustments to avoid existing utilities within the roadway, and centered approximately 1.5 to 2 feet from the rock ledge. Tied-back anchors were installed at 45 degrees, consisting of 1-inch or 1.375-inches diameter SAS thread bars (ASTM A722, ultimate tensile strength f_u = 150 ksi) in 3.5 to 4-inches diameter holes. Toe pins were drilled vertically 5 feet deep below the pile toes, through pipe sleeves attached to the soldier piles, to secure the piles during excavation below the pile toes. Toe pins consisted of 1-inch diameter SAS thread bars (ASTM A722, f_u = 150 ksi) and were installed in 4-inches diameter drilled holes. The face of the rock cut below the soldier piles were stabilized using rock dowels inclined at 15 degrees, consisting of 1-inch diameter SAS thread bars (ASTM A722, f_u = 75 ksi) in 3-inches diameter drilled holes. Toe anchors for the CIP concrete wall comprised 1.375-inches diameter SAS thread bars in 4-inches diameter holes. All anchor and dowel holes were backfilled with 5000 psi cementitious grout.

 © Deep Foundations Institute 2025

ROCK ANCHOR PERFORMANCE

Entrance 1, 63rd Street Station

Pullout tests were carried out on 8 rock anchors at 63rd Street Station (Table 1). Loads were applied in increments of 20% of the maximum test load and locked off at the working load. Creep was observed for 10 mins. Piers 1 to 4 bear on very dense sands while Piers 5 to 8 bear on the rock. Figure 4 shows the load-displacement plots for these tests. As can be seen, the displacements were larger for any given applied load at Piers 1, 2, 3, 7 and 8 (with 12 feet bond lengths in rock) in comparison with the much stiffer response at Piers 4, 5 and 6 (with 14 to 22 feet bond lengths in rock). Anchor displacements generally ranged from 0.31 to 0.46 inches at maximum test load, except for P-4N which registered only 0.11 inches. Observed creep at maximum test load was less than 0.014 inches or 8.0 x 10^{-5} ins/kip in general (creep was not observed for P-4N). The grout-rock bond resistance was estimated assuming the contribution of the anchor length in soil is small.

Table 1. Proof tests on tied-back rock anchors at Entrance 1, 63rd Street Station

Anchor No.	Anchor Rod Diameter (d)	Inclination from Horizontal (α)	Anchor Length (L_T)	Free Length (L_f)	Bond Length in Soil (L_s)	Bond Length in Rock (L_b)	Hole Diameter (D)	Maximum Test Load (T_{max})	Lock Off Load (T_{LO})	Ratio of Test Load to Lock Off Load (T_{max}/T_{LO})	Estimated Bond Resistance in Rock ($f_{b,\,max}$)
	inches	degree	feet	feet	feet	feet	inches	kips	kips		psi
P-1N	3.0	76	41.4	10	19.4	12	5	180	70	2.6	79.6
P-2N	3.0	76	41.4	10	19.4	12	5	180	70	2.6	79.6
P-3N	3.0	76	41.4	10	19.4	12	5	180	70	2.6	79.6
P-4N	3.0	76	43.4	10	19.4	14	5	190	80	2.4	72.0
P-5N	3.0	76	48.7	10	20.7	18	5	310	230	1.3	91.4
P-6N	3.0	76	52.7	10	20.7	22	5	320	270	1.2	77.2
P-7W	3.0	76	42.7	10	20.7	12	5	175	130	1.3	77.4
P-8W	3.0	76	42.7	10	20.7	12	5	175	130	1.3	77.4

1. Anchor designations N and W denote anchors installed in the North and West faces of excavation pit.
2. Piers 1 to 4 bear on very dense sand with allowable bearing capacity of 8 to 10 ksf.
3. Piers 5 to 8 bear on Class 1d or better rock (NYCBC, 2008).

Ho (2019) presented the results of tension load tests on drilled rock-socketed micropiles installed in Manhattan Schist as part of the retrofit program for 63rd Street Station. The average bond resistance mobilized in the rock sockets ranged from 173.4 to 213.6 psi, which were much higher than indicated in the present anchor proof tests (maximum 91.4 psi). These higher values could be attributed to the difference in drilling methodology. These micropiles were drilled with a permanent casing to the top of rock thereby improving drill hole stability. Tricone bits or down-the-hole hammers were used for drilling the micropiles, hence roughness of the drill hole could have enhanced the interface resistance. In the current case, the anchors were not cased within the overburden soils, and the anchors were installed using a self-drilling anchor and grouted in place.

 © Deep Foundations Institute 2025

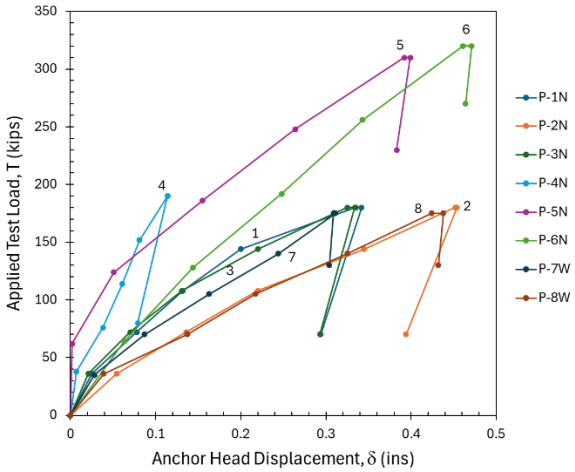


Fig. 4. Pullout tests for rock anchors at Entrance 1 (63rd Street Station).

Ancillary 2, 86th Street Station

Proof tests were carried out on 15 rock anchors within the 86th Street Station shaft in accordance with ASTM D 4435. The anchors were proof loaded to 1.5 times the design load and locked off to 80% of the working load. The test load was incrementally applied in steps of 25% of the working load. The load was held for 10 minutes at the maximum test load to evaluate creep movements. Table 2 summarizes the test results for these anchors (designated TA and TB). Additional test results for 4 rock dowels (RD series) and 2 pre-tensioned toe anchors (A series) for the CIP concrete support of excavation wall are also included for comparison. The maximum mobilized grout-rock bond resistances were 98.4 psi for tied-back rock anchors, 56 psi for rock dowels, and 90.7 psi for pre-tensioned toe anchors.

Figure 5 shows the load-displacement plots for tied-back rock anchors and rock dowels located at the North, South and West faces of the excavation pit. As can be seen, the load-displacement relationship was approximately linear for most of the tests with maximum displacement of less than 0.17 inches, indicating reasonably stiff elastic behavior. It was also obvious that the rock dowels exhibited a stiffer response than the tied-back rock anchors since the dowels were fully grouted. It was observed that the variation in load-deformation response of the tied-back anchors was much greater in the West face than the other two faces, indicating more variable rock quality and potentially weaker rock on the West face.

Figure 6 shows the performance of the two vertical pre-tensioned toe anchors installed for the CIP concrete SOE wall. A2-14 was an abandoned anchor. As can be seen, A2-14 exhibited significant displacement as the test load was applied. It subsequently failed to maintain load beyond 128.1 kips. The pre-failure maximum displacement reached was approximately 1.2 inches. The unexpected poor performance of A2-14 was attributed to lack of drill hole cleanliness due to weak rock conditions encountered in the West face. Corrective action was implemented for the subsequent replacement anchor A2-14-1 (drilled 1 foot away) by flooding the hole with water and blowing with compressed air to remove loosened rock at the grout-rock interface prior to grout placement. After grouting was completed, any observed loss of grout was topped off. The replacement anchor A2-14-1 performed normally and could be loaded to the full test load of 153.8 kips with a displacement of 0.44 inches.

 © Deep Foundations Institute 2025

Table 2. Proof tests on tied-back anchors and rock dowels at Ancillary 2, 86th Street Station

Anchor No.[1]	Anchor Rod Diameter (d)	Inclination from Horizontal (α)	Total Anchor Length (L_T)	Free Length (L_f)	Rock Bond Length (L_b)	Hole Diameter (D)	Maximum Test Load (T_{max})	Lock Off Load (T_{LO})	Ratio of Test Load to Lock Off Load (T_{max}/T_{LO})	Estimated Bond Resistance in Rock ($f_{b,\,max}$)
	inches	degree	feet	feet	feet	inches	kips	kips		psi
TA-2S	1.0	45	18.7	11.9	6.8	4	67.5	36	1.9	65.8
TA-4S	1.0	45	20.4	13.6	6.8	4	67.5	36	1.9	65.8
TA-5S	1.0	45	20.9	13.7	7	3.5	67.5	36	1.9	73.1
TA-9W	1.0	45	22.6	15.5	7	3.5	19.5	10	2.0	21.1
TA-10W	1.0	45	22.5	15.5	7	3.5	19.5	10	2.0	21.1
TA-14EN	1.0	45	22.9	15.9	7	3.5	15	8	1.9	16.2
TA-14WN	1.0	45	23	16	7	3.5	15	8	1.9	16.2
TA-15N	1.0	45	21	14.2	6.8	4	67.5	36	1.9	65.8
TA-17N	1.0	45	21.6	14.8	6.8	4	67.5	36	1.9	65.8
TB-6S	1.375	45	27.4	15.4	12	3.5	135	72	1.9	85.3
TB-8S	1.375	45	27.4	15.4	12	3.5	135	72	1.9	85.3
TB-9W	1.375	45	25.8	15.4	10.4	3.5	135	NR[4]	-	98.4
TB-10W	1.375	45	25.8	15.4	10.4	3.5	135	NR[4]	-	98.4
TB-11N	1.375	45	27.4	15.4	12	3.5	135	72	1.9	85.3
TB-13N	1.375	45	27.3	15.3	12	3.5	135	72	1.9	85.3
RD1-S	1.0	15	15	0	15	3	95	-	-	56.0
RD2-N	1.0	15	15	0	15	3	95	-	-	56.0
RD1-N	1.0	15	15	0	15	3	95	-	-	56.0
RD1-W	1.0	15	15	0	15	3	95	-	-	56.0
A2-14W[2]	1.375	90	28	13	15	4	128.1	-	-	75.5
A2-14-1W[3]	1.375	90	28	13	15	4	153.8	82.0	1.9	90.7

1. Designations N, S and W denote anchors installed in the North, South and West faces of excavation pit.
2. Anchor A2-14 could not be loaded to the specified test load and was abandoned.
3. Replacement anchor A2-14-1W was installed 1 foot away from A2-14W.
4. NR = Not Recorded

 © Deep Foundations Institute 2025

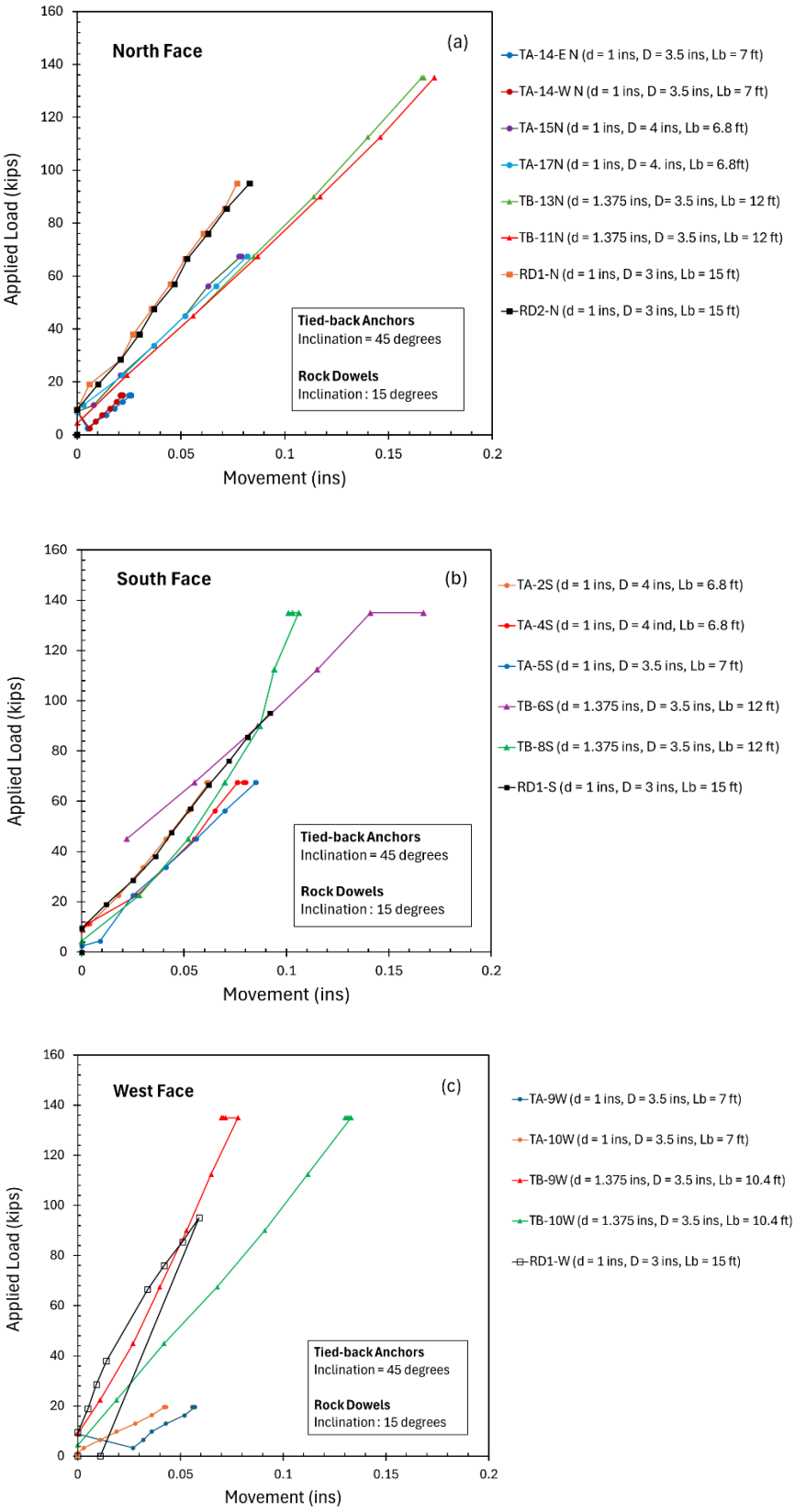


Fig. 5. Tied-back anchors and rock dowels at Ancillary 2 (86th Street Station).

In comparing the pre-tensioned toe anchor AW-14-1 for the CIP SOE wall with the tied-back anchors braced against soldier piles in Fig. 6, the vertically installed toe anchor displayed a softer load-displacement response relative to the tied-back anchors which were inclined at 45 degrees. This reflects greater effectiveness of load transfer in inclined anchors by bearing against passive resistance behind the soldier piles as opposed to reacting against a vertically loaded concrete wall in end bearing on the rock.

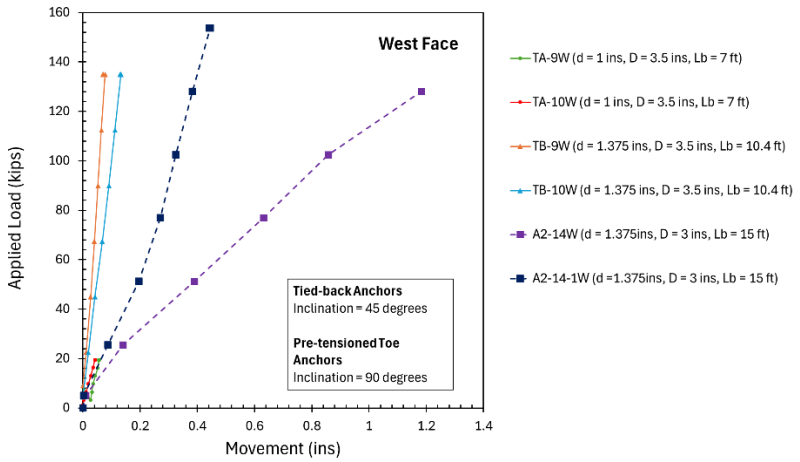


Fig. 6. Toe anchors and tied-back anchors on West face at Ancillary 2 (86th Street Station).

SITE SPECIFIC GEOLOGICAL FEATURES

Manhattan Schist is a crystalline metamorphic rock and is generally categorized as Class 1a Hard Sound Rock (RQD > 85%) to C1ass 1b Medium Hard Rock (50% < RQD < 85%) in the New York City Building Code (NYCBC, 2008). However, this qualitative description cannot be easily applied in design practice as the geological character of Manhattan Schist can be quite complex (Snee et al. 2004). It is known that the behavior of rock masses will be influenced by the geological features in a significant manner and will result in lower overall strength of the rock mass compared to its intact rock strength. A more quantitative approach would be necessary for evaluating rock mass strength based on consideration of site-specific geological features.

The rock encountered in this project can be broadly described as medium hard to very hard, fresh to slightly weathered, fine-grained to coarse-grained quartz-mica-garnet schist, with very thin to thin convoluted, crenulated, sub-horizontal to sub-vertical foliations. The joints and fractures were generally rough, very closely to moderately closely spaced and slightly weathered, and may be stained with iron-oxide and chloride. Occasionally, the rock was penetrated by intrusions of very hard, fresh quartz-feldspar pegmatite. A comprehensive testing program was performed at the 86th Street Station site to characterize the Manhattan Schist. Figure 7 shows the distribution of intact rock strengths (σ_c) obtained. Ignoring the single high value of 13.52 ksi, the computed mean intact rock strength was 7.95 ksi, with a standard deviation of 1.85 ksi.

 © Deep Foundations Institute 2025

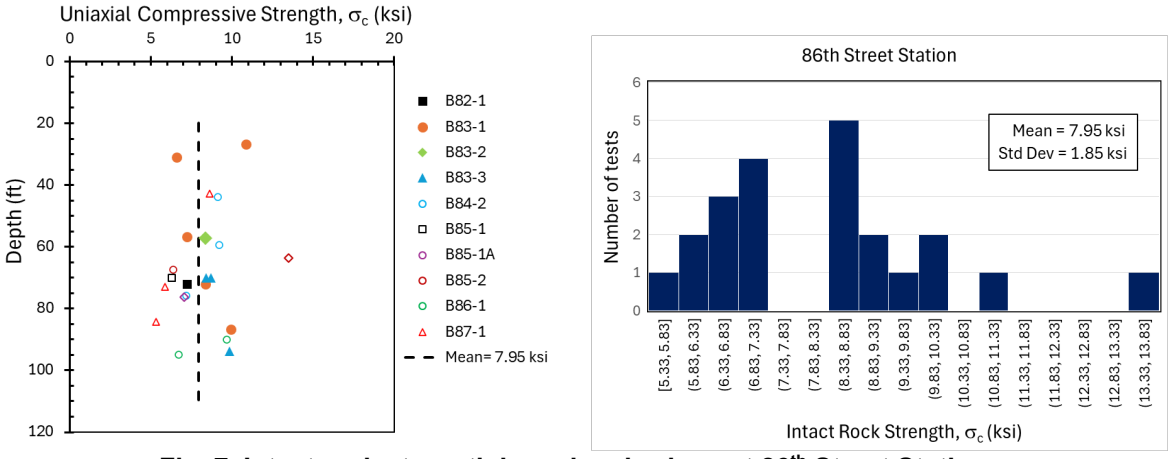


Fig. 7. Intact rock strength based on borings at 86th Street Station.

Figure 8 shows the rock conditions at Entrance 1 (63rd Street Station). Borings B63-7 and B63-8 were drilled along the alignment of the proposed excavation support wall within the street sidewalk on 3rd Avenue and 63rd Street respectively (Fig. 2a). Total core recovery (TCR) generally varied between 74% and 100% for the two borings with an overall mean of 97%. No strength test was performed on rock cores in these borings. It was assumed a mean intact rock strength of 7.95 ksi for the Manhattan Schist was reasonably applicable at the 63rd Street Station site. In this paper, RMR ratings adopted were based on a dry condition (R = 15) and without adjustment for joint orientation (R = 0) as recommended by Hoek and Brown (1988). As can be seen, the spread of RQD values was much wider than the RMR values. The rock anchors were installed within the top 25 feet of rock. Evaluated RQD values within the rock anchor zone ranged from 45% to 100% (mean = 75%) and with observed joint/fracture spacing varying between 0.16 feet to 2.5 feet (mean = 0.68 feet). The corresponding RMR values within the rock anchor zone varied between 59 and 83 (mean = 70) indicating fair to very good rock (Bieniawski, 1979).

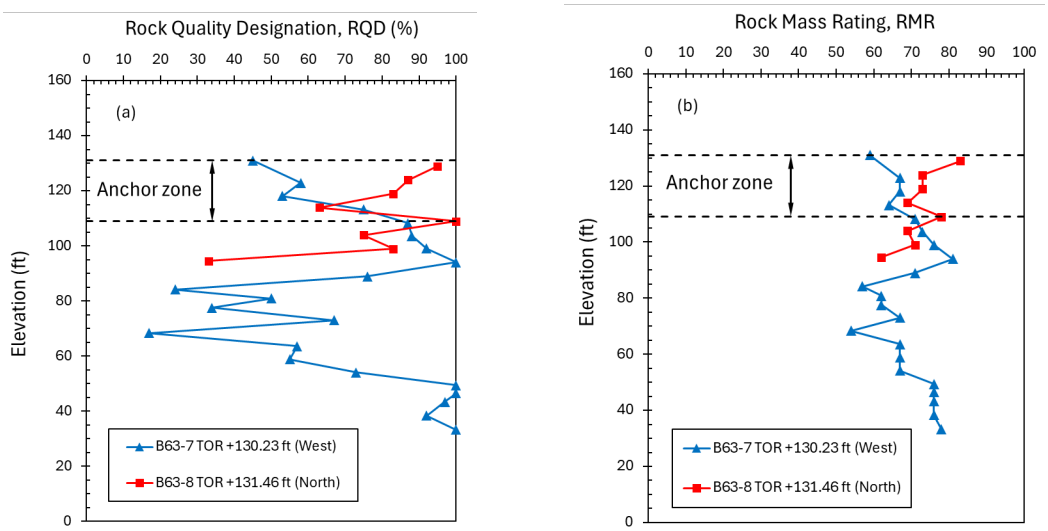


Fig. 8. RQD and RMR for Entrance 1 (63rd Street Station).

Figure 9 shows the RQD and RMR values observed at Ancillary 2 (86th Street Station) based on the borings in the vicinity of the excavation (Fig. 3a). Overall TCR for all borings ranged from 66% to 100% with a mean of 98%. The RQD values varied significantly on each face of the excavation, suggesting weaker rock on the West face and better rock conditions for the North and South faces. Boring B3-1 located in the middle of the excavation pit indicated the best rock conditions. Similar to the previous observation at 63rd Street

Station, the RMR values varied within a much narrower band compared to the RQD values. The rock anchors were embedded within the upper 15 feet of rock. RQD values within the rock anchor zone ranged from 8% to 100% (mean = 56%) with observed joint/fracture spacing of between 0.01 feet to 0.71 feet (mean = 0.31 feet). RMR values within the rock anchor zone was based on the mean intact rock strength of 7.95 ksi obtained for this site, and the respective RQD and observed joint conditions in the individual borings at each excavation face. The overall RMR values within the rock anchor zone ranged from 54 to 75 (mean = 66) indicating fair to good rock.

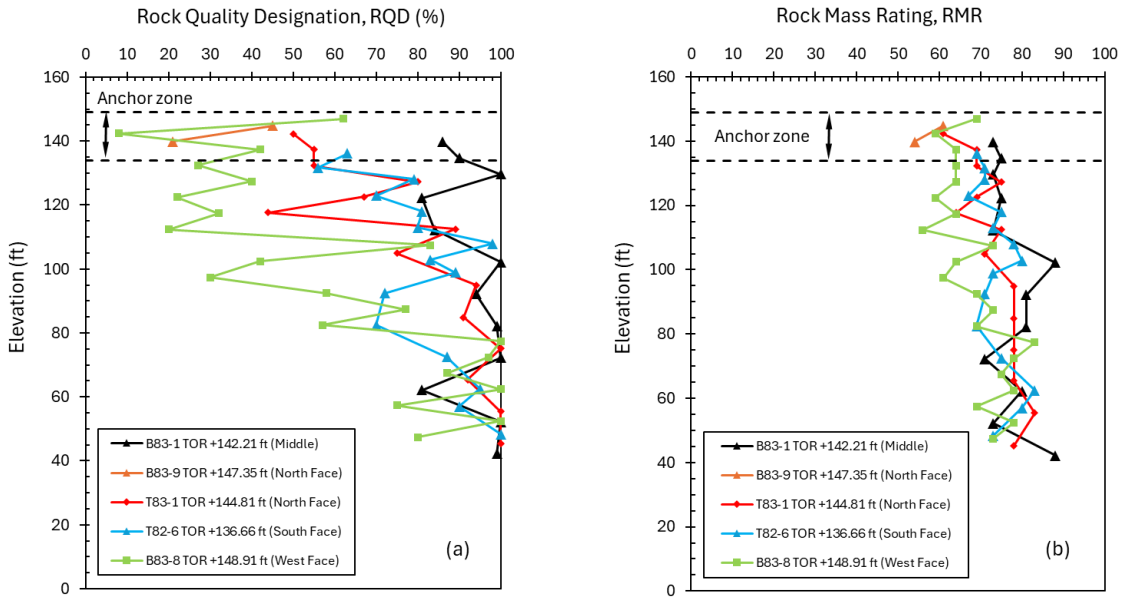


Fig. 9. RQD and RMR for Ancillary 2 (86th Street Station).

ROCK MASS STRENGTH

This section reviews the different methods for evaluating rock mass strength. Kulhawy and Goodman (1987) proposed that compressive strength of a rock mass (σ_{cm}) can be evaluated based on RQD, assuming $\sigma_{cm} = 0.33\sigma_c$ for RQD < 70%, and increasing linearly to $\sigma_{cm} = 0.8\sigma_c$ at RQD = 100%, where σ_c is the uniaxial compressive strength of intact rock. AASHTO (1996) recommends that $\sigma_{cm} = 0.15\sigma_c$ for RQD < 64%, then increasing linearly with RQD in accordance with the equation $\sigma_{cm} = \alpha_\sigma \sigma_c$ where $\alpha_\sigma = 0.0231$ RQD – 1.32. Zhang (2010) proposed a more generalized expression in the form $\alpha_\sigma = 10^m$, where m = 0.013 RQD – 1.34, based on test results that covered the full range of RQD from 0 to 100%. Figure 10a shows the variation of the rock mass strength ratio (α_σ) with RQD for the above proposed methods. As can be seen, all three relationships are in general agreement for RQD > 70%. However, the constant values proposed by Kulhawy and Goodman (1987) for RQD < 70% and AASHTO (1996) for RQD < 64% respectively are less realistic. It is proposed that the relationship by Zhang (2010) be adopted for design as it is more representative of rock mass strength over the full range of RQD.

Hoek and Brown (1988) proposed that rock mass strength of reasonably undisturbed or interlocked rock masses can be evaluated based on the Hoek-Brown Failure Criterion using RMR: $\sigma_{cm} = \sigma_c \sqrt{s}$ where $s = e^n$ and n = (RMR-100)/9 (Brown and Hoek 1988). The Hoek-Brown Failure Criterion assumes isotropic rock behavior and is applicable to intact rock or jointed rock with four or more discontinuity sets. When using this criterion, Hoek and Brown (1988) recommended adopting RMR ratings compatible with a dry condition and without adjustment for joint orientation. Figure 10b shows the variation of α_σ with RMR.

 © Deep Foundations Institute 2025

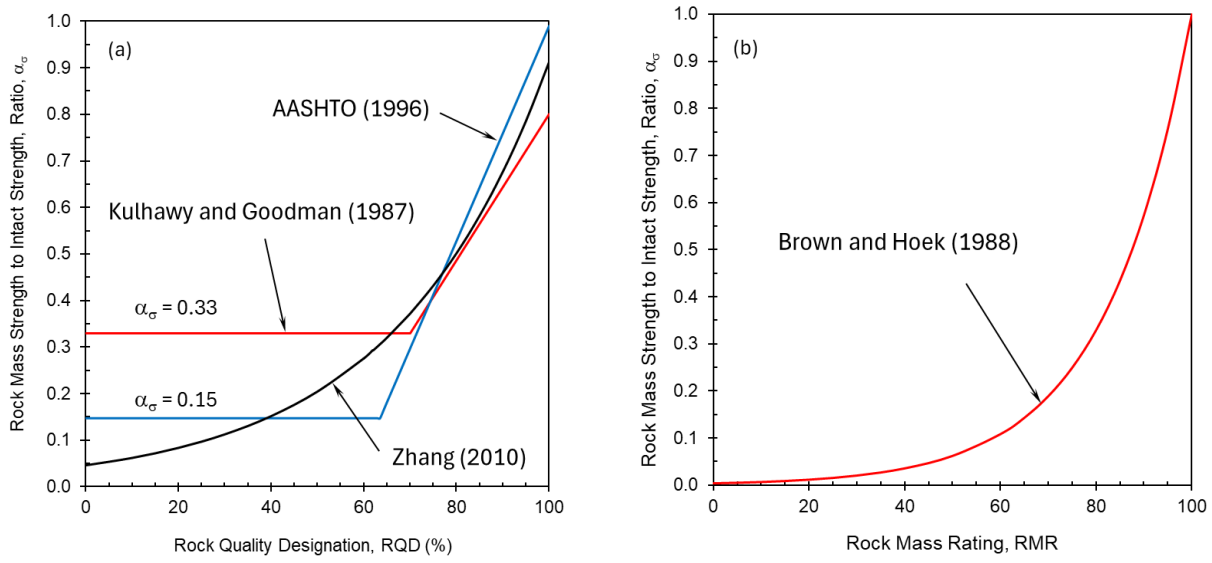


Fig. 10. Variation of rock mass strength ratio with rock quality: (a) RQD, (b) RMR

GROUT-ROCK BOND RESISTANCE

Current practice in rock anchor design in competent rock relies on guidance based on FHWA (1999) and PTI (2014). These documents recommend grout-rock ultimate bond resistance (f_b) of 250 to 450 psi for Granite and Basalt, 200 to 300 psi for Dolomite Limestone, 150 to 200 psi for Soft Limestone and 120 to 200 psi for Slates and Hard Shales. PTI (2014) indicates the ultimate bond resistance can be estimated as 10% of the intact rock strength up to the limit of 600 psi. These ranges are quite wide and do not provide guidance with respect to rock quality. A factor of safety of 2.0 is recommended for permanent rock anchors based on PTI (2014). FHWA (1999) recommends a factor of safety of 3.0 for competent rock to account for discontinuities in the rock mass (joints, fractures and clay-filled fissures).

In this paper, it is proposed that grout-rock bond resistance be evaluated using Horvath and Kenny's empirical relationship, f_b (psi) = $\beta\sqrt{q_u}$ where β varies from 3 (lower bound) to 4 (upper bound) and q_u (in psi) is the unconfined compressive strength of the weaker material (either grout or rock). This relationship was derived from linear regression curve fitting of load test data for small diameter rock-socketed drilled piers (D = 3.3 to 12 inches) and rock anchors (D = 1.5 to 7 inches) for material strength up to approximately 6000 psi (Horvath and Kenney, 1979). This is consistent with the typical limits of grout strength (5000 to 6000 psi) used in rock anchor design practice. Table 3 summarizes the lower bound and upper bound f_b values obtained using this relationship, assuming q_u = rock mass strength (σ_{cm}). The rock condition behind each excavation face was determined based on the nearest relevant borings. The rock mass strengths corresponding to the anchor zones shown in Figs. 8 and 9 were evaluated using Zhang (2010) and Hoek and Brown (1988) and used in the calculation of grout-rock bond resistance.

 © Deep Foundations Institute 2025

Table 3. Estimated and maximum mobilized grout-rock bond resistance

Facility	Wall Face	Intact Rock Strength (σ_c)	Mean RQD[5]	Mean RMR[5]	Rock Mass Strength (σ_{cm})		Ultimate Grout-Rock Bond Resistance[3] (f_b)		Maximum Mobilized Grout-Rock Bond Resistance[4] (f_{bm})	Ratio of Ultimate to Mobilized Bond Resistance (R_f)	
					Zhang (2010)[1]	Brown and Hoek (1988), Hoek and Brown (1988)[2]	Based on RQD	Based on RMR		Based on RQD	Based on RMR
		ksi	%		psi	psi	psi	psi	psi		
Entrance 1 (63rd St. Station)	North (B63-8)	7.95	64	66	2468.1 (α_σ = 0.310)	1202.4 (α_σ = 0.151)	149.0 to 198.7	104.0 to 138.7	91.4	1.6 to 2.2	1.1 to 1.5
	West (B63-7)	7.95	86	75	4768.3 (α_σ = 0.6)	1982.4 (α_σ = 0.249)	207.2 to 276.2	133.6 to 178.1	77.4	2.7 to 3.6	1.7 to 2.3
Ancillary2 (86th St. Station)	North (B83-9 and T83-1)	7.95	45	63	1397.5 (α_σ = 0.176)	1017.8 (α_σ = 0.128)	112.2 to 149.5	95.7 to 127.6	85.3	1.3 to 1.8	1.1 to 1.5
	South (T82-6)	7.95	67	70	2700.0 (α_σ = 0.340)	1501.6 (α_σ = 0.189)	155.9 to 207.8	116.2 to 155.0	85.3	1.8 to 2.4	1.4 to 1.8
	West (B83-8)	7.95	37	64	1099.9 (α_σ = 0.138)	1075.9 (α_σ = 0.135)	99.5 to 132.7	98.4 to 131.2	98.4	1.01 to 1.3	1.0 to 1.3

1. Rock mass strength based on Zhang (2010) using RQD
2. Rock mass strength based on Brown and Hoek (1988) and Hoek and Brown (1988) using RMR
3. Ultimate grout-rock bond resistance based on Horvath and Kenney (1979), f_b = 3 to 4 $\sqrt{\sigma_{cm}}$
4. Maximum values obtained from rock anchor tests in each excavation face
5. Mean RQD and RMR refers to values over the embedded anchor zones in rock based on individual borings

Table 3 shows the rock mass strength obtained using RMR were consistently lower than that based on RQD in all cases, except for the West face at Ancillary 2 (86th Street Station) where both values were very similar for the weaker rock conditions. This implies that for medium to hard rock formation such as Manhattan Schist, which is characterized by significant geological features, the RMR approach appears to better reflect the conditions of the rock mass. The ratio of estimated ultimate bond resistance calculated based on RMR to the maximum value mobilized in the anchor tests (R_f) ranged from 1.0 to 1.7 (using $\beta = 3$) and 1.3 to 2.3 (using $\beta = 4$). Clearly, the load-displacement responses of these tests (Figures 4 to 6) suggest the maximum mobilized bond resistances were well within the failure limit. The values calculated based on $\beta = 3$ appear to be conservative since it predicted failure was reached for the anchors in the West face at 86th Street Station. It is proposed that $\beta = 4$ be used to provide a more realistic estimate of the bond resistance in Manhattan Schist when using RMR. This study indicates for temporary anchors, a minimum factor of safety of 1.3 seems appropriate when using the modified equation $f_b = 4\sqrt{(\sigma_{cm})}$, assuming reasonably good workmanship. A higher factor of safety may be required for permanent anchors if long term creep is critical. However, it is important to recognize that anchor performance could be compromised by poor workmanship (drilling technique, hole cleaning and grout placement). As demonstrated by A2-14 (Figure 6), a deficient anchor due to poor workmanship may result in large displacements and premature slippage failure. Based on the estimated ultimate bond resistance of 131.2 psi for A2-14-1 and the failure stress of 75.5 psi for A2-14, the reduction in bond resistance amounted to 42.5%.

CONCLUSIONS

The performance of rock anchors embedded in Manhattan Schist is reviewed in this paper based on proof load test results obtained for the Second Avenue Subway project at 63rd Street Station and 86th Street Station. The influence of geological features on rock anchor performance in Manhattan Schist is

 © Deep Foundations Institute 2025

highlighted. The conventional use of intact rock strength (σ_c) and rock quality designation (RQD) is insufficient to describe complex rock formations such as Manhattan Schist. Hoek and Brown (1988) proposed that rock mass strength (σ_{cm}) of reasonably undisturbed or interlocked rock masses can be evaluated based on the Hoek-Brown Failure Criterion using Rock Mass Rating (Bieniawski 1979). Brown and Hoek (1988) recommend $\sigma_{cm} = \sigma_c \sqrt{s}$ where $s = e^n$ and $n = (RMR-100)/9$. The Hoek-Brown Failure Criterion assumes isotropic rock behavior and is ideally suited for intact rock or jointed rock with four or more discontinuity sets. When using this criterion, Hoek and Brown (1988) recommends adopting RMR ratings compatible with a dry condition and without adjustment for joint orientation. Rock mass strengths obtained using RMR are more closely bounded than for RQD. It is proposed that grout-rock bond resistance for rock anchor design in Manhattan Schist be based on a modified version of Horvath and Kenney (1979) equation using $f_b = 4\sqrt{(\sigma_{cm})}$ with σ_{cm} derived from RMR. In using this methodology, a minimum factor of safety of 1.3 is recommended for temporary anchors assuming reasonably good workmanship for anchor installation. A higher factor of safety may be required for permanent anchors. It was demonstrated that deficiency in workmanship due to poor drill hole cleanliness can cause 42.5% reduction in bond resistance.

REFERENCES

ASSHTO, 1996. Standard Specifications for Highway Bridges, 16th Edition, American Association of State Highway and Transportation Officials, Washington D.C.

ASTM D4435, 1998. Standard Test Method for Rock Bolt Anchor Pull Test, American Society of Testing and Materials, Pennsylvania.

Brown E. T., and Hoek, E., 1988. Discussion of "Determination of the shear failure envelope in rock masses", Journal of Geotechnical Engineering Division, ASCE, 114 (3), 371-373.

FHWA, 1999. Geotechnical Engineering Circular No.4 Ground Anchors and Anchorage Systems, Report No. FHWA-IF-99-015, Federal Highway Administration, Washington D.C.

Garavito-Bruhm, E., Napoli. A., and Towell, N., 2012. Second Avenue Subway Project, New York: refurbishment of an existing underground station, Proceedings of Structures Congress 2012, Chicago, IL, ASCE.

Ho, C. E., 2019. Rock-socketed micropiles for subway improvement in Manhattan Schist. Proceedings of the 16th Pan American Conference on Soil Mechanics and Geotechnical Engineering, Cancun, Mexico, ISSMGE, 1026-1033.

Hoek, E., and Brown, E. T., 1988. The Hoek-Brown failure criterion - a 1988 update, Proceedings of the 15th Canadian Rock Mechanics Symposium, 31-38.

Horvath, R.G., and Kenney, T.C., 1979. Shaft Resistance of Rock-Socketed Drilled Piers, Proceedings of the Symposium on Deep Foundations, Atlanta, GA, ASCE, 182-214.

Kiernan, J., Stokes, M., and Freitas, J., 2014. Manhattan underground – rapid SEM mining by drill and blast of Second Avenue Subway's 86th Street Station. Proceedings of the North American Tunneling Conference 2014, Los Angeles, CA, SME, 1069-1080.

Nasri, V., Hoffman, S., and Parikh, A., 2013. Design and construction of 86th Street Station Rock Caverns in New York. Proceedings of the Rapid Excavation and Tunneling Conference 2013, Washington, DC, SME, 2-10.

 © Deep Foundations Institute 2025

NYCBC, 2008. New York City Building Code, New York City Department of Buildings.
PTI, 2014. Recommendations for Prestressed Rock and Soil Anchors, 5th Edition, Post-Tensioning Institute, Michigan.

Snee, C. P., Ponti, M.A, and Shah, A, N, 2004. Investigation of complex geologic conditions for the Second Avenue Subway tunnel alignment in New York City, New York. Proceedings of the North American Tunneling Conference, SME, 357-362.

Voorwinde, M., Giffen, R., and Powers, R., 2014. Second Avenue Subway Project: design and construction of 72nd Street Station and G3/G4 Cavern Final Linings. Proceedings of the North American Tunneling Conference 2015, Los Angeles, CA, SME, 29-39.

Voorwinde, M., Garavito-Bruhn, E., Dalton, L., and Giffen, R., 2015. Second Avenue Subway Project: design and construction of large cavern linings and penetrations at 86th Street Station. Proceedings of the Rapid Excavation and Tunneling Conference 2015, New Orleans, LO, SME, 29-39.

Zhang, L. 2010. Estimating the strength of jointed rock masses. Rock Mechanics and Rock Engineering, 43 (4), 391-402.

 © Deep Foundations Institute 2025

INNOVATIVE APPROACHES TO ASSESSING UNKNOWN PILE LENGTHS: ENSURING CLEARANCE AND STABILITY FOR URBAN TUNNELING PROJECTS

Hamed Layssi, FPrimeC Solutions Inc., Richmond Hill, Canada, hamed@fprimec.com
Farid Moradi, FPrimeC Solutions Inc., Richmond Hill, Canada, farid@fprimec.com
Mohammadhossein Afsharipour, FPrimeC Solutions Inc., Richmond Hill, Canada, afshar@fprimec.com
Richard Malantic, FPrimeC Solutions Inc., Richmond Hill, Canada, richard@fprimec.com
Kambiz Daneshvar, FPrimeC Solutions Inc., Richmond Hill, Canada, kambiz@fprimec.com

ABSTRACT

With the growing prevalence of tunneling projects in urban centers worldwide, where tunnels are excavated beneath existing structures and infrastructures, safeguarding existing buried structural systems, particularly bridge piles and deep foundations, has become a critical engineering challenge. Accurate knowledge of pile length and foundation details is essential to ensure sufficient clearance from proposed tunnel alignments and to mitigate risks to structural stability during construction. However, many older structures lack reliable design or as-built documentation, leaving foundation lengths and conditions uncertain. This uncertainty poses significant risks to the integrity of these foundations, especially when they intersect with new tunneling activities. This paper addresses the challenges of evaluating unknown pile lengths in the context of protecting existing buried infrastructure during urban tunneling projects. It presents three case studies where foundation investigations were required due to inadequate as-built information. To determine pile lengths and ensure safe clearances, three Non-Destructive Testing (NDT) techniques were employed: Parallel Seismic (PS), advanced surface Guided Waves (GW), and Length Inductive Testing (LIT). These techniques were selected and adapted based on specific site conditions, including access constraints, soil profiles, and surrounding structural configurations. Each case study highlights the methodologies used to assess pile lengths, the considerations for adapting NDT techniques to site-specific challenges, and the practical implications for maintaining the stability of existing foundations during tunneling. The paper evaluates the advantages and limitations of each NDT method, emphasizing their role in mitigating risks to buried infrastructure and facilitating safer integration of modern tunneling projects with legacy systems. This work provides valuable insights into the importance of tailored investigative approaches in urban environments, where preserving the integrity of critical infrastructure is paramount.

Keywords: Urban Tunneling, Unknown Pile Lengths, Non-Destructive Testing (NDT), Structural Stability, Buried Infrastructure.

INTRODUCTION

In dense urban environments, where underground infrastructure projects such as tunnel boring operations intersect with legacy foundations, understanding the characteristics of existing deep foundations is critical to ensuring structural safety (Haijian and Longxiang, 2011). One of the most vital parameters in this context is the tunnel influence zone and its distance from existing foundations (Lim et al., 2023) which highlights the importance of the embedded length of piles supporting adjacent buildings or bridge structures. Uncertainty in pile length can lead to inaccurate assessments of clearance between the tunneling machine and the foundation toe. In case of insufficient clearance, ground deformation that occurs during tunnel construction could have a major impact on nearby existing piles. This deformation influences both the stability and performance of the piles, altering their behavior. As a result, the piles may experience increased axial settlement and lateral displacement, along with additional axial loads and bending moments. These effects can compromise the integrity of the foundation system and potentially cause damage to the structure it supports (Ayasrah et al., 2021).

 © Deep Foundations Institute 2025

Some existing pile foundations might not have adequate design documentation or accurate as-built construction records. Evaluating such foundations come with certain practical and technical challenges. These existing foundations are often inaccessible, buried deep and heavily coupled with existing structural components (Hossain et al., 2013). In these scenarios, obtaining accurate information about the length, geometry and integrity of existing deep foundations will be crucial.

Various Non-Destructive Testing (NDT) methods are available to assess unknown foundations, with the choice of method depending on its specific applicability and the foundation type under investigation (Hossain et al. 2013). Some of these NDT methods include Parallel Seismic (PS), Length Inductive Testing (LIT), Borehole Sonic, and Borehole Radar. Recently, advanced solutions based on the guided wave theory, and dispersion analysis have been developed and used for pile length estimation (Cui S. et al., 2023, Cui S., et al, 2024).

This paper aims to present the capabilities and challenges in estimating or verifying the length of existing foundations in three different case studies. Each case poses certain technical and practical challenges that would impact the selection of the test methods, and the accuracy and reliability of the pile length estimates.

METHODOLOGY

Parallel Seismic: The Parallel Seismic (PS) method is a non-destructive testing technique widely used to determine unknown foundation depths. It operates on the principle that an impact on the exposed structure generates wave energy traveling down the foundation, which is tracked by receivers in a nearby cased borehole parallel to the structure (ASTM D8381M−21, Olson et al., 1998b; Sack and Olson, 2009; Hossain et al., 2013). For testing, a short-duration, high-energy impact is applied vertically or horizontally to the side or top of the foundation using an instrumented hammer (i.e., a hammer instrumented by a geophone or accelerometer). The wave energy travels through the foundation, refracts into the soil, and is detected by hydrophone receivers. The hydrophone, sensitive to pressure changes, is suspended in a water-filled cased borehole placed 0.9 to 1.5 meters from the foundation edge to ensure accuracy

In practice, if site constraints prevent access to pile heads, impacts can be applied to column sides supported by piles. The impact is directed toward the borehole-facing side of the column, maintaining a consistent 0.3-meter distance from the slab level. Stress waves (P-Wave) generated by an instrumented hammer are captured by the hydrophone for waveform analysis, The versatility and accuracy of the PS method make it a reliable tool for evaluating various foundation systems (Hossain et al., 2013). Parallel Seismic method has demonstrated high accuracy, with reported variations typically within ±5% of the actual pile length (Roman et al. 2008). The field operational setup and a schematic drawing for the PS test can be seen in Figs. 1, 2, and 3.

Length Inductive Testing: The Length Inductive Testing method is a non-destructive procedure designed to determine the embedded depth of metallic piles such as sheet piles, H-piles, and pipe piles. Similar to a metal detector, the induction test operates by detecting disturbances in a magnetic field caused by nearby metallic targets. The test involved drilling an access borehole parallel to the pile that extents well beyond the presumed pile length. An induction probe is then inserted in the access boreholes and lowered gradually. As probe moves downward parallel to the metallic pile, the voltage is recorded. Once the probe passes across the pile toe, the signal strength changes significantly. This change in signal strength is used to estimate the depth of existing steel pile (Robinson, 2008). A schematic for the test set-up is presented in Fig. 4.

Guided Waves: The Guided Waves method is a non-destructive testing approach used to estimate the length of unknown pile foundations. It operates by generating surface guided waves that travel through a

 © Deep Foundations Institute 2025

pile and analyzing the wave behavior as it interacts with the pile's toes and the surrounding soil. This method leverages the principles of wave propagation, where the generated waves move along the pile and reflect when encountering changes in material properties or geometric boundaries. In the context of pile length estimation, the guided wave method involves placing sensors on the lateral or top surfaces of the pile to capture the wave responses. The phase difference between the signals collected by these sensors is analyzed using a dispersion relation, which describes how wave velocity changes with frequency. By interpreting the periodic patterns in the phase difference and wavenumber relationship, the method can accurately determine the pile length.

This approach is advantageous because it does not require an exposed pile head, and the test can be executed even when only the lateral side of the pile is accessible. The method's accuracy is enhanced through the use of advanced computational techniques, such as the Spectral Element Method (SEM) and modified Ridders' algorithm (Cui and Maghoul 2023, Cui et a,. 2024). The utilized test set-up for this method is presented in Figs. 1 and 2.

CASE STUDIES

Case Study 1 – Estimating unknown length of piles in condominium building, Toronto

The design and construction of a tunnel in downtown Toronto involved boring underneath an existing condominium structure in dense urban area. According to the existing documents, the structure was a reinforced concrete structure supported on drilled shafts; however, design documents did not specify any information regarding the length and diameter of the piles. The main objective of this study was to assess whether there was adequate clearance between the pile toe and the alignment of the tunnel.

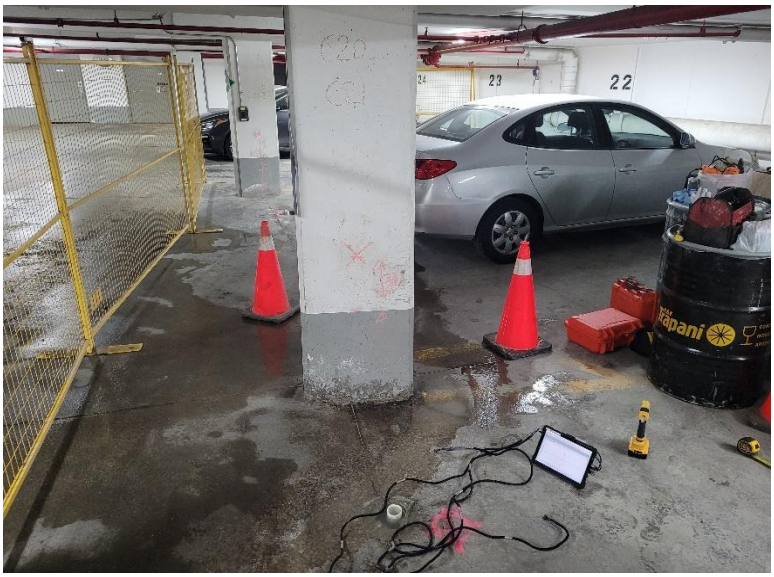


Fig. 1. Column on top of Pile foundation under investigation.

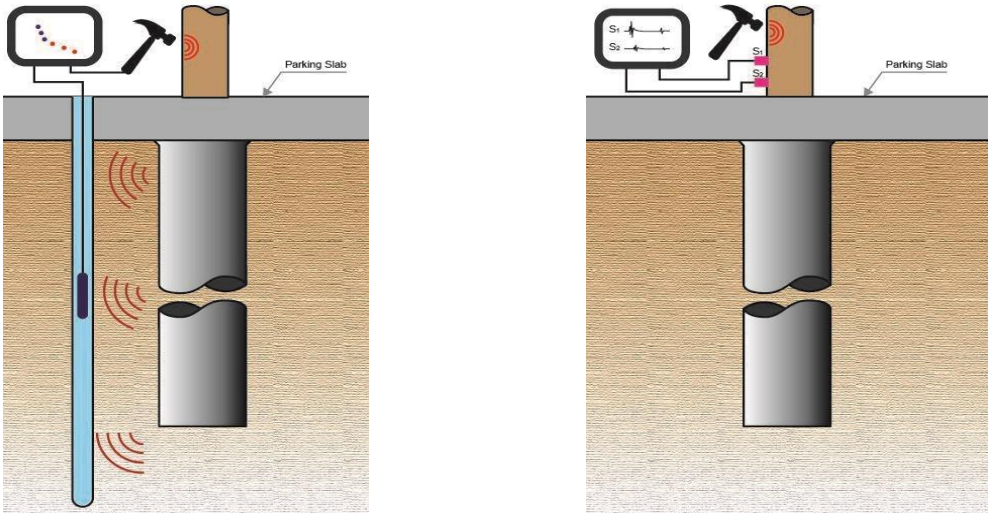
Two different non-destructive evaluation methods were considered for this assessment. The test methods were selected to accommodate the special site condition and the type of the deep foundation (concrete drilled shaft):

- Parallel Seismic
- Dispersion Analysis of Surface Waves

 © Deep Foundations Institute 2025

A small rig was used for drilling the access borehole parallel to the piles for the parallel seismic test. Access to the pile cap was not feasible at the time of study. The strikes were applied to the connected concrete column, close to the ground level. A hydrophone was gradually lowered in the access borehole and the arriving wave was recorded using the PS apparatus.

For Dispersion Analysis, two accelerometers were installed on the connected column, and the column was struck to create the surface waves. Figure 1 presents the test set-up for this case study.



a) b)

Fig. 2. Pile Length Test Setup: a) Parallel Seismic; b) Dispersion Analysis of Surface Waves.

Case Study 2 – Validating The Length of Helical Piles Under Bridge Abutment, GTA

The design and construction of another tunnel in GTA involved boring underneath an existing pedestrian bridge. The steel bridge was supported over East and West abutment walls, and the footings of the abutment walls were supported on a series of vertical and inclined helical piles. The minimum design length of helical piles was provided in the design document, however, no further evidence on the actual length of these piles was available at the time of this study.

 © Deep Foundations Institute 2025



Fig. 3. West abutment wall of the pedestrian bridge. The edge of the footing is accessible.

The main objective of this case study was to assess whether there is adequate clearance between the pile toe and the alignment of the tunnel. Two NDT methods were used to verify the length of helical piles. Since access to the pile head was not feasible, the test methods were limited to the procedures that could be accomplished through an access borehole.

Four access boreholes were drilled near to the abutment wall, as close as possible to the location of the helical piles. The following testing methods were considered for this assessment:

- Parallel Seismic Test
- Length Induction Test

The boreholes were drilled starting from ground level. They extended below the footing elevation, and the drilling continued for about 3 meters past the presumed pile toe. Figure 4 shows the different test setups used in this case.

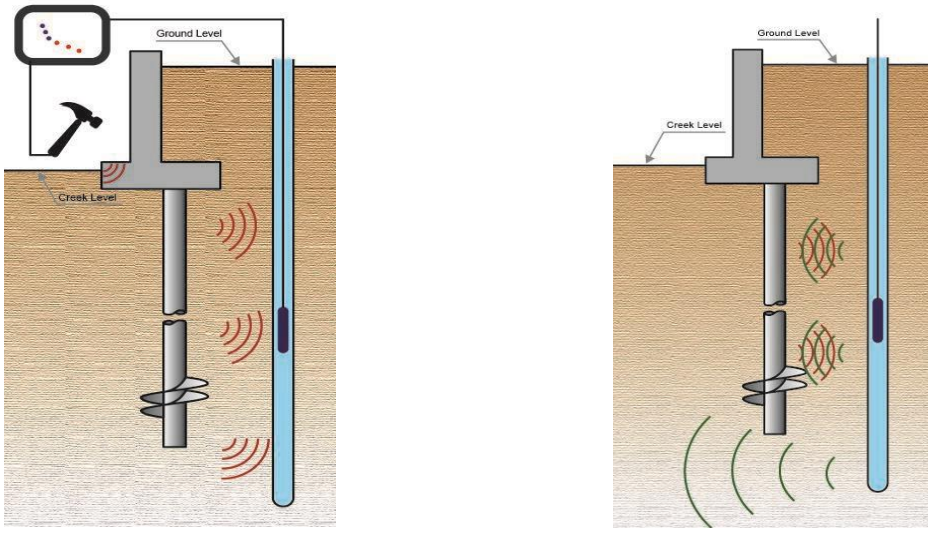


Fig. 4. Pile Length Test Setup: a) Parallel Seismic, b) Length Induction Test.

 © Deep Foundations Institute 2025

Case Study 3 – Verifying The Length of Existing H-Piles of Transmission Line, Edmonton

The design and construction of a water pipeline involved boring underneath a transmission line lattice tower. The tower was supported over a series of H-Piles. The minimum design length of piles was provided in the design document, however, no further evidence on the actual length of these piles was available at the time of this study. The main objective of this study was to assess whether there was adequate clearance between the pile toe and the alignment of the pipeline.



Fig. 5. H-Pile foundations of the Lattice Tower (Transmission Line)

Three NDT methods were used to verify the length of helical piles:

- Parallel Seismic Test
- Length Induction Test
- Dispersion Analysis of Surface Waves

Figure 6 presents the various test set-up for this case study.

 © Deep Foundations Institute 2025

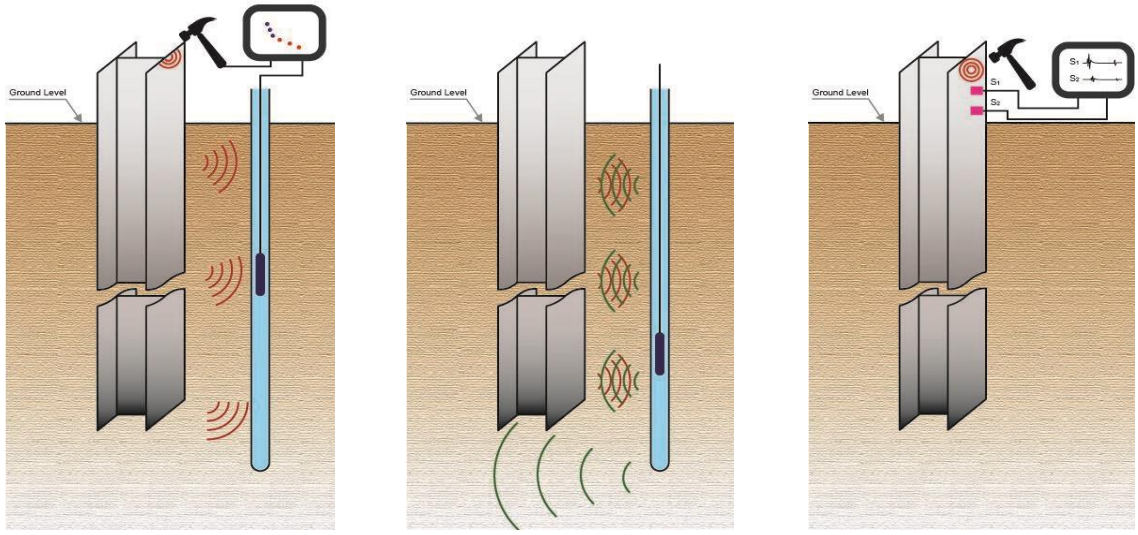


Fig. 6. Pile Length Test Setup: a) Parallel Seismic, b) Length Induction Test, c) Dispersion Analysis of Surface Waves

Test Results and Discussions

Case 1

The Parallel Seismic test results for Pile P2 are presented in Fig. 7. Two distinct lines were fitted to the top and bottom part of the arrival times. The intersection of these two lines was marked as the potential pile toe. The estimated pile length from the PS method was approximately 6.5 m from the ground surface.

The Guided Wave test was carried out on two locations (North and South sides) on the pile of interest. The estimated length of the pile when the Guided Waves test was carried out on the North side was 9.2 m and on the South side was 8.0 m from the ground level. The average estimated pile length was determined as 8.6 m. The pile length measured from the PS test were in good agreement with the existing information about the depth of bedrock in the case study, however, the test did not provide further information whether rock socketing has been used. The results from the Guided waves provided a longer pile length. In the absence of further information, the two values were used as the low and high boundaries for pile length estimation. In the context of this project (clearance underneath the pile toe), the larger pile length estimate would allow for a more conservative risk assessment.

 © Deep Foundations Institute 2025

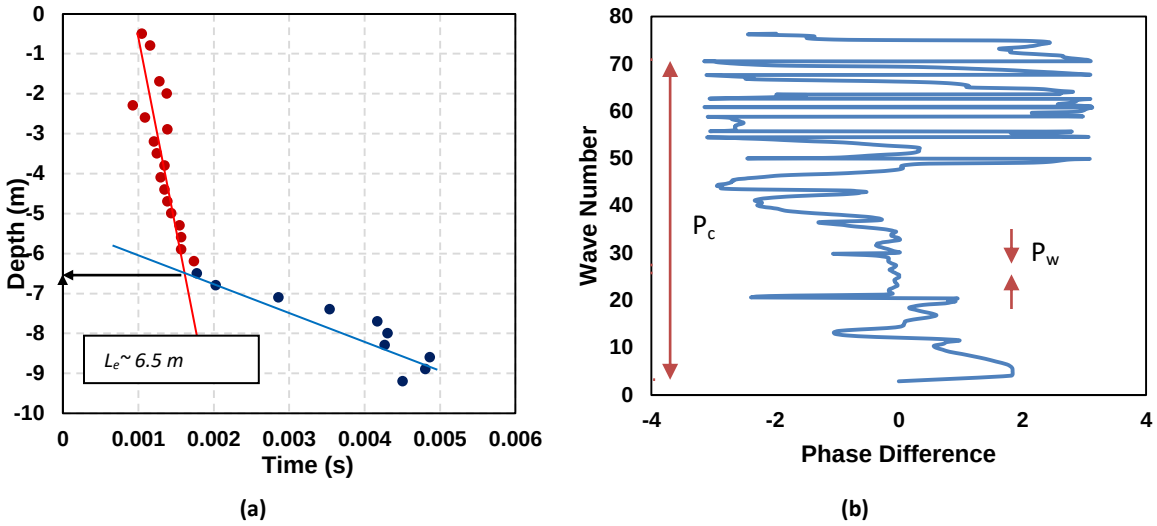


Fig. 7. Test results for the pile of interest in Case 1. a) PS results, b) Guided Waves results.

Case 2

The parallel seismic test results for this case are shown in Fig. 8a. The traditional analysis was slightly challenging for this case, since the first arrival times appear to align along a single line. In order to develop an unbiased pile length evaluation procedure, the two lines were fitted in two different approaches. For the top part, the first arrivals from the depths of 3m to 6 meters were used to develop a linear regression. The line was extended well below the presumed pile length. The second line was developed based on regression line on the first arrivals at the depth of 13 m and lower. The intersection of these two linear regression lines were identified at 10.5 m and marked as the estimated pile length.

The length induction test results are presented in Fig. 8b. The data appear to be generally consistent with no major fluctuation in the voltage measurements. However, for one pile (where the borehole distance to the pile was minimum 0.45 m), the voltmeter registered an abnormally higher voltage. This abnormal peak was calculated to be at the depth of 10 m to 10.5 m, measured from the ground level, and could potentially be associated with a helix. It is the understanding of the authors that increased cross-section of the pile due to presence of helix is potentially correlated with the localized increase in the voltage. The depth was reported as the estimated pile length. The estimated length was in good agreement with the existing design documents.

 © Deep Foundations Institute 2025

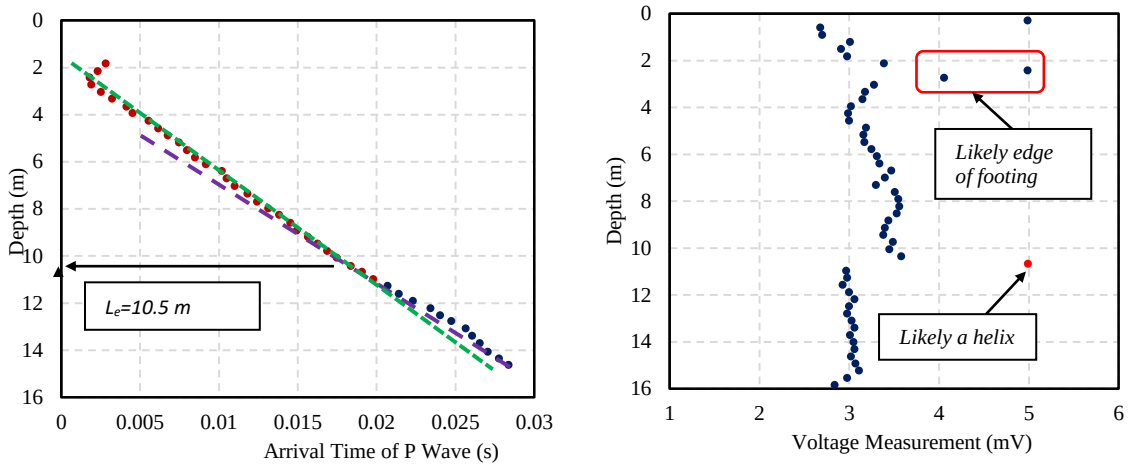


Fig. 8. Test results for the pile of interest in Case 2: a) PS results, b) LIT test results.

Case 3

The Parallel Seismic test results on the pile of interest in this case are presented in Fig. 9a. In a similar way to case #2, two distinct lines were fitted to the top and bottom part of the arrival times. The intersection of these two lines was marked as potential pile toe. The parallel seismic test suggested a pile length of approximately 19 m. The results were in good agreement with the existing information based on historical cases for similar lattice towers.

The Length Induction Test result on the pile is presented in Fig. 9b. The data appear to be generally inconclusive. The voltages increase with the depth and abruptly decreases towards the average value on or around the depth of 16 m, however the nature of these changes is not consistent with what is expected from typical LIT test next to H-Piles (see Robinson, B and Webster, S., 2008). In the absence of more detailed information, the findings of the LIT on the foundation remained inconclusive.

Guided Wave test on H1 is presented in Fig. 9c. The estimated length using this method was estimated as determined as 20.5 m. The pile length measured from the PS test are in good agreement with the existing information about the depth of bedrock in the job site, and the guided waves, similar to case #1, provide a conservative estimate of the length of the pile.

 © Deep Foundations Institute 2025

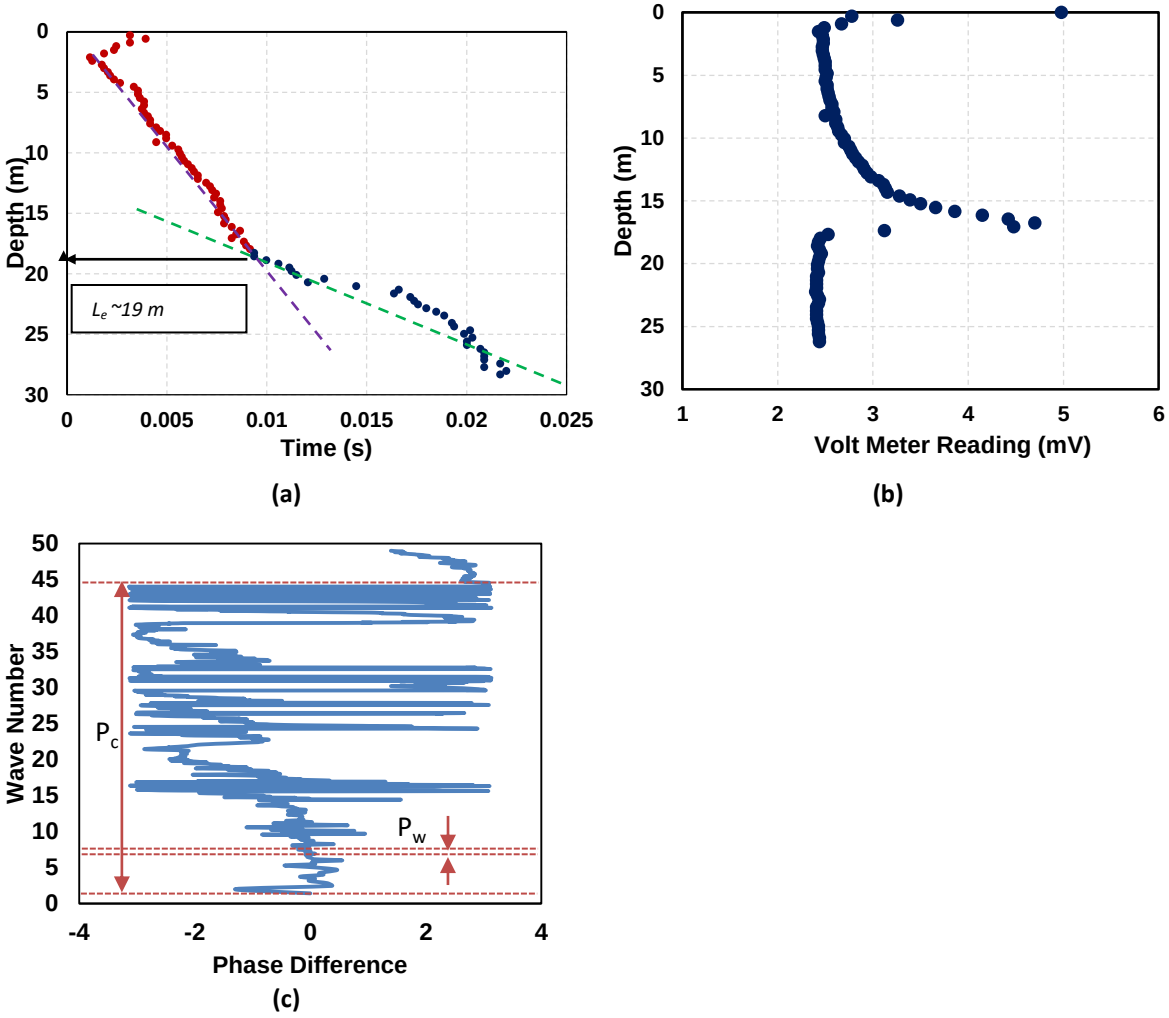


Fig. 9. Test results for the pile of interest in Case 3: a) PS results, b) LIT test results, c) Guided Waves results.

CONCLUSIONS

Non-destructive testing and evaluation (NDT-E) methods offer significant potential for assessing the unknown length of existing foundations, particularly in scenarios where direct access is limited or intrusive methods are impractical. This becomes especially critical in tunnel boring operations in densely developed rural areas, where maintaining sufficient clearance from pile toes is a major concern for both designers and contractors.

Excavation and daylighting of deep foundations to determine pile length are often not feasible due to logistical, safety, and cost constraints. In such cases, the application of NDT-E methods provides a valuable alternative, enabling engineers and contractors to gather essential information about the physical dimensions and integrity of piles without invasive procedures.

Among the available techniques, the Parallel Seismic method has demonstrated high accuracy, however, it requires access boreholes and the pile head or pile cap conditions that are not always achievable, especially in structures under service load. The Length Induction method showed mixed results in the

 © Deep Foundations Institute 2025

case studies presented. Literature suggests it requires an access borehole within 450 mm of the pile, a requirement that is often challenging in real-world applications.

Alternatively, the Guided Wave method presents an alternative approach that requires minimal exposure near the pile head. When preliminary data such as design pile length is available, this method serves as an effective tool for validation of pile length and integrity. Recent experiments show that the method produces reliable outcomes in the case of concrete and timber piles, however, the results on steel piles are generally more complicated due to an increase in the noise to signal ratio.

Overall, while individual NDT-E methods each have their limitations, a multi-technology approach enhances the accuracy and reliability of foundation evaluations. Selecting the appropriate combination of methods, tailored to site-specific constraints and available data, is essential for achieving reliable assessments in complex engineering environments.

REFERENCES

Ayasrah, M., Qiu, H., & Zhang, X. (2021). Influence of Cairo Metro Tunnel Excavation on Pile Deep Foundation of the Adjacent Underground Structures: Numerical Study. Symmetry, 13(3), 426. https://doi.org/10.3390/sym13030426

Cui, Shihao, Hongwei Liu, and Pooneh Maghoul. 2023. “Pile Length Estimation Based on Guided Wave Theory and Dispersion Analysis for Reuse of Foundations.” International Journal of Solids and Structures 283 (November):112486. https://doi.org/10.1016/j.ijsolstr.2023.112486.

Cui, S. , Maghoul, P., Layssi, H, Moradi, F. 2024. Steel hollow pile length estimation based on guided waves, 17th Pan-American Conference on Soil Mechanics and Geotechnical Engineering (XVII PCSMGE), , La Serena Chile, 2024.

Du, Ye, Chunyu Song, Longzhu Chen, and Jun Yang. 2016. “PS Wave Based Parallel Seismic Test for Pile Length Assessment.” Soils and Foundations 56 (3): 440–48. https://doi.org/10.1016/j.sandf.2016.04.010.

Fereshtehnejad, Ehsan, Gianluca Gazzola, Pratik Parekh, Chirag Nakrani, and Hooman Parvardeh. 2022. “Detecting Anomalies in National Bridge Inventory Databases Using Machine Learning Methods.” Transportation Research Record 2676 (6): 453–67. https://doi.org/10.1177/03611981221075028.

He Haijian and Ma Longxiang, "Safety risk evaluation of buildings and structures influenced by construction of adjacent underground engineering," 2011 International Conference on Electric Technology and Civil Engineering (ICETCE), Lushan, China, 2011, pp. 646-650, doi: 10.1109/ICETCE.2011.5775422.

Hertlein, Bernard H, and William H Walton. 2000. “Assessment and Reuse of Old Foundations.” Transportation Research Record 1736 (1): 48–52.

Hossain, MS, MS Khan, J Hossain, G Kibria, and T Taufiq. 2013. “Evaluation of Unknown Foundation Depth Using Different NDT Methods.” Journal of Performance of Constructed Facilities 27 (2): 209–14.

Liao, Shu-Tao, Jian-Hua Tong, Cheng-Hao Chen, and Tsung-Tsong Wu. 2006. “Numerical Simulation and Experimental Study of Parallel Seismic Test for Piles.” International Journal of Solids and Structures 43 (7): 2279–98. https://doi.org/10.1016/j.ijsolstr.2005.03.057.

 © Deep Foundations Institute 2025

Lim, C. X., Jusoh, S. N., Lim, C. B., Abdullah, R. A., & Yunus, N. Z. M. (2023). Tunnel depth effect to pile in Tunnel's influence zone. Physics and Chemistry of the Earth, Parts A/B/C, 129, 103298. https://doi.org/10.1016/j.pce.2022.103298

Lu, Zhi Tang, Zhi Liang Wang, and Dong Jia Liu. 2013. “A Study on the Application of the Parallel Seismic Method in Pile Testing.” Soil Dynamics and Earthquake Engineering 55 (December):255–62. https://doi.org/10.1016/j.soildyn.2013.09.021.

Mulla, Mohammed A. 2014. “Evaluating Bridges with Unknown Foundations for Vulnerability to Scour.”

Ni, Sheng-Huoo, Yan-Hong Huang, Xian-Min Zhou, and Kuo-Feng Lo. 2011. “Inclination Correction of the Parallel Seismic Test for Pile Length Detection.” Computers and Geotechnics 38 (2): 127–32. https://doi.org/10.1016/j.compgeo.2010.10.002.

Niederleithinger, Ernst. 2012. “Improvement and Extension of the Parallel Seismic Method for Foundation Depthmeasurement.” Special Issue on IS-Kanazawa 9th International Conference on Testing and Design Methods for Deep Foundations 52 (6): 1093–1101. https://doi.org/10.1016/j.sandf.2012.11.023.

Roman, E. & Olson, L. & Sack, D. (2008). Determining the Length of H and Sheet Piles Using the Parallel Seismic Method. Symposium on the Application of Geophysics to Eng ineering and Environmental Problems 824-828. 10.4133/1.2963324.

Sack, Dennis A, and Larry D Olson. 2009. “Combined Parallel Seismic and Cone Penetrometer Testing of Existing Foundations for Foundation Length and Evaluation.” In Contemporary Topics in Deep Foundations, 544–51.

Zhang, Jing-Yi, Long-Zhu Chen, and Jinying Zhu. 2016. “Theoretical Basis and Numerical Simulation of Parallel Seismic Test for Existing Piles Using Flexural Wave.” Soil Dynamics and Earthquake Engineering 84 (May):13–21. https://doi.org/10.1016/j.soildyn.2016.01.017.

Zhang, Jing-Yi, and Xiaoqin Lei. 2018. “Numerical Modeling of Parallel Seismic Method for Detecting Existing Piles in Layered Soil.” Soils and Foundations 58 (1): 134–45. https://doi.org/10.1016/j.sandf.2017.11.009.

Brent Robinson, Scott Webster (2008) Proceedings of The Fifth Highway Geophysics - NDE Conference, Charlotte, NC, pp 101-110

 © Deep Foundations Institute 2025

INNOVATIVE SECANT PILE EXCAVATION SUPPORT: WEAPONS STORAGE AND MAINTAINANCE FACILITY – MALMSTROM AIR FORCE BASE

Seth T. Hoffman, PE, SE, Brierley Associates, Aurora, IL, USA, 630-822-5739,
shoffman@brierleyassociates.com
Bill Zietlow, PE, Brierley Associates, Denver, CO, USA, 303-903-7178,
bzietlow@brierleyassociates.com
Brendan Harkins, PE, Condon-Johnson & Associates, Kent, WA, USA, 206-396-4819,
bharkins@condon-johnson.com

ABSTRACT

The United States Air Force is constructing a new facility to consolidate weapon maintenance, storage, and training to support intercontinental ballistic missile operations at Malmstrom Air Force Base in Montana. Part of the new facility requires an approximately 30 ft by 75 ft by 40 ft depth basement to house significant mechanical equipment, with a thick ground-level structural concrete slab above. Concurrent construction of other portions of the structure on all sides precluded open cut or offset temporary support. A single pass system of reinforced concrete secant walls was selected to overcome these constraints. In the completed condition, these walls span between the bottom floor slab and ground-level structural slab, however the upper slab could not be constructed until after the major mechanical equipment was installed inside the basement, requiring alternate means of lateral support during construction. The design team considered several alternatives, including temporary internal steel wale frames and top-down construction with block-outs for equipment installation, but none provided adequate access for equipment installation. Grouted tiebacks were also evaluated, but deemed infeasible due to numerous adjacent drilled shaft foundations. Ultimately, the team devised a hybrid system utilizing three different methods of lateral support: cantilever secants, shallow tie-rods to temporary deadmen shafts, and tie-rods anchored to the adjacent permanent structure foundations. This facilitated successful construction and equipment installation with no obstructions inside the excavation, while meeting all performance objectives.

Keywords: Deep Excavation, Permanent Secant Piling, Complex Sequence, Large-Diameter Drilled Shafts, Dense Construction

INTRODUCTION

The United States Air Force is constructing a new facility to consolidate weapon maintenance, storage, and training to support intercontinental ballistic missile operations at Malmstrom Air Force Base in Montana, which includes heavy reinforced concrete building structures. One of the structures includes a 30 ft by 75 ft by 40-ft deep basement to house significant mechanical equipment. The basement will have a thick ground-level structural concrete slab above that is contiguous with the surrounding building structure. The general configuration of this basement structure is illustrated in Figs. 1 and 2.

The construction schedule and sequencing required concurrent construction of other portions of the structure on all sides of the basement, which precluded open cut excavation or conventional support of excavation (SOE) and construction of conventional cast-in-place formed concrete basement walls. The prime contractor, Archer-Western Federal JV subcontracted Condon-Johson & Associates to design and construct a single-pass SOE and permanent basement wall system and the required temporary supports until the permanent supporting structure was complete. Condon-Johnson & Associates engaged Brierley Associates to provide the required design and construction-phase services to successfully complete the work.

 © Deep Foundations Institute 2025

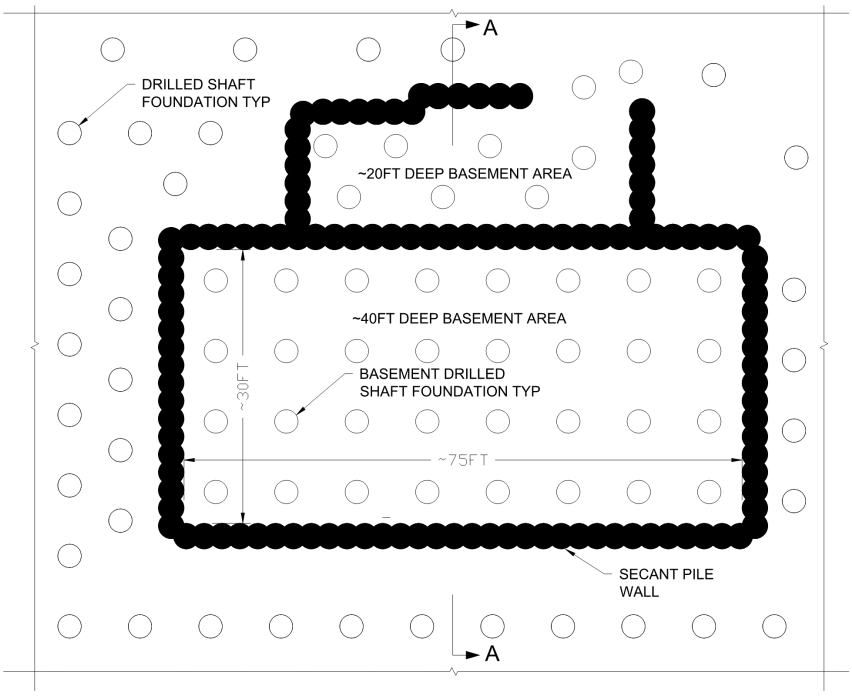


Fig. 1. Basement Structure Plan View

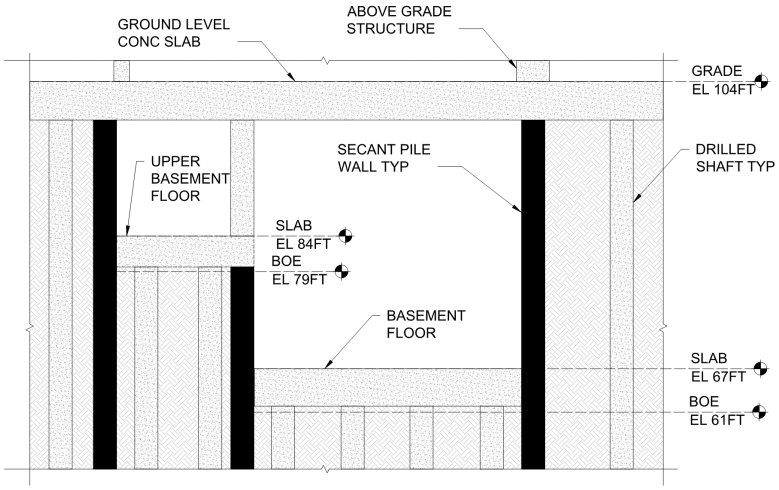


Fig. 2. Basement Structure Section A-A

This paper focuses on the concept development, alternatives analysis, and selection of the preferred SOE/permanent wall system and its successful construction. Due to the proximity to adjacent drilled shaft foundations and concurrent construction, the contract documents specified secant pile basement walls with size, reinforcement, connection to the permanent top slab, and temporary support delegated to the contractor. Condon-Johnson and Brierley considered a wide variety of alternatives, ultimately devising a hybrid system utilizing three different methods of lateral support: cantilever secants, shallow tie-rods to temporary deadmen shafts, and shallow tie-rods anchored to the adjacent permanent structure foundations. This facilitated successful construction and equipment installation with no obstructions inside the excavation, while meeting all performance objectives.

 © Deep Foundations Institute 2025

Schedule was a significant challenge and required preparation for construction prior to completing design. Furthermore, Brierley and Condon-Johnson were not initially aware of all design constraints, particularly those associated with the installation of mechanical equipment within the basement, as well as embeds and block-outs. These constraints were discovered during the design review process and coordination meetings with the project design team and required creative solutions to adapt the designs after construction was underway. Condon-Johnson worked closely with Brierley to ensure that design solutions employed readily available equipment and materials to minimize delays and disruptions.

SITE CONDITIONS

The construction site was located on the Malmstrom Air Force Base near Great Falls, Montana. The site geology consists of surficial sand and glacial lakebed clays overlying glacial till clays. Sandstone, clay shale, and shale underly the glacial till clays, generally at depths on the order of 75 ft.

Based on recommendations from the project geotechnical report, a uniform cohesive design soil profile was used, with a total unit weight of 125 pcf and undrained shear strength of 1,875 psf, as shown in Fig. 3. Groundwater was not encountered in the subsurface exploration, so design for hydrostatic loads or dewatering was not required and therefore not recommended.

Layer No.	Depth	USCS Classification	Parameter	Recommended Value
1	0.0 to 73.0	CL, CH	Effective Unit Weight, γ	125 pcf
			Undrained Shear Strength, Su	1,875 psf
			K-value	1000 pci (static) 400 pci (cyclic)
			Strain, ε_{50}	0.005

Fig. 3. Design Soil Parameters

SUPPORT OF EXCAVATION CONCEPTS AND SELECTION

As previously introduced, the contract drawings envisioned the SOE as a single-pass secant-pile system, with the final configuration of the structure utilizing the walls spanning vertically between the ground-level and basement slabs. The secant piles would be installed prior to excavation, but since the top and bottom slabs could not be completed until after excavation, means to laterally support the secants in their interim conditions would be required. Since Brierley and Condon-Johnson were responsible for designing the secants, we had considerable freedom in sequence and methods to accomplish the work, subject to the site, construction sequences, and other constraints. However, each approach had differing tradeoffs, such as cost, schedule, and complexity, particularly with coordination with other trades and related construction. Thus, to thoroughly evaluate each option, we prepared a total of six initial concepts for consideration, which were:

1. Grouted Tiebacks
2. Tie-Rods and Deadman Anchors
3. External Wale and Deadman Anchor Shafts
4. Internal Temporary Wale Frame – Below the Top Slab
5. Internal Temporary Wale Frame – Above the Top Slab
6. Top-Down Construction

 © Deep Foundations Institute 2025

All these options would utilize similar reinforced concrete secant piles, but with varying means to support the tops of the secant piles until the top and bottom floor slabs could be completed to provide the permanent load path. Since the permanent condition required the secant pile walls to span the full height from the bottom to the top slab, and Brierley/Condon-Johnson was responsible for both the permanent and temporary design cases, all options were based on a single level of temporary supports at or near the top of the secants. The following sections summarize each of the options considered with their respective advantages and disadvantages.

Grouted Tiebacks

The grouted tiebacks option had the advantage of allowing a fully open excavation plan with no interior obstructions. However, due to the number and pattern of surrounding drilled shafts (which had to be installed prior to excavation) the permissible paths for tiebacks were impractical, requiring precise alignment at many varying angles, and would likely have struck drilled shafts during installation.

Tie-Rods and Deadman Anchors

To address the complexity and risk of drilling inclined grouted tiebacks through the surrounding drilled shafts, this option utilized shallow buried horizontal (or slightly inclined) tie-rods, anchored to buried deadman walls. However, the permissible paths for the tie-rods were still challenging, and would require precise and varying angular orientation of anchor trumpets in the secant piles. Furthermore, preliminary calculations indicated that developing adequate capacity in the deadman walls would require significant depth, and also conflict with planned surrounding construction activities.

External Wale and Deadman Anchor Shafts

The previous tieback and tie-rod options utilized one rod in each (reinforced) secondary secant pile. To reduce the complexity of threading so many rods between the surrounding drilled shafts, this option introduced external wale beams that allowed reducing the number of tie-rods by approximately half, which provided easier positioning around the surrounding drilled shafts. Instead of conventional wall-type deadmen, this option also introduced large-diameter drilled shafts as deadman anchors. These were required at greater depth, but installation would be easier and less disruptive.

Internal Temporary Wale Frame – Below the Top Slab

To eliminate the interference with surrounding construction activities and additional external elements of the previous three options, an alternative that utilized a conventional internal wale frame was developed. The wale frame would be located several feet below the top slab, allowing completion of the excavation, base slab, and top slab, after which the frame would be cut up and removed through openings in the top slab. The secant piles would be designed to have adequate structural capacity as a cantilever during excavation to the relatively shallow depth before the wale frame would be installed.

Internal Temporary Wale Frame – Above the Top Slab

To avoid the complexity of constructing the top slab falsework around the wale frame, a modified version of the previous option was devised that used a similar internal steel wale frame but located at an elevation above the top slab. This would utilize heavy steel W-shapes embedded vertically into the reinforced secondary secants, extended to carry the lateral load to the steel frame above. The construction sequence would be similar to that for the previous internal frame below the top slab, except that the top slab would be poured around the W-shape pile extensions, after which they would be cut off flush with the top slab, or in a shallow pocket that could be patched with grout to conceal them.

Top-Down Construction

Lastly, a concept using top-down construction was developed. The secants would be installed followed by the permanent top slab poured on prepared grade with a smooth formwork surface (such as plyform on grade) to provide the top support load path before commencing any excavation. Block-outs in the top slab sufficient to gain access with small excavation equipment (e.g. mini-excavators and skidloaders) would be left, but small enough to maintain adequate strength in the top slab to provide the required support to the secant pile walls. The excavation would then be performed below the top slab, after which the base slab would be poured, internal mechanical equipment installed, followed by infilling the top slab block-outs. The primary disadvantage of this method was the slower and more costly excavation process, necessitated by using small equipment and working below the top slab.

Selected Design Alternative

Due to the simplicity and minimal impact on surrounding construction activities, the top-down approach was the favored method by most of the construction team, including the general contractor, and was progressed to an initial design submittal. However, after submittal, the specialty mechanical equipment installer indicated that this method would not be compatible with installing their equipment inside the basement, as they required nearly the entire top slab to remain open until after their equipment was installed. This requirement also eliminated feasibility of both internally-braced options, as the required wale frame members could not be designed around the clear space required for equipment installation.

This required the design team to re-design and use an approach with an external means of support. The selected option for final design was a version of the third option, utilizing external tie-rods to deadman shafts, but with further refinement and optimization.

SUPPORT OF EXCAVATION DESIGN

Secant Pile Diameter Selection and Tolerances

Condon-Johnson's original bid utilized 3ft diameter shafts for the secant piles, installed using 900mm sectional casing. This was to match the drilled shaft foundations Condon-Johnson was also constructing on the project and allowed for shared drill tooling. This original approach also utilized a mid-height internal wale frame to reduce demands until the base slab was installed. When it became clear that internal bracing was not possible, and the concepts for a single level of support at the top of the secants were being developed (as described in the previous section), it became evident that the higher moments resulted in dense rebar cages and inefficient use of reinforcement. To increase the capacity of the shafts and reduce congestion to meet best practices for concrete placement, the secant piles were upsized to 1m diameter.

Secant pile placement tolerances were selected to be 1" plan location at ground surface and 1% maximum out-of-plumbness. The spacing between adjacent reinforced secondary secants in the shallower portion of the basement was set at 5'-0" (to provide approximately 9" of overlap between each primary and secondary), and at a closer 4'-6" (to provide approximately 12" of overlap) with piles in the deeper section, to ensure adequate overlap at the bottom of the excavation after placement tolerances.

Secant Pile Design

After the secant pile size and layout was established, design groups were identified, which included four basic pile types and corresponding design cross-sections. All walls were designed with reinforced secondary secant piles carrying the entire tributary load based on their spacing, with unreinforced primary piles acting only as lagging. All walls were required to carry some permanent vertical loading from the structure above, with some wall portions subjected to higher loads.

 © Deep Foundations Institute 2025

Since the secant piles acted as both temporary SOE and permanent basement structural walls, load cases were prepared that captured all conditions that would be encountered, from the beginning of construction through the service life of the structure. As boundary conditions varied throughout these periods, the applicable earth pressure theories varied as well. During construction, when piles were in a cantilever condition, active lateral earth pressure was used, and when temporary construction conditions utilized a support at the top of the wall, apparent earth pressure profiles were used. In the permanent condition, lateral earth pressures were taken as at-rest values, along with lateral seismic pressure and soil swell pressure. Lateral pressures from relevant surcharge loads were included as well, including from construction equipment.

Each secant pile design case was analyzed for all load and boundary conditions throughout its lifecycle, and the resulting demand envelopes (shear, moment, and axial) were used to design reinforcement that provided adequate capacity for all conditions. See Fig. 5 for an example.

Longitudinal (vertical) reinforcement was designed with conventional deformed Grade 60 reinforcement. Due to uncertainty in prompt availability of reinforcement for the project, a variety of bar options were analyzed, including #11, #14, and #18 bars. The final design provided options for both #11 and #18 bars, which required bundling bars in both cases to provide adequate clearance for concrete placement due to the ratio of reinforcement required in the highest-demand zones (See Fig 4). Some of the bundled longitudinal bars were terminated in lower-demand zones to economize steel and reduce congestion.

Transverse reinforcement was designed using Grade 80 spiral bars to minimize congestion. Typical pitch varied between 6 in. and 12 in., depending on location and corresponding shear demand.

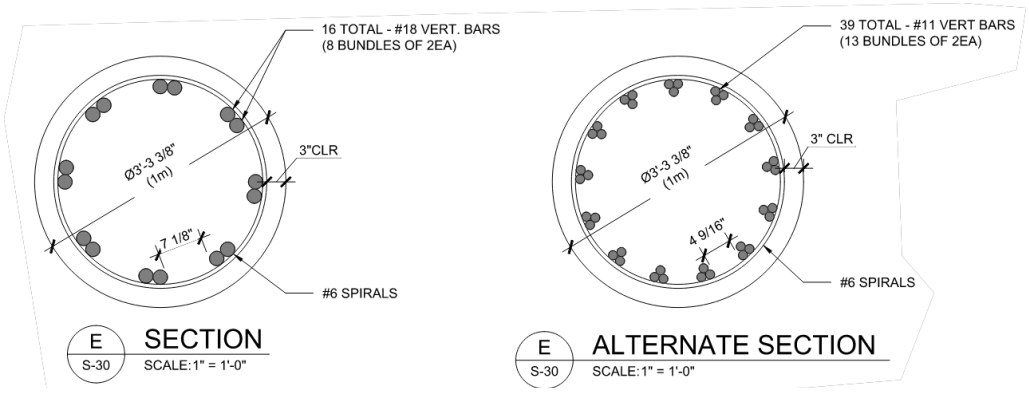


Fig. 4. Example Secant Pile Reinforcement Cross-Sections

Reinforced Concrete Wale Design

The design used external tie-rods at approximately every other reinforced secondary secant pile, requiring a wale beam. This was provided as a reinforced concrete beam integral with the top of the secant piles, just below the permanent top slab. The beam was designed to share the top 4'-0" height of the secant piles, with reinforcement detailed to pass through each other uninterrupted, as shown in Fig. 6.

The wale was designed for continuity around corners, which reduced the number of tie-rods near corners. To provide continuity and minimize differential wall deflection, it was also extended around the entire perimeter of the basement, including through the secant piles that were designed only as cantilevers.

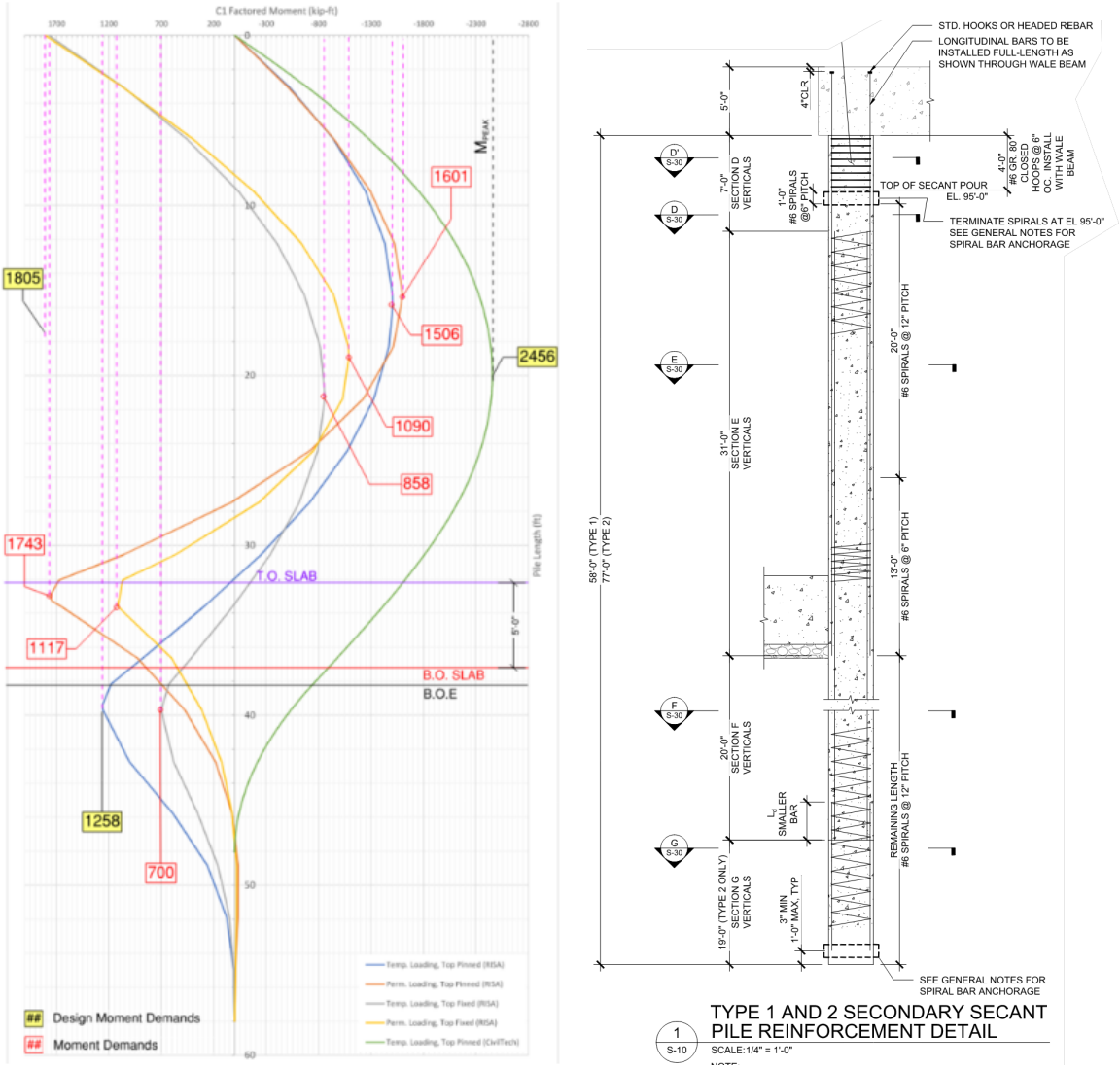


Fig. 5. Example Secant Pile Bending Moment Envelope and Reinforcement

Tie-Rods, Deadman Shafts and Anchor Points

On the east and west sides, the tie-rods supporting the wale beam were anchored by reinforced concrete deadman piles. These were 6 ft diameter drilled shafts, 50-ft deep. They were designed as laterally-loaded shafts and analyzed using LPile to determine their capacity at an acceptable deformation and structural demands for which their reinforcement was designed. They were offset from the secant pile walls

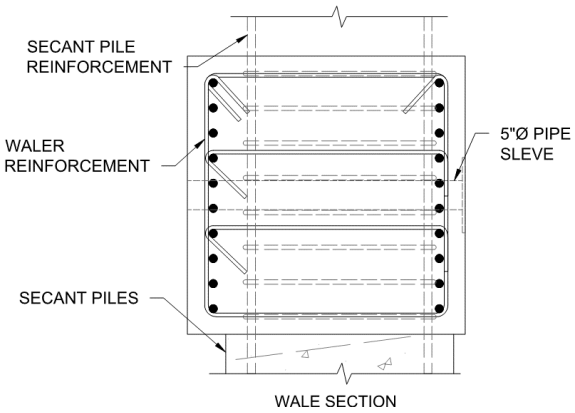


Fig. 6. Example Wale Beam Cross-Section

 © Deep Foundations Institute 2025

(80 ft) to ensure the full capacity could be mobilized. The tie-rods and tops of the deadman shafts were located at an elevation that avoided conflicts with surrounding future construction in the area, which permitted abandonment in place after they were no longer required.

On the south side of the secant pile basement structure, a large permanent reinforced concrete slab was located with a dense array of permanent drilled shafts. With approval from the permanent structure designer, this portion of the structure was utilized as an anchor, avoiding the use of temporary deadman shafts. Since the secant pile excavation was a schedule priority, the minimum required number of drilled shafts required was calculated, which permitted only a portion of the overall slab to be poured and reach strength before it could be utilized as an anchor. The tie-rods were located below the permanent slab and connected to the slab with a cast-in-place corbel secured to the bottom of the slab with reinforcement dowels. All tie-rods were proof-loaded and pretensioned to 250 kips. See Fig. 7.

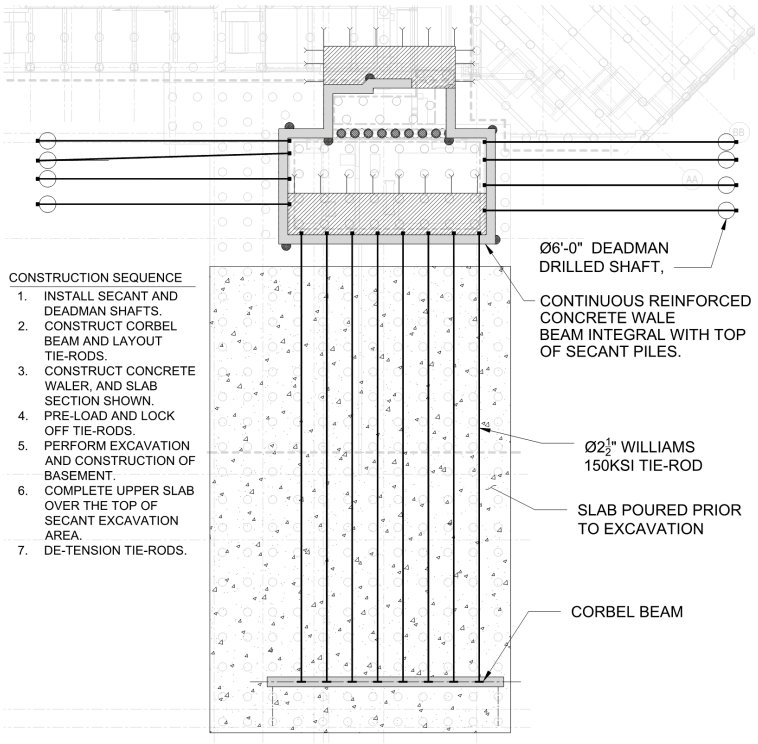


Fig. 7. Tie-Rod, Deadman Pile, and Anchor Beam Plan

CONSTRUCTION

Secant Pile Installation

A reinforced concrete guidewall was constructed prior to drilling the secant piles to ensure they were all located with the proper overlap. The guidewall also aided with the vertical alignment of the piles, particularly the secondaries when the casing was coring through the adjacent piles.



Fig. 8. Secant Pile Drilling

The consistent and uniform stiff clays on this site were ideal for open hole drilling. Condon-Johnson was able to install all primary piles in this manner, including depths near 80ft, with negligible groundwater. The secondary piles were installed using 1M sectional casing. This casing cored through the adjacent piles creating the interlock between the primary and secondary piles. The casing also aided in maintaining vertical alignment. The stiff clays on this project

 © Deep Foundations Institute 2025

allowed the casing to be removed prior to reinforcement and concrete placement, which greatly simplified the installation process and increased production rates. All concrete was placed using free fall methods. Both primary and secondary secant piles were poured only up to the bottom of the wale beam to allow its construction after the secants were complete. The transverse reinforcement in the top 4ft of the secants was designed with Grade 80 closed hoops that were installed with the wale beam rebar, rather than the continuous spirals used in the rest of the secant length below.

Deadman Drilled Shaft and Tie-Rod Installation

The deadman shafts were drilled using open hole drilling methods. For ease of tie-rod installation, a steel trumpet was installed in the reinforcement cage prior to shaft construction. Once these shafts were installed, and prior to all the wale beam reinforcement being placed, the tie-rods were installed. Shallow trenches were dug for each tie-rod between the wale and the deadman shafts and corbel beam. The tie-rods were connected at the deadman shafts and corbel beam and laid in the trench to within 4 ft of the back face of the wale. Leaving the tie-rods a few feet behind the wale ensured that the trumpets were correctly oriented and located within the wale, but eliminated the need to drill holes in the wale formwork. The tie-rods were encased in a PVC sleeve within the buried trench portion to allow free elongation during stressing and minimize disturbance to the surrounding soils during tensioning and detensioning.



Fig. 9. Tie-Rod Installation to Deadman Shafts



Fig. 10. Excavation at Final BOE

The tie-rods and corbel beam below the 5-ft thick on grade mat slab to the south were placed and constructed prior to the slab. After the deadman shafts on the east/west sides and corbel and anchor slab on the south had reached strength, the tie-rods were proof-loaded and locked-off at 250 kips. A week after locking-off the tie-rods, a lift off test was performed

 © Deep Foundations Institute 2025

on each tie-rod to determine if creep deflection of the deadman shafts or anchor slab was causing any decline in lock-off load. The results showed negligible decrease in lock-off loads.
After the remainder of construction within the basement area is complete, including cast-in-place lining, interior dividing walls, a mezzanine structure, and placement of mechanical equipment, the top slab over the secant excavation will be constructed on falsework. After it reaches strength, it will provide the permanent support at the top of the secant pile walls, so the tie-rods will no longer be necessary, at which they will be detensioned, cut off at the wale, and block-out holes in the final lining wall will be patched over them.

Construction Challenges and Solutions

The site was graded to the elevation of the bottom of the 5-ft thick mat slab. The secant reinforcement extended up into this mat slab, and secant reinforcement cages were spaced less than 5 ft on center. This prevented Condon-Johnson from utilizing an oscillator to extract the sectional casing during concrete placement without a substantial amount of cribbing. Fortunately, the favorable soil conditions allowed Condon-Johnson to overcome this issue by extracting the casing with the drill rig prior to reinforcement and concrete placement.

SUMMARY AND CONCLUSIONS

The basement area structural construction was completed in mid-June 2025, with permanent top slab complete and having reached design strength, at which time tie-rods were detensioned, leaving the structure in its permanent configuration. Detensioning went smoothly as planned.

This paper focuses on the innovative approaches used to design and construct the basement structure on the new Weapons Storage and Maintenance facility on Malmstrom Air Force Base, and how these approaches enabled efficient construction, despite a challenging schedule and physical constraints. By considering a wide variety of concepts at the beginning of the project, the design and construction team was able to identify the best methods and ultimately combine portions of multiple preliminary concepts to arrive at the best solution, even after unexpected new constraints were introduced. The selected design used a superimposed concrete wale beam to support the top of the secant piles, along with buried tie-rods and deadman drilled shafts, which was able to avoid all conflicts and impediments to the permanent construction, particularly the unique and challenging installation of the mechanical equipment within the basement area. Use of a portion of the permanent structure and foundations provided cost and schedule savings in lieu of installing additional temporary-use deadman anchor shafts. The careful planning and design allowed a smooth and successful construction process, and a system that performed as intended and met all project goals.

ACKNOWLEDGMENTS

Brierley and Condon-Johnson would like to acknowledge the contributions of the Walsh/Archer-Western Federal team, Army Corps of Engineers and Black & Veatch. The success of the project is due in large part to the strong communication channels between all parties on the project, and the results-oriented and collaborative attitude of the project team.

REFERENCES

- Sketches and figures by Brierley and Condon-Johnson

- Photos courtesy of Condon-Johnson and Archer-Western Federal/Walsh

 © Deep Foundations Institute 2025

NYCDOT BUILDS A BRIDGE UNDER A BRIDGE UNDER A BRIDGE IN BROOKLYN

Anthony Loreto, Underpinning & Foundation Skanska, Queens, New York, USA, 929-303-7287, anthony.loreto@skanska.com
Lisa Papandrea, PE, Underpinning & Foundation Skanska, Queens, New York, USA, 929-581-0394, lisa.papandrea@skanska.com

ABSTRACT

A roadway bridge in a residential Brooklyn neighborhood is an unlikely poster child for the complexity of New York City's dense web of infrastructure. However, the NYCDOT's reconstruction of the 5th Avenue Bridge in Bay Ridge, Brooklyn certainly fits the bill: micropiles, H piles, soldier piles, subways, railroads, a petroleum pipeline, an interstate highway viaduct… and about twenty feet of working headroom.

This case study addresses the load testing and construction of deep foundations that were employed to support the south integral abutment of the new roadway bridge, which will span 170 feet across active LIRR and NYCT subway tracks below and replace the existing 106-year-old bridge in its exact location. To maintain two-way traffic at all times, the foundations were constructed from underneath the existing bridge prior to its staged demolition. Working under 12 to 23 feet of headroom, eighteen (18) HP16x183 H-piles, twenty-four (24) 24-inch diameter pipe soldier piles, and thirty-eight (38) hollow-bar micropiles were installed up to 65 feet deep in dense sands.

Solutions employed to overcome the challenges of the confined environment without adversely impacting nearby sensitive infrastructure are presented, with particular focus on the H piles and the micropiles. The H piles were driven using a forklift-mounted hydraulic impact hammer and were dynamically load tested. For the micropiles, an alternative hollow-bar bond zone installation method was proposed by the pile subcontractor and subjected to a static load test program.

INTRODUCTION

The New York City Department of Transportation (NYCDOT) is reconstructing the Fifth Avenue vehicular bridge at 65th Street in Bay Ridge, Brooklyn. The existing Fifth Avenue bridge, first constructed in 1915 and last rehabilitated in 1962, will be replaced with a single-span integral abutment bridge. The bridge spans north-south approximately 170 feet over five active Metropolitan Transportation Authority (MTA) railroad lines: three Long Island Railroad (LIRR) tracks and two New York City Transit (NYCT) N Line tracks. Above the bridge spans another bridge: the Gowanus Expressway viaduct (Interstate Highway I-278), runs east-west approximately 19 feet above the southern half of the Fifth Avenue bridge. A general plan and elevation of the existing bridge are depicted in **Fig. 1** and **Fig. 2.**

To maintain two-way vehicular travel lanes and sidewalk on 65th Street and Fifth Avenue throughout the construction phase, the reconstruction was sequenced concurrently with the staged demolition of the existing structure. While the traffic plans allowed the north integral abutment to be constructed from street level, the south integral abutment had to be fully constructed from track level, below the existing bridge deck. Multiple types of deep foundation elements were constructed and load tested in these highly confined conditions. Methods utilized to overcome the site constraints proved successful and provided meaningful lessons for future applications.

 © Deep Foundations Institute 2025

SOUTH INTEGRAL ABUTMENT OVERVIEW

The contract documents included a boring location plan, geologic section and corresponding boring logs. The subsurface at the proposed south integral abutment consists of 20 feet of silty sand over 60 feet of gravelly sand with some silt, as shown in **Fig. 2**. The silty sand layer has an average SPT N-value of 20 blows per foot. The gravelly sand layer has an average SPT N-value of 30 blows per foot, with noted nested cobbles and locations of roller bit refusal in the geotechnical borings. Groundwater information was not provided in the contract documents but is estimated to be approximately 40 feet below track level grade, based on public data.

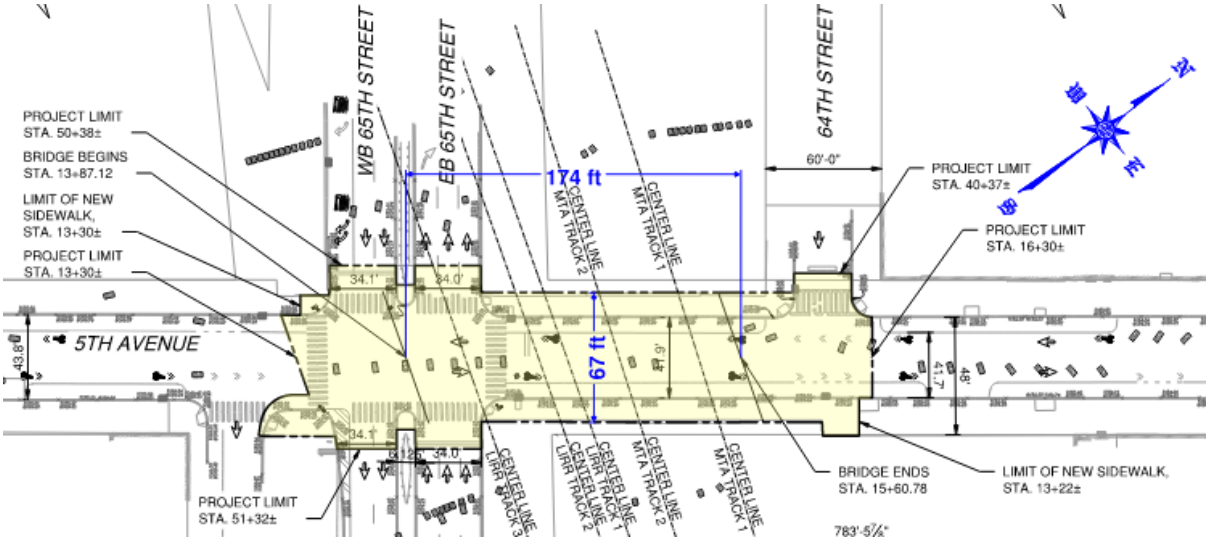


Fig. 1. General Plan of 5th Avenue Bridge

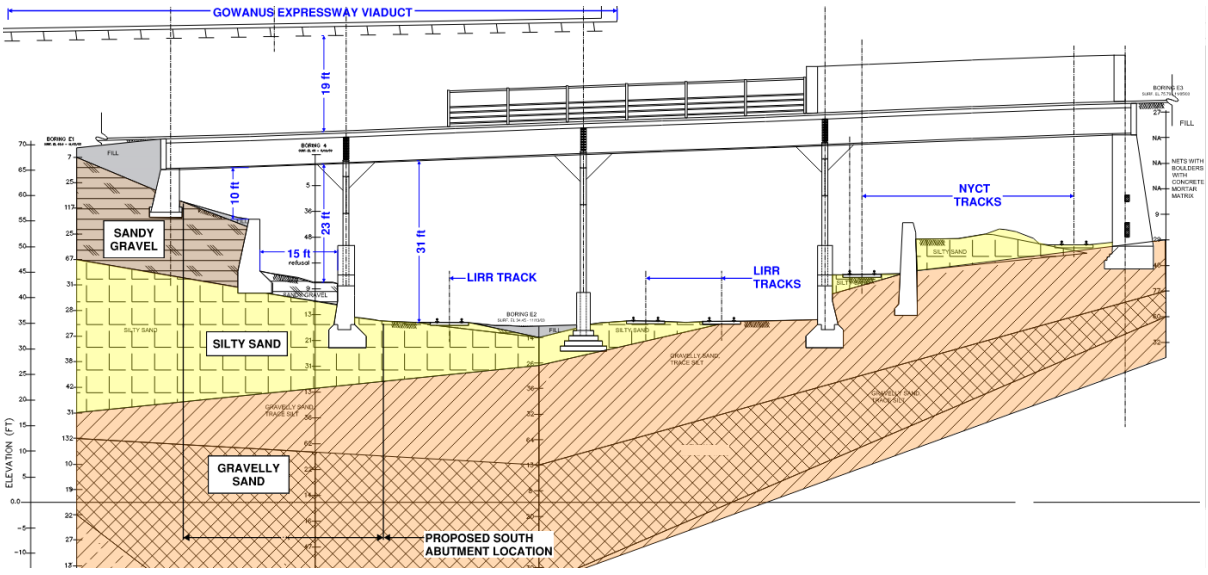


Fig. 2. Existing 5th Avenue Bridge Elevation (looking west)

The contract design for the south integral abutment foundations included three types of deep foundation elements, as shown in **Fig. 3**: driven HP16x183 steel piles to support the integral abutment stem, drilled 12.75” diameter micropiles to support the abutment wingwalls, and drilled 24” diameter by 1” thick pipe

 © Deep Foundations Institute 2025

soldier piles to retain the backfill around the abutment piles. Piles were located to clear the existing south abutment gravity walls, bridge piers and Gowanus Expressway viaduct column foundations, consisting of battered timber pile groups. The soil design parameters used for the proposed foundation design were not provided in the contract documents.

As shown in the section in **Fig. 3**, the H-piles and soldier piles are located within the 15-ft wide "mezzanine" level between an existing bridge pier and an existing gravity wall, with about 23 feet of headroom. The wingwall micropiles are located partially on the "mezzanine" level and partially on the "balcony" level, with about 12 feet of headroom.

Equipment and material deliveries were limited to one access point on 64th Street and Fourth Avenue, across the multitude of railroad tracks and one avenue (approximately 1000 feet) west of the south abutment site.

Upon award, the contractor considered various enabling works, alternative designs, and alternative means and methods to overcome the confined conditions. An option to install the piles from the existing bridge deck (although still limited by the Gowanus Expressway viaduct deck above) was abandoned due to its impact on the traffic plans. Underpinning the existing south abutment and gravity wall was considered in order to excavate and create more headroom, but did not offer enough headroom to be viable. Drilled piles in lieu of H piles were evaluated, but could not provide the relative high flexural strength and corresponding low flexural rigidity required for an integral abutment. Ultimately, means and methods were selected to perform the work with minimal enabling works and thus minimal disturbance to surrounding structures and foundations.

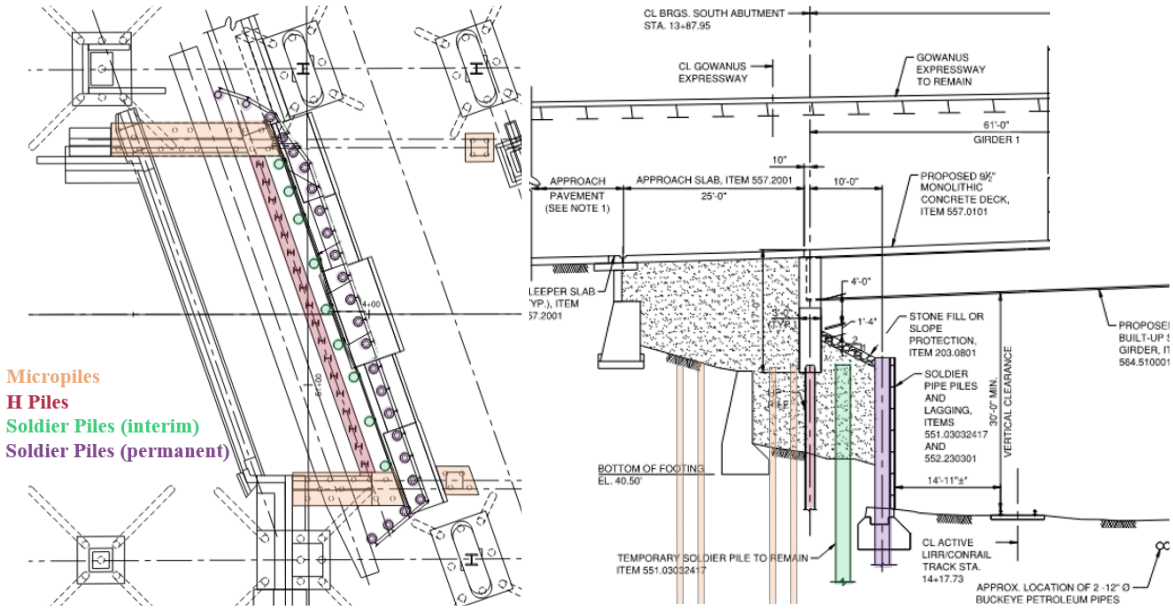


Fig. 3. South Abutment Foundation Plan and Section (looking west)

MICROPILE DESIGN AND LOAD TESTING

The factored axial compression loads for the micropiles were 80 kips factored axial compression (145 kips nominal resistance) at the west wingwall and 60 kips (110 kips nominal resistance) at the east wingwall.

 © Deep Foundations Institute 2025

Design criteria also included 30 kips factored uplift and 20 kips nominal lateral resistance. The contract design was a 45-ft cased length with 12.75” outside diameter by 0.5” thick steel casing, and a gravity-grouted (Type A) bond length with a full-length #14 Grade 75 center reinforcing threaded bar and 8,000 psi grout. The specified bond lengths were 25 feet at the west wingwall and 20 feet at the east wingwall. Two static compression load tests were required, one in the vicinity of each wingwall, on non-production piles.

An alternative hollow bar (Type E) bond zone design was proposed by the contractor and accepted by NYCDOT. While the hollow bar system typically has higher material costs than conventional micropiles, it was well suited for the site’s subsurface conditions and space constraints.

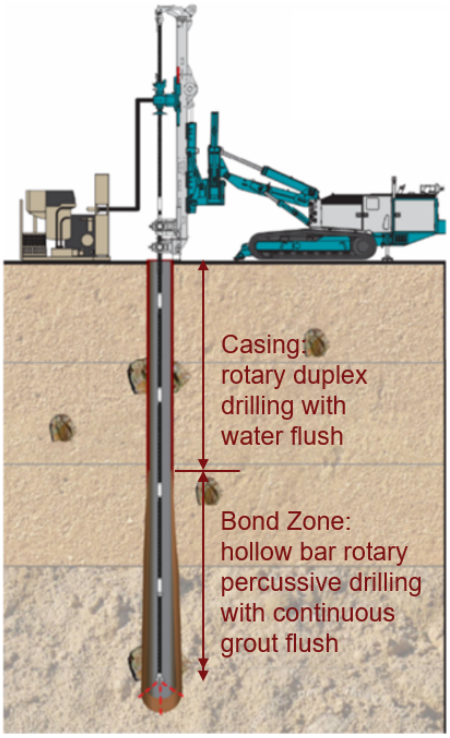
To construct the specified Type A bond zone in soil, the casing must first be advanced to the tip of the bond zone to keep the borehole stabilized. Then, the cased borehole is filled with grout and the casing is slowly withdrawn to the top of the bond zone. The above-grade section of casing is then removed and the central reinforcing bar is set into the fluid grout.

For a Type E bond zone, depicted in **Fig. 4**, a threaded hollow-core steel bar with a sacrificial drill bit is advanced to the tip of the bond zone with continuous pressurized grout injection through ports in the drill bit. The bar is advanced by rotary percussion using a top hammer (also called a drifter). The grout injection serves to flush drill cuttings, to stabilize the borehole, and to scour and penetrate the surrounding soil for bond strength. The hollow bar and grout constitute the final structural elements of the pile’s bond zone. Prior to the hollow bar bond zone construction, the permanent casing is installed to the top of the bond zone.

By eliminating the need to extract temporary casing, a relatively smaller drill rig could be used, making the micropile constructible with only 12 feet of headroom. Risk of the casing getting stuck due to binding with nested cobbles was eliminated, as well as the risk of grout setting during withdrawal and removal of the segmental casing sections, prior to placement of the center bar. Additionally, the hollow bar drilling system has the ability to advance through cobbles and boulders without requiring any retooling, or use of an air-powered downhole hammer. Since grout is used as the drill fluid instead of water or air, the hollow bar system mitigates the potential for ground disturbance and voids.

The alternative hollow bar design consisted of a 76 mm (3 inch) outer diameter by 51 mm (2 inch) inside diameter hollow bar (minimum yield stress 78 ksi) with 5,000 psi grout. The permanent casing remained the same as the original design to provide equivalent flexural strength and stiffness. The effective diameter of a hollow bar bond zone is dependent on the soil properties, the diameter of the sacrificial drill bit, and the hollow bar advancement rate during installation. To maintain the same bond lengths as the contract design, an 8” diameter cross-cut drill bit was selected. For medium dense sands with some silt and gravel, a design bond zone diameter of 1.5 times the drill bit, or 12 inches, was assumed, in accordance with AASHTO guidelines. The design micropile cross sections are shown in **Fig. 5**.

 © Deep Foundations Institute 2025



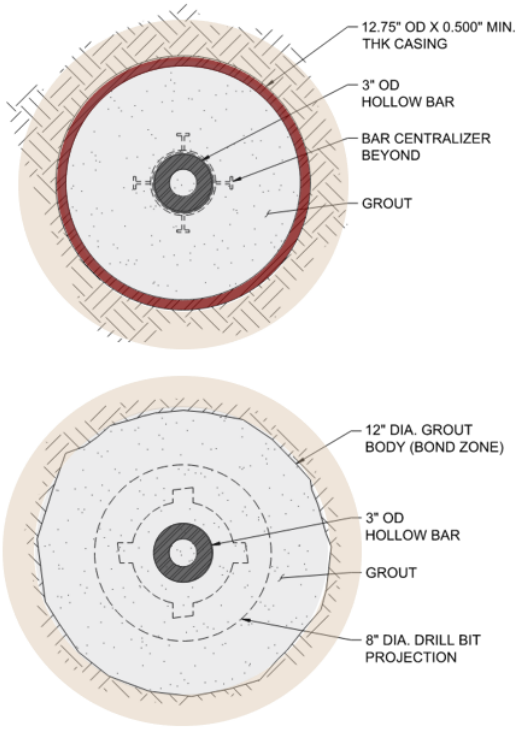


Fig. 4 (Left). Type E Micropile schematic section
Fig. 5 (Right). Design cased length (Top) and bond zone (Bottom) cross-sections

Prior to commencement of production micropiles, two non-production static load tests were successfully performed. The first load test, at the east wingwall, was a static compression load test with nonproduction reaction piles. In accordance with NYCDOT standard specifications, the pile was tested to 4 times the design load (4 x 60 kips = 240 kips). For the second load test, at the west wingwall, space constraints and nearby existing bridge substructures limited the available footprint for sacrificial reaction piles. Therefore, the contractor proposed an uplift test in lieu of a compression test, testing to 2.5 times the design load (2.5 x 80 kips = 200 kips) to minimize the ground bearing pressure from the test behind existing gravity retaining walls. A comparison of the bond length parameters and nominal resistances of the contract design, the alternative final design, and the load test results are presented in **Table 1**. Note that neither load test resulted in failure of the test pile or significant pile top displacement, therefore the actual ultimate grout-to-ground resistance of the test piles is undetermined. For reference, the typical range of nominal grout-to-ground bond resistance provided in AASHTO for Type E bond zone in medium-very dense sand is 2.5 ksf to 7.5 ksf.

 © Deep Foundations Institute 2025

Table 1. Bond Zone Design Parameters and Load Test Data

	Contract Design	Alternate Design	Alternate Design Load Test Results	
	Type A Bond Zone (Gravity-Grouted)	**Type E Bond Zone (Hollow Bar System)**	**Load Test 1 (Uplift Test)**	**Load Test 2 (Compression Test)**
Grout-to-Ground Resistance	2.0 ksf[1]	2.5 ksf[1]	2.5 ksf[2]	3.8 ksf[2]
Bond Zone Diameter	11.82 inches	12 inches	12 inches (assumed)	12 inches (assumed)
Bond Length	25 feet	25 feet	25 feet	20 feet
Nominal Bond Zone Resistance	157 kips	196 kips	200 kips (test load)	240 kips (test load)
Net Displacement	-	-	0.08 inches (uplift)	0.05 inches (settlement)

1. Lower-Bound Presumptive Nominal Grout-to-Ground Bond for Preliminary Micropile Design, for Sand (some silt, gravel; fine-coarse, medium-very dense) [reference: AASHTO Table C10.9.3.5.2-1].
2. Calculated from the maximum test load.

MICROPILE CONSTRUCTION

Micropile installation took place across multiple work platforms with varying elevations, requiring strategic planning of logistics, equipment staging, and execution methods to ensure smooth operations and quality assurance.

As shown in **Fig. 3**, all micropile drilling occurred below the existing Fifth Avenue Bridge deck within close proximity to the existing gravity wall abutment foundations, pier wall footings, and Gowanus Expressway battered pile-supported column foundations. To avoid undermining these existing substructures, minimal changes to the existing grade elevations were made. Therefore, the wingwall micropiles closest to the existing bridge abutment were drilled with 12 feet of headroom, the remaining wingwall micropiles were drilled from the “mezzanine” area with 23 feet of headroom, and micropiles for two temporary column foundations were drilled from track level, between railroad tracks, with 31 feet of headroom. Because of the extremely confined conditions under the bridge, the grout plant required for drilling the hollow bar system was set on top of the Fifth Avenue Bridge deck, directly above the drilling site. This layout required close coordination between grout delivery operations and drilling crews to maintain continuous production. Additionally, once the drill rig was mobilized to the drilling site, there was insufficient space to feed additional drilling equipment to the operation. Therefore, all drilling tools, casing, and support materials must be staged to the drill rig upon setting up on the pile location.

Two dedicated rigs were utilized to streamline micropile installation. Both were Comacchio 8D drill rigs designed for limited access sites with removable power units and telescopic masts. One rig was tooled for rotary drilling to advance the 12.75-inch steel casing to the design casing tip elevation using duplex rotary drilling with internal water flush to remove the soils from inside the casing (**Fig. 6**). The second rig was fitted with a drifter head to advance the 76 mm hollow bar beyond the tip of the casing and to the design tip of the bond zone via rotary percussive drilling with continuous grout injection (**Fig. 7**). This two-rig system reduced downtime by allowing work to continue seamlessly between casing installation and hollow bar drilling without the need to modify rig configurations mid-process. In some areas, it also allowed for

 © Deep Foundations Institute 2025

several micropile casings to be drilled in succession, followed by the respective hollow bar installations, minimizing the required moves of the rigs.

Depending on the headroom at each location, micropile casings were drilled in either 5-foot sections or 2.5-foot sections, with threaded joints flush with the casing outside diameter. For micropiles where casing threaded joints were located with the upper 3 feet of the micropile, a 9-inch outer diameter by 0.5-inch thick, 8-foot long steel pipe was set inside the grouted annulus between the outer casing and hollow bar after completion of grouting. This inner pipe provided supplemental flexural reinforcement at the top of the pile, to offset the reduction in flexural capacity at the threaded joint locations.





Fig. 6 (Left). Comacchio 8D with rotary head installing casing.
Fig. 7 (Right). Comacchio 8D with drifter head installing hollow bar.

The hollow bar system proved a suitable bond zone construction method for the site constraints and soil conditions. After the casing is installed and cleaned out to the design casing tip elevation at 45-feet depth, the hollow bar, fitted at the tip with an 8-inch diameter cross-cut drill bit with grout injection ports, is lowered into the cased borehole. The hollow bar is installed in 5-ft long sections and connected with full-strength couplers as each section is lowered into the borehole. The hollow bar then advances beyond the casing tip to construct the bond zone with continuous grout injection and rotary percussive force delivered by the rig's drifter head. After reaching the design bond zone tip, grout injection continues until clean, rich grout is observed flowing from the top of the pile, to verify that all cuttings and spoils were successfully removed from the borehole. Grout cube samples were taken both at the grout plant and at the return grout at top of pile to confirm that the design grout mix's specific gravity and strength were obtained.

Advantages of the hollow bar method included: ability to penetrate through natural obstructions such as nested cobbles and boulders, elimination of the requirement of installing casing temporarily to the tip of the bond zone and extracting the casing to the top of the bond zone after grouting, and minimal disturbance of surrounding soils and foundations due to borehole stabilization with continuous grout injection. One

 © Deep Foundations Institute 2025

challenge of the hollow bar method, particularly for a confined work site, was spoils management, which required construction of temporary shallow trenches to divert grout and spoils away from the borehole and away from active railroad tracks. Another challenge was management of grout deliveries and grout mix workability, since it was essential to have enough grout batched to complete a pile once hollow bar drilling commences, and it was essential that the grout maintain workability until completion of the bond zone. The quantity of grout required varied for each pile location, since continuous grout injection was required throughout the drilling process, and the drilling duration would increase if an obstruction or hard drilling was encountered. Grout consumption varied from 1.5 to 4.5 times the theoretical pile volume (2.7 times on average).

H PILE DESIGN CRITERIA AND EQUIPMENT SELECTION

The deep foundations for the south integral abutment stem consisted of eighteen (18) HP16x183 ASTM A709 Grade HPS 70W (70 ksi minimum yield stress) driven piles with a nominal geotechnical compression capacity of 250 kips. To achieve this capacity, the design estimated a pile length of 60 feet, with one production pile specified for dynamic testing with a pile driver analyzer (PDA) in accordance with ASTM 04945 to establish pile driving criteria. The pile layout is shown in **Fig. 8**. Given the known headroom constraints, the contract design specified a complete-joint penetration welded splice detail along the HP16 flanges and web, as shown in **Fig. 9**. Pile cutoff elevation was approximately 10 feet above existing grade, therefore the pile was to be driven to about 50 feet penetration. As per integral abutment design guidelines in NYCDOT's Bridge Design Manual, the webs of the piles were oriented parallel to the centerline of the bridge superstructure beams, so that primary bending takes place about the strong-axis of the pile.

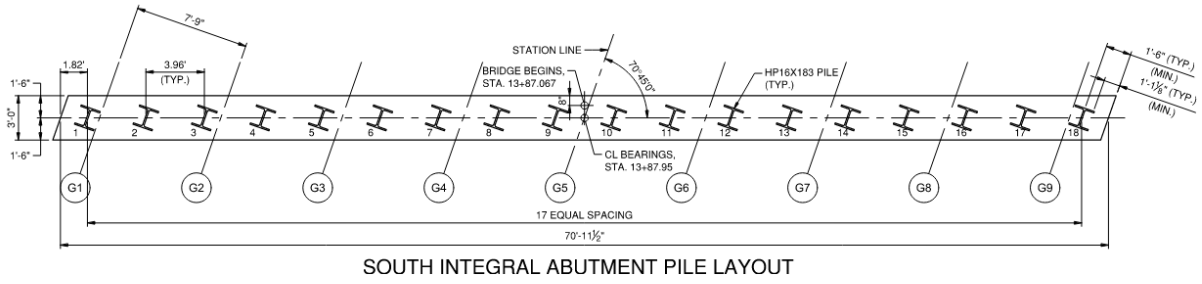


Fig. 8. South Integral Abutment Pile Layout

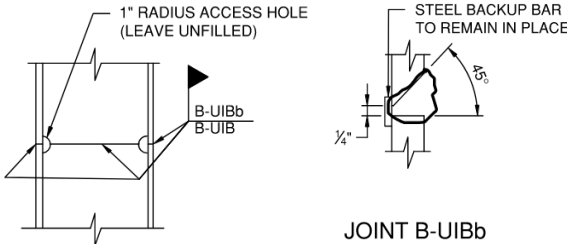


Fig. 9. Pile Splice Details

The overarching challenge was to find an impact hammer with enough energy to drive such a heavy pile through 50 feet of dense sand while still being compact enough to fit and operate within the 15-foot wide by 23-foot high work zone. Wave Equation (WEAP) Analyses using GRLWEAP14 software were performed to evaluate the suitability of several hammers, including both hydraulic impact hammers and

 © Deep Foundations Institute 2025

vibratory hammers. In the case of the vibratory hammer, it would be used to penetrate the initial 40 feet, then an impact hammer would be used for the final drive in order to properly measure penetration resistance.

Although it was predicted that a vibratory hammer could drive the pile sections in significantly less time than an impact hammer, the small site made the use of multiple hammers impractical. Initial WEAP analyses concluded that an APE 7-3 low-headroom hydraulic impact hammer (rated energy 42,000 ft-lbs) could deliver adequate energy to drive the pile through the dense sand stratum. The contractor ultimately selected the APE 8-3 low-headroom hydraulic impact hammer (rated energy 48,000 ft-lbs) to provide more flexibility in case a denser soil matrix was encountered. For the selected APE 8-3 hammer, the final WEAP analyses estimated that for a hammer drop height of 2 feet and penetration depth of 50 feet, a penetration resistance of approximately 18 blows per foot correlates to approximately 250 kips nominal capacity, with 23 kip-ft transferred energy. H pile models with 50% soil plug and 0% soil plug were evaluated, with both models rendering comparable results.

Given the hammer size and the headroom limitations, each pile had to be driven in approximately 10-ft sections, therefore requiring five complete-joint penetration welds. Considering a welded joint thickness of 1.13 inches (i.e., the flange and web thickness of the HP16x183) and providing time for requisite ultrasonic testing of the weld, it was initially estimated that a single welded splice would take on the order of 3 hours with one welder. Therefore, it was critical to develop a logistics plan that allowed for piledriving to continue while welding was in progress on other pile sections.

H PILE CONSTRUCTION

The H piles were located within the 15-feet wide “mezzanine” level underneath the existing bridge deck, bounded on the north and south by existing shallowly founded bridge retaining walls. Due to site topography and the various substructures from the Fifth Avenue Bridge and Gowanus Expressway viaduct, installation equipment such as pile drivers and excavators could only enter and exit the “mezzanine” from the eastern side of the existing bridge. The selected low-headroom hydraulic impact hammer needed to be mounted to equipment capable of maneuvering through this narrow, one-way alley.

Mounting the hammer on a conventional piledriving rig or excavator was not feasible with the space constraints, so the hammer was mounted to a forklift. The Kalmar DCE 150-6 Forklift (with an operating weight of 33,000 lbs and total width of 8.3 feet) was selected and fitted with custom leads to support the 22,500-lb hammer, as shown in **Fig. 10** and **Fig. 11**.

Prior to the start of the H-pile installation, the team constructed temporary engineered sheeted pits at each pile location, 10 feet deep and 4 feet square, as shown in **Fig. 12**. To protect and maintain the existing concrete gravity wall adjacent to the pile locations, the sheeted pits were constructed in sequence similar to conventional concrete underpinning pits, where every other pit was backfilled with lean concrete with a cylindrical opening in the middle to receive the pile. The primary benefit of the “starter pit” was that it allowed the team to use a 20-foot long pile starter section set into the pit, thus eliminating a time-consuming full penetration welded splice. Another benefit was that any shallow obstructions that may impede piledriving were removed during the pre-excavation for the starter pits, which mitigated potential deviations from the design plan location and orientation of the piles. The effect of the starter pit on the overall pile penetration resistance at end of drive was concluded to be negligible based on revised WEAP analyses.

 © Deep Foundations Institute 2025

After the starter section was driven to working grade with the forklift-mounted hammer, the next 10-foot section was set on top with an excavator, where typically two welders worked concurrently to complete the full penetration welded splice. Once the weld was inspected and approved, the forklift-mounted hammer positioned onto the pile to continue driving. Each pile was driven to the design estimated penetration without any major obstructions or issues with the hammer setup.





Fig. 10 (Left). The Kalmar DCE 150-6 Forklift with APE 8-3 Hydraulic Impact Hammer
Fig. 11 (Right). Driving an H-pile (looking east)

 © Deep Foundations Institute 2025

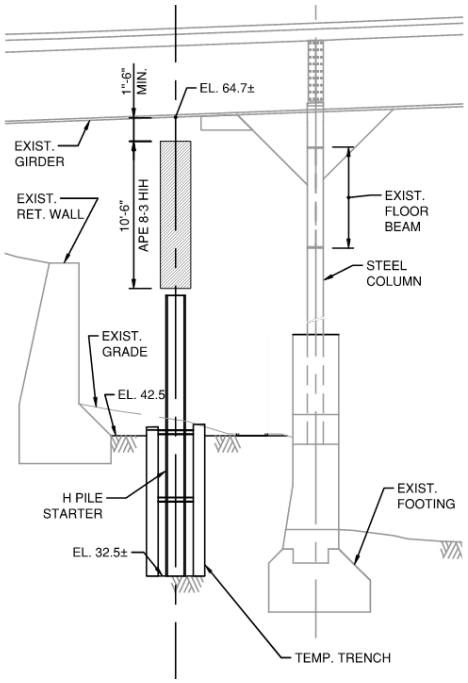


Fig. 12. Section (looking west) of starter pile section in temporary trench

H PILE DYNAMIC TESTING

The contract design specified that one production pile shall be driven with dynamic testing using PDA, with one restrike after 24 hours. However, the mobilized Case Method capacity of the first pile (S18) on initial drive, driven to the estimated tip elevation at 14 blows per foot (bpf), was only 203 kips compared to the 250 kips required nominal capacity. An additional 5-foot section was welded to the pile and the pile was driven deeper on the following day to 16 bpf, but the resulting Case Method capacity was unchanged and the computed CAPWAP capacity was only 154 kips. Rather than continuing to extend and drive the pile, which would require significant time to weld the splices and significant additional material costs, the project team decided to wait for potential soil setup before performing the next restrike. Restrike 1 was performed one day after the first restrike, resulting in a Case Method and CAPWAP capacity of 225 kips and 196 kips respectively. Restrike 2 was performed 13 days after the first restrike, in which the required nominal capacity was exceeded (262 kips Case Method capacity, 255 kips CAPWAP capacity).

During the setup period for the first pile, additional piles were driven to the estimated design tip, all with PDA on initial drive, with varying results. Piles S1 through S8, S10 and S16 exceeded the nominal capacity at end of initial drive. The remaining piles (S9, S11 through S15, and S17) reached capacity on restrikes ranging from 3 days to 20 days after initial drive. The variation in the PDA data and the indication of soil setup were unexpected given the similar penetration resistances and similar subsurface conditions based on geotechnical borings. Additionally, significant soil setup was not anticipated given the low silt content in the gravelly sand stratum.

Most likely, the PDA data was not representative of the actual geotechnical capacity of the piles due to issues related to the confined work site: the forklift-mounted hammer, unable to rotate, could not align with the orientation or as-driven verticality of the H Piles, making it impossible to guarantee concentric impact of the piles with the hammer. Additionally, some piles were driven with short follower sections since pile

 © Deep Foundations Institute 2025

sections needed to be driven low enough for the forklift to traverse over, resulting in a likely loss of energy during transfer from hammer to follower to pile. As an additional verification, a refined WEAP analysis was performed, which used the PDA data to calibrate the WEAP model and better correlate penetration resistance (bpf) with capacity, resulting in 14 bpf for 250 kips nominal geotechnical capacity. **Table 2** shows the Case Method capacity, CAPWAP capacity and Refined WEAP analysis capacity determined for each pile.

Table 2. Summary of HP16x183 PDA data and derived capacities.

Pile No.	Penetration Depth (feet)	Penetration Resistance (BPI) (BPF)	Mobilized Case Method Capacity Estimate, RX7 JC=0.7 (kips)	Mobilized Case Method Capacity Estimate, RX9 JC=0.9 (kips)	Refined WEAP Estimated Capacity (kips)	CAPWAP CAPACITY		
						Shaft (kips)	Toe (kips)	Total (kips)
S1	48.0	2 Blows / 1" 24 BPF	323	312	350+	-		
S2	48.0	2 Blows / 0.5" 48 BPF	383	321	350+	-		
S3	48.0	2 Blows / 0.5" 48 BPF	307	303	350+	-		
S4	48.1	2 Blows / 1" 24 BPF	309	292	350+	-		
S5	48.1	2 Blows / 1" 24 BPF	303	303	350+	-		
S6	48.1	2 Blows / 1" 24 BPF	264	257	350+	-		
S7	48.0	2 Blows / 1" 24 BPF	269	267	350+	-		
S8	48.0	1 Blow / 0.5" 24 BPF	307	302	350+	-		
S9	48.0	2 Blow / 1.75" 14 BPF	283	260	250	-		
S10	48.0	1 Blow / 0.5" 24 BPF	256	250	350+	-		
S11	48.0	1 Blow / 0.75" 16 BPF	306	303	280	-		
S12 (EOID)	46.0	13 BPF	105	105	160	-		
S12 (BORS)	46.1	1 Blow / 0.5" 24 BPF	301	291	350+	-		
S13	48.4	1 Blow / 1" 12 BPF	351	329	220	-		
S14	48.6	1 Blow / 1" 12 BPF	273	260	220	170	80	250
S15 (EOID)	48.0	16 BPF	191	191	200	114	74	188
S15 (BORS)	48.1	2 Blow /1.5" 16 BPF	274	265	280	-		
S16	48.0	3 Blow / 1.5" 24 BPF	274	274	350+	-		
S17	48.7	3 Blow /3" 12 BPF	260	259	220	180	72	252
S18 (EOID)	51.0	16 BPF	206	196	200	115	39	154
S18 (BORS)	52.1	4 Blows / 1.75"	258	254	350+	140	118	258

CONCLUSION

All driven and drilled piles for the Fifth Avenue Bridge south integral abutment were completed within the project schedule and without exceeding any threshold vibratory or deformation values for adjacent infrastructure. During pre-construction, meticulous logistical planning and engineering were performed to ensure appropriate equipment and installation methods were selected. During construction, a coordinated effort and communication between the contractor's team and the owner's team made it possible to quickly adapt to unforeseen conditions and implement proposed optimizations. The work is a representative case study of deep foundation installation in extremely confined urban sites.

The hollow bar micropile alternative proved effective and safe within the site constraints, and additionally provided increased geotechnical capacity compared to the gravity-grouted bond zone specified in the original design. It also offered increased risk mitigation compared to conventional pressure-grouted bond zones, as installation and extraction of temporary casing to the bond zone tip is not required and formation

of voids is less likely since the borehole is stabilized by continuous grout injection. For similar projects, hollow bar micropiles should be considered in the design phase so that shorter bond lengths and the resulting potential cost and schedule savings can be realized.

The driven H pile operation was also a lesson regarding pile installation in confined spaces. Although the selected equipment was suitable for the site constraints, geotechnical conditions, and pile size, it was an unexpected challenge to collect reliable PDA data and verify that the piles met the design requirements. Although not typically cost-effective on the average site, perhaps a static load test in lieu of PDA would have been a more reliable and less time-consuming option. Alternatively, by understanding the mobility limitations of a forklift-mounted hammer, certain measures should be taken for future projects with PDA such as measuring the verticality of the pile to be struck to account for eccentricity, or designing a follower to use for all piles and to instrument the follower and pile to measure the energy transfer.

REFERENCES

AASHTO (American Association of State Highway and Transportation Officials). (2017) *AASHTO LRFD Bridge Design Specifications*, Publication Code LRFD-8. AASHTO, Washington, D.C.

Brooklyn Public Library. (1914). “Looking southeast from 64th St. showing reconstruction of 5th Ave. bridge [picture].” <https://catalog.brooklynpubliclibrary.org/record=b114919 26>

DeJesus, Jaime. “DOT previews 65th Street bridge reconstruction.” *Brooklyn Reporter*, <https://brooklynreporter.com/2021/03/dot-previews-65th-street-bridge-reconstruction/> (March 4, 2021).

Ischebeck USA Inc. (2019). *Titan Micropiles Design and Construction*. Naples, FL.

Sabatini, Paul J., Burak Tanyu, Tom Armour, Paul Groneck, and James Keeley. (2005). *Micropile Design and Construction (Reference Manual for NHI Course 132078)*. National Highway Institute, Federal Highway Administration, U.S. Department of Transportation. Report No. FHWA-NHI-05-039. Washington, D.C.

State of New York Department of Transportation Geotechnical Engineering Bureau. (2020). *Geotechnical Control Procedure: Static Pile Compressive Load Test Manual*, GCP-18. Revision #5.

New York State Department of Transportation. (2021). *Bridge Manual*.

 © Deep Foundations Institute 2025

RISK-BASED ANALYSIS OF THE LOAD-BEARING CAPACITY OF CONTINUOUS FLIGHT AUGER (CFA) PILES

David A. Cabral , Author , Flavia S. Cabral, Co-author, REDAV Company, Rio de Janeiro, Rio de Janeiro, Brazil,

ABSTRACT

The allowable load of a pile is influenced by soil characteristics, structural requirements, and foundation-related risks. In deep foundations, such as piles, accurate estimation of both the allowable load and pile length is critical, as these parameters directly affect construction costs and structural safety. This paper presents a comparative analysis of two allowable load assumptions for continuous flight auger (CFA) piles with a 50 cm diameter. The discussion emphasizes the importance of balancing safety and cost-effectiveness in foundation design, considering both direct construction expenses and the financial impact of geotechnical risk.

Keywords: risk analysis, bearing capacity, continuous flight auger pile, geotechnical design, foundation engineering

INTRODUCTION

The allowable load of a pile must be defined based on the specific conditions of each project. Key influencing factors include:

- Local soil characteristics;
- Structural configuration and load requirements;
- Foundation risk level;
- The vulnerability of the structure to foundation-related failures.

A foundation is considered statically stable when applied loads (S) are lower than the available resistances (R). Instability arises when loading exceeds resistance or when displacements surpass serviceability limits. Therefore, the estimation of foundation resistance and allowable load is a critical step in geotechnical design and dimensioning of the foundation elements.

In the context of deep foundations, the design process typically involves estimating the allowable load (P_{adm}) and the optimal pile length (L). The interaction between Padm and L has a significant impact on the final design, influencing both the financial and safety aspects of the project.

Allowable load is commonly calculated by dividing the ultimate bearing capacity by an appropriate factor of safety. As such, conservative or aggressive assumptions directly affect pile length and cost.

This study analyzes two scenarios for a CFA pile with a diameter of 50 cm:

- **Scenario 1**: Traditional allowable load of 800 kN;
- **Scenario 2**: Higher allowable load of 1,200 kN.

The ideal solution is the one that minimizes total cost, accounting for both the direct cost of pile installation and the financial implications of potential structural failure.

 © Deep Foundations Institute 2025

METHODOLOGY

This study investigates the optimal relationship between Allowable Load (P_{adm}) and Ideal Pile Length (L_{ideal}) from a risk analysis perspective, assessing its impact on the overall safety of the foundation system.

The analysis focuses on a continuous flight auger (CFA) pile with a diameter of 50 cm, considering two different design load scenarios:

- Scenario 1 – Sk_1 = 800.00 kN
- Scenario 2 – Sk_2 = 1,200.00 kN

The ideal pile length is defined as the depth at which the pile reaches a competent bearing stratum capable of supporting the allowable load, accounting for pile-soil interaction, wich is the resistance surface.

To evaluate average pile resistance, the analysis considers a variation of ±1.00 m around the depth at which the pile achieves a safety factor of 2.00. This approach reflects the influence of geotechnical variability on foundation performance and risk.

The pile's load-bearing capacity is estimated using the semi-empirical method developed by Cabral (1986). This method has been calibrated through static load testing, ensuring the reliability of the predicted values.

LOAD CAPACITY – CABRAL'S PROPOSED METHOD (1986)

The method proposed by Cabral (1986) for estimating pile capacity is based on in-situ Standard Penetration Tests (SPT). In this method, soil properties are inferred from the SPT N-values, which represent the soil's resistance to the penetration of a standard sampler.

The total ultimate load capacity (Q_{ult}) is calculated as the sum of two components: the shaft resistance and the tip resistance, as shown in Equation 1 and illustrated in Fig. 1.

$$Q_{ult} = Q_{l,ult} + Q_{p,ult} \quad [1]$$

Where:

- Q_{ult} = Ultimate load capacity
- $Q_{l,ult}$ = Shaft (skin) resistance at failure
- $Q_{p,ult}$ = Tip (base) resistance at failure

This formulation allows for a comprehensive estimation of pile capacity, reflecting both frictional resistance along the pile shaft and end-bearing resistance at the pile tip. The method is particularly suitable for CFA piles in stratified soils where SPT profiles provide reliable input data.

 © Deep Foundations Institute 2025

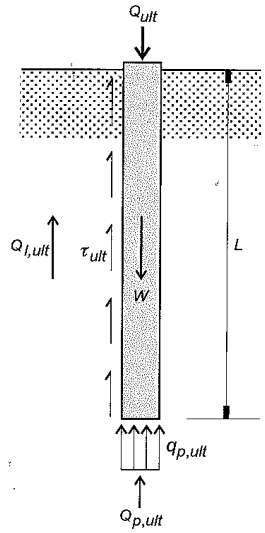


Fig. 1. Distribution of Shaft Resistance and Tip Resistance along the pile

The shaft resistance at failure ($Q_{l,ult}$) is calculated using Equation 2:

$$Q_{l,ult} = \pi\, D \sum (N\, \beta_1)\, \Delta_L \quad [2]$$

Where:

- D = Pile diameter;
- N = Standard Penetration Test (SPT) blow count;
- β1 = Shaft resistance coefficient, which varies according to soil type (see Table 1);
- ΔL = Thickness of the soil layer.

The tip resistance at failure ($Q_{p,ult}$) is estimated using Equation 3:

$$Q_{p,ult} = \beta_2\, N_p \left(\frac{\pi\, D^2}{4}\right);\ \beta_2\, N_p \leq 4{,}00\ \text{Mpa} \quad [3]$$

Where:

- N_p = SPT blow count at the pile tip;
- β_2 = Tip resistance coefficient, dependent on soil type (see Table 1)

These equations reflect the total ultimate load-bearing capacity of the pile as the sum of lateral friction along the shaft and end-bearing resistance at the pile tip. The coefficients β_1 and β_2 are empirically derived based on soil classification and local calibration from load tests.

Table 1. β_1 and β_2 values function of type of the soil

SOIL	β_1(%)	β_2
Sand	4,0 - 5,0	2,0 - 2,5
Silte	2,5 - 3,5	1,0 - 2,0
Clay	2,0 - 3,5	1,0 - 1,5

 © Deep Foundations Institute 2025

GEOTECHNICAL RISK ANALYSIS

In general, geotechnical risk analysis aims to identify potential foundation-related risks through a systematic approach that supports the following objectives:

- Determining the most appropriate foundation depth based on soil behavior;
- Ensuring foundation safety, even in the presence of unforeseen variations in subsurface conditions;
- Reducing overall project costs and minimizing the likelihood of failure or the need for corrective actions during construction.

Risk analysis is conducted from a probabilistic perspective, using Gaussian (normal) distribution curves to represent both soil resistance and applied load.

Each curve is characterized by a mean (μ) and a standard deviation (σ), where:

- μ_R = Mean value of load-bearing capacity (resistance);
- μ_S = Mean value of applied load;
- σ_{pR} and σ_{pS} = Standard deviations associated with μ_R and μ_S, respectively.

From the resistance and load curves, the safety margin distribution can be derived. This allows for the determination of both the mean safety factor and the probability of failure of the foundation system.

The mean safety factor is defined as the ratio between the mean load-bearing capacity and the mean applied load, as shown in equation [4].

$$SF = \frac{\mu_R}{\mu_S} \quad [4]$$

The reliability index (β) quantifies the safety margin in probabilistic terms and is calculated using equation [5].

$$\beta = \frac{\mu_R - \mu_S}{\sqrt{\sigma_{pR}^2 + \sigma_{pS}^2}} \quad [5]$$

The probability of failure (r) is determined by the area under the normal distribution curve associated with the calculated reliability index β.

The total cost of the foundation system is obtained by multiplying:

- The direct construction cost, and
- The financial cost of failure (C_R), calculated by Equation (6):

$$C_R = \rho \times \upsilon \times C \quad [6]$$

Where:

- ρ = Probability of failure;
- υ = Vulnerability index of the structure;
- C = Estimated cost of structural repair or replacement in case of failure.

The vulnerability index (υ) reflects the potential consequence of foundation failure on the structure and ranges from 0 to 8:

 © Deep Foundations Institute 2025

- 0 = The integrity of the element is maintained regardless of the failure event;
- 8 = Extreme potential for exposure, where failure leads to irreversible damage and the affected element cannot react in time to mitigate consequences, including significant environmental harm.

This probabilistic framework enables engineers to account for both uncertainty in geotechnical parameters and consequences of structural failure, supporting optimized and risk-aware foundation design

CASE STUDY

To conduct this study, three borehole from a site located in Barra da Tijuca, in the West Zone of Rio de Janeiro, Brazil, were analyzed.

The SPT reflects the stratified soil conditions, which typically include alternating layers of sands, silts, and soft clays.

CALCULATION OF THE IDEAL PILE LENGTH (L_{ideal})

The required length of the 50 cm diameter continuous flight auger (CFA) pile was calculated using the Cabral method (1986) for two design load cases: Sk_1 = 800.00 kN and Sk_2 = 1,200.00 kN.

The results of these calculations are presented in Table (2) below.

 © Deep Foundations Institute 2025

Table 2. Calculation of the ideal pile length

Depth	SP 01			SP 02			SP 03		
m	N_{SPT}	P_R (kN)	P_{adm} (kN)	N_{SPT}	PR (kN)	Padm	N_{SPT}	P_R (kN)	P_{adm} (kN)
1,00	3,00	240,00	120,00	10,00	800,00	400,00	12,00	960,00	480,00
2,00	2,00	160,00	80,00	8,00	640,00	320,00	10,00	800,00	400,00
3,00	4,00	320,00	160,00	2,00	160,00	80,00	8,00	640,00	320,00
4,00	4,00	320,00	160,00	3,00	240,00	120,00	6,00	480,00	240,00
5,00	6,00	480,00	240,00	5,00	400,00	200,00	8,00	640,00	320,00
6,00	14,00	1.120,00	560,00	6,00	480,00	240,00	4,00	320,00	160,00
7,00	8,00	640,00	320,00	14,00	1.120,00	560,00	5,00	400,00	200,00
8,00	9,00	720,00	360,00	16,00	1.280,00	640,00	6,00	480,00	240,00
9,00	6,00	480,00	240,00	6,00	480,00	240,00	6,00	480,00	240,00
10,00	9,00	720,00	360,00	5,00	400,00	200,00	7,00	560,00	280,00
11,00	13,00	1.040,00	520,00	8,00	640,00	320,00	9,00	720,00	360,00
12,00	13,00	1.040,00	520,00	9,00	720,00	360,00	4,00	320,00	160,00
13,00	14,00	1.120,00	560,00	8,00	640,00	320,00	10,00	800,00	400,00
14,00	15,00	1.200,00	600,00	6,00	480,00	240,00	16,00	1.280,00	640,00
15,00	12,00	960,00	480,00	9,00	720,00	360,00	16,00	1.280,00	640,00
16,00	14,00	1.120,00	560,00	13,00	1.040,00	520,00	18,00	1.440,00	720,00
17,00	14,00	1.120,00	560,00	15,00	1.200,00	600,00	22,00	1.760,00	880,00
18,00	20,00	1.600,00	800,00	14,00	1.120,00	560,00	24,00	1.920,00	960,00
19,00	18,00	1.440,00	720,00	16,00	1.280,00	640,00	20,00	1.800,00	900,00
20,00	28,00	2.240,00	1.120,00	16,00	1.280,00	640,00	20,00	1.800,00	900,00
21,00	24,00	1.920,00	960,00	20,00	1.600,00	800,00	24,00	2.160,00	1.080,00
22,00	20,00	1.600,00	800,00	28,00	2.240,00	1.120,00	22,00	1.980,00	990,00
23,00	18,00	1.440,00	720,00	22,00	1.760,00	880,00	20,00	1.800,00	900,00
24,00	20,00	1.600,00	800,00	26,00	2.470,00	1.235,00	24,00	2.160,00	1.080,00
25,00	16,00	1.520,00	760,00	32,00	3.040,00	1.520,00	24,00	2.160,00	1.080,00
26,00	26,00	2.470,00	1.235,00	29,00	2.610,00	1.305,00	26,00	2.340,00	1.170,00
27,00	26,00	2.470,00	1.235,00	26,00	2.340,00	1.170,00	34,00	3.060,00	1.530,00
28,00	28,00	2.660,00	1.330,00	29,00	2.610,00	1.305,00	32,00	2.880,00	1.440,00
29,00	32,00	3.040,00	1.520,00	35,00	3.150,00	1.575,00	36,00	3.240,00	1.620,00
30,00	34,00	3.230,00	1.615,00	38,00	3.420,00	1.710,00	38,00	3.420,00	1.710,00
31,00	39,00	3.705,00	1.852,50	40,00	3.600,00	1.800,00	45,00	4.050,00	2.025,00
32,00	35,00	3.325,00	1.662,50	45,00	4.050,00	2.025,00	50,00	4.500,00	2.250,00

It can be observed that the bearing stratum for Scenario 1 has an average depth of 20.00 meters, while for Scenario 2, the average depth is approximately 25.00 meters, as shown in Fig. (2).

 © Deep Foundations Institute 2025

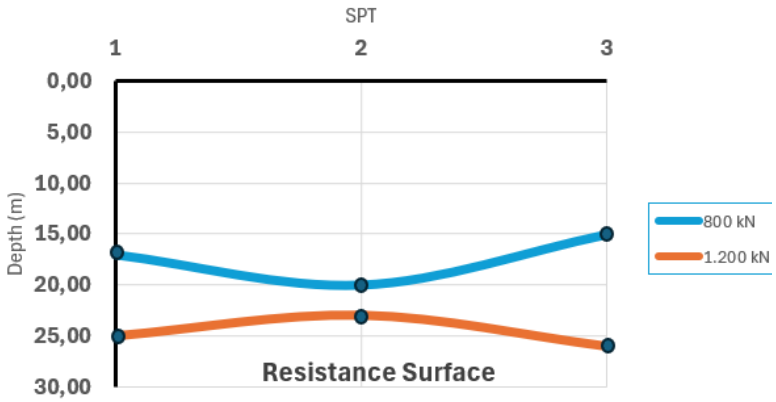


Fig. 2. Resistance Surface for 800kN and 1.200 kN scenarios.

DESIGN SAFETY CALCULATION

Based on the data presented in Table 3, for the three boreholes and considering Scenario 01 with an allowable load P_{adm} = 800.00 kN, the following parameters were obtained:

Scenario 800,00kN	
Medium load capacity (μ_R)	1.760,00 kN
Minimum load capacity	1.280,00 kN
Characteristic load capacity	1.130,04 kN
Standard deviation (s_{pR})	328,77 kN
Average request load (μ_S)	800,00 kN
Standart deviation of the requestion load (s_{pS})	100,00 kN
Reliabillity factor (β)	2,75
Probability of failure (r)	0,30%
Safety factor	2,20
Average depth considered	20,00 m

 © Deep Foundations Institute 2025

Financial economic risk analysis	
Cost of the work	$ 100.000,00
Probability of failure (r)	0,30%
Vulnerability (n)	4
Cost of geotechnical risk	$ 1.181.038,00
Number of piles	450
Unit cost of the pile	$ 20.000,00
Foundation cost with geotechnical risk	$ 10.161.038,00
Cost-to-investment ratio	9,0%
Acceptable risk (investor)	2,5%
Acceptable risk value	$ 2.500.000,00
Safety Factor	2,20
Failure occurrence ($1/P_f$)	338,69

Based on the values above we can conclude that the risk is acceptable.

SCENARIO 1.200,00kN	
Medium load capacity (μ_R)	2.445,56 kN
Minimum load capacity	1.520,00 kN
Characteristic load capacity	1.321,74 kN
Standard deviation (s_{pR})	501,02 kN
Average request load (μ_S)	1.200,00 kN
Standart deviation of the requestion load (s_{pS})	100,00 kN
Reliabillity factor (β)	2,49
Probability of failure (r)	0,65%
Safety factor	2,04
Average depth considered	25,00 m

 © Deep Foundations Institute 2025

Financial economic risk analysis	
Cost of the work	$ 100.000,00
Probability of failure (r)	0,65%
Vulnerability (n)	4
Cost of geotechnical risk	$ 645.901,00
Number of piles	345
Unit cost of the pile	$ 25.000,00
Construction Cost Reduction	$2.300.000,00
Foundation cost with geotechnical risk	$ 8.625.000,00
Cost-to-investment ratio	8,6%
Acceptable risk (investor)	2,5%
Acceptable risk value	$ 2.500.000,00
Safety Factor	2,04
Failure occurrence (1/Pf)	154,82

Scenario 01 results in an equivalent cost of $ 10,570,000.00.

Scenario 02, with fewer piles, allows for a reduction in the size of pile caps and a shorter construction schedule, leading to a lower equivalent cost of $ 8,900,000.00.

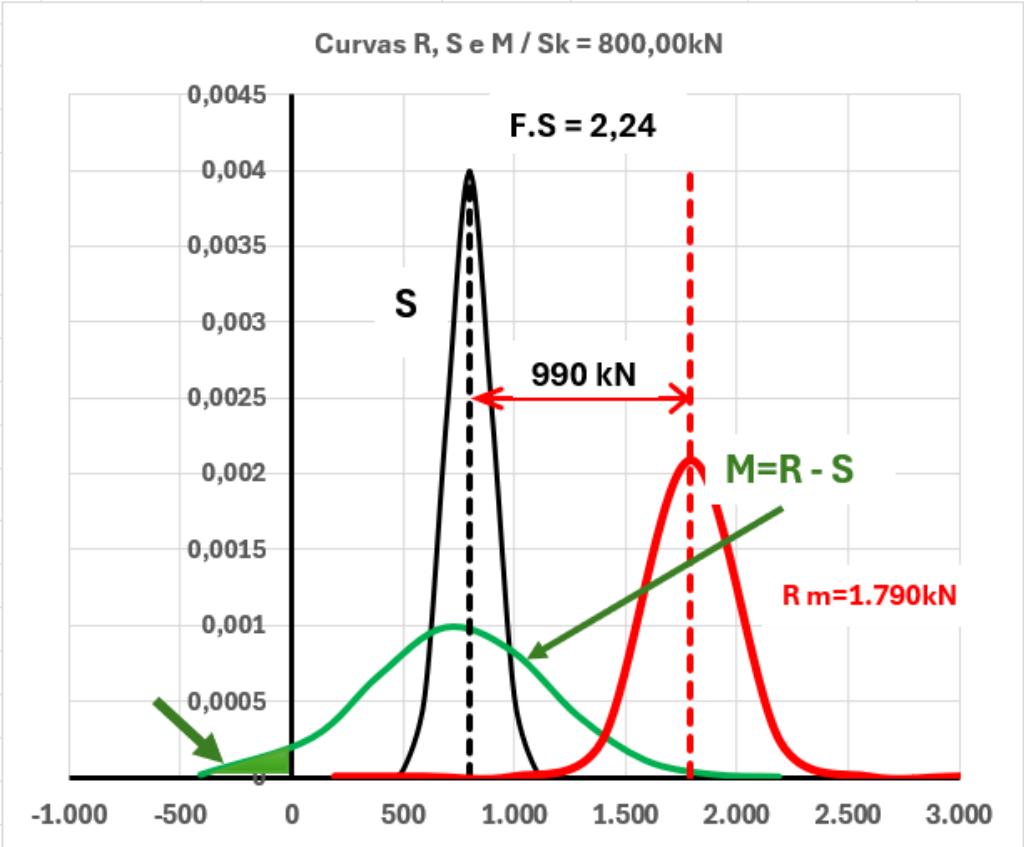
It is important to note that this type of pile can exhibit significant variation in tip resistance, making it essential to carefully analyze shaft friction.

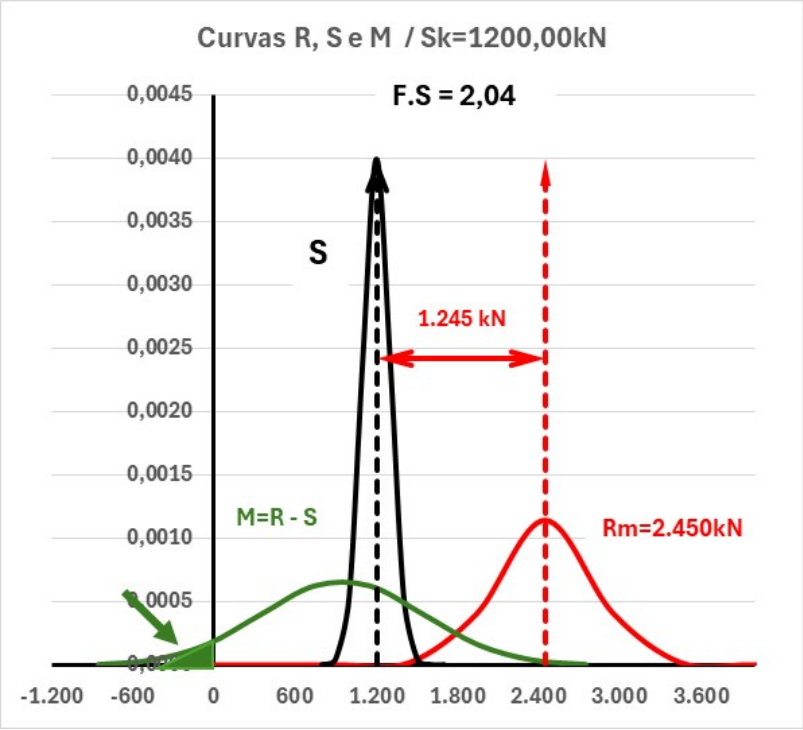
The definition of the optimal design load should also consider additional potential savings, such as:

- Reduction in pile cap volumes
- Shorter foundation execution time

 © Deep Foundations Institute 2025

Curve MS





 © Deep Foundations Institute 2025

CONCLUSION

This study highlights the importance of integrating geotechnical risk analysis into foundation design. Comparing two allowable load hypotheses for 50 cm CFA piles, the analysis reveals that:

- A higher allowable load assumption may reduce direct costs but increase long-term risk.
- Conservative design, although costlier upfront, may offer greater reliability in uncertain geotechnical contexts.
- The optimal solution balances cost, performance, and acceptable risk thresholds.

By applying a risk-based approach, engineers can make informed decisions that ensure structural safety while maintaining cost efficiency—ultimately delivering more robust and responsible engineering solutions.

This study demonstrated the importance of incorporating geotechnical risk analysis into the design of CFA pile foundations. By comparing two admissible load scenarios—800 kN (Scenario 01) and 1,200 kN (Scenario 02)—it was possible to evaluate not only the technical feasibility but also the economic and safety implications of each design alternative.

While Scenario 01 offers a lower probability of failure (1 in 250), it results in higher overall construction costs ($ 10.57 million). On the other hand, Scenario 02, despite presenting a slightly higher failure probability (1 in 155), leads to significant cost savings ($ 8.9 million) by reducing the number of piles, pile cap volumes, and foundation execution time.

Given that the risk level of Scenario 02 remains within acceptable limits for typical structural vulnerability levels, it can be considered a viable and cost-effective design solution. Moreover, the findings reinforce the relevance of considering shaft friction variability and adopting risk-informed decision-making to optimize both safety and efficiency in pile foundation projects.

REFERÊNCIAS

ABNT. NBR 6122 – Projeto e execução de fundações - Procedimento. ABNT, 1996. ABNT. NBR 8681 – Ações e segurança nas estruturas - Procedimento. ABNT, 2003.

ANG, A.H-S & TANG, W. (1984). Probability concepts in engineering planning and design. Volume II: Decision, Risk and Reliability. John Wiley & Sons. New York. 562 p.

AOKI, N. (1997). Aspectos geotécnicos da interação estrutura – maciço de solos. XXVIII Jornadas Sul-americanas de Engenharia Estrutural, São Carlos – SP, Brasil. v.1, p.VII-XX.

AOKI, N. (2002). Probabilidade de falha e carga admissível de fundação por estacas. Revista Militar de Ciência e Tecnologia, V. XIX, Brasil, p. 48-64.

AOKI, N.; CINTRA, J.C.A. (1996). Influência da variabilidade do maciço de solos no comprimento de estacas. III Seminário de Engenharia de Fundações Especiais e Geotecnia, São Paulo, Brasil, ABEF/ABMS, v.1, p.173-184.

BENJAMIM, J.R. & CORNELL, C.A. (1970). Statistics and Decision for Civil Engineering.

 © Deep Foundations Institute 2025

McGraw-Hill Book Company.

FUSCO, P. B. (1974). Conceitos estatísticos associados à segurança das estruturas. Estruturas de concreto, Vol.1, 2ª. Parte. São Paulo.

OLIVEIRA, S. K. F. & AOKI, N. (1998). Análise da segurança no projeto de fundações por estacas: método dos estados limites. XI COBRAMSEG – 10º Congresso Brasileiro de Mecânica dos Solos e Engenharia Geotécnica, Brasília.

SCHIEL, F. (1957). Estática de estaqueamentos. Publicação nº. 10. Escola de Engenharia de São Carlos – USP, São Paulo.

SHIGLEY, J.E. & MISCHKE, C. R. (1989). *Mechanical Engineering Design*. 5th ed., McGraw Hill, Inc, New York, (ISBN: 0-07-056899-5, Library of Congress: TJ 320.S5 1989)

SILVA, F.C. (2003). *Análise de segurança e confiabilidade de fundações profundas em estacas.* Dissertação de mestrado. Escola de Engenharia de São Carlos – USP. Vol.1/2, 565 p.

WHITMAN, R. V. (1984). *Evaluating calculated risk in geotechnical engineering.* Journal of Geotechnical Engineering, ASCE, Vol. 110, No. 2, February, p. 145-188.

ZAGOTTIS, D. (1981). *Pontes e grandes estruturas: IV Introdução da segurança no projeto estrutural.* Departamento de Engenharia de Estruturas e Fundações – USP. São Paulo – Brasil, 237 p.

Aoki, N. (2009). Desafio da Geotecnia em Momentos de Crise. Palestra de Abertura.

 © Deep Foundations Institute 2025

THE IMPORTANCE OF COLLABORATIVE PROJECT DELIVERY- LOOKING BACK WHILE LOOKING FORWARD

Luca Barison, PE, Nicholson Construction Company, Denver CO USA, 617) 970-4544
Luca.Barison@nicholsonconstruction.com
Brad Long, PE, Brentwood TN USA, (615) 766-7739
Tom Pullen, PG, Brierley Associates, Cottage Grove, MN USA, (607) 244-3010
Tpullen@brierleyassociates.com

ABSTRACT

The Deep Foundations Institute's (DFI) mission continues to bring together professionals with unique skillsets and organizations from varied disciplines to create a shared vision and consensus for the deep foundations industry. Looking back over the past 50 years since the founding of DFI, the geo-industry often had to navigate difficult questions, such as if conventional price-driven procurement model(s) satisfy what we need in the geotechnical construction market and as individual members of DFI. Procurement method(s) have evolved to meet an ever-changing need and have included bringing in Contractors early in the procurement process to provide input/benefit/shared solution(s). What are the opportunities for DFI members to be involved with this process?

While each of us benefit from the challenges learned over the past 50 years, we all have an opportunity to shape a pivotal time in our institute. The industry is seeing an evolution in project delivery, one that reflects an increased willingness to share risks and adapt design and schedule strategies for improved outcomes. We each bring new lessons learned and perspectives from challenging projects, we also shape the collaboration among stakeholders, and we share the commitment to improving risk management in project delivery.

This paper will offer the audience an opportunity to see what the authors as DFI members have learned while navigating and shaping the past few decades of project delivery and their thoughts on the next 50 years of continued change with project delivery in a collaborative environment.

Keywords : Design Build, Design Bid Build, Construction Management at Risk, Early Contractor Involvement, Owner, Designer, Engineer, Constructor, Geotechnical Contractor, Collaboration

1. THE EVOLUTION OF COLLABORATION IN PROCUREMENT MODELS

This paper does not intend to introduce new procurement methods or to compare existing ones. Rather, its primary objective is to underscore the critical role of collaboration within procurement models when applied to geotechnical construction,

Throughout its history, Deep Foundations Institute (DFI) has witnessed a transformation in the way projects are conceived, designed, and delivered. The construction industry has evolved from a contractor risk biased process of designing and constructing complex construction projects to a more integrated, collaborative, and risk-conscious approach involving Owner, Designer, and Constructor at different stages of delivery. This shift has been shaped by technological advances, increasing project complexity, risk informed decision making, and a growing demand for cost-effective, time-efficient delivery models that require thinking outside the conventional norms of construction contracting.

 © Deep Foundations Institute 2025

The Owner, Designer, General Contractor, and Geotechnical Contractor each play a role in successful project delivery. Early alignment across these parties is an essential part of delivering projects on time, budget, and with reduced risk. This evolution encourages all parties to collaboratively share risk and deliver projects based on lessons learned. As parties gain more experience with alternative forms of project delivery, they will all benefit. This paper also invites Owners to consider how procurement models influence collaboration and long-term project success.

In the last few decades, the conventional price-driven procurement models (i.e., Design-Bid-Build, Low-Bid Tendering, Lump Sum / Fixed Price Contracts, Unit Price Contracts, Competitive Bidding with Prequalification) have served as a primary form of project delivery. Their linear, segmented structure offered apparent predictability, typically clear contractual roles, and the appearance of fairness through competitive bidding. However, as projects have become more complex—both technically and contractually—these models have struggled to keep pace with reasonable risk sharing and needs of the project team as well as modern construction.

Over the past two decades, there has been a marked shift toward more collaborative models such as Construction Manager/General Contractor (CM/GC), Construction Manager at Risk (CMAR), Design-Build (DB), and Progressive Design-Build (PDB). These delivery methods have emerged in response to growing demands for faster schedules, fewer claims, and a more adaptive design development and are becoming the norm in many construction markets across the globe.

These project delivery methods share several key characteristics:

- Early Contractor Involvement: All methods involve engaging the Contractor or Design-Builder early in the process to improve project outcomes.
- Collaboration Focus: They emphasize varying levels of collaboration between the Owner, Designer, and Builder, with PDB and CM/GC offering the highest levels.
- Risk Allocation: Each method strategically distributes design and construction risks between the Owner and the Contractor, aiming to balance responsibility and accountability.
- Procurement Flexibility: Most use a qualifications-based or two-phase procurement process to select teams that align with project goals beyond just cost.

Several trends have accelerated the move toward collaborative procurement:

- Increased project complexity, especially in urban environments and underground construction, where uncertainty is high and traditional scoping is inadequate.
- Heightened risk sensitivity among Owners, who seek early input on constructability, site constraints, and potential schedule threats.
- Demand for innovation, particularly around sustainability, cost efficiency, and speed-to-market.
- Availability of progressive contract structures that support iterative design and phased development.
- More certainty with regards to schedule and cost.

2. LIMITATIONS OF CONVENTIONAL PRICE-DRIVEN PROCUREMENT MODELS

In certain situations, the conventional price-driven procurement model appears to create separation between design and construction in the name of objectivity and fairness. It is a process where Owners could be motivated by risk transfer, cost certainty, schedule implications, and roadblocks to a successfully constructed project. However, this same separation becomes a liability when the project involves significant underground uncertainty. Designers are often challenged with codes, standards, and processes that could impact the intentions of the Owner and the team until later in the design stage or at construction contract award when it may present incredible impacts. Specifically, Geotechnical Contractors are often introduced after design decisions have already been made – placing some impact on their ability to bring recognizable value.

While collaborative delivery models are gaining momentum, traditional price-driven approaches still dominate many sectors. In this approach to geo-structural design, Engineers often proceed with creating plans and specifications before gathering detailed, site-specific information or consulting with the construction teams who will carry out the work. Designers may be bound by a stricter budget that drives the services provided during the pre-construction phase. As a result, they must rely on assumptions about critical factors such as subsurface conditions (e.g., soil type, rock layers, groundwater levels), constructability and construction methods (the techniques and equipment that will be used). These assumptions are made without direct input from field investigations or early recommendations by construction experts. Once excavation or construction begins, real-world conditions may differ significantly from what was assumed. This can lead to design changes or delays, increased costs, safety risks and disputes between stakeholders.

Although the following points apply broadly to the project team, this paper specifically focuses on how such models impact DFI Contractors in the following ways:

Delayed Engagement

Without a role in preconstruction planning, geotechnical construction teams often receive finalized designs with limited flexibility—constraining their ability to propose alternate approaches or flag high-risk design assumptions.

Prescriptive Design, Limited Adaptability

The conventional price-driven procurement model tends to lock in designs before any field insight from construction partners is available. This is particularly problematic in subsurface work, where on-site conditions are inherently variable and require adaptable solutions.

Lowest Bid ≠ Best Value

The conventional price-driven procurement model emphasizes competitive low-cost bidding to help reduce costs. Although this can work for multiple reasons, it can often become counterproductive for complex, risk-heavy projects especially those involving challenging ground conditions. This is often due to:

 © Deep Foundations Institute 2025

- Proposals are evaluated almost exclusively on cost—not innovation, not constructability, not risk mitigation.
- Geotechnical Contractors have limited to no opportunity to engage meaningfully in the design process and therefore discuss alternatives.
- Geotechnical Contractors are typically bidding to meet prescriptive specifications, with limited incentive to propose potentially better solutions, especially when such alternatives could shift additional risk to the Contractor and require explicit approval from the Owner.

This method of procurement becomes challenging and risky for Geotechnical Contractors often bidding in the blind and needing to cover risk with contingencies while trying to remain cost competitive. Without access to data or design documents, the result can be a race to the bottom. Unfortunately, the experience, ideas, and ability of Geotechnical Contractors to optimize are often missed and/or under-utilized during conventional price-driven procurement.

Reactive vs. Proactive Project Management

One of the major pitfalls of conventional price-driven procurement model is that it often places the Owner in a reactive role. When issues emerge during construction—be it groundwater, unstable soils, or unsuitable fill—the team must respond to problems that were not anticipated and planned for.

3. WHY COLLABORATIVE DELIVERY CAN BENEFIT ALL PARTIES

In collaborative delivery, the emphasis shifts from "What is the cheapest way to meet these specs?" to "What is the smartest way to deliver this project?"—and that shift directly benefits the Owner.

Over the last few decades, specific collaborative delivery methods have emphasized integration, transparency, and shared goals. These models encourage early contractor involvement and create space for each stakeholder's expertise to shape the project before it is locked in.

A proactive approach through collaborative delivery affords:

- The planning and execution of site-specific investigations and test programs developed jointly with input from all the parties which help gather actual site condition information.
- The design team, GC/CM, and Geotechnical Contractor(s) to have the ability to co-develop a plan based on actual site conditions and elements of the design that have been agreed to as they were developed, minimizing assumptions.
- The project to have a shared risk, not transferred risk. It is priced with input from the people who should typically know how to build in those conditions based on their experience.
- The project team to function as a unified body.

For the Owner, this could result in fewer surprises and typically more control and confidence in both budget and schedule.

 © Deep Foundations Institute 2025

Benefits to the Team

As procurement evolves, so does the opportunity for Owners and Designers to implement a more comprehensive and collaborative involvement with all the key players of the project, such as the Geotechnical Contractors, largely involved in the overall project success.

In these delivery models:

- Owners can be transparent up front and lay out their priorities that influence successful delivery of a project.
- Designers can communicate design needs and the standards (codes, policy, etc.) that will be required or recommended to be incorporated in the design and construction. They can clearly state what the performance requirements of the design are without necessarily trying to prescribe construction methods.
- Throughout the design and review process – both Owner and Designer can partner with the Geotechnical Contractor to ensure goals are being met. This is a significant advantage of collaborative procurement – to utilize the expertise of each stakeholder to the fullest and from the project's inception to maximize the benefit to the Owner in terms of cost, schedule, quality, safety, environment, and overall project delivery.
- Geotechnical Contractors can participate in early constructability reviews and risk workshops, where their field knowledge adds tremendous value.
- Ground-related risk is not simply transferred down the contracting chain—it is identified and addressed collaboratively, reducing disputes and inefficiencies.
- Innovation is encouraged, not discouraged. Firms that can bring new methods, technologies, or insights to the table are rewarded—not penalized for being different.

4. How Geotechnical Contractors can Influence Delivery

Early Identification of Risks

Geotechnical Contractors can be involved with the plan to perform early investigations (for example the location of the borings, how many borings, depth of borings, the type and quantity of laboratory testing on soils and rock samples), help interpret geotechnical data and co-develop mitigation strategies before finalizing the design. This avoids late-stage rework and improves the quality of bid packages.

Shared Understanding of Site Conditions

By aligning expectations between the Owner, Designer, and Geotechnical Contractor, the team is afforded an opportunity to reduce the chances of scope disputes, claims, or adversarial dynamics that could occur later as the project progresses.

Innovation in Design and Construction

When involved early, Geotechnical Contractors can suggest better foundation systems, earth retention and ground improvement methodologies, value engineering options, and efficient construction methods that may otherwise be missed.

 © Deep Foundations Institute 2025

Influence with Decision-Making

With key voices at the table decisions are made using actual, site-specific data, not assumptions or generic models. As a result, the is a more reliable decision making on risk and schedule which allows the project to stay on track, avoiding costly delays caused by rework, re-evaluation, or redesign when unexpected conditions arise.

Schedule and Cost Control

The scope of work often handled by Geotechnical Contractors typically lies on the project's critical path, making their involvement essential from the outset. Their input is crucial in evaluating and identifying opportunities to expedite and optimize geotechnical activities. Ideally, he collaborative approach not only enhances efficiency but also provides a solid foundation for assessing the project costs more accurately as the estimates are typically based on an optimized and coordinated schedule agreed upon by are typically based on an optimized and coordinated schedule agreed upon by a re typically based on an optimized and coordinated schedule agreed upon by all parties.

For Owners, this has helped:

- Avoid overdesign (excessive foundations, suboptimal support of excavation or unnecessary ground treatment)
- Understand real-world constructability limitations
- More accurately allocate areas of risk
- Reduce change orders and construction-phase disputes

5. HOW DESIGNERS CAN INFLUENCE EARLY INVOLVEMENT

Designers play a pivotal role in shaping early contractor involvement within the geotechnical construction industry by bridging technical insight with constructability. Their early participation in project planning enables a more accurate assessment of subsurface risks, refinement of design parameters, and selection of appropriate construction methods tailored to site-specific conditions. Innovation is often less restricted by contractual terms, scope, budget, etc. By collaborating with Contractors during the conceptual and preliminary design phases, Engineers help identify potential challenges early on—such as soil variability, groundwater conditions, or slope stability issues—and incorporate practical, cost-effective solutions into the project. This is key in the early design phases (just at a 50% or later milestone). This proactive involvement not only reduces the likelihood of costly design changes or delays during construction but also fosters innovation, improved safety, and optimized project delivery through a more integrated and informed approach.

6. HOW OWNERS CAN INFLUENCE EARLY INVOLVEMENT

Require Geotechnical Contractor Engagement in Collaborative Delivery Teams

The authors encourage Owners to critically examine this key shift in procurement strategy, as it represents a foundational change with the potential to significantly improve project delivery outcomes. In CMGC, CMAR, DB or PDB projects, it is essential that Owners consider stipulating requirements that ensure

 © Deep Foundations Institute 2025

Geotechnical Contractors are embedded in the initial team and play a significant role in how the team is selected for award. Ensure their input is considered in design development, constructability reviews, and risk allocation. There are also benefits involving other key subcontractors in this process as well.

Use Qualifications-Based Selection

In the procurement process, Owners must also mandate a qualifications-based selection for key specialty Contractors. Geotechnical expertise should be evaluated based on project-specific relevance, technical depth, and ability to contribute to collaborative processes—not solely on cost.

Foster Room for Collaboration

Include Geotechnical Contractors in design meetings, risk workshops, and value engineering sessions. They have insight that directly informs design and sequencing decisions.

Incentivize Risk Sharing

Use contract structures that reward early risk identification and mitigation. Consider shared contingencies, pre-construction services contracts, or phased scopes that allow iterative input as information becomes available.

7. IS COLLABORATIVE DELIVERY ALWAYS RIGHT AND APPROPRIATE?

While the authors make the case that in geo-structural design and construction collaborative delivery models offer significant advantages, they are not universally applicable. Their effectiveness depends on several project-specific factors.

Collaborative models are most beneficial for projects with high geotechnical or constructability risk, complex stakeholder environments and evolving scopes or performance-based outcomes. We believe they also require Owner's involvement and input, experienced design and construction firms in the various types of procurement, transparency in the collaboration and a true buy-in on the teams' goals. When applied strategically, these models can unlock substantial value; when misapplied, they can introduce inefficiencies and risk.

For simpler, well-defined projects that Owners can easily design, plan and budget, more conventional models may be more cost-effective and administratively efficient. For some Geotechnical Contractors, participating in early preconstruction phases of a project demands a significant commitment of time and personnel—an investment they may be unwilling to make. As a result, they often prefer to follow more traditional procurement methods.

It is important to recognize that collaborative procurement is not a one-size-fits-all solution; each firm must evaluate whether it is the right fit for their approach and capabilities.

 © Deep Foundations Institute 2025

8. CONCLUSION: STRONGER FOUNDATIONS START WITH SMARTER AND COLLABORATIVE PROCUREMENT

Since onset, early contractor involvement within the procurement process has seen both successes and challenges. In the construction industry, early collaborative procurement has become standard practice for General Contractors but not for Geotechnical Contractors. The evolution towards a more collaborative approach to procurement has helped to shift progress and will continue to shape our construction industry. It represents a fundamental opportunity for Geotechnical Contractors to reposition themselves not as risk absorbers, but as risk managers, innovators, and strategic partners.

As DFI continues to see a quiet and steady transformation, we each must play a role in shaping its continued evolution. Collaborative delivery models will continue to enable early integration of Contractors and Owners, allowing them to proactively manage risk, drive innovation, and enhance project outcomes from the outset. In this context, for the next 50 years and beyond the expertise and contributions of DFI companies are not only valuable—they are essential.

 © Deep Foundations Institute 2025